UFFC ◆IEEE

2015

IUS

IEEE International Ultrasonics Symposium

21-24 OCTOBER, 2015, TAIPEI, TAIWAN

ABSTRACT BOOK

2015

IEEE International
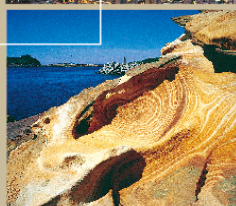## Ultrasonics Symposium

Date
October, 21-24, 2015

Venue
Taipei International Convention Center

TAIPEI
TAIWAN

Table of Contents

Oral Sessions, Thursday, October 22, 2015:

Poster Sessions, Thursday, October 22, 2015:

Awards Sessions, Thursday, October 22, 2015:

Oral Sessions, Friday, October 23, 2015:

Poster Sessions, Friday, October 23, 2015:

Oral Sessions, Saturday, October 24, 2015:

Poster Sessions, Saturday, October 24, 2015:

Message from the 2015 IEEE International Ultrasonics Symposium General Chair

Pai-Chi Li

Distinguished Professor and the Taiwan Bio-Development Foundation (TBF) Chair in Biotechnology

National Taiwan University, Taipei, Taiwan

Welcome to Taipei!

For the first time, the IEEE International Ultrasonics Symposium will be held in Taiwan. It is our great pleasure to invite you to participate in this event that brings together people from all around the world to share the latest advancements in the field of ultrasonics, inspiring new ideas and promoting collaborations.

This year there are around 800 papers to be presented, once again demonstrating active worldwide participation. These presentations cover the five main focus areas of this symposium: Medical Ultrasonics, Sensors, NDE & Industrial Applications, Physical Acoustics, Microacoustics: SAW, FBAR & MEMS, and Transducers & Transducer Materials. There are 21 invited talks, including three clinical talks to be presented by leading clinical experts from Taiwan, Japan and Korea. The poster presentations include 18 student poster competition finalists. There will also be a special session on "Ultrasonics in Biometrics" – this session is jointly organized by the IEEE Biometrics Council and the UFFC Society. I am confident this will be a very informative and inspiring meeting. I particularly would like to thank the entire organizing committee for their remarkable efforts to make the symposium an unforgettable event.

The venue, Taipei International Convention Center, is in the heart of Taipei. Before, during and after the symposium, I hope that you will have a chance to enjoy the rich cultures, the scenery, the food and the hospitality of Taiwan. We are looking forward to seeing you in Taipei.

CONFERENCE VENUE

Taipei International Convention Center

Venue Address:

1 Hsin-Yi Road, Sec.5, Taipei 11049

Tel: +886(2)2725-5200

⭐ Taipei International Convention Center (TICC)

● TICC $\xrightarrow{\text{500M – 5 min walk}}$ Taipei 101 Tower
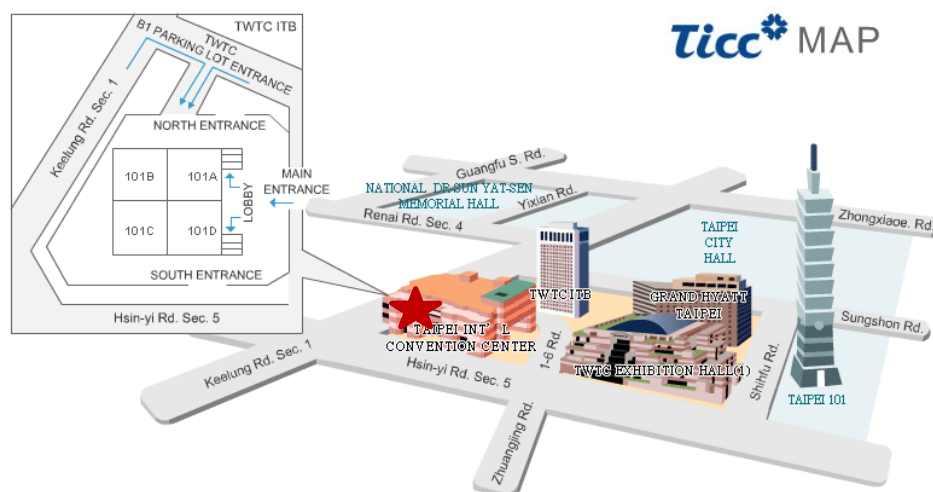
For additional information of public transit to TICC, please review the TICC website:

http://www.ticc.com.tw/Traffic/Content/ticcmrten.aspx

REGISTRATION AND FEES ($USD)

IUS 2015 Registration Fee		
Registration Status	Before Sep 15, 2015	After Sep. 15, 2015
IEEE Members*	US$ 665	US$ 815
Non-IEEE Members*	US$ 890	US$ 1040
Student*	US$ 250 (IEEE Member) US$ 400 (Non-IEEE Member)	US$ 400 (IEEE Member) US$ 550 (Non-IEEE Member)
Retiree*	US$ 250	US$ 400
Life IEEE Member*	US$ 250	US$ 400
One-Day Registration**	US$ 400	US$ 400
Short Courses***	US$ 250 (One Short Course) US$ 400 (Two Short Courses)	US$ 350 (One Short Course) US$ 500 (Two Short Courses)
Student & Retiree Short Courses***	US$ 150 (One Short Course) US$ 250 (Two Short Courses)	US$ 250 (One Short Course) US$ 400 (Two Short Courses)
Guest****	US$ 150	US$ 150
* Registration as Students must be accompanied with a proof of status. (e.g. Student ID) ** Registration as Life IEEE Member must be accompanied with a proof of status. (e.g. Member Card)* **Life Member is defined by IEEE as at least 65-year old and the age plus years of IEEE membership should be equal or greater than 100. Life members should show their IEEE Life Member card or evidence of Life Membership when getting registration materials.*		
Symposium Proceedings DVD	US$ 25	US$ 25
Symposium Banquet *Banquet ticket is included (expect for one day, short course and guest registration). You may purchase additional tickets for accompanying guests.*	US$ 90	US$ 90

Entitlement

*<u>**Registration fees for IEEE Members, Non-IEEE Members, Student, Retiree and Life IEEE Member**</u>*

- Admission to all scientific sessions and exhibition
- Admission to symposium social programs (Welcome Reception & Banquet)
- Symposium program and abstract book on USB
- Conference scheduling App miraMOBILE (search iTunes Apple store or Google Play)
- Refreshment during the symposium

- Password-protected internet access to the conference proceedings for a period of one year for downloading the papers.
- All students are entitled to free Taipei 101 Observatory Tour.

**Registration fees for One Day Registrants*

- Password-protected internet access to the conference proceedings for a period of one year for downloading the papers
- Ticket to the Welcome Reception

***Registration fees for Short Course(s) Registrants*

- Includes password-protected internet access to the conference proceedings for a period of one year for downloading the papers

****Registration fees for Guest*

- Admission to symposium social programs
- Refreshment during the symposium

Refund Policy

General attendees (non-author) are eligible for a registration refund. Notification of cancellation and request for refunds must be sent in writing to the IUS 2015 Symposium Secretariat. The following cancellation and refund policies will apply:

- Before Sep. 01, 2015: **Refund** of prepaid fees except for an administrative charge of **US$50**.
- After Sep. 01, 2015: **No** refund is applicable.
- Authors who have uploaded their papers are **not** entitled to any refunds.
- *All refund will be processed after the conference has concluded.*

CONFERENCE PROCEEDINGS

IMPORTANT NOTE: The paper submission deadline is October 7th, 2015 (two weeks before the conference).

In order for the 2015 IEEE International Ultrasonics Symposium to be published in a timely manner, it is important that authors follow the submission instructions to the best of their ability. Conference attendees will receive electronic access to the conference proceedings containing all the papers presented at the conference as part of their full registration fee.

As the Proceedings is a record of the 2015 IEEE International Ultrasonics Symposium, only those papers which are actually presented and defended at the Symposium by the author at either an oral or a poster session will be accepted for publication in the Proceedings. In the event that an author is unable to personally present the paper, she/he MUST be represented in either poster or oral sessions by an individual who is qualified to discuss the technical material in the paper and who will remain in attendance for the full session in which the paper is presented. All the session chairpersons will be recording the presenters attendance, both oral and poster, and sending the results to the Proceedings Editor.

All presenters, both oral and poster, are encouraged to publish in the conference proceedings. Full paper submissions are limited to four (4) single-side pages in the required two-column format. Invited papers can be up to ten (10) pages in length. For all papers: two (2) extra pages may be used at an excess page charge of $125/page. Payments for excess page charge are part of the paper submission process.

Instructions for the generation of the conference papers can be found at the IEEE Proceedings Author Tools Box at the following website:

http://www.ieee.org/conferences_events/conferences/publishing/templates.html. Here you will find Manuscript Templates for Conference Proceedings, IEEE Citation Reference, and IEEE Keyword Guidelines.

Part of the paper submission process involves standard conversion to PDF, and the authors will be given the opportunity to approve the converted files before the completion of the submission process. As part of the submission process, the author will have to indicate that they have read and conformed to the IEEE Proceedings formatting standards. Authors may risk having their paper not included in the proceedings if there is excessive deviations from the IEEE format standards. Our publication schedule will not allow the authors to make changes to their manuscripts after the deadline. If the papers deviate from the standard format they will be removed from publication.

The paper submission deadline is October 7th, 2015 (two weeks before the conference). IEEE takes the protection of intellectual property seriously. Accordingly, all submissions will be screened for plagiarism using CrossCheck. By submitting your work you agree to allow IEEE to screen your work. For more information please visit: http://www.crossref.org/crosscheck/index.html.

VISA ASSISTANCE

Citizens from the following countries are eligible for visa-exempt entry to Taiwan for 90 days:
Andorra, Australia, Austria, Belgium, Bulgaria, Canada, Croatia, Cyprus, Czech Republic, Denmark, Estonia, Finland, France, Germany, Greece, Hungary, Iceland, Ireland, Israel, Italy, Japan, Republic of Korea, Latvia, Liechtenstein, Lithuania, Luxembourg, Malta, Monaco, the Netherlands, New Zealand, Norway, Poland, Portugal, Romania, San Marino, Slovakia, Slovenia, Spain, Sweden, Switzerland, U.K., U.S.A. and Vatican City State.

The nationals of the following countries are eligible for the visa exemption program, which permits a duration of stay up to 30 days:
Malaysia, Singapore.

Citizens from India, Thailand, Philippines, Vietnam, and Indonesia: Visitors are from above countries also eligible for visa-empty entry if having a valid visa or permanent residence certificate issued by U.S.A., Canada, Japan, U.K., Schengen Convention countries, Australia or New Zealand. However, an advanced registration shall be completed through "Advance Online Registration System for the Visitors of Nationals from Five Southeast Asian Countries to Taiwan." (https://niaspeedy.immigration.gov.tw/nia_southeast/)

Visitor Visa for Attending Conference
Participants who aren't eligible for visa-empty entry MUST apply for visitor visa in advance.

For detail of the visitor visa application, please visit the Bureau of Consular Affairs' (BOCA) website at http://www.boca.gov.tw/mp.asp?mp=2 and/or http://www.boca.gov.tw/ct.asp?xItem=1443&ctNode=779&mp=2

If you need a personal letter of invitation to attend the Conference, please provide the following information as stated below:

- salutation (Mrs. / Mr.)
- title (Prof. / Dr. / ...)
- complete name   (first, middle, last name)
- complete mailing address (company/institution, street, city, state/province, postal code, country)
- e-mail address
- whether you are author/co-author (including ID# of your contribution)
- whether you have already registered AND paid your registration fee (incl. Invoice #), and any other details that US or your country of residence requires for your visa application

Then, contact the Conference Coordinators by email at:

    Ms. Kira Yeh

    2015 IUS Registration Office

    ius2015.reg@elitepco.com.tw

    Telephone: +886-2-8502-7087

Visa for Mainland China Passport Holders For further information, you could visit:

http://ewh.ieee.org/conf/ius/ius_2015/CrossStrait.html

IEEE Visa Guidelines

According to IEEE's guidelines for providing visa letters such formal letters of invitation will only be issued to:

- People the committee knows
- Speakers/Presenters
- Committee members
- Attendees/Exhibitors who have paid their registration fee in full

The Conference cannot contact or intervene with any Embassy or Consulate office abroad on your behalf so please begin your visa application process as soon as you determine that you want to attend the 2015 IEEE International Ultrasonics Symposium.

STUDENT TRAVEL SUPPORT

Student Travel Support will be available beginning Friday, October 23rd, 1:00 pm in the registration area. Please have identification and travel receipts available.

PRESIDENT'S STUDENT RECEPTION

Students attending the Conference are invited to attend a complimentary breakfast on Friday, October 23rd from 7:00 am to 8:00 am. This is an opportunity for students to network with other students and with the Administrative Committee members of the UFFC Society.

WOMEN IN ENGINEERING LUNCHEON

Women active in the technical areas of the UFFC conference are invited to attend a complimentary lunch and networking event organized by the women in UFFC group on Saturday, October 24th from 12:00 to 13:00. Katherine Ferrara, Distinguished Professor of Biomedical Engineering at the University of California, Davis, will offer a highlight presentation on securing, pursuing and maintaining an academic career while drawing upon your creative edge and attaining a good work-life balance.

For additional information please contact IEEE UFFC liaison to WIE, Dr. Lori Bridal, at lori.bridal@upmc.fr .

IEEE EVENT PHOTOGRAPHY STATEMENT

No flash photography may be used. Video recording by participants and other attendees during any portion of the conference is not allowed without special prior written permission of IEEE. Photographs of PowerPoint or other slides as well as posters are not permitted.

IEEE NON-DISCRIMINATION POLICY

IEEE is committed to the principle that all persons shall have equal access to programs, facilities, services, and employment without regard to personal characteristics not related to ability, performance or qualification as determined by IEEE policy and / or applicable laws

WELCOME RECEPTION

Thursday, October 22nd, 2015
Time: 6:00 pm – 8:00 pm

Location: Taipei International Convention Center, Third floor
The Conference Reception will be held at the Banquet Hall. Student Paper Competition winners will be announced during the reception.

BANQUET

Friday, October 23rd, 2015
Time: 6:00 pm – 9:00 pm

Location: Taipei International Convention Center, Third floor
The Conference Banquet will be held at the Banquet Hall.

Entertainment:
Time: 6:00 pm – 7:00 pm
Location: Taipei International Convention Center, Third floor
The Conference Banquet Entertainment will be held at the Plenary Hall.

U-Theatre: Founded in Taiwan by Ms. Ruo-Yu Liu, its present art director, in October 1988, and joined by its drumming master and music director, Mr. Chih-Chun Huang, since 1993, U-Theatre has presented rigorous works of aesthetic beauty rooted in the disciplined study and practice of meditation, drumming, martial arts, Tai-Chi, dance, and acting. Uniting East and the West, the ancient and the modern, the spiritual and the soulful, U Theatre lives and breathes 'Excellence" as embodied by the meaning of the Chinese character "U". Over the last decade the U-Theatre has been invited to perform at the world stage including Barbican Center (UK), Cultuurcentrum Brugges (Belgium), Avignon Festival, Biennale de la Danse (France), and the Next Wave Festival at BAM (NYC).

The performance at the 2015 IEEE IUS consists of the following three parts:
Surging: As a part of *The Sound of Ocean*, *Surging* is marked by ritual-like choreography and overwhelmingly intense music. With a full blast of highly enthusiastic and vibrant drumming, this piece reveals a force that is capable of bringing together and elevating the spirits of the audience. In a certain way, *Surging* can be compared to making a brushstroke in Chinese calligraphy. With a stroke of the pen, the debut is made, as if a mountain were falling and the ground breaking apart, resulting in cracks that reveal springs, which symbolize the birth of man. The water flows down, following the structure of the landscape that symbolizes the course of human life.

Sword of Spirits: The performance combines sticks, drums and martial arts to form a dance. In the middle of the stage, the hero turns around, stares at, or concentrates on striking the drums with a stick. All these gestures are blended into rhythms. Together with the women surrounding him who strike their drums from the side, they form a picture where there is tenderness in the middle of rigidity, and there is rigidity in the middle of tenderness. Long and short sticks fall simultaneously or in alternation on the top of the drum or the drum body, and together with the vocal singing reveal an extraordinary diverse music.

Sword of Wisdom: This piece is inspired by the story of Manjusri Bodhisattva who holds a sword in one hand, and scripts in the other. When the hero is granted wisdom, it is as if he had several selves, with his power multiplied. On the stage are five heroes, who in reality represent the strength of one hero. The heroes strike the drums and the ground with swords, and, by throwing and spinning them, make different sounds on the top, the body, the middle of the top of different drums or by striking on the ground, symbolizing ubiquitous wisdom. On the stage, martial arts, long sticks and drumbeats, and the turning around, rotating and jumping and leaping of the performers, together with richly diverse singing, produce a visual sensation of «blending together» in stereo. This is a new drumming form developed and practiced rigorously by U People. Striking the drums with long sticks produces an intimate relationship between performers, drums and rhythms, obtaining a form of performance that combines hands, eyes, the body and gestures into one whole. The performers are fully absorbed in each and every gesture and drumbeat; their concentration and the unity of their body and mind are visible to the spectators.
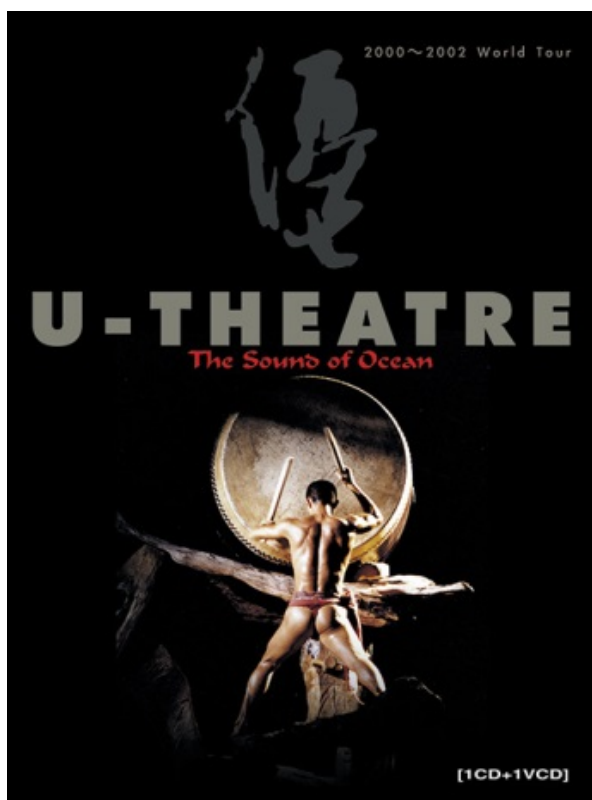
TOURS

	Tamsui Half-Day Mini Tour - NTD1,300/person		Jiu Fen One-Day Tour - NTD2,350/person
	Yehliu Geopark One-Day Tour - NTD2,430/person		Hualien Two Days Tour - NTD7,600/person
	Tainan Two Days Tour - NTD9,550/person		Sun Moon Lake Two Days Tour - NTD9,500/person

Please find more options to explore Taiwan on the IUS 2015 website
(http://ewh.ieee.org/conf/ius/ius_2015/TravelInformation.html) or contact our travel agent:

Taddy Lee
E-mail: taddyle@liontravel.com

＊ The tour desk will be available besides the registration desk. There will also be travel
agents at the desk to provide tour information and arrangement services.

➢ **Free Taipei 101 Observatory tours for students**
Student tours are scheduled during the conference on following dates and time:

Wednesday, October 21st 2015

Time: 7:00pm-10:00pm

Thursday, October 22nd 2015
Time: 8:30pm-10:00pm

Friday, October 23rd 2015
Time: 9:00pm-10:00pm

Saturday, October 24th 2015
Time: 6:00pm-10:00pm

The attendance is only available for the students who had registered online for his/her participation. The ticket will be issued with the presence of FREE Taipei 101 Observatory Tour coupon, half an hour before the beginning of tour in front of the observatory ticket booths on the 5th floor of Taipei 101 Shopping mall, please be on time to ensure your entitlement.

Description: FREE Taipei 101 Observatory Tour

At 382 meters above the ground, the 89th floor Observatory offers visitors a commanding view of the city and Taipei Basin at all directions. The world's largest damper, weighing 660 metric tons, is also exhibited at this level. The Observatory is equipped with high - power binoculars, drinks bar, image services, pre-recorded audio tour guides in seven languages, & souvenir shops.

TAIPEI 101 Observatory's elevators are Guinness Record - breaking high-speed pressurized elevators in 2004, with a speed of 1010 meters per minute. It takes only 37 seconds to reach the 89th floor.
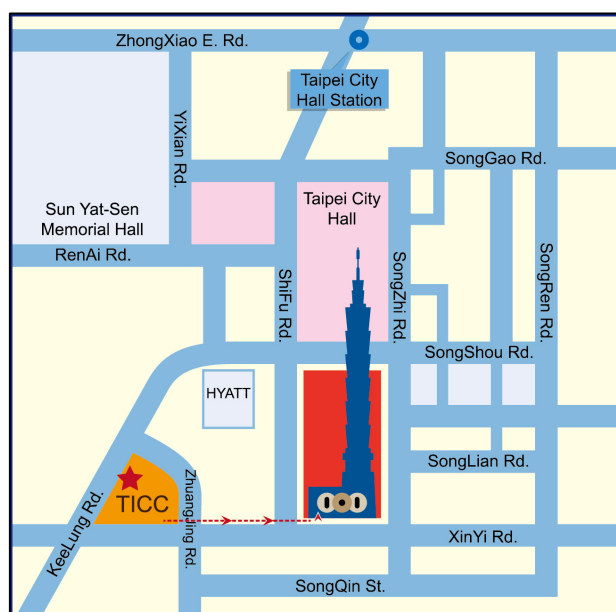
EXHIBITORS LIST

Gold Level Exhibitor Information

Verasonics, a technology company based in Kirkland, Washington USA, was founded in 2002. Verasonics designs, manufactures and sells state-of-the-art ultrasound research systems for academic and commercial investigators. These real-time, software-based ultrasound systems simplify the data collection and analysis process to facilitate accelerated research and development.

Verasonics systems support emerging applications requiring high frequencies, high frame rates, high power and high channel count for medical and industrial applications such as earth sciences and non-destructive testing NDT/NDE.

Verasonics licenses its technology, sells research systems and software components, and provides consulting services.

Exhibitor and Satchel Insert Sponsor

S-Sharp is dedicated to providing cutting edge solutions to preclinical and clinical research ultrasound. Our core competence is the ability to leverage rapid advancement of electronics technologies and powerful software computations into biomedical ultrasound and to address our customer's needs. Our preclinical ultrasound imaging product, Prospect, in an open platform designed to streamline the workflow and enhance the quality of small animal research. In addition, Prospect's unique imaging technologies, including shear wave elasticity measurements and Analog Doppler, assist users to perform high quality preclinical research that was not possible before. Our array ultrasound imaging product, Prodigy, shares the same core technologies and innovations. It is aimed to provide the highest research values to most people in need.

Exhibitor and Welcome Reception Sponsor

Weidlinger Associates is the developer of PZFlex, the premier finite element simulation software for piezoelectric and ultrasound analyses. Specifically written for this class of problems, PZFlex displays efficiencies that allow multi-million element models to be solved rapidly on a desktop PC. For nearly 20 years PZFlex has been the simulation tool of choice of the ultrasound imaging, SONAR, NDT, sensor and actuator communities.

Coffee Break for One Day Sponsor

As one of the world-leading manufacturers for Real-Time VOC analyzer, TricornTech possesses critical technology, which leverages the advanced electronic technologies, nano-materials, and innovative sensing architecture to create its significance in the market.

With strong force of Self-R&D capabilities and innovative technologies, TricornTech successfully presents the leading-edge MiTAP series (Miniaturized Total Analysis Platform), enabling on-site analytical monitoring capability and providing multiple merits of specificity, portability, accuracy, cost-effectiveness and more to achieve state-of-the-art performance.

TricornTech is committed to providing integrated, cost-effective and constructive solutions to assist our valued customers solving problems. Not only do we offer a wide product range from high-tech portable instruments to integrated online systems, we also provide a comprehensive software custom made to each and every customer. Our solutions make an excellent foundation for a proactive approach to maintenance, integrated in customers' normal maintenance activities. On Customers' request, we put together the monitoring equipment package best suited to your economic and technical requirements.

Exhibitor Information

	Acoustic Life Science Co., Ltd. (ALS) is a high-tech Chinese company dedicated to the research, develop, production and application of advanced medical ultrasound technology. With cutting-edge technology, professional management team and comprehensive facilities, ALS is a fast-growing company specialized in ultrasound probe technology. We value our talents, patents, as well as key techniques, which are the cornerstones to enable the sustainable development of the company. Ultrasound probes and interventional ultrasound products are two main categories of ALS's portfolio. Leading in ultrasound materials, manufacturing process and new application, we continue to innovate and develop state-of-the-art techniques to build next generation medical ultrasound products.
	Founded in 2007 as a value innovator providing comprehensive ultrasound solutions, ALPINION has been dedicated to technological and user-driven innovation in medical ultrasound transducers, diagnostics, research, and therapeutic ultrasound (US-guided HIFU). With its acoustic engineering superiority, ALPINION strives to provide customers with uniform and fundamentally excellent imaging performance throughout the whole product lifetime.
	BK Ultrasound's Sonix brand has been a leading provider of ultrasound research systems for researchers and entrepreneurs for more than 10 years. Our full diagnostic ultrasound research systems give users an access to the specialized software development kits, software updates and unlimited access to our knowledge database.
	Advanced OEM Solutions (AOS) designs, develops, and manufactures cutting-edge phased array and conventional multi-channel boards (modules) for the NDT industry, especially integrator for AUT inspection solution. Our products are designed to be compact, open (source code is included in SDK), cost effective, and easy to use. For detail, pls. go to our website.

Founded in 1997, Shanghai Apex Electronics Technology Co., Ltd. (Abbreviated to APEX) is the leading company for designing, development and manufacturing medical ultrasonic transducers (probes), and provides related technical services.

The mission of Apex is to provide advanced acoustic technologies, superior qualities, high acoustic performance and low cost products to satisfy increasing customer demands.

APEX is dedicated to excellence through quality by ensuring the solid commitment that our quality standards must be higher than the quality specified and expected by our customers.

Apex offers a complete series of diagnostic medical ultrasound products for a broad range of clinical application including micro-convex, linear arrays, curved

Spun off from the Industrial Technology Research Institute (ITRI) of Taiwan, R.O.C. in 2002, Broadsound Corporation is a medical ultrasound equipment company with research, development, manufacturing, marketing, and sales, focusing on medical diagnostic ultrasound transducers and ultrasound imaging & instrumentation system development platform; the main products and services include the following:

1. New Ultrasound Replacement Transducers
2. Custom-made Ultrasound Transducers
3. Custom-designed Services
4. Ultrasound Transducer Automation Test System
5. Ultrasound Transducers Repair Service

Launching the marketing in 2007, we have now successfully sold the Broadsound new replacement transducers and established good relationships with highly satisfied partners in more than 100 countries globally. Broadsound Corporation offers excellent quality, high performance, and cost-effective ultrasound transducers covering convex array, linear array, phased array, and endo-cavity array. Pioneering in the sector of new ultrasound replacement transducer, so far Broadsound Corporation is the sole company in the world who has the European Union CE0197 mark, U.S. FDA 510(k) Marketing Clearance, and registration to other countries such as Russia and Brazil etc. on the new ultrasound replacement transducer.

	Cephasonics is a medical- and industrial-device technology leader utilizing ultrasound and the power of the cloud to bring about the ubiquitous adoption of ultrasound-based measurement products that improve the quality of life. Launched with a management buyout in March 2012 and headquartered in Santa Clara, Calif., Cephasonics' ultrasound technology, including its AutoFocus™ beamforming technology, has won multiple industry awards for innovation. Additional information about Cephasonics can be found at www.cephasonics.com.
	The Department of Medical Ultrasound of the Fraunhofer Institute for Biomedical Engineering IBMT technologically implements the scalability of ultrasound in a new unique modular ultrasound beamformer, which can be easily adapted to a variety of applications in research and product development. In addition to the ultrasonic hardware, the department applies innovative software solutions that enable us to use ultrasound in medicine, biotechnology, the NDT and sonar. Specialities are systems and methods that work with very high frequencies, are adapted to specific environmental conditions (hybrid imaging on MRI/pressure neutrality for use in AUVs and ROVs), use optical laser combined with ultrasound (optoacoustics) or are extremely compact for use with mobile devices.
	IMASONIC is an independent, privately-owned company that develops and produces ultrasonic transducers for health and safety applications. Since its creation in 1989, IMASONIC has been contributing to improving ultrasonic technology by designing and manufacturing transducers based on customer's requirements for medical (HIFU, diagnosis and monitoring) and industrial applications (NDT and measurement). Located in France, the company has 90 employees.
	IPPT PAN is a government funded scientific institute conducting research in theoretical and applied physics, mechanics of materials and structures, computational methods, electronics, and ultrasonics. Professional Electronic Lab (http://us4us.eu) is dedicated to

provide advanced electronic design services as well as R&D on medical and industrial applications of ultrasound. Implemented certified quality management systems ISO-9001/ISO-13485 enable us to design, produce and introduce medical devices on the EU market.

Our flagship product is a Versatile Ultrasound Research Platform, which enables real-time implementation and testing of the most computational intensive ultrasound algorithms, thanks to the GPU processing.

Kolo Medical is a world leader in next generation silicon ultrasound transducer technology. We are the first company to make CMUT a practical alternative to PZT transducers, and thus, uniquely positioned to set a new performance standard in clinical diagnostic imaging. Our design and engineering innovations will establish the silicon age of ultrasound imaging.

Kolo has brought together a team of world-class talent from the medical ultrasound and semiconductor industries. Our founders, originally from the research group at Stanford University that invented the CMUT technology, have more than 30 years' experience in silicon transducer innovation. Their expertise in developing the most advanced innovations in this field puts Kolo in an enviable position, with more than 40+ issued patents and impressive IP. Our management team is comprised of seasoned executives and world-renowned technology pioneers from market leading companies, known for their experience in developing and commercializing emerging innovative technologies.

Kolo's proprietary transducer technology delivers an unprecedented level of performance in the area of ultra-high resolution imaging. We offer a portfolio of innovative transducers to meet our customers' diagnostic imaging needs and enable new applications in areas that are not currently developed due to limitations of existing PZT transducer technology.

Our facility in Kvistgaard, Denmark, formerly known as Ferroperm Piezoceramics (www.ferroperm-piezo.com, www.insensor.com), specialises in manufacturing advanced piezoelectric ceramic components and integrated piezoelectric thick film devices.

ONDA	ONDA is the global leader in ultrasound measurement instrumentation and services. Our products are used to acoustically test devices in the medical, industrial, and electronic markets. Over 3,000 hydrophones have been used around the world to support a broad range of applications including medical imaging, therapeutic ultrasound, ultrasonic cleaning, and non-destructive testing. Onda has served over 1,000 unique customers in over 35 countries representing Fortune 10 companies, government research centers, and the most prominent universities.
Polytec	For over 45 years Polytec has provided high-technology, laser-based measurement solutions to researchers and engineers. Our commitment is to provide the most precise and reliable optical instruments and sensors available for non-contact measurement, setting Polytec apart from the competition as the gold standard in the design and manufacture of vibrometer and velocimeter systems. Our innovations answer many pressing manufacturing and engineering challenges.
PRECISION ACOUSTICS	Precision Acoustics (PA) manufactures acoustic measurement products for medical and NDT industries and is the leading global supplier of test and measurement equipment for the MHz ultrasound markets in the range 40 kHz to 50 MHz. PA products include needle, membrane and fibre-optic hydrophones, single element PVdf and piezo-ceramic ultrasound transducers and the automated Ultrasonic Measurement System (UMS) for beam plotting and NDT scanning. In addition Precision Acoustics offers a consultancy service for the development of bespoke ultrasound measurement and generation solutions, including custom transducers, ultrasonic materials characterisation and automated test and measurement systems. Precision Acoustics maintains a close working relationship with the acoustics group of the National Physical Laboratory, London as well as with several leading research institutions worldwide.
scia systems	scia Systems manufactures advanced ion beam and plasma processing equipment. The systems are used in the production of microelectronics, MEMS and precision optical

components, in both, high volume production as well as applications in research and development.

Key applications are frequency and thickness trimming to Angstrom precision, in manufacturing of BAW/SAW devices, with the industry proven scia Trim 200 system. Furthermore the scia Magna 200 deposits SiO2 temperature compensation films and piezoelectric AlN films. High homogeneity, rapid deposition rates and excellent material properties can be achieved, due to its unique Double Ring Magnetron architecture.

scia Systems provides highly reliable tools together with a superior technology support. The tools are flexible and modular in design. Several vacuum process chambers can be combined into cluster or in-line solutions, according to customer-specific requirements.

Sonic Concepts, Inc. manufactures high-power, wide-bandwidth ultrasound transducers and related equipment. SCI supplies single- or multi-element transducers, as well as annular, linear, and 2D arrays, transmit electronics, passive cavitation detectors, high-intensity hydrophones, radiation force balances, water degassing equipment, and more. SCI supports customer orders from initial prototyping into full-scale production.

TRUST Bio-Sonics is one of the leading companies in providing the ultrasound contrast agents. Through our innovative technologies, we offer a series of the world's smallest (micron/nano-sized) bubble agents for contrast-enhanced perfusion imaging, ultrasound-mediated drug/gene delivery and more advanced theranostic applications.

We strive to improve the quality of human life by developing novel technologies and offering a product portfolio for ultrasound-based early diagnosis and therapy. To make breakthroughs of ultrasound technologies, you are welcome to join our open platform and lead your own innovations!

The SAMPL lab, led by Prof. Yonina Eldar, is a lab within the EE department at the Technion, Israel institute of Technology. SAMPL research focuses on new design paradigms in which sampling and processing are designed jointly in order to exploit signal properties already in the sampling stage.

The laboratory facilitates the transition from pure theoretical research to the development, design and implementation of prototype systems.

Zurich Instruments makes lock-in amplifiers and phase-locked loops that have revolutionized instrumentation in the high-frequency and ultra-high-frequency ranges by combining frequency-domain tools and time-domain tools within each product. This reduces the complexity of laboratory setups, thus removing sources of potential problems and so allows researchers to focus on their experiments. The new MFLI instrument for low-frequencies makes these advantages available to a wider range of users.

Acknowledgements

FUTURE CONFERENCE

2016
ieee
IUS
INTERNATIONAL ULTRASONICS SYMPOSIUM
september 18-21, Tours, France

September 18-21, TOURS, FRANCE
ieee INTERNATIONAL ULTRASONICS SYMPOSIUM

General Chair
Ayache Bouakaz,
Université F. Rabelais de Tours,
Inserm, France

Technical Chair
Ton van der Steen,
Biomedical engineering,
Erasmus MC, Rotterdam,
The Netherlands

Finances Chairs
Christelle Vibrac,
Université F. Rabelais de Tours and
Dan Stevens Treasurer IEEE

Exhibits Chairs
Oliver Keitmann,
Siemens AS, Denmark and
Jean Luc Gennisson
Institut Langevin, Paris

Short courses Chairs
Nico de Jong,
Erasmus MC, Rotterdam and
Lori Bridal, LIB Paris

Communication - Sponsor Chairs
Nicolas Felix,
VERMON Tours and
Cyril Lafon, LabTAU, Lyon

Audio - Video Chair
Jean-Marc Grégoire,
Université F. Rabelais de Tours

**Local / student / Travel / Visa
arrangements Chair**
Jean-Michel Escoffre,
Université F. Rabelais de Tours and
Hervé Liebgott, CREATIS Lyon

Publication Chair
Steve Freear,
University of Leeds, Leeds,
United Kingdom

The annual 2016 IEEE International Ultrasonics Symposium will be held at the **the VINCI Convention Center, TOURS, FRANCE, from September, 18-21, 2016**. Oral and poster presentation formats will be used at the symposium. Papers are solicited for this conference describing original work in the field of ultrasonics from the following subject classifications:

◄ Group 1: Medical Ultrasonics

MBB	Medical Beamforming and Beam Steering
MBE	Biological Effects & Dosimetry
MBF	Blood Flow Measurement
MCA	Contrast Agents
MEL	Elastography
MIM	Medical Imaging
MPA	Medical Photoacoustics
MSD	System & Device Design
MSP	Medical Signal Processing
MTC	Medical Tissue Characterization
MTH	Therapeutics, Hyperthermia, and Surgery

◄ Group 2: Sensors, NDE & Industrial Applications

NAF	Acoustics Microfluidics
NAI	Acoustic Imaging
NAM	Acoustic Microscopy
NAS	Acoustic Sensors
NDE	General NDE Methods
NEH	Energy Harvesting
NFM	Flow Measurement
NMC	Material & Defect Characterization
NPA	Photoacoustics
NPC	Process Control
NSP	Signal Processing
NTD	Transducers: NDE and Industrial
NUA	Underwater Acoustics
NWP	Wave Propagation

◄ Group 3: Physical Acoustics

PAT	Acoustic Tweezers and Particle Manipulation
PNL	Nonlinear Acoustics
PGP	General Physical Acoustics
POA	Opto-acoustics
PPN	Phononics
PTF	Thin Films
PMI	Magnetic/Electromagnetic Interactions
PUM	Ultasonic Motors & Actuators

◄ Group 4: Microacoustics: SAW, FBAR, MEMS

ADA	Device Applications
ADD	Device Design
ADM	Device Modeling
AMP	Materials & Propagation
AMS	Microacoustic Sensor Devices & Applications

◄ Group 5: Tranducers & Transducer Materials

TMC	Materials Fabrication and Characterization
TMO	Modeling (Analytical & Numerical)
TFT	Thin and Thick Piezoelectric Films
TMU	Micromachined Ultrasonic Transducers
TMI	Biomedical Diagnostic and Imaging Transducers
TTT	Biomedical Therapeutic Transducers
THF	Front-end and Integrated Electronics
TFI	High Frequency Transducers
TPF	Applications of Piezoelectrics & Ferroelectrics

IEEE ULTRASONICS, FERROELECTRICS,
AND FREQUENCY CONTROL SOCIETY

◆ IEEE

ewh.ieee.org/conf/ius/ius_2016/

CONFERENCE ORGANIZING COMMITTEE

General Chair:

Pai-Chi Li

National Taiwan University

Taipei, Taiwan

Technical Program Chair:

Stanislav Emelianov

Georgia Institute of Technology and

Emory University Medical School, USA

Finance Chair:

Mark Schafer

Sonic Tech, Inc.

Ambler, PA, USA

Publication Chair:

Steve Freear

University of Leeds

Leeds, United Kingdom

Short Course Chair:

Hairong Zheng

Shenzhen Institute of Advanced Technology,

Chinese Academy of Science, Shenzhen, China

Exhibits Chair:

Tsung-Tsong Wu

National Taiwan University

Taipei, Taiwan

Publicity Chair:

Ken-Ya Hashimoto

Chiba University

Chiba, Japan

Web Chair:

Chih-Kuang Yeh

National Tsing-Hua University

Hsinchu, Taiwan

Local Arrangements Chair:

Che-Chou Shen

National Taiwan University of Science and Technology

Taipei, Taiwan

Audio-Visual Chair:

Chih-Chung Huang

National Cheng-Kung University

Tainan, Taiwan

SHORT COURSES

1A: 08:00am-12:00pm   **Ultrasound Imaging Systems: from Principles to Implementation**

Instructor: Kai Thomenius**,** Massachusetts Institute of Technology, USA

1B: 08:00am-12:00pm   **Elasticity Imaging: Methods and Applications**

Instructor: Mark Palmeri**,** Duke University, USA

1C: 08:00am-12:00pm   **Ultrasonic Therapy: Mechanism, Methods, and Application**

Instructor: Kullervo Hynynen**,** Sunnybrook Health Sciences Centre, Canada

1D: 08:00am-12:00pm   **Signal Processing and System-on-Chip Designs for Ultrasonic Imaging, Detection and Estimation Application**

Instructors: Jafar Saniie**,** Department of Electrical and Computer Engineering, Illinois Institute of Technology, USA an**d** Erdal Oruklu, Department of Electrical and Computer Engineering, Illinois Institute of Technology, USA

1E: 08:00am-12:00pm   **Laser Interferometric Measurement of Acoustic Surface and Bulk Waves: Application for SAW&FBAR Components**

Instructor: Kimmo Kokkonen, Aalto University, Finland

1F: 08:00am-12:00pm   **Medical Transducers (with Electronics)**

Instructors: L. Scott Smith, GE Global Research and David Cowell, University of Leeds, UK

2A: 1:00pm-5:00pm   **Ultrafast Imaging in Biomedical Ultrasound: Principles and Applications**

Instructors: Mickael Tanter and Mathias Fink, Institut Langevin, ESPCI, France

2B: 1:00pm-5:00pm   **Ultrasound Contrast Agents: Fundamentals and Application to Molecular Imaging, Gene and Drug Delivery**

Instructors: Nico de Jong, Erasmus MC, The Netherlands and Michel Versluis, University of Twente, The Netherlands

2C: 1:00pm-5:00pm   **Biomedical Photoacoustics: From Bench to Bedside**

Instructor: Michael Kolios, Department of Physics, Ryerson University, Canada

2D: 1:00pm-5:00pm   **Acoustical Imaging; from Acoustic Field Equations to Imaging and Inversion**

Instructor: Koen W.A. van Dongen, Laboratory of Acoustical Wavefield Imaging, Faculty of Applied Sciences, Delft University of Technology, the Netherlands

2E: 1:00pm-5:00pm   **A Modern Approach to Modelling and Simulation of Micro-acoustic Devices**

Instructor: Alireza Baghai-Wadji, University of Cape Town, South Africa

2F: 1:00pm-5:00pm   **High Frequency Transducers (with Materials)**

Instructors: Sandy Cochran, University of Dundee, UK and Qifa Zhou, University of Southern California, USA

TECHNICAL PROGRAM COMMITTEE

Group 1: Medical Ultrasonics

TPC Vice Chair
Georg Schmitz
Ruhr-Universität
Bochum, Germany

Members

- Ayache Bouakaz, INSERM, France
- Lori Bridal, University Pierre and Marie Curie, France
- Charles A. Cain, University of Michigan, USA
- Jean-Yves Chapelon, INSERM, France
- Paul A. Dayton, University North Carolina/NCSU, USA
- Nico de Jong, Erasmus Medical Centre, The Netherlands
- Chris de Korte, Catholic University of Nijmegen, The Netherlands
- Jan Dhooge, Catholic University of Leuven, Belgium
- Emad Ebbini, University of Minnesota, USA
- Stanislav Emelianov, Georgia Institute of Technology and Emory University, USA
- Kathy Ferrara, University of California Davis, USA
- Stuart Foster, University of Toronto, Canada
- Steven Freear, University of Leeds, UK
- Caterina Gallipi, University of North Carolina, USA
- James Greenleaf, Mayo Clinic, USA
- Christopher Hall, Philips Research, USA
- Peter Hoskins, University of Edinburgh, UK
- John Hossack, University of Virginia, USA
- Kullervo Hynynen, University of Toronto, Canada
- Jørgen Arendt Jensen, Technical University Denmark , Denmark
- Hiroshi Kanai, Tohoku University, Japan
- Jeff Ketterling, Riverside Research , USA
- Michael Kolios, Ryerson University, Canada
- Elisa Konofagou, Columbia University, USA
- Nobuki Kudo, Hokkaido University, Japan
- Pai-Chi Li, National Taiwan University, Taiwan

- Hervé Liebgott, CREATIS, France

- Jian-yu Lu, University of Toledo, USA

- Tom Matula, University of Washington, USA

- James G. Miller, Washington University, USA

- Helen Mulvana, University of Glasgow, UK

- Kathy Nightingale, Duke University, USA

- Svetoslav Nikolov, BK Medical, Denmark

- William D. O'Brien, University of Illinois, USA

- Michael Oelze, University of Illinois, USA

- Georg Schmitz, Ruhr-Universität Bochum, Germany

- Ralf Seip, Philips Research, USA

- Mickael Tanter, INSERM, France

- Kai Thomenius, GE Corporate R&D, USA

- Hans Torp, University of Science and Technology, Norway

- Piero Tortoli, University Firenze, Italy

- Ton van der Steen, Erasmus Medical Centre, The Netherlands

- Kendall Waters, Silicon Valley Medical Instruments, USA

- Keith Wear, Food and Drug Administration, USA

- Wilko G. Wilkening, Siemens Medical Solutions , USA

- Chih-Kuang Yeh, National Tsing Hua University, Taiwan

- Hairong Zheng, Shenzhen Institutes of Advanced Technology, China

Group 2: Sensors, NDE, and Industrial Application

TPC Vice Chair
David Greve
Carnegie Mellon University
USA

Members

- Robert C. Addison, Rockwell Science Center

- Walter Arnold, Fraunhofer Institute for NDT

- James Blackshire, Air Force Research Laboratory

- Ramazan Demirli, Villanova University

- James Friend, UCSD

- Eric S. Furgason, Purdue University

- David Greve, Carnegie Mellon University

- Edward Haeggstrom, University of Helsinki

- Jacqueline Hines, Applied Sensor R&D Corporation

- Patrick Johnston, NASA Langley Research Center

- Lawrence W. Kessler, Sonoscan Inc.

- Pierre T. Khuri-Yakub, Stanford University

- Mario Kupnik, Technische Universität Darmstadt

- Roman Maev, University of Windsor

- Kentaro Nakamura, Tokyo Institute of Technology

- Erdal Oruklu, Illinois Institute of Technology

- Nishal Ramadas, Elster Instromet

- Jafar Saniie, Illinois Institute of Technology

- Gangbing Song, University of Houston

- Bernhard Tittman, Pennsylvania State University

- Jiromaru Tsujino, Kanagawa University

- John F. Vetelino, University of Maine

- Paul Wilcox, University of Bristol

- William Wright, University College Cork

- Donald E. Yuhas, Industrial Measurement Systems

- Jennifer Michaels, Georgia Institute of Technology

Group 3: Physical Acoustics

TPC Vice Chair
Vincent Laude
Centre National de la Recherche
Scientifique, France

Members

- Arthur Ballato, Clemson University, USA

- Anne Bernassau, University of Glasgow, UK

- Jan Brown, JB Consulting, USA

- Charles Courtney, University of Bath, UK

- Emmanuel Defay, CRP G. Lippmann, Luxemburg

- Jianke Du, Shanghai Jiaotong University, China

- David Feld, Avago Technologies, USA

- Tao Han, Shanghai Jiao Tong University, China

- Fred Hickernell, Motorola, Inc., USA

- Takefumi Kanda, Okayama University, Japan

- Eun Sok Kim, University of Southern California, USA

- Minoru K. Kurosawa, Tokyo Institute of Technology, Japan

- Amit Lal, Cornell University, USA

- John Larson, Avago Technologies, USA

- Vincent Laude, FEMTO-ST / CNRS, France

- Andreas Mayer, Hochschule Offenburg, Germany

- Farid G. Mitri, Chevron, USA

- Roy H. Olsson III, Sandia National Laboratories, USA

- Mihir Patel, Schlumberger-Doll Research,, USA

- Yan Pennec, IEMN / Universite de Lille 1, France

- Susan Schneider, Marquette University, USA

- Bikash Sinha, Schlumberger-Doll Research,, USA

- Masaya Takasaki, Muroran Institute of Technology, Japan

- Koen W.A. Van Dongen, Delft University of Technology, Netherlands

- Jorg Wallaschek, Leibniz Universitat Hannover, Germany

- Ji Wang, Ningbo University, China

- Tsung-Tsong Wu, National Taiwan University, Taiwan

- Takahiko Yanagitani, Nagoya Institute of Technology, Japan

- Yook-Kong Yong, Rutgers University, USA

- Jiun Der Yu, Epson Research & Development Inc., USA

Group 4: Microacoustics - SAW, FBAR, MEMS

TPC Vice Chair
Karl Wagner
TDK Corporation
Munich, Germany

Members

- Ben Abbott, Qorvo Inc. , USA

- Robert Aigner, Qorvo Inc. , USA

- Sylvain Ballandras, freq 'n' sys SAS, France

- Kushal Bhattacharjee, Qorvo Inc. , USA

- Sunil Bhave, Cornell University, USA

- Sergey Biryukov, IFW Dresden, Germany

- Paul Bradley, Avago Technologies, USA
- Jidong Dai, Murata Electronics, Inc., USA
- Omar Elmazria, Universite de Lorraine, France
- Gernot Fattinger, Qorvo Inc., USA
- Gerhard Fischerauer, University of Bayreuth, Germany
- Ken-ya Hashimoto, Chiba University, Japan
- Shitang He, IACAS, China
- Michio Kadota, Tohoku University, Japan
- Jyrki Kaitila, Avago Technologies, Germany
- Kimmo Kokkonen, Aalto University, Finland
- Jan Kuypers, Qorvo Inc. , USA
- Don Malocha, University of Central Florida, USA
- Hiroyuki Nakamura, Skyworks-Panasonic Corp., Japan/USA
- Natalya Naumenko, Nat. University of Science & Technology MISIS, Russia
- Tuomas Pensala, VTT, Finland
- Mauricio Pereira da Cunha, University of Maine, USA
- Maximilian Pitschi, TDK Corporation, Germany
- Leonard Reindl, Albert-Ludwigs-University Freiburg, Germany
- Richard Ruby, Avago Technologies, USA
- Marc Solal, Qorvo, Inc , USA
- Shuji Tanaka, Tohoku University, Japan
- Masanori Ueda, Taiyo Yuden, Japan
- Karl Wagner, TDK Corporation, Germany
- Robert Weigel, University of Erlangen-Nuremberg, Germany
- Sergei Zhgoon, National Research University, Russia

Group 5: Transducers and Transducer Materials

TPC Vice Chair
Sandy Cochran
University of Dundee
UK

Members

- Sandy Cochran, University of Dundee, UK
- David Cowell, University of Leeds, UK
- Christopher Daft, River Sonic Solutions, USA

- Loriann Davidsen, Philips Healthcare , USA

- Levent Degertekin, Georgia Institute of Technology, USA

- Christine Démoré, University of Dundee, UK

- Charles Emery, Ulthera Inc., USA

- Arif Sanli Ergun, TOBB University, Turkey

- Lynn Ewart-Paine, NUWC, USA

- Tomas Gomez, CSIC, Madrid, Spain

- Anne-Christine Hladky, Institut Supérieur d'Electronique et du Numérique, France

- Xiaoning Jiang, North Carolina State University, USA

- Ho-yong Lee, Ceracomp Co., Ltd, Korea

- Reinhard Lerch, Friedrich-Alexander-Universität Erlangen-Nuremberg, Germany

- Richard O'Leary, University of Strathclyde, UK

- Omer Oralkan, North Carolina State University, USA

- Wei Ren, Xi'an Jiaotong University, China

- Paul Reynolds, uBeam, USA

- Yongrae Roh, Kyungpook National University, Korea

- Ahmad Safari, Rutgers University, USA

- Jean-Francois Saillant, Areva, France

- Mark Schafer, Sonic Tech Inc., USA

- Scott Smith, GE Global Research, USA

- Wallace Smith, Office of Naval Research, USA

- Yasuhito Takeuchi, Kagoshima University, Japan

- Susan Trolier-McKinstry, Pennsylvania State University, USA

- Jian Yuan, Philips Shanghai Apex, USA

- Shujun Zhang, Pennsylvania State University, USA

- Qifa Zhou, University of Southern California, USA

PLENARY LECTURE

Thursday, October 22nd, 2015 8:00 am – 9:30 am, Plenary Hall

Pan-Chyr Yang, MD, PhD, President, National Taiwan University

Ultrasound and Translational Pulmonary Medicine

Dr. Yang currently is the President of National Taiwan University and Professor in the Department of Internal Medicine, National Taiwan University College of Medicine. His major research interests are pulmonary and critical care medicine, molecular and cellular biology, lung cancer genomics and personalized cancer therapy. He was elected member of Academia Sinica in 2006 because of his contributions in leading the translational research and implementation of precision therapy for lung cancer in Taiwan, which have significantly improved the survival in lung cancer patients. His research group identified novel genes and pathways that associated with lung cancer progression. They established new platform for development of lung cancer stem cell directed therapy and discovered the autocrine-paracrine interaction between the lung cancer stem cell with cancer microenvironment. They also identified specific gene expression and microRNA biomarkers that might be beneficial for precision therapy of lung cancer patients.

ABSTRACT

Ultrasound technology is a powerful diagnostic and therapeutic tool in clinical medicine. Here I summarize the progress of ultrasound technology in translational pulmonary medicine in the past decades. Air-containing lung is not a good ultrasound-transmitting medium. By scanning through the acoustic window created by consolidated disease lung, ultrasound is a very useful and reliable tool to evaluate the nature of the lesions of the chest wall, pleural cavity, diaphragm, mediastinum, hilum, and peripheral lungs. A precise puncture transducer can be used to perform ultrasound-guided transthoracic needle biopsy (TNB) with real-time visualization of the biopsy needle and the lesion. The accuracy of ultrasound-guided TNB for peripheral pulmonary nodules, chest wall lesions, and mediastinal tumors is 88% to 100%. Ultrasound-guided TNB is also useful for histologic diagnosis of tumors causing superior vena cava syndrome, Pancoast's tumors, pulmonary consolidation of unknown etiology, and tumors with obstructive pneumonitis. Moreover, transthoracic needle aspiration under ultrasound guidance can provide adequate specimens for microbiologic diagnosis of lung abscesses, necrotizing pneumonia, and parapneumonic effusions. Color Doppler imaging further extends the diagnostic spectrum of ultrasound, allowing the hemodynamics and neovascularization of a pulmonary lesion to be assessed noninvasively. Pulmonary arteriovenous malformations, pulmonary sequestration, and pulmonary infarctions can be diagnosed easily with color Doppler ultrasound. The color Doppler ultrasound puncture guiding device can improve the safety of ultrasound-guided TNB by simultaneously displaying blood vessel information, the needle shaft, and the puncture route. The recent development of endobronchial ultrasound (EBUS) further extends the accessibility of ultrasound for evaluating and sampling of lesions adjacent to the airways and mediastinum and improves the staging of lung cancer. In combination of "omic technology", ultrasound has become indispensable diagnostic and therapeutic tool for translational pulmonary medicine.

CLINICAL SPEAKERS

1E-1 Ultrasound-guided high intensity focused ultrasound: clinical experience

Jae Young Lee**,** Seoul National University Hospital, South Korea

Friday, October 23rd, 2015 10:30am – 11:00am, Plenary Hall, 3F

1E-2 Clinical Application of Liver Elastography

Yi-Hong Chou and Hsin-Kai Wang, Taipei Veterans General Hospital, Taiwan

Friday, October 23rd, 2015 11:00am – 11:30am, Plenary Hall, 3F

1E-3 Ultrasound Fusion Imaging of Liver Tumor: Recent Progress and Clinical Relevance

Masatoshi Kudo, Kinki University, Japan

Friday October 23rd, 2015 11:30am – 12:00pm, Plenary Hall, 3F

INVITED SPEAKERS

Group 1: Medical Ultrasonics

1A-1 Elasticity measurement of carotid artery atherosclerotic plaque

Chris de Korte, Medical UltraSound Imaging Center (MUSIC), Department of Radiology and Nuclear Medicine, Radboud University Medical Center, Netherlands

October 22nd, Thursday, 10:30am - 10:45am, Plenary Hall, 3F

1B-3 Handheld photoacoustic imaging with integrated diode lasers

Georg Schmitz, Hans-Martin Schwab, Martin Beckmann, Chair for Medical Engineering, Ruhr-Universität, Germany

October 22nd, Thursday, 1:30am - 1:45am, Plenary Hall, 3F

1C-3 Super-resolution imaging of microbubble contrast agents

Robert Eckersley, King's College, UK

October 22nd, Thursday, 4:00am - 4:15am, Plenary Hall, 3F

1D-5 Shear wave elasticity imaging for preclinical research on small animals and 3D cell cultures

Pai-Chi Li, National Taiwan University, Taiwan

October 23rd, Friday, 9:00am – 9:15am, Plenary Hall, 3F

2G-1 Nonlinear beamforming of aperture domain signals

 Brett Byram, Biomedical Engineering, Vanderbilt University, USA

 October 23rd, Friday, 3:30pm – 3:45pm, VIP Room, 4F

2I-1 Ultrafast vector flow imaging

 Damien Garcia, University of Montreal, Canada

 October 24th, Saturday, 10:30am - 10:45am, VIP Room, 4F

Group 2: Sensors, NDE & Industrial Applications

5B-1 Quantitative phased array modeling and imaging

 Lester Schmerr Jr., Center for NDE, Iowa State University, USA

 October 22nd, Thursday, 1:00pm - 1:15pm, Room 103, 1F

5D-1 In-chip GHz ultrasonic pulses for information processing

 Amit Lal, SonicMEMS, Electrical and Computer Engineering, Cornell University, USA

 October 23rd, Friday, 8:00am – 8:15am, Room 103, 1F

5H-1 SAW synthesis with inverse filter and IDT Arrays for microfluidic and biological applications: one ring to rule them all

 Michaël Baudoin, Antoine Riaud, Jean-Louis Thomas, Adrien Bussonière, Olivier Bou Matar, IEMN, University of

 Lille, EC Lille, CNRS, INSP, France

 October 24th, Saturday, 8:00am - 8:15am, Room 103, 1F

Group 3: Physical Acoustics

6B-1 Phonon dynamics in electromechanical resonators

 Imran Mahboob, Hirsohi Yamaguchi, NTT Basic Research Laboratories, Japan

 October 22nd,Thursday, 1:00pm - 1:15pm, Room 201AF, 2F

6D-1 Depth-profiling of acoustic, optic and acousto-optic spatial inhomogeneities by technique of picoseconds ultrasonic interferometry

 Vitalyi Gusev, LAUM, UMR-CNRS 6613, LUNAM, Université du Maine, Le Mans, France

 October 23rd, Friday, 8:00am – 8:15am, Room 201AF, 2F

6G-1 Finite element analysis of BAW devices: principles and perspectives

 Robert Thalhammer, John Larson, Avago Technologies, Munich, Germany, Avago Technologies, USA

 October 23rd, Friday, 3:30pm – 3:45pm, Room 201AF, 2F

Group 4: Microacoustics - SAW, FBAR, MEMS

7A-1 GaN MEMS resonators and oscillators
    D. Weinstein, MIT, USA
    October 22nd, Thursday, 10:30am – 10:45am, Room 105, 1F

7C-1 Current developments and future trends in mobile terminal frontend architectures
    Harald Pretl, DMCE GmbH & Co KG, Austria
    October 22nd, Thursday, 3:30pm - 3:45pm, Room 105, 1F

7E-1 Heterogeneous integration technology using wafer-to-wafer transfer
    Shuji Tanaka, Department of Bioengineering and Robotics, Tohoku University, Japan
    October 23rd, Friday, 10:30am – 10:45am, Room 105, 1F

Group 5: Transducers & Transducer Materials

8A-5 Wearable ultrasound applicators for wound healing and noninvasive drug delivery
    Peter A. Lewin, Youhan Sunny, Christopher Bawiec, Leonid Zubkov, Michael Neidrauer,
    Michael S. Weingarten, David J. Margolis, Drexel University, University of Pennsylvania,
    USA
    October 22nd, Thursday, 11:30am – 11:45am, Room 102, 1F

8F-1 Reliability measurements of CMUT arrays of a semiconductor manufacturer
    Christophe Antoine, Erik Tarvin, Sushil Bharatan, Urvi Shah, Rob O'Reilly, Michael Judy,
    Analog Devices Inc., USA
    October 23rd, Friday, 1:00pm – 1:15pm, Room 102, 1F

8J-1 Current Status and Future Prospects of High Performance Piezoelectric Single Crystals:
Bridgman Method vs. Solid-state Single Crystal Growth (SSCG) Method
    Ho-yong Lee, Ceracomp Co. Ltd, Republic of Korea
    October 24th, Saturday, 1:00pm - 1:15pm, Room 102, 1F

STUDENT PAPER COMPETITION

Student Paper Competition Chairs:

Stanislav Emelianov

PA-1 *Low flow rate spraying using a torsional ultrasonic transducer*

Shunsuke Tsuyuki[1], Takefumi Kanda[1], Koichi Suzumori[2], Shin-ichiro Kawasaki[3], Shoki Ofuji[1], [1]Okayama University, Okayama, Japan, [2]Tokyo Institute of Technology, Tokyo, Japan, [3]National Institute of Advanced Industrial Science and Technology, Miyagi, Japan

PA-2 *Fast wave velocity measurement by Brillouin scattering using induced phonon from ScAlN piezoelectric thin film*

Masahiko Kawabe[1], Takahiko Yanagitani[2], Hayato Ichihashi[1], Shinji Takayanagi[1], Masashi Suzuki[3], Mami Matsukawa[1], [1]Doshisha University, Kyoto, Japan, [2]Waseda University, Tokyo, Japan, [3]Nagoya Institute of Technology, Nagoya, Japan

PA-3 *High order mode polarity inverted Al-polar (0001) ScAlN/O-polar (000-1) ZnO film resonator*

Takeshi Mori[1], Takahiko Yanagitani[2], Masashi Suzuki[1], [1]Nagoya Institute of Technology, Japan, [2]Waseda University, Tokyo, Japan

PA-4 *Multiphysics Modeling of BAW Filters*

Andreas Tag[1], Dominik Karolewski[2], Bernhard Bader[3], Maximilian Pitschi[3], Robert Weigel[1], Amelie Hagelauer[1], [1]Institute for Electronics Engineering, University of Erlangen-Nuremberg, Erlangen, Germany, [2]Institut für Mikroelektronik- und Mechatronik-Systeme gemeinnützige GmbH, Germany, [3]TDK Corporation, Germany

PA-5 *Evaluation of Acoustic Properties of $CaTiO_3$-(K,Na)NbO_3 Film Using Microfabricated Structure*

Ryosuke Kaneko[1], Michio Kadota[1], Yuji Ohashi[2], Jun-ichi Kushibiki[1], Shinsuke Ikeuchi[3], Shuji Tanaka[1], [1]Graduate school, Tohoku University, Sendai, Miyagi, Japan, [2]Institute for Material Research, Tohoku University, Sendai, Miyagi, Japan, [3]Devices Development, Murata Manufacturing Co., Ltd., Nagaokakyo, Kyoto, Japan

PA-6 *SAW Characteristics of AlN/SiO_2/3C-SiC Layered Structure with Embedded Electrodes*

Qiaozhen Zhang[1], Tao Han[1], Jing Chen[1], Kenya Hashimoto[2], [1]Electronic Information and Electrical Engineering, Shanghai Jiao Tong University, Shanghai, Shanghai, China, People's Republic of, [2]Graduate School of Engineering, Chiba University, Japan

PA-7 *Dual-Mode Integrated Circuit for Imaging and HIFU With 2-D CMUT Arrays*

Ji Hoon Jang[1], Anshuman Bhuyan[1], Hyo-Seon Yoon[1], Jung Woo Choe[1], Amin Nikoozadeh[1], Douglas Stephens[2], Butrus Khuri-Yakub[1], [1]Electrical Engineering, Stanford University, Stanford, California, USA, [2]Biomedical Engineering, University of California, Davis, Davis, California, USA

PA-8 *Capsule-based Ultrasound-mediated Targeted Gastrointestinal Drug Delivery*

Fraser Stewart[1], Antonella Verbeni[2], Yongqiang Qiu[1], Benjamin Cox[1], Jan Vorstius[3], Sandy Cochran[1], [1]Institute for Medical Science and Technology, University of Dundee, United Kingdom, [2]The BioRobotics Institute, Scuola Superiore Sant'Anna, Italy, [3]School of Engineering, Mathematics and Physics, University of Dundee, United Kingdom

PA-9 *Design of High-Efficiency, Miniaturized Ultrasonic Receivers for Powering Medical Implants with Reconfigurable Power Levels*

Ting Chia Chang[1], Marcus Weber[1], Jayant Charthad[1], Amin Nikoozadeh[1], Butrus T. Khuri-Yakub[1], Amin Arbabian[1], [1]Electrical Engineering, Stanford University, Stanford, CA, USA

PA-10 *Photoacoustic properties of plasmonic-nanoparticle coated microbubbles*

Adam Dixon[1], Song Hu[1], Alexander Klibanov[1], John Hossack[1], [1]Biomedical Engineering, University of Virginia, Charlottesville, Virginia, USA

PA-11 *Joint compressive sampling and deconvolution in ultrasound medical imaging*

Zhouye Chen[1], Adrian Basarab[1], Denis Kouamé[1], [1]IRIT, UMR CNRS 5505, University of Toulouse, France

PA-12 *Automatic Mouse Embryo Brain Ventricle Segmentation, Gestation Stage Estimation, and Mutant Detection from 3D 40-MHz Ultrasound Data*

Jen-wei Kuo[1], Yao Wang[1], Orlando Aristizabal[2,3], Daniel H. Turnbull[3], Jeffrey A. Ketterling[2], Jonathan Mamou[2], [1]Electronics and Computer Engineering, Polytechnic School of Engineering, New York University, Brooklyn, USA, [2]F. L. Lizzi Center for Biomedical Engineering, Riverside Research, New York, USA, [3]Skirball Institute of Biomolecular Medicine, New York University School of Medicine, New York, USA

PA-13 *Robust Sound Speed Estimation for Hepatic Steatosis Assessment*

Marion Imbault[1], Alex Faccinetto[2], Bruno-Félix Osmanski[1], Mathias Fink[1], Jean-Luc Gennisson[1], Valérie Vilgrain[2], Mickaël Tanter[1], [1]Institut Langevin, ESPCI ParisTech, PSL Research University, CNRS UMR 7587, INSERM U979, Paris, France, [2]Department of Radiology, Beaujon Hospital, Paris, France

PA-14 *In vivo magnetomotive ultrasound imaging of rat lymph nodes – a pilot study*

Maria Evertsson[1], Magnus Cinthio[1], Pontus Kjellman[2,3], Sarah Fredriksson[2], Roger Andersson[1], Hanna Toftevall[2], Hans W Persson[1], Tomas Jansson[4,5], [1]Biomedical Engineering, Faculty of Engineering, LTH, Lund University, Lund, Sweden, [2]Genovis AB, Sweden, [3]Medical Radiation Physics, Clinical Sciences Lund, Lund University, Lund, Sweden, [45]Biomedical Engineering, Clinical Sciences Lund, Lund University, Lund, Sweden, [5]Medical Services, Skåne University Hospital, Lund, Sweden

PA-15 *Ultrafast Pulsed Magnetomotive Ultrasound Imaging of Sentinel Lymph Nodes: Small Animal Study*

Yu-Chun Huang[1], Jieh-Yuan Houng[1], Yi-Da Kang[2], San-Yuan Chen[2], Meng-Lin Li[1,3], [1]Dept. of Electrical Engineering, National Tsing Hua University, Hsinchu, Taiwan, [2]Dept. of Materials Science and Engineering, National Chiao Tung University, Taiwan, [3]Institute of Photonics Technologies, National Tsing Hua University, Taiwan

PA-16 *Ultrasound flow mapping for the investigation of crystal growth*

Norman Thieme[1], Richard Nauber[1], Hannes Beyer[1], Hannes Radner[1], Lars Büttner[1], Paul Bönisch[2], Kaspars Dadzis[2], Lamine Sylla[2], Dagmar Meier[3], Olf Pätzold[3], Jürgen Czarske[1], [1]Laboratory for Measurement and Sensor System Techniques, Dresden University of Technology, Dresden, Germany, [2]SolarWorld Innovations GmbH, Freiberg, Germany, [3]Institut für Nichteisen-Metallurgie und Reinststoffe, Technische Universität Bergakademie, Freiberg, Germany

PA-17 *Non-contact mass measurement of droplet based on free oscillation under ultrasonic levitation*

Sae Ito[1], Ryohei Nakamura[1], Hiroki Tanaka[1], Yosuke Mizuno[1], Marie Tabaru[1], Kentaro Nakamura[1], [1]Precision and Intelligence Laboratory, Tokyo Institute of Technology, Yokohama, Japan

PA-18 *Ultrasound Image-based Absolute Concentration Measurement Technique for Materials with Low Scatterer Concentration*

John H. Lee[1], Javier Jimenez[2], Xiang Zhang[1], Duane S. Boning[1], Brian W. Anthony[1], [1]Massachusetts Institute of Technology, Cambridge, MA, USA, [2]Madrid-MIT M+Vision Consortium, Massachusetts Institute of Technology, Cambridge, MA, USA

POSTER PRESENTATION GUIDE

Posters will be on display in the Poster Area located in the **4F Corridor**. This year we will have three full day poster sessions. Each poster session is divided into two time slots, as follows:

Mornings: 09:30 am to 10:30 am (posters with odd numbers will be presented)
Afternoons: 2:30 pm to 3:30 pm (posters with even numbers will be presented)

Posters must be posted in the morning between 7:30 am to 8:00 am. They must be removed between 5:00 pm to 5:30 pm at the end of the day. Therefore, each poster will be displayed for a full day (8:00 am – 5:00 pm)

Student Paper Competition (SPC) posters will be displayed in **Room 101** on the **first floor**. To recognize an outstanding work of the students and their accomplishment, SPC posters will be on display for all three (3) days of the conference. Student authors are required to be present for all six poster sessions to describe their work. Judges will review the SPC posters on Thursday only.

Poster Size and Instructions

- One poster board is allocated to each presentation. The recommended poster size is 36 inches high by 48 inches wide (92 cm x 122 cm).
- Posters must be mounted using supplies provided by the organizing committee.
- Each poster presenter is required to defend his/her poster during the respective poster session slot for the paper to be included in the conference proceedings.
- Simply posting the pages of your written version of the proceedings paper is not effective and thus not acceptable for your poster.
- The title of your poster paper should be done in block letters which are at least 8 to 10 cm (3 to 4 inches) high.
- All text must be easily readable from a distance of 1 to 2 meters. Make the lettering at least 1 cm high, smaller lettering will not be legible from a distance of 1 to 2 meters.
- All graphs and charts should be least 25 X 30 cm (approximately 8.5 x 11 inches) or larger.
- It is a good idea to sequentially number your materials in the poster. This will indicate to the viewer a logical progression through your poster.
- Provide an introduction (outline) and a summary or conclusion for your poster.
- Prepare your poster carefully so that it can be used as the basis to explain and answer questions from the viewers.
- It is helpful to have copies of your proceedings paper available for those who may want to study specifics of your work in more detail.
- Have your business cards or contact information available for those who may wish to contact you at a later date.
- Bring along a notepad to use for a discussion of technical details relating to your poster.

ORAL PRESENTATION GUIDE

Observing Your Allotted Time

- The total time allotted to each speaker is 15 minutes. You should plan to speak for 12 minutes and leave 3 minutes for questions.
- Invited speakers have twice this time, 30 minutes in total, and they should plan to speak for about 25-27 minutes leaving 3-5 minutes for questions.
- There is no excuse for using more than your allotted time. Rehearse your presentation several times; projecting slides and doing anything else you would otherwise expect to do at the meeting. It is a discourtesy to your audience, the Session Chair and the other speakers to exceed your allotted time. The Session Chairs are instructed to adhere to the printed schedule for the session. With many parallel sessions this is critical to the overall success of the conference.

Organization of Oral Sessions

- There are six to eight parallel sessions in the conference and the Technical Program Committee will ensure minimal conflicts of topics between the parallel sessions.
- Audio and Video Equipment Provided at the Conference: The conference will be equipped with a computer video projector and a computer that is connected to the projector for each oral presentation room. Normal audio equipment such as microphones will be provided.
- Software Used in the Conference: The computers are equipped with Windows 7 as well as **Microsoft PowerPoint 2010 (Office 2010)** and **Adobe Acrobat Reader**. The PowerPoint 2010 is the preferred projection software offered at the conference.
- It is strongly recommended to all authors to check their presentation in the Speaker Ready Room for compatibility and proper operation.
- Avoid Font Problems: Since your computer may have sophisticated fonts (such as special equation symbols) that the conference computers do not have, it is suggested that when you save your PowerPoint presentations, use "Save As" from your "File" pull-down menu. When a dialog box pops up, click on the "Tools" menu on that dialog box and select "Save Options". Then, check the option "Embed true type fonts". Click "OK" and then click "Save". This allows you to include the fonts you are using in your presentations to minimize the font incompatibility problems. Otherwise, any fonts that are not recognized by the conference computers would be incomprehensible. In addition to the default ".pptx" file format, we suggest that you also save a copy of your presentations in the ".ppsx" (PowerPoint Show) format for safe (the ".ppsx" version may also include some of the special fonts in your presentations). If you have a full version of Adobe Acrobat, we suggest you also save (or print) your presentations into a ".pdf" format and thus you will be able to use the free Adobe Reader software to present in case nothing else would work.
- Movies or Videos: If you have movies or videos, the best way to present them properly is to use your own laptop computers since the conference computers may not have the Code/Decode

(Codec) software that is necessary to play your movies or videos. If you do not wish to bring your own computers, you may have to convert all of your movies and videos to the Moving Picture Experts Group 1 (MPEG1) format to ensure a cross-platform compatibility. In addition, the movie or video files should be placed where the links in your presentations are pointing to. To make it easy, you could place the movies and videos in the same folder as your ".pptx" or ".ppsx" files when you prepare your presentations and then copy all these files together to a folder or the desktop of the conference computers.

- USB Thumb Drives: Nowadays it is convenient to save your PowerPoint presentations in a USB 2.0 thumb drive. The conference computers will be equipped with the USB 2.0 interfaces. However, some USB drives may have security or driver issues that may prevent the drives from being recognized by the conference computers. Please scan your USB drives to remove viruses if there are any before you bring them to the conference.

- CD or DVD Backup: You could also save a copy of your presentation on a CD-R, CD-RW, DVD+/-R, or DVD+/-RW as a backup in case your USB thumb drives do not work with the conference computers (such as missing drivers or having security protections). When you use CD or DVD media, you should "close" (not be able to add any more files) them to increase the chance that these media could be read by the conference computers. If you use Direct CD to save your presentations, please make sure they are readable in a computer without Direct CD software installed.

- VGA Adapters: The conference computer projectors will be equipped only with a standard 15-pin analog Video Graphic Array (VGA) connector. If you decide to bring your laptop computers that do not have a VGA port, it is your responsibility to bring all necessary video output adapters with you so that your computers can be connected to the projectors (your computer vendors usually sell or ship such converters with your computers). In addition, the highest resolution of the computer projectors is 1024 x 768 pixels and the resolution of your laptop computers may need to be adjusted properly.

- 100V-240V Voltage Converters: Taiwan uses 110V/60Hz as its power standard. If your laptop computers do not work with 110V/60Hz, it is your responsibility to bring all necessary power converters. In addition, please plug the power adapters into the power strips so that your laptop computers will not run out of power during your presentations. Please also notice that the plug of the power adapter of your laptop computer may not necessarily fit with the 110V power strip. In this case, international converters/adaptors may be needed for you to use the power strips.

- Backup Your Laptop Computers: We suggest you make a copy of your presentations on a USB thumb drive in case your computers are damaged, lost, or cannot be used for whatever reasons.

Good Practices

- Show no more than 1 slide per minute of speaking time. This means approximately 10-12 slides maximum for the 12 minutes of presentation at the symposium. Remember, the last three minutes of the presentation are for questions from the audience. It detracts from the quality of the

presentation to flash numerous graphs, equations, or tables on the screen in rapid sequence in an effort to squeeze a presentation into its allotted time.

- Make the letters on your slides sufficiently big – suggested minimum font size is 14.
- Put no more than 12 lines of text or 4 curves on any slide.
- Avoid lengthy tabulations of numerical data and limit equations to those for which the terms can be properly defined.
- Your audience needs time to interpret the data that you present. While you are very familiar with the data displayed, the audience is not. Describe the abscissa, coordinates, units and the legend for each curve.
- When you display a curve, tell the audience what they should be looking for in order to grasp the point you are trying to make. The audience will not have time to figure it out for themselves.
- Use repetition in your talk to ensure the facts are understood by the audience.
- In addition to the body of the talk, present an introduction and a summary or conclusion.
- Include only information or data that can be properly explained in the allotted time.
- Repeat any questions that are posed to you.
- If a question requires a lengthy reply, suggest that you and the person asking the question meet after the presentation. Then take the discussion out of the meeting room.

SPEAKER READY ROOM

Speaker Ready Room is located at Room 203 on the 2nd floor of the Taipei International Convention Center (TICC). The schedule of the speaker ready room is as follows:

October 21:	7:00 AM – 5:00 PM
October 22:	7:00 AM – 5:00 PM
October 23:	7:00 AM – 5:00 PM
October 24:	7:00 AM – 5:00 PM

Please follow closely the instructions on the "Oral Presentation Guide" to prepare your presentation and to avoid any technical difficulties.

2015 IUS CONDENSED PROGRAM

2015 IUS CONDENSED PROGRAM					
Wednesday, October 21, 2015					
Time	**102** **1st floor**	**105** **1st floor**	**103** **1st floor**	**201AF** **2nd floor**	**201BC** **2nd floor**	**201DE** **2nd floor**
08:00 - 12:00	Short Course 1A Ultrasound Imaging Systems: from Principles to Implementation	Short Course 1B Elasticity Imaging: Methods and Applications	Short Course 1C Ultrasonic Therapy: Mechanism, Methods, and Application	Short Course 1D Signal Processing and System-on-Chip Designs for Ultrasonic Imaging, Detection and Estimation Application	Short Course 1E Laser Interferometric Measurement of Acoustic Surface and Bulk Waves: Application for SAW&FBAR Components	Short Course 1F Medical Transducers (with Electronics)
12:00 - 13:00	Lunch Break					
Time	**102** **1st floor**	**105** **1st floor**	**103** **1st floor**	**201AF** **2nd floor**	**201BC** **2nd floor**	**201DE** **2nd floor**
13:00 - 17:00	Short Course 2A Ultrafast Imaging in Biomedical Ultrasound: Principles and Applications	Short Course 2B Ultrasound Contrast Agents: Fundamentals and Application to Molecular Imaging, Gene and Drug Delivery	Short Course 2C Biomedical Photoacoustics: From Bench to Bedside	Short Course 2D Acoustical Imaging; from Acoustic Field Equations to Imaging and Inversion	Short Course 2E A Modern Approach to Modelling and Simulation of Micro-acoustic Devices	Short Course 2F High Frequency Transducers (with Materials)

2015 IUS CONDENSED PROGRAM							
Thursday, October 22, 2015							
Time	**Plenary Hall** **3rd floor**	**VIP Room** **4th floor**	**201BC** **2nd floor**	**201DE** **2nd floor**	**103** **1st floor**	**201F** **2nd floor**	**201A** **2nd floor**	**102** **1st floor**
08:00 - 09:30	Opening Plenary (Plenary Hall, 3rd floor)							
09:30 - 10:30	Coffee Break (101, 1st floor) & Poster Display (West Corridor, 4th floor)							
10:30 - 12:00	Session 1A MEL: Carotid elasticity measurement techniques	Session 2A MCA: Molecular imaging	Session 3A MBF: Advances in flow imaging methods	Session 4A MBB: Beamforming I	Session 5A Ultrasonics in Water and Air	Session 6A Acoustic Tweezers and Particle Manipulation	Session 7A MEMS and FBAR Oscillators and innovative applications	Session 8A Medical Applications of Transducers
12:00 - 13:00	Lunch Break							
Time	**Plenary Hall** **3rd floor**	**VIP Room** **4th floor**	**201BC** **2nd floor**	**201DE** **2nd floor**	**103** **1st floor**	**201F** **2nd floor**	**201A** **2nd floor**	**102** **1st floor**
13:00 - 14:30	Session 1B MPA: Photoacoustic systems	Session 2B MEL: New shear wave imaging techniques	Session 3B MTH: Treatment monitoring	Session 4B MIM: Advances in vascular imaging	Session 5B Arrays	Session 6B Phononics	Session 7B Microacoustic Modeling	Session 8B CMUT Design
14:30 - 15:30	Coffee Break (101, 1F) & Poster Display (West Corridor, 4F)							
15:30 - 17:00	Session 1C MCA: High temporal and spatial resolution contrast imaging	Session 2C MBF: New vascular mapping tools	Session 3C MTH: Brain	Session 4C MBB: Beamforming II	Session 5C NDE	Session 6C Nonlinear Acoustics	Session 7C RF frontend devices	Session 8C Transducer Design, Fabrication and Applications
18:00 - 20:00	Welcome Reception (Banquet Hall, 3F)							

	2015 IUS CONDENSED PROGRAM						
	Friday, October 23, 2015						
Time	**Plenary Hall** 3rd floor	**VIP Room** 4th floor	**201BC** 2nd floor	**201DE** 2nd floor	**103** 1st floor	**201F** 2nd floor	**201A** 2nd floor	**102** 1st floor
08:00 - 09:30	Session 1D MEL: Elasticity imaging of small structures	Session 2D MCA: Microbubbles and nanodroplets applications	Session 3D MPA: Photoacoustic imaging of atherosclerosis and cancer	Session 4D MIM: Image fusion and classification methods for improved diagnostics	Session 5D Frontiers of Ultrasonics	Session 6D Opto-acoustics	Session 7D Reduction of TCF	Session 8D Transducers for IVUS
09:30 - 10:30	Coffee Break (101, 1st floor) & Poster Display (West Corridor, 4th floor)						
10:30 - 12:00	Session 1E Clinical Ultrasound	Session 2E MEL: Characterizing vascular disease	Session 3E MTH: Bubbles and HIFU	Session 4E MBB: Beamforming III	Session 5E Signal Processing	Session 6E General Physical Acoustics & Ultrasonic Motors & Actuators	Session 7E Emerging technologies	Session 8E Front-end and Integrated Electronics
12:00 - 13:00	Lunch Break						
Time		**VIP Room** 4th floor	**201ABC** 2nd floor	**201DE** 2nd floor	**103** 1st floor	**201F** 2nd floor		**102** 1st floor
13:00 - 14:30		Session 2F Ultrasonics in Biometrics	Session 3F MEL: Mechanical characterization of the heart	Session 4F MSP: Compressive sensing and image reconstruction	Session 5F Industrial Applications	Session 1F MSD: Novel imaging systems		Session 8F Applications of CMUTs
14:30 - 15:30	Coffee Break (101, 1st floor) & Poster Display (West Corridor, 4th floor)						
15:30 - 17:00		Session 2G MBB: Beamforming IV	Session 3G MEL: New applications of elasticity imaging	Session 4G MIM: Medical imaging I	Session 1G MTC: High frequency tissue characterization	Session 6G Physics of Thin-Film Resonators		Session 8G Transducers for Therapy
18:00 - 19:00	Banquet Performance Plenary Hall, 3rd floor						
19:00 - 21:00	Symposium Banquet (Banquet Hall, North Lounge & South Lounge, 3rd floor)						

	2015 IUS CONDENSED PROGRAM						
	Saturday, October 24, 2015						
Time		**VIP Room** 4th floor	**201ABC** 2nd floor	**201DE** 2nd floor	**103** 1st floor	**201F** 2nd floor		**102** 1st floor
08:00 - 09:30		Session 2H MBB: Beamforming V	Session 3H MEL: Methods for elasticity imaging	Session 4H MTH: Ultrasound-mediated agent delivery	Session 5H Microfluidics	Session 1H MSP: Medical signal processing		Session 8H Transducer Applications
09:30 - 10:30	Coffee Break (101, 1st floor) & Poster Display (West Corridor, 4th floor)						
10:30 - 12:00		Session 2I MIM: Advances in vascular and flow imaging	Session 3I MEL: Towards clinical application of elasticity imaging	Session 4I MTH: Histotripsy, shockwaves and liquefaction	Session 5I MBE: Bioeffects and dosimetry	Session 1I MTC: Tissue characterization		Session 8I CMUTs and Signal Processing
12:00 - 13:00	Lunch Break						
Time		**VIP Room** 4th floor	**201ABC** 2nd floor	**201DE** 2nd floor	**103** 1st floor	**201F** 2nd floor		**102** 1st floor
13:00 - 14:30		Session 2J MPA: Photoacoustic imaging and reconstruction	Session 3J MTC: Cardiovascular tissue characterization	Session 4J MTH: Taming cancer, tumors, and bacteria	Session 5J Sensors and sensing	Session 1J MBF: 3D imaging and flow simulations		Session 8J Materials Fabrication and Characterization
14:30 - 15:30	Coffee Break (101, 1st floor) & Poster Display (West Corridor, 4th floor)						
15:30 - 17:00		Session 2K MIM: Medical imaging II	Session 3K MEL: Fundamental elastography studies	Session 4K MCA: Contrast perfusion imaging	Session 5K Flow Measurement	Session IK MSD: Novel high-frequency systems		Session 8K More Medical Transducer Applications

TAIPEI INTERNATIONAL CONVENTION CENTER FLOOR PLANS

First Floor Map: (Registration, Exhibitions, Oral Sessions, Student Poster Competition)
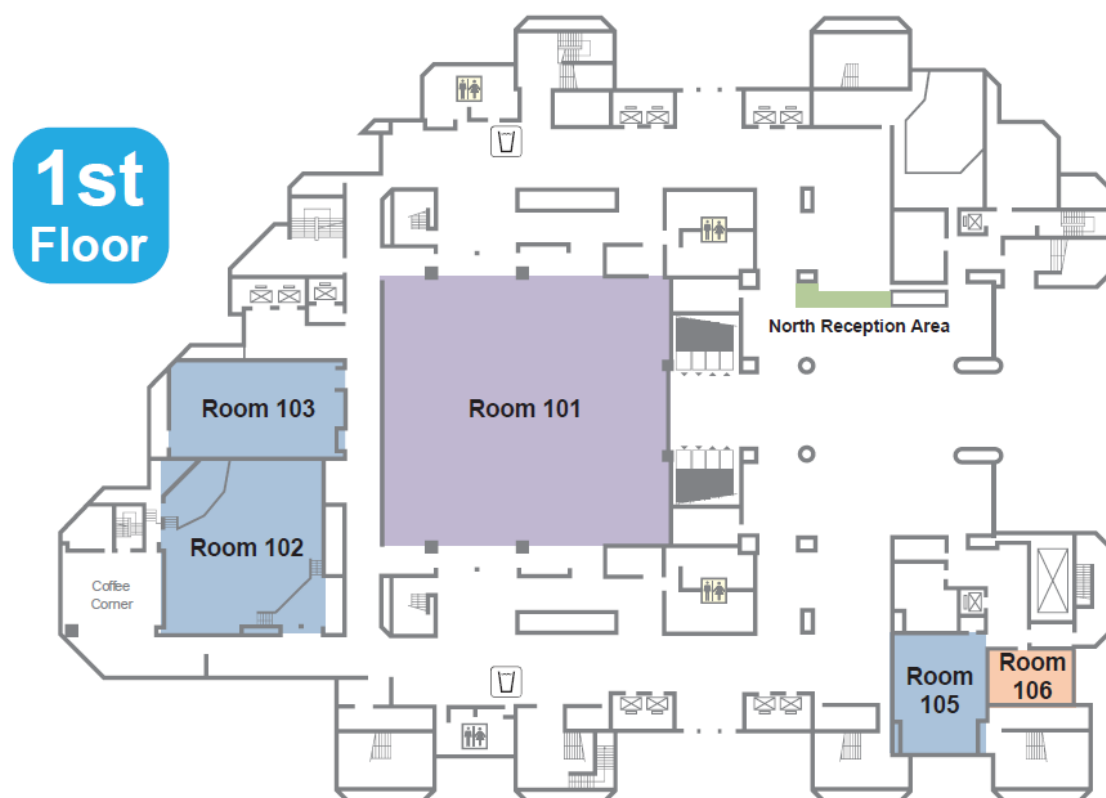
Session Rooms / Function Spaces	
Room 101	Exhibition & Student Poster Competition & Exhibitors Breakfast
Room 102	Oral Sessions & Short Course
Room 103	Oral Sessions & Short Course
Room 105	Oral Sessions & Short Course
Room 106	Family Room
North Reception Area	Registration Desk

Second Floor Map: (Oral Sessions – 10/22~23AM, Speaker Ready Room, Secretariat Room)
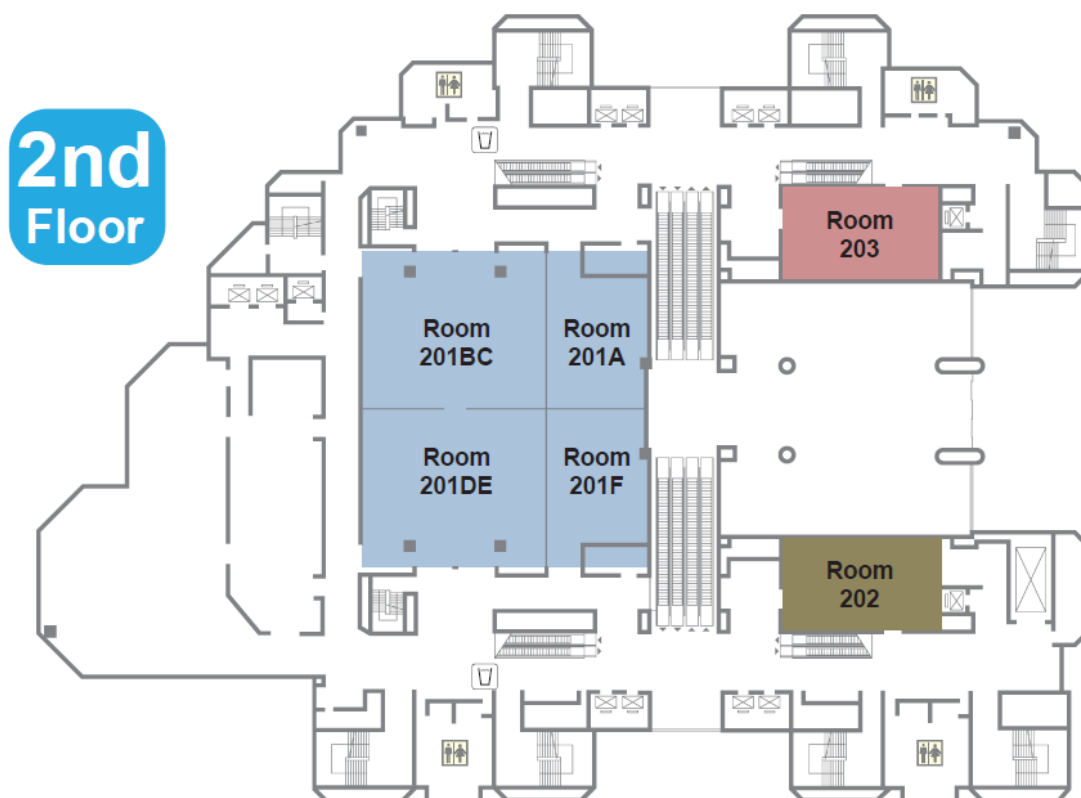
Second Floor Map: (Oral Sessions – 10/23PM~24, Speaker Ready Room, Secretariat Room)
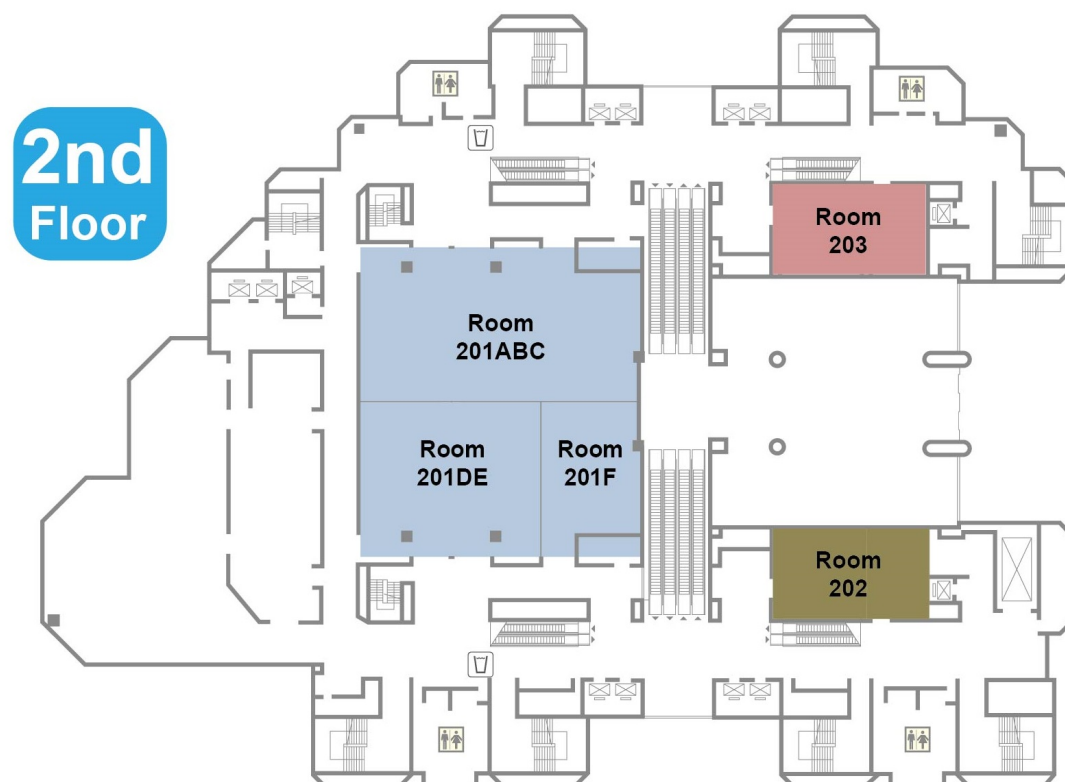
Session Rooms / Function Spaces	
Room 201 A	Oral Sessions
Room 201 BC	Oral Sessions & Short Course
Room 201 ABC	Oral Sessions
Room 201 DE	Oral Sessions & Short Course
Room 201 AF	Short Course
Room 201 F	Oral Sessions
Room 202	Secretariat Room
Room 203	Speaker Ready Room

Third Floor Map: (Opening Ceremony, Plenary Lecture Social Events)
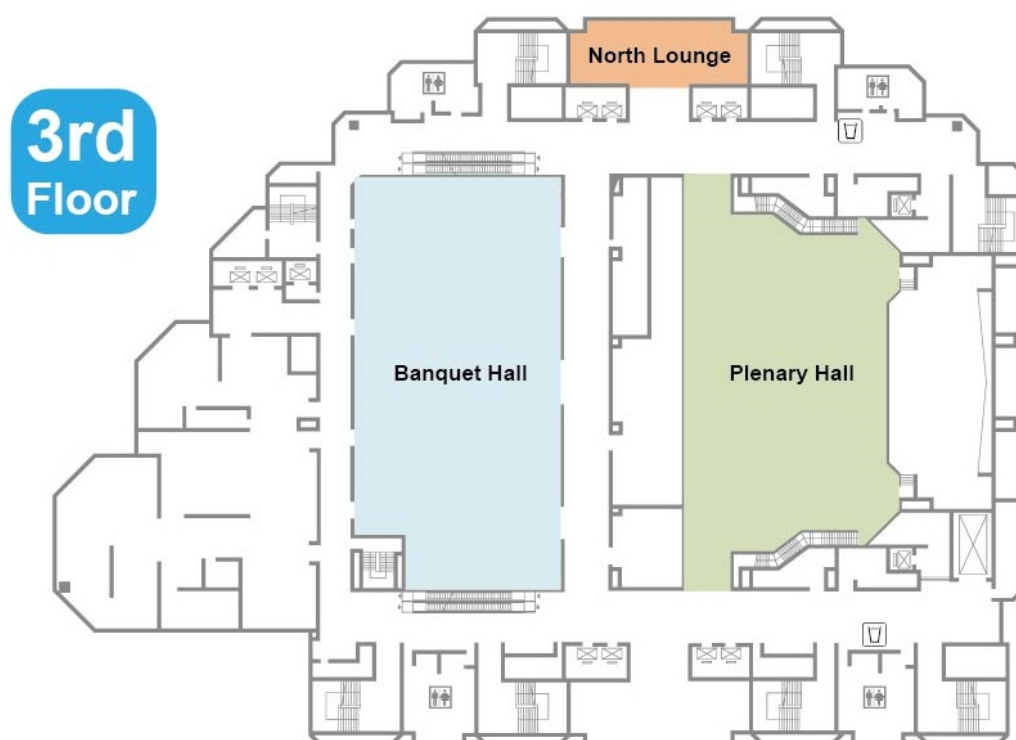
Session Rooms / Function Spaces	
Plenary Hall	Opening Ceremony & Plenary Lecture & Banquet Performance
Banquet Hall	Welcome Reception & Banquet & WIE Luncheon & President's Student Reception
North Lounge	President's Reception

Fourth Floor Map: (Oral Sessions, Poster Sessions)
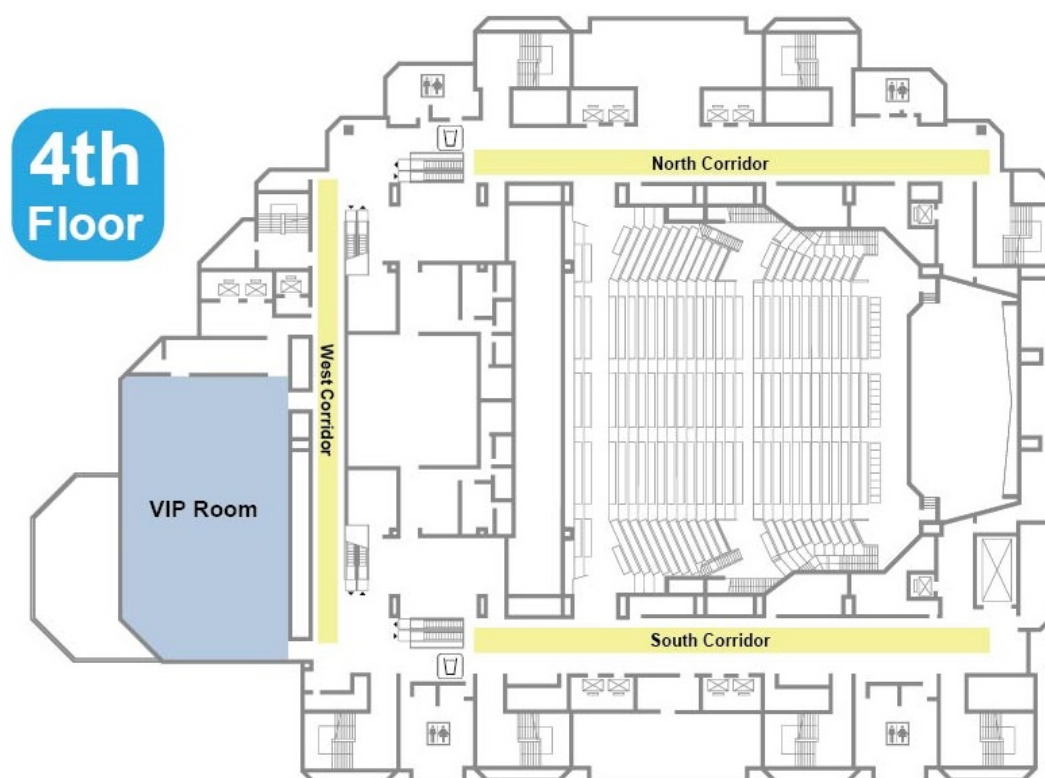
Session Rooms / Function Spaces	
VIP Room	Oral Sessions
West Corridor	Poster Sessions
North Corridor	Poster Sessions
South Corridor	Poster Sessions

1A - MEL: Carotid Elasticity Measurement Techniques

Plenary Hall

Thursday, October 22, 2015, 10:30 am - 12:00 pm

Chair: **Ton van der Steen**
Erasmus Medical Centre

1A-1

10:30 am   Elasticity measurement of carotid artery atherosclerotic plaque

Chris de Korte[1]; [1]*Medical UltraSound Imaging Center (MUSIC), Department of Radiology and Nuclear Medicine, Radboud university medical center, NIjmegen, Netherlands*

Background, Motivation and Objective

Cardiovascular disease is a leading cause of death. In the majority of cases this is due to the formation of atherosclerotic plaques in arteries. Initially, thickening of the inner layer of the arterial wall occurs. Continuation of this process leads to plaque formation. The risk of a plaque to rupture and thus to induce an ischemic event is directly related to its composition. Consequently, characterization of the plaque composition as well as its proneness to rupture are of crucial importance for risk assessment and treatment strategies.

Statement of Contribution/Methods

The carotid is an excellent artery to be imaged with ultrasound because of its superficial position. Using conventional echography, the Intima Media Thickness (IMT) can be quantified. There is a wealth of studies describing the relation between IMT and the risk for myocardial infarction and stroke. Also the diameter change over the cardiac cycle (distensibility) can quantified using ultrasound, providing a surrogate marker for the cross sectional mechanical properties. With Pulse Wave Velocity (PWV) assessment, the propagation of the pressure pulse over the arterial bed is quantified. PWV is a marker for global arterial stiffness. Recently, an ultrasound based method to estimate the local PWV have been introduced. Although all these parameters are associated with cardiovascular disease, they do not easily translate to the risk of the individual patient.

Other techniques focus on characterization of plaques. With ultrasound elastography, the strain in the plaque due to the pulsatile pressure can be quantified. This technique was initially developed using intravascular catheters to image coronaries, but recently non-invasive methods were successfully developed. A high correlation between the measured strain and the risk for rupture was established. Acoustic Radiation Force Imaging (ARFI) also provides characterization of local plaque components based on mechanical properties. However, both elastography and ARFI provide an indirect measure of the elastic modulus of tissue. With shear wave imaging (SWI), the elastic modulus can be quantified, although the carotid artery is one of the most challenging tissues for this technique due to its size and geometry. Prospective studies still have to establish the predictive value of these techniques for the individual patient.

Validation of ultrasound-based mechanical characterization of arteries and plaques remains challenging. Ex vivo mechanical testing provides accurate modulus values but lacks the mimicking in vivo boundary conditions. MRI is often used as gold standard for plaque characterization, but its limited resolution only renders global characterization of the plaque. Histology still is the gold standard but is only available if tissue is excised.

Results/Discussion

In conclusion, ultrasound is an excellent technique to characterize the different stages of vascular disease.

1A-2

11:00 am   Shear wave elastography for lipid content detection in transverse arterial cross-sections

Hendrik Hansen[1], Mathieu Pernot[2], Simon Chatelin[2], Mickael Tanter[2], Chris de Korte[1]; [1]*Medical UltraSound Imaging Center (MUSIC), Department of Radiology and Nuclear Medicine, Radboud university medical center, Nijmegen, Netherlands,* [2]*Institut Langevin, École Supérieure de Physique et de Chimie Industrielles, Paris, France*

Background, Motivation and Objective

A main cause of stroke is the rupture of atherosclerotic plaques in carotid arteries. Plaques with a large soft lipid-rich core are more prone to rupture than predominantly fibrous, stiff plaques. Monitoring the presence of lipids in plaques noninvasively, fast, and relatively inexpensive remains challenging. Ultrasound shear wave elastography has these properties and experimental studies showed that it enables detection of locally softer regions in vessel-mimicking phantoms. However, these studies only report imaging in a longitudinal imaging plane. Since it is not possible to detect lipids over the full vessel circumference when imaging in a longitudinal plane, this study investigates the feasibility of shear wave elastography in transverse imaging planes.

Statement of Contribution/Methods

A SuperSonic Imagine Aixplorer equipped with a linear array probe (SL10-2, f_c = 6 MHz) was used to induce shear waves in vessel-mimicking polyvinylalcohol phantoms of varying dimensions and Young's moduli using a single focused ultrasonic push (300 μs). The push was followed by 0° plane wave acquisitions (n = 100, PRF ≥ 10 kHz) to detect the axial motion induced in the vessel wall. To visualize the generated circumferentially propagating shear waves, axial motion maps were created showing the axial phase shift as a function of circumferential position for a circular path in the vessel wall.

Results/Discussion

As the figure shows, approximately linearly propagating wave fronts were observed for all phantoms indicating circumferentially propagating shear waves. For homogeneous phantoms (A), one wave was observed, which made a roundtrip, whereas a slow and a fast wave were observed for 'soft plaque' phantoms (B-C). Thus, detection of a soft region within a stiff wall seems possible in transverse imaging planes. In (C), the slow wave even disappeared in the segment where no soft inner layer was present, suggesting that the technique might also be used to estimate lipid-core size. (D) shows a preliminary in vivo result in a volunteer obtained with a Verasonics V1 system with a linear array probe (L7-4, f_c = 5 MHz, 100 μs push) which confirms that circumferentially travelling shear waves can be created in vivo. Based on these observations we conclude that shear wave elastography in transverse imaging planes is feasible and promising for lipid-core detection in plaques of superficial arteries.
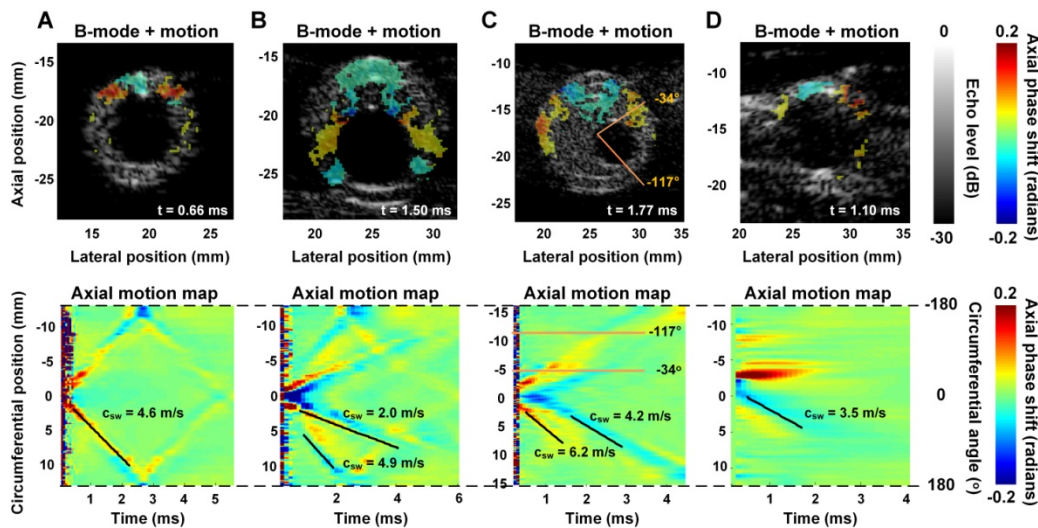
1A-3

11:15 am   Carotid artery wall dynamics captured with multi-plane high-frame-rate imaging

Pieter Kruizinga[1], Frits Mastik[1], Johannes G Bosch[1], Antonius FW van der Steen[1,2], Nico de Jong[1,2]; [1]*Thorax Center - Biomedical Engineering, Erasmus Medical Center, Rotterdam, Netherlands*, [2]*Faculty of Applied Sciences - Acoustical Wavefield Imaging, Delft University of Technology, Delft, Netherlands*

Background, Motivation and Objective

Plaques within the carotid artery (CA) show different dynamic behaviour during fast pressure waves that propagate along the wall [1]. These dynamic wall-wave interactions can be captured in a longitudinal view of the CA using high-frame-rate ultrasound imaging (HFRI). A major disadvantage of this approach is that out-of-plane motion causes misinterpretation of the true wall motion. Here we describe a new imaging setup comprising three intersecting HFR imaging planes which allows us to capture velocities along the CA wall with high temporal resolution in multiple planes simultaneously.

Statement of Contribution/Methods

We imaged the left CA of a volunteer using simultaneously 3 linear array transducers (Acuson L7, Siemens). The transducers were connected to a research ultrasound system (Verasonics Vantage 256). Every 4th element (32 in total) of each transducer was connected to one channel of the Verasonics system. A customized mount kept the transducers under a 45, 0 and -45 degree angle. The imaging planes intersected at a depth of 20mm. One transducer would transmit (TX) one plane-wave and all transducers would receive (RX) the echoes. This TX-RX acquisition was repeated with the other transducers at a repetition rate of 10kHz. Three TX-RX acquisitions were processed into one multi-plane frame acquired at a 1kHz frame-rate. We imaged the CA for a period of 2.4s. The axial displacement analysis was done by RF phase difference processing as described in our previous paper [1]. From the displacement analysis we derived 6 velocity images of the artery wall (3 x anterior + 3 x posterior wall). These images (channels x frames) were then used to estimate the motion of the CA wall with high temporal resolution in multiple planes simultaneously.

Results/Discussion

For visualization we mapped the artery wall velocity images on a cylindrical surface. Figure 1(a) shows this surface at one multi-plane frame. In (b) we show tissue velocity curves at one location on the anterior and posterior wall. Interestingly an oscillatory velocity pattern seems present that is in antiphase between the left and right imaging plane (red and blue), which indicates that this corresponds to a lateral vibrating motion, instead of a diameter change.

[1] Kruizinga P, et al. "High-Definition Imaging of Carotid Artery Wall Dynamics. UMB 40.10 (2014)

Carotid artery in longitudinal view imaged with multi-plane high-frame-rate imaging.
(a) Carotid artery wall velocities at one multi-plane frame (frame #1455, 1.455s) are mapped on a 3D cylindrical surface. (b) Tissue velocity curves of the anterior and posterior wall at 7.2 mm. Oscillatory motion indicates lateral motion of the carotid artery.

THURSDAY ORAL

1A-4
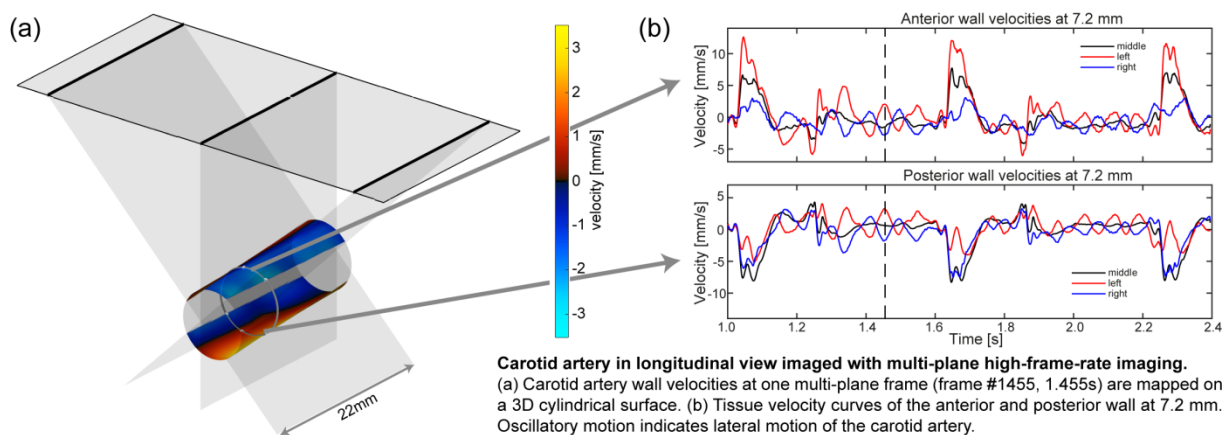
11:30 am Comparison of Different Pulse Waveforms for Local Pulse Wave Velocity Measurement in Healthy and Hypertensive Common Carotid Arteries In Vivo

Chengwu Huang[1], Yuan Su[2], Hong Zhang[2], Lin-Xue Qian[2], Jianwen Luo[1]; [1]*Department of Biomedical Engineering, Tsinghua University, Beijing, China, People's Republic of,* [2]*Department of Ultrasound, Beijing Friendship Hospital, Capital Medical University, Beijing, China, People's Republic of*

Background, Motivation and Objective

Pulse wave velocity (PWV), a measurement of arterial stiffness, is predictive of cardiovascular disease and all-cause mortality. Pulse wave imaging (PWI) is an ultrasound-based technique aiming at measuring the local PWV within the image field-of-view (Luo et al, IEEE TUFFC 2012; Huang et al, IEEE TUFFC 2014). By determining the time delay of the pulse waveforms for a known distance as measured in the ultrasound image, local PWV can be calculated. There exist three possible methods of PWV estimation that are based on the distension waveforms, the displacement waveforms of the anterior (near) wall or posterior (far) wall, respectively. However, the performance of these methods has not been compared. The objective of this study was to characterize the *in-vivo* performance of the three PWV estimation methods in common carotid arteries (CCAs) of both healthy and hypertensive subjects.

Statement of Contribution/Methods

Ultrasound radiofrequency (RF) signals were acquired on both left and right CCAs from 13 heathy subjects (25 ± 3 yo) and 14 hypertensive subjects (57 ± 6 yo) using a SonixMDP system (Ultrasonix). The displacement waveforms of the anterior and posterior walls were estimated from RF-based speckle tracking, and then the distension waveform was derived. The local PWVs at both systolic foot (PWV_{sf}) and dicrotic notch (PWV_{dn}) were determined for each of the three methods. Mean PWV and coefficient of variation (CV) were estimated from about 15 cardiac cycles for each artery.

Results/Discussion

Higher precision of PWV estimation was found by using the distension waveform method than the other two methods in both the healthy and hypertensive groups, as indicated by the smallest CV. Both PWV_{sf} and PWV_{dn} were significantly higher in the hypertensive group compared to the heathy group using the distension waveform method (PWV_{sf}: 5.85 ± 1.59 m/s vs. 4.61 ± 1.03 m/s, p<0.001; PWV_{dn}: 7.65 ± 2.16 m/s vs. 5.03 ± 0.85 m/s, p<0.001, Fig. 1), while no significant difference was found between the two groups using the other two methods (all p>0.01). Thus the expected difference in arterial stiffness between the two groups can be discriminated well by the distension waveform method, but not by the anterior or posterior wall waveform method. The local PWV estimated from the distension waveform might be a promising index for local arterial stiffness characterization and hypertension management.
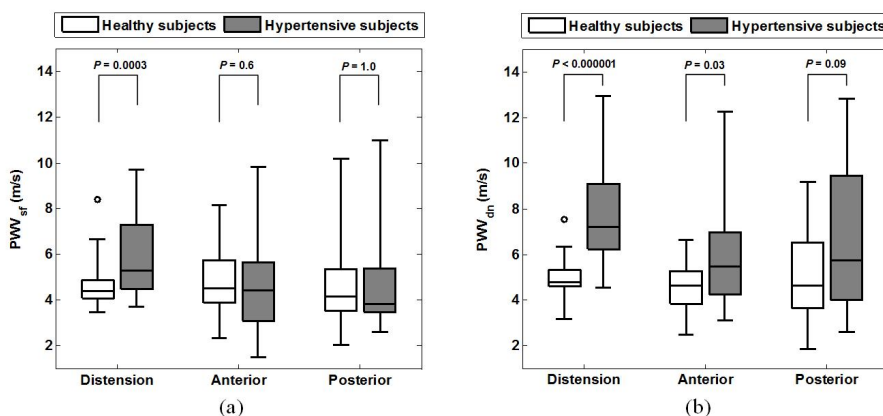

Fig.1. Difference in (a) PWV_{sf} and (b) PWV_{dn} estiamtion between the healthy and hypertensive subjects for each of the three methods. Distension, distension waveform method; Anterior, anterior waveform method; Posterior, posterior waveform method.

1A-5

11:45 am In Vivo Carotid Plaque Stiffness Measurements with ARFI Ultrasound in Endarterectomy Patients

Tomasz Czernuszewicz[1], Jonathon Homeister[2], Melissa Caughey[3], Mark Farber[4], Joseph Fulton[4], Peter Ford[4], William Marston[4], Raghuveer Vallabhaneni[4], Timothy Nichols[2,3], Caterina Gallippi[1,5]; [1]*Joint Department of Biomedical Engineering, University of North Carolina and North Carolina State University, Chapel Hill, NC, USA,* [2]*Department of Pathology and Laboratory Medicine, University of North Carolina, Chapel Hill, NC, USA,* [3]*Department of Medicine, University of North Carolina, Chapel Hill, NC, USA,* [4]*Department of Surgery, University of North Carolina, Chapel Hill, NC, USA,* [5]*Department of Electrical and Computer Engineering, North Carolina State University, Raleigh, NC, USA*

Background, Motivation and Objective

Stroke is commonly caused by thromboembolic events originating from the carotid vasculature. It has been shown that plaques in the carotids composed of large, mechanically-soft necrotic cores covered by thin fibrous caps have a propensity to rupture and induce cerebrovascular accidents. To improve plaque characterization with ultrasound, our group has been investigating Acoustic Radiation Force Impulse (ARFI) imaging, which has shown promise in early animal and human studies. We herein report results for in vivo carotid ARFI imaging with matched histology in patients undergoing endarterectomy.

Statement of Contribution/Methods

Patients were consented and recruited from UNC Hospitals (N = 16) and imaged with ARFI on a Siemens Acuson Antares. Imaging was performed pre-operatively by focusing on the surgical plaque. After surgery, the extracted specimen was imaged with μCT, decalcified, and sectioned according to noted arterial geometry for spatial registration to the ultrasound imaging plane. The sections were stained with H&E, combined Masson's elastin (CME), and Von Kossa for calcium, and compared to parametric 2D ARFI images of peak displacement (PD).

Results/Discussion

From 16 patients, 15 intact plaque samples (11 from symptomatic patients) were collected with matched ARFI images. Fig. 1 shows an ARFI PD image from a 45 y/o symptomatic female with spatially-matched histology (stained with CME). The ARFI image shows a focal stenosis with plaque in both proximal and distal walls. Plaque in the proximal wall appears to displace far (10.8 ± 11.7 μm) and is covered by a low-displacing region (2.8 ± 0.9 μm, 0.93 ± 0.4 mm thick) suggesting necrotic core and fibrous cap. Plaque in the bottom wall appears to have a focal region of relatively higher displacement (3.0 ± 1.6 μm) also covered by a stiffer region (1.5 ± 0.5 μm, 0.56 ± 0.1 mm thick). Histology confirms the presence of necrotic core and fibrous cap in both proximal and distal walls (with cap thicknesses of 0.91 ± 0.1 mm, and 0.60 ± 0.1 mm, respectively). Out of the 15 plaque samples, 8 were ruptured with significant thrombus. In general, regions of rupture had higher PD, and ARFI imaging was able to directly visualize rupture in some cases as a discontinuity in the low-displacing cap. These results suggest that ARFI is relevant to characterizing plaque via mechanical stiffness and may be used to improve plaque risk stratification.
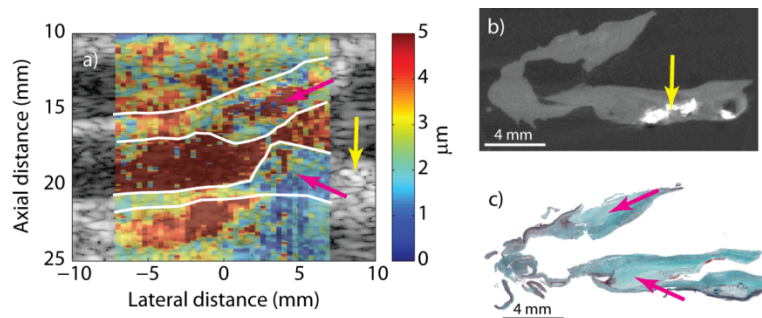
Figure 1: (a) B-mode with ARFI peak displacement image overlaid. Significant stenosis is visible due to plaque in both the proximal and distal wall. In the proximal wall, an area of large displacement (top magenta arrow) is observed, covered by a lower displacing cap. Relatively larger displacements are also seen in the distal wall, but with smaller absolute magnitude (bottom magenta arrow). (b) μCT showing minor calcification in the distal wall (yellow arrow), that matches spatially with bright spot on B-mode. (c) CME stain showing necrotic core in both proximal and distal wall (magenta arrows).

2A - MCA: Molecular Imaging

VIP

Thursday, October 22, 2015, 10:30 am - 12:00 pm

Chair: **Helen Mulvana**
          University of Glasgow

2A-1

10:30 am   The use of acoustic radiation force decorrelation weighted pulse inversion (ADW-PI) in enhancing microbubble contrast

Elizabeth Herbst[1], Sunil Unnikrishnan[1], **Shiying Wang[1]**, Alexander Klibanov[1], Will Mauldin[1], John Hossack[1]; [1]*Biomedical Engineering, University of Virginia, Charlottesville, Virginia, USA*

Background, Motivation and Objective

Microbubble-based ultrasound contrast agents can be targeted to cancer disease markers present on the endothelium, providing molecular-based contrast between normal and diseased tissue. Imaging methods, such as contrast pulse sequence (CPS) and pulse inversion (PI), are capable of capturing the non-linear acoustic reflections from microbubbles, but tend to also capture harmonic signal from echogenic tissue interfaces. In this study, acoustic radiation force (ARF) was applied during simultaneous PI and B-mode imaging to capture signal decorrelation based on microbubble motion. The decorrelation characteristics of microbubble-bound tissue were then used to create a filter isolating microbubble signal from bright tissue signal, in a new method termed ARF-decorrelation-weighted pulse inversion (ADW-PI).

Statement of Contribution/Methods

Microbubbles conjugated with anti-VEGFR2 antibody were targeted to subcutaneous hindlimb tumors in C57BL/6 mice. Microbubbles were administered via bolus injection and allowed to bind to VEGFR2 receptors. Tumors were then imaged using a combination of B-mode imaging, synthetic aperture virtual source element imaging, and PI, at a frequency of 11 MHz. A train of ARF waveforms (Freq = 4.4 MHz, Duration = 875 μs, Ten 15-cycle pulses, PRF = 11.4 kHz) was applied between image acquisitions at a mechanical index less than 0.1. CPS images were acquired with a Siemens Sequoia clinical scanner. Correlation coefficients between paired B-mode images were used to generate decorrelation maps, which were then multiplied with corresponding PI data to generate a final filtered image (Fig 1).

Results/Discussion

Tissue regions containing bound microbubbles showed approximately six-fold higher decorrelation than normal static tissue. ADW-PI effectively suppressed PI tissue signal by >80 dB, increasing microbubble-to-tissue contrast by at least 50 dB compared to CPS images. These results demonstrate that ADW-PI is effective at suppressing non-linear signal from harmonic tissue interfaces while preserving microbubble signal, and is demonstrably superior to existing approaches for isolating the contrast agent signal from background tissue.
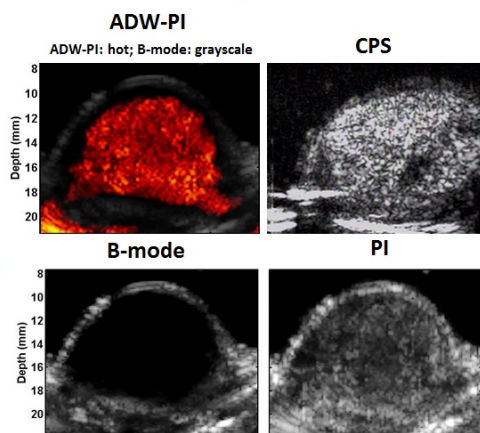

Figure 1: Demonstration of the ability of ADW-PI to suppress harmonic tissue signal while preserving microbubble signal. The CPS and PI images both show significant harmonic signal from the mouse femur. When a bilateral filter multiplying B-mode decorrelation by PI image intensity, the high-decorrelation, high-intensity microbubble region is amplified while the high-intensity, low decorrelation tissue regions are suppressed. The top left image shows the ADW-PI filtered image overlaid in a heatmap on top of the original B-mode.

2A-2

10:45 am   Quantification of the binding kinetics of targeted ultrasound contrast agent for molecular imaging of cancer angiogenesis

Simona Turco[1], Peter J. A. Frinking[2], Hessel Wijkstra[1,3], Massimo Mischi[1]; [1]*Electrical Engineering, Eindhoven Univeristy of Technology, Eindhoven, Netherlands*, [2]*Bracco Suisse S.A., Geneva, Switzerland*, [3]*Urology, Academic Medical Center, University of Amsterdam, Amsterdam, Netherlands*

Background, Motivation and Objective

Cancer growth requires angiogenesis; imaging of angiogenesis holds thus great potential for improved cancer detection and treatment. In this context, ultrasound molecular imaging permits the visualization of cancer angiogenesis by use of novel targeted contrast agents (tCA). These consist of ligand-bearing microbubbles (MB) designed to specifically bind molecular angiogenic expressions, thus providing selective enhancement especially in the late phase. Discrimination between bound and free MB is crucial to assess the degree of binding and thus quantify angiogenesis. Currently, binding is assessed by the differential targeted enhancement (dTE), i.e., the difference in signal enhancement in the late phase before and after the application of a destructive pulse. However, this method is not quantitative, and it requires long acquisitions and a high-pressure pulse, which may damage the endothelial tissue. To overcome these limitations, here we propose a new method for quantification of the MB binding kinetics by fitting a dedicated compartmental model to the tCA first-pass.

Statement of Contribution/Methods

The tCA concentration in each pixel of tissue is described by a dilution model where the kinetics of free and bound MB are described as a convective-dispersion process and a well-mixed compartment, respectively. A time-intensity curve (TIC) is measured at each pixel and fitted by the proposed model for the quantitative assessment of MB binding by the estimation of the binding rate Kb. The feasibility of the method is investigated in two prostate tumor-bearing rats by performing contrast-specific ultrasound imaging after a bolus injection of BR55 tCA (Bracco, Suisse).

Results/Discussion

Figure 1a-b compares the late-phase enhancement with the parametric map of Kb in the prostate of a tumor-bearing rat, while Fig. 1c shows an example of TIC with corresponding model fit. The proposed method enables quantitative estimation of MB binding by assessment of the first pass tCA binding kinetics, reducing the acquisition time with no need for the high-pressure pulse. Further validation is necessary to clarify the value of the proposed quantitative binding parameter for angiogenesis imaging in the context of cancer diagnostics and therapy monitoring.

Figure 1: a. Late phase enhancement in the prostate of a tumor-bearing rat injected with BR55. **b.** Parametric map of the binding rate K_b. **c.** Example of TIC measured at one pixel with corresponding model fit.

2A-3

11:00 am   Molecular acoustic angiography: Demonstration of in vivo feasibility for high resolution superharmonic ultrasound molecular imaging

Brooks Lindsey[1], Sarah Shelton[1], James Tsuruta[2], F. Stuart Foster[3], Paul Dayton[1,4]; *[1]Joint Department of Biomedical Engineering, University of North Carolina-Chapel Hill and NC State University, Chapel Hill, NC, USA, [2]Department of Pediatrics, University of North Carolina-Chapel Hill and NC State University, Chapel Hill, NC, USA, [3]Sunnybrook Research Institute, Toronto, ON, Canada, [4]Biomedical Research Imaging Center, University of North Carolina-Chapel Hill, Chapel Hill, NC, USA*

Background, Motivation and Objective

The value of a molecular imaging technique in revealing tissue pathophysiology may be greatly enhanced by combining it with anatomical imaging in order to visualize the distribution of the marker, as in PET-CT systems. While B-mode images typically provide anatomical information in ultrasound molecular imaging, a vascular anatomical reference provided by superharmonic imaging of free microbubbles with acoustic angiography can provide additional information on the relationship between microbubble targeting and vessel size. In this work, we analyze the tradeoffs necessary for performing superharmonic imaging in vivo and assess this targeting-vessel diameter relationship using sequential scans of free and targeted microbubbles.

Statement of Contribution/Methods

Lipid shelled microbubble contrast agents were prepared which are targeted to the $\alpha_v\beta_3$ integrin. For in vivo studies, the following parameters were studied: 1) Effect of peak negative transmit pressure from 700-1200 kPa; 3) Effect of repeated scans at each pressure; 2) Effect of microbubble size distributions centered at 2 μm and 4 μm.

5 female Fischer 344 rats with fibrosarcoma tumors implanted subcutaneously in the right flank were imaged when tumors reached ~1 cm according to an IACUC-approved protocol. Animals received a bolus of 5×10^7 cyclic RGD microbubbles; free bubbles were allowed to clear for 12 minutes. 3D molecular images were then acquired using the VisualSonics 770 with a prototype dual-frequency transducer which transmits at 4 MHz and receives at 30 MHz. A second dual-frequency scan was performed using a constant infusion of 1.5×10^8 #/min of non-targeted microbubbles. Vessels in angiography images were segmented offline to compare the spatial distribution of targeted microbubbles and vascular structure.

Results/Discussion

Images of targeted and free microbubbles were fused offline into a single high contrast, high resolution projection visualization (Fig. 1) of both microvascular anatomy and $\alpha_v\beta_3$ targeting. While 65% of molecular image intensity is lost from the first to the second scan at 1200 kPa, use of larger microbubbles yields a 56% increase in initial image intensity. After analyzing molecular and angiography volumes, 66% of targeting occurs within 50 μm of the centerline of a vessel in the range of 150-350 μm, indicating the majority of targeting occurs within resolvable vessels.
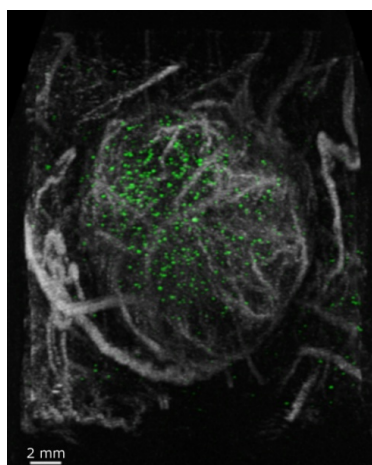
2A-4

11:15 am   Ultrasound Molecular Imaging with Modulated Acoustic Radiation Force-based Beam Sequence in Mouse Abdominal Aorta: A Feasibility Study

Shiying Wang[1], Sunil Unnikrishnan[1], Alexander L Klibanov[1,2], F William Mauldin Jr[1], John A Hossack[1]; *[1]Biomedical Engineering, University of Virginia, Charlottesville, Virginia, USA, [2]Division of Cardiovascular Medicine, University of Virginia, Charlottesville, Virginia, USA*

Background, Motivation and Objective

Ultrasound molecular imaging has been developed for pre-clinical applications including detection of cancer and cardiovascular disease. We recently introduced a novel modulated Acoustic Radiation Force (ARF)-based beam sequence for detection of targeted adhesion using short imaging protocols without necessitating control measurements in large blood vessels [1-2]. In this study, *in vivo* validation of the sequence was accomplished for the first time in the mouse abdominal aorta for detection of inflammation.

Statement of Contribution/Methods

Upregulation of P-selectin in C57/BL6 mouse was achieved by intraperitoneal injection of tumor necrosis factor-α (0.5 µg/mouse) 2 hours before imaging. Biotinylated lipid-perfluorobutane microbubbles (MBs, Ø ≈ 2 µm) conjugated to P-selectin antibody (RB40.34) were used as targeted MBs. Control MBs were biotinylated MBs without antibodies. The beam sequence [1-2] was programmed on a Verasonics scanner equipped with a L22-14v transducer. In the sequence, ARF was applied for 70 s while imaging lasted for 180 s. Bolus injection of 25×10^6 MBs was administered through a tail vein catheter while imaging. The signal magnitude of the bottom wall of the abdominal aorta was detected. The residual-to-saturation ratio (R = residual MB / saturated MB) extracted from the signal magnitude curve was used to differentiate control and targeted groups.

Results/Discussion

The initial 3 s of the sequence captured the baseline signal intensity from the bottom wall without MBs. After MB injection (3 s), the signal intensity of the wall dropped immediately due to shadowing from the MBs in the lumen. During application of ARF (10 – 80 s), the signal intensity increased. After cessation of ARF, the signal intensity decreases to baseline level in the control group, while remaining at a high residual level in the targeted group. The R parameter could be used to separate the control (≈ 10%) and targeted (≈ 60%) groups. In conclusion, feasibility was demonstrated for rapid (3 min) detection of inflammation in mouse abdominal aorta using our new modulated ARF-based beam sequence. This method has potential for clinical applications that may include the early assessment of abdominal aortic aneurysm (AAA) risk, which currently is significantly under diagnosed.

[1] Wang *et al*, Phys Med Biol, 2014; 59(2): 465-484

[2] Wang *et al*, Ultrasound Med Biol, 2015; 41(1): 222-234
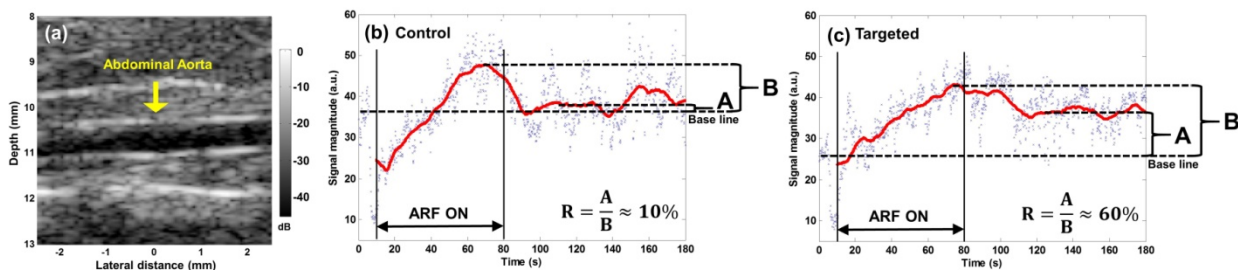
Figure. (a) B-mode image demonstrates the abdominal aorta of mouse. Region of interest was defined in the middle of bottom vessel wall. (b) Signal magnitude curve of control experiment (R ≈ 10%). (c) Signal magnitude curve of targeted experiment (R ≈ 60%). Red lines indicate the moving average of raw data. ARF pulses were applied from *t* = 10 to 80 s.

2A-5

11:30 am   A Theoretical Model for the Interaction of an Ultrasound-Activated Contrast Microbubble with a Wall at Arbitrary Separation Distances

Alexander Doinikov[1], **Ayache Bouakaz**[1]; *[1]Inserm U930, Université François-Rabelais, Tours, France*

Background, Motivation and Objective

Both *in vitro* and *in vivo*, contrast microbubbles usually move near bounding surfaces, such as the wall of an experimental container or the wall of a blood vessel, which affect the acoustic response of microbubbles in both imaging and therapeutic applications. This problem inspires interest in theoretical models that are able to predict the effect of a wall on the ultrasound dynamics of a contrast microbubble. At present, there are models for the case where the distance between a bubble and a wall is large compared to the bubble size and for the case where a bubble is adherent to a wall. The aim of our study is to develop a generalized model that describes the dynamics of a contrast microbubble at arbitrary distances from a wall and makes thereby it possible to simulate the acoustic response of the bubble starting from large distances up to direct contact between the bubble and the wall.

Statement of Contribution/Methods

The derivation of the model is based on the multipole expansion of the bubble velocity potential, the image source method and the Lagrangian formalism. The model consists of two coupled differential equations. The first equation is a modified Rayleigh-Plesset equation for the bubble radial oscillation and the second equation describes the translational displacement of the bubble center. Numerical simulations are made to determine how the acoustic response of a contrast microbubble depends on separation distance near walls of different types: rigid, plastic, arterial, etc. The dynamics of the bubble encapsulation is described by the Marmottant shell model.

Results/Discussion

The simulations show that the magnitude of the bubble resonance frequency near a wall depends on both the separation distance and the wall material properties. In particular, the OptiCell and the arterial walls cause the resonance frequency to increase with decreasing separation distance. The model is validated by comparing with experimental data obtained for phospholipid-shelled bubbles near a compliant agarose gel boundary [Helfield *et al.*, PMB **59**, 1721–1745, 2014; JASA **136**, EL40–EL46, 2014]. The comparison is performed for two data sets. In the first case, the simulated and measured values of the bubble resonance frequency and the scattered pressure are compared as a function of bubble diameter, using the experimental data for bubbles with diameters ranging from 2.3 µm to 4 µm, insonified at 30 kPa in the frequency range from 4 to 13.5 MHz. In the second case, the simulated and measured values of the maximum scattered pressure amplitude are compared as a function of distance from the agarose boundary, using the experimental data for a 2.3-µm-diameter bubble insonicated at 69 kPa and 11 MHz. In both cases, the theoretical model correctly predicts the qualitative behavior of the measured quantities and the quantitative level of their values.

2A-6

11:45 am   Modelling of ultrasound contrast agent oscillations in vessels based on an infinite mirror image method

Martin Ward[1,2], Yesna Yildiz[2], Virginie Papadopoulou[2], Robert Eckersley[3], Meng-Xing Tang[2]; [1]*Department of Mathematics, Imperial College London, London, United Kingdom,* [2]*Department of Bioengineering, Imperial College London, London, United Kingdom,* [3]*Biomedical Engineering Department, Division of Imaging Sciences, King's College London, United Kingdom*

Background, Motivation and Objective

Understanding the oscillations of microbubble ultrasound contrast agents (UCAs) in vessels of various diameters is important for quantitative contrast enhanced ultrasound imaging and therapy. Current studies either consider the vessel wall effect from a single side [1] or use a linear perturbation method in which case they are dependent on UCA-to-vessel size ratio and require the bubble to be placed centrally [2].

Statement of Contribution/Methods

We propose to model oscillations of UCAs in arbitrary locations within a small vessel by extending the mirror image method for a bubble near a wall [1] and simulating a microvessel as cross-sectionally square. By including an infinite grid of images for the UCA's reflections, we allow for asymmetrical UCA placement in microvessels. The influence of vessel cross-sectional shape is also investigated using a polygonal cross-section.

Results/Discussion

Results show that the radial oscillations of the UCA reduce when it is in a smaller vessel or closer to a vessel wall. The radial oscillations decreased 3-74% for vessel sizes of 50-10μm with the UCA 2 radii away from one edge, compared to only one boundary and using the same parameters as in [1]. These results offer new possibilities for better understanding and quantification of UCA behaviour in large versus smaller vessels.

Fig.1: a) Maximum radial excursions of a 2 um radius UCA in vessels of different diameters using 3 models. The microbubble is placed 2 radii away from a vessel wall and insonated with a 1-cycle, 4 MHz, 210 kPa pulse. The shell parameters used are as in [1]. 'Free bubble' refers to a microbubble in free space, '1-wall' is the model used in [1], '4-wall' is the model presented here with an infinite grid of mirror images to model the effect of vessel walls on the radial oscillations of a microbubble in microvessels. b) Maximum radial excursion of a 2 um UCA in a 50 um diameter vessel with respect to the UCA position in the vessel (same ultrasound and shell parameters).

[1] A.A. Doinikov, S. Zhao, P.A. Dayton, Ultrasonics, 49 (2009) 195-201.

[2] S. Qin, K. Ferrara, UMB, 33 (2007) 1140-1148.
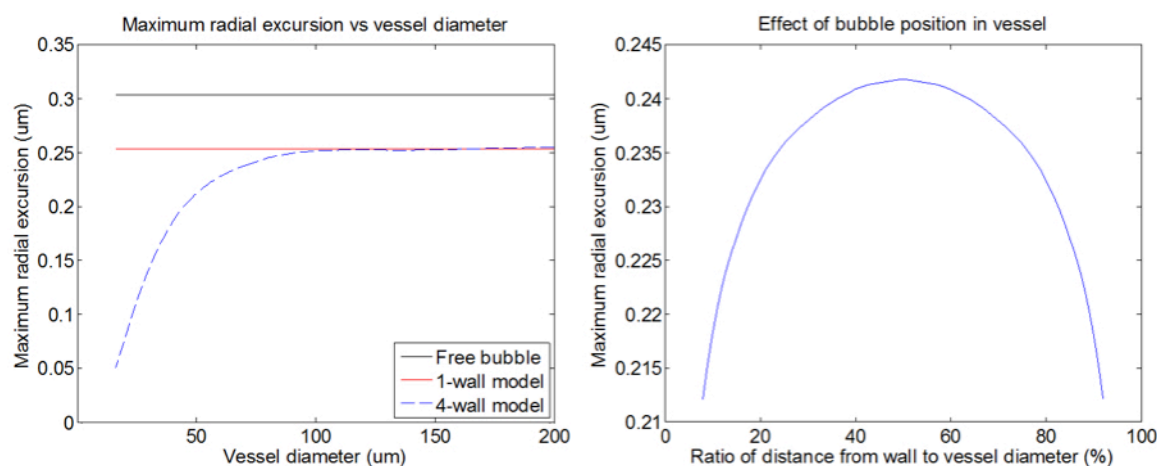
3A - MBF: Advances in Flow Imaging Methods

201BC

Thursday, October 22, 2015, 10:30 am - 12:00 pm

Chair: **Piero Tortoli**
Università di Firenze

3A-1

10:30 am **Adaptive Spectral Estimation Methods in Color Flow Imaging**

Yücel Karabiyik[1], Ingvild Kinn Ekroll[1,2], Jørgen Avdal[1], Hans Torp[1], Lasse Løvstakken[1]; [1]*Department of Circulation and Medical Imaging, Norwegian University of Science and Technology, Trondheim, Norway,* [2]*St. Olavs Hospital, Trondheim, Norway*

Background, Motivation and Objective

Clutter rejection for color flow imaging (CFI) remains a challenge due either to a limited amount of temporal samples available or because of non-stationary tissue clutter. This is particularly the case for interleaved CFI and B-mode acquisitions. Low velocity blood signal is attenuated along with the clutter due to the long transition region of the available clutter filters, causing regions of biased mean velocity estimates or signal dropouts. This issue will limit the ability to measure low blood velocities along the vessel walls as needed for wall shear rate/stress estimation.

**Statement of Contribution/Methods**

In this work we investigate how adaptive spectral estimation methods, the Capon and Blood Iterative Adaptive Approach (BIAA), can be used to estimate the mean velocity in CFI without prior clutter filtering. The approach is based on confining the clutter signal in a narrow spectral region around the zero Doppler frequency, made possible by the low spectral sidelobe levels of the adaptive estimators. The clutter signal was removed by an ideal and adaptive filter in the frequency domain. The mean frequency was estimated using the autocorrelation methods in the frequency domain and compared to conventional autocorrelation method using suitable polynomial regression filters and for varying SNR and packet size. The filter orders and the ideal filter cutoff were chosen to minimize the bias due to the clutter. The proposed methods are evaluated using computer simulations, *in vitro* flow phantom experiments and *in vivo* recordings from the common carotid of a healthy volunteer.

Results/Discussion

Capon and BIAA methods can display low blood velocities which would be attenuated by the polynomial regression filter and can potentially give better estimation of mean velocities for CFI at a higher computational cost. The results below are generated using packet size 12. Simulation results show that the BIAA has the highest variance of the methods for small packet size and low SNR (see figure) and it is considerably more computationally demanding. In the velocity range 2 – 10 cm/s, autocorrelation, Capon and BIAA have 1.9, 0.5 and 0.8 cm/s maximum absolute bias and 2, 0.4 and 3 cm/s mean standard deviation respectively. *In vitro* and *in vivo* results showed that the Capon method provided color flow images and flow profiles with lower variance especially in the regions close to the artery wall.
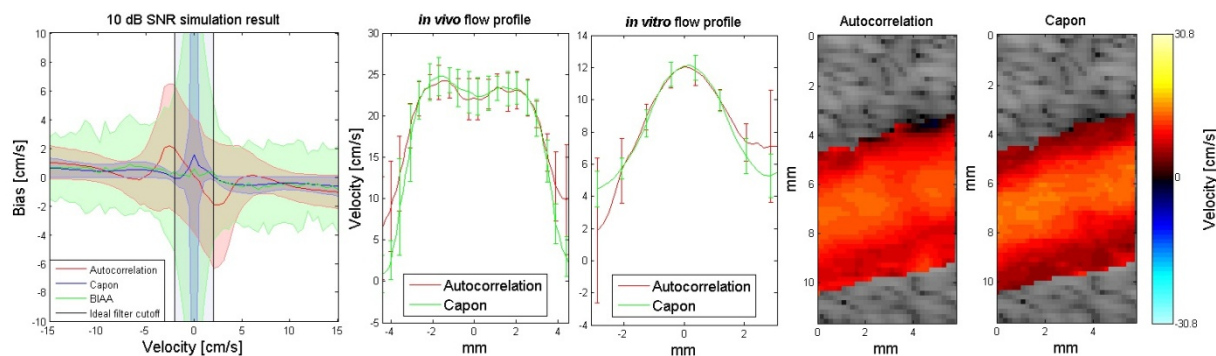
3A-2

10:45 am **Robust Estimator Design for High Frame Rate Flow Vectorgraphy: The Least-Squares Vector Doppler Technique**

Billy Y. S. Yiu[1], Alfred C. H. Yu[1]; [1]*Medical Engineering Program, University of Hong Kong, Pokfulam, Hong Kong*

Background, Motivation and Objective

A known prerequisite for tracking complex flow using ultrasound is the need to derive flow vectors at sub-ms time resolution. Although such a task can possibly be achieved by combining plane wave imaging with cross-beam vector Doppler estimation, the results are prone to significant variance in cases with weak blood signal, which typically is the case since plane waves are unfocused in nature. To avoid this pitfall, we have been generalizing plane wave vector Doppler to a multi-Tx, multi-Rx angle formulation that allows flow vector computation to be realized through least-squares estimation. The current work aims to test the robustness of our method through analyzing the performance of different Tx-Rx angle pairs, and evaluate the practical need for robust flow vector estimation in the context of dynamic flow visualization.

Statement of Contribution/Methods

Least-squares vector Doppler was realized using a SonixTouch system for Tx operations (to fire steered plane waves), a SonixDAQ tool for Rx data acquisition, and an L14-5 linear array. To test each configuration with M-Tx and N-Rx angles, a rotational flow phantom was developed. It consisted of a 2.5 cm well embedded within a cast of tissue mimicking agar. Placed within the well was blood mimicking fluid, and to create circulating flow, a magnetic stirrer was placed at the well bottom (1.4 rev/s). Flow vectorgraphy maps were generated from this setup (using 5 MHz frequency; 3-cycle pulses; 10 kHz PRF; -10 to +10 deg angle span) to analyze estimation consistency at both local scale (whether individual vectors are correct) and global scale (whether rotational flow can be accurately tracked). Visualization performance was also assessed by using the flow vector results as input to the vector projectile imaging (VPI) framework established recently (involving dynamic inter-frame updates of vector position).

Results/Discussion

With the use of least-squares vector Doppler, circulatory motion can be consistently tracked (Fig a: representative case with 5Tx-5Rx). These vector estimates, when used as input for VPI visualization, gave projectile tracks that were aligned with the expected circular route. In contrast, the simple 2Tx-1Rx config led to various spurious vectors (Fig b), and the projectile tracks deviated significantly away from expected route. Related VPI cineloops will be shown at the meeting.

(a) 5 Tx & 5 Rx　(b) 2 Tx & 1 Rx

15

0
[cm/s]
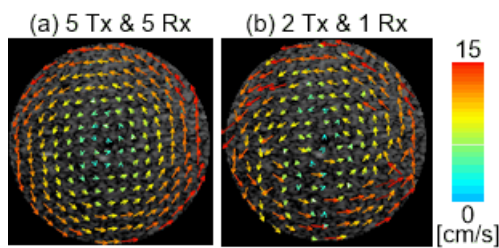
3A-3

11:00 am   Unaliased vector Doppler imaging from unsteered plane waves

Damien Garcia[1], Shahrokh Shahriari[2], Daniel Posada[2], Julia Faurie[2]; [1]Department of radiology, University of Montreal, Canada, [2]University of Montreal, Canada

Background, Motivation and Objective

Vascular velocity measures by conventional duplex ultrasound can be unreliable since color Doppler is affected by aliasing and beam/flow angle. Several strategies were developed for vector flow imaging (VFI). To provide reliable time-resolved VFI, we propose an unaliased unsteered technique based on plane wave ultrasound imaging.
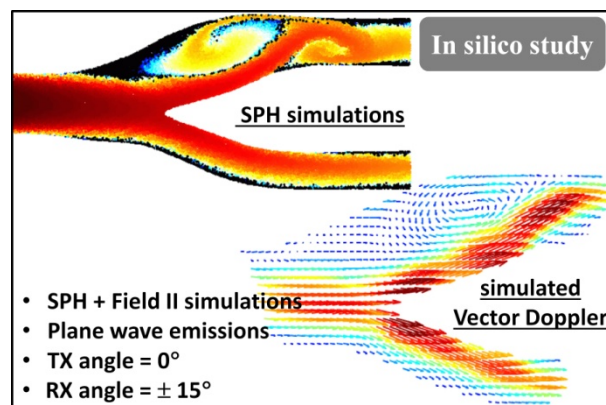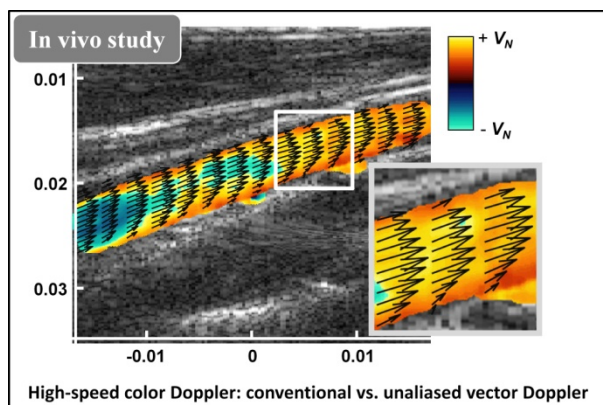
Statement of Contribution/Methods

Plane waves were transmitted to obtain duplex images. B-mode images were generated by coherent compounding of steered emissions. Unsteered plane waves (no Tx delay) were produced for color Doppler. We used staggered double-PRF transmits to obtain unaliased Doppler fields. In staggered PRF, lags between successive transmits change in an alternating way. The IQ-demodulated signals were migrated at two opposite receive angles before Doppler analysis. Clutter filtering was spatially adaptive to obtain optimal blood velocities. Unaliased unsteered vector Doppler imaging was tested 1) *in silico*, 2) *in vitro*, 3) *in vivo* (Verasonics scanner + 5 MHz linear array):

1) We coupled SPH (smoothed particle hydrodynamics) with Field II to simulate Doppler images in a carotid bifurcation.

2) We carried out experiments in a spinning disk.

3) We imaged the carotid of a healthy volunteer.

Results/Discussion

Although the errors were five times larger in the cross-beam direction, we obtained a good agreement between the ground-truth and Doppler-based vector fields, both *in silico* and *in vitro*. Optimal *in vivo* receive angles (± 15°) and f-number (3) were chosen based on the *in silico* and *in vitro* results. The *in vivo* carotid flow was adequately dealiased by the staggered technique. We observed a very consistent flow vector field. According to our results, unaliased unsteered vector Doppler might be a reliable tool for comprehensive flow imaging.

--

In vivo study

$+ V_N$

$- V_N$

0.01

0.02

0.03

-0.01　　0　　0.01

High-speed color Doppler: conventional vs. unaliased vector Doppler

In silico study

SPH simulations

- **SPH + Field II simulations**
- **Plane wave emissions**
- **TX angle = 0°**
- **RX angle = ± 15°**

simulated Vector Doppler

3A-4

11:15 am   Time-resolved Doppler vortography in the left ventricle

Julia Faurie[1], Daniel Posada[1], Amir Hodzic[2], François Tournoux[2], Damien Garcia[3]; [1]University of Montreal, Canada, [2]Department of echocardiography, University of Montreal Hospital, Canada, [3]Department of radiology, University of Montreal, Canada

Background, Motivation and Objective

A large flow vortex forms in the left ventricle during diastolic filling. Clinical studies based on contrast-enhanced speckle tracking showed that the vortex flow pattern can reflect the diastolic cardiac function. With the purpose of improving diastology, we recently devised Doppler vortography to estimate the core vorticity of the main intraventricular vortex. This technique is limited by the low frame rates (< 20 fps) given by conventional Doppler-echo. In the present work, we adopted ultrafast ultrasound to get time-resolved Doppler vortography. We also addressed the aliasing issues using an approach proposed by our team.

Statement of Contribution/Methods

Doppler vortography is based on the recognition of the Doppler field antisymmetry created by a vortex flow. It returns a map called Blood Vortex Signature (BVS), from which vortex center and core vorticity can be deduced. Ultrafast Doppler vortography was tested *in vitro* (2-cm-Ø spinning disk) and *in vivo* (left heart of volunteers) using a Verasonics scanner with a 2.5 MHz phased array. Wide circular waves were generated to insonify the whole regions of interest at high frame rates. We used staggered double-PRF transmits to obtain alias-free color Doppler. Staggered PRF is an emission process where lags between successive pulse transmits change in an alternating way. Clutter filtering was spatially adaptive to obtain optimal Doppler velocities: we used polynomial regression models whose degree was determined by minimizing the Akaike information criterion AIC. The core vorticity of the main vortex was finally estimated from the color-Doppler-derived BVS map.

Results/Discussion

We observed a strong correlation between the *in vitro* vorticities determined by ultrafast Doppler vortography and the angular velocities of the spinning disk ($r^2 = 0.99$). We successfully tracked the main vortex in three different healthy subjects during the whole cardiac cycle. The main vortex appeared in diastole after the onset of rapid filling, during ventricular relaxation. Its core vorticity followed a biphasic waveform related to ventricular relaxation and atrial contraction (E and A waves). The vortex persisted

during isovolumic contraction then vanished during ejection. Ultrafast Doppler vortography can decipher the vortex flow dynamics and thus could be of clinical relevance for early assessment of diastolic function.
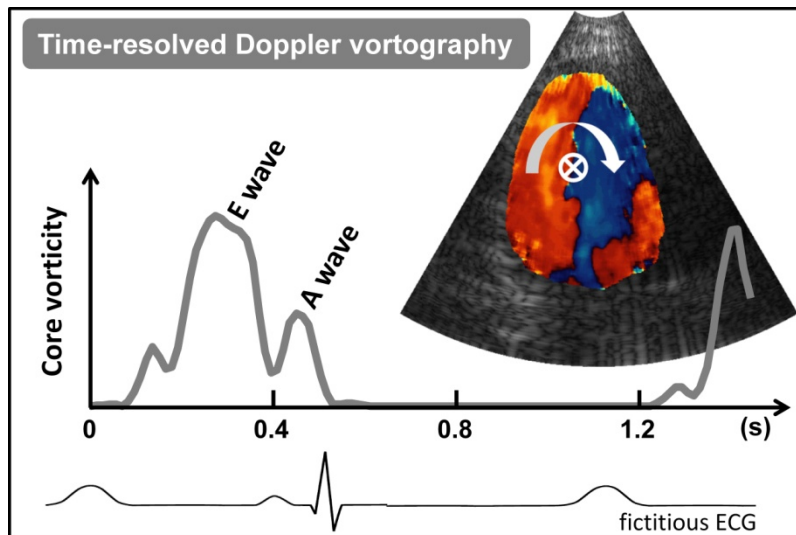
3A-5

11:30 am   Improved Vector Velocity Estimation using Directional Transverse Oscillation for a Convex Array

Jørgen Arendt Jensen[1]; [1]*Dept. of Elect. Eng., Center for Fast Ultrasound Imaging, Technical University of Denmark, Lyngby, Denmark*

Background, Motivation and Objective

A method for estimating vector velocities using transverse oscillation (TO) combined with directional beamforming is presented. It avoids having to predict the lateral wavelength, which makes it self-calibrating and increases the accuracy of vector velocity estimates.

Statement of Contribution/Methods

A normal focused field is emitted and the received signals are beamformed in the lateral direction transverse to the ultrasound beam. A lateral oscillation is obtained by having a receive apodization waveform with two separate peaks. The IQ data are obtained by making a Hilbert transform of the directional signal, and the standard TO estimator can be used to find both the lateral and axial velocity. The approach is self-calibrating as the lateral oscillation period directly is estimated from the directional signal through a Fourier transform. The approach was implemented on the SARUS scanner using a BK Medical 8820e transducer with a focal point at 105.6 mm (F#=5) for VFI. A 6 mm radius tube in a circulating flow rig was scanned and the parabolic volume flow of 112.7 l/h (peak velocity 0.55 m/s) measured by a Danfoss Magnetic flow meter for reference.

Results/Discussion

Examples of velocity estimates for the new TO approach are shown below for 32 emissions at a 90 degrees beam to flow angle. The top left figure shows the estimated angle and the bottom figure shows the mean of the 40 estimated profiles +/- one std at a vessel depth of 30 mm. The std drops from 9.14% to 5.4%, when using the new approach. The bias is -5.05% and the angle is found within +/- 3.93 degrees. The self-calibrating feature of the approach is demonstrated on data from a vessel at 70 mm show in the right figure. The same beamforming scheme is used, and a relative std of 7% is obtained, the bias is -1.74%, and the angle is found within +/- 2.6 degrees.

3A-6

THURSDAY ORAL
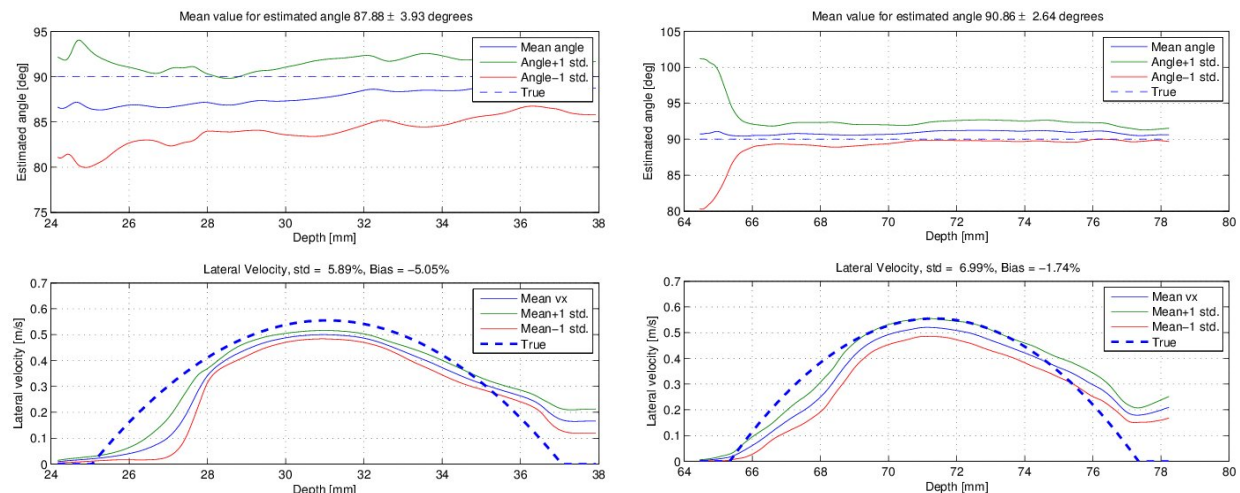
11:45 am   Small-diameter Vasculature Detection with Coherent Flow Power Doppler Imaging

You Li[1], Jeremy Dahl[2]; [1]*Department of Biomedical Engineering, Duke University, Durham, North Carolina, USA,* [2]*Department of Radiology, School of Medicine, Stanford University, Stanford, California, USA*

Background, Motivation and Objective

Power Doppler (PD) imaging is a widely used method for flow detection in clinics, and is utilized as an adjunct tool for prenatal/placental vessel evaluation. However, the sensitivity of PD in small vessel detection is limited by the small-diameter and slow flow of the placental vasculature, where abnormalities are indicative of disorders including preeclampsia, fetal growth restriction, and early pregnancy loss. In order to provide more sensitive detection of placental vasculature, a coherent flow imaging technique, termed coherent flow power Doppler (CFPD), is characterized and evaluated.
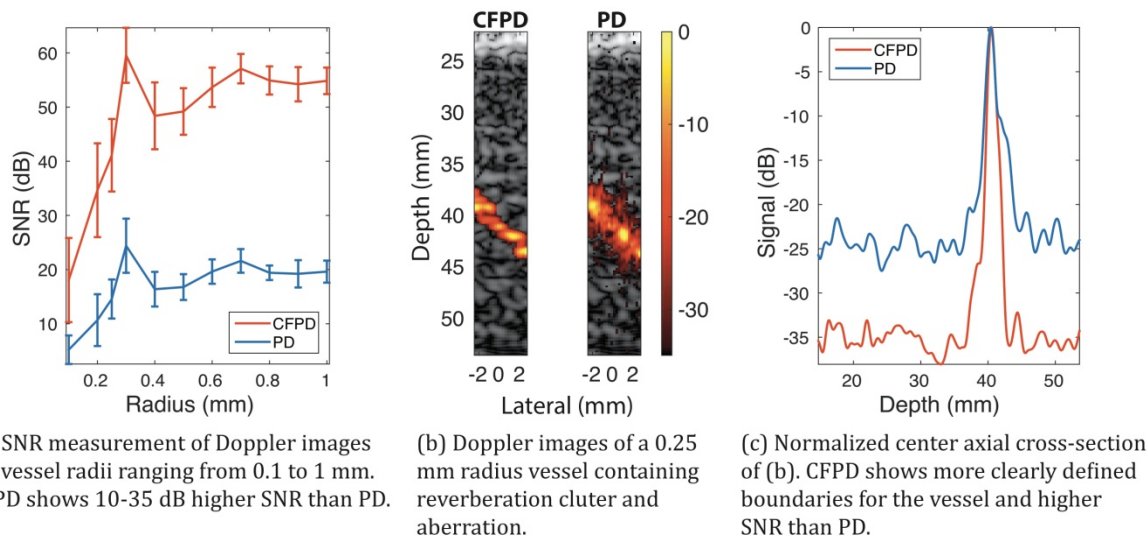
Statement of Contribution/Methods

The CFPD method detects flow based on the spatial coherence of backscattered echoes from blood. Because the signal produced by CFPD is dependent on the spatial coherence of blood echoes instead of the field amplitude, CFPD can suppress spatially incoherently noise including thermal noise and reverberation clutter. Performance of CFPD in small vessel detection is characterized with Field II and nonlinear full-wave simulations. In these simulations, the vessel radii varied from 0.1 to 1 mm with a flow velocity of 10 mm/s, which are typical diameters and flow speeds associated with the maternal spiral arteries in the placenta. These simulations were repeated with the addition of a human abdominal wall model to assess the impact of reverberation clutter and aberration on small vessel detection with CFPD.

Results/Discussion

Simulations with Field II show that CFPD yielded a 10-35 dB increase of SNR over conventional PD imaging (Fig. (a)). The improvement in SNR enables CFPD to detect flow in smaller vessels than PD. With a channel SNR of 30 dB, CFPD can detect vessels with radii as small as 0.1 mm, limited by the resolution of the system, while PD is unable to provide sufficient SNR for detection for vessels with radii below 0.25 mm. Simulations with reverberation clutter and aberration generated by the full-wave simulations and human abdominal data show that the Doppler images produced with CFPD have more clearly defined boundaries and higher SNR than PD (Fig. (b) and (c)), indicating that CFPD is less susceptible to reverberation clutter. These results imply that CFPD can play a major role in the detection and observation of the maternal spiral arteries, which significantly impact preeclampsia.

(a) SNR measurement of Doppler images for vessel radii ranging from 0.1 to 1 mm. CFPD shows 10-35 dB higher SNR than PD.

(b) Doppler images of a 0.25 mm radius vessel containing reverberation cluter and aberration.

(c) Normalized center axial cross-section of (b). CFPD shows more clearly defined boundaries for the vessel and higher SNR than PD.

4A - MBB: Beamforming I

201DE

Thursday, October 22, 2015, 10:30 am - 12:00 pm

Chair: **Jesse Yen**
University of Southern California

4A-1

10:30 am   Coherence Beamforming Applied to Velocity Estimation and Partially Coherent Signals

Jeremy Dahl[1], You Li[2], Dongwoon Hyun[2]; *[1]Radiology, Stanford University, Palo Alto, CA, USA, [2]Biomedical Engineering, Duke University, Durham, NC, USA*

Background, Motivation and Objective

Time-delay and phase-shift estimators are often utilized in context of tracking speckle to estimate parameters such as strain, displacement, and velocity. These estimators rely on the beamformed RF signal to accurately estimate time and phase shifts. Partially coherent targets such as speckle, however, introduce variance and bias errors into the estimation because the delay-and-sum beamformer does not adapt to the spatial variation of the sampled waveform. In addition, the presence of acoustic and thermal noise can exacerbate this problem. We introduce a theory describing the delay-and-sum beamforming process as a function of the coherence between the element signals of the transducer array and show how partial coherence introduces variance and bias into the estimates of velocity and displacement estimation.

Statement of Contribution/Methods

We demonstrate this theory in the context of velocity estimation. Pulsed Doppler simulations of a 2 mm vessel at a 60° angle and a flow rate of 10 mm/s were performed in Field II with a 5 MHz linear array to evaluate this theory. Simulated acoustic noise was added to the channel signals of the array. Velocity was estimated between RF channel signals, rather than beamformed RF signals, using Kasai's autocorrelation method. Velocity was estimated as a function of spatial lag and the bias and variance were measured. Experiments in tissue-mimicking flow phantoms using a 4 mm vessel and a 5 MHz linear array were compared to the simulation results.

Results/Discussion

By eliminating incoherent information (large spatial lags) in Kasai's velocity estimator, bias was reduced in high noise environments. Limiting the signal to high coherence signals (≤ 13 spatial lags), the bias was reduced from 8.3% (9.17 mm/s) with conventional color flow (CF) to 0.6% (9.94 mm/s) with coherent color flow (CCF) at 10 dB noise relative to the blood signal (see figure). The standard deviation of the velocity estimates dropped from 3.38 mm/s to 0.96 mm/s. In general, variance and bias of the velocity information increased with increasingly incoherent (larger spatial-lags) information added into the beamformed signal. Low noise yielded smaller variance and bias. Phantom experiments demonstrated similar variance to low noise (-20 dB noise; bias could not be accurately estimated). Although this method improves bias and variance, it sacrifices spatial resolution.
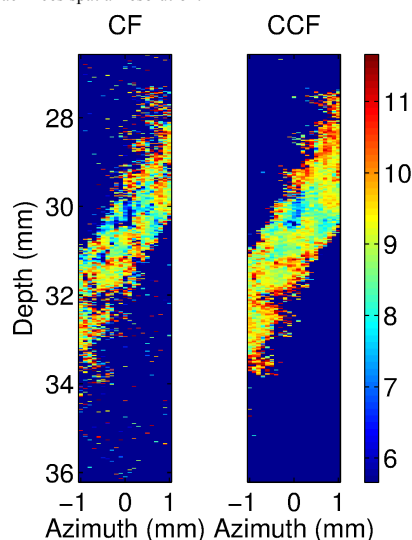
4A-2

10:45 am   Acoustic clutter suppression with weighted phase-difference coherence factor

Zijian Guo[1], Ting-Lan Ji[2], Albert Gee[1], Dave Napolitano[1], Ching-Hua Chou[1], Yuling Chen[1], D-L Donald Liu[2], Glen McLaughlin[1]; *[1]Zonare Medical Systems, Mountain View, CA, USA, [2]Mindray North America, Mountain View, CA, USA*

Background, Motivation and Objective

Various forms of coherence factors have been proposed to improve spatial resolution and suppress acoustic clutters. In one form, coherence factor was defined as the ratio of the coherent sum to the incoherent sum of the aperture data. In another form, phase coherence factor computes the inverse of the standard deviation of the phases of the aperture data. Regardless of the forms of definition, coherence factors evaluate focusing quality at given field points based on the degrees of coherence of the aperture data. These methods work effectively for coherent sources such as pin targets, whose correlation length is infinite. For incoherent sources with finite correlation lengths, however, the coherence factors suffer from the decorrelation effect from the source. As a consequence, most of the coherence factors tend to introduce large speckle variance. In this paper, we propose the weighted phase-difference coherence factor and its computation-efficient form vector coherence factor, in an attempt to suppress acoustic clutters while preserving tissue speckles.

Statement of Contribution/Methods

The weighted phase-difference coherence factor (WPD-CF) is defined as the inverse of the weighted standard deviation of the phase differences between signals from adjacent channels, where the weighting factors are the signal magnitudes. Since the element spacing between adjacent channels is shorter than the correlation lengths, the phase differences are not affected by the decorrelation effect. By evaluating the degrees of coherence of the phase differences rather than the absolute phases, WPD-CF preserves signals from the mainlobe for both pin targets and tissue speckles. On the other hand, the phase differences show high variations in the presence of phase

aberrations. As such, WPD-CF differentiates the true signals from the random acoustic clutters. The reliability of the method was further improved by employing signal magnitudes as weighting factors. Several computation-efficient forms of WPD-CF, named vector coherence factors (VCF), were derived based on the fact that the cosine of the angle between two vectors is proportional to their dot product.

Results/Discussion

The advantages of WPD-CF were demonstrated by the phantom and in vivo imaging results, as shown in the Figure. We believe WPD-CF and VCF have great potential in cardiac and vascular imaging applications.

a) Original   b) CF-weighted   c) WPD-CF-weighted
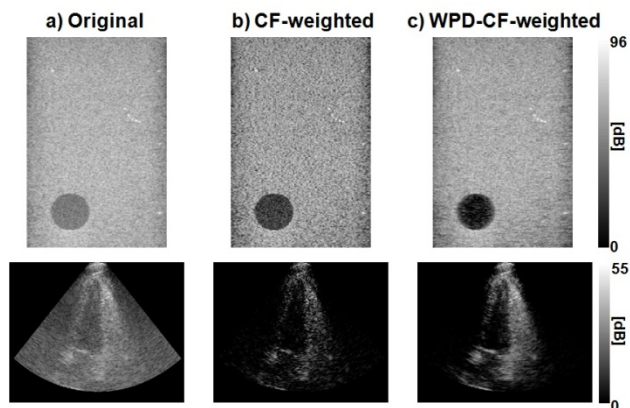
Comparison between a) the original images, b) CF-weighted, and c) WPD-CF-weighted images. The WPD-CF-weighted method suppressed the clutter in the chamber while preserved tissue speckle.

4A-3

11:00 am   **Adaptive Imaging with Multi-Phase Apodization with Cross-correlation: Phantom and In-vivo Results**

Junseob Shin[1], **Jesse Yen[2]**; *[1]Earth and Environmental Sciences, Los Alamos National Laboratory, Los Alamos, NM, USA, [2]Biomedical Engineering, University of Southern California, Los Angeles, CA, USA*

Background, Motivation and Objective

We previously introduced a beamforming method called Dual Apodization with Cross-correlation (DAX), which utilizes two distinct receive amplitude apodizations to intentionally introduce out-of-phase grating lobes that allow for clutter suppression. Our previous work demonstrated its utility in suppressing off-axis clutter and phase aberration effects. However, its effectiveness would likely diminish in the presence of near-field reverberation clutter whose magnitude can be much greater than those of off-axis clutter and phase aberration effects. In this work, we propose a new method, called Multi-Phase Apodization with Cross-correlation (MPAX), which benefits from added phase diversity in multiple pairs of random phase apodizations for increased effectiveness in suppressing both off-axis and reverberation clutter.

Statement of Contribution/Methods

RF channel data were acquired from a custom sponge phantom having a 4 *cm*-diameter hole using a Verasonics system and a 64-element ATL P4-2 phased array with center frequency of 2.5 MHz, 50% bandwidth, and a pitch of 0.32 *mm*. To mimic the near-field reverberation clutter artifacts, a 1 *cm*-thick copper wire mesh was placed at the face of the array. The MPAX weighting matrix was created by averaging n sets of cross-correlation coefficient matrices computed from n independent realizations of complementary random phase apodization pairs having a peak-to-peak phase delay $m = 4$ radians. To maximize the quality of the weighting matrix, spatial smoothing was introduced via subarray averaging with a subarray size $L=16$ elements. Hence, a total of $n=64-L+1=49$ coefficients were computed from each subarray and were averaged. Performance of MPAX was evaluated in terms of improvement in contrast-to-noise ratio (CNR). Initial results for echocardiography from a normal healthy volunteer are also presented to demonstrate feasibility in-vivo.

Results/Discussion

In both sponge phantom and in-vivo cardiac images, MPAX was shown to effectively suppress reverberation clutter, yielding CNR improvements of 144% and 63%, respectively (Fig 1). The amount of additional CNR improvements associated with further increasing the number of phase apodization pairs is minimal for the specific choice of our m value. For future work. further optimization of MPAX parameters will be investigated and a pilot study on human subjects is underway.

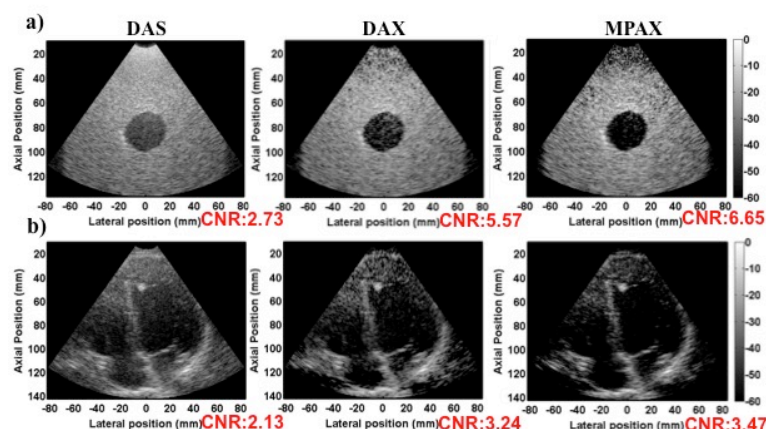**Fig 1.** Performance comparison between DAS, DAX, and MPAX from **a)** a custom sponge phantom with a copper wire mesh and **b)** *in-vivo echocardiography* data from a normal healthy volunteer. In both cases, MPAX showed the highest CNR values.

4A-4

11:15 am A comparison of analytical and numerical approaches for CT-based aberration correction in transcranial ultrasound: application to passive acoustic imaging

Ryan Jones[1,2], Kullervo Hynynen[1,2]; [1]*Medical Biophysics, University of Toronto, Canada,* [2]*Physical Sciences Platform, Sunnybrook Research Institute, Canada*

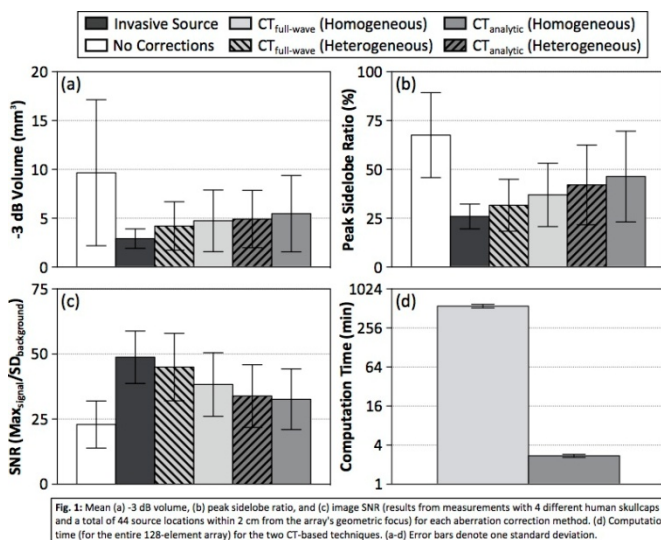**Background, Motivation and Objective**

During clinical focused ultrasound (FUS) brain treatments, pre-treatment computed tomography (CT) scans of the patient's head are analyzed to derive driving signals for the phased array elements that mitigate focal distortions upon propagation through the skull. Recently, our group has demonstrated that an analogous approach can be performed during beamforming on receive, with an array of hydrophones, to allow for passive acoustic imaging within the skull cavity. The objective of the current study was to compare analytical and numerical approaches for calculating aberration corrections based on CT data, with a particular focus on their application to passive imaging in the brain.

Statement of Contribution/Methods

A sparse hemispherical receiver array [O'Reilly *et al.*, *IEEE TBME* (2014)] was used to passively listen through *ex vivo* human skullcaps to emissions from a fixed source emitter. The raw RF waveforms were captured and passive beamforming was performed to render spatial maps of source activity. Measurements were taken at various locations within the cranial cavity by moving the source around the field using a 3D positioning system. Two different CT-based aberration correction models were investigated: an analytical method [Clement & Hynynen, *UMB* (2002)] similar to that currently employed by commercial FUS brain systems for transmit focusing, and a 3D full-wave model [Connor & Hynynen, *PMB* (2002)] based on the Westervelt equation. Images generated using CT-based skull corrections were compared with those obtained through an invasive source-based approach, as well as images formed without skull corrections.

Results/Discussion

Both CT-based techniques provided improvements in image quality over the case where no aberration correction is performed [Fig. 1]. For each model, corrections achieved by allowing for heterogeneous skull acoustical parameters in simulation outperformed the corresponding case where homogeneous parameters were assumed [Fig. 1]. Of the CT-based methods, the full-wave model provided the best imaging results, at the cost of having a larger computational burden [Fig. 1]. These results highlight the importance of accurately modeling trans-skull propagation when calculating CT-based aberration corrections. Although presented in an imaging context, our results may be applicable to the problem of transmit focusing through the skull.

Fig. 1: Mean (a) -3 dB volume, (b) peak sidelobe ratio, and (c) image SNR (results from measurements with 4 different human skullcaps and a total of 44 source locations within 2 cm from the array's geometric focus) for each aberration correction method. (d) Computation time (for the entire 128-element array) for the two CT-based techniques. (a-d) Error bars denote one standard deviation.

4A-5

11:30 am Adaptive Beamformer Incorporating with Element Directivity

Hideyuki Hasegawa[1], Hiroshi Kanai[2]; [1]*Graduate School of Science and Engineering for Research, University of Toyama, Toyama, Japan,* [2]*Graduate School of Engineering, Tohoku University, Sendai, Japan*

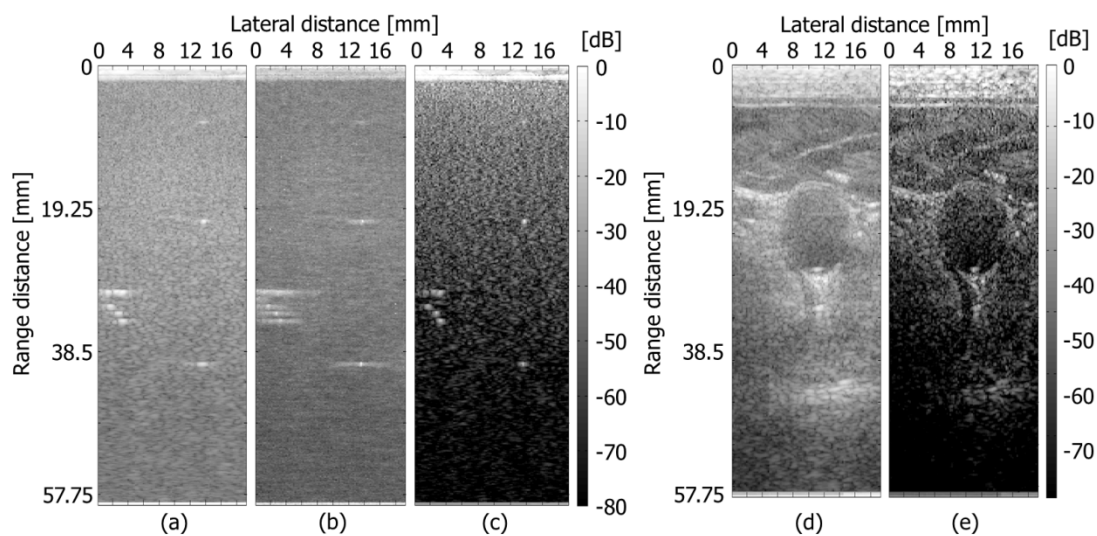**Background, Motivation and Objective**

High frame rate ultrasound is an emerging technique for medical ultrasound imaging. However, spatial resolution and contrast are degraded compared to conventional beamforming using focused transmit beams. In the present study, a kind of minimum variance beamformer, namely, amplitude and phase estimation (APES) beamformer, was examined for improvement of the spatial resolution.

Statement of Contribution/Methods

The APES beamformer estimates the desired signal, i.e., echo from the focal point, using delay-and-sum beamforming without considering the element directivity and removes it from the spatial covariance matrix. By omitting the element directivity, the error in estimation of the desired signal increases and, as a result, more part of the desired signal remains in the spatial covariance matrix. Consequently, sub-array averaging is necessary for further suppressing the desired signal contained in the spatial covariance matrix. In the present study, the APES beamformer was modified so as to consider the element directivity in estimation of the desired signal. Also, the proposed APES beamforming was further modified to be applied to outputs of sub-aperture beamforming to reduce dimension of the spatial covariance matrix.

Results/Discussion

The effect of the element directivity on APES beamforming was evaluated by a basic experiment using a phantom. In parallel beamforming with the conventional DAS, lateral spatial resolution, which was evaluated from the lateral full width at half maximum of the amplitude profile of an echo from a fine wire, was 0.50 mm (Fig. (a)). Using conventional APES, the lateral spatial resolution was improved to 0.26 mm (Fig. (b)). Lateral spatial resolution was further improved to 0.25 mm using the modified APES (Fig. (c)). In both APES beamforming, sub-array averaging was not used, and outputs from 6 sub-apertures were processed. Figures (d) and (e) show B-mode images of a carotid artery obtained by DAS and modified APES, respectively. Undesired echoes are suppressed significantly by the modified APES. In the present study, the element directivity was considered in APES beamforming. Spatial resolution of an ultrasound image was improved without sub-array averaging. Also, by combined with sub-aperture beamforming, the computational load was significantly reduced compared with sub-array averaging.

4A-6

11:45 am   Model-based clutter suppression in the presence of phase-aberration from *in vivo* data and simulations

Kazuyuki Dei[1], Brett Byram[1]; [1]*Biomedical Engineering, Vanderbilt University, TN, USA*

**Background, Motivation and Objective**

Recent studies reveal that multipath scattering sources may significantly degrade ultrasound images. However, during *in vivo* imaging it is difficult to differentiate whether degradation is from multipath or off-axis scattering or from phase aberration. To compare the relative contributions of scattering clutter and phase aberration, we apply our aperture domain model image reconstruction (ADMIRE) method that suppresses off-axis and reverberation clutter, while preserving channel data so that aberration profiles can be estimated after decluttering.

Statement of Contribution/Methods

We applied ADMIRE to *in vivo* channel data. We used this data to generate B-mode images and measured contrast pre- and post-ADMIRE, and we measured near-field phase-aberration profiles and corrected for the aberration both pre- and post-ADMIRE to determine the relative impact of aberration before and after ADMIRE. We also quantified the aberration profile's autocorrelation full-width half-max (FWHM) and the root-mean square (RMS) before and after ADMIRE. Finally, in order to validate our *in vivo* results we performed Field II simulations with aberrated wavefronts, and we determined measured aberration profile errors as a function of degrees of freedom (DOF) allowed in ADMIRE.

Results/Discussion

The contrast of post-ADMIRE images showed 6.5±1.1 dB improvement from the original data, whereas when applying phase-aberration post-ADMIRE there was a negligible additional improvement in contrast (-.15±1.3 dB). We found that contrast decreased 1.3±2.4 dB when applying aberration correction alone. The aberration profiles' FWHM before and after ADMIRE are 1.6±.76 mm and 3.1±.34 mm, respectively (higher is better). The average RMS values pre- and post-ADMIRE are 34±10 ns and 16±4.5 ns, respectively (lower is better). Results show ADMIRE decreased measured aberration levels. This by itself suggests that off-axis and multipath scattering may substantially impact aberration measurements. To test this hypothesis, we applied ADMIRE with different DOF to the Field II simulated aberrated wavefronts. Three wavefront reconstructions are shown below (left) for three different DOFs in the model-fit. We quantified the error of measured aberration profiles as a function of DOF (right). These results suggest that ADMIRE itself can suppress aberration depending on the DOF of the decomposition.
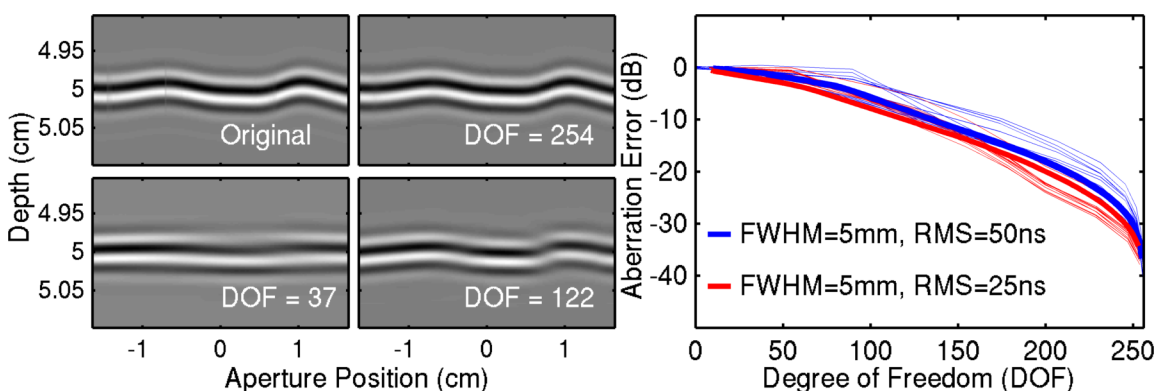
5A - Ultrasonics in Water and Air

103

Thursday, October 22, 2015, 10:30 am - 12:00 pm

Chair: **Jiromaru Tsujino**
Kanagawa University

5A-1

10:30 am   Shear wave generation in soft tissues using electrolysis-induced bubbling

Sandra Montalescot[1], **Stefan Catheline**[2], Ali Zorgani[3], Benedicte Roger[1], Rémi Souchon[1]; *[1]INSERM, University of Lyon, France, [2]INSERM, University of Lyon, Lyon, France, [3]University of Lyon, France*

Background, Motivation and Objective

In the field of elastrography, shear waves are usually generated in soft tissues using either external vibrators or the acoustic radiation force. In a recent article the possibility to generate shear waves in conductive tissues using the Lorentz force was demonstrated. In this study, we present a new method based on electrical currents in conductive tissues containing water: the electrolysis-induced bubbling.

Statement of Contribution/Methods

The experiments were conducted on homemade 10%-gelatin phantoms containing NaCl (10%) to achieve a high electrical conductivity and US-scattering agar particles (0.3%) to allow displacement field imaging in the phantom using speckle-tracking algorithms. A sinusoidal electrical pulse is applied to the phantom with brass electrodes. This electrical current causes copper oxidation on the anode and water reduction into gaseous dihydrogen on the cathode. The resulting bubbling pushes the surrounding gelatin, which induces a shear wave in the phantom. This wave is then filmed with an ultrafast scanner.

Results/Discussion

Displacement maps (fig 1) clearly show the propagation of a shear wave right after the electrical pulse.

Our model of bubble thickness on the electrode predicts a comparable evolution and a magnitude compatible with the experimental results.

Discussion and conclusions

This study proves that it is possible to generate shear waves in soft matter using electrolysis-induced bubbling and proposes a model to predict the amplitude of the waves. However, we used highly salted phantoms with an around ten times higher electrical conductivity than biological tissues. The efficiency of this method shall therefore be optimized in order to use it in biological tissues.
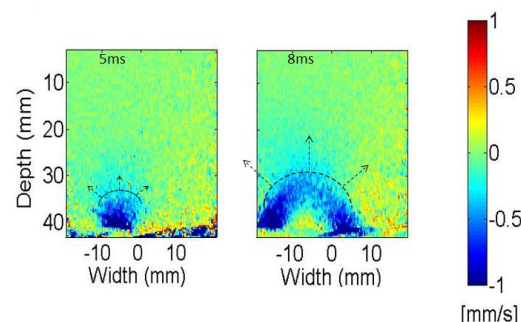

Figure 1 : Shear wave emission from the cathode. The transient bubble growing creates a displacement field in the direction of the ultrasound probe (t = 5 ms) placed at the depth origin. Mechanical motion is then transported in the bulk mainly as a shear wave (t = 8 ms)

5A-2

10:45 am   Measurement of human body surface displacement by breathing using airborne ultrasound

Shinnosuke Hirata[1], Hiroyuki Hachiya[1]; *[1]Dept. of Mechanical and Control Engineering, Tokyo Institute of Technology, Meguro-ku, Japan*

Background, Motivation and Objective

There is a growing need for remote monitoring of vital information. We have been studied non-contact measurement of human body surface displacement by breathing using ultrasonic pulse-echo method. In the case of a standing human, the displacement by breathing is as smaller as that by body movement. Furthermore, they are equal to or smaller than the wavelength of typical airborne ultrasound. Therefore, measurement of the displacement by only breathing using airborne ultrasound is typically difficult. In the proposed method, a small displacement can be estimated by tracking the phase difference of echo signals. Then, displacements are measured from the front and back of the human body. The displacement by breathing can be calculated using the front and back displacements.

Statement of Contribution/Methods

To improve the echo reflected from the human body, pulse compression using M-sequence is employed in the proposed method. Therefore, sine waves which are modulated by binary words in the M-sequence code are periodically transmitted from the front and back of the human body. Received signals are correlated with the transmitted M-sequence code. Each displacement is estimated from the phase difference between temporally adjacent echo signals. The displacement by body movement is cancelled by the difference between the front and back displacements.

Results/Discussion

The M-mode image of echoes from the front of the human body is illustrated in Fig. (a). Displacements of breathing and body movement are included in the echo motion. The front and back displacements which were estimated from phase differences are illustrated in Fig. (b). Identification of the displacement by breathing from each displacement is difficult because the displacement by body movement was larger than that by breathing in the experiment. The difference between 2 displacements of Fig. (b) is illustrated in Fig. (c). The displacement by breathing of several millimeters seems to be measured by the proposed method. Furthermore, the amplitude spectrum of the displacement of Fig. (c) is also illustrated in Fig. (d). The breathing frequency seems to be approximately 0.13 Hz.
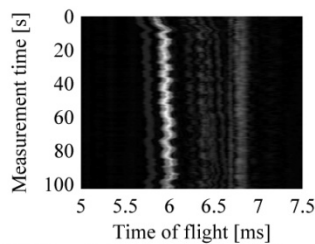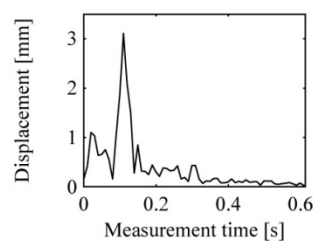
(a) M-mode image of echo from front surface
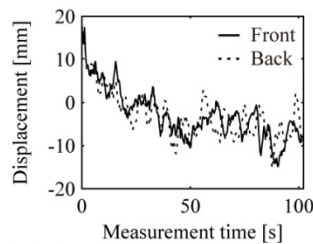
(b) Displacement estimated from phase difference
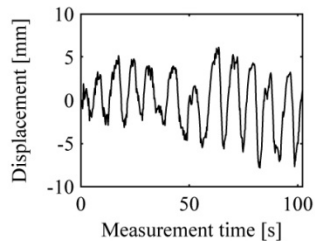
(c) Difference between front and back displacements

(d) Amplitude spectrum of (c)

5A-3

11:00 am **Phased array transducer for emitting 40-kHz air-coupled ultrasound without grating lobes**

Eric Konetzke[1], Matthias Rutsch[2], **Maik Hoffmann[1]**, Alexander Unger[2], Rene Golinske[1], Dirk Killat[1], Sivaram Nishal Ramadas[3,4], Steve Dixon[3], Mario Kupnik[2]; *[1]BTU Cottbus-Senftenberg, Germany, [2]Technische Universität Darmstadt, Germany, [3]University of Warwick, Coventry, United Kingdom, [4]Elster-Instromet, Belgium*

Background, Motivation and Objective

We succeeded in fabricating a versatile 1D phased array transducer, capable emitting directed air-coupled ultrasonic waves at 40 kHz without any grating lobes. It is well known, that this achievement is only possible when each transducer element is small enough for an element pitch that is equal half of the wavelength, i.e. 4.3 mm. Grating lobes limit the opening angle of the array [Harput, 2008] and they require a significant portion of the available energy. Efficient and commercially available single element transducers, such as the widely used MA40 series from Murata Seisakusho, Japan, are too large in diameter (> 10 mm) to simply form a 1D phased array by arranging several of them in an array configuration with proper element pitch. Thus, to the best of our knowledge, there is no efficient phased array transducer available that is capable to fulfill the half-wavelength criteria for air-coupled ultrasound at a frequency as low as 40 kHz, resulting in ultrasonic propagation with low attenuation.

Statement of Contribution/Methods

Therefore, in this work we demonstrate a solution by extending an approach, demonstrated by Takahashi et al, ICMT, 2007. Instead of trying to form the phased array transducer with small emitting transducer elements directly, we employ acoustic waveguides. The main idea is that these waveguides separate the larger acoustically active sources from the effective acoustic apertures of the phased array transducer elements. Using an aluminum mold, we manufactured these waveguides using shrinking tubes. The waveguides have circular-shaped openings for the housed single-element transducers (MA40S4, Murata) with a diameter of 10 mm and are then tapered and bent, over a defined and optimized length of 67.1 mm to a rectangular-shaped element aperture of 4.3 x 6 mm at the other end. Combining twelve of these arrangements on a PCB to form one of eight channels gave us the finished phased array transducer with superior acoustic performance.

Results/Discussion

By using a volumetric characterization system [Hoffmann et al, IUS 2013], the phased array transducer was tested. The main lobe is narrow and symmetric and it can be steered over an opening angle of 110° without any grating lobes - exactly as expected from theory. In addition, we measured a maximum sound pressure level of 142 ±1 dB at a distance of 30 cm, which can be explained by the fact that the waveguides concentrate the acoustic energy into a smaller effective aperture. Such an array will be essential for numerous ultrasonic applications, which did not benefit from beam steering capability so far. Example applications are gas flow metering, range finding, anemometry, gesture sensing, ultrasonic communication, acoustic tweezing in air, and acoustic imaging of entire rooms, to name a few. The approach is compatible with 3D printing techniques for fabricating the waveguide layer. For future work, we plan extending the approach to build an air-coupled fully populated 2D phased array transducer.

5A-4

11:15 am **Laser-ultrasound imaging of material porosity with a kHz rate fiber-optic pump-probe system**

Ivan Pelivanov[1,2], Matthew O'Donnell[1]; *[1]Bioengineering, University of Washington, Seattle, Washington, USA, [2]Physics Faculty, Moscow State University, Moscow, Russian Federation*

Background, Motivation and Objective

Material porosity is a very important problem directly affecting material strength and life time. Ultrasound (US) is one of the primarily NDE methods to quantify porosity, where US speed/attenuation are usually used to estimate void content. However, most US approaches require a sample with plane, parallel and relatively smooth surfaces to correctly measure the attenuation and speed, but such conditions are not always fulfilled in practice. In addition, US methods cannot directly image porosity as X-rays do. Here we present a method to evaluate porosity using non-contact laser-ultrasound (LU) images obtained with at least a 1 kHz A-scan rate. This system can also be used in US speed/attenuation measurements at high scan rates.

Statement of Contribution/Methods

The method is based on laser-ultrasound generation of ultra wide band probe US signals at the surface of a sample under study and non-contact, high resolution, point-like detection of back-scattered transients.

The main components of the system are a compact, high (up to 100 kHz) pulse repetition rate nanosecond laser to generate probe US signals at the surface of a sample under study and a custom designed, fiber-optic based Sagnac interferometer for non-contact detection of back scattered ultrasound [I. Pelivanov et al, Photoacoustics, 2 (2), p. 63, 2014; I. Pelivanov et al, J. Appl. Phys., 115(11), p. 113105, 2014; I. Pelivanov et al, IEEE Tran. UFFC, in press]. The sample is fixed on a XY translation platform, which can be moved at a linear translation speed of 100 mm/s in both lateral directions. The A-scan stepping accuracy is 1 μm.

The laser-generated probe US pulse propagates through the sample, partially reflecting off of the sample structure and reflecting off of the back wall. All acoustic waves propagating back to the front wall of the sample (including reflections from voids) are detected with the interferometer. A-scan signals are processed to determine US speed and attenuation, and material porosity is imaged as filtered B-scans.

Results/Discussion

High resolution B-scans obtained for graphite-epoxy composites illustrated in Fig.1 clearly exhibit a strong correlation between the image brightness of heterogeneities with material porosity as assessed gravimetrically and with US speed. These results strongly suggest that pores can be directly imaged in composites using the wideband LU system developed here.
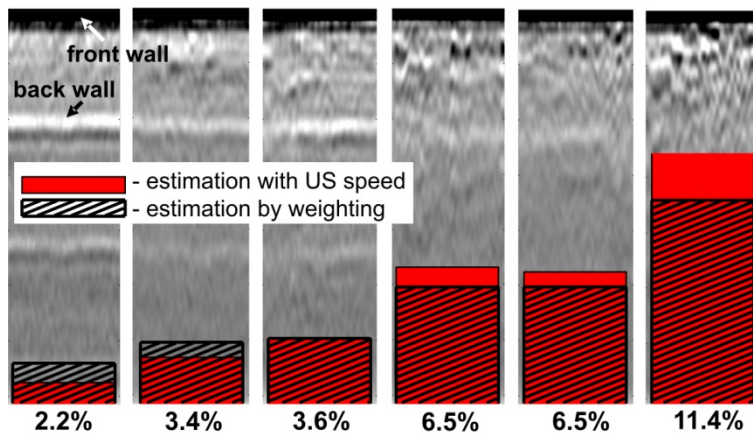

Fig.1. LU B-scan images in graphite-epoxy composite samples with different void content. Evaluation of porosity with US speed and by weighting is shown for comparison.

5A-5

11:30 am   Investigation of Lamb Waves in Solid-Liquid Layers

Detlef Pape[1], Miklos Lenner[1], Tobias Kaufmann[1]; [1]*Corporate Research, ABB Switzerland Ltd., Baden-Daettwil, Switzerland*

**Background, Motivation and Objective**

Lamb waves are used in non-destructive testing to detect defects or corrosion of pipe walls or other sensitive constructions. Depending on the used mode of the Lamb wave the propagation of the waves can be influenced by the presence of liquids as for example in liquid filled pipes. The leaky Lamb waves occurring in this regime have already been investigated in the past. However, even in non-filled pipes, liquids can cover the wall either due to condensation out of a saturated gas phase or due to remains of water in a former filled pipe. The liquid then covers the wall partly or fully as a layer and can influence the propagation of the Lamb waves. In this paper we investigate the propagation of Lamb waves in partially or fully covered plates with liquid layers.

Statement of Contribution/Methods

For the investigation, different modes of Lamb waves were generated in a 1x1m2 size Aluminum plate which was covered by layers of water of different sizes L and thicknesses dl of several mm. The propagation time as well as the signal strength of the different modes were measured. The propagation of Lamb waves was also simulated numerically and the results were compared with the measurements and with theoretical descriptions.

Results/Discussion

The results show a clear effect of the water on the propagation of the Lamb waves in the plate. For leaky modes as the zero order asymmetric mode the main part of the wave is coupled into the water layer and propagates in this layer. By the variation of the layer size the properties of the propagation in the liquid phase could be determined. These propagation properties are additionally influenced by the thickness of the water layer. But also normally non-leaky or only weakly leaky waves as the symmetric mode at lower frequencies are influenced by the water layer. So liquid layers can influence the sensitivity and measurement precision of defect detection in solid walls.
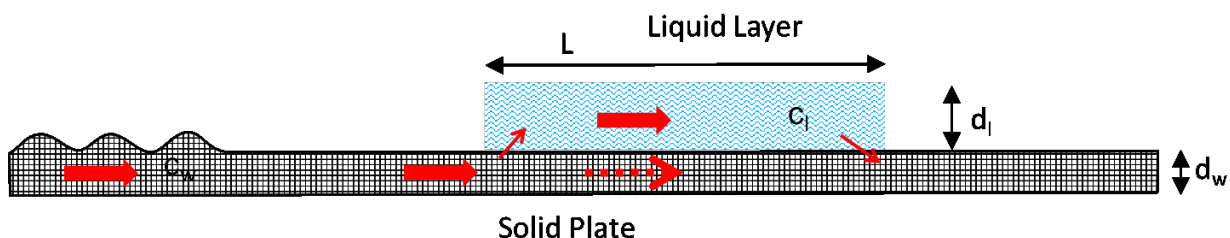
5A-6

11:45 am   Transducer beam diffraction effects in sound transmission near leaky Lamb modes in elastic plates at normal incidence

Magne Aanes[1,2], Kjetil Daae Lohne[2], Per Lunde[1,2], Magne Vestrheim[1]; [1]*Department of Physics and Technology, University of Bergen, Bergen, Norway,* [2]*Christian Michelsen Research AS, Bergen, Norway*

Background, Motivation and Objective

The plane-wave theory of fluid-embedded viscoelastic plates is often used in waveguide applications, and to estimate wall thickness and sound velocities in plates and pipe walls. In normal-incidence through-transmission measurements, frequency shift and increased sound transmission as compared to plane-wave theory, have been observed for certain leaky Lamb modes. These phenomena and the underlying physics are here studied using a system model accounting for 3D description of the transducer's sound field.

Statement of Contribution/Methods

Finite element modeling, combined with an angular spectrum method, is used to simulate the signal propagation through a system consisting of a piezoelectric transducer and a water-embedded steel plate. This includes description of the transducer (its electro-acoustic coupling, vibration, and radiation in water), excitation of viscoelastic leaky Lamb modes in the plate, and the subsequent transmitted sound field in water. The model, capable to accurately describe the measured sound field phenomena, is used to investigate the observed deviations between measurements and plane-wave theory, by varying the longitudinal and shear wave velocities of the plate in a case study.

Results/Discussion

Fig. 1 shows frequency spectra of beam transmission through the plate, compared to plane-wave transmission coefficients. Fig. 2 shows the pressure field (beam) distribution through the plate at 457 kHz, close to the S1 Lamb mode. Such and other results are analyzed in relation to phase and group velocity curves for leaky Lamb modes close to normal incidence. Use of the 3D system model demonstrates that the measured phenomena are caused by beam diffraction effects.

Fig. 2 — Pressure field distribution from the transducer, incl. transmission through plate

Fig.1 — Beam transmission spectra compared to plane-wave transmission coefficients
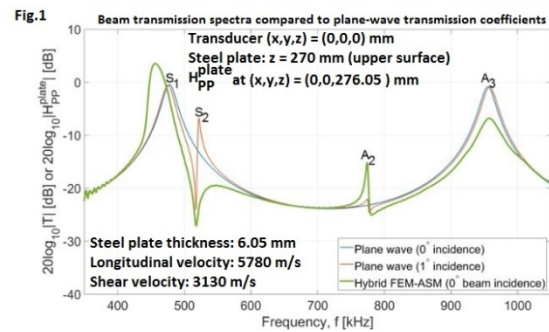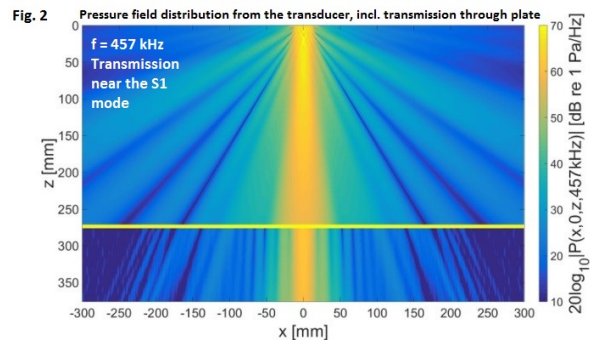
6A - Acoustic Tweezers and Particle Manipulation

201AF

Thursday, October 22, 2015, 10:30 am - 12:00 pm

Chair: **Amit Lal**
Cornell Univeristy

6A-1

10:30 am Dynamic Acoustic Field for Tuneable and Scalable Particle Sorting

George Skotis[1], David Cumming[1], Jemma Roberts[1], Mathis Riehle[1], **Anne Bernassau[2]**; *[1]University of Glasgow, United Kingdom, [2]Heriot-Watt University, United Kingdom*

Background, Motivation and Objective

Separating and isolating cells and micro-organisms from a heterogeneous mixture is a fundamental step in basic biological, chemical and clinical studies, enabling regenerative medicine, stem cell research, clinical sample preparation and improved food safety. Achieving cell separation utilizing ultrasonic manipulation by frequency sweeping has been previously demonstrated; however, this method has several critical disadvantages: unstable forces, small particle displacement, lack of flexibility due to the frequencies that can be used.

In this paper, we demonstrate a flow-less dynamic acoustic field (DAF) method that can be used to separate particles depending on their size or density within a sample volume. We also study the discriminative ability of the method for particles of different sizes or densities. The application of DAF to primary pig dorsal root ganglion neurons as a contact-less means of separating these neurons from debris and smaller cells, which results from tissue digestion, is demonstrated. To prove the scability of our DAF method, we also demonstrate sorting polystyrene particle in mid-air.

Statement of Contribution/Methods

When two opposing acoustic transducers are excited, a linear interference pattern of nodes and antinodes is formed in the interstitial media. As a result, the micro-particles are trapped at the minima of the potential acoustic energy density. Electronically shifting the excitation phase of one of the transducers, with respect to the other, proportionally translates the linear interference pattern in the direction of the added phase delay. The DAF technique relies on a repeated cycling pattern of the phase difference between the two excited transducers from 0˚ to 360˚. Within each cycle the phase is swept completely through 360˚ over a time t_{ramp} and then allowed to rest for a period t_{rest} before commencing the next cycle. The interplay between the rate at which the phase is swept, and the length of the rest time, is at the core of the separation technique.

Results/Discussion

We first demonstrate the method for the separation of particles with different diameters between 6 and 45 μm and secondly particles of different densities in a heterogeneous medium. The dynamic acoustic field is then used to separate dorsal root ganglion cells. The shearless, label-free and low damage characteristics make this method of manipulation particularly suited for biological applications. Advantages of using a dynamic acoustic field for the separation of cells include its inherent safety and biocompatibility, the possibility to operate over large distances (centimetres), high purity (ratio of particle population, up to 100%), and high efficiency (ratio of separated particles over total number of particles to separate, up to 100%).

This DAF method has proved to be scalable and sort polystyrene particles of 3 mm and 1.5 mm diameter in mid-air.

6A-2

10:45 am Traveling Standing Waves: a Feasibility Study

Paul van Neer[1], Ludwig Rasmijn[2], Armin Rasidovic[3], Arno Volker[1]; *[1]Process and Instrumentation Development, TNO, Delft, Zuid-Holland, Netherlands, [2]TNO, Netherlands, [3]Applus RTD, Netherlands*

Background, Motivation and Objective

Lately, there has been significant interest in the noninvasive manipulation of particles and liquids. The reported acoustic techniques rely on either the acoustic radiation force or acoustic streaming. The former allows for particle manipulation based on their density, compressibility and size. Acoustic streaming can be used in developed flows to induce fluid velocities angled to the liquid flow direction. These methods often use standing wave fields induced locally through continuous compressional waves aimed perpendicular to a hard reflector. This has a drawback for industrial applications (i.e., continuous flow reactors): the standing wave field is excited only locally, whereas it should be excited along the entire length of a pipe. Solving this by using numerous actuators along the pipe length is impractical and cost prohibitive.

In this work the feasibility of using guided waves to induce a standing wave field over a pipe's radius, but traveling along a pipe's length, is investigated.
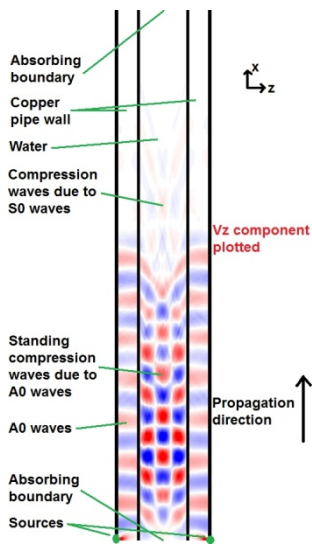
Statement of Contribution/Methods

The method worked by exciting Lamb waves in the wall of a liquid filled pipe, which partially refracted into the liquid. The frequency was chosen such that: 1) a radial resonance was excited in the liquid, and 2) the reflected waves in the liquid added constructively with the refracted wave energy.

The experimental geometry consisted of a copper pipe – length 1m, ID 4mm, WT 1mm. For transmission a radially vibrating piezo was mounted on the pipe. Its dimensions were such that at 830 kHz A0 waves were excited and S0 waves were suppressed. The Lamb waves were measured using a 2nd radially vibrating piezo. The pressure in the liquid was measured with a custom built hydrophone. The induced wave fields were investigated using finite difference simulations.

Results/Discussion

The figure shows a simulated example of a 3rd order standing wave field. The standing compressional wave field caused by refracted A0 wave energy, traveling along the pipe, is visible. The 7th, 8th, 9th and 10th order standing wave fields were calculated to exist in the liquid at frequencies of 625, 830, 1020 and 1185 kHz, respectively. These resonances were measured at 625, 769, 1037 and 1194 kHz, respectively. The differences were caused by the hydrophone/transmitter transfer functions. The measurements show the feasibility of inducing radial standing wave fields traveling along a pipe.

Absorbing boundary
Copper pipe wall
Water
Compression waves due to S0 waves
Vz component plotted
Standing compression waves due to A0 waves
A0 waves
Propagation direction
Absorbing boundary
Sources

6A-3_____

11:00 am   Phononic crystal guided parallel particles transport

Fei Li[1,2], Feiyan Cai[1], Chen Wang[1], Long Meng[1], Chaowei Xu[1], Liufeng Geng[1], Chengxiang Zhang[1], Hairong Zheng[1]; *[1]Paul C. Lauterbur Research Centre for Biomedical Imaging, Shenzhen Institutes of Advanced Technology, Shenzhen, Guangdong, China, People's Republic of, [2]Shenzhen Key Laboratory of Nanobiomechanics, Shenzhen Institutes of Advanced Technology, Shenzhen, Guangdong, China, People's Republic of*

Background, Motivation and Objective

Rapid and precise transportation of microparticles is a crucial functional module in microfluidic devices, where a sample can be pumped to flow through processing areas. In general, microparticles are transported in micro-channels by micro-pumps and micro-valves, which need complex fabrication and high cost. In addition, the micro-channel may be clogged by suspended particles, thus limit the number of measurements and throughput per chip. In order to overcome the above drawbacks, in this paper, we proposed a novel method that particles were aligned and directionally transported on a pure flat surface by the modulated acoustic field through phononic crystal plate (PCP).

Statement of Contribution/Methods

As shown in figure 1, the stainless steel PCP had a pattern of parallel polygonal lines with a constant distance and a 120 degrees intersection angle, and consisted of periodic structures (alternate grooves and stubs) fabricated by chemical-etching processes. The PCP had a resonance frequency of 3.77 MHz by acoustic transmission measurements, and located in a water chamber constructed by PDMS walls, a quartz substrate and a piece of glass cover. The acoustic field on the PCP planar surface was scanned by a commercial 3D ultrasound scanning system. Chirp pulses with a frequency range of 3.77MHz-3.98MHz were generated by a programmable arbitrary waveform generator to excite a PZT adhering to the substrate. Manipulated polystyrene (PS) spheres with a diameter of 15μm were added onto the pure flat PCP surface with a micropipettor. Particles movements in the PCP tuned acoustic field were recorded by a CCD camera.

Results/Discussion

We observed that PS spheres were aligned into parallel lines due to standing waves generated from the interference of the periodic stubs. And aligned particles were transported along the designed paths with a 120 degrees corner by the acoustic streaming, which originated from A0 mode Lamb wave excited by the offset acoustic source. This system might provide particles transport with a simple, disposable, scalable and parallel microfluidic device without micro-channels, pumps and valves.
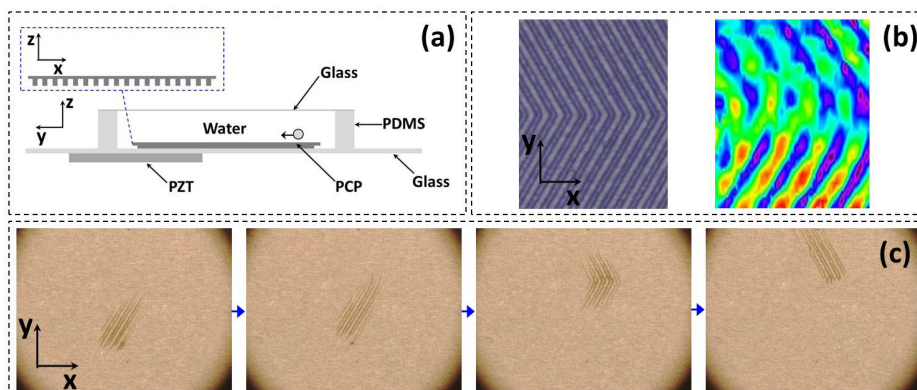

Figure 1 (a) Scheme of experimental setup in yz plane and another view of the PCP in xz plane; (b) etched artificial periodic structures (left) and the acoustic field on the planar surface of the PCP (right); (c) transport snapshots of aligned PS particles guided by the PCP along the designed route with a corner of 120 degrees.

6A-4

11:15 am Self-acoustophoresis of metallic microparticles in ultrasonic standing waves: new tricks with old hats

Wei Wang[1]; [1]*School of Materials Science and Engineering, Harbin Institute of Technology, Shenzhen Graduate School, Shenzhen, Guangdong, China, People's Republic of*

Background, Motivation and Objective

Acoustophoresis, the migration of objects in an acoustic field, forms the basis for acoustic manipulation of microparticles, and sits at the core of acoustic separations and devices such as acoustic tweezers. Despite the extensive research on the fundamental understanding and applications of acoustophoresis, there still remain new territories uncharted in this seemingly old field.

In this presentation we would like to describe our discoveries of metallic microparticles propelled into autonomous directional motion and fast spinning by MHz ultrasonic standing waves. These observations introduce a new class of microparticle behaviors in ultrasound that are completely different from previous reports, and represent brand new opportunities that remain to be explored and exploited. On the other hand, the complicated interplay among the geometry and composition of the particles, hydrodynamic effects and acoustic forces calls for the collective wisdom of researchers from multiple disciplines in order to elucidate the mechanisms behind the observed effects.

Statement of Contribution/Methods

Our experiments were conducted in a homemade acoustic chamber consisting of a rigid substrate, which had a piezoelectric disk glued to the back, tape with a hole at the center, and a function generator that was connected to the ceramic disk. The height of the chamber is roughly 200 µm. When sine waves of appropriate frequencies were applied, an ultrasonic standing bulk wave was formed in the chamber that produced a nodal plane at its center. The behaviors of microparticles in the chamber were observed and recorded using an optical microscope equipped with CCD cameras.

Results/Discussion

We observed strong and surprising behaviors of metallic microrods (3 µm by 300 nm) in ultrasonic standing waves. These microparticles were levitated onto the nodal plane where they exhibited fast axial propulsion at 200 µm/s. Importantly such motion was completely different from the typical acoustophoresis where particles collectively migrate towards a specific spot. Rather, the individual particles had seemingly random trajectories that were independent of each other. Additionally the microrods could dynamically align into long and organized chains of one rod in width that spontaneously span, and on a larger scale these chains formed ring structures with diameters of hundreds of micrometers.
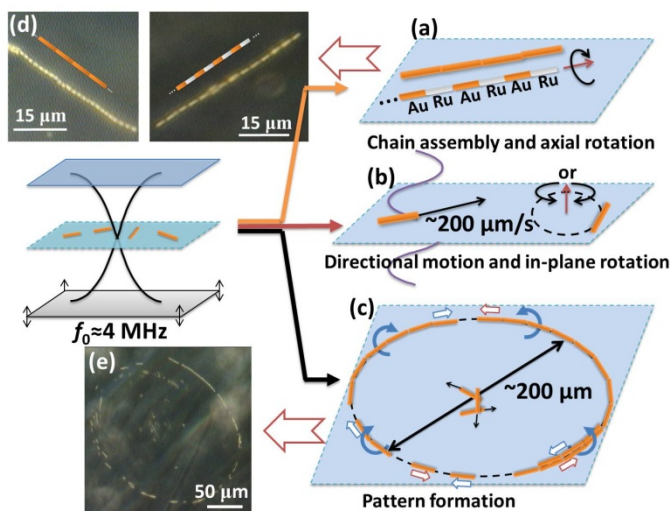
6A-5

11:30 am Recent advances in developing biomedical applications of single beam acoustic tweezers

Ying Li[1,2], Changyang Lee[1,2], Ruimin Chen[1,2], Hae Lim[1,2], Ming-Yi Lin[3], Kwok Ho Lam[4], Kirk Shung[1,2]; [1]*Biomedical Engineering, University of Southern California, Los Angeles, USA,* [2]*NIH Resource Center on Medical Ultrasonic Transducer Technology, University of Southern California, USA,* [3]*Zilkha Neurogenetic Institute, University of Southern California, USA,* [4]*Department of Electrical Engineering, Hong Kong Polytechnic University, Hong Kong*

Background, Motivation and Objective

The feasibility of single beam acoustic tweezers (SBAT) was first theoretically and experimentally demonstrated in our laboratory. Major efforts have been devoted to fabricate various types of SBATs and explore their applications. In the latest effort, the feasibility of in vivo application of SBAT was demonstrated by trapping microparticles in excised blood vessels in vitro. One of 300MHz SBATs fabricated in our laboratory has been shown to possess exceptional precision in manipulating nanoparticles. Besides, a novel method with better accuracy was purposed to calibrate the trapping force of SBATs. Those recent advances in SBAT technology will be reported in this article and following by a discussion of potential biomedical applications of SBATs.

Statement of Contribution/Methods

The potential of in vivo applications of SBAT were demonstrated by two in vitro experiments. A polyimide tubing (Fig.1A) and a rat aorta (Fig.1B) were used to mimic the geometry and properties of blood vessels in vivo. The tubing and the rat aorta were filled with distilled water and fluorescent polystyrene beads size of 3 µm diameter, respectively. Fluorescence imaging were applied to allow better visualization. A 40 MHz SBAT was applied to externally manipulate those polystyrene beads. Furthermore, trapping force of the SBAT was calibrated by a novel method. The SBAT and a micropipette were controlled by two XYZ positioners, respectively. Both of them were applied to manipulate a same 5µm polymer bead, but in opposite directions (Fig.1C). The aspiration force generated by a micropipette could be precisely controlled by a pressure controller (Ez-gSEAL 100B Pressure, Neobiosystems). Therefore, the acoustic trapping force could be balanced and estimated by adjusting the aspiration force.

Results/Discussion

SBAT has been shown to be capable of manipulating microparticles on a curved surface, and after it penetrating through a blood vessel wall. It is highly possible that the SBAT can be applied to in vivo studies involving small animal like rat and mice following additional development. The new calibration method could better describe the trapping force on microparticles of a size at the cell level. It will help to better evaluate the trapping performance of high frequency and high resolution SBATs, and allow SBAT to serve as a noninvasive force measuring tool for biological applications.
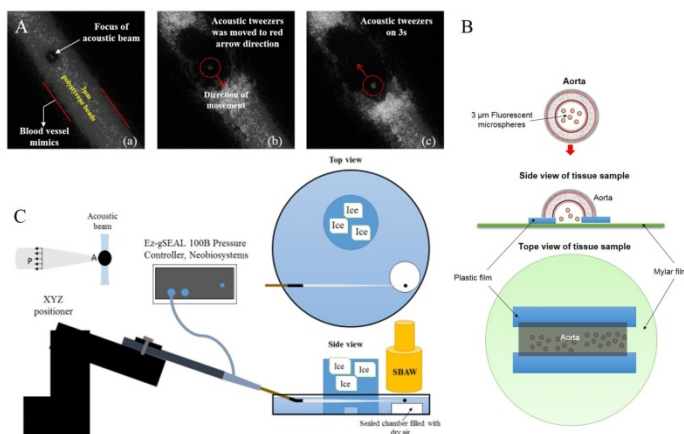
Fig.1 A: Aggregated fluorescent polystyrene microspheres of 3μm size were manipulated by acoustic tweezers inside of a blood vessel mimicking tube. B: A rat aorta tissue sample for an *in vitro* experiment to demonstrate the feasibility of *in vivo* applications of SBAT. C: Experimental configuration for calibrating the trapping force of SBAT by micropipette.

6A-6

11:45 am Cell deformation by acoustic trapping with a single-element high-frequency ultrasound transducer: Potential to determine invasiveness of breast cancer cells

Jae Youn Hwang[1], Jinman Park[1], Chi Woo Yoon[2], Hae Gyun Lim[2], Jungwoo Lee[3], K. Kirk Shung[2]; [1]*Daegu Gyeongbuk Institute of Science & Technology (DGIST), Daegu, Korea, Republic of,* [2]*Biomedical Engineering, University of Southern California, USA,* [3]*Electronic Engineering, Kwangwoon University, Korea, Republic of*

Background, Motivation and Objective

Various acoustic trapping techniques have been developed to manipulate a tiny particle and a live cell. In our recent work, single beam acoustic trapping has been shown to be promising as an alternative method towards various biomedical applications. However, the development of more meaningful biomedical applications of single beam acoustic trapping techniques is still needed. In this study, we thus experimentally demonstrate the potential of our single beam acoustic trapping technique to measure mechanical properties of breast cancer cells with different phenotypes. We here show that acoustic trapping induces deformation of a trapped cell and moreover its deformability depends on the mechanics of a trapped cell. Furthermore, we investigate whether the deformability of a trapped breast cancer cell is related to its invasion potential.

Statement of Contribution/Methods

A press-focused single-element LiNbO3 transducer at a center frequency of 30 MHz was utilized to trap human breast cancer cells, including MDA-MB-231, BT-474, SKBR-3, and MCF-7, and a 10 um microbead. The deformation of an acoustically trapped cell was monitored by using bright-field imaging and compared with the deformation of an acoustically trapped microbead at different acoustic pressures. In addition, the deformabilities of acoustically trapped cells with different invasiveness were examined, quantitatively.

Results/Discussion

In this study, it was found that the acoustic trapping at 30 MHz deforms the trapped individual breast cancer cells, not the microbead as well as the deformability of the trapped cells depends on their mechanical properties. Interestingly, it was observed that the deformability increased as the applied acoustic pressure increased. We have also shown that the highly invasive cancer cells exhibited larger deformability than the weakly invasive cancer cells due to acoustic trapping, thus indicating that the deformability of a trapped cancer cell may be related to their invasion potentials. Typically, the mechanical characteristics of cancer cells have been shown to be highly correlated with its invasiveness. Particularly, many previous studies have shown that a highly invasive cancer cell is softer than a weakly invasive cancer cell. Thus, our proposed approach may be beneficial to determine the invasion potential of a cancer cell.
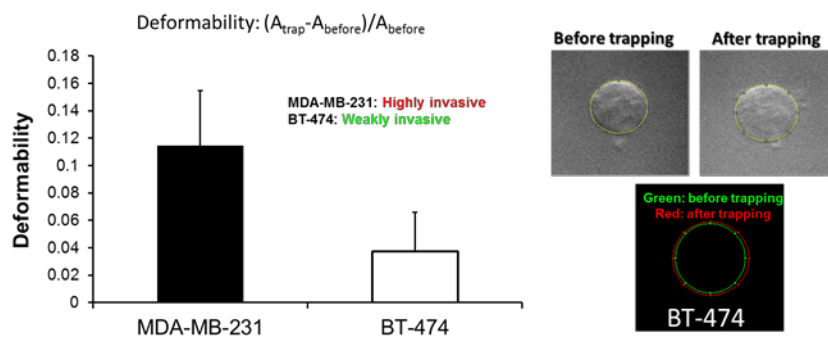
7A - MEMS and FBAR Oscillators and Innovative Applications

105

Thursday, October 22, 2015, 10:30 am - 12:00 pm

Chair: **Shuji Tanaka**
Tohoku University

7A-1

10:30 am   GaN MEMS Resonators and Oscillators

D. Weinstein[1]; [1]*MIT, Cambridge, MA, USA*

Background, Motivation and Objective

As a wide band-gap semiconductor with large breakdown field and saturation velocity, gallium nitride (GaN) has been used increasingly in high-power, high-frequency electronics and monolithic microwave integrated circuits (MMICs). GaN also has excellent electromechanical properties, including high acoustic velocities and low phonon losses. Together with a strong piezoelectric coupling (up to 2%), these properties make GaN ideal for RF MEMS resonators, and offers a platform for seamless integration of high performance RF MEMS resonators with high frequency and high power electronics. This monolithic integration of MEMS resonators with ICs leads to reduced parasitics and matching constraints, enabling low phase-noise clocks and frequency-selective filters for signal processing and high-frequency wireless communications.

Statement of Contribution/Methods

replace

Results/Discussion

We present the design, optimization and fabrication of multi-frequency piezoelectric MEMS resonators that achieve the highest frequency-quality factor product in GaN to date. Additionally, we implement unique transduction capabilities of GaN, such as the ability to use the 2D electron gas (2DEG) as a switchable electrode for transduction. These high performance resonators are used as building blocks to demonstrate the first monolithic GaN MEMS-based oscillators, where active HEMTs along with passives and resonators are all integrated on the same chip. We will discuss our recent results of monolithic Pierce and Colpitts oscillators using 1 GHz GaN MEMS resonators. This first demonstration of low-phase noise, small foot-print monolithic GaN-MEMS oscillators paves the road towards compact and power efficient RF front-ends for wireless communication systems

7A-2

11:00 am   Oven Controlled FBAR Oscillator

Rich Ruby[1], Kannan Sankaragomathi[2], Suresh Sridaran[3], Reed Parker[3]; [1]*avago technologies, Menlo Park, Ca, USA*, [2]*GoogleX, Google, CA, USA*, [3]*avago technologies, USA*

Background, Motivation and Objective

As remote sensors increase due to the popularity of "Internet of Things", there is a need for these remote sensors to receive and transmit packets of data to an ad-hoc network. One such network would be 'Bluetooth Low Energy' or BLE. BLE works on all Android phones and should an Android phone be near a sensor, they will establish contact, data will be uploaded to the phone and then sent over the airwaves. The radio for transmitting BLE must work at the ISM band 2400 MHz to 2483 MHz. The radio must be low power, and small. The current solution is to use a quartz resonator placed inside a ceramic package. However, this is big, and the resonator height is critical in many applications. The problem of a crystal oscillator is its frequency is around 35 to 50 MHz. Power-hungry PLLs are needed to multiply the signal up.

Statement of Contribution/Methods

An FBAR oscillator oscillates directly at 2.4GHz, thus eliminating multiplication of frequency. The problem of FBAR oscillators is that the stability necessary for a BLE radio is on the order of +/- 50 ppm. This is challenging as the FBAR resonator will drift as much as 3000 ppm for a standard FBAR and +/- 150 ppm for a zero drift FBAR resonator (or ZDR). In the case of a ZDR, the freq vs. Temp curve is parabolic with a maximum frequency at the 'Turn over Temperature' or TOT. Near TOT, the delta frequency is very small for small temperature fluctuations. But, a ZDR can be held at nearly constant frequency if the temperature of the resonator is held to a specific temperature. If the TOT of the resonator is chosen properly, the accuracy and placement of the TOT can be greatly relaxed. Given these properties the FBAR oscillator using a ZDR with an on-resonator heater (as an example to keep temperature constant) can both generate a clean low phase noise oscillator (essential for radio signal integrity) and a stable frequency.

Results/Discussion

An ultra stable ZDR resonator (Ruby et al.,"A Comparison of FBAR Oscillators with Standard Resonators and Stress Relieved Resonators", IUS 2013). is suspended in space held by a central pin that supports the resonator and brings in both RF lead to top and bottom electrodes and can also be used to bring in both a heater coil and a heater sensor. The heater coil and sensor are on opposite sides of the resonator (another version uses a cantilever design) and are part of a feedback circuit (with Wheatstone bridge) to keep the temperature (i.e. the sensor resistor) at one temperature (value). We chose a local resonator temperature and TOT to be ~ 90C. With heater off, we measured ~300 ppm (-40C to 90C) and with heater and feedback on, a stability of +/-1 ppm over temperature. The phase noise was not degraded and is acceptable for BLE. Heater power varied linearly and inversely with ambient temperature (~14 mW at -40C to 0 mW at 90C). This circuit can be implemented in an FMOS type die (Gilbert et al. "Sub-10 fs Jitter S-Band Oscillators and VCOs in a 1X1X0.23 mm3 Chip Scale Package", IFCS 2013).

7A-3

11:15 am   Towards a CMOS Compatible Acoustic Delay Line Memory

Justin Kuo[1], Jason Hoople[1], Amit Lal[1]; [1]*School of Electrical and Computer Engineering, Cornell University, Ithaca, New York, USA*

Background, Motivation and Objective

In this paper, we present the concept and demonstrate the use of recirculating ultrasonic pulses as memory elements, stored in the thickness of the silicon wafer. This memory can be integrated directly with CMOS to provide a 3D ultrasonic memory (1A). Recently we demonstrated the use of thin film aluminum nitride (AlN) piezoelectric transducers on silicon for on-chip ultrasonic communication, phased arrays for reconfigurable communication, and ultrasonic TSVs for 3D chip stacking. In this paper, we use the ultrasonic pulses to store digital information. We show that thin film RF transducer frequencies in the GHz range and CMOS scaling of operating frequencies can be combined to form sonic bulk memory. We have opened a new opportunity for utilizing this type of memory directly on a chip with densities and power levels comparable to conventional memories, advancing the field of ultrasonic delay line memory. Our memory, when integrated with CMOS elements, can be used to accelerate the real time computation of images, which requires a large memory to store pixels in a serial stream, allowing for faster processing at lower power/area than traditional FPGAs to reduce one of the bottlenecks for real time computer vision.
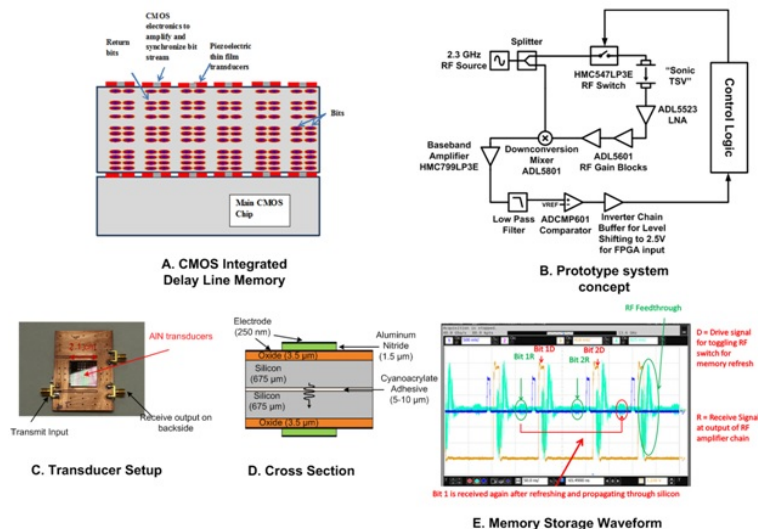
Statement of Contribution/Methods

The AlN transducers were fabricated on a double side polished silicon wafer with Sandia National Lab's RF MEMS process. The delay line memory cells were implemented by bonding two chips with an acoustically thin layer of cyanoacrylate adhesive, and using 100x100um AlN transducers as the transmit/receive elements (1C, D).

Results/Discussion

The memory bit feedback electronic system was implemented using off-the-shelve electronics(1B). At present, we are designing CMOS integrated versions of this memory, which would eliminate all off-chip components. The transmit pixel was driven with an RF pulse of 16 ns at 2.3 GHz. Receive signals prior to amplification were on the order of 1 mV in amplitude. The received signals were demodulated using a RF demodulator and a comparator to distinguish bits. The comparator output is processed in a FPGA, which then pulses the transmit transducer again, forming a recirculating loop. Using this setup, 2-bits of memory were successfully stored into the silicon channel (1D). The number of bits in this system was limited by electronic latency and bandwidth, and can be extended by CMOS integration in the future.

A. CMOS Integrated Delay Line Memory

B. Prototype system concept

C. Transducer Setup

D. Cross Section

E. Memory Storage Waveform

7A-4 _____

11:30 am   Chipscale GHz Ultrasonic Channels for Fingerprint Scanning

Jason Hoople[1], Justin Kuo[1], Mohamed Abdel-moneum[2], Amit Lal[1]; *[1]Electrical and Computer Engineering, Cornell University, USA, [2]Intel Corporation, USA*

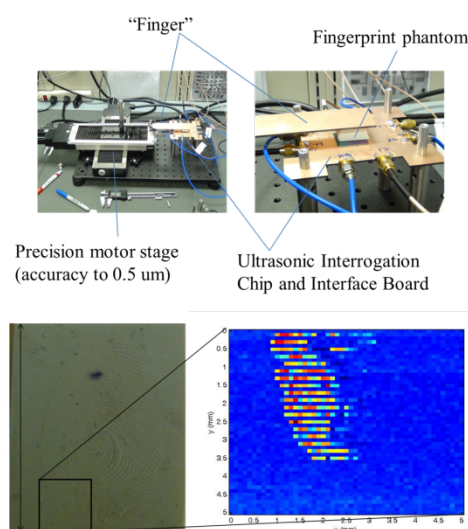**Background, Motivation and Objective**

In this paper we present high-frequency GHz ultrasonic interrogation of surface ultrasonic impedance for imaging fingerprints (Figure 1a). Previously we have investigated the use of high frequency (>1GHz) ultrasonic generation and detection within silicon chips. Ultrasound waves generated by the transducers in the top layers of the chip are confined within the silicon due to the large acoustic mismatch between silicon and air. If the ultrasonic impedance boundary condition changes, such as when human tissue is in direct touch with the silicon die, then part of the confined energy will leak and is transmitted into the tissues reducing the amount of acoustic energy reflected back. This method could be used to detect a fingerprint since the ridges of the finger would present an absorptive impedance and the valleys are full of air and resulting in lower ultrasonic absorption. Additionally, CMOS processing electronics could be integrated with the transducer and are not at risk of ESD since the active area is on the backside of the chip. With such a high frequency; small, power efficient transducers can be fabricated in very high density allowing for a much higher resolution, without the need for any large DC biases.

Statement of Contribution/Methods

The 1.5 micron thick aluminum nitride transducers were fabricated on a double side polished silicon wafer with Sandia National Lab's RF MEMS process. A pulse generator was used to generate RF pulses with Vpp of 4Vpp at 2.7 GHz, with 100 ns long pulses. In order to test the device repeatedly in a predictable repeatable setup, a rubber phantom of a fingerprint was formed. The fingerprint was scanned over an array of pixels to measure the response as a function of transducer position.

Results/Discussion

After scanning the fingerprint across the backside of the chip the amplitude of the received signal is measured. This is then plotted spatially against the known x-y position stage location. When air was the backing material signals on the order of 700 μV were measured, when the phantom ridge was under the transducer signals on the order of 300-400 μV were measured, easily distinguishing the two states. This results in the image of the fingerprint as seen in the abstract figure. The response due to different amount of pressure applied to the phantom also showed our ability to measure the pressure applied during fingerprinting.

"Finger"
Fingerprint phantom

Precision motor stage
(accuracy to 0.5 um)

Ultrasonic Interrogation
Chip and Interface Board

7A-5

11:45 am   Pt-Ni / Pt-Zr Electrodes for Stable SAW Resonator Operation During Repeated Temperature Cycling up to 1000°C

Mauricio Pereira da Cunha[1], Anin Maskay[1], Robert Lad[1], David Frankel[1], Scott Moulzolf[1], Michael Call[1], George Bernhardt[1]; [1]*Laboratory for Surface Science and Technology, University of Maine, Orono, ME, USA*

Background, Motivation and Objective

The appropriateness of wireless surface acoustic wave (SAW) technology has been verified recently in multiple high-temperature harsh-environments, such as turbine engines, power plant gas burners, municipal solid waste power plant water walls, and other industrial applications requiring stable device operation above 500°C. Many technological challenges arise in such environments, such as: (i) device ability to withstand shocks in temperature; (ii) packaging design and resilience to insure operational integrity during significant temperature excursions; (iii) SAW substrate stability and endurance for long-term operation; and (iv) identification of thin-film electrode materials for SAW interdigital transducers (IDTs) and reflectors capable of stable operation to 1000°C and above.

Statement of Contribution/Methods

This paper focuses on the implementation and characterization of a new type of Pt-alloy electrode used for SAW IDTs and reflectors. The thin film electrodes are comprised of a 140nm to 190nm thick Pt-Ni / Pt-Zr multi-layer conducting structure patterned on langasite substrates. This electrode configuration enables stable SAW device operation for over 300 hours of thermal cycling and soaking profiles up to 1000°C. The devices were also successfully operated for short terms (12 hours) up to 1100°C.

Results/Discussion

In addition to operation for long times at a fixed high-temperature, thermal cycling is key for verifying harsh environment SAW device stable operation. One-port SAW resonators tested in a box furnace were exposed to four temperature cycles between 300 and 1000ºC (soaking 1h at the minimum and maximum temperatures); 48h soaking at 1000°C; and four additional 300-1000°C thermal cycles, as measured by a K-type thermocouple (right-hand axis of the figure). The left-hand axis shows the peak frequency for one of the SAW resonators tested. To confirm stable operation, this heating profile was repeated three times for a total of 300h of testing. The real and imaginary parts of the device impedance response and their behavior with temperature and time will also be discussed in the paper and compared to other films previously fabricated by the University of Maine group. The results confirmed SAW device stability up to 1000°C for high-temperature harsh-environment sensor and frequency control applications.
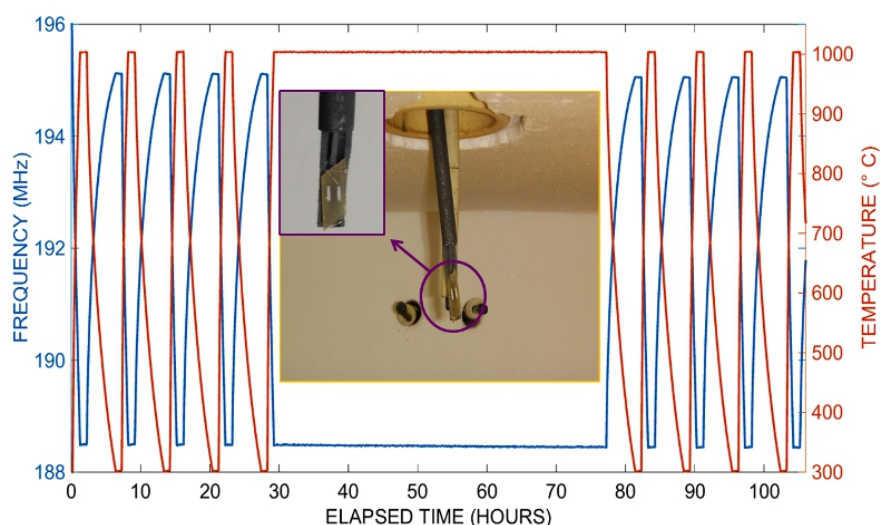
8A - Medical Applications of Transducers

102

Thursday, October 22, 2015, 10:30 am - 12:00 pm

Chair: **Mark Schafer**
             PhotoSonix Medical, Inc.

8A-1

10:30 am   *In-vivo* **navigation of neurosurgical biopsy needles using microultrasound transducers with M-mode imaging**

Rachael McPhillips[1], Yun Jiang[2], Zhen Qiu[1], Syed Osama Mahboob[1], Han Wang[1], Carl Meggs[2], Giuseppe Schiavone[3], Daniel Rodriguez-Sanmartin[4], Sam Eljamel[1], Marc P. Y. Desmulliez[3], Christine E.M. Démoré[1], Tim Button[2], Sandy Cochran[1]; [1]*University of Dundee, Dundee, United Kingdom,* [2]*University of Birmingham, Birmingham, United Kingdom,* [3]*Heriot Watt University, Edinburgh, United Kingdom,* [4]*Applied Functional Materials Ltd, Birmingham, United Kingdom*

Background, Motivation and Objective

The use of interventional tools in neurosurgery presently relies on stereotactic guidance allied to pre-operative MRI or CT imaging. A need for a real-time, portable imaging modality which provides safe navigation of tools such as needles to a region of interest is evident. Conventional ultrasound probes require a relatively large craniotomy to accommodate the necessary probe aperture to image deep within the tissue. Integrating a microultrasound (μUS) transducer at the tip of a needle, however, has the potential to overcome this problem as a minimally invasive, high resolution imaging tool allowing the surgeon to maneuver safely to a target in the brain. This paper presents single element composite transducers fabricated within brain needles and demonstrates the feasibility of using real-time M-mode imaging as a means of guiding these needles to a target within in-vivo brain tissue.

Statement of Contribution/Methods

Two imaging transducers were fabricated within needles of 1.8 mm inner diameter to provide forward and side viewing orientations respectively. Viscous polymer processing (VPP) based fabrication was used for the composite material utilized as the active material in the transducers, achieving pillars with a width of ~20 μm and kerf of ~8 μm. To determine the performance of these devices, miniature targets were inserted into fresh porcine brain and the brain of a soft-embalmed human cadaver, as shown in Fig.1. Using an experimental set-up which allowed the user to observe a real-time M-mode image, the forward facing and side facing needles were inserted and manipulated within the brain to locate the targets and explore the ease with which they could be identified when varying the distance from the tip of the needle.

Results/Discussion

MRI scans of the brains determined their condition before and after soft-embalmed human cadaver and fresh ex vivo porcine skulls were penetrated. μUS M-mode images were acquired, displaying how the depth of the target in the brain tissue varied as a function of time. These images demonstrated the capability of the imaging needle devices to detect the position of the targets. Combining the device with M-mode imaging was an effective measure of assessing the feasibility to navigate in brain tissue with μUS and has established a foundation for future work with ultrasound arrays in needle packages and the significant potential of such devices.
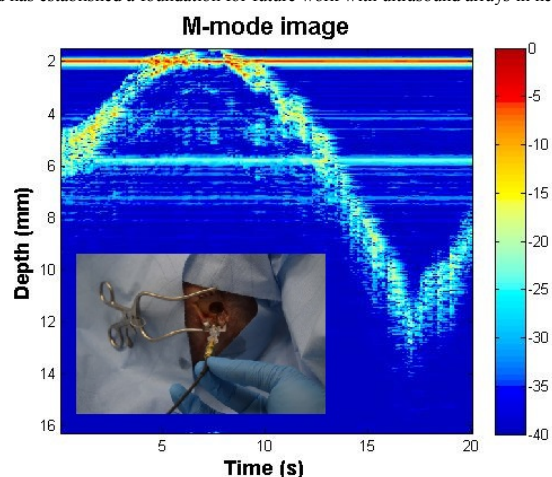

Figure 1: M-mode image of target position as the distance from the needle tip is varied. Inset shows the insertion of the needle into the skull.

8A-2

10:45 am   **3/15 MHz Dual-layer Co-Linear Array for Transrectal Acoustic Angiography**

Sibo Li[1], Jinwook Kim[1], Sandeep Kasoji[2], Paul Dayton[2], Xiaoning Jiang[1]; [1]*Mechanical and Aerospace Engineering, North Carolina State University, Raleigh, North Carolina, USA,* [2]*Joint Department of Biomedical Engineering, University of North Carolina and North Carolina State University, Chapel Hill, North Carolina, USA*

Background, Motivation and Objective

Prostate cancer is the second leading cause of cancer death of American men, and still lacks effective method in clinical evaluation. In recent years, with benefits of real time exam and non-invasive manner, transrectal ultrasound (TRUS) already plays a substantial role in diagnosis and management of prostate cancer. Gray-scale ultrasound is commonly used for biopsy guidance, although traditional ultrasound imaging has poor sensitivity and accuracy in detecting the disease itself. In comparison with conventional ultrasound, contrast-enhanced ultrasound (CEUS) provide high-resolution imaging of the microvasculature and estimation of blood perfusion in organs, tissues, and in tumors. Recent progress on contrast enhanced acoustic angiography suggested that microbubbles can be excited at 2 -4 MHz, and the nonlinear responses from microbubbles can be detected at frequency > 10 MHz, leading to high signal to noise, high-resolution contrast imaging, and providing exceptional sensitivity to unique tumor microvessel structural characteristics. In this paper, a 3 MHz/15 MHz ultrasound array was developed, for the first time, for transrectal acoustic angiography.

Statement of Contribution/Methods

The co-linear array (85-tx/170-rx elements) was designed and fabricated for 3 MHz transmit and 15 MHz receive. Two high dielectric constant PZT active layers were stacked with a low acoustic impedance isolation layer and a customized flexible circuit in between. The pitch of the transmission array and receiving array are 270 μm and 135 μm, respectively. The KLM model was used for backing and matching layer design, and the fractional bandwidth and sensitivity for individual element was obtained.

The Field II program was used for acoustic field simulation to obtain the beamforming and imaging resolution. Pulse-echo tests were conducted for elements of the low frequency transmission and high frequency receiving arrays. The transmitting array was also evaluated by measuring the acoustic pressure profile of single element and multi-elements using a hydrophone. The contrast test was performed by exciting micro-bubbles in a micro-tube using the 3 MHz transmitting array and detecting the super harmonic responses from microbubbles using the 15 MHz receiving array. Finally, comprehensive phantom imaging was performed with a Verasonics System.

Results/Discussion

The pulse-echo test results showed that at 1uJ input the pulse-echo amplitudes are 200 mV and 40 mV, and the -6 dB fractional bandwidth are 40 % and 34 %, respectively, for the 3 MHz transmitting and 15 MHz receiving elements. For low frequency transmission elements, the transmission peak negative pressure sensitivity reaches 40 kPa/Vpp with single burst excitation, which is sufficient to excite non-linear responses from microbubbles. The contrast tests and phantom imaging are being performed and the details will be reported in the full paper.

8A-3

11:00 am   Fabrication and Characterization of 15 MHz Concave Array Transducers for Ophthalmic Imaging

Jung Hyui Cha[1], Byungwoo Kang[2], Jihun Jang[2], Jin Ho Chang[1,2]; [1]*Interdisciplinary Program of Integrated Biotechnology, Sogang University, Seoul, Korea, Republic of,* [2]*Department of Electronic Engineering, Sogang University, Seoul, Korea, Republic of*

Background, Motivation and Objective

Ophthalmic imaging is one of the most popular applications in high frequency ultrasound imaging. The commercial ophthalmic imaging systems employ either single element or annular array transducers with mechanical scanning; they are not capable of providing high frame rate and color Doppler images. Although not only the linear but also the convex array transducers have been previously proposed to overcome those problems, high refraction and reflection from the anterior segment can degrade image quality. Thus, as a remedy, 15 MHz 128-element concave array transducers, fitting well to the inherent spherical shape of the eye, are fabricated and characterized for effective ophthalmic imaging in this paper.

Statement of Contribution/Methods

Major parameters for fabricating the concave array are 15 mm radius of curvature, 148 μm pitch and 7.5 mm elevation width. In order to image the retinal region of interest in the posterior segment, 30 mm geometric focus was decided. As an active layer, the 1-3 piezo-composite with a ceramic width of 56 μm and a kerf width of 18 μm was fabricated due to bidirectional, i.e., lateral and azimuth, curvature and its high coupling coefficient. One element was formed by two ceramic posts at the ceramic volume fraction of approximately 56%. Double matching layers and an epoxy backing were also used.

Results/Discussion

From a typical element of the finished array, the pulse-echo response had the center frequency of 15.95 MHz and the -6 dB fractional bandwidth of 67.8% with electrical tuning applied. The measured crosstalk level for the adjacent elements was less than -25 dB. Thus, the evaluation results demonstrated that the developed concave array transducer can be a possible alternative for high frequency ophthalmic imaging with desired capability.
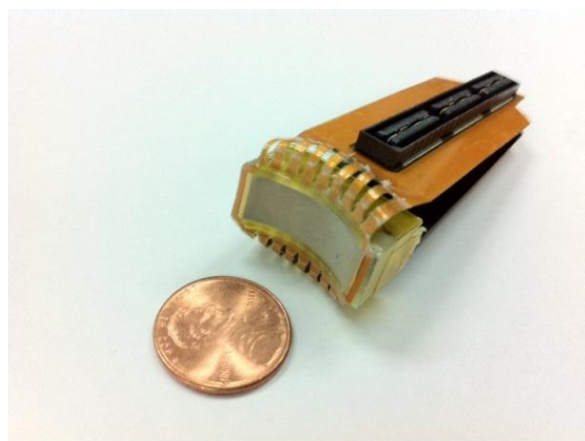

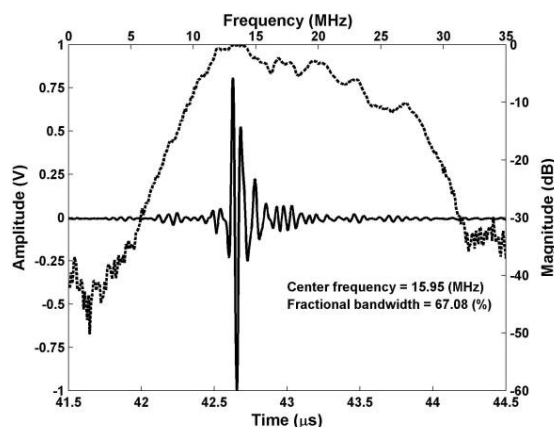Fig. 1. A photograph of the finished 15 MHz 1-3 piezo-composite concave array.

Fig. 2. Measured pulse-echo response of a typical element of the 15 MHz concave array: waveform in time domain and spectrum in frequency domain.

8A-4

11:15 am   Programmable delivery of macromolecules using high frequency ultrasound

Sangpil Yoon[1], Min Gon Kim[1], Yingxiao Wang[2], K. Kirk Shung[1]; [1]*Department of Biomedical Engineering, University of Southern California, Los Angeles, California, USA,* [2]*Department of Bioengineering & Institute of Engineering in Medicine, University of California, San Diego, USA*

Background, Motivation and Objective

An approach to deliver macromolecules into the cytoplasm of cells has been developed using highly focused high frequency ultrasound. Single-cell level targeting capability of the proposed technique was demonstrated by selectively delivering desired macromolecules only into targeted cells from a monolayer of cells. Human embryonic stem cells (hESCs) and induced pluripotent stem cells (iPSCs) are invaluable sources for regenerative medicine. Gene editing of hESC and iPSC-derivation from human somatic cells need stable and efficient delivery methods of macromolecules. Gentle massages of target cells using highly focused and high frequency ultrasound may induce transient holes on cell plasma membrane, which lead to the cytoplasmic introduction of macromolecules.

Statement of Contribution/Methods

3 kDa dextran labeled with Cascade Blue (B), Tetramethylrhodamine (Y), and Alexa 488 (G) were chosen as macromolecules to be delivered into cytoplasm of HeLa cells. An ultrasonic transducer with 215 MHz center frequency was integrated with epi-fluorescence microscope to induce intracellular delivery and to monitor treated cells as shown in Figs. 1(a) and (b). First, 3 kDa dextran labeled with three different fluorescence molecules (B, Y, and G) were delivered into three different individual cells, located adjacent with each other. Next, one cell was targeted to deliver three different kinds of 3 kDa dextrans labeled with B, Y, and G fluorescence. One pulse was applied to a target cell with a peak-to-peak voltage of 47 V and pulse durations of 5 μs and 7 μs. After the treatment, cells were incubated in cell growth medium for 30 minutes to ensure the recovery of cell membrane. By using epi-fluorescence microscope, Y, G, and B fluorescence, emitted from target cells, were captured.

Results/Discussion

Three different kinds of 3 kDa dextran labeled with B, Y, and G were successfully delivered into three different individual cells as shown in Fig. 1(c) and one cell as shown in Figs. 1(d). The proposed technique for the intracellular delivery of macromolecules can selectively delivery desired molecules into targeted individual cells.
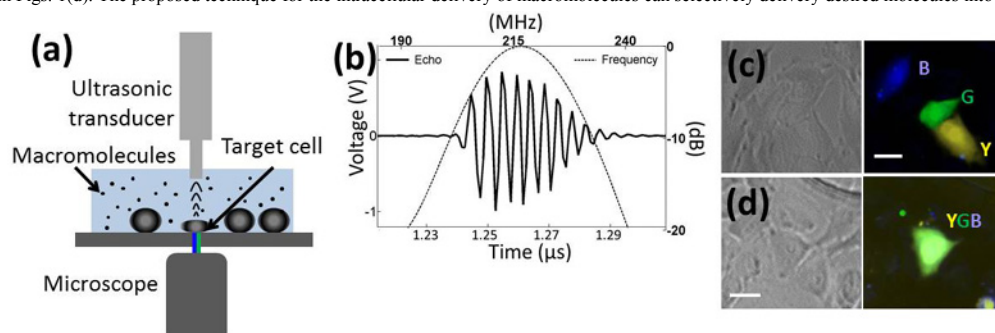

Fig. 1. (a) Schematic diagram of intracellular delivery system. Epi-fluorescence microscope and ultrasonic transducer control stage were integrated to treat and monitor cells. (b) Echo response of high frequency ultrasonic transducer and its spectrum. Center frequency was measured to be 215 MHz. Programmable delivery of macromolecules using high frequency ultrasound was demonstrated using 3 kDa dextran labeled with Cascade Blue (B), Tetramethylrhodamine (Y), and Alexa 488 (G) into (c) three different individual HeLa cells and (d) one HeLa cell. Scale bars indicate 20 μm.

8A-5

11:30 am   Wearable ultrasound applicators for wound healing and noninvasive drug delivery

Peter A. Lewin[1], Youhan Sunny[1], Christopher Bawiec[1], Leonid Zubkov[1], Michael Neidrauer[1], Michael S. Weingarten[1], David J. Margolis[2]; *[1]Drexel University, USA, [2]University of Pennsylvania, USA*

Background, Motivation and Objective

This talk examines the challenges associated with the design of clinically viable ultrasound applicators operating at the relatively low frequency (20 kHz) and intensity (<100 mW/cm2, spatial peak, temporal peak) levels, and tailored to treatment of chronic wounds, such as venous or diabetic ulcers. These challenges were associated with the transducer architecture and weight, and principle and efficiency of operation, including electrical power consumption. Over 500,000 patients are treated for venous ulcers alone annually at the cost exceeding $2,400 per month; this cost excludes the expenses due to limited productivity and quality of life issues related to pain and depression. Hence, there is a need to develop a non-invasive low-cost technology that would allow therapeutic treatment of chronic wounds and be able to reduce the current high cost of their management.

Statement of Contribution/Methods

This need was realized by designing a fully wearable Band-Aid™-like, customizable, dial-in delivery, battery-operated ultrasound applicator. The clinically proven device features light weight (<100g), is powered by 10-12V fully rechargeable lithium-ion batteries and can operate for up to 4 hours between re-charging. To emphasize the uniqueness of the design, it might be useful to note that typically, the thickness of the capacitive piezoelectric element is inversely proportional to the frequency, therefore a 20 kHz element would need to be 10 cm thick. Such element would be bulky and require hundreds of volts (demanding a large power amplifier), in excitation signal thus eliminating any chance of being a portable design. To overcome this, a mechanical displacement amplifier, which translates 2 MHz ultrasound waves into 20 kHz output at the desired pressure amplitude (55 kPa; i.e. 100 mW/cm2), with only 12 volts excitation was chosen as a preferred solution.

Results/Discussion

The applicator was successfully validated in clinical environment; the results of the small pilot clinical study showed a net reduction in venous ulcer wound size after just four weeks. In contrast, patients who didn't receive ultrasound treatment had an average increase in wound size during the same time period. The group receiving 15 minutes of 20 kHz ultrasound showed the greatest improvement, with all five patients experiencing complete healing by the 4th treatment.

In another, pre-clinical study obtained using animal model the feasibility of using this applicator design for non-invasive transdermal drug delivery was verified. More specifically, the study outcome indicated that ultrasound is capable of reducing inflammation in a mouse model of rheumatoid arthritis. The combination of ultrasound exposure with topical application of inflammation mediating gel, exhibited statistically significant ($p < 0.05$) enhanced anti-inflammatory properties in comparison with the delivery of the drug or ultrasound treatment alone. Support: NIH R01EB009670 and NSF 1064802.

1B - MPA: Photoacoustic Systems

Plenary Hall

Thursday, October 22, 2015, 01:00 pm - 02:30 pm

Chair: **Stas Emelianov**
Univ. of Texas at Austin

1B-1

1:00 pm   Optimization of the laser irradiation pattern in a high frame rate integrated photoacoustic / ultrasound (PAUS) imaging system

Soon Joon Yoon[1], Bao-Yu Hsieh[1], Chen-wei Wei[1], Thu-Mai Nguyen[1], Bastien Arnal[1], Ivan Pelivanov[1,2], Matthew O'Donnell[1]; *[1]Department of Bioengineering, University of Washington, Seattle, Washington, USA, [2]International Laser Center, Moscow State University, Russian Federation*

Background, Motivation and Objective

To integrate real-time photoacoustics (PA) into ultrasound (US) scanners and accelerate clinical translation of combined PAUS imaging, we have showed that a high frame rate can be achieved with a portable, low-cost, low pulse energy (a few mJ), high-repetition rate laser (~1kHz) and rapid scanning of a narrow (~ a few mm in diameter) laser beam over the imaging area, keeping the same image quality achieved with a conventional wide beam approach [IEEE Transactions on UFFC 62(2), 391-328, 2015]. As a proof of concept, we used a 1D galvo-mirror to perform beam scanning but observed that it must be replaced by a fiber-optic light delivery system (see Fig.1) for clinical translation. This work is aimed at optimizing the laser irradiation pattern which the fiber-optic system should provide, including both 1D (laterally, Fig.1a) and 2D (with elevation added, Fig1b) patterns to provide the most efficient light penetration into tissue and the highest possible imaging frame rate under permissible exposure limits.

Statement of Contribution/Methods

3D Monte-Carlo simulation is used to optimize the light penetration into tissue. To confirm potential optimal patterns, an experimental system using a 2D galvo-mirror scanner with variable beam shape is employed. A nanosecond diode-pumped laser (TECH-1053 Specific, Laser-Export Co. Ltd., Moscow, Russia, 1053 nm wavelength) with a 2.3 mJ pulse at a 960 Hz pulse repetition rate is used as the light source. An US linear array transducer (AT8L12-5 50 mm, Broadsound Corp., Taiwan) interfaced with an US scanner (Verasonics, Redmond, WA) is used for interleaved PAUS imaging. Finally, a simple model of needle guidance and drug delivery is used to test overall system performance.

Results/Discussion

PA and US images were collected within exposure limits for both pulse fluence and average radiance. Fig.1c shows a typical integrated PAUS image from a PVA phantom with a needle inserted. In the PA image, the needle is clearly visualized from the background. This result is obtained at (but not limited by) a 60 Hz frame rate for both interleaved US and PA modalities and thereby shows great potential for clinical translation.
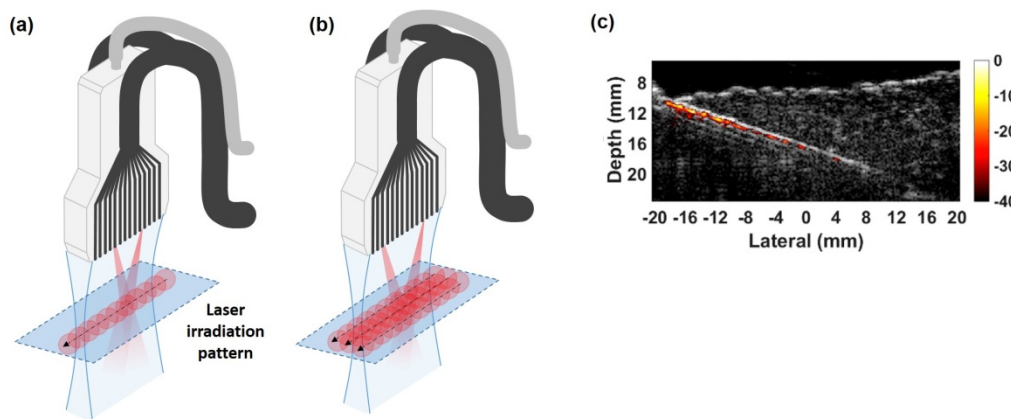

Fig. 1. Schematic diagram for an integrated PAUS imaging system using (a) 1D and (b) 2D laser scanning. (c) Combined PAUS images of a needle in a PVA phantom. Field of view is 40 x 20 mm^2 (lateral x depth).

1B-2

1:15 pm   Optimizing a Single-Sided Reflection Mode Photoacoustic Setup for Clinical Imaging

Martin F Beckmann[1], Hans-Martin Schwab[1], Georg Schmitz[1]; *[1]Chair for Medical Engineering, Ruhr-Universität Bochum, Bochum, Germany*

Background, Motivation and Objective

Reflection mode setups are photoacoustic setups where light source and transducer are placed on the same side of the imaged object. They are more suitable for clinical applications than transmission mode setups or tomographic setups, but they are also more subject to problems such as clutter. In some systems, it is not possible to apply light on both sides of the transducer, e.g. due to price or size considerations. The goal of this contribution is to optimize a reflection mode setup using single sided illumination and demonstrate the results experimentally for a handheld combined diode laser photoacoustic probe (FULLPHASE system) described by Daoudi et al. [1].

Statement of Contribution/Methods

3D Monte Carlo light simulations were employed to calculate the absorbed radiant energy density within the imaging area. The simulations were repeated at several illumination angles. In addition, the sensitivity of a 7.5 MHz linear array transducer in the illuminated volume was determined by 3D acoustic simulations. Both simulations were combined to assess the expected spatial sensitivity of the complete photoacoustic system. Additionally, the simulations were validated in an experiment using the FULLPHASE system inside a scattering medium.

Results/Discussion

The experiments (left fig.) show good agreement with the simulations (center fig.). Both show a strong displacement between ultrasound- and photoacoustic imaging regions. In the experiments, an up to 5 dB lower sensitivity was found on the acoustical axis than at locations in the same axial distance from the transducer but closer to the light source, shifting the most sensitive region by over 1 mm elevationally.

The shift is strongly reduced, when an acoustic standoff is placed between transducer and skin. Additionally, this moves the imaging region closer to the elevational focus of the transducer (right fig.). If an acoustic standoff causes the light to be centered beneath the transducer, the asymmetry becomes negligible. Thus, we suggest moving the transducer away from the skin and illuminate close to the acoustic detection. Additionally, the simulations suggest steep angles of incidence; however the influence of the location of incidence is far greater.

[1] K. Daoudi et al.: "Handheld probe integrating laser diode and ultrasound transducer array for ultrasound/photoacoustic dual modality imaging", Opt. Expr. 22, 2014
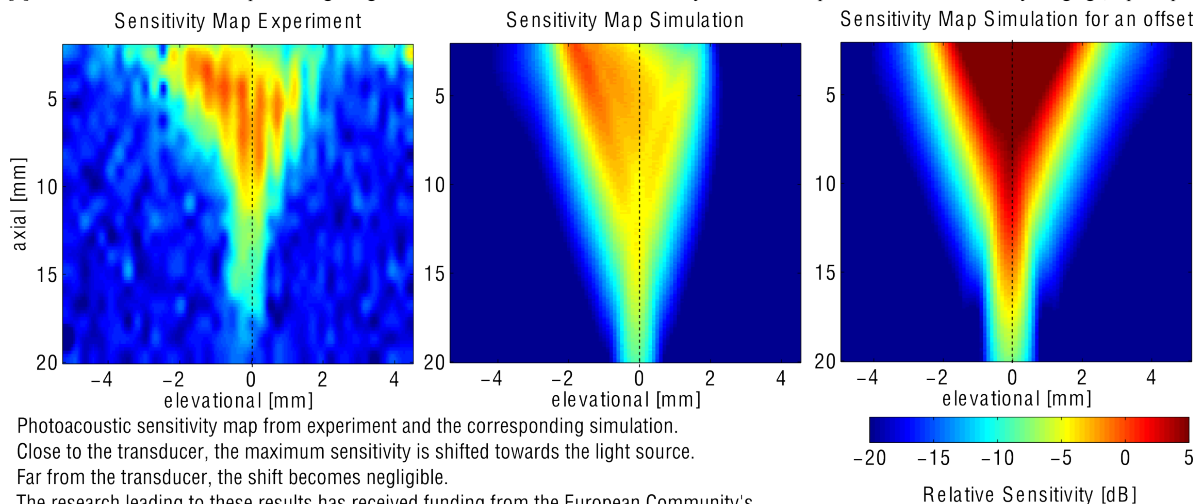
Photoacoustic sensitivity map from experiment and the corresponding simulation.
Close to the transducer, the maximum sensitivity is shifted towards the light source.
Far from the transducer, the shift becomes negligible.
The research leading to these results has received funding from the European Community's Seventh Framework Programme (FP7/2007-2013) under grant agreement no 318067.

1B-3

1:30 pm   Handheld Photoacoustic Imaging with Integrated Diode Lasers

Georg Schmitz[1], Hans-Martin Schwab[1], Martin Beckmann[1]; *[1]Chair for Medical Engineering, Ruhr-Universität Bochum, Bochum, Germany*

Background, Motivation and Objective

Photoacoustic imaging has demonstrated great potential for clinical imaging in the past and several commercial preclinical photoacoustic or hybrid photoacoustic/ultrasound scanners are already available. For clinical scanning, dedicated tomographic scanners and reflection mode scanners similar to current ultrasound systems are under development. The advantage of hybrid ultrasound and photoacoustic scanners is their capability of morphological, functional and contrast agent imaging. For widespread acceptance and application the systems should be suitable for point-of-care use, be robust and have low purchasing and maintenance cost.

Statement of Contribution/Methods

For this reason, this paper's focus is on a hybrid photoacoustic ultrasound system with a handheld combined laser/ultrasound probe and specifically addressing the corresponding signal processing algorithms that aim at optimal use of the maximal permitted laser exposure. The handheld probe used is developed in the European project FULLPHASE and is equipped with high power laser diodes. Pulse energies of the laser diodes are currently at 0.56 mJ and aim for 1 mJ per pulse with a pulse repetition rate up to 10 kHz. The system aims at multispectral imaging with a fixed set of wavelengths. Because of the lower pulse energies compared to solid state lasers the high pulse repetition rate of the laser diodes can be exploited by transmitting coded light sequences, also with several wavelengths excited simultaneously. Additionally, clutter originating mostly from strong photoacoustic signals from the skin surface have to be reduced by signal processing. Acoustic plane-wave pulse echo measurements can be used to identify these unwanted signals using appropriate reconstruction methods and reduce them.

Results/Discussion

First preclinical images demonstrate the feasibility of clinical photoacoustic scanning with the handheld scanner and show the limitations in penetration depth imposed by the laser safety rules clinical systems have to comply with. Coding strategies and clutter reduction techniques allow to improve the images quality and the achievable SNR significantly and are the key to clinical application of photoacoustic imaging.

Research was funded by the European Community's Seventh Framework Programme (FP7/2007-2013) under grant agreement n° 318067

1B-4

2:00 pm   In vitro and in vivo dynamic blood volume assessment using photoacoustics

H.M. Heres[1], M.Ü. Arabul[1], F.N. Van de Vosse[1], M.C.M. Rutten[1], R.G.P. Lopata[1]; *[1]Biomedical Engineering, Cardiovascular Biomechanics Group, Eindhoven University of Technology, Netherlands*
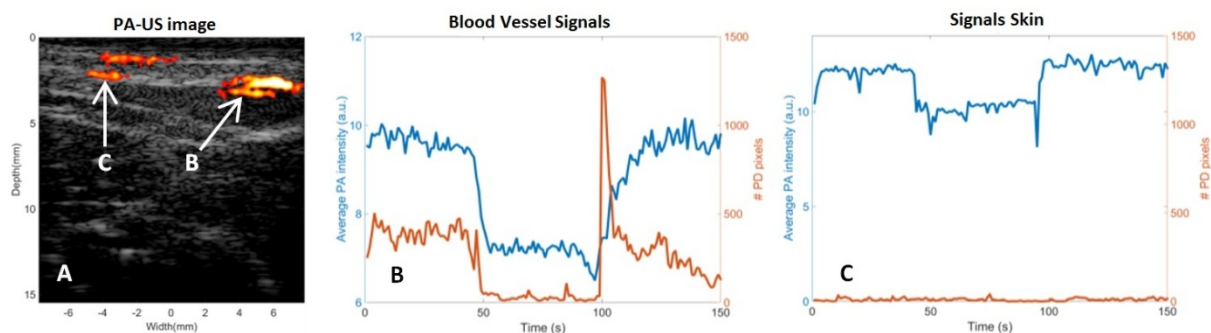
Background, Motivation and Objective

Skin perfusion is a possible marker for skin diseases such as scleroderma and dermatomyositis. Photoacoustic (PA) imaging is a promising tool for the assessment of skin perfusion due to its high sensitivity to blood. Recently, a handheld PA probe was presented (FULLPHASE), which incorporates a diode laser ($\lambda = 805$ nm, 1.0 mJ/pulse) and ultrasound probe. In this study, the detection of blood volume changes using PA imaging was examined in vitro and demonstrated in vivo and compared to Power Doppler (PD).

Statement of Contribution/Methods

Perfusion phantoms were developed using cylindrical moulds (length = 50 mm, Ø = 15 mm) filled with gelatin. Needles (Ø = 180 μm) were inserted in the gelatin to create perfusion channels after removal. By changing the number of channels, the partial blood volume (PBV) of the phantoms was varied in the physiological range (0.8 to 3.4%). The optical and acoustic absorption and the scattering coefficients of the gelatin were matched to those of skin. The phantoms were perfused with blood mimicking fluid. For in vivo measurements, the perfusion response to occlusion of the forearm was measured in 5 healthy volunteers. During a measurement of 150 s, the arterial blood flow was occluded for 45 s using a pressure cuff (p = 160 mmHg). In both experiments, cross-sectional images were obtained during the measurement using PA with a frame rate (FR) of 30 Hz and PD (PRF = 250 Hz (in vitro)/ 1.3 kHz (in vivo), FR = 20 Hz). The average PA intensity and number of PD pixels were calculated in the perfused area of the phantoms, and in specific regions of the forearm identified as skin and vessel, respectively.

Results/Discussion

Phantom measurements revealed a linear signal increase in both PA and PD with PBV. PD signals saturated at a PBV of 2.5% due to resolution limitations. Good SNR from skin and vessels was obtained in vivo in the PA images. The signal intensities in these regions typically showed a decrease after occlusion and normalization after release of the cuff (Fig 1). For PD, signal variations were only measured in the arteries, while no signal was obtained in the skin. In this study, PA detection of dynamic blood volume changes in skin was demonstrated using a handheld probe. Compared to PD, PA shows an advantage in sensitivity and spatial resolution. Future studies include combined PA imaging and motion tracking, since tissue movement affected the signal analysis in vivo.

1B-5

2:15 pm   Photoacoustic microscopy using four-wave mixing in a multimode fiber

Margaret Ferrari[1], Jessica Farland[1], **Takashi Buma[1]**; [1]*Union College, USA*

Background, Motivation and Objective

Many applications in photoacoustic microscopy (PAM) use contrast agents that preferentially absorb light at wavelengths other than 532 nm. This usually requires the use of expensive dye or optical parametric oscillator (OPO) lasers. We have previously demonstrated a cost-effective alternative using an inexpensive 532 nm laser and a photonic crystal fiber, where multiple wavelengths are produced by stimulated Raman scattering.

**Statement of Contribution/Methods**

In this paper, we demonstrate a new source using four-wave mixing (FWM) in a conventional step-index multimode fiber. FWM between multiple spatial modes of the fiber produces a broad spectral continuum.

Our Q-switched Nd:YAG laser produces 2 ns duration pulses at 532 nm with 21 uJ of energy at a 10 kHz repetition rate. The laser pulses are coupled into a 100 meters of a step-index fiber that is designed to be single-mode at 1060 nm. At 532 nm, the fiber supports only a few spatial modes. The fiber output goes through a dielectric filter, where the selected spectral window is sent to a PAM system employing optical focusing and laser scanning.

Results/Discussion

The attached figure shows the optical spectrum from the multimode fiber source. Significant FWM occurs in the fiber, as shown by the narrowly spaced spectral lines near 532 nm as well as the broad continuum that extends to 900 nm. Although the input laser most likely excites the fundamental (LP01) spatial mode, the fiber output has a "doughnut" shape characteristic of the next higher spatial mode (LP11). This suggests that wavelength generation is primarily achieved by phased matched FWM between the LP01 and LP11 fiber modes. Dielectric filters were used to select either a 750-900 nm (0.5 uJ pulse energy) or 532-700 nm (0.4 uJ pulse energy) spectral window. PAM imaging of a USAF target produced an image resolution of 13 um in both spectral windows. Imaging experiments are performed on two silicone tubes, one filled with diluted red ink and the other with 200 uM of IR-820 dye. Both images are shown over a 2.1 x 2.6 mm field of view and 10 dB scale. The IR-820 tube is clearly visible at long wavelengths and is faint at short wavelengths. The red ink tube produces negligible signal at long wavelengths.

The advantages of this multi-wavelength optical source are the very simple apparatus, the flexibility in choosing the desired spectral range, and the use of a very inexpensive optical fiber.
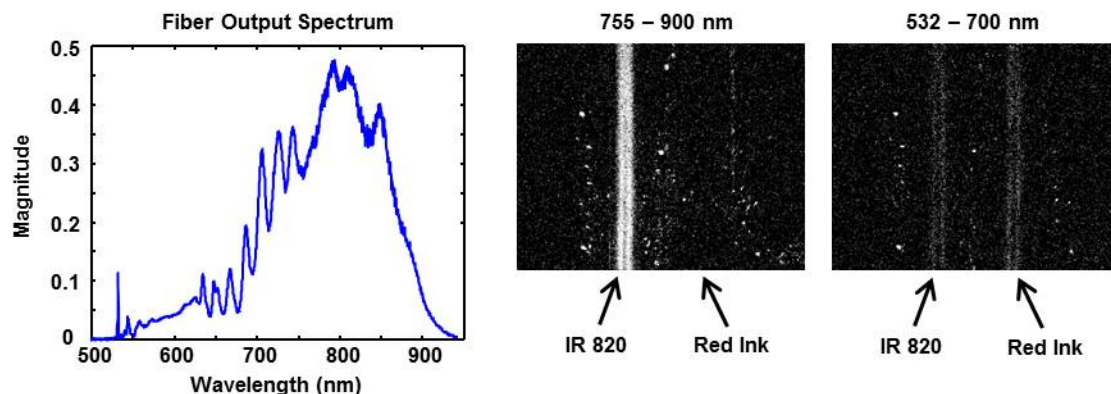
2B - MEL: New Shear Wave Imaging Techniques

VIP

Thursday, October 22, 2015, 01:00 pm - 02:30 pm

Chair: **Mickael Tanter**
INSERM

2B-1

1:00 pm **Shear wave elastography with fast single-push multi-angle compounding**

Heechul Yoon[1], Salavat Aglyamov[1], R. Andrew Fowler[1], Stanislav Emelianov[1]; [1]*Biomedical Engineering, The University of Texas at Austin, Austin, Texas, USA*

Background, Motivation and Objective

Mechanical properties of tissue can be assessed by many techniques, such as supersonic shear imaging (SSI), acoustic radiation force impulse (ARFI), and, more recently, comb-push ultrasound shear elastography (CUSE). However, elasticity contrast is overestimated when the push beam is applied over the inclusion. Therefore, these approaches require either a-priori knowledge of the target location, or multiple pushes to exclude on-target interrogation, reducing frame rate of imaging. In addition, part of the energy of push beam(s) is lost due to the generation of grating lobes (Fig. 1). Here we introduce a single-push multi-angle shear wave elasticity imaging (SWEI) technique to overcome the current limitations of dynamic elasticity imaging techniques.

Statement of Contribution/Methods

Our single-push multi-angle SWEI method uses the mainlobe and grating lobes to produce pushing beams with variable magnitude (Fig. 1). Shear wave speed (SWS) maps reconstructed from these push beams cover an entire FOV in a single acquisition. This approach does not require prior knowledge of the target size and location – the maps of SWS can be uncoupled using directional filtering, avoiding contribution of on-target pushing and overestimation of elasticity contrast. Furthermore, this method uses the acoustic energy of grating lobes as pushing beams, and produces high-quality elasticity images with angular compounding.

Push beams controlled by phase of the transmit wave on each element were analyzed numerically (Field II) and confirmed by hydrophone measurements of the pressure field (L11-4v transducer, 4.5 MHz, 600 µs pushing pulse). Ultrafast imaging studies (Verasonics Vantage 128 system, 5.2 MHz) of CIRS breast phantom with hard inclusion ($\mu/\mu0=3.0$) were performed with 12.5 kHz frame rate. Ultrasound IQ data were captured and then processed off-line.

Results/Discussion

Magnitudes of main and grating lobes were adjusted by varying transmit phase (Fig. 1). A comparison of shear elasticity maps (contrast, SNR and CNR) between our and other techniques was performed (Fig. 2). Single-push multi-angle SWEI approach provides comparable elasticity maps ($\mu/\mu0=2.96\pm0.05$) at higher frame rate and does not require any prior assumptions. Our approach allows user selection of angular spacing, magnitude and number of pushing beams optimized for specific clinical applications.
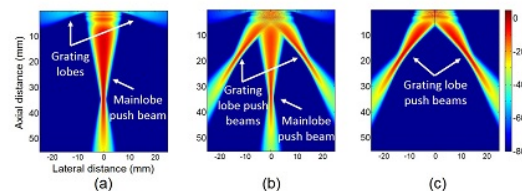

Fig. 1. Field II simulation of acoustic pressure fields in medium with 0.3 dB/cm/MHz attenuation coefficient. (a) Conventional ultrasound: mainlobe produces single push beam, grating lobes are negligible, (b) Transmit phase was adjusted to produce equal magnitude of main and grating lobes acting as multi-angle push beams, and (c) Transmit phase was used to cancel the mainlobe such that, only grating lobes act as push beams.
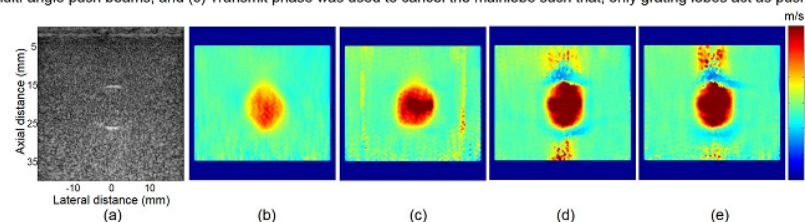

Fig. 2. (a) B-Scan of the CIRS breast phantom with a single hard inclusion. Shear wave speed maps obtained using (b) single push multi-angle SWEI, (c) CUSE, (d) ARFI, and (e) SSI. Note that with on-target push, CUSE, ARFI, and SSI overestimate the elasticity contrast.

2B-2

1:15 pm **Magnetic Resonance-guided transient shear wave imaging using constructive multi-pulse transmission**

Yu Liu[1], Brett Fite[1], Josquin Foiret[1], Erik Dumont[2], Katherine Ferrara[1]; [1]*Biomedical Engineering, UC Davis, Davis, California, USA*, [2]*Image Guided Therapy, Pessac, France*

Background, Motivation and Objective

The goal of this study is to use constructive multi-pulse transmission to improve visualization of transient shear wave propagation by Magnetic Resonance (MR) imaging. MRI provides a three-dimensional view of the surrounding anatomy during interventions and therefore the development of MRI-based interventional strategies is desirable for multiple clinical applications. Our ultimate goal is to detect changes in tissue properties following ablation.

Statement of Contribution/Methods

A 3 MHz 16-element annular array transducer (Imasonic SAS, France, 300 kHz bandwidth, 120 W peak acoustic power, 48 mm diameter, 35 mm radius of curvature, adjustable focal depth, $0.5 \times 0.5 \times 2$ mm^3 focal volume at -6 dB), controlled by an embedded MR-compatible 2-dimensional positioning and ultrasound system (Image Guided Therapy, France), was integrated within a 7T MR scanner (Biospec 70/30 USR, Bruker Biospin, Germany). Three pulses (3 MHz, 450 ms pulses with 4.5 mm spacing between transmit foci, 29 watts acoustic power, 10 MPa PNP) were sequentially excited along the beam axis creating planar shear waves in an 8% gelatin phantom which were imaged with MRI (Fig. 1A, TR/TE/FA = 500ms/22ms/180°). For shear wave velocity estimation, a delay t was programmed into the MR shear imaging sequence after the ultrasound excitation and before the motion encoding gradient. The shear wave velocity was validated using ultrafast ultrasound imaging with a Vantage 256 (Verasonics, WA, USA) and a Phillips L7-4 probe. To generate the shear wave, the central 96 elements of the array were used to transmit 4.3 MHz, 100 µs pulses with 4.3 mm spacing between transmit foci with 10 MPa PNP. Ultrasound images were obtained with 5.2 MHz center frequency, using 30 acquisitions of 50 frames in flash imaging mode with a PRF of 5000 Hz.

Results/Discussion

The shear wave velocity in an 8 % gelatin phantom was estimated as 1.80 m/s using the multi-pulse transmission and MR imaging sequence, which agreed with the estimate of 1.78 m/s obtained using an MR-ARFI sequence and 1.70 m/s obtained using ultrasound shear wave measurements. The propagating shear waves were readily visualized with both MRI and ultrasound (Fig. 1). In conclusion, visualization of transient shear wave propagation is achieved using the combination of an MR shear imaging sequence and multi-pulse transmission. Ongoing work is aimed at the detection of ablation foci.
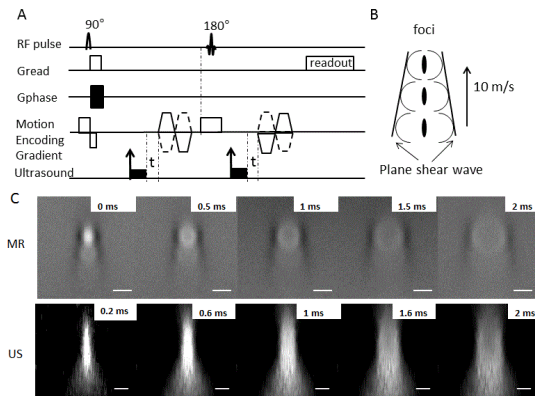
Figure1. (A) Magnetic Resonance shear imaging sequence used to image the transient shear wave propagation. The delay time t, varied from 0 to 2 ms with a 0.5 ms increment, was added between the ultrasound excitation and Motion Encoding Gradient. (B) Three ultrasound pulses were sequentially transmitted along the beam axis and plane shear waves were formed. (C) Comparison of the results of shear wave propagation with both MR (first row) and ultrasound (second row) imaging guidance. Scale bar: 5 mm.

2B-3

1:30 pm   Moving beam shear wave reconstruction for both ultrasound and optical coherence tomography applications

Bao-Yu Hsieh[1], Shaozhen Song[1], Thu-Mai Nguyen[1], Soon Joon Yoon[1], Tueng Shen[2], Ruikang Wang[1,2], Matthew O'Donnell[1]; *[1]Department of Bioengineering, University of Washington, Seattle, Washington, USA, [2]Department of Ophthalmology, University of Washington, Seattle, Washington, USA*

Background, Motivation and Objective

Phase-sensitive speckle tracking can image shear wave propagation using both ultrasound (US) and optical coherence tomography (OCT) systems. Shear wave imaging (SWI) is used for quantitative elastography. In image regions where there is no speckle, for example within the crystalline lens for OCT studies and in cyst and cyst-like structures within the breast for US studies, elastic properties cannot be directly reconstructed from tracked displacements. The purpose of this study is to develop a method to reconstruct the elastic properties in speckle-less regions using a moving acoustic radiation force (mARF) source and a limited set of detection positions within speckle-generating areas near that region. Our immediate motivation is to obtain the elastic properties of the crystalline lens to help guide minimally invasive treatment of presbyopia.

Statement of Contribution/Methods

A linear US array interfaced with a programmable US system launched shear waves by synthesizing a mARF source. Push beams were electronically controlled and sequentially stepped laterally. The generation system was synchronized with the appropriate imaging system depending on the application, where the same array was used for US detection and a phase-sensitive OCT (PhS-OCT) system operating at a 125 kHz A-line rate was used for optical detection. For either system, local displacements are calculated and stacked sequentially based on the distance between shear source and detection beams. The local shear wave speed was then reconstructed by a time-of-flight algorithm. To initially verify the performance of this approach, we performed experiments on tissue-equivalent phantoms and a porcine crystalline lens.

Results/Discussion

Typical mARF data acquisition is shown in Figure 1 (b), where M-mode snapshots of shear wave propagation in a phantom detected by PhS-OCT are illustrated when the source is 3.0, 4.2, and 5.4 mm away from OCT detection. The ability to reconstruct shear wave speed in a heterogeneous US phantom (Figure 1 (c)) is illustrated in Figures 1(d) and (e), where the shear speed reconstructed using a conventional approach (continuous tracking – (d)) is contrasted to the moving beam approach (single detection spot – (e)). These preliminary results suggest that mARF reconstruction may be an effective way to assess the elastic properties in speckle-less regions of both US and OCT images.
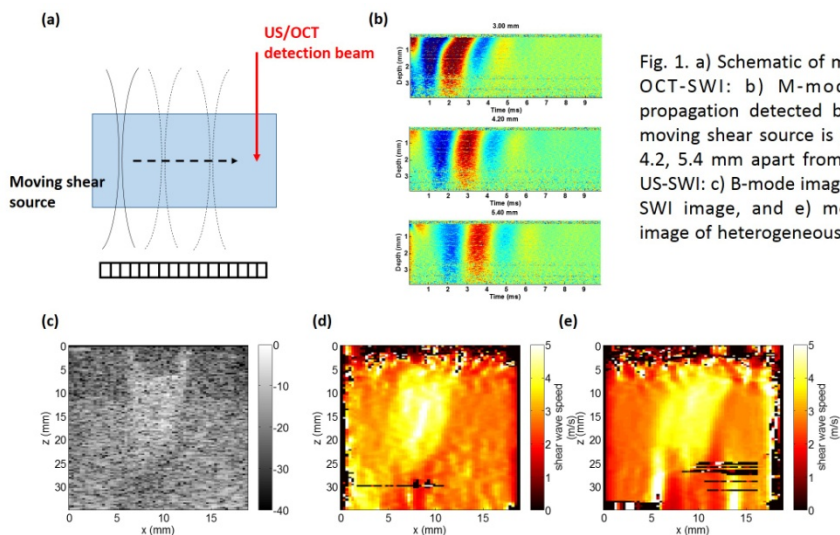
Fig. 1. a) Schematic of moving beam SWI; OCT-SWI: b) M-mode shear wave propagation detected by PhS-OCT when moving shear source is positioned at 3.0, 4.2, 5.4 mm apart from detection beam. US-SWI: c) B-mode image, d) conventional SWI image, and e) moving beam SWI image of heterogeneous gelatin phantom.

2B-4

1:45 pm   Eliminating Speckle Noise with Three-dimensional Single-Track-Location Shear Wave Elasticity Imaging (STL-SWEI)

Peter Hollender[1], Samantha Lipman[1], Gregg Trahey[1,2]; *[1]Biomedical Engineering, Duke University, Durham, North Carolina, USA, [2]Radiology, Duke University Medical Center, Durham, North Carolina, USA*

Background, Motivation and Objective

Conventional multiple track location shear wave elasticity imaging (MTL-SWEI) is a powerful tool for noninvasively estimating tissue elasticity. The resolution and noise of MTL-SWEI systems, however, are limited by speckle noise. Single track location SWEI (STL-SWEI) is a novel variant which fixes the position of the tracking beam and modulates the push location to cancel out the effects of speckle bias. We present a 3D STL-SWEI system which provides full suppression of lateral and elevation speckle bias for high resolution elasticity imaging.

Statement of Contribution/Methods

We mounted a HIFU piston with a hole in the center to a translation stage. We positioned a matrix array ultrasound transducer to point through the hole into the target, aimed within the scanning grid (but not necessarily aligned). The scanner, HIFU piston, and stage were synchronized by a laptop. The HIFU piston generated a 1.1 MHz push, and the matrix array was used to track the resulting displacements over a three-dimensional field of view through the center of the piston. The HIFU piston was then translated in 0.25 mm steps between each acquisition over a 12 mm by 12 mm lateral-elevation grid, repeating the measurement at each position. For each voxel in the tracking field of view, a c-scan of the arrival times was formed, with lateral and elevation positions defined by the push indices. The radial component of the spatial (push location) gradient of the arrival times, relative to the track position computed in each scan, was then used to make velocity estimates. The steered parallel beams provided overlapping estimates of shear wave velocity.

Results/Discussion

The 3D STL-SWEI system builds volumes of shear wave velocity estimates with less noise than the equivalent MTL-SWEI images, owing to the elimination of the speckle bias. By adaptively detecting the effectively track beam location, the effects of elevation speckle bias are also eliminated – a feature not available in 2D STL-SWEI. The tracking transducer to perform 3D STL-SWEI does not need to be 3D itself because the tracking positions are treated as unknown, but using a matrix array allows for comparison of performance to MTL-SWEI. STL-SWEI will require electronically-steerable pushes to achieve clinically relevant framerates in 3D, but makes much higher resolution images than MTL-SWEI.

2B-5
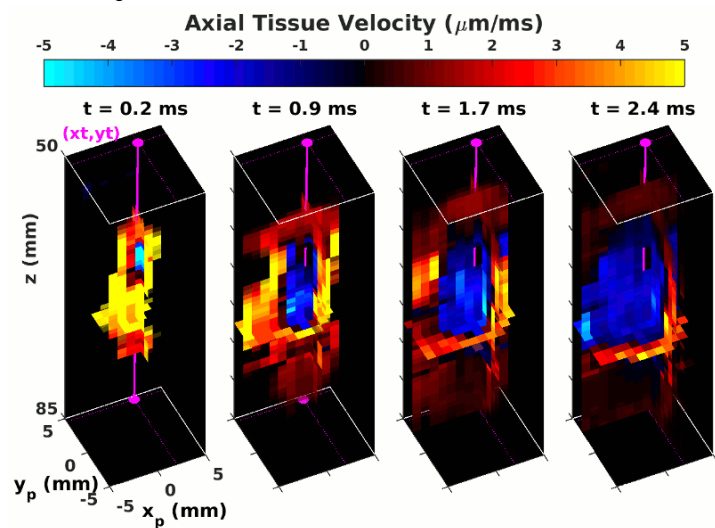
2:00 pm   Implementation of Shear Wave Elastography on Pediatric Cardiac Transducers with Pulse-inversion Harmonic Imaging and Time-aligned Sequential Tracking

Pengfei Song[1], Xiaojun Bi[2,3], Daniel C. Mellema[1], Armando Manduca[1], Matthew W. Urban[1], Shigao Chen[1], James F. Greenleaf[1]; *[1]Department of Physiology and Biomedical Engineering, Mayo Clinic College of Medicine, Rochester, Minnesota, USA, [2]Department of Cardiovascular Diseases, Mayo Clinic College of Medicine, Rochester, Minnesota, USA, [3]Department of Medical Ultrasound, Tongji Hospital Medical College, Wuhan, Hubei, China, People's Republic of*

Background, Motivation and Objective

Monitoring myocardial stiffness changes with shear wave elastography (SWE) has significant potential for assessing chemo-induced cardiotoxicity for pediatric cancer patients. While B-scan with adult cardiac probes on children is commonly acceptable, SWE can be challenging due to the narrow intercostal spaces of children, which hinders the effective transmission of the push beam for shear wave generation. This study aimed at addressing this challenge by implementing cardiac SWE on a pediatric cardiac probe with pulse-inversion harmonic imaging (PIHI) and time-aligned sequential tracking (TAST).

Statement of Contribution/Methods

A pediatric cardiac phased array P7-4 (Philips Healthcare) and a Verasonics Vantage system were used in this study. For PIHI detection, the P7-4 transmits at 3 MHz (f_t) and receives at 6 MHz (f_r). For TAST, the P7-4 sequentially transmits 3 plane waves steered at different angles to form 3 detection zones. Shear wave signals from each zone were then aligned and combined following the method proposed in Song, IEEE UFFC 62(2), 2015. For comparison, a fundamental imaging (f_c = 5 MHz) TAST detection on the P7-4 and a PIHI-TAST detection (f_t = 2 MHz, f_r = 4 MHz) on an adult probe P4-2 were also used in this study. The three detection methods were tested on a healthy child (age = 5) to measure end-diastolic myocardial stiffness.

Results/Discussion

Figure 1 shows the example ECG-gated B-mode images and shear wave signals in end-diastole on the same subject. While the adult P4-2 B-scan quality is acceptable, no robust shear wave signals could be detected. One possible reason is the severe blockage of the push beam by the narrow intercostal space. The P7-4 fundamental-TAST could not detect any shear wave signals due to severe noise contamination of the myocardium by the blood clutter, as indicated by the B-mode image. The P7-4 PIHI-TAST could detect robust shear wave signals from the same subject thanks to the smaller footprint which provides better access through the narrow rib gap, and the harmonic detection signals which reject the clutter noise effectively. The success rate of shear wave detection was almost 0% for P4-2 and P7-4 fundamental, and close to 100% for P7-4 PIHI-TAST. The high quality shear wave signals from P7-4 PIHI-TAST are promising for robust assessment of myocardial stiffness and monitoring chemo-induced cardiotoxicity for cancer children.
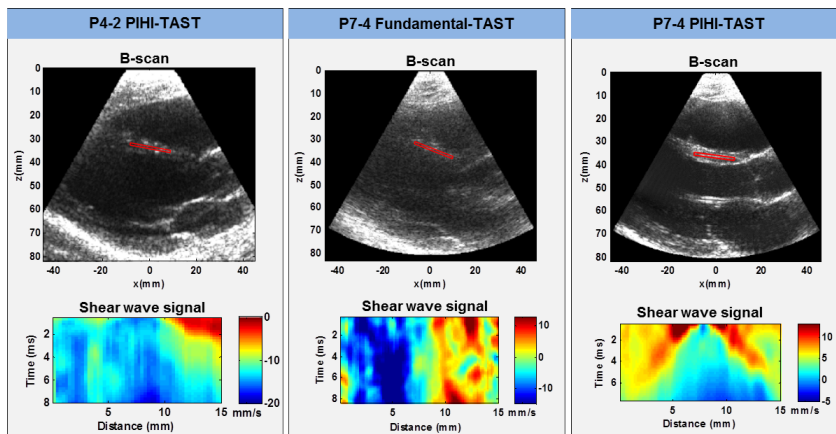
Figure 1. Shear wave motion detection comparisons among the adult cardiac probe P4-2 with PIHI-TAST shear wave detection (left column), the pediatric cardiac probe P7-4 with fundamental-TAST shear wave detection (middle column), and the P7-4 with PIHI-TAST shear wave detection (right column). The upper row shows the synchronized B-mode images (acquired ~80 ms before shear wave sequence) in end-diastole. The red boxes indicate the regions of myocardium where shear wave signals (lower row) were extracted.

2B-6

2:15 pm   Storage and Loss moduli imaging in soft solids using Supersonic Shear Imaging technique

Eliana Budelli[1,2], Javier Brum[3], Miguel Bernal[1], Thomas Deffieux[1], Mickael Tanter[1], Patricia Lema[2], carlos negreira[3], jean-luc Gennisson[1]; *[1]Institut Langevin, Paris, France, [2]Instituto de Ingeniería Química, Uruguay, [3]Laboratorio de Acústica Ultrasonora, Uruguay*

Background, Motivation and Objective

Non invasive evaluation of rheological behavior of soft tissues may provide an important diagnosis tool. Nowadays, available commercial ultrasound systems only provide shear elasticity estimation by shear wave speed assessment under hypothesis of a purely elastic model. However, to fully characterize the rheological behavior of tissues, through storage (G') and loss (G") moduli, it is necessary to estimate also shear wave attenuation. Shear waves generated in the Supersonic Shear Imaging (SSI) technique is not plane. Consequently, a diffraction correction is needed to estimate the shear wave attenuation. The use of a cylindrical wave approximation to take into account diffraction was already proposed [1, 2]. Here such approximation is revisited experimentally and through numerical simulation to validate and to calculate maps of G' and G" for an isotropic and homogeneous viscoelastic medium.

Statement of Contribution/Methods

A Green's function algorithm (anisotropic and viscoelastic) [3] was carried out to establish the validity of the cylindrical approximation. This approximation is valid in the center of the pushing line and at distance x equivalent to k*x >1, being k the shear wave number. Experiments were conducted in an agar-gelatin phantom. Shear waves were generated in two different ways: using a vibrating plate generating plane shear wave (Transient elastography technique TE) at different frequencies (100-600 Hz) or using the SSI technique, both with an 8MHz probe (SL 15-4, Supersonic Imagine (SI)). The shear wave propagation was followed with an ultrafast ultrasound scanner (Aixplorer, SI). For both techniques, the shear wave velocity (V) and attenuation (α) at a single frequency were recovered from the phase and amplitude decay versus distance respectively. αSSI was calculated by applying the diffraction correction. VTE and αTE were used as references.

Results/Discussion

αSSI was calculated for each frequency (100-500 Hz). As an example, at 300Hz <αSSI> = 44±6 Np/m was in good agreement with αTE = 46±2 Np/m. Fig.1 shows maps of G' and G'' (b) calculated from VSSI and αSSI maps at 300 Hz (a) [4]. Then maps of G' and G" were calculated for each frequency in the shear wave bandwidth. Using any chosen rheological model, elasticity and viscosity maps of the medium can be deduced. The application of this technique is currently under investigation in vivo in human liver.
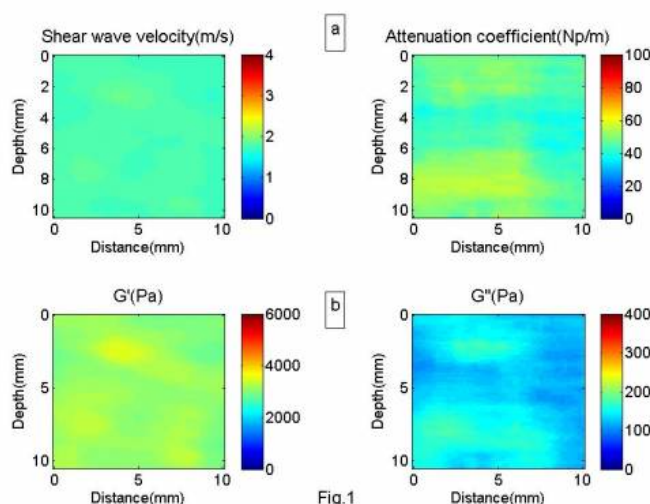

Fig.1

Ref: [1] Deffieux, IEEE TMI 2009 [2] Nenadic, IEEE IUS 2014 [3] Chatelin PMB 2015 [4] Gennisson, UMB 2006

3B - MTH: Treatment Monitoring

201BC

Thursday, October 22, 2015, 01:00 pm - 02:30 pm

Chair: **Ayache Bouakaz**
           Inserm

3B-1

1:00 pm   10 MHz Catheter-based Annular Array for Thermal Strain Guided Intramural Cardiac Ablations

Douglas Stephens[1], Josquin Foiret[1], Steven Lucero[1], Katherine W. Ferrara[1], Kalyanam Shivkumar[2], Pierre Khuri-Yakub[3]; *[1]Biomedical Engineering, University of California, Davis, California, USA, [2]University of California, Los Angeles, USA, [3]Stanford University, USA*

Background, Motivation and Objective

A yearly global population of well over 100,000 ventricular tachycardia patients could benefit from guided cardiac ablation of otherwise untreatable intramural arrhythmogenic substrates. A guided catheter-based HIFU device used epicardially with a subxiphoid approach is proposed which is placed with electroanatomical mapping. After the HIFU device is positioned, the thermal strain feedback at low intensities can confirm myocardial contact and establish a projected power titration guideline for full HIFU ablation. This PZT based spherical array design is an early demonstration prototype of a fully steerable CMUT array design in development at Stanford.

Statement of Contribution/Methods

The multifunctional catheter is designed to direct an axially steerable 10 MHz HIFU beam into the myocardium without damaging the epicardium itself and the vitally important coronary vessels. The spherical array is 7 mm in diameter with a radius of curvature of 7 mm; it is housed in a custom 3D printed tip housing (see figure) which is 10 mm in total diameter and 4 mm in profile and joined to a 7 Fr (2.3 mm) catheter shaft. The prototype array is water cooled and has a built-in thermistor to monitor transducer temperature. The ablation axial steering addresses the 4 to 10 mm depth range, while 10 MHz can produce a high focus gain to produce a 23 C rise in temperature with bursts of 200 msec durations. A unique feature of this work is the use of the Verasonics Vantage 256 system as both the HIFU power source and thermal strain echo data receiver; a custom 32 channel power combiner/splitter (4 annuli x 8:1) interface was built to permit this development.

Results/Discussion

Two 10 MHz 7 mm prototype spherical devices have been built and tested. Both are made from PZT-5A with no backing material and only a 100 micron EPOTEK-301 epoxy front matching/insulation layer. The first device is a 9.6 MHz single element spherical HIFU transducer which was driven with an ENI amplifier and produced heating intensities sufficient to visibly ablate (0.5 mm ablation diameter by 1.5 mm length, or 0.3 mm^3) beef tissue in a room temperature bath in less than 0.5 sec. The second device is a 10.4 MHz spherical four element annular array which has been used to collect thermal strain echo data from a laboratory phantom. Continued development is underway to demonstrate both heating and thermal strain data from *in-vivo* animal experiments.
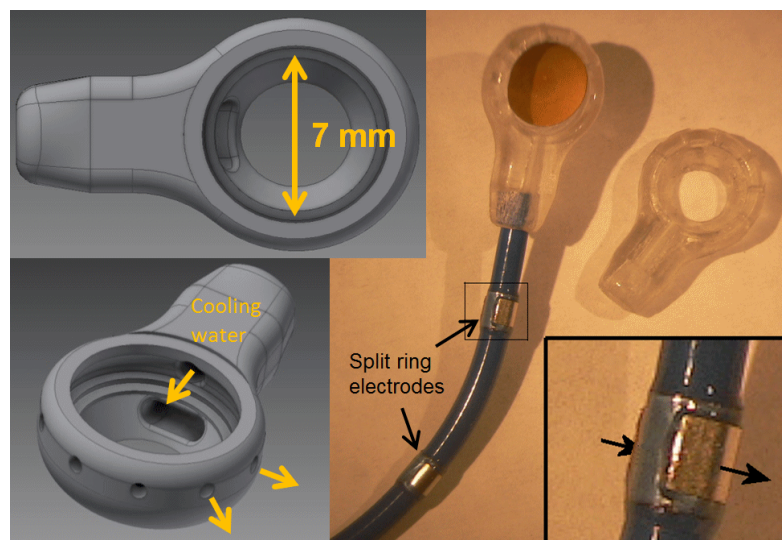
3B-2

1:15 pm   Real-Time Feedback System for High-Intensity Focused Ultrasound Treatment Using Decorrelation Maps of RF Echoes with Plane - Wave Transmission

Ryo Takagi[1], Hayato Jinbo[2], Ryosuke Iwasaki[1], Shin Yoshizawa[2], Shin-ichiro Umemura[1]; *[1]Biomedical Engineering, Tohoku University, Japan, [2]Communications Engineering, Tohoku University, Japan*

Background, Motivation and Objective

In our previous study, motion-compensated detection of tissue coagulation using correlation between RF frames was suggested in the monitoring of high-intensity focused ultrasound (HIFU) treatment. The real time capability of this method to detect coagulation was demonstrated for exposure with single focus. However, it has not been demonstrated for sequential exposure with multiple foci, which is more practical but requires more robust feedback because the tissue can be overheated. In this study, such feedback at a high frame rate was developed to detect tissue coagulation while preventing overheating.

Statement of Contribution/Methods

The correlation coefficient maps between RF frames during HIFU exposure were used for the treatment feedback system. Figure.1 (a) shows the timing chart of this system. The ROI around the HIFU focus in the correlation coefficient map and the threshold of the decorrelation within the ROI were set to determine the completion of the treatment. A stage to place an excised block of tissue (chicken fillet) was controlled by a PC to scan the HIFU focus mechanically. When the correlation coefficient,

calculated at a rate of 5 Hz during HIFU exposure at 3.38 MHz, was below the preset threshold, the exposure was discontinued and the stage was mechanically moved for the next location of the focus. This sequence of exposure automatically performed HIFU treatment with multiple foci.

Results/Discussion

Figure.1 (b) shows the relationship between the positions of HIFU foci and the exposure time to complete the treatment at each focus. It also shows a slice of the tissue sample after the series of HIFU exposure. The focal positons are numbered with the order of exposure. As shown in Fig.1 (b), the exposure time was the longest at the first HIFU focus because the initial exposure cannot utilize the residual heat from the previous exposure. The exposure time was further decreased in the second row due to the residual heat. As shown Fig.1, the tissue was coagulated homogeneously as the result of setting the appropriate threshold. A frame rate (5 Hz), more than an order of magnitude higher than the inverse of exposure time needed for coagulation, seemed to be important for monitoring and feedback to prevent overheating the tissue. The result implies that the proposed monitoring system is useful for the real-time monitoring of HIFU treatment.
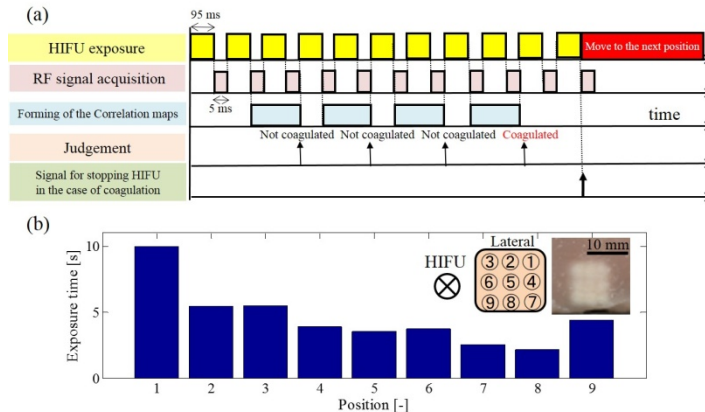
Fig.1 (a) The timing chart of this real-time feedback system. (b) The relationship between the positions of HIFU foci and the exposure time to complete the treatment at each focus and the slice of the tissue sample in lateral direction after the series of HIFU exposure

3B-3

1:30 pm   **Visualization of 3D temperature distribution caused by exposure of HIFU with thermo-chromic liquid crystal phantom**

Toshihide Iwahashi[1], Kazuhiro Matsui[1], Tang Tianhan[1], Keisuke Fujiwara[2], Kazunori Itani[2], Takashi Azuma[1], Kiyoshi Yoshinaka[3], Akira Sasaki[1], Shu Takagi[1], Yoichiro Matsumoto[1], Ichiro Sakuma[1]; [1]*The University of Tokyo, Japan*, [2]*Hitachi-Aloka Medical, Japan*, [3]*National Institute of Advanced Industrial Science and Technology, Japan*

Background, Motivation and Objective

HIFU (High Intensity Focused Ultrasound) is one of a promising minimally invasive treatment method. It is expected that energy concentration causes heat coagulation around focal area, while dispersion does not give a damage outside focus area. To establish temperature contorol technique, it is importnt to investigate three dimensional temperature around the target. For this purpose we developed a temperature distribution meaurement visualization method. In clinical practice, visualization of temperature distribution produced by clinical therapeutic ultrasonic devices is useful for ensuring clinical efficacy and patient safety. In this study, 3D temperature measurement phantom with MTLC (micro-capsuled thermo-chromic liquid crystal) was propsed, and its performance was demonstrated.

Statement of Contribution/Methods

MTLC is micro capsule whose diameter is 30 micro meters and its specific gravity is 1000 kg/m3. Its reflectance spectrum depends on temperature. Reflected light changes from the red to purple as temperature goes up. When a transparent material with which MTLC was mixed is illuminated with a light sheet, the temperature distribution of the illuminated section can be visualized. 3D temperature distribution can be acquired with scanning with a light sheet. Transparent urethane phantom which contain three kinds of MTLC (15-25 degrees, 25-35 degrees, 35-45 degrees) was used. Room temperature was 21 degrees. A light sheet whose thickness was 4mm was reflected by a galvanometer mirror whose frequency was 1Hz and its position was scanned. Illuminated sections were captured by a CCD camera (30fps).

Results/Discussion

Illuminated section showed two kinds of MTLC colored. MTLC (35-45 degrees) colored in an elliptical form around focal area and MTLC (25-35 degrees) colored around the entrance surface. A cross section image given by 3D reconstruction showed MTLC (25-35 degrees) colored in a toroidal form around the entrance surface. Elastic discontinuity at the entrance surface may cause a local heating through viscous dissipation. In the presentation, the reason of observed surface heating will be discussed.

3B-4
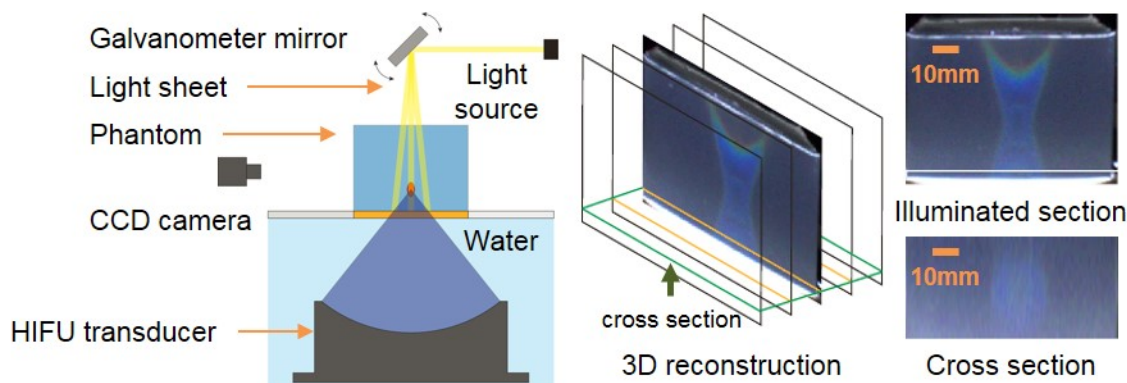
1:45 pm   Monitoring of Radiofrequency Ablation with Shear Wave Delay Mapping

William Shi[1], Ajay Anand[1], Shriram Sethuraman[1], Sheng-Wen Huang[1], Hua Xie[1], Gary Ng[2]; *[1]Philips Research North America, Briarcliff Manor, NY, USA, [2]Philips Ultrasound, Bothell, WA, USA*

Background, Motivation and Objective

Real-time monitoring of radiofrequency ablation (RFA) is essential to ensure adequate treatment coverage of liver tumors. As a widely used guidance tool, ultrasound imaging is a natural option for ablation monitoring. During RFA procedures tissue stiffness is elevated due to thermal necrosis. The high stiffness contrast between treated and non-treated tissue has led to the use of ultrasound elastography for coagulation zone visualization. A highly sensitive shear wave delay mapping approach has been developed for better lesion boundary detection than the conventional shear modulus based elastography, especially, in the presence of a rigid ablation needle. The purpose of this study is to investigate the feasibility of the new technique for monitoring RFA-induced thermal lesion formation.

Statement of Contribution/Methods

A proof-of-concept experimental setting for shear wave delay mapping was developed on a commercial ultrasound system iU22 with a curvilinear transducer C5-1 (Philips Healthcare). Shear waves were generated with 2.5 MHz pushing pulses while their propagation was detected with 3.5 MHz imaging pulses. Beamformed imaging data were streamed to an external computer for offline processing. Ablation-induced changes in shear wave delays were displayed as surrogate measures of stiffness maps. Such stiffness maps were updated every 20 seconds, which was sufficiently fast for tracking ablation boundary expansion over 10 to 25 minutes. Furthermore, in-vivo breathing artifacts were minimized with a motion gating algorithm. A total of 6 thermal lesions were generated ex-vivo on bovine or porcine livers and 4 thermal lesions produced in-vivo on porcine livers (around 45 mm in depth) by a commercial RFA electrode (Angiodynamics). After each experiment, the liver was cut open at the imaging plane to confirm the pathological changes caused by RFA.

Results/Discussion

The progression of thermal lesions during RFA was observed (more clearly in-vivo than ex-vivo) on shear wave delay maps. Tissue softening was seen ex-vivo for non-perfused livers, but not observed in-vivo for live livers with 'cooling' blood perfusion. In-vivo lesion sizes (measured laterally on stiffness maps), both at the end of ablation and 10 minutes after ablation, were 9.6±1.4 mm (83%±13% of respective pathological sizes of 11.6±1.8 mm), while ex-vivo lesion sizes at the end of ablation (with the temperature still elevated) and 10 minutes after ablation (after cool down) were 10.8±1.0 mm (68%±10%) and 13.0±1.0 mm (82%±12% of respective pathological sizes of 16.2±2.4 mm), respectively. Overall, the shear wave delay mapping technique appears feasible for monitoring the progression of thermal lesion boundary. Additional investigations will be required to establish the relationship between the shear wave delay mapping, clinical stages of tumor cell destruction, and ablative safety margin.

3B-5

2:00 pm   Advances in thermal strain imaging: 3D motion and tumor validation studies

Josquin Foiret[1], Katherine W. Ferrara[1]; *[1]Department of Biomedical Engineering, University of California, Davis, USA*

Background, Motivation and Objective

Targeted drug delivery therapies involving temperature sensitive vehicles and localized mild hyperthermia are emerging as an efficient way to non-invasively treat cancer [1]. To this end, control of hyperthermia is essential to efficiently release drug while avoiding thermal damage to healthy tissue. In previous work, thermal strain imaging (TSI) with motion compensation was validated on a tissue-mimicking phantom for 2D motion and used to control hyperthermia using a proportional-integral-derivative (PID) loop [2]. In this work, real time TSI with motion compensation is validated for 3D translational motion in a tissue mimicking phantom. The ultimate goal is to use TSI to non-invasively control hyperthermia *in vivo* and preliminary results obtained on a tumor bearing mouse are presented.

Statement of Contribution/Methods

A 5 MHz single element transducer (IL0508HP, Valpey-Fischer, MA) was used to generate a mild temperature increase (+4°C) in a calibrated agarose-based phantom. Ultrasound data were acquired with a Vantage ultrasound research system (Verasonics, USA) with a 5 MHz array (L7-4, Philips ATL, USA). The imaging array was mounted on a 3D linear stage and positioned at 90° from the heating transducer. TSI was processed in real time at 4 Hz using 2D speckle tracking routines as previously described [2]. A 3D translational motion reaching a maximum velocity of 8.7 mm/s with a periodicity of 4 s was simulated. Preliminary data were also collected on a tumor bearing mouse (studies were approved by the UC Davis Institutional Animal Use and Care Committee) using a 10 MHz compact array (CL15-7, Philips ATL, USA).

Results/Discussion

On the phantom, the algorithm tracked temperature changes in the presence of 3-D motion while showing oscillations related to the out-of plane displacement of the imaging array (Fig. 1). A good agreement was found between the maximum and minimum values of the oscillations compared to the absolute temperature at the extrema of the motion. The noise introduced by the 3D motion was estimated to be 0.15°C. *Ex vivo* and *in vivo* application of the technique on tumor bearing mice is underway (Fig. 2). A colinear therapeutic/imaging array designed for pre-clinical drug delivery studies is currently under construction.

[1] Kheirolomoom et al., J. Cont. Rel., 172, 2013.
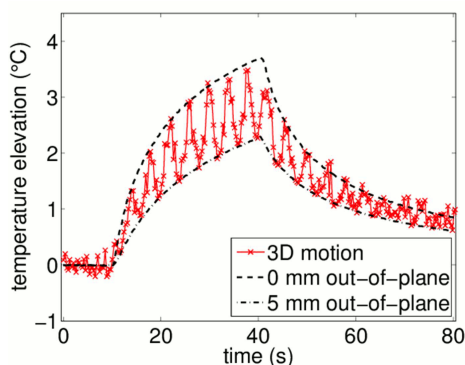
[2] Foiret et al., IEEE IUS, 2014.

Figure 1. Estimated temperature elevation in a tissue-mimicking phantom with a periodic 3D translational motion of the imaging array. Oscillations account for the out-of-plane motion of the array with respect to the fixed heated region.
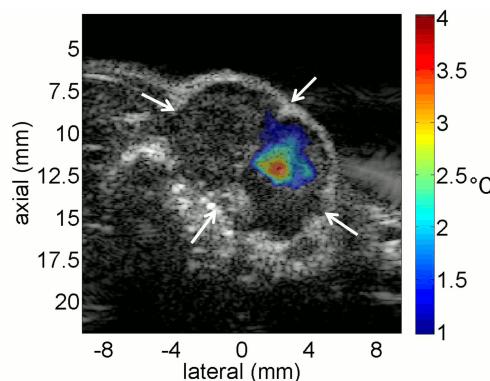
Figure 2. Temperature map superimposed on B-mode image of a mouse tumor after 20 s of mild heating at a fixed location with 0.5x0.5x2 mm beam within a larger tumor (arrows indicate the tumor position).

3B-6

2:15 pm   Monitoring of Lesions Induced by Cavitation-Enhanced High-Intensity Focused Ultrasound Using Shear Wave Elastography

Ryosuke Iwasaki[1], Ryo Takagi[1], Ryo Nagaoka[1], Hayato Jimbo[2], Shin Yoshizawa[2], Yoshifumi Saijo[1], Shin-ichiro Umemura[1]; *[1]Biomedical Engineering, Tohoku University, Sendai, Japan, [2]Communications Engineering, Tohoku University, Sendai, Japan*

Background, Motivation and Objective

Acoustic cavitation bubbles accelerate the High-Intensity Focused Ultrasound (HIFU) treatment through enhancing the heating effect of ultrasound, but they may also damage the tissue mechanically. The thermal coagulation of tissue in HIFU treatment has been reported to be quantitatively detected by Shear Wave Elastography (SWE). However, the mechanical change of the tissue may make the detection difficult if cavitation is involved. In this study, the feasibility of SWE to detect the coagulation induced by HIFU enhanced by cavitation.

Statement of Contribution/Methods

Ultrasound was generated by a 256-element array therapeutic transducer. The target samples were excised chicken breasts placed in a water tank. The intensity of high-intensity short pulses for cavitation inception and lower-intensity longer bursts for tissue heating were set to 64 and 2.2 kW/cm^2, respectively, at a driving frequency of 1 MHz. The focal spots were scanned at each corner of a regular hexagon 3 mm each side. The sequence was repeated for about 22 s at a repetition frequency of 7.3 Hz. After HIFU exposure, ultrasonic beams focused at 5 different depths from 23 to 39 mm were insonated to create shear sources. Then, RF echo frames was acquired after plane wave pulse transmission at a PRF of 5 kHz. The axial displacements were calculated from the phase shift between adjacent frames. The shear wave velocity at each point was estimated via a time-of-flight algorithm applying the least-square method.

Results/Discussion

Figure (a) maps the shear wave velocity in a chicken breast tissue before HIFU exposure. The actual coagulated area was approximately 10 mm in diameter and centered at a depth of 28 mm and +11 mm from the axis. Figure (b) maps the shear wave velocity after tissue coagulation, where the dotted circle encloses the coagulated region. Figure (c) shows the subtraction B-mode image between before and after HIFU, where high brightness represents remaining bubbles. The result suggests that it is possible to detect coagulated regions using SWE even in the presence of microbubbles induced by cavitation-enhanced HIFU heating.
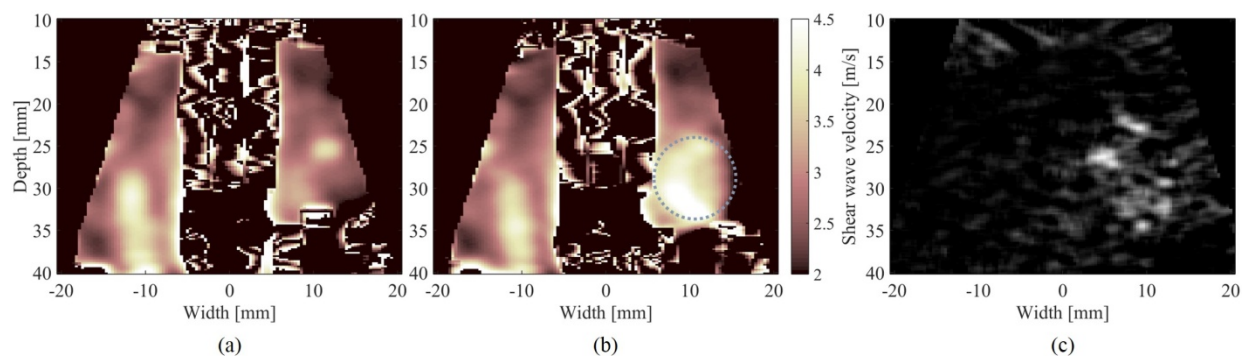
4B - MIM: Advances in Vascular Imaging

201DE

Thursday, October 22, 2015, 01:00 pm - 02:30 pm

Chair: **Ton van der Steen**
          Erasmus Medical Centre

4B-1

1:00 pm   Coherent RF-data processing to enhance the Intima-Lumen interface

Alfonso Rodriguez-Molares[1], Lasse Lovstakken[1], Julio Martin-Herrero[2], Tore Gruner Bjastad[3], Hans Torp[1]; [1]*Circulation and Medical Imaging, Norwegian University of Science and Technology, Trondheim, Norway,* [2]*Signal Theory and Communications, University of Vigo, Vigo, Spain,* [3]*GE Vingmed Ultrasound, Horten, Norway*

Background, Motivation and Objective

Many computer applications have been proposed to segment the carotid artery wall in ultrasound images and produce automated measurement of the intima-media thickness (IMT), one of the most widely used risk indicator of cardiovascular disease. Automatic IMT measurement is a challenging problem due to high levels of reverberation noise, and negative contrast ratio between the signal reflected at the intima-lumen (IL) interface and the reflection at the adventia-media (AM) interface.

Statement of Contribution/Methods

The IL interface can be recognized in subsequent RF-lines as a sequence of slightly delayed pulses. Providing that those delays can be estimated, it is possible to coherently add scanlines to produce a coherent profile of the vessel wall. The IL pulse in the coherent profile should present a higher SNR and contrast ratio respect to the reflection at the AM boundary, which often overshadows the reflection at the IL and hinders its detection.

The aforementioned delays are estimated here semi-automatically. A seed is inserted at one point of the image in the vicinity on the IL boundary. By analysis of the short-lag peaks in the crosscorrelation of adjacent scanlines the most probable path for the IL interface is determined. Restrictions to the searching area are imposed based on the transmitted pulse characteristics and local regularization of the IL interface. Once that the delays are estimated, coherent profiles of the vessel walls are produced by delay and sum. Coherent profiles can be used to detect the IL interface or to enhance its visualization in B-mode images.

Results/Discussion

The main thesis of this approach has been tested with in vivo images of healthy volunteers acquired with a GE-Vingmed scanner and 9L probe. The leftmost Figure shows a B-mode image of the carotid artery of one of the volunteers. There the near and far wall profile regions, obtained from the semiautomatic delay estimation algorithm, are shown enclosed by a green line. The mean processing time of the delay estimation algorithm is 16 ms/frame, without multithreading.

Coherent and incoherent profiles are are shown in the central panel. Those are produced as the amplitude of the average RF-line and the average RF-line amplitude, respectively. In the coherent profiles the amplitude of the IL pulse is typically increased by 12 dB to 18 dB respect to incoherent profile, which confirms the thesis of this approach.

The rightmost Figure exemplifies how coherent profiles can be used to enhance the visualization of the IL interface by an heuristic combination of the coherent profile and the original image.
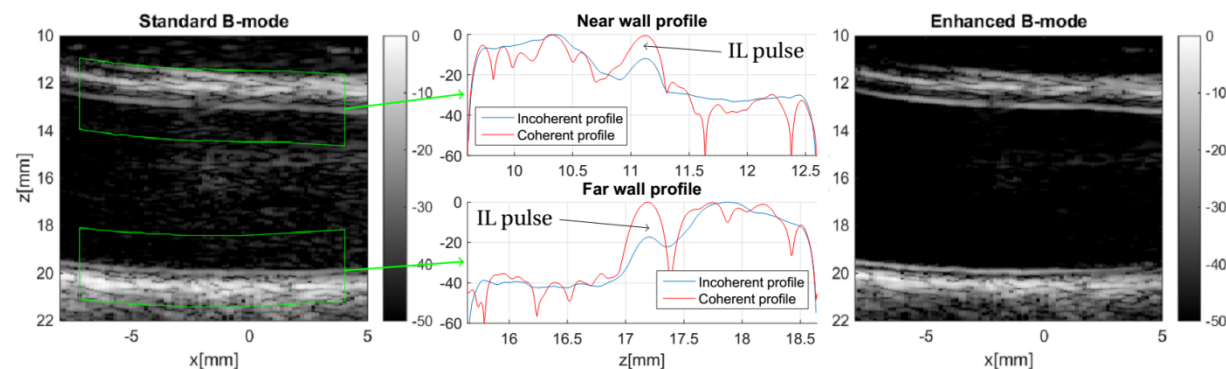
4B-2

1:15 pm   Estimation of arterial wall motion using ultrafast imaging with transverse oscillations: in-vivo study

Sebastien Salles[1], Damien Garcia[2], Alfred Yu[3], Didier Vray[1], Hervé Liebgott[1]; [1]*Creatis, France,* [2]*RUBIC, Canada,* [3]*EEE Department The University of Hong Kong, Hong Kong*

Background, Motivation and Objective

Over the past decade, the pulse wave imaging and the pulse wave velocity estimation (PWV) have shown to be relevant means to characterize the elastic parameters of artery walls. Because of the difficulty in estimating small displacements in the direction perpendicular to beam axis, the PWV is usually estimated without taking into account the longitudinal motion of the intima-media complex (IMC). We thus proposed in a previous phantom study to combine (1) ultrafast ultrasound imaging, (2) transverse oscillation (TO) and (3) a 2D phase-based motion estimator. Here our objective was to evaluate the proposed technique in vivo for the estimation of the PWV. A second objective was to highlight the propagation of a longitudinal motion and estimate the corresponding bulk wave velocity (BWV) along the carotid IMC.

Statement of Contribution/Methods

1) Plane-wave imaging was implemented on the SonixTouch system (14.084 frames/s). Pre-beamformed radio-frequency (RF) data were acquired with the 128-channel Sonix DAQ

2) TO were produced by filtering the beamformed RF signals, to ensure an optimal control of the TO parameters.
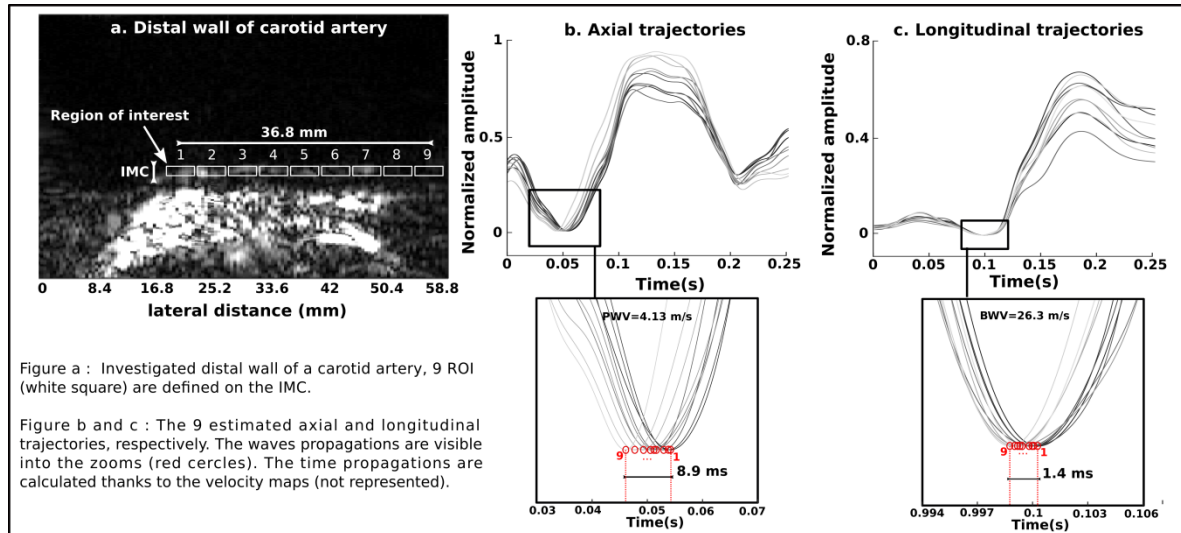
3) 2D Motion vectors were estimated using a phase-based approach: two single quadrant spectra were used to derive two phase images, which were combined to estimate the local displacements between two consecutive images.

The same carotid artery of a healthy subject was investigated twice during two cardiac cycles. The proximal and distal IMCs were tracked using our method. The PWV and BWV were then estimated along the carotid wall and used to derive the Poisson's ratio and Young's modulus of the carotid IMC using the modified Moens–Korteweg equation.

Results/Discussion

The PWV and BWV were estimated by tracking the foot (i.e., fiduciary point) of the wall velocity waveform defined as the inflection point at which the temporal derivative of the velocity attains its maximum. The mean PWV and BWV estimation of the carotid wall were respectively 4.13 m/s and 26.3 m/s. The Poisson's ratio and the Young's Modulus estimation were respectively 0.487 and 91 kPa.

In this study, we have shown that our technique was able to estimate the PWV taking into account the longitudinal motion of the IMC and for the first time the BWV in the carotid wall in-vivo. This allowed us to estimate the Poisson ratio and the Young's modulus of the carotid IMC which are closed to standards for such healthy arteries.

Figure a : Investigated distal wall of a carotid artery, 9 ROI (white square) are defined on the IMC.

Figure b and c : The 9 estimated axial and longitudinal trajectories, respectively. The waves propagations are visible into the zooms (red cercles). The time propagations are calculated thanks to the velocity maps (not represented).

4B-3

1:30 pm   Intra-plaque stiffness mapping in carotid stenosis patients in vivo using high-frame rate Pulse Wave Imaging

Ronny Li[1], Iason Apostolakis[2], Edward Connolly[3], Elisa Konofagou[2,4]; [1]*Department of Biomedical Engineering, Columbia University, USA,* [2]*Biomedical Engineering, Columbia University, USA,* [3]*Neurological Surgery, Columbia University, USA,* [4]*Radiology, Columbia University, USA*

Background, Motivation and Objective

In current clinical practice, the risk of stroke is based heavily on the degree of arterial lumen narrowing. However, there is a growing body of evidence indicating plaque structure and composition as more direct predictors of future cerebrovascular ischemic events. The purpose of this study is to introduce a method for mapping the internal stiffness of carotid plaques using a previously developed arterial Pulse Wave Imaging (PWI) method.

Statement of Contribution/Methods

The atherosclerotic common carotid artery of three (N = 3) stenosis patients were imaged using a plane wave sequence (Verasonics, Redmond, WA, USA) with a 5 MHz linear array at 1500-2000 FPS. The channel data from the 128-element transducer was beamformed using a delay-and-sum method. Inter-frame axial displacements were estimated offline using a 1D cross-correlation-based motion estimation method. 30 manually-initiated wall traces were automatically generated between the outer and inner layers of the anterior wall. For each trace, an adaptive linear-fitting method was used to track the 50% waveform upstrokes on the spatio-temporal PWI displacement map over one cardiac cycle, generating a piece-wise array of PWV measurements. The thickness and diameter along each trace were used along with the corresponding PWV to derive the incremental Young's modulus based on the modified Moens-Korteweg equation. 1D interpolation was performed along each scan line to upsample in the axial direction, resulting in a resolution of ~ 25 microns.

Results/Discussion

Fig. 1 shows the internal PWV map, modulus map, and CT angiogram in patients 1 (M, 56) and 2 (M, 79). The blue rectangle in the CT images represents the ultrasound imaging plane. In patient 1, the PWV map (1a) and modulus map (1b) reveal two regions of high stiffness contrast (pink circles), which appear to correlate with two bright areas on the CT (1c) caused by calcification. In patient 2, the PWV map (1d) and modulus map (1e) show a region of low stiffness contrast in the center of the plaque, possibly indicating a vulnerable necrotic core that is not apparent from the CT (1f). These preliminary findings demonstrate the potential of the PWI technique to internally map plaque stiffness, allowing for the identification of features such as calcifications and lipid pools that may not be detectable by other imaging modalities. This work is funded by NIH R01-HL098830.
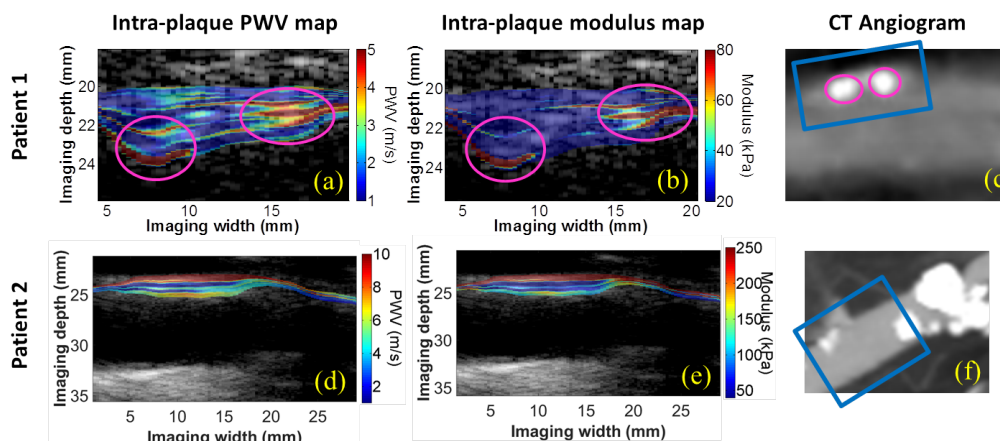

Figure 1. Intra-plaque PWV (a,d) and modulus (b,e) maps for two carotid stenosis patients and their corresponding CT angiograms (c,f). The blue rectangle in the CT images represents the ultrasound imaging plane. The pink circles in (a-c) represent regions of high stiffness contrast due to calcifications within the plaque.

4B-4

1:45 pm   **Dual-frequency intravascular ultrasound imaging of *vasa vasorum*: *Ex vivo* and *in vivo* demonstration**

Brooks Lindsey[1], K. Heath Martin[1], Jianguo Ma[1,2], Zhuochen Wang[1,2], Xiaoning Jiang[1,2], Paul Dayton[1,3]; [1]*Joint Department of Biomedical Engineering, University of North Carolina-Chapel Hill and NC State University, Chapel Hill, NC, USA,* [2]*Department of Mechanical & Aerospace Engineering, North Carolina State University, Raleigh, NC, USA,* [3]*Biomedical Research Imaging Center, University of North Carolina-Chapel Hill, Chapel Hill, NC, USA*

Background, Motivation and Objective

Cardiovascular disease is the leading cause of death in the United States according to the CDC. In order to identify vulnerable plaques—those most likely to rupture and result in heart attack or stroke—we have developed a mechanically-steered, dual-frequency intravascular ultrasound (IVUS) system for imaging *vasa vasorum*, microvasculature ≤200 µm in diameter whose presence is correlated with plaque vulnerability. This system uses a novel prototype dual-frequency transducer to excite microbubble contrast agents within *vasa vasorum* at 5.5 MHz and receive harmonic echoes at 35 MHz.

Statement of Contribution/Methods

Imaging system penetration depth was evaluated using excised coronary arteries (8.1 mm Ø) from hypercholesterolemic pigs. Specimens were prepared by denuding the connective tissue external to the adventitial layer and cutting to ~ 8 mm in length. Vessels were sutured to a screw-driven spreader to ensure patency and immobility. A 200 µm cellulose tube was positioned outside of the vessel to mimic *vasa vasorum* and infused with microbubbles at 1 mL/hr. 3D imaging was performed in a tank filled with phosphate buffered saline with a motion stage providing pullback along the vessel lumen.

Imaging system resolution and contrast-to-tissue ratio (CTR) were evaluated in an *in vivo* environment using the chorioallantoic membrane (CAM) of chicken embryos, which has vessel sizes similar to the human *vasa vasorum*. B-mode and dual-frequency scans were acquired in 17 embryos at 2 weeks gestation using a 1 mL/hr infusion rate of microbubble contrast agents.

Results/Discussion

B-mode images in porcine arteries provide arterial anatomy as in conventional IVUS imaging but with poor detection of the 200 µm tube (circled, Fig. 1a), while dual-frequency images map *vasa vasorum* alone (Fig. 1b), which can be added to the grayscale IVUS image (shown in red, Fig. 1c) and can be visualized in 3D (Fig. 1d). CAM vessels with diameters as low as 250 µm were identified with clear boundaries in dual-frequency contrast mode. CTR measured over time from the beginning of microbubble infusion shows significant improvement in CTR at all post-injection time points in dual-frequency images. Dual-frequency contrast-enhanced IVUS demonstrates sufficient penetration, sensitivity, and resolution in realistic *ex vivo* and *in vivo* imaging environments for mapping *vasa vasorum*.
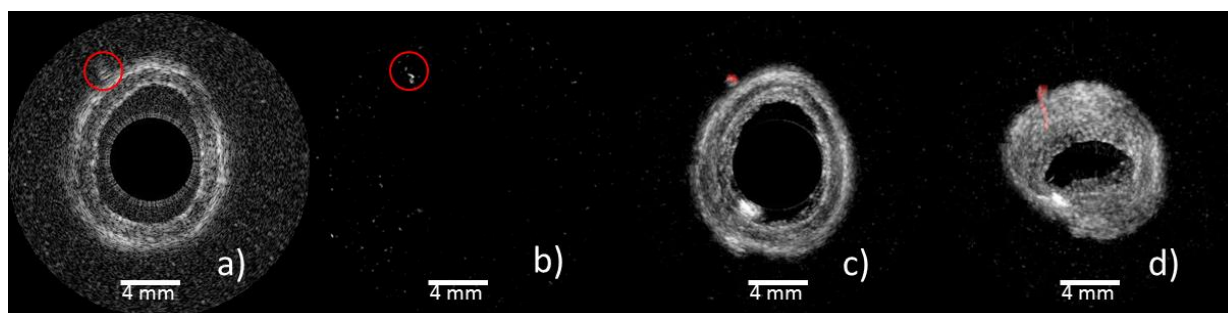
4B-5

2:00 pm   **Improved Estimation of Thermal Strain Using Pulse Inversion Harmonic Imaging: An Ex Vivo Human Tissue Study**

Xuan Ding[1,2], Man Nguyen[2], Isaac James[3], Kacey Marra[1,3], J. Peter Rubin[1,3], Steven Leers[4,5], Kang Kim[1,2]; [1]*Department of Bioengineering, University of Pittsburgh School of Engineering, Pittsburgh, PA, USA,* [2]*Center for Ultrasound Molecular Imaging and Therapeutics, University of Pittsburgh School of Medicine, Pittsburgh, PA, USA,* [3]*Department of Plastic Surgery, University of Pittsburgh School of Medicine, Pittsburgh, PA, USA,* [4]*Heart and Vascular Institute, University of Pittsburgh School of Medicine, Pittsburgh, PA, USA,* [5]*Department of Surgery, University of Pittsburgh Medical Center, Pittsburgh, PA, USA*

Background, Motivation and Objective

Ultrasound thermal strain imaging (TSI) and non-invasive thermometry are similar in principle. Studies have shown that TSI is able to identify lipids in ex vivo human plaques and in an in vivo rabbit model. In future in vivo human studies, clutter will degrade image quality and concerns about thermal safety will prevent further temperature increases. Here, we show that even in the presence of clutter and for the same temperature rise, pulse inversion harmonic (PIH) imaging is able to improve the strain signal to noise ratio (SNR) and contrast to noise ratio (CNR) for TSI.

Statement of Contribution/Methods

TSI was performed on a Vantage (Verasonics Inc.) system with an L7-4 linear array. Fundamental images at 3.3 MHz and 6.6 MHz were acquired. A PIH image was formed by summing received data from two 3.3 MHz 180o phase shifted transmits. For heating, a multi-foci beamforming was used to obtain a broad heating beam thereby allowing imaging and heating to be implemented using a single transducer.

A homogeneous gelatin phantom was imaged with TSI using heating duty cycles (DC) from 0.1-10%. The temperature rise was measured with a thermocouple (MT-23/5, Thermoworks). Whole human abdominal fat and a carotid endarterectomy sample were obtained with IRB approval and embedded in gelatin. TSI was performed using a 5% DC with and without clutter which was generated using a copper mesh. After TSI, the carotid tissue was stained with Oil red O (ORO). Temporal shifts were tracked with a 1.5λ kernel using Loupas' estimator and a 0.44 X 0.89 mm (axial X lateral) median filter was applied. The strain was estimated using linear regression over a 4 mm window.

We define $\lambda_{eff} = (du/dz)/\Delta T$. ΔT is the measured temperature rise. du/dz is the thermal strain. The strain SNR and CNR were calculated.

Results/Discussion

Fig. 1a shows that, in the homogeneous phantom λ_{eff}, while converges to nearly -0.1 %/oC for all imaging methods, PIH-TSI has smaller spatial variation. Fig. 1b shows that the strain SNR for PIH-TSI is 36% greater than the SNR for fundamental TSI. Fig. 1c shows that even with clutter, PIH-TSI provides a strain estimate consistent with the shape of the heating beam. Without clutter, the CNR in the fat was 0.80 (3.3 MHz), 0.98 (6.6 MHz), 1.05 (PIH). With clutter, the CNR was 0.62 (3.3 MHz), 0.87 (6.6 MHz), and 1.09 (PIH). Fig. 1d shows that PIH TSI improves lipid contrast in the ex vivo carotid.
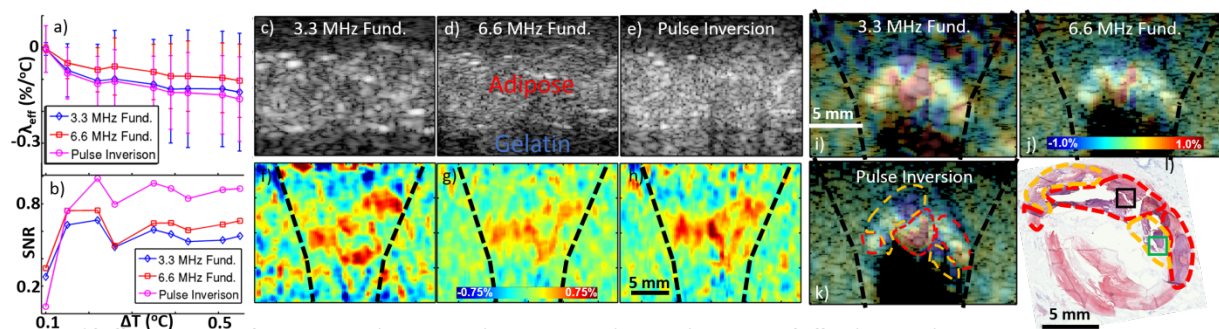
Fig. 1: a) λeff as a function of temperature change. Error bars represent the spatial variation in λeff within a single image. b) Strain SNR as a function of temperature change. Strain SNR converges for ΔT > 0.25°C and is 36% higher for PI-TSI. c) – h) B-mode and TSI images of *ex vivo* human fat. Dotted black lines indicate the shape of the heating beam measured with a hydrophone. Red indicates positive strain corresponding to fat. i) – l) *Ex vivo* carotid endarterectomy samples with matching ORO histology where red dashed areas indicate lipid rich areas and green dashed areas indicate water based tissue. Shadowing present below the artery due to heavy calcific deposits within the plaque. These pixels were masked in the strain overlay. Pulse Inversion images demonstrate improved contrast between lipid and water based tissues and better agreement with histology. Magnified views of the dashed boxes in l) are shown in panels m) and n).

4B-6

2:15 pm   In-vivo Demonstration of High-speed Integrated Intravascular Ultrasound and Optical Coherence Tomography Imaging on Atherosclerosis Animal Model

Teng Ma[1], Jiawen Li[2], Mingyue Yu[1], Dilbahar Mohar[3], Pranav M. Patel[3], K. Kirk Shung[1], Zhongping Chen[2], Qifa Zhou[1]; *[1]NIH Resource Center for Medical Transducer Technology and Department of Biomedical Engineering, University of Southern California, USA, [2]Department of Biomedical Engineering, University of California Irvine, USA, [3]Division of Cardiology, University of California Irvine, USA*

Background, Motivation and Objective

Recently, the integrated intravascular ultrasound (IVUS) and optical coherence tomography (OCT) system, a multi-modality and multi-scale intravascular imaging method, has demonstrated its improved capability of assessing the morphological feature of atherosclerotic plaques. This synergistic approach that combines the complementary characteristics carried by IVUS of deep-penetration to visualize the entire coronary artery volume, and OCT of high resolution to portray microstructure of luminal tissues, is a promising technology to be translated into clinical practice. However, this translational strategy is obstructed by the great imaging speed gap between IVUS and OCT. The aim of this study is to develop a high speed integrated IVUS-OCT hardware-software platform to enable real-time co-registered multimodal intravascular imaging.

Statement of Contribution/Methods

The high-speed integrated IVUS-OCT system is modified with stronger mechanical design of the catheter and optimized data processing algorithm. The imaging catheter is fabricated based on the back-to-back arrangement of a 45 MHz IVUS transducer and a ball-lens OCT probe with an OD of 0.9 mm to facilitate automatic imaging co-registration. Ex vivo imaging of cadaver human coronary artery sample was performed to validate the hybrid imaging system's capability to characterize atherosclerotic plaque at a high imaging speed. Moreover, in vivo imaging of aortic de-endothlialization rabbit model for atherosclerosis was also performed to adequately evaluate the design of such high speed IVUS-OCT imaging system.

Results/Discussion

We successfully acquired integrated IVUS-OCT imaging ex vivo and in vivo at a rotational imaging speed of 50 frames per second with 1000 A-lines per frame, and a pull-back imaging speed of 1.25 cm per second. Representative IVUS-OCT image pairs and histology of coronary artery segments with a confirmed calcified plaque were shown in Fig.1 (A-D). The successful demonstration in vivo of the integrated high speed IVUS-OCT imaging has proved that this technology holds promise for improving diagnosis of atherosclerosis and translating into clinical benefit.
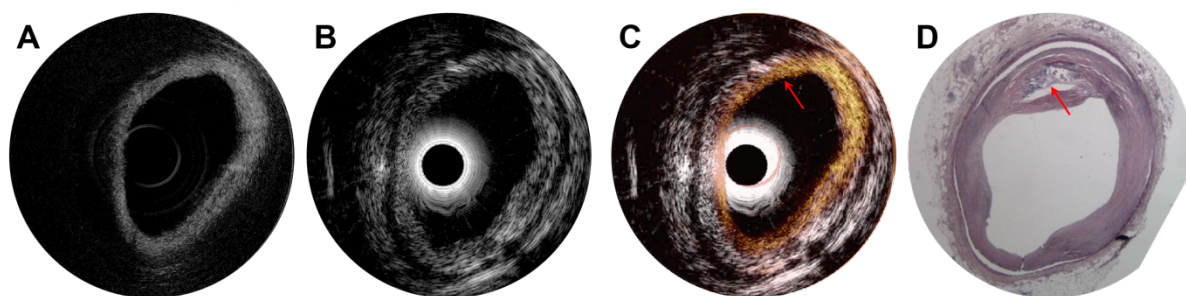

Figure 1. OCT Image(A), IVUS Image(B), Hybrid IVUS-OCT Image(C) and H&E histology image (D) of a human atherosclerotic coronary artery. The red arrow indicates the site of a calcified plaque.

5B - Arrays

103

Thursday, October 22, 2015, 01:00 pm - 02:30 pm

Chair: **Robert Addison**
Rockwell Science Center

5B-1

1:00 pm   Quantitative Phased Array Modeling and Imaging

Lester Schmerr[1]; [1]*Center for NDE, Iowa State University, Woodward, Iowa, USA*

Background, Motivation and Objective

For over two decades there has been a worldwide effort to develop ultrasonic nondestructive evaluation (NDE) models and demonstrate their use in simulating and designing NDE inspections. These efforts have led ultimately to the development of complete ultrasonic measurement models that have been used by the NDE community for a wide range of ultrasonic NDE applications and have been the basis for performing quantitative ultrasonic NDE measurements. Ultrasonic measurement models in essence provide an explicit functional relationship for the received voltage, V, measured in an NDE inspection in terms of the characteristics of the interrogating system and sensors and the properties of the flaw being examined, i.e.

$V = f$ (flaw, system, sensors)   (1)

Although measurement models were originally developed for single element transducers, they also can be constructed for phased arrays. In the form of Eq. (1), such phased array measurement models are forward models, i.e. they predict, for a given flaw and inspection setup the measured voltage. However, in practice we want to invert those models in some fashion to extract information on the flaw. Phased array imaging methods, for example, try to extract flaw geometry explicitly in the form of an image. Unfortunately, most of the commonly used imaging methods form an image directly from the received voltage. In this case it can be seen from Eq. (1) that the image, I, will depend not only on the flaw but on the system and sensor properties as well, i.e.

$I = g(V) = g[f(\text{flaw, system, sensors})]$ (2)

Methods such as the synthetic aperture focusing method (SAFT) and the total focusing method (TFM) are examples of such an approach.

Statement of Contribution/Methods

Here, we will show that with a few physical assumptions about the response of flaws we can in fact invert the measurement model relationship of Eq.(1) to form a flaw image, where the resulting image depends on the flaw properties alone, i.e.

$I(\text{flaw}) = f^{-1}$ (V, system, sensors)(3)

An image formation process of this type we will call an ultrasonic imaging measurement model (IMM).Depending on the array elements involved, we will show that SAFT and TFM are filtered versions of this flaw image and demonstrate the explicit properties of this filter. For small flaws, our IMM can also be shown to reduce to the Physical Optics Far Field Inverse Scattering (POFFIS) method originally developed by Bojarski and later modified by Bleistein. Thus, an ultrasonic IMM provides for the first time a unified framework for understanding some of the most commonly used phased array imaging approaches.

Results/Discussion

Examples will be given that demonstrate that the flaw response that is being imaged with all these methods is the front surface specular response(for volumetric flaws)or the edge diffracted signals(for cracks). All other flaw responses are artifacts of the imaging process and cannot be reliably used for quantitative flaw characterization purposes.

5B-2

1:30 pm   Imaging Beyond Aliasing

Paul van Neer[1], Arno Volker[1]; [1]*Process and Instrumentation Development, TNO, Delft, Zuid-Holland, Netherlands*

Background, Motivation and Objective

Proper spatial sampling is critical for high quality imaging. If the sampling criterion is not met, artifacts appear in the image, generally referred to as grating lobes. For inspection efficiency the width of the field of view is becoming larger leading to an increase in the number of elements and therefore transducer complexity and cost. The development of volume scanning methods in the medical field poses its own problems. Here a matrix of piezoelements is used to scan a volume using electronic beam steering. The challenge is to connect 2500+ elements using <256 channels. Most solutions use prebeamforming to reduce the data at a cost of image quality. Another option may be to reconstruct the non-aliased data from spatially aliased data. In this work a novel method to reconstruct nonaliased radio-frequency (RF) data from strongly spatially aliased RF data is investigated using simulations.

Statement of Contribution/Methods

The reconstruction method involves an iterative scheme using wave field extrapolation. No medium assumptions are made. It has the following steps: 1) A matrix containing zeros at the locations where signals need to be interpolated is created such that no aliasing occurs. 2) The dataset is inversely extrapolated to focus the wave energy. 3) A threshold is applied to the extrapolated data selecting such that aliasing artifacts are excluded. 4) The dataset is forward extrapolated such that the input data is obtained. Now the empty traces contain signal. 6) The original RF dataset is copied into the reconstructed dataset. 7) Steps 2 – 6 are performed iteratively using a progressively lower threshold.

Aliased and non-aliased datasets were modeled based on point diffractors and diffractors of increasing width. The datasets were imaged using a wavenumber-frequency domain mapping.

Results/Discussion

The figure shows a reconstruction example. An imaged aliased dataset – a factor of 4 undersampled – based on diffractors of increasing widths is shown on the left, the imaged reconstructed dataset is shown in the middle and the reconstruction error is shown on the right. The error after reconstruction was 0.77%, 4.2% and 43%, for undersampling of a factor 2, 4 and 8, respectively. For point diffractors the reconstruction error was 0.9%, 3.0% and 7.2%, respectively. These results show the method's potential. It may also be used to reconstruct signals for dead array elements.
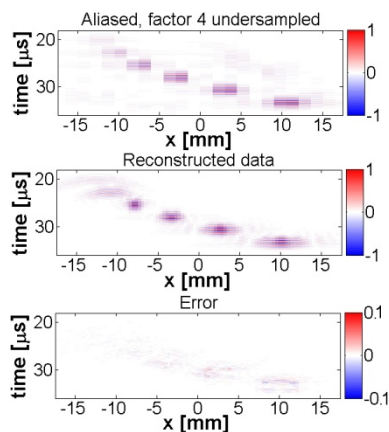
5B-3

1:45 pm   Flexural Transducer Arrays for Industrial Non-Contact Applications

Tobias Eriksson[1], Sivaram Ramadas[1,2], Alexander Unger[3], Maik Hoffmann[4], Mario Kupnik[3], Steve Dixon[1]; *[1]University of Warwick, United Kingdom, [2]Elster-Instromet, Belgium, [3]Technische Universität Darmstadt, Germany, [4]BTU, Cottbus-Senftenberg, Germany*

Background, Motivation and Objective

Many industrial, non-contact, ultrasonic applications require a robust, intrinsically-safe transducer that is simple to construct, has low energy consumption, a good impedance match to the load medium, and tuneable characteristics (frequency, bandwidth etc.). In the case of an array device, one also requires low inter-element cross-talk, and that field directivity constraints are satisfied. The motivation of this work is to design, build, and test an efficient, flexural, ultrasonic transducer array, applicable to industrial non-contact applications where the transducer is in direct contact with a fluid.

Statement of Contribution/Methods

A simple design is used, in which the piezoelectric ceramic element is mounted directly onto a thin metal sheet, which is subsequently assembled into a complete flexural array device and tested in the 50 to 500 kHz frequency range. The analytical model of an edge clamped plate was used to estimate the axi-symmetric device resonance frequencies. The effect of variation in design parameters, such as the aspect ratios of the piezoelectric and flexural membrane, was studied in further detail using finite element (FE) modelling, demonstrating that the optimal diameter of the driving element depends on the vibrational mode of the transducer. For the prototype transducer used in this study, the optimal diameter was 6 mm, which is close to the diameter of the 2nd anti-node of the vibrational mode.

We focus on inter element cross-talk and mechanisms to reduce them via special baffle design. A prototype 100 kHz, 2D array device was fabricated by bonding 6 mm diameter, 0.25mm thick piezoelectric discs onto a 0.25 mm thick stainless steel sheet. A machined acrylic back plate is used to separate elements within the array and provide the rigid clamping required for each flexural element. Experimental analysis of the prototype array behaviour, including field directivity measurements using a microphone, laser interferometry, and pulse-echo/pitch-catch experiments were conducted.

Results/Discussion

Individual elements on the experimental prototype yielded an average pressure of 2.3 Pa p-p, at a distance of 24 cm from the source, when driven by a 100 kHz, 10 V p-p, 3 cycle, sinusoidal signal. Waves from each individual element superpose to give roughly 20 Pa p-p, when the entire 3x3 array was used in the same setup. A custom built, low frequency phased array controller was developed to demonstrate steering in air using these flexural arrays. Significant cross-talk was observed, with displacements in neighbouring inactive elements reaching up to 25% of the maximum displacement of the excited element. However, several techniques for decreasing cross-talk, have been found through FE modelling, and these will be experimentally evaluated in future work. Our results illustrate that it is possible to design efficient, low cost, ultrasonic transducer arrays that are applicable to many real-world, industrial, non-contact applications.

5B-4

2:00 pm   High Resolution Autofocused Virtual Source Imaging (AVSI)

Jorge Camacho[1], **Jorge F. Cruza**[1]; *[1]Ultrasonic Systems Group, Spanish National Research Council (CSIC), Madrid, Madrid, Spain*

Background, Motivation and Objective

It is well known that synthetic aperture focusing technique (SAFT) provides improved lateral resolution and can be used with array transducers. But, when a coupling medium used, refraction at the interface complicates the computation of the ultrasound time-of-flight (TOF) from every element to every imaged point. This slows down the imaging process since there are not general formulae for arbitrarily shaped interfaces.

The objective of this research was to find new techniques that avoid the complications of refraction and, at the same time, improve SNR and resolution with lower cost equipment. This is achieved by creating virtual source/receivers at automatically detected interface points, a process we call Autofocused Virtual Source Imaging (AVSI).

Statement of Contribution/Methods

A first pulse-echo trigger determines the normal incidence point at the interface for a given array sub-aperture. Such point acts as a virtual source, producing an approximately cylindrical wavefield into the part. The same active aperture focused at the virtual source is used to beamform the received echoes. Emission and reception is achieved by a conventional delay-and-add procedure, while SAFT processing is applied to the beamformed A-scans. The approach followed is depicted in Fig. 1.

Since several elements are simultaneously triggered and focused in emission and reception at the interface normal incidence point, SNR is improved with regard to traditional SAFT. Besides, since the virtual source lies at the interface, SAFT processing is carried out in the second medium only, thus avoiding the complications of refraction.

Results/Discussion

AVSI was implemented in a conventional phased array instrument (SITAU-311, Dasel S.L., Spain) with fixed focus at the auto-detected normal incidence point. SAFT processing was carried out by software in an external computer. Active apertures were chosen to get the theoretical useful opening angle needed for every inspection.

Results show a constant resolution, significantly higher than that obtained with phased array and the same active aperture. In fact, the resolution is that of a full-parallel phased array system, but only a fraction of that hardware is required. SNR is high and the process is carried out without prior knowledge of the inspected part shape, thus demonstrating the auto-focusing capability of the AVSI technique.
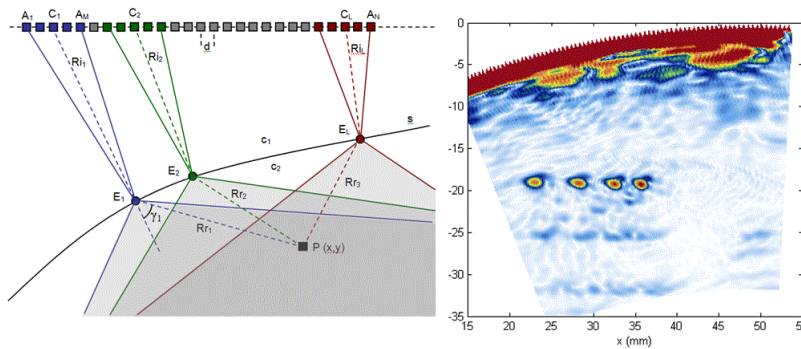
Fig 1. (Left) Principles of the AVSI technique, showing three active apertures with virtual sources/receivers and sound coverage over the pixel P(x,y). (Right) AVSI image of a curved surface aluminum block with 1.5 mmm side-drilled holes.

5B-5

2:15 pm   Fast Calculation of Wideband Beam Pattern for Designing Large Planar Array

Cheng Chi[1], Zhaohui Li[2]; [1]Depatment of Electronics, Peking University, Beijing, China, People's Republic of, [2]Deparment of Electronics, Peking University, China, People's Republic of

Background, Motivation and Objective

Being able to provide more information than two-dimensional (2D) imaging, wideband real-time three-dimensional (3D) acoustic imaging is becoming more and more important in underwater observation, nondestructive testing, medical diagnosis and other fields.

When using a fully sampled uniform array, tens of thousands of sensors are needed, which leads to over-high hardware cost and complexity of array processing. Therefore, it becomes necessary to design large sparse wideband planar arrays for real-time 3D acoustic imaging.

By now, some sparse array design methods whose iterative procedures of calculating beam pattern may be used for hundreds of thousands of times, have only been employed to design sparse planar arrays by using narrowband beam pattern (BP). Impeded by the high time consumption of calculating wideband beam pattern, these method rarely employ wideband BP. However, the planar arrays designed by using narrowband BP could not guarantee the achievement of the best results in the wideband case.

Therefore, our objective is to propose a fast calculation method of wideband BP of arbitrary large planar arrays, to make the methods which need massive iterations available for designing wideband large planar arrays.

Statement of Contribution/Methods

Our study proposes a fast method of calculating wideband BP of arbitrary planar arrays. Compared with Field II which is commonly-used, the calculation speed of the proposed method is increased by about three orders of magnitude with comparable accuracy.

The proposed fast method is mainly on the basis of two fast transforms: nonuniform fast Fourier transform (NUFFT) and short inverse fast Fourier transform (IFFT).

Results/Discussion

An equispaced planar array with 10000 sensors was employed to demonstrate the efficiency and accuracy of the proposed method of calculating wideband BP.

The mean relative error between the results of the proposed method and Field II is evaluated, which is kept within 3%. The calculation time required by the two methods is also extracted: 7s for the proposed method and 3440s for Field II. The calculation time of the proposed method is approximately lower 500 folds than that of Field II.

A spiral array design example is also given to verify that the proposed method enables the massive iterations of wideband BPs and can help design better wideband large planar arrays.
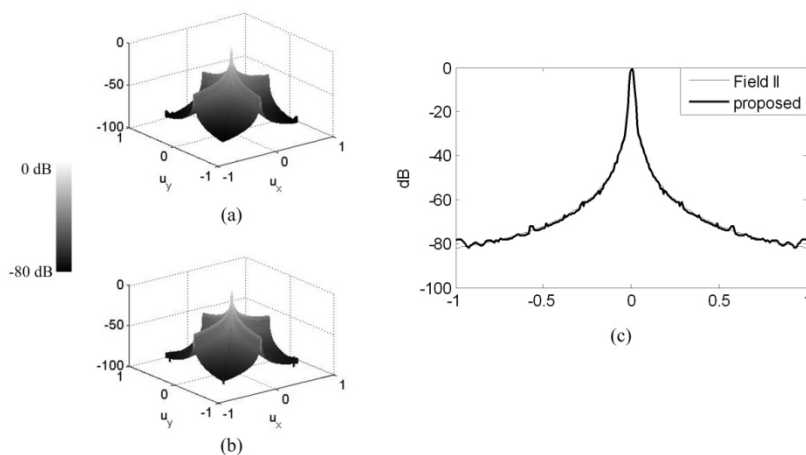

Fig. Wideband BPs calculated by the proposed method and Field II (a) Field II; (b) the proposed method; (c) the diagonal lines of the two wideband BPs.

6B - Phononics

201AF

Thursday, October 22, 2015, 01:00 pm - 02:30 pm

Chair: **Tsung-Tsong Wu**
National Taiwan University

6B-1

1:00 pm   Phonon Dynamics in Electromechanical Resonators G3 topic: Phononics (PPN)
Imran Mahboob[1], Hirsohi Yamaguchi[1]; *[1]NTT Basic Research Laboratories, Japan*

Background, Motivation and Objective
Phonon dynamics in electromechanical resonators

Electromechanical resonators, consisting of a mechanically compliable element embedded in an electrical transduction circuit, provide an almost perfect acoustic cavity in which phonons can be confined in the guise of a tangible mechanical vibration on times scales greatly exceeding the vibration period. Consequently, the interactions of this phonon ensemble can be dynamically engineered enabling far from equilibrium nonlinear dynamics to be explored.

Here I will first review the GaAs/AlGaAs based electromechanical resonators which provide the ideal platform in which nonlinear phononics can be developed by controlling the phonon ensemble via piezoelectrically induced mechanical strain fields. I will then briefly describe concepts such as parametric resonance and parametric amplification, inspired by photonics, which have been developed in this platform. Indeed the ultimate nonlinear photonic system is the laser, and as specific example, I will describe how a phonon laser can also be executed in this system by utilising the atom-like spectrum of discrete mechanical vibrations namely phonon modes.

These results vividly demonstrate that concepts from photonics can be translated to phononics in the electromechanical resonator platform and they pave the way towards a new class of technology based on ultra-pure acoustic vibrations.

[1] I. Mahboob and H. Yamaguchi, Bit storage and bit flip operations in an electromechanical oscillator, Nature Nanotechnology 3, 275 (2008)

[2] I. Mahboob, E. Flurin, K. Nishiguchi, A. Fujiwara and H. Yamaguchi, Interconnect-free parallel logic circuits in a single mechanical resonator, Nature Communications 2, (2011) 198

[3] I. Mahboob, K. Nishiguchi, H. Okamoto and H. Yamaguchi, Phonon-cavity electromechanics, Nature Physics 8, 387 (2012)

[4] I. Mahboob, K. Nishiguchi, A. Fujiwara and H. Yamaguchi, Phonon Lasing in an Electromechanical Resonator, Phys. Rev. Lett. 110, 127202 (2013)

[5] H. Okamoto, A. Gourgout, C-Y. Chang, K. Onomitsu, I. Mahboob, E. Y. Chang and H. Yamaguchi, Coherent phonon manipulation in coupled mechanical resonators, Nature Physics 9, 480 (2013)

[6] D. Hatanaka, I. Mahboob, K. Onomitsu and H. Yamaguchi, Phonon waveguides for electromechanical

circuits Nature Nanotechnology 9, 520 (2014)

[7] I. Mahboob, H. Okamoto, K. Onomitsu and H. Yamaguchi, Two-Mode Thermal-Noise Squeezing in an Electromechanical Resonator, Phys. Rev. Lett. 113, 167203 (2014)

[8] I. Mahboob, N. Perrissin, K. Nishiguchi, D. Hatanaka, Y. Okazaki, A. Fujiwara, and H. Yamaguchi, Dispersive and Dissipative Coupling in a Micromechanical Resonator Embedded with a Nanomechanical Resonator, Nano Lett. Article ASAP (2015)

Statement of Contribution/Methods

Results/Discussion

6B-2

1:30 pm   The generation of impulses from narrow bandwidth signals using resonant spherical chains
David Hutchins[1], Jia Yang[1], Omololu Akanji[1], Peter Thomas[1], Lee Davis[1], Steven Freear[2], Sevan Harput[2], Nader Saffari[3], Pierre Gelat[3]; *[1]School of Engineering, University of Warwick, Coventry, United Kingdom, [2]School of Electronic and Electrical Engineering, University of Leeds, Leeds, United Kingdom, [3]3Department of Mechanical Engineering, University College London, London, United Kingdom*

Background, Motivation and Objective
It is possible to observe non-linear acoustic propagation along a chain of spheres that are in contact with each other. As dispersion is also present, solitary waves can be generated. In long chains, these waves have known characteristics. However, in shorter chains their form is less well-known. In particular, the case of harmonic excitation (i.e. with a narrow bandwidth) has not been studied for finite chain lengths, where resonances within the chain would be expected. The objective was to transform sinusoidal signals into a set of wide bandwidth impulses. Acoustic signals generated by such signals may be relevant to biomedical applications.

Statement of Contribution/Methods
An ultrasonic horn, operating at 73 kHz, was used to excite one end of a chain of steel spheres. The vibration transmitted along the chain was measured at the far end using a laser vibrometer. Various chain lengths, ranging from 2-10 spheres, were studied. It was found that when certain conditions were met, a set of impulses were generated that seemed to be enhanced by reflection within the chain. This required the spheres to be just touching, with a minimal pre-compression force. Both harmonics and sub-harmonics could be observed. Theoretical models were developed, which are based on the relevant equations of motion, including the end conditions imposed by both the horn and the cylindrical holder used to maintain the spheres in the correct orientation.

Results/Discussion
The impulses were observed to be generated only when certain numbers of spheres were used. This was required so as to establish the nonlinear normal modes (NNMs) of the system by reflection at both ends of the chain. This resonant condition was needed to establish the impulses, which contained various harmonics and sub-harmonics of the excitation frequency, depending on the chain length – the longer the chain, the wider the bandwidth of each impulse, and the greater the time spacing between impulses. The results are compared to theoretical predictions, and it was observed that the main features agreed with theory. Figure 1 below shows the
experimental output for a chain of 6 spheres of 1 mm diameter, compared to the resonant input waveform from the ultrasonic horn.

It is thus established that a gated sinusoidal input can be transformed into a set of impulses, of great interest to many applications in biomedical ultrasound and elsewhere.
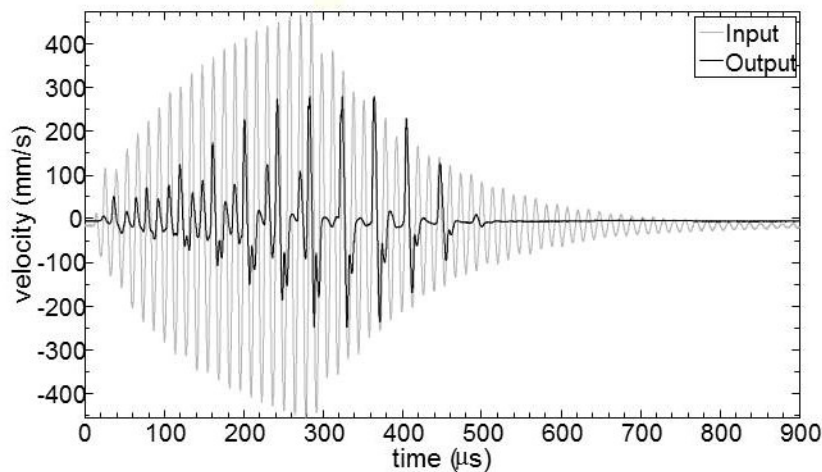
6B-3

1:45 pm **Tunable Bragg band gaps in piezocomposite phononic crystals**

Charles CROËNNE[1], Marie-Fraise PONGE[1], Franck LEVASSORT[2], Lionel HAUMESSER[2], Mai PHAM THI[3], **Anne-Christine HLADKY**[1]; [1]*IEMN, UMR 8520 CNRS, ISEN Department, Lille, France,* [2]*François-Rabelais University, GREMAN UMR 7347 CNRS, Tours, France,* [3]*Thales Research and Technology, Palaiseau, France*

Background, Motivation and Objective

Phononic Crystals (PCs) have received a great deal of interest for the last decades and recent studies have introduced significant breakthroughs in the domain of tunable PCs. In particular, it has been shown numerically and experimentally that a 1D structure made of a stack of identical piezoelectric materials can exhibit a Bragg gap with exceptional tunability properties, when the electric boundary conditions on periodically placed transverse electrodes are modified [S. Degraeve et al, J. Appl. Phys. 115, 194508 (2014)]. The width of the gap in such an all-piezoelectric PC is directly related to the electromechanical coupling factor of the piezoelectric material. However, in order to avoid the parasitic modes (radial mode, flexural modes …) that can deteriorate the band-gap effect, the piezoelectric elements must be rods or plates, with severe constraints on the aspect ratios.

Statement of Contribution/Methods

In order to overcome this limitation while maintaining a good efficiency for the device, it is proposed to use piezoelectric composites with 1-3 connectivity. They are made of a periodic arrangement of piezoelectric rods immersed in a passive matrix such as a polymer. The rod section can be circular or square and the piezoelectric composite is poled along its thickness. These two-phase structures present improved properties in comparison with bulk piezoelectric materials: in particular, depending on the filling fraction of the piezoelectric phase, a higher electromechanical coupling factor is obtained. The calculation of the dispersion curves of the device is performed using the Finite Element Method. When the ratio between the thickness of the rods and the periodicity is greater than 3, then the main vibration mode of the piezocomposite corresponds to a thickness mode of the piezoelectric rod that is not disturbed by transverse modes. In that case, an analytical model exploiting homogenized material parameters can also be used for the calculation of the dispersion curve.

Results/Discussion

The piezocomposite under interest is made of PZT4 rods embedded in a polymer. The thickness of each layer is large enough to avoid parasitic lateral modes. In the dispersion curve, a band gap for the longitudinal waves appears at the boundary of the Brillouin zone when the electrodes are in short circuit, whereas no gap is observed when they are in open circuit. All intermediate cases can be obtained by connecting the electrodes through capacitances of a given value. Finally a stack containing 20 plates is considered. The device is excited using the first layer of the piezocomposite. By using the finite element method and the analytical model, the transmission as well as the electrical potential on the last layer are calculated as a function of frequency, when the intermediate layers are in open circuit or short circuit. They clearly exhibit a band gap related to the electrical connections. Finally, a device has been fabricated and first experiments are presented.

6B-4

2:00 pm **Tunability of the band structure of a piezoelectric phononic crystal using electrical negative capacitance**

Bruno Morvan[1,2], Sid Ali Mansoura[1,2], Pierre Maréchal[1,2], Paul Bénard[1,2], Anne-Christine Hladky-Hennion[2,3], Bertrand Dubus[2,3]; [1]*LOMC UMR 6294 CNRS, Le Havre, France,* [2]*FANO FR CNRS 3110, France,* [3]*IEMN UMR 8520 CNRS, ISEN, Lille, France*

Background, Motivation and Objective

These last years, numerous applications have emerged from the research field of Phononic Crystal (PC) : frequency filters, wave collimation, super-resolution lenses… These applications are based on unusual dispersion properties of the waves in a periodic structured material (anisotropy, forbidden frequencies band, negative or zero angle refraction, hybridization gap, …). Recently the use of active materials has been proposed in order to extend or simply adjust the properties of the PC in frequency. Among all the proposed solutions, those using an electrical control have received a great deal of interest because of their ease of use. The aim of our study is to demonstrate the possibility of using piezoelectric material coupled to a negative capacitance charge to obtain an efficient control of the wave propagation in the PC.

Statement of Contribution/Methods

In a first step, a theoretical and experimental study of a unit block of the PC constituted by a piezoelectric plate connected to a negative capacitance is performed in the MHz frequency range. Mason's model is considered for the characterization of the piezoelectric plate and the expression of the resonance and antiresonance frequencies are evaluated according to the value of the electrical connected negative capacitance. In a second step, an electrical circuit based on the current feedback operational amplifiers is proposed in order to achieve experimentally the negative capacitance. Measurements are performed demonstrating the possibility to obtain a large range of tuning of the antiresonance frequency. In a second time, the transmission of waves through a phononic crystal constituted by a stack of piezoelectric layers connected to negative capacitance is studied.

Results/Discussion

The preliminary study of a piezoelectric layer alone shows large variations of the antiresonance frequency with the value of the added negative capacitance. This tunability is experimentally demonstrated in the MHz frequency range. These variations induce changes in the band structure of the PC. In particular, the acoustic transmission through the PC shows some significant shifts of the frequency stop bands in very good agreement with theoretical results.

6B-5

2:15 pm   Phononic crystal based liquid sensor governed by localized defect resonances

Aleksandr Oseev[1], Marc-Peter Schmidt[1], Ralf Lucklum[1], Mikhail Zubtsov[1], Soeren Hirsch[2]; *[1]Institute of Micro and Sensor Systems (IMOS), Otto-von-Guericke University Magdeburg, Magdeburg, Germany, [2]Department of Engineering, University of Applied Sciences Brandenburg, Brandenburg, Germany*

Background, Motivation and Objective

Phononic crystal sensors are promising for liquid sensor applications. We have shown already that the frequency of narrow transmission bands depends on properties of liquids confined within a 2D phononic crystal.

In comparison to almost all liquid sensor platforms where sensors respond to effects very close to the sensor, e.g. mass load due to absorption of molecules in a recognition layer, the objective of the liquid cavity resonators is the determination of volumetric (bulk) properties of the liquid.

Statement of Contribution/Methods

The quality factor is the most crucial parameter of sensor performance. Therefore classical microacoustic resonance sensors must avoid radiation of acoustic energy into the liquid. The phononic crystal sensor concept tailors acoustic wave propagation in a way to excite a specific mode within the band gap of the phononic crystal.

We apply surface acoustic wave (SAW) devices as reliable platform for the phononic crystal sensor realization. It performs both excitation of a selected liquid cavity resonance and its detection. The liquid cavity microchannel is realized within an overlayer of the SAW device. The liquid in the microchannel becomes a part of vibrating overlayer and determines its acoustic properties.

Results/Discussion

The sensor development contains three parts: development of the SAW platform including etching of periodic elements, design of the overlayer containing the microchannels, and optimization of acoustic coupling between the two elements. Fig. 1 shows a simulation result of the overlayer with acoustic field penetrating the liquid. Fig. 2 shows the SAW substrate featuring a phononic crystal structure with well defined shape and depth of holes etched into quartz. They prove the correctness of our approach.

Liquid microchannels

20 µm   EHT = 20.00 kV   WD = 23.0 mm
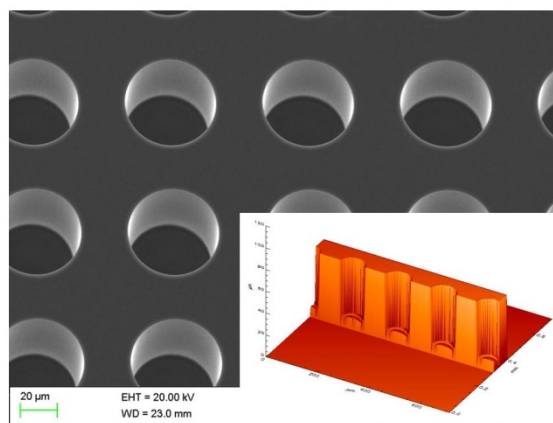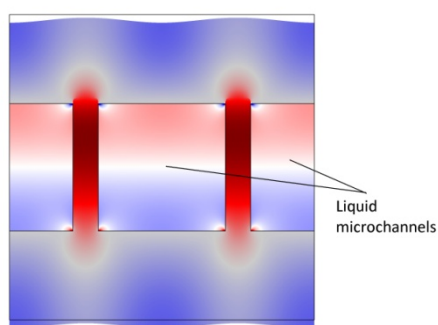
7B - Microacoustic Modeling

105

Thursday, October 22, 2015, 01:00 pm - 02:30 pm

Chair: **Ken-ya Hashimoto**
Chiba University

7B-1

1:00 pm   Efficient and Accurate WLP SMT SAW Duplexer EM Simulation in Module Integration

Hao Dong[1], Kevin Gamble[2], Jean Briot[2], Thor Thorvaldsson[2]; [1]*Qorvo, Apopka, Florida, USA*, [2]*Qorvo, USA*

Background, Motivation and Objective

With the SAW die getting smaller and more bands included in the module, the full EM co-simulation of filter die and laminate is required to catch all the parasitic effects which have the impact on insertion loss, rejection and isolation. But the final EM model can be very complex and takes more computation time and more memory. Sometimes the complex EM model can easily lead to unreasonable simulation time and even false results. On the other hand, it's difficult to run full EM co-simulation due to different tool in die and laminate design, different sites or companies in some cases. We are working on the efficient and accurate EM simulation method to simplify the model and reduce the simulation time. For flexibility, we separate the die EM and laminate EM, then combine both EM results in schematic to get the final response. This paper discusses the efficient and accurate method to do it and keeps the similar modeling accuracy compared with full EM co-simulation of die and laminate.

Statement of Contribution/Methods

Different from packaged SAW filter, WLP SMT SAW die doesn't have the package and no common ground pad. Usually we do WLP SMT SAW die EM by defining a perfect electric conductor (PEC) under the die as the ground reference and laminate EM with floating PEC for landing pads. The PEC introduces extra parasitic effects and this makes WLP die very sensitive to the coupling between ground pads and PEC plane. The discrepancy can be clearly observed on the isolation. The efficient and accurate method we found is considering the implementation on the laminate, define a ground plane for WLP SMT SAW die, and eliminate the ports for ground pads. By doing this, we reduce the ground pads sensitivity in die EM, and we don't need to define the floating PEC for landing pads in laminate EM. We simplify the EM setup, and no more concerns about the difference of port ground reference. The simulation speed is improved and the design cycle time is reduced too.

Results/Discussion

Our full EM simulation of die and laminate matches the measurement very well, so we take the full EM simulation data as the reference. The following plot shows the comparison of B20 isolation among full EM simulation of die and laminate, separate die EM and laminate EM with extra PEC, and the new method without PEC. The new method shows good agreement with reference, and it takes less simulation time, and provide the flexibility in die and laminate design.

-     Reference, full EM co-simulation of die and laminate
-     Separated die EM and laminate EM with PEC as port reference
-     Separated die EM and laminate EM without PEC, new method
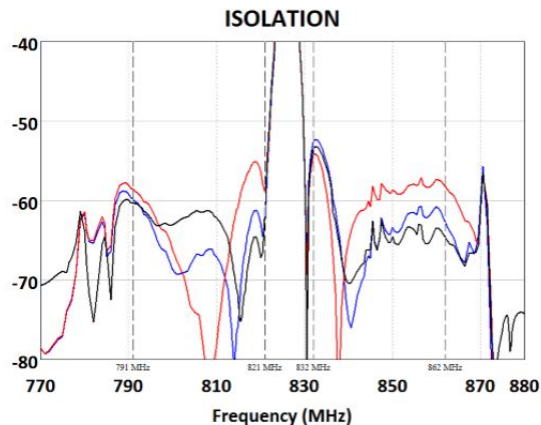
7B-2

1:15 pm   Study on Generation Mechanisms of Third-Order Non-Linearity in SAW Devices

Ryo Nakagawa[1,2], Takanao Suzuki[1], Hiroshi Shimizu[1], Haruki Kyoya[1], Katsuhiro Nako[1], Ken-ya Hashimoto[2]; [1]*Murata Manufacturing Co., Ltd, Japan*, [2]*Graduate School of Engineering, Chiba University, Japan*

Background, Motivation and Objective

Importance of linearity of the RF front-end in cellular phone handsets has been getting strong in recent years. Thus, ultimate linearization of the SAW duplexer which is one of the main components of the RF front-end is strongly desired. In this situation, better understanding the generation mechanism and behavior of nonlinear signal are crucial.
In this work, we propose a simulation technique of nonlinear signals of SAW devices, and by using it, the generation mechanisms of third-order non-linearity are discussed.

Statement of Contribution/Methods

First, the linear strain S_L and linear electric field E_L are calculated by the conventional COM analysis. Then the non-linear stress T_N and non-linear electric flux density D_N are calculated from the constitutive equations expressed in third-order polynomials with respect to S_L and E_L. Then T_N and D_N are treated as voltage and current sources, respectively, in an equivalent circuit model of an interdigital transducer, and as the result, non-linear signal levels at external terminals are calculated. Coefficients appearing in the constitutive equations are determined by fitting the calculated results with the measured ones. Determination of the coefficients is relatively straightforward when the driving conditions are properly chosen because influence of each coefficient varies with the driving conditions.

Results/Discussion

Fig. 1 compares experimental and simulated non-linear outputs of a one-port SAW resonator under various conditions. Identical non-linear coefficients were used for the simulations. It is seen that the agreement is well. We also examined other conditions, and the accuracy was verified to this degree. Through the investigation, it became clear that (a) D_N is a major non-linearity source for the out-band output, (b) influence of T_N is significant only when a non-linear signal is generated close to the resonance, (c) non-linear terms only governed by S_L give strong contribution to T_N and D_N only when all the driving frequencies are close to the resonance, and (d) non-linear terms only governed by E_L are dominant in T_N and D_N when all the driving frequencies are far from the resonance.
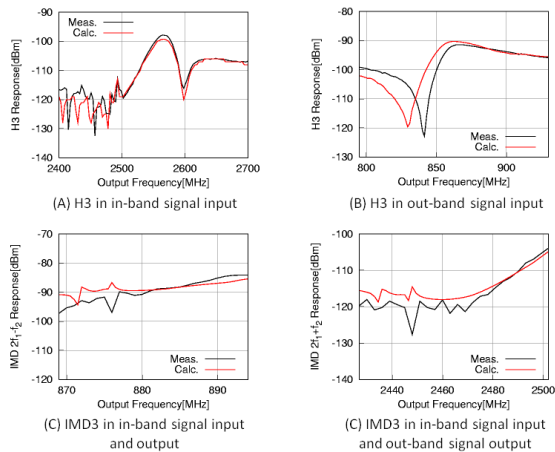
Fig 1. Measurement and simulation results of non-linear signals in various input and output frequencies.

7B-3

1:30 pm   Effective nonlinear constants for SAW devices from FEM calculations

Andreas Mayer[1], Elena Mayer[1], **Markus Mayer[2]**, Philipp Jaeger[2], Werner Ruile[2], Ingo Bleyl[2], Karl Wagner[2]; *[1]Hochschule Offenburg, Germany, [2]TDK corporation, Munich, Germany*

Background, Motivation and Objective

The importance of suppressing nonlinear signals in filtering devices grows with increasing number of simultaneously active frequency bands and continuing miniaturization. Substantial progress in simulating nonlinearities in SAW filters has been achieved in the last years. Recently we demonstrated that a single frequency independent constant in a P-Matrix approach is sufficient to describe the IMD3 of a variety of devices on lithium tantalate (YXl)/42, including test devices and duplexers and highlighted the role of the metallization ratio.

Statement of Contribution/Methods

In this work we investigate this effective nonlinear constant in more detail. Starting from a FEM simulation we calculate the linear fields and combine them with the help of nonlinear tensors to get the nonlinear fields. The latter are the source terms for nonlinear current at the output ports. By analyzing the input voltage and the resulting nonlinear current, an effective nonlinear constant can be obtained and used in a P-Matrix approach.

Results/Discussion

In the case of LiNbO3 an effective nonlinear constant for IM3 is calculated and used in a P-Matrix calculation. A comparison between the calculated and measured IMD3 is made and discussed.

7B-4

1:45 pm   Thermal Modeling of WLP-BAW Filters – Power Handling and Miniaturization

Michael Fattinger[1], Paul Stokes[1], Gernot Fattinger[1]; *[1]BAW R&D, Qorvo, Apopka, Florida, USA*

Background, Motivation and Objective

The continuing miniaturization and increasing feature density of modern mobile devices is a main driving force for research and development of new technologies like Bulk Acoustic Wave devices. This can lead to thermal complications in many BAW filter applications. The decrease in volume and therefore increase in power density, in combination with technologies like flip-chip wafer level packaging (WLP), which are less favorable from a thermal point of view, induce challenges in the design and fabrication of such devices.

The ladder filter design of BAW filters naturally results in unbalanced power dissipation across the different contributing resonators, thus giving rise to hot spots on the die. The design of the die and the accompanying laminate can help to provide a low thermal resistivity path to cool the die. The laminate layout is already mainly governed by electrical considerations, which further narrows the design options. Also the durability of the parts benefits from cooler operation. Thus proper thermal design has an immediate impact on higher quality of the resulting products.

Statement of Contribution/Methods

The development of a thermal model to predict the performance of BAW resonators and filters is the main focus of this work. A model of resonator self-heating with corresponding cross-heating used on filter designs provides a reliable forecast of maximum filter temperatures, power handling capabilities and pass-band shape degradation on different filter designs prior to first builds.

The material parameters and thermal properties of our dies and modules used for the simulation have been identified by experiments and are backed by 3D FEM simulations of BAW dies, laminates and whole modules.

Results/Discussion

The model is embedded into the standard simulation of electrical characteristics that is used to design BAW filters, thus it is already providing information to identify thermal problems during the first design iteration. Besides lifetime and power handling considerations the heating of resonators has direct influence on the pass-band shape. The frequency shift of the dissimilar tempered resonators can lead to degradation of filter performance at the edge of the pass-band.

The benefits of using the model during early design stages, easing design decisions and the successful prediction of failing resonators in slam-tests as well as the prediction of resonator temperatures and consequential shift in frequency are shown. The challenges of collecting and distilling simple but meaningful thermal parameters for use in the cross-heating section of the model are presented.

7B-5

2:00 pm **Theoretical and Experimental Investigation of Spurious Modes in a SAW Delay Line Based on Langasite**

Natalya Naumenko[1,2], Pascal Nicolay[3], Jochen Bardong[3]; [1]*Acousto-optical Research Center, National University of Science and Technology, Moscow, Russian Federation,* [2]*MTUCI, Moscow, Russian Federation,* [3]*Carinthian Tech Research (CTR AG), Villach, Austria*

Background, Motivation and Objective

SAW delay lines are widely used for wireless passive sensing of various quantities, like pressure and temperature. To reach the maximum sensitivity, the sensor signal must be of the highest possible clarity. It is therefore important to separate the desired signal from the overlapping spurious signals. However, the identification of spurious modes as well as the understanding of their physical nature may be a complicated problem, especially when the corresponding signals overlap with each other and/or with the main SAW signal in time and/or frequency domains. The number and type of spurious modes depend on the substrate material and geometry of the device. This work focused on the development of a systematic approach to investigate spurious modes in SAW delay lines. The method combines different theoretical and experimental techniques. It is applied to the analysis of an experimental delay line based on YX-Langasite (LGS).

Statement of Contribution/Methods

The analysis of the test YX-LGS delay line started with measurements of its transfer function (S21), whose spectrogram was then plotted in the time-frequency domain. The spectrogram displays the energy distribution over delay times and frequencies, which makes it possible to quickly localize the different propagating modes. To identify the spurious signals caused by bulk acoustic waves (BAWs) propagating along the surface, the measured frequency responses were compared to simulated responses obtained using the SDA-FEM-SDA numerical technique. Simulations for a substrate of finite thickness with non-zero propagation losses in LGS provided good agreement with experimental frequency responses, including multiple normal modes propagating in LGS plate. The signals caused by tilted BAWs reflected from the bottom were identified via rigorous analysis of the BAW slowness surface and comparison with the spectrogram obtained for the device with suppressed SAW signals. The anisotropy of LGS in the YX plane, which manifests itself through the concavity of the fast shear BAW sheet of the slowness surface and the fast variation of polarization vectors around the X+30° direction, results in the strong radiation of BAWs along X and X+60° directions and the coupling between the fast and slow shear BAWs propagating obliquely to the surface. These interfering modes generate few spurious signals in the spectrogram, whose position agree with simulation results.

Results/Discussion

A combination of numerical and experimental techniques was applied to the analysis of spurious signals in a SAW delay line based on YX-LGS. The identification of the physical nature of the spurious signals will enable designers to easily avoid the overlapping between the main and some of the strongest spurious signals by fine-tuning the geometrical parameters of the delay line. The developed approach will be further applied to other LGS orientations used in wireless sensors operating at high temperatures.

7B-6

2:15 pm **Analysis of the Spurious Lamb modes in Temperature Compensated LSAW hybrid Substrates**

Patrick Turner[1], Ventsislav Yantchev[2], Sean McHugh[1], Victor Plessky[3]; [1]*Resonant Inc., Santa Barbara, USA,* [2]*Uppsala University, Uppsala, Sweden,* [3]*GVR Trade SA, Chez-le-Bart, Switzerland*

Background, Motivation and Objective

Bonded LiTaO$_3$ (LT) wafers have demonstrated a reduced temperature coefficient of frequency while retaining (or even improving) the electromechanical coupling and wave-guiding properties of the leaky SAW IDTs. However, the performance of LSAW resonators fabricated on bonded wafers can be compromised by the existence of spurious modes in the vicinity of the resonant and anti-resonant frequencies of the IDT. Suppression of these modes is desirable, and various hybrid substrates have been studied with this in mind [1]. Here, we identify and analyze these spurious modes in LT/Si hybrid substrates using COMSOL finite element analysis, with the aim of minimizing their disruptive effects.

Statement of Contribution/Methods

Two types of spurious modes were identified, both are well guided within the LT plate: high order Lamb waves polarized predominantly in the sagittal plane, and quasi-shear plate modes. Lamb modes are excited in the vicinity of the resonator stopband and cause unwanted spurious responses. There are indications that inside the stopband, interaction between Lamb modes and LSAW take place due to the finite device dimensions, which in turn leads to an increased coupling to these modes. The effects of LT anisotropy on the Lamb wave localization are also studied here (see the Figure below).

Results/Discussion

The theoretical predictions are found to be in good agreement with the experiment. Furthermore, RF filter simulations including the excitation of spurious Lamb modes will be demonstrated. Design strategies to minimize ripples in the filter passband will be discussed.

[1] K. Y. Hashimoto, et al. "Recent development of temperature compensated SAW devices" Proc. IEEE Int. Ultrason. Symp. 2011.
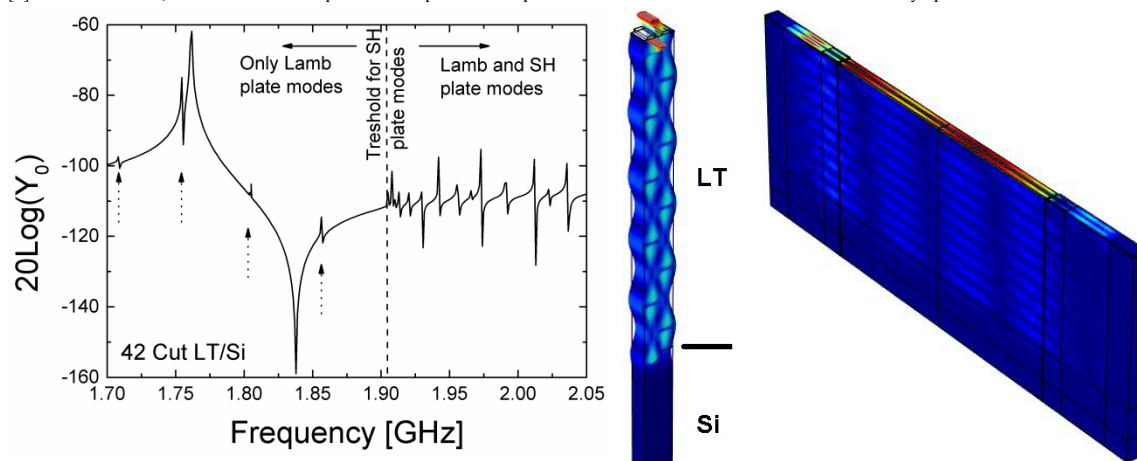
8B - CMUT Design

102

Thursday, October 22, 2015, 01:00 pm - 02:30 pm

Chair: **Levent Degertekin**
Georgia Institute of Technology

8B-1

1:00 pm **Experimental Study of Mutual Acoustic Coupling in CMUTs with Substrate-Embedded Springs**

Byung Chul Lee[1], Amin Nikoozadeh[1], Butrus T. Khuri-Yakub[1]; [1]*Stanford University, USA*

Background, Motivation and Objective

A CMUT with substrate-embedded springs, called PCMUT, has been demonstrated that provides non-flexural parallel-plate piston movement and improves the transducer performance (B.C. Lee et al, IUS 2014). Our 2D PCMUT element under investigation is composed of four unit cells that exhibit mutual acoustic coupling. Similar to a conventional CMUT array element, these cells′ interactions have to be carefully taken into account. In this paper, we report on the experimental measurements of the mutual acoustic coupling between PCMUT cells. We also experimentally evaluate the effect of a viscoelastic polymer on the mutual acoustic coupling of the PCMUT cells.

Statement of Contribution/Methods

We fabricated a single 2D PCMUT element composed of four cells using our second generation PCMUT fabrication process (B.C. Lee et al, IUS 2014). The 2D PCMUT element is designed for a full 2D array with a pitch of 280μm for a center frequency of 1.5MHz. A variety of measurements have been conducted on the fabricated device. The plate displacement of each PCMUT cell was measured with a laser Doppler vibrometer (LDV, Model OFV-511, Polytec GmbH). A hydrophone (Model HGL-0200, ONDA Corp.) was used to measure acoustic transient response of the device in vegetable oil. After evaluating the performance of the PCMUT device without viscoelastic polymer coating, we encapsulated the device with a 500μm layer of polydimethylsiloxane (PDMS, Dow Corning Sylgard 160). We compared hydrophone measurements with and without PDMS passivation in the far field to evaluate the effect of the viscoelastic polymer over the cell-to-cell interaction.

Results/Discussion

A scanning electron microscope image of the single 2D PCMUT element with four cells is shown in figure 1(a). The LDV measurement of the device shows the mutual coupling between cells (Fig. 1(b)). The acoustic transient responses and their corresponding frequency spectra from the hydrophone measurements with and without PDMS are depicted in figure 1(c). It is seen that the PDMS encapsulation widens the -3dB fractional bandwidth from 81% to 98% by suppressing the mutual interaction. Currently, we are working on simulating the effect of PDMS using our 3D finite element analysis model to further investigate the inter-element acoustic interactions in our 2X2, 2D PCMUT array elements.

This work is supported by National Institutes of Health and Analog Devices.

(a)   (b)   (c)
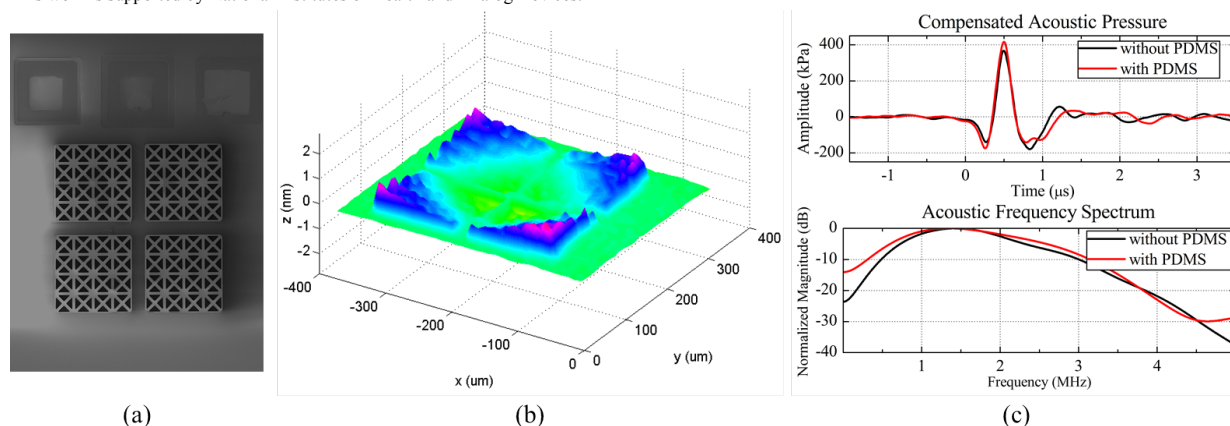
8B-2

1:15 pm **Fabrication of Capacitive Micromachined Ultrasonic Transducers with Through-Glass-Via Interconnects**

Xiao Zhang[1], F. Yalcin Yamaner[2], Omer Oralkan[1]; [1]*Department of Electrical and Computer Engineering, NCSU, Raleigh, North Carolina, USA, [2]Department of Electrical and Electronics Engineering, Istanbul Medipol University, Istanbul, Turkey*

Background, Motivation and Objective

The integration of CMUT transducers with supporting electronic circuits is critical for the overall efficiency of the CMUT-based imaging systems and for a compact form factor. The current interconnection methods for hybrid integration are based on TSV interconnects. Those strategies require a complicated insulation process to reduce the parasitics and also cause roughness and stress problems. An alternative method is to fabricate conducting pillars under each element by creating isolation trenches in a highly conducting silicon substrate. This process is also complicated and creates reliability problems. In this study, we present a fabrication process to make CMUT arrays with through-glass-via (TGV) interconnects. This new approach simplifies the overall fabrication process and helps reduce the parasitic interconnect capacitance and resistance, improving device performance and reliability.

Statement of Contribution/Methods

We demonstrated a novel fabrication method for CMUTs amenable to 3D integration by building MEMS structures directly on a TGV substrate. The fabrication process has 3 critical steps. First, hermetically sealed through-glass-via interconnects are formed by filling laser-drilled through channels in a 0.7-mm borosilicate glass wafer using a copper paste with a thermal coefficient of expansion matched to glass. The wafer is then sintered and polished until a smooth glass surface and a good copper-to-glass surface co-planarity are obtained. Second, 250-nm cavities are formed by plasma etching the glass and wet etching the copper vias to the same depth. A 140-nm Cr/Au layer is deposited in the cavities as the patterned bottom electrodes, which are connected to dedicated vias for each array element. Third, the device layer of an SOI wafer with a 200-nm PECVD silicon-nitride insulation layer on top is anodically bonded to the processed glass wafer to form the vibrating plate over the cavities.

Results/Discussion

The individual devices are probed from the backside for impedance measurements after grounding the top electrode through a Cr/Au contact evaporated on the conductive silicon-plate. A preliminary impedance measurement of a 2D array element shows the functionality of the fabricated device. The open-circuit resonant frequency of the CMUT element is measured as 4.47 MHz at -40-V DC voltage. Spring softening is observed as expected.

Borosilicate Glass   Copper   Chromium/Gold
Silicon Nitride   Silicon
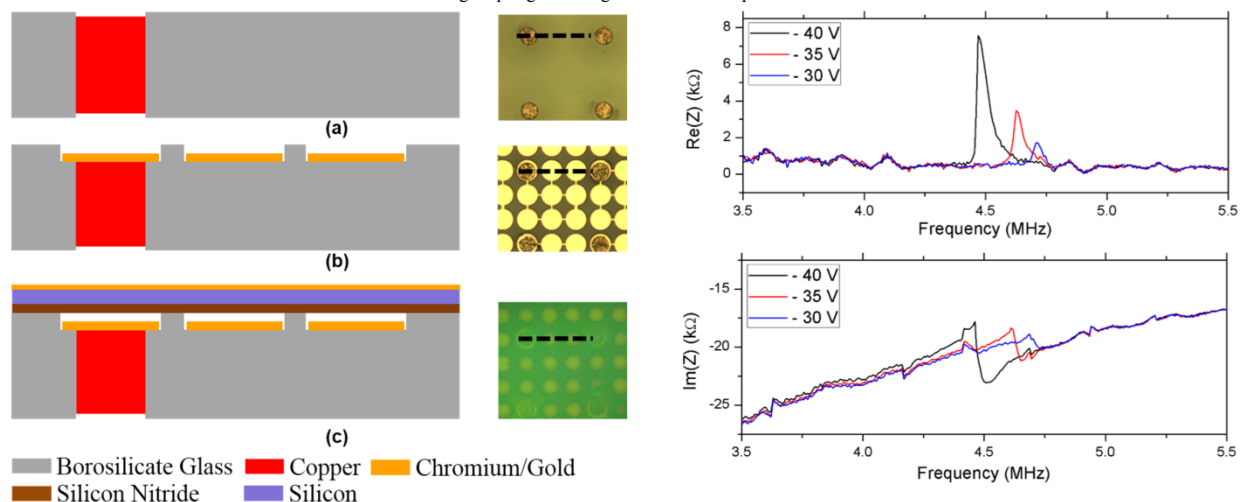
8B-3

1:30 pm   Highly Reliable CMUT Cell Structure with Reduced Dielectric Charging Effect

Shuntaro Machida[1], Taiichi Takezaki[1], Takashi Kobayashi[1], Hiroki Tanaka[1], Tatsuya Nagata[2]; *[1]Hitachi, Ltd., Tokyo, Japan, [2]Hitachi Aloka Medical, Ltd., Tokyo, Japan*

Background, Motivation and Objective

Capacitive micro-machined ultrasonic transducers (CMUTs), as an alternative of conventional piezoelectric transducers, have various advantages such as superior imaging quality and potential capability of circuit integration. However, CMUTs are hardly operated at high voltage to generate enough ultrasound power because the electrical charging effect of dielectrics in the CMUT cell degrades the receiving sensitivity after a long term operation. We propose a highly reliable CMUT cell structure which resolves the dielectric charging effect.

Statement of Contribution/Methods

The proposed CMUT cell structure reducing the dielectric charging effect has a spacer beneath the membrane and a partial opening in the top electrode just above the spacer. The fabricated CMUT cell was stressed by superimposed DC and AC voltages for a constant time. Before and after the stress, C-V characteristic of the CMUT cell was measured to evaluate the charging effect. The trapped charge (Q_{trap}) in the dielectrics was extracted from the shift of the voltage at the minimum capacitance value in the C-V curve.

Results/Discussion

The Q_{trap} in the conventional CMUT cell started to increase just after the maximum operating voltage (V_{max}) exceeded the collapse voltage (V_c) ($V_{max} / V_c > 1$). On the other hand, the Q_{trap} in the proposed CMUT cell remained almost constant up to $V_{max} / V_c = 1.4$ showing a drastic reduction of the dielectric charging effect.

The high endurance against the charging effect in the proposed CMUT cell structure is described as follows: The spacer limits the direct contact of the membrane with the bottom of the cavity even when the V_{max} exceeds the V_c. The direct current flow in the dielectrics between the electrodes is reduced by limiting the contacting area of the membrane. Moreover, the partial opening in the top electrode reduces the electric field around the spacer where the distance between the electrodes is closest at the maximum membrane displacement. Consequently, we reduced the dielectric charging effect in the CMUT cell structure realizing a high voltage operation of CMUTs with high reliability.
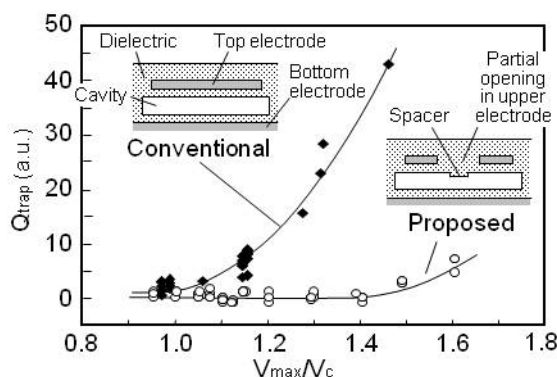
8B-4

1:45 pm   Fabrication of polymer bonded capacitive micromachined ultrasonic transducers (CMUTs)

Zhenhao Li[1], Albert I. H. Chen[1], Shuai Na[1], Lawrence Wong[1], John T. W. Yeow[1,2]; *[1]Systems Design Engineering, University of Waterloo, Waterloo, Ontario, Canada, [2]Waterloo Institude of Nanotechnology, University of Waterloo, Waterloo, Ontario, Canada*

Background, Motivation and Objective

Wafer bonding is often a preferred method over surface micromachining for CMUT fabrication because the resulting membrane layer is more uniform and can be easily optimized. Previously reported fusion bonding methods include SOI to SiO2 wafer and LPCVD SiN to SiN wafer. However, RMS roughness at the bonding interface is usually required to be less than 1 nm. While purchased SOI and SiO2 wafer pairs meet the roughness requirement, LPCVD SiN wafers need to be chemical mechanical

---

polished (CMP) to smoothen the surface. Although SiN is preferred as membrane material due to its high Young's modulus and electrical insulating property, the difficulties of CMP limit the use of SiN. Therefore, our objective is to fabricate CMUTs with LPCVD SiN membrane, but with no need of CMP.

Statement of Contribution/Methods

The polymer bonded CMUT is fabricated by:

1) Use LPCVD SiN wafer as top wafer and p+ Si wafer as bottom wafer.

2) Photosensitive bisbenzocyclobutene (photo-BCB) is spin coated on both the top and the bottom wafers with top wafer patterned with cavities.

3) Top and bottom wafers are then brought into contact in a vacuum chamber.

4) BCB curing at 150°C for 15 minutes followed by 250°C for 1 hour with compress pressure of 0.4 MPa.

5) KOH wet etching for SiN membrane release.

6) Cr/Al electrode deposition and patterning.

The resonant frequencies of the CMUTs are measured in air using a vibrometer. Acoustic characterizations include both pitch-catch and pulse-echo measurements done in immersion.

Results/Discussion

Initial attempts to fabricate photo-BCB CMUTs result in functional devices, with the resonant frequencies in the range of 10 to 20 MHz in air. The proposed process has three advantages: 1) Cavities patterning process is simplified by using photo-BCB; 2) Conformal coating of BCB lessens the wafer bonding requirement on surface roughness; 3) A maximum process temperature of 250°C (for BCB curing) results in a low temperature process that is suitable of monolithic integration of CMUTs on microelectronic circuits. While more characterizations still need to be done, initial results suggest that the proposed technique can be an attractive alternative for CMUT fabrications.

8B-5

2:00 pm   CMUTs with vented cavities and non-uniform squeeze films

Nikhil Apte[1], **Amin Nikoozadeh[1]**, Butrus (Pierre) T. Khuri-Yakub[1]; *[1]E. L. Ginzton Laboratory, Stanford University, USA*

Background, Motivation and Objective

CMUTs typically have a wide bandwidth when immersed in a liquid medium like water which makes them quite attractive for applications like medical ultrasound imaging. However, in airborne applications, CMUTs have a very narrow bandwidth. Previously we had proposed CMUTs with the cavity between the plate and the substrate vented to the ambient environment. Such CMUTs have additional damping due to the viscous and thermal losses in the squeeze film formed under the CMUT plate. In addition, such CMUTs also see some squeeze film stiffening due to the compression and rarefaction of the fluid during the motion of the CMUT plate. The design of such CMUTs involves optimizing these damping and stiffening effects.

Statement of Contribution/Methods

The squeeze film damping and stiffening effect depends largely on the squeeze number (σ) associated with it, where $\sigma=(12\mu\omega R^2)/(Ph^2)$. When designing the CMUT for a particular application, the plate radius (R) and gap height (h) can be selected to get a particular squeeze number. However the CMUT plate's radius is often constrained since it also controls the CMUT's frequency and its diffraction loss. Also it is usually desired to keep the gap height as small as possible for high transduction efficiency. This leaves very little room to optimize the squeeze film effect seen by the CMUT. To overcome this, we are proposing a squeeze film which has a non-uniform thickness. One way to achieve this is by etching holes or trenches in the substrate. By varying the size and location of these trenches, we can optimize the squeeze film effect.

Results/Discussion

We designed CMUTs with trenches etched in the substrate such that they form multiple cylindrical posts under the CMUT plate. The gap between the posts and the CMUT plate was kept small to increase the transduction efficiency. At the same time, the width of the trenches was varied to vary the squeeze film stiffening and damping effect. Our finite element model predicts that the bandwidth, sensitivity and frequency of the device can be varied significantly by varying the trench area. We have fabricated these devices and are currently characterizing them.
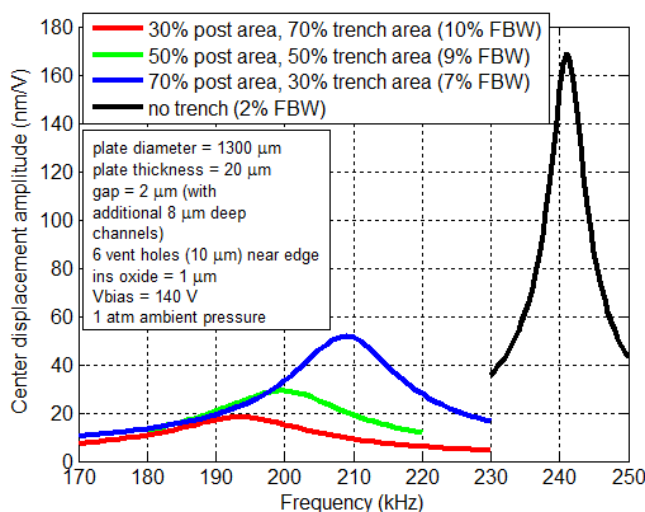
8B-6

A Commercialized High Frequency CMUT Probe for Medical Ultrasound Imaging

Danhua Zhao[1], Steve Zhuang[1], Ron Daigle[2]; *[1]Kolo Medical Inc, USA, [2]Verasonics Inc, USA*

Background, Motivation and Objective

CMUT probes have been introduced to the medical ultrasound imaging field for two decades. Compared to traditional PZT probes, CMUT probes have a number of advantages: wide bandwidth, easy volume fabrication, and high thermal efficiency. Despite many ultrasound equipment companies having spent great efforts developing commercial CMUT probes, few succeeded due to some of the well-known challenging problems associated with making CMUT transducers. Kolo Medical Inc, a CMUT

---

technology pioneer, has developed a number of advanced CMUT technologies to make commercial quality CMUT probes. Kolo has collaborated with Verasonics Inc to integrate CMUT probes into their state-of-art imaging system Vantage 128. This paper presents a 15 MHz CMUT linear array and its imaging results.

Statement of Contribution/Methods

One of the CMUT limitations is its low sensitivity when compared to its PZT counterpart. A. Savoia and his colleagues used a preamplifier (MAX4805) in their CMUT probe to boost the sensitivity [1]. Although the preamplifier can increase sensitivity, it can also produce unnecessary heat and lower the center frequency. Kolo Medical Inc. has recently developed a proprietary technology that combines CMUT fabrication and probe optimization to significantly increase sensitivity without utilizing a preamplifier for commercialization.

A commercial ready 15 MHz CMUT linear array probe was made with the advanced technology. The probe has 256 elements. A 2:1 multiplexer is utilized to connect the 256 elements to the 128 channels of the Verasonics Vantage 128 system. A DC-to-DC convertor is placed inside the ZIF connector to convert a low DC voltage ranging between +3.3 V and +12 V to any desired high bias voltage ranging from +120V to +250V.

Results/Discussion

The probe was tested both in water tank and on a phantom. A measured acoustic waveform is plotted in Fig. 1(a). The corresponding spectrum is plotted in Fig. 1(b). The center frequency is 15.7 MHz and the bandwidth is 93%. Fig. 1(c) shows a phantom image generated by a 10 MHz PZT probe while Fig. 1(d) shows the same phantom image generated by the 15 MHz CMUT probe on the Vantage 128 system. The detail resolution of the 15 MHz CMUT is significantly better than that of the 10 MHz PZT probe as expected.

(a)   (b)

(c)   (d)
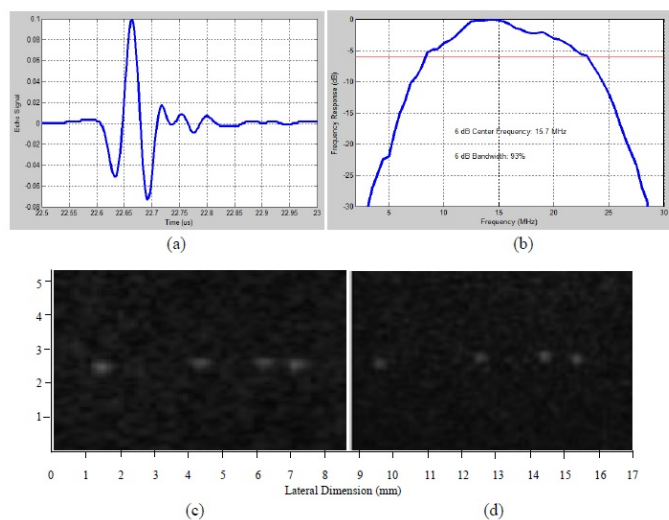
1C - MCA: High Temporal and Spatial Resolution Contrast Imaging

Plenary Hall

Thursday, October 22, 2015, 03:30 pm - 05:00 pm

Chair: **Ayache Bouakaz**
Inserm

1C-1

3:30 pm   **High Frame Rate Contrast-Enhanced Flow Vectorgraphy with Wide Velocity Estimation Dynamic Range Based on Multi-Band Processing**

Alfred C. H. Yu[1], Billy Y. S. Yiu[1]; *[1]Medical Engineering Program, University of Hong Kong, Pokfulam, Hong Kong*

Background, Motivation and Objective

While high frame rate (HFR) flow mapping is nowadays possible using plane waves, it remains non-trivial to accurately track flow patterns with high spatiotemporal variations. In particular, due to the inherently low signal from blood, it is not straightforward to design an effective flow vector estimator that can perform consistently over a wide range of flow speeds. Here, we report a new contrast-enhanced HFR flow vectorgraphy method to enable high dynamic range flow vector estimation. It is intended to achieve fine slow-time resolution needed for slow-flow detection while accounting for fast-flow Doppler aliasing.

Statement of Contribution/Methods

Our method involved three key principles: 1) plane wave excitation; 2) multi-harmonic slow-time analysis of contrast echoes; 3) multi-angle vector Doppler. A 3Tx-3Rx plane wave steering configuration was adopted (–10, 0, +10 deg; 10kHz PRF), as realized with an L14-5 probe on a SonixTouch scanner equipped with SonixDAQ. A 5 MHz Tx freq. was used to excite intravascular microbubbles (Definity-like; from 3% bolus injections) to elicit their harmonics. After beamforming, multi-harmonic slow-time processing was performed at each pixel as follows for each Tx-Rx angle pair. First, a filter bank was used to extract contrast-specific harmonics (5 bands between 4-9 MHz; 1 MHz steps). Next, for each band, mean Doppler freq. was estimated using the Kasai method (with 64-sample sliding windows). Linear regression was then performed on these Doppler estimates to derive unaliased flow estimate for that Tx-Rx angle pair. To derive the flow vector, the unaliased flow estimates from all Tx-Rx angle pairs were used as input to a 9 equations, 2 unknowns algebraic problem. The process was repeated at all time points to obtain HFR flow vectorgraphy cineloops. To test the framework's performance, we have conducted experiments on a bifurcation model with 50% stenosis (pulsatile flow; peak flow rate: 15ml/s).

Results/Discussion

The peak jet velocity measured using our method was 100 cm/s, while recirculation flow speed was as low as 3 cm/s. The resulting vectorgraphy maps consistently depicted flow jet and recirculation (Fig a), while those estimated from flow echoes only at fundamental freq. showed various spurious artifacts (Fig b). These findings show that multi-band contrast processing can enhance the robustness of HFR flow vector estimation.
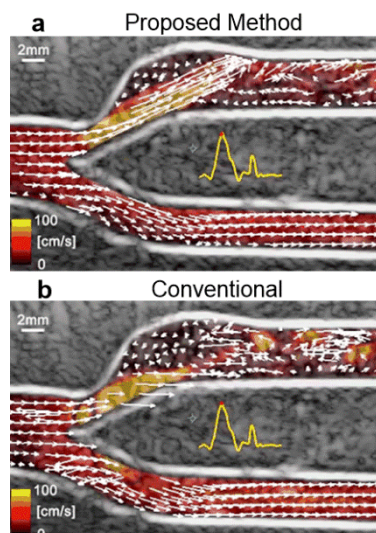
1C-2

3:45 pm   **Visualizing tumour perfusion with plane-wave contrast-enhanced Doppler: concepts and trade-offs**

Charles Tremblay-Darveau[1], Ross Williams[2], Paul S. Sheeran[1,2], Laurent Milot[2,3], Matthew Bruce[4], Peter N. Burns[1,2]; *[1]Medical Biophysics, University of Toronto, Toronto, Canada, [2]Sunnybrook Research Institute, Toronto, Canada, [3]Department of Medical Imaging, University of Toronto, Toronto, Canada, [4]Supersonic Imagine, Aix-en-Provence, France*

Background, Motivation and Objective

We demonstrated previously [1] that high frame-rate (5kHz or more) plane-wave ultrasound enables combined colour Doppler and contrast-enhanced (CE) imaging. The conduit flow can then be segmented from the capillary perfusion while maintaining imaging frame rate above 60Hz. Whereas accurate velocity estimates requires long driving pulses, short acoustic pulses must be used in CE-Doppler to maintain sufficient echo coherence over repeated insonation, thereby introducing new limitations in velocity estimates with autocorrelators. In this work, we demonstrate that the microbubble response can drastically affect the center frequency of the echo for broadband driving pulses. A model predicting the variance of autocorrelator-based velocity estimations with microbubbles is developed, and validated in vitro. Lastly, a mapping of the perfusion of a VX-2 tumour is produced as a proof of principle.

Statement of Contribution/Methods

A pulse-inversion Doppler (PID) [2] vector was acquired by repeatedly insonating Definity microbubbles with 4.5MHz center frequency low pressure plane-wave pulses of alternating polarity at high pulse repetition frequency (1-8kHz) using an Aixplorer scanner. Axial velocity estimation was performed using a 1D autocorrelator, and the standard deviation of the flow was then computed for a region of interest encompassing the center region of the vessel.

Results/Discussion

As a consequence of the large RF bandwidth, the center frequency of the nonlinear microbubble echo was recorded at 5.6 ± 0.3 MHz, which is lower than for the surrounding nonlinear tissue echo (7.5 ± 0.8 MHz). It follows that the center frequency must be compensated in order to avoid bias in velocity estimates with microbubbles. In addition, the experimental error on autocorrelator-based velocity estimates with microbubbles (Fig 1a) agrees with the proposed theoretical model (solid line), and depends only upon the SNR and coherence of the Doppler signal. Finally, the perfusion in a VX-2 tumour was assessed using PID. The resulting power Doppler (Fig1b) and combined perfusion-Doppler overlay (Fig1c) revealed more anatomic information than conventional CE-imaging, and opens the path to new imaging possibilities with ultrasound.

[1] C. Tremblay-Darveau et al. IEEE UFFC (2014), 61 (12), p. 1988-2000

[2] D. Hope Simpson et al. IEEE UFFC (2001), 48 (6), p.1483-1494
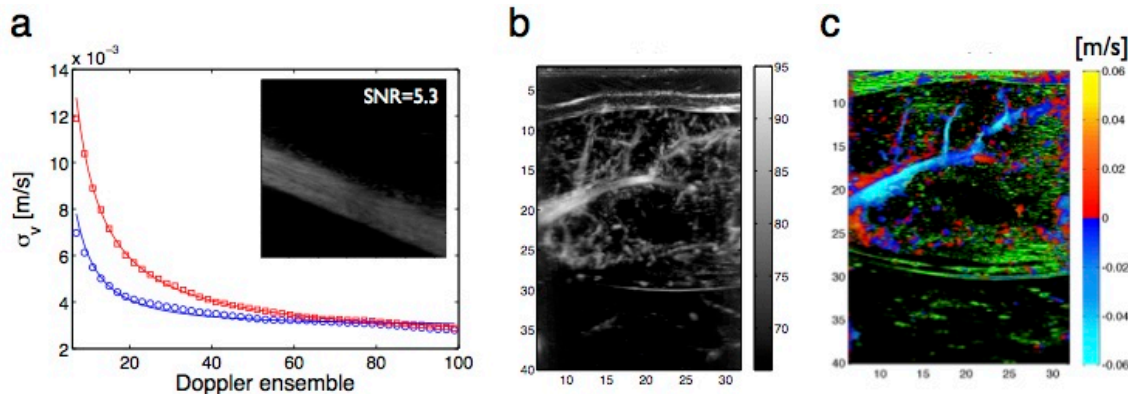
Fig1: a) Experimental velocity standard error evaluated from linear (blue circles) and nonlinear (red squares) signal. The solid lines are the theoretical predictions. b) Power Doppler and c) combined colour Doppler and perfusion (green colour map) imaging of a VX-2 tumour (Frame rate = 80Hz) in a rabbit.

1C-3

4:00 pm   Superresolution imaging of microbubble contrast agents

Robert Eckersley[1], K. Christensen-Jeffries[1], M. X. Tang[2], J. V. Hajnal[1], P. Aljabar[1], C. Dunsby[3, 4], *[1] Biomedical Engineering Department, Division of Imaging Sciences, King's College London, London SE1 7EH, UK., [2] Department of Bioengineering, Imperial College London, London SW7 2AZ, UK. , [3] Department of Physics, Imperial College London, London SW7 2AZ, UK, [4] Centre for Histopathology, Imperial College London, London W12 0NN, UK.*

Background, Motivation and Objective

Many diseases, such as those associated with diabetes, coronary heart disease, and the growth and metastasis of tumors exhibit architectural changes in micro-vascular structure, as well as variations in vascular flow. Current clinical imaging modalities such as MRI, PET, CT and Ultrasound cannot easily resolve the microvasculature. Although optical light microscopy is able to resolve structures on the scale of microvasculature, the restricted imaging depth of this approach is a major limitation. Thus, there is a clinical need for the development of new imaging techniques that can fill this resolution gap.

Statement of Contribution/Methods

Borrowing from ideas in super-resolution optical microscopy [1], the objective of our research is to enable 3D super-resolution ultrasound imaging of microvascular morphology and flow, using low MHz frequency ultrasound with high sensitivity, accuracy and depth penetration. This review will place our work in context with that of other groups working on related aspects [2,3] and describe our findings to date.

Results/Discussion

In previously published work [4,5] we used an unmodified clinical Ultrasound system in a standard contrast enhanced mode and demonstrated super-resolution imaging, in 2D, through the use of a low concentration of a microbubble contrast agents. The technique works through identification of individual bubble signals and the precise localisation of the origin of these signals. We included the first *in vivo* demonstration of this technique where structures under 20 μm are resolved using an US wavelength of 230 μm, and we extended our technique to enable velocity measurement in the detected microvasculature. More recent progress, that we have made, in terms of extension to 3D localization and improvements in microbubble identification and signal processing will also be discussed.

[1]   Stefan W Hell, Microscopy and its focal switch. Nature Methods Vol. 6 No. 1 January 2009
[2]   M. A. O'Reilly and K. Hynynen, "Super-resolution ultrasound method for brain vascular mapping," *Medical Physics* vol. 40, no. 11, *110701,* 2013.
[3]   Y. Desailly, O. Couture, M. Fink, M. Tanter, "Sono-activated ultrasound localization microscopy," *Appl. Phys. Lett.,* vol. 103, no. 17, pp. 174107, 2013.
[4]   O. M. Viessmann et al., "Acoustic super-resolution with ultrasound and microbubbles," *Phys. Med. Biol.,* vol. 58, no. 18, pp. 6447-6458, 2013.
[5]   K. Christensen-Jeffries et al., "In Vivo Acoustic Super-Resolution and Super-Resolved Velocity Mapping Using Microbubbles," IEEE Trans. Med. Imaging, 2014.

1C-4

4:30 pm   Ultrafast ultrasound localization microscopy of the living brain vasculature at the capillary scale

Claudia Errico[1], Juliette Pierre[1], Sophie Pezet[2], Yann Desailly[1], Zsolt Lenkei[2], Mickael Tanter[1], Olivier Couture[1]; *[1] Intitut Langevin, (ESPCI-ParisTech,CNRS UMR7587, INSERM ERL U979), Paris, France, [2] Brain Plasticity Unit (ESPCI-ParisTech, CNRS UMR 8249), Paris, France*

Background, Motivation and Objective

The resolution of conventional ultrasound imaging is diffraction limited and corresponds roughly to the ultrasonic wavelength (100 μm). We have previously introduced the concept of ultrasound localization microscopy (ULM) by extracting precise positions for thousands of individual microbubbles per second from their punctual echo in ultrafast images [Couture et al. 2011, Desailly et al. 2013], allowing to surpass the diffraction-limit by an order of magnitude.. Since intravenously injected microbubbles perfuse the entire vascular bed, the accumulation of their superlocalized echoes could precisely highlight the vasculature, in vivo at the microscopic scale. In this work, we show that ULM permits to overcome the trade-off between resolution and penetration, leading to a spatial reconstruction of the living rat brain vasculature down to the capillary level (<10 μm).

Statement of Contribution/Methods

The skull of anesthetized Sprague-Dawley rats was thinned and fixed in a stereotactic frame. Boluses of 200 μL microbubbles (2*10^9 microbubbles/mL) were delivered in the jugular vein. A linear array (15MHz, 128 elements) connected to an ultrafast clinical scanner (SSI, France) was placed coronally on the rat head at Bregma -1mm. Plane wave illumination continuously insonified the rat brain for 150s at 500Hz frame rate. Spatiotemporal filtering separated the fast decorrelation of the microbubble signal from the signals of slow moving blood and skull. Microbubbles were observed as unique and distinct sources. By deconvolving their individual point-spread-function, the axial position of microbubbles was localized one-by-one in depth. As the microbubbles could be observed over several images, their motion was also tracked over tens of milliseconds to determine the magnitude and orientation of their velocity vector.

Results/Discussion

In the rat brain cortex, up to 1 million individual bubble events could be detected within 150 s. The resulting map of microbubble positions was reconstructed with a resolution of λ/10 (10 μm), down to 3.5 mm in depth. In a coronal plane, vessels between 15 and 65 micron diameter were highlighted by several passing microbubbles. Branching vessels could be resolved starting from 16 um separation distance. The quantification of down and upstream flows further facilitated the discrimination between individual vessels. Bubble velocities ranged between 2 to 14 mm/s, which is consistent with the observed microvessel diameters. In conclusion, the millisecond time-resolution combined with the micrometric spatial resolution of ULM allows the comprehensive reconstruction of the vascular map of entire organs within tens of seconds, paving the way to ultrasound localization microscopy in preclinical and clinical studies.

1C-5

4:45 pm   Parametric Perfusion Imaging with Single-pixel Resolution and High Signal to Clutter Ratio

Diya Wang[1], Xuan Yang[1], Hong Hu[1], Hui Zhong[1], Lei Zhang[1], Mingxi Wan[1]; *[1]The Key Laboratory of Biomedical Information Engineering of Ministry of Education, Department of Biomedical Engineering,School of Life Science and Technology,Xi`an Jiaotong University, Xi`an, Shaanxi, China, People's Republic of*

Background, Motivation and Objective

Parametric perfusion imaging (PPI) extracted from time-intensity-curves (TICs) can depict quantitatively the spatial distribution of tumor perfusion information in liver cancer research. Its accuracy is related to signal-to-clutter ratio (SCR) of TICs and color-coded threshold. However, this SCR is limited by the malposition of region-of-interest (ROI) and TIC fluctuations induced by respiratory motion, which is exacerbated during selecting single-pixel ROI to obtain PPI with the highest resolution. And color-coded threshold decreases because the selected PPI region includes lots of invalid TICs from regions without microbubbles (MBs). The objective of this study was to obtain PPI accurately with single-pixel resolution by respiratory motion compensation combined with TICs filtration and denoising.

Statement of Contribution/Methods

First, a sequence of dynamic contrast images was divided into equal-sized ROIs of 1×1 pixel. Malpositions of all single-pixel ROIs were then corrected by motion displacements of targeted ROI estimated by a modified block matching algorithm. Next, TICs were then obtained from these corrected single-pixel ROIs, and invalid TICs whose correlation coefficients were lower than a correlation threshold decided by typical region without MBs were eliminated. Whereas the valid reserved TICs were filtered by the detrended fluctuation analysis and fitted to a lognormal bolus model to improve their SCR. Finally, color-coded PPI images were obtained based on the perfusion parameters extracted from these TICs with higher SCR.

Results/Discussion

Disturbances from respiratory motion and regions without MBs were effectively removed by our combined methods. SCR of TICs of a typical patient with gallbladder carcinoma invasion into the liver was improved by 5.49 ± 0.34 dB, and operation time of PPI decreased $50.4 \pm 0.1\%$. Hot spots distribution, perfusion detailed and edge characteristics of neovascularization in the invasion area were accurately distinguished and depicted by PPI with single-pixel resolution, especially the time to peak and wash out time. In summary, our combined methods can contribute to accurately make a clinical decision in liver cancer diagnoses using PPI with single-pixel resolution and sufficient perfusion information.
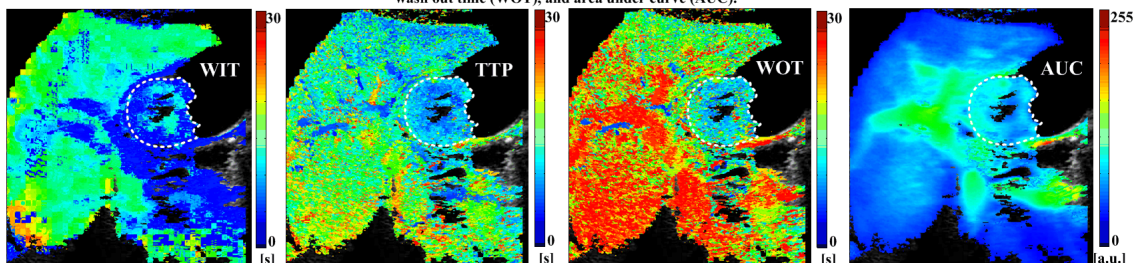

a) Typical dynamic contrast enhanced ultrasound images of a patient with gallbladder carcinoma invasion into liver
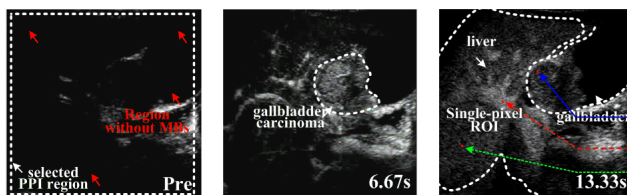
B) Single-pixel TICs in carcinoma area, hepatic vein and lobe
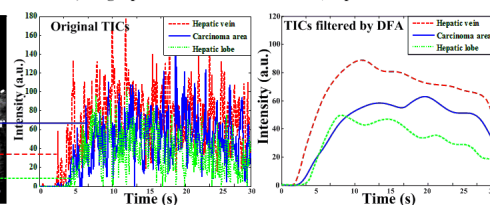
C) Parametric Perfusion images with single-pixel resolution including wash in time (WIT), time to peak (TTP), wash out time (WOT), and area under curve (AUC).

2C - MBF: New Vascular Mapping Tools

VIP

Thursday, October 22, 2015, 03:30 pm - 05:00 pm

Chair: **Damien Garcia**
University of Montreal

2C-1

3:30 pm **Functional connectivity of the mouse brain using transcranial functional ultrasound (fUS)**

Elodie Tiran[1], Jérémy Ferrier[2], Bruno-Félix Osmanski[1], Thomas Deffieux[1], Sophie Pezet[2], Zsolt Lenkei[2], Mickaël Tanter[1]; [1]*Institut Langevin, ESPCI-ParisTech, PSL University, INSERM U979, CNRS UMR7587, France*, [2]*Laboratoire de Neurobiologie, ESPCI-ParisTech, PSL University, CNRS UMR8249, France*

Background, Motivation and Objective

Recently, functional ultrasound (fUS) has been introduced as a powerful method to image intrinsic connectivity in the living rat brain through a thinned-skull window (Osmanski et al 2014). Resting state functional connectivity is of great medical interest since it is affected by neurological and psychiatric disorders such as schizophrenia, Alzheimer's disease, or depression. For pre-clinical studies, mouse is the reference animal model as a wide range of genetic models for neurological diseases is available. We investigated whether non-invasive mouse brain imaging is possible, i.e. without craniotomy or thinning the skull.

Statement of Contribution/Methods

A 15 MHz ultrasonic probe (0.110 mm pitch, 128 elements) with an ultrafast scanner (Aixplorer, SSI, France) was used to perform transcranial ultrafast imaging (5 tilted plane waves [-4 -2 0 2 4] °, 2500 Hz pulse repetition frequency) in anesthetized C57BL/6J RJ mice. 200 images were acquired for 0.4 s every 2 s during 10 min. Tissue signal was then removed by high-pass filtering of each 200 images block to get a single Doppler image every 2 s.

Two connectivity analysis approaches were investigated and compared: seed based connectivity analysis based on ROIs cross-correlations and unsupervised analysis based on Singular Value Decomposition (SVD) of Doppler data.

Results/Discussion

Transcranial mouse brain imaging (N=5) yielded very high Doppler image quality even through the skin (fig (a-b)). Both seed based correlation matrices and unsupervised modes could be obtained (fig (c-d): r [-0.03 0.87]). The link between both connectivity analysis approaches is investigated. Acquisition noise was found to affect mainly correlations involving deep and small structures, which required additional normalization.

Acquisition settings were optimized by assessing the stability of the correlation matrix coefficients versus repetition and acquisition times. According to our preliminary results, 180 s acquisition time seems to be a good compromise with a standard deviation of correlation coefficients of less than 0.1 versus a full acquisition (fig (e)).

In conclusion, we demonstrate high-quality non-invasive transcranial imaging of functional connectivity in the living mouse brain. This method is a promising tool for the functional analysis of the transgenic mice models of neurological and psychiatric disorders.
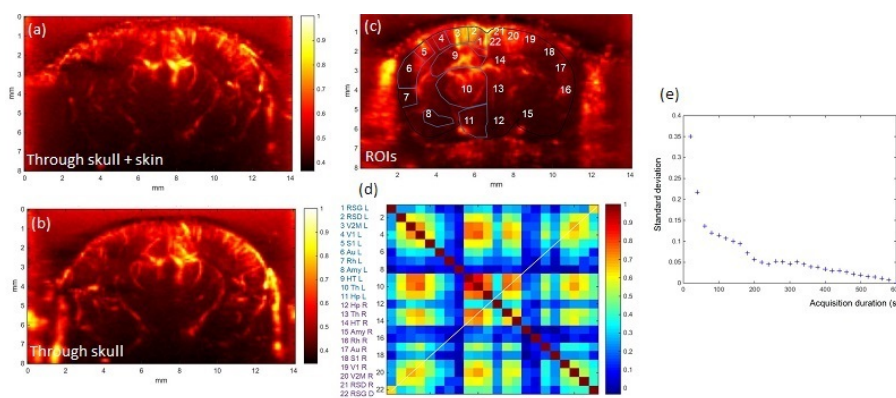
Figure: Transcranial Ultrafast Doppler images acquired on an anesthetized (ketamine 50mg/kg/h + medetomidine 0.5 mg/kg/h) mouse brain (a) through skull and skin or (b) through skull after removal of the skull skin. (c) Regions Of Interest (ROIs) mapping in a chosen imaging plane (~Bregma -2.3 mm) acquired on an anesthetized mouse and (d) the corresponding seed based correlation matrix. (e) Standard deviation of the difference matrix between a correlation matrix computed over the N first seconds of the acquisition and the correlation matrix computed over the whole acquisition duration (600 s).

2C-2

3:45 pm **Investigating functional ultrasound imaging for in vivo dissection of the visual pathway using light stimulations.**

Marc Gesnik[1], Laura Zamfirov[2], Paul-Henri Prevot[2], Laëtitia Duhamel[2], Serge Picaud[2], José-Alain Sahel[2], Mathias Fink[1], Thomas Deffieux[1], Jean-Luc Gennisson[1], Mickaël Tanter[1]; [1]*Institut Langevin, Paris, France*, [2]*Institut de la Vision, Paris, France*

Background, Motivation and Objective

Functional ultrasound (fUS) imaging of the brain is a recently developed technique for in vivo neurosciences with unprecedented spatial and temporal resolution. Thanks to an ultrafast scanner, the cerebral blood volume (CBV) can be acquired and mapped with a very high sensitivity. This sensitivity allows to detect subtle changes in CBV due to neurovascular coupling in areas of the brain where an evoked neuronal activity has been triggered. [1-2]

In this study, we designed a fUS set-up aiming to follow the spatiotemporal functional response of different visual stimuli patterns on in vivo rodent brains in 3D.

Statement of Contribution/Methods

In vivo experiments were performed on 11 anesthetized (urethane 1g/kg) and trepanned rats. A 15MHz ultrasonic probe (128 elements, 0.11mm pitch, Vermon, France), driven by an ultrafast scanner (Aixplorer, Supersonic Imagine, France) is translated on top of the brain over both visual cortex thanks to a motorized system (PI micos, VT80) .The ultrasonic sequence lasts 10 min, with every 2s, 200 frames acquired at 500 frames/s. Each frame is a coherent compounding of 11 planes waves with a 5500 Hz

pulse repetition frequency. The visual stimuli are created with a white LED in front of either the right or the left eye. One stimulus consists in 10s of flickering light at 5Hz repeated every minutes. Acquired data were high-pass filtered and correlated to the visual stimulation pattern to produce activation maps. Repeatability of the response for different patterns was studied to prepare for 3D scans.

Results/Discussion

Figure 1 presents the cerebral response induced in right and left hemisphere by illuminating the left and right eye respectively. A repeatable increase in CBV of $4.4\% \pm 2.4\%$ in vision involved areas is measured (N=18 acquisitions) and can be detected from a single flash (fig 1.c). Correlation coefficients up to 0.6 allow us to determine spatially the activated areas. We manage to access deep visual functions in brain, such as the colliculi, which are not accessible by classical techniques.

This work demonstrates the ability of fUS to reliably measure activation of cerebral visual areas using flickering light. FUS imaging could thus prove to be a valuable tool for research in visual restauration or visual disorders.

[1] Macé, Nat. Methods 2011 [2] Osmanski, Neuroimage 2014
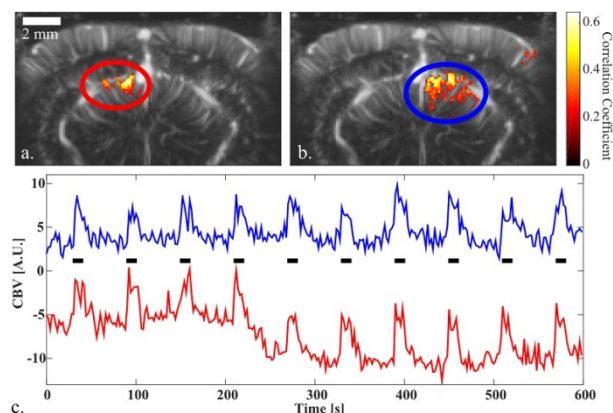
Figure 1: Functional activity of the brain in response to visual stimuli. a-b) Overlay of cerebral activation (colour scale) and brain vasculature (grey scale), a) (resp. b) activation of left (resp. right) hemisphere after stimulating right (resp. left) eye. Activated areas correspond to left and right colliculi. c) Time course of sensory-evoked activity for one acquisition. Blue (resp. Red) line: CBV in right (resp. left) colliculus after stimulating left (resp. right) eye, Black rectangles: periods of stimulation.

2C-3

4:00 pm   Non-invasive Estimation of Intravascular Pressure Changes using Ultrasound

Jacob Bjerring Olesen[1], Carlos Armando Villagómez-Hoyos[1], Marie Sand Traberg[1], Carsten Erik Thomsen[2], Jørgen Arendt Jensen[1]; [1]*Center for Fast Ultrasound Imaging, Dept. of Elec. Eng. DTU, Kgs. Lyngby, Denmark,* [2]*Dept. of Radiology, Copenhagen University Hospital, Copenhagen, Denmark*

Background, Motivation and Objective

Abnormal changes in intravascular blood pressure are an indication of a diseased vessel. Measuring the pressure variations is therefore used clinically as a diagnostic marker in assessing the physiological state of a vascular region. Today, pressure is assessed by inserting pressure sensing wires or catheters. These procedures suffer some severe limitations as they are highly invasive and require the use of ionising radiation for guidance. Further, literature has shown that catheters induce disturbances to the pressure field they are measuring leading to inaccuracies of up to 24%. This abstract presents a non-invasive method, which accurately displays the intravascular pressure distribution without the use of ionising radiation or having to undergo a surgical procedure.

Statement of Contribution/Methods

The proposed method estimates pressure from 2D vector velocity fields using a model based on the Navier-Stokes equations. Scans of a carotid phantom (Shelley Medical Imaging Technologies) with a 70% constriction are performed using a linear array transducer (BK8670, BK Medical) connected to the experimental scanner SARUS. Angle-independent velocity fields are acquired to a depth of 3cm using directional synthetic aperture flow imaging on series of 8 low-resolution images recorded with an fprf of 15 kHz. The performance of the estimator is evaluated by comparing its results to a 3D simulation model, where the geometry is reconstructed from MRI data.

Results/Discussion

The study showed pressure changes across the constricted phantom varying from -5 Pa to 7 Pa with a standard deviation of 4%. The proposed method had a normalised root-mean-square error of 10%, which is an improvement factor of 2.5 compared to invasive catheters. The figure shows intravascular pressure changes through three cardiac cycles. The center displays the individual pressure gradients along the white line seen on the B-mode image. Summing the individual gradients yields the drop in pressure that exists across the constricted region; this is plotted to the left. The result demonstrates that non-invasive pressure measurements are obtainable without the use of invasive devices and ionizing radiation. It further shows pressure estimates with an accuracy superior to invasive catheters while maintaining a frame rate in the order of kilohertz.
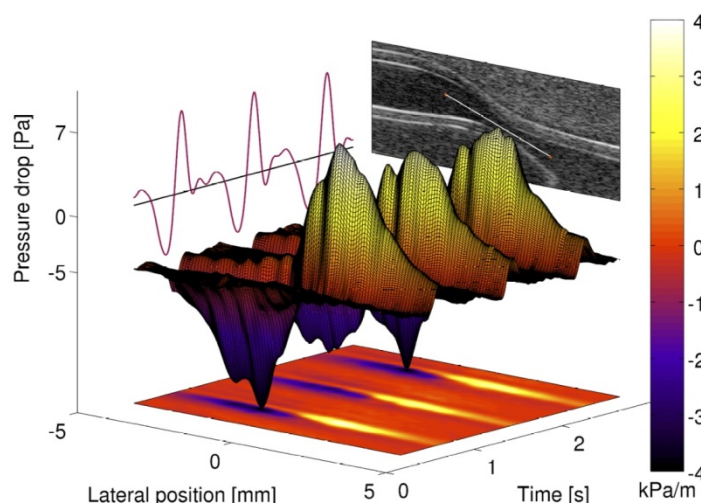
2C-4

4:15 pm   Ultrafast Doppler imaging of intramyocardial coronary arteries

David Maresca[1], Mafalda Correia[1], Olivier Villemain[1], Bijan Ghaleh[2], Mickael Tanter[1], Mathieu Pernot[1]; *[1]Institut Langevin, ESPCI ParisTech, CNRS UMR 7587, INSERM U979, Paris, France, [2]INSERM U955 Equipe 03, Université Paris Est Créteil et Ecole Nationale Vétérinaire d'Alfort, Maisons-Alfort, France*

Background, Motivation and Objective

Transthoracic echocardiography is recommended by international guidelines to assess wall motion abnormalities suggestive of coronary artery disease (CAD). As conventional Doppler imaging is not sensitive enough to assess myocardial perfusion, the risk stratification of CAD patients can be enhanced by performing myocardial contrast echocardiography (MCE). Unfortunately, MCE is scarcely used in clinical practice [1]. Here, we implemented ultrafast Doppler imaging combined with cardiac motion correction on a conventional 3 MHz cardiac phased array probe and successfully imaged intramyocardial coronary arteries without any contrast agent injection. In addition, the sensitivity of ultrafast Doppler imaging to changes in myocardial perfusion was positively assessed by measuring Doppler intensity in the myocardium during occlusion and reperfusion of the left circumflex (LCx) and left anterior descending (LAD) coronary territories.

Statement of Contribution/Methods

We used a 3 MHz phased array probe (96 elements, pitch of 0.2 mm) connected to a programmable ultrafast ultrasound scanner (Aixplorer, Supersonic Imagine, France). We insonified open chest pig hearts (N=3) in diastole with a dedicated ultrafast Doppler imaging sequence consisting of 8 diverging wave transmissions at a pulse repetition frequency of 1 kHz. Electrocardiograms and coronary volumetric flow rates measured invasively were registered during ultrasound acquisitions. Ultrafast datasets were beamformed and tissue clutter was separated from coronary signals with a sliding multidimensional filter based on spatiotemporal coherence analysis. Tissue Doppler imaging of the cardiac wall motion and ultrafast Doppler images of intramyocardial coronary arteries were computed and overlaid on ultrafast Bmode images to cross anatomical and functional information.

Results/Discussion

We successfully imaged intramyocardial coronary arteries in open chest pig hearts in early and late diastole. Time windows (< 100 ms) for coronary imaging corresponded to phases of the heart cycle where wall motion does not exceed 2 cm/s as assessed by Tissue Doppler. Ultrafast Doppler intensity changes in the myocardium during LCx and LAD occlusion and subsequent reperfusion were of the order of 70 percent which correlated positively with coronary flow rates measured invasively, whereas no significant drop was observed in Bmode intensities. Intramyocardial artery cross sections measured with ultrafast Doppler imaging went down to 150 µm. Next, ultrafast Doppler imaging of the coronary no-reflow mechanism will be investigated. Thanks to its very high sensitivity, ultrafast Doppler imaging of intramyocardial coronary arteries demonstrates strong clinical potential as an ultrasound-based coronarography technique free of any contrast agent injection.

[1] Montalescot G et al, 2013 ESC guidelines on the management of stable coronary artery disease. European heart journal 34 (2013)

2C-5

4:30 pm   Velocity measurement of the main portal vein with Transverse Oscillation

Andreas Hjelm Brandt[1], Kristoffer Lindskov Hansen[1], Michael Bachmann Nielsen[1], Jørgen Arendt Jensen[2]; *[1]Dept. of Radiology, Copenhagen University Hospital, Rigshospitalet, Denmark, [2]Center for Fast Ultrasound Imaging, Technical University of Denmark, Denmark*

Background, Motivation and Objective

The European Federation of Societies for Ultrasound in Medicine and Biology recommends examination of patients with suspected liver disease using Spectral Doppler Ultrasound (SDU) to evaluate blood flow in the main portal vein. Reduced velocities can indicate liver cirrhosis. Velocity measurements obtained with SDU are unreliable, when the insonation angle is >70 degrees to the main portal vein. The vector velocity method Transverse Oscillation (TO) measures velocity independently of the insonation angle. The hypothesis of this study is that TO can provide accurate velocity estimates in the main portal vein when compared to SDU.

Statement of Contribution/Methods

TO velocity measurements were performed with a 3 MHz convex probe (BK medical 8820e, Herlev, Denmark) connected to the experimental ultrasound scanner SARUS. SDU velocity measurements were performed with a commercial ultrasound scanner (UltraView 800, BK Medical, Herlev Denmark) and a convex probe (BK medical 6C2, Herlev, Denmark). Five healthy volunteers were scanned, and recordings of several heartbeats were conducted with two views. TO peak velocities and angle spread were calculated and averaged along the center line of the vessel. SDU peak velocities were gathered with the standard spectral Doppler setup. Each participant was scanned with both techniques within 5 min. TO and SDU peak velocities were compared using a paired t-test.

Results/Discussion

Results of all scans are shown in Table 1. TO peak velocities were not significantly different from SDU peak velocities (TO=0.250m/s, SDU=0.246m/s, (p=0.91), indicating that TO can provide accurate peak velocities in the main portal vein. SDU assumes a fixed insonation angle, but this angle fluctuates depending on irregularity of the vessel, irregular flow, and breathing pattern. Accuracy for TO has previously been reported to be around 3°, but the measured angle span was 12.7°- 67.7°. There is thus a large angle variability, when measuring flow in the portal vein. This greatly effects the peak velocity and cannot be detected with SDU. The TO convex array implementation

provides the first vector velocity measurements below 60 mm, and is a useful angle independent alternative for flow estimation in abdominal ultrasound. It may provide new information of abdominal fluid dynamics and yield both velocity and angle estimates for a more realistic flow characterization.

Table 1:

Intercostal views	VFI peak velocity (confidence interval) [m/s]	SDU peak velocity [m/s]	Mean insonation angle VFI (+/-SD) [deg]	SDU Angle correction [deg]	TO scan depth [mm]
Pat 1	0.25(0.22-0.29)	0.306	20.27 (+/-30.11)	53	85
Pat 2	0.31(0.28-0.35)	0.20	26.72 (+/-25.16	4	72
Pat 3	0.23(0.22-0.23)	0.24	26.41 (+/-12.70)	21	77
Pat 4	0.21(0.12-0.37)	0.19	4.16 (+/- 54.76)	8	76
Pat 5	0.18(0.17-0.19)	0.30	16.81 (+/-20.68)	15	81
Subcostal views	VFI peak velocity (confidence interval) [m/s]	SDU peak velocity [m/s]	Mean insonation angle VFI (+/-SD) [deg]	SDU Angle correction [deg]	NA
Pat 2	0.26(0.04-0.68)	0.15	72.74 (+/-67.68)	21	61
Pat 3	0.327(0.26-0.41)	0.36	99.77 (+/-36.88)	66	68
Pat 5	0.24(0.11-0.54)	0.23	77.56 (+/-63.77)	15	62

2C-6

4:45 pm   Intraoperative vector flow imaging of the ascending aorta: Is systolic backflow and atherosclerosis related?

Kristoffer Lindskov Hansen[1], Hasse Møller-Sørensen[2], Jesper Kjaergaard[3], Maiken Jensen[2], Jens Lund[4], Jørgen Arendt Jensen[5], Michael Bachmann Nielsen[1]*; [1]Department of Radiology, Rigshospitalet, Copenhagen University Hospital, Copenhagen, Denmark, [2]Department of Cardiothoracic Anesthesiology, Rigshospitalet, Copenhagen University Hospital, Copenhagen, Denmark, [3]Department of Cardiology, Rigshospitalet, Copenhagen University Hospital, Copenhagen, Denmark, [4]Department of Cardiothoracic Surgery, Rigshospitalet, Copenhagen University Hospital, Copenhagen, Denmark, [5]DTU Elektro, Center for Fast Ultrasound Imaging, Technical Univercity of Denmark, Lyngby, Denmark*

Background, Motivation and Objective

In the ascending aorta, atherosclerotic plaque formation, which is a risk factor for cerebrovascular events, most often occurs along the inner curvature. Atherosclerosis is a multifactorial disease but the predilection site for the aortic vessel degradation is probably flow dependent. To better understand the aortic flow and especially the complex flow patterns, the ascending aorta was scanned intraoperatively with the angle-independent and real-time vector velocity ultrasound method Transverse Oscillation (TO), in patients undergoing coronary by-pass surgery. The aim of the study was to analyze systolic backflow in relation to atherosclerosis.

Statement of Contribution/Methods

Thirteen patients with normal aortic valves were included in to the study (12 males and 1 female, mean age 66.1 y.o., range 41-80 y.o.). TO implemented on a conventional US scanner (ProFocus 2202 UltraView, BK Medical, Herlev, Denmark) with a linear array transducer (8670, BK Medical, Herlev, Denmark) was used intraoperatively on the ascending aorta in a long axis view. The presence of systolic backflow, visualized with TO, was correlated to aortic atherosclerosis, to systolic velocities obtained with transesophageal echocardiography and cardiac output obtained with pulmonary artery catheter thermodilution, to age, aortic diameter, left ventricular ejection fraction (LVEF) and previous myocardial infarctions (MI).

Results/Discussion

Systolic backflow in the ascending aorta was present for 38% (n=5) of the patients (Fig 1). The location of the backflow was strongly associated to the location of the plaques ($p<0.005$) and backflow was associated to high systolic velocities ($p<0.05$). Neither cardiac output ($p<0.52$), age ($p<0.49$), aortic diameter ($p<0.79$), LVEF ($p<0.59$) nor previous MI ($p<0.79$) were associated to systolic backflow. It was shown that systolic backflow is a common flow feature in the ascending aorta, and that backflow is strongly associated to atherosclerotic plaques and systolic velocities. The study indicates that vector flow imaging using TO can provide important blood flow information in the assessment of atherosclerosis.

Fig 1: Systolic backflow and atherosclerotic plaques along the inner curvature of the ascending aorta. The color map and vector arrows define velocity and direction of the flow. The black arrows mark the atherosclerotic plaques.
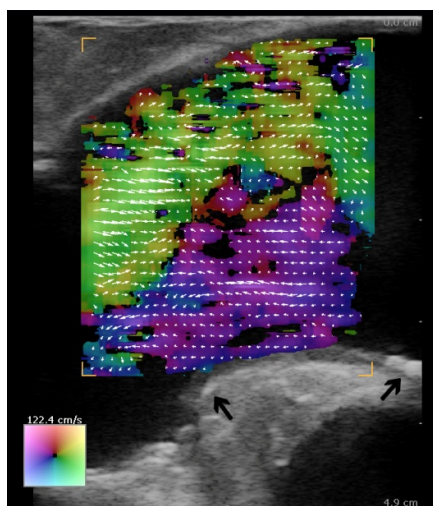
3C - MTH: Brain

201BC

Thursday, October 22, 2015, 03:30 pm - 05:00 pm

Chair:　　**Kullervo Hynynen**
　　　　　Univ. of Toronto

3C-1

3:30 pm　　**Pupil dilation and motor response elicitation by ultrasound neurostimulation**

Hermes Kamimura[1,2], Shutao Wang[1], Hong Chen[1], Qi Wang[1], Christian Aurup[1], Camilo Acosta[1], Antonio Carneiro[2], Elisa Konofagou[1]; [1]*Columbia University, New York, NY, USA,* [2]*University of Sao Paulo, Brazil*

Background, Motivation and Objective

Focused ultrasound (FUS) neurostimulation is a promising technique to drive neuronal activity. It has been presented as an alternative to overcome limitations of other techniques such as implantation of electrodes when using Deep Brain Stimulation, the poor spatial resolution ($\approx$1cm), inadequate depth penetration and short lasting effects (milliseconds) of Transcranial Magnetic Stimulation, and the gene modification required by optogenetics. Here, we explored motor- and cognitive-related brain regions of mice using US neurostimulation. The eye movements and pupil dilation were recorded to monitor the neural circuit activation of the mice.

Statement of Contribution/Methods

The experiments were performed in C57BL-6 anesthetized mice with intraperitoneal injection of sodium pentobarbital (65 mg/kg). The anesthesia level was assessed by the pedal reflex and vital signs recordings. FUS in the MHz range was used to achieve higher spatial resolution. The sonications of motor- and cognitive-related brain regions were carried out at 1.9 MHz with 50% duty cycle, pulse repetition frequency of 1 kHz, pulse duration of 1s, interval interstimulus of 1 s for 10 repetitions. Muscle activity was measured using an electromyography system with 26-gauge electrodes placed 5-mm apart in the biceps femoris in both hindlimbs and the ground electrode on the tail. The eye movements and pupil dilation were measured by a high-resolution camera focused the mouse eyes.

Results/Discussion

Motor responses including paws and tail movements were recorded on videos synchronized with the FUS. Contralateral muscle activity recorded on EMG signals was observed when the US neurostimulations were carried out at +2 mm of Lambda and ± 2 mm lateral of midline. Ipsi-lateral movements were observed in other regions of the sensory cortex. The minimum pressure to elicit movements was 2.26 MPa (calibrated in water). Higher pressures increased the success rate from 20% (at the threshold) to 70% (2.78 MPa). The estimated latency was 266 ± 37 ms. The sonication of eye-motor related and anxiety related regions of the brain elicited eyeball movements and pupil dilations of up to 20%. The superior colliculus region required a lower pressure threshold (1.6 MPa) to elicit pupil dilation. Other regions that are anxiety-related such as the hippocampus and locus coeruleus required higher pressure thresholds (>2.7 MPa) to elicit pupil dilations. The motor responses indicated the successful target specificity of the FUS neurostimulation using frequencies in the MHz-range. The pupil dilation response elicited by the FUS neurostimulation has important implications for cognition. Therefore, this technique may become an important tool for functional brain mapping to understand the brain complex network activity and connectivity.

3C-2

3:45 pm　　**Linearity of the Targeting Parameters and Gray-to-White-Matter Ratio Dependence on the Focused-Ultrasound Induced Blood-Brain Barrier Opening Volume across Non-Human Primates**

Maria Eleni (Marilena) Karakatsani[1], Gesthimani Samiotaki[1], Matthew Downs[1], Vincent Ferrera[2], Elisa Konofagou[1,3]; [1]*Biomedical Engineering, Columbia University, New York, NY, USA,* [2]*Neuroscience, Columbia University, New York, NY, USA,* [3]*Radiology, Columbia University, New York, NY, USA*

Background, Motivation and Objective

The application of FUS coupled with the systemic administration of microbubbles has been proved to open the Blood-Brain Barrier (BBB) locally, transiently and non-invasively in non-human primates (NHP). In this study, the dependence of the V_{BBB} on the FUS pressure, the incidence angle and the underlying structure of the brain region targeted is being established. The refraction angle, the shift in the geometric focus due to the skull aberrations and the dependence on the gray-to-white-matter ratio at the focus were also investigated.

Statement of Contribution/Methods

Five NHPs were sonicated using FUS (F_O: 500kHz; PRF: 2Hz; duration 120s; PNP 275-600 kPa) while being intravenously administered with monodisperse (4-5 micron in diameter), lipid-coated, gas-filled microbubbles. The NHPs were scanned in a 3T MR system (Achieva, Philips) acquiring 3D T1-weighted (T1w) post-contrast images for visualization of the induced opening. The estimation of the incidence and refraction angles as well as the center of the targeted region were established by projecting the ultrasound beam and the focus onto the BBB opening site detected on post-contrast T1w images. The opening size was scaled according to the skull thickness, through which the beam propagated, to account for energy losses. To quantify the shift, an automated intensity-based algorithm was designed to identify the centroid of the targeted region and the V_{BBB}. Finally, the opening was overlaid onto the brain region in a segmented T1w image to quantify the amount of gray matter (GM) and white matter (WM) that exhibited BBB opening.

Results/Discussion

It was found that the V_{BBB} increased linearly from 81.48±20 mm^3 to 454.86±50 mm^3 with an incidence angle ranging from 73.25±0.19° to 88.05±0.19° at 400 kPa. When the incidence angle was fixed at 76.62±0.19°, the V_{BBB} increased from 250.02±50 mm^3 to 858.05±50 mm^3 within the pressure range of 300-600 kPa. Repeated sonications at the same incidence angle and pressure, 81.24±0.66° and 300kPa, respectively, yielded consistent opening volumes of the order of 544.1±20mm^3. The determination coefficient between the incidence angle, the pressure and the V_{BBB} was 0.8243 (n=15), 0.84 (n=23) for the caudate and putamen regions and 0.9 (n=26) for the putamen region of the first day post sonication scans. The opening-to-targeting-shift varied from 2.08±1 mm to 4.2±2 mm axially and 0.7±0.5 mm to 2.6±2 mm laterally within a FUS beam incidence angle range of 17.4°, from 72.32° to 89.77° and an angle shift of 5.2±2.2° while the skull thickness ranged from 1.3±0.15 to 2.5±0.15 mm. Finally, although the targeting was planned in a region of 51.48±13.16% GM and 48.44±13.08% WM, the induced opening in the GM accounted for an average of 81.3±8.9% of the opening cases, while 19.2±9.1% occurred in the WM. This parametric optimization study identified thus the incidence angle range with the highest reproducibility and lowest aberration effects for NHP BBB opening in vivo.

3C-3

4:00 pm   **Enhanced intranasal brain drug delivery by focused ultrasound-activated microbubbles**

Hong Chen[1], Camilo Acosta[1], Carlos Sierra Sánchez[1], Marilena Karakatsani[1], Elisa Konofagou[1]; [1]*Columbia University, New York, NY, USA*

Background, Motivation and Objective

Neurotrophic factors are essential for the development, survival and function of neurons; however, their therapeutic use in the treatment of central nervous system diseases has been limited by their low blood-brain barrier (BBB) permeability and rapid breakdown in circulation. Intranasal (IN) administration is a promising approach for delivering neurotrophic factors directly to the brain, bypassing the BBB. However, IN delivery has low efficiency and does not provide localized delivery to specific brain sites. It has been assumed that the most likely mechanism for the widespread distribution of IN-administered drugs in the brain is the convective flow induced by the expansion and contraction of the perivascular spaces with the cardiac cycle, namely "perivascular pump" effect. Microbubble cavitation can also cause expansion and contraction of the perivascular spaces. Our previous study demonstrated the feasibility of using focused ultrasound (FUS) in combination with microbubbles for enhancing the delivery efficiency of IN-administered drugs in a targeted region. The objective of this study was to test the hypothesis that microbubble cavitation serves as microbubble-enhanced "perivascular pump", leading to enhanced drug transport within cerebral perivascular spaces.

Statement of Contribution/Methods

To test this hypothesis, wild-type mice were divided into two groups: (1) IN administration followed by FUS sonication (IN+FUS) and (2) FUS sonication followed by IN administration (FUS+IN). The hypothesized microbubble-enhanced "perivascular pump" effect only affected drug delivery outcomes in group 1, but not in group 2. In the IN+FUS group, IN administration of fluorescently-labeled 40 kDa dextrans was followed by FUS treatment of the caudate-putamen at one hemisphere in the presence of systemically administered microbubbles. In FUS+IN group, the same protocol was used with the only difference that pretreatment by FUS and microbubbles was followed immediately by IN-administration of dextrans. For both groups, the contralateral, non-treated caudate-putamen was used as control with IN only. Dextran delivery outcomes were evaluated using ex vivo fluorescence imaging.

Results/Discussion

The results showed that both IN+FUS and FUS+IN groups achieved enhanced dextran delivery at the FUS-targeted caudate-putamen region compared to the contralateral control with IN only. However, the fluorescence intensity of the IN+FUS group was on average 302% higher than the control with IN only; the FUS+IN group was only 121% higher than the control with IN only. The area of fluorescence enhancement achieved by the IN+FUS group was 2.4 times of that achieved by the FUS+IN group. The higher drug delivery obtained with IN+FUS over FUS+IN suggested that microbubble cavitation may serve as the microbubble-enhanced "perivascular pump", leading to enhanced delivery of IN-administered drugs. Supported by NIH grants R01 EB009041 and R01 AG038961.

3C-4

4:15 pm   **Dopaminergic neuron regeneration after Neurturin delivery through the FUS-induced BBB opening in a Parkinsonian model**

Gesthimani Samiotaki[1], Camilo Acosta[2], Maria Eleni Karakatsani[2], Shutao Wang[1], Elisa Konofagou[1]; [1]*Columbia University, New York, NY, USA*, [2]*Columbia University, USA*

Background, Motivation and Objective

FUS in conjunction with systemically administered microbubbles has been previously shown to open the Blood-Brain Barrier (BBB) locally, non-invasively and reversibly while the enhanced trans-BBB delivery of Neurturin has already been established in wild-type mice. Neurturin is a neurotrophic factor with regenerative effects on dopaminergic neurons, which are profoundly affected in Parkinson's disease. The objective of this study is to investigate the regenerative effects of NTN on the MPTP mouse model of PD following FUS-induced BBB opening.

Statement of Contribution/Methods

A total of 24 wild-type mice received a sub-acute MPTP regimen, and the lesions were allowed to stabilize for 4 weeks. Mice then received sonication or not and NTN or saline, they were divided in 3 groups, and they were allowed to survive for 4 weeks. The caudate-putamen and the substanita nigra were targeted using FUS (1.5 MHz, PRF: 10 Hz, 0.45 MPa, 10,000 cycles, 60 s) immediately after the IV administration of monodisperse bubbles. Following sonication, post-contrast T1-weighted, 3D MR images were acquired for detection of opening. Animals were survived for 28 days after treatment in order to allow for any neuroregeneration to occur. Animals were then sacrificed and their brains were collected for immunohistochemistry. To visualize the effect of the MPTP and the NTN treatment, brain samples were stained with an anti-TH antibody, a marker of DA neurons. Stereologically unbiased methods were performed in order to estimate the total number of TH-IR neurons in the SN in a standard manner. In the CP, a thresholding technique was used in order to visualize the difference in TH-immunoreactivity between the ipsilateral and the contralateral hemispheres, after the images were converted to grayscale. Two-way, mixed-factorial ANOVA was performed to detect the effects of FUS and NTN. Statistical significance was determined at an alpha level of 0.05. A post-hoc paired t-test within each group, were the FUS- side served as the intra-animal control in each case, in order to detect any difference in the number of TH+ cells in the FUS+ side.

Results/Discussion

Immunohistochemistry revealed more DA in the ipsilateral (FUS+) substantia nigra and caudate putamen (CP) only in the group where NTN was administered. Since the MPTP lesions and the DA neuronal apoptosis preceded NTN delivery, neuroregeneration was concluded for this group. Regarding the CP, some differences between the two sides were detected only in that group as well, as detected following thresholding. In this study, the neuroregenerative effects of the Neurturin neurotrophic factor through the FUS-induced BBB opening in a Parkinsonian mouse model were shown for the first time, suggesting the potential of this technique in the reversibility of the PD phenotype. A single administration of NTN achieved subtle but consistent increase in the number of neurons on the side of FUS-induced BBB opening, four weeks post-treatment.

3C-5

4:30 pm   **Improving targeting of ultrasound-mediated blood-brain barrier opening using chirp and random-based modulations**

Hermes Kamimura[1,2], Shutao Wang[1], Shih-Ying Wu[1], Marilena Karakatsani[1], Camilo Acosta[1], Antonio Carneiro[2], Elisa Konofagou[1]; [1]*Columbia University, New York, NY, USA,* [2]*University of Sao Paulo, Brazil*

Background, Motivation and Objective

The skull may distort the focused ultrasound (FUS) beam compromising accurate targeting of transcranial therapeutic ultrasound (US) applications. Large array transducers with phase and amplitude corrections of the signals have been proven capable of correcting aberration effects caused by the skull in *in vivo* studies. The use of short US pulses has also been reported to suppress standing wave formation in the brain *in vivo*. However, the efficacy of the random or chirp modulations have only been assessed in simulations or phantoms where many other parameters are disregarded such as the heterogeneity of the soft tissue, the variability of the drug uptake and clearance among subjects. In this study, the capability of the chirp- and random-based coded ultrasonic excitation in improving the targeting is investigated using an FUS-mediated blood brain barrier (BBB) opening protocol in mice.

Statement of Contribution/Methods

A FUS transducer (radius: 30 mm, focal length: 60 mm) was driven by an arbitrary waveform generator loaded with the chirp- and random-based coded ultrasonic excitation signals. The mice were positioned in a stereotaxic frame where a mixture of 1% isoflurane and oxygen was constantly delivered at 0.8 L/min through a mask. The mice were divided into 3 groups (n=15). Two groups were sonicated with the chirp and random coded excitation methods each with the same frequency bandwidth: 1.5-1.9 MHz, pressure: 0.52 MPa and duration: 30 s. The third group was sonicated with monofrequency pulsed US with frequency: 1.5 MHz, pressure: 0.52 MPa, burst duration: 20 ms, and equivalent duration: 5 min. All mice received tail vein injections of polydisperse microbubbles immediately before each sonication. The groups were sonicated in the

right caudate putamen with the left side kept as the control. Passive Cavitation Detection detected the bubble activity in real time inside the mice's brain. T1-weighted MRI using gadolinium confirmed the BBB opening and hematoxylin and eosin staining histology evaluated the safety.

Results/Discussion

The mean BBB opening volumes were 9.38 ± 5.71 mm^3, 8.91 ± 3.91 mm^3 and 35.47 ± 5.10 mm^3 for the chirp, random and conventional sonications, respectively. The mean cavitation levels were 55.40 ± 28.43 V.s, 63.87 ± 29.97 V.s and 356.52 ± 257.15 V.s for the chirp, random and conventional sonications, respectively. The coded excitation methods improved the targeting precision, generating lower cavitation levels and smaller opening volumes than the conventional sonication. Larger bandwidths produced more precise targeting but were limited by the frequency response of the transducer, the skull attenuation and the microbubbles optimum frequency range. The coded excitation methods may thus enable more precise drug delivery and it may benefit other FUS applications, such as ablation, that use higher-pressure levels and require precision to ablate or stimulate the targeted region without causing damage to the normal tissue.

3C-6

4:45 pm   Optimization of ultrasound-microbubble mediated drug transport in a new and realistic model of the human blood-brain barrier in vitro

Charles SENNOGA[1], Aya Zeghimi[1], Kayathiri Ganeshamoorthy[2], Pierre-Olivier Couraud[2], Ignacio Romero[2], Babette Weksler[2], Ayache Bouakaz[1]; *[1]Inserm U930, Université François-Rabelais de Tours, France, [2]Inserm 1016, Institut Cochin, Paris, France*

Background, Motivation and Objective

Non-invasive macromolecular transport across the blood-brain barrier (BBB) remains clinically challenging. As a result, a significant number of biotechnology agents engineered for brain therapeutics and/or diagnostics have limited efficacy *in vivo*. Although focused ultrasound (FUS) and microbubbles has been shown, not only to facilitate the transient opening of the BBB, but also to potentiate drug delivery into the brain parenchyma, the temporal and acoustic parameters needed to maintain physiological cell viability whilst ensuring efficient drug transport across the BBB have not been sufficiently optimized. Here we systematically examine the influence of insonation parameters on the permeability and post-sonication viability of a new and realistic human cerebral microvascular endothelial cell (hCMEC/D3) line. We use our findings to shed light on the mechanism(s) underlying ultrasound-induced opening of the BBB.

Statement of Contribution/Methods

hCMEC/D3 cells were cultured (5% CO_2, 37°C, 75% humidity) on 12-well inserts (0.4 µm size pores), until confluent. Permeability assays were performed by insonating hCMEC/D3 cell monolayers in the presence of 50 µM of the fluorescent drug mimic, *Lucifer Yellow* (lucY) and either BR14, MM1 (Bracco Research, Switzerland) or our in-house microbubble agent CT537 at 5 microbubbles/cell. hCMEC/D3 cell monolayers were insonated by using a calibrated transducer with a centre frequency of 1MHz (SoniGene sonoporator, VisualSonics, Inc), variable pressure, duty cycle (DC) and time. Protocol (1) 550 kPa, 1% DC, 120 sec; (2) 450 kPa, 3% DC, 60 sec, (3) 300 kPa, 10% DC, 60 sec. Successful BBB trans-migration of lucY was assessed by quantifying fluorescence emissions at 536 nm by using a microplate reader. All emissions were normalised against 1M Mannitol (without insonation) which is known to transiently destabilize hCMEC/D3 tight junctions (TJs). Cell viability was assessed by using propidium iodide. Ultrasound-induced opening of the BBB was assessed by using a combination of TEM, SEM and confocal epi-fluorescence.

Results/Discussion

Mannitol showed 100% effective transport of lucY and did not compromise cell viability. Protocols (1) and (2) exhibited significantly higher ($p<0.05$) rates of cell permeability and lucY transport (21%) as compared with Protocol (3) with lower permeability and transport (10.2%). Under similar insonation parameters, BR14 and MM1 microbubbles exhibit similar results, while the in-house microbubbles (CT537) returned comparatively lower lucY transport. TEM, SEM and confocal microscopy showed a strong correlation with increased hCMEC/D3 permeability, disruption of TJs and successful transport of lucY, suggesting that drug transport is potentially mediated by disruptions of TJs.

4C - MBB: Beamforming II

201DE

Thursday, October 22, 2015, 03:30 pm - 05:00 pm

Chair: **Jeremy Dahl**
Stanford University

4C-1

3:30 pm   Synthetic aperture imaging using a semi-analytic model for the transmit beams

Svetoslav Ivanov Nikolov[1], Jens Munk Hansen[1]; [1]*BK Ultrasound, Herlev, Denmark*

Background, Motivation and Objective

Many modern high-end scanners use some form for coherent synthesis of image lines by combining beams acquired with different transmissions, such as retrospective dynamic transmit focusing (Acuson / Siemens), nSIGHT (Philips), and Zone imaging (Zonare). There are two major strategies described in the literature to uniformly focus both transmit and receive beams throughout the field of view -using virtual sources, and by applying spatial matched filtration. The virtual source model is precise, when the transmit is either strongly focused (f-number 1, 2) or images are formed using circular or spherical waves. The spatial matched filtration can be used also with weakly focused transmissions, but requires the measurement and storage of the response of point targets within the limits of the transmit beam.

Statement of Contribution/Methods

This paper presents a semi-analytic model for the transmitted field, which can be applied to synthetic transmit imaging. The model is more precise than the virtual source concept, does not require the measurement of the transmit field as matched filtration methods do, and can be applied to both strongly and weakly focused transmissions. Furthermore, the model is applicable to tissue harmonic and contrast enhanced ultrasound imaging.

Results/Discussion

The paper presents the development of the model using the principles of diffraction, and its validation using computer simulations and measurements on a phantom. In Fig. 1, the model is validated against Field II simulations for varying f-numbers and focal depths. In Fig. 2, the model is used for synthetic aperture tissue harmonic in-vivo imaging. The same emissions are used for the two images, dynamic receive focusing (left), synthetic transmit aperture using the proposed model (right)

Fig. 1
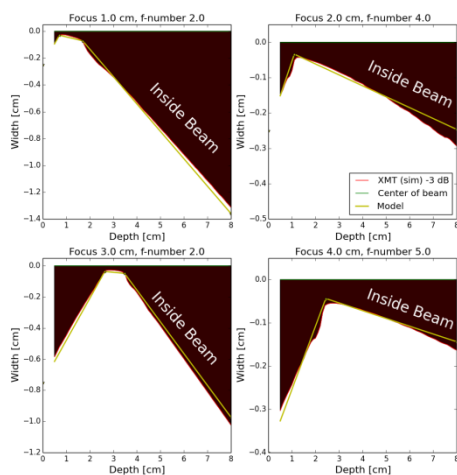
Fig. 2
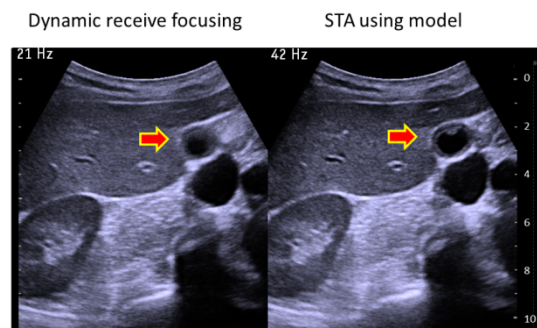
4C-2

3:45 pm   Increasing the Robustness and Convergence Rate of the Kaczmarz Method in Reconstructing the Speed of Sound (SoS) in Solid Materials using Analytical Signals

Leili Salehi[1], Georg Schmitz[2]; [1]*Department of Medical Engineering, Ruhr Universität Bochum, Bochum, Germany,* [2]*Department of Medical Engineering, Ruhr Universität Bochum, Germany*

Background, Motivation and Objective

To determine the mechanical properties and morphology of solid materials, tomographic imaging at relatively low frequencies is a promising option. However, mode conversions between compressional and shear waves require the use of non-linear tomographic methods taking multiple scattering into account. For this reason, we have presented an approach based on the Kaczmarz method. A necessary condition of convergence is that the accumulated phase difference between a wave propagating through the background medium and the correct solution has to be smaller than 2π. It means that the higher the contrasts the lower the imaging frequency has to be chosen.

In this work, we demonstrate that this restrictive convergence condition is mainly due to calculating the adjoint operator for the real wave field instead of its analytical extension to a complex wave field.

Statement of Contribution/Methods

A pseudo spectral time domain simulation for the complex wave field is performed for the forward propagation in a solution space of 91 mm × 91 mm full of a soft material with a convolutional perfectly matched layer on the borders. A set of simulated measurement data is obtained from a computer phantom. 36 point transducers for transmit and receive are distributed on a circle around the object with varying compressibility, shear modulus, and mass density. The object is insonified with pulse excitation (center frequency 100 kHz, bandwidth 87 kHz) using all transducers, consecutively.

The nonlinear forward wave propagation operator mapping the spatially varying bulk and shear moduli to the measurements on the borders is linearized by its Fréchet derivative. The error between the measured data and the outcome of the linearized operator on the borders is propagated back to the medium. Reconstruction is done applying the complex adjoint of the linearized forward operators to the wave field simulation data considering a constant mass density.

Results/Discussion

Figure 1 shows the Longitudinal SoS maps of the phantom (a), the reconstruction with complex and real calculations after 3600 iterations (b, c), and the SoS reconstruction errors using the same update step sizes (d). The results show that applying the complex calculations gives more robustness to the method and helps to increase the convergence rate choosing larger steps. However, the memory demand doubles for the complex calculations.

Figure 1.
a) Longitudinal SoS in Phantom (m/s)
b) Reconstructed Longitudinal SoS using Complex Data (m/s)
c) Reconstructed Longitudinal SoS using Real Data (m/s)
d) Reconstruction Errors (m/s)
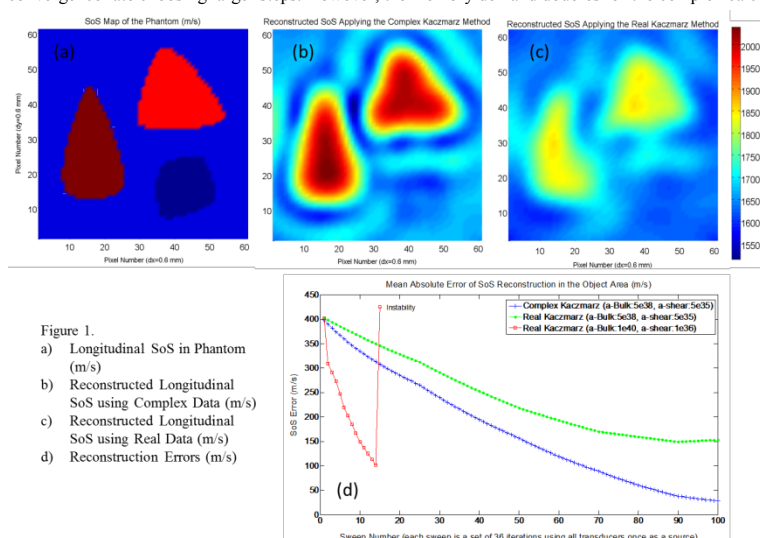
4C-3

4:00 pm   **Phantom and *in vivo* demonstration of swept synthetic aperture imaging**

Nick Bottenus[1], Will Long[1], David Bradway[1], Gregg Trahey[1,2]; *[1]Biomedical Engineering, Duke University, Durham, North Carolina, USA, [2]Radiology, Duke University, Durham, North Carolina, USA*

Background, Motivation and Objective

Ultrasound imaging of deep targets suffers from low lateral resolution due to limited aperture size and low-frequency transmit pulses. Mechanically sweeping the transducer in the imaging plane and coherently combining the backscattered echoes from all positions forms large synthetic transmit and receive apertures, increasing lateral resolution. Expected challenges in implementation include positioning accuracy, tissue motion and aberration. We present the first phantom and *in vivo* images produced using this swept synthetic aperture (SSA) technique.

Statement of Contribution/Methods

For each acquisition, channel data were acquired using a 3 MHz phased array transducer and a Verasonics ultrasound scanner at a pulse repetition frequency of 1 kHz for a duration of 1 second. The transducer was attached to a rotating aluminum arm at a distance of 10 cm from the center of rotation, manually swept in the imaging plane over approximately 45 degrees and tracked by a rotary encoder synchronized with the scanner. 3-D synthetic aperture beamforming was performed using a measured calibration of the transducer position relative to the axis of rotation and the known rotation angle to produce a high-resolution image in the plane of the sweep. A single-position full synthetic aperture image was acquired immediately before the sweep for comparison. Wire targets at a depth of 7.7 cm in 1540 m/s fluid were imaged to measure resolution. A fetal phantom and *in vivo* human arm in 1540 m/s fluid were imaged at depths of 10 cm and 7 cm respectively.

Results/Discussion

The -6 dB width of the wire target phantom was reduced by 80.5%, from 1.94 mm to 0.38 mm. The attached figure shows a comparison between a conventional, single-position synthetic aperture and SSA images. The SSA image of the fetal phantom target (left) demonstrates improved edge resolution of the ventricles and skull and finer speckle texture from the improved resolution produced by the larger effective aperture. Contrast between the ventricles (yellow circle) and background (cyan circle) was improved by 2.7 dB and contrast-to-noise ratio was improved by 66.3%. Clutter is present in the SSA image at depth due to strong reflection off the glass tank present across multiple imaging angles. Finer tissue layer structures are resolved in the *in vivo* arm image (right). We also discuss the k-space coverage and speckle texture of the resulting SSA image.

THURSDAY ORAL

4C-4
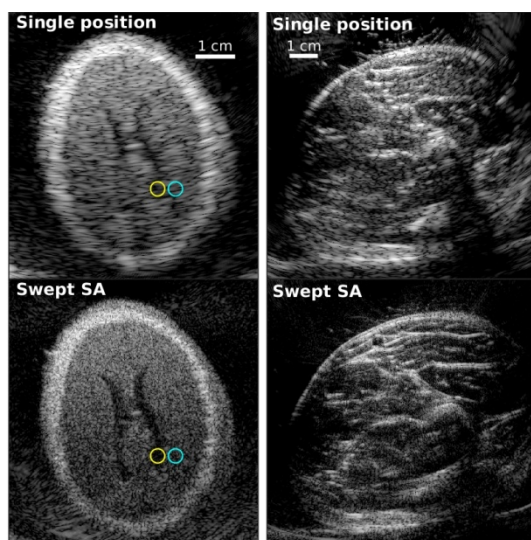
4:15 pm   **Real-time Channel Data Compression for Improved Software Beamforming Using Micro-beamforming with Error Compensation**

U-Wai Lok[1], Huai-Shun Shih[1], Pai-Chi Li[2]; [1]Biomedical Electronics and Bioinformatics, National Taiwan University, Taipei, Taiwan, [2]Electrical Engineering, National Taiwan University, Taipei, Taipei, Taiwan, Taiwan

Background, Motivation and Objective

GPU-based software beamforming has advantages over hardware-based beamforming because it is more programmable and complicated imaging algorithms can be efficiently implemented. However, the need for a high data transfer rate from the hardware front end to the software back end is a major technical challenge. To mitigate this issue, a micro-beamforming approach is proposed to reduce the data size by pre-steering and summing the channel data over small sub-apertures (Fig. A). However, grating lobes and other artifacts may appear and degrade image quality. In this study, we propose a modified micro-beamforming approach to achieve real-time date compression while minimizing the artifacts. First, the RF data are converted to baseband and micro-beamforming is only applied to the amplitude data while the phase data is unchanged. Second, a compensation factor is derived and applied to the sub-aperture amplitude beam sum at the software back end. Results show that the proposed approach can be implemented in real-time with minimal compression errors.

Statement of Contribution/Methods

As previously described, baseband data are converted from in phase/quadrature phase data to amplitude/phase data before micro-beaming is applied. The errors associated with the micro-beamforming approach is modeled as zero mean Gaussian distribution with a variance of σ^2. The compensation factor is derived by the centroid of the single-sided Gaussian distribution and this factor is applied to the micro-beamformed data at the software back end (Fig. B). For real-time implementation, the standard deviation is computed and a header is added at the hardware front end. Each micro-beamformed sample is compensated at the GPU software back end.

Results/Discussion

The micro-beamforming approach with and without error compensation was applied to the amplitude data from a tissue mimicking phantom to investigate its performance. Fig. C shows that lower mean square errors can be obtained for each beam data when the proposed compensation method is used. In addition, the peak-signal-to-noise ratio (PSNR) with error compensation has approximately 4 dB improvement as compared with the PSNR without compensation. However, lower compression ratio is achieved due to the need to include headers as shown in Fig. D. A compression ratio from 3.18 to 4 is achieved.

Conditions	Results
Compression ratio (amplitude data) w/o compensation	4
Compression ratio (amplitude data) with compensation	3.18
PSNR w/o compensation (dB)	60.52
PSNR with compensation (dB)	64.13
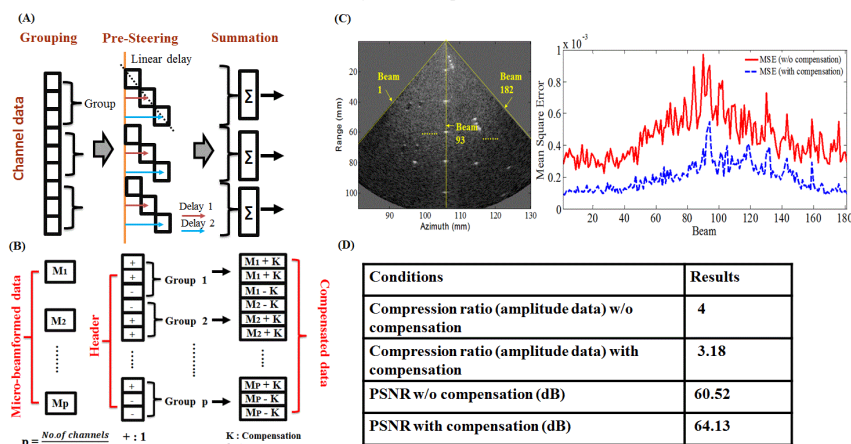
Figure **(A)** Illustration diagram of micro-beamforming approach, **(B)** Error compensation at the GPU back end, **(C)** Mean square errors of each beam data with and without the proposed method, and **(D)** PSNR and compression ability with and without the proposed compensation method where each group consists of 4 samples in this experiment.

4C-5

4:30 pm   **Real-Time High-Framerate In Vivo Cardiac SLSC Imaging on a GPU-Based Beamformer**

Dongwoon Hyun[1], Gregg Trahey[1], Jeremy Dahl[2]; [1]Biomedical Engineering, Duke University, Durham, NC, USA, [2]Radiology, Stanford University, Stanford, CA, USA

Background, Motivation and Objective

Coherence-based beamforming techniques such as short-lag spatial coherence (SLSC) have demonstrated clutter-suppressing capabilities in simulation, phantom, and *in vivo* experiments. However, the computational cost of SLSC has restricted these experiments to offline processing, or, with the aid of graphics processing unit (GPU) based computing, low frame rates on the order of <10 frames per second (fps). These frame rates are inadequate for fast-moving targets such as the heart. Our previous work has shown that spatial coherence estimation on uniform arrays is highly redundant, and that nearly identical coherence estimates can be obtained by making efficient use and approximations of the coherence function.

Statement of Contribution/Methods

A Verasonics research ultrasound scanner was used to acquire raw channel data using a P4-2v phased array transducer. A GPU-based beamformer was used to focus and beamform the data in real-time. Spatial downsampling of the aperture signals and single-sample covariance estimation, approximated from the phase difference of the channel signals, was utilized to improve computational speed on the GPU beamformer while improving axial resolution of SLSC images. Side-by-side B-mode and SLSC images, video clips, and frame rates were acquired from the real-time system in phantoms and *in vivo* hearts and livers.

Results/Discussion

With the efficient techniques, real-time SLSC imaging rates improved from 7 fps to up to 40 fps for a fixed field of view. The SLSC images demonstrated reduced clutter and yielded heart chamber CNR improvements of 49% compared to B-mode imaging. Fig. 1 shows a screenshot of the real-time system imaging a heart *in vivo*, with 30 dB of dynamic range for B-mode and SLSC values from 0 to 0.8. For an acquisition depth of 18 cm and 65 imaging lines, a frame rate of 17 fps was achieved with a relatively weak GPU (NVIDIA Quadro K620). The frame rate was inversely related to the number of image pixels: at 12 cm, the frame rate increased to 24 fps. Furthermore, the fps increased linearly with respect to the spatial downsampling factor and more than doubled with single-sample coherence estimation. Combined with the efficient coherence estimation techniques, software beamforming provides sufficient frame rates for real-time *in vivo* cardiac B-mode and SLSC imaging.
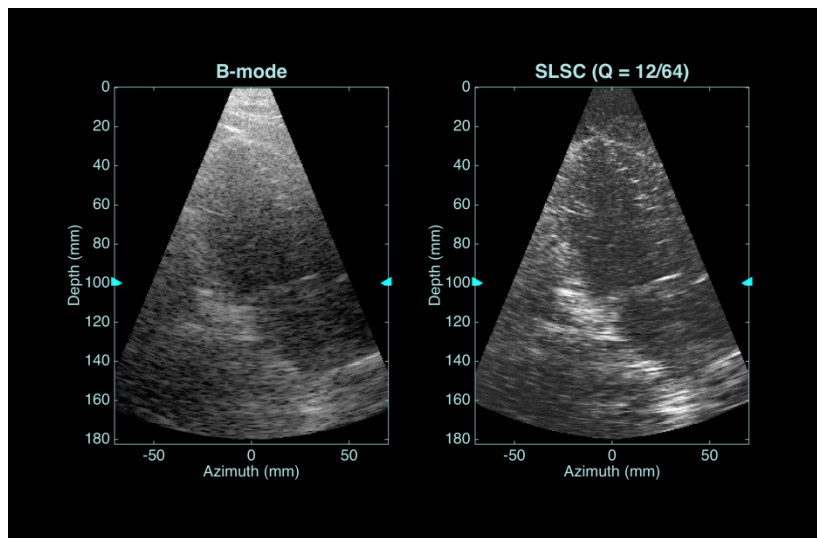
4C-6_____

4:45 pm   Linear Array Beamformation Using Virtual Sub-wavelength Receiving Elements

Shao-Yu Peng[1], Meng-Lin Li[1,2]; *[1]Dept. of Electrical Engineering, National Tsing Hua University, Hsinchu, Taiwan, [2]Institute of Photonics Technologies, National Tsing Hua University, Taiwan*

Background, Motivation and Objective

Generally, the grating-lobe artifacts can be avoided with array pitch smaller than one half of wavelength; however, due to cost or physical limitations, such a condition is hard to be satisfied in multi-dimension or high frequency array transducers. Besides grating lobes, sidelobe signals also affect imaging contrast and quality. To suppress the sidelobes, the window method such as Tukey window and Hamming window is widely used.

Statement of Contribution/Methods

To suppress grating lobes and sidelobes associated with linear arrays, we propose a novel linear array beamformation method based on a concept of virtual sub-wavelength receiving elements. Each array element is virtually divided into multiple sub-elements with sub-wavelength pitch. The signal detected by each virtual sub-element contributes to that of its physical element at different arrival time. Therefore, the signals of the virtual sub-elements from the same physical elements are approximated using the same signal received by their physical element. Delay-and-sum beamformation on receive is then done with the approximated signals and corresponding delays of the virtual sub-elements instead of using those of physical elements. Such a beamformation synthesizes a non-uniform sampled receive aperture with its mean effective array pitch smaller than one wavelength; thus the grating lobes can be suppressed. The sub-wavelength mean effective array pitch implies that better receive delay estimation, because of smaller effective receive elements, can be achieved, which plays the role of sidelobe suppression.

Results/Discussion

Wire phantom experiments using a research ultrasound engine (Prodigy, S-Sharp Corp., Taiwan) were performed to verify our idea. The figure showed the projected beampatterns of single plane wave imaging for a wire located at the depth of 12.5 mm, which were produced with a 128-element linear array transducer working at 6 MHz center frequency. The array pitch was 0.308 mm (~1.2 wavelength). Our method provided at least 5-dB suppression of the grating lobe and sidelobes, and rivaled the window method. Our method works for coherent plane wave compounding as well. Optimal sub-wavelength dividing of each physical element will also be presented.
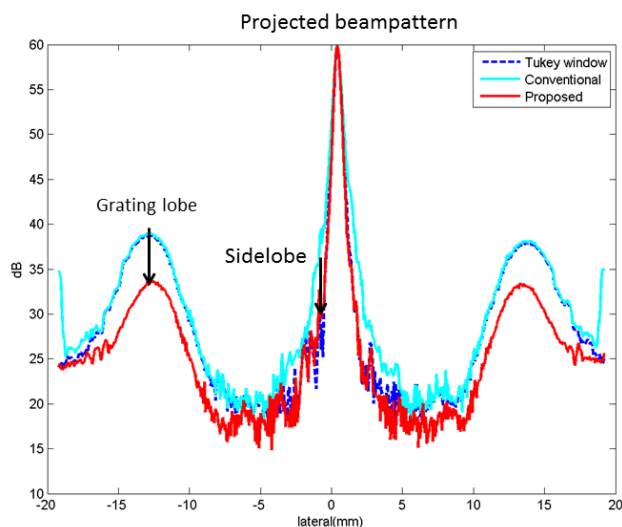
5C - NDE

103

Thursday, October 22, 2015, 03:30 pm - 05:00 pm

Chair: **Lawrence Kessler**
Sonoscan Inc.

5C-1

3:30 pm   **Measurement of the Clamping Force Applied by Load-Bearing Bolts Using a Combination of Compression and Shear Ultrasonic Waves**

Johan E. Carlson[1], Peter Lundin[2]; *[1]Div. of Signals and Systems, Lulea University of Technology, Lulea, Sweden, [2]Swerea KIMAB, Kista, Sweden*

Background, Motivation and Objective

Rods and bolts are commonly used as structural elements in a variety of applications. In the automotive and aviation industry they are used in engines and suspensions and in the energy industries they are used in reactor tanks, generator turbines etc. In infrastructural constructions, load bearing rods and bolts are used e.g. in railings and bridges. Concerning underground constructions, rock bolts are used to secure the stability of tunnels. To use a sufficient number of bolts with appropriate specifications and to mount them correctly is therefore of great importance not only for safety but also for economic reasons. Accurate methods for characterizing and monitoring the conditions of rock bolts and other structural elements would, in addition to increasing the safety, also enable an optimized use of the bolts as well as the whole structure.

Statement of Contribution/Methods

This paper presents laboratory results from using a combined compression and shear wave ultrasonic technique for measuring the torque applied to a rock bolt. When the bolts are loaded, the time of flight of compression and shear wave pulses are affected differently, since the dispersion due to the wave guide effects affect the two modes differently. Previous research suggests, however, that the ratio of the time of flight varies linearly with the applied torque. The main challenge is therefore to accurately estimate the time of flight of the two wave modes, even in the presence of dispersion and noise.

Results/Discussion

The paper show experimental results on a 1.1 m long 1" diameter epoxy covered rock bolt (Pretec AB, Göteborg, Sweden). A 5 MHz dual element transducer was used to transmit both the compression and shear wave pulse (Olympus D7066) and different methods for estimating the time of flights were evaluated. The figure below shows the ratio between the shear and compression time of flight as a function of the torque applied to the bolt. In this case the time of flight was estimated from pulses which propagated two and three times back and forth through the bolt, i.e. the propagated distance was 4.4 and 6.6 m, respectively.
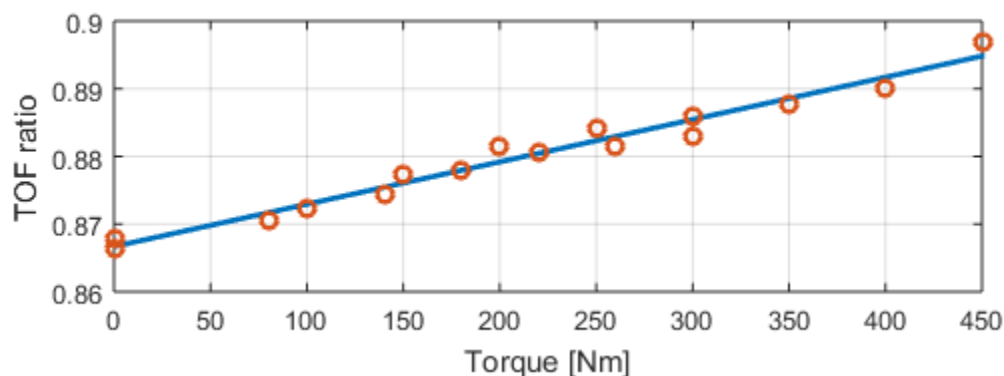
5C-2

3:45 pm   **Development and Application of Guided Wave Technology for Buried Piping Examination in Nuclear Power Plant**

Kuang-Chih Pei[1], Hung-Fa Shyu[1], Bing-Hung Lee[2], Jean-Chung Toung[3]; *[1]Nondestructive Testing Lab.,NFMD, Institute of Nuclear Energy Research, Taoyuan City, Taiwan, [2]Taiwan Metal Quality Control CO., Taiwan, [3]Taiwan Power Company, Taiwan*

Background, Motivation and Objective

Guided wave (GW) technology, well used in petrochemical industries and academic field for pipeline inspection, were studied on assessing the integrity of buried pipes in nuclear power plant (NPP). Since GW does not require direct access to the entire examination surface and can be used to screen relatively large component areas from a single probe location, this provides a potential method to examine inaccessible portions of the pipeline, such as the buried pipes. However, the damping, due to the anticorrosive coating, soil texture and pressure, certainly caused serious attenuation during GW propagation. A considerable range of inspection could be reduced.

Statement of Contribution/Methods

In this research, a field experiment was conducted to verify and quantify the attenuation rate caused by different coatings, soil pressures and pipe sizes. The site inspection could offer not only the data for analysis but the uncertainty study of the underground environment for process development. The GW records from a series of examinations on 10 different pipes were compared and analyzed after a designed process for inter-pipe normalization.

Results/Discussion

The test results indicate the relation (equation) between soil pressure and attenuation rate, so as the influence over GW attenuation by the different pipe coating under different GW main frequencies. More than the field tests, real GW inspection was applied on an abandoned 10-inch raw-water pipeline buried for NPP construction 40 years ago. Three positions were excavated for inspections. The results shown here demonstrate a successful evaluation using the GW method on a buried pipe in NPP environment.
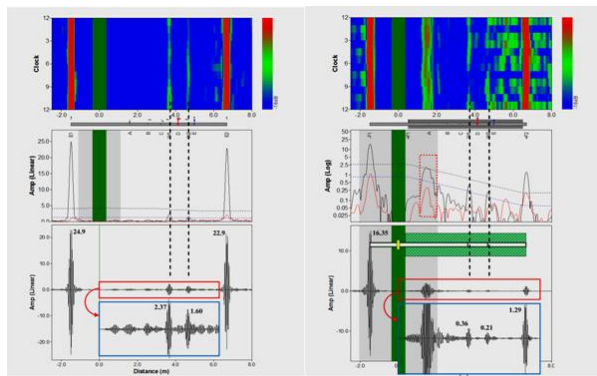
The difference of GW signals in 6-inch bare pipe (left) and buried pipe (right)
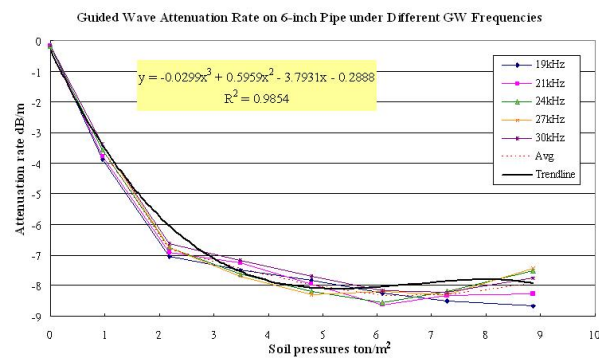
5C-3

4:00 pm   Attenuation and Phase Compensation for Guided Wave Based Inspection Using a Filter Approach

Christian Kexel[1], **Joel Harley[2]**, Jochen Moll[1]; [1]*Department of Physics, Goethe University of Frankfurt, Germany,* [2]*Department of Electrical and Computer Engineering, University of Utah, Salt Lake City, UT, USA*

Background, Motivation and Objective

Structural health monitoring using guided waves (GW) has received great attention recently. However, detecting and characterizing defects in plate-like structures by means of GW is complicated due to their dispersive nature. Imaging, e.g. based on compressed sensing, benefits from dispersion compensation due to the reduced computational burden of requiring fewer atoms in the dictionary matrices. Yet, most current dispersion compensation methods require prior knowledge about the guided wave's dispersive properties. For many scenarios, this information is unavailable. In this paper, we present a new, *data-driven* dispersion compensation method that requires no a priori information.

Statement of Contribution/Methods

We analyze data obtained by a scanning laser doppler vibrometer (SLDV) of an isotropic aluminum plate. We propose a time-domain preprocessing step comprised of the generation of a non-dispersive reference signal and a FIR filter, which reconstructs the amplitude and phase of the measured signal by solving a least-squares problem involving both signals. The reference signal is modeled as a tone burst (with some center frequency and number of cycles) and the group velocity is estimated in a data-driven manner from an early subset of the measurements. An efficient implementation of our processing via shared-memory parallelisation is shown in Figure 1.

Results/Discussion

We demonstrate the compensation of attenuation and phase-effects between the measured and filtered pulse in Figure 2. The figure shows that the measured data is transformed into three identical, delayed pulses. In our paper, we discuss the limitations of our approach as well as its application for enhancing the resolution of current acoustic wavefield imaging methods.
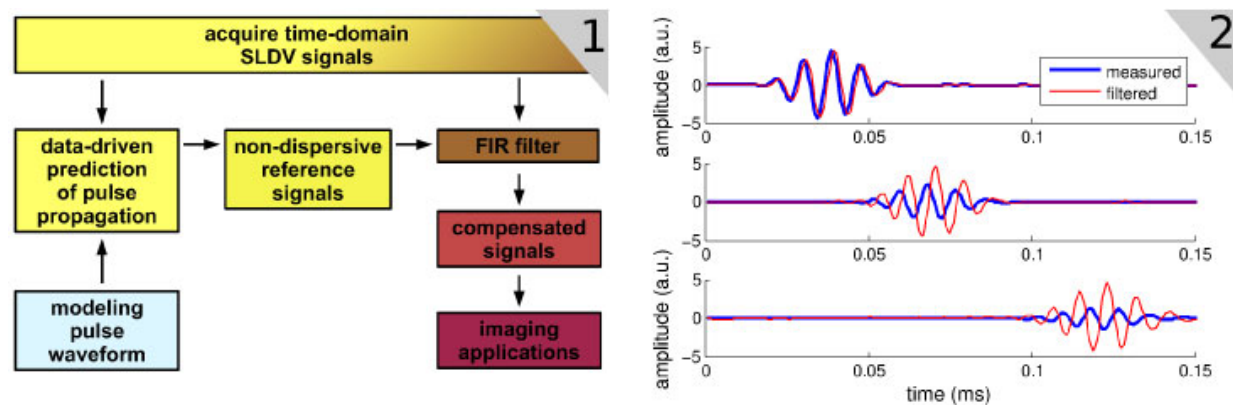
5C-4

4:15 pm   Numerical simulations of ultrasonic flexural waves in cased wellbores and evaluations of the cement bond quality

Xiao He[1], Hao Chen[1], Xiuming Wang[1]; [1]*State Key Laboratory of Acoustics, Institute of Acoustics, Chinese Academy of Sciences, Beijing, China, People's Republic of*

Background, Motivation and Objective

Cement bond quality is significant to productivity and security of a cased wellbore in the oil/gas field. The ultrasonic flexural-wave evaluation is a potential way to detect the debonding which appears at the cement sheath interfaces. In this paper, we present the ultrasonic wavefields in a multilayered cased hole and reveal the flexural wave responses to defects at the cement annulus.

Statement of Contribution/Methods

To excite and record Lamb waves of the flexural modes, an inclined pitch-catch sonic system is arranged inside the steel casing. The wavefields in the layered media are modeled by the 2D/3D finite difference methods. The following kinds of models are considered: (1) the cased hole is well bonded; (2) debonding appears at the casing-cement interface; (3) debonding appears at the cement-formation interfaces; and (4) sector defects exist in the annulus. We also investigate the influence of cement acoustic impedance on the evaluation results.

Results/Discussion

It is found that two groups of flexural waves are prominent in the wavefields. They are the primary flexural (PF) waves arriving early and the secondary flexural (SF) modes received by the transducers later. If a fluid-filled channel appears at the casing-cement interface, the PF-wave attenuation will decrease with the increasing width of the debonding. In contrast, the energy of SF waves will be greatly enhanced if the channel is located between the cement and the formation (Fig. 1). For a 250-kHz sonic transmitter, the resolution of detection for a sector defect is about 5-10 degrees. Hence it is possible to effectively evaluate the bond quality of the cement annulus by extracting the properties of ultrasonic flexural waves.
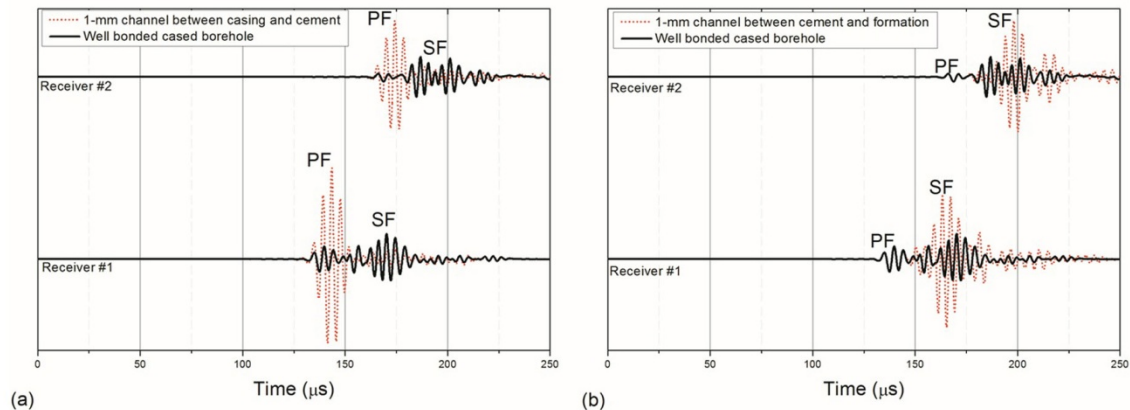
Fig. 1. Numerical simulations of ultrasonic flexural wave responses. (a) Well bonded cased hole and borehole with debonding at the casing-cement interface. (b) Well bonded cased hole and borehole with debonding at the cement-formation interface.

5C-5

4:30 pm   Laser ultrasound imaging of defects in curved structures with a flexible ultrasonic transducer

Makiko Kobayashi[1], Chin-Chi Chen[2], **Tai-Chieh Wu[2]**, Po-Hsieh Tung[2], Che-Hua Yang[2]; [1]*Graduate School of Science and Technology, Kumamoto University, Japan,* [2]*College of Mechanical and Electrical Engineering, National Taipei University of Technology, Taiwan*

Background, Motivation and Objective

In the manufacturing industrial structures with curved surfaces such as pipes, non-destructive testing during operation has been desired since defects and interior cracks could happen due to impact shock and vibration. Laser ultrasound visualization (LUV) system, which employs the pulsed laser to scan over the surface of monitoring area and an ultrasonic transducer to detect defects, could be an ideal solution since laser can generate all modes of ultrasound including guided waves so that it is suitable for fast scanning of large area. However, the traditional transducers generally lack curved surface adaptability, high temperature durability and broad bandwidth and it counteracts advantages of laser usage.

Statement of Contribution/Methods

The LUV system employs a gyro-scanning laser for the generation of ultrasonic waves which are detected with a contact transducer on a curved surface. A high temperature broadband flexible ultrasonic transducer (FUT) was employed for LUV system instead of a traditional transducer. Piezoelectric film of the FUT was made by PZT/PZT sol-gel composite. The mixture of PZT sol-gel solution and PZT powders was sprayed on 55µm thickness stainless steel substrate. The heating processes were operated after spray coating process and those processes were repeated until the desired thickness was reached. ~9MHz FUT was incorporated with LUV system for acoustic wave propagation monitoring along the tube with 50 mm diameter and 3 mm thickness. In this experiment, the tube specimen had an internal defect with 2 mm diameter and 2 mm depth.

Results/Discussion

A sequence of imaging frames captured by the LUV system are shown in Fig. 1. At least two guided modes are observed. Echoes from the defect can be observed for the faster mode (L(0,2)) at 6.04 µs, and for the slower mode (L(0,1))in the later frames with larger amplitude. The wave fronts of reflected echoes and scattered echoes from the defect was clearly observed from these images. Therefore, it could be concluded that LUV system with FUT is a novel technique and it has excellent potential in inspection applications.

5C-6
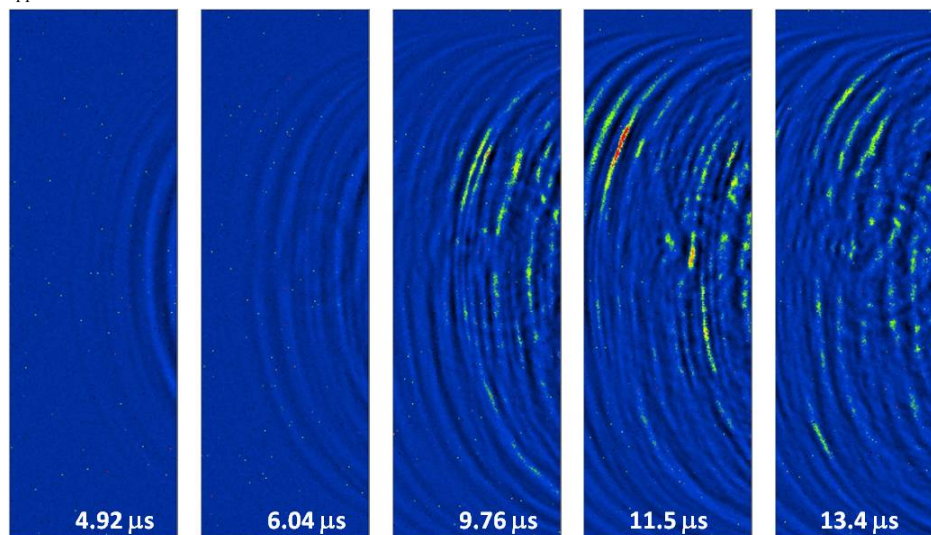
4:45 pm   A novel split inductively coupled piezoelectric transducer for flaw detection in pipes

David Greve[1], Peng Gong[2], Irving Oppenheim[2]; [1]*Department of Electrical and Computer Engineering, Carnegie Mellon University, Pittsburgh, PA, USA,* [2]*Civil and Environmental Engineering, Carnegie Mellon University, Pittsburgh, PA, USA*

Background, Motivation and Objective

Damage to pipes by erosion or cracking can lead to catastophic failure. Of particular concern are particular pipes and other components used in fracking, where internal pressures can be as high as 15000 psi and localized erosion can result from particulate matter. We seek to develop a robust mounted transducer that can be permanently mounted at critical locations and that will insonify the entire circumference of the pipe.

Statement of Contribution/Methods

Inductively coupled transducers have been previously proposed. These transducers eliminate the need for electrical connectors that are highly vulnerable to damage. However when a single piezoelectric element is mounted on the surface of a pipe the return pulses are dominated by reflections from the internal wall. We propose instead the use of a split piezoelectric element. When driven in series the emission of waves normal to the transducers are strongly suppressed. Emitted waves consist primarily of bulk and surface waves which readily insonify the entire circumference of the pipe.

Transient simulations have been performed using COMSOL of a split transducer, each element 0.4 cm x 2 mm, mounted to a 1.9 in ID. 2.8 in OD steel pipe. Simulations show primarily the emission of surface waves and longitudinal waves at an angle with respect to the transducer normal.

Transients were observed experimentally at a frequency of 800 kHz. As expected, early arrivals from the internal wall were strongly suppressed. Strong pulses were observed at about 110 and 220 µs, corresponding to traversing the entire circumference one and two times with a velocity near 3000 m/sec.

Results/Discussion

The split transducer effectively insonifies the entire circumference of the pipe while suppressing early returns from the internal surface. Generation of surface waves is dominant; consequently detection of erosion of the internal surface does not appear to be practical.
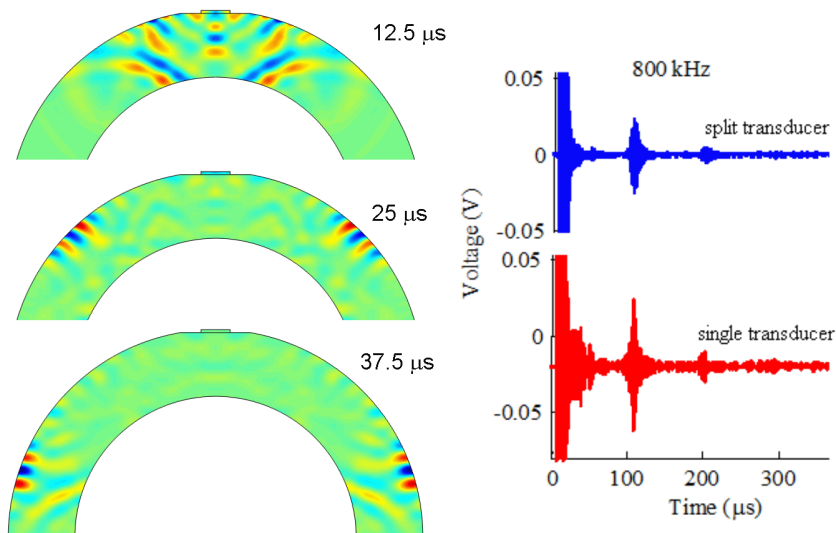
6C - Nonlinear Acoustics

201AF

Thursday, October 22, 2015, 03:30 pm - 05:00 pm

Chair: **Koen W.A. Van Dongen**
Delft University of Technology

6C-1

3:30 pm **Nonlinear Acoustic Pulse Evolution at the Edge of a Silicon Crystal**

Alexey M. Lomonosov[1,2], Pavel D. Pupyrev[1,3], Peter Hess[2], **Andreas P. Mayer[3]**; [1]*General Physics Institute, Moscow, Russian Federation*, [2]*University of Heidelberg, Heidelberg, Germany*, [3]*HS Offenburg - University of Applied Sciences, Gengenbach, Germany*

Background, Motivation and Objective

Acoustic waves guided by the tip of a crystal edge are non-diffractive by their nature. The strain field of a sinusoidal edge wave is localized within distances from the apex line of the order of magnitude of a wavelength. Also, acoustic edge waves are non-dispersive, if the quality of the tip is sufficiently high. In view of these properties, strong cumulative nonlinear effects may be expected. However, at rectangular edges of isotropic elastic media with Poisson ratios corresponding to practical materials, edge waves are of flexural character, and the presence of resonant second-order nonlinearity is forbidden by symmetry. This is also the case for high-symmetry configurations in anisotropic media, and this is the reason why in the past, second-order nonlinear effects of appreciable magnitude were not observed with edge waves.

The goal of this study is to demonstrate experimentally strong second-order nonlinear effects at crystal edges. The following prerequisites had to be satisfied:

- An edge configuration without reflection symmetry with respect to the midplane of the edge in an anisotropic medium, which guarantees sufficiently strong second-order nonlinearity,

- A high-quality tip,

- Large strains,

- Sufficiently low damping.

These requirements were met at a rectangular silicon edge with a (1 1 1) and a (1-1 0) surface, fabricated by cleavage, and laser excitation of the edge waves.

Statement of Contribution/Methods

High-intensity acoustic pulses were generated at the tip of the edge by a pulsed laser source. As they propagate along the apex line, their shape was observed by probe-beam deflection at two observation points at the tip with different distances from the source.

Comparison of the pulse shapes at the two observation points revealed strong second-order nonlinear effects, namely pulse compression, spiking and wave-front steepening with a clear tendency towards shock formation.

Numerical simulations were carried out on the basis of an evolution equation containing second-order nonlinearity. The integral kernel of the nonlinear term was calculated from the second-order and third-order elastic moduli of silicon.

Results/Discussion

It was found to be predominantly the phase of the complex kernel that governs the specific qualitative change of shape the pulses undergo during propagation. For this, good agreement was found between the experiment and the simulation of the pulse evolution from the first to the second observation point.

Accounting for small attenuation, simulations have been carried out of acoustic pulse propagation far beyond the distance corresponding to shock formation in the inviscid case. Inspection of the Fourier spectra of the nonlinear acoustic edge pulses revealed a power law behavior at high frequencies, which is analyzed on the basis of the nonlinear evolution equation.

6C-2

3:45 pm **Application of electrode stress for improving frequency-temperature behavior of UHF quartz resonators**

Yook-Kong Yong[1], Jianfeng Chen[1], Randall Kubena[2], Deborah Kirby[2], David Chang[2]; [1]*Rutgers University, Piscataway, NJ, USA*, [2]*HRL Laboratories, Malibu, CA, USA*

Background, Motivation and Objective

The effect of stress in the electrode films of quartz resonators is well known. This electrode stress effect is significant in ultra high frequency (UHF) quartz resonators because the thickness of electrodes when compared to the thickness of quartz plate is much more than in lower frequency resonators. We study the effect of electrode stress in a UHF 1 GHz, AT-cut quartz resonators with the objective of improving their frequency temperature behavior.

Statement of Contribution/Methods

Currently, quartz plate resonators are analyzed and designed by assuming the electrode films as mass loading films. The effects of electrode film stress are then treated empirically. We study the UHF thickness shear resonators as composite plate resonators wherein not only the mass loading effects but the electrode films material properties such linear and nonlinear elastic constants, temperature derivatives of elastic constants and thermal expansion coefficients are incorporated into a COMSOL model for vibrations of a composite plate superposed on initial strains due to temperature change and bonding stress in electrodes.

Results/Discussion

Fig. 1 shows the frequency shift effect of electrode stress due to bonding in a UHF 1 GHz, AT-cut quartz resonator where the 10 MPa tensile stress in the aluminum electrodes (green curve) shifts the frequency upwards of 13 KHz.

Fig. 2 shows the composite effects of two electrode films, aluminum and chrome respectively, on the frequency-temperature (f-T) curve of the UHF 1 GHz, AT-cut quartz resonator. The aluminum electrode causes the f-T curve (red) to rotate clockwise from the curve with mass loading only (blue). We can improve the f-T curve by adding a chrome film that will rotate the curve (green) counter-clockwise. These results were observed experimentally in literature

Fig.1: Effects of initial stress in the aluminum electrodes of the 1 GHz UHF AT-cut quartz (S1X) resonator

- no initial stress in electrodes
- 0.1 MPa initial tensile stress in electrodes
- 10 MPa initial tensile stress in electrodes

Rutgers
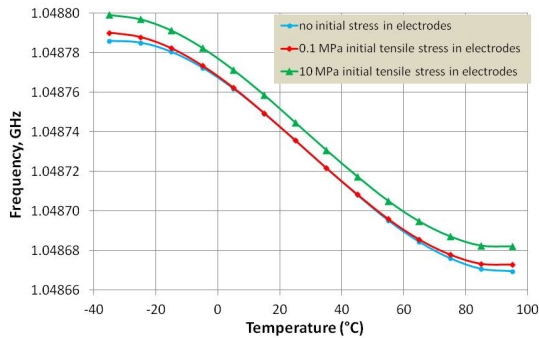
Fig.2: Frequency-Temperature behavior of the 1 GHz UHF composite plate resonator consisting of the AT-cut quartz plate sandwiched between aluminum and chromium electrode films.

- massloading
- composite plate_Al=.04μm
- composite plate_Cr=.02μm & Al=.04μm

Rutgers
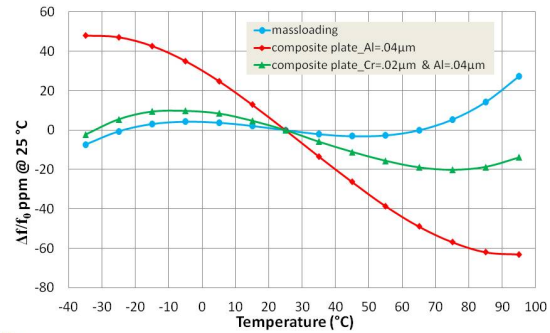
6C-3

4:00 pm **Temperature control of a droplet on disposable type microfluidic system based on a surface acoustic wave device for blood coagulation monitoring**

Noriyuki Ohashi[1], **Jun Kondoh[1]**; [1]*Shizuoka University, Hamamatsu-shi, Japan*

Background, Motivation and Objective

Monitoring of the blood coagulation is important for the screening of hemophilia. The blood coagulation can be classified endogenous and exogenous coagulations. Hemophilia is one of endogenous diseases. Activated partial thromboplastin time (APTT) is the test to measure the coagulation time of the blood. Normally, impedance change during blood coagulation is measured. However, the instruments for measuring the coagulation are expensive and a volume of sample is several ml. Therefore, if a coagulation process is measured with several μl, point of care testing of the blood coagulation is possible. As coagulation factor in the human plasma is activated at 37 °C, sample heating is required. The droplet heating is possible using a surface acoustic wave [1]. Also, we proposed disposable digital microfluidic system (DMFS), which consists of a cover glass/liquid layer/128YX-LiNbO3. When an electrochemical sensor is fabricated on the sensor plate, impedance change can be monitored under the temperature controlled conditions. In this research, we applied the DMFS for monitoring blood coagulation process at 37 °C.

Statement of Contribution/Methods

A water droplet of 2 μl was placed on the 128YX-LiNbO3, on which an interdigital transducer (IDT) was fabricated. Water droplet of 2 μl was placed on the 128YX-LiNbO3. Then the glass was placed onto it. The droplet automatically spread. This is the preparation method of the DMFS. An electrochemical sensor was fabricated on the glass. Burst signal was applied to the IDT. Applied power and duty factor were modified. The longitudinal wave is radiated from the SAW at water/128YX-LiNbO3 interface. When the longitudinal wave is reflected at the glass/water interface, high-order Lamb wave is generated in it. Nonlinear phenomena in a droplet on the glass are caused by the Lamb wave. A droplet was placed on the glass surface. The droplet is heated by the radiated longitudinal wave from the leaky Lamb wave. The temperature was measured using thermocouple thermometer.

Results/Discussion

First, water droplet of 10 μl was placed on the glass. Temperature of droplet was measured by changing applied power or duty factor. Linear relationships were obtained between the temperature obtained 1min after the SAW was generated and applied power or duty factor. From the results, combinations of applied power and duty factor were decided to keep at 37 °C. Then, three aqueous solutions of human plasma, reagent for coagulation, and CaCl2 were mixed. The volume of each solution was 5 μl. The measurement time of blood coagulation is 10 min. Optimum combination of applied power and duty factor was 1.5W and 80%, respectively. Then the impedance changes during the coagulation were measured. As the temperature was kept at 37 °C and the solutions were uniformly mixed by the longitudinal wave radiated, reproducible results were obtained.

[1] J. Kondoh, et al., Sen&Act A, 149, pp. 292-297, 2009.

6C-4

4:15 pm **Numerical simulation of nonlinear attenuation in bubbly mediums**

Amin Jafarisojahrood[1], Raffi Karshafian[2], Michael C. Kolios[2]; [1]*Physics, Ryerson University, Canada*, [2]*Ryerson University, Toronto, Canada*

Background, Motivation and Objective

The acoustic response of microbubbles (MBs) is non-linear and complex. The presence of MBs in a medium changes the medium's acoustic properties and increases the attenuation of the bubbly medium.

The existing models of ultrasound attenuation in a bubbly medium are based on linear approximations (very small amplitude MB oscillations). However, most of the applications (e.g. MB enhanced diagnostic imaging, therapeutic ultrasound and sonochemistry) employ higher pressures which result in high amplitude nonlinear MB oscillations. Thus linear models are not valid in many regimes used in applications.

In order to optimize the use of MBs, the attenuation of a medium in the presence of the MBs should be investigated and classified with the nonlinear oscillations of the MBs incorporated in the model.

Statement of Contribution/Methods

In this study, using the methods of nonlinear dynamics, we have classified the behavior of MBs for a wide range of frequencies and applied pressures. The Hoff model for encapsulated MB oscillations is coupled to a thermal dissipation model and is numerically solved and the results are visualized by the aid of the bifurcation diagrams of the radial oscillations of the MBs as a function of the incident pressure. A model to incorporate the nonlinear attenuation and sound speed is developed by deriving the complex wave number from the model developed by Calfish for the propagation of acoustic waves in a bubbly medium.

Results/Discussion

Results showed that depending on the frequency of the ultrasound wave , the nonlinear oscillations of the MBs can be classified into 5 main categories in which the MBs oscillations exhibit: 1. Linear resonance (fr), 2. pressure dependent resonance (fs), 3. Sub Harmonic (SH) resonance (fSH), 4. Pressure dependent SH resonance and 5. Higher order SH resonance oscillations (fn). Results show that when MBs are sonicated by their fr, the effective attenuation of the medium can potentially decrease as the pressure increases, in good agreement with experimental observations. When sonicated with their fs, the effective attenuation of the medium is smaller than in the case of fr. This happens only below a pressure threshold which corresponds to the saddle node bifurcation in the corresponding bifurcation diagram. Above this pressure, the effective attenuation and sound speed increase abruptly by ~5 and ~2 fold respectively. In the other classified sonication regimes (3-5), the attenuation and sound speed changes are negligible below the threshold corresponding to the SH oscillations. As soon as the pressure increases above the threshold for SH oscillations (e.g. period doubling in the

---

bifurcation diagram), the effective attenuation increases abruptly (~ up to 5 fold), however the maximum exhibited attenuation is ~10 to 100 folds smaller than the maximum attenuation in case of sonication with fr and fs.

6C-5

4:30 pm   Dynamic behaviour of laser nucleated bubbles in a focused ultrasound field

Lian Sheng Wang[1], Gianluca Memoli[1], Mark Hodnett[1], Bajram Zeqiri[1]; [1]*National Physical Laboratory, Teddington, United Kingdom*

Background, Motivation and Objective

The United Kingdom National Physical Laboratory (NPL) is embarked on research intended to establish a reference facility, based on hybrid (i.e. optical/acoustical) cavitation of single bubble/controlled bubble clouds. Ultimately, this will assist in developing the metrological framework to define a traceable unit of cavitation, hence underpinning and supporting advanced manufacturing and healthcare applications exploiting high power ultrasound.

Statement of Contribution/Methods

The facility consists of: a Litron Nano-TRL850Q-switched Nd:YAG laser operated at 532 nm and 10 Hz;   an optical beam splitting system able to form either single beam or multiple beams; a high speed camera (16 frames, up to 330 million fps) and cuboid acoustical chamber with optical glass walls. Four Tonpilz transducers (nominally 28, 36 and 80 kHz) are used to generate an acoustic field coincident with the position of the bubble/ bubble cloud. Using the laser/optical system, single bubble or small bubble clouds of 4x4x4 and 5x5x5 can be generated in the water-filled chamber. The overlapping acoustic beams of the transducers are aligned specifically to generate a superposition of their acoustic fields, generating acoustic pressures sufficient to cavitate water at a focal point where bubbles are seeded by the laser/optical system, and to drive the generated bubbles into oscillation and collapse. Hydrophones and cavitation sensors are positioned at various locations inside the chamber to measure both the driving acoustic field and broadband acoustic emissions created by cavitating bubbles. Three fixed-position pressure sensors are mounted on the chamber walls to monitor the generated acoustic signals.

Results/Discussion

To precisely measure the acoustic field pressures driving the bubbles, the depth profile of the acoustic field along the central axis of the acoustic chamber was measured using a Reson 4038 hydrophone. The bubble size generated by the laser against delivered energy was determined experimentally for a range of suitable sizes. The dynamic behaviour of bubbles from non-cavitation, to non-inertial and inertial cavitation has been investigated optically under various acoustic fields, in order to quantify the response of a laser-nucleated bubble cloud to a driving acoustic field. The results of bubble-bubble interactions (secondary Bjerknes forces) have been studied in terms of cloud deformation, both in the direction of the driving field and perpendicular to it, and the shape development of individual bubbles within a cloud under various inter-bubble distances/laser energies and negative peak acoustic pressures will be discussed. Acoustic emission from cavitating bubbles has been monitored into the megahertz range with pressure sensors employed to provide quantitative measurements of cavitation thresholds for both non-inertial and inertial cavitation. Results are compared with the optical observations.

6C-6

4:45 pm   Experimental results on the Pressure Dependence of the Minnaert Resonance Frequency for three different Gases in Water

Jarle Andre Johansen[1], Bern Inge Hansen[1]; [1]*Department of engineering and safety, UiT The Arctic University of Norway, TROMSO, Norway*

Background, Motivation and Objective

Early gas leak detection at deep sea levels is of prime importance as more offshore gas fields are being developed. Many passive and active (ultra)sonic methods exists for detection and characterization of gas bubbles in water[1]. Here we examine the passive emission of sound from medium size gas bubbles in water. The natural oscillation frequency for bubbles in this regime follows the Minnaert formula[2]: $v=(2\pi a)^{-1} (3\kappa p_0/\rho)^{1/2}$, v is frequency, a is radius, κ is polytropic index, p_0 is ambient pressure, and ρ is water density. Very few have presented experimental results on frequency dependence of ambient pressure. We have previously reported this for nitrogen gas bubbles by simulating depths down to more than 300m. Here we expand this by examining two more gases, helium and CO_2.

Statement of Contribution/Methods

We contribute with new experimental results for the pressure dependence of the natural frequency of the sound emitted from gas bubbles in water. We compare our previously reported results using nitrogen gas with new results using helium and CO_2, hence testing also the polytropic index dependence of the natural frequency in the Minnaert equation.

We use hydrophones and specially developed near-hydrophone charge amplifiers and low impedance line drivers for low noise and robust signal transport.

We simulate the water depth by a controlled pressure vessel. Gas bubbles are released through a nozzle by setting the supply gas pressure slightly higher than inside the vessel. We estimate bubble size by photographic techniques. Bubble oscillations are captured using a high speed camera.

Results/Discussion

We present the oscillation frequency for medium sized bubbles, with radii ca 1.5 mm, released in water.

We use three gases with different molecular complexity and polytropic index. Helium with $\kappa_{He}=1.66$, Nitrogen with $\kappa_{N2}=1.404$, and Carbon dioxide with $\kappa_{CO2}=1.3$

Ambient pressure was varied from ca 100-4000 kPa, resulting frequencies ranged from ca 2800-17300 Hz.

Discussion and Conclusions

Our experiment was the first systematic test of the pressure dependence of the Minnaert frequency for nitrogen gas in water under the described conditions. These results have been reported previously[3]. The main uncertainty is the estimation of the actual bubble size. This has been accounted for using error estimation.

In this study two more gases with different polytropic index are added into the experiment.

Our new results show that both pressure and ploytrophic gas constant dependence can be explained well by the Minnaert equation.

[1]TG Leighton, The acoustic bubble, Academic Press 1994

[2]M Minnaert, On the musical air bubbles and sounds of running water, Phil Mag 1933 16

[3]BI Hansen & JA Johansen, Experimental Results on the Pressure Dependence of the Minnaert Resonance Frequency for Nitrogen Gas Bubbles in Water, Proceedings IEEE IUS 2011

7C - RF Frontend Devices

105

Thursday, October 22, 2015, 03:30 pm - 05:00 pm

Chair: **Jidong Dai**
Murata Electronics, Inc.

7C-1

3:30 pm **Current developments and future trends in mobile terminal frontend architectures**
Harald Pretl[1]; [1]*DMCE GmbH & Co KG, Austria*

Background, Motivation and Objective

The RF frontend is a crucial component of every mobile device requiring cellular communication capabilities. Usually consisting of antennas, switches, filters, duplexers and power amplifiers (PA) it consumes a sizeable part of the available PCB area and budget. Ever increasing requirements in number of supported bands and features drive a concurrent improvement need in both size and cost. The features driving front-end complexity are performance-enhancement measures like antenna-tuning or envelope-tracking (ET) for PA and carrier-aggregation (CA) for LTE.

Statement of Contribution/Methods

This talk provides an overview of the state-of-the-art and some recent developments in mobile terminal front-end architectures, enabled by advancements in the frontend component area as well as improvements in cellular transceiver architectures. The different requirements in market segments like low-, mid- and high- tier are discussed and it is shown how this affects the implementation of the frontend. The introduction of CA in 3GPP Release 10 and thereby simultaneous radio operation in different frequency bands increases the complexity in the frontend considerable. Implementation of ET to lower the power dissipation of the PA for high crest-factor transmit signals creates specific issues in the frontend as well. The implications of CA and ET are analyzed and the impact to the frontend component specifications are shown.

Results/Discussion

In the final part of the presentation an outlook is provided how future technologies like MEMS or novel concepts like tunable filters and circulator-based frontend architectures could help to tackle some of the issues arising in mobile terminals due to ever increasing cost and miniaturization pressure and the steadily growing number of frequency bands and requirements driven by new 3GPP releases.

7C-2

4:00 pm **Full band 41 filter with high Wi-Fi rejection – design and manufacturing challenges**
Susanne Kreuzer[1], Alexandre Volatier[1], Gernot Fattinger[1], Fabien Dumont[1]; [1]*BAW R&D, Qorvo, Apopka, Florida, USA*

Background, Motivation and Objective

Within the last 5 years the latest standard of 4G LTE was established worldwide, where providers built up and steadily expanded their network coverage supporting many different FDD and TDD bands. Band 41 is one of the most important LTE bands regarding its huge demand in the Asian market where all major service providers own specific channels, as well as in the USA where Sprint, recently acquired by Softbank, launched its new LTE network using band 41 which encompasses the XGP band from Japan.

Band 41 is a 194 MHz wide TD-LTE band operating from 2496MHz to 2690MHz. Thus, it covers a large spectrum and enables the increasing demand of higher download and upload rates in the booming smart-phone and tablet industry.

Statement of Contribution/Methods

While there exist filters that cover only parts of the whole B41 spectrum we present a single full band high performance BAW filter in a small package size of 2 x 2 x 0.83 mm with a low insertion loss of typical 2.1 dB over the most part of the passband. Thus, the number of RF components to support the full band 41 in a phone is reduced.

As the band 41 operating frequency regime is close to Wi-Fi's active spectrum the need of a highly selective filter to meet the strict LTE rejection requirements is obvious, where our filter shows an excellent Wi-Fi rejection of typical 43dB up to channel 11.

Results/Discussion

In this article we will present a full band 41 filter using state-of-the-art BAW technology. Due to the wide band and the resulting wide separation of shunt and series resonators the low insertion loss in the passband can not be realized by common design strategies as used for narrower bands.

Also we discuss how to cope with the challenges arising due to the tough Wi-Fi rejection requirements on the design side as well as on the manufacturing side. The steepness of the filter's lower edge plays a major role to fulfill the tight constraints of the B41-Wi-Fi coexistence under operating conditions, where the use of high-Q BAW technology is indispensable. Additional challenges arise in order to be able to achieve the accuracy needed in manufacturing to guarantee the filter's high rejection selectivity as well as its low loss performance over the whole band 41.

7C-3

4:15 pm **Study of power durability measurement of RF SAW devices for IEC standardization**
Tatsuya Omori[1], Shunsuke Ohara[1], Chang-Jun Ahn[1], Ken-ya Hashimoto[1]; [1]*Electrical & Electronics Engineering, Chiba University, Chiba, Chiba, Japan*

Background, Motivation and Objective

Power durability is one of the most important characteristics of SAW/BAW RF devices. Although the acceleration test in terms of applied power and/or chip temperature is mandatory to estimate their time-to-failure (TTF), the test procedures have not been standardized yet. They should be highly repeatable and applicable to various devices such as FBARs.

This paper reports a trial of the TTF estimation of SAW devices for the IEC standardization. Automated TTF measurement system was developed, and it was checked how the TTF changes with the acceleration parameters. RF wafer probes were used for the experiment so as to monitor the chip temperature accurately.

Use of the cutoff frequency of the BAW radiation is also investigated for monitoring the chip temperature in packaged SAW devices.

Statement of Contribution/Methods

The figure shows developed TTF measurement system for RF SAW filters used in this work. During the power irradiation mode, an RF signal amplified by a PA is applied via a wafer probe to the DUT mounted on a temperature controlled stage. Power of the output signal is monitored by a power meter. Device failure is detected by rapid

change in the output power. During the monitor mode, input power is monitored by the power meter and 2-port scattering parameters of the DUT are acquired by a vector network analyzer (VNA). The monitoring is performed every 10 minutes, and the operation mode can be toggled by an electromechanical switch array. Whole sequences are automatically controlled by a PC, which also collect all the measured data.

Results/Discussion

A large number of ladder type SAW filters in the 2 GHz range were fabricated in a $LiTaO_3$ wafer, and their TTFs were measured under various conditions. The experiments showed that the acceleration by temperature and applied power obeys the Eyring model well. Then the acceleration factors of the test devices were successfully extracted.

It was also demonstrated that the chip temperature can be estimated from the cutoff frequency of the BAW radiation, which is insensitive to the surface conditions such as contamination and is identified easily from the VNA data. The temperature coefficient was much larger than that of the SAW response. This technique seems quite feasible to monitor chip temperature of packaged RF SAW devices during the TTF measurements because no modification is necessary for the SAW device design.
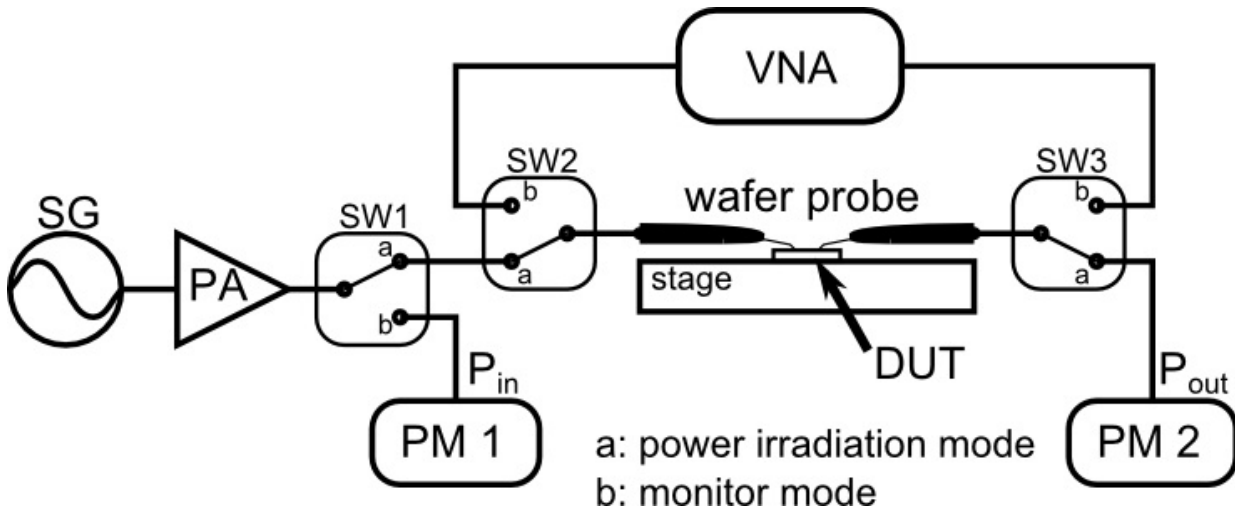
7C-4

4:30 pm   Design Considerations for High Power BAW Duplexers for Base Station Applications

Jeff Galipeau[1], Rodolfo Chang[1]; *[1]QORVO, Apopka, Florida, USA*

Background, Motivation and Objective

BAW filters & duplexers have become prolific in the Mobile Handset and Smartphone market in recent years. The purpose of this work is to leverage the BAW/SMR superior power handling and robustness attributes to address the Small Cell Base Station market.

These Base Stations are used to address cellular coverage in buildings and congested urban areas. These Base Stations use a duplexer based architecture much like a mobile phone with transmit (Tx) and receive (Rx) roles reversed. Thus, the Tx filter must handle higher power levels, provide higher reliability and higher isolation in the Rx band than the handset counterpart. The transmit power dictates the addressable cell size.

The goal of this study is to provide a duplexer solution for Band 1 & Band 7 (2.1 and 2.6 GHz respectively) where the Tx path is capable of withstanding an input power of 2.5 Watts for a minimum of 87,600 device hours at 95C. This market is currently addressed by cavity filters which are large and expensive but offer high performance and high reliability. The market is pushing for a smaller, more cost effective solution, where the performance is still very high.

Statement of Contribution/Methods

This study examines the upper limits of power handling using a standard BAW/SMR stack. Since miniaturization of the BAW die in the Base Station is not as critical as in a Handset, a design technique that spreads the power over a greater area of the BAW die is employed. This work employs resonator power dissipation models, thermal heat flow models to predict self- heating of the duplexer under high power. IR thermal scans, accelerated life tests, both thermal and power, and failure analysis are used to quantify the improvements. Also we examine the usage of highly thermally conductive (hi-K) laminates and hi-K attachment methods to create a full hi-power duplexer module. ALSO, care has to be taken in the design of the phasing matching circuit at the antenna port, because of the high level of power injected at the larger TX BAW die. We examine the advantages of using "double" T-type matching circuit at the antenna port in order to further isolate the smaller Rx BAW die from thermal damage without degradation on the Insertion Loss.

Results/Discussion

We have shown that carefully designed BAW duplexer can dissipate substantially higher power levels for longer device life than standard BAW duplexer counterparts. Our B7 and B1 duplexers are rated for 2.5W for 40k+ hours. Preliminary power accelerated test for Band 1 shows that is possible to significantly extend the power handling of a standard BAW/SMR stack. This work shows that thermal considerations of BAW die itself, as well as Antenna Phasing Matching circuit design, die attachment methods, laminate design and heat-sink considerations are all important to improve the life of the device. We believe that High Power BAW technology could be potentially disruptive to cavity type filters in the Small Cell base station market.

7C-5

4:45 pm   A zero TCF band 13 SAW duplexer

Yiliu Wang[1], Marc Solal[1], Taeho Kook[1], Jean Briot[1], Ben Abbott[1], Alan Chen[1], Timothy Daniel[1], Svetlana Malocha[1], Keqi Qin[1], Kurt Steiner[1], William Wu[1]; *[1]Qorvo Inc., USA*

Background, Motivation and Objective

RF spectrum is becoming a very sparse resource and several systems have to coexist while separated by small frequency gaps. For example, public safety band NS07 is 2.5 MHz below the LTE band 13 TX band. Standard SAW and typical Temperature Compensated SAW (TC-SAW) filters do not provide enough rejection in this band, especially within the required operating temperature range. The only way, when not using an NS07 compliant duplexer, to avoid noise radiation into the public safety band is to reduce their transmitted power when the public safety network is activated.

  To be compliant with NS07, the band 13 TX filter needs to have a very steep transition. Therefore, high quality factors as well as low temperature coefficient of frequency (TCF) are required. To reduce the TCF, the current standard approach is to bury the electrodes inside a silicon oxide overlay. Since silicon oxide has a positive TCF while piezoelectric substrates have negative TCFs, compensation is possible. Usually, TC-SAW filters on lithium niobate substrates have a TCF in the range of -20 to -25 ppm/°C. This corresponds to a frequency shift of 2 MHz at 800 MHz for a temperature range of 100°C. This is too large for applications requiring steep transitions bands.

Statement of Contribution/Methods

A band 13 duplexer meeting the NS07 rejection requirement is presented. The substrate utilized is lithium niobate with an orientation close to Y+128°. The oxide thickness is increased enough to obtain full temperature compensation. Piston mode transducers are used in order to suppress the transverse modes and to reduce the losses. By increasing the silicon oxide thickness, it is possible to reduce TCF toward some targeted ppm/degC value. The drawback is a reduction by about 40% of the coupling factor and thus, of the possible relative bandwidth. However, band 13 is narrow enough to be compatible with this approach.

Results/Discussion

The resulting temperature compensation produces a frequency shift smaller than 200 kHz p.p. within the 100°C temperature range. Quality factors in the 1500 range are obtained. Typical results are a rejection of 25dB in the NS07 band within the temperature range with an insertion loss better than 3dB.

It is understood that this duplexer is the first band 13 SAW duplexer meeting the NS07 rejection specification.
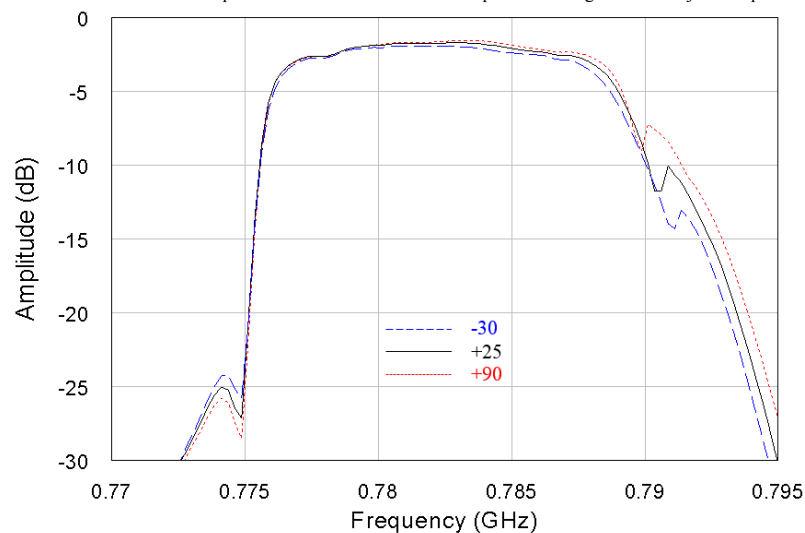
8C - Transducer Design, Fabrication and Applications

102

Thursday, October 22, 2015, 03:30 pm - 05:00 pm

Chair: **Sandy Cochran**
University of Dundee

8C-1

3:30 pm **Piezoelectric Micromachined Ultrasonic Transducers with Increased Coupling Coefficient via Series Transduction**

Yipeng Lu[1], **Qi Wang[1]**, David Horsley[1]; *[1]University of California, Davis, Davis, CA, USA*

Background, Motivation and Objective

This work demonstrates a new electrode configuration for piezoelectric micromachined ultrasonic transducers (PMUTs) with increased electromechanical coupling coefficient (k_t^2). The electrodes, a center electrode surrounded by a ring electrode, are identical to those used in differential PMUTs. Unlike a differential PMUT, where the two top electrodes (TEs) are referenced to a common ground electrode, here only the two TEs are used, effectively putting the two piezoelectric transducers in series. The benefit of series readout is that the transducer's electrical capacitance is halved, doubling the receive sensitivity and k_t^2.

Statement of Contribution/Methods

PMUTs were fabricated using a cavity-SOI process, Fig. 1. Transduction is based on two series piezoelectric capacitors formed between the two TEs (TE-1 and TE-2) and a floating bottom electrode. Voltage applied to TE-1 and TE-2 results in opposite electric fields, creating opposite curvature beneath these electrodes and exciting the PMUT's vibration mode. While the displacement per volt is unchanged, k_t^2 is doubled because the series capacitance is halved, reflecting the design's greater power efficiency as a transmitter and increased SNR as a receiver.

Results/Discussion

Devices were characterized using laser Doppler vibrometry and electrical impedance measurements, Fig. 2. The 50 μm diameter PMUT membrane is composed of 1.1 μm PZT on 2.5 μm Si, resulting in 12 MHz resonant frequency in air. The peak displacement per volt is slightly lower than that of the single-electrode design due to imperfect electrode layout. Electrical impedance measurements, confirm that the capacitance is halved (from 158 pF to 75 pF), resulting in k_t^2 increasing from 14% to 27% after calibration to remove parasitic capacitance caused by bond pads.
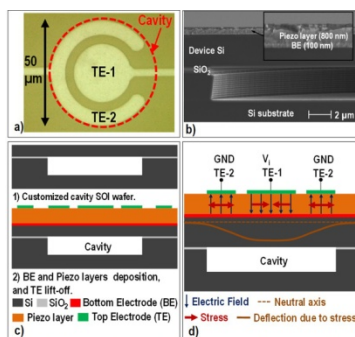
Fig. 1: (a) top-view optical image and (b) cross-section SEM image of the proposed PMUT; (c) fabrication process flow based on cavity SOI wafers with only 1 more mask to pattern top electrode (TE); (d) PMUT operation principle in transmit mode: voltage between electrodes TE-1 and TE-2 generates opposite electric field beneath them, which results in opposite stresses inside the film and bending moment to deflect the membrane. The proposed PMUT eliminates the need to pattern BE, and due to large coupled membrane area, its coupling coefficient is 2× increased without differential driving and sensing.
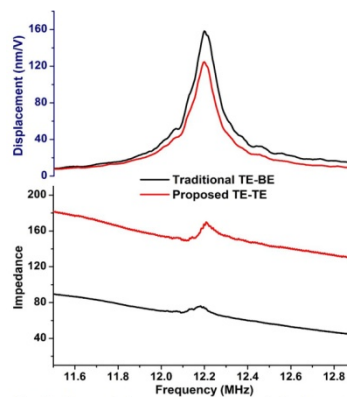
Fig. 2: Measured frequency responses of displacement sensitivity and electrical impedance. Compared with traditional PMUT (driven through TE and BE), the proposed PMUT (driven through two TEs) has ~20% reduced displacement sensitivity due to imperfect electrode layout of outer ring TE, but 2× increased coupling coefficient k_t^2, from 14% to 27% after calibration to remove parasitic capacitance caused by bond pads.

8C-2

3:45 pm **Micro-replication using Photoresist Moulds for Wafer-scale Fabrication of Fine-scale Piezocomposites**

Yun Jiang[1], Hana Hughes[2,3], Tanikan Thongchai[1], Carl Meggs[1,3], Tim Button[1,2]; *[1]School of Metallurgy and Materials, University of Birmingham, Birmingham, United Kingdom, [2]Central European Institute of Technology, Brno, Czech Republic, [3]Applied Functional Materials Ltd, Birmingham, United Kingdom*

Background, Motivation and Objective

Piezocomposites operating above 30 MHz are in demand to improve spatial resolution for ultrasound imaging and other applications. However, increasing the operational frequency of these materials poses a considerable challenge for conventional dicing techniques, as ultrafine dimensions are required. As promising alternatives, micro-moulding methods involving various mould materials and mould filling techniques are being developed, but are still at the laboratory stage, generally limited by the poor strength of the ceramic/binder system, the achievable geometries, dimensions and aspect ratios of the mould and/or prohibitive cost. In this work, an innovative mask-based moulding strategy combining novel ceramic processing and photolithographic micro-mould fabrication is demonstrated, offering a versatile and cost-effective approach for the fabrication of high frequency piezocomposites that can be scalable for industrial production.

Statement of Contribution/Methods

Water-based gel casting systems of both lead-based and lead-free piezoceramics were optimised to have low viscosity and high solids loading in order to facilitate the moulding process, as well as high green strength to retain the integrity of fine structures during demoulding. Thick positive and negative photoresists were employed for the micro-sized mould fabrication. Different moulding strategies were evaluated and achievable feature shapes and sizes were investigated for both resists by adjusting the photolithographic processing parameters. Suitable demoulding conditions were explored whilst minimising any adverse effect of stripping solutions on the gel-cast ceramic.

Results/Discussion

Resist moulds with a range of pattern designs have been fabricated. The achieved mould thicknesses vary from 30 μm to 120 μm with aspect ratios of 10. The ability to strip the positive photoresist in the presence of the gel-cast ceramic has been demonstrated by successfully achieving piezocomposite structures of both upstanding regular pillars and randomised segments with lateral feature sizes <5 μm. The success of these moulding methods suggests that they will be particularly applicable to the production of a wide range of fine ceramic structures, and as both the photolithographic and gel-casting processes can be automated, this technique has the potential for utilisation in mass production.
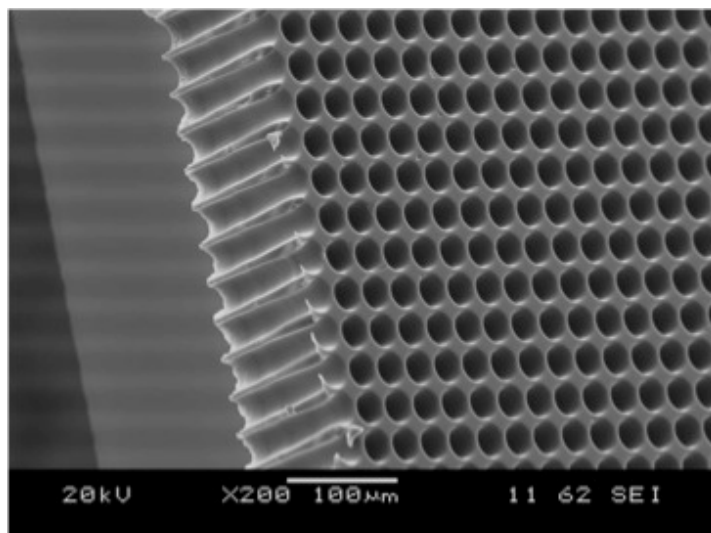
8C-3

4:00 pm   Gas Coupled Polymeric Capacitive Transducers via Pad Printing

Richard O'Leary[1]; [1]*University of Strathclyde, United Kingdom*

Background, Motivation and Objective

Capacitive ultrasonic transducers (cUT) comprise a substrate patterned with a regular array of uniformly dimensioned cavities above which a membrane is positioned. Micropatterning of polymer substrates has been shown to be effective methodology for the manufacture of such cUT has recently been demonstrated [1]. The method involves creating a positive mask of sessile liquid droplets on a polymer substrate. The droplets define the cavity dimensions and spatial distribution, a subsequent processing stage independently defines the cavity depth. Droplets can be defined in a variety of ways – a 3D CNC machine equipped with a piezoelectric droplet generator has been found to be most robust. This paper describes a new method for the patterning of the polymer substrate via a pad-printing technique.

Statement of Contribution/Methods

The printing pad is manufactured using 3D printing technique, an example pad is illustrated in Figure 1 – essentially the pad comprises an array of styli. The lateral dimensions and spatial distribution of the styli are replicated via the pattern of deposited droplets. In the current investigation only cylindrical styli have been investigated. The morphology of the styli tips has been explored: planar; convex and concave tips were all investigated.

Droplets are deposited onto the polymer substrate by a dip and place method. Interestingly, the planar tips were found to create droplet patterns with the highest fidelity with respect to the pad.

After solvent processing to create cavities [1,2], substrates were air-dried and washed with purified water, electroded and packaged with a membrane to form capacitive transducers.

Results/Discussion

Single element air coupled devices, 600kHz nominal centre frequency, were constructed and evaluated experimentally. Transducer bandwidths in excess of 100% were observed with two-way insertion loss of 60dB being typical. Laser vibrometery confirms uniform surface dilation of the excited membrane.

Since the methodology affords the independent control of cavity spatial distribution, depth and lateral dimensions with significant potential for the rapid high volume manufacture of capacitive transducer structures for a range of applications.

[1] O'Leary et al Proc 2013 IEEE IUS, pp1113-16 doi 10.1109/ULTSYM.2013.0285
[2] O'Leary et al Proc 2014 IEEE IUS, pp177-180 doi 10.1109/ULTSYM.2014.0045
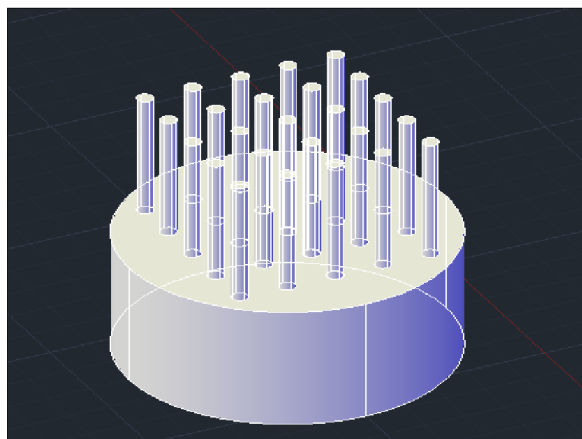
Figure 1 CAD model of an example print pad

8C-4

4:15 pm   Extending the receive performance of phased micromachined ultrasonic transducer arrays in air down to 40 kHz and below

Matthias Rutsch[1], Eric Konetzke[2], **Alexander Unger[1]**, Maik Hoffmann[2], Sivaram Nishal Ramadas[3,4], Steve Dixon[3], Mario Kupnik[1]; *[1]Technische Universität Darmstadt, Germany, [2]BTU Cottbus-Senftenberg, Germany, [3]University of Warwick, Coventry, United Kingdom, [4]Elster-Instromet, Belgium*

Background, Motivation and Objective

We investigate the approach of how to build a 1D phased micromachined ultrasonic transducer array that is able to receive directed ultrasonic waves in air over a wide opening angle at frequencies of 40 kHz and below. Such a low frequency range is beneficial because of the low attenuation. It is challenging, however, to directly fabricate a receiving micromachined ultrasonic transducer array, such as a CMUT array, that fulfills both the maximum receive sensitivity at 40 kHz or below and an element pitch of half the wavelength, i.e. 4.3 mm, for zero grating lobes associated with a wide opening angle. For example, a circular-shaped wafer-bonded CMUT element with evacuated cavity, with a 40-µm-thick silicon plate, can barely be brought down to < 45 kHz. One has to limit the plate diameter to about 4 mm for an element pitch of 4.3 mm (for sufficient bonding area). Further thinning down the plate thickness does not work either due to non-linear geometry effects (stress-stiffening), resulting in an increasing resonance frequency.

Statement of Contribution/Methods

Therefore, we test the hypothesis whether intentionally separating the active aperture from the receiving transducer elements will allow us to gain additional design flexibility. In comparison to previous work from [Takahashi, ICMIT 2007], we focus on receiving mode. We propose an additional layer consisting of many tapered waveguides. This additional layer (smart packaging layer) can be 3D-printed or fabricated by using shrinking tubes in combination with an aluminum mold, as used for our first prototype. The array features eight channels with twelve 4.3 x 6 mm rectangular-shaped effective aperture elements, with an optimum element pitch of 4.3 mm. As preliminary test receivers at the other end of each waveguide, we use commercially available ultrasonic transducers (40 kHz) with a diameter of 10 mm (MA40S4R, Murata, Japan). The array is rotated in steps at the distance of 1.5 m in front of a large aperture emitter, consisting of 222 ultrasonic transducers connected in parallel of the same type. A 40 kHz sinusoidal burst signal with 80 cycles and 10 VRMS was applied to the emitter. The received signals of the eight channels were recorded using parallel-triggered digital oscilloscopes and post processed in MATLAB for receive-beam forming.

Results/Discussion

The received signals had an SNR of 37.8 dB and, as theory predicts, for this setup the phased array is able to receive with a sensitivity of -55.9 dB (0 dB equal 1 V/Pa) within an opening angle of 110° without any significant grating lobes exceeding -10 dB. These results prove that intentionally separating the active aperture of a phased array from the receiving transducer elements by using a smart packaging layer, consisting of many waveguides, will be useful for many air-coupled ultrasound applications, for which receive beam steering at frequencies as low as 40 kHz and below is required.

8C-5

4:30 pm   Spiral array inspired multi-depth cost function for 2D sparse array optimization

Emmanuel Roux[1,2], Alessandro Ramalli[2], Marc Robini[1], Hervé Liebgott[1], Christian Cachard[1], Piero Tortoli[2]; *[1]CREATIS, Université de Lyon, CNRS UMR 5220, INSERM U1044, Université Claude Bernard Lyon 1, INSA-Lyon, Villeurbanne, France, [2]Ingenieria dell'informazione, Università degli studi di Firenze, Firenze, Italy*

Background, Motivation and Objective

During the last decade, the increasing interest in 3D ultrasound imaging pushed the development of 2D-matrix arrays. In particular, state-of-the-art methods for 2D sparse array footprint optimization use simulated annealing (SA) to reduce the number of elements and to find their best position, intensity and size [Trucco, 99] [Cheng, 10] [Diarra,13]. The typical cost function to be minimized measures the fidelity of the beam simulated from the current footprint solution to a template beam pattern (TBP). However, the simulations have been so far limited to the focal depth. In this work, we investigate the performance obtainable using a multi-depth cost function.

Statement of Contribution/Methods

Since the Blackman-tapered 256-element spiral array has 3D homogeneous performance over the volume [Ramalli,14], we let its related beam be the TBP. It was evaluated at three depths (R_1=15, R_2=25 and R_3=35 mm) where the -30dB main lobe widths were 8.3°, 5.5° and 13.5°, respectively. The multi-depth cost function aimed at minimizing the maximum side and grating lobe levels (SLL and GLL) outside the main lobe region.

The 256 elements positions of two 7MHz sparse arrays were optimized using SA with $2.56 \cdot 10^9$ iterations. The first solution (*opti1d*) was obtained by optimizing the beam pattern only at the focal depth (R_2), as in literature, whereas the second solution (*opti3d*) was optimized at R_1, R_2, and R_3. During the optimization, the simulations were done using FIELD II, and all arrays had a 6 mm aperture radius, λ-size square elements and focal point at 25 mm on z-axis.

Finally, their performance in terms of beam patterns, SLL, resolution, and sensitivity was compared to that of the spiral array. Beams produced by a 2D dense array (2292 elements) are also taken as a reference.

Results/Discussion

As reported in Table 1, *opti3d* is 1.2dB more sensitive than *opti1d*. Furthermore, even though *opti1d* achieves an optimal behavior at 25 mm (Figure 1) its beam profiles are 18.5 dB and 12.2 dB higher than in *opti3d* at 15mm and 35mm depths, respectively. This outlines the risks connected to single depth optimization with no control out of the

focal depth. Compared to the spiral array, *opti3d* is 1dB less sensitive but it has comparable SLL and resolution (Table 1). The median distances between the spiral and the *opti3d* arrays beam profiles are 2.13dB, 0.56dB, and 0.81dB at R_1, R_2, and R_3 respectively.

Figure 1: Multi-depths beam profiles of dense, spiral, opti1d and opti3d arrays (focusing at 25 mm on z-axis)
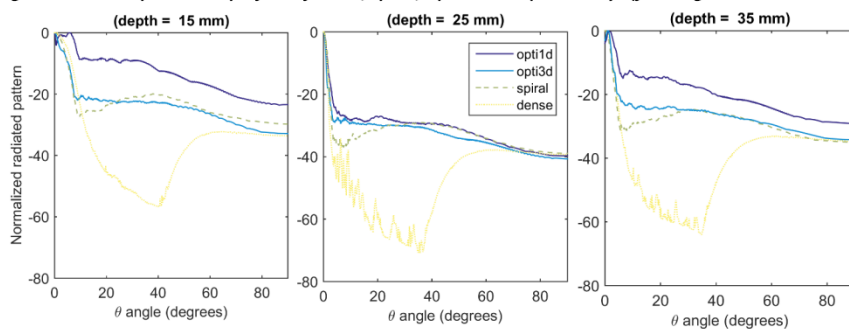
Table 1: Median values of the side lobe (SLL), resolution and sensitivity of dense, spiral, opti1d and opti3d arrays computed at all depths [10-40] mm over 81 steering angles ([-32°, +32°] in both elevation and azimuthal directions)

	SLL (dB)	**resolution** *(-6dB)*		**sensitivity** (dB)
		degrees	mm	
Dense array ($N_e = 2292$)	-21.5	3.23	1.41	0.00
Spiral array ($N_e = 256$)	-15.6	2.91	1.27	-5.88
Opti1d array ($N_e = 256$)	-14.0	2.48	1.08	-8.09
Opti3d array ($N_e = 256$)	-16.1	2.98	1.30	-6.89

8C-6

4:45 pm   **Design and fabrication of relaxor-ferroelectric single crystal PIMNT/epoxy 2-2 composite based array transducer**

Qingwen Yue[1]; [1]*Shanghai Institute of Ceramics,Chinese Acadmy of Science, China, People's Republic of*

Background, Motivation and Objective

Relaxor-based ferroelectric single crystals Pb(Mg1/3Nb2/3)O3-PbTiO3 (PMNT) and Pb(In1/2Nb1/2)O3-Pb(Mg1/3Nb2/3)O3-PbTiO3 (PIMNT) have attracted considerable attention because of their extremely high piezoelectric and electromechanical coupling coefficients near the morphotropic phase boundary (MPB) (d33~2000pC/N, d31~-2000pC/N, d15~6000pC/N, k33~0.92, k31~0.94, k15~0.97)[7,8,9]. Among these high performance relaxor-based ferroelectric single crystals, ternary single crystal PIMNT exhibits increasing competiveness due to their ultrahigh piezoelectric properties and improved thermal stability such as the increased MPB temperature (>120 ¡ãC), Curie temperature (>180 ¡ãC), and coercive field (> 5 kV/cm), in comparison to the PMNT single crystals.It was an important breakthrough for the 1-3 and 2-2 piezoelectric composites consisting of finite-sized piezoelectric single-crystal or ceramic bars and beams embedded respectively in a passive polymer matrix in overcoming the limitations of acoustic impedance matching, relative pulse-echo sensitivity, and operating bandwidth in monolithic single-crystal and ceramic-based ultrasonic transducers and transducer arrays.

Statement of Contribution/Methods

In this paper, we report the design, preparation, and electromechanical properties of a 65 vol% PIMNT/epoxy 2¨C2 composite as well as the design, fabrication, and performance of a 10 MHz PIMNT/epoxy 2¨C2 composite linear array transducer. The results of the developed PIMNT/epoxy 2¨C2 composite and ultrasonic transducer are compared with those of the PIMNT single crystal based array transducer at the same working frequency.

Results/Discussion

By designing the size of the single crystal beam in 2-2 composite, pure height-extensional mode was achieved. Based on the improved flexibility of the composite, a 12-elements high frequency array transducer was fabricated. A broad bandwidth(127.7%) and relative high pulse-echo sensitivity has been obtained. The results suggest a new approach to fabricate broadband ultrasonic array using 2-2 composite of relaxor-based ferroelectric single crystals.
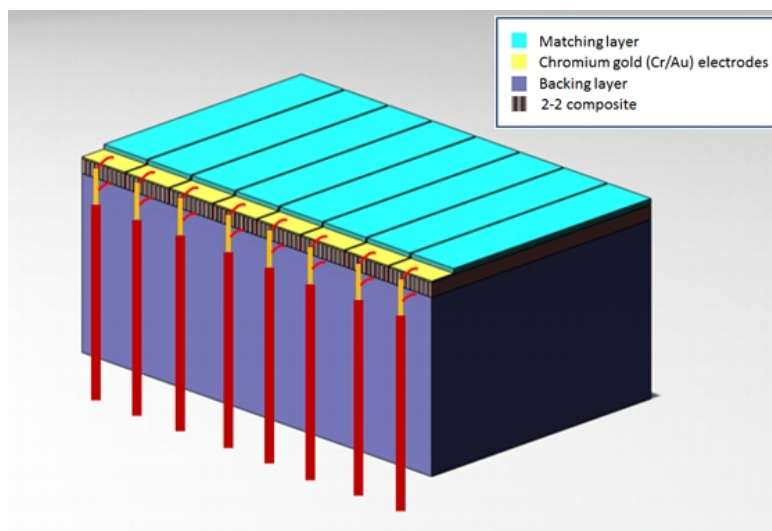
P1A1 - MEL: Elasticity Imaging: Simulations and Experimental Studies

4th floor

Thursday, October 22, 2015, Posters displayed 08:00 am - 05:00 pm. Authors must be present at their poster from 9:30 - 10:30am (odd number posters) and 14:30 – 15:30pm (even number posters).

Chair: **Brett Byram**
Vanderbilt University

P1A1-1

8:00 am   RSNA QIBA Ultrasound Shear Wave Speed Phase II Phantom Study in Viscoelastic Media

Mark Palmeri[1], Shigao Chen[2], Ted Lynch[3], Kathryn Nightingale[1], Ned Rouze[1], Pengfei Song[2], Matthew Urban[2], Hua Xie[4], Keith Wear[5], Brian Garra[5], Andy Milkowski[6], Paul Carson[7], Richard Barr[8], Vijay Shamdasani[9], Michael Macdonald[10], Yasuo Miyajima[11], Timothy Hall[12]; [1]*Biomedical Engineering, Duke University, Durham, NC, USA*, [2]*Mayo Clinic, USA*, [3]*CIRS, Inc., USA*, [4]*Philips Research, USA*, [5]*US Food and Drug Administration, USA*, [6]*Siemens Healthcare, USA*, [7]*University of Michigan Ann Arbor, USA*, [8]*Radiology Consultants, Inc., USA*, [9]*Philips Healthcare-Ultrasound, USA*, [10]*GE Healthcare, USA*, [11]*Toshiba Medical Research Institute USA, Inc., USA*, [12]*Medical Physics, University of Wisconsin Madison, Madison, WI, USA*

Background, Motivation and Objective

Significant intersystem variability in liver shear wave speed (SWS) measurements precludes meaningful comparison of measurements performed with different systems. The RSNA Quantitative Imaging Biomarker Alliance (QIBA) ultrasound SWS committee has been developing elastic and viscoelastic (VE) phantoms to evaluate system dependencies of SWS estimates used to non-invasively characterize liver fibrosis. Previous elastic phantom studies (Phase I) demonstrated intersystem variability ranging from 6-12% in elastic phantoms with nominal SWS of 1.0 and 2.0 m/s. A source of intersystem variability not characterized in the Phase I study was the impact of viscosity that can lead to phase velocity differences between imaging systems. The objective of our Phase II phantom study is to perform a systematic comparison of ultrasound imaging system-based SWS estimation in phantoms that have VE behavior similar to that observed in normal and fibrotic liver.

Statement of Contribution/Methods

CIRS, Inc. (Norfolk, VA) fabricated 3 phantoms (A1, B3, C1) using a proprietary oil-water emulsion infused in a Zerdine hydrogel. These phantoms were characterized by their phase velocity (200 Hz) and a linear fit of phase velocity as a function of temporal frequency (100-400 Hz) to provide an empirical, quantitative metric of their dispersion that is not dependent on an assumed viscoelastic material model. These metrics were compared to human data acquired by Duke and the Mayo Clinic/Philips Research. The 3 phantoms have been circulated to different academic, government and industry sites for measurement on different systems at focal depths of 3, 4.5 and 7 cm.

Results/Discussion

The 3 phantoms match the VE behavior of human data well (Fig. 1(a)). There is greater intrasystem SWS variance at the deeper depths (Fig. 1(b)), while there are statistically-significant differences across all the systems, with the greatest differences being in the most viscous phantom (C1). These data are expected to inform our parallel effort of developing calibrated VE digital phantoms to further understand the sources of bias and variance in these imaging systems. *Disclaimer: The mention of commercial products, their sources, or their use in connection with material reported herein is not to be construed as either an actual or implied endorsement of such products by the Department of Health and Human Services.*
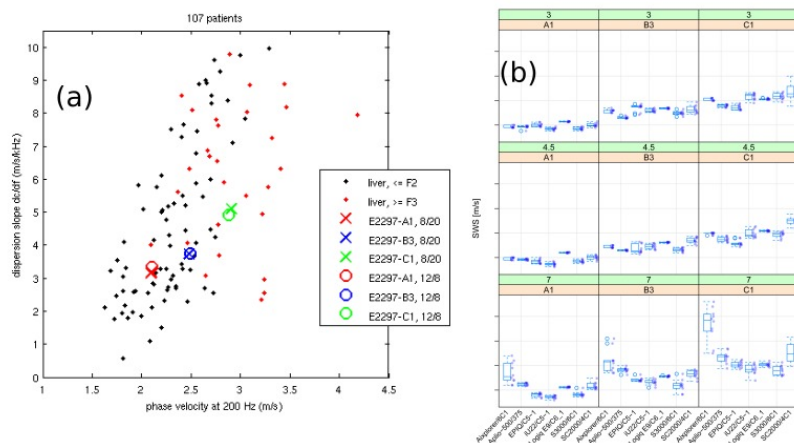
Figure 1: (a) CIRS phantom measurements (circles and crosses) made with a research SWS imaging system on different dates compared to human data categorized by fibrotic disease severity.
(b) Intersystem variability across different phantoms [A1, B3, C1] and imaging depths (3, 4.5, 7 cm). Absolute SWS values have been withheld due to the ongoing, blinded nature of the study.

P1A1-2

8:00 am   Estimation of degree of anisotropy in transversely isotropic (TI) elastic materials from acoustic radiation force (ARF)-induced peak displacements (PD)

Md Murad Hossain[1], Caterina Gallippi[1,2]; [1]*Joint Department of Biomedical Engineering, University of North Carolina, Chapel hill, North Carolina, USA*, [2]*Electrical and Computer Engineering, North Carolina State University, Raleigh, North Carolina, USA*

Background, Motivation and Objective

A TI material is defined by an axis of symmetry (AoS) perpendicular to a plane of isotropy. The mechanical properties (Young's modulus, shear modulus, and Poisson's ratio) are different in along versus across the AoS. In shear wave elastography imaging (SWEI), the anisotropy of the tissue is estimated as the ratio of shear wave velocity (SWV) along versus across the AoS. The objective of this work is to present a novel way of describing the anisotropy of a TI material using ARF induced peak displacements. We defined the anisotropy as the ratio of PD when the AoS is oriented along versus across the elevational dimension of an asymmetric ARF point spread function (PSF). Our hypothesis is that PD will relate degree of anisotropy in both Young's and shear moduli.

Statement of Contribution/Methods

To find the effect of Young's and shear modulus on anisotropy, eleven TI elastic materials were modeled using LS-DYNA3D with the following range of elastic constants: E_T= 15.35- 54 kpa; E_L=27.73-441 kpa; μ_T=4.01-15.85 kpa; μ_L=16 -36 kpa; ν_LT=0.51-0.96; ν_TT was kept constant to 0.499 (incompressible TI materials); where E = Young's modulus, μ= shear modulus, υ= Poisson's ratio, L= along the AoS, and T= across the AoS. The materials were excited with ARF excitations, modeled using Field II as the 3D acoustic intensity fields associated with a Siemens VF7-3 linear array transducer centered at 4.21 MHz with F/1.5 focal configuration. The ARF magnitude was kept constant at same region of excitation for 70 µs. Simulations were performed for a total time of 3.5 ms with a 10 kHz PRF.

Results/Discussion

The anisotropy (PD when AoS is oriented along elevation / PD when AoS is oriented across elevation) of a TI material (E_L=47.25 kpa,E_T=30.24 kpa,μ_L=16 kpa,μ_T=9 kpa and ν_LT=0.68) was 1.23 (15.67 µm/12.69 µm), whereas the SWEI technique gave an anisotropy value of 1.33 (4 ms^(-1)/3 ms^(-1)). When only the Young's modulus was varied (E_L=216 kpa,E_T=34.56 kpa), without changing the shear modulus value, the SWEI technique gave the same value of anisotropy 1.33. However, anisotropy measured using PD gave value of 1.25 (15.03 µm/11.98 µm). The correlation between ARF PD ratio and material shear modulus ratio was 0.96 in the eleven simulated TI materials. When Young's modulus was considered in the definition of material anisotropy as: $(-(\nu\_TT*E\_L +\nu\_LT*E\_T)*\mu\_L*\mu\_T +(f\_lat*\mu\_T+f\_ele*\mu\_L)*E\_L*E\_T)/(-(\nu\_TT*E\_L +\nu\_LT*E\_T)*\mu\_L*\mu\_T +(f\_ele*\mu\_T+f\_lat*\mu\_L)*E\_L*E\_T)$ where f_ele/f_lat is the ratio of the elevational to the lateral spatial extent of the ARF PSF, the correlation between PD ratio and material anisotropy increased to 0.98. This finite element analysis illustrates that the ratio of ARF-induced PD can be used as a measure of anisotropy in TI materials and that the anisotropy measure is sensitive to both Young's and shear moduli. However, a numerical solution is needed to directly relate PD ratio to specific degrees of anisotropy in Young's and shear moduli.

P1A1-3

8:00 am　　**Experimental study on the effect of the cylindrical vessel geometry on arterial shear wave elastography**

Darya Shcherbakova[1], Annette Caenen[1], Simon Chatelin[2], Clement Papadacci[2], Mathieu Pernot[2], Abigail Swillens[1], Patrick Segers[1]; *[1]iMinds Medical IT, IBiTech-bioMMeda, Ghent University, Ghent, Belgium, [2]Institut Langevin, ESPCI ParisTech, CNRS UMR7587, INSERM U979, Paris, France*

Background, Motivation and Objective

Supersonic shear wave imaging (SSI) in arteries is typically applied in the longitudinal view, as this facilitates acquisition of shear wave (SW) propagation. However, the collagen fibers in arteries are mainly circumferentially oriented to bear the load, leading to typical pressure-induced stiffening. As such, assessing the SW propagation along the fiber direction (circumferential view) might be a more sensitive and meaningful measurement. We investigated the influence of these two imaging planes (longitudinal/circumferential), focusing on the geometrical effect of the cylindrical vessel shape on SW propagation, by using an in-vitro PVA hydrogel phantom lacking arterial fibers.

Statement of Contribution/Methods

We created a polyvinyl alcohol (PVA) hydrogel tubular phantom (6 mm inner diameter, 2.5 mm wall thickness), freeze-thawed twice at -20/20°C. The submerged phantom was pressurized with a water column at 0, 30 and 60 mmHg. SSI measurements were performed in longitudinal and circumferential directions using the Aixplorer system, at a depth 6 to 18 mm and 8 MHz push, with duration of 250 µs. The SW group speed was derived using a time-of-flight algorithm at each pressure level in the circumferential and longitudinal views. Mechanical testing of a PVA-sample yielded a Young's modulus ($E \approx 3\mu$) of 72.6 kPa.

Results/Discussion

Examples of SW propagating in the axial-lateral plane in time are shown in Fig. 1A. Presence of the second circumferential wave in the longitudinal excitation view is clearly visible at time points of 2.0 ms, 2.2 ms and in the corresponding shear wave speed (SWS) map. In the circumferential direction wave interference is visible with 2 pairs of shear wave fronts, looping towards each other and hence imposing limited time window for time-of-flight algorithm estimation (after ≈1 ms fronts first interfere). As can be seen from the SWS maps, more dispersion occurs in the circumferential direction, making group speed estimation more challenging.

Longitudinal wave fronts
Circumferential wave fronts moving counterclockwise
Circumferential wave fronts moving clockwise
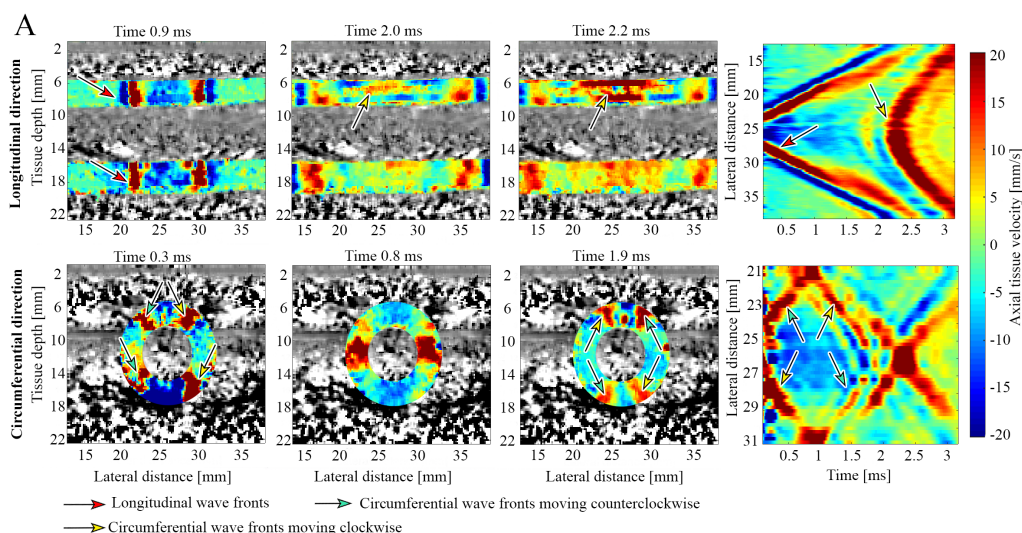
P1A1-4

8:00 am　　**High line-density pulse wave imaging for local pulse wave velocity estimation using motion matching: A feasibility study on vessel phantoms**

Fubing Li[1], **Qiong He[1]**, Chengwu Huang[1], Jianwen Luo[1]; *[1]Department of Biomedical Engineering, Tsinghua University, Beijing, China, People's Republic of*

Background, Motivation and Objective

High frame rate (FR) (>200 Hz) is required in pulse wave imaging (PWI) to estimate regional pulse wave velocity (PWV) of arteries, and can be achieved by sparse imaging or plane wave imaging at the expense of spatial resolution or signal-to-noise ratio (SNR). However, both high line-density (LD) and high FR are required when mapping local PWV variations along inhomogeneous arteries. In this study, a motion matching method was developed to obtain high LD data at high FR. The feasibility of this method was tested and its performance was compared with those with sparse imaging and plane wave imaging.

Statement of Contribution/Methods

A homogeneous and 3 half-soft-half-stiff polyvinyl alcohol cryogel vessel phantoms were made. The phantom was connected with a pulsatile pump to generate pulse waves and scanned by a SonixMDP system (Ultrasonix) with an L14-5/38 probe. A 38-mm imaging field of view (FOV) was divided into 4 sub-sectors, each with 34 beams including a common beam. For each sector, high LD and high FR (~507 Hz) RF data were acquired for several pulse cycles. The full FOV (128 beams, 38 mm) data was reconstructed from the sub-sector frames by aligning the estimated vessel motion along the common beam. The composite RF frames were then post-processed using PWI technique. Local PWV was estimated within a sliding kernel of ~10 mm along the vessel wall. For comparison, the sparse imaging (32 beams, 38 mm) and plane wave imaging (128 beams, 38 mm) methods were also implemented.

Results/Discussion

For the homogeneous phantom, local PWV measurements show good agreement between the sparse imaging and proposed method, with slightly lower standard deviations (SDs) when using the proposed method. More fluctuations of local PWV measurements are found with plane wave imaging (Fig. 1(a)). In addition, in the low SNR condition (with a plastic sheet inserted above the phantom), the proposed method obtains significantly smaller SDs than sparse imaging (Fig. 1(b)). For the inhomogeneous phantoms, significant difference of local PWV measurements between the stiffer and softer regions is found, and the proposed method obtains the lowest SDs (Fig. 1(c)). The proposed method is capable of obtaining simultaneously high LD (128 beams within 38 mm) and high FR (>500 Hz) data and mapping local PWV variations. Its performance is found to be superior to the sparse imaging and plane wave imaging methods.
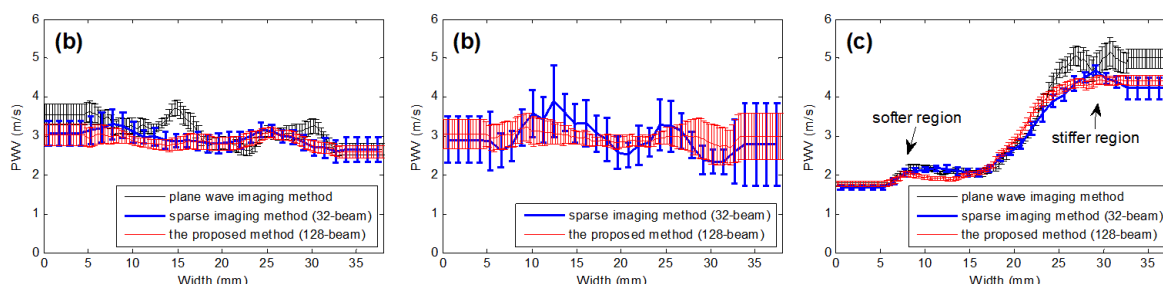
Fig. 1 Local PWV variations of the homogeneous phantom in (a) high SNR and (b) low SNR conditions, and of (c) the inhomogeneous phantom. The mean and SD of the local PWVs were estimated from data in 10 pulse cycles.

P1A1-5

8:00 am   Viscoelastic tissue mimicking phantom validation study with shear wave elasticity imaging and viscoelastic spectroscopy

Carolina Amador[1], Randall Kinnick[1], Matthew Urban[1], Mostafa Fatemi[1], James Greenleaf[1]; *[1]Department of Physiology and Biomedical Engeenering, Mayo Clinic College of Medicine, Rochester, Minnesota, USA*

Background, Motivation and Objective

Acoustic radiation force shear wave elasticity imaging (SWEI) methods are being used to characterize soft tissue pathologies by assessing the viscoelastic (VE) properties of tissue. Tissue mimicking phantoms are frequently used in the evaluation of SWEI methods. To adequately evaluate the SWEI methods, it is extremely important to characterize the VE properties of tissue mimicking phantoms with an independent method. In this study, we developed VE tissue mimicking phantoms that were then tested with SWEI and VE spectroscopy methods.

Statement of Contribution/Methods

VE tissue mimicking phantoms consisting of 8% gelatin (Sigma-Aldrich, St. Louis, MO), 1% potassium sorbate (Sigma-Aldrich), 1% cellulose (Sigma-Aldrich), 6% propylene glycol and 0.5% xanthan gum were made by volume concentration. To vary the VE properties, two phantoms were made with 5% (Phantom 2) and 10% (Phantom 3) of Vanicream Lite (Pharmaceutical Specialties, Inc., Rochester, MN). The control phantom (Phantom 1) did not have Vanicream. From a given batch, each phantom mixture was poured into 3 cylinders (9.4 mm diameter and 44 mm height) for VE spectroscopy measurements and in a cube with 40 mm x 60 mm x 38 mm (width x length x height) dimensions for SWEI measurements. For the VE spectroscopy experiments, a RheoSpectris C500 (Rheolution, Inc., Montreal, QC, Canada) with the cylinder fixture was used to measure complex modulus with frequencies between 10 Hz and 2000 Hz. For SWEI experiments, a Verasonics ultrasound system (Verasonics, Inc., Kirkland, WA) equipped with a linear array transducer (L11-4v, Verasonics, Inc., Kirkland, WA) was used. Experiments were completed one day and one week after phantom preparation. Phantoms were covered with paraffin film and stored at room temperature in between the study dates. A Kelvin-Voigt fractional derivative (KVFD) model was fit to VE spectroscopy measurements and SWEI measurements at frequencies from 100 - 500 Hz. The KVFD model parameters μ_1 [Pa], μ_2 [Pa·s], α and the fit's mean squared error (MSE) from SWEI and VE spectroscopy were compared.

Results/Discussion

One week post phantom preparation, the KVFD model parameters (μ_1 [kPa], μ_2 [Pa·s], α) for Phantom 1 were 3.95, 1.8, 0.8 for SWEI and 3.71, 2.4, 0.77 for VE spectroscopy, for Phantom 2 were 3.89, 2.4, 0.8 for SWEI and 3.79, 3.11, 0.75 for VE spectroscopy and for Phantom 3 were 3.76, 10, 0.6 for SWEI and 3.8, 8.5, 0.63 for VE spectroscopy. The MSE for all fits was less than 0.01. In this study, we have proposed a new formulation for VE tissue mimicking phantoms and evaluated the complex modulus of these phantoms with two independent methods. The study found that for the proposed VE phantoms, one week of aging after phantom preparation is required for material stability. The results showed an increasing viscosity (μ_2) as the Vanicream concentration increased from 0% to 10%. (This study was supported in part by NIH grants R01DK092255 and R01CA168575).

P1A1-6

8:00 am   Comparison of techniques for estimating shear-wave velocity in arterial wall using shear-wave elastography - FEM and phantom study

Jun-keun Jang[1], Kengo Kondo[1], Takeshi Namita[1], Makoto Yamakawa[1], Tsuyoshi Shiina[1]; *[1]Graduate School of Medicine, Kyoto University, Kyoto, Japan*

Background, Motivation and Objective

Shear-wave elastography (SWE) enables us to calculate the Young′s modulus of soft tissue directly from the shear-wave velocity (C_S) that can generally be estimated by the time-of-flight method (TM). However, shear waves in the arterial wall, a thin-layered tubular medium, are influenced by strong dispersion effects. Recent studies have overcome this limitation using the Lamb-theory-based method (LM). In this work, we performed both experimental and finite- element (FE) analyses for thin-layered media to evaluate the advantage of LM over TM.

Statement of Contribution/Methods

PZFlex® FE analysis software applied the axial pressure shown in Fig. 1 (a). The generated shear waves then propagated in the lateral direction. After axial velocity data was obtained from the FE analysis, each C_S was estimated by TM and LM. To validate FE results, we conducted an experiment on the thin-layered phantom (Fig. 2 (a)). After

obtaining IQ data with an Aixplorer® ultrasound system and a 7.5MHz linear probe, we measured axial velocity data with a 2D autocorrelator and then estimated each C_S using the two methods.

Results/Discussion

Figures 1 (b) and 2 (b) illustrate the results of TM; Figs. 1 (c) and 2(c) illustrate those of LM. C_{S_MEAN} in Fig. 1 (b) was not equal to C_T in Fig. 1 (a) and exhibited a non-uniform distribution despite being a homogeneous medium. In contrast, LM accurately estimated C_S in Fig. 1 (C). There was a considerable discrepancy between C_{S_MEAN} in Fig. 2 (b) and the previously measured C_S (=5.6m/s) of a bulk sample of a 1.5% agar phantom, but Fig. 2 (c) did not exhibit any significant difference in C_S. In conclusion, LM can accurately estimate C_S for thin-layered media, but TM is suitable only for unbounded media. The result of a tube phantom will be discussed later to further validate our findings.
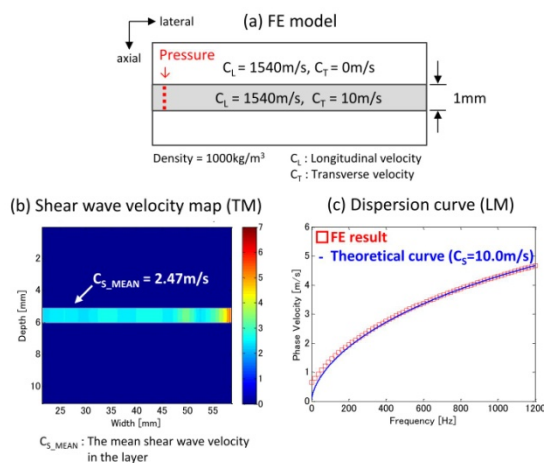
Figure 1. The result of FE analysis
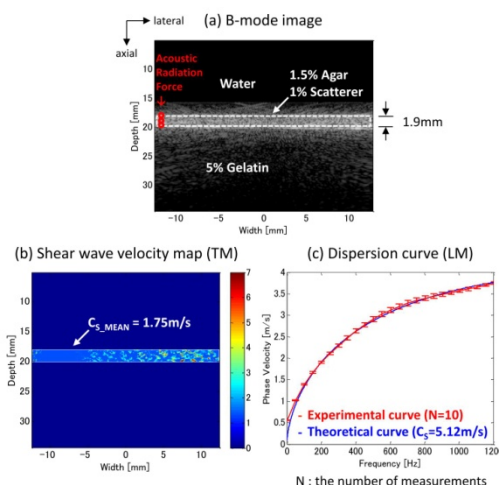
Figure 2. The result of phantom experiment

P1A1-7 _____

8:00 am **Viscoelasticity and shear wave velocity of liver tissue evaluated by dynamic mechanical analysis**

Kenoh Murakami[1], Kenji Yoshida[2], Kazuya Kawamura[2], Mariko Tsukune[3], Yo Kobayash[4], Masakatsu Fujie[5], Riwa Kishimoto[6], Takayuki Obata[6], Tadashi Yamaguchi[2]*; [1]Graduate School of Engineering, Chiba University, Chiba, Japan, [2]Center for Frontier Medical Engineering, Chiba University, Chiba, Japan, [3]Graduate School of Science and Engineeringand Institute of Advanced Active Aging Research, Waseda University, Tokyo, Japan, [4]Research Institute for Science and Engineering, Waseda University, Tokyo, Japan, [5]Faculty of Science and Engineering, Waseda University, Tokyo, Japan, [6]Research center for charged particle therapy, National Institute of Radiological Science, Chiba, Japan*

Background, Motivation and Objective

In shear wave elastography (SWE) of liver, the frequency dependence of shear wave velocity is significant information for evaluating viscoelastic character of tissue relating to fibrosis. Although Voigt model has been often used in viscoelastic analysis, several studies showed that the experimental data was not consistent with the theoretical prediction. To experimentally investigate the frequency dependence of viscoelasticity of liver tissue, dynamic mechanical analysis (DMA) tests of rat and pig livers are conducted using a rheometer, and shear wave velocity is calculated from the result of DMA tests.

Statement of Contribution/Methods

The storage and loss modulus of sample were measured by a rheometer (AR-G2, TA-Instruments). In the DMA tests, the columnar sample with diameter of 8 mm and thickness of 2.5 mm was sandwiched by parallel plate and twisted by sinusoidally-varying torque. The frequency of the torque was swept from 0.1 Hz to 10 Hz. The homogenous acrylamide gel phantom, rat and pig livers were prepared for the tests. Shear wave velocity was calculated from the storage and loss modulus assuming that the density of sample is 1000 [kg/m3].

Results/Discussion

Assuming of Voigt model, there is no frequency dependence in storage modulus. Loss modulus is proportional to the frequency. Figure 1(a) show that storage modulus of rat and pig liver increase with increasing in the frequency although that of gel phantom has no frequency dependence in the range of 0.1 - 3 Hz. In Fig. 1(b), loss modulus of all sample have approximately-same frequency dependence although they do not obey the Voigt model. As a result, shear wave velocity has frequency dependence as shown in Fig.1(c). It is interesting that the frequency dependence below 3 Hz is different from that above 3 Hz. In measured range of 0.1 - 10 Hz, the frequency dependence of share wave velocity results from that of storage modulus because loss modulus is typically much smaller than storage modulus. The future task is to interpret the physical meaning of measured frequency dependence for modeling viscoelastic behavior of liver.

(a) Storage modulus (b) Loss modulus (c) Shear wave velosity
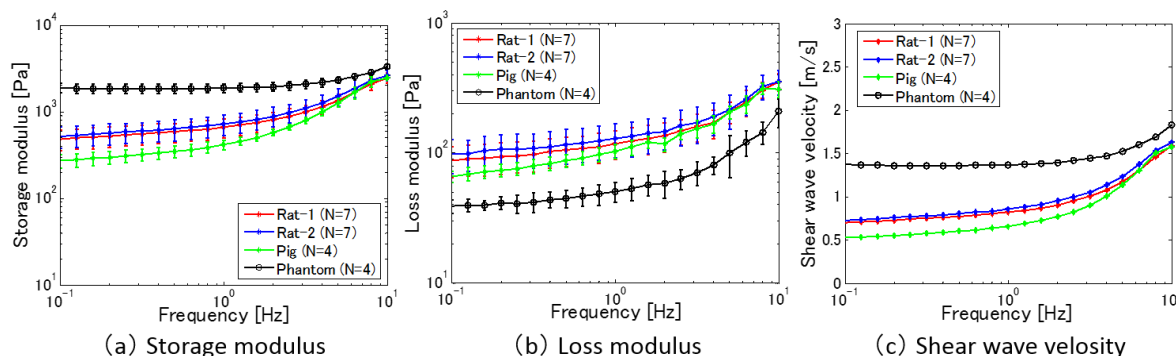
Fig. 1 Frequency dependence of each object

8:00 am   Feasibility of micro-elastography for tissue surrounding phase-change microbubbles using bubble wavelet transform

Runna Liu[1], Rui Huo[1], Hong Hu[1], Shanshan Xu[1], Supin Wang[1], Mingxi Wan[1]; *[1]The Key Laboratory of Biomedical Information Engineering of Ministry of Education, Department of Biomedical Engineering,School of Life Science and Technology,Xi'an Jiaotong University, Xi'an, Shaanxi, China, People's Republic of*

Background, Motivation and Objective

Pathological states of soft tissue are usually correlated with changes in its mechanical properties. Currently, several sonoelastographic methods have been developed to evaluate the elastic properties. However, applicability of sonoelastography for small targets such as tissues surrounding tumor angiogenesis, is limited because of poor resolution and difficulty in producing detectable strain by external induction or internal physiological fluctuations. We propose to explore the possibility of quantifying the viscoelastic properties of soft tissues through phase-change microbubble dynamic in tissue and bubble wavelet transform detection method.

Statement of Contribution/Methods

The proposed method was first validated by phantom experiments. Two transparent homogeneous tissue-mimicking phantoms with different rigidity (15% and 30%) were prepared, namely soft and hard phantom, respectively, in which nanoparticles of perfluoropentane (F2 Chemicals Ltd., Preston, UK) were evenly distributed. Sparsely distributed phase-change microbubbles were produced by a focused single element concave transducer (a 100 mm diameter, a geometric focal length of 75 mm and a working frequency of 1.6 MHz, Imasonic, Besancon, France). A Sonix-Touch ultrasound scanner with a 5 MHz linear array (Ultrasonix, Burnaby, BC, Canada) was used for acquisition of backscattering signals.

Firstly, a mother wavelet named bubble wavelet was constructed according to Keller-Miksis equation incorporating the Voigt model, which was accounting for large-amplitude bubble oscillations in viscoelastic media. With different viscoelastic parameters including shear elasticity and viscosity, a series of bubble wavelets were constructed. Secondly, continuous wavelet transform at various resolution levels was used to analyze the correlation between the backscattering signals and bubble wavelets. The wavelet coefficients were then used to replace the backscattering signals and obtain a series of images with the post-processing producer, including logarithmic compression, coordinate transformation, and grayscale scan conversion. Thirdly, signal-to-noise ratio (SNR) of images was served as an index to evaluate this method quantitatively and defined as the ratio of the power backscattering signals from the phase-change microbubbles to that from the noise. The optimal image with high SNR was obtained after comparison. Finally, the relationship between SNR, shear elasticity and viscosity revealed the viscoelastic properties of the phantoms.

Results/Discussion

The values for shear elasticity and viscosity were 0.61 MPa and 0.009 Pa.s for the soft phantom and 1.13 MPa and 0.012 Pa.s for the hard phantom. These measured values of shear elasticity revealed the difference in the rigidity of the phantoms. Further studies are needed to evaluate the proposed method by comparison with other methods.

P1A2 - MBE: Bioeffects in Cells and Tissue

4th floor

Thursday, October 22, 2015, Posters displayed 08:00 am - 05:00 pm. Authors must be present at their poster from 9:30 - 10:30am (odd number posters) and 14:30 – 15:30pm (even number posters).

Chair: **Jonathan Mamou**
           Riverside Research

P1A2-1

8:00 am   Study the Cell Death Induced by Subcellular Localized Sonodynamic Therapy

Yongmin Huang[1], Zhihai Qiu[1], Yaoheng Yang[1], Cheng Liu[1], SUN Lei[1]*; [1]The Hong Kong Polytechnic University, Hong Kong*

Background, Motivation and Objective

Sonodynamic therapy (SDT), based on the synergistic effects of low intensity ultrasound and sonosensitizer, is a potential noninvasive approach for the treatment of cancers. Although several mechanisms have been proposed, the most commonly understood one is that SDT can induce cancer cells to produce reaction oxygen species, especially the singlet oxygen ($^1O_2$). As a toxic agent, $^1O_2$ can interact with a wide range of molecules and organelles and cause cancer cells death. Considering the complexity of a cell, the possible responses are diverse when $^1O_2$ is produced in different subcellular localization. For example, $^1O_2$ produced in the cell membrane elicits a different response from $^1O_2$ produced in the cell mitochondria. To optimize the SDT treatment requires a better understanding of the intrinsic sonodynamic functional mechanism in different subcellular localization.

Statement of Contribution/Methods

During the SDT experiments, breast cancer cells MCF-7 were incubated with sonosensitizer protoporphyrin IX (PpIX, targeted on cell membrane) and 5-aminolevulinic (ALA, targeted on cell mitochondria). After incubation, PpIX and ALA subcellular distribution was imaged by confocal microscopy. Then both cells were treated by low intensity ultrasound (frequency of 1.0MHz, Ispta of 500mW/cm2, duty circle of 20%) for 10 minutes. Following ultrasound treatment, part of the MCF-7 cells were loaded with singlet oxygen sensor green (SOSG) and performed confocal microscoopy to probe $^1O_2$ subcellular spatial distribution. Meanwhile, the rest of the MCF-7 cells undergo Hoechst 33342/PI stain and flow cytometry every 30 minutes for the analysis of the necrosis and apoptosis ratio.

Results/Discussion

Confocal images showed that PpIX and ALA adhered to the cell membrane and mitochondria, respectively. It was also confirmed that $^1O_2$ was produced in membrane and mitochondria after ultrasound treatment. Hoechst 33342/PI stain and flow cytometry results demonstrated that there were more necrosis when loaded with PpIX and more apoptosis when loaded with ALA. Such results indicated that the production of $^1O_2$ in membrane tends to induce necrosis, in contrast, the production of $^1O_2$ in mitochondria tends to induce apoptosis. In conclusion, the subcellular localized SDT can result in different cell death pathway and provide us a multi-choice method to enhance the SDT effect.

P1A2-2

8:00 am   Impact of Microbubble-to-cell Parameters on Heterogeneous Sonoporation at the Single-Cell Level

Peng Qin[1], Yutong Lin[1], lifang Jin[2], Lianfang Du[2], Alfred C H Yu[3]*; [1]Instrumentation Science and Engineering, shanghai Jiao Tong University, Shanghai, China, People's Republic of, [2]Department of Ultrasound, Shanghai Jiaotong University Affiliated the First People's Hospital, Shanghai, China, People's Republic of, [3]Medical Engineering Program, The Univeristy of Hong Kong, Hong Kong*

Background, Motivation and Objective

Sonoporation as transient plasma membrane perforation elicited by ultrasound and microbubble has been shown great potential for drug delivery. However, the heterogeneity of sonoporation causes complexity and challenge in the realization of controllable and predictable delivery. The aim of this work is to understand how the non-acoustic microbubble-to-cell parameters lead to variable sonoporation.

Statement of Contribution/Methods

Using a customized ultrasound exposure and fluorescence imaging platform, we observed sonoporation dynamics at the single-cell level and quantified exogenous molecular uptake level to evaluate the extent of sonoporation. Sonovue microbubbles with different concentration were introduced to passively regulate the microbubble-to-cell parameters, i.e. distance, number and size. One MHz ultrasound with 10 cycle duration (10 Îs) and 0.5 MPa peak negative pressure (calibrated by a needle hydrophone) were applied to trigger the collapse of bubbles. The time-lapse fluorescence images of PI (for sonoporation tracking) were acquired at 30 sec interval over 10 min period after exposure, and then the mean fluorescence intensity was measured to determine PI uptake level. Cell viability was evaluated by calcein blue fluorescence images at 10 min.

Results/Discussion

Our results revealed the impact of microbubble-to-cell parameters on the heterogeneity of sonoporation.1) when the bubble diameter (D) is less than 5.5 um, no sonoporation (Type I) was observed when d/D > 1 (d refers to the distance of microbubble from the cell) while reversibly mild sonoporation (Type II) occurred by the localized collapse of bubble when d/D < 1. 2) The bubble exhibited translational movement with collapse when D > 5.5 um. The translation toward the cellular surface or along the plasma membrane could lead to reversibly moderate sonoporation (Type III) or irreversibly intense sonoporation (Type IV). The translation in the opposite direction away from the cell would generate Types I or II sonoporation. 3) The number of bubbles is positively correlated with the degree of sonoporation when D < 5.5 um and d/D < 1. Localized collapses of two to three bubbles would result in Types II or III sonoporation while Type IV was found after the collapse of four or more bubbles. Our study suggests non-acoustic parameters are essential for the application of sonoporation in drug delivery.

A. Single Bubble (0 < D < 5.5 μm)

B. Single Bubble (D > 5.5 μm)

C. Multiple Bubbles (0 < D < 5.5 μm; d/D < 1)

Symbol	Meaning
Ultrasound	
Microbubble	
Cell	
PI molecule	
D	Cell Diameter
d	The distance of bubble from cell
Type I	No sonoporation
Type II	Mild sonoporation
Type III	Moderate sonoporation
Type IV	Intense sonoporation
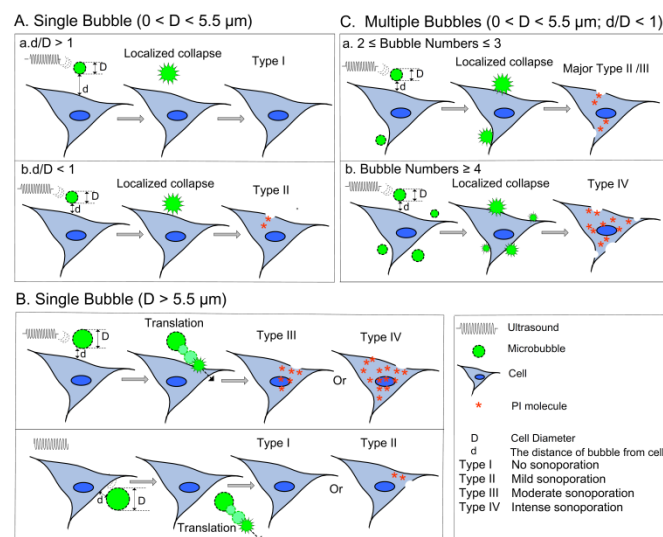
P1A2-3

8:00 am   Effects of low-intensity pulsed ultrasound on nerve growth factor-induced neurite outgrowth and signaling in PC12 cells

Lu Zhao[1], Yi Feng[1], Mingxi Wan[1]; *[1]The Key Laboratory of Biomedical Information Engineering of Ministry of Education, Department of Biomedical Engineering,School of Life Science and Technology,Xi'an Jiaotong University, Xi'an, Shannxi, China, People's Republic of*

Background, Motivation and Objective

Nerve growth factor (NGF) therapy has been considered as potential therapeutic approach for the treatment of neural injury and degeneration. However, the high concentration of NGF may exert adverse effects on other cell types and long period treatment of NGF raises an issue of medical cost. Thus, investigating combination of NGF therapy with other approach to promote neurite outgrowth is of great interest. In this study, we intend to explore the possibility and associated molecular mechanisms of combining NGF and low-intensity pulsed ultrasound (LIPUS) in promoting neurite outgrowth, which is an essential process in neural regeneration.

Statement of Contribution/Methods

PC12 cells, which will differentiate into neurons upon NGF stimulation, were seeded on the polylysin-coated well plate as the in vitro model. LIPUS were applied to PC12 cells for 10 min every other day with spatial average intensity 50 mW/cm2, 20% duty cycle, 100 Hz pulse repetition frequency and 1 MHz ultrasound, and then incubated with NGF (50 ng/ml). PC12 cells were photographed on the second, forth, sixth days after LIPUS treatment using light microscopy and harvested at seventh day for Western Blot analysis.

Results/Discussion

LIPUS alone could not significantly induce neurite outgrowth in PC12 cells. However, LIPUS could significantly enhance the neurite length but not attachment point, indicating that its primary effect on neurite elongation instead of initiation. In addition, LIPUS increased the phosphorylation levels of ERK1/2 and CREB in the presence of NGF, but not change the levels of Akt and STAT3. We also found that ERK1/2 inhibitor PD98059 significantly attenuated LIPUS-induced neurite outgrowth. Moreover, LIPUS increased NGF-induced expression of neurotrophic cofactor thioredoxin (Trx), a downstream effector of ERK1/2-CREB. Taken together, these results provide important insights that LIPUS synergistically enhances NGF-induced ERK1/2-CREB-Trx pathway to promote neurite outgrowth. The combination therapy of LIPUS and NGF could potentially be considered for the improvement of nerve regeneration.

P1A2-4

8:00 am   Sonodynamic Therapy of Breast Tumor by Using of IR-780 Dye

Fei Yan[1], Yekuo Li[2], Zhiting Deng[1], Hairong Zheng[1]; *[1]Paul C. Lauterbur Research Center for Biomedical Imaging, Shenzhen Institutes of Advanced Technology, China, People's Republic of, [2]Guangzhou General Hospital, China, People's Republic of*

Background, Motivation and Objective

Sonodynamic therapy (SDT) is developing as a new modality for cancer therapy through activating certain chemical sensitizers by ultrasound. Discovery and development of novel sonosensitizers is one of the most essential factors in SDT and is attracting extensive attentions in this research field. The aim of this work was to introduce IR-780 iodide, a lipophilic cation heptamethine dye with peak absorption at 780 nm, as SDT agents for breast cancer treatment.

Statement of Contribution/Methods

The in vitro cellular uptake, cell viability, and the generation levels of reactive oxygen species (ROS) were examined by using of 4T1 breast cancer cells incubated with various concentrations of IR-780 followed by US irradiation. Also, the tissue permeability and distribution of IR-780 in the tumor-bearing mice by a whole animal NIR imaging system were examined in order to determine the optimal time for in vivo SDT using IR-780. Moreover, the in vivo efficacy of IR-780 as a sonosensitizer against breast tumor was tested.

Results/Discussion

Our results showed that there was a dose- and time-dependence for cellular uptake of IR-780 iodide in 4T1 cancer cells. Significant lower viabilities and more necrotic/apoptotic cells were found when these cancer cells were treated with IR-780 iodide and US irradiation. Further analyzing the generation of ROS demonstrated the significantly increased levels of 1O2 and H2O2, but not •OH in the SDT-treated cells. The fluorescence signals of mice receiving intratumoral injection of IR-780 increased gradually as IR-780 diffusing in the tumor tissue, reaching a maximum tumor coverage area after 1 h. The in vivo anti-tumor efficacy of SDT with IR-780 revealed the great tumor growth inhibition of xenografts of 4T1 cancer cells. It was further confirmed by histological analysis and TUNEL staining. Our study strongly supported the notion that SDT with IR-780 will provide a promising ultrategy for tumor treatment with minimal side effects.

P1A2-5

8:00 am   DNA packing by low-intensity ultrasound

Donghee Park[1], Gillsoo Song[2], Hyunjin Park[3], Hyungbeen Lee[2], Ji-Young Jang[1], Han-Sung Kim[2], Chul-Woo Kim[1], Jongbum Seo[2]; [1]*Cancer Research Institute, Seoul National University College of Medicine, Seoul, Korea, Republic of,* [2]*Department of Biomedical Engineering, Yonsei University, Wonju, Korea, Republic of,* [3]*School of Electronic Electrical Engineering, Sungkyunkwan University, Suwon, Korea, Republic of*

Background, Motivation and Objective

Low-intensity ultrasound (hundreds of mW/cm^2) has been used as an effective modality to accelerate the osteogenic differentiation response in fracture healing. Even small DNA related structures including chromatin architecture can be transiently influenced by low-intensity ultrasound. We hypothesized that the proper low-intensity ultrasound sonication could physically and effectively compact a large population of free DNA in fluid. These findings indicate that ultrasound has the potential to alter the topology of DNA in the submicro- to micrometer range. In this study, we focused on the direct manipulation of DNA topology and retentivity of transiently influenced DNA using very low-intensity ultrasound.

Statement of Contribution/Methods

The 4.2-kbp pEGFP-C1(Roche Applied Science) were amplified in Escherichia coli and purified by Endo-free plasmid mega. Low-intensity ultrasound was applied to the purified pEGFP, then the topology change of pEGFP due to ultrasound was observed by atomic force microscopy (AFM). A single-element transducer with a 1/2-inch diameter aperture was used in the experiment at 1.12 MHz. An acoustic pressure of 126 kPa on the surface of the transducer with 1% duty cycle and 100 Hz pulse repetition frequency was used to generate the ultrasound intensity of 5.4 mW/cm^2 for 30 to 300 seconds. The AFM images of pEGFPs were quantitatively analyzed by the degree of bending based on image processing approaches.

Results/Discussion

In AFM images of normal pEGFP, some of the pEGFPs are supercoiled, while others are more relaxed to an extent that they appear open circular. On the other hand, most of sonicated pEGFP in results of AFM image seem tightly condensed. Comparing normal pEGFP and sonicated pEGFP in AFM image, the degree of supercoiling seems quite different. Considering that most of purified pEGFPs are already in supercoiled form, these results indicate that low-intensity ultrasound packs the supercoiled pEGFPs into a tighter form.

Degree of folding, designated as folding index, was measured using curvature values of the contours of the pEGFP. The mean values of the folding index were 181.3, 262.63, 311.7, 494.1, and 640.7 in control, 30-second, 60-second, 120-second, and 300-second group, respectively. The energy increased by increasing sonication time at a fixed duty cycle caused denser supercoiling of pEGFPs in the AFM images. The mean value of the folding index increases in a proportional manner as the sonication time increase. Additionally, the folding index in the control group did not change significantly (130 (one hour) -> 150 (one week)) while the folding index in the 30-second group reduced significantly (203 (one hour) -> 154(one week)) considering the SD value. We observed that the degree of folding decreased as time passed.

This study provides the first evidence to show that low-intensity ultrasound can directly alter DNA topology.

P1A2-6

8:00 am   On the thermal effect in biological tissues exposed to ultrasound of longer pulse duration after administration of contrast agents

Kazuki Akai[1], Yasunao Ishiguro[2], Naotaka Nitta[3], Hideki Sasanuma[2], Nobuyuki Taniguchi[4], Iwaki Akiyama[1]; [1]*Faculty of Life and Medical Sciences, Doshisha University, Kyotanabe, Kyoto, Japan,* [2]*Department of Surgery, Jichi Medical University, Shimotsuke, Tochigi, Japan,* [3]*Human Technology Research Institute, National Institute of Advanced Industrial Science and Technology, Tsukuba, Ibaraki, Japan,* [4]*Department of Clinical Laboratory Medicine, Jichi Medical University, Shimotsuke, Tochigi, Japan*

Background, Motivation and Objective

Acoustic radiation force impulse (ARFI) has recently been used to evaluate the stiffness of tissues. Typically, the ultrasound pulse used on this technology uses longer pulse durations (PD) and higher acoustic intensities compared with typical diagnostic ultrasound. Under WFUMB guidelines for safety criteria of diagnostic ultrasound, the maximum Mechanical Index (MI) value permitted is 1.9 and the I_{spta} is 720 mW/cm^2. Furthermore, when ultrasound contrast agents (UCA) are present during a HIFU, temperature rise have been observed. However, it is not yet clear how much the temperature increases with the ultrasound intensity level used in ARFI. Therefore, the purpose of this study was to identify the effects of temperature rise using the UCA (Sonazoid®) exposed to longer PD of ultrasound under regulation limits. This paper includes a phantom experiment and an animal experiment in order to find if ultrasound exposure increases the temperature in tissues due to the presence of microbubbles.

Statement of Contribution/Methods

Two types of tissue mimicking material (TMM) based on IEC60601-2-37 were used. One of these included fixed Sonazoid® microbubbles.

The experimental system as shown in Figure 1 has a focused transducer (2.5 MHz, focal length of 25 mm and an f-number of 2). The transducer has a hole in the center where a thermo-couple passes through.

In both experiments, the ultrasound exposure safety parameters were established within the aforementioned regulation limits (MI of 1.8 and I_{spta} of 715 mW/cm^2). The PD and pulse repetition time were determined as follows: 4.24ms, 2s; 10.6ms, 5s and 21.2ms, 10s. In the animal experiment, rabbits under general anesthesia were exposed to the same conditions. After a drip infusion of the UCA, the temperature rise of the liver was measured by placing the transducer on the rabbit′s abdomen.

Results/Discussion

The phantom experiment results are shown in Figure 2. From these results, the temperature rise was proportional to the PD with and without microbubbles. The temperature rise measured in the phantom with microbubbles was approximately 20 percent higher than the phantom without them. Nevertheless, as shown in Figure 3 a significant difference in the temperature rise due to the presence of microbubbles was not observed in the animal experiment. This is because the microbubbles collapsed by exposure to the high intensity ultrasound.
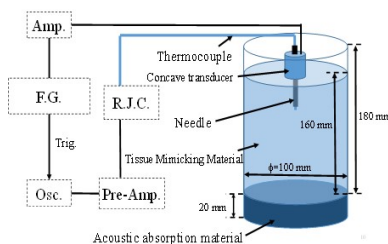
Fig. 1 Experimental system for measurement of temperature rise.
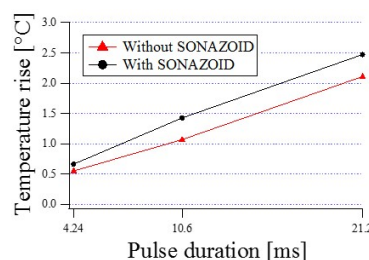
Fig. 2 The relationship between pulse duration and temperature rise (Phantom experiments).
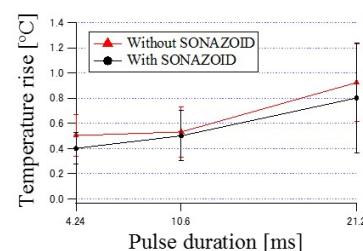
Fig. 3 The relationship between pulse duration and temperature rise (Animal experiments,n=5).

THURSDAY POSTER

8:00 am   Controlled thermal-sensitive liposomes release on a disposable microfluidic device

Long Meng[1], Zhiting Deng[1], Lili Niu[1], Feiyan Cai[1], Hairong Zheng[1]; *[1]Shenzhen Institutes of Advanced Technology, Chinese Academy of Sciences, Shenzhen, China, People's Republic of*

Background, Motivation and Objective

The recent technology that high intensity focused ultrasound (HIFU) can be used to trigger drug released from its carriers thermally has been considered as a promising approach for targeted drug delivery. Release of encapsulated drugs from nano-carriers such as liposomes under the stimulus of temperature elevation due to ultrasound absorption can achieve higher local drug concentration and reduce the toxicity. However, the complex and microscopic interactions between ultrasound and cells have proven to be difficult to reveal the mechanism of HIFU-mediated drug delivery. In this paper, HIFU is used in a microfluidic device to enable controlling the release of temperature-sensitive liposomes (TSL) and investigating the influence of thermal effects on the drug delivery.

Statement of Contribution/Methods

The source of Micro-HIFU (MHIFU) used in this study is a single element unidirectional transducer (SPUDT) with curved electrodes to concentrate the acoustic energy into a focused zone. The PDMS cavity was placed on the LiNbO3 substrate directly and the center of the PDMS cavity was located at the focal position of MHIFU. The thermal distribution of fluid medium in the PDMS cavity was visualized by a thermal infrared imager. Encapsulation of Doxorubicin (DOX) into the TSL was carried out using a remote loading protocol. The AFM image of the topography of the membrane were acquired at a scan field of 5µm×5µm.

Results/Discussion

Fig. 1A shows the evolution and the spatial distribution of PDMS cavity at as function of time. The results show that the temperature of sample in PDMS cavity increased quickly from 26 °C to 42°C within less than one minute. Fig. 1B shows the uptake of DOX by 4T1 cells at 30 min after MHIFU treatment. When the fluid in PDMS cavity was heated by MHIFU at 42°C, the cells emitted strong red fluorescence and the blue fluorescence was lo-localized with DOX, indicating DOX accumulated in nuclei. At 4 h after MHIFU mediated drug delivery at 42°C, the cell surface showed a kind of squamous structure with more uniform size and some depressions also could be found (Fig.1C). Combined microfluidic and AFM technologies may offer a promising alternative method for investigation of the complex dynamics between ultrasound and living cells in a microscopic scale.
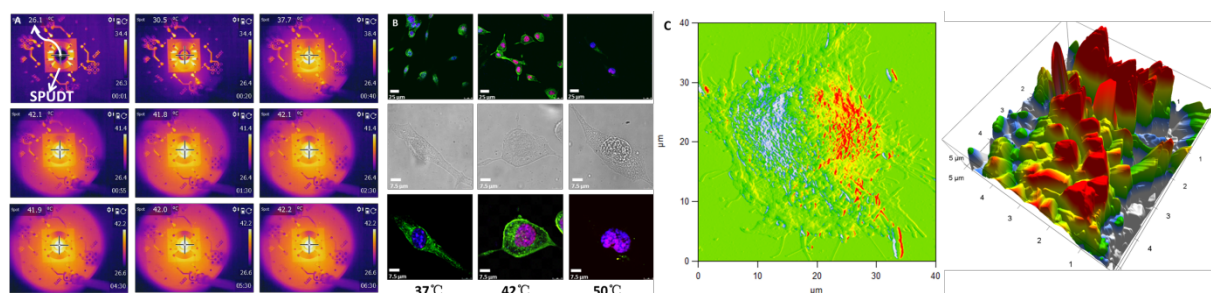
Figure1. (A) The temperature variation with the time induced by MHIFU (30 MHz, 20 V_{p-p}).(B) The fluorescence image shows the drug has entered into the cellular nuclei after MHIFU irradiation at 42 ° C while the nuclear fragmentation and myofilament destruction were occurred at 50° C. (C) At 4h after MHIFU-mediated drug delivery at 42 ° C, the membrane surface was full of squamous structures with more uniform size.

8:00 am   The Contribution of Shear Wave Absorption to Ultrasound Heating in Bones: Coupled Elastic-Thermal Modeling Using the k-Wave Toolbox

Bradley Treeby[1], Teedah Saratoon[1]; *[1]Medical Physics and Biomedical Engineering, University College London, London, United Kingdom*

Background, Motivation and Objective

There are many applications of therapeutic ultrasound in which ultrasound waves interact with bone. These include high-intensity focused ultrasound (HIFU) therapies delivered through the ribs or skull, HIFU treatments targeted at bone metastasis for pain relief, and low-intensity ultrasound used in physiotherapy. In these applications, the heating of bone and surrounding tissue needs to be controlled; either to avoid thermal damage, or to ensure adequate treatment delivery. However, the heating of bone is complicated by the presence of a fluid / solid interface. In this case, the generation, propagation, and absorption of shear waves within the bone must also be considered. The absorption in bone is considerably higher than in the surrounding soft tissue, and the shear absorption coefficient is approximately twice that of the compressional wave. In this work, the contribution of shear wave absorption to ultrasound heating in bones was quantified.

Statement of Contribution/Methods

A Kelvin-Voigt viscoelastic model was used to compute wave propagation from focused and unfocused transducers with CW excitation incident on bone. The model was discretised using the Fourier collocation spectral method as implemented in the open-source k-Wave acoustics toolbox. The volume rate of heat deposition was calculated from the magnitude of the steady state particle velocity. Due to the different absorption coefficients, individual contributions to the heating term were computed by splitting the particle velocity into compressional and shear components using a k-space dyadic and storing these separately. The volume rate of heat deposition was then used within a thermal model to calculate the temperature after a 30 second sonication assuming no perfusion. The simulations were repeated for angles of incidence between 0 (normal incidence) and 60 degrees. Two bone geometries were considered: an idealised cylindrical bone, and an anatomical long bone derived from a CT scan. Simulations were repeated with the shear properties set to zero to examine the heating when shear waves are ignored.

Results/Discussion

For both transducers, for angles close to normal incidence, the contribution of shear wave absorption to bone heating was almost zero. In this case, ignoring shear waves in the simulation had little effect on the final temperature (< 0.3 K). In contrast, when the incidence angle was increased past 15 degrees, the contribution of shear wave absorption increased rapidly, becoming the dominant component of the heat deposition at approximately 40 degrees. For angles of incidence beyond 45 degrees, the difference in the final temperature when shear waves were ignored in the simulation was > 5 K, illustrating the significant contribution of shear wave absorption to ultrasound heating in bones at non-normal incidence. These results have particular importance for patient selection and treatment planning for ultrasound therapy in the region of bones.

P1A3 - MIM: Ultrasound Image Formation

4th floor

Thursday, October 22, 2015, Posters displayed 08:00 am - 05:00 pm. Authors must be present at their poster from 9:30 - 10:30am (odd number posters) and 14:30 – 15:30pm (even number posters).

Chair: **Gregg Trahey**
           Duke University

P1A3-1 _____

8:00 am   6-DOF Free-hand Navigation Interface for Volumetric 3-dimensional Ultrasound Imaging: Preliminary Results

JongJun LEE[1], Jeeun KANG[1], Tai-kyong SONG[1]; [1]*Department of electronic engineering, Sogang university, Seoul, Korea, Republic of*

Background, Motivation and Objective

Volumetric 3-dimensional ultrasound imaging have been expected to provide more realistic morphological information in several diagnostic applications such as circulatory system, obstetrics, and gynecology. However, conventional interface suffers from the limited degree-of-freedom (DOF) in providing arbitrary cross-sections, which may be valuable to users in ultrasound diagnosis. Here, we present the 6-DOF free-hand navigating interface for volumetric 3-dimensional ultrasound imaging.

Statement of Contribution/Methods

The proposed system consists of magnetic sensor-based 6-DOF tracking system (TrakSTAR system, Ascension Tech. Corp., USA) connected to a workstation powered by Intel i7-3820(3.6GHz) and Nvidia GTX690, which reconstructs the arbitrarily-selected cross-sections from the volumetric data obtained by ultrasound research package (SonixTouch Corp., Canada). The three magnetic sensors (Model 800, Ascension Tech. Corp., USA) attached to the back of the hand, thumb, and little finger of user allow the continuous motion tracking and magnification of the arbitrarily-selected cross-sections for fine examination.

Results/Discussion

For performance test of the proposed navigation interface, volumetric scanning was conducted on 3D abdominal phantom (057A, CIRS. Corp.) by using motorized stage and commercial ultrasound imaging system and probe (C5-3/60, Ultrasonix Corp.). As a results, our volume-navigating interface successfully provides the arbitrary cross-sections of abdominal phantom with over 60 frame-per-second (fps). Our future works will be focused on developing real-time data acquisition and volume navigating interface using real-time 3-D imaging transducers.
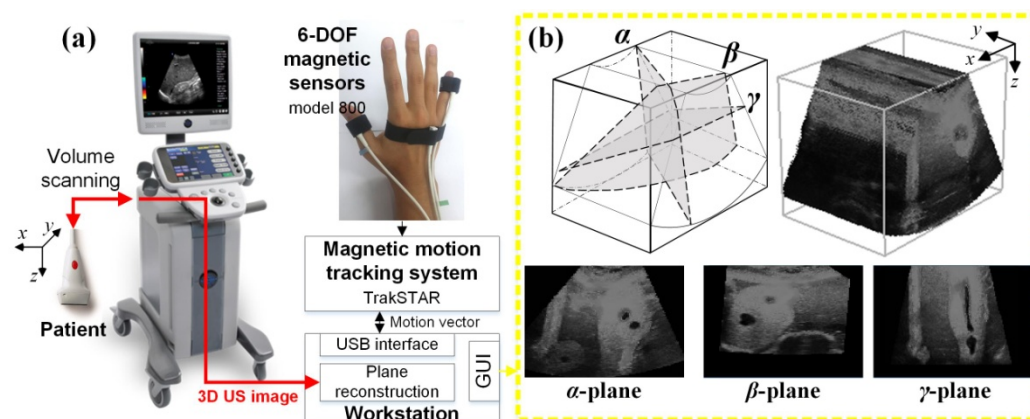
Fig. 1 (a) Block diagram of the developed volume navigating system (b) Volume rendered 3-D image and arbitrarily-selected cross-sections (α-, β-, and γ-planes)

P1A3-2 _____

8:00 am   Advanced Automated Gain Adjustments for *In-Vivo* Ultrasound Imaging

Ramin Moshavegh[1], Martin Christian Hemmsen[1], Bo Martins[2], Andreas Hjelm Brandt[3], Thor Bechsgaard[3], Kristoffer Lindskov Hansen[3], Caroline Ewertsen[3], Michael Bachmann Nielsen[3], Jørgen Arendt Jensen[1]; [1]*Electrical engineering, Technical University of Denmark, Lyngby, Denmark, [2]BK Medical ApS, Herlev, Denmark, [3]Department of Radiology, Copenhagen University Hospital, Copenhagen, Denmark*

Background, Motivation and Objective

Automating the TGC on the ultrasound scanners reduces the number of settings on the interface and therefore the unnecessary user adjustments. TGC becomes highly challenging when large fluid collections are present causing drastic attenuation distribution changes within the scan plane. This paper presents an automated hierarchical TGC (AHTGC) algorithm that adapts to the large attenuation variation between different types of tissues and large fluid collections.

Statement of Contribution/Methods

The novelty stems from incorporating several physical estimates of the underlying tissue as constituents of the compensation strategy. It relies on estimates of tissue attenuation, scattering strength, and SNR. First, the received signal is calibrated for the shape of the beam profile to ensure all the scanned media is evenly highlighted. Second, a 2-D SNR map is generated for each frame, and a histogram based feature (F_1) is computed for deciding whether the frame contained large anechoic regions (Type 1) or not (Type 2). Third, a TGC curve is computed automatically and used to compensate for the gains in the frame. Finally, a 2-D attenuation map is generated and used to correct the adjusted gains inside the anechoic regions after applying the TGC curve. Nine healthy subjects were scanned using a newly-launched scanner BK3000 (BK Medical, Denmark), and a total of 45 abdominal sequences each containing 50 frames were acquired. The AHTGC was applied to these *in-vivo* sequences.

Results/Discussion

Matching pairs of *in-vivo* sequences, unprocessed and processed with the AHTGC, were evaluated side-by-side by three radiologists and rated based on the image quality. Wilcoxon signed-rank test was applied to the ratings provided by radiologists. The average VAS score was highly positive 12.16 (p-value: 2.09×10^{-23}) favoring the compensated data with the AHTGC. The discrimination power of feature F_1 was also evaluated in a classification experiment using a logistic regression. The area under ROC curve was 87.22 ± 0.021, indicating that feature F_1 accurately classified the two types of scans. The left figure shows an unprocessed sagittal view of a human gallbladder and inferior vena cava. The right figure shows the same scan after applying the AHTGC. The radiologists reported that the tissue homogeneity is increased in the AHTGC images, and the anechoic regions are better identified.
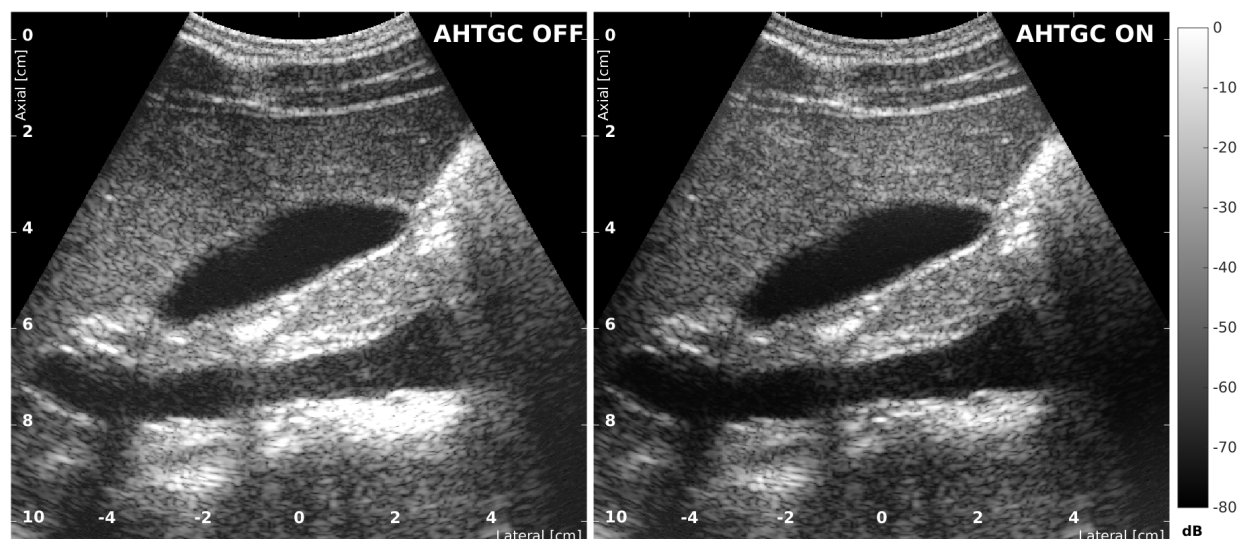
P1A3-3

8:00 am   Quantifying the benefit of elevated acoustic output in harmonic imaging

Yufeng Deng[1], Mark Palmeri[1], Ned Rouze[1], Kathryn Nightingale[1]; *[1]Duke University, Durham, North Carolina, USA*

Background, Motivation and Objective

Tissue Harmonic Imaging (THI) techniques have been proposed to reduce the clutter and improve image quality in B-mode imaging and shear wave tracking; however, THI penetration depth is limited by decreased signal-to-noise ratio (SNR) at depth from low incident harmonic pressures and high attenuation. This work evaluates THI data quality over a range of Mechanical Indices (MI). The goal is to quantify the effect of increasing MI on image quality and penetration depth, and to determine if there is clinical benefit in exceeding the current FDA guideline of MI 1.9 in the context of hepatic imaging.

Statement of Contribution/Methods

M-mode THI data at two MI values (1.6 and 2.2) was acquired using a 4C1 curvilinear transducer and a modified Siemens SC2000 ultrasound scanner in a tissue mimicking phantom and in the livers of 26 patients evaluated for potential liver diseases. Expecting zero displacement between subsequent M-mode lines, tissue displacement correlation coefficient (CC) and jitter were used as image quality metrics. Additionally, B-mode THI images were acquired using a modified Siemens S3000 scanner and a 4C1 transducer in the livers of patients and volunteers over a range of MI values (1.0-2.5). Mean pixel brightness and contrast-to-noise ratios (CNR) of hypoechoic structures were calculated at each MI. Pulse-inversion harmonics were used in all sequences.

Results/Discussion

Preliminary results are illustrated in Figure 1: (a) displacement jitter level at MI = 2.2 is significantly lower than that at MI = 1.6, measured in a phantom. (b) M-mode CCs measured at 50 mm and 75 mm axially from a patient with a body mass index of 31 kg/m². CC at MI = 2.2 is higher than CC at MI = 1.6 at both depths. In addition, CC decreased more significantly from 50 mm to 75 mm at MI = 1.6. These results indicate that data obtained at the higher MI has higher SNR and higher penetration. (c) and (d) show the B-mode images of the livers of 2 healthy volunteers. The boxes indicate the regions of interest for brightness and CNR calculation. (e) and (f) show that pixel brightness (and thus SNR, assuming a constant level of electronic noise) increases with increasing MI in both volunteers. (g) and (h) demonstrate a strong correlation between CNR and MI. These results support the hypothesis that exceeding MI of 1.9 would enable improved THI hepatic image quality.
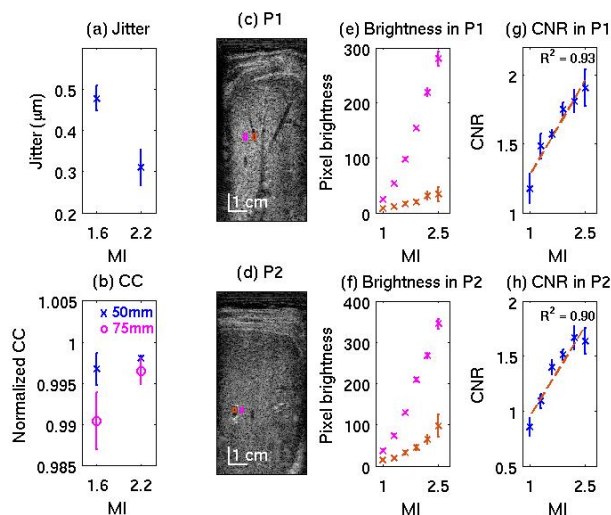
P1A3-4 _____

8:00 am   **3D Super-Resolution Ultrasound using Microbubbles**

Kirsten Christensen-Jeffries[1], Meng-Xing Tang[2], Joseph V Hajnal[1], Paul Aljabar[1], Christopher Dunsby[3,4], Robert J Eckersley[1]; *[1]Biomedical Engineering, Division of Imaging Sciences, Kings College London, London, United Kingdom, [2]Bioengineering, Imperial College London, London, United Kingdom, [3]Department of Physics, Imperial College London, London, United Kingdom, [4]Centre for Histopathology, Imperial College London, London, United Kingdom*

Background, Motivation and Objective

The structure of microvasculature cannot be resolved using standard clinical ultrasound (US) imaging frequencies due to the fundamental diffraction limit of US waves. Having the ability to resolve complex micro-vascular structures containing microbubbles would be crucial in the assessment of tumor microvasculature and other angiogenic diseases using clinical US. Recently, our group has demonstrated 2D super-resolution both *in vitro* and *in vivo* in a mouse ear by localizing isolated US signals from microbubbles flowing within vessels, where vessel structures as fine as 19 µm are clearly visualized *in vivo* [1, 2]. Visualisation of more complex 3D vasculature requires an acquisition strategy which can localize bubbles in the elevational plane to high precision.

Statement of Contribution/Methods

The translation of super-resolution to 3D has been achieved by transmission and reception of fast plane wave contrast pulse sequences from a 2D linear array transducer (ULA-OP system, University of Florence, Italy), with simultaneous detection of scattered signals by a second synchronized passive system. Coincident scatter events from isolated US microbubble signals are then identified and localized using post-processing algorithms to visualize micro-vessel structures in 3D.

Results/Discussion

3D super-resolution allows localization of bubble signals in three dimensions with localization precision equal to 1.9 µm in axial and elevational planes, and 11 µm in the lateral plane with respect to the active transducer, compared to 211 µm, 820 µm and 680 µm as the three dimensions of the point spread function for the original imaging system. The plane wave contrast acquisition strategy allows fast, 3D, high resolution imaging of micro-vessel structures at depth.

[1] O. M. Viessmann et al., "Acoustic super-resolution with ultrasound and microbubbles," Phys. Med. Biol., vol. 58, no. 18, pp. 6447-6458, 2013.

[2] K. Christensen-Jeffries et al., "In Vivo Acoustic Super-Resolution and Super-Resolved Velocity Mapping Using Microbubbles," IEEE Trans. Med. Imaging, 2014, doi:10.1109/TMI.2014.2359650.

P1A3-5 _____

8:00 am   **A Study for B-Mode Imaging using 100-MHz-Range Ultrasound through a Fused Quartz Fiber**

Takasuke Irie[1,2], Masasumi Yoshizawa[3], Norio Tagawa[1], Tadashi Moriya[4]; *[1]Graduate School of System Design, Tokyo Metropolitan University, Tokyo, Japan, [2]Microsonic Co., Ltd., Japan, [3]Metropolitan College of Industrial Technology, Japan, [4]Tokyo Metropolitan University, Tokyo, Japan*

Background, Motivation and Objective

The tissue diagnosis in the current pathological examination has two drawbacks. (1) It takes a long time because it requires a tissue sample obtained by the biopsy and the observation using an optical microscope, and (2) it gives burden on the patient. The main objective of the study is to enable an operator to observe directly microscopic images of the tissue in real time without taking out the tissue sample from the patient. To achieve the objective, we are developing a needle type ultrasonic microscope that uses a thin fiber as an ultrasound probe.

Statement of Contribution/Methods

We reported that the microscopic C-mode images of the tissue samples (mucosal layer of the stomach and kidney) were obtained using a focused ultrasound beam radiated from a tapered quartz fiber. In the experiment, it took a considerable amount of time to obtain the image. In this paper, we describe that a B-mode image of an animal bone (body of vertebra of pig) in water was obtained in a short time. In the experiment, we used the same system as the previous one. We measured the amplitude of the ultrasonic wave radiated from the fiber using the reflected echo from a stainless steel plate in water. The fiber was moved to the vertical (*Z*) direction, and the same measurement was repeated. Then, we performed the B-mode imaging of a stainless steel mesh in order to estimate the spatial resolution and an animal bone (body of vertebra of pig). The scanning of ultrasound beam in B-mode imaging was performed with 5 µm intervals and 2 mm length in the single (*X*) direction. The stainless steel mesh with 13 µm wire in diameter was placed at the focal point of ultrasonic beam in water.

Results/Discussion

The measured propagation distance of the ultrasound in water was approximately 1 mm from the end of the fiber. The B-mode image of the stainless steel mesh and the animal bone were obtained. In the image of the stainless steel mesh, it was shown that the spatial resolution of the image was approximately up to 13 µm. As shown in Fig.1, the measured propagation distance of the ultrasound in the animal bone was approximately 150 µm due to the attenuation of ultrasound. The frequency band of the image was approximately 80-170 MHz. As the results of the experiment, we expect that the microscopic image of the tissue can be seen directly in real time.

P1A3-6
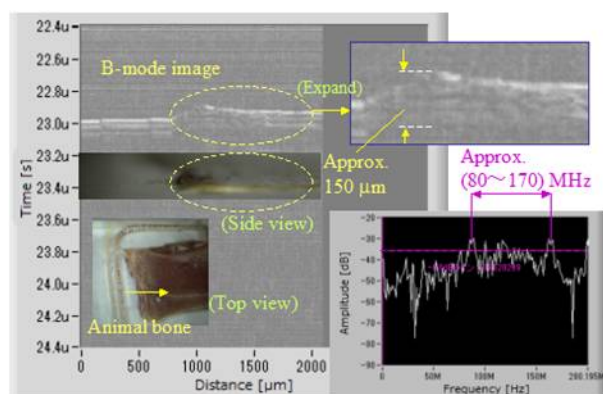
8:00 am   **Assessment of the Potential of Beamforming for Needle Enhancement in Punctures**

Stefanie Dencks[1], Georg Schmitz[1]; *[1]Chair for Medical Engineering, Ruhr-Universität Bochum, Germany*

Background, Motivation and Objective

In sonography the visibility of a needle becomes poor for deep puncture targets because the angle of incidence of the ultrasound wave increases. In [1] we showed with simulations and measurements that despite large puncture angles an unexpectedly good needle visibility in some image sectors can be generally explained by resonant scattering modes of the needle. As a first step to assess the potential of needle enhancement by a beamformer adapted to the needle specific signals, we investigate the RF signals which are received at the transducer's single elements.

Statement of Contribution/Methods

Measurements were performed with a Verasonics Vantage 256 research ultrasound system and a linear L12-3v array (8.9 MHz center frequency). The puncture angle of the needle (Pajunk UniPlex Nanoline, 20G) was varied between 0° and 60°. For each measurement, a segment of 32 transducer elements was driven to transmit an ultrasound wave focused on the needle without steering angle. The arriving RF signals were recorded at 128 elements including the transmit elements. For a measurement series (one puncture angle), the segments of transmission were shifted along the transducer in steps of 20 elements and the focus was set according to the real distance of the needle to the center of the segment.

In a first step, for each measurement the envelopes of the recorded RF signals were summed up according to 1) a standard delay-and-sum (D&S) beamforming and 2) an adapted algorithm based on the detected real time-of-flights (TOF).

In a second step, the RF signals were analyzed regarding their frequency components. For this, the spectrogram of each RF signal was computed and the main frequency components identified. The dominant frequencies, their TOFs and amplitudes were evaluated along the transducer elements.

Results/Discussion

The detected TOFs of the RF signals do not coincide with the hyperbola which is assumed for the standard D&S beamforming. Using the energy contained in the RF signals applying the adapted algorithm 2), the amplitude could be improved by a mean of 5dB for 0° and up to a mean of 26dB for 60°. Each RF signal contains several frequency peaks. These peaks vary along the elements regarding their frequency and TOF changing also their amplitudes.

Analyzing the RF signals it becomes obvious that they contain energy that is not exploited until now but can be used to improve needle visibility up to 26dB. The frequency dependent TOFs are an indication for resonant guided waves excited in the needle and reradiated into the medium (see [2]). If so, the travel paths and sound velocities depend on the modes and orders of the resonances and have to be systematically evaluated to design an adaptive beamformer.

[1] Dencks et al.: Needle visibility for deep punctures with curved arrays, IUS, 2014.

[2] León et al.: Scattering of an obliquely incident acoustic wave by an infinite hollow cylindrical shell, JASA, 1992.

P1A3-7

8:00 am   **Pulse inversion based multi-subharmonic composite cavitation imaging**

Hui Zhong[1], Mingxi Wan[1]; *[1]Xi'an Jiaotong University, Xi'an, Shaanxi Province, China, People's Republic of*

Background, Motivation and Objective

Cavitation monitoring imaging is necessary for safety and efficiency during HIFU therapy. It is known that subharmonic imaging could be used in contrast-enhanced imaging for its great ability of suppression of tissue scattering. However, it is rather difficult to generate subharmonic for encapsulated microbubbles especially for single imaging pulse. In contrast, unencapsulated cavitation bubbles have greater nonlinearity, which could make it easier to generate subharmonics. Since the generation of subharmonics is related to bubble size, which is in a wide range, it is difficult to detect cavitation bubbles with various sizes by using only 1/2 subharmonic. Therefore, a multi-subharmonic composite cavitation imaging method was proposed in this study for suppression of tissue scattering and improvement of cavitation imaging sensitivity.

Statement of Contribution/Methods

Several components including 1/2, 1/3 and 1/4 subharmonic were extracted by bandpass filters with corresponding center frequency respectively. The pulse inversion technique was used to eliminate the fundamental component confused with subharmonics. To image all the subharmonic components in one image, different subharmonic components whose intensities were greater than 50 percent of corresponding maximum intensity were coded with different colors and displayed simultaneously. Imaging pulses with different pressure (0.15~1.2 MPa) and cycle number (1~5 cycles) were used to obtain the composite cavitation images to investigate the effect on sensitivity of imaging parameters.

Results/Discussion

The proposed method was validated with the experiments of porcine muscle in vitro. It was found that the obtained composite cavitation images can greatly suppress the tissue scattering, and have higher sensitivity than PI-based second harmonic and 1/2 subharmonic images. Moreover, the composite cavitation images can reflect the distribution of cavitation with respect to bubble size. In general, all the subharmonic components increased with HIFU treatment time. The highest intensities of subharmonic components were obtained when cycle number is 4 or 5 and pressure is about 0.75 MPa. The results imply that the subharmonics are difficult to be generated with low acoustic energy of imaging pulse and high acoustic energy could make cavitation bubble collapse causing decrease of subharmonics.
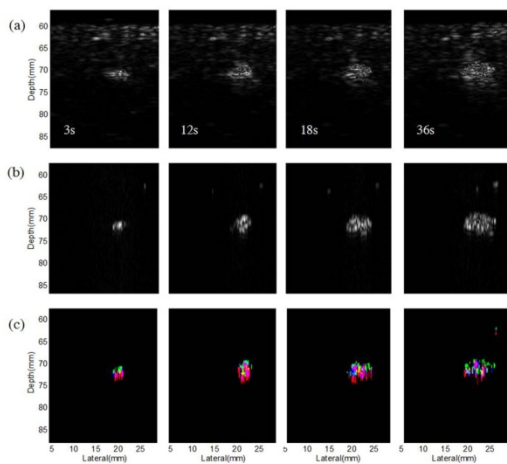
Fig. Dynamic monitoring cavitation images at 3, 12, 18 and 36s after HIFU exposures with the power of 100W. The imaging pulse cycle number is 2, and acoustic pressure is 1.2 MPa: (a) PI-based second harmonic images, (b) PI-based 1/2 subharmonic images, (c) composite cavitation images (green, blue and red colors indicating 1/2, 1/3 and 1/4 subharmonic components respectively)

P1A3-8 _____

8:00 am **Contrast-enhanced ultrasound tomography using the cumulative phase delay between second harmonic and fundamental component**

Libertario Demi[1], Ruud J.G. van Sloun[1], Hessel Wijkstra[1,2], Massimo Mischi[1]; *[1]Biomedical Diagnostics Lab., Eindhoven University of Technology, Netherlands, [2]Academic Medical Center Amsterdam, Netherlands*

Background, Motivation and Objective

Standard dynamic-contrast enhanced ultrasound (DCE-US) imaging detects and estimates ultrasound-contrast-agent (UCA) concentration based on the amplitude of the harmonic components generated during ultrasound (US) propagation through UCAs. However, harmonic generation is not specific to UCAs, as it also occurs for US propagating through tissue. Moreover nonlinear artifacts affect standard DCE-US imaging, causing contrast to tissue ratio (CTR) reduction, and resulting in possible tissue misclassification and misinterpretation of UCA concentrations [1]. Especially when focusing on US tomography, no contrast-specific modality exists, and in particular speed-of-sound changes due to UCAs are well within those caused by different tissue types [2].

Recently, a new marker for UCAs has been introduced [3]. A cumulative phase delay (D) between the second harmonic (2H) and fundamental (F0) component is in fact observable for US propagating through UCAs, and is absent in tissue. In this paper, tomographic US images based on D are presented and compared to standard US tomography. Finally, the clinical application of these results is discussed.

Statement of Contribution/Methods

The ULA-OP platform and Esaote LA332 linear array were used to image a gelatin phantom containing a PVC plate (used as a reflector) and a cylindrical cavity (7 mm diameter) filled with 240 µL/L SonoVue® UCA dilution, which was placed in between the probe and PVC plate.

A frequency f_0 = 2.5 MHz and a mechanical index MI = 0.05 were used. Echoes obtained from the PVC plate were processed to obtain, line by line, a measure of D = $2\Pi\Delta t f_0$, with Δt the time delay between 2H and F0. Next, a sinogram was constructed from consecutive US frames as obtained from different observation angles, and an image generated by filtered back-projection. These images were compared to speed of sound and dispersion-based US tomography.

Results/Discussion

Our results show the applicability of the marker D for contrast specific US imaging, with D images showing superior CTR (16.1 dB) as compared to speed of sound (0.03 dB) and dispersion (2.3 dB) US tomographic images. These results open possibilities to DCE-US tomography with potential applications to breast imaging for cancer localization.

[1] Tang et al, IEEE Tr. UFFC 53, pp 2406-15, 2006

[2] Hibbs et al, IEEE IUS, pp 1829-32, 2009

[3] Demi et al, JASA 136, pp. 2968-75, 2014
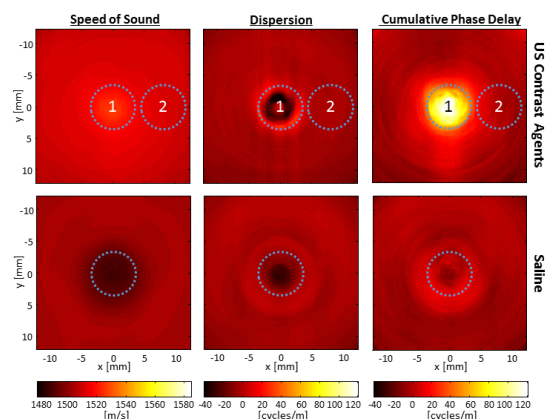
Tomographic images based on Speed of Sound, Dispersion, and Cumulative Phase Delay (column 1, 2 and 3, respectively) as obtained in case the cavity was filled with 240 µL/L UCA concentration diluted in saline, and saline only (row 1 and 2, respectively). CTR values have been calculated for area 1 with respect to area 2.

P1A3-9

8:00 am   Microultrasound Capsule Endoscopy Inflammatory Imaging: Phantom Studies

Benjamin F Cox[1], Vipin Seetohul[1], Holly Lay[1], Sandy Cochran[1]; *[1]Imaging & Technology, University of Dundee, Dundee, United Kingdom*

Background, Motivation and Objective

Inflammatory bowel conditions such as coeliac disease (CD) often present in discrete and optically obscure patches. We aim to improve the diagnosis and management of CD and similar proximal small bowel disorders with the development of a tethered microultrasound (μUS) capsule endoscope (CE). The capsule has a high frequency, single element curved transducer and a micromotor with a flat rotating mirror, giving a 360° scan. Complementing engineering developments are concurrent μUS qualitative and quantitative imaging studies of small bowel. Our objective is to characterise CD using tissue phantoms and relate results to current pathologic scoring systems to improve image-based diagnosis.

Statement of Contribution/Methods

Abattoir samples of porcine small bowel were perfused with phosphate-buffered saline and 10 μm diameter polystyrene beads to simulate an influx of lymphocytes. Tissue was scanned using a single element 45 MHz transducer on a mechanical scanner. Images were reconstructed and analysed for impedance (Z), random attenuation (RA) and back-scatter coefficient (BSC) using MATLAB (The Mathworks, Cambridge, UK). Tissue was then fixed in formalin, stained and microscopically examined for comparison with the Marsh classification.

Results/Discussion

Our analysis demonstrated qualitative and quantitative changes to the small bowel. Visually apparent changes included an increased mucosal signal with concomitant decrease in the prominent smooth muscle signal. Quantitative changes resulted in significant changes to Z, RA and BSC. Imaging correlated well with histological examination. Results indicate qualitative and quantitative methods of tissue analysis can be employed as a means of enhancing capsule endoscopic diagnosis with μUS. Methods established from these proximal bowel studies may be applied to more remote areas to negate biopsy need with an autonomous CE. This would allow greater reliance on image guidance to make treatment decisions, as needed with Crohn's disease.

Figure 1. Pre and post perfusion images, left and right respectively. Right image inset: optical image of 10 μm diameter fluorescent beads. Note loss of prominent Muscularis propria and agar signal with bead influx. Lower image is a reproduction of the Marsh classification (courtesy of Mayo Foundation for Medical Education and Research, Diagnostic Challenges of Celiac Disease).
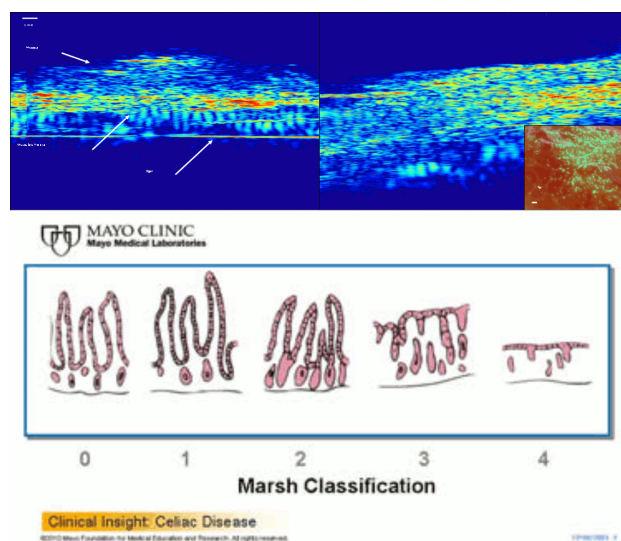
P1A4 - MBB: Beamforming I

4th floor

Thursday, October 22, 2015, Posters displayed 08:00 am - 05:00 pm. Authors must be present at their poster from 9:30 - 10:30am (odd number posters) and 14:30 – 15:30pm (even number posters).

Chair: **Meng-Lin Li**
           National Tsing Hua University

P1A4-1 _____

8:00 am   Dual-Domain Compressed Beamforming for Medical Ultrasound Imaging

Bo Zhang[1], Jean-Luc Robert[2], Guillaume David[3]; [1]*Medisys, Philips Research France, Suresnes, France,* [2]*Philips Research North America, Briarcliff, USA,* [3]*Columbia University, New York, USA*

Background, Motivation and Objective

Since recently, the compressed sensing (CS) technique has drawn great interest in the ultrasound community due to its capacity of reconstructing images with many fewer measurements than conventional techniques such as Delay-And-Sum (DAS) beamforming. In this paper, we propose a novel beamforming approach based on a dual-domain CS technique. We want to achieve: (1) a much higher frame rate by using substantially fewer transmissions than required by DAS; (2) in the same time, a better image quality than DAS, and standard CS reconstructions with a single image-representation domain.

Statement of Contribution/Methods

We model the acoustic data as a linear spectral solution to Born's diffraction equation. The CS-based beamforming requires a good sparsity-promotion representation of the image. For this purpose, we model the image as a combination of geometry information and a low-contrast residue. The beamforming is formulated as depth-dependent optimization problems, which are solved by Augmented Lagrangian successively in wavelet domain to capture the overall geometry, and in the image domain for preserving the low contrasts.

Results/Discussion

We evaluate our approach on simulated Field-II data, on real speckle phantom, and on real cardiac scans. In addition, targeting more practical conditions, we specifically consider only few iterations for iterative solvers. We find that our method requires typically only 3 or 4 plane-wave transmissions to achieve comparable or better image quality, than DAS using more than 10 transmissions. Overall, we attain a theoretical frame rate over 1KHz at depth of 15cm. Compared to the CS beamforming using a single image-representation domain, the dual-domain approach preserves better weakly contrasted signals and produces less holey-tissue artifacts.
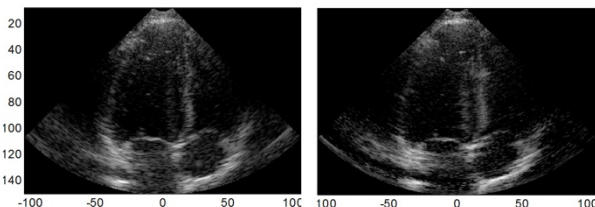
Figure 2. Image reconstructed from a real cardiac phased-array scan (2.6 MHz). (Left) Result of DAS using 11 plane-wave TX; (Right) Result of our approach using only 4 TX and no more than 20 iterations in any domain. Our method achieves a theoretical frame rate of 1.3 KHz, a comparable image quality inside the ventricle, and a much better contrast in the far field.
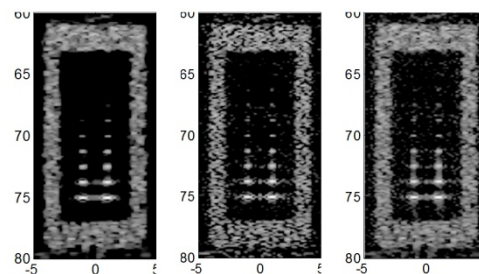
Figure 1. Image reconstructed from a simulated Filed-II scan using a linear probe (6 MHz) with a single plane-wave TX. The simulated data consist of a rectangular tissue frame enclosing 18 diffusers of amplitudes ranging from -50dB to 0dB. No more than 20 iterations are used for any domain. (Left) CS-beamforming in the wavelet domain with good geometry reconstruction but limited contrast sensitivity on the isolated diffusers; (Middle) CS-beamforming in the image domain with good contrast sensitivity but holey-tissue artifacts on the frame; (Right) Dual-domain CS-beamforming combining the advantages of both domains.

P1A4-2 _____

8:00 am   Efficiency of Multi-look compounding of MVDR and APES Beamformers under Strong Wave Aberration Conditions

Teiichiro Ikeda[1], Shinta Takano[1], Hiroshi Masuzawa[1]; [1]*Hitachi Ltd., Tokyo, Japan*

Background, Motivation and Objective

In diagnostic ultrasound systems, the transmitted wave is severely aberrated as propagating through the human body. Previously we proposed the mode vector compounding (MVC) in adaptive beamformers for suppressing the effect of aberration [1]. In the MVC, the compounded outputs of the multi-look mode directions yield suppressed unwanted responses. To obtain maximized desired signals while suppressing unwanted responses, the invariance on the multi-look directions is very important. In this work, we evaluate the dependence on mode directions of different adaptive beamforming algorithms and the implication to the MVC performance is discussed.

Statement of Contribution/Methods

The MVC uses normal DAS (delay and sum) output which is constructed from one transmission event. Then adaptive weights are calculated for virtually oriented several mode vector directions. Finally we get compounded output by summing the weighted signals. Here we compare the two types of beamforming algorithms, MVDR (minimum variance distortionless response) and APES (amplitude and phase estimation) for estimating the adaptive weights for different mode directions. The ultrasound pulses propagating through spatially dispersed aberrators with different speeds of sound to the surrounding medium were calculated. The time history of pressure at the location of the receiving array was taken as the aberrated RF signals and then processed by the offline beamforming programs.

Results/Discussion

Figure shows the B-mode images of DAS, MVDR and APES beamformers. For MVDR and APES, the different mode directions are compounded. In the case of the compounded MVDR, compared with DAS, the point reflector images are much diffused in space whereas the compounded APES yield tightly focused two point images. The line profiles show the responses for different (-2 , 0 and 2 degree) mode directions. In the case of MVDR, the peak amplitude is dragged to the mode direction which causes diffused images. In the case of compounded APES, independent on the mode directions, the peak amplitudes of -2 and +2 degree are almost the same as of 0 degree. The invariance of APES beamformer thought to comes from the subtracting process of in-phase response in calculating the correlation matrix and the feature is strong advantages for suppressing the aberration in ultrasound images.

[1] Ikeda T. et al., Proc. on IEEE IUS, pp. 1674-77(2014).

DAS

MVDR (compounded)

APES (compounded)
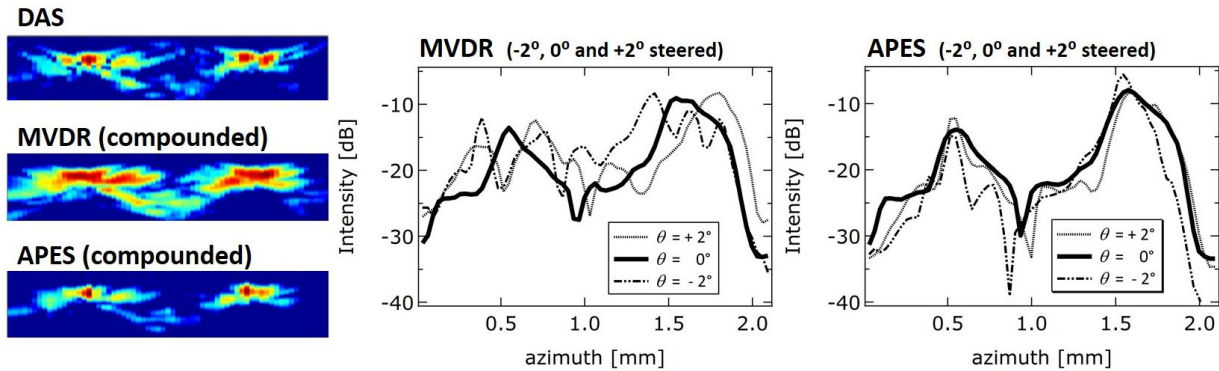
P1A4-3

8:00 am   **Hadamard-Encoded Synthetic Transmit Aperture Imaging with a Reduced Number of Receiving Channels**

Ying Li[1], Ping Gong[1], Michael C. Kolios[1], Yuan Xu[1]; *[1]Biomedical Physics, Ryerson University, Toronto, ON, Canada*

Background, Motivation and Objective

Synthetic transmit aperture (STA) imaging has been widely studied in ultrasound imaging. Usually the number of receiving channels is the same as the number of the array elements. When the number of receiving channels is large, such as in a matrix array for 3D imaging, the system cost will be high due to the receive electronics for each element. Therefore, it is desirable to reduce the number of receiving channels while keeping a large number of transmit channels to ensure adequate SNR. However, a reduced number of receiving channels in the standard STA will lead to reduced image quality. Therefore, we propose a novel technique designed to maintain image quality with a reduced number of receiving channels.

Statement of Contribution/Methods

In standard STA, the signal received at *i*-th receiver and transmitted by the *j*-th transmitter is equivalent to the signal received at *j*-th receiver and transmitted by the *i*-th transmitter ($S_{ij}=S_{ji}$). To lower the number of receiving channels, we utilized this symmetry property of RF signal with the encoded measurement data to solve for the equivalent data in traditional STA. The Hadamard matrix was used to encode this transmission process. The receiving elements were also combined to reduce the number of receiving channels. In the decoding process, we applied the pseudoinverse to decode for the equivalent data in the traditional STA. After decoding, ultrasound images were reconstructed using the standard image reconstruction method in STA.

The simulation RF data was generated for a 64-element, 2 cm wide, 5 MHz linear array by using Field II. The phantom contained one hypo-echoic inclusion, one hyper-echoic inclusion, and one point target. We also simulated the standard STA with only 16 receiving channels to compare with the proposed new method.

Results/Discussion

Fig. 1 shows the log envelope images of (a) standard STA, (b) standard STA with regular-selected 16 receiving channels, the proposed new method with (c) 17 receiving channels, and (d) with 9 receiving channels. The reconstruction result shows better contrast in the hypo-echoic lesion compared to the regular-selected sparse array. The image quality using the new method was comparable with the standard STA for the tested phantom.
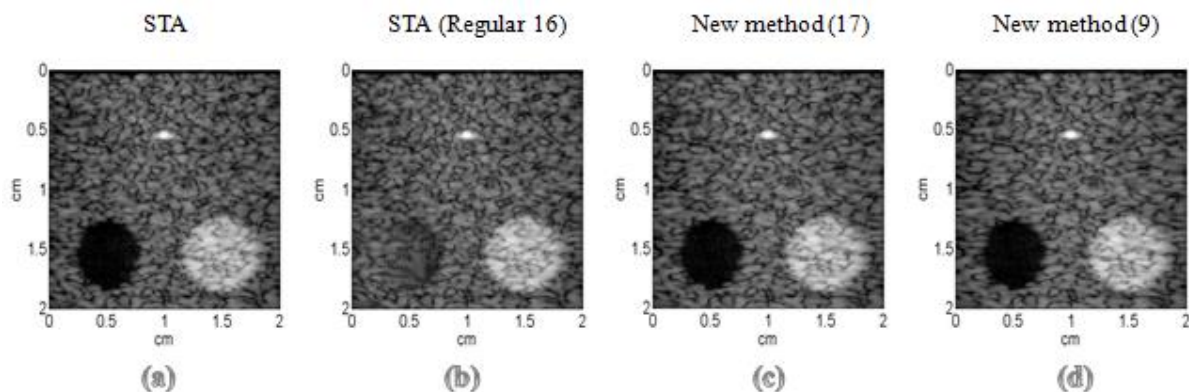
P1A4-4

8:00 am   **Compressive Adaptive Beamforming in 2D and 3D Ultrafast Active Cavitation Imaging**

Chen Bai[1], Shanshan Xu[1], Bowen Jing[1], Miao Yang[1], Mingxi Wan[1]; *[1]The Key Laboratory of Biomedical Information Engineering of Ministry of Education, Department of Biomedical Engineering,School of Life Science and Technology,Xi'an Jiaotong University, Xi'an, Shaanxi, China, People's Republic of*

Background, Motivation and Objective

Ultrafast active cavitation imaging (UACI) based upon wide beam have been developed to detect cavitation bubbles dynamics, in which adaptive beamforming can be utilized to improve resolution and signal-to-noise ratio (SNR). However, regular adaptive beamforming continuously updates the spatial filter for each sample point, which requires a huge amount of calculation, especially in the case of a high sampling rate and, moreover, 3D imaging. In order to achieve UACI rapidly with satisfactory resolution and SNR, this paper proposed an adaptive beamforming on the basis of compressive sensing (CS), retaining the quality of adaptive beamforming but reduce the calculating amount substantially.

Statement of Contribution/Methods

After presteering on radiofrequency (RF) signals of cavitation bubbles detected by wide beam, adaptive beamforming was accomplished on 40% points selected randomly from a certain bandwidth rather than on every sample point in the frequency domain, as ultrasonic signal was modulated on a carrier with the useful information occupying only a portion of the entire spectrum. Then, using the Fourier basis, the beamformed data for UACI in the frequency domain was reconstructed by the CS technique. Finally, the UACI was achieved by transforming the data into the time domain and then performing the imaging procedure.

     Institute of Electrical and Electronics Engineers

Results/Discussion

Among the different beamforming methods in 2D UACI based upon wide beam, and simulation of 3D UACI based upon slightly focused wide beam to improve the sensitivity, the SNR of proposed method in both 2D and 3D images increased by about 27dB and 12dB, compared with the delay-and-sum (DAS) and regular adaptive beamforming, respectively. According to the corresponding autocorrelation functions, lateral resolution of the proposed method, roughly the same as regular one, was 3.74 times of that of DAS. Nevertheless, time consuming, comparable to DAS, for the proposed method in 2D and 3D UACI respectively accounted for only 14.31% and 15.05% of that for regular method. In summary, our proposed method has been proved to achieve about sevenfold reduction in time consuming with equivalent good performance as regular adaptive beamforming, demonstrating that this method can promptly accomplish either 2D or 3D UACI with high quality.

(a) 2D UACI based on different beamforming methods

(b) Simulation of 3D UACI based on the proposed method

(c) Resolutions

(d) Time consuming
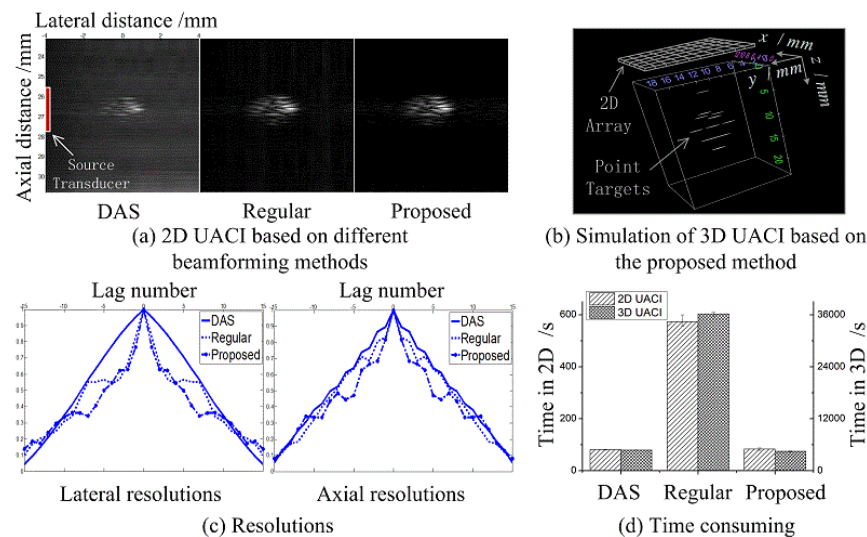
P1A4-5

8:00 am   Compressed Sensing-Synthetic Focusing for High Frame Rate, High Resolution and High Contrast Ultrasound Imaging

Jing Liu[1], Qiong He[1], Jianwen Luo[1]; [1]*Department of Biomedical Engineering, Tsinghua University, Beijing, China, People's Republic of*

Background, Motivation and Objective

Compressed sensing (CS) allows much lower sampling rate than the Nyquist sampling rate. Recently it has been applied in ultrasound imaging to reduce the data size. In linear acoustics, a plane wave firing is a linear combination of synthetic focusing (SF) firings. Therefore, we propose a novel beamforming technique, named compressed sensing-synthetic focusing (CS-SF), to speed up the acquisition of ultrasound imaging, without compromising the image quality.

Statement of Contribution/Methods

Ultrasound transducer transmits plane wave with different apodizations for m times and receives the corresponding echoes. The full dataset of SF is then recovered from the recorded echoes using a CS reconstruction algorithm. Finally, a standard SF beamforming is performed on the dataset. When m is less than the number of SF firings, higher frame rate is achieved. In addition, CS-SF maintains the high resolution of SF because of the CS recovered full dataset of SF, and improves the contrast due to plane wave firings. The feasibility and performance of CS-SF were investigated in Field II simulations of both point and cyst models with a 7.5 MHz, 128-element linear array. Phantom experiments were also performed in both CIRS and Gammex phantoms using a Verasonics system with a 7.5 MHz, 128-element linear array.

Results/Discussion

Simulations demonstrate the feasibility of CS-SF to recover the full dataset of SF. In the point model, the normalized root mean square errors of the full dataset of SF and its recovered version from CS-SF with m=32, 64, 128 firings are as low as 0.98%, 0.42% and 0.01%, respectively. Phantom experiments manifest that CS-SF achieves comparable or higher lateral resolution (LR) than SF, and comparable contrast-to-noise ratio (CNR) to the conventional focused mode besides higher frame rate. In the CIRS phantom, the average LR of CS-SF with m=64 firings (CS64-SF), SF and focused mode at the depths between 20 and 50 mm is 0.47, 0.52 and 0.59 mm; the CNR of CS64-SF, SF and focused mode is -1.65, -9.06 and -2.55 dB (for cysts), respectively. Both the LR and CNR of CS64-SF are better while its frame rate is twice higher. When m decreases to 32 (CS32-SF), the LR slightly decreases to 0.48 mm and the CNR decreases to -5.86 dB, while the frame rate is 4 times higher. The proposed CS-SF method is thus proven to obtain simultaneously high frame rate, high resolution and high contrast ultrasound imaging.
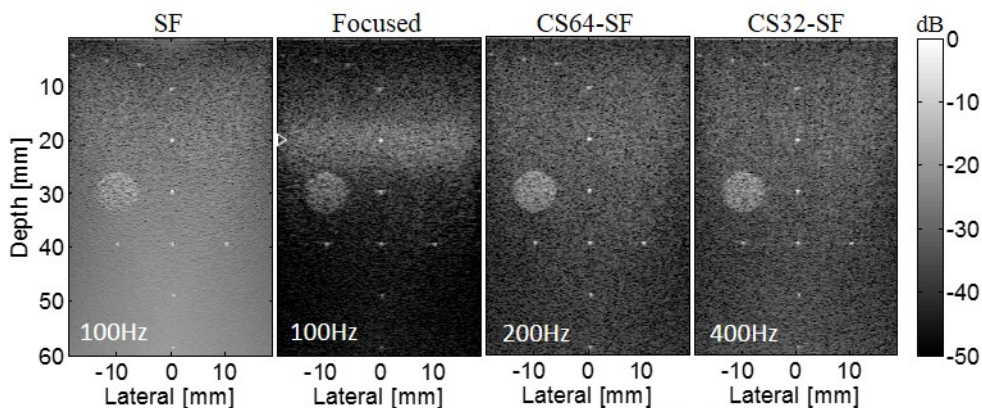
Figure 1. B-mode images for the wire region of the CIRS phantom.

8:00 am   Plane-wave Ultrasound Imaging Based on Compressive Sensing with Low Memory Occupation

Congzhi Wang[1], Hairong Zheng[1]; [1]*Shenzhen Institutes of Advanced Technology, Chinese Academy of Sciences, China, People's Republic of*

Background, Motivation and Objective

Coherent compounding method for plane-wave ultrasound imaging has been widely used in many frontier research areas in medical ultrasound. However, it still needs to find a compromise between the frame rate and image quality, which restricts its wider implementation. How to maintain the high frame rate and at the same time improve the image quality, has become a significant issue on plane-wave imaging technique. Although several methods based on compressive sensing (CS) have been proposed in previous studies, they still have some limitations, especially on the memory occupation and the amount of computation side.

Statement of Contribution/Methods

In this paper, a novel CS-based beamforming method used for plane-wave ultrasound imaging is proposed and its image quality has been verified on several simulated phantoms. In this method, only the relationship between the time-delay information and the spatial distribution of the scatterers is considered when establishing the encoding matrix. In addition, the encoding matrix is expressed totally in time-domain with a dictionary-searching concept, and can be sparse-expressed with very low memory occupation. The imaging results have been compared with the traditional DAS method and the coherent compounding method.

Results/Discussion

Images were obtained with CS method and DAS method on three phantoms: 1) with 5 point scatterers in it; 2) with 6 circle bright or dark regions in it; and 3) established from a biopsy photograph of human kidney. The image quality of CS method has been verified to be better than the traditional DAS method and even the coherent compounding method, on both lateral resolution and image contrast. In addition, comparing to the other existing CS methods, the memory occupation of our method is significantly reduced, since the encoding matrix can be sparse-expressed (e.g. 1.57 GB for ours vs. approx. 283 GB for another existing method). And the time-delay of the echo signals are expressed directly in time-domain, thus avoiding the errors induced by the short-time Fourier translation calculation in those frequency-domain methods. The proposed method can be easily implemented on some low-cost hardware platforms, and can obtain ultrasound images with both high frame rate and good image quality, which make it has a great potential for clinical application.
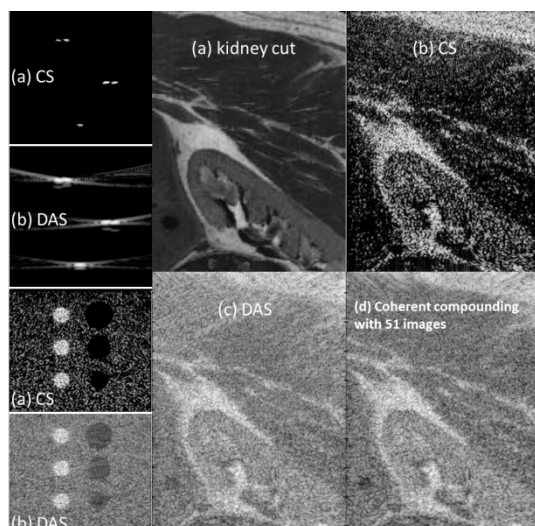
8:00 am   Fourier Beamformation of Multistatic Synthetic Aperture Ultrasound Imaging

Elahe Moghimirad[1], Carlos A. Villagomez Hoyos[2], Ali Mahloojifar[1], Babak Mohammadzadeh Asl[1], Jørgen Arendt Jensen[2]; [1]*Dep. of Elec. and Comp. Eng., Tarbiat Modares University, Tehran, Iran,* [2]*Center for Fast Ultrasound Imaging, Dept. of Elec. Eng., Bldg. 349,Technical University of Denmark, Denmark*

Background, Motivation and Objective

Conventional ultrasound imaging is performed using line-by-line focused transmissions. However, synthetic aperture (SA) imaging has a better resolution and contrast at the cost of more computational load. To overcome this problem, Delay-And-Sum (DAS) reconstruction has been replaced by the Fourier beamformation (FB) algorithms in radar and sonar. The FB algorithm is extended here to multistatic medical ultrasound imaging, compensating for the effects from bandwidth, beam width, and imaging depth.

Statement of Contribution/Methods

The method consists of 4 steps: a 2D fast Fourier transform of the data, frequency shift of the data to baseband, interpolation to convert polar coordinates to rectangular ones, and returning the data to the spatial-domain using a 2D inverse Fourier transform. In addition, apodization and a beam width correction algorithm were used to compensate for the effects of a wide beam width especially in the near field. Experiments were performed using Field II simulated data with a 96-element linear transducer with $\lambda/2$ pitch which was excited at 4MHz. Each imaging sequence was performed using one element transmitting and all of them receiving. A simulated point target was used to evaluate the result in terms of axial and lateral resolution. Also, to study more realistic conditions concerning the contrast ratio, a cyst phantom of size 10 mm ×10 mm ×10 mm was simulated centered at 30 mm depth with 3 mm radius.

Results/Discussion

The point spread function of simulated point target at 40 mm depth is shown in Figure 1(a). The lateral resolution is 0.82 mm and 0.75 mm for DAS and FB, respectively. The axial resolution is also 0.35 mm for DAS and 0.33 mm for FB. Figure 1(b) shows the cystic resolution of point target at different depths for -20 dB and -6 dB demonstrates a better resolution for FB at all depths. The cyst phantom was also used to calculate the contrast ratio which is 94.04% and 94.72% for DAS and FB, respectively. To calculate the computational complexity, a $M \times N$ pixel final image was assumed. The number of calculations for making one low resolution image assuming 8 digit real numbers (16 digit complex numbers) is $MN^2 \times 296$ for DAS and $MN[1056 + 24 log_2 (MN)]$ for FB which results in a 20 times improvement in process time for FB on the typical 2000×100 pixels image. The results show that FB has a better performance with less computational complexity in comparison with DAS.
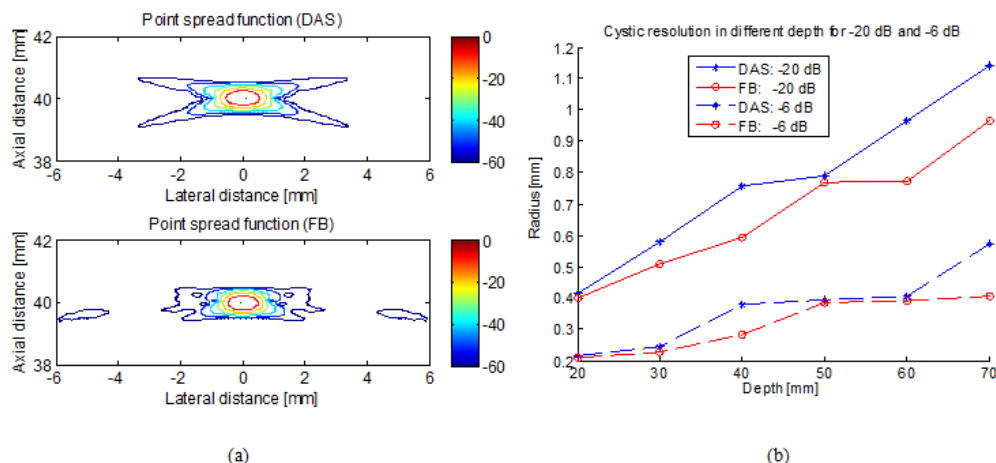
Figure1: Simulated point target (a) point spread function of DAS (top) and FB (bottom), and (b) cystic resolution in different depth for -20 dB and -6 dB for DAS (blue lines) and FB (red lines).

P1A4-8

8:00 am   Comparison of spatial and temporal averaging on Ultrafast Imaging in presence of quantization errors

Asraf Mohamed Moubark[1], Zainab Alomari[1], Sevan Harput[1], **Steven Freear[1]**; [1]*School of Electronic and Electrical Engineering, University of Leeds, Leeds, United Kingdom*

Background, Motivation and Objective

In Ultrafast imaging, both Compound Plane Wave Imaging and Plane wave imaging pave the way in producing high frame rates.The compounding operation is effectively a spatial averaging filter that reduces the speckles of the image and increases the lateral resolution. Although spatial averaging often improves CPWI image quality, quantization errors introduced during beam steering degrade this improvement. It is also possible to improve the image quality by applying temporal averaging in conjunction with PWI, which is not prone to beam steering errors. In this study, the effect of temporal and spatial averaging on speckle noise reduction and spatial resolution in ultrafast ultrasound imaging is evaluated.

Statement of Contribution/Methods

In figure 1 it can be observed clearly the presence of a stair case pattern on the wave front of steered plane wave while the wave front of plane wave don't show any.Simulations were carried out by using the Field II software in Matlab. The effect of spatial averaging technique in the presence of quantization error on the image quality has been evaluated by transmitting three different plane waves steered from ±30° with angular steps of 0.1°, 0.5° and 1.0°. As for temporal averaging technique, a set of three plane waves were transmitted at 0 degrees. Simulations were performed with a sampling frequency of 160 MHz for a 128 element linear probe with a center frequency of 5.5MHz, bandwidth of 5 MHz, and inter element spacing of λ.

Results/Discussion

It is demonstrated in this paper that spatially averaged and coherently compounded CPWI provides a good quality image when compared with temporally averaged PWI with the presents of quantization errors. In CPWI, the spatially averaged and coherently compounded echoes signal improve the signal to noise ratio (SNR) of the image amplitude in a region of interest (ROI) from speckle noise by the maximum factor of $\sqrt{N}$, where N is the number of compounded frames. However, the quantization errors degrade the overall performance by $\beta(N-1)$, where β is the error factor produced by different angular steps. Even though this problem does not occur in PWI where the transmitted wave front always remains constant perpendicular to all the elements but CPWI improve the SNR better than PWI.
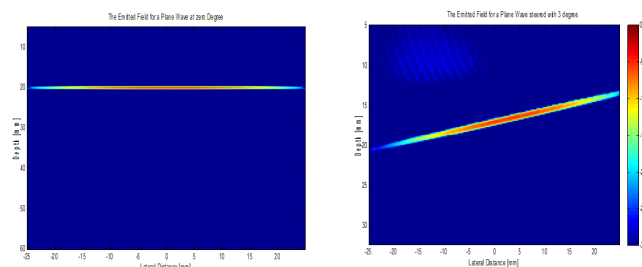
Figure 1: Plane wave and Steered plane wave at 3°.

8:00 am   Single transmission plane wave compounding for ultrafast ultrasound imaging

Natan Pages[1], Barbara Nicolas[1], **Herve Liebgott[1]**; *[1]CREATIS, France*

Background, Motivation and Objective

Coherent compounding of low resolution images obtained from different insonnification angles is the state of the art technique to improve the quality of ultrafast plane wave (PW) images. The main drawback of this method is the frame rate decrease as several acquisitions ($\approx$ 10) are required. On the other hand, frequency division multiplexing or pseudo-random coded excitations have been used in synthetic aperture imaging to accelerate the acquisition rate.

The objective of this work is to improve the image quality in PW imaging without decreasing the frame rate, using coded excitations.

Statement of Contribution/Methods

We propose to emit several PW simultaneously with different angles. Each PW is carrying a specific excitation signal, here m-codes are used.

With the knowledge of all emitted codes, a linear model of the problem is build where each received signal is expressed as a matrix product with a convolution matrix containing the delayed codes.

Before beamforming, decoding is achieved to separate the different PW.

In our approach the influence of scatterrers situated inside the so-called blind region close to the probe and outside the imaging region is taken into account. Due to their specific position, the echoes of these scatterrers cannot be collected entirely which leads to an ill posed problem that cannot be inverted. Pseudo-inverse based on truncated SVD has been used to separate the different PW.

Finally angle compounding is achieved with the decoded signals

Results/Discussion

Our technique has been validated using Field II simulations of a linear 128 elements array with f0=8 MHz. Resolution and CNR have been evaluated and compared with conventional PW compounding. To validate the technique two PW are encoded and transmitted simultaneously. Figure 1 shows the PSF images obtained after 3 transmissions corresponding to 3 angles in the conventional approach and 6 in our technique. The resolution is clearly improved.

The CNR as a function of number of transmissions is evaluated: [1-10] angles in the classical approach corresponding to [2-20] angles with the proposed method. Again at a given frame rate, our technique obtained better results (Fig 1c).

This study validates the feasibility of coded excitation PW imaging as a mean to improve the spatial image quality in ultrafast PW imaging. Future works include extendind the method to more than 2 simultaneous PW transmissions.
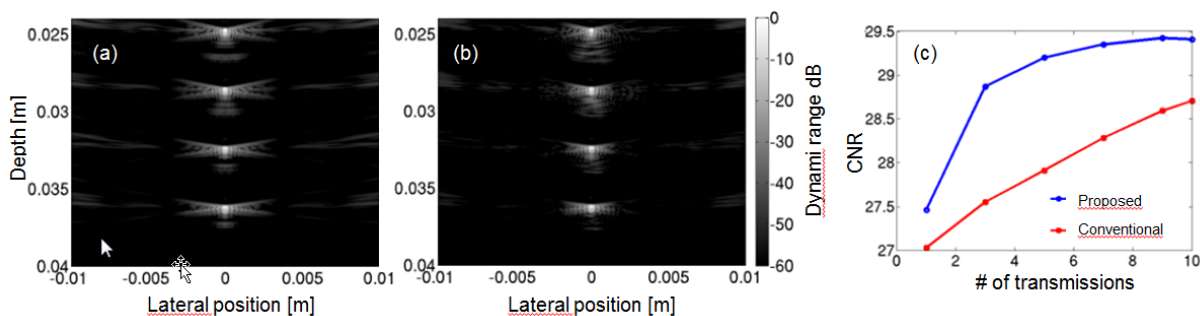
Figure1: (a) and (b) represent the PSF images obtained from 3 transmissions corresponding to 3 and 6 angles in the conventional and proposed method, respectively. (c) represents the CNR for the conventional and proposed technique for different number of transmissions between 1 and 10 corresponding to 2 to 20 angles with the proposed method.

8:00 am   Increased frame rate for plane wave imaging without loss of image quality

Jonas Jensen[1], Matthias Bo Stuart[1], Jørgen Arendt Jensen[1]; *[1]Dept. of Elect. Eng, Technical University of Denmark, Kgs. Lyngby, Denmark*

Background, Motivation and Objective

Plane Wave (PW) and Synthetic Aperture (SA) imaging have the potential of producing high-quality images and velocity estimates of both slow and fast flow at high frame rates. However, linear array transducers produce grating lobe artifacts in transmission and reception, which affect the image quality and/or frame rate. These artifacts are undesirable for high-quality imaging and flow estimation, because a high frame rate is needed for fast flow estimation. This paper demonstrates that a transducer with $\lambda/2$-pitch produces PW images at a higher frame rate than a λ-pitch transducer without loss of image quality.

Statement of Contribution/Methods

A 3.5 MHz 128 element phased array transducer with $\lambda/2$-pitch and a 64 element λ-pitch transducer were simulated using Field II. All elements were used to generate steered plane waves for acquisition of low-resolution images, which were combined to obtain high-resolution images. An optimization procedure based on reducing the FWHM and cystic resolution was executed for selecting the optimal steering angle and number of emissions. The approach was implemented on the SARUS scanner using transducers with the same parameters as in the simulations. Scans of a wire phantom and a phantom containing water filled cysts were conducted to investigate image quality and effects of transmit-grating lobes. The image quality was assessed in terms of FWHM and cystic resolution.

Results/Discussion

Figure (a) shows a point target at 10 mm measured with the λ-pitch (top) and $\lambda/2$-pitch (bottom) transducer. Based on the optimization, 17 PWs equally spaced between ±20 deg. are used for the images. The cystic resolution for 20 deg. steering is shown in figure (b) as a function of the number of emissions for a measured and simulated point target. To obtain a cystic resolution of -27 dB, only 9 emissions are required with the $\lambda/2$-pitch transducer, while 33 emissions are required with the λ-pitch transducer, which has a direct effect on the frame rate. The influence of the transducer pitch is profound at depths from 0-20 mm, which is the interesting region for superficial vessels. Furthermore, the cyst phantom simulation shows that the λ-pitch transducer produces artifacts with undesirable strengths of -30 to -40 dB for a low number of emissions. It is therefore recommended to use a transducer with $\lambda/2$-pitch to increase the frame rate in plane wave imaging.

(a)   (b)
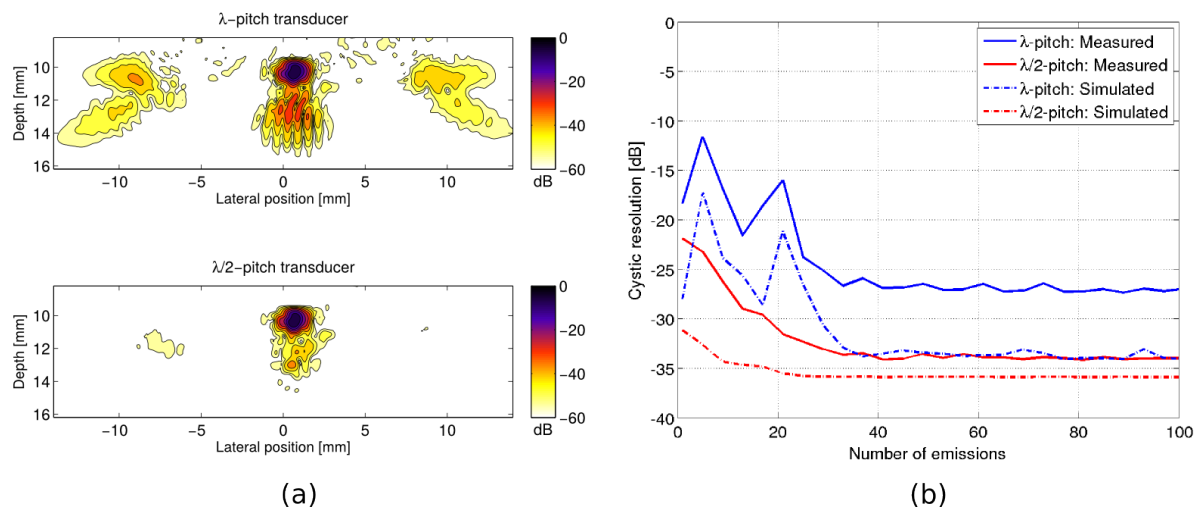
P1A4-11

8:00 am   Motion-Corrected Coherent Compounding for Improved Beamforming in Ultrafast Imaging

Jean Provost[1], Mafalda Correia[1], Mickael Tanter[1], Mathieu Pernot[1]*; [1]Institut Langevin, ESPCI, Paristech, INSERM, France*

Background, Motivation and Objective

Coherent compounding of multiple successive emissions such as tilted plane waves can significantly improve contrast and resolution in Ultrafast Ultrasound Imaging. However, compounding is typically carried out under the assumption that the scatterers' motion is small and negligible during the compounding operation. In this study, we propose a novel beamforming approach that ensures both the spatial and temporal coherence prior to compounding. More specifically, we demonstrate in phantoms and in humans in vivo that by correcting for the translation of the scatterers in between emissions, improved tissue motion estimation is obtained at a limited computational cost.

Statement of Contribution/Methods

We first demonstrated that, unlike when using focused beams, speckle decorrelation occurs due to translation motion when using standard coherent compounding and how this decorrelation can be corrected for by applying a specific apodization function along the slow-time dimension. This novel approach called Motion-Corrected Coherent Compounding (MCCC) was then compared against standard and sliding-window coherent compounding in simulations, in a phantom study, and for cardiac shear wave elastography in the human heart. An Aixplorer system (Supersonic Imagine, Aix-en-Provence, France) was used to perform Shear Wave Imaging at 2300 frames/s using a 3-MHz phased array probe in a breast phantom (059, CIRS, Norfolk, VA). A similar sequence was used transthoracically in the heart of a healthy volunteer.

Results/Discussion

Simulations revealed that MCCC effectively provided motion correction in all three directions, i.e., axial, lateral, and elevational. Additionally, MCCC consistently provided better motion estimates both in phantoms (Fig. 1) and in vivo. Indeed, by taking into account the temporal dimension when performing compounding, improved coherence of the point-spread function resulted in enhanced motion estimation quality, which could be obtained at the pulse repetition frequency. MCCC is particularly attractive as it can be used to compound a large class of 2D and 3D emission types, and can be implemented at a limited computational cost.
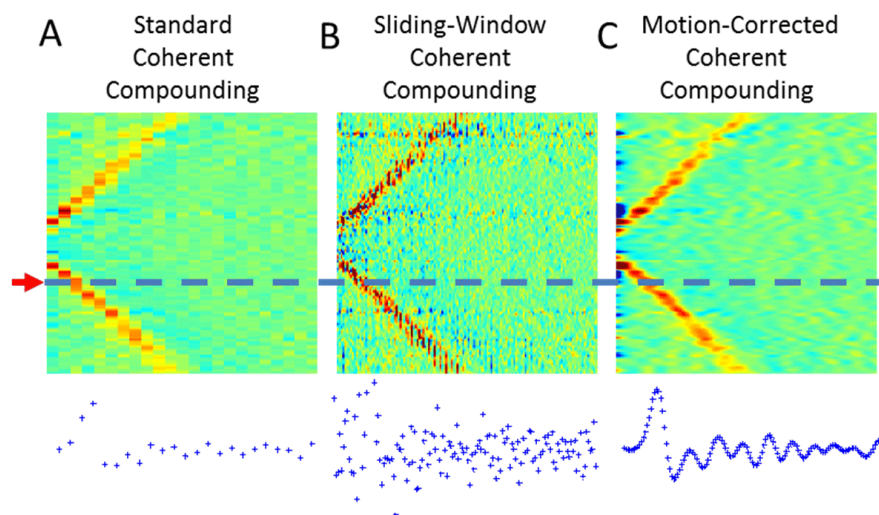
P1A5 - MTH: Therapeutic Methods

4th floor

Thursday, October 22, 2015, Posters displayed 08:00 am - 05:00 pm. Authors must be present at their poster from 9:30 - 10:30am (odd number posters) and 14:30 – 15:30pm (even number posters).

Chair: **Helen Mulvana**
           University of Glasgow

P1A5-1

8:00 am   New cancer treatment method utilizing intratumoral drug distribution control with mechanical effects of cavitation

Ken-ichi Kawabata[1], Takashi Maruoka[1], Rei Asami[1], Hideki Yoshikawa[1], Reiko Ashida[2]; *[1]Hitachi, Ltd., Tokyo, Japan, [2]Osaka Medical Center for Cancer and Cardiovascular Diseases, Osaka, Japan*

Background, Motivation and Objective

Mechanical effects of ultrasound have potentials for drug delivery system (DDS). Previously, we proposed to use liquid droplets containing superheated perfluorocarbons as sensitizers to destroy tissue structures which exist as barriers for drug delivery in combination with pulsed exposure of ultrasound at conventional HIFU intensity range. It was found that such droplets can induce spatially controlled ultrasonic mechanical effects with acoustic intensity of several kW/cm^2 ex vivo and in vitro. In this study, we investigated in vivo antitumor effects of the mechanical effects induced in such a way in the presence of antitumor agents. Further, the possibility of ultrasonic monitoring of the therapeutic process was investigated.

Statement of Contribution/Methods

Pulsed HIFU (pHIFU) exposures were performed using a focused ultrasound transducer with a diameter of 78 mm and F number of 1.0 at 1.1 MHz. Typically, ultrasound pulses with an intensity of 3 kW/cm^2 (pulse duration: 300 cycles, PRF: 1 kHz, total exposure time: 60 s) was applied to samples or animals in a water tank filled with degassed water kept at 37 °C. In vivo experiments were performed with CDF1 mice subcutaneously inoculated with Colon 26 tumor tissues. Before ultrasound application, a superheated perfluorocarbon droplet (PCND) and/or an anti-tumor drug (Adriamycin) were injected into the tumor. For evaluating the changes in tissue properties by pHIFU exposure, Realtime Tissue Elastography®, a strain imaging, was applied.

Results/Discussion

When pHIFU were applied to tumor tissues without PCNDs injection, only short-term (2-3 days) delay in tumor growth was observed. At the same ultrasound conditions, the injection of PCNDs prior to the pHIFU resulted in an enhanced tumor growth delay for about a week. When PCNDs and Adriamycin instead of PCNDs alone were injected to the tumor and the pHIFU was then applied, a drastic tumor growth inhibition was observed. The tumor growth was completely prohibited for two weeks. In three of four examinations, no regrowth was observed during 30 days. No significant anti-tumor effects were observed when Adriamycin was injected and pHIFU was not applied. Further, it was shown that lesions by pHIFU and PCNDs were clearly visualized as soft regions in strain imaging, suggesting the possibility of realtime monitoring of the therapeutic process with echographic methods (Fig. 1).

(a) Gross image   (b) B-mode image   (c) Strain image
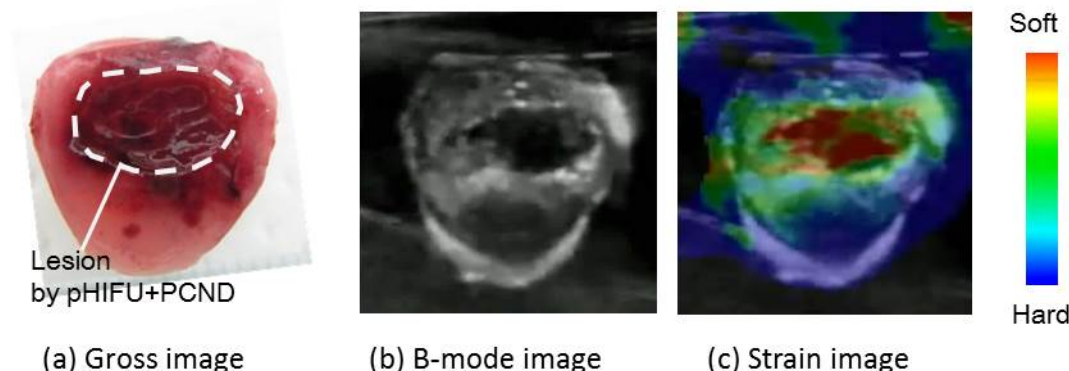
Figure 1 Gross and echographic appearances of pHIFU induced lesion in tumor tissue

P1A5-2

8:00 am   High resolution coagulation size estimation with multiple modulation frequencies for localized motion imaging

Takashi Azuma[1], Ryusuke Sugiyama[1], Chen Optatovsky[1], Mika Seki[1], Hideki Takeuchi[1], Keisuke Fujiwara[2], Kazunori Itani[2], Kiyoshi Yoshinaka[3], Shu Takagi[1], Yoichiro Matsumoto[1]; *[1]The University of Tokyo, Japan, [2]Hitachi Aloka Medical, Japan, [3]National Institute of Advanced Industrial Science and Technology, Japan*

Background, Motivation and Objective

A real-time ultrasound (US) coagulation monitoring system for coagulation size control based on acoustic radiation force is described in this paper. US imaging to facilitate HIFU has advantages with respect to portability, cost effectiveness and spatiotemporal resolution. Localized motion imaging (LMI) is one of the techniques based on US to detect a change of tissue mechanical properties caused by its thermal coagulation. In this paper, our purpose is to improve sensitivity to small coagulation using a square wave amplitude modulation (AM) including multiple frequencies.

Statement of Contribution/Methods

In LMI, acoustic radiation force (ARF) generated by a transducer is used as a mechanical input to deform tissue at the focus. The ARF is modulated by changing the US intensity. The size of localized oscillation area can be controlled by AM frequency. In this study, square-wave modulation was used to achieve a multiple-frequency AM. The amplitude of the oscillating tissue can be measured by a cross-correlation between echo signals in consecutive frames. After coagulation, the tissue stiffness changes are detected as changes of tissue oscillation. A coagulated area is estimated from decrease ratios of the amplitude between before and after coagulation.

A prototype real-time one-dimensional LMI system was constructed. AM frequencies of square wave modulation, HIFU frequency, time interval in coagulation size estimation were 34 Hz, 2 MHz, 1s respectively. The sonication time was 30s. The target porcine liver tissue was embedded in polyacrylamide gel. In the square wave AM, coagulation size based on 3rd and 5th harmonics component of vibration frequency were also estimated.

Results/Discussion

Figure shows time-lapse changes of estimated coagulation size using the different frequency components. The highest frequency was suitable for detection of coagulation beginning. The middle frequency were suitable for track of coagulation expansion. The lowest frequency did not show good result in current case. However, if coagulation size will exceed vibration area of the middle frequency, this lowest condition has a potential to track of coagulation expansion.

In the proposed square wave AM, combination of higher and lower AM frequency could successfully detect coagulation beginning and track coagulation expansion in the latter part of sonication duration.
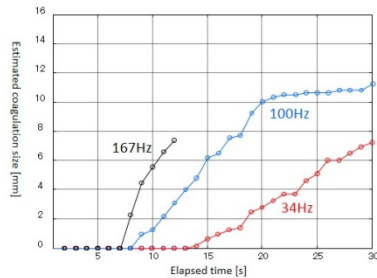
P1A5-3

8:00 am   Temperature distribution analysis for High Intensity Focused Ultrasound Breast Cancer Treatment by Numerical Simulation

Mingzhen ZHANG[1], Takashi AZUMA[1], Kohei OKITA[2], Xiaolei QU[1], Ryuta NARUMI[1], Hidemi FURUSAWA[3], Junichi SHIDOOKA[3], Shu TAKAGI[1], Yoichiro MATSUMOTO[1]; *[1]Graduate School of Engineering, The University of Tokyo, Japan, [2]College of Industrial Technology, Nihon University, Japan, [3]Breastopia Medical Corporation, Breastopia Namba Hospital, Japan*

Background, Motivation and Objective

Breast cancer incidence is dramatically increasing in Japan. High intensity focused ultrasound (HIFU) is a low-invasive treatment method for breast cancer. It could produce irreversible tissue thermal coagulation in focus position. To improve coagulation region accuracy, most previous studies tried to control focus position and make the target position have maximum acoustic pressure. However, direct reason for coagulation is not high pressure but temperature. This study tried to numerically analyze temperature distribution for HIFU breast cancer treatment.

Statement of Contribution/Methods

Spatial and temporal temperature distribution for HIFU breast cancer treatment was numerically analyzed, and it was compared to acoustic pressure distribution. Due to pressure sharpness spatially varying, heat diffusion was spatially different. As the result, temperature-rise speeds in different locations were expected to be different.

To implement the numerical analysis, there were four steps. First, breast models were obtained by segmentation of real patient MRI image. Second, HIFU radiation was opened. Third, pressure field was spatially calculated. Finally, temperature distribution was simulated both spatially and temporally.

In the simulation, time-step of ultrasound propagation was 6.74 ns(t). The propagation was simulated by Eq.1: $1/(\rho_m c^2_{sm})p'_t+\text{div }\mathbf{u}=f_p A\cos(\omega t)$, and Eq.2: $\rho_m \mathbf{u}'_t=\text{div}\{-p\mathbf{I}+\zeta_{vm}\text{tr}(\mathbf{e})\mathbf{I}+2\mu_{vm}(\mathbf{e}-1/3\text{tr}(\mathbf{e})\mathbf{I})\}$.

Time-step of temperature-rise was set at 6.74 ms(τ), which was 10^6 times of propagation time-step. And the temperature-rise was simulated by Eq.3: $\rho_m C_{pm}T'_\tau=\text{div}(\kappa_m\text{grad}(T))+\zeta_{vm}\{\text{tr}(\mathbf{e})\mathbf{I}\}^2+2\mu_{vm}(\mathbf{e}-1/3(\text{tr}(\mathbf{e})\mathbf{I})^2\}$.

In the above equations, Eq.1 is mass conservation equation with sound source on the right side. Eq.2 is momentum equation in isotropic fluid model. And Eq.3 is heat equation with these two terms from right as heat source from viscous dissipation.

Results/Discussion

Fig.(a) and (b)-1~3 showed acoustic pressure and thermal temperature distribution of one patient. (b)-4 showed temperature ratio of other region to focus region dramatically increased as exposure time increased. Thus, too long exposure time may cause thermal damage out of focus region, even when the temperature is not able to cause coagulation. We will apply same analysis to 6 patients data and discuss these results in the presentation.
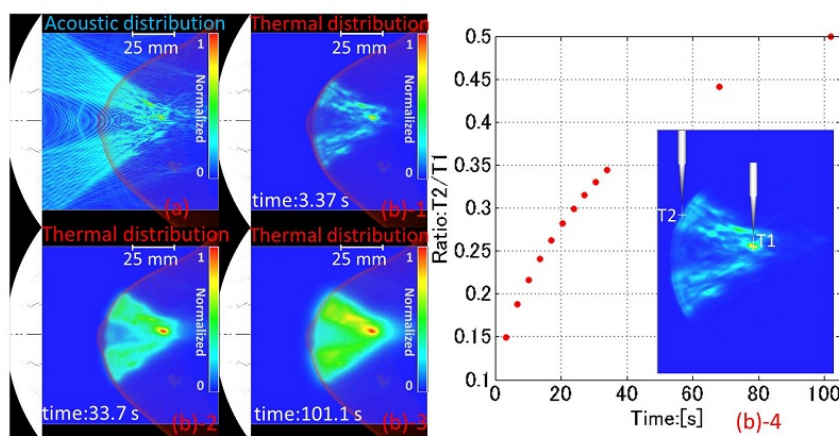
Fig.(a), Acoustic distribution; **(b)-1, (b)-2, (b)-3,** Thermal distribution at radiation time of 3.37 s, 33.7 s, 101.1 s; **(b)-4,** Temperature ratio of other region to focus region as exposure time increase

P1A5-4

8:00 am **Generation of calibration curve with pulse compression technique for ultrasound-based temperature estimation**

Su A Lee[1], Jong Seob Jeong[1]; [1]*Medical Biotechnology, Dongguk University, Gyeonggi-do, Korea, Republic of*

Background, Motivation and Objective

Although ultrasound imaging has been attracting attention as an image guidance for high intensity focused ultrasound (HIFU) therapy, the function of temperature estimation is not accurate. In order to solve this problem, the speckle tracking method based on echo shifts in time domain has been proposed by some researchers. However, the accuracy of this algorithm is low especially at higher temperature (above 50 °C) because echo shifts are essentially related to the speed of sound. To minimize those errors and improve accuracy, the calibration curve was introduced and it should be applied to speckle tracking method. Since the echo shift information is obtained by the peak amplitude of the backscattered signal, increasing the amplitude within the intensity regulation is a critical factor for precise temperature measurement. Hence, in this study, a pulse compression technique by using the chirp signal is presented to increase SNR (signal to noise ratio).

Statement of Contribution/Methods

To verify the adequacy of the proposed method, 1-cycle sinusoidal signal was employed as a reference, and the chirp waveform (with a sweep range from 2 to 8 MHz, 5 μs time duration, and 5 MHz center frequency) was designed by using a MATLAB program. The performance was experimentally demonstrated by in-vitro measurements on a sliced porcine liver. The propagation speed and tissue thickness were measured by transferring the specimen from a heating bath to a measurement bath per each temperature. Note that the temperature range was from 25 °C to 70 °C, and the calibration curve was then generated by combining speed of sound and tissue expansion effects.

Results/Discussion

The amplitude of the compressed signal was much higher than that of the sinusoidal signal as shown in Figure 1. In a front-side case, 14.6 times and 8.5 times higher at 25 °C and 70 °C, respectively. In a rear-side case, 12.3 times and 6.6 times higher at 25 °C and 70 °C, respectively. A speed of sound, normalized tissue expansion using tissue thickness, and the calibration curve are also shown in Figure 1. Owing to the poor sensitivity of the sinusoidal signal, irregular patterns are observed with much higher errors. On the other hand, the curve performed by the pulse compressed signal had smaller errors in higher temperatures. Therefore, the pulse compression method can be useful for precise temperature estimation during HIFU surgery.

P1A5-5 _____

8:00 am   Visualization of the intensity field of a high intensity focused ultrasound (HIFU) source in situ

Trong Nguyen[1], Minh Do[1], **Michael L. Oelze**[1]; [1]*Electrical and Computer Engineering, University of Illinois at Urbana-Champaign, USA*

Background, Motivation and Objective

High intensity focused ultrasound (HIFU) can provide a means of noninvasive ablation of tissues such as tumors. However, currently the gold standard for monitoring HIFU is MRI temperature mapping. Because of the expense, lack of portability and slow update of temperature maps from MRI, ultrasonic solutions to monitoring of HIFU remain an important clinical goal. Real-time visualization of the field distribution of the HIFU source during treatment would allow the localization of the intersection of the beam with the tissue. Real-time visualization of the beam in the context of the tissue is important for proper placement of therapy especially during tissue motion. To visualize the HIFU field in a tissue, a reconstruction technique was employed using a Fourier-domain f-k migration approach with a linear array system co-aligned with the HIFU source. The reconstruction technique used the scattered signal from the medium to reconstruct the intensity field pattern of the HIFU field in situ and superimpose the intensity field image on a B-mode of the scattering medium.

Statement of Contribution/Methods

A 6-MHz single-element transducer (f/3) was used as the HIFU source and aligned perpendicular to the field of a linear array (L14-5) operated by a SonixRP system equipped with a Sonix-DAQ. The array had 128 elements and a measured center frequency of 6.5 MHz. The 6-MHz HIFU source was pulse excited and the fields scattered from a sample, i.e., a homogeneous tissue-mimicking phantom or a chicken breast, were received by each element of the linear array. Beam forming based on Fourier-domain f-k migration techniques were applied to the channel data to reconstruct the intensity field pattern from the HIFU source. For comparison, a wire target was placed in the field and the intensity field pattern was reconstructed by moving the wire throughout the focal region. The intensity field pattern reconstructed from the sample was compared to the field characteristics of the 6-MHz source characterized by the wire technique. The intensity field pattern was then superimposed on a registered B-mode image of the sample acquired using conventional B-mode imaging with the linear array and the SonixRP to provide context to the therapy beam placement.

Results/Discussion

The -6-dB beam width estimates at the HIFU focus using the in situ reconstruction technique and the wire technique were 1.7 mm and 1.5 mm, respectively. The -6-dB depth of field estimates for the in situ reconstruction technique and the wire technique were 20.1 mm and 19.0 mm, respectively. Therefore, the novel reconstruction technique was able to accurately visualize the field of a focused source in the context of the interrogated medium. The visualization technique would allow real-time adjustment of the HIFU beam location in tissues during therapy.

P1A5-6 _____

8:00 am   Inducing antivascular effects in tumors with ultrasound stimulated micron sized bubbles

Naomi Matsuura[1], Minseok Seo[2], Niroo Sivapalan[2], Siqi Zhu[2], Ben Leung[2], **David Goertz**[3,4]; [1]*Medical Imaging, University of Toronto, Canada*, [2]*Sunnybrook Research Institute, Canada*, [3]*Sunnybrook Research Institute, Toronto, ON, Canada*, [4]*Medical Biophysics, University of Toronto, Canada*

Background, Motivation and Objective

It has been demonstrated that relatively low intensity ultrasound in combination with microbubbles is capable of inducing a vascular shutdown in preclinical tumors, and that this can lead to growth inhibition. In previous reports we have shown that this effect can be coupled with anticancer agents to achieve potent antitumor effects, by a means that is not linked to increases in drug uptake (Todorova et al Int J Cancer 2013; Goertz et al Plos One 2012). Work to date has been conducted with commercial agents such as Definity or experimental formulations that are designed to be comprised substantially of bubble sizes that are resonant at the exposure frequencies employed (0.5-3 MHz). Here we investigate the potential of an experimental agent comprised of micron to submicron sized bubbles to induce antivascular effects in tumors.

Statement of Contribution/Methods

Experiments were conducted with KHT sarcoma tumors initiated intramuscularly in the hind legs of C3H mice and grown to approximately 200 mm3 in size. Control and treated groups were evaluated (n=5-6/ group), with ultrasound exposures conducted at 1 MHz with a 0.00024 duty cycle and peak negative pressure of 1.6 MPa). An experimental in house agent lipid (DPPC/DPPA, DPPE-mPEG5K, perfluorbutane) encapsulated agent with a volume peak at 0.9 microns was employed, with injection gas volume fraction matched to Definity doses. Agent was monitored withheld a Philips L12-5 probe in contrast mode. Tissue was harvested after a presacrifice perfusion stain injection (DiOC7). Agent characterization experiments included frequency dependant attenuation measurements (1-40 MHz) and cavitation detection and analysis.

Results/Discussion

The agent frequency response was such that insonations occurred well below the resonant frequency and the exposures were at a level the produced wideband acoustic emissions associated with inertial cavitation. Rapid perfusion reductions were observed in the tumors after treatments as evidenced by perfusion staining and contrast imaging (Fig. 1). These perfusion reductions were comparable to those that we have previously reported with Definity under similar exposure conditions in the same tumor type. The particular characteristics of micron sized formulations may however offer advantages in the context of clinical implementations.
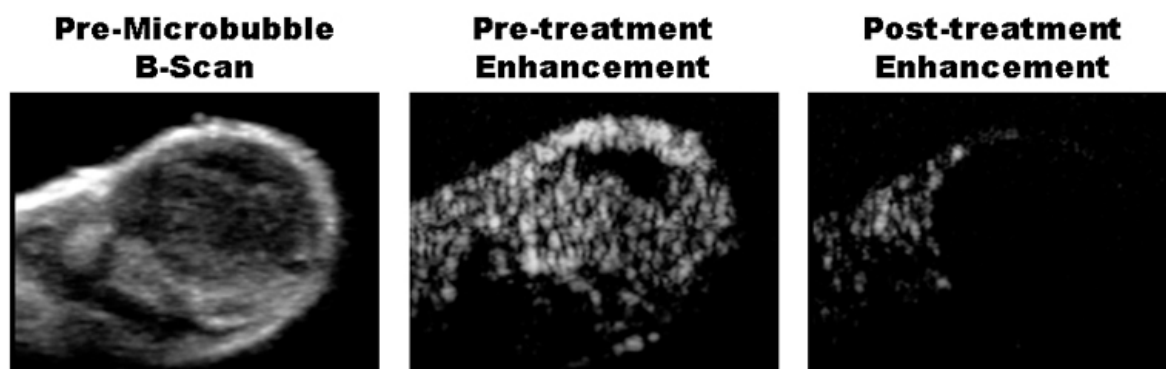
Figure 1. Left: B-scan image of tumor. Middle: contrast image pre-treatment. Right: contrast image post-treatment shows a pronounced vascular shutdown within the tumor. Image width=15mm.

P1A5-7

8:00 am   **Enhanced Cavitation Activities from Axial Split Foci Using Second/Third-Harmonic Superimposition for Focused Ultrasound Surgery**

Mingzhu Lu[1], Yubo Guan[1], Yujiao Li[1], Mingxi Wan[1]; *[1]Department of Biomedical Engineering,School of Life Science and Technology,Xi'an Jiaotong University, The key Laboratory of Biomedical Information Engineering of Ministry of Education, Xi'an, Shaanxi, China, People's Republic of*

Background, Motivation and Objective

Inertial cavitation can accelerate heating up in focused ultrasound surgery. Furthermore, the superimposing of two frequency pressures at confocal region can enhance nucleation cavitation and inertial cavitation activity, thus speed up heating rate for shortening treatment time. This study aims at enhancing cavitation heating by using dual-frequency modes of second-harmonic and third-harmonic superimposition for high-efficient focused-ultrasound surgery.

Statement of Contribution/Methods

The transducer consists of two element arrays, both are spherical annular, one is stimulated with 1.1 MHz, and the other with 3.3 or 2.2 MHz. By controlling the ratio of dual-frequency acoustic powers, the superimposing of two frequency pressures result in split foci along beam axial within confocal region, and the maximal peak intensity of split focus can reach about 2 times the sum of two frequency intensities, indicating strong wave interference. The 1.1 MHz/3.3 MHz and 1.1 MHz/2.2 MHz modes have thirteen (see Fig.1 (a)) and nine split foci respectively (within about 7-mm axial focal region). Under inertial cavitation condition, the cavitation clouds at neighbor foci will interfere with each other, so enhancing cavitation heating greatly. When using 60° phase shift in 1.1 MHz/3.3 MHz case, both negative and positive peak pressures reach maximum, this is due to that peak-negative pressures of two frequencies occur at same time, as well as peak positive pressures meeting, resulting strongest cavitation activities. In 135° phase shift with 1.1 MHz/2.2 MHz, the negative peak pressure reach maximum.

Results/Discussion

When using 1.1 MHz/3.3 MHz frequency, 60° phase shift, 65 W/20 W acoustic power, 100 Hz pulse-repetition frequency, and 0.4 duty factor, the BSA gel-phantom experiment results show the largest lesion size of 4.4×9.5 mm (lateral×axial), the earliest lesion-inception time is 0.2 s. In 1.1 MHz/2.2 MHz setting case, using 135° phase shift, 65 W/26 W acoustic power, the results show 3.9×8.5 mm lesion size, 0.5-s lesion inception time. High speed imaging shows the cavitation clouds occurring at split foci (see Fig.1 (b)). The filtered-PCD mean square waveforms indicate the inertial cavitation energy, so Fig.1 (c) reveals that the strong inertial-cavitation activities involves in both cases, and that the strongest activity achieves with 60° phase and 1.1 MHz/3.3 MHz.
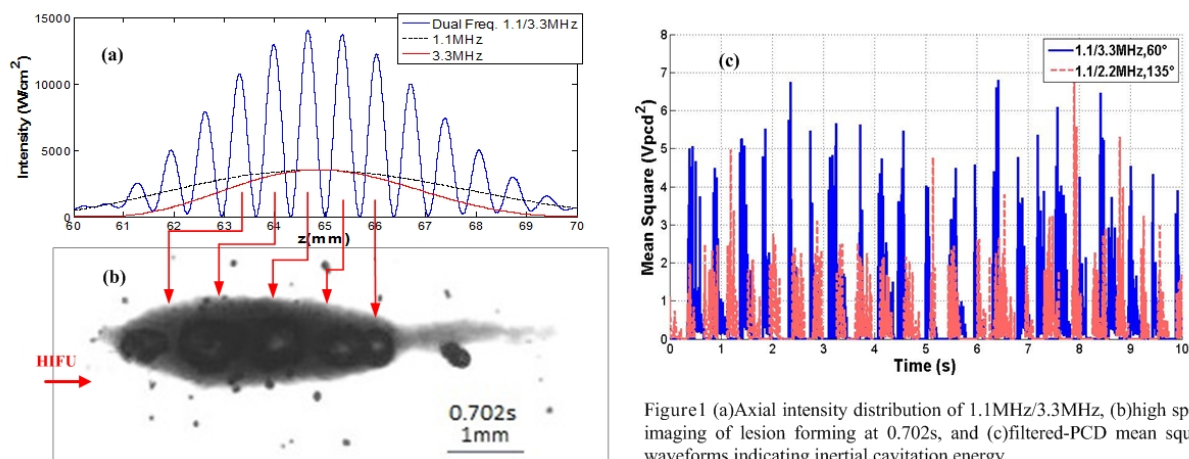
Figure1 (a)Axial intensity distribution of 1.1MHz/3.3MHz, (b)high speed imaging of lesion forming at 0.702s, and (c)filtered-PCD mean square waveforms indicating inertial cavitation energy.

P1A5-8

8:00 am   **New discovery of thin catheter movement under acoustical field of focused transducer**

Takashi Mochizuki[1], Nobuhiro Tsurui[1], Naoto Hosaka[1], Kohji Masuda[1]; *[1]Tokyo University of Agriculture and Technology, Tokyo, Japan*

Background, Motivation and Objective

We have developed the control method of a thin catheter (less than 1 mm diameter) using acoustic radiation force, in which method it was pushed on the acoustic radiation direction. However, it is not clinical satisfaction to move the catheter injected to the human body to the direction of percutaneous ultrasound beam, therefore it is desired to manipulate the catheter to arbitrary direction. Under the needs, we could discover the phenomenon that the catheter displaced to the perpendicular angle of the radiation direction near the acoustic focal zone of ultrasound.

Statement of Contribution/Methods

Figure 1 shows the experimental setup, which consists of a focused transducer (the central frequency of 3.36 MHz, the diameter of 40 mm, and the focal distance of 40 mm) and a thin catheter (the diameter of 0.4 mm). The tip of the catheter is observed to measure the displacement in YZ-plane upon ultrasound emission, where the length of the catheter is 44 mm, as shown in Fig.1. First ultrasound is emitted to bend the catheter in Z-axis (1 to 2 in Fig.1 (a)), before the transducer is moved in Y-direction (2 to 3 in Fig.1 (b)) with keeping the emission of ultrasound. Although the displacement d_Z in the Z-direction is always positive, the displacement d_Y in Y-direction ranges both of positive and negative. We have recorded the maximum displacements d_{Ymax} and d_{Zmax} according to the initial distance , which indicates between the tip of the catheter and the transducer.

Results/Discussion

The graph in Fig.1(c) shows the displacement d_{Ymax} versus the initial distance ζ with maximum sound pressure of 300 kPa-pp, where $\zeta = 37$ mm was the boundary to show that the catheter was pulled and pushed with $\zeta < 37$ mm and $\zeta > 37$ mm, respectively. Figure 1(d) shows the photo of the tip of the catheter with $d_{Ymax} = 0.46$ mm and $d_{Zmax} = 4.9$ mm. Making use of the phenomena, there is a possibility to bend the thin catheter in perpendicular angle to the ultrasound propagation, which suggests that more complicate control of the catheter could be possible with three-dimensional design of acoustic field.
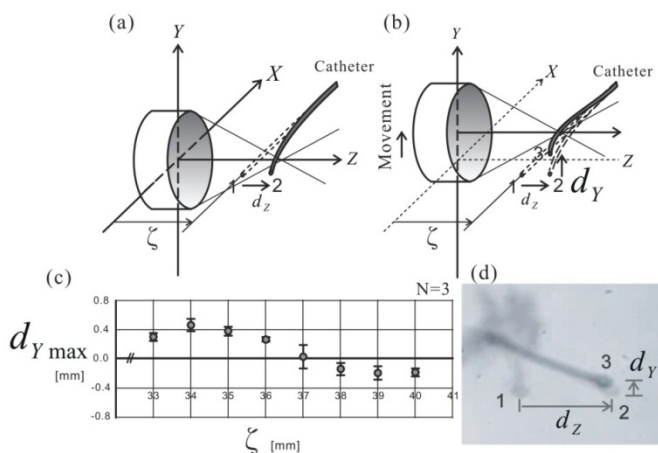
Fig.1. Lateral displacements of catheter in association with the movement of ultrasound transducer.

P1A5-9

8:00 am   Features of acoustic radiation function on thin catheter as a tube

Takashi Mochizuki[1], Nobuhiro Tsurui[1], Kohji Masuda[1]; *[1]Graduate school of Bio-Application & System Engineering, Tokyo University of Agriculture and Technology, Tpkyo, Japan*

Background, Motivation and Objective

We have developed methodology of thin catheter (diameter<1mm) control inside the human body using acoustic radiation force to supply directly anticancer drug to the tumor. It has been known that the acoustic radiation force on thin catheter is related to product ka of wave number k and catheter radius a. However, it was mainly the studies of simulation with the model of a pole shape but not a tube. In this paper, the relation between actually measured data using a tube and the theory is discussed.

Statement of Contribution/Methods

The catheter (outer and inner diameters are 0.45mm and 0.35mm, respectively) is used. In accordance with Langevin theory, the acoustic radiation force comes out of the acoustic pressure difference Δp between P_A (front side pressure of the catheter) and P_B (back side pressure). However, when the diameter of catheter becomes near wavelength, the force becomes complicate. So, we have adopted acoustic radiation function (ARF) as an evaluation. It is defined as ratio of the acoustic force (Fa) and the force (Fc) actually measured from the displacement of the catheter which results from Δp using cantilever theory. Fa is calculated from acoustic pressure, which was measured in advance before the experiment.

Results/Discussion

Figure 1 shows graphs of ARF on the catheter in cases, inner filled with air and water, respectively. In data of air case, the characteristics are discussed in next three categories: 1) In case ka>>2, diffraction effect of ultrasound is small, so the acoustic pressure P_B is almost zero because of sound shadowing, that is, Δp=P_A. Therefore, it pushes the catheter. 2) In case ka=2, the phase of both side pressures, P_A and P_B is coincident, therefore, Δp becomes zero. In this case, Fc should be zero in theory, but in actual measurement result, two minimum points were observed around ka=2. From this, it is assumed that a little ultrasound goes through the catheter because the catheter is a tube constructed with thin material, and a little force comes out of its leak sound. 3) In case ka<<2, the wave length is enough long in comparison with the diameter of the catheter, so Δp becomes small and the force is small.

In case of inner filled with water, the graph monotonically increases, but is lower than date of air case in all rage of ka. From this fact, it is considered that the ultrasound wave goes through the catheter inside, and therefore, it results in decreasing Δp .
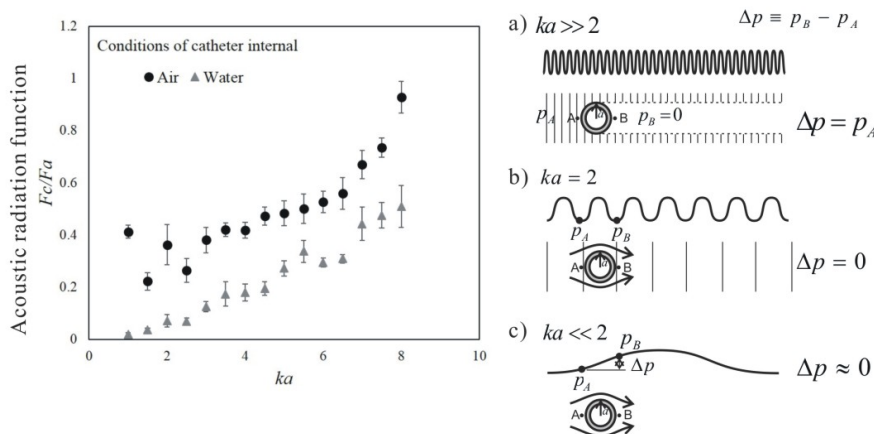
Fig.1. Features of Acoustic radiation function.

P1A5-10 _____

8:00 am   Ultrasound image-based dynamic fusion modeling for estimating the impact of organ motion on HIFU therapies and evaluating motion compensation strategies

W. Apoutou N'DJIN[1], Jean-Yves CHAPELON[1], David MELODELIMA[1]; *[1]LabTau, Inserm, U1032; Université de Lyon, Lyon, France*

Background, Motivation and Objective

Organ motion is a key component in the treatment of abdominal tumors by High Intensity Focused Ultrasound (HIFU), since it may influence the safety, efficacy and treatment time. Here we report the development in a porcine model of an Ultrasound (US) image-based dynamic fusion modeling method for estimating the effect of in-vivo motion on intraoperative HIFU treatments performed in the liver in conjunction with surgery, and evaluating motion compensation strategies.

Statement of Contribution/Methods

The performances of a toroidal HIFU focusing strategy involving single 40-second exposures were evaluated in-vivo in a porcine liver model during breathing and apnea. The HIFU device was a 3 MHz toroidal-shaped transducer embedding a 7.5 MHz curvilinear phased-array US imaging probe for real-time guidance. After HIFU exposures, US images of the liver were acquired with a higher resolution using a 12 MHz linear array US imaging probe. A US speckle tracking method was used at 2 different times of the study to quantify in-vivo liver motions: (i) during post-processing on high resolution US imaging data for fusion modeling of toroidal HIFU treatments; (ii) during the treatment to provide a liver motion feedback in real-time to the user. Fusion modeling of HIFU ablations was implemented by merging dynamic in-vivo motion data in a numerical modeling of HIFU treatments. Large single lesions (7 cm3) were generated with a 40s-exposure and the ability to increase HIFU lesion volumes by juxtaposing precisely multiple single lesions during respiration was studied.

Results/Discussion

Liver motions during breathing were spatially homogenous and could be approximated to a rigid motion mainly encountered in the cranial-caudal direction (f=0.20Hz, magnitude >13mm). Elastic liver motions due to cardiovascular activity, although negligible, were detectable near millimeter-wide sus-hepatic veins (f=0.96Hz, magnitude <1mm). The fusion modeling quantified the effects of respiratory motions on the size and homogeneity of large single lesions usually predicted after a 40-second single toroidal HIFU exposure in stationary tissues. Although their shapes was slightly modified (DSC>75%), lesions remained homogeneous and the ablation rate was little affected by the breathing (<5%). Real-time liver motion feedback allowed controlling manually the probe position to juxtapose accurately 9 single lesions and create homogeneous HIFU ablations (40 cm3 in 14 min). Post-operative fusion modeling accounting for residual motions confirmed experimental observations. This technique may show promise along with the emergence of virtual navigation for evaluating numerically focusing strategies and assist image-guided HIFU interventions. This work was supported by the Lyon Auvergne Rhône Alpes Canceropôle (CLARA), the French General Directorate for Health Care (DGOS) and the French National Cancer Institute (INCA) within the Integrated Research Site of Lyon (LYRIC).

P1A5-11 _____

8:00 am   Enhanced spatio-temporal control of acoustic cavitation during flow using a novel short-pulse ultrasonic pulse sequence and passive acoustic mapping

Antonios Pouliopoulos[1], Marc Tinguely[2], Caiqin Li[1], Mengxing Tang[1], Valeria Garbin[2], James Choi[1]; *[1]Bioengineering, Imperial College London, United Kingdom, [2]Chemical Engineering, Imperial College London, United Kingdom*

Background, Motivation and Objective

Pre-formed microbubbles exposed to focused ultrasound (FUS) pulses can generate acoustic cavitation that results in clot dissolution, sonoporation, and capillary opening (e.g., blood-brain barrier opening). However, control of cavitation has hitherto been limited to controlling its persistence (stable vs. transient), type (non-inertial vs. inertial), and magnitude by adjusting the pressure. Here, we present a novel range of acoustic pulse shapes and sequences that have the additional ability to control cavitation distribution and duration in physiologically relevant flow conditions. In vivo evidence of its ability to enhance drug delivery distribution has been previously shown (Choi et al., PNAS 2011) and we will explore a wider range of parameters with analysis performed with 2D passive acoustic mapping (PAM).

Statement of Contribution/Methods

Traditional therapeutic parameters are composed of a 10-100ms long pulse to generate cavitation. In flow conditions, this results in over- and under-treated regions, upstream and downstream respectively, due to the rapid destruction of microbubbles within the first few milliseconds and the continued microbubble replenishment upstream to the focal volume (Pouliopoulos et al., Phys Med Biol 2014). Our pulse shape and sequence exploits the presence of flow by applying short pulses separated by off-time intervals on the scale of μs to facilitate inter-pulse microbubble movement. A 0.5MHz FUS transducer sonicated flowing microbubbles while a linear array orthogonal to the FUS beam captured acoustic emissions. The type, magnitude, duration and distribution of cavitation activity were determined using imaging with PAM and high-speed optical microscopy.

Results/Discussion

PAM experiments showed that our short-pulse sequences improved the spatio-temporal uniformity of the acoustic cavitation activity during a 100ms burst by reducing the upstream bias produced by continuous wave sonication (figure). High-speed microscopy revealed that this is due to the increased lifetime and mobility of the microbubbles as they flowed through the focal volume. Microbubbles not only translate between successive pulses, but also can be sonicated multiple times throughout a burst. Our demonstration of improved spatio-temporal control of cavitation may have impact on the design of parameters in a wide range of therapeutic applications.
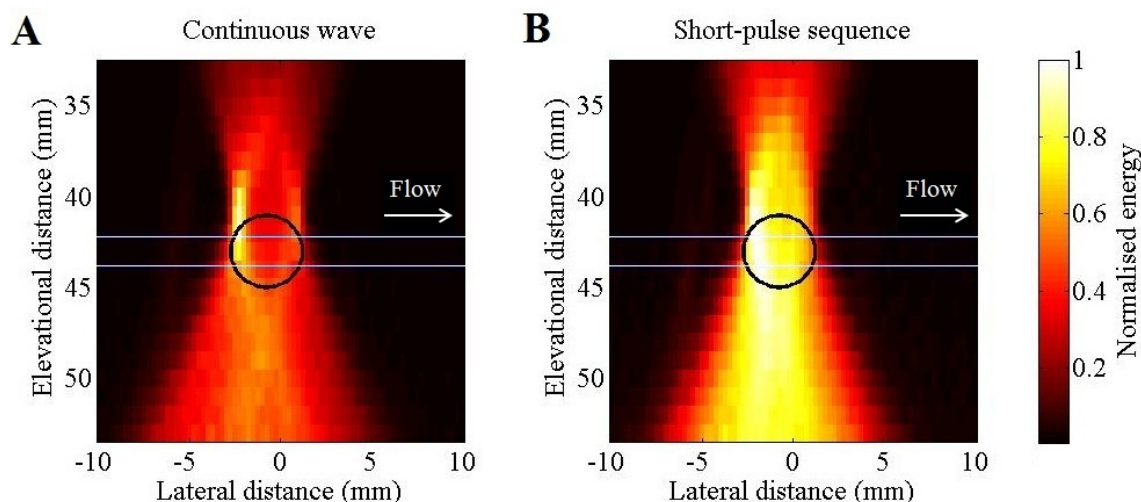
8:00 am **The dynamic excitation of a chain of pre-stressed spheres for biomedical ultrasound applications: contact mechanics finite element analysis and validation**

Pierre Gelat[1], Nader Saffari[1], David Hutchins[2], Jia Yang[2], Omololu Akanji[2], Peter Thomas[2], Lee Davis[2], Steven Freear[3], Sevan Harput[3]; *[1]UCL Mechanical Engineering, University College London, United Kingdom, [2]School of Engineering, University of Warwick, United Kingdom, [3]School of Electronic and Electrical Engineering, University of Leeds, United Kingdom*

Background, Motivation and Objective

There has been recent interest in the transmission of acoustic signals along a chain of spheres to produce waveforms of relevance to biomedical ultrasound applications. Effects which arise as a result of Hertzian contact between adjacent spheres can potentially change the nature of the signal as it propagates down the chain. The possibility thus exists of generating signals with a different harmonic content to the signal input into one end of the chain. This transduction mechanism has the potential to be of use in both diagnostic and therapeutic ultrasound applications, and is the object of the study presented here.

Statement of Contribution/Methods

The nonlinear dynamics of granular chains can be treated using discrete mechanics models. However, in cases where the underlying assumptions of these models no longer hold, and where geometries are more complex, a more comprehensive numerical solution must be sought. Problems pertaining to contact mechanics can efficiently be treated using the finite element method. The latter was used to investigate the dynamics of a pre-stressed chain of six 1 mm diameter stainless steel spheres excited at one end using a tone burst displacement signal with a fundamental frequency of 73 kHz. The final sphere of the chain was assumed to be in contact with a cylindrical matching layer radiating into a half-space of fluid with the properties of water. This configuration mimicked an experimental set-up in which a resonant ultrasonic horn transducer was used to excite one end of a six-sphere chain, with the final sphere radiating into water via a matching layer.

Results/Discussion

The finite element model was initially validated in absence of fluid loading with a discrete mechanics approach, demonstrating good agreement between both methods. After addition of the fluid loading, predicted radiated acoustic pressures in the medium were compared with experimental results obtained using a calibrated hydrophone. Good agreement between theory and experiment was obtained, demonstrating that finite element analysis is a suitable tool for investigating this novel transduction mechanism, which will be used to model and optimise more complex configurations.

8:00 am **Extracorporeal Acute Cardiac Pacing by High Intensity Focused Ultrasound in Practice and Theory**

Amit Livneh[1], Eitan Kimmel[1], Dan Adam[1]; *[1]Biomedical Engineering, Technion-Israel Institute of Technology, Haifa, Israel*

Background, Motivation and Objective

Extracorporeal acute cardiac pacing by high intensity focused ultrasound (HIFU) could be a disruptive technology in the field of cardiology. Recently, we published results demonstrating premature ventricular contraction (PVC) induction in anesthetized rats; PVC induction was demonstrated temporally throughout the entire cardiac cycle outside of the absolute refectory period and spatially throughout the entire left ventricle (LV). These results suggest membrane currents as the dominant cellular level mechanism and cavitation as the dominant ultrasound tissue interaction mechanism. The minimal peak negative pressure that was applied for eliciting PVCs was 1.53 MPa, and the duration between HIFU insonation onset and the resulting PVCs' ECG-q wave had a population median of 7.62 ms, much shorter than the applied insonation duration.

Statement of Contribution/Methods

A mathematical model is presented, for HIFU induced intermembrane cavitation and ion current dynamics in a genie pig LV cardiomyocyte.

Results/Discussion

The figure below summarizes simulation results of a sequence of 3 cardiac cycles. The blue trace in panel A shows 3 cardiac action potentials (AP), the 1st and 3rd APs were electrically paced by the stimulation presented in the brown trace, the AP at 300ms is a simulated HIFU paced PVC. The HIFU paced PVC was induced by the simulated 2.5ms insonation pattern presented in panel B. Our intra membrane cavitation model was applied for simulating the resulting membrane displacement (C), and temporal change in membrane capacitance (D). Panels (E-G) show the intracellular ion concentrations (blue) and ionic currents (brown) of Ca^{+2}, Na^+, and K^+ respectively. Panels (H-J) zoom in on the ionic concentrations and currents during the HIFU PVC induction. The Na+ currents of all the APs were almost identical (F), the Ca^{+2} traces of the HIFU paced PVC were similar to those of the proceeding AP (E), yet the HIFU induced K^+ current was significantly higher than those in the electrically paced APs (G). The HIFU PVC was induced by Na^+ current, as is noted in the gradual incline in its magnitude (I) vs. a decline in the K^+ current (J).

Numerical simulation results reconstructed our measurements, suggesting new insights in the study of HIFU pacing. These results, may also be supportive, of the suggested role that intramembrane cavitation plays in mediating ultrasonic neural modulation.
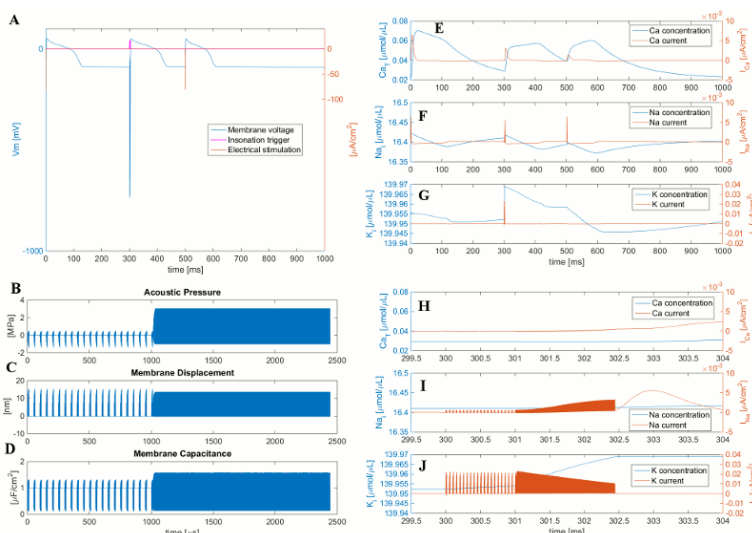
8:00 am   HIFU real-time feedback control using localized motion imaging with dynamic cross correlation window

Xiaolei Qu[1], Takashi Azuma[1], Ryusuke Sugiyama[1], Kengo Kanazawa[1], Mika Seki[1], Akira Sasaki[1], Hideki Takeuchi[1], Keisuke Fujiwara[2], Kazunori Itani[2], Satoshi Tamano[3], Shu Takagi[1], Ichiro Sakuma[1], Yoichiro Matsumoto[1]; *[1]The University of Tokyo, Japan, [2]Hitachi Aloka Medical, Ltd., Japan, [3]Tohoku University, Japan*

Background, Motivation and Objective

High intensity focused ultrasound (HIFU) is a minimally invasive treatment modality for cancerous tumors. Real-time monitoring is extremely important for it. Our group had developed a HIFU real-time feedback control system monitored by Localized Motion Imaging (LMI) which based on Harmonic Motion Imaging method [1] and improved the detection sensitivity for small coagulation area. However, previous LMI wasn't robust to noise, it always overestimated coagulation region size since noise. In this study, a HIFU real-time feedback control system using a novel noise robust LMI was developed.

Statement of Contribution/Methods

A HIFU transducer mounted with an imaging array in its center was used to induce localized motion and thermal coagulation, and obtain 1D echo signal. The obtained signal was transformed to a PC and processed by LMI Matlab code. While the detected coagulation size was larger than 10 mm, HIFU would be stopped.

 LMI imaged tissue stiffness change by detecting change of tissue motion induced by HIFU. For the detection, cross correlation with constant window size was employed for temporal neighbor echo images. The window size was a compromise between noise robustness and deformation map resolution. Larger window size is more robust and smaller has higher resolution. However, different image local regions may have totally different SNR which depends on the depth, tissue structures and so on. Therefore, LMI with local dynamic cross correlation window size was proposed in this study. For the proposed method, the window size was increased until the obtained maximum cross correlation similarity large enough.

Results/Discussion

The developed HIFU real-time feedback system could obtain 16 frames less than 0.1 s and calculate coagulation size less than 0.9 s. Thus, coagulation size was estimated in each second for real-time feedback. Fig.1 compared estimated coagulation size by previous and proposed LMI. Since overestimation, previous LMI stopped HIFU while the real coagulation size was only 9 mm but not expected 10 mm. However, proposed LMI not only estimated the real size at last, but also gave more smooth size increasing. We had already developed HIFU real-time feedback system monitored by previous LMI, and we will give experiment result by the system using proposed LMI until the presentation.

Ref.: [1]. E. E. Konofagou, K. Hynynen, Ultrasonics. Symp., 2002, p. 1895.
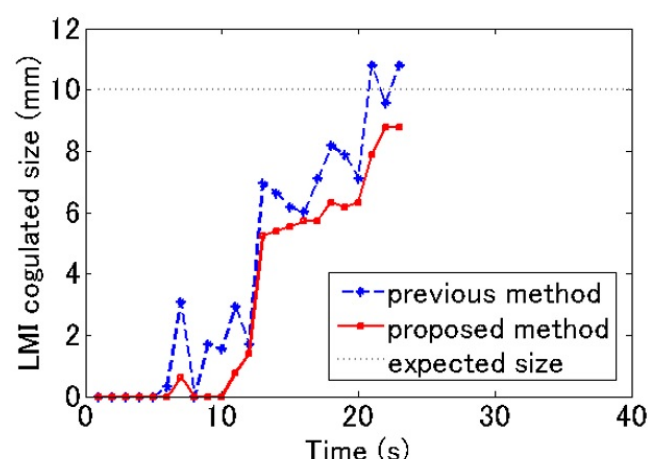
Fig. 1 LMI coagulation size estimation in HIFU real time feedback control system.

8:00 am   Pulse Inversion Technique for HIFU Treatment Monitoring in Real Time

Byungwoo Kang[1], Hyuncheol Kim[2,3], Jin Ho Chang[1,3]; *[1]Electronic Engineering, Sogang University, Korea, Republic of, [2]Chemical and Biomolecular Engineering, Sogang University, Korea, Republic of, [3]Interdiciplinary Program of Integrated Biotechnology, Sogang University, Korea, Republic of*

Background, Motivation and Objective

In ultrasound image guided HIFU, the large amplitude HIFU signals received by an ultrasound (US) imaging transducer creates an interference pattern in US images, thus hampering real-time monitoring of HIFU treatment. To overcome the problem, we have recently proposed a real-time monitoring method in which the alternate firing of the 180¡Æ phase difference HIFU pulses is conducted, just like the pulse inversion used in tissue harmonic imaging. By adding the HIFU pulses received by an imaging transducer, the fundamental and odd harmonic components of the HIFU interference can be removed, so that it is possible to secure the desired spectral bandwidth used to construct US images for HIFU treatment monitoring. One drawback of the method is degradation of spatial resolution of US monitoring images as HIFU pulse length becomes short. In this paper, we propose an alternative real-time HIFU monitoring method using pulse inversion.

Statement of Contribution/Methods

In the proposed method, instead of alternate firing of HIFU pulses, US monitoring signals are fired in accordance with the general pulse-inversion sequence and the received signals are subtracted from each other as shown in Fig. 1(a). Since the HIFU interferences are the same phase, the subtraction makes it possible to completely eliminate the interferences theoretically. Therefore, we can use the full spectral bandwidth of an US imaging transducer and thus no degradation of spatial resolution of US monitoring images occurs. To evaluate the performances of the proposed method, a bovine serum albumin (BSA) gel phantom was fabricated and a custom-built HIFU treatment system was used to generate HIFU interference signals. As a monitoring system, a commercial US scanner equipped with a curved linear array was used. The RF image data received by the scanner were stored and monitoring images was constructed using MATLAB.

Results/Discussion

Fig. 1(b) shows the conventional US monitoring image containing strong HIFU interferences. Due to the interference, the treatment area was hardly seen in the image. After applying the proposed method to the acquisition of US monitoring image data and the signal processing, it was observed that the HIFU interference pattern disappeared in the image (see Fig. 1(c)). The experimental results demonstrated that the alternative method proposed here also works well to remove HIFU interferences.
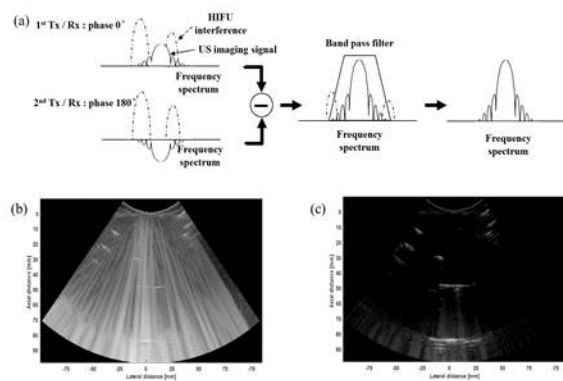
P1A6 - MSP: Medical Signal Processing

4th floor

Thursday, October 22, 2015, Posters displayed 08:00 am - 05:00 pm. Authors must be present at their poster from 9:30 - 10:30am (odd number posters) and 14:30 – 15:30pm (even number posters).

Chair: **Martin Hemmsen**
Technical University of Denmark

P1A6-1 _____

8:00 am **Sub-sampled Doppler ultrasound reconstruction using block sparse Bayesian learning**

Oana Lorintiu[1], Hervé Liebgott[1], Olivier Bernard[1], Denis Friboulet[1]; *[1]Université de Lyon, CREATIS ; CNRS UMR5220 ; Inserm U1044 ; INSA-Lyon ; Université Lyon 1, Lyon, France*

Background, Motivation and Objective

Duplex Doppler is an echographic mode that allows visualizing at the same time a B-mode image and the blood flow, for which a strategy for alternating velocity and B-mode emissions is required. In a recent study ([1], J. Richy et al., IEEE TMI, 2013) we have shown that compressed sensing-based reconstruction of Doppler signal allowed reducing the number of Doppler emissions and yielded better results than traditional interpolation. However, in this study the reduction of Doppler emission has to be limited to 60% in order to produce satisfying reconstruction (i.e. a PSNR > 20 dB). We propose here to improve over this study using the block sparse Bayesian learning (BSBL) framework to reconstruct Doppler signals.

Statement of Contribution/Methods

Compressed sensing (CS) allows the reconstruction of a signal $x \in R^n$ from a linear combination of a small number of random measurements by assuming that x has a sparse representation in some model basis, i.e. the vector v gathering the coefficients of x in this basis has only $s < m < n$ non zero coefficients. The proposed BSBL approach is applied to the v s-sparse signal. This framework allows reducing the amount of data needed for reconstruction by adaptively learning and modeling the intra-block correlation of v.

The Doppler signal is reconstructed segment by segment using the Fourier basis as the sparsifying transform.

Results/Discussion

Using the FIELD II program, we simulated the blood flow in a femoral artery. The PRF was set to 5 kHz for a mean velocity of 0.15 m/s, a femoral radius of 2 mm and a beam/flow angle of 60°.

The reconstruction quality was assessed for varying subsampling rates (20 to 80%) through the PSNR computed from the reconstruction obtained with the fully sampled Doppler data as a reference. The results provided by the proposed method were compared to the classic CS reconstruction proposed in [1].

Figure 1 compares the sonograms achieved for CS reconstructions at a 50% and 80% subsampling rate for a segment length of 256 and an overlap of 128 samples.

The results show that with this method the subsampling rate can be increased up to 80% while producing satisfying reconstruction quality, thereby considerably improving the results obtained with classic CS reconstruction in [1].

Moreover, we observed that the shape of the spectrogram is well preserved at high subsampling rates whereas it is lost in the classic CS reconstruction scheme.
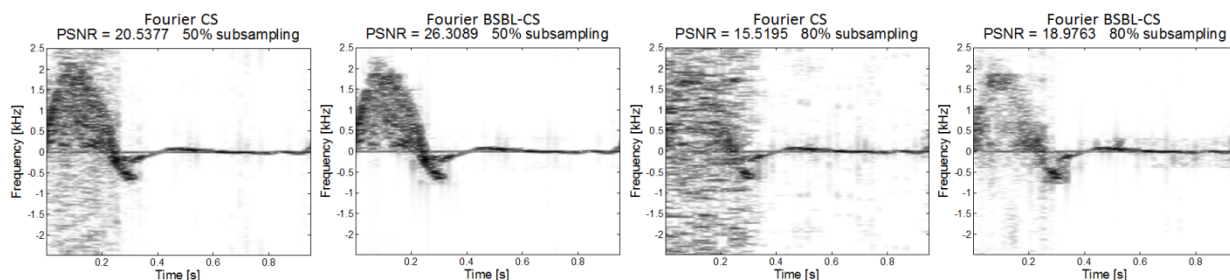
Figure 1: Sonograms of Fourier based classic CS and BSBL-CS reconstructions for 50% and 80% subsampling.

P1A6-2 _____

8:00 am **B-field energy dependent phase lag dispersion in Magnetomotive ultrasound imaging**

Roger Andersson[1], Magnus Cinthio[1], Maria Evertsson[1], Hanna Toftevall[2], Anders Wahlström[3], Sarah Fredriksson[4], Göran Nybom[5], Tomas Jansson[6,7]; *[1]Biomedical Engineering, Lund University, Lund, Sweden, [2]Geccodots AB, Lund, Sweden, [3]Lundinova AB, Lund, Sweden, [4]Genovis AB, Lund, Sweden, [5]JOIN Business & Technology AB, Lund, Sweden, [6]Clinical Sciences Lund, Biomedical Engineering, Lund University, Sweden, [7]Medical Services, Skåne University Hospital, Lund, Sweden*

Background, Motivation and Objective

Magnetomotive ultrasound (MMUS) imaging is a method that enables the use of superparamagnetic iron oxide nanoparticles (SPIO NP) as an ultrasound contrast agent. In MMUS the contrast is achieved by virtue of a time-varying external magnetic field whereby embedded NPs are set in motion.

We have noted a phase lag between the excitation signal and the detected NP magnetomotion, as well as a wider distribution of these phases the smaller the magnetic field. Our objective is to study the effects of phase distribution depending on the magnitude of the applied magnetic field.

Statement of Contribution/Methods

Experimental phantom was made from 5% by weight ballistic gel. The ballistic gel solution was poured into a phantom mold, and a cylinder creating hollow where a ballistic insert of matching diameter, was placed when the first batch had cross-linked. Phantoms with different SPIO NP concentrations of the cylinder were prepared, (0.1, 0.2, 0.3 mg/ml).

The MMUS imaging system utilize a Visualsonics Vevo 2100 for detection, a solenoid (in-house construction) and a function generator, together with a power supply to control the applied magnetic field, by means of a square-wave over the solenoid.

Signal processing was performed on recorded signal to quantify response related to the magnetic field, using our previously published phase and frequency discriminative algorithm. The reference signal from the function generator was fed to the ultrasound system via the ECG-input.

For each spatial position in the image a phase estimate was deduced in relation to the magnetic field by use of quadrature detection over the recorded time sequence.

Results/Discussion

The interval for the deduced MMUS phase estimate ranged ±π and was color coded (Panel A). A histogram of these phase estimates over the entire image area is seen in Panel B. The peak at 1 radian corresponds to magnetomotion. The location of this peak seen to vary on phantom design or some other hitherto unknown parameter. Increase of B-field energy narrows the NP response to a smaller phase range (Panel C). Lower NP concentration and/or reduced magnetic field yields less significant pronounced phase peak.

We hypothesize that the width of the phase shift is a characterization of higher concentration and higher magnetic force and a measure of how well the nanoparticles are synchronized.

Panel A

Panel B

Panel C
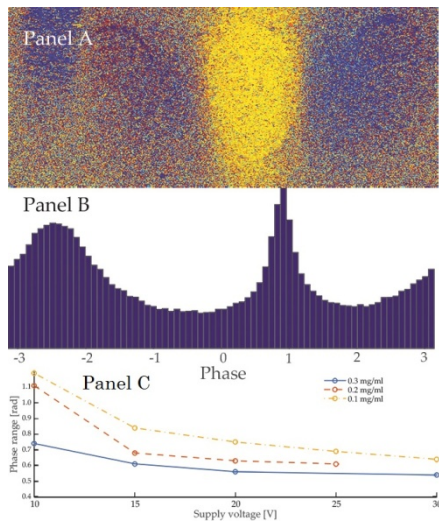
P1A6-3

8:00 am   **Discover layered structure in ultrasound images with a joint sparse representation model**

Junbo Duan[1], Hui Zhong[1], Bowen Jing[1], Siyuan Zhang[1], Mingxi Wan[1]; *[1]The Key Laboratory of Biomedical Information Engineering of Ministry of Education, Department of Biomedical Engineering,School of Life Science and Technology,Xi`an Jiaotong University, Xi'an, Shaanxi, China, People's Republic of*

Background, Motivation and Objective

The axial resolution of ultrasound device is related to the duration of impulse generated by transducer. Deconvolution can eliminate the limit-band effect of transducer, and therefore improve the resolution significantly. However, traditional methods carry out the deconvolution scan line by scan line independently, and the information embedded within neighbor scan lines are unused, especially for those materials with layered structure.

Statement of Contribution/Methods

The proposed model combines the deconvolution along the axial direction with a sparse-favoring constraint along the lateral direction. Along the axial direction, RF data are modeled as the convolution between scatters with the impulse waveform, and therefore could be formulated as the multiplication between a Toeplitz matrix generated from the impulse waveform, and a column vector representing the axial distribution of scatters. A l-1 norm regularized least square problem can recover the sparse representation of scatters robustly. To incorporate the information embedded within neighbor scan lines, along the lateral direction we introduce an extra l-1 norm regularization term into the model, yielding a joint sparse representation model. This extra term constrains two scatter vectors of neighbor scan lines to have nonzero entries with approximate axial coordinates, and therefore the concurrence of echo along the lateral direction can be captured, which is a characteristic of layered structure. As a result, by accumulating this lateral information, we can discover layered structure much easier.

Results/Discussion

The proposed method was tested on both simulated and real data. Since the two regularization parameters (Lagrangian multipliers corresponding to two l-1 norm regularization terms) control the trade-off between data fitting fidelity and sparsity, and therefore have impact on the performance of proposed method, in the simulation we first tuned these two parameters by Monte-Carlo method, and found the best setting that achieves the least mean square error between the estimate and the ground truth. Then the best setting was used to process real data, which is the SonixTouch RF data of muscle tissue sampled at 40 MHz with impulse central frequency 5.4 MHz. Compared with B-mode imaging, results show that the proposed method can discover layered structure with high axial resolution.
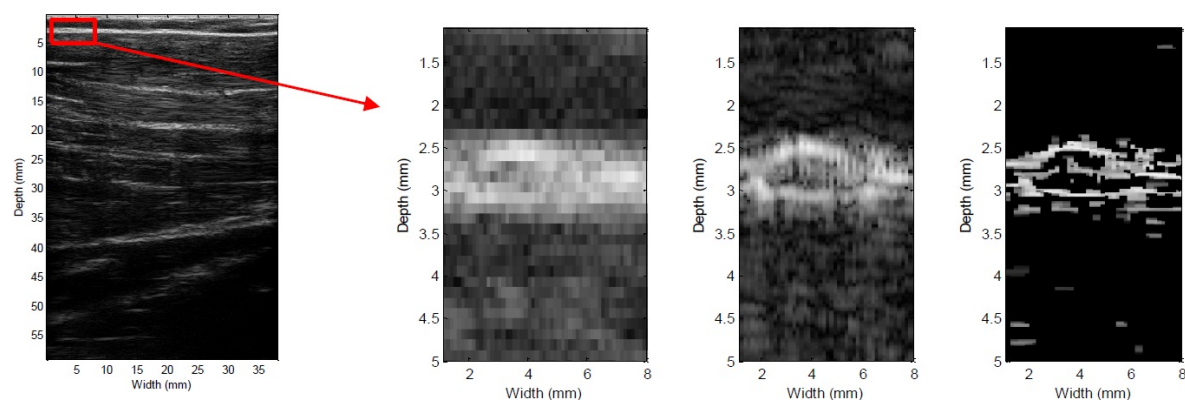
(a) muscle tissue, (b) (c) and (d) show the zoom in of the red box

(b) b8 of SonixTouch

(c) b-mode image of RF data

(d) proposed method

8:00 am   A Sub-Nyquist Sampling Analog Front-End with Mixer-Based Subarray Beamforming for B-Mode Ultrasound Imaging

Jonathon Spaulding[1], Boris Murmann[1]; *[1]Stanford University, Stanford, California, USA*

Background, Motivation and Objective

Traditional ultrasound imagers suffer from a large data rate between their analog to digital converter (ADC) front-end and digital beamforming backend. This high aggregate data rate (~30 Gb/s) is holding back the design of imagers with small form factors and high transducer count (for 3D imaging). This work implements an analog front-end (AFE) which uses information known *a priori* to reduce the data rate by more than a factor of 30.

Statement of Contribution/Methods

Our 32-channel AFE samples received reflections at their innovation rate, which is many times lower than the physical signal bandwidth would suggest. This is accomplished by mixing the signal to baseband and low-pass filtering it to acquire only a small fraction of its bandwidth. Narrowband acquisition enables a mixer-based dynamic subarray beamforming topology (time delays are well-approximated by phase shifts for small bandwidths). This reduces the ADC count, leading to further reductions in the data rate. Offline, full-rate signals are recovered from these beamformed low-rate samples using compressed sensing algorithms.

Results/Discussion

The first figure shows the system architecture for our sub-Nyquist sampling AFE. For the final demonstration, the pre-recorded signal source will be replaced with a commercial ultrasound machine. The second figure shows A-scan data taken with this system. Pre-recorded data from a phantom was input to the AFE hardware, sampled at a low rate, reconstructed, and compared against the input for accuracy. The input signal (blue) is comprised of 2250 real samples at a rate of 15 MS/s, our reconstruction (red) was created from 299 complex samples taken at a rate of 2 MS/s. Using a subarray size of 8 elements, we reduce the data rate by a factor of 30.
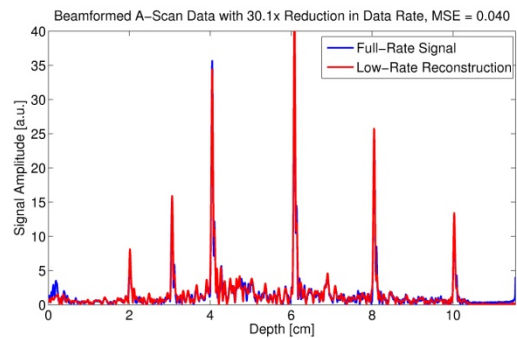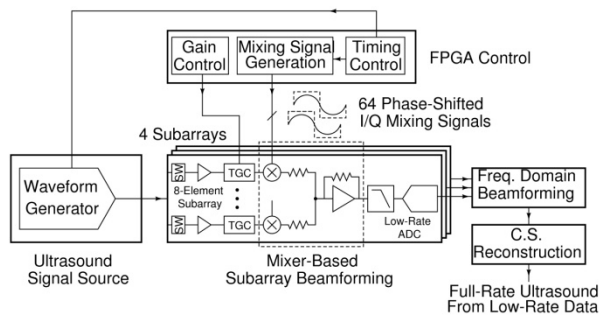
8:00 am   Combined use of edge-detection and tissue Doppler for robust left ventricle segmentation

Sigurd Storve[1], Fredrik Orderud[2], Hans Torp[1]; *[1]Department of Circulation and Medical Imaging, Norwegian University of Science and Technology, Norway, [2]GE Vingmed Ultrasound, Norway*

Background, Motivation and Objective

In quantitative echocardiography, a robust and accurate automatic segmentation of the left ventricle (LV) is important. Poor image quality and the rapid motion of the mitral valve plane make this task difficult. Automatic segmentation algorithms typically perform edge-detections on the B-mode images in order to estimate the boundary contour. By using tissue Doppler imaging (TDI), velocities in the myocardium can also be acquired. We have investigated if the combined use of edge-detection and displacements computed from tissue Doppler velocities improves the segmentation robustness.

Statement of Contribution/Methods

We used the Real-time Contour Tracking Library (RCTL, GE Vingmed Ultrasound), which is a Kalman filter-based automatic segmentation tool. Tissue Doppler velocities from two points in the mitral valve plane were integrated between successive B-mode frames and the resulting displacements were used together with displacements from the edge detectors to update a 2D LV spline model. The accuracy with and without the use of TDI was assessed by computing the Modified Hausdorff Distance (MHD) between manual reference segmentations and automatic segmentations for all B-mode frames in 11 recordings, each containing one cycle. In addition, the tracking accuracy in the mitral valve plane region was quantified for each recording by computing the maximum distance, over all frames, between the midpoint of the lower part of the estimated contour and the reference segmentation. The recordings were looped and Doppler displacements were enabled after one cycle of warming up by using only edge-detections. The two TDI sampling points were placed in the myocardium, 5mm from the model.

Results/Discussion

The mean ± std. MHD were 3.5 ± 1.4 mm (without TDI) and 3.4 ± 1.1 mm (with TDI). The improved tracking of the valve plane when using Doppler displacements is illustrated in the figure and can be explained by an increased ability to react to fast motion and also a better rejection of detected edges on the mitral valve, which sometimes can pull the base of the model upwards. The bar chart shows the influence of TDI on the maximum valve plane error for all 11 recordings. Use of TDI reduced the mean from 8.0 to 6.5mm. The overall MHD was only slightly reduced by the use of TDI. We conclude that the use of TDI can make the tracking more robust. Results from a larger dataset will be ready for the conference.
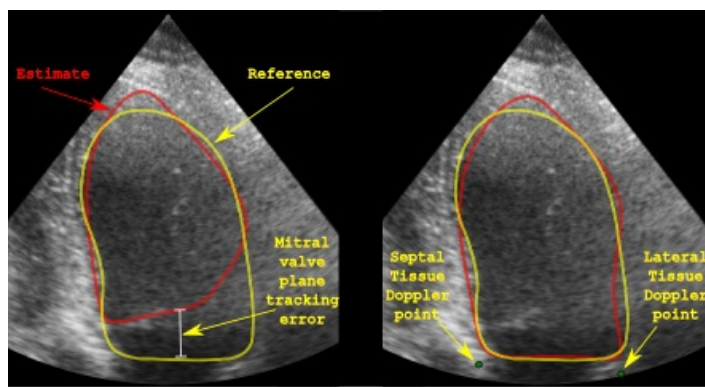
Comparison of tracking results for the same frame with (right) and without (left) the use of tissue Doppler displacements. When used, the base of the model is correctly located in the mitral valve plane.
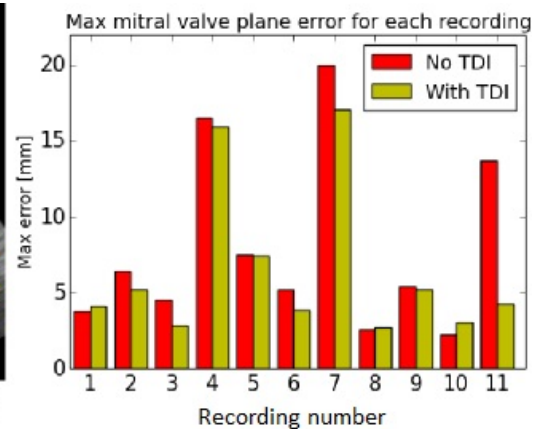
P1A6-6

8:00 am   **Streak artifact reduction for blind deconvolution of multibeam image**

Kangwon Jeon[1], Hyuntaek Lee[1], Munkyeong Hwang[1], Yongsup Park[1]; *[1]Digital Media & Communications R&D Center, Samsung Electronics, Suwon, Gyeonggi, Korea, Republic of*

Background, Motivation and Objective

In ultrasound imaging, blind deconvolution technique is used to enhance image resolution. This technique boosts high frequency signal using deconvolution kernel estimated from the image itself. However, when there is a scanline which has different characteristics from others, the estimated kernel will not be smooth along lateral direction, causing streak artifact on the result image.

Most of recent ultrasound imaging systems use multibeam techniques to provide dense scanlines. However, the beam patterns of the multibeam scanlines are slightly different from each other. This difference causes the streak artifact when used with blind deconvolution although it is a not significant in basic B-mode image. Our objective is to improve the image quality by reducing streak artifact of blind deconvolution technique in multibeam condition.

Statement of Contribution/Methods

In this paper, we propose a scanline grouping method to reduce the streak artifact of blind deconvolution technique. The scanlines with similar characteristics are grouped together, and blind deconvolution is applied to each group separately. Estimated deconvolution kernel has smooth characteristic along lateral direction and reduces the streak artifact. All of the processed scanlines need to be un-grouped as the original input image at last. The block diagram of the proposed method is shown in Fig. 1.

Results/Discussion

IQ data of *in-vivo* abdomen was acquired using Samsung Medison RS80A ultrasound system with convex probe (CA1-7A). The blind deconvolution results with and without scanline grouping method are shown in Fig. 2. The proposed method has correlation of 0.86 between neighboring scanlines, compared to 0.81 for the conventional method, indicating reduced streak artifact.

The proposed method is expected to work effectively with other adaptive signal processing techniques also, especially 2D or lateral direction filters.
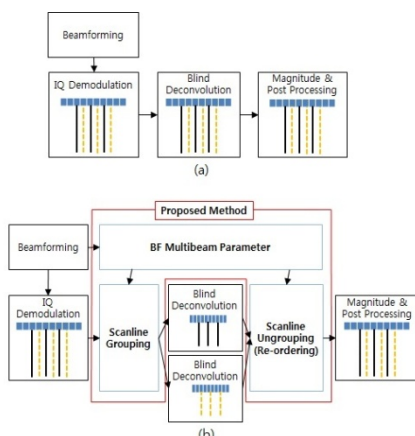
Fig 1. Block diagram (a) Conventional method, (b) Proposed method
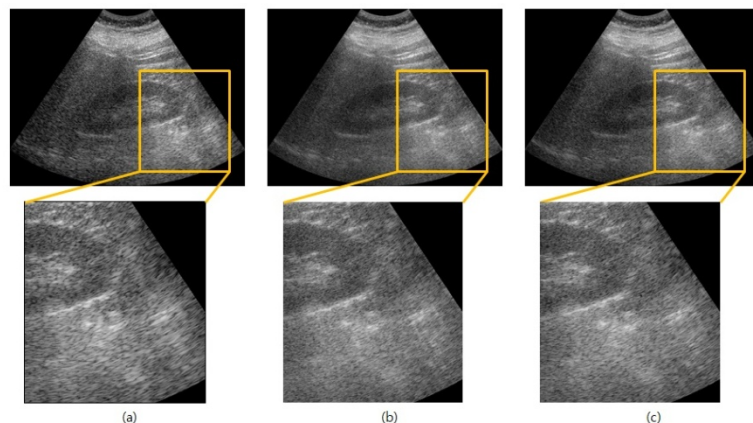
Fig 2. Image comparision (a) Original input, (b) Conventional reuslt, (c) Proposed result

---

P1A6-7

8:00 am   **Dynamic Baseband Pulse Compression for Coded Excitation Imaging**

Yeajin Kim[1], Jinbum Kang[1], Yangmo Yoo[1,2]; *[1]Electronic Engineering, Sogang University, Seoul, Korea, Republic of, [2]Interdisciplinary Program of Integrated Biotechnology, Sogang University, Korea, Democratic People's Republic of*

Background, Motivation and Objective

Coded excitation can improve the signal-to-noise ratio (SNR) in medical ultrasound imaging. To preserve axial resolution, effective pulse compression (PC) techniques are important. PC can be achieved with radio-frequency and complex baseband data (i.e., PC_{RF} and PC_{CBB}, respectively). While PC_{CBB} can reduce the computational complexity compared to PC_{RF}, it suffers from the degraded SNR due to tissue attenuation. The dynamic quadrature demodulation (DQDM) can be applied to compensate tissue attenuation. However, the conventional $PC_{CBB-Fixed}$ deteriorates the location of targets after PC. In this paper, a new dynamic baseband pulse compression ($PC_{CBB-Dynamic}$) method is presented which can improve SNR while preserving the location of targets.

Statement of Contribution/Methods

In the PC$_{CBB-Dynamic}$ method, DQDM is first applied to RF data for compensating depth-dependent attenuation. The coefficients for PC$_{CBB}$ are generated with the dynamically changed demodulation frequencies. The obtained PC$_{CBB-Dynamic}$ coefficients are independently applied for compressing in-phase and quadrature components of complex baseband data. To evaluate the proposed PC$_{CBB-Dynamic}$ method, RF data were captured with a custom-built ultrasound research platform, which can transmit arbitrary waveforms, by exciting a 16-cycle Gaussian-windowed chirp signal centered 2.3-MHz with the fractional bandwidth of 60%. The performance of the PC$_{CBB-Dynamic}$ method was compared with the PC$_{RF}$ and PC$_{CBB-Fixed}$ methods.

Results/Discussion

Figs. 1(a)-1(c) shows the reconstructed B-modes from three PC methods. As shown in Fig. 1(a)-1(c), three PC methods show the comparable image quality. Unlike PC$_{RF}$, the PC$_{CBB-Fixed}$ method changes the location of point targets as shown in Figs. 1(d) and 1(e) since it doesn′t account for the change in demodulation frequencies in DQDM. The mean change in the location of point targets with PC$_{CBB-Fixed}$ is 0.931mm+0.630 and it becomes severe as the depth increases (up to 1.952 mm for the target at 19 cm). On the other hand, the proposed PC$_{CBB-Fixed}$ method preserves the target locations unlike PC$_{CBB-Fixed}$. In addition, it shows the comparable SNR and axial resolution with the PC$_{RF}$. These results indicate that the proposed PC$_{CBB-Fixed}$ method can be used for effective pulse compression in coded excitation while reducing computational complexity and target location errors.
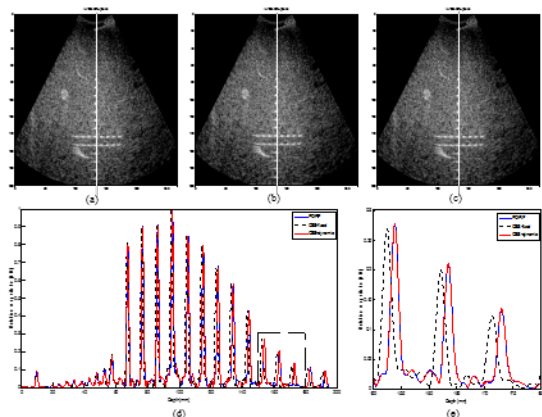
Figure 1. (a)-(c) B-mode image in phantom study obtained by PC-RF, CBB-fixed, and CBB-dynamic, respectively. (d) Results of envelope signals along A-line using each methods and (e) the beam profile of points in 15-18cm (dashed line in (d)).

P1A6-8

8:00 am   A Multiparametric Approach Integrating Vessel Diameter, Wall Shear Rate and Physiologic Signals for Optimized Flow Mediated Dilation Studies

Alessandro Ramalli[1], Michal Byra[2], Alessandro Dallai[1], Carlo Palombo[3], Kunihiko Aizawa[4], Piero Tortoli[1]; *[1]Information Engineering Department, University of Florence, Firenze, Italy, [2]Department of Ultrasound, Institute of Fundamental Technological Research PAS, Warsaw, Poland, [3]Department of Surgical, Medical, Molecular, and Critical Area Pathology, University of Pisa, Pisa, Italy, [4]Diabetes and Vascular Medicine Research Centre, NIHR Exeter Clinical Research Facility, University of Exeter Medical School, Exeter, United Kingdom*

Background, Motivation and Objective

Flow Mediated Dilation (FMD) is widely used to assess the endothelial function by ultrasound. Ideally, both the brachial artery wall shear stress (stimulus) and diameter change (effect) shall be estimated and monitored for 10 minutes, while blood flow is restricted by a cuff and then suddenly released. An inherent difficulty of the method is maintaining the linear array probe aligned with the artery over such a long time. The problem is here faced by an integrated hardware/software approach that displays in real-time both spatial velocity profiles and diameter changes, and acquires raw data all over the exam.

Statement of Contribution/Methods

The software of the ULA-OP research scanner (Fig. 1 top) was modified to include a processing module that estimates and shows in real-time the diameter of the selected blood vessel (Fig. 1d). The module analyses up to 100 B-Mode frames/s and, for each frame, locates the walls of the vessel by means of a robust edge detection algorithm [DOI: 10.1109/TMI.2006.891477].

The hardware was equipped with a custom acquisition board that embeds a 16 GB memory card to acquire the raw imaging and Doppler echo-data as well as physiologic auxiliary signals (e.g. ECG, arterial pressure, breath) during the exam. A Matlab® based software platform (Fig. 1 bottom) was developed to describe, by multiple parameters, the time-course and amplitude of changes in the vessel diameter and wall shear rate.

Results/Discussion

During the exam, the real-time display shows the B-mode image with markers highlighting the vessel walls, the diameter trend, the multigate spectral Doppler data as well as aux signals. Possible probe/arm movements produce a corresponding change in the diameter graph and in the spectral profiles shape, so that the correct probe position can be quickly restored. The integrated FMD system is currently used in a multicenter study addressed to investigate the relations between diameter and wall shear rate changes in subjects with or without cardiovascular risk factors or clinical events (FP7-IMI Project "SUMMIT"). Data from the first 85 volunteers were acquired, and for each of them up to 25 parameters were extracted, quantifying absolute and relative changes, timing and rate of changes. Work is in progress to determine characteristic patterns and reference values in young healthy volunteers as prerequisite to clinical studies in patients.
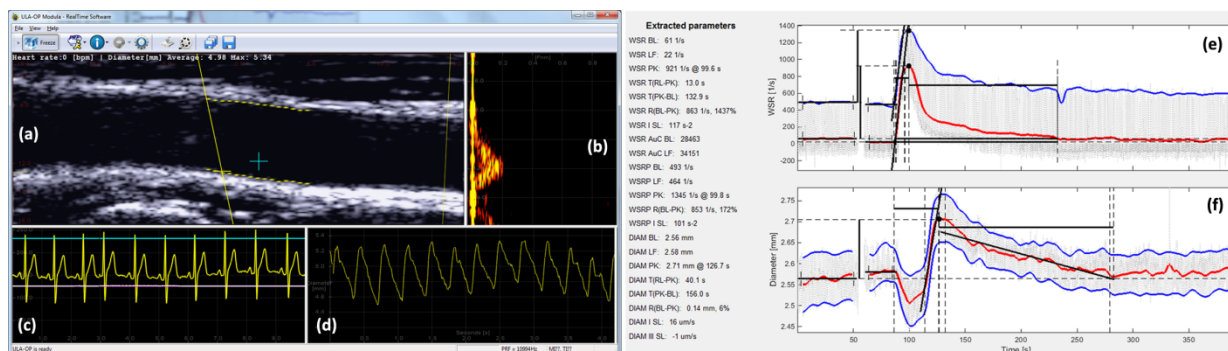
Fig. 1 - ULA-OP real-time application window during FMD acquisition (left): B-mode image (a), Multigate Spectral Doppler Profile (b), auxiliary ECG signal (c), and diameter trend (d). Matlab based software platform for multiple parameter extraction (right): wall shear rate (e) and diameter (f) analysis over 7 minutes.

P1A6-9

8:00 am   **A Novel Side Lobe Estimation Method in Medical Ultrasound Imaging Systems**

Mok Kun Jeong[1], Sung Jae Kwon[1]; *[1]Electric, Electronic and communication engineering, Daejin University, Pocheon, Kyeonggi, Korea, Republic of*

Background, Motivation and Objective

Ultrasound signals impinging on an array transducer manifest themselves as sinusoids whose spatial frequency varies as a function of the incident angle. The received channel data from the main lobe direction have a spatial frequency of zero when considered across all the channels because the individual channel data have the same phase in the temporal domain, while those from the side lobe directions have a spatial frequency that is not zero and varies with the ultrasound beam incident direction. Thus, the received channel data can be modeled as a sum of sinusoidal waveforms that have a specific frequency depending on the incident angle.

Statement of Contribution/Methods

In modeling the received channel data as a sinusoid, we define the number of cycles across an aperture as cycles per aperture (CPA). In the ultrasound field response, signals coming from the side lobe directions have a frequency of an integer plus a half, while those coming from the null directions have an integral frequency. We note that a sinusoid of an integral frequency can be canceled out by adding the individual channel data in the focusing process, but that a sinusoid that has a CPA of an integer plus a half cannot be canceled by adding, leaving only a half-cycle sinusoid, which becomes a clutter that has adverse effects on ultrasound image quality. To remove the channel data whose CPA is an integer plus a half, we estimated the waveform of the channel data. In order to model the sinusoid that has a CPA of an integer plus a half as one with an integral CPA, we have appended zeros to the channel data to extend its length. By taking the Fourier transform of the extended channel data, we estimated the side lobe amplitude and determined the waveform of the side lobe in the channel data.

Results/Discussion

We determined the side lobe amplitude from the PSF of a wire target at a depth of 35 mm using our new side lobe estimation method. We estimated the 1st to 20th side lobes depending on the incident angles. By subtracting the estimated side lobes from the received channel data, we were able to achieve a reduction in side lobe levels by 14 dB. The figure from top to bottom compares both the PSF of the wire target and the 1st to 5th side lobe levels, all log compressed over a 50 dB scale. Higher-order side lobes appear at different locations according to the incident angles.
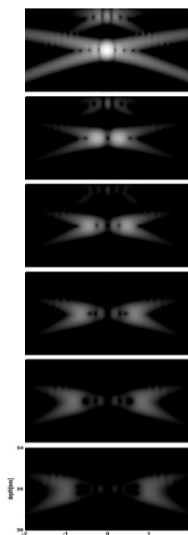
P1A6-10

8:00 am   **Estimation of Arteriovenous Fistula Stenosis by Quantitative Doppler Ultrasound Using Adaptive Gray Relation Method**

Jian-Xing Wu[1], Tainsong Chen[2]; *[1]National Synchrotron Radiation Research Center, Hsinchu, Taiwan, [2]Department of Biomedical Engineering, National Cheng Kung University, Tainan, Taiwan*

Background, Motivation and Objective

Arteriovenous fistula (AVF) is a vascular access and very import in hemodialysis that is a treatment for patients suffering from end-stage renal disease. Stenosis is considered the major cause of dysfunction of AVF. Despite the relatively low thrombosis rates of AVF, surveillance programs are necessary for detection of stenosis. The objective of this study was to develop an estimation system using adaptive gray relation method for AVF stenosis on hemodialysis patients by quantitative Doppler ultrasound.

Statement of Contribution/Methods

We extracted the quantitative blood flow parameters from Doppler Ultrasound signal included supracritical Reynolds (Ratio) and the resistive (Res) indexes in three sites (arterial, venous anastomosis and middle of loop) of fistula on arm (Fig. A). The quantitative parameters are the input for analysis and the processing flowchart is shown in Fig. B. The adaptive gray relation method, that could possess with a flexible pattern mechanism and does not require inference rules, is chosen as the kernel for classification. In order to verify the accuracy, we recruited 50 patients (18 females and 32 males, stenosis range 10% to 90%) for testing and confirming by the degrees of stenosis (DOS) that measured by B-Mode ultrasound or angiography images. Those experiments followed IRB approval procedure.

Results/Discussion

DOS is 1 means total occlusion, over 0.5 usually means need to be surgical treatment and between 0.3 to 0.5 means it may have effect upon the efficiency during hemodialysis. Therefore, we followed clinical comment to design three different groups for classification that included DOS < 0.3, $0.3 \leq DOS \leq 0.5$ and DOS > 0.5. The testing results show that the system output has high correlation (R square is 0.91) with DOS. Also, three different groups has statistical difference (p<0.01) with each other (Fig. C). The percentage of correct selection in our data is about 83%. These results indicated that the proposed system using adaptive gray relation method could discriminate the different DOS groups efficiently and correctly. Furthermore, the proposed method is robust and low cost for implementation, it has high potential to be applied in a portable system for routine examinations or home care applications.
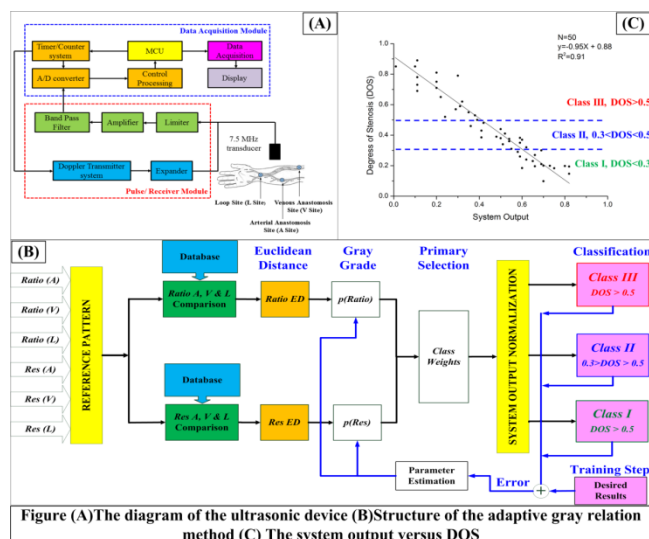
Figure (A)The diagram of the ultrasonic device (B)Structure of the adaptive gray relation method (C) The system output versus DOS

P1A7 - MBF: Performance Investigations and Phantom Design

4th floor

Thursday, October 22, 2015, Posters displayed 08:00 am - 05:00 pm. Authors must be present at their poster from 9:30 - 10:30am (odd number posters) and 14:30 – 15:30pm (even number posters).

Chair: **Lasse Løvstakken**
NTNU

P1A7-1 _____

8:00 am ***In vivo* Investigation for Accuracy Estimation of Vector Flow Mapping**

Tomohiko Tanaka[1], Takashi Okada[2], Tomohide Nishiyama[2], Yoshinori Seki[2], Ken-ichi Kawabata[1]; *[1]Hitachi, Ltd., Japan, [2]Hitachi Aloka Medical, Ltd., Japan*

Background, Motivation and Objective

Vector flow mapping (VFM) is a promising tool for capturing 2D flow vectors in the left ventricle (LV) and opening up new prospectives. By using color flow mapping (CFM) and a fluid physical law, VFM estimates azimuth velocities under assumed 2D planar flow. Besides typical CFM artifacts, a major factor causing VFM uncertainty is flow through the image plane. Since through-plane flows (TPFs) differ according to each measurement, VFM accuracy also depends on each measurement, implying that VFM-based diagnosis might be unreliable. Given that the accuracy of each VFM measurement is known, the quality of VFM-based diagnosis can be improved by rejecting or retaking unreliable VFM results.

In a previous report [1], *a posteriori* VFM accuracy estimation (VAE) was proposed, and *in vitro* validation using an LV phantom with particle image velocimetry (PIV) confirmed that the estimated VFM uncertainty by VAE agrees with that measured by PIV [1]. In the present study, VAE was applied to a human subject to investigate the validity of VAE *in vivo*.

 [1] Tanaka et al., IEEE IUS 2013

Statement of Contribution/Methods

An ultrasound scanner with a sector probe was used to capture flows in a healthy human heart. While VFM calculates azimuth velocity by using a weighted averaging of two different calculations, namely, right and left integrations, VAE calculates VFM uncertainty by using two-calculation discrepancies (TCDs). VFM uncertainty was estimated by dividing the standard deviation of the TCDs in an image by the square root of six. Uncertainty was normalized by a CFM range of 1.2 m/s.

Results/Discussion

Ultrasound images are shown in Figs. 1 (a)-(c), and their TCD maps are shown in Figs. 1 (d)-(f). The discrepancy denotes the magnitude of VFM uncertainties along an integration path, and it changes according to paths, or depth. For a wall motion artifact (Fig. 1(a)), the uncertainty becomes larger, i.e., 8%, since its TCD map indicates a high value on the path where the artifact is. For a short-axial view (Figs. 1(b)), strong TPFs existing in the short-axial view also cause large uncertainty of 9%, and the TCD map indicates high values in the entire domain. For a long-axial view in the filling phase (Fig. 1(c)), VAE indicates a small uncertainty (i.e., less than 5%) because the flow is possibly along the imaged plane. As shown above, VAE reasonably reflects VFM uncertainties for unreliable VFM data sets.
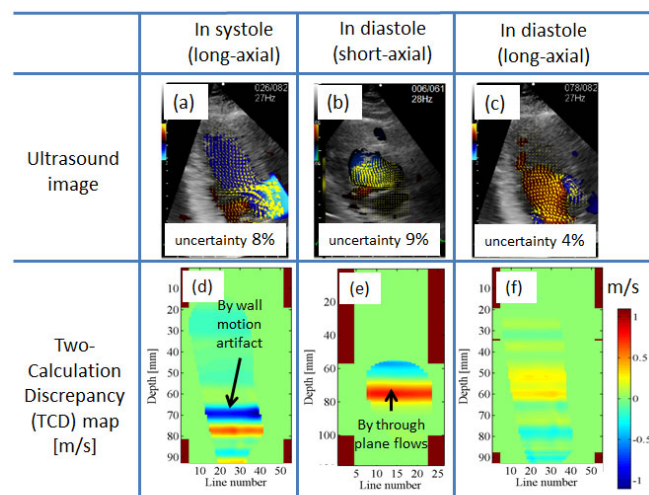
Figure 1 VAE results for *in vivo* investigation

P1A7-2 _____

8:00 am **Validation of a novel vector method for blood peak detection in an anthropomorphic phantom**

Riccardo Matera[1], **Stefano Ricci**[1], Alfred C.H. Yu[2], Billy Y.S. Yiu[2], Piero Tortoli[1]; *[1]Information Engineering Dept., Università di Firenze, Florence, Italy, [2]Medical Engineering Program, University of Hong Kong, Pokfulam, Hong Kong*

Background, Motivation and Objective

The peak blood velocity is a parameter of high medical interest used, for example, in the determination of carotid stenosis grade. The standard approach, which typically exploits the maximum frequency detectable in the Doppler spectrum, is prone to two main sources of errors: the ambiguity of the Doppler angle and the spectral broadening. Recently a novel method (doi: 10.1109/TUFFC.2013.2798) was introduced that, based on a mathematical model, is unaffected by the spectral broadening problem and automatically corrects for the angle through a vector Doppler approach. The method directly measures the max velocity component in a large sample volume that includes all the vessel section. The method offered good results when verified in-vitro in straight tubes, but tests in a more realistic configuration are necessary for an accurate validation.

.

Statement of Contribution/Methods

A carotid bifurcation phantom with a 50% eccentric stenosis narrowing at the entrance to the internal artery is used. The phantom is fabricated using a lost-core casting approach. Its vessel lumen was of a co-planar bifurcation geometry (6 mm, 3 mm, and 4 mm diameter respectively for common (CCA), internal (ICA), and external carotid artery branches). A polyvinyl alcohol cryogel is used as the phantom's tissue mimic (120 kPa elastic modulus; 1518 m/s sound speed; 0.24 dB/(cm MHz) attenuation). A programmable pump moves a blood mimicking fluid through the phantom. A linear array probe is positioned in the plane of the bifurcation and connected to the ULAOP research scanner. ULAOP is programmed for generating the TX/RX sequences for the method under test (MUT), and for other 2 methods used as reference: Multigate Vector Doppler (MGVD, doi: 10.1109/TUFFC.2014.6722616) and multigate Spectral Doppler (MSD, doi:10.1109/TUFFC.2009.1303). In MSD the Doppler angle is evaluated in the B-mode image.

.

Results/Discussion

Measurements in the CCA and ICA, 10 mm before the bifurcation and on the stenosis, respectively (see figure, top), were performed with different pump settings. The figure (bottom) reports an example of measurement in the CCA, where the MUT shows a good agreement with both the references (+2.2% and +5.2% mean error vs. MGVD and MSD, respectively). In the ICA a higher overestimation was measured (+15% and +20%, respectively). The coefficient of variability was below 1.5% in all of the tests.

.
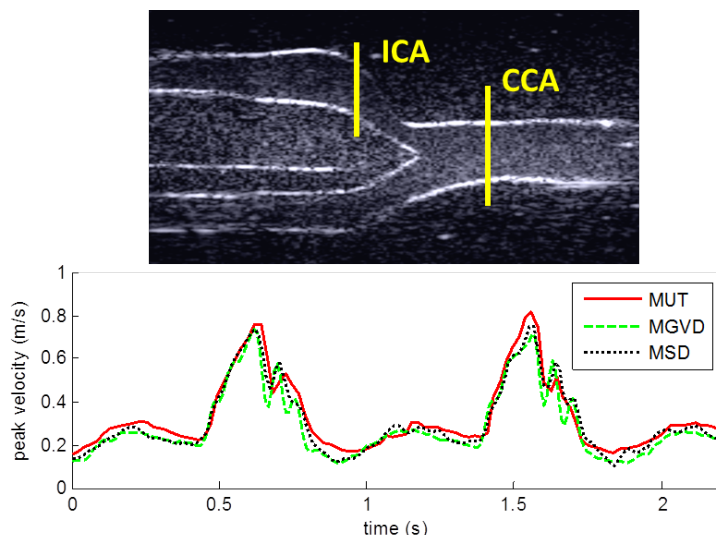
P1A7-3

8:00 am   Novel Design of Patient-Specific Cerebral Aneurysm Phantoms for Intraoperative Ultrasound Investigations

C. K. Ho[1], Adrian J. Y. Chee[1], Billy Y. S. Yiu[1], Anderson C. O. Tsang[2], K. W. Chow[3], Alfred C. H. Yu[1]; *[1]Medical Engineering Program, University of Hong Kong, Pokfulam, Hong Kong, [2]Department of Surgery, University of Hong Kong, Pokfulam, Hong Kong, [3]Department of Mechanical Engineering, University of Hong Kong, Pokfulam, Hong Kong*

Background, Motivation and Objective

During neurosurgery, intraoperative imaging can serve to provide feedback on cerebrovascular hemodynamics and help monitor procedures such as the placement of flow-diverting stents near an aneurysm. Ultrasound can potentially play a major role here given its real-time scanning capability. However, its proper use is known to require extensive user training, and to do so it would be beneficial to create phantoms that can be leveraged as emulation tools for operator skills development. As such, we have sought to devise a novel framework for fabricating ultrasound-compatible cerebral aneurysm phantoms based on patient-specific vascular information.

Statement of Contribution/Methods

The preoperative cerebral vasculature of a patient was first scanned using CT. The data was used to construct a patient-specific aneurysm geometry using MIMICS, and inlet-outlet flow connectors were added using SolidWorks. The drafted geometry was then prototyped using a fused deposition modelling system with polylactic acid (PLA) as the construction material. Subsequently, the PLA-built aneurysm model was mounted onto a case, and a 15% polyvinyl alcohol (PVA) solution was poured into the case to serve as an elastic tissue mimic (the PVA would turn into cryogel after one 24-hr freeze-thaw cycle). Afterward, the PLA material that corresponds to the aneurysm lumen was dissolved using chloroform, thereby producing a wall-less aneurysm phantom. To put the phantom into operation, its inlet and outlets were connected to a pulsatile pump (carotid pulse; 1.2 Hz rate) that fed blood mimicking fluid into the phantom. B-mode images and Doppler power maps were acquired using a SonixTouch scanner and an L14-5 linear array (5 MHz freq; 3.3 kHz PRF).

Results/Discussion

As illustrated by B-mode images from two orthogonal planes [Figs (a) & (b)], ultrasound-compatible cerebral aneurysm phantoms with geometry specific to an actual patient can be fabricated for the first time. Also, flow within this phantom can be suitably detected using power Doppler [Figs (c) & (d)]. We anticipate that, besides using this phantom as a training platform for intraoperative imaging during neurosurgery, it can also serve as a novel investigative tool to evaluate the performance of new flow imaging techniques, particularly high frame rate imaging methods and flow vector visualization innovations.
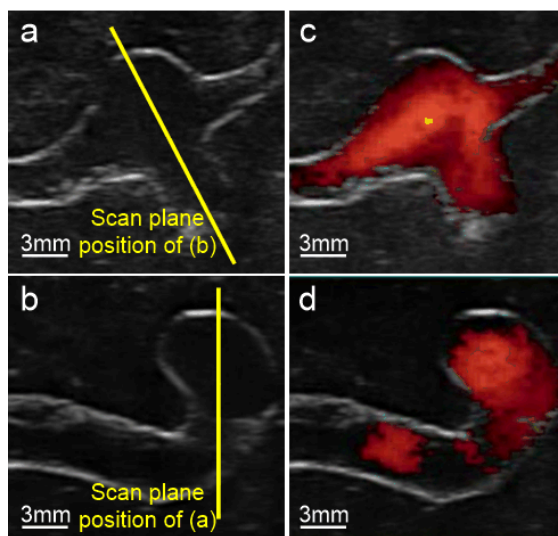
P1A7-4

8:00 am   Implementation and evaluation of slow-time Golay decoding for pre-clinical high-frequency color Doppler imaging in mice

Che-Chou Shen[1], Jyun-Gong Yu[1], Gency Jeng[2]; [1]*Electrical Engineering, National Taiwan University of Science and Technology, Taipei, Taiwan, [2]S-Sharp Corporation, Taiwan*

Background, Motivation and Objective

Golay Complementary Sequence (GCS) can compensate the high attenuation of high-frequency ultrasound by elevating signal level with low range side lobe and low implementation cost. However, due to potential motion artifact, it is conventionally regarded as not applicable to blood flow detection. In our previous study, it has been demonstrated that the Doppler spectrum of GCS has the main-lobe signal apart from the side-lobe signal by half of the pulse-repetition-frequency (PRF). Therefore, GCS decoding can be performed by low-pass filtering in slow-time domain with cutoff frequency of PRF/4 to eliminate any motion artifact from side-lobe in Doppler imaging.

Statement of Contribution/Methods

In this work, the proposed GCS Doppler has been implemented in a commercial high-frequency (> 20 MHz) ultrasound imaging system for pre-clinical examinations. The two waveforms of GCS are transmitted in an interspaced manner when the motor drives the transducer to laterally scan the kidney vessel and the abdominal aorta of ICA mice with transmit frequency ranging from 30 MHz to 40 MHz. The un-coded Doppler and the GCS Doppler are compared for color Doppler quality and signal-to-noise ratio (SNR) while all other parameters are kept unchanged.

Results/Discussion

The in-vitro results in Fig. (A) show that, when the Doppler shift is within PRF/4, the GCS not only improves the SNR but also retains comparable Doppler information to conventional un-coded counterpart. In the in-vivo 40-MHz imaging of mouse¡¦s kidney of Fig.(B), GCS Doppler increases the penetration from 13.5 mm to 14.2 mm but minor aliasing might be identified in some high-velocity vessel branches. For the abdominal aorta, GCS Doppler allows the increase the transmit frequency from 30 MHz to 35 MHz without compromising Doppler sensitivity.
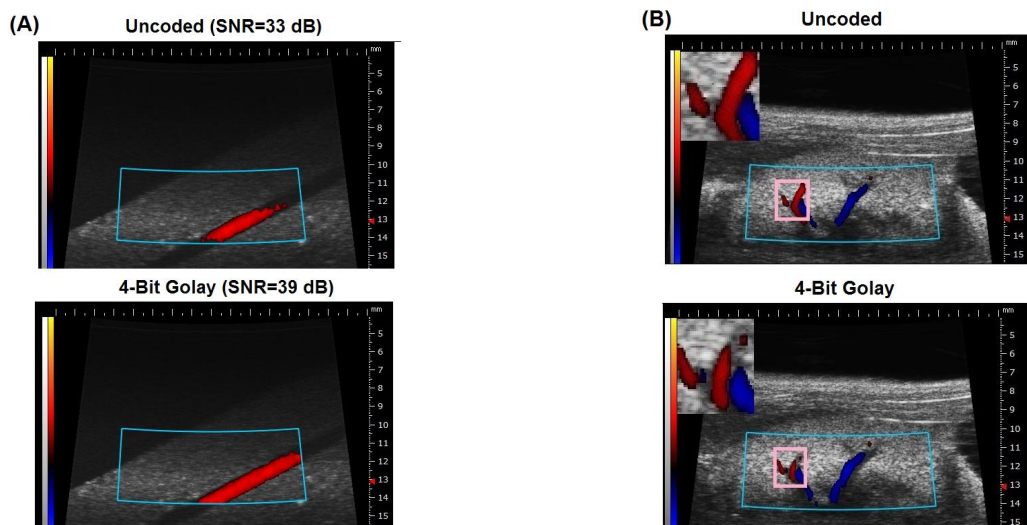
P1A7-5

8:00 am   Thin-Walled Carotid Bifurcation Phantom Systems for Vascular Strain-Flow Imaging Investigations

Adrian J. Y. Chee[1], Billy Y. S. Yiu[1], Alfred C. H, Yu[1]; [1]*Medical Engineering Program, The University of Hong Kong, Hong Kong*

Background, Motivation and Objective

Vascular phantoms are well regarded as essential experimental tools in the development of new ultrasound techniques for assessing wall mechanics and blood flow. Straight-tube models are the simplest (used in strain measurement studies), but they lack resemblance of actual arterial geometries. Bifurcation models have also been reported (in flow imaging studies); yet, current designs are either wall-less or have walls that lack ultrasound compatibility and elastic tunability, so they are ill-suited for assessing

integrative imaging methods that seek to concurrently assess biomechanics and hemodynamics. In this work, we seek to devise a multi-purpose vascular phantom system with: 1. anthropomorphic geometry; 2. tunable vessel wall elasticity; 3. stenosis features.

Statement of Contribution/Methods

Our new phantom system uses a tuning-fork co-planar vessel as the geometric model mimicking the carotid bifurcation; wall thickness was set to 1.5 mm. Its fabrication first involved the generation of negative outer mold of the vessel and inner core with 3D printing. To create a stenosis site, the core diameter at internal carotid artery (ICA) inlet was reduced, providing room to form a locally thicker inner wall. Next, the inner core was mounted within the negative outer mold, and the cavity between them was injected with PVA solution to form the vessel wall; wall stiffness was controlled the number of freeze-thaw cycles (1 to 5; elastic modulus ranged between 80-180 kPa). The inner core was removed afterward. At last, the bifurcation vessel was mounted onto a container, and gelatin was cast as tissue mimic. During operation, the phantom was connected to a flow circuit that was driven by a gear pump with carotid pulse and 72 bpm rate.

Results/Discussion

As demo, two bifurcation geometries with 80 kPa elastic modulus were fabricated: a healthy model and one with 50% stenosis at the ICA inlet. Both models exhibited 6% distension in the common carotid artery (based on M-mode plots from SonixTouch with 5 MHz Tx freq). On the other hand, at the ICA inlet, the stenosed model distended merely by 1% while the healthy model distended by 5%. Color flow images (acquired using SonixTouch) showed the appearance of flow jet in the stenosed ICA as expected (see figure). We anticipate that these phantom systems would be useful for investigations in studying fluid structure interactions at arterial branches.

a Healthy Bifurcation

b Bifurcation with 50% Stenosis
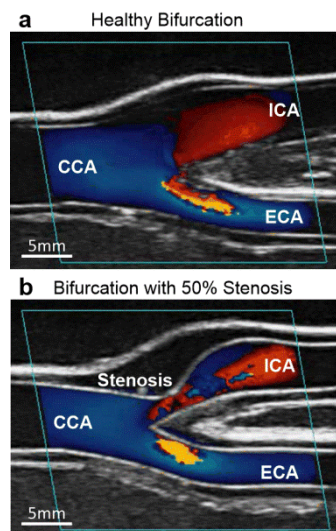
P1A7-6

8:00 am   Receiver Operating Characteristics Analysis of Eigen-Based Clutter Filters for Ultrasound Color Flow Imaging

Adrian J. Y. Chee[1], Alfred C. H. Yu[1]; [1]*Medical Engineering Program, University of Hong Kong, Pokfulam, Hong Kong*

Background, Motivation and Objective

In color flow imaging (CFI), achieving robust flow detection in the presence of tissue motion remains a long-standing challenge to be properly addressed. Key to tackling this problem is the effective suppression of slow-time clutter originating from tissue echoes that contain non-zero frequency contents whenever tissue displaces during data acquisition. For some time, eigen-based clutter filtering has been tipped as an emerging solution, and it works by adaptively suppressing tissue clutter based on principal component analysis. However, the field is distinctly short of data on how much gain in flow detection sensitivity and specificity can be achieved with the use of eigen-filters. In this work, our aim is to systematically investigate the flow detection impact of eigen-filters through the undertaking of receiver operating characteristic (ROC) analyses, so as to substantiate the merit of this CFI clutter suppression method.

Statement of Contribution/Methods

A novel vascular phantom testbed has been devised to serve as an investigate tool for CFI eigen-filtering in cases with tissue motion due to both intrinsic (arterial pulsation) and extrinsic (human induced) factors. It was equipped with three features: (i) a compliant vessel wall with elasticity resembling human arteries (PVA material; 1.5 mm wall thickness; 6 mm inner diameter; 80 kPa elastic modulus), (ii) pulsatile flow behavior that resembles cardiac circulation (72 bpm rate; 6.5 ml/s systolic flow rate), and (iii) tissue vibrations that mimic extrinsic motion such as tremor (piezoelectric vibrator; 10 Hz frequency). During the experiment, an L14-5 array was positioned to image the phantom's short axis, and raw CFI-RF data was acquired from a SonixTouch system. Eigen-filtering was then performed on the CFI-RF data, and the post-filter Doppler power distribution was compiled for: 1. flow region (within vessel lumen; power supposed to remain high after filtering), and 2. tissue region (power should be low if clutter was adequately suppressed). From these power distributions, we derived, for different power thresholds (i.e. color gain), the true positive rate (% of flow pixels above threshold) and false alarm rate (% of tissue pixels above threshold). The corresponding ROC curve was plotted, and the area under ROC curve (A') was calculated as a detection metric. Results were compared against the polynomial regression filter typically used in CFI.

Results/Discussion

Throughout the pulse cycle, eigen-filters yielded post-filter power distributions that have limited overlap between tissue and flow regions. Accordingly, there exists a color gain that can minimize false positives while maximizing flow detection sensitivity. The A' of eigen-filter was found to range between 94% (systole) and 89% (diastole). In contrast, the performance of polynomial regression filter was inferior (A' merely ranged between 76% and 68%). These findings serve to attest the use of eigen-filters in CFI.

P1A7-7

8:00 am   Wall Shear Rate Method Validation Through Multi-physics Simulations

Stefano Ricci[1], Abigail Swillens[2], Alessandro Ramalli[1], Patrick Segers[2], Piero Tortoli[1]; [1]*Information Engineering Dept., Università di Firenze, Florence, Italy,* [2]*IBiTech-bioMMeda, iMinds Medical IT, Gent University, Belgium*

Background, Motivation and Objective

The Wall Shear Rate (WSR) represents the radial variation of blood velocity close to the vessel walls. The WSR is related to the tangential force that blood applies to the vessel surface, and is indicated as a potential biomarker for the early assessment of cardiovascular diseases. Unfortunately, the direct measurement of the WSR is hampered by the clutter that hides the weak Doppler signal near the wall, i.e. where the WSR should be evaluated. We recently proposed an algorithm that recovers the velocity trend

near the wall, and thus the WSR, by exploiting the simultaneous measurement of the part of velocity profile not ruined by clutter, and the wall positions. An accurate validation of the algorithm requires the comparison between the measurement and the corresponding ground-truth, which is available only when suitable simulations are used.

.

Statement of Contribution/Methods

A carotid bifurcation model based on a MRI scan of a patient is considered. The flow/tissue scatterers move according to complex fluid-structure interaction (FSI) simulations that account for both flow and wall movement. The B-mode images and the Doppler signal are generated by FIELD II based on the simulated scatterers' positions. The wall-movement produces a realistic clutter overlapped to the Doppler signal, which is partially removed by a 50Hz wall filter. The radial velocity profile is obtained by the Welch estimator applied to the Doppler spectra. The profile section corrupted by clutter is reconstructed through a 2-step interpolation, and the WSR is calculated at the wall positions dynamically detected from the B-mode frames. The calculated WSR is finally compared to the ground-truth provided by simulations.

.

Results/Discussion

The WSR is measured and checked in the common (CCA) and internal (ICA) regions of the carotid artery at about 0.8 mm before and after the bifurcation, respectively. The picture shows the measured WSR (continuous red) compared to the ground-truth (dashed blue) for both the proximal (top) and distal (bottom) wall. The diameter is reported below for reference. The error on the WSR peak value is between -0.1% to -16% with an average value of -6%. The RMS error over the whole heart cycle, relative to the peak value, is between 5% and 12% (average: 8.2%).

.
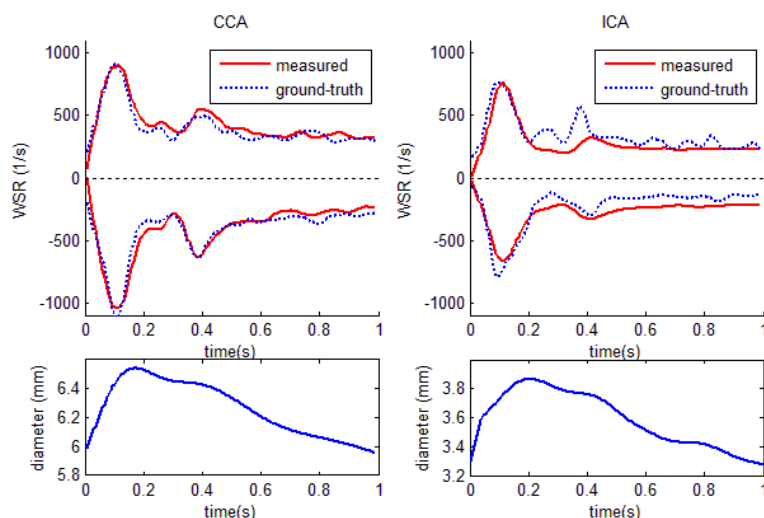
P1A7-8

8:00 am **Investigation of Twinkling Artifact by Controlling Oscillating Disturbance**

Yu Naito[1], Masayuki Tanabe[1], Masahiko Nishimoto[1], Hiroshi Hashimoto[2], Takao Jibiki[2], Tadashi Shimazaki[2]; *[1]Graduate School of Science and Technology, Kumamoto University, Kumamoto, Japan, [2]GE Healthcare Japan Corporation, Japan*

Background, Motivation and Objective

The twinkling artifact is a phenomenon that rapidly alternating color pixels behind a stationary strongly reflecting medium where an acoustic shadow is expected in Doppler mode. Although this phenomenon has a potential in clinical diagnosis for example early detection of microcalcification in dense breast, the occurrence mechanism has not been clarified yet. There have been several hypotheses for underlying mechanism of this phenomenon: surface roughness of calcification, phase jitter noise of the ultrasound machine, and oscillation of reflecting medium. In this study, *in-vitro* experiments were conducted, and the effects of the oscillating disturbance on a microcalcification embedded in soft tissue were investigated.

Statement of Contribution/Methods

A transparent poly (vinyl alcohol) hydro (PVA-H) gel soft tissue-mimicking phantom containing embedded a glass bead with the diameter 311 μm was used. All scanning were performed using a medical ultrasound machine (LOGIQ S8 pilot unit, GE Healthcare) with a linear array probe (ML6-15, GE Healthcare). To control the oscillating environment, the probe was fixed in a clamp attached to a 3-axis stage, and the stage was placed on the vibration-isolated table and far enough away from all oscillating machine including the ultrasound machine. The color Doppler mode was applied and pulse repetition frequency was set to 600 Hz. the other ultrasound machine conditions were set as the twinkling artifact arise in out-of-control oscillating environment. Both the finally displayed images and the I/Q signals of successive packets were obtained and analyzed.

Results/Discussion

When the stage was placed on the same table with the ultrasound machine, the twinkling artifact appeared, and stable Doppler shift components appeared in the peak values of the amplitude of successive I/Q signals. When the oscillating disturbance was isolated, the twinkling artifact and Doppler shift components were suppressed. Suppression of the twinkling artifact by control of oscillating environment demonstrated that the twinkling artifact generates from variability among the acoustic signals, not phase jitter or surface roughness of microcalcificaiton. Furthermore, the variability would be caused by the microcalcificaiton oscillations excited by environmental disturbance.
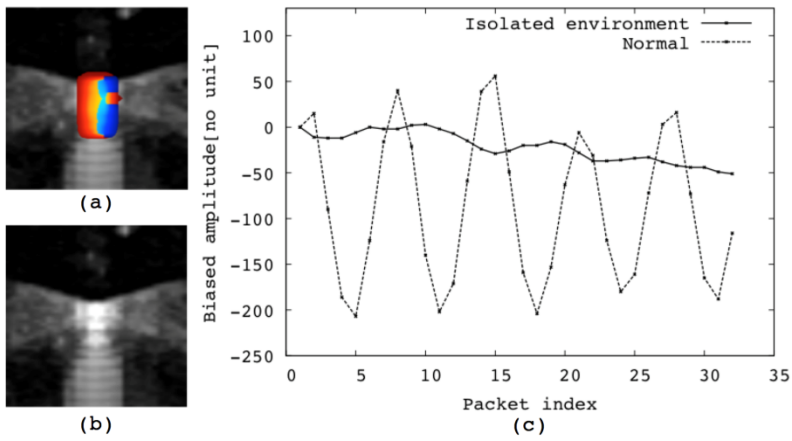
Color Doppler images in (a)normal and (b)isolated environments, and (c)their peak values in successive packets.

THURSDAY POSTER

P2A1 - Ultrasonics in Air and Water

4th floor

Thursday, October 22, 2015, Posters displayed 08:00 am - 05:00 pm. Authors must be present at their poster from 9:30 - 10:30am (odd number posters) and 14:30 – 15:30pm (even number posters).

Chair: **Jiromaru Tsujino**
Kanagawa University

P2A1-1 _____

8:00 am **Ultrasonic transducer characterization in air based on an indirect acoustic radiation pressure measurement**

Anastasia Guseva[1], Maik Hoffmann[1], Alexander Unger[2], Silvia Zulk[3], Mohamed Balla El Amien[4], Ennes Sarradj[1], Mario Kupnik[2]; *[1]BTU Cottbus-Senftenberg, Germany, [2]Technische Universität Darmstadt, Germany, [3]Leibniz Universität Hannover, Germany, [4]University of Sharjah, United Arab Emirates*

Background, Motivation and Objective

The well-known non-linear effect of acoustic radiation pressure, present in front of an emitting ultrasonic transducer, results in a net force that pushes the transducer in the opposite direction. In immersion, this force is quite large (mN-range), and, thus, relatively simple to measure. An interesting example, described in [Tan et al., OCEANS 2010], uses the effect to generate acoustic thrust to maneuver small vessels, diving in water. In air, however, the resulting forces acting on the ultrasonic transducer is about one order of magnitude smaller (μN-range), due to the low density of air compared to water. Usual air-coupled transducers weigh several grams, aggravating a direct measurement on a sensitive scale or in some other form of force measurement setup. Therefore, we present proof-of-concept measurement results from a simple indirect method that allows us to determine such small resulting forces.

Statement of Contribution/Methods

Our method utilizes resonance magnification of a clamped aluminum cantilever beam (20x2x850 mm) with the ultrasonic transducer mounted at the tip of the beam. One by one, we test two types of air-coupled ultrasonic transducers (MA40S4S with 10 mm diameter and MA40B8S with 16 mm diameter, both from Murata, Japan), operating at a resonance frequency of 40 kHz. The systems self-resonance frequency is 2 Hz with a quality factor exceeding 300. Strain gauge signals are used in combination with a self-tuning electronic circuit to derive a gate signal, turning on and off the ultrasonic transducer at the appropriate times. Therefore, the small force in the μN-range is sufficient to force the beam into steady-state oscillation with simple to measure deflection amplitudes in the mm range, after a long transient startup phase (resonance magnification). The configuration is modeled by a simple mass-spring-dashpot system. The four parameters (natural frequency, spring constant, modal mass, and damping constant) are extracted from preceding characterization steps. Then, Fourier method is employed to calculate the amplitude of the force signal (unipolar square-shaped, 50% duty cycle), required to reach a given beam deflection amplitude. In addition, the sound pressure levels were measured by using a calibrated microphone (B&K 4138).

Results/Discussion

The maximum forces determined are 153 μN (7 mm deflection) and 52 μN (3 mm deflection) for the large and small ultrasonic transducer, respectively. For each transducer, the input signals have been varied up to the manufacturer specified maximum amplitudes of 40 Vpp and 20 Vpp, respectively. In addition, a comparison to the measured sound pressure levels revealed good correlation to the forces measured. This indicates that the method has potential to be used in future to characterize different types of air-coupled ultrasonic transducers in terms of their total efficiency rate, i.e. electrical to acoustic energy.

P2A1-2 _____

8:00 am **Side Lobe Suppression for Air-Coupled Ultrasonic Transducers with Parabolic Horn**

Koji Ibata[1], Rokuzo Hara[1], Tomonori Kimura[1], Toru Fukasawa[1], Hiroaki Miyashita[1], Satoru Inoue[1]; *[1]Mitsubishi Electric Corporation, Japan*

Background, Motivation and Objective

Air-coupled ultrasonic transducers which consist of piezo-electric ceramics and metal housing, generate and detect an ultrasonic wave in air. They are widely used for object detection system because they make composition of the system simple. Recently they have been used for object detection system in cars. The detection range for the present object detection system in cars is a few meters, because they should be able to detect objects only around cars. In late years the blind spot warning system and the collision avoidance system and so on are demanded because the interest in the car safety increases. For these purposes, the object detection system are required more high-performance. For realization of these functions, it is necessary to extend the detection range of air-coupled ultrasonic transducers. In general the acoustic impedance of air-coupled ultrasonic transducers is very high compared to that of the air. Therefore, the radiation efficiency of the transducer decreases because the acoustic mismatching between the transducer and air is very large. As a result, the detection range is short. In order to expand detection range, it is necessary to improve the radiation efficiency of the transducer.

Statement of Contribution/Methods

There are some methods for improving the radiation efficiency of the transducer. In this papers, we discuss the improving the radiation efficiency of the transducer by the horn. The horn is a tapered ultrasonic wave guide designed to provide the acoustic impedance matching between the transducer and the air. The horn is superior in the environmental worthiness because it is generally made of the metal or the resin. So it is effective to improve the radiation efficiency of the transducer for the object detection system in cars by the horn. We have adopted the parabolic horn and the effect of it has been investigated by the calculation and the experiment. And also we proposed the method of suppressing the side lobe caused by attaching the horn.

Results/Discussion

As a result, the sound pressure level in the front direction of the transducer has become 16.7dB greater and the directional pattern has been sharpened. And also we have presented about the side lobe suppression, which is caused by attaching the horn. We have shown that the acoustic absorption material which is attached the edge of the horn is effective for suppressing the side lobe.

P2A1-3 _____

8:00 am **Calibration of ultrasonic hydrophones based on spherically focused self-reciprocity technique**

Guangzhen Xing[1], Ping Yang[2], Pengcheng Hu[1]; *[1]Institute of Ultra-precision Optoelectronic Instrument Engineering, Harbin Institute of Technology, Harbin, Heilongjiang, China, People's Republic of, [2]Division of Mechanics and Acoustics, National Institute of Metrology, Beijing, Beijing, China, People's Republic of*

Background, Motivation and Objective

High frequency hydrophone has been applied widely in the field of clinical applications. To determine the hydrophone sensitivity precisely has vital importance on keeping safty of medical ultrasound equipments and is necessary for evaluation of ultrasonic transducers.

THURSDAY POSTER

Statement of Contribution/Methods

A method using spherically focused transducers based on self-reciprocity technique to calibrate hydrophones was proposed in this article. In self-reciprocity calibration of focused transmitters, a numerical calculation using Rayleigh integral was used to estimate the diffraction loss of the transmitted ultrasonic beam. The pressure detected could also be significantly influenced by spatial averaging effect of the hydrophone, especially when a focused transducer was used. The active element size of the hydrophone, which could be different with the nominal was measured to evaluate the spatial averaging effect. One way to estimate the reflection coefficient of focusing beams on heterogeneous interface was depicted. Also, a new measurement method using first echo current and open-circuit voltage was utilized for self-reciprocity technique, avoiding the drawback of possibility of damaging the electrical unit by measuring short-circuit current.

Results/Discussion

The calibration results agreed well with the report given by National Physical Laboratory (NPL). In theory, spherically focused self-reciprocity technique could reach a higher signal to noise ratio compared with traditional reciprocity using plane piston transducers. Additionally, the correction of water attenuation is not necessary in this experimental arrangement, which may result in a wider application especially in high frequency hydrophone calibrations.

Institute of Electrical and Electronics Engineers
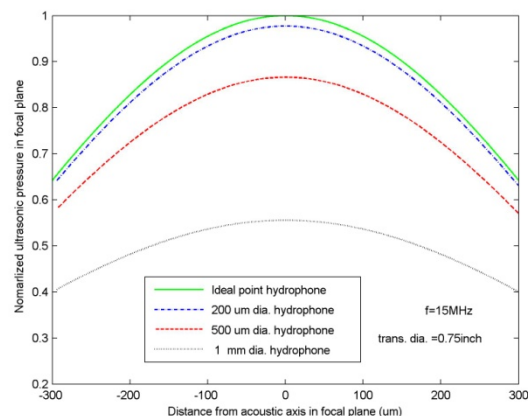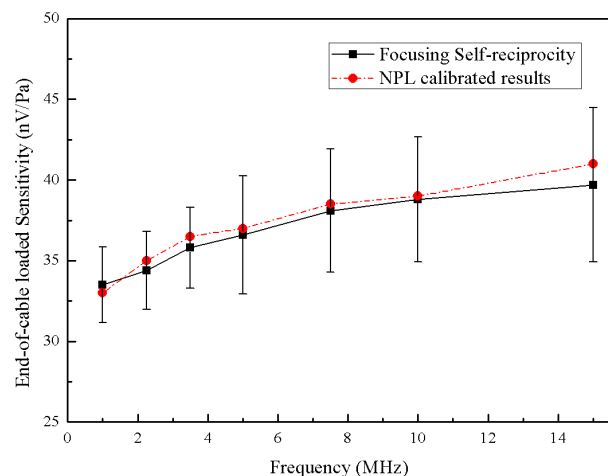
P2A2 - SHM in Concrete

4th floor

Thursday, October 22, 2015, Posters displayed 08:00 am - 05:00 pm. Authors must be present at their poster from 9:30 - 10:30am (odd number posters) and 14:30 – 15:30pm (even number posters).

Chair: **Joel Harley**
University of Utah

P2A2-1 _____

8:00 am **Low Frequency Coded Waveform for the Inspection of Concrete Structure**

M.N.I.B. Mohamed[1], S. Laureti[1,2], M. Ricci[2], L.A.J. Davis[1], P. Burrascano[2], D.A. Hutchins[1]*; [1]School of Engineering, University of Warwick, Coventry, United Kingdom, [2]Polo Scientifico Didattico di Terni, Università degli Studi di Perugia, Terni, Italy*

Background, Motivation and Objective

It is very difficult to inspect thick sections of concrete and related material using ultrasound. The problem is mainly scattering from aggregate and other types of inclusions. This often limits the depth of penetration, but also causes a poor signal to noise ration (SNR) to be present in a single-sided inspection. The objective was to develop a system at low frequencies (100- 400 kHz), which had good penetration, but also had a reasonable bandwidth and SNR. This required the correct combination of transducer, excitation waveform and an additional signal processing method in term of defect location could be optimised.

Statement of Contribution/Methods

Low frequency piezocomposite transducers have been used in combination with pulse compression methods to penetrate 35 cm into concrete-type materials. A chirps signal with frequency range 100-200 kHz and of 10 ms duration was used to excite a pair of 54 mm diameter piezocomposite transducer in pitch-catch mode. The centre frequency of the transducers was 170 kHz. Using this arrangement, good signal could be obtained, but there was a problem with variability due to high degree of scattering - even small changes in transducer location changed and the measurement. Thus, in addition signal processing method was introduced, whereby the total energy reaching the receiver was calculated as a function of time from the cross-correlation outputs.

Results/Discussion

Measurement on a wide range of samples with different compositions (in terms of aggregate size and composition)indicated that rectified cross-correlation output could be used to indicate the location of cracks. However, this was not repeatable; although the main back wall echoes were observed at the expected locations, the output was still dominated by larger peaks arising from scattered signal at other times from aggregate and inclusions. These unwanted signal changed with transducer location. However using a running average of total energy, average over a number of measurements, led to a good estimate of thickness of a cracked sample. Results for undamaged (red line) and cracked (black line) sample are shown in the figure below, where a threshold line shows a clear difference between the two. This method is likely to be of much interest to the NDE of thick concrete samples, where the location of useful data can be very difficult.
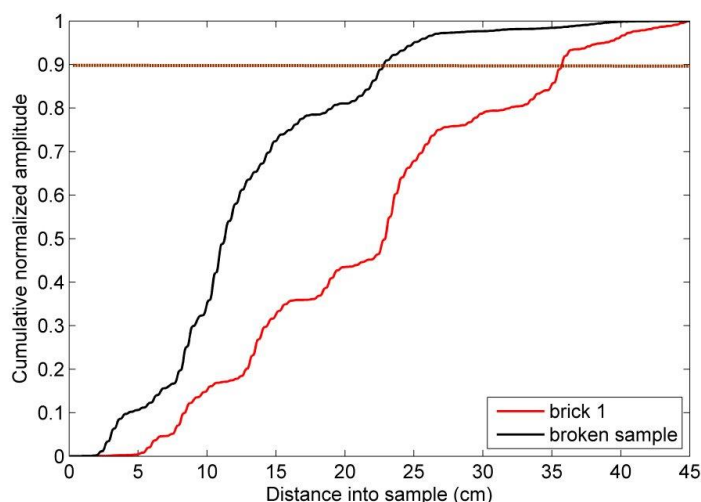
P2A2-2 _____

8:00 am **Reverse Time Migration Based Ultrasonic Imaging of Rebars Embedded in Concrete**

Surendra Beniwal[1], Abhijit Ganguli[1]*; [1]Civil Engineering, Indian Institute of Technology Delhi, Delhi, India*

Background, Motivation and Objective

The Reverse Time Migration (RTM) algorithm has been applied extensively for geophysical subsurface imaging, using both acoustic and elastic wave inversion methodologies. In this technique, the explored medium is excited at certain locations by surface based acoustic sources. The signals reflected from the interior of the medium are recorded on the surface. These signals are subsequently time reversed and fed back into a simulated medium (utilizing known material and geometric properties of the medium) at the receiver locations. The resulting wave propagation is simulated via a Finite Difference in Time Domain (FDTD) or Finite Element (FE) based numerical scheme. A second simulation, involving the forward migration of the source field, is also performed by feeding signals at the respective source positions. The fields, resulting from the forward and the time reversed simulations, are stored at each time step and at each spatial location in the simulated medium. A subsurface image of the medium is generated, using the two fields obtained in the above two steps, by applying an Imaging Condition. In the field of Non-Destructive Evaluation (NDE) of concrete, application of the RTM algorithm is a relatively new area of research.

Statement of Contribution/Methods

In the current work, the RTM algorithm is applied on experimental ultrasonic data, acquired on a concrete block with embedded rebars. Some of the closely spaced steel rebars are in bonded (healthy) condition and some of them are artificially debonded from the concrete, thereby simulating a delaminated situation. The ultrasonic data was

obtained in a Full Matrix Capture (FMC) scheme and the RTM calculations were performed using the elastic as well as the acoustic wave propagation modality. To the best of the authors' knowledge, the application of RTM using ultrasonic FMC data (collected on a physical concrete medium) to image and to evaluate the steel rebar condition has not been yet explored in the literature.

Results/Discussion

The RTM based images are able to locate the steel rebars and distinguish between the delaminated and the bonded conditions of the rebars.

RTM generated Image (Acoustic propagation)   RTM generated Image (Elastic propagation)
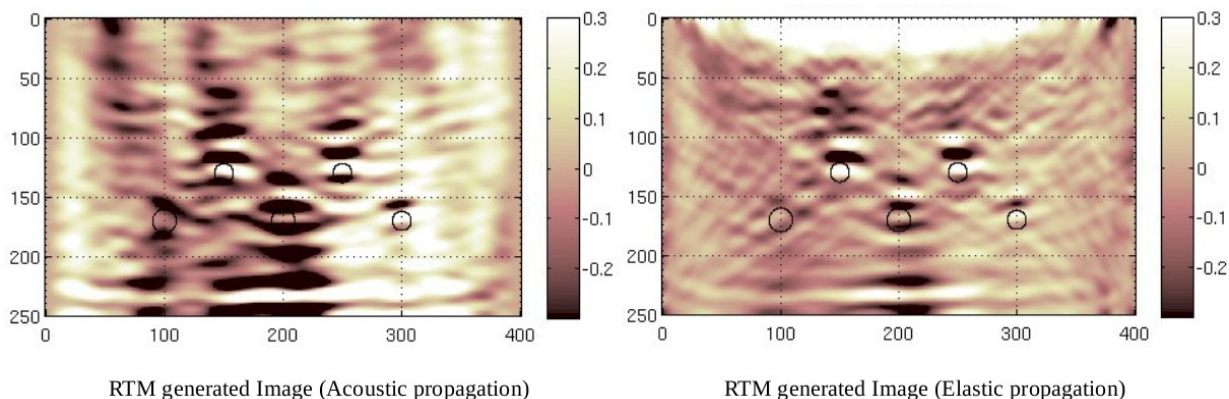
P2A2-3

8:00 am   Study on Non-Contact Acoustic Imaging Method for Concrete Structures -The 2nd Construction Method using a Strong Ultrasonic Sound Source-

Tsuneyoshi Sugimoto[1], Kazuko Sugimoto[2], Noriyuki Utagawa[3], Kageyoshi Katakura[4]; [1]*Graduate School of Engineering, Toin University of Yokohama, Yokohama, Japan,* [2]*Graduate School of Engineering, Toin University of Yokohama, Japan,* [3]*SatoKogyo Co., Ltd., Japan,* [4]*Meitoku Engineering, Japan*

Background, Motivation and Objective

The long distance non-contact acoustic inspection method with defective detection accuracy comparable as the hammer method has been examined. This is the technique of having combined a scanning laser Doppler vibrometer (SLDV) and a long-distance acoustic device (LRAD). Although the directional characteristics of the LRAD itself are excellent in 1 kHz with ±15 degree. There are problems such as angular dependence nature to a subject and noise to the circumference at the time of considering practical use. Then, the case where a strong ultrasonic sound source and LDV for a single point were combined as the 2nd construction of the non-contact acoustic inspection method was examined.

Statement of Contribution/Methods

The strong ultrasonic wave sound source with the investigation performance in a practical distance was made as an experiment (diameter 600mm, focal distance 5m). This sound source is constituted by 3200 ultrasonic elements with a resonance frequency of 40.35 kHz. In order to set the same axis as a sound wave and laser light, a hole 40 mm in diameter was opened in the center of the sound source. A single point LDV (Polytec Corp. OFV-505) is arranged in the back of the sound source.

Results/Discussion

The inspection experiment was carried out using 500 to 7100 Hz tone burst waves to the circular defective part (dia. 300mm, depth 80 mm) and the healthy part of the concrete test object. From the experimental result, a clear flexural resonance peak can be observed on the defective part.

It became clear that the strong ultrasonic sound source can generate sufficient sound pressure for non-destructive investigation of concrete even with a 5m distance. From now on, occupying a very important position as a sound source of this method is expected.
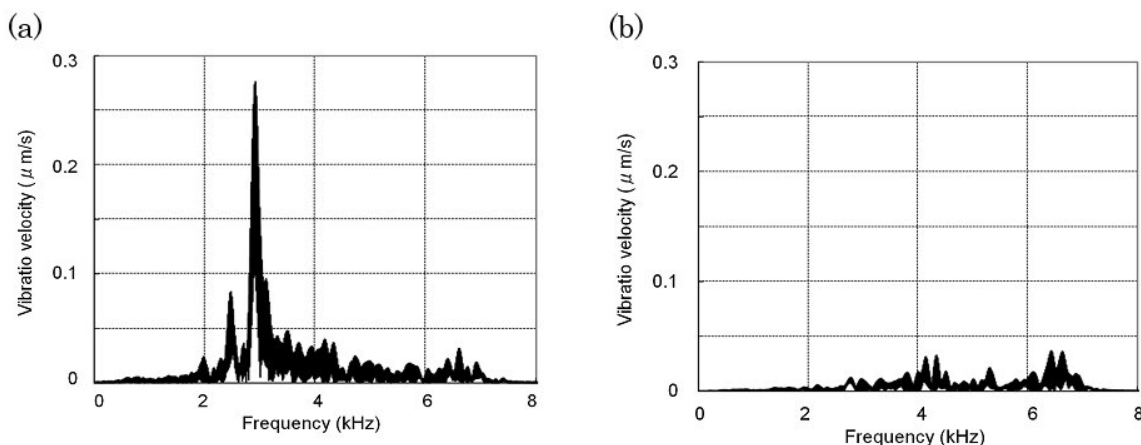
Vibration velocity spectrum. (a) Defective part, (b) healthy part.

P2A2-4

8:00 am   **Detection of Delamination in Concrete Medium Using Rayleigh Waves**

Debdutta Ghosh[1], **Surendra Beniwal[1]**, Abhijit Ganguli[1]; *[1]Civil Engineering, Indian Institute of Technology Delhi, Delhi, India*

Background, Motivation and Objective

Concrete is a heterogeneous cement-based material and when ultrasonic waves propagate through it, the waves exhibit a high degree of attenuation and scattering. This makes ultrasonic damage detection in concrete a difficult task. However, despite these difficulties, evaluation of concrete structures, using ultrasonic compressional waves, is quite popular and widespread. In this paper, we explore the feasibility of utilization of Rayleigh waves for near-surface damage detection or rebar assessment in reinforced concrete slabs.

Statement of Contribution/Methods

To the best of the authors' knowledge, this is a relatively less explored research area. The imaging of the near-surface defects is performed, using scattered Rayleigh wave information, by operating an ultrasonic array with transducer elements, having center frequency of 100 kHz. An artificial delamination, originating from a rebar, is embedded inside a laboratory based concrete slab to simulate a radial crack, approaching the slab surface. The Synthetic Aperture Focusing Technique (SAFT) is used for image reconstruction using experimental surface wave data collected on this slab surface. Two operations are performed for combining the SAFT images corresponding to individual sources: a) the Summation approach and b) the Multiplication approach.

Results/Discussion

The results show that the Multiplication algorithm generates better results than the conventional Summation algorithm. The difficulties, associated with Rayleigh wave imaging of the near surface defects, are also discussed in the paper.

SAFT image (Summation algorithm)   SAFT image (Multiplication algorithm)
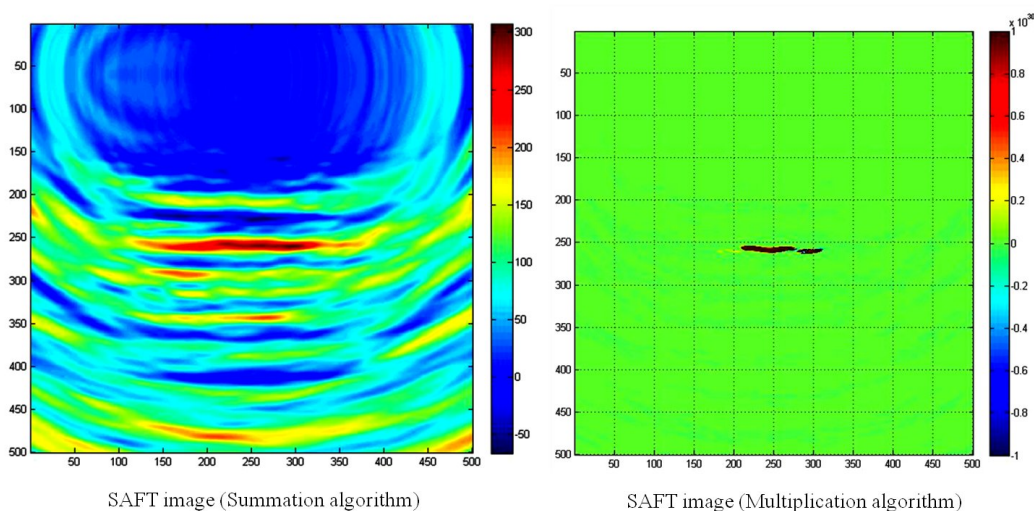
P2A3 - Flaw Detection

4th floor

Thursday, October 22, 2015, Posters displayed 08:00 am - 05:00 pm. Authors must be present at their poster from 9:30 - 10:30am (odd number posters) and 14:30 – 15:30pm (even number posters).

Chair: **Erdal Oruklu**
Illinois Institute of Technology

P2A3-1 _____

8:00 am   Nonlinear Rayleigh Surface Acoustic Waves for Determining Yielding of Alloys

Kui Yao[1], Shifeng Guo[1], Lei Zhang[1], Shuting Chen[1], Yi Fan Chen[1], Meysam Sharifzadeh Mirshekarloo[1], Huajun Liu[1], Zhiyuan Shen[1]; *[1]Institute of Materials Research and Engineering, A*STAR(Agency for Science, Technology and Research), Singapore*

Background, Motivation and Objective

Overloading exceeding yielding strength of metallic materials will lead to permanent plastic deformation and defects. The mechanical yielding irreversibly modifies the structure and mechanical behavior, and possibly leads to unknown structure life and even induces catastrophic accident if not detected in advance. Non-destructive test (NDT) method for effectively identifying yielding in such a manner that the integrity of the structures under test remains intact is highly demanded. Yielding of a metallic material is always accompanied by some microstructural changes, such as the appearance of dislocations, slip bands, and micro-cracks. Such microstructural changes can lead to changes in various macroscopic and microscopic mechanical properties that could affect propagation of ultrasonic wave in the material, including nonlinear ultrasonic wave behaviors. In this work, nonlinear Rayleigh surface acoustic wave was used to determine plastic deformation at varying strain levels of titanium and aluminum alloys.

Statement of Contribution/Methods

Experiments were conducted using piezoelectric transducers to generate and detect tone burst ultrasonic Rayleigh surface waves in our standard testing samples. The amplitudes of the fundamental and second harmonic waves were measured to obtain the acoustic nonlinearity at different strain levels on both materials. Microscopically, the plastic deformation in a metal was manifested by the formation of dislocations. Transmission electron microscopy (TEM) was used to determine dislocation density. A theoretical model that links the dislocations with the stress and strain relationship is developed.

Results/Discussion

The results of the nonlinear ultrasonic measurements showed an increased acoustic nonlinearity with the degree of strain levels in both Ti and Al specimens.

The increased dislocation density was found in the samples with higher degree of plastic deformation. The theoretical model correlates the acoustic nonlinear parameter with the microscopic damages.

Figure 1 A typical frequency spectrum showing the magnitude of the fundamental and second order harmonic ultrasonic signals in a sample with plastic deformation.
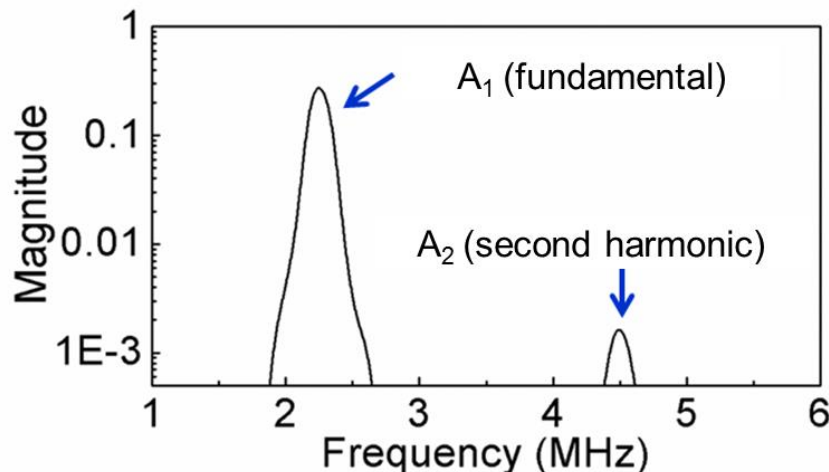
P2A3-2 _____

8:00 am   Combination of direct, half-skip and full-skip TFM to characterize multi-faceted crack in weld

Xiaoli Han[1], Wentao Wu[1,2], Ping Li[1], Jing Lin[2]; *[1]Institute of Acoustics, Chinese Academy of Sciences, China, People's Republic of, [2]State Key Laboratory for Manufacturing System Engineering, Xi'an Jiaotong University, Sha'anxi, China, People's Republic of*

Background, Motivation and Objective

Crack is one of the most dangerous process defects in welded joint. Ultrasonic method is one of the most popular means of NDE of weld. The estimation of the depth of crack allows a better estimate of the risk which the crack poses to the equipment, which is very important for weld defect ratings.

In the conventional sizing of embedded cracks by TFM (total focusing method) imaging, only the direct ray paths between the imaging point and the array are used, so for a vertical extended and multi-faceted crack, it can only capture the indications of part of the crack because only a narrow area can be reached by the direct ray and few specular reflection from the crack faces is captured. Thus the accuracy of sizing for a multi-faceted crack is limited and usually the sizing result is underestimated.

The motivation is mainly to improve the characterizing accuracy of a vertical extended and multi-faceted crack embedded in a weldment with two flat parallel surfaces through combining direct, half-skip and full-skip TFM for the inspection case involving an inclined wedge.

Statement of Contribution/Methods

Direct, half-skip and full-skip TFM can image different crack areas for the case of multi-faceted cracks in butt weld inspection using an inclined wedge. A combination of images of different crack surfaces from the three TFM modes is used to determine the extending trend in vertical direction, and eventually crack depth can be quantified more accurately.

Firstly, FMC (full matrix capture) data set is obtained by ultrasonic phased array system. Secondly, transmission delay corresponding to the three TFM modes is calculated and B-scan images of target area using the three modes are obtained respectively. Thirdly, indication of different crack areas is identified and the different crack areas are sized respectively according to the intensity distribution in different modes. Finally, image areas used for sizing are extracted and displayed together according to the corresponding positions and the extending trend in vertical direction is made out, and sizing along the depth direction is given.

Simulation is done for notches with three facets in vertical direction to prove the validity of the method. For the experiment validation, notches and real cracks with multi facets are characterized to further verify the stability and limit of the method.

Results/Discussion

Results show that the hybrid TFM in determining the extension trend and estimating the equivalent depth in the vertical direction is feasible for actual cracks with multi facets. The hybrid TFM can give more information in characterizing such cracks on the same array position, which is very important for weld rating. There are challenging aspects to be further discussed. For example, certain points in the crack may be redundantly indicated in more than one TFM modes or no strict distinction between areas two ray paths of different TFM modes can reach.

P2A3-3 _____

8:00 am **Optimal Lamb wave mode and frequency selection for assessment of creep damage in titanium alloy plates**

Yanxun Xiang[1], Fu-Zhen Xuan[2]; *[1]East China University of Science and Technology, Shanghai, Shanghai, China, People's Republic of, [2]East China University of Science and Technology, China, People's Republic of*

Background, Motivation and Objective

Solid plate structures and large diameter pipes usually have been used in many practical engineering situations at elevated temperatures with complex loading conditions.It would be helpful to make a good decision for maintenance and reparation of components by developing a more precise assessment method of creep damage.Lamb waves offer a convenient method of evaluating these damaged materials.However,optimal guided wave mode and frequency selection usually has been a tough problem in practical applications of ultrasonic Lamb wave inspection.

Statement of Contribution/Methods

The present study focuses on the characterization of creep damage in titanium alloy using Lamb waves. First, the relationship between the out-plane displacement of Lamb waves and the creep damage states of titanium alloys has been theoretically analyzed, in which the creep damage was theoretically calculated by a creep damage variable D obtained by micro-tensile test of materials. Then, the amplitude-frequency sweep method was used to acquire Lamb wave spectrum in the creep deformed materials, where the optimal Lamb mode and frequency can be determined. In addition, some specified Lamb modes selected by this method have been carried out for inspection of the creep damaged specimens to make a validation and comparison with the theoretical results.

Results/Discussion

It can be found that the amplitude-frequency curves V(f) measured by frequency sweep method display a clear variation to different creep damage states for a certain Lamb wave mode in titanium alloy.The creep degradation of Ti60 specimens can be characterized by variations of color level of the Lamb wave amplitude spectra, in which some Lamb modes with specific phase velocity and frequency thickness product (FTP) sensitive to the damage can be determined.

According to the results of theoretical analysis and the amplitude-frequency sweep, some specified sensitive Lamb modes could be considered optimal for assessment of creep damage in Ti60 plates, which have a feature that undergoes a relative larger change in amplitude with the creep deformation. For instance,the measured data of S2 mode with a FTP of 6.0 MHz•mm shows a monotonically decreasing trend with respect to the creep life fraction, which is in good accordance with the theoretical calculation and is relatively easy to correlate with the creep deterioration. Note that the optimal S2 mode gives about 40% reduction in amplitude compared with the initial value (the virginal state).

In an experimental perspective, the amplitude-frequency sweep method shows a great promise for mode optimization of guided wave inspection, which can be of a guideline for mode choice of Lamb wave and frequency selection. The amplitude-frequency sweep method is an excellent and potential tool for tackling problems with unknown material properties, or for problems where only estimates of material properties are available.

P2A3-4 _____

8:00 am **Detection of Low-frequency Components in Ultrasonic Waves Transmitted through Contact Solids**

Yuji Kato[1], Hirotaka Tanaka[1], Toshihiko Sugiura[1]; *[1]Keio University, Japan*

Background, Motivation and Objective

In structural inspection, it is important to detect closed cracks difficult to find by conventional ultrasonic techniques. Use of nonlinear ultrasonic waves can be a promising way, though their basic phenomena are complicated and not clear yet. In our previous research of nonlinear ultrasonics, instead of nonlinear signals, we found some low-frequency components appearing only in propagated waves through contact surfaces, though the generation mechanism of such low-frequency components is not clarified. In this study, we attempt to reveal the cause of the low-frequency components, investigating effects of the contact surfaces, and suggest that the low-frequency components found in our experiments can be used as a new inspection method of closed cracks.

Statement of Contribution/Methods

We experimentally examined transmission of ultrasonic waves through contact surfaces. Two metal blocks were stacked and loaded by a compressor in order to simulate a closed crack. We measured propagation time of received waves and also analyzed frequency spectra of those received wave signals. Further, we did experiments using two different configurations of blocks, limiting the propagation route of ultrasonic waves in different ways: one is only straight down from the transmitter to the receiver, and the other is only oblique direction. Moreover, we also carried out numerical simulation of this modeling with contact surfaces by using the finite element method (FEM) and compared obtained results with experimental ones.

Results/Discussion

The propagation time of ultrasonic waves transmitted through the contact surfaces was slightly longer than that for one block without contact surfaces. Low-frequency components were observed only in the received waves transmitted in the oblique direction. These results agree with numerical ones obtained by FEM. The slight delay in wave detection implies that ultrasonic waves transmitted through the contact surfaces propagate not only normal to the surfaces but also oblique to them. It means that some of diffused ultrasonic waves change the propagation direction at the contact surfaces towards the receiver. Because of frequency dependence of the wave directivity, if some of the received ultrasonic waves have propagated in the oblique direction, the proportion of low-frequency components in those waves can become larger. In conclusion, ultrasonic waves transmitted through the contact surfaces can propagate obliquely to the receiver, and thus the received waves can contain larger proportion of low-frequency components. Measuring such low-frequency components can be useful for detecting a closed crack in structures.

P2A3-5 _____

8:00 am   Reconfigurable and Programmable System-on-Chip Hardware Platform for Real-time Ultrasonic Testing Applications

Pramod Govindan[1], Boyang Wang[1], Pingping Wu[1], Ivan Palkov[1], Vidya Vasudevan[1], **Jafar Saniie[1]**; *[1]Electrical and Computer Engineering, Illinois Institute of Technology, Chicago, Illinois, USA*

Background, Motivation and Objective

Present day ultrasonic signal processing applications such as medical imaging and non-destructive testing has stringent requirements on low cost and portability to provide high quality diagnostics and characterization at real-time pace. Advancements in the field of digital signal processing, embedded computing, and semiconductor technologies, have significantly assisted ultrasound researchers in the development of low-cost, portable, and computationally efficient systems. In this study, a reconfigurable and programmable System-on-Chip (SoC) based hardware platform is designed and developed to effortlessly test and evaluate a wide variety of ultrasonic signal processing applications.

Statement of Contribution/Methods

This reconfigurable platform comprises of 2 major components: (i) a programmable Analog Front-End (AFE) for performing beamforming and signal conditioning, and (ii) Xilinx Zynq SoC for dynamically reconfiguring the AFE and also to execute computationally complex ultrasonic signal processing algorithms. AFE consists of a Texas Instruments (TI) LM96550 HV Pulser, LM96530 Transmit/Receive (T/R) Switch, LM96570 Beamformer over TX-SDK-V2 EVM, a programmable low noise filter/amplifier and a programmable gain control amplifier VCA8500, and an Analog Devices ADC AD9467. VCA8500 receives ultrasound echoes from TX-SDK-V2 and forwards to the AD9467, which interfaces with Zynq SoC through a LVDS (low voltage differential signaling) interface. VCA8500 incorporates a Low Noise Pre-amplifier and a Variable Gain Amplifier for controlled amplification and noise filtering of the raw analog data. Zynq SoC combines all programmable logic and powerful dual-core ARM processing unit to provide very high speed data processing. ARM processor triggers the ultrasonic excitation. The high speed ADC acquires ultrasonic data at 250 MSPS, which is transferred to the memory via high performance AXI bus interface. Furthermore, an efficient software design flow based on serial peripheral interface (SPI) mastered by Zynq SoC has been developed for optimal configuration of the ultrasonic testing system.

Results/Discussion

After programming AFE components, the ARM processor triggers a transducer, and acquires data from a steel block test specimen, which is dynamically transferred to the Zynq SoC via high speed ADC. Based on the quality of received echo, certain parameters of AFE are automatically re-programmed to ensure high quality signal processing. Capabilities of reconfigurable ultrasonic testing platform is analyzed and evaluated by implementing discrete wavelet transform based data compression using 2 different architectural configurations: (i) hardware-only, and (ii) software-only. In hardware-only design, the Zynq programmable logic compresses 33 MB of acquired ultrasonic data into 0.4 MB in 0.25 seconds, whereas in software-only design the ARM processor within Zynq executes the compression algorithm in 1 minute.

P2A3-6 _____

8:00 am   Model-based parameter estimation for defect characterization in ultrasonic NDE applications

Yufeng Lu[1], **Jafar Saniie[2]**; *[1]Electrical and Computer Engineering, Bradley University, Peoria, Illinois, USA, [2]Electrical and Computer Engineering, Illinois Institute of Technology, Chicago, Illinois, USA*

Background, Motivation and Objective

In ultrasonic structural health monitoring, the received ultrasonic response is commonly used to characterize defects and unravel their physical information including locations, orientations and sizes. Signal modeling is not only an important way of analyzing ultrasonic signal, but also plays an important role in NDE of materials. Various flaw scattering models/theories have been utilized to describe different types of flaws including void and solid inclusion. There have been benchmark studies aiming to quantitatively evaluate manufactured flaws such as side-drilled hole, flat-bottom hole, etc. Both planar and focused transducers are used for contact or immersion ultrasonic testing. Nevertheless, it is challenging, yet favorable, to decompose ultrasonic signals into echo wavelets and use estimated echo parameters for defect classification.

Statement of Contribution/Methods

Chirplet is a model often used in the signal processing applications such as radar, sonar, and ultrasound. By using six parameters a broad range of signals such as dispersive or non-dispersive, symmetric or skewed, narrowband or broadband can be represented. In this investigation, chirplet model-based signal decomposition algorithm is used to decompose ultrasonic signals into a linear combination of chirplets. In addition, estimated chirplet parameters are used to quantify defect evaluation. In this experimental study, ultrasonic benchmark data have been evaluated to test a variety of defects including different sizes of side-drilled hole and planar defect with different lengths and heights. It has been demonstrated that the chirplet-based algorithm not only accurately decomposes the ultrasonic signal, but also characterizes the defect shape and size.

Results/Discussion

In this paper, chirplet model is used for signal decomposition and parameter estimation. Extensive benchmark results indicate that the model-based algorithm offers an efficient way of characterizing defects. This method successfully associates the estimated chirplets and their parameters as a quantitative technique to characterize defects. Additionally, this type of study can be utilized in ultrasonic NDE to assess the structural integrity of materials.

P2A3-7 _____

8:00 am   Instrument for Rock Bolt Inspection by Means of Ultrasound

Tadeusz Stepinski[1], Karl-Johan Mattsson[2]; *[1]WIMR, AGH Univ. of Science and Technology, Krakow, Poland, [2]Geosigma AB, Sweden*

Background, Motivation and Objective

When a mine, tunnel or other rock facility is constructed, one of the key issues is staff safety as well as minimizing the risk of interference during the work. The most important activity after the rock surface has been scaled is to reinforce the roof and the walls. The most common way of doing this is installation of rock bolts that are grouted in boreholes and application of shotcrete over the surface. There are many types of anchor rock bolts; typically, they take the form of several meters long steel bars with diameter in the range of one inch. Nondestructive inspection of rock bolts after their installation is a vital issue to ensure safety of staff working at the rock facility as well as sustainable rock reinforcing.

Statement of Contribution/Methods

In this paper we present a new digital ultrasonic instrument for nondestructive inspection of rock bolts using guided waves. The Rock Bolt Tester (RBT) instrument applies long-range ultrasound to investigate bolt's status, especially its grouting condition. RBT features an application tailored ultrasound probe that transmits high-energy, low frequency (below 100kHz) guided waves and is capable of receiving weak echoes reflected from the discontinuities at the bolt surface as well its end-echo that have propagated in the range of up to four meters. The RBT is a portable instrument that consists of specially designed analog electronics for generation and reception of guided waves and an embedded digital computer for signal processing, operator communication and data storage. In the paper we will focus on advanced processing techniques applied to enhance tiny echo signals received by the probe.

Results/Discussion

Results of the RBT's evaluation using prepared rock bolts installed at a number of sites (tunnels and mines) are presented in the paper. The test bolts with different lengths in the range of 2 to 4 m were manufactured by shielding a certain steel bolt length with plastic tube sealed with silicon. Plastic end cups were installed on many bolts to create uniform conditions for end echo measurements.

Approximately 3,000 tests have been conducted; selected results are presented in the paper for illustration and comparison of the results of the applied signal processing techniques.

P3A1 - General Physical Acoustics

4th floor

Thursday, October 22, 2015, Posters displayed 08:00 am - 05:00 pm. Authors must be present at their poster from 9:30 - 10:30am (odd number posters) and 14:30 – 15:30pm (even number posters).

Chair: **Yook-Kong Yong**
           Rutgers University

P3A1-1 _____

8:00 am   **LATERAL ELECTRIC FIELD EXCITED RESONATOR BASED ON PZT CERAMICS**

Andrey Teplykh[1], Boris Zaitsev[1], Iren Kuznetsova[2]; *[1]Kotel'nikov Institute of Radio Engineering and Electronics of RAS, Saratov Branch, Saratov, Russian Federation, [2]Kotel'nikov Institute of Radio Engineering and Electronics of RAS, Moscow, Russian Federation*

Background, Motivation and Objective

At present lateral electric field excited resonators are widely used for development of liquid and biological sensors. The main problem in development of such resonators is suppression of parasitic oscillations which strongly deteriorate their resonant properties. For solving this problem researchers use the electrodes of special shape or damping layer deposited on the certain part of resonator. By now aforementioned resonators were developed on such materials as lithium niobate, lithium tantalate, and quartz. But possibility of use of lead zirconate titanate piezoceramics (PZT) was not studied although this material has high value of electromechanical coupling coefficient. In this paper the resonators with lateral electric field based on pointed piezoceramics was first developed. It has been found that these resonators are characterized by good quality of series and parallel resonances at low-frequency range. These properties are very important for development of various acoustic sensors.

Statement of Contribution/Methods

We used the plates of piezoceramics with shear dimensions of 18*20 mm, and thickness of 2 mm. One side of plate was deposited by thin film of aluminum with gap in the center which was oriented so that excited lateral electric field was directed along crystallographic axis Z of piezoceramics. We studied three samples with gap width of 2, 3 and 4 mm. With the help of LCR-meter the frequency dependencies of impedance and admittance were measured. It has been found that good quality of series and parallel resonances are watched in frequency range 90-100 kHz. These dependencies allowed finding the corresponding values of Q-factor and resonant frequencies allowed to determine the effective electromechanical coupling coefficient. The theoretical analysis based on finite element method allowed finding values of frequencies of series and parallel resonances for each case which turned out to be in a good agreement with experiment.

Results/Discussion

Is has been found experimentally that Q-factors of series (140-160) and parallel (180-190) resonances practically do not depend on the width of gap between electrodes. However, effective value of electromechanical coupling coefficient increases with increase the width of gap between electrodes from 11 up to 16%. Today obtained values of electromechanical coupling coefficient are record because the known values for lithium niobate do not exceed 4%. At that it should be noted that good qualities of resonances was achieved without use of any special methods for suppression of parasitic oscillations. Theoretical analysis has shown that dominant component of mechanical displacement of oscillations is tangential one.

P3A1-2 _____

8:00 am   **"Inverse method for evaluation of elastic parameters in functionally graded materials using ultrasonic Love waves"**

Piotr Kielczynski[1], Marek Szalewski[1], Andrzej Balcerzak[1], Krzysztof Wieja[1]; *[1]Polish Academy of Sciences, Poland*

Background, Motivation and Objective

Functionally graded materials (FGM) are heterogeneous media, in which the mechanical parameters are functions of the distance from the surface into the bulk of the material. FGMs can provide elevated mechanical properties (e.g., high strength and hardness) and superior exploitation characteristics (e.g., crack, wear and corrosion resistance). Love waves may be used to study spatial profiles changes in mechanical properties (e.g., modulus of elasticity) of FGMs. Love wave penetration depth depends on the frequency. Thus, by changing the frequency of the wave one can probe subsurface profiles of materials. Love wave energy is concentrated near the surface of the waveguide. For this reason, any disturbance in the material parameters in the surface region have considerable impact on the dispersion characteristics of the Love wave (i.e., velocity and attenuation). Therefore, the Love waves are particularly convenient to study the physical properties of inhomogeneous graded materials. Conventional methods for investigation the elastic properties of FGM are destructive methods. By contrast, Love wave method used to investigate the elastic properties of the FGM is a non-destructive method.

Statement of Contribution/Methods

The aim of this study was to evaluate the inverse procedure to determine profiles (as a function of depth) of the mechanical properties of inhomogeneous FGM resulting from the application of various technological processes of surface treatment. First, the Direct Sturm-Liouville Problem for Love waves propagating in elastic graded materials with various profiles of the shear stiffness as a function of the distance from the surface, has been solved using the Finite Difference Method and Transfer Matrix Method (Haskell-Thompson method). Love wave dispersion curves were evaluated in the frequency range from 1 to 20 MHz. The inverse problem was formulated as an optimization problem with appropriately constructed objective function that depended on the material properties of an elastic waveguide of the Love wave and the experimental data. To minimize the considered objective function, optimization procedures of the Nelder-Mead type from Scilab software package were employed.

Results/Discussion

The Inverse Problem has been solved for two types of FGM: 1) nonhomogeneous layer on the homogeneous half-space, 2) nonhomogeneous half-space. The accuracy of the results obtained from the solution of the Inverse Problem using the evaluated objective function for the dispersion curves corrupted by noise, is good. The results of this work may also find application in geophysics, seismology and underground acoustics to investigate the internal structure of Earth (crustal and subcrustal region near the Earth surface). These results can be also applied in exploration of natural resources (e.g., mineral oils, gases and minerals).

P3A1-3 _____

8:00 am   **"Ultrasonic studies of physicochemical parameters of biofuels in a broad range of pressures and temperatures"**

Piotr Kielczynski[1], Marek Szalewski[1], Andrzej Balcerzak[1], Krzysztof Wieja[1], Aleksander Rostocki[2], Ryszard Siegoczyñski[2], Stanislaw Ptasznik[3]; *[1]Polish Academy of Sciences, Poland, [2]Warsaw University of Technology, Poland, [3]Institute of Agricultural and Food Biotechnology, Poland*

Background, Motivation and Objective

The aim of the study was to determine thermodynamic parameters of biofuel components by using ultrasonic methods on the example of methyl and ethyl esters of fatty acids, in a wide range of pressures (from atmospheric pressure to 600 MPa) and for various temperatures from 20 to 50 °C. Knowledge of physicochemical parameters of

biofuels at high pressures is of great importance in the design of injection systems in modern diesel engines (common rail). Direct measurement of thermodynamic parameters of liquids under high pressure, using classical methods, is very difficult. To overcome this disadvantage, the authors applied ultrasonic methods, which in contrast to the classical methods allow in a relatively simple way the determination of thermodynamic parameters of the liquid under high pressure. Phase transitions of first order that occur under high pressure have been also examined.

Statement of Contribution/Methods

Ultrasonic wave velocity, density and viscosity of the liquid as a function of pressure for various temperatures, have been measured. The measured curves of velocity, density and viscosity as a function of pressure and temperature are approximated by the analytical expressions. On this basis, the thermodynamic parameters of the investigated liquid, such as: isothermal compressibility, adiabatic compressibility (and its reciprocal adiabatic bulk modulus), thermal expansion coefficient, specific heat at constant pressure, etc. were evaluated. Ultrasonic wave velocity was determined from the time of flight measurement by using the cross-correlation method. Ultrasonic wave velocity measurement was carried out at a frequency $f = 5$ MHz. Viscosity was measured by the original method that uses ultrasonic surface waves of the Love and Bleustein-Gulyaev type, developed by the authors at the Institute of Fundamental Technological Research in Warsaw. The density of the liquid subjected to high pressure was determined from the change in volume of the test sample liquid in the high pressure chamber.

Results/Discussion

The results of measurements and calculations and their interpretation will allow a better understanding of the physicochemical properties and the nature of molecular interactions in the investigated liquids. These results will also be useful in the development of models of the physicochemical phenomena occurring in liquids exposed to high pressures. It is also very important to find out the presence of high-pressure phase transitions in liquids, especially the value of pressure at which the transformation begins. Using the results of measurements and calculations, one can determine the empirical equation of state in the analytical form as the implicit function of three variables (p, V, T).

P3A1-4

8:00 am　Experimental Investigation on the Jet-like Acoustic Streaming in front of an Oscillating Circular Piston

Arturo Santillan[1]; [1]*Department of Technology and Innovation, University of Southern Denmark, Odense M, Fyn, Denmark*

Background, Motivation and Objective

Nonlinear effects can be observed in a sound field of very high energy density; one of these effects is a resulting time average of the particle velocity of the fluid being different from zero. The time average of the particle velocity is called the acoustic streaming. Moreover, associated with the acoustic streaming is a net flow of mass of the fluid. In this paper, the acoustic streaming produced by a propagating sound wave in air under free field conditions is studied experimentally: the strong jet-like wind generated by a beam of sound radiated by a powerful ultrasonic source.

The main motivation of the work has been to confirm the results of numerical simulations presented in a previous paper. Those simulations were obtained by means of the finite-difference time-domain method, and the results showed that a significant flow of air can be produced in front of the radiating piston by the acoustic propagating wave. The simulations also indicated that the flow of air has its maximum magnitude along the axis.

The general objective of the work described in this paper has been to determine experimentally the acoustic streaming produced by a sound wave radiated by a circular piston, and to compare the experimental data with numerical simulations presented previously by the author.

Statement of Contribution/Methods

Although the jet-like wind effect produced by a beam of sound has been known for several decades, the information on this phenomenon available on the literature is scarce. The magnitude of the generated flow of air can be strong enough to blow out a candle; however, the velocities are predicted to be relatively low, less than one meter per second, which complicates its measurement. In this paper, the use of the viscous drag force on a sphere is investigated to determine the air velocity produced by the sound beam and the associated flow of mass.

The experimental investigation is extended to study the effects on the generated acoustic streaming due to the diameter of the piston and the presence of a baffle.

The work to be presented contributes to further understand the strong jet-like wind effect produced by a propagating wave of high intensity and the associated physical mechanisms involved.

Results/Discussion

The results of the experimental investigation show that the flow of air produced by the acoustic wave along the symmetry axis that has been determined experimentally corresponds quite well with the numerical predictions. There is a good agreement in the spatial distribution and the magnitude of the acoustic streaming along the axis between the experimental and the numerical data. This agreement was obtained with sources of different diameter. It has also been confirmed that the use of a rigid baffle increases the acoustic streaming. The obtained experimental results show that the finite-difference time-domain method can be used to simulate both the evolution in time of a high-amplitude propagating wave and the associated nonlinear effects.

P3A1-5

8:00 am　Dyadic Universal Functions and Simultaneous Near-field/Far-field Regularization of Elasto-dynamic Dyadic Green's Functions for 3D Mass-loading Analysis in Micro-acoustic Devices

alireza baghai-wadji[1]; [1]*Electrical Engineering, University of Cape Town, Cape Town, South Africa*

Background, Motivation and Objective

Last year it was rigorously shown that the Green's functions arising in three dimensional (3D) electrostatic field analysis in micro-acoustic devices can be simultaneously regularized in the near- as well as the far-field. Furthermore, it was demonstrated that geometry-independent Universal functions can be constructed and pre-calculated for high-performance computation of the self- and mutual interaction matrix elements, in the boundary element method applications.

Statement of Contribution/Methods

This contribution extends the above-mentioned results to 3D elasto-dynamic mass-loading vector field problem in micro-acoustic devices and constructs the corresponding dyadic Universal functions. The intermediate calculations in acoustics are by orders of magnitudes more complex; however, in principle, they follow the same recipe. The resulting dyadic Universal functions, being the ultimate product of the computations, are astonishingly smooth and can be stored, retrieved, processed, and easily added to existing software packages, readily enabling 3D mass-loading analysis in micro-acoustic devices. The calculation of dyadic Universal functions follows the following automatable steps: i) standard calculation of dyadic Green's functions; ii) construction of problem-specific eta-regularized integral representations for Dirac's delta functions; iii) Construction of eta-regularized dyadic Green's functions (regularization of the near-field in spatial domain); iv) selection of appropriate expansion- and testing functions; v) setting up expressions for the calculation of self- and mutual interaction elements in the boundary element method applications; vi) Hadamard-like regularization of the expressions of self- and mutual interaction elements (regularization of the far-field in spatial domain); vii) construction of eta-regularized, and Hadamard-like regularized dyadic Universal functions; viii) calculation of the self- and interaction elements in the boundary element method applications.

Results/Discussion

The manipulations involved will be rigorously supported by a series of lemmata. Universal functions for aluminium and gold electrodes will be constructed, and their functional properties compared and interpreted.

P3A1-6

8:00 am   Ultrasonic batch processing of ultra heavy crude oil for viscosity reduction on the industrial scale

Delong Xu[1], Jingjun Deng[1], Weijun Lin[1], Chao Li[1], Lixin Bai[1]; [1]*Institute of Acoustics, Chinese Academy of Sciences, Beijing, China, People's Republic of*

Background, Motivation and Objective

Due to the shortage of the fossil fuel and with the increasing demand for it, the global demand for crude oil had a remarkable yearly growth rate from 1% to 1.8% (International Energy Agency, 2009) in the first decade of the 21st century. Therefore, the unconventional oil and gas such as heavy crude oil (HCO) and ultra heavy crude oil (UHCO) whose density is less than 10API and 20API respectively are getting more and more attentions in the world. But their properties of heavier density, higher viscosity, and worse fluidity make it very difficult to produce and transport them, especially when the temperature is low. To solve the problems of their production and transportation which are still very difficult technically in the world, the economical and effective methods which can be used to reduce viscosity of UHCO must be developed. Meanwhile the mechanisms of effects of ultrasonic wave on the viscosity reduction of UHCO will be emphatically investigated in this paper.

Statement of Contribution/Methods

Ultrasonic processing (UP) can be used to improve rheological properties of UHCO among the traditional methods of heating, injecting light crude oil or hydrocarbon and adding viscosity reudcer which all have bottleneck problems for batch processing on the industrial scale.In this paper, the effects of ultrasonic wave on viscosity reduction for Fengcheng ultra heavy oil in Xinjiang oil field are studied. Four types of the oil-in-water (O/W) of ultra heavy oil examples are prepared for experiments in lab. In the experiments, these four types of examples are irradiated by ultrasonic horn (18kHz). The electrical power input for UHCO in the lab is 150w and the viscosity is measured through viscometer (Brookfield RVDV-III).

According to the experiments in the lab, an ultrasonic batch processing prototype is designed and used for the practical production in the Xinjiang oil field for reducing the viscosity of UHCO on the industrial scale. 10 tons UHCO can be processed per day. The electrial power input of the prototype is 10kw.

Results/Discussion

The results are as following:

1.The obvious viscosity reduction effects of ultrasonic wave on reducing viscosity can be observed for examples whose viscosity irradiated by ultrasonic wave is 25% lower than that un-irradiated at 20 centigrade and 20% less quantity of active macromolecule viscosity reducer is needed. And the reason of the phenomenon observed in this paper is analyzed qualitatively.

2.According to the results in the oil field, the prototype of ultrasonic batch processing for the UHCO can be used to reduce the viscostiy of UHCO on the industrial scale. And some improvements need to be made for the further practical industrial production.

The results obtained in this paper can provide fundamental basis for the development of new ultrasonic technologies of reducing the viscosity of UHCO, which is helpful for improving and keeping good fluidity of HCO and UHCO during their extraction and pipe transportation.

P3A1-7

8:00 am   A basic study of technique for stirring of liquid in non-contact way using high-intensity aerial ultrasonic waves

Taichi Urakami[1], Ayumu Osumi[1], Youich Itoh[1]; [1]*Nihon University, Japan*

Background, Motivation and Objective

The operation of stirring reagent is an experimental technique used very well in the field of chemistry experiment.

If the reagent handling is small, the conventional stirring method reduce amount of reagent because a small amount reagent adhered a stirring device.

Therefore, it is necessary to do accurately stirring experiment by non-contact way.

We have investigated non-contact techniques for stirring liquid using high-intensity ultrasonic waves.

Statement of Contribution/Methods

In the experiment, high-intensity aerial ultrasonic waves were irradiated to the wall surface of the fluid vessel containing a liquid, and the behavior of the liquid was carefully observed.

A point-converging acoustic source with a stripe-mode vibration plate (frequency: 26.8 kHz) was used to generate high-intensity aerial ultrasonic waves.

The sound pressure of aerial ultrasonic waves generated by the sound source was about 25 kPa at the supplied electric power of 150 W in free field.

We prepared the 0.2 mm thick PET (polyethylene terephthalate) plate (width, 10 mm; length, 50 mm; thickness, 3 mm).

The observation of liquid stirring was confirmed using video camera when blue ink was dropped into the pure water in the container under ultrasonic irradiation.

Results/Discussion

Figure 1 shows the result.

The stirring of the liquid was observed at 5 seconds after the sound wave irradiation start.

As a result, It was confirmed that the proposed method realized the non-contact stirring of the liquid in the container.

Case of normal

Case of
Ultrasonic irradiation

0 sec   10 sec   20 sec
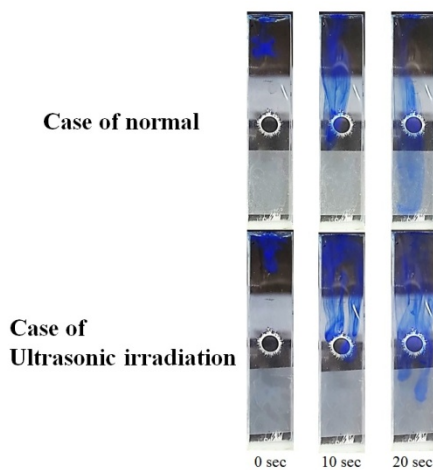
Fig.1

P3A1-8

8:00 am   Composite Lateral Electric Field Excited Piezoelectric Resonator

Boris Zaitsev[1], Alexander Shikhabudinov[1], Andrey Teplykh[1], Irina Borodina[1], Iren Kuznetsova[2]; *[1]Saratov Branch, Kotel'nikov's Institute of Radio Engineering and Electronics of RAS, Russian Federation, [2]Kotel'nikov's Institute of Radio Engineering and Electronics of RAS, Russian Federation*

Background, Motivation and Objective

Piezoelectric resonators with lateral electric field are widely used for development of biological and liquid sensors. However as before the problem of suppression of parasitic oscillations is relevant. For that the electrodes of the special form are used but their sizes depend on orientation and shear dimensions of plate. Other method which has been successfully realized for longitudinal wave is based on the deposition of the damping layer on the certain part of the resonator. But for liquid sensors the most preferable is shear acoustic wave without radiation loss. In the paper the lateral electric field excited resonator of shear acoustic wave based on the plate of 128 YX lithium niobate of thickness of 0.5 mm was developed.

Statement of Contribution/Methods

For this plate orientation the deposition of the damping layer did not lead to the total suppression of parasitic oscillations. So the spatial separation of the source of HF electric field and resonant piezoelectric plate by the air gap was suggested. The analyzed structure consisted of two plates. The first glass plate was the holder of two rectangular electrodes with sizes 10×5 mm and gap between them of 2 mm. The second plate of 128 YX lithium niobate was set near the glass plate so that electric field was oriented along axis X. It is apparent that the lateral components of electric field in the second plate had the maximum amplitude because they are continuous on the interface of two dielectric media. The normal components which were the sources of parasitic oscillations significantly attenuated in the second plate. The frequency dependencies of the real and imaginary parts of the electrical impedance and admittance were measured for different values of gap width between plates.

Results/Discussion

It has been found that for values of gap width of 0.1, 0.2, 0.3 and 0.5 mm the parallel resonance existed without parasitic oscillations. As for series resonance the frequency dependencies of real and imaginary parts of the electrical admittance in all cases excluding gap width of 0.1 mm turned out to be split near the resonant frequency. But for gap width of 0.1 mm the pronounced series resonance was found. At that the values of Q-factor for both resonances were equal ~15000 with electromechanical coupling coefficient of ~ 2%. It should be noted that the maximum values of Q-factors for parallel and series resonances obtained previously in lithium niobate were equal 1800 and 13000, respectively. So the composite piezoelectric resonator with lateral electric field allows to achieve the record values of the Q-factor of parallel and series resonances. For values of gap width less than 0.1 mm all frequency dependencies of electrical impedance and admittance had several resonant peaks due to strong influence of the normal components of electric field.

P3A1-9

8:00 am   Influence of Liquid on Properties of Backward Acoustic Waves in Piezoelectric Plates

Iren Kuznetsova[1], Boris Zaitsev[2], Ilya Nedospasov[1], Anastasia Kuznetsova[2]; *[1]Moscow Department, Kotel'nikov Institute of RadioEngineering and Electronics of RAS, Moscow, Russian Federation, [2]Saratov Department, Kotel'nikov Institute of RadioEngineering and Electronics of RAS, Saratov, Russian Federation*

Background, Motivation and Objective

The backward acoustic waves propagating in bounded media have been the subject of investigation more than 50 years. The distinguished feature of the backward wave is the opposite orientation of the phase and group velocities. For cutoff frequency, the group velocity of these waves vanishes, whereas the phase velocity remains finite. It has been shown that among large quantities of symmetric and antisymmetric acoustic Lamb modes in isotropic plates only some of them have the properties of backward waves near the cutoff frequency. As for acoustic waves of higher orders propagating in piezoelectric plates, a few papers theoretically predicted the possibility of the existence of backward waves in such materials as lithium niobate, potassium niobate, high symmetric crystals of class C6v. However, the investigation of influence of different mechanical and electric boundary conditions on the properties of backward acoustic waves in piezoelectric plates has not been provided. Therefore, the purpose of this paper is theoretical investigation of the influence of nonconducting and nonviscous liquid on properties of the backward acoustic Lamb and shear-horizontal waves of the higher orders in the plates of various piezoelectric crystals. The materials under study were lithium niobate and potassium niobate.

Statement of Contribution/Methods

In this work the theoretical study of backward acoustic waves of higher order in structure "liquid - piezoelectric plate" was performed. For analysis of wave propagation we used the motion equation, Laplace's equation, and constitutive equations for piezoelectric medium and liquid, and appropriate mechanical and electrical boundary conditions. The dependencies of the velocity and attenuation of the waves under study were found.

Results/Discussion

As a result of the performed analysis the conditions of existence of backward waves in piezoelectric plate contacting with liquid were obtained. It has been found, for example, that the presence of liquid on the surface of the Y-X lithium niobate plate leads to the reducing of the parameter hf (h – plate thickness, f – frequency) region where S1 backward wave is exist

P3A1-10

8:00 am **A Conservative Edge-free and Corner-free Finite Difference Method Formulation for Analysing Mass-loading Problems in Three Dimensions**

Ireka Ikenna[1], Mebratu Fenta[1], **alireza baghai-wadji**[2]; [1]*Department of Mathematics and Applied Mathematics Mathematics, University of Cape Town, Cape Town, South Africa,* [2]*Electrical Engineering, University of Cape Town, Cape Town, South Africa*

Background, Motivation and Objective

It is desirable to gain a deeper understanding of the mass-loading phenomenon in micro-acoustic devices beyond customary brute-force application of the Finite Element Method (FEM). The gained insights are expected to allow the design of more accurate approximate techniques in addition to illuminating the underlying physical phenomenon itself. At last year's conference a method was proposed which eliminated the corner-points from the analysis by applying the spectral domain Finite Difference Method (FDM) to the mass-loading problem in two dimensional (2D) models of rectangular metallic electrodes. The superiority of the method against an optimized FEM code was firmly established.

Statement of Contribution/Methods

This paper extends last year's work in three aspects. i) The method applies to 3D models of massive electrodes. ii) The technique permits anisotropic elastic media. iii) The geometrical constraints imposed by rectangular shape of the electrodes will be relaxed. Each of these steps deserves particular attention. a) The transition to three dimensions introduces discontinuity of the normal derivatives not only at the corners but also along the edges. The proposed theory eliminates all the edge- and corner points from the analysis. This result will be presented for the first time in literature. b) The inclusion of the anisotropic property has been realized via diagonalization of the elasto-dynamic governing equations. This idea extends existing formulations in the FDM applications. c) The geometrical flexibility has been enabled by adapting the conservative finite difference formulation to vector fields.

Results/Discussion

Thin or thick, rectangular or non-rectangular, isotropic or anisotropic electrodes attached to elastic substrates have been analysed using the proposed edge-free corner-free finite difference formulation. The numerical results have been tested against numerical data obtained by customized FEM software specifically developed in the lab.

P4A1 - Sensors & Applications I

4th floor

Thursday, October 22, 2015, Posters displayed 08:00 am - 05:00 pm. Authors must be present at their poster from 9:30 - 10:30am (odd number posters) and 14:30 – 15:30pm (even number posters).

Chair: **Mauricio Pereira da Cunha**
University of Maine

P4A1-1 _____

8:00 am **Investigation of langasite surface acoustic wave pressure sensors with a structure of reinforcing its pressure sensitivity**

Honglang Li[1], Yabing Ke[1], Yiyu Zhao[1], Lina Cheng[1], Shitang He[1]; *[1]Institute of acoustics, China, People's Republic of*

Background, Motivation and Objective

Langasite (LGS) surface acoustic wave (SAW) pressure sensors can be utilized as battery-free wireless sensors in harsh environments (e.g., rotating cars and truck tires, hermetically sealed chambers) [1]. Much theoretical and experimental works has been performed to analyze its pressure sensitivity of sensors with the structure of a sealed cavity adjacent to a substrate and uniform pressure loading, which indicate that large size and small height of substrate are beneficial to reinforce the pressure sensitivity. However this methods are impractical for application. A structure to reinforce the pressure sensitivity is utilizing a deforming force applied to the substrate at one point so that to enlarge the pressure-induced deformation[2]. This structure has already adopted for quartz substrate. Its application for LGS substrate have not been studied yet.

In this paper, LGS SAW pressure sensors utilizing the above second structure is investigated. The FEM and perturbation method are adopted to analyze its pressure sensitivity. Experiments are also performed to verify the theory.

Statement of Contribution/Methods

In theory, a FEM model of the above second structure is build to analyze the pressure-induced deformation. With the strain and stress derived from the FEM model, the pressure sensitivity can be derived by the perturbation method.

In experiment, the package of sensors adopts the above second structure. Three resonators with propagation angles of 74°, 80° and 80° respectively in Z-cut LGS substrate are adopted to measure the temperature and pressure together.

Results/Discussion

Fig.1 shows the experimental pressure response at different temperature, and the experimental and theoretical temperature response. The experimental and theoretical pressure sensitivity are about 0.04MHz/MPa and 0.046MHz/MPa respectively. Experimental results agree well with theoretical results, which demonstrate the accuracy of theory.

This work firstly investigates the LGS SAW pressure sensors utilizing the structure of high sensitivity in theory and experiment. Problems including bad pressure response at high temperature and not high pressure sensitivity need further research.

[1] Scott C. Moulzolf, et al., IEEE Ultrason. Symp. Proceedings. 2012: 1224-1227.

[2] Victor Kalinin, et al., IEEE Ultrason. Symp. Proceedings. 2003: 1412-1415.

(a)   (b)
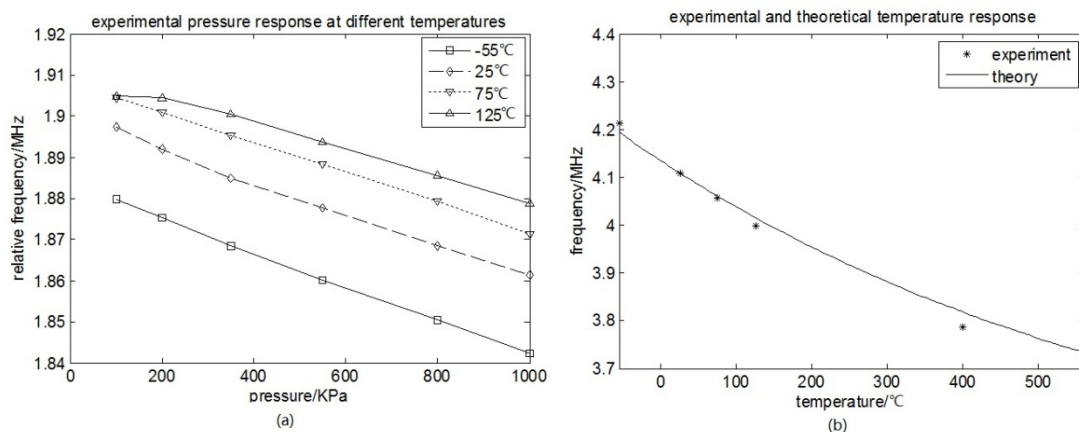
P4A1-2 _____

8:00 am **Development of SAW current sensor based on the magnetomechanics effect**

Yana Jia[1], Wen Wang[1], Xinlu Liu[1], **Shitang He**[1]; *[1]Chinese Academy of Sciences, Institute of Acoustics, Beijing, China, People's Republic of*

Background, Motivation and Objective

SAW current sensor exhibits some excellent properties as fast response, simple structure, strong anti-jamming, long working-life, and low cost, especially the wireless and passive measurement. The developed SAW current sensor is composed of a differential delay line oscillator, and a rare earth giant magnetostrictive TbDyFe film coated onto the sensing device as the magnetic sensitive material (Fig. 1). The response mechanism of the sensor utilizing magnetomechanics effect were investigated theoretically, high sensitivity, large dynamic range and good linearity were observed in the calculation.

Statement of Contribution/Methods

TbDyFe film was deposited along the SAW propagation path of the sensing device by RF magnetron sputtering. Because of the magnetomechanical nature of TbDyFe film, magnetostrictive strain and ΔE effect are induced by the magnetic field from the desired current, hence, resulting in the changes of the TbDyFe film thickness, young's modulus, and following the shift of the SAW phase velocity. The sensor signal was characterized by using the differential oscillation frequency. Referring to the theory of acoustic wave propagation in layered medium and the effective dielectric constant method, the response mechanism of the TbDyFe coated SAW current sensor is

performed.In the sensor experiments, the current is created by the Helmholtz coil, and the differential oscillation frequency signal is picked by using the frequency acquisition module.

Results/Discussion

Fig. 2 (a) shows the SAW dispersion depending on the various current intensity of 0, 300A, 600A and 900A. The SAW phase velocity depending on current intensity with different TbDyFe film thickness of 0.2 um, 0.3 um, 0.4 um and 0.5 um are described in Fig. 2 (b). Larger sensor response will be achieved when higher operation frequency and larger TbDyFe thickness are applied. With the increase of the current intensity, the SAW phase velocity decreases monotonically, linear sensor response will be expected. The current sensitivity of 45.3771 KHz/A in the range of [0,900A] can be concluded theoretically in case 0.5um TbDyFe thickness and 500Mhz operation frequency are applied. The experimental results will be shown soon.
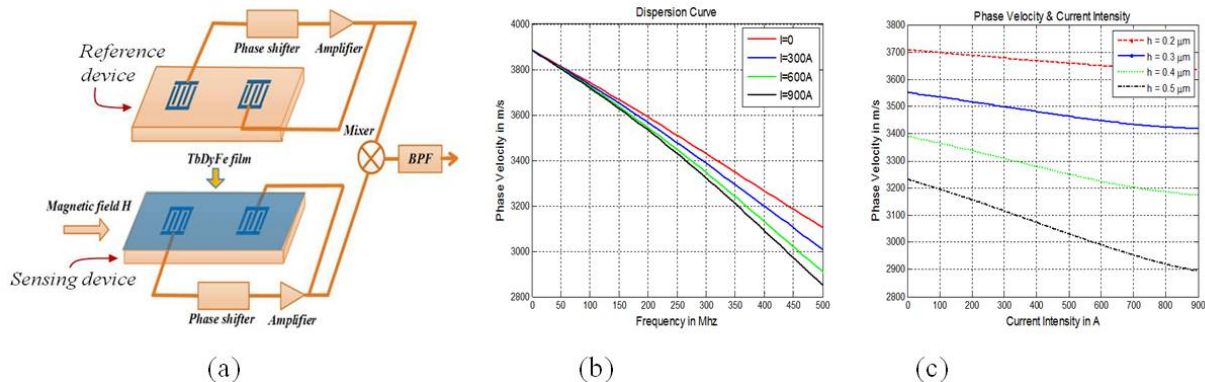
Fig. 1 (a) Scheme of SAW current sensor, (b) SAW dispersion depending on the various current intensity, and (c) SAW velocity change depending on TbDyFe film thickness

P4A1-3

8:00 am   Development of practical ball surface acoustic wave trace moisture analyzer by undersampling

Toshihiro Tsuji[1], Toru Oizumi[1], Nobuo Takeda[1], Singo Akao[1], Yusuke Tsukahara[1], Kazushi Yamanaka[1]*; [1]Tohoku University, Sendai, Japan*

Background, Motivation and Objective

Ball surface acoustic wave (SAW) sensor is expected to realize a compact, fast, and sensitive trace moisture analyzer[1] by temperature compensation using two-frequency measurement (TFM)[2]. The TFM uses harmonic devices, where relative delay time change at the third harmonic frequency is subtracted by that at the fundamental frequency. However, the measurement systems were expensive for the requirement of high-speed analog-digital converter (ADC) or double systems of heterodyne circuits. In this study, we aim to solve the problem by undersampling (US).

Statement of Contribution/Methods

In the TFM system using US (Fig.1), a transmission signals to the sensor (f_1=80MHz, f_2=240MHz) synchronizes with a clock of ADC (f_s=100MHz). US generates aliasing outputs expressed by f_{image}=|f-Nf_s|, where f represents f_1 or f_2, and N is a non-zero integer. The aliasing outputs at f_{u1} and f_{u2} corresponding to f_1 and f_2, respectively, are extracted by band-pass filters (BPFs). In the experiment, US and BPFs were simulated by a decimation of oversampling (OS) waveform (5GHz) by a factor of 50 and a wavelet transform with the Gabor function (γ=50), respectively.

Results/Discussion

Figure 2 shows the waveforms observed at positions A-D in Fig.1. A is OS waveform and B is BPF one with a bandwidth of 0.15f_2. The degradation of signal-to-noise ratio by US (C) was significantly improved by the wavelet transform (D). An application to trace moisture measurement is shown in Fig.3. The temperature compensation was attained by the subtraction of outputs between f_{u2} and f_{u1} (Fig.3(b)), and the sensor response comparable to the case of OS was obtained even when using US (Fig.3(c)). Thus, practical ball SAW trace moisture analyzer could be developed by US.

Fig. 1 TFM system using US in ball SAW sensor
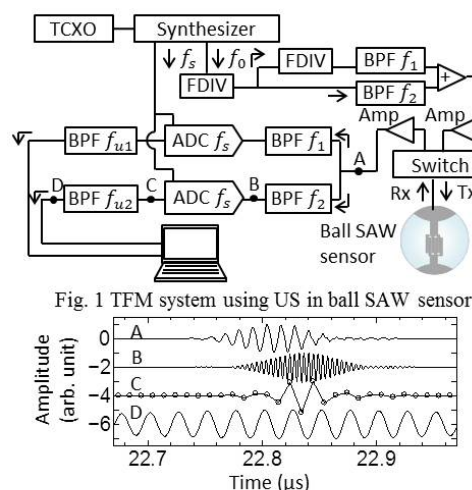
Fig. 2 Change in waveform by US simulated at A-D in Fig.1
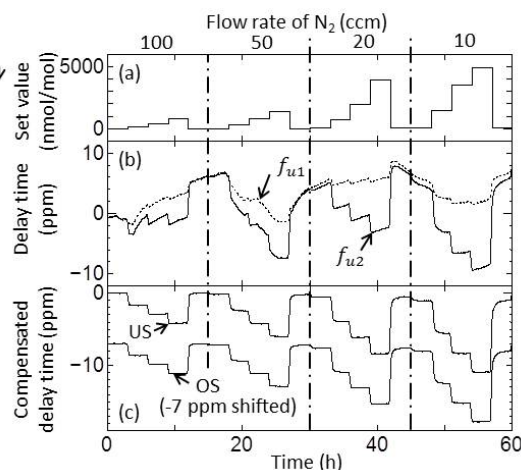
Fig.3 Temperature compensation (a)set value (b) US outputs (c) compensated outputs of US and OS

P4A1-4 _____

8:00 am   Stabilization of SAW atomizer for a wearable olfactory display

Kazuki Hashimoto[1], Takamichi Nakamoto[1]; *[1]Tokyo Institute of Technology, Kanagawa-Ken, Japan*

Background, Motivation and Objective

An olfactory display, a gadget to generate odors and to deliver them to a user can be useful in human interface. In our olfactory display, micropumps provide several kinds of odor liquids to the SAW device, followed by the atomization based on the SAW streaming. A user can sniff the smell immediately due to the atomization, as is shown in Fig.1. However, the atomization was not stable enough to be used for an olfactory display.

Statement of Contribution/Methods

When we atomized odor liquid by the SAW device, atomization capability deteriorated in a few tens of seconds. We measured the temperature of the SAW device in operation, and then it was found that it reached more than 60 Celsius degrees in 10 seconds. We hypothesized that SAW velocity change due to its temperature variation caused the resonance frequency shift. Thus, we constructed frequency control system where the temperature of the SAW device is measured and is sent to a CPU core in a FPGA. Then CPU core determines adequate frequency based on calibration data collected in advance and sends compensated frequency value to direct digital synthesizer module in the FPGA, which generates the driving signal of SAW device.

Results/Discussion

We evaluated the system by a quartz crystal microbalance sensor, since its oscillation frequency decreases with the amount of adsorbed droplets due to atomization. We used water as a sample liquid since its atomization can be visually observed. It was found from Fig.2 that atomization deteriorated 15 seconds after starting SAW device in operation without the compensation, whereas atomization using the compensation system did not stop. Thus, we concluded that constructed compensation system worked well and should be embedded to our wearable olfactory display.
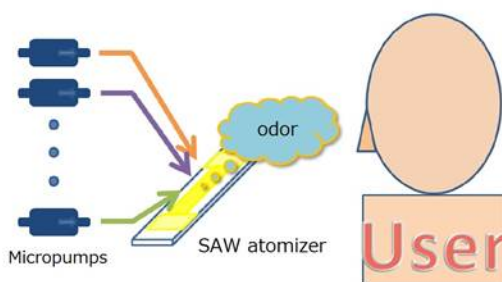
Fig1.Basic idea of our olfactory display
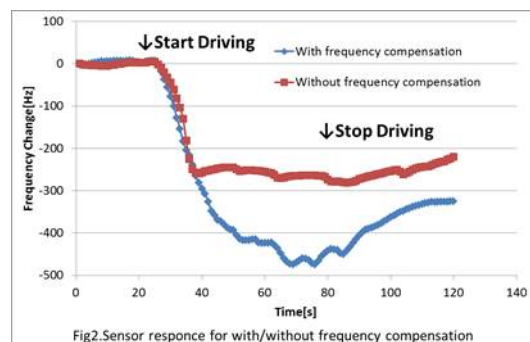
Fig2.Sensor responce for with/without frequency compensation

P4A1-5 _____

8:00 am   Conductivity measurement of liquid by SH-SAW sensor consisting of IDT/(11-20) oriented ZnO film/silica glass substrate

Shoko Hiyama[1], Takahiko Yanagitani[2], Shinji Takayanagi[1], Mami Matsukawa[1]; *[1]Wave electronics research center, Laboratory of Ultrasonic Electronics, Doshisha university, Kyoto, Japan, [2]Waseda University, Tokyo, Japan*

Background, Motivation and Objective

Because SH-SAW can propagate without the energy leakage into liquid, it is suitable for the liquid sensor to measure conductivity. (11-20) oriented ZnO films whose c-axis is oriented parallel to the substrate plane can excite SH-SAW. We have demonstrated the excitation of SH-SAW using the ZnO film[1]. At the electrically conductive interface, SH-SAW velocity decreases due to the weak of piezoelectric stiffening effect. Therefore, the conductivity of liquid can be detected as the SAW velocity change. In this study, we detected the electrical conductivity of liquid using the SH-SAW sensor.

Statement of Contribution/Methods

Our numerical simulation provided that the IDT/(11-20) ZnO (0°, 90°, 55°)/silica glass substrate structure had the highest K^2 value[2]. The (11-20) oriented ZnO film were grown by a sputtering system. IDT electrodes consistied of 54 finger pairs with the wavelength of 23 μm and propagation path of 3 mm. To keep solutions on propagation path, a pool made of silicone rubber was fabricated between the transmitter and receiver IDTs. SH-SAW excitation was observed at 138 MHz by a network analyzer. We input a signal by a digital signal generator, and observed an output signal by an oscilloscope. Then, SH-SAW velocity changes due to conductivity were calculated from arrival times of output signal. The input signal was a eight cycle sinusoidal wave electric pulse at 138 MHz with an amplitude of 2 V_{p-p}. KCl solutions with different conductivity (5.9×10^{-3} to 11.2 S/m) were prepared.

Results/Discussion

Fig. 1 (a) shows the changes of SH-SAW velocity due to conductivity from experiment and theoretical calculation. SH-SAW velocity decreased as the conductivity of KCl solution increased. This tendency correspond to the theoretical SH-SAW velocity changes. Fig. 1 (b) shows the theoretical energy loss and the change of the maximum amplitude due to conductivity. The amplitude is at minimum at a certain conductivity. This tendency also correspond to the theoretical energy loss. Fig. 1 shows that this SH-SAW sensor was driven by the weak of stiffening effects. This sensor can detect conductivity around 1 S/m. The measurement accuracy will be enhanced and more conductivity solution will be measurement.

[1] T. Yanagitani, et al., *IEEE TUFFC.*, **52**, 3140 (2005).

[2] A. Tanaka, et al., *IEEE TUFFC*, **55**, 2709 (2008).
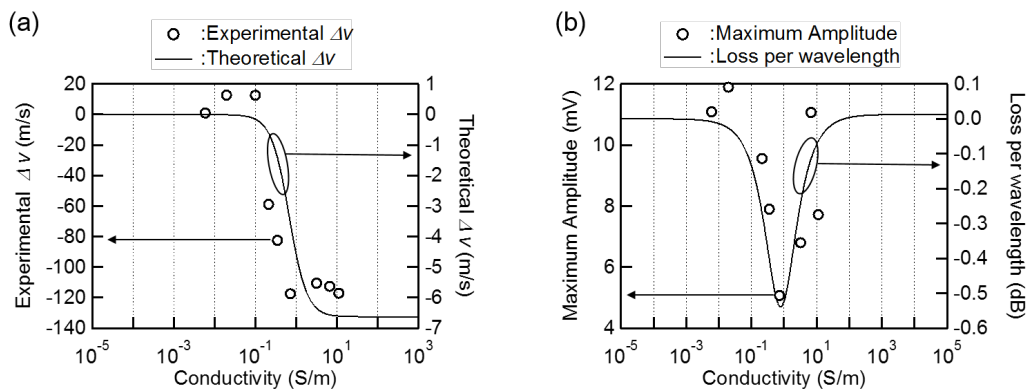
Fig. 1 (a) Experimental and theoretical SH-SAW velocity changes as a function of the electrical conductivity.
(b) Maximum amplitude and loss per wavelength as a function of the electrical conductivity.

P4A1-6

8:00 am **Currently extracting title from uploaded file...**

Ivan Antcev[1], **Sergei Bogoslovsky[1]**, Gennadiy Sapozhnikov[1], Sergei Zhgoon[2], Alexander Shvetsov[2]; *[1]Joint Stock Company "NPP "Radar mms", St Petersburg, Russian Federation,* *[2]MPEI, Moscow, Russian Federation*

Background, Motivation and Objective

Implantable temperature sensors find application in surgery and traumatology. The main problem of implantable sensors is the electromagnetic wave propagation loss inside biological objects. The other problem is the requirement of high measurement accuracy that is in the range of 0.1 degree C.

Statement of Contribution/Methods

Compact biologically compatible sensors have been designed and fabricated on the basis of single crystal quartz. Two separate approaches were adopted. The first approach uses a pair of SAW resonators for the frequency range of 915 MHz. The quartz cut is 70°Y and the orientations are 70°Y-90°X for the BGS wave and 70°Y-80°X for the Rayleigh wave (the TCF difference is close to 140 ppm/°C). The second approach uses a single 5.28 MHz bulk wave resonator made with Y-cut (the TCF is greater than 80 ppm/°C). Both types of sensors are hermetically sealed with a proprietary flip-chip technique using metallized frames at the die edges. Miniature antennas with different designs were incorporated into the packages and tested. Variants of the interrogators with a single common antenna and with separate antennas for the transmitter and for the receiver were studied. In order to increase the working distance interrogating signals were designed to maximize the reflected energy, the regimes of initial and precise reading were implemented. Interrogators use the signal processing approach based on optimum solving rule for discrete signal classification.

Results/Discussion

Extensive testing of both systems brought a lot of valuable practical information on their performance. Experiments on sheep have shown the possibility of reading information from the sensors with the implantation depth up to 20 cm. The specifications of the system stated that the working distance from the sensor location to the interrogator antenna may reach up to 60 cm. This distance to the implanted sensor required the interrogator average and impulse power levels of 10 mW and 2 W respectively. Because of the lower level of the electromagnetic wave propagation loss at lower frequencies inside living objects and of the higher resonator Q-factor the system based on BAW resonators has shown better performance in this range of distances. The paper discusses the details of the system implementation for SAW and BAW sensors and their operation characteristics comparison.

Embodiments of 915 MHz SAW sensors

Embodiments of 5.28 MHz BAW sensors

P4A2 - Microacoustic Resonators

4th floor

Thursday, October 22, 2015, Posters displayed 08:00 am - 05:00 pm. Authors must be present at their poster from 9:30 - 10:30am (odd number posters) and 14:30 – 15:30pm (even number posters).

Chair: **Maximilian Pitschi**
              TDK Corporation

P4A2-1 _____

8:00 am   Optimized Response of AlN Stack For Chipscale GHz Ultrasonics

Jason Hoople[1], Justin Kuo[1], Jeffrey Soon Bo Woon[2], Navab Singh[2], Amit Lal[1]; [1]*Electrical and Computer Engineering, Cornell University, USA,* [2]*Institute of Micoelectronics, Singapore*

Background, Motivation and Objective

In this paper we present designs of an aluminum nitride (AlN) based mechanical stack for transmit/receive applications in silicon. By optimal design of the mechanical layer thicknesses and properties the channel gain, center frequency and bandwidth can be controlled to allow for the use lower gain and power electronics to conduct a number of on-chip ultrasonic information processing operations. Previously, we reported on the use of thin film AlN transducers on silicon chips for on-chip ultrasonic communication. Within all these applications it is important to design the mechanical structure to best couple acoustic energy from the transducer (AlN) to the channel (silicon). Though this is a classical design problem for NDE applications the frequency range (>1GHz) and fabrication techniques (microfabrication) allow for a greater degree of freedom due to the precise control of thicknesses. The design choices for electrode materials is limited in order to maximize electromechanical coupling of the piezoelectric thin film. In this paper we present numerical modeling of the transducer stack, and experimental verification.

Statement of Contribution/Methods

The aluminum nitride process flow was developed in conjunction with the Institute for Microelectronics Engineering (IME) in Singapore, this stack can be seen in Fig(A) below. Certain materials in the stack, such as molybdenum metal electrodes, were fixed due to IME's processing capabilities; however the thicknesses and additional passive layer materials could still be modified. Analytical MATLAB simulations were run to verify the effect of each layer on the voltage transfer function of a pulse echo. These simulations were verified in the FEA software PZFlex.

Results/Discussion

Materials on the back side of the transducer reduced the center frequency and bandwidth of the transducer, however using these materials shifts the center frequency and allows transducers with lower output impedance to be used at those frequencies. Additionally the bottom layers demonstrate behavior consistent with a quarter wave length matching layer. While these layers do not affect the center frequency of the devices they do affect the bandwidth. An example of one layer is Fig (D). Original aluminum nitride samples from IME resulted in return signals on the order of 200 µV at 1.3 GHz, the new stack produces return signals of 9 mV at 1.3 GHz.

A: Composition of stack

B: Material Properties

	Characteristic Impedance (MRayls)	Speed of Sound (m/s)
SiO_2	12.7	5760
Mo	58.2	5657
AlN	36.4	8500
Si	17.4	7470

C: Experimental Results 1.3 GHz T/R
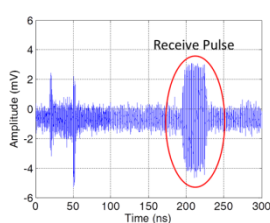
D: Top SiO2 Thickness Effects
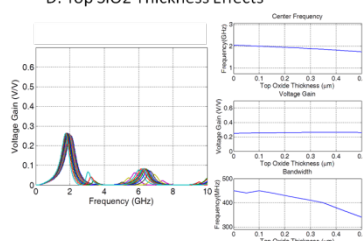
P4A2-2 _____

8:00 am   Low Loss and Wide Band Filters Using New Dispersive☐@Interdigital Transduceres with Floating Electrodes

Kazuhiko Yamanouchi[1]; [1]*Acoustic Wave Labo.,Ltd, Japan*

Background, Motivation and Objective

In order to obtain the high performance of Surface Acoustic Wave (SAW) devices, it is very important for the interdigital transducer (IDT) to be made the unidirectional ones (UIDT) with SAW materials. Especially the mobile communication and UWB communication systems require the high efficient unidirectional IDT for the phase linear, wide band, low-loss filters at GHz-ranges.

Statement of Contribution/Methods

Many types of unidirectional transducers are proposed. That is (1) UIDT with Multi-phase shifters, (2)Single Phase UIDT, (a) Mass loading and Coupling difference internal reflection type UIDT, Thin film grating type UIDT, Acoustic distribution internal reflection ,and Grating strip reflection type UIDT,(c) Natural UDT using anisotropy of substrate and (d) electrode reflection type UIDT, et al. The UDTs of (1) have some demerits of phase shifters and air gap electrodes, meander line with high resistivity. Also The UIDT of (1) have some demerits to be used the multi-photolithograhy technqeues. The UDTs of (3) have some demerits of low transduction and small reflectivity, with many spurious signals and using the special substrate.

Dispersive interdigital transducers (DIDT) have sharp cut-off and flat wide band frequency characteristics. Unfortunately, the conventional dispersive interdigital transducers have the uni-directionalty only to the down-chirp direction (DUDIDT). Therefore the non-dispersive filter with low insertion loss can not be obtained. If the up-chirp unidirectional dispersive IDT (UUDIDT) are obtained, phase linear and the very low loss filters are obtained by combining DUDIDT and UUDIDT.

In this paper, DUDIDT and UUDIDT were investigated by using floating electrodes with the open and shorted electrodes inserted between the inderdigital transducers.

The large deirectivity of DUDIDT is obtained by inserting the open floating electrode between the negative and positive electrodes. The UUDIDT is obtained by inserting the open and short floating electrodes between the divided negative electrode, and the negative and positive electrodes.

Results/Discussion

The theoretical results showed the large directivity around 12dB in the floating electrode type DUDIDT compared with the directivity of 6dB in the only DUIDT. The short and open floating electrode type UUDIDT showed the up-ward directivity of 10dB compared with the down-ward dirctivity of 6dB in the conventional DUDIDT. The filters with non-dispersive, phase linear, flat band of wide bandwidth of 3%-30%, sharp cut off and low insertion loss of below 2dB are obtained. The experimental results show almost the good agreement with the theoretical ones.

P4A2-3

8:00 am   Acoustic Micro-resonator Utilizing Hemispherical Air Cavity for Sensitivity Enhancement

Anton Shkel[1], Eun Sok Kim[1]; [1]Electrical Engineering, University of Southern California, Los Angeles, CA, USA

Background, Motivation and Objective

Acoustic transducers with high quality-factor are preferable in a variety of applications including ranging, ultrasonic imaging, and acoustic signature detection. This paper proposes coupling a mechanical resonator with an air cavity as a passive amplification approach for enhancing desirable characteristics.

Statement of Contribution/Methods

We report the modelling, feasibility study, parametric design, and fabrication approach for an acoustic resonator amplified by an air cavity. The device features a cantilever with sputter-deposited zinc oxide for piezoelectric sensing coupled to a microfabricated hemispherical chamber. The coupled air-acoustic microsystem exhibits the Helmholtz acoustic resonance effect, amplifying the sensed pressure wave. A cross section of the proposed device is shown in Figure 1a.

A multiphysics model was developed for both the cantilever and air cavity. An optimized design was derived for the intended 22.6 kHz resonance frequency of the air-acoustic system, with paddle dimension of D=348 μm, thickness of t=2 μm, and a hemisphere radius of R=825 μm.

The acoustic sensor is fabricated using a two-wafer approach (Figure 1ai). An SOI wafer with 2 μm thick device layer is used for fabrication of the cantilever-based piezoelectric sensing element. The SOI's buried oxide layer serves as an etch-stop for KOH backside etching. The sensing layers consist of evaporated Al electrodes, sputter-deposited ZnO, and PECVD SiN for electrical isolation. DRIE is used for the final release of the paddles.

The Helmholtz resonance chamber is fabricated on a second wafer (Figure 1aii). Silicon nitride serves as an etch mask for HNA isotropic wet etching of silicon. Gold is deposited on the hemisphere and the wafers are fused by eutectic bonding between gold and silicon (Figure 1aiii).

Results/Discussion

Preliminary measurements indicated that sensitivity of cantilever-based acoustic sensors can be increased by a factor of 13.9 with the use of a matched resonant air cavity. Acoustic simulations in COMSOL demonstrated that the differential pressure on the cantilever is amplified by about 41 dB at the resonance frequency, indicating a potential sensitivity enhancement by two orders of magnitude (Figure 1b). These preliminary results support the use of air-acoustic amplification as a potential mechanism for optimization of acoustic sensors.
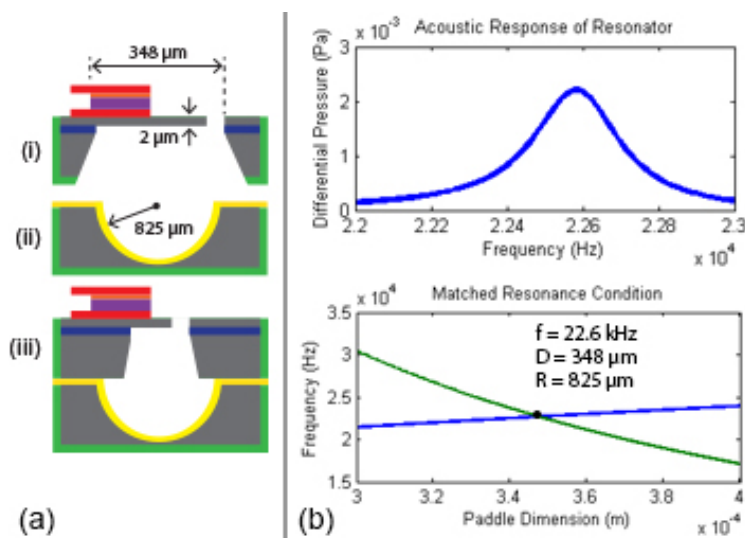
P4A2-4

8:00 am   High-Q piezoelectric Lamb wave resonators based on AlN plates with chamfered corners

Chih-Ming Lin[1], Jie Zou[1], **Yung-Yu Chen**[2], Albert Pisano[3]; [1]Mechanical Engineering, University of California, Berkeley, CA, USA, [2]Mechanical Engineering, Tatung University, Taipei, Taiwan, [3]Mechanical and Aerospace Engineering, University of California, San Diego, CA, USA

Background, Motivation and Objective

Piezoelectric resonators usually exhibit a large coupling coefficient which leads a small motional resistance, but unfortunately they show a medium Q. Various loss mechanisms existing in piezoelectric resonators have been investigated recently where the interfacial loss, causing from the stress jump at the interface and the anchor loss, representing the acoustic energy leakage via the support tethers, are considered as the primary loss mechanisms. The metal-to-piezoelectric stress can be minimized with the optimized deposition conditions. The anchor loss can be reduced by different approaches, such as positioning the tethers at nodal locations in the vibration mode or using different materials for the support and vibrating body to form acoustic impedance mismatch.

Statement of Contribution/Methods

In this work, a novel Lamb wave resonator utilizing an AlN plate with chamfered corners is investigated to reduce the anchor loss without introducing unwanted spurious modes. Fig. 1(a) illustrates an AlN LWR based on a rectangular plate. As shown in Fig. 1(b), an AlN LWR composed of the same transducer configuration, but a chamfered-corner plate is used to reflect the acoustic waves toward the plate. The perfectly matched layer (PML)-based FEA approach is employed to analyze the anchor Q of the LWRs. The obvious displacement occurring in the tether indicates a part of acoustic energy is lost via the tether vibrations so the predicated anchor Q of the conventional LWR is as 5,997. The simulated anchor Q of the AlN LWR using the chamfered-corner plate can be significantly increased to 21,555.

Results/Discussion

In order to have large electromechanical coupling of the S0 mode in the plate, a 5-μm-thick AlN plate is employed herein. Fig. 2 compares the measured frequency responses of the resonators with 13 finger electrodes on the rectangular and chamfered AlN plates. The 829.4-MHz LWR on the chamfered- corner plate yields a loaded Q of 3,016, representing a 1.48× enhancement over the 829.3-MHz LWR on the rectangular plate. The effective coupling of the piezoelectric LWR on the AlN plate with chamfered corners is 1.00%, slightly lower than 1.03% observed in the rectangular one, presenting that the thick AlN plate increases the electromechanical coupling of the S0 mode. More importantly, the resonance frequency of the AlN LWR on the chamfered-corner plate is almost the same as that on the rectangular plate, verifying the chamfered corners don't introduce unwanted spurious modes.

Figure 1: Illustration of (a) a Lamb wave resonator (LWR) employing a rectangular AlN plate and (b) a LWR using an AlN plate with chamfered corners.
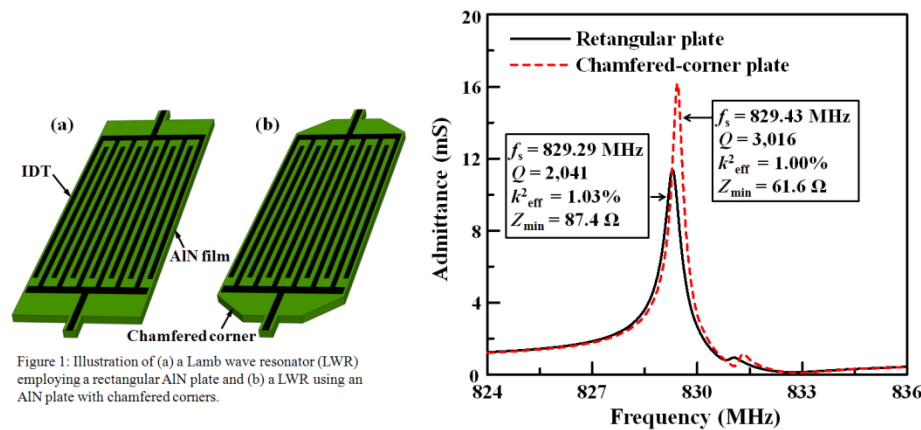
Fig. 2 Comparison of measured frequency responses of the AlN LWRs on the rectangular and chamfered-corner plates.

THURSDAY POSTER

P4A2-5

8:00 am   HBAR AS HIGH FREQUENCY HIGH STRESS GENERATOR

Tanay Gosavi[1], Evan MacQuarrie[1], Gregory Fuchs[1], Sunil Bhave[2]; [1]*Cornell University, NY, USA,* [2]*Analog Devices Inc, Woburn, MA, USA*

Background, Motivation and Objective

In this paper we report on High-Overtone Bulk Acoustic Resonator (HBAR) as high stress generator by measuring f-Q product of tones and overtones from room temperature to 80K. We show that due to high Q HBARs can generate up to 20MPa AC stress with small drive voltages at GHz frequencies. This capability is instrumental in manipulating spin-defect qubits in materials like Diamond [1] and Silicon Carbide[2] and is key for developing solid-state wafer-scale hybrid quantum systems.

Statement of Contribution/Methods

Circular HBARs of radii 250μm and 75μm were fabricated on Diamond chips and SiC wafers.Also HBARs of radius 75μm were fabricated on Silicon for benchmarking. The dimensions of HBARs are shown in Fig 1A. Fig 1B and 1C show f-Q products of HBARs made in all three materials measured at temperatures 295K and 80K over a range of frequencies. Qs shown are computed from the measured S11 spectra using Q-Circle method [3].

Results/Discussion

In Fig 1B (295K) f-Q for HBARs in SiC scales with frequency but are an order of magnitude lower then the theoretical limit. Measured f-Q for Diamond were approximately two orders of magnitude lower than theoretical limit. This may be due to the small chip size which is a practical limitation of Diamond and NV-center technology. Fig 1C (80K), shows an outstanding 10x improvement in f-Q of SiC HBAR. Plotting Q of the 3.4GHz resonance in SiC over the temperature range (Fig 1D), we see that Q increases proportional to $1/T^{-1.556}$. The exponent -1.556 indicates that Q is partially anchor loss limited and that the resonator is in Landau-Rumer Regime [4][5]. Stress generated by the HBAR shown in Fig 1E, calculated using an analytical model, prove that HBARs are efficient high frequency high stress transducers. It's important to note that amplitude of stress in HBARs doesn't increase linearly with Q; this has also been verified using FEA simulations.

In conclusion, our study of f-Q and Q of acoustic modes in different semiconductors identifies SiC HBAR as a clear winner for generating stress at GHz frequencies.

References

[1] E. R. MacQuarrie, et al., Physical Review Letters 111, 227602 (2013).

[2] A. L. Falk, et al., Physical Review Letters 112, 187601 (2014).

[3] D. A. Feld, et al., Ultrasonics Symposium 2008, pp. 431.

[4] R. Tabrizian, et al., Transducers'09, pp.2131,2134.

[5] V. B. Braginsky, et al., Systems with Small Dissipation, The University of Chicago Press, 1985.
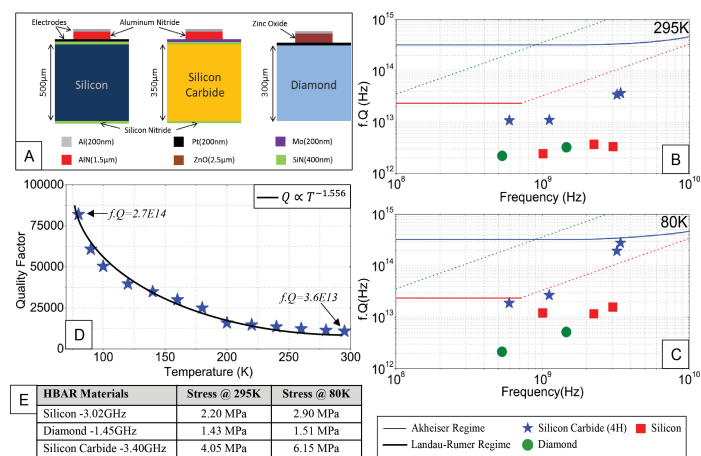
Figure 1: A) Device geometries for HBARs fabricated on (100) Silicon, (8" of 1120)) 4H-Silicon Carbide, and Type IIA CVD (100) Diamond substrates. Frequency-Quality factor product vs. Frequency graphs of HBAR resonances measured at temperatures 295K (B), and 80K (C). Data points on the plots represent measured resonances of Silicon(red), Diamond(green) and Silicon Carbide(blue) HBARs. The lines on the graph represent the two different phonon-phonon dissipation limited fQ values calculated for these materials at room temperature. In case of Diamond we only see Landau-Rumer regime of damping as it has high thermal conductivity. D) Quality Factor v/s Temperature of 3.4GHz mode of Silicon Carbide HBAR. Quality factor scales from 10800 at 295K to 82000 at 80K. E) Calculated peak stress generated by HBAR resonators on different substrates for a 1V drive.

THURSDAY POSTER

P4A3 - Materials & Propagation

4th floor

Thursday, October 22, 2015, Posters displayed 08:00 am - 05:00 pm. Authors must be present at their poster from 9:30 - 10:30am (odd number posters) and 14:30 – 15:30pm (even number posters).

Chair: **Sergei Zhgoon**
National Research University Moscow Power Engineering Institute

P4A3-1

8:00 am   **Investigation on Surface Acoustic Wave propagation for a non-planar piezoelectric thin film device**

Mohanraj Soundara pandian[1], Eloi Marigo Ferrer[1], Muniandy Shunmugam[1], Rubiyatulniza Binti Hussain[1], Charlie Tay Wee Song[1], Jazril Bin Jamil Din[1], Chan Buan Fei[1], Venkatesh Madhaven[1], Arjun Kumar Kantimahanti[1], Aamir Farooq Malik[2], Varun Jeoti[2]; *[1]SilTerra Malaysia Sdn Bhd, Kulim, Kedah, Malaysia, [2]Universiti Teknologi PETRONAS, Malaysia*

Background, Motivation and Objective

The actual trend in microelectronics industry to expand the capabilities of the standard CMOS technologies into other areas opens new opportunities for new devices and new challenges to face. SAW devices fabricated in a CMOS compatible technology using Aluminum Nitride (AlN) thin film possesses high potential in the field of integrated SAW sensors. AlN thin film process is well established and fully integrated with the circuits for MEMS and FBAR applications. However not fully understood and explored for SAW applications. In this paper we present a study on the surface acoustic wave propagation performance and coupling coefficient for a non-planar AlN thin film device.

Statement of Contribution/Methods

As shown in the Figure 1a, piezoelectric AlN thin film is deposited on top of Interdigital Transducers (IDT) by Physical Vapor Deposition (PVD) process. The effect on SAW properties and its mechanism is studied in detail. The test vehicle consists of a 1μs delay line of two ports with an acoustic wavelength (λ) of 4μm. First the IDT layer is deposited, patterned and etched employing three different thicknesses t1 > t2 > t3. Then AlN 1μm thick is deposited, patterned and etched to form the electrical access to the IDT layers. X-SEM image of the fabricated devices is shown in Figure 1b, non planar AlN layer is clearly seen.

Results/Discussion

Employing a network analyzer to characterize the delay line, the S21 magnitude graph from Figure 2a is obtained for the three different IDT thickness conditions. Extracting the resonance frequency and computing the piezoelectric coefficient through Y11 parameter, the graph from Figure 2b is obtained. First and second conditions correspond respectively to thicknesses with high non conformal topography whilst the third one has almost flat AlN layer topography. This conformal effect plays a major role on the crystal lattice orientation of the piezoelectric layer, modifying their acoustic and electrical properties. Maximum frequency achieved is 1.02GHz which provides 1.3μs of delay between input and output ports. The coupling coefficient of 0.26% falls in the range reported for AlN on Si subtrate. The measurements prove that a conformal AlN deposition provides a frequency closer to the theoretical value with a higher coupling coefficient.
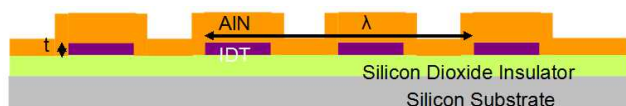
Figure 1a
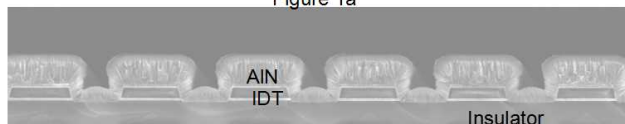
Figure 1b
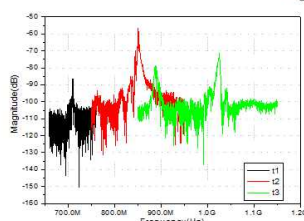
Figure 2a
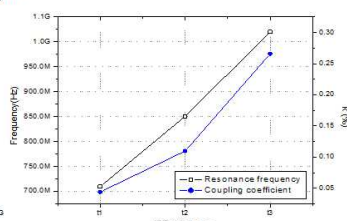
Figure 2b

P4A3-2

8:00 am   **Effect of Sintering temperature on the Dielectric and Piezoelectric Properties of (Na0.525K0.443Li0.037)(Nb0.883Sb0.08Ta0.037)O3 Ceramics for piezoelectric Actuators**

Gwang Min Lee[1], Ju Hyun Yoo[1,2], Yeong Ho Jeong[3], Lark Hoon Hwang[1]; *[1]semyung university, Korea, Republic of, [2]electrical engniering, semyung university, jecheon, chungbuk, Korea, Republic of, [3]Korea National University of Transportation, Korea, Republic of*

Background, Motivation and Objective

Recently, lead-based piezoelectric ceramics have been widely used because of their excellent electrical properties such as piezoelectric actuators, piezoelectric sensors and transducers. However, PZT-based piezoelectric ceramic causes a serious problem for the environment and human health. Accordingly research on lead-free piezoelectric compositions has become more and more active in recent years. Lead-free piezoceramics have received considerable attention as a promising candidate for the PZT ceramics because of their high phase transition temperature and excellent electromechanical coupling factor(kp) properties. However, it is difficult to obtain the dense NKN ceramics because of high hygroscopic and the volatilization of the alkali element during their sintering process.

Statement of Contribution/Methods

Therefore, Sintering temperature of the ceramic should be decreased to prohibit the volatilization of them. In this study, in order to decrease sintering temperature, Bi2O3 and Fe2O3 as sintering aids were added. Also, in order to find the optimum sintering temperature, dielectric and piezoelectric properties were investigated as a function of sintering temperature change.

Results/Discussion

In this study, (Na0.525K0.443Li0.037)(Nb0.883Sb0.08Ta0.037)O3 (abbreviated as NKL-NSTO3-Bi2O3-Fe2O3) ceramics were fabricated as a function of sintering temperature by the traditional solid state sintering process in order to develop the excellent lead-free piezoelectric ceramics.

The results are as follows: For the NKL-NSTO3-Bi2O3-Fe2O3 ceramics sintered at temperatures of 1020~1060¡É, the improved piezoelectric and dielectric properties of d33=343 pC/N, kp=0.520, Qm=56.1 and ¥år=1473 was obtained for specimens sintered at 1040¡É for 3h. These results show that the sintering temperature plays an important role in piezoelectric properties.

P4A3-3

8:00 am   Plate Modes in Langasite

Natalya Naumenko[1]; [1]*Acousto-optical Research Center, National University of Science and Technology, Moscow, Russian Federation*

Background, Motivation and Objective

Resonators based on Lamb waves and other modes propagating in thin crystal plates or piezoelectric films find widening application in the last few years. The simplicity of plate mode excitation with common interdigital transducers combined with recent achievements in fabrication of thin crystal plates makes this type of devices attractive for wireless communication systems and sensors. Compared to surface acoustic waves (SAWs) plate modes provide much wider ranges of wave characteristics in the same material and allow optimization of device performance via variation of orientation, plate thickness and geometrical parameters of electrode structure. The previously reported Lamb wave resonators using AlN films and thin plates of LiNbO$_3$ demonstrated superior performance compared to SAW resonators using the same materials. Langasite (LGS), which is attractive for high-temperature applications, is less investigated as potential material for plate mode resonators, though thin plates of LGS have been already successfully fabricated in 90-ties [1]. This paper studies plate modes in LGS in order to estimate their typical and best characteristics and find optimal orientations for plate mode resonators.

Statement of Contribution/Methods

The characteristics of plate modes propagating in a plate of thickness h under Pt grating were extracted from the admittance functions simulated at different temperatures. Analysis starts from zero-order quasi-symmetric (qS0) and quasi-antisymmetric (qA0) modes propagating along X-axis in rotated Y-cuts of LGS. At the fixed thickness $h/2p$=0.3, where p is a periodicity of a grating, both modes demonstrate zero temperature coefficient of frequency (TCF) in certain orientations and maximum coupling 1.7%, which grows in thinner plates up to 2.2%. Zero TCF can be combined with k^2 about 1.5%. Due to the LGS symmetry, shear horizontally polarized (SH) modes have negligible coupling in Y-cuts, X-propagation, but high coupling for X+90° propagation direction. In the latter orientations only SH waves can be efficiently excited. The coupling of SH1 mode can be enhanced by deposition of a metal electrode at the plate bottom surface. With variation of a plate thickness k^2≈1.8% can be combined with nearly zero TCF and V≈12,000 m/s. The variations of the plate mode characteristics with LGS thickness are analyzed in YX and YZ cuts as typical examples of YX and Y,X+90° cut families.

Results/Discussion

The study of zero-order and higher-order plate modes propagating under Pt grating in rotated Y-cuts of LGS with X- and X+90° propagation directions revealed that electromechanical coupling of these modes can be 4-5 times higher than maximum SAW coupling in LGS. In thin LGS plates zero TCF can be combined with k^2>1.8%. Orientations providing optimal combinations of wave characteristics were found for qA0, qS0 and high-velocity SH1 modes.

[1] M. Sato, K. Moroishi, S.Ishigami et al., Proc. 1996 IEEE Int. Freq. Contr. Symposium, pp. 379-383.

P4A3-4

8:00 am   Measurements of Acoustical Physical Constants for Ca$_3$Nb(Ga$_{0.75}$Al$_{0.25}$)$_3$Si$_2$O$_{14}$ Single Crystal Using the Ultrasonic Microspectroscopy System

Yuji Ohashi[1], Yuui Yokota[1], Tetsuo Kudo[1], Shunsuke Kurosawa[1], Kei Kamada[1,2], Akira Yoshikawa[1,2]; [1]*Tohoku University, Japan,* [2]*C&A Co., Japan*

Background, Motivation and Objective

Ca$_3$NbGa$_3$Si$_2$O$_{14}$ [CNGS] single crystal has attractive features such as higher electro-mechanical coupling factors, no phase transition up to melting point around 1300°C, comparable temperature coefficient of frequency (TCF), and smaller impedance as compared to quartz. Therefore, CNGS is one of promising piezoelectric materials for combustion sensor and small-size oscillator with low electrical consumption. Recently, however, prices of raw materials composed of rare elements are rising because of an increase of their demands for various applications and there is an attempt to reduce usages of such rare elements in various fields. Especially, Ga$_2$O$_3$ powder is extremely expensive among composing elements of CNGS. In the case of La$_3$Ta$_{0.5}$Ga$_{5.5}$O$_{14}$ [LTG] crystal, on the other hand, there were some reports about Al doping to Ga site in the LTG crystal and the Al doping improved some piezoelectric properties such as electrical resistivity and piezoelectric constant. So we have tried to grow Al-doped CNGS crystal by the Czochralski method resulting in successful growth of 1 inch Ca$_3$Nb(Ga$_{0.75}$Al$_{0.25}$)$_3$Si$_2$O$_{14}$ [CNGAS] bulk crystal.

In this study, we measured acoustical physical constants (elastic, piezoelectric, and dielectric constants, and density) for CNGAS single crystal by the ultrasonic microspectroscopy (UMS) technology.

Statement of Contribution/Methods

From the CNGAS single crystal ingot mentioned above, we prepared 5 substrates with 2-mm thick (X-, Y-, Z-, 40.24°Y-, 144.98°Y-cut) for measuring bulk wave velocities. For these specimens, we measured longitudinal and shear wave velocities around room temperature with the UMS system. Dielectric constants were determined from measurements of capacitances for X- and Z-cut plates with 0.5-mm thick. Density was measured for the remained parts without any cracks based on the Archimedes′ principle.

Results/Discussion

Measured density was 3967.3 kg/m^3 corresponding to 3.7% decrease of that for CNGS. Elastic constants and piezoelectric constants were determined from measured bulk wave velocities. It is noteworthy that piezoelectric constants increase by 5.9% in e$_{11}$ and 39.7% in e$_{14}$ as compared with those of CNGS due to Al substitution effect exhibiting e$_{11}$=0.374 C/m^2 and e$_{14}$=-0.415 C/m^2. From this result, it is hoped that acoustic devices with higher coupling factor and lower cost will be made by higher doping of Al in CNGS.

P4A3-5

8:00 am   Loss Reduction of Leaky Surface Acoustic Wave by Loading with High-Velocity Thin Film

Shoji Kakio[1], Keiko Hosaka[1]; [1]*Interdisciplinary Graduate School of Medicine and Engineering, University of Yamanashi, Japan*

Background, Motivation and Objective

Leaky surface acoustic waves (LSAWs) offer a number of beneficial characteristics such as a larger electromechanical coupling factor (K^2) and higher phase velocity than Rayleigh waves. However, LSAWs have an inherent attenuation because they lose energy by continuously radiating the bulk wave into the substrate. For the longitudinal-type LSAW, the authors have shown, theoretically and experimentally, that its attenuation can be reduced by loading the substrate with an aluminum nitride (AlN) thin film

---

with a higher velocity than that of the substrate [1]. In this study, the propagation properties of LSAWs on LiNbO$_3$ (LN) substrates loaded with an AlN thin film were investigated theoretically and experimentally. 10° Y-X LN with a large K^2 for the LSAW was used as the substrate.

Statement of Contribution/Methods

First, the phase velocity and attenuation of the LSAW on a rotated Y-X LN substrate with an AlN thin film were calculated by a numerical method. The independent elastic constants of the AlN thin film were assumed to be c_{11} and c_{44} because AlN thin films deposited by RF magnetron sputtering in this study were nonpiezoelectric and polycrystalline. Next, the propagation properties of an LSAW on a 10° Y-X LN substrate were measured using an interdigital transducer (IDT) pair. The single-electrode IDT pair with period λ of 8 μm was fabricated using a 0.015-λ-thick Al film. To evaluate the propagation loss *PL*, samples with propagation path lengths of *L*=10, 25, and 50 λ were fabricated. Then, the AlN thin film was deposited on the IDT pair and the metallized propagation path by RF magnetron sputtering.

Results/Discussion

From the theoretical calculation, it was found that the rotation angle from the Y axis giving zero attenuation shifts toward 0° from around 60° as the film thickness is increased for the metallized interface. This means that the anisotropy of the substrate can be changed by loading it with a high-velocity thin film. When the rotation angle was 10°, the calculated attenuation was reduced to zero from the 0.36 dB/λ for the case without a film by loading the substrate with an AlN thin film approximately 0.1 λ thick. Then the attenuation increased with film thickness. The calculated phase velocity increased monotonically with film thickness. The film thickness dependence of the measured *PL* was similar to the calculated value. After the deposition of the AlN thin film 0.125 λ thick, the measured insertion loss of the IDT pair with *L*=50 λ decreased from the 29.7 dB for the sample without a film to 9.6 dB, and the measured *PL* decreased from the 0.40 dB/λ for the sample without a film to 0.02 dB/λ.

[1] F. Matsukura and S. Kakio: Jpn. J. Appl. Phys. 53 (2014) 07KD04.

P5A1 - Transducer Materials

4th floor

Thursday, October 22, 2015, Posters displayed 08:00 am - 05:00 pm. Authors must be present at their poster from 9:30 - 10:30am (odd number posters) and 14:30 – 15:30pm (even number posters).

Chair: **Yasuhito Takeuchi**
Asahikawa Medical University

P5A1-1

8:00 am   Novel Spring-Mass Matching Layer Fabrication for Ultrasound Transducers

Mikel Gorostiaga[1], Matthias C. Wapler[1], Ulrike Wallrabe[1]; *[1]Department of Microsystemsengineering, Laboratory for Microactuators, IMTEK - University of Freiburg, Freiburg im Breisgau, Germany*

Background, Motivation and Objective

Spring-mass matching layers consisting of a thin polymer layer ("massless spring") covered by a metal foil ("incompressible mass") can be designed to any desired acoustic impedance by adjusting the layer thicknesses. In the past, readily available polymer and metal foils have been bonded together with epoxy, which affects the response due to the epoxy thickness (e.g. ~8 µm) and the limited thickness control of available polymer foils. This problem worsens with decreasing spring layer thicknesses at high frequencies (e.g. 10 µm PDMS at 4MHz). In view of these limitations, we present a new method to produce well-controlled spring-mass layers.

Statement of Contribution/Methods

The new approach is to spin-coat Sylgard184 PDMS directly on top of a Stainless Steel foil, which has been previously coated with Dow-Corning 92-0023 primer for enhanced PDMS-metal bonding. After curing, the PDMS-metal composite is structured with an UV laser to avoid the edge effect of the coating and match the geometry of the transducer. Finally, the PDMS-metal layer and the transducer are bonded together using the same PDMS in a press to ensure a constant thickness of the spring layer, a flat metal foil and a single, homogeneous polymer layer.

This was demonstrated with a 35µm metal/20µm polymer structure on top of a 500µm PZT transducer with 20mm diameter. The layers were flat up to a small tilt of 0.3mrad. In spite of this, the electric impedance of the transducer measured in air agreed well with KLM model simulations, when accounting for ~10% depolarization due to the soldering of the connecting wires and their parasitic impedance.

Results/Discussion

A novel method for the creation of pure spring-mass matching layers has been developed by spin-coating PDMS (spring) on top of steel foils (mass), and structuring the resulting composite with an UV laser. This process offers a straightforward, repeatable and controllable way to create matching layers without epoxy bonding. Due to the difficulty of handling very thin metal foils (<10µm), the approach is limited to frequencies below approximately 10MHz, after which other fabrication methods such as PVD or sputtering are more suitable.
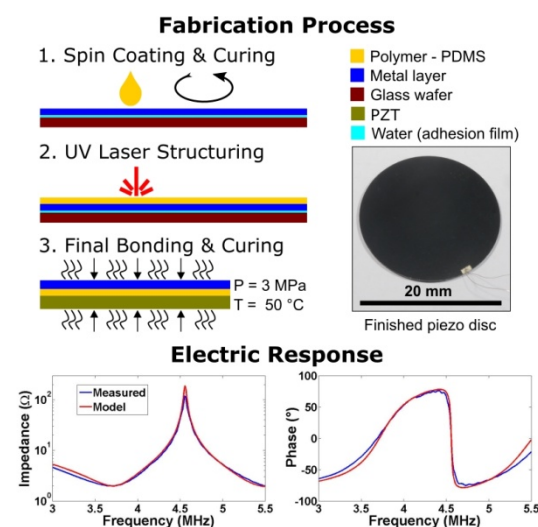
P5A1-2

8:00 am   Additive manufacture of impedance matching layers for air-coupled ultrasonic transducers

Sivaram Nishal Ramadas[1,2], Michael Hunter[1], John Thornby[3], Chris Purssell[4], Simon Leigh[4], Steven Dixon[1]; *[1]Physics, University of Warwick, United Kingdom, [2]Elster Instromet, Belgium, [3]WMG, University of Warwick, United Kingdom, [4]School of Engineering, University of Warwick, United Kingdom*

Background, Motivation and Objective

A key problem in designing an efficient ultrasonic transducer for operating in a low acoustic impedance medium such as air, is the large impedance mismatch between the active piezoceramic material and the load medium. While matching layers (typically micro-balloon loaded epoxy) can be added to the face of the piezoelectric material, their reliability and associated manufacturing difficulties can impact upon the longevity and cost of the resultant transducer. In this paper, we adopt an advanced additive manufacturing technique, known as micro-stereolithography (µSL) and develop a new µSL material system to produce impedance matching layers for use in air-coupled ultrasonic transducers.

Statement of Contribution/Methods

A custom built µSL apparatus, employing an inverted method of fabrication whereby the uncured, liquid photopolymer is held in a tray with an optically transparent base and a silicone layer on its uppermost surface, was used in this study. The tray is mounted above a structured light source (an LED digital light projector with a digital micro-mirror device) to photo-polymerise the resin at addressable locations on the two-dimensional focal plane of the source. Photo-curable resins for the µSL comprise of a

diacrylate functionalised oligomer, acrylate functionalised cross linker and a photo initiator. In order to reduce the acoustic impedance of the µSL matching layers, glass micro balloon filler was added to the photo-curable resin.

Results/Discussion

Numerous trials were carried out to determine optimum µSL parameters (such as exposure time, and layer thickness). The fabricated matching layers were tested non destructively using X-ray CT, and it was observed that the layer porosity is consistent at about 28% and there were polymer rich boundaries between layers. A series of transducers with µSL matching layers were fabricated and their behaviour was analysed experimentally in the lab. The prototype device performance is consistently comparable or better (both in terms of sensitivity & bandwidth) with matching layers produced conventionally – while using only very little raw materials without any wastage. Matching layers were also printed directly on an active piezoceramic substrate to eliminate any additional gluing required in the transducer assembly. This is a significant benefit not only to improve the energy transfer into the load medium, but also in improving the reliability of the complete transducer fabrication process, as faults in the matching layer bond line is often one of the main modes of failure in an ultrasonic transducer. Results to date are very encouraging, and could result in a robust, reproducible, economical and improved fabrication method for industrial air-coupled transducers. The µSL technique could potentially eliminate (or at-least minimise significantly) any post processing required (i.e. lapping, machining, and gluing) in a typical matching layer fabrication process.

P5A1-3

8:00 am **1-3 piezocomposites based on super-cell structuring for transducer applications**

Remi Rouffaud[1], **Franck Levassort[1]**, Mai PhamThi[2], Claire Bantignies[3], Marc Lethiecq[1], Anne-Christine Hladky-Hennion[4]; [1]*GREMAN UMR 7347 CNRS, François-Rabelais University, Tours, France, [2]Thales Research & Technology, Palaiseau, France, [3]VERMON SA, Tours, France, [4]ISEN, IEMN UMR 8520 CNRS, Lille, France*

Background, Motivation and Objective

In ultrasound transducers, the most popular fabrication method for 1-3 piezocomposites (i.e. aligned piezoelectric rods in a polymer matrix) is the « Dice and Fill » Method (DFM) where lateral periodicity p is introduced which leads to the occurrence of lateral modes. These spurious modes can drastically damage the performance of the device if they appear near its thickness (h) mode frequency, thus limiting the effective frequency range. Several conditions were defined in the literature to reduce the influence of these modes, in particular minimum values of the ratio h/p according to the piezoelectric phase volume fraction. The modification of the rod shape, the minimization of the kerf value or a random distribution of rods were also studied but for in most of these cases, specific and costly manufacturing processes are required. In order to overcome these limitations while maintaining a good electromechanical efficiency for the 1-3 piezocomposites, a new fabrication method is proposed which is compatible with existing tools already employed for the DFM.

Statement of Contribution/Methods

The new fabricated 1-3 piezocomposite is partially regular but with a Super-Cell structure (13SC). The chosen cell shape allows numerical modeling to be performed (ATILA software) with periodic conditions and reasonable calculation time. The retained fabrication process is based on the lamination method [1]. The representative cell is composed of 5 rods with equivalent square sections. The proposed configuration is realized with 47% volume fraction of PZT and the matrix is epoxy resin. Two lateral periodicities as well as two different pitches in one direction are defined to minimize the effect of spurious modes. For comparison, two regular 1-3 piezocomposites, with the same materials, are fabricated by DFM using identical piezoelectric volume fraction and the two lateral periodicities values.

[1] F. Wang et al., Materials Chemistry and Physics, vol. 105, pp. 273-277, 2007.

Results/Discussion

In the experimental procedure, nine regular thinnings were carried out to increase the thickness frequency and thus study the evolution of the characteristics (bandwidth and sensitivity) of the three composites considered as a transducer, through the measurements of their electro-acoustic responses in water. This procedure covers, for the two regular piezocomposites, a h/p ratio between 2 and 0.8 where the lower limit of this ratio is theoretically defined at 1.25 for good operating conditions in thickness mode. For 13SC composite, the h/p range is lower according to the two lateral periodicity values. This study is performed in the frequency range 0.4-1.3 MHz. Experimental results confirm those obtained with the numerical simulations, showing that the 13SC composite can be used in this entire frequency range unlike regular composites, while keeping similar sensitivity and bandwidth.

P5A1-4

8:00 am **Design and Fabrication of Lead-free BNT Film High Frequency Ultrasound Transducers**

Wei Ren[1]; [1]*Electronic Materials Research Laboratory, Key Laboratory of the Ministry of Education, Xi'an Jiaotong University, China, People's Republic of*

Background, Motivation and Objective

Intravascular ultrasound (IVUS) has been used for diagnosis of coronary diseases. According to the outstanding transducer performance, $Ba_{0.5}Na_{0.5}TiO_3$ (BNT)-based piezoelectric materials are good candidates for the IVUS applications.

Statement of Contribution/Methods

In this paper, lead-free BNT piezoelectric 0-3 composite thick film has been employed to fabricate a linear array transducer. The BNT based transducer array has 2×16-element patterns with the length of 3 mm and width of 24 µm for each element. To reduce the cross-talk between the elements, the width between elements is designed at 12 µm. The PiezoCAD software has been employed to analyze the performance of the array.

Results/Discussion

The simulation results shows that the BNT film array has a center frequency of 82.87 MHz and a -6 dB bandwidth of 79.3%. In the process of fabrication of transducers, micro-machining technologies have been adopted. The thin films of Si_3N_4 and SiO_2, are used as etching masks, and patterned by reactive etching and buffered oxide etch (BOE), respectively. After that, the part of Si not covered by the patterned masks is etched by 30% KOH solution. BNT slurry being prepared by mixing BNT solution and BNT powder has been deposited on the substrate by spin coating and then thermally treated to obtain 0-3 composite thick film. Then by patterning the top electrode, Cr/Au, which is deposited by sputtering, and filling backing material, the kerfless linear array can be fabricated. The results indicate that the high-frequency BNT film array is a promising ultrasound transducer for IVUS and other medical applications.

P5A2 - Thick and Thin Films

4th floor

Thursday, October 22, 2015, Posters displayed 08:00 am - 05:00 pm. Authors must be present at their poster from 9:30 - 10:30am (odd number posters) and 14:30 – 15:30pm (even number posters).

Chair: **Yasuhito Takeuchi**
          Asahikawa Medical University

P5A2-1

8:00 am   (100)-Textured Lead-free KNN-based Thick Film for IVUS£¨>50MHz£©Imaging

benpeng zhu[1], Teng Ma[2], Yongxiang Li[3], Xiaofei Yang[1], K.kirk Shung[2], Qifa Zhou[2]; *[1]Huazhong University of Science and Technology, China, People's Republic of, [2]Department of Biomedical Engineering, NIH Transducer Resource Center, University of Southern California, USA, [3]Key Laboratory of Inorganic Functional Materials and Devices, Chinese Academy of Sciences, China, People's Republic of*

Background, Motivation and Objective

Intravascular ultrasound (IVUS) plays a critical role in diagnosing coronary artery disease which is one of the major causes of human morbidity and fatality. In order to enhance the imaging resolution, increasing IUVS central frequency to higher than 50MHz is thought to be an effective way, sacrificing to a certain extent the penetration depth. Up to now, only limited IVUS studies have been carried out at such high frequencies, because it is a great challenge to fabricate highly sensitive miniaturized transducers. Due to its excellent piezoelectric behaviors, lead-based piezoelectric layer has been the most popular for IVUS (>50 MHz) applications. However, the toxicity of lead is a severe issue in view of the environmental protection and human body safety. Therefore, the development of lead-free piezoelectric layer to replace lead-containing one for IVUS (>50 MHz) imaging is of urgent importance.

Statement of Contribution/Methods

In this study, we present the preparation of 35um free-standing (100)-textured KNN-based thick film with enhanced piezoelectric property, the fabrication process of a highly sensitive miniaturized high frequency (>50MHz) transducer and the imaging of the rabbit aorta.

Results/Discussion

The (100)-textured KNN-based thick film exhibited similar piezoelectric behavior to lead containing materials: a longitudinal piezoelectric coefficient (d33) of ~150 pm/V and an electromechanical coupling coefficient (kt) of 0.42. Based on this thick film, a 52 MHz side-looking miniature transducer with a bandwidth of 61.5% at -6 dB was built for intravascular ultrasound (IVUS) imaging. As shown in Fig.1, in comparison to 40 MHz PMN-PT single crystal transducer, the rabbit aorta image had better resolution and higher noise-to-signal ratio, indicating that lead-free (100)-textured KNN-based thick film may be suitable for IVUS (>50 MHz) imaging.

Fig. 1. IVUS imaging of healthy rabbit aorta from (A) 52 MHz KNN-based thick film transducer; and (B) 40 MHz PMN-PT single crystal transducer
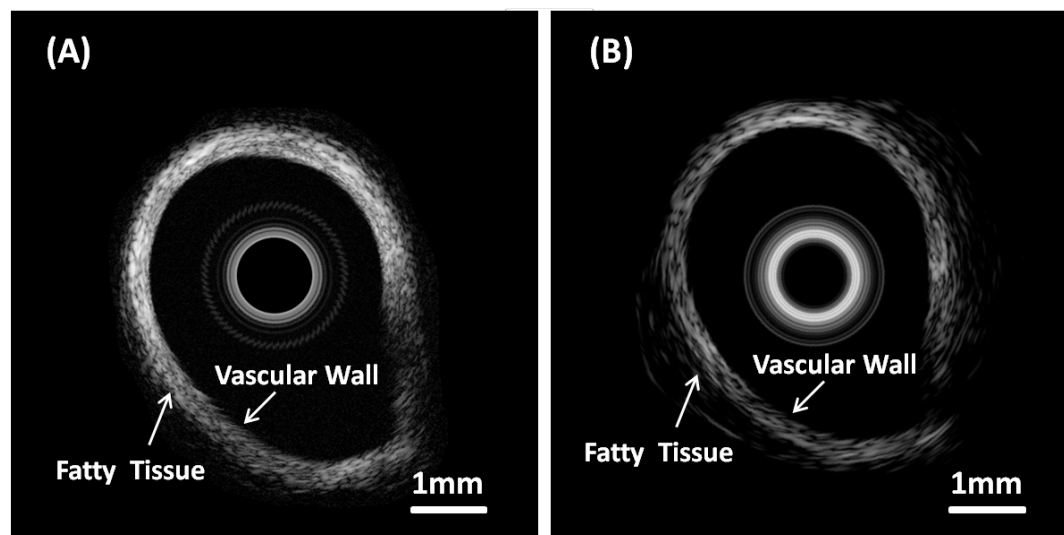
P5A2-2

8:00 am   Domain Engineering in Epitaxial Ferroelectric Thin Films

Mahamudu Mtebwa[1], **Nava Setter**[1]; *[1]Ceramics Laboratory, EPFL, Lausanne, Switzerland*

Background, Motivation and Objective

The term Domain Engineering is commonly used to describe the process of poling ferroelectric single crystals with the poling field applied off the polar direction of the crystal. Such poling typically results in a poled multi-domain structure. Domain engineered crystals of relaxor-ferroelectrics such as PMN-PT and PZN-PT show exceptionally high piezoelectric response and are used in medical transducers.

Moreover, some evidence exists in the literature that domain engineered crystals, particularly BaTiO3, exhibit enhanced piezoelectric activity (d33 and d31) that increases as a function of domain wall density: The smaller is the distance between domain walls, the higher is the piezoelectric coefficient.

Ferroelectric thin films typically exhibit reduced piezoelectric coefficients relative to the bulk crystals. There are several reasons for this, not the least is the clamping of the domain walls by the substrate. Domain engineering in ferroelectric thin films has been hardly explored so far, while this process might improve the piezoelectric response in a similar way it does in bulk crystals. We present our investigation of this problem.

Statement of Contribution/Methods

Highly tetragonal compositions of PZT were grown on (110) SrTiO3 monocrystalline substrate, coated with La0.7Sr0.3MnO3 (LSMO) conductive film epitaxially grown on the substrate and having thickness of 10 nm. The so-grown PZT films were smooth, tetragonal monocrystalline films. The films consisted each of a single domain with polarization pointing away from the substrate (inclined by 45% to it). Voltage in the direction towards the substrate was applied through a conductive AFM tip which was then scanned across the film.

Results/Discussion

By varying the thickness of the film (in the range 30- 100 nm), the applied voltage, and the scanning direction, various domain patterns developed, including periodic patterns of domains (Fig 1), sometimes with width of domain stripes as small as 13 nm. Piezoelectric measurements are being performed by piezo-force microscopy and by conventional d33 measurements using samples covered by Pt top electrode. Results will be presented. So far, enhancement of piezoelectric properties has not been demonstrated. The methodology to obtain periodic patterns of ultrafine domains was well developed and will be reported.

Fig 1: Periodic domains in tetragonal (110) PZT
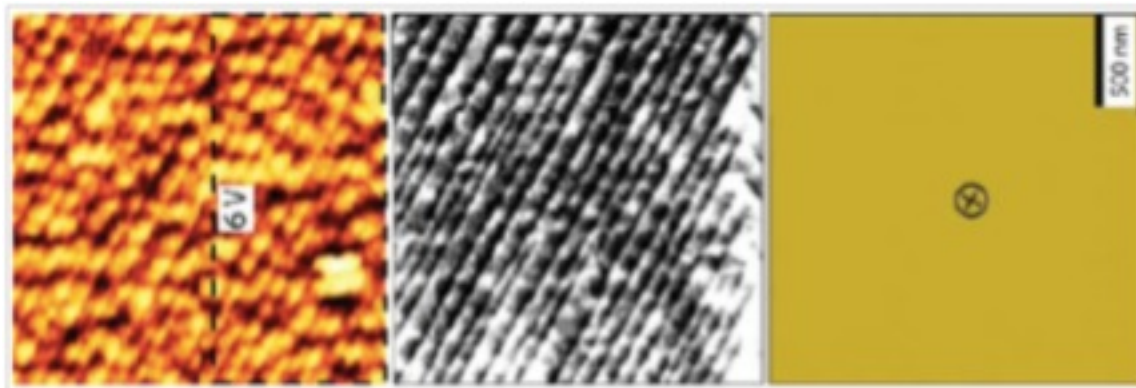
P5A2-3 _____

8:00 am　　**High power piezoelectric characteristics of KNbO3 thick films by hydrothermal method.**

Mutsuo Ishikawa[1], Yousuke Uchida[1], Motoko Shibuya[1], Nobuaki Kosuge[1], Minoru Kurosawa[2], Hiroshi Funakubo[2]; *[1]Toin Univ. of Yokohama, Japan, [2]Tokyo inst. of Tech., Japan*

Background, Motivation and Objective

Recently, high-frequency ultrasonic transducer is proposed for medical applications using piezoelectric crystal. For high power application such as ultrasonic cleaner or actuators, it is important to have high piezoelectric constant and higher limitation of vibration velocity.

Therefore we measured limitation of vibration velocity of Potassium Niobate (KN) thick films by the hydrothermal method that is reported for low temperature process and without polarization treatment. The limitation of vibration velocity obtained was 5m/s, it was twice as higher the hard type PZT.

Statement of Contribution/Methods

The KN films were deposited at 240 ºC on (100)c Nb-SrTiO3 substrates by the hydrothermal method. An autoclave (PARR, 4748) that contained an inner vessel made of Teflon to resist high alkali solutions was utilized for the hydrothermal growth. A 20 ml solution of 10 mol/l KOH (Kantokagaku) and 1.0 g of niobium oxide powder (Nb2O5, purity 99.95%, Kantokagaku) were used as source materials of K and Nb, respectively. The (100)c Nb-SrTiO3 substrate was kept facing down with a Teflon folder in the inner vessel, and the above-mentioned source materials were mixed and placed in the autoclave. The autoclave was shut tight and placed in a constant-temperature oven (Yamato DS-400) maintained at 240 ºC for a hydrothermal chemical reaction. The thickness of KN films obtained was approximately 150 micro meters.

Next, ultrasonic transducers with thickness vibration mode were fabricated by the KN thick films that were separated from Nb-SrTiO3 substrate.

And vibration velocity of surface of the ultrasonic transducers were measured by Laser Doppler Velocimetry (Polytec OFV-3001).

Results/Discussion

The frequency characteristics were measured for the prototype ultrasonic transducer using hydrothermal KN 150 micro meters thick films. A peak was observed at approximately 10.3 MHz. The frequency response was analyzed using Mason's equivalent circuit. According to the result, the 10 MHz peak is excited by thickness mode of piezoelectric effect. Next, the limitation of the vibration velocity was measured. The obtained result was 5m/s at 1.5kVp-p. Moreover, Moreover, under the same conditions, the radiation ultrasound from the prototype ultrasonic transducer was over 4MPa in the degassed water. We will present the reason for the hydrothermal KN films are able to drive at large vibration velocity.

P5A2-4 _____

8:00 am　　**Fundamental Study on the Miniature Coiled Stator-UltraSound Motor with hydrothermally synthesized lead zirconate titanate poly-crystalline film transducer for medical applications**

Seiya Ozeki[1], Toshinobu Abe[1], Tadashi Moriya[2], Takasuke Irie[3], Minoru Kurosawa[4], Shinichi Takeuchi[1]; *[1]Clinical Engineering, Toin University of YOKOHAMA, Yokohama, kanagawa, Japan, [2]Tokyo Metropolitan University, Hino, Tokyo, Japan, [3]Microsonic Co., Ltd., Kokubunji, Tokyo, Japan, [4]Interdisciplinary Graduate School of Science and Engineering, Tokyo Institute of Technology, Yokohama, Kanagawa, Japan*

Background, Motivation and Objective

Recently, intravascular diagnosis like intravascular ultrasonography (IVUS) has been used clinically in medical field. The ultrasound probe should be rotated within the vessel for these medical applications. A driving device such as a motor for the ultrasound probe is placed outside the patient's body. A nonuniform rotation and the rupture of the shaft for rotating device occur owing to the undesired mechanical load. For this reason, the operating time should be limited to short time. Therefore we have developed a helical coil type ultrasound motor (CS-USM: Coiled Stator Ultrasound Motor) using piezoelectric ceramic transducer as a miniature ultrasound motor for rotating the ultrasound probe for use in blood vessels in order to solve these problems. Also, we previously reported the torque-revolution speed characteristics of the CS-USM with the diameter of about 2.5 mm, which was fabricated by using a piezoelectric ceramic transducer.

 However, it is difficult to fabricate smaller CS-USM than our current CS-USM with the diameter of about 2.5 mm. Therefore, we tried to develop the smaller CS-USM by using hydrothermally synthesized lead zirconate titanate polycrystalline film instead of piezoelectric ceramic transducer in this study. Because the advantage of hydrothermal synthesis is that the lead zirconate titanate poly-crystalline film can be deposited easily even on the surface of tiny titanium substrate.

Statement of Contribution/Methods

Hydrothermally synthesized lead zirconate titanate poly-crystalline film was deposited on the titanium substrate in order to fabricate the driving ultrasound transducers for the new CS-USM. Material of the acoustic waveguide was stainless steel or titanium, and the substrate of the driving ultrasound transducers was the titanium, and they were welded by spot welding. We measured the revolution speed of fabricated CS-USM by using a laser Doppler Velocimeter: LDV. The continuous sinusoidal waves were applied to the fabricated driving ultrasound transducer using hydrothermally synthesized lead zirconate titanate poly-crystalline film.

Results/Discussion

The operation of the fabricated CS-USM using hydrothermally synthesized lead zirconate titanate poly-crystalline film transducer was confirmed and its revolution speed of CS-USM were measured in this study. The maximum revolution speed of CS-USM with hydrothermally synthesized PZT film transducer was obtained at frequencies of 26.4, and 33.9 kHz. The measured maximum revolution speed of CS-USM was 1100 rpm. However, rotational speed of the fabricated CS-USM in this study was lower than the CS-USM using piezoelectric ceramic transducer. In addition, the torque of the CS-USM in this study was too small to measure. In order to improve the torque and revolution speed of the CS-USM, we should reconsider the structure of the CS-USM and deposition method of hydrothermally synthesized lead zirconate titanate poly-crystalline film.

P5A2-5

8:00 am   Electrical and Acoustic Characreization of Scandium Aluminum Nitride (ScAlN) Piezoelectric Micromachined Ultrasonic Transducers (PMUT)

Panu Koppinen[1], Sergey Gorelick[1], Feng Gao[1], James Dekker[1], Tommi Riekkinen[1], Alessandro Caspani[2]*; [1]Knowledge Intensive Products and Services, VTT Technical Research Centre of Finland Ltd, Espoo, Finland, [2]Dipartimento di Elettronica, Informazione e Bioingegneria, Politecnico di Milano, Milano, Italy*

Background, Motivation and Objective

Micromachined ultrasonic transducers (MUTs) are an emerging class of MEMS devices, which can be used in a wide variety of potential applications such as in gesture recognition and range finding, in medical applications and in personal healthcare as well as in different types of sensors based on ultrasonics such as gas sensors. The miniaturization of ultrasonic transducers provide several advantages which can make them attractive even for mobile applications, these are low power consumption, small size and good coupling to the medium (air or liquid). MUTs are divided into two different categories, CMUTs (capacitive micromachined transducers) and PMUTs (piezoelectric micromachined transducers). Typically, PMUT devices are fabricated either with aluminum nitride (AlN) or lead zirconium titanate (PZT). We will present a novel type of devices fabricated with scandium doped AlN (ScAlN). The main advantage of ScAlN is a stronger piezoelectric coupling than AlN, while it still has the same order of magnitude dielectric constant, and thus reduced parasitic capacitance of the device compared to e.g. PZT.

Statement of Contribution/Methods

Our PMUT device consists of a released membrane with SiO2/Mo/ScAlN/Mo stack, with SiO2 and ScAlN layer thickness of 1 um and bottom and top Mo electrode thicknesses of 150 nm and 250 nm, respectively. ScAlN film was sputter deposited on top of the bottom electrode with Sc concentration of 26%. In addition, we have also fabricated reference devices with AlN, which is a more conventional piezoelectric material. The reference AlN devices have the same stack thicknesses and electrode geometries as ScAlN

devices to allow us to make a feasible comparison of the acoustic and electrical properties of the devices. Devices were fabricated on a 6" (150 mm) wafers containing membrane diameters from 130 um to 240 um. Electrical impedance and acoustic transmission characteristics are measured on selected dies on different locations of the wafer to determine the process uniformity.

Results/Discussion

Typical resonance frequencies of the measured devices were from about 500 kHz up to 1.4 MHz. Electrical impedance measurements of the PMUT devices show about two orders of magnitude higher piezoelectric coupling factor k^2 for ScAlN devices compared to AlN devices with the same device geometry and stack thickness.

P5A2-6

8:00 am   Development of anti-cavitation hydrophone with hydrothermal PZT film -Estimation of durability-

Michihisa Shiiba[1,2], Nagaya Okada[3], Minoru Kurosawa[4], Shinichi Takeuchi[1]*; [1]Toin University of Yokohama, Japan, [2]Research Fellow of Japan Society for the Promotion of Science, Japan, [3]Honda Electronics Co., Ltd., Japan, [4]Tokyo Institute of Technology, Japan*

Background, Motivation and Objective

Recently, ultrasound treatment methods such as sonoporation for gene transfer, high-intensity focused ultrasound (HIFU) for cancer therapy and sono dynamic therapy (SDT) are developed and used actively. Furthermore, ultrasound cleaners and ultrasonic particle dispersion systems are used in the industrial field. There is a tendency that ultrasound is irradiated frequently in these applications. These acoustic field distributions should be measured with a hydrophone. However, electrodes or piezoelectric elements of the hydrophones were broken by effect of high sound pressure and acoustic cavitation when acoustic fields formed by ultrasound apparatus with high intensity ultrasound like ultrasound cleaner or HIFU device were measured by using normal commercial hydrophones. Therefore, it was difficult to measure such high intensity acoustic field by using normal commercial hydrophone.

The novel anti-cavitation hydrophones were fabricated by deposition of hydrothermally synthesized lead zirconate titanate (PZT) polycrystalline film on the reverse side of titanium front plate. These hydrophones were not damaged by measurement of acoustic field formed by HIFU device.

Statement of Contribution/Methods

We fabricated new hydrophones using titanium membrane front plate (acoustic receiving surface) and titanium backing material with specific acoustic impedance of 27 MRayl for measurement of high intensity ultrasound in this study.

A durability test on our fabricated anti-cavitation hydrophone was performed by exposure to the ultrasound acoustic field with the generation of acoustic cavitation in the water tank of an ultrasound cleaner (Honda Electronics HCL-280A) at 22.5 kHz. The maximum input electric power of the ultrasound cleaner is 48 W. Output voltages from the hydrophone under test were measured at 3.5 MHz for the durability test.

Results/Discussion

The receiving sensitivity of our fabricated hydrophone did no decrease even after ultrasound cleaner exposure for 5 hours. The frequency characteristics of the receiving sensitivity was not changed. The electrode (titanium membrane front plate) of our fabricated anti-cavitation hydrophone was not damaged at all even after sonication. However, the epoxy resin seal surrounding the edge of the titanium membrane front plate was dropped off by peeling from tip of the fabricated hydrophone. Elucidation of the problems of stable fabrication method of hydrophone are our near future works.

P5A2-7

8:00 am   **Influence of Tough Hydrophone Shapes with Titanium Front Plate and Hydrothermal PZT Thick Film on Distribution of Acoustic Bubbles around Focal Point of HIFU Transducer**

Nagaya Okada[1], Michihisa Shiiba[2], Minoru K. Kurosawa[3], Shinichi Takeuchi[2]; *[1]Research and Development Div., HONDA ELECTRONICS CO., LTD., Japan, [2]Department of Clinical Engineering, Faculty of Biomedical Engineering, Toin University of Yokohama, Japan, [3]Interdisciplinary Graduate School of Science and Engineering, Tokyo Institute of Technology, Japan*

Background, Motivation and Objective

Recently, ultrasound applications with the assistance of high-intensity ultrasound pulse are used increasingly in medical systems. It is necessary to measure the distribution of ultrasound intensity to ensure low-risk treatment. We have developed a pointed tough hydrophone by the deposition of a hydrothermally synthesized lead zirconate titanate (PZT) thick film with 16 μm on the reverse surface of Ti plate. The deposited film is protected from acoustic cavitation by the Ti plate. This hydrophone was prevented from damage at a high pressure field (15 MPa) at a focal point of a concave HIFU transducer driven CW with input power to the sound source up to 50 W. However, the acoustic bubbles are observed at a region of the concave transducer and the tough hydrophone at the focal point. These are caused by a standing wave because the shape of the tough hydrophone tip is flat with 3.5 mm in diameter. Accordingly, this study is aimed at influence of existence of the tough hydrophone on their ultrasound field and the spacial distribution of the acoustic bubbles.

Statement of Contribution/Methods

The influence of the tough hydrophone shapes on the spacial distribution of acoustic bubbles around focal area of the concave transducer was investigated using visualization by luminol and ultrasound system. Changing the acoustic bubbles was observed depending on hydrophone tips that have needle shape, curvature shape and lip stick shape compared to the tough hydrophone tip with flat surface installed at the focal point.

Results/Discussion

As the result of the visualization by luminol with existence of the tough hydrophone with flat shape tip, a stripe pattern derived from the standing wave was observed. Similarly, the trapping acoustic bubbles derived from the standing wave and moving acoustic bubbles derived from acoustic radiation forces were observed in figurer. By contrast, as the result of the observation using needle type hydrophone, the amount of the trapping acoustic bubbles reduced, while the moving bubbles remained and thinned in shape. The present shape of tough hydrophone tip was good use for low frequency ranges several tens kHz, whereas the influence of existence of tough hydrophone with round shape tip was reduced as compared to that with flat shaped tip at high frequency.
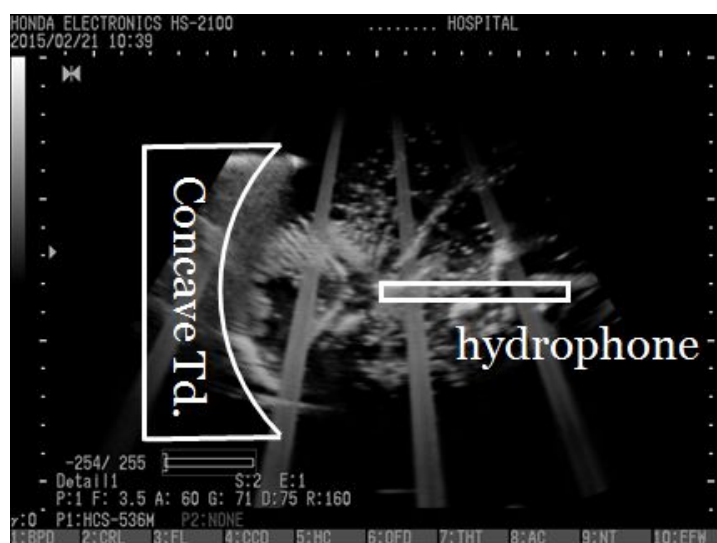
P5A2-8

8:00 am   **Characterization of a MEMS 3D Piezoelectric Ultrasound Transducer for Portable Imaging Systems**

Corina Nistorica[1], Dimitre Latev[1], Deane Gardner[1], Darren Imai[1], Chris Daft[2]; *[1]FUJIFILM Dimatix, Inc, USA, [2]River Sonic Solutions, USA*

Background, Motivation and Objective
Statement of Contribution/Methods

Piezoelectric micromachined transducers are a novel approach for the construction of miniaturezed, low-power portable ultrasound imaging systems and catheter transducer arrays. Here we report on the performance of a 3D MEMS ultrasound transducer. High performance PZNT film was implemented in 3D dome-shaped structures, which form the basic resonating cells of the transducer. Adjustable frequency response can be achieved by mixing the basic cells and modifying the dimensions of the flexible dome-shaped membranes by lithography. Such domes having various dimensions and various resonant frequencies are built into a parallel network of resonators taking advantage of overlapping frequency spectra of multiple resonators similar to a high order linear filter. The construction of the dome-shaped structure and the electrical and acoustic properties are described. A linear array with a center frequency of 5MHz was fabricated and desirable features such as wide-bandwidth frequency response of 97% at -6dB, high sensitivity of 300kPa/V at 5mm depth in water and a two way insertion loss of -50 dB are demonstrated. Additionally, low voltage operation compatible with CMOS integration of 5V to 20V and low impedance (less than 50 ohms) are also demonstrated. Uniformity of the elements in the array was also characterized. A linear array with 64 elements was used to image targets in a tissue phantom producing an axial resolution of 0.5mm and axial resolution of 0.8mm. Such a transducer can be incorporated in miniaturized medical imaging and therapeutic systems such as ICE, IVUS, and even phased array probe for HIFU ultrasound.

Results/Discussion

P5A3 - Transducer Design and Modeling

4th floor

Thursday, October 22, 2015, Posters displayed 08:00 am - 05:00 pm. Authors must be present at their poster from 9:30 - 10:30am (odd number posters) and 14:30 – 15:30pm (even number posters).

Chair: **Yasuhito Takeuchi**
Asahikawa Medical University

P5A3-1

8:00 am Design of a bullet beam pattern of an ultrasound transducer by use of a multifocal lens and a shaded electrode

Euna Choi[1], Yongrae Roh[1]; *[1]School of Mechanical Engineering, Kyungpook National University, Daegu, Korea, Republic of*

Background, Motivation and Objective

Ultrasonic imaging transducer is often required to compose a beam pattern of a low sidelobe level and a small beam width over a long focal region to achieve good image resolution. Usually, ultrasound transducers have many channels along its azimuth, which allows easy formation of the sound beam into a desired shape. However, common 1D array transducers have no control of the beam pattern along their elevation. In order to overcome this difficulty, many kinds of acoustic lens have been developed and patented such as Fresnel lens and Hanafy lens. In this work, a new method is proposed to manipulate the beam pattern by using an acoustic multifocal lens and a shaded electrode on top of the piezoelectric layer.

Statement of Contribution/Methods

The shading technique split the initial uniform electrode into several segments and combined those segments to compose a desired beam pattern. The beam patterns were calculated by the finite element method using PZFlex. For a given elevation width and frequency, the optimal pattern (number and dimension) of the split electrodes was determined by means of the OptQuest-Nonlinear Program (OQ-NLP) algorithm to achieve the lowest sidelobe level.

The requirement to achieve a small beam width with a long focal region was satisfied by employing an acoustic lens of three multiple focuses. Optimal geometry of the multifocal lens such as the radius of curvature and aperture diameter for each focal point was also determined by the OQ-NLP algorithm. For the optimization, a new index was devised to evaluate the on-axis response: focal region ratio = focal region / minimum beam width. The larger was the focal region ratio, the better was the beam pattern.

Combining the shaded electrode of the optimal pattern with the multifocal lens of the optimal geometry showed the sidelobe level of -20.2 dB and the focal range ratio of 45.7. In comparison, the basic transducer with a uniform electrode and a flat lens had the sidelobe level of -13.0 dB and the focal region ratio of 38.3. Validity of these results have been verified through experiments. Figure 1 compares the measured beam patterns of the designed transducer and the basic transducer.

Results/Discussion

We developed a new design method to achieve the bullet beam pattern of an ultrasound transducer by use of a multifocal lens and shaded electrodes. Efficacy of the design has been confirmed by the experimental data in Fig. 1.
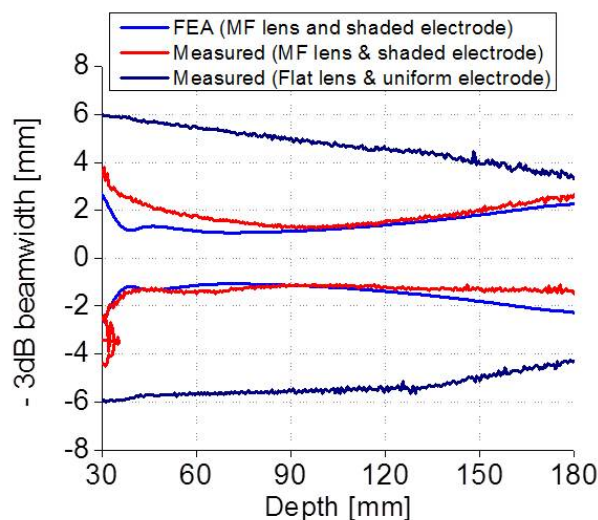
P5A3-2

8:00 am Impedance Conversion of Matching Layer for Air Ultrasonic Transducers

Minoru Toda[1], **Minoru Toda[2]**; *[1]Sensor Solution, TE Connectivity, USA, [2]TE Connectivity, USA*

Background, Motivation and Objective

Typical air ultrasonic transducers (> 100kHz) often consist of thickness mode PZT and a front $\lambda/4$ matching layer which offers impedance conversion, efficient energy transfer and broader bandwidth. Traditional design approaches use matching layers of impedance Zm targeted at converting high impedance of PZT $Zp= 30 \times 10^6$ Rayl to low impedance of Air $Za= 447$ Rayl, or vice versa. However, recent experiments have revealed that converted impedance at the front of PZT Z1, is nearly identical in vacuum or air.

Statement of Contribution/Methods

An analysis of air loaded matching layer has been conducted. Traditional design method defines impedance at the front of PZT as $Z1=Zm^2/Za = Zp$. This requires $Zm=0.12$ MRayl from $Zm =\sqrt{(ZpZa)}$. This equation holds for zero loss or infinite Qm (mechanical quality factor of matching layer). When loss is assumed, a new relation is found and the impedance Z1 is expressed by $Z1=(4/\pi)ZmQm$. This relation does not include Za, consistent with observation.

Results/Discussion

Electrical input impedance of a typical air transducer has been measured. In addition to the peaks at resonance and anti-resonance of the PZT, an extra peak was observed at the center frequency of λ/4 matching layer. This peak was observed when testing in both air and vacuum (left Fig.). Impedance curves were calculated using Mason Model and varying Qm. Calculated curves were consistent with the measured values when Zm = 0.3 MRayl and Qm = 80-100 (right Fig.). In traditional designs, Zm = 0.3 MRayl results in Z1 = 200 MRayl. However, in this work Zm = 0.3 MRayl results in Z1= 30 MRayl representing the desired result for PZT. In air transducers the matching layer does not work as a traditional impedance converter, instead, a resonator with internal loss much greater than radiation loss.
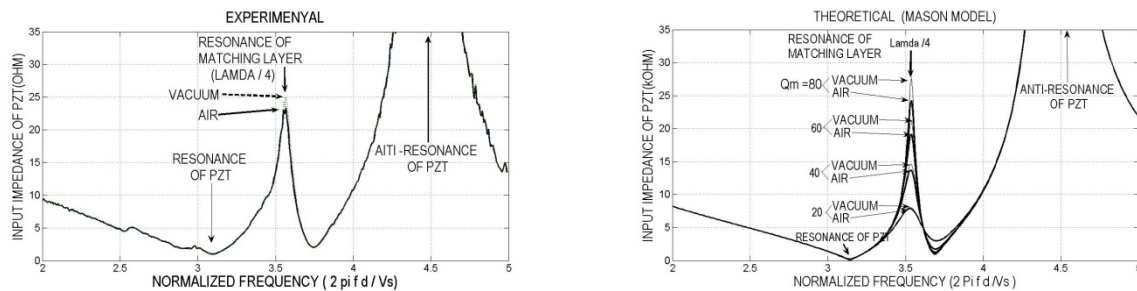
P5A3-3

8:00 am   **Diffraction loss calculation based on boundary element method for an air-coupled phased array**

Rene Golinske[1], Maik Hoffmann[1], Eric Konetzke[1], Alexander Unger[2], Matthias Rutsch[2], Mario Kupnik[2]; *[1]BTU Cottbus-Senftenberg, Germany, [2]Technische Universität Darmstadt, Germany*

Background, Motivation and Objective

We present an efficient numerical method to analyze the diffraction loss of a 1D phased ultrasonic transducer array for airborne applications to an arbitrary located and oriented receiving aperture. The array features a layer of waveguides that separate the larger acoustically active sources from the effective acoustic apertures of the phased array transducer elements, with the goal to fulfill the half-wavelength criteria also for a lower frequency range [Konetzke et al., IUS 2015]. The efficient calculation of diffraction loss for a specific application of such an array, excited with arbitrary input signals on all channels and different beam steering angles is essential for testing and characterizing these type of arrays. Available methods, such as Field II or FOCUS, Michigan State, provide the pressure field in front of the phased transducer array, i.e. they assume a point source receiver. Our calculation method, however, is focused on efficiently calculating the diffraction loss to a given receiving aperture, such as a microphone or a receiving transducer, with arbitrary location and orientation.

Statement of Contribution/Methods

Our model is based on the integral expression of the wave equation in the time domain, which has no closed form solution. The boundary element method (BEM) is used for a numerically efficient calculation of the diffraction loss. The entire model is implemented in the commercially available software package Mathematica V10 from Wolfram Research. The 1D phased array, that we model and that we use for validation measurements [Hoffmann et al., IUS 2013], consists of eight channels with 12 rectangular-shaped element apertures, 4.3 x 6 mm in size each, i.e. there are 96 elements in total. These emitting elements are discretized by the Distmesh-algorithm with a starting number of 10 elements per wavelength [P.-O. Persson, 2004]. In the model, each of these elements can be excited by an arbitrary transient signal. Similar as in our validation experiments, we use a sinusoidal burst signal with 80 cycles and a true time delay for beam steering over an opening angle of 110°. As the receiving aperture, we assume a circular-shaped microphone membrane with a diameter of 3 mm, representing a B&K 4138 microphone used in our experimental setup. The location and orientation of the receiving aperture is arbitrary. Again, the receiving aperture is discretized by the Distmesh-algorithm, with a starting number of 10 elements per wavelength.

Results/Discussion

After testing for convergence, we determined the performance of the model for moving the receiving aperture within an entire 3D volume at different locations. The calculation of the diffraction loss for one microphone location requires 50 seconds on a regular 64-Bit quad core machine. The direct comparison to the volumetric measurement results showed good agreement, which validates the model. Such a model will help to optimize phased array transducers for air-coupled applications.

P5A3-4

8:00 am   **Optimization of the Structure of 1-3 Piezocomposite Materials to Maximize the Performance of an Underwater Transducer**

Yongrae Roh[1], **Haejune Park[1]**; *[1]School of Mechanical Engineering, Kyungpook National University, Daegu, Korea, Republic of*

Background, Motivation and Objective

Recently, 1-3 piezocomposites are widely used in underwater acoustic transducers to overcome the limitation of conventional piezoceramics. However, the structure of the piezocomposites should be carefully designed to achieve the superiority in transducer performance. In this paper, an underwater acoustic transducer was designed using the 1-3 piezocomposites to have good Transmitting Voltage Response (TVR), -3dB Fractional Bandwidth (FBW), and Receiving Voltage Sensitivity (RVS).

When the piezocomposite plate vibrates in a thickness mode, inter-pillar resonant modes are likely to occur, which is likely to couple with the thickness mode. For the sake of transduction efficiency, it is very important to design the piezocomposite transducer not to have the inter-pillar mode of vibration.

Statement of Contribution/Methods

The underwater transducer in this work consisted of the piezocomposite plate, a front acoustic matching layer, and a backing layer attached to a thick steel plate. The performance of the transducer was analyzed by presenting the transducer with an equivalent circuit. Then, the structure of the 1-3 piezocomposite plate was optimized to maximize the magnitude of objective functions while preventing the occurrence of the inter-pillar mode. Three different objective functions were tried in the design. The first function, TFR, was used to maximize both TVR and RVS responses while preserving a wide FBW. The second function was to maximize only the TVR while preserving a wide FBW. The third function was to maximize only the RVS. The selected design variables were volume fraction of the ceramic (VF), elastic modulus of the polymer (Y), thickness of the composite (t), and aspect ratio of the composite (AR). The objective functions were maximized by the OptQuest-Nonlinear Program algorithm. After the optimization, a finite element model of the transducer was constructed with the commercial package ANSYS to follow the optimized structural variables, and was used to check any occurrence of the inter-pillar mode. If the occurrence were observed, the variation ranges of the design variables were adjusted to shift the inter-pillar mode away from the frequency range of interest.

The transducer of the optimized structure showed significant improvement in its performance. For example, the transducer optimized to have the highest TFR had the TVR of 165.3 dB, FBW of 43.9%, and RVS of -171.3 dB without any mode coupling while those of the initial transducer were 152.6 dB, 4.9%, and -175.7 dB, respectively.

Results/Discussion

We determined the optimal structure of the 1-3 piezocomposite plate to maximize the particular performance of interest of an underwater acoustic transducer while preventing the occurrence of the inter-pillar mode within the frequency range of operation. The optimal design method is applicable not only to the specific structure in this work but also to general underwater acoustic transducers of various structures.

P5A3-5

8:00 am   A feasibility study of angled backing structure using FEM Simulation for lightweight ultrasound transducer

Seon Mi Ji[1], Sung Min Kim[1], Jong Seob Jeong[1]; *[1]Medical Biotechnology, Dongguk University, Gyeonggi-do, Korea, Republic of*

Background, Motivation and Objective

In the ultrasonic transducer, a backing layer is generally made of composite material using metal powder and polymer to provide proper attenuation coefficient and acoustic impedance. Also, the thickness of the backing layer is usually thick enough to attenuate incoming and reflecting waves. Thus, the weight of the backing layer is one of the key parameters for fabrication of the lightweight ultrasound transducer. To reduce the weight of the backing layer while maintaining the performance, in this study, we suggested the angled backing structure and demonstrated the performance by using FEM (finite element method) simulation.

Statement of Contribution/Methods

The FEM simulation by using PZFlex tool was conducted for designing a 5.5 MHz transducer. PMN-32%PT single crystal and E-Solder 3022 (5.9 MRayl) were used for a piezoelectric layer and a backing layer, respectively. No matching layer was used to monitor the isolated effect of the backing layer (Figure 1(a)). To demonstrate the performance of the proposed angled backing structure, the grooved backing well known structure for CMUT transducer was also implemented and their performance was compared to each other ((Figure 1(b)).

Results/Discussion

Under the condition of one-wavelength thickness of the backing layer, both the grooved structure and the angled structure show that the pulse echo signals had reduced ripples compared to the conventional signal (Figure 1(b)). The angles of the proposed backing structure affected the direction of the incoming wave based on scattering and reflection. Thus, the angled backing can prevent the distortion of the wave expecting improved bandwidth and reducing weight. In the angled structure, the effects of the degree and size of the triangle were small resulting in reduced fabrication complexity of the proposed angled structure. Hence, the proposed backing structure may be a possible method for decreasing the weight of the ultrasound transducer and increasing bandwidth. We will experimentally demonstrate the performance of the proposed method in the future.
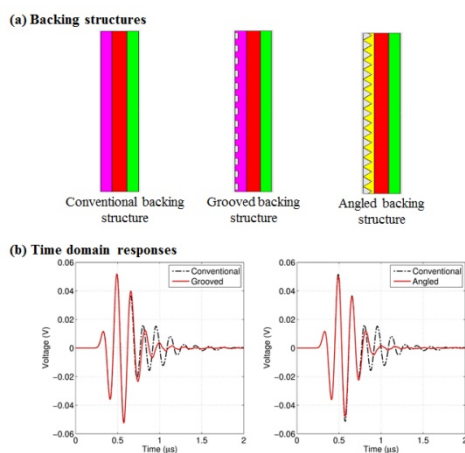
Figure 1. (a) Design of three types of transducers: conventional, grooved, and suggested angled structure. Note that green color is water medium. (b) Time domain responses of grooved structure (left) and angled structure (right) compared with conventional structure in both cases.

PA - Student Paper Competition Finalists

Student Paper Competition Room

Thursday, October 22, 2015, 08:00 am - 06:00 pm

PA-1 _____

8:00 am   **Low flow rate spraying using a torsional ultrasonic transducer**

Shunsuke Tsuyuki[1], Takefumi Kanda[1], Koichi Suzumori[2], Shin-ichiro Kawasaki[3], Shoki Ofuji[1]; *[1]Okayama University, Okayama, Japan, [2]Tokyo Institute of Technology, Tokyo, Japan, [3]National Institute of Advanced Industrial Science and Technology, Miyagi, Japan*

Background, Motivation and Objective

In many industrial fields, a spraying of coating materials with a low flow rate is expected for the coating quality improvement. When the flow rate of the spraying is low, the pressure applied to coating materials have to be diminished. An ultrasonic vibration can effectively assist to enlarge a spray angle and atomize of materials even if the pressure is low. In this research, we propose the ultrasonic atomization by using a torsional vibration mode transducer. We have evaluated on the low flow rate spraying by using a bolt-clamped transducer.

Statement of Contribution/Methods

Figure 1 shows a schema of ultrasonic transducer for the spraying. This transducer can oscillate the tip of nozzle in perpendicular to the flow direction. Generally, the atomization condition is dominated by Weber number. From the macroscopic view the surface tension is changed when the nozzle is oscillated. Therefore we can control the atomization of the liquid by changing the Weber number. In this research, we have fabricated the torsional transducer to evaluate the effect of the atomization. We have observed the spray angle and atomization condition at the low flow rate. Additionally, the results of have been compared with those by using a longitudinal transducer.

Results/Discussion

Figure 2 shows the relationship between flow rates and spray angle when water was sprayed. In the case of torsional vibration mode, when the driving frequency, the applied voltage, and the flow rate were 18.3 kHz, 60 Vp-p, and 15 ml/min, the water has been successfully atomized. In addition, although the ethylene glycol has higher viscosity, we have succeeded in atomizing ethylene glycol effectively. As a result, the torsional vibration has generated a stable atomizing condition than the longitudinal vibrational mode in a low flow rate spraying.

Fig. 2 Relationship between flow rates and spray angle when water was sprayed

Fig. 1 Structure of bolt-camped transducer for spraying

PA-2 _____

8:00 am   **Fast wave velocity measurement by Brillouin scattering using induced phonon from ScAlN piezoelectric thin film**

Masahiko KAWABE[1], Takahiko YANAGITANI[2], Hayato ICHIHASHI[1], Shinji TAKAYANAGI[1], Masashi SUZUKI[3], Mami MATSUKAWA[1]; *[1]Doshisha University, kyoto, Japan, [2]Waseda University, Tokyo, Japan, [3]Nagoya Institute of Technology, Nagoya, Japan*

Background, Motivation and Objective

Brillouin scattering enables a nondestructive and noncontact technique to measure the hypersonic wave velocity in thin materials. However, weak thermal phonons result in the long time and low accuracy measurement. To overcome this problem, a technique with artificially induced phonons is suggested using a piezoelectric film. In this study, we have tried to induce strong longitudinal phonons by ScAlN films deposited on the surface of a bulk sample. The ScAlN film is suitable for excitation of phonons owing to the excellent piezoelectric character.

Statement of Contribution/Methods

Longitudinal phonons were induced by a Sc0.41Al0.59N piezoelectric film [1]. The film was grown by an RF magnetron sputtering on DC sputter-deposited Ti metal film (150 nm)/ sample (5 × 5 × 25 mm, ED-H, Tosoh Corp.). The crystalline c-axis of the film was aligned with the normal. The film (4 μm thick) was deposited on one side of a sample. On another side of the sample, an Al film (300 nm) was deposited as a light reflector for the RIΘA scattering geometry. We induced phonons by applying an electric field on Ti electrode using a signal generator (E8257D, Agilent technologies). The scattering light was measured by a Tandem Fabry-Perot Interferometer (JRS) with a laser (wavelength; 532nm, Laser Quantum). Here, the laser beam hit the sample at the position of 1 mm from the ScAlN film, with the angle of 2 degrees from the normal direction to the sample surface. The phonons were excited at 760 MHz (the primary resonance of ScAlN film).

Results/Discussion

Figure 1 shows a typical spectrum of a Brillouin peak from the induced phonons. The intensity of Anti-Stokes peak was about 22,666 counts (input power: 10 dBm), which was 1,079 times as intense as the peak before excitation. Velocity can be obtained easily by the fixed frequency and the angle of incident light. Because ScAlN has excellent piezoelectric properties, the intensity of the excited Brillouin peak was 6 times stronger than that excited from a ZnO film [2]. The obtained velocity was 602×10 m/s, which was equal to the reported velocity of the sample. The intensity of Brillouin scattering dramatically improved by the induced phonons radiated from the ScAlN film. With this technique, rapid and precise velocity measurements can be achieved.

[1] T. Yanagitani, and M. Suzuki, Appl. Phys. Lett. 105, 122907 (2014).

[2] T. Yoshida et al., IEEE TUFFC, 58,(6), 1255(2011).

STUDENT PAPER COMPETITION

(a)Measurement specimen

(b)Brillouin spectra before and after excitation
(Number of interferometer scans: 100 times)

Fig. 1 Specimen and measured spectra

PA-3

8:00 am   **High order mode polarity inverted Al-polar (0001) ScAlN/O-polar (000-1) ZnO film resonator**

Takeshi Mori[1], Takahiko Yanagitani[2], Masashi Suzuki[1]; *[1]Nagoya Institute of Technology, Japan, [2]Waseda University, Tokyo, Japan*

Background, Motivation and Objective

Polarization-inverted multi-layer resonators are attractive for high order mode excitation and high power operation. In the ultrasonic microscope applications, *n*-fold low capacitance of *n*th polarization-inverted multi-layer enables *n*-fold increase of emission area in the transducer without sacrificing impedance matching between the transducer and 50Ω measurement system. Large emission area leads to a concentration of the ultrasonic. Previously, we reported the control of the polarity in ScAlN and ZnO films by ion beam irradiation during film growth, and we found that the usual ScAlN and ZnO films grown by a standard planar sputtering possess (0001) Al-polarity and (000-1) O-polarity, respectively [1,2]. In this study, we considered that the polarization-inverted (0001)/(000-1) multi-layer can be easily obtained by depositing usual (0001) Al-polar ScAlN film on usual (000-1) O-polar ZnO film. To check this assumption, we fabricated two layer (0001) ScAlN/(000-1) ZnO film resonator by a conventional magnetron sputtering.

[1] M. Suzuki et al., APL 104 172905 (2014)
[2] R. Hashimoto et al., IUS 2013, IUS3-H-6.

Statement of Contribution/Methods

c-axis oriented ZnO films (approximately 4.2 *μ*m) were grown on (0001) Ti films/silica glass substrate by off-axis deposition geometry. c-axis oriented ScAlN films (approximately 3.9 *μ*m) was grown on the ZnO films by on-axis deposition geometry. The polarities of the layers were determined by a press test using an oscilloscope. We also investigated longitudinal wave conversion loss of the ScAlN/ZnO film HBARs to determine the resonance mode.

Results/Discussion

As shown in Fig. 1, positive response indicating O-polarity, was observed in the first layer ZnO film when the compressive stress was applied, whereas the, negative response, indicating Al-polarity, was observed in the second layer ScAlN film.

As shown in Fig. 2, two layered (0001) ScAlN/(000-1) ZnO film excited the 2nd mode resonance at 0.72 GHz with suppression of the 1st mode resonance at 0.27 GHz. The experimental conversion loss curve agreed well with the theoretical one calculated by Mason's model including the effects of polarity inversion. This indicates that the polarization direction of the second layer and the first layer are perfectly inverted. Minimum conversion loss of 1.8 dB is smaller than that of typical single layer ScAlN film HBAR.

Fig. 1 Opposite piezoelectric responses of the usual ScAlN and usual ZnO films when compressive stress is applied

Fig. 2 Longitudinal wave conversion loss curves of the ScAlN/ZnO HBAR, showing perfect polarity inversion

8:00 am   Multiphysics Modeling of BAW Filters

Andreas Tag[1], Dominik Karolewski[2], Bernhard Bader[3], Maximilian Pitschi[3], Robert Weigel[1], Amelie Hagelauer[1]; *[1]Institute for Electronics Engineering, University of Erlangen-Nuremberg, Erlangen, Germany, [2]Institut für Mikroelektronik- und Mechatronik-Systeme gemeinnützige GmbH, Germany, [3]TDK Corporation, Germany*

Background, Motivation and Objective

Bulk Acoustic Wave (BAW) filters are commonly used at high power levels and need to fulfill strict specifications like tight transition bandwidths. A part of the applied power will dissipate and lead to a temperature increase within the filter and, thus, to a significant frequency shift of the filter's transfer function. To be able to design filters fulfilling the challenging transition bandwidths at high power levels accurate multiphysics modeling techniques are required.

Statement of Contribution/Methods

Multiphysics (electromagnetic (EM) acoustic thermal) 3 D finite element methods (FEM) are not suitable for single BAW resonators, not to mention a filter, due to the tremendously high calculation times. The solutions presented in the literature do not take the spacial distribution of the temperature and dissipated power into account since they are based on measured TCFs and the dissipated power is calculated from the S-parameters. In our previous works, we have presented modeling approaches taking the spatial distributions of the temperature and the different kinds of the dissipated powers into account in order to remarkably improve the modeling of BAW resonators at high power levels. In this work, the modeling approach has been extended enabling precise and at the same time fast multiphysics simulations of whole BAW filters at high power levels.

Results/Discussion

The acoustic is modeled by an extended 1D modeling approach allowing efficient calculation times and providing the distribution of the viscous losses within each layer together with the lateral leaking power for each resonator, respectively. EM is modeled with a 3D FEM simulation program providing the spatial distribution of the EM losses.

The spatially distributed losses are transferred to the thermal 3D simulation. The result of the thermal simulation is the spatial temperature distribution being used for modification of the geometry of each resonator and the material within each layer in each resonator. Finally, the acoustic and EM simulations are repeated with all the modifications. An example is shown in Fig. 1. The high accuracy of the modeling approach was verified by measurements of the S-Parameters and the temperature distribution by the infrared thermography during high power loads. The developed multiphysics modeling approach enables effective design of modern BAW filters for high power levels.

Fig. 1 Left hand side: Simulation results for the transfer function of a solidly mounted BAW filter without power load, with 33 dBm power load at the frequencies of 1839 MHz and 1914 MHz, respectively. Right hand side: Simulation results of the lateral temperature distribution within two different layers of the resonator for two power loads. The temperature distribution is quite different within the different layers and the power loads at different frequencies.

STUDENT PAPER COMPETITION

8:00 am   Evaluation of Acoustic Properties of CaTiO₃-(K,Na)NbO₃ Film Using Microfabricated Structure

Ryosuke Kaneko[1], Michio Kadota[1], Yuji Ohashi[2], Jun-ichi Kushibiki[1], Shinsuke Ikeuchi[3], Shuji Tanaka[1]; *[1]Graduate school, Tohoku University, Sendai, Miyagi, Japan, [2]Institute for Material Research, Tohoku University, Sendai, Miyagi, Japan, [3]Devices Development, Murata Manufacturing Co., Ltd., Nagaokakyo, Kyoto, Japan*

Background, Motivation and Objective

$Pb(Zr,Ti)O_3$ (PZT) is the most widely used for piezoelectric devices, because it has high piezoelectric constants over a wide range of temperature. However, it contains lead at high concentration. Nowadays, lead-free piezoelectric films have been widely studied for the next-generation piezoelectric devices. $(K,Na)NbO_3$ (KNN) is one of the candidates of the replacement, because its d_{31} is around 100 pm/V, which is equivalent to that of PZT. However, the material constants and acoustic properties of the KNN film have not been measured yet. In this research, we develop a method to measure the acoustic properties of a (001)-oriented KNN film deposited on a blanket platinum film.

Statement of Contribution/Methods

We used a 1.7 μm thick $CaTiO_3$-doped KNN film on Si (500 μm)/SiO2 (150 nm)/Ti (10 nm)/Pt (100 nm) [1]. First, we fabricated piezoelectric resonators on the KNN film by microfabrication technology. Fig. 1 shows length extension mode and radial/longitudinal thickness modes resonators. The radial and longitudinal thickness modes are generated on the same resonator. The resonance and antiresonance frequencies of each mode are measured using a network analyzer. The velocity of leaky Lamb wave in a KNN diaphragm of 2 mm diameter covered with 200 nm thick Al is measured using an acoustic microscope.

Results/Discussion

The following material constants were extracted from measured results of the resonators; $s_{11}^E = 9.27 \times 10^{-12}$ /Pa, $s_{12}^E = -3.06 \times 10^{-12}$ /Pa, $s_{66}^E = 24.7 \times 10^{-12}$ /Pa, $k_{31}^2 = 0.06\%$, $k_t^2 = 13.5\%$, $d_{31} = -119$ pC/N, Poison ratio $\sigma_{12}^E = 0.33$, $\varepsilon_{33}^T/\varepsilon_0 = 1,226$. The phase velocity of length extension mode is 4,905 m/s. The phase velocity of A_0 and S_0 mode of Lamb waves in the KNN diaphragm of 0.2-0.3λ thickness were measured by ultrasonic microscopy as 1,491 m/s and 5,370-5,180 m/s, respectively, as shown in Fig. 2. The developed method can be basically applicable to any piezoelectric blanket films unlike our previous study [2], where ScAlN was deposited on a patterned platinum layer.

[1] S. Ikeuchi et al., "Preparation of (K,Na)NbO₃-CaTiO₃ film by RF magnetron sputtering", IEEE Ultrason. Symp. 2014, pp. 1578-1581.

[2] Akira Konno et al., "Determination of Full Material Constants of ScAlN Thin Film from Bulk and Leaky Lamb Waves in MEMS-based Samples", IEEE Ultrason. Symp. 2014, pp. 273-276.

(a) Length Expander mode
resonator: $l = 200 \sim 600 \ \mu m$

(b) Radial/Longitudinal thickness modes
resonator: $d = 30 \sim 200 \ \mu m$

Fig. 1 Fabricated piezoelectric transducers.

Fig. 2 Measured phase velocity of
leaky Lamb wave on KNN diaphragm
as a function of KNN thickness.

PA-6

8:00 am **SAW Characteristics of AlN/SiO₂/3C-SiC Layered Structure with Embedded Electrodes**

Qiaozhen Zhang[1], Tao Han[1], Jing Chen[1], Kenya Hashimoto[2]; *[1]Electronic Information and Electrical Engineering, Shanghai Jiao Tong University, Shanghai, Shanghai, China, People's Republic of, [2]Graduate School of Engineering, Chiba University, Japan*

Background, Motivation and Objective

Layered structure consisting of AlN thin film combined with 3C-SiC substrate has been paid much attention because of their high SAW velocity. It has been demonstrated that the AlN/3C-SiC layered substrate shows better performance in terms of electromechanical coupling coefficient (K^2) and temperature coefficient of delay (TCD) when configured with embedded inter-digital transducer (IDT) electrodes. However, this configuration results in poor step coverage of AlN thin films since the edge discontinuities of the patterned IDT electrodes, which harms AlN crystalline growth and causes cracks in AlN thin films. Therefore, a novel sandwich structure with flattened underlayer for AlN growth by filling amorphous silicon dioxide (SiO_2) in the groove between the electrodes is proposed as shown in Fig.1, and the temperature compenation function can also be expected.

Statement of Contribution/Methods

The SAW characteristics on the proposed AlN/SiO₂/IDT/3C-SiC structure is modeled and analyzed by employing finite element method (FEM). The input admittance of the infinitely-long IDT SAW is calculated, and the phase velocity (V) and coupling factor (K^2) curves have been calculated according to the resonance and anti-resonance frequencies. The temperature coefficient of frequency (TCF) of the structure is predicted using the thermo-mechanical coupling modeling based on COMSOL FEM software.

Results/Discussion

Fig.1 shows simulation results of the phase velocity and coupling factor curves as a function of the normalized AlN thickness (h_{AlN}/λ) for Rayleigh mode propagates along AlN/SiO₂/IDT/3C-SiC structure with embedded electrodes. It can be seen that the high V of 5500m/s and enhanced K^2 of 1.43% are simultaneously obtained when the normalized AlN thickness is 0.5. Fig.2 shows the frequency-temperature curves as a function of temperature for the Rayleigh mode on this proposed layered structure with the normalized AlN thickness of 0.4 and the normalized SiO₂ thickness of 0.5%. As it is shown, the first order TCF equals to 0.28ppm/°C and the second order equals to -2ppb/ °C² for the temperature ranging from -20 °C to 100 °C. The proposed structure enables the growth of highly quality AlN thin films feasible and shows great potential for achieving high velocity, relative large K^2 and temperature compensated SAW applications.
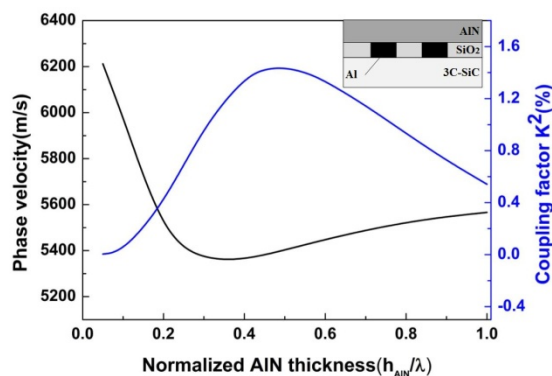
Fig.1. SAW properties of AlN/SiO₂/IDT/3C-SiC structure for Rayleigh mode.
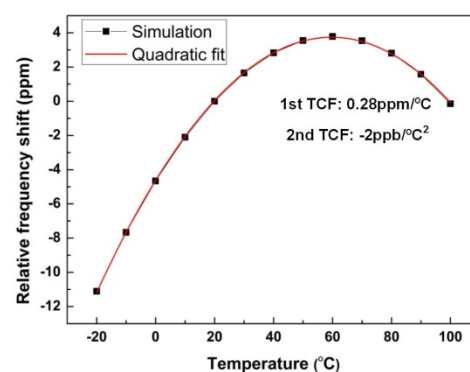
Fig.2. Frequency-temperature dependence of AlN/SiO₂/3C-SiC structure for Rayleigh mode ($h_{AlN}/\lambda = 0.4$, $h_{SiO_2}/\lambda = 0.5\%$).

PA-7

8:00 am **Dual-Mode Integrated Circuit for Imaging and HIFU With 2-D CMUT Arrays**

Ji Hoon Jang[1], Anshuman Bhuyan[1], Hyo-Seon Yoon[1], Jung Woo Choe[1], Amin Nikoozadeh[1], Douglas Stephens[2], Butrus Khuri-Yakub[1]; *[1]Electrical Engineering, Stanford University, Stanford, California, USA, [2]Biomedical Engineering, University of California, Davis, Davis, California, USA*

Background, Motivation and Objective

For successful high intensity focused ultrasound (HIFU) operation, it is important to have a reliable guidance and monitoring method such as magnetic resonance imaging (MRI) and ultrasound imaging. However, MR-guided HIFU systems are typically bulky, and the imaging-guided HIFU systems use separate ultrasound transducers and electronics. In this paper, we present a dual-mode integrated circuit (IC) that can perform both ultrasound imaging and HIFU with a single 2D capacitive micromachined ultrasonic transducer (CMUT) array.

Statement of Contribution/Methods

The dual-mode IC consists of pulsers, transmit beamforming circuitry, and low-noise amplifiers for imaging mode and switches for HIFU mode. In the imaging mode, only the 64 diagonal CMUT elements are used as receivers without significant loss of image quality, and the other 960 elements transmit the ultrasound beam. In the HIFU mode, each of the 1024 CMUT elements is assigned to one of the eight HIFU channels based on the phase delay from it to the desired focal point using a dedicated high-voltage switch. The eight HIFU channels are connected to an eight-channel phase generating system for a fixed focal point in front of the CMUT array. We can alternate between the imaging and HIFU modes on demand by turning the switch network on and off (Fig. 1).

Results/Discussion

The dual-mode IC was fabricated in the 0.18-µm, high-voltage process. We previously fabricated a 250-µm-pitch, 32×32-element CMUT array that has a center frequency of 5 MHz using the sacrificial release process, and flip-chip bonded this CMUT array to the IC. The integrated assembly is connected to a custom-designed printed circuit board (PCB) to interface the IC to an 8-channel phase generating system, an image reconstruction system, and a field-programmable gate array (FPGA). The phase generating system consists of digital synthesizers and power amplifiers to drive eight HIFU channels. The imaging system processes the data received by the 64 receive channels to reconstruct real-time ultrasound images. The FPGA sends the beam patterns to the IC and control signals to switch the modes. We have successfully demonstrated the functionality of all the individual components. We are currently working on demonstrating interleaved imaging and HIFU using a single 2D CMUT array. This work was supported by the National Institutes of Health (NIH) under grant R01HL117740

PA-8

8:00 am   Capsule-based Ultrasound-mediated Targeted Gastrointestinal Drug Delivery

Fraser Stewart[1], Antonella Verbeni[2], Yongqiang Qiu[1], Benjamin Cox[1], Jan Vorstius[3], Sandy Cochran[1]; *[1]Institute for Medical Science and Technology, University of Dundee, United Kingdom, [2]The BioRobotics Institute, Scuola Superiore Sant'Anna, Italy, [3]School of Engineering, Mathematics and Physics, University of Dundee, United Kingdom*

Background, Motivation and Objective

Focused Ultrasound (FUS) has a variety of potential uses, including therapeutic treatment of the gastrointestinal (GI) tract. Capsule endoscopy is already a key interest for researchers for the diagnosis of GI conditions such as inflammation, Crohn's disease and neoplasms and has the potential to be developed for treatment by incorporating a FUS transducer and associated drug delivery (DD). This paper describes a tethered capsule for targeted drug delivery (TDD) of GI conditions. We also compare piezo-ceramic (PZ) materials for the transducer to be housed in the capsule.

Statement of Contribution/Methods

Miniature bowls made with PZ54 and PZ26 (Meggitt Sensing Systems, Kvistgaard, Denmark) with frequencies of 4 MHz and 3.5 MHz respectively were selected and characterised to find the most suitable candidate for TDD. Both bowls have an outer diameter of 5 mm and focal distance of 15 mm, making them ideal to be embedded in a therapeutic capsule made with rapid prototyping and also including CMOS camera, LED illumination and DD channel (Fig. 1a). The DD channel pathway beyond the capsule is confocal with the transducer (Fig. 1a) with the intention to deliver drugs and increase cell membrane permeability through sonoporation. Functional tests included running microbubbles (MB) through the DD channel and monitoring the behaviour at the ultrasound (US) focus.

Results/Discussion

The PZ54 transducer provided an acoustic pressure P_{ac} = 125 kPa (PZ54 pressure mapping shown in Fig. 1b)and mechanical index MI = 0.063 with a beam diameter BD = 0.75 mm at the focus and the corresponding figures for the PZ26 transducer were P_{ac} = 157 kPa, MI = 0.084 and BD = 1.35 mm, both transducers were driven at 4 V_{pp}. Values for P_{ac} in the range $50 < P_{ac} < 300$ kPa ($0.05 < MI < 0.3$) are suitable for reversible sonoporation [1], and both PZ26 and PZ54 transducers fall in this range. The PZ54 transducer was selected due to its BD allowing a smaller area to be sonicated; PZ54 is also more suitable for FUS purposes because it has a higher permittivity than PZ26, which is better for electrical impedance matching. Functional tests showed that the MB egress was heavily influenced by the FUS, with their course of travel redirected due to acoustic radiation force. This suggests that a capsule configured as we have has potential in biomedical and DD applications.

[1] Qiu et al (2012) J. of Bio. Mech. 45(8) 10.1016

Figure 1(a)

Figure 1(b)

PA-9

8:00 am   Design of High-Efficiency, Miniaturized Ultrasonic Receivers for Powering Medical Implants with Reconfigurable Power Levels

Ting Chia Chang[1], Marcus Weber[1], Jayant Charthad[1], Amin Nikoozadeh[1], Butrus T. Khuri-Yakub[1], Amin Arbabian[1]; *[1]Electrical Engineering, Stanford University, Stanford, CA, USA*

Background, Motivation and Objective

Millimeter and sub-mm sized implantable medical devices with high available power are attractive for many novel therapeutic applications. Ultrasonic power delivery can be used to shrink down the dimensions of an implant and eliminate the need for batteries and wires, while achieving high power levels (> 1 mW) for great depths in the body. Compared to RF wireless powering, ultrasonic energy transfer has several advantages: high acoustic-electrical power conversion efficiency (PCE), lower losses through tissue, superior energy focusing, and favorable impedance to interface with integrated circuits. To design for desired impedance and high PCE, we investigate ultrasonic receivers with different piezoelectric materials; and we propose an electrical matching technique in the operating region to optimize efficiency over various load power from different operation modes of an implant.

Statement of Contribution/Methods

Ultrasonic receivers are made with PZT4, PZT5H, and BaTiO₃ and sized to 1.5 mm thick and 1.1 mm wide on the sides. Air backing is utilized to increase the harvesting efficiency. We do not use acoustic matching layers for the ease of implementation and because a large instantaneous bandwidth is not required for the design of receiver. To study the energy harvesting capability for typical loads of active circuits (1 kΩ to 100 kΩ), impedance and PCE are measured and simulated using the 3-D finite element method. Mineral oil is used to imitate acoustic impedance of tissue in the measurement.

Results/Discussion

The receivers exhibit inductive impedance between the fundamental series and parallel resonances; moreover, the real part mimics typical implant loads, allowing for efficient overall impedance matching with capacitors. When the receiver's electrical matching is appropriately adapted, high PCE of 40% - 60% is achieved over a wide band (~300 kHz) for both PZT4 and PZT5H; and PCE of 40% - 50% is predicted for BaTiO₃ in simulation. The receiver can be designed to operate for a given implant load, and we can also program switched-capacitor network (without bulky inductors) to match to varying load powers. As a result, the proposed system can harvest acoustic power efficiently over large dynamic range of loads to enable miniaturized and complex medical implants.

Fig. 1. Measured (solid) and simulated (dash) real impedance and PCE of the receiver with (a) PZT4 (b) PZT5H. The impedance is inductive in the shaded region. (c) Proposed system diagram with tunable switched capacitor network.

PA-10

8:00 am   Photoacoustic properties of plasmonic-nanoparticle coated microbubbles

Adam Dixon[1], Song Hu[1], Alexander Klibanov[1], John Hossack[1]; *[1]Biomedical Engineering, University of Virginia, Charlottesville, Virginia, USA*

Background, Motivation and Objective

We present the design of a multimodality contrast agent for photoacoustic and ultrasound imaging comprising microbubbles coated with optically absorbing gold nanorods (AuMBs). We hypothesized that coupling nanorods to the microbubble shell would drive thermal expansion of the microbubble's gaseous core and result in an amplified photoacoustic emission following excitation by 5 nanosecond pulsed laser irradiation (λ=750 nm). Results of both in vitro and in vivo ultrasound/photoacoustic dual-modality imaging are presented.

Statement of Contribution/Methods

Gold nanorods were covalently attached to the microbubble shell using a gold-thiol bond. The behavior of single AuMBs following excitation by a single nanosecond-duration laser pulse was characterized by high-speed video microscopy, analysis of the photoacoustic emission, and finite element numerical modeling.

STUDENT PAPER COMPETITION

Results/Discussion

We identified two-distinct AuMB responses to pulsed laser excitation. At low laser fluence (below 5 mJ/cm2), microbubble wall motion was not detectable via high speed microscopy and photoacoustic emissions were relatively weak. At higher laser fluence, the microbubble diameter expanded by several hundred nanometers and photoacoustic emissions were over 10-fold greater than photoacoustic emissions from comparable concentrations of freely dispersed gold nanorods. Rapid microbubble expansion was hypothesized to result from water vapor formation at the gold nanorod-water interface. Thermal modeling of the gold nanorod/water/microbubble system confirmed that temperatures sufficient for water vaporization were reached at the nanorod surface (above 600 K). Finally, we demonstrated 9 dB photoacoustic contrast enhancement derived from the presence of AuMBs in the murine kidney.

(a): Geometry and results of finite-element simulations of heat transfer from a single gold nanorod to the microbubble gas core. Note temperatures rise above the critical point of water. (b) Top: temperature of the gas core. Bottom: radial oscillations of the microbubble.

PA-11

8:00 am   Joint compressive sampling and deconvolution in ultrasound medical imaging

Zhouye Chen[1], Adrian Basarab[1], Denis Kouamé[1]; *[1]IRIT, UMR CNRS 5505, University of Toulouse, France*

Background, Motivation and Objective

Compressive Sampling (CS) and ultrasound (US) image deconvolution are two research tracks explored in the literature. CS seeks to reduce the volume of acquired data, but an image quality degradation of the restored images from a low number of samples was observed in practice. Deconvolution aims at improving the quality (spatial resolution, contrast, SNR) of US images. Combining these two frameworks (Compressive Deconvolution (CD)) is an interesting alternative for high quality CS reconstructions. The benefit of CD is the joint volume reduction of the acquired data and the image quality improvement. We propose herein a novel scheme of CD and its application to US imaging.

Statement of Contribution/Methods

The model of CD is given in eq. (1) (top of Fig 1), where **y** is the RF image, **x** is the tissue reflectivity function (TRF) to be estimated, **H** is a matrix representing the PSF, **Φ** is a rectangular random matrix commonly used in CS and **n** is a Gaussian noise. To solve (1), we reformulate it as the optimization problem in (2): the first term represents the data fidelity, the second enforces the sparsity of RF data in wavelet domain **ψ** [Liebgott, Ultrasonics'11] and the third imposes a Laplacian prior on the TRF [Michailovich, IEEE TIP'07]. The resulting restoration problem is far more difficult than those addressed in CS or deconvolution separately.

To solve (2), we propose a novel numerical scheme based on the alternating direction method of multipliers that allows us to split the three terms in (2) into three sub-problems and to solve them separately.

Results/Discussion

We compare our method with the only existing approach on CD [Amizic, IEEE TIP'13] **on simulated data**. The results (Fig 1 and Table 1) show that our method performs better in terms of PSNR and Structure SIMilarity for different data reduction ratios. Our method was then applied to **in vivo data** showing a mouse bladder acquired with a 20 MHz single-element probe (Fig 2). The PSF was previously estimated following [Michailovich, IEEE TMI'05]. Despite the data reduction, we remark that our method is able to restore images with better contrast (CNR is computed between the two red blocks in Fig 2) than the native B-mode image.

Future work will explore different priors on the TRF (e.g. generalized Gaussian [Alessandrini, IEEE UFFC'11]), compressive blind deconvolution (joint TRF and PSF estimation) and validation on further experimental data.

Fig.1 Comparison results (SNR=40dB, CS ratio=80%)

Table. 1 Quatitative comparison results
(Average metrics for 10 experiments for each CS ratio)

CSratio	20%	40%	60%	80%		CSratio	20%	40%	60%	80%
[Amizic,	SSIM	17.79	48.67	67.35	74.35	Proposed	SSIM	23.98	56.53	70.86	77.92
IEEE,TIP'13]	PSNR	19.80	21.57	22.39	22.89		PSNR	21.09	22.97	23.79	24.45

Fig.2 Results on in-vivo data

8:00 am **Automatic Mouse Embryo Brain Ventricle Segmentation, Gestation Stage Estimation, and Mutant Detection from 3D 40-MHz Ultrasound Data**

Jen-wei Kuo[1], Yao Wang[1], Orlando Aristizabal[2,3], Daniel H. Turnbull[3], Jeffrey A. Ketterling[2], Jonathan Mamou[2]; *[1]Electronics and Computer Engineering, Polytechnic School of Engineering, New York University, Brooklyn, USA, [2]F. L. Lizzi Center for Biomedical Engineering, Riverside Research, New York, USA, [3]Skirball Institute of Biomolecular Medicine, New York University School of Medicine, New York, USA*

Background, Motivation and Objective

Volumetric analysis of brain ventricles (BVs) is important to the study of normal and abnormal development of the central nervous system (CNS) of mouse embryos. High-frequency ultrasound (HFU) is frequently used to image embryos because HFU is real-time, non-invasive, and provides fine-resolution images. However, manual segmentation of BVs from 3D HFU volumes remains challenging and time consuming. Therefore, automatic segmentation, staging, and brain phenotypes detection algorithms are needed for studies with large embryo counts.

Statement of Contribution/Methods

Volumetric ultrasound data were acquired in utero and in vivo from pregnant mice using a 5-element, 40-MHz annular array. A 5-channel pulser was used to consecutively excite each array element. The 25 resulting transmit/receive signals processed using delay-and-sum beamforming which yielded a depth of field sufficient to cover the entire head of the embryo. An automatic segmentation algorithm called nested graph cut (NGC) was developed to segment the BVs, head, amniotic fluid, and uterus. To define the missing boundary between objects (e.g., head and uterus), NGC only applied predefined structural information and, thus, did not require any training. After segmentation, it is possible to stage embryos or detect mutants with a BV phenotype based on the volume ratio between the BVs and head (Fig. 1a) and BV morphology (Fig. 1b). Mutations caused by the loss of midbrain tissue (Fig. 1b) were automatically detected by extracting and quantifying the skeleton geometry of the third and fourth BV.

Results/Discussion

The NGC algorithm was applied to 40 wild type embryos spanning from days E10.5 to E14.5 and the Dice similarity coefficient (DSC) was used to quantitatively compare automatic and manual segmentations. The average DSC was 89±5% for BV segmentation and 90±3% for head segmentation. The NGC algorithm also showed better performance than region growing, active shape model (ASM), and our previous work, which refines the ASM result by shape-constrained region growing. In addition, NGC permitted to automatically detect mutants from stage-matched wild-type embryos. Therefore, our NGC-based framework could be invaluable in streamlining development biology studies requiring quantitative CNS assessment, staging, and mutant detection.

Fig. 1: (a) BVs-Head volume ratio automatically computed from NGC-based segmentation can be used to stage embryos. (b) Mid-sagittal section of E12.5 embryos showing the expected loss of mid-brain tissue (arrows) in an Engrailed 1 (En1) mutant compared to a wild-type littermate. 3D renderings generated from NGC segmentation results also reveals an increase in BV volume for the EN1 mutant due to loss of midbrain tissue.

8:00 am **Robust Sound Speed Estimation for Hepatic Steatosis Assessment**

Marion Imbault[1], Alex Faccinetto[2], Bruno-Félix Osmanski[1], Mathias Fink[1], Jean-Luc Gennisson[1], Valérie Vilgrain[2], Mickaël Tanter[1]; *[1]Institut Langevin, ESPCI ParisTech, PSL Research University, CNRS UMR 7587, INSERM U979, Paris, France, [2]Department of Radiology, Beaujon Hospital, Paris, France*

Background, Motivation and Objective

Hepatic steatosis is a common condition, the prevalence of which is increasing along with non-alcoholic fatty liver disease (NAFLD). Currently, the most accurate noninvasive imaging method for diagnosing and quantifying hepatic steatosis is MRI, which estimates the Proton-Density Fat Fraction (PDFF) as a measure of fractional fat content (Leporq, 2013). However MRI has several limitations including cost, contra-indications and poor availability that could be overcome by using ultrasound. Although conventional ultrasound is widely used by radiologists for hepatic steatosis assessment, it remains qualitative. It is well known that speed of sound within soft tissues varies slightly with fat content. The objective of this study is to assess the accuracy for steatosis detection and staging of a specific ultrasonic sequence for sound speed estimation (SSE). A preliminary clinical trial was undertaken, with PDFF measurement as a gold standard, to test this new sequence based on the assessment of spatio-temporal properties of the local speckle noise for SSE.

Statement of Contribution/Methods

Prospectively, 10 patients underwent MRI (3T Philips Ingenia), conventional ultrasound examination and specific ultrasound sequence acquisition; the later two using an abdominal curved probe (SC6-1, Supersonic Imagine (SI)) driven by an ultrafast ultrasound scanner (Aixplorer, SI). We implemented a new ultrasonic sequence for SSE based on time reversal processing of local speckle noise and focusing criterion (Montaldo, 2011). As steatosis can be considered as a homogeneous diffuse disease, only one single region of interest at 6 cm depth in the right liver was required for each patient. Fat and muscle layers thickness were measured with conventional ultrasound and were integrated in the calculation of the final SSE in the liver.

Results/Discussion

Our approach enables an accurate estimate of the ultrasonic sound speed in the liver with a standard deviation below 2.4 %. We obtained SSE ranging from 1.43 ± 0.01 mm/µs to 1.56 ± 0.01 mm/µs for patients with PDFF from 28.17% to 0.18% respectively. Strong correlation for quantification of hepatic steatosis was observed between the decrease of SSE and the increase of PDFF ($R^2 = 0.92$) (Fig. 1). In conclusion, this first pilot study demonstrates the feasibility of hepatic steatosis detection and staging with SSE in patients with NAFLD.

Fig. 1: Correlation between sound speed estimation (SSE) and proton density fat fraction (PDFF) for ten patients. Patients without steatosis are characterized by PDFF<2.5%. We observe that speed of sound in liver decreases when fat fraction increases.

PA-14

8:00 am *In vivo* **magnetomotive ultrasound imaging of rat lymphnodes – a pilot study**

Maria Evertsson[1], Magnus Cinthio[1], Pontus Kjellman[2,3], Sarah Fredriksson[2], Roger Andersson[1], Hanna Toftevall[2], Hans W Persson[1], Tomas Jansson[4,5]; *[1]Biomedical Engineering, Faculty of Engineering, LTH, Lund University, Lund, Sweden, [2]Genovis AB, Sweden, [3]Medical Radiation Physics, Clinical Sciences Lund, Lund University, Lund, Sweden, [4]5Biomedical Engineering, Clinical Sciences Lund, Lund University, Lund, Sweden, [5]Medical Services, Skåne University Hospital, Lund, Sweden*

Background, Motivation and Objective

We have previously developed a frequency and phase tracking algorithm which is able to detect superparamagnetic iron oxide nanoparticles (SPIO NPs) using magnetomotive ultrasound imaging, with our primary aim being to detect sentinel lymph nodes (SLNs) in breast cancer surgery. Recently we have shown detection of SPIO laden rat SLNs *in situ* (IEEE T-UFFC, 61:1276-1283). Here we present the feasibility of *in vivo* detection of SLNs in rats and how the signal-to-clutter-ratio is affected by magnetic coil excitation.

Statement of Contribution/Methods

Three Wistar rats were subcutaneously injected with 0.1 mL 35 nm NP solution in concentrations of 0.1, 0.2, 0.3 mg iron oxide/mL in their right hind paws. 24 hours post injection the animals were anaesthetized and scanned with a high frequency ultrasound scanner (Visualsonics VEVO 2100). For each rat the location of the popliteal lymph node, proximal to the injection site, was positioned between the transducer (center frequency 30 MHz) and a coil producing a time varying magnetic field. The AC-voltage (5 Hz) applied on the coil was varied between 5-60 V, in steps of 5 V. The RF IQ cineloops were processed offline in Matlab where our algorithm was implemented. Signal-to-Clutter-Ratios (SCR), defined as magnetomotive displacement amplitude in the lymph node divided by that in the rest of the ultrasound image, were calculated.

Results/Discussion

The SPIO-NP laden sentinel lymph nodes in all three rats were successfully imaged using MMUS and our phase-gated algorithm. Panel A shows a graph of SCR versus excitation voltage. The SCR increases with higher voltage and after 20-30 V the SCR stabilizes and only a small increase can be seen. This is primarily due to magnetic saturation of the iron core at higher voltages. The mean SCR for the three rats (conc. 0.1, 0.2 and 0.3 mg Fe/ml) were 15.7 dB, 23.5 dB and 18.2 dB respectively. This indicates inter-subject variation in SPIO-NP uptake in the sentinel lymph node and/or geometrical differences. Panel B and C show the SLN in rat 2 at 55 V. Panel B shows the total movement in the ultrasound image at all frequencies and phases and panel C shows the frequency and phase gated image obtained using our algorithm. The color represents displacement, note the different scales on the color bars. The SCR was 28.2 dB. In panel B, observe the bright area to the left of the SLN, stemming from the popliteal artery.

PA-15

8:00 am **Ultrafast Pulsed Magnetomotive Ultrasound Imaging of Sentinel Lymph Nodes: Small Animal Study**

Yu-Chun Huang[1], Jieh-Yuan Houng[1], Yi-Da Kang[2], San-Yuan Chen[2], Meng-Lin Li[1,3]; *[1]Dept. of Electrical Engineering, National Tsing Hua University, Hsinchu, Taiwan, [2]Dept. of Materials Science and Engineering, National Chiao Tung University, Taiwan, [3]Institute of Photonics Technologies, National Tsing Hua University, Taiwan*

Background, Motivation and Objective

Sentinel lymph nodes (SLNs) are the first draining lymph nodes while the metastatic cancer cells are spreading. A noninvasive imaging modality for SLN identification with fine needle aspiration biopsy (FNAB) would be beneficial for staging the axillary lymph nodes without surgical intervention. Recently, photoacoustic imaging has shown its feasibility of SLN mapping. However, it is not available for clinical use yet, and involves laser safety issues. MRI has been tried with superparamagnetic iron oxide nanoparticles (SPIOs) for SLN imaging. Because of its high cost and low imaging rate, MRI is not a good solution for SLN FNAB.

Statement of Contribution/Methods

Here we propose an alternative solution – ultrafast pulsed magnetomotive ultrasound (pMMUS) for noninvasive SLN identification, which leverages the MRI SPIOs and offers real-time imaging capability for SLN FNAB. Ultrafast pMMUS is based on plane wave imaging, which frame rate is fast enough for tracking of the magneto-motion of the SPIOs induced by a magnetic pulse. Ultrafast pMMUS localizes the SPIOs drained to the SLNs and thus identify the SLNs. Experiments on rats were carried out to verify the feasibility. Each rat was injected intradermally on the hind paw pad with 0.1 ml of SPIO solution under anesthesia. Ten minutes post injection, ultrafast pMMUS with a 5-kHz frame rate and a 6-ms magnetic pulse was performed postmortem using a clinical ultrasound research platform (Prodigy, S-Sharp, Taiwan). Matched filtering with the measured magnetic pulse was applied to improve the pMMUS contrast deteriorated by false motion estimation and magnetic field inhomogeneity.

Results/Discussion

Fig. (a) showed the B-mode image of the SPIO-laden SLN and its surrounding fat tissue where the SLN was hard to be localized. Ultrafast pMMUS displacement mappings at 0- and 6.4-ms when the magnetic pulse being applied were shown in Figs. (b) and (c), respectively. The SLN was identified in Fig. (c), and was confirmed by the methylene blue assay. The dynamic response of the excited SPIOs was visualized and compared with the measured magnetic pulse (Fig. (d)). Overall, we demonstrated the feasibility of the proposed ultrafast pMMUS for noninvasive SLN identification. Proper SPIO particle size, time window of imaging, and motion-tracking algorithm will be studied to further improve the performance of the proposed method.

(a) B-mode image

(b) Ultrafast pMMUS at t=0 msec

(c) Ultrafast pMMUS at t=6.4 msec

(d) Normalized displacement curve

PA-16

8:00 am   Ultrasound flow mapping for the investigation of crystal growth

Norman Thieme[1], Richard Nauber[1], Hannes Beyer[1], Hannes Radner[1], Lars Büttner[1], Paul Bönisch[2], Kaspars Dadzis[2], Lamine Sylla[2], Dagmar Meier[3], Olf Pätzold[3], Jürgen Czarske[1]; [1]*Laboratory for Measurement and Sensor System Techniques, Dresden University of Technology, Dresden, Germany,* [2]*SolarWorld Innovations GmbH, Freiberg, Germany,* [3]*Institut für Nichteisen-Metallurgie und Reinststoffe, Technische Universität Bergakademie, Freiberg, Germany*

Background, Motivation and Objective

The production of high quality solar cells requires a deep understanding of the solidification process. Especially when time-dependent magnetic fields are used to improve the material and heat transfer in the melt, the resulting flow structures are complex and unsteady. Hence, numerical simulations are used to gain an insight into the melt flow. For the calibration of the numerical simulations, model experiments at room temperature are used. This requires a comprehensive flow mapping of complex and unsteady flow phenomena. Commercial flow instrumentation systems usually utilize only one or a few single element probes that are operated strictly in sequential multiplex. This leads to low frame rates and limits their application to quasi-static flow fields.

Statement of Contribution/Methods

We present an ultrasound array Doppler velocimeter (UADV) suited for model experiments with solidification in crucibles with a 220 x 220 mm² base. The UADV is equipped with four ultrasound arrays with 42 elements each. Due to its modular set-up various arrangements of the ultrasound arrays are feasible, for example, measuring two horizontal 2d-2c flow fields. The melt flow is strongly influenced by the melt height, that constantly decreases during a solidification process. Hence, measuring the position and the shape of the solidification front is required for an understanding of the melt flow. The vertical position of the solidification front is measured with nine single US transducers which are placed on top of the melt.

The signal processing is done by a FPGA enabling long running measurements of up to one day, which is required for solidification processes. The 2d-2c flow fields are composed of two orthogonal 2d-1c flow fields. This composition requires an exact knowledge of the relative positions of the ultrasound arrays. The relative positions are determined by a novel spatial self-calibration that uses mutual time of flight measurement.

Results/Discussion

The UADV was applied to solidification experiments with gallium in a crucible with a 220 x 220 mm² base and an external magnetic field. Measurement results including the measurement of the solidification front will be shown. A comparison with numerical simulations will be provided. The figure shows an exemplary flow and solidification interface measurement with GaInSn and a mock-up solidification interface.

PA-17 _____

8:00 am   Non-contact mass measurement of droplet based on free oscillation under ultrasonic levitation.

Sae Ito[1], Ryohei Nakamura[1], Hiroki Tanaka[1], Yosuke Mizuno[1], Marie Tabaru[1], Kentaro Nakamura[1]; *[1]Precision and Intelligence Laboratory, Tokyo Institute of Technology, Yokohama, Japan*

Background, Motivation and Objective

Recently, non-contact manipulation is much in demand for the area of drug development, biotechnology and new material sciences. Ultrasonic levitation of droplet is one of the promising methods for non-contact transport, mixing and dispensing. [Y.Ito et al., Acoust. Sci. Technol., 31 (2010)420.] Evaluating mass is also an essential issue. We challenge, in this report, to measure the mass of a small droplet suspended in ultrasonic field in air from the free oscillation around the nodal position of the standing waves.

Statement of Contribution/Methods

A droplet suspended at the node of the pressure standing wave field will vibrate near the nodal position if some disturbance is applied to the droplet. The natural frequency of the free oscillation is determined by the mass of the droplet and the slope of the potential force. Thus, we can estimate the mass by measuring the frequency of the free oscillation, provided the force acting on the droplet is known.

A droplet is levitated in the standing wave between a vibrating horn of 30 mm in diameter, and a reflector. The distance between the horn and the reflector was adjusted to a half wavelength (7 mm at 27.4 kHz). First, we levitated five solid samples with different mass and diameter and observed the oscillation to obtain the calibration curve. Oscillation was caused by rising slightly the drive voltage of the transducer for a short time (0.07 s). The droplet was illuminated with a collimated light, and then, the shadow of the droplet was projected on a quarter- divided photo detector. The oscillation displacement was recorded as the output voltages of the element detectors. The sound pressure was measured using a thin piezoelectric element bonded on the surface of the reflector. The sound pressure was kept constant for various sample droplets by changing the driving voltage.

Results/Discussion

We demonstrated the mass estimation for ethanol and water droplets with different volumes. The average measurement error was 21%. The error might be attributed to the difference in the actual sound pressure near the droplet because the shape of the droplet was deviated from sphere due to acoustic radiation pressure. We need to compensate this pressure discrepancy to achieve higher accuracy. We believe that this experiment is a useful challenge to estimate the mass of droplet under totally non-contact condition.

STUDENT PAPER COMPETITION

8:00 am   Ultrasound Image-based Absolute Concentration Measurement Technique for Materials with Low Scatterer Concentration

John H. Lee[1], Javier Jimenez[2], Xiang Zhang[1], Duane S. Boning[1], Brian W. Anthony[1]; *[1]Massachusetts Institute of Technology, Cambridge, MA, USA, [2]Madrid-MIT M+Vision Consortium, Massachusetts Institute of Technology, Cambridge, MA, USA*

Background, Motivation and Objective

Ultrasound-based measurement of absolute concentration of scatterers has a wide range of potential applications such as in microbiology, cell culture, and blood work. When the material is dilute and the scatterer size is similar to the wavelength of ultrasound, individual scatterers can be distinguished in the image. While the number of scatterers in the image can be counted, quantifying the image volume is challenging since the exact slice thickness is unknown. We propose a method for estimating the volume of image of a dilute monodispersed sample acquired with a mechanically scanned single element transducer. The method does not require prior characterization of the transducer or the setup.

Statement of Contribution/Methods

For a disk transducer the beam shape is the same in the azimuth and elevation directions due to radial symmetry. Therefore, the resulting beam of a mechanically scanned disk transducer will have a slice profile identical to the azimuthal beam shape. The azimuthal beam width can be estimated from the spreading of an individual scatterer, which depends on the point spread function and properties of the scatterer.

Images are acquired with a linearly scanned 75-MHz spherically focused transducer. The samples consist of 10-μm polystyrene particles in distilled water with concentration ranging from 5 - 50 particles/μL. After envelope detection, the particle echoes are detected (Fig. 1a) and characterized by fitting to a 2D Gaussian. From the population of particles, beam widths are mapped as a function of axial position and used to estimate the image volume. Concentration is calculated for each frame and combined to produce the final measurement.

Results/Discussion

Fig. 1b shows a plot of beam width vs. axial position. Slice thickness is estimated from the upper boundary in the plot, which represents the maximum observable beam width at a given axial position. This method is compared to hemocytometer measurements. While the means show good agreement, the proposed ultrasound method shows smaller variance (Fig. 1c).

The proposed method enables the measurement of absolute concentration of dilute sample using only ultrasound image data with significantly better performance than the widely accepted hemocytometer method. Currently, this method is limited to mechanically scanned single element imaging, but work to extend the method to array imaging is ongoing.

Figure 1. (a) B-mode image showing the detected particles (yellow). (b) Scatter plot of extracted beam width vs. axial position. (c) Comparison of absolute concentration measurement between the proposed method and the hemocytometer.

1D - MEL: Elasticity Imaging of Small Structures

Plenary Hall

Friday, October 23, 2015, 08:00 am - 09:30 am

Chair: **Kathy Nightingale**
Duke University

8:00 am   Characterizing Sclerotic Skin Stiffness with Acoustic Radiation Force Impulse (ARFI) and Shear Wave Elasticity Imaging (SWEI)

Mark Palmeri[1], A. Rambi Cardones[2], Seung Yun Lee[1], Kathryn Nightingale[1]; [1]*Biomedical Engineering, Duke University, Durham, NC, USA,* [2]*Dermatology, Duke University, Durham, NC, USA*

Background, Motivation and Objective

Sclerotic skin diseases are associated with inflammation and fibrosis in the dermis, and these diseases lack a non-invasive imaging technology to diagnose and evaluate their severity. The associated change in skin collagen content with disease progression makes this pathology amenable to being characterized with Acoustic Radiation Force Impulse (ARFI) and Shear Wave Elasticity Imaging (SWEI) methods. The objective of this study was to characterize skin stiffness in healthy individuals at repeated 3 month intervals and to compare sclerotic to healthy skin stiffness.

Statement of Contribution/Methods

ARFI and SWEI were implemented using a Siemens 14L5 linear array on an ACUSON S2000™ scanner, focused at 5.5 mm with an F/1 focal configuration and offset from the skin using a gel bridge to keep the dermis in the focal zone. A single dermatologist performed all imaging. Harmonic tracking (6,15/12.3 MHz) was used to improve B-mode image quality with reduced clutter and higher resolution using a pulse inversion technique with a pulse repetition frequency of 8.9 kHz. SWEI shear wave speeds were reconstructed over a 7 mm lateral extent confined to the dermis for 5.7 ms.

Twenty-two patients were imaged in an IRB-approved study, with normal and sclerotic skin stiffness characterized by (1) mean ARFI displacement magnitude, and (2) group shear wave speed estimated using a Radon sum of shear wave velocity data. Imaging was performed at different anatomic sites, including the upper and lower back, arm, forearm, abdomen, thigh and calf. Five repeat data acquisitions were performed in each anatomic location. The ratios of ARFI displacement and SWEI-derived shear wave speed were calculated between sclerotic lesions and unaffected contralateral skin in the same anatomic site.

Results/Discussion

ARFI displacement and SWEI shear wave speeds were reconstructed in 85% of all acquisitions, with most failures attributed to regions of interest that extended beyond the dermis into the subcutaneous fat. Restricting regions of interest to the dermis yielded a 96% success rate. ARFI and SWEI metrics showed no significant difference between contralateral imaging locations across different anatomic sites in healthy skin ($p < 0.05$). Mean shear wave speeds were >200% greater in sclerotic lesions than in contralateral healthy skin in patients with graft-vs-host disease (GVHD) ($p < 0.01$), and 25% greater in patients with morphea. ARFI displacements exhibited greater variability than shear wave speed in characterizing sclerotic skin, showing a 61% decrease compared to healthy skin in GVHD patients ($p < 0.05$) and a 19% decrease in morphea patients ($p < 0.05$). ARFI and SWEI are able differentiate sclerotic skin lesions from healthy skin, and studies are underway to evaluate their utility in longitudinally monitoring disease progression and response to therapy.

8:15 am   Model-based assessment of the mechanical properties of the animal crystalline lens in situ using acoustic radiation force and optical coherence elastography system

Chen Wu[1], Zhaolong Han[1], Shang Wang[1,2], Jiasong Li[1], Manmohan Singh[1], Chih-hao Liu[1], Stanislav Emelianov[3], Fabrice Manns[4,5], Kirill Larin[1,2], **Aglyamov Salavat**[3]; [1]*Biomedical Engineering, University of Houston, Houston, Texas, USA,* [2]*Molecular Physiology and Biophysics, Baylor College of Medicine, Houston, Texas, USA,* [3]*Biomedical Engineering, University of Texas at Austin, Austin, Texas, USA,* [4]*Bascom Palmer Eye Institute, University of Miami Miller School of Medicine, Miami, Florida, USA,* [5]*Biomedical Engineering, University of Miami College of Engineering, Miami, Florida, USA*

Background, Motivation and Objective

A better understanding of presbyopia is a fundamental requirement for the development of effective correction techniques. According to the most widely accepted theory, presbyopia results from an increase in stiffness of the crystalline lens. However, the exact relation between lens stiffness and presbyopia remains to be established. Therefore, there is a need for a clinical method capable of assessing biomechanical properties of the crystalline lens in situ and noninvasively. In our previous studies, we used acoustic radiation force to probe laser-induced micro-bubbles as a way to remotely assess the viscoelastic properties of the crystalline lens. In this work, we extend this approach to the case where the acoustic radiation force is applied to the anterior surface of the crystalline lens to create a short spatially localized deformation, while displacement of the lens surface is measured using phase-sensitive optical coherence tomography (OCT) system.

Statement of Contribution/Methods

We have developed model-based approach to assess the biomechanical properties of the lens and applied this approach for measuring age-related changes in biomechanical properties of the lens in intact rabbit eyes in situ. The crystalline lens was modeled as a viscoelastic medium and an external acoustic load was considered as an axisymmetric force applied to the upper surface of the medium. An analytical solution of this problem was obtained using the Hankel transform. A 3.5 MHz single element transducer was used to remotely disturb the anterior surface of the young (2-3 months old, n=3) and mature (over 6 months old, n=4) rabbit lenses through the cornea and the aqueous humor. In the phase-sensitive OCT system, a superluminescent laser diode was utilized as the light source with a central wavelength of ~840 nm and bandwidth of ~50nm. The A-line acquisition rate of this system was 25 kHz. Ultrasound transducer and OCT system were co-focused, and the measurements of the displacement were performed at the focal point.

Results/Discussion

Results of the measurements demonstrated a significant difference between the maximum displacements of the young and the mature lenses, which were 3.3±0.1 µm and 1.6±0.4 µm, respectively. The reconstruction results show the Young's modulus (2.5±0.5 kPa) and shear viscosity (0.37±0.7 Pa s) of the young lenses are both less than the ones of the mature lenses (7.4±0.8 kPa and 0.57±0.9 Pa s). In the mature lenses, both experimental and theoretical displacements demonstrate saturation at the end of the acoustic pulse, which happens when the elastic response of the medium compensated for the acoustic force. In summary, the optical coherence elastography system, which combines acoustic radiation force loading and phase-sensitive OCT, was demonstrated as a promising tool for noninvasive assessment of the biomechanical properties of the lens.

8:30 am   Factors Impacting Detection of Untethered Scatterers within Viscoelastic Background by ARFI Surveillance of Subcutaneous Hemorrhage (ASSH): In Silico Demonstration

Tomasz Czernuszewicz[1], Robert Hinson[1], Caterina Gallippi[1,2]; *[1]Joint Department of Biomedical Engineering, University of North Carolina/North Carolina State University, Chapel Hill, NC, USA, [2]Department of Electrical and Computer Engineering, North Carolina State University, Raleigh, NC, USA*

Background, Motivation and Objective

ARFI Surveillance of Subcutaneous Hemorrhage (ASSH) is a method for noninvasively detecting and monitoring subcutaneous hemorrhage, in vivo. In ASSH, acoustic radiation force (ARF) is used to mechanically excite tissue surrounding a vascular injury, and regions of hemorrhage are identified by elevated variance in the measured tissue acceleration profiles. The elevated variance is attributed to RF signal decorrelation due to untethered blood scatterers that do not experience elastic recovery following ARF excitation. However, increased variance, or jitter, can be caused by a number of factors nonspecific for the presence of hemorrhage, such as low ultrasonic SNR or small tracking-kernel size. In this work, a model of low-reflection-amplitude, untethered scatterers (mimicking red blood cells) under ARF excitation is developed using FEM simulation and Field II, and the model is utilized to quantify the detection performance of ASSH.

Statement of Contribution/Methods

Soft-tissue dynamics in response to an ARF impulse were simulated using LS-DYNA and ultrasonically tracked using Field II. To mimic hemorrhaged blood, additional scatterers were added to the Field phantom with amplitudes 10 times smaller than background scatterers and assigned a random amount of residual motion following peak displacement (either ±1 μm or ±5 μm). The untethered scatterers were arranged in a hemispherical lesion that grew from 0.96 mm^2 to 15.3 mm^2 over six times steps, and 2D ASSH images were simulated with 10 independent scatterer realizations. White Gaussian noise was added to RF lines to achieve 5-50 dB SNR, and data sets were motion tracked with six kernel sizes (1.5λ, 2.5λ, 3.5λ, 5λ, 7λ, and 10λ). Profiles of displacement were converted to acceleration, and variance of acceleration (VoA) was calculated. Finally, ROC analysis determined optimal VoA thresholds to maximize ASSH sensitivity and specificity.

Results/Discussion

Performance analysis showed that at 40 dB SNR ASSH could achieve high sensitivity (≥0.9) and specificity (≥0.95) when the untethered scatterer area was ≥15.3 mm^2, and residual motion and concentration were ±5 μm and 45-60%, respectively. Even in the cases of lower scatterer concentrations (15%) and smaller hemorrhage area (0.96 mm^2), mean sensitivity and specificity were greater than 0.8 and 0.9, respectively, when the residual scatter motion was ±5 μm. However, when residual scatterer motion was ±1 μm, performance decreased. Kernel size had substantial impact on ASSH performance, particularly when scatterer residual motion was low (±1 μm); mean AUC increased approximately 10 percentage points between the 1.5λ and 10λ simulations. These results suggest that, given adequate system SNR and optimal threshold and kernel selection, ASSH achieves high performance (≥0.9 AUC) for detecting untethered scatterers.

FRIDAY ORAL

8:45 am   High Frequency Point Shear Wave Elastography (HF-pSWE): A Novel Technique for High Resolution Soft Tissue Elasticity Mapping

Pei-Yu Chen[1], Chih-Chung Huang[1], Ma Teng[2], Qifa Zhou[2], K. Kirk Shung[2]; *[1]Department of biomedical engineering, National Cheng Kung University, Taiwan, [2]Department of Biomedical Engineering, University of Southern California, USA*

Background, Motivation and Objective

Shear wave elastography (SWE) is a novel imaging technique that assesses the mechanical properties of soft tissue by tracking the shear wave propagation speed. The shear wave speed can directly relate to the stiffness of tissue. Currently, several ultrasonic shear wave approaches have been proposed to detect the elastic properties of tissue, such as transient elastography, supersonics shear imaging, and comb-push ultrasound shear elastography. However, most of above methods cannot provide enough resolution for imaging the vessel, skin, and ophthalmic tissues due to their operational frequency. In order to increase the resolution of shear wave image for estimating the elastic properties of these micro-structure tissues, a HF pSWE imaging technology was developed in present study.

Statement of Contribution/Methods

A novel triple elements transducer was fabricated for HF pSWE in this study. The larger element with a frequency of 8 MHz was used to generate acoustic radiation force to induce shear wave propagation in tissue, and the shear wave speed can be detected by another two 32 MHz detecting elements using pulse-echo mode. By moving the triple element transducer, the shear wave speed of multiple locations can be obtained to reconstruct a two-dimension image by calculating the time shift between two detecting points, so-call HF pSWE. Experimental setup and the signal processing procedures are shown in Fig. 1(b).

Results/Discussion

The B-mode images and their corresponding HF-pSWE images from two layer gelatin phantoms are shown in Fig. 1(c) and (d), respectively. The dimension of HF-pSWE images are 1.5 by 1.5 mm for both top-bottom and right-left phantoms. The average values of shear wave propagation speed are about 0.82 m/s for 7% and 0.35 m/s for 2% gelatin phantom, respectively. It is difficult to recognize the stiffness distribution of phantoms from B-mode images, however, the stiffness within two-layer phantoms can be observed clearly by HF pSWE images. A HF-pSWE technique was successfully developed in this study. The experimental results demonstrate the feasibility of using this novel triple elements transducer for high resolution shear wave imaging. In the future, this technique will be further verified by scanning in vitro and in vivo tissues of animal to demonstrate the feasibility for clinical applications.
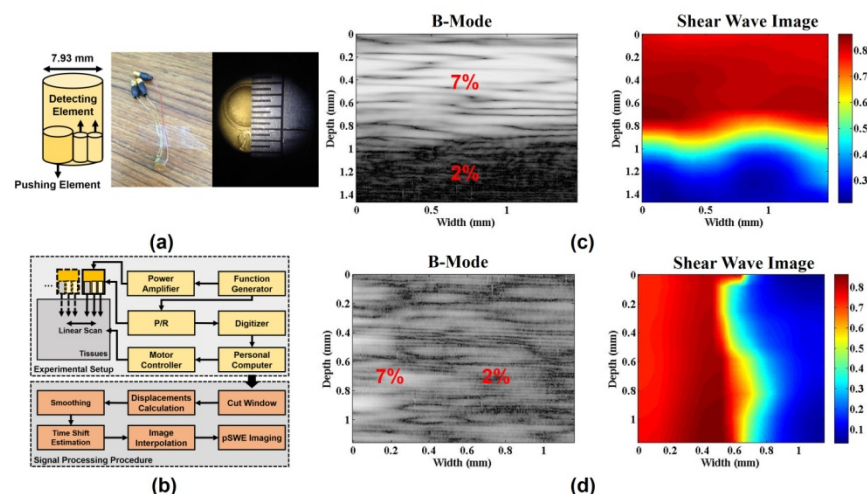
Fig. 1

1D-5

9:00 am   Shear Wave Elasticity Imaging for Preclinical Research on Small Animals and 3D Cell Cultures

Pai-Chi Li[1]; [1]*National Taiwan University, Taipei, Taipei, Taiwan, Taiwan*

Background, Motivation and Objective

Shear wave elasticity imaging (SWEI) has exhibited widespread clinical success. Several methods such as transient elastography (TE), acoustic radiation force impulse (ARFI) imaging, and supersonic shear imaging (SSI) have been developed based on shear waves created by either using an external vibrator on the body surface or generating an acoustic radiation force inside the body by a focused ultrasound beam. However, the applications of SWEI have been relatively limited for preclinical studies of small animals because of its poor spatial resolution and the need to generate a strong radiation force with a narrow beam at a shallow depth. In addition to small animal studies, the other important field in preclinical research is mechanobiology in which 3D cell cultures recapitulating in vivo cell behaviors in response to various types of mechanical stimuli are of particular interest. One example is stiffening of the extracellular matrix resulting from cell remodeling potentiates many pathological conditions, including advanced cancers. Again, an effective tool is needed for measuring the elastic properties of such 3D cell cultures without directly contacting the samples.

Statement of Contribution/Methods

A high-frequency imaging platform has been developed using a 40 MHz single-element transducer for imaging and a separate 20 MHz excitation transducer for producing the radiation force and the associated shear waves. It was used to evaluate liver fibrosis in C57BL/6 (B6) mice and the results demonstrate that the high-frequency SWEI platform can yield quantitative viscoelastic properties for diagnosing various fibrosis stages in mice. The original high frequency SWEI setup is similar to the array configuration, in which the push beam is fixed while shear wave propagation in the image plane is tracked. An alternative near field SWEI setup has also been developed in which the push beam and the shear wave detection beam are kept close to each other over the image plane. Results demonstrate that SWEI resolution and accuracy can be greatly improved. The SWEI platform has also been applied to 3D cell culture systems for quantitatively evaluating the spatiotemporal dynamics of the elasticity of a matrix remodeled by cells cultured in 3D environments. The elasticity changes of a 3D matrix grown with various cell types were measured and the principal mechanism underlying the stiffening of matrices remodeled by highly invasive cancer cells was delineated. The described approach has shown to be an effective tool in fields involving cell-matrix mechanotransduction, and also has potential as a useful drug screening platform.

Results/Discussion

The high frequency SWEI platform has shown to be an effective tool for preclinical research on both small animals and 3D cell cultures. It will also be compared with other potential approaches, including the optical shear wave detection method based on laser speckle contrast imaging.

FRIDAY ORAL

2D - MCA: Microbubbles and Nanodroplets Applications

VIP

Friday, October 23, 2015, 08:00 am - 09:30 am

Chair: **Nico de Jong**
Erasmus Medical Centre

2D-1

8:00 am   Live Cytodynamics Imaging During Single-Site Sonoporation: Rapid Activation of Annexin Self-Defense Response by Vibrating and Collapsing Microbubbles

Wenjing Zhong[1], Alfred C. H. Yu[1]; [1]*Medical Engineering Program, University of Hong Kong, Pokfulam, Hong Kong*

Background, Motivation and Objective

While the use of microbubble (MB) contrast agents to induce sonoporation is well heard of and the pertinent cavitation dynamics has been often studied, the biophysics involved in the process has remained to be a poorly understood topic. The field is particularly short of knowledge on the biophysical dynamics at the sonoporation site: i.e. whether and how the cell would actively respond to cavitational forces. In this work, we aim to investigate how cellular self-defense machinery would be activated when a MB adjacent to the cell vibrates (stable cavitation) or collapses (inertial cavitation). Focus is placed on probing cytoplasmic annexin proteins, as they bind strongly to phospholipids and calcium ions.

Statement of Contribution/Methods

To study the annexin self-defense machinery, first we prepared YFP plasmids specific to the annexin-A1 gene. They were presented to HEK-293 cells that were seeded inside a cell chamber tailored for live confocal imaging (20x28 mm base; 1 mm height). The plasma membrane was co-labeled using CellMask. Targestar P MBs were then added as single-site sonoporation agents (1:1 cell-bubble ratio), which would passively adhere to the membrane. Subsequently, the cell chamber was mounted on an acoustically coupled confocal imaging system, and the dynamics of membrane and annexin-A1 were tracked live over the course of sonoporation (with 40x oil lens). During the experiment, the ultrasound unit of our platform would send a single shot of 10-cycle, 1 MHz ultrasound pulse (through a cone waveguide) to trigger the onset of sonoporation. Two peak negative pressures were used: 0.2 MPa (to induce MB vibration without rupture), and 0.85 MPa (to induce MB collapse).

Results/Discussion

In cases with large pore size (2.7 um peak gap size in this case), annexin-A1 was found to persistently accumulate at the sonoporation site and along the membrane periphery. See figure for a set of annexin-A1 images (scan plane at cell's mid-height) in a sonoporation case due to MB collapse (inertial cavitation). Similar findings were observed in sonoporation induced by vibrating MBs. The trend was found to be reversible for smaller sonoporation sites (~1 um diameter). These direct observations represent the first evidence that the cellular self-defense machinery is recruited in sonoporation, suggesting that the cell-bubble interaction is by no means biologically passive.
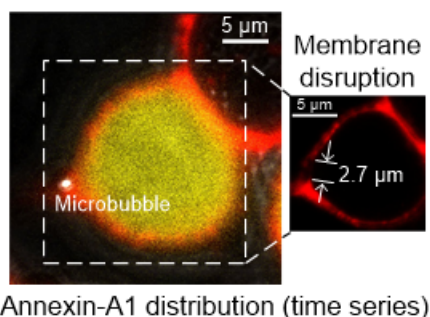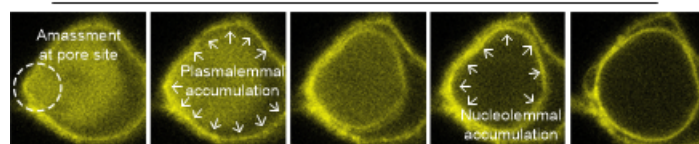
2D-2

8:15 am   Effect of shell loading on the mechanical properties and dynamic response of Optison™ microbubbles.

Camilo Perez[1,2], Yujin Zong[3], Cheng-Hui Wang[4], Jarred Swalwell[5], Juan Tu[6], Thomas Matula[2]; [1]*Bioengineering, University of Washington, Seattle, Washington, USA,* [2]*Center for Industrial and Medical Ultrasound- Applied Physics Laboratory, University of Washington, Seattle, Washington, USA,* [3]*Department of Biomedical Engineering, Xian Jiaotong University, Xi'an, China, People's Republic of,* [4]*Institute of Applied Acoustics, Shaanxi Normal University, Xi'an, China, People's Republic of,* [5]*Oceanography, University of Washington, Seattle, Washington, USA,* [6]*Physics, Nanjing University, China, People's Republic of*

Background, Motivation and Objective

Some microbubbles (MBs) incorporate materials (drugs or fluorescent markers) either loaded to the native bubble shell or dissolved within the layers of the shell, thus modifying their shell properties. Understanding how loading affects a MB's response is important for imaging and therapeutic applications. The objective of this study was to determine the relative effect of loaded vs. unloaded MBs with a statistically large sample.

Statement of Contribution/Methods

A flow cytometer modified with a PZT transducer (UFFC, Vol. 58, pg. 955, 2011) was used to extract the shell properties of statistically significant numbers of MBs. We incorporated Evans blue fluorescent dye (which has a strong binding with albumin) to the shell of Optison™ and confirmed the shell loading via fluorescent microscopy and flow cytometry. Size stability was performed using coulter multisizer before and after dye loading. The viscoelastic properties of Optison™ MBs (dye-loaded vs unloaded) driven at 1 MHz were measured at 50kPa and 100kPa peak-positive pressures.

Results/Discussion

Our statistically significant results with protein MBs agree with previous findings for lipid shelled MBs (UMB Vol. 38 pg. 2174, 2012). Loaded MBs exhibited increased shell viscosity both as a function of MB size and shear rate (Fig 1A, 1B, respectively) over unloaded MBs. In addition, spectral analysis of hundreds of MB R(t) curves in the mean size range (R= 1.5-2.5 µm) revealed a statistically significant enhancement of +4.5, 5.5, 6.4 and 7.7dB increase in the second, third, fourth and fifth harmonic of the loaded MB spectra compared to the unloaded MB (averaged for N=340 MB in each group). Increasing the driving pressure did not change the viscosity and shear rate trends shown in Fig1A and B. The shell elastic modulus did not show statistically significant differences between groups (Fig 1C). Loading (Fig. 1D) did not significantly change MB size distribution. These results suggest that there is a size dependent (and thus frequency dependent) effect with loading that affects the viscosity and shear rate of the bubble, and also that loaded MBs may enhance contrast signal strength.
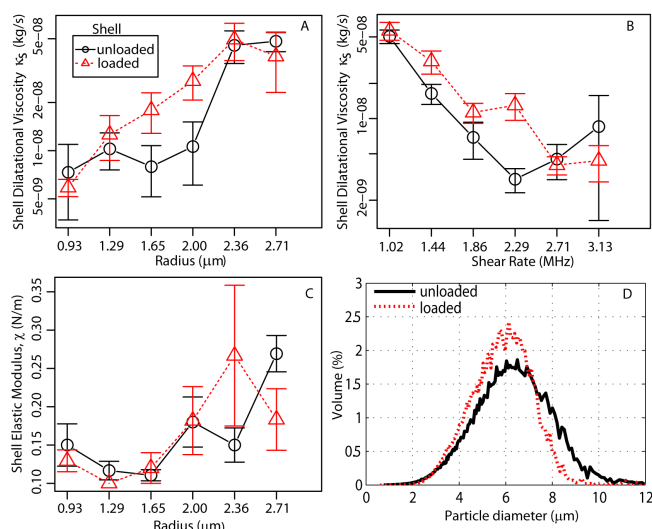
2D-3

8:30 am   **Effects of the Microbubble Shell Physicochemical Properties on Ultrasound-Mediated Drug Delivery to the Brain**

Shih-Ying Wu[1], Cherry Chen[1], Yao-Sheng Tung[1], Oluyemi Olumolade[1], Elisa Konofagou[1,2]; *[1]Biomedical Engineering, Columbia University, New York, USA, [2]Radiology, Columbia University, New York, USA*

Background, Motivation and Objective

Lipid-shelled microbubbles have been used in ultrasound-mediated drug delivery. The physicochemical properties of the microbubble shell could affect the delivery efficiency since they determine the microbubble mechanical properties, circulation persistence, and dissolution behavior during cavitation. Therefore, the aim of this study was to investigate the shell effects on drug delivery efficiency in the brain via blood-brain barrier (BBB) opening in vivo using monodisperse microbubbles with different phospholipid shell components.

Statement of Contribution/Methods

The physicochemical properties of the microbubble (median diameter: 4-5 µm) shell monolayer were varied by using phospholipids with different hydrophobic chain lengths (C16, C18, and C24), with the same lipopolymers (DSPE-PEG2000) and gas core (perfluorobutane). The dependence on the molecular size (3 and 40 kDa dextran) and acoustic energy (both pressure: 225-600 kPa and pulse length: 67 and 670 µs) were investigated in wild-type mice (n=123), using a single element focused ultrasound (FUS) transducer (excitation frequency: 1.5 MHz, pulse repetition frequency: 5 Hz, duration: 1 min) for sonication, with a pulse-echo transducer for passive cavitation detection (PCD) in order to uncover the physical mechanisms. The animals were sacrificed 1 hr after sonication, and the brains were processed for fluorescence imaging and hematoxylin and eosin staining in order to evaluate delivery efficiency and safety, respectively.

Results/Discussion

Our results showed that a relatively small increase in the microbubble shell rigidity resulted in a significant increase in the delivery of 40-kDa dextran, especially at higher pressures. Smaller (3 kDa) dextran did not show significant difference in the delivery amount, suggesting the observed shell effect was molecular size-dependent. In studying the impact of acoustic energy on the shell effects, it was found that they occurred most significantly at pressures causing microbubble destruction (450 kPa and 600 kPa); by increasing the pulse length to deliver the 40-kDa dextran, the difference between C16 and C18 disappeared while C24 still achieved the highest delivery efficiency. These indicated that the acoustic energy could be used to modulate the shell effects. The acoustic cavitation emission revealed the physical mechanisms associated with different shells that the intensity of stable and inertial cavitation increased with hydrophobic chain length especially at higher pressures. Overall, lipid-shelled microbubbles with long hydrophobic chain length could achieve high delivery efficiency for larger molecules especially with high acoustic energy. Our study, for the first time, offered evidence directly linking the microbubble monolayer shell with their efficacy for drug delivery in vivo.

2D-4

8:45 am   **High-Speed Fluorescence Microscopy of Near-Wall Shedding of Drug-Lipid Complexes from Phase-Change Droplets**

Shih-Tsung Kang[1], Tsung-Lun Chang[1], Chih-Kuang Yeh[1]; *[1]Department of Biomedical Engineering & Environmental Sciences, National Tsing Hua University, Hsinchu, Taiwan*

Background, Motivation and Objective

Phase-change droplets can undergo acoustic droplet vaporization (ADV) to release drug payloads under ultrasound (US) exposure. However, understanding the spatiotemporal dynamics of drug-surfactant distribution in response to ADV is challenging, since ADV is a microsecond process hardly resolved with conventional microscope. Herein, we used high-speed fluorescence imaging at up to 225 kfps to study the drug-surfactant distribution on single droplets during ADV and the effects of transient bubble motion and flow perturbation.

Statement of Contribution/Methods

Perfluoropentane droplets (3–10 µm in diameter) were stabilized by a shell of DSPC and DSPE-PEG2000 embedded with DiI (8 mol%) as a model lipophilic drug. The experiments were conducted in a specialized optical inverted microscopy system that allowed for concurrent laser and US excitation under high-speed imaging. Single US pulses (5 MHz, 3 cycles, 10 MPa) were transmitted to induce ADV of single droplets in a 200-µm tube at the optical focus. A 532 nm laser pulse was simultaneously

transmitted to produce laser exposure with a FWHM width of 80 µm at the optical focus. This achieved a peak intensity of 25 kW/cm^2 to produce sufficient DiI fluorescence for imaging at 225 kfps. Droplets in different positions against the tube wall were selected for observation in a bottom or side view.

Results/Discussion

The results showed pronounced lateral diffusion of DiI fluorescence on a vaporizing droplet. In the bottom view, the DiI-lipid complexes diffused outward along the bubble surface to the periphery in 4.4 µs with a mean velocity of ~1 m/s. They later flowed back to the center of the bubbles, resulting a converging flow impact at 30.8 µs to trigger the shedding of DiI-lipid complexes. The results captured in the side view revealed that the converging effect was caused by the downward interfacial shear flow due to the rapid droplet expansion against the wall. These findings suggest that ADV-based drug delivery features a near-wall preference of payload release. The effects of droplet size and ultrasound parameters will be discussed in this study, which is anticipated to provide valuable information for the optimization of ADV-based drug delivery.

FRIDAY ORAL
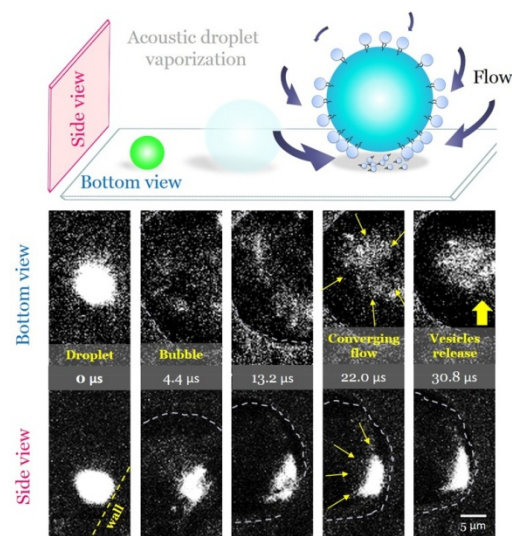
2D-5

9:00 am   **Image-Guided Characterization of Phase-shift Droplets at Pre-clinical Frequencies *In Vitro* and *In Vivo***

Paul S. Sheeran[1,2], Kimoon Yoo[3], Ross Williams[1], Yasaman Daghighi[1], Emmanuel Cherin[1], F. Stuart Foster[1,2], Peter N. Burns[1,2]; [1]*Physical Sciences, Sunnybrook Research Institute, Toronto, Canada,* [2]*Medical Biophysics, University of Toronto, Toronto, Canada,* [3]*Chemical Engineering, University of Waterloo, Waterloo, Canada*

Background, Motivation and Objective

Perfluorocarbon droplets that change state by acoustic and/or optical energy have been proposed for applications of medical ultrasound. Studies have primarily characterized droplet activation at frequencies common in human medicine. Motivation exists to design droplets for the higher frequencies used with superficial targets and small animal imaging (20-40 MHz). In this study, we measure high-frequency *in vitro* vaporization thresholds of phase-shift droplets on a pre-clinical platform and validate these measurements *in vivo*.

Statement of Contribution/Methods

Decafluorobutane (DFB) droplets near 200 nm in diameter were prepared by a previously published 'microbubble condensation' method. Size-selected emulsions (SSE) were prepared by removing the largest precursor microbubbles from native emulsions (NE) through decantation prior to condensation. Microbubble and droplet diameters were measured by Coulter counter and dynamic light scattering, respectively. Vaporization thresholds at 37°C were measured in droplet-embedded polyacrylamide phantoms. Using standard settings on a VisualSonics Vevo2100, bubble production was characterized with increasing power at 20, 30, and 40 MHz for both NE and SSE. In vivo performance was evaluated using C3H mice administered a 100 µL droplet bolus followed by 100 µL saline. Contrast production from vaporized droplets was measured in various organs with single-plane and volumetric acquisitions as a function of output power and time after injection.

Results/Discussion

DFB droplets were vaporized using high-frequency B-mode imaging sequences at pressures within the diagnostic range (MI < 1.9). Comparison between NE and SSE revealed that outliers present orders of magnitude less in concentration can significantly skew reported vaporization thresholds by as much as 2 MPa. *In vivo* thresholds were comparable to phantom measurements, though impacted by tissue attenuation (**Figure 1**). Enhancement from vaporization varied with organ and time after injection. Significant qualitative and quantitative differences were observed between NE and SSE. Data highlighted the extended circulation of DFB droplets, with vaporization continuing past 1 hour. Phase-shift droplets can be extended to high-frequency imaging platforms, creating new diagnostic and therapeutic possibilities that may assist with clinical translation.
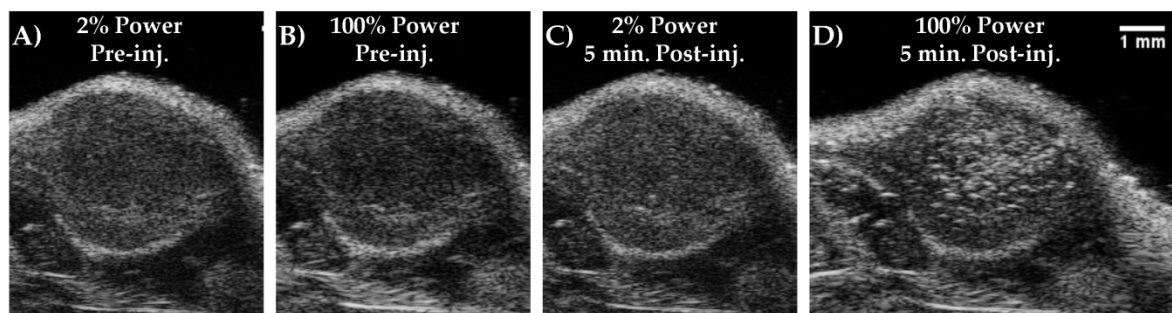
Figure 1. B-mode images of a KHT-C hindlimb xenograft tumour on a VisualSonics Vevo2100 (MS-550D probe; 40 MHz, 1-cycle pulse, 3 foci at 4, 5, 6 mm). Baseline images were taken prior to intravenous injection at A) 2% and B) 100% power. C) Five minutes after injection, circulating droplets provided minimal contrast enhancement at 2% power (below the vaporization threshold). D) Increasing power to 100% vaporized the droplets in plane, generating a high degree of contrast within the tumour.

2D-6

9:15 am   High-speed imaging of vaporization and recondensation dynamics of ICG-loaded PFP droplets irradiated by a short pulse laser

Jaesok Yu[1,2], Xucai Chen[1], Flordeliza S. Villanueva[1], Kang Kim[1,2]; [1]*Center for Ultrasound Molecular Imaging and Therapeutics, University of Pittsburgh School of Medicine and University of Pittsburgh Medical Center, Pittsburgh, PA, USA,* [2]*Department of Bioengineering, University of Pittsburgh School of Engineering, Pittsburgh, PA, USA*

Background, Motivation and Objective

Phase transition droplets have been proposed as promising contrast agents for ultrasound and photoacoustic imaging. A short pulse laser activated perfluoro-based droplets, especially when they are in the medium with temperature below their boiling point undergo phase changes of vaporization and recondensation in response to pulsed laser irradiation. Here, we report and discuss the optical observation of vaporization and recondensation dynamics of droplets in response to short pulsed laser using a high speed camera.

Statement of Contribution/Methods

Droplets with perfluoropentane (PFP) core were synthesized. Indocyanine green (ICG) was added to the core encapsulated by bovine serum albumin shell. Liquid droplets of 0.5-5.0 μm were diluted and injected into the optical chamber under high-speed microscopy (UPMC Cam) interfaced with a tunable Q-switched Nd:YAG laser. The laser pulse was delivered through an optical fiber and was aligned and tightly focused to 40 μm by a 60× objective lens. The laser fluence was estimated to be about 1.2 J/cm^2. To investigate the effect of temperature on the vaporization process, the optical chamber was mounted on a temperature controlled water reservoir. Vaporization event was recorded at 5 million frames per second and analyzed using imageJ software.

Results/Discussion

As shown in the snap shots of the movie frames, most of the droplets within the laser beam area rapidly expanded as soon as they were exposed to the laser pulse. The vaporization and recondensation processes occurred within 3 μs. In five consecutive laser pulses to the same area, the vaporization/recondensation processes were consistently reproduced. As the temperature of the media was increased above the boiling point of the PFP, the droplets did not recondensate and remained in gas phase. The fast dynamics of optical droplet vaporization/recondensation process has been imaged for the first time at sub-microseconds time scale, which will help understand the underlying processes and eventually guide the optimal design of phase transition droplets as a contrast agent.
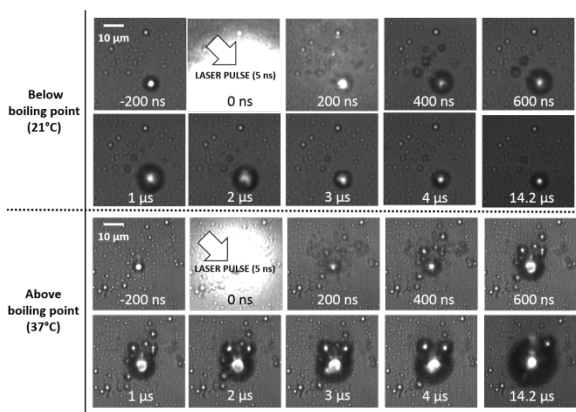
Figure 1 Snap shots of captured high-speed movie of vaporization and recondensation dynamics of ICG-loaded PFP droplets; Recondensation of vaporized droplets occurred within 3 μs after vaporization at temperature below boiling point 21°C (TOP). At temperature above boiling point 37°C, droplet was continuously expanding after vaporization (BOTTOM)

3D - MPA: Photoacoustic Imaging of Atherosclerosis and Cancer

201BC

Friday, October 23, 2015, 08:00 am - 09:30 am

Chair: **Georg Schmitz**
Ruhr-Universität Bochum

3D-1

8:00 am   Ex-vivo photoacoustic imaging of atherosclerotic carotid plaques

M.U. **Arabul**[1], H.M. Heres[1], M.C.M. Rutten[1], M.R.H.M. van Sambeek[2], R.G.P. Lopata[1]; [1]*Cardiovascular Biomechanics Group, Department of Biomedical Engineering, Technical University of Eindhoven, Netherlands,* [2]*Vascular Surgery, Catharina Hospital Eindhoven, Netherlands*

Background, Motivation and Objective

Vulnerability assessment of carotid plaques is vital to prevent atherosclerosis-related mortality and disability. Photoacoustic imaging (PAI) may have the ability to reveal the composition and the anatomical structure of the plaque, which determines its mechanical properties and vulnerability. In this study, we used PAI and ultrasound (US) imaging to image endarterectomy samples ex-vivo and compare the results with those obtained in healthy porcine carotids.

Statement of Contribution/Methods

A fully integrated hand-held photoacoustic probe was used, consisting of a pulsed diode laser (QUANTEL, FR) and a linear array transducer (ESAOTE, NL). The laser has a 130 ns pulse duration and 1 mJ pulse energy at 808 nm. The linear array transducer has a central frequency of 7.5 MHz. Four porcine carotid arteries and six carotid plaque samples were obtained from respectively a local slaughterhouse and hospital, and were mounted in a mock circulation setup. The intact plaque samples were pressurized in the physiological range with a phosphate buffered saline (PBS) solution. In both static and pulsatile cases, ultrasound and photoacoustic images were acquired. Due to calcifications and the limited optical penetration depth, images were mostly limited to the proximal wall of the samples.

Results/Discussion

Photoacoustic images of plaque samples revealed morphological information that is not visible in US images. Blood clots were found in the medial layer of the plaque samples, which can be extensions of vasculature in the plaque or the result of trauma inflicted on the medial vascularization, as well as intra-plaque hemorrhage (Fig. 1B). Data of 6 endarterectomy samples revealed that PAI of carotid plaques at 808 nm wavelength is capable of quantifying these blood clots, and luminal blood as seen in the overlay image (Fig. 1C-D). The porcine carotids revealed no hemorrhaging, which was corroborated by the lack of PAI contrast.

Due to the non-invasive nature of photoacoustic imaging, this ex-vivo study may elucidate the pre-clinical studies towards the in-vivo, non-invasive vulnerability assessment of the atherosclerotic carotid. Future studies will include more samples and the use of multi-wavelength PAI. Furthermore, to obtain more data on morphology, samples will be rotated around the longitudinal axis and scanned in the transverse plane for the multi-wavelength excitations.
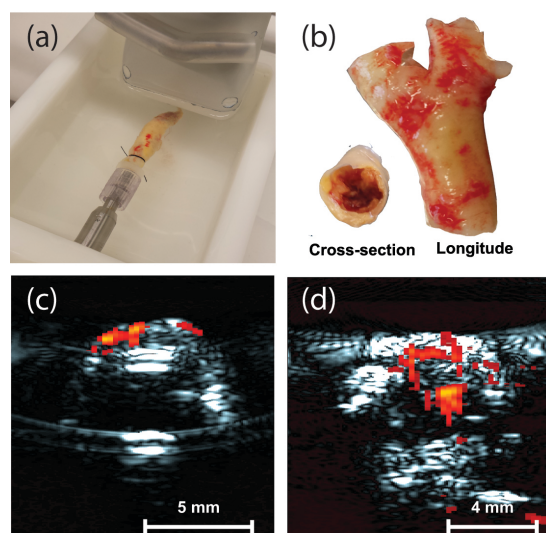
Figure 1:
(a) Mock circulation setup

(b) Picture of the plaque with blood clots on the surface and intra-plaque hemorrhage.

(c-d) Overlay image of plane wave ultrasound and photoacoustic images.

3D-2

8:15 am   Optical and acoustic spectroscopy of atherosclerotic plaque photoacoustics

Verya Daeichin[1], **Min Wu**[1], Antonius F. W. van der Steen[1,2], Gijs van Soest[1]; [1]*Erasmus MC, Rotterdam, Netherlands,* [2]*Interuniversity Cardiology Institute of the Netherlands, Netherlands*

Background, Motivation and Objective

The identification of vulnerable atherosclerotic plaques in the coronary artery is emerging as an important tool for guiding percutaneous coronary interventions, and may enable preventive treatment of such plaques in the future. Vulnerability of a plaque is determined by its structure and composition. While intravascular ultrasound (IVUS) reveals structural information, spectroscopic photoacoustic (sPA) imaging can visualize the atherosclerotic plaque composition on the basis of the optical absorption contrast. The visibility of PA imaging of plaques in IVUS frequency range (> 20MHz) has been reported1-2. However, whether such a high frequency is optimal for lipid detection has not been investigated yet.

Statement of Contribution/Methods

In an ex vivo study on human coronary arteries (7 samples, 36 locations), we combined PA spectroscopy and analysis of frequency content of the received signals. Utilizing two transducers (0.25-20 MHz and 10-35 MHz), we covered a large frequency range below the typical IVUS frequency band (0.25-35 MHz) for receiving the PA signal. sPA imaging was performed at wavelengths ranging from 1125 to 1275 nm with a step of 2 nm, allowing differentiation between plaque lipids and peri-adventitial fat tissue (Fig.1). Moreover, a k-Wave3 simulation was used with initial pressure source obtained from human coronary plaque histological images stained for fat (Oil Red O). We also compared these simulation results to the ex vivo experimental results.

Results/Discussion

Optical and acoustical spectroscopy of an atherosclerotic coronary artery sample, are depicted in Fig. 1. The acoustic spectroscopy of such a sample agrees well with the simulation results in Fig.1 e and f. Our data shows that more than 60% of the PA energy of the coronary plaque lipids lies in the frequency band below 5 MHz.

Although the PA signal of plaque lipid is a very broadband and can be detected in the IVUS frequency range, its amplitude is lower by 20 dB at frequencies > 10MHz. This frequency information can be critical for the choice of the transducer element used for PA catheter fabrication especially in a real-time imaging system where averaging is not affordable.

Fig. 1. Spectroscopy photoacoustic imaging of an atherosclerotic coronary artery sample ex vivo acquired with the two transducers (a and b are using 0.2-20 MHz transducer and c and d are using 10-35MHz transducer) and acoustic spectroscopy of an atherosclerotic coronary artery sample compared to the simulation results (amplitude in e and power in f).

References
1. Jansen, K., et al., Opt Lett, 2011. 36(5): p. 597-9.
2. Wang, B., et al., Opt Lett, 2012. 37(7): p. 1244-6.
3. Paul, C.B., et al., 2009, CRC Press. p. 25-34.

3D-3

8:30 am   Photoacoustic microscopy of lipids using a graded-index multimode fiber amplifier

Jessica Farland[1], Margaret Ferrari[1], **Takashi Buma[1]**; *[1]Union College, USA*

Background, Motivation and Objective

Photoacoustic microscopy (PAM) of lipid-rich tissue has applications such as identifying atherosclerotic plaques and visualizing myelinated peripheral nerves. Many lipids have an optical absorption peak in the 1200 nm spectral range, which is typically produced with very expensive optical parametric oscillator (OPO) lasers. We have previously demonstrated that an inexpensive 1064 nm laser and nonlinear fiber optics can produce pulses in the 1200 nm spectral range.

Statement of Contribution/Methods

In this paper, we demonstrate an improved system producing a ten-fold increase in pulse energy at a wavelength (1215 nm) near the optical absorption peak of lipids. A key factor is the use of a graded-index multimode fiber (GIMF), where the fiber core has a parabolic refractive index profile. The large GIMF core simplifies coupling of the input laser beam. GIMFs also exhibit an interesting "beam cleanup" effect where the nonlinearly generated wavelengths occupy the fundamental spatial mode. To our knowledge, this is the first demonstration of a GIMF-based pulsed optical source for PAM.

Our system consists of a 1047 nm Q-switched Nd:YLF laser producing 14 ns pulses with 150 uJ of energy at a 1 kHz repetition rate. The laser pulses are coupled into a 250 meter long GIMF (0.2 NA, core diameter = 50 um). Stimulated Raman scattering produces four spectral lines at 1095, 1150, 1215, and 1275 nm. A dielectric band-pass filter selects the desired wavelength for PAM. Our PAM system weakly focuses the laser beam into the object. A two-axis stepper motor system scans the laser and the 25 MHz f/2 transducer over the object. Imaging experiments are performed on a lipid phantom consisting of a small strip of butter placed between approximately 1.2 mm thick pieces of chicken breast meat.

Results/Discussion

The GIMF output pulse energies at 1047, 1095, 1150, 1215, and 1275 nm are measured to be 59.0, 9.6, 6.0, 4.8, and 4.1 uJ, respectively. The attached figure shows PAM images taken at each wavelength. Each C-mode image covers a 2 x 1 mm region and shown over the same 20 dB scale. No signal averaging is performed. The butter region is only visible at 1215 nm, which is consistent with the optical absorption peak of lipids.

The combination of a 1047 nm pulsed laser and a GIMF offers a cost-effective approach to perform PAM of lipids. The pulse energy at 1215 nm is sufficiently high for many in vivo imaging applications.

FRIDAY ORAL

3D-4
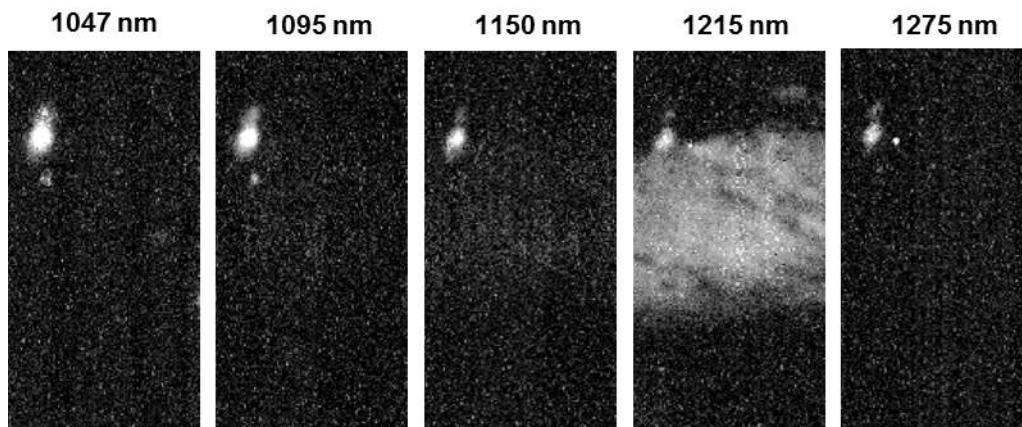
8:45 am Photoacoustic assessment of spatially and temporally varying oxygen saturation and perfusion in an orthotopic rat model of human hepatocellular carcinoma

Katherine Dextraze[1,2], Nina Munoz[3], Steven Huang[3], Tomas Figueira[3], Andrew Heinmiller[4], Rony Avritscher[3], Richard Bouchard[1,2]; [1]*Imaging Physics, University of Texas MD Anderson Cancer Center, Houston, TX, USA,* [2]*University of Texas at Houston Graduate School of Biomedical Sciences, Houston, TX, USA,* [3]*Interventional Radiology, University of Texas MD Anderson Cancer Center, Houston, TX, USA,* [4]*FUJIFILM VisualSonics, Inc., Toronto, Canada*

Background, Motivation and Objective

Oxygen saturation variations have been linked to tumor aggressiveness and poorer prognosis. A spatial map of oxygen saturation and perfusion within the tumor may serve as an important biomarker to improve guidance of tumor biopsies or inform treatment options. The goal of this study was to compare multi-wavelength photoacoustic-ultrasonic (PAUS) imaging and microbubble-based perfusion imaging to blood-oxygen-level dependent (BOLD) and DCE MRI to assess spatio-temporal variations in oxygen saturation and perfusion within an in vivo orthotopic rat tumor.

Statement of Contribution/Methods

Four rats inoculated with an orthotopic model of human hepatocellular carcinoma were imaged while inhalation gas was switched from medical air (20% oxygen) to pure oxygen at 10 min intervals. MRI BOLD and DCE imaging was performed on a 4.7T animal scanner (Biospec 47/40, Bruker Biospin). PAUS imaging was performed with the Vevo LAZR system using a 15-MHz prototype transducer with a 1-mm fiber bundle. Under medical air and pure oxygen, 3D B-mode, 3D Doppler, and 3D multi-wavelength PA data were acquired. To perform perfusion imaging, 150 microliters of MicroMarker microbubbles were then injected. PA-based oxygen saturation was obtained using the 750nm/850nm ratio, while BOLD estimates were achieved by subtracting T2* maps (oxygen to medical). PAUS data were approximately coregistered with MRI and histology data at the midsection of each tumor. After imaging, animals were sacrificed and gross histologic analysis was performed using pimonidazole staining.

Results/Discussion

The lower-frequency probe was able to obtain reliable PA-based oxygen saturation estimates in excess of 1 cm in the rat tumor. The spatial variation observed in PA-based oxygen saturation estimates - varying from 36-65% (medical air) to 61-90% (oxygen) at the tumor midsection - generally mirrored BOLD MRI results. The figure shows matched (B & E and C & F) slices from a tumor; red arrows (B & D) indicate regions of increased PA-based oxygen saturation that are similarly indicated in the BOLD images (E & F). Although microbubble and DCE acquisitions yielded similar results, they did not always correlate with oxygen saturation variations. This initial work shows the potential of using PAUS-based assessment of oxygenation saturation and perfusion for interrogation of an orthotopic rat tumor microenvironment.

3D-5
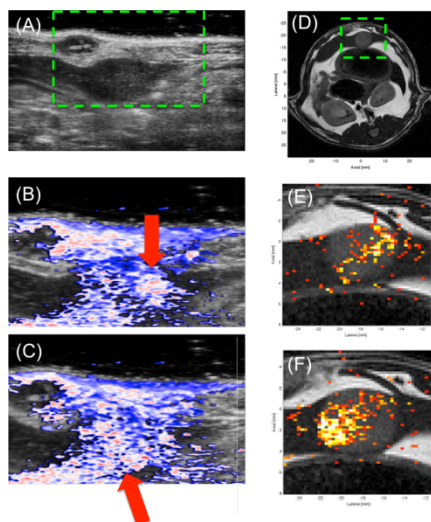
9:00 am Detection of Lipid in Ex-Vivo Atherosclerotic Rabbit Vessels using a Dual-Frequency Intravascular Imaging Probe for Ultrasound and Frequency Domain Photoacoustic Imaging

Robin Castelino[1,2], Hyunggyun Lee[2], F. Stuart Foster[1,2]; [1]*Medical Biophysics, University of Toronto, Canada,* [2]*Imaging Research, Sunnybrook Research Institute, Canada*

Background, Motivation and Objective

Although routinely used, intravascular ultrasound (IVUS) imaging is reported to have low sensitivity in the detection of thrombus and lipid-rich lesions due to the limited acoustic contrast of soft tissues. Intravascular photoacoustics (IVPA) has shown potential to characterize lipid-rich structures based on the optical absorption contrast of these tissues at 1210nm and 1720nm. Imaging is most commonly performed using an expensive pulsed laser, however, it can be achieved with inexpensive continuous wave (CW) laser diodes in a technique known as frequency domain intravascular photoacoustics (FD-IVPA). In this study, we image rabbit ex-vivo atherosclerotic vessels using a dual-frequency multimodal intravascular imaging probe for simultaneous IVUS and FD-IVPA imaging.

Statement of Contribution/Methods

The dual-frequency multimodal imaging probe consists of two back-to-back transducers viewing outward at 180°. The IVUS transducer has an active area of 0.5mm by 0.5mm and centered at 40MHz (53% BW). The active area of the FD-IVPA transducer is 0.5mm by 0.6mm, centered at 23MHz (60% BW) and co-aligned with a 400μm fiber delivering 1.5W over an amplitude modulated linear chirp from 16-25MHz for 0.5ms. The entire assembly is housed within a 4.5Fr hypotube. An atherosclerotic rabbit aorta was harvested and divided into six sections measuring 1cm in length. Each section were imaged at three locations with both IVUS and FD-IVPA at 1210nm, totalling 18 acquisitions across the vessel. A healthy rabbit aorta vessel, used as a control, was also imaged in the same manner.

Results/Discussion

IVUS and FD-IVPA A-lines were acquired and reconstructed separately. To create a combined IVUS image with a FD-IVPA overlay one image was rotated by 180°. The average increase in FD-IVPA signal intensity was measured to be 6.4 ± 1.4dB as compared to the control. The results indicate that FD-IVPA imaging has the potential to detect fatty deposits within vessel walls at 1210nm. This capability may enable more optimised detection of vulnerable plaque in future coronary catheter development.

Control

Diseased

IVUS   FD-IVPA   IVUS + FD-IVPA   Oil Red O
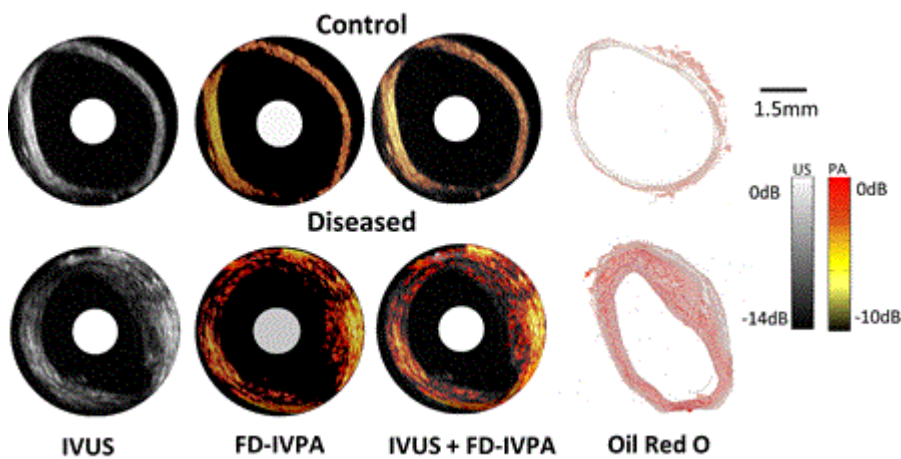
3D-6

9:15 am   Tri-modal imaging for surgical guidance: preliminary *in vivo* experiment

Jeeun Kang[1], Jin Ho Chang[1,2], Brian C. Wilson[3,4], Sun Mi Kim[5], Hak Jong Lee[5], Tai Kyong Song[1]; [1]*Electronics Engineering, Sogang University, Seoul, Seoul, Korea, Republic of,* [2]*Sogang Institute of Advanced Technology, Korea, Republic of,* [3]*Princess Margaret Cancer Centre, University Health Network, Canada,* [4]*Medical Biophysics, University of Toronto, Canada,* [5]*Department of Radiology, Seoul National University of Bundang Hospital, Korea, Republic of*

Background, Motivation and Objective

Multi-modality approach is increasingly being required for both preclinical and clinical applications as it enables complementary information from each modality. In this paper, we report the preliminary in vivo experimental results for surgical guidance using our all-in-one tri-modal imaging system to provide molecular/functional information from photoacoustic (PA) and fluorescence (FL) imaging as well as morphological information from ultrasound (US) imaging.

Statement of Contribution/Methods

The tri-modal imaging system uses the same custom high-frequency ultrasound transducer (Humanscan Co. Ltd., Korea) for both US and PA imaging connected to ultrasound imaging system (GE Ultrasound Korea, Korea), bringing the pulsed laser light generated from a movable Nd:YAG laser pumped optical parametric oscillator (OPO) system (Hanbit Laser, Corp., Korea) into a compact probe by fiber optic bundles. The FL subsystem is separated from the US/PA combined system but the front end that delivers and collects the FL light is physically integrated into the same handpiece. In *in vivo* experiments assuming surgical situation, a cocktailed contrast dye of methylene blue and fluorescein for PA and FL imaging is injected into a femoral muscle of a rabbit model (tumor in realistic surgery) to intentionally enhance the contrast on the connected lymph vessels. Note that the animal study is performed under the approval by the Institutional Review Board of Seoul National University Bundang Hospital (BA1407-157/037-01).

Results/Discussion

The *in vivo* experimental results indicates that the tri-modal imaging system can successfully support surgical guidance. Following the injection of the contrast dye, the temporal change in contrast on lymph vessels can be clearly visualized in PA imaging as shown in Fig. 1(c) as well as morphological information of US imaging in Fig. 1(b). During an operation, the contrast from the lymph vessels can also be augmented in FL imaging as in Fig. 1(d). Therefore, the results indicate that the tri-modal imaging can support the surgical application; For example in lumpectomy, the US images will localize overall tumor, the PA images will add molecular contrast to guide the tumor excision, while the FL imaging will assist the removal of any potential existence of residual tumor cells in the surrounding lymph vessels within the lumpectomy cavity.
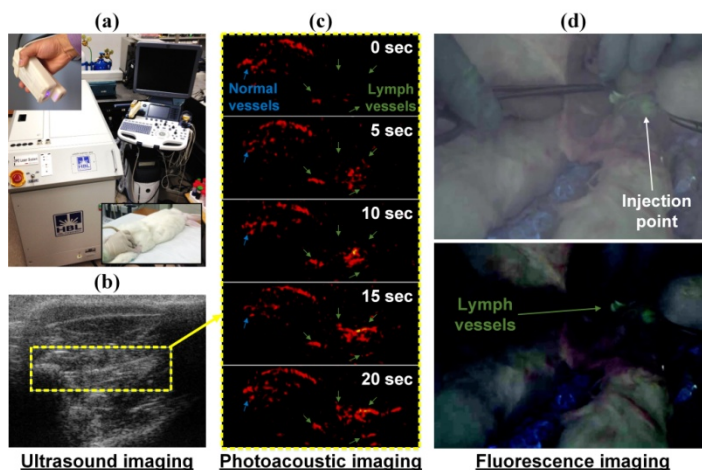
Fig. 1. (a) External appearance of the tri-modal imaging system, probe, and rabbit model examined, (b) ultrasound and (b) photoacoustic images, and (c) fluorescence images during *in vivo* surgery

FRIDAY ORAL

4D - MIM: Image Fusion and Classification Methods for Improved Diagnostics

201DE

Friday, October 23, 2015, 08:00 am - 09:30 am

Chair: **Hans Bosch**
Erasmus Medical Center

8:00 am   Spatiotemporal registration of 3D volumetric echocardiographic images

Adriyana Danudibroto[1,2], Jørn Bersvendsen[2,3], Olivier Gerard[2], Oana Mirea[1], Jan D'hooge[1], Eigil Samset[2,3]; *[1]Dept. of Cardiovascular Sciences, KU Leuven, Belgium, [2]GE Vingmed Ultrasound, Oslo, Norway, [3]University of Oslo, Oslo, Norway*

Background, Motivation and Objective

Fusion of 3D echocardiographic images has been shown to overcome inherent limitations of this modality such as signal dropouts and limited field of view. Prior to fusion, accurate temporal and spatial registration are essential. We previously reported on a multi-scale 3D Farnebäck optic flow methodology for the spatial registration. The aim of this study was bi-fold: i) validate this methodology using in-vivo recordings, ii) extend the methodology to allow for temporal alignment.

Statement of Contribution/Methods

From 7 healthy subjects, 19 apical 3D recordings were taken from differing transducer positions using a GE E9 system and the first frame was spatially registered using the proposed method. For each recording, the endocardial border on the first frame was manually contoured, hence the mean absolute distance (MAD) and Hausdorff distance (HD) between the segmented surfaces could be calculated prior and after registration.

For temporal registration, the normalized cross correlation (NCC) between the first frame and each consecutive frame was computed for the floating and reference sequences. The elastic temporal alignment was then modeled as a 1D cubic B-spline and solved by minimizing the squared differences between the aligned NCC-over-time functions. To quantify the temporal alignment results, NCC between corresponding frames for each recorded pair was computed prior and after temporal registration and the timing of mitral valve opening (MVO) was annotated for all recordings.

Results/Discussion

An example of fusion of two recordings can be seen in Figure 1. Spatial registration of the recordings reduced the MAD from 6.5 ± 1.6 mm to 2.3 ± 0.7 mm, HD from 17.4 ± 4.8 mm to 8.5 ± 2.8 mm which were statistically significant ($p<0.01$) and comparable to registration using Procrustes alignment based on the manual contours. Temporal registration significantly increased the NCC by 0.1% ($p<0.05$) in comparison to linear time interpolation and the temporal misalignment for MVO was 20 ± 14 ms which was less than half of the inter frame time. This study thus presents a new frame work for spatiotemporal alignment of 3D ultrasound recordings. Coupling the space-time registration methodologies is the topic of ongoing work.
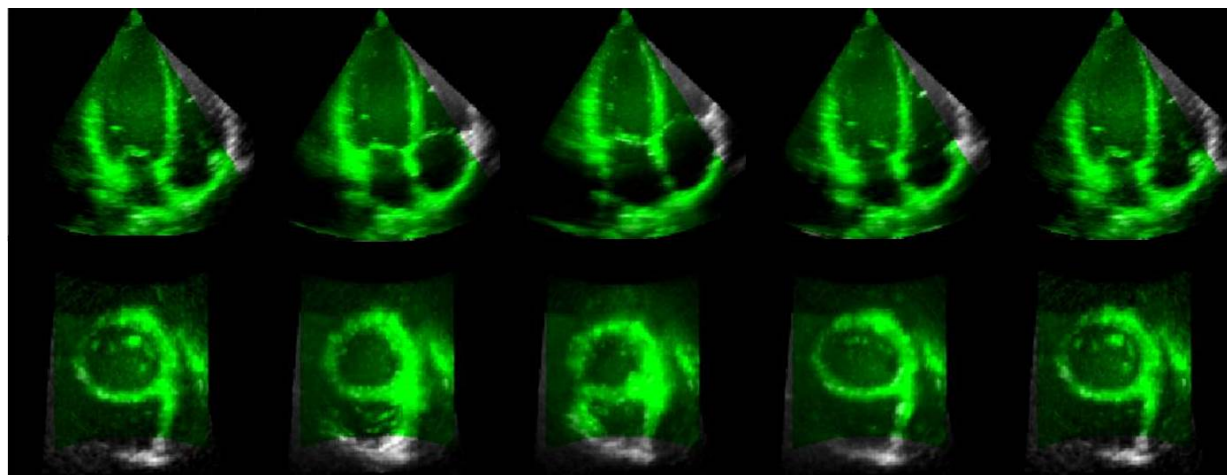
Figure 1: Fusion of two recordings across phases of the cardiac cycle. Reference volume is highlighted in green.

8:15 am   Anatomically Verified Algorithm for Image Fusion of 3D Echocardiography and Coronary Computed Tomography Angiography

Tim Nordenfur[1], Aleksandar Babic[2,3], Ivana Bulatovic[4], Anders Giesecke[4], Jonaz Ripsweden[4], Eigil Samset[2,3], Reidar Winter[4,5], Matilda Larsson[1]; *[1]Medical Engineering, KTH Royal Institute of Technology, Stockholm, Sweden, [2]University of Oslo, Oslo, Norway, [3]GE Vingmed Ultrasound, Oslo, Norway, [4]Karolinska Institutet, Stockholm, Sweden, [5]Department of Cardiology, Danderyd Hospital, Stockholm, Sweden*

Background, Motivation and Objective

Coronary artery disease, caused by stenosis of the arteries supplying the myocardium, remains the most common cause of death in the world. The treatment decision is often based on two separate investigations: 1) stenosis morphology and location, and 2) effect on cardiac function. The resulting images are viewed side-by-side and integrated mentally by the clinician. However, visualization of both morphological and functional information together, fused into a single image, might provide incremental diagnostic value.

Our aim was therefore to develop and verify a semi-automatic image fusion algorithm to combine morphological 3D images from cardiac computed tomography angiography (CCTA) and functional information from transthoracic 3D+time echocardiography (3DE).

Statement of Contribution/Methods

13 patients with suspected coronary artery disease underwent CCTA (Light Speed VCT XT, GE Healthcare) and 3DE (4VD, 27-55 fps, 1.7/3.3MHz, Vivid E9, GE Healthcare) at Karolinska University Hospital (Stockholm, Sweden). The left-ventricular (LV) endocardium was segmented in each 3DE dataset by two cardiologists separately using EchoPac 4D Auto-LVQ and in each CCTA image using a model-based edge-detection algorithm. The CCTA and 3DE images in matching cardiac phase were fused through a rigid transform such that the base centroid, base-to-apex line and three-chamber plane from one modality would coincide with those from the other.

The anatomical feasibility of the fusion algorithm was evaluated by manual landmark identification in the CCTA and 3DE datasets by a third cardiologist before fusion. In each fused 3D image, the distance between corresponding CCTA and 3DE landmarks were measured.

Results/Discussion

A fused image containing the coronary artery tree from CCTA and the LV endocardium from 3DE for one patient can be seen in fig. 1b. Fig. 1c shows the fused LV endocardium surfaces from CCTA and 3DE.

The anatomical verification study showed that the images were correctly fused up to an error of 1-2 cm for any landmark, as seen in fig. 1a. The results indicate that the developed CCTA/3DE image fusion algorithm is feasible and provides anatomically correct results. It remains to investigate how the fused images can improve treatment strategy decision and patient outcome.

Measure	Mean ± SD (n=13)	
	clinician A	clinician B
Distance between (cm)		
endocardial apices	1.7 ± 0.5	1.6 ± 0.6
mitral valve centers	1.2 ± 0.7	1.0 ± 0.4
aortic valve centers	2.3 ± 1.2	2.2 ± 0.9
Angle between (degrees)		
mitral-apex lines	7.9 ± 4.9	6.8 ± 4.2
(a)	(b)	(c)
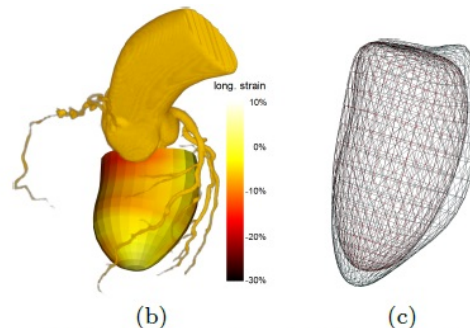
Figure 1: (a) Anatomical verification results from fused images of 13 patients based on 3DE segmentation by two clinicians. (b) Fused image of the coronary artery tree from CCTA and the LV endocardium with color-coded instantaneous strain from 3DE in end-diastole. (c) Fused image of segmented LV endocardium surfaces from CCTA (cyan) and 3DE (red) in end-diastole.

4D-3

8:30 am   **Simultaneous Positron Emission Tomography and Ultrafast Doppler Imaging in vivo**

Jean Provost[1], Anikitos garofalakis[2], Thomas Viel[2], Damien Bouda[2], Joevin Sourdon[2], Mathieu Pernot[3], Bertrand Tavitian[2], Mickael Tanter[3]; [1]*Institut Langevin, ESPCI ParisTech, INSERM, Paris, France,* [2]*PARCC INSERM UMR 970, France,* [3]*Institut Langevin, ESPCI ParisTech, INSERM, France*

Background, Motivation and Objective

The development of novel diagnostic tools and treatments for our most pressing healthcare challenges such as cancer can tremendously benefit from a complete understanding of the multifactorial, multi-scale biological underpinnings involved. In this study, we introduced a novel device capable of simultaneously performing Positron Emission Tomography (PET) and Ultrafast Ultrasound Imaging (UUI). PET is the most sensitive molecular imaging modality and as such can be used to characterize subtle biological pathways in vivo but cannot image tissue structure and suffers from poor spatial and temporal resolution. UUI, on the other hand, can be performed at thousands of images per second with a 100-micron resolution to quantitatively map function (such as blood flow) and the structure of tissues. The objective of this study was to demonstrate the feasibility of simultaneous PET/UUI imaging in small animals for pre-clinical studies.

Statement of Contribution/Methods

The PET/UUI device was built by combining an Aixplorer system (Supersonic Imagine, France) with a PET/CT Nano-PET scanner (Mediso, Hungary). A 15-MHz ultrasound probe (Vermon, France) was motorized within the PET tube using a single-axis linear stage (Physik Instrumente, Germany). Ultrafast Doppler Imaging was performed using repeated 2D 400-ms-long, 500-fps compounded tilted plane wave acquisitions (-10 to 10 degrees with a 2 degree increment) over an elevational scanning range of 1 cm with a 200-um step size. The PET acquisition lasted 15 minutes. A CT scan was performed prior to the PET/UUI acquisitions for spatial co-registration and PET attenuation correction. A bi-modality flow phantom consisting of a twisted tygon tube filled with a blood phantom mixed with a controlled concentration of fludeoxyglucose-F-18 (FDG) put in motion using a syringe pump was used to assess the effect on the quantification capabilities of PET in the presence of an ultrasound probe near the photodetectors. The PET/UUI Power Doppler sequence was then applied in vivo in a subcutaneous allografted tumor model in a nude mouse after the intravenous administration of 10 MBq.

Results/Discussion

The phantom study demonstrated that Ultrafast Doppler Imaging and PET imaging could be performed simultaneously. While the ultrasound probe did modify the PET image, its effects were deemed insignificant after CT-based attenuation correction. The in vivo study demonstrated the feasibility of simultaneously displaying the CT scan of the bone structure of the mouse; the PET image of the FDG accumulation in the tumor; and the Ultrafast Power Doppler image of the vasculature surrounding the tumor. These initial results demonstrate the feasibility of simultaneous PET and Ultrafast Doppler Imaging for the study of the relationship between angiogenesis and metabolism in tumors and more generally the viability of a PET/UUI approach.

4D-4

8:45 am   **Detection and Characterization of Sentinel Lymph Node using Contrast-Enhnaced Ultrasound and Photoacoustic Imaging**

Stanislav Emelianov[1], Alexander Hannah[1], Geoffrey Luke[1]; [1]*University of Texas at Austin, Austin, Texas, USA*

Background, Motivation and Objective

In cancer patients, evaluation of regional lymph node for metastases is of paramount importance. Unfortunately, there is no single imaging approach that can reliably detect sentinel lymph node(s) and identify micrometastases in lymph nodes. Previously, we reported that changes in blood oxygen saturation in lymph nodes correlate with metastatic invasion. Here, we present an ultrasound contrast agent, ultrasound imaging protocol and image processing algorithm to identify location of sentinel lymph node thus completing the comprehensive imaging approach to identify the lymph nodes and to detect lymph node metastases.

Statement of Contribution/Methods

An optically activated contrast nanoagent (Fig. 1A) for ultrasound imaging (Fig. 1B) consists of a liquid perfluorohexane nanodroplet encased in a surfactant shell and encapsulating a near infrared optical absorber. This droplet vaporizes in response to a pulsed laser irradiation, induces phase-change ultrasound contrast, and immediately recondenses due to its high boiling point relative to body temperature. By imaging the droplets using ultrafast ultrasound, we captured this rapid phase-change "blinking" behavior. Given the laser pulse repetition rate, an autocorrelation applied to the differential ultrasound intensity was used to discern the nanodroplets from the surrounding tissue and provide a background-free map of the particles.

Results/Discussion

The experiments were performed using a metastatic murine model of oral squamous cell carcinoma. First, the ultrasound images of the known lymph nodes were acquired (Fig. 1C). Then the laser activated nanoagents were injected near the primary tumor and allowed to drain into lymph nodes. The lymph nodes were imaged using ultrasound transducer interfaced with the laser source (Vevo LAZR, Visualsonics, Inc.). The resulting set of high frame rate ultrasound images were used to discern the nanodroplets from the surrounding tissue and provide a background-free map of the particles within sentinel lymph node (Fig. 1D). Finally, the metastases within the lymph node of a mouse were confirmed by measuring blood oxygen saturation (Fig. 1E) using US-sPA imaging. Overall, the developed approach form a foundation for a comprehensive approach capable of immediate localization of sentinel lymph node(s) and accurate assessment of sentinel lymph node micrometastases.
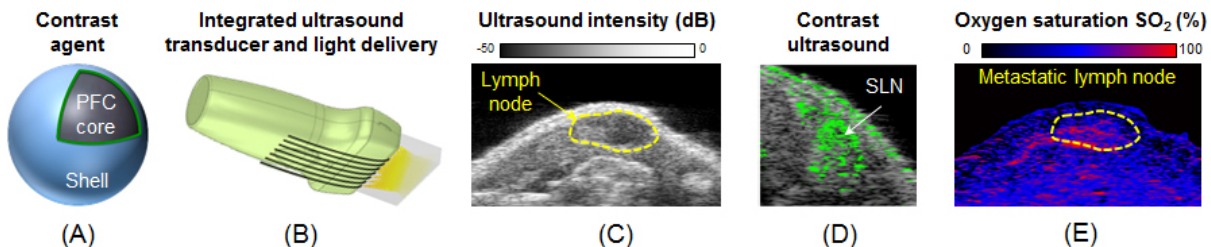
Figure 1: (A) Optically-activated ultrasound contrast agent – PFC nanoDroplet; (B) Ultrasound imaging transducer integrated with light delivery system; (C) Ultrasound image of the lymph node; (D) Contrast-enhanced ultrasound localizes the sentinel lymph node (SLN); (E) Oxygen saturation map identifies the detected sentinel lymph node as metastatic.

4D-5

9:00 am   Random Forest Classification and Local Region-Based, Level-Set Segmentation for Quantitative Ultrasound of Human Lymph Nodes

Thanh Minh BUI[1], Alain Coron[1], Jonathan Mamou[2], Emi Saegusa-Beecroft[3], Junji Machi[3], Lori Bridal[1], Ernest Feleppa[2]; *[1]Sorbonne Universités, UPMC Univ Paris 06, INSERM, CNRS, LIB, Paris, France, [2]F. L. Lizzi Center for Biomedical Engineering, Riverside Research, New York, NEW YORK, USA, [3]University of Hawaii and Kuakini Medical Center, Honolulu, Hawaii, USA*

Background, Motivation and Objective

To detect metastatic foci in excised human lymph nodes (LNs) using three-dimensional (3D), high-frequency quantitative ultrasound (QUS), it is essential to accurately segment three media in the 3D envelope data: LN parenchyma (LNP), fat and normal saline (NS). However, automatic segmentation of the 3D data remains challenging because of speckle noise as well as low contrast and intensity inhomogeneity caused by attenuation and focusing effects.

Statement of Contribution/Methods

We present a novel method to automatically segment the three media in LN envelope data consisting of two steps: initialization and refinement. In the first step, a 3-class, Random Forest (RFo) classification framework is employed to label the 3 media. Thirteen features (e.g., median envelope, cumulative sum of backscattered power, statistical gamma distribution parameters, imaged depth, local phase, etc.) are computed for the cubic region centered at each voxel. In the second step, the initialization is refined by a 3-phase, local region-based, level-set segmentation method that integrates the gamma probability density function (PDF) of the envelope data. To handle depth-dependent data inhomogeneity efficiently, PDF parameters are computed once per depth-range-slice for each medium. From a database of 54 representative LNs acquired from colorectal-cancer patients, 12 LNs were used to train the RFo classifier, and the 42 remaining LNs were used for testing. The Dice similarity coefficient (DSC) was used to compare automatic and manual segmentation.

Results/Discussion

RFo initialization alone: DSCs of 0.922 ± 0.022, 0.801 ± 0.075 and 0.959 ± 0.013 for LNP, fat and NS, respectively. Initialization and refinement: significantly better DSCs were obtained: 0.937 ± 0.021, 0.824 ± 0.074 and 0.961 ± 0.009 (Wilcoxon signed rank test). Figs. 1a and 1b show representative results. Furthermore, QUS estimates from LNs segmented using the automatic segmentation were very close to those obtained when manual segmentation was used (e.g., as indicated in Fig. 1c, for the average-effective-scatterer-size, D, the mean of the differences of D estimated with the 2 segmentation methods was 0.02 μm and the 95% limits of agreement (MEAN $\pm$ 1.96*STD) were -1.06 and 1.11 μm). Thus, accurate QUS-based cancer detection in excised LNs can be obtained without operator-dependent segmentation.
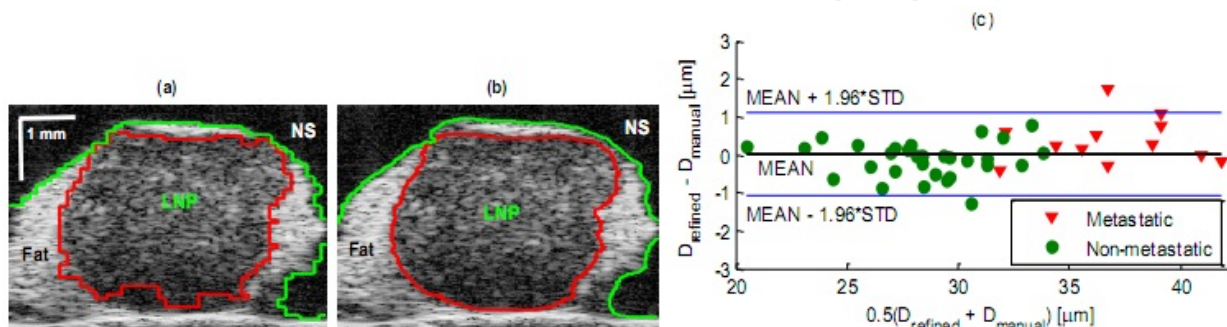
Fig. 1. (a) Initialization by the RFo classification alone overlaid on the log-compressed B-mode image (40 dB dynamic range) extracted from a representative, 3D segmentation. (b) Refined segmentation using the depth-adapted, level-set segmentation overlaid on the B-mode image; the DSCs of the refined segmentation were 0.934, 0.843 and 0.948 for LNP, fat and NS, respectively. (c) Difference vs. the mean for D estimated on 42 human LNs segmented with the two different methods (refined vs. manual).

4D-6

9:15 am   Automatic detection of ischemic myocardium by spatio-temporal analysis of echocardiographic strain and strain rate curves

Mahdi Tabassian[1,2], Martino Alessandrini[2], Lieven Herbots[2], Oana Mirea[2], Jan Engvall[3], Luca De Marchi[1], Guido Masetti[1], Jan D'hooge[2]; *[1]Department of Electrical, Electronic and Information Engineering, University of Bologna, Bologna, Italy, [2]Department of Cardiovascular Sciences, Laboratory of Cardiovascular Imaging and Dynamics, KU Leuven, Belgium, [3]Department of Medical and Health Sciences, Linkoping University, Sweden*

Background, Motivation and Objective

Echocardiographic strain (rate) imaging allows quantifying regional myocardial function. In clinical applications, most often, end-systolic strain and peak systolic strain rate have been used as techno-markers to classify disease. However, as these values characterize the strain (rate) curve at a single time point potentially important diagnostic information in the temporal behavior of these curves gets lost. The aims of this study were therefore bi-fold: 1) to build a statistical model enabling a compact representation of the temporal strain (rate) profiles and, 2) to use this compact representation to build a feature vector to detect disease.

Statement of Contribution/Methods

Longitudinal strain and strain rate traces were extracted for each LV segment (18 segments model) on a set of 60 normal subjects and 60 patients with acute infarction imaged with a GE VingMed Vivid 7 (2.5MHz, 180 frames/s). Statistical modeling of the strain (rate) curves was performed with Principal Component Analysis (PCA). Two separate PCA models were built with the segmental strain and strain rate curves to capture their temporal behavior. For each subject, the eigenvalues of the first 15 principal components of all 18 segments were concatenated into a single feature vector to account for mechanical interactions between segments thereby providing a spatio-temporal representation of the global LV function. The K-Nearest Neighbor (KNN) method was then used as classifier. To assess the benefit of PCA features as compared to traditional markers, the classification task was repeated by using segmental end-systolic strain and peak-systolic strain rate values as features. Classification results were obtained using 10-fold cross-validation. Hereto, subjects were randomly divided into 10 equal-size folds. Nine folds were used for training and the last one was used for testing the classifier.

Results/Discussion

The best accuracy rates obtained by the employed features are listed in Table 1. The PCA features extracted from the strain rate traces yielded the best outcome and significantly enhanced the classification results achieved by the traditional markers to detect ischemic heart disease. Taking the spatio-temporal behavior of the strain (rate) profiles into account can thus improve clinical decision making. Testing this concept in other disease states is the topic of active work.

Table 1. The best average classification accuracies and their corresponding sensitivity and specificity values (%) achieved with the spatio-temporal and traditional features.

	Accuracy	Sensitivity	Specificity
Spatio-temporal features			
Strain	70	78.33	61.66
Strain rate	85.83	86.67	85
Traditional features			
Strain	64.17	40	88.33
Strain rate	67.5	80	55

FRIDAY ORAL

5D - Frontiers of Ultrasonics

103

Friday, October 23, 2015, 08:00 am - 09:30 am

Chair: **David Greve**
Carnegie Mellon University

FRIDAY ORAL

5D-1

8:00 am   In-chip GHz Ultrasonic Pulses for Information Processing

Amit Lal[1]; [1]*SonicMEMS, Electrical and Computer Engineering, Cornell Univeristy, Ithaca, NY, USA*

Background, Motivation and Objective

Combining of piezoelectric thin films with CMOS enable high frequency (> 1GHz) sonars that can be used to communicate within and across CMOS chips. The chip-scale sonar will enable communications in one chip, or through IC stacks, forming a user defined communications layer for 3D ICs. The added interconnect capability would allow the programmers to use ultra-high fan-out and fan-in capabilities, often needed to implement algorithms in associative pattern recognition algorithms. These associative processing approaches may lead to brain like computing devices.

Statement of Contribution/Methods

Two dimensional arrays of piezoelectric AlN pixels were used to form a phased array of sonic pulses, launched into the bulk of the silicon wafers. Coherent addition of the pulses at GHZ frequencies results in directivity in data transmission. The reflected pulses are detected on receiver piezoelectric pulses.The spatial extent of pulses enables information transfer not only within the chip, but also across chip boundaries. The latter enables information communication across chips forming ultrasonic through silicon vias. Recirculating ultrasonic pulses through the wafer can also sustain delay line memory.

Results/Discussion

We demonstrate chip-scale sonar for communications at > 100Mbit/s, sonic memory with 2 bits across a wafer thickness, and ultrasonic vias across chips. We have also developed high frequency ultrasonic imaging of surface acoustic impedance. Ongoing work on integrating all necessary circuitry on a single chip will enable compact and programmable GHz ultrasonic transducers for industrial, medical, and information processing applications.

5D-2

8:30 am   Mechanical Properties of Comet 67P/Churyumov-Gerasimenko Measured by CASSE and DIM on Board Rosetta's Lander Philae

Walter Arnold[1,2], Thomas Albin[3], Claudia Faber[4], Hans-Herbert Fischer[5], Alberto Flandes[6], Attila Hirn[7], Martin Knapmeyer[4], Harald Krüger[3], Alexander Loose[3], Diedrich Möhlmann[4], Klaus-Jürgen Seidensticker[4], Klaus Thiel[8]; [1]*Department of Materials and Materials Technology, Saarland University, Saarbrücken, Germany,* [2]*I. Phys. Institut, Georg-August Universität, Göttingen, Germany,* [3]*Max Planck Institute for Solar System Research, Germany,* [4]*DLR Institute of Planetary Research, Germany,* [5]*DLR MUSC Cologne, Germany,* [6]*Instituto de Geofísica, Mexico,* [7]*MTA Centre for Energy Research, Hungary,* [8]*University of Cologne, Germany*

Background, Motivation and Objective

In August 2014 the ESA spacecraft Rosetta encountered the comet 67P/Churyumov-Gerasimenko. Rosetta carried the lander Philae that landed on the comet's nucleus on November 12th 2014. Philae has ten different instruments on board including the Surface Electric Sounding and Acoustic Monitoring Experiment (SESAME) comprising CASSE, DIM, and PP. The objective of the Rosetta mission is to determine physical, chemical, and geophysical properties of comet 67P by the instruments on board of the Rosetta Orbiter and the Lander Philae.

Statement of Contribution/Methods

The Comet Acoustic Surface Sounding Experiment (CASSE) is housed in the six soles of Philae's landing feet. It consists of three piezoelectric tri-axial accelerometers, and three transducers. This allows for both passive listening to the comet's seismic activity and active sounding of the comet surface. The deceleration signal occurring in the first milliseconds of the touchdown at an impact velocity of approx. 1 m/s was recorded by CASSE. It contains information on the elastic (modulus) and on the crushing strength of the cometary soil. The analysis is based on a recently developed inversion scheme exploiting extended Hertzian contact mechanics which in turn is based on calibration using laboratory tests of the landing on different materials.

The Dust Impact Monitor (DIM) on board of Philae is a cube with three of its sides covered with PZT detectors. DIM is aimed to derive the elastic-plastic properties and the flux of the millimeter-sized dust-particle population that moves near the surface of the comet nucleus. Calibration experiments between -40 deg C and 20 deg C were performed to analyze the response of DIM based on Hertzian contact mechanics.

Results/Discussion

In this contribution, we will give an overview of the data recorded so far by CASSE and DIM at the time of submission of this abstract, their interpretation and relation to the measurement techniques employed in non-destructive materials characterization based on ultrasonics. The data support the concept that the elastic and strength properties of the comet material corresponds to very porous solids with porosities up to 80% and of agglomerates of regolith particles.

5D-3

8:45 am   Magnetic sensing by ultrasonic excitation

Kenji Ikushima[1], Hisato Yamada[1], Miki Uehara[1]; [1]*Department of Applied Physics, Tokyo University of Agriculture and Technology, Tokyo, Japan*

Background, Motivation and Objective

All ferromagnetic materials exhibit hysteresis in the variation of flux density B with magnetic field H. Hysteretic properties, such as permeability, coercivity, remanence, and hysteresis loss are known to be sensitive to such factors as stress, strain, grain size, and heat treatment. Because hysteresis measurements yield a number of independent parameters of materials, they have been used in the determination of material properties, in stress sensor applications, and in nondestructive evaluation (NDE) of large-scale structures.

Recently, we presented a magnetic detection technique that incorporated ultrasonic inspection [1,2]. The principle of this technique is based on the generation of acoustically stimulated electromagnetic (ASEM) fields through magnetomechanical coupling.

Statement of Contribution/Methods

A specimen (JIS G 3101 SS400; size: 50 × 50 × 0.8 mm) is subjected to external magnetic fields along the direction of one edge of the plate by using a commercial electromagnetic coil. The ultrasonic focal point (focal spot size: 0.8 mm) scans the whole area of the specimen by moving the transducer with an integrated pick-up loop

antenna (tuned frequency: 8.9 MHz; diameter: 10 mm) while holding the distance r constant ($r \approx 15$mm). The steel plate specimen with an artificial defect (a 1 mm hole) is placed in a focused zone at a distance of about 40 mm from a 10 MHz transducer (diameter: 20 mm).

Results/Discussion

Magnetic hysteresis loops are measured by ultrasonic techniques and used in visualizing the magnetic-flux distribution in a steel plate. The differential piezomagnetic coefficient determines the amplitude of acoustically stimulated electromagnetic (ASEM) fields, yielding the hysteresis behavior of the intensity of ASEM response. By utilizing the high correspondence of the ASEM response to the magnetic-flux density, we image the specific spatial patterns of the flux density formed by an artificial defect of a steel plate specimen. Magnetic-flux probing by ultrasonic waves is thus shown to be a viable method for nondestructive material inspection.

[1] K. Ikushima et al., Appl. Phys. Lett. 89, 194103 (2006).

[2] H. Yamada et al., Rev. Sci. Instrum. 84, 044903 (2013).

5D-4

9:00 am   Non-contact mass measurement of droplet based on free oscillation under ultrasonic levitation.

Sae Ito[1], Ryohei Nakamura[1], Hiroki Tanaka[1], Yosuke Mizuno[1], Marie Tabaru[1], Kentaro Nakamura[1]; *[1]Precision and Intelligence Laboratory, Tokyo Institute of Technology, Yokohama, Japan*

Background, Motivation and Objective

Recently, non-contact manipulation is much in demand for the area of drug development, biotechnology and new material sciences. Ultrasonic levitation of droplet is one of the promising methods for non-contact transport, mixing and dispensing. [Y.Ito et al., Acoust. Sci. Technol., 31 (2010)420.] Evaluating mass is also an essential issue. We challenge, in this report, to measure the mass of a small droplet suspended in ultrasonic field in air from the free oscillation around the nodal position of the standing waves.

Statement of Contribution/Methods

A droplet suspended at the node of the pressure standing wave field will vibrate near the nodal position if some disturbance is applied to the droplet. The natural frequency of the free oscillation is determined by the mass of the droplet and the slope of the potential force. Thus, we can estimate the mass by measuring the frequency of the free oscillation, provided the force acting on the droplet is known.

A droplet is levitated in the standing wave between a vibrating horn of 30 mm in diameter, and a reflector. The distance between the horn and the reflector was adjusted to a half wavelength (7 mm at 27.4 kHz). First, we levitated five solid samples with different mass and diameter and observed the oscillation to obtain the calibration curve. Oscillation was caused by rising slightly the drive voltage of the transducer for a short time (0.07 s). The droplet was illuminated with a collimated light, and then, the shadow of the droplet was projected on a quarter- divided photo detector. The oscillation displacement was recorded as the output voltages of the element detectors. The sound pressure was measured using a thin piezoelectric element bonded on the surface of the reflector. The sound pressure was kept constant for various sample droplets by changing the driving voltage.

Results/Discussion

We demonstrated the mass estimation for ethanol and water droplets with different volumes. The average measurement error was 21%. The error might be attributed to the difference in the actual sound pressure near the droplet because the shape of the droplet was deviated from sphere due to acoustic radiation pressure. We need to compensate this pressure discrepancy to achieve higher accuracy. We believe that this experiment is a useful challenge to estimate the mass of droplet under totally non-contact condition.

5D-5

9:15 am   High sensitivity liquid sensor based on slotted phononic crystal

Liufeng Geng[1,2], Feiyan Cai[2], Fei Li[2], Long Meng[2], Chen Wang[2], Shuhong Xie[1], Hairong Zheng[2]; [1]*School of Materials Science and Engineering, Xiangtan University, Xiangtan, Hunan, China, People's Republic of,* [2]*Shenzhen Institutes of Advanced Technology, Chinese Academy of Sciences, China, People's Republic of*

Background, Motivation and Objective

The ability of confining an acoustic wave in an ultrasmall region of sub-wavelength dimensions can extend phonon's lifetime, break the diffraction limit and enhance the acoustic wave-matter interaction, which is also critical for the applications of acoustic sensor. In recent study, we have demonstrated that a strong localized mode exists in a subwavelength slot between two plates immersed in liquid. In addition, this mode can be efficiently excited by a plane wave by introducing periodic grooves at the upper or lower side of individual plate. We name this system as slotted phononic crystal (SPC). Here, we will further investigate the properties of this system for liquid sensor.

Statement of Contribution/Methods

The SPC consists of a slot between two glass plates drilled with two periodical square grooves arrays in the single outer side of the individual plate. The transmission spectrums are carried out by the finite element methods (COMSOL Multiphysics) for SPC immersed in tested liquid of 1-propanol for a set of molar ratios, and then the quality factor $Q=fm/\Delta fFWHM$ (fm and $\Delta fFWHM$ represent the resonant frequency and full-width at half-maximum(FWHM) of the resonant peak) and the sensitivity of the system $S=\Delta f/\Delta x$ (Δf is the resonant frequency shift, and Δx is the molar ratio change) are calculated based on the transmission spectrums. In addition, the density and speed of sound of 1-propanol mixtures are also shown as a reference.

Results/Discussion

The transmission spectrums of SPC immersed in 1-propanol mixtures of molar ratios with 0, 0.056 and 0.507 are shown in Fig. 1(a). It is clearly shown that the quality factor Q of the SPC immersed in water is as high as 10259, and the sensitivity S is large as 0.2854 MHz for the ratio as 0.056. As shown in Fig. 1(b), it's worth noting the dependence of the molar ratio of 1-propanol on the frequency of transmission dip and speed of sound is not similar. Both the changes of density and speed of the liquid mixtures are influence on the frequencies of the transmission dips. Thus, this SPC can be a promising platform for liquid properties sensor with high sensitivity and high Q-factor.
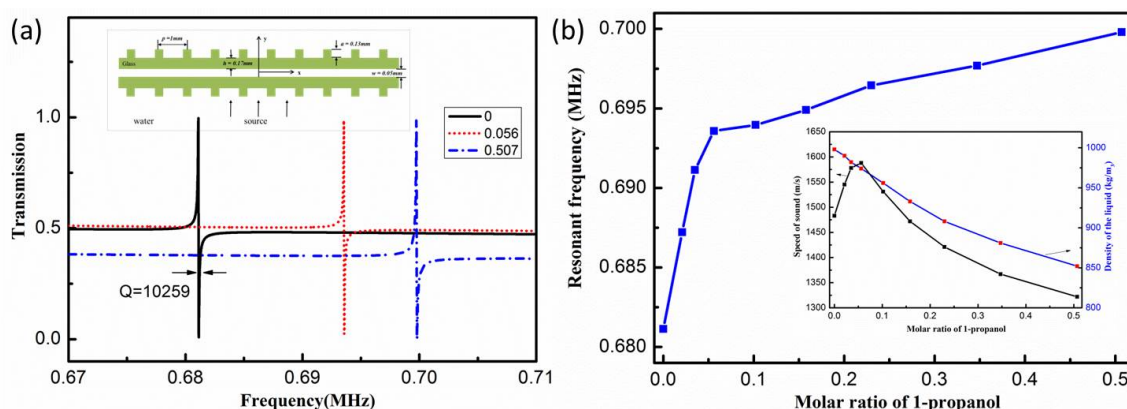
Figure 1 (a) The transmission spectrums of SPC for different molar ratios of 1-propanol mixtures and the inset displays the schematic structure graph for the SPC system. (b) Resonant dip frequency vs molar ratio of 1-propanol in the liquid mixtures, and inset shows the speed of sound and the density of the liquid vs molar ratio of 1-propanol in the liquid mixtures.

6D - Opto-Acoustics

201AF

Friday, October 23, 2015, 08:00 am - 09:30 am

Chair: **John Larson**
                Avago Technologies

6D-1

8:00 am   Depth-Profiling of Acoustic, Optic and Acousto-Optic Spatial Inhomogeneities by Technique of Picosecond Ultrasonic Interferometry
Vitalyi Gusev[1]; *[1]LAUM, UMR-CNRS 6613, LUNAM, Université du Maine, Le Mans, France*

Background, Motivation and Objective

In picosecond laser ultrasonics ultra-short laser pulses are used both for the generation and detection of the acoustic pulses with a typical length from 100 nm down to several nanometres. These acoustic pulses could be applied for the depth profiling, i.e., spatially resolved imaging, of the inhomogeneous materials.

Statement of Contribution/Methods

Picosecond acoustic interferometry or time-domain Brillouin scattering technique, which monitors temporal evolution of a single frequency component of wide-frequency-band acoustic pulses, provides opportunity for the depth-profiling of the optically transparent spatially inhomogeneous materials with sub-μm to nm spatial resolution, for revealing individual micro-crystallites in optically isotropic polycrystalline aggregates and for monitoring the nonlinear transformation of the finite amplitude acoustic pulses of GHz frequency range. In an inhomogeneous medium, the time-domain Brillouin scattering signal at each time instance contains information on the local parameters of the medium in the spatial position of the laser-generated light-scattering acoustic pulse at this time instance. The spatial resolution of the method can be controlled either by the spatial scale of the linear laser-generated picosecond acoustic pulse propagating inside the tested material or the spatial width of the weak shock front in the nonlinear acoustic pulse. These scales are much shorter than optical wavelength.

Results/Discussion

Applications include depth-profiling of the nano-porous low-k materials for microelectronics and polycrystalline aggregates of H2O ice at Magabar pressures in diamond anvil cell.

[1] C. Mechri, P. Ruello, J. M. Breteau, M. R. Baklanov, P. Verdonck, V. Gusev, Appl. Phys. Lett. 95, 091907 (2009).

[2] V. Gusev, A. M. Lomonosov, P. Ruello, A. Ayouch, G. Vaudel, J. Appl. Phys. 110, 124908 (2011).

[3] A. M. Lomonosov, A. Ayouch, P. Ruello, G. Vaudel, M. R. Baklanov, P. Verdonck, L. Zhao, and

V. E. Gusev, ACS Nano 6, 1410 (2012).

[4] C. Klieber, V. E. Gusev, T. Pezeril, K. A. Nelson, Phys. Rev. Lett. 114, 065701 (2015).

[5] V. E. Gusev, J. Appl. Phys. 116, 064907 (2014).

[6] S. M. Nikitin, N. Chigarev, V. Tournat, A. Bulou, D. Gasteau, B. Castagnede, A. Zerr, V. E. Gusev, Sci. Rep. 5, 9352; DOI:10.1038/srep09352 (2015).

6D-2

8:30 am   Fast wave velocity measurement by Brillouin scattering using induced phonon from ScAlN piezoelectric thin film
Masahiko KAWABE[1], Takahiko YANAGITANI[2], Hayato ICHIHASHI[1], Shinji TAKAYANAGI[1], Masashi SUZUKI[3], Mami MATSUKAWA[1]; *[1]Doshisha University, kyoto, Japan, [2]Waseda University, Tokyo, Japan, [3]Nagoya Institute of Technology, Nagoya, Japan*

Background, Motivation and Objective

Brillouin scattering enables a nondestructive and noncontact technique to measure the hypersonic wave velocity in thin materials. However, weak thermal phonons result in the long time and low accuracy measurement. To overcome this problem, a technique with artificially induced phonons is suggested using a piezoelectric film. In this study, we have tried to induce strong longitudinal phonons by ScAlN films deposited on the surface of a bulk sample. The ScAlN film is suitable for excitation of phonons owing to the excellent piezoelectric character.

Statement of Contribution/Methods

Longitudinal phonons were induced by a Sc0.41Al0.59N piezoelectric film [1]. The film was grown by an RF magnetron sputtering on DC sputter-deposited Ti metal film (150 nm)/ sample (5 × 5 × 25 mm, ED-H, Tosoh Corp.). The crystalline c-axis of the film was aligned with the normal. The film (4 μm thick) was deposited on one side of a sample. On another side of the sample, an Al film (300 nm) was deposited as a light reflector for the RIΘA scattering geometry. We induced phonons by applying an electric field on Ti electrode using a signal generator (E8257D, Agilent technologies). The scattering light was measured by a Tandem Fabry-Perot Interferometer (JRS) with a laser (wavelength; 532nm, Laser Quantum). Here, the laser beam hit the sample at the position of 1 mm from the ScAlN film, with the angle of 2 degrees from the normal direction to the sample surface. The phonons were excited at 760 MHz (the primary resonance of ScAlN film).

Results/Discussion

Figure 1 shows a typical spectrum of a Brillouin peak from the induced phonons. The intensity of Anti-Stokes peak was about 22,666 counts (input power: 10 dBm), which was 1,079 times as intense as the peak before excitation. Velocity can be obtained easily by the fixed frequency and the angle of incident light. Because ScAlN has excellent piezoelectric properties, the intensity of the excited Brillouin peak was 6 times stronger than that excited from a ZnO film [2]. The obtained velocity was 602×10 m/s, which was equal to the reported velocity of the sample. The intensity of Brillouin scattering dramatically improved by the induced phonons radiated from the ScAlN film. With this technique, rapid and precise velocity measurements can be achieved.

[1] T. Yanagitani, and M. Suzuki, Appl. Phys. Lett. 105, 122907 (2014).

[2] T. Yoshida et al., IEEE TUFFC, 58,(6), 1255(2011).

FRIDAY ORAL

(a)Measurement specimen

(b)Brillouin spectra before and after excitation
(Number of interferometer scans: 100 times)

Fig. 1 Specimen and measured spectra

6D-3

8:45 am   Fourier synthesis and timbre tuning of radio frequency nanomechanical pulses

Achim Wixforth[1], Florian Schuelein[2], Hubert Krenner[2]; *[1]Institute of Physics, University of Augsburg, Augsburg, Germany, [2]University of Augsburg, Germany*

Background, Motivation and Objective

The concept of Fourier synthesis provides the foundation for both everyday consumer electronic products and fundamental research. In the latter, so called pulse shaping is nowadays key to dynamically initialize, probe and manipulate the state of classical or quantum systems. In nuclear magnetic resonance, for instance, shaped pulses have a long-standing tradition and the underlying fundamental concepts have subsequently been successfully extended to optical frequencies and even to implement quantum gate operations. Transfer of these paradigms to nanomechanical systems, requires tailored nanomechanical waveforms (NMWFs) for mechanically mediated coherent control schemes.

Statement of Contribution/Methods

Here, we report on a novel additive Fourier synthesizer for NMWFs based on monochromatic surface acoustic waves (SAWs). As a proof of concept, we electrically synthesize four different elementary NMWFs from a fundamental SAW at $f1 \approx 150$ MHz using a superposition of up to three discrete harmonics fn.

Results/Discussion

We employ these shaped pulses to interact with an individual sensor quantum dot (QD) and detect their deliberately and temporally modulated strain component via the quantum- and opto-mechanical QD response. As a very attractive feature and in contrast to the commonly applied direct mechanical actuation by bulk piezoactuators, SAWs provide more than two orders of magnitude larger frequencies > 20 GHz to resonantly drive mechanical motion. Thus, our technique uniquely allows coherent mechanical control of localized vibronic modes of optomechanical and phoXonic crystals, most tantalizing even in the quantum limit when cooled to the vibrational ground state.

6D-4

9:00 am   Surface-wave resonance on substrates with copper nanowires

Hirotsugu Ogi[1], Shoichi Masuda[1], Akira Nagakubo[1], Masahiko Hirao[1]; *[1]Osaka University, Japan*

Background, Motivation and Objective

Recent advances in fabrication technologies accelerates miniaturization of acoustic devices, and detailed experiments and analysis are required for their successful operations. High-frequency surface-acoustic-wave (HF-SAW) devices are representative acoustic devices for bandpass filters and sensors. Because of shortened wavelength, propagation behavior of HF-SAW is highly affected by structures on substrate, even their dimensions are in nanometers, showing complicated dispersion relationships.

Statement of Contribution/Methods

Here, we fabricate copper nanowires on silicon and glass substrates using electron-beam lithography method, and detect HF-SAW resonances with picosecond ultrasonics. We then propose a theoretical model for explaining the unique dispersion behavior, involving the interfacial stiffness between the nanowire and substrate surface.

Results/Discussion

We detected HF-SAW resonances up to 10 GHz with a error within 3.5%. They are highly dispersive for Si and less dispersive for glass substrates, and existing models, considering stiffness and mass of the nanowire, failed to explain the anomalous dispersion behaviors. Our model, involving the interfacial stiffness, favorably explained them, indicating the reliability of the proposed model to analyze dispersion relations of HF-SAWs. The dispersion of HF-SAW can be thus used for evaluation of adhesion quality.

6D-5

9:15 am   THz acoustic spectroscopy by using GaN-based double quantum wells as the acoustic transducer

Jun Wei Fan[1], Jinn-Kong Sheu[2], Kung-Hsuan Lin[1]; *[1]Institute of Physics, Academia Sinica, Taipei, Taiwan, [2]Department of Photonics, National Cheng Kung University, Tainan, Taiwan*

Background, Motivation and Objective

InGaN/GaN heterostructures have been used to efficiently generate and detect coherent acoustic waves between 100 GHz and 2 THz [1-3]. By using single quantum well structure as the acoustic transducer, broad band acoustic spectra can be obtained [3]. However, the acoustic signal initiated in the single quantum well by the femtosecond optical pulses is usually embedded in the transient electronic signals at around zero time delay. For many cases of acoustic analysis, it is important to measure the acoustic energy excited within the acoustic transducer. Multiple quantum wells have also been used to generate THz acoustic phonons [1, 2]. The acoustic signals can be enhanced by

the number of quantum well, and the specific frequency can be amplified by the spatial period of the wells. It is also possible to obtain the generation signals. However, the first oscillation cycle around zero time delay is still embedded in the electronic signals. In addition, the studied frequency components are limited compared with the broadband spectrum from single quantum well structure.

Statement of Contribution/Methods

In this presentation, we demonstrate that double quantum well structure can not only get the information of the generated signals but also obtain the broadband acoustic spectrum in single trace measurement. The concept is shown in Fig. 1 (a). After the acoustic pulses are generated in quantum wells at T=0, the pulses propagate out from the quantum well regions. According to our calculation, the acoustic signals at $T=t_1$ and at $T=t_3$ can be treated as the generated and reflected signals.

Results/Discussion

We have used this technique to study temperature-dependent acoustic attenuation of GaN for frequency up to 1.3 THz as shown in Fig. 1 (b). According to the dependence of temperature and frequency, we analyzed the contributions of acoustic attenuation in GaN such as anharmonic decay, defect scattering, and surface roughness. This technique can also be applied to THz acoustic spectroscopy of other materials such as glass on the top of the GaN cap layer. More details will be discussed in the presentation.

References

[1] K.-H. Lin *et. al.*, IEEE Trans. Ultrason. Ferroelectr. Freq. Control **52**, 1404 (2005).

[2] A. A. Maznev *et. al.*, Ultrasonics **52**, 1 (2012).

[3] Yu-Chieh Wen *et. al.*, Appl. Phys. Lett. **99**, 051913 (2011).

FRIDAY ORAL
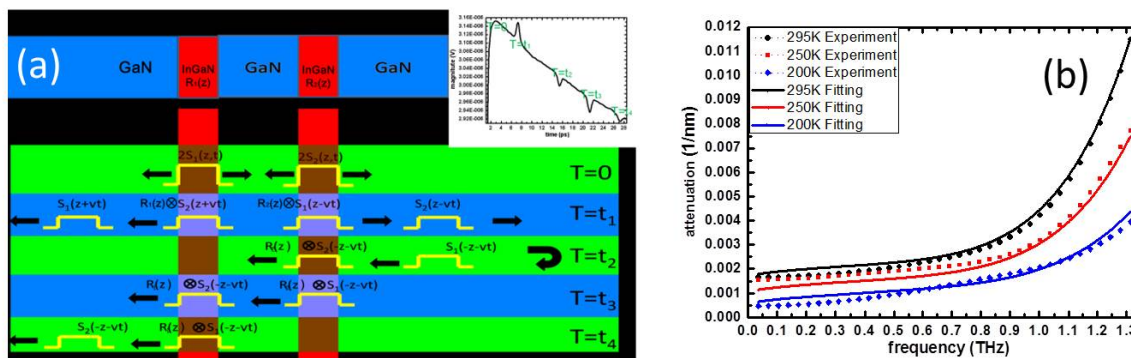
7D - Reduction of TCF

105

Friday, October 23, 2015, 08:00 am - 09:30 am

Chair: **Robert Aigner**
Qorvo Inc.

7D-1

8:00 am   The study of the anomalous thermomechanical effect of fluorine-doped silicon dioxide (FSG) films using temperature dependent FTIR measurements

Matthias Knapp[1,2], Philipp Jäger[2], Werner Ruile[2], Matthias Honal[2], Ingo Bleyl[2], Leonhard M. Reindl[1]; [1]*Department of Microsystems Engineering, University of Freiburg, Freiburg, Germany*, [2]*TDK Corporation, Munich, Germany*

Background, Motivation and Objective

The improvement of filter performance in recent years has lead to a rapid development of layered systems for surface acoustic wave (SAW) filters. Despite properties like passivation or wave guiding, especially temperature compensation techniques are a field of interest. Typically, silicon dioxide (SiO_2) thin films are used as a functional layer, because it becomes stiffer when heated. Recently, fluorine-doped silicon dioxide thin films are reported to be a possible replacement of SiO_2 in surface acoustic wave devices, due to its higher anomalous thermomechanical behaviour compared to silicon dioxide. The objective of this work is to investigate the anomalous thermomechanical behaviour of fluorine-doped silicon dioxide using temperature dependent Fourier transform infrared spectroscopy (FTIR) measurements.

Statement of Contribution/Methods

A fluorine-doped silicon dioxide thin film was deposited on a silicon wafer. Five different temperatures were applied to the wafer using a heating foil. At these temperatures the FTIR measurement was performed in order to measure the typical Si-O vibration peaks.

Results/Discussion

The Si-O bending motion ω_3 and stretching motion ω_4 absorption peaks shift linearly towards lower wave numbers with increasing temperature of the wafer (see Fig. 1). These results can be transformed into changes of the geometrical parameters of the SiOF network, which are the Si-O-Si intertetrahedral angle θ and the stretching force constant α, using the central force model as described by J. T. Fitch et al. We try to explain the small thermal expansion of the fluorine-doped silicon dioxide from purely geometrical considerations and the anomalous thermal coefficient of elasticity by thermodynamic consideratins. The explanations match well with experimental results from differential delay line evaluation.
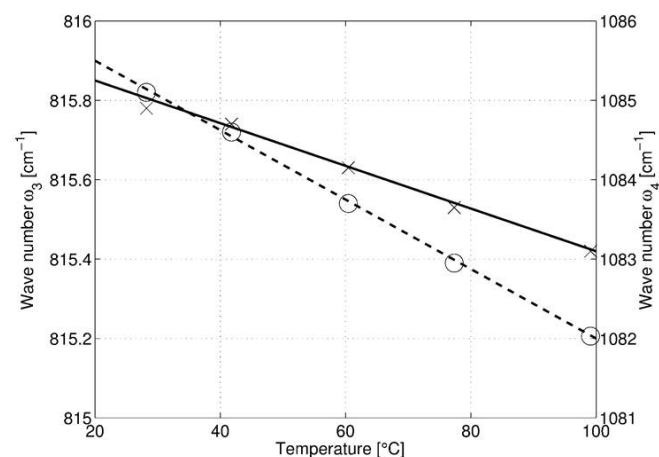
Fig. 1: Temperature dependent shift of the Si-O absorption peaks of SiOF thin films measured with FTIR spectroscopy

---

7D-2

8:15 am   Increased Piezoelectric Coupling Factor in Temperature Compensated Film Bulk Acoustic Resonators

Tokihiro Nishihara[1], Shinji Taniguchi[1], Masanori Ueda[1]; [1]*TAIYO YUDEN CO.,LTD., Japan*

Background, Motivation and Objective

Temperature compensation techniques have been demanded for RF filters and duplexers.

Though several kinds of TC-FBARs have been reported, those effective coupling factors have been only 4-5.6%, compared to 6.3-7.1% of the conventional FBARs.

Therefore, the applications of TC-FBAR filters have been restricted to the bands with the narrow fractional bandwidths under 1.5%.

However RF filters and duplexers with the fractional bandwidths over 2.5% have been mainly used in wireless communication services.

Our objective is to enhance the effective coupling factor of TC-FBAR for such filters and duplexers.

Statement of Contribution/Methods

We have shown the feasibility of fluorine-doped SiO2 (SiOF) material as temperature compensated material [1].

The deposition conditions and the quality of SiOF films have been improved for higher temperature coefficient of elasticity.

The insertion position of SiOF film and each film thickness in TC-FBAR were optimised.

The fabrication process of TC-FBAR with SiOF was also developed.

Results/Discussion

The temperature coefficient of elasticity (c33) was increased from 60 ppm/°C of SiO2 film to 210 ppm/°C of SiOF film.

Our developed TC-FBAR with SiOF film were fabricated and compared against the conventional TC-FBAR with SiO2.

The effective coupling factor of 6.1% and TCF of -10 ppm/°C were achieved in the 2 GHz TC-FBAR with SiOF.

In contrast, 4.4% and -10 ppm/°C were obtained respectively in the 2 GHz TC-FBAR with SiO2.

TC-FBAR with SiOF film will be suitable for RF filters and duplexers with the fractional bandwidth of around 3%.

[1] S.Matsuda et al., Proc. 2011 IEEE IUS, pp.76-78.

7D-3

8:30 am   c-Axis parallel oriented ScAlN films grown by ion-beam assisted RF magnetron sputtering

Mineki Oka[1], Shinji Takayanagi[1], Takahiko Yanagitani[2], Mami Matsukawa[1]; *[1]Doshisha University, Kyotanabe, Japan, [2]Waseda University, Tokyo, Japan*

Background, Motivation and Objective

Recently, Akiyama et al. found that doping scandium into AlN film dramatically increases the piezoelectric coefficient d_{33} [1]. We previously reported the Sc-doped AlN film. And when concentration of doping became 35%, the electromechanical coupling coefficient k_{33} became 0.36. c-Axis parallel oriented AlN film was grown by irradiation of ion beam during AlN deposition [2]. However, whether or not electromechanical coupling coefficient k_{15} is raised in ScAlN film have never been investigated. In this study, we prepared c-axis parallel oriented ScAlN films by using ion beam assisted RF magnetron sputtering and observed shear wave excitation with ScAlN films.

Statement of Contribution/Methods

At first, Al film were fabricated as a bottom electrode. ScAlN film was deposited on the silica glass substrate by RF magnetron sputtering. Scandium ingot grains were put on an Al target. During sputtering deposition, we irradiated nitrogen and argon mixed ion beam from ECR ion source to substrate. The crystalline orientation of the films were determined by XRD analyses and shear mode conversion losses were measured by a network analyzer. Sc concentration in the films were measured by Energy dispersive X-ray spectrometry and those were 0, 8, 12, and 18%, respectively.

Results/Discussion

Fig. 1(a) shows AlN (0002) X-ray pole figure of the $Sc_{0.18}Al_{0.82}N$ film. c-Axis of all film samples were parallel to the substrate and aligned along the direction of ion beam. The FWHM value of φ was 9-16°. Fig. 1(b) shows frequency responses of the conversion losses in $Sc_xAl_{1-x}N$ films. When the Sc concentration was 8%, the conversion loss was the better than the one of 18%.It might be effect of some ion from scandium ingot grain. However, this ScAlN film could excite pure shear wave and shear mode conversion loss was lower than that of the pure AlN film.

[1] M. Akiyama, et, al: Adv. Mater., vol. 21, no. 5 (2009) pp. 593-596.
[2] M.Suzuki, et al: IEEE Int Ultrason Symp., (2011) pp. 262
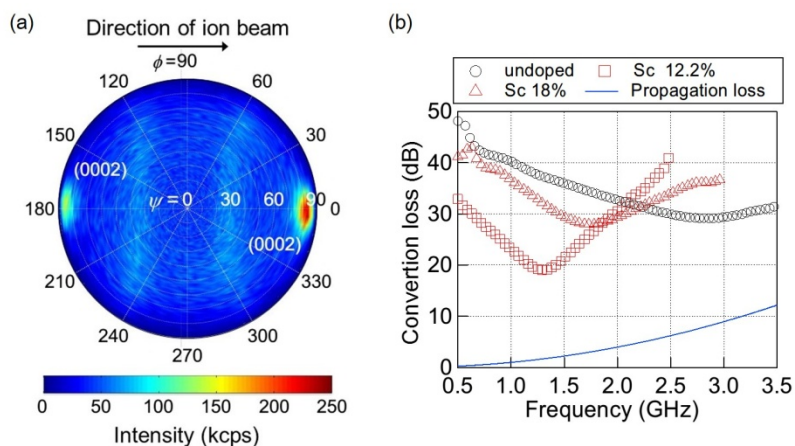
Fig. 1 (a) (0002) pole figure of $Sc_{0.18}Al_{0.82}N$ film
and (b) shear mode conversion loss in Sc-doped and undoped AlN film.

7D-4

8:45 am   Estimation of temperature dependence of C_{44} elastic constant in 42°Y-X cut LiTaO3 single crystals

Minerva Gonzalez[1,2], Fabien Henrot[1], Florent Bassignot[1], Ausrine Bartasyte[1], Bernard Dulmet[1], Sylvain Ballandras[3], Claudia Kajiyama[4], Ingo Bleyl[5], Jean Michel Brice[2]; *[1]Institut FEMTO-ST, Besançon, France, [2]TDK Electronics France SAS, Valbonne Sophia Antipolis, France, [3]Frec|n|sys SASU, Besançon, France, [4]Epcos Inc. (a TDK group company), San Jose, CA, USA, [5]TDK Corporation, Munich, Germany*

Background, Motivation and Objective

42° rotated Y-cut X propagating LiTaO3 (42°Y-X LT) is widely used as substrate for Surface Acoustic Wave (SAW) devices due to its piezoelectric properties such as good electromechanical coupling factor (K2= 7-10% for SAW devices) and a relatively low Temperature Coefficient of Frequency (TCF). The SAW performance of a 42°Y-X LT filter device is strongly influenced, in particular, by the C44 elastic stiffness element. Although it has been previously shown in the literature that the K2 and the elastic constants depend on the Li composition at room temperature, and that these properties also depend on ferroelectric domain structure in LT, a thorough study that correlates the temperature dependence of the stiffness coefficients to different lithium compositions is lacking.

Statement of Contribution/Methods

In this work, K2 and TCF of several types of bulk acoustic wave (BAW) resonators based on 42°Y-X LT and Z-cut LT single crystals with different stoichiometries and ferroelectric domain structures were studied experimentally and by finite element analysis.

FRIDAY ORAL

Results/Discussion

Initially, finite element analysis was carried out to determine the most suitable configurations for generation of acoustic modes in tests devices based on 42°Y-X LT and Z-cut LT. Thickness and lateral field excitations were modeled in piezoelectric plates, as well as thickness field excitation of shear modes in high aspect ratio ridge structures. The latter shows the highest K2 and shear modes that are mainly dependent on C44, and this result was confirmed experimentally. However, the measured frequency response of such structures exhibited many spurious resonances, making difficult the extraction of acoustical parameters. In order to improve the quality of the frequency response, the geometrical parameters of the ridge structures were optimized. Moreover, an elaborate fitting procedure that allows taking into account several resonances occurring simultaneously in a restricted frequency range was used. The temperature dependence of C44, K2 and TCF of ridge structures were determined for crystals with different Li concentrations and ferroelectric domain structures and results obtained are discussed.

7D-5

9:00 am   Multiphysics Modeling of BAW Filters

Andreas Tag[1], Dominik Karolewski[2], Bernhard Bader[3], Maximilian Pitschi[3], Robert Weigel[1], Amelie Hagelauer[1]; [1]*Institute for Electronics Engineering, University of Erlangen-Nuremberg, Erlangen, Germany,* [2]*Institut für Mikroelektronik- und Mechatronik-Systeme gemeinnützige GmbH, Germany,* [3]*TDK Corporation, Germany*

Background, Motivation and Objective

Bulk Acoustic Wave (BAW) filters are commonly used at high power levels and need to fulfill strict specifications like tight transition bandwidths. A part of the applied power will dissipate and lead to a temperature increase within the filter and, thus, to a significant frequency shift of the filter's transfer function. To be able to design filters fulfilling the challenging transition bandwidths at high power levels accurate multiphysics modeling techniques are required.

Statement of Contribution/Methods

Multiphysics (electromagnetic (EM) acoustic thermal) 3 D finite element methods (FEM) are not suitable for single BAW resonators, not to mention a filter, due to the tremendously high calculation times. The solutions presented in the literature do not take the spacial distribution of the temperature and dissipated power into account since they are based on measured TCFs and the dissipated power is calculated from the S-parameters. In our previous works, we have presented modeling approaches taking the spatial distributions of the temperature and the different kinds of the dissipated powers into account in order to remarkably improve the modeling of BAW resonators at high power levels. In this work, the modeling approach has been extended enabling precise and at the same time fast multiphysics simulations of whole BAW filters at high power levels.

Results/Discussion

The acoustic is modeled by an extended 1D modeling approach allowing efficient calculation times and providing the distribution of the viscous losses within each layer together with the lateral leaking power for each resonator, respectively. EM is modeled with a 3D FEM simulation program providing the spatial distribution of the EM losses.

The spatially distributed losses are transferred to the thermal 3D simulation. The result of the thermal simulation is the spatial temperature distribution being used for modification of the geometry of each resonator and the material within each layer in each resonator. Finally, the acoustic and EM simulations are repeated with all the modifications. An example is shown in Fig. 1. The high accuracy of the modeling approach was verified by measurements of the S-Parameters and the temperature distribution by the infrared thermography during high power loads. The developed multiphysics modeling approach enables effective design of modern BAW filters for high power levels.

Fig. 1 Left hand side: Simulation results for the transfer function of a solidly mounted BAW filter without power load, with 33 dBm power load at the frequencies of 1839 MHz and 1914 MHz, respectively. Right hand side: Simulation results of the lateral temperature distribution within two different layers of the resonator for two power loads. The temperature distribution is quite different within the different layers and the power loads at different frequencies.

7D-6

9:15 am   SAW Characteristics of AlN/SiO₂/3C-SiC Layered Structure with Embedded Electrodes

Qiaozhen Zhang[1], Tao Han[1], Jing Chen[1], Kenya Hashimoto[2]; [1]*Electronic Information and Electrical Engineering, Shanghai Jiao Tong University, Shanghai, Shanghai, China, People's Republic of,* [2]*Graduate School of Engineering, Chiba University, Japan*

Background, Motivation and Objective

Layered structure consisting of AlN thin film combined with 3C-SiC substrate has been paid much attention because of their high SAW velocity. It has been demonstrated that the AlN/3C-SiC layered substrate shows better performance in terms of electromechanical coupling coefficient (K^2) and temperature coefficient of delay (TCD) when configured with embedded inter-digital transducer (IDT) electrodes. However, this configuration results in poor step coverage of AlN thin films since the edge discontinuities of the patterned IDT electrodes, which harms AlN crystalline growth and causes cracks in AlN thin films. Therefore, a novel sandwich structure with flattened underlayer for AlN growth by filling amorphous silicon dioxide (SiO_2) in the groove between the electrodes is proposed as shown in Fig.1, and the temperature compenation function can also be expected.

Statement of Contribution/Methods

The SAW characteristics on the proposed AlN/SiO₂/IDT/3C-SiC structure is modeled and analyzed by employing finite element method (FEM). The input admittance of the infinitely-long IDT SAW is calculated, and the phase velocity (V) and coupling factor (K^2) curves have been calculated according to the resonance and anti-resonance frequencies. The temperature coefficient of frequency (TCF) of the structure is predicted using the thermo-mechanical coupling modeling based on COMSOL FEM software.

Institute of Electrical and Electronics Engineers

Results/Discussion

Fig.1 shows simulation results of the phase velocity and coupling factor curves as a function of the normalized AlN thickness (h_{AlN} /λ) for Rayleigh mode propagates along AlN/SiO$_2$/IDT/3C-SiC structure with embedded electrodes. It can be seen that the high V of 5500m/s and enhanced K^2 of 1.43% are simultaneously obtained when the normalized AlN thickness is 0.5. Fig.2 shows the frequency-temperature curves as a function of temperature for the Rayleigh mode on this proposed layered structure with the normalized AlN thickness of 0.4 and the normalized SiO$_2$ thickness of 0.5%. As it is shown, the first order TCF equals to 0.28ppm/^{o}C and the second order equals to -2ppb/ ^{o}C^2 for the temperature ranging from -20 ^{o}C to 100 ^{o}C. The proposed structure enables the growth of highly quality AlN thin films feasible and shows great potential for achieving high velocity, relative large K^2 and temperature compensated SAW applications.

Fig.1. SAW properties of AlN/SiO$_2$/IDT/3C-SiC structure for Rayleigh mode.

Fig.2. Frequency-temperature dependence of AlN/SiO$_2$/IDT/3C-SiC structure for Rayleigh mode (h_{AlN}/ λ =0.4, h_{SiO2}/ λ =0.5%).

8D - Transducers for IVUS

102

Friday, October 23, 2015, 08:00 am - 09:30 am

Chair: **Qifa Zhou**
University of Southern California

8D-1

8:00 am   **High Frequency Single Crystal Composite for Ultrasound Applications**

Jian Tian[1], Kevin Meneou[1], Brandon Stone[1], Pengdi Han[1], Stephen Dynan[1]; *[1]CTG Advanced Materials, Bolingbrook, Illinois, USA*

Background, Motivation and Objective

Piezoelectric single crystal lead magnesium niobate-lead titanate (PMN-PT) has been widely accepted in premium medical ultrasound-imaging systems operating at MHz frequency range, with significantly improved image quality. The advantage of single crystal is limited when used as monolithic crystal at high frequency (e.g., > 30 MHz). Crystal composite offers an effective means to full exploit the excellent properties of single crystals at high frequency. It is until recently that crystal composite becomes commercially available. In this paper we present design, fabrication, and characterization of crystal composite with frequency around 50 MHz for intravascular ultrasound (IVUS) application.

Statement of Contribution/Methods

Crystal composite has improved electromechanical coupling than monolithic single crystal. To maximize the coupling, crystal pillars in a composite need to have a large thickness /width aspect ratio. On the other hand, it is preferable to have crystal pillars of low aspect ratio for subsequent mechanical finishing. To cope with these competing requirements, crystal composite is specially designed to have optimized coupling while being production friendly. Other design considerations include crystal pillar geometry, arrangement, crystal composition and orientation, filling epoxy, and specific transducer requirements. Semiconductor techniques including photolithography and reactive ion etching were used to create crystal pillars and 1-3 composite structure. Etched crystals then go through routine piezoelectric composite fabrication process such as epoxy filling, lapping, coating, poling and testing. Parylene is coated on transducers before acoustic test.

Results/Discussion

Selected dielectric and piezoelectric properties of the crystal were measured on an Agilent 4294A impedance analyzer. Crystal composite demonstrates excellent properties, with the electromechanical coupling factor up to 0.8. Enhanced coupling factor increases the energy conversion efficiency between electrical and acoustic energies, which allows a higher sensitivity and broader bandwidth for composite based transducers. Acoustic test on a 50 MHz crystal composite transducer showed high senility and broad bandwidth. The excellent property of the crystal composite has led to the new generation of IVUS transducers.

8D-2

8:15 am   **A PMN-PT Micromachined 1-3 Composite IVUS Ultrasound Array**

Sibo Li[1], Zhuochen Wang[1], Jinwook Kim[1], Wenbin Huang[1], Jian Tian[2], Pengdi Han[2], Chao Zhang[3], Xiaoning Jiang[1]; *[1]North Carolina State University, Raleigh, North Carolina, USA, [2]CTG Advanced Materials, Bolingbrook, Iliinois, USA, [3]Tsinghua University in Shenzhen, Shenzhen, Guangdong, China, People's Republic of*

Background, Motivation and Objective

PMN-PT 1-3 composite has been increasingly used in medical imaging transducers due to its low impedance, high piezoelectric coefficients and high electromechanical coupling coefficients (kt). Fabrication of composite material for transducers above 25 MHz has been difficult by using traditional dice-and-fill method until the development of piezo-composite micromachined ultrasound transducer technique (PC-MUT). By using micromachining technique, PMN-PT 1-3 composites with frequency of 15 MHz-> 75 MHz have been reported for intravascular ultrasound imaging (IVUS), ophthalmic imaging and non-destructive testing. In this paper, we present a 64-element 40 MHz micromachined 1-3 composite IVUS array.

Statement of Contribution/Methods

Micromachined technique was utilized for the 1-3 composite fabrication. Key processes include photolithography, electro-plating, deep reactive ion etching (DRIE), kerf filling and precision lapping. The final fabricated composite consists of 15 μm wide posts and 6 μm wide kerfs filled with Epotek 301 epoxy. The composite was lapped to 32 μm in thickness, followed by impedance and phase spectrum measurements. The KLM model was used for design of backing and matching layers. The array was designed with the pitch of 80 μm and 64 elements. After the array was interconnected with a custom flexible circuit, it was wrapped to a circular array with 1.5 mm in diameter. The array was then mounted to a fixture for the pulse echo test and phantom imaging experiments.

Results/Discussion

The fabricated composite showed the resonance of 40 MHz and kt of 0.67. From the KLM model, the initial results showed the -6dB fractional bandwidth of 55% and sensitivity of 8 mVpp/V. The pulse echo test showed 500 mVpp sensitivity and -6 dB fractional bandwidth of ~60% using the Olympus 5900R pulser/receiver with the 1 μJ excitation. Those results hold great potential for IVUS imaging.
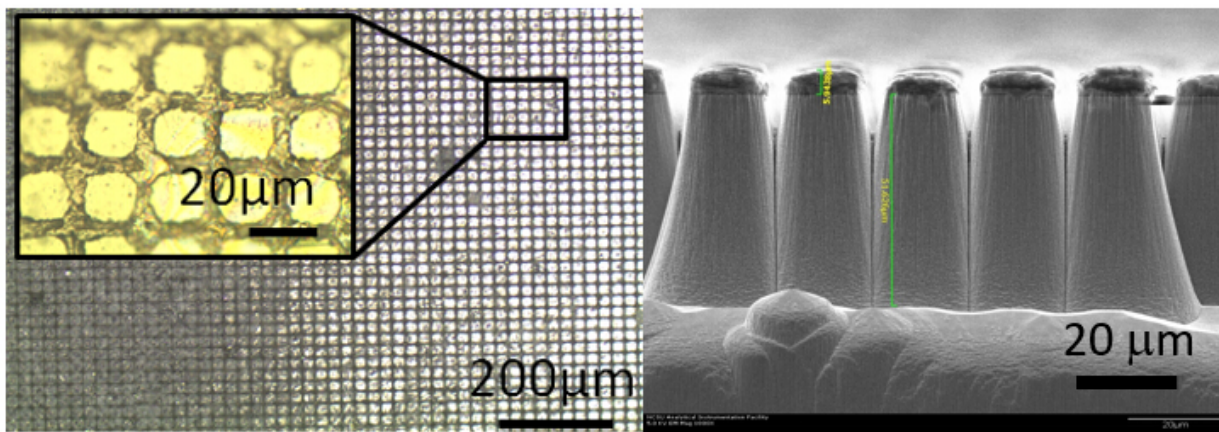
Left: Top view of a typical composite.
Right: Side view of etched PMN-PT single crystal micro-array under SEM

8D-3

8:30 am   Intravascular Acoustic Radiation Force Imaging: Feasibility Study

Carl Herickhoff[1], Mark Palmeri[2], Jeremy Dahl[1]; *[1]Radiology, Stanford University, Palo Alto, CA, USA, [2]Biomedical Engineering, Duke University, Durham, NC, USA*

Background, Motivation and Objective

Coronary heart disease (CHD) affects 15.4 million people and is the leading cause of death in the U.S. CHD involves plaque buildup along the vessel wall, narrowing and hardening arteries (atherosclerosis) and restricting the supply of blood and oxygen to the heart muscle. Plaques characterized by a thin fibrous cap and a soft, lipid-rich necrotic core are vulnerable to rupture, which can result in a heart attack or stroke. Our long-term goal is the development of an intravascular ultrasound (IVUS) probe capable of high-resolution acoustic radiation force imaging in the coronary arteries, to identify and characterize vulnerable plaque. We investigate the feasibility of this approach through construction of a prototype transducer and finite-element simulation of vessel plaque response to an acoustic radiation force (ARF) excitation.

Statement of Contribution/Methods

Our design concept augments a 3.5-Fr, 0.75-mm long cylindrical phased array of a Volcano Eagle Eye IVUS catheter with a 2.2-mm long cylindrical transducer to generate ARF pushes. A prototype transducer was fabricated from a 4.6-Fr tube of radially-poled PZT-4: the tube was cut to 2.2 mm, bonded to a length of stainless steel needle tubing, and electrically connected to a micro-coaxial cable. Optimal drive frequency was determined by measuring the acoustic field at a range of 6 mm with a hydrophone in a water tank. The transducer was placed in a gel phantom (2.9 kPa stiffness, 1.0 m/s shear wave speed) and driven by a Verasonics system at 7.5 MHz, with a 111-µs long, 96 V peak-to-peak transmit pulse. Field II was used to simulate ARF excitation (6-MHz, 2.2-mm cylinder) and tracking (20-MHz Volcano array) with 0.5 dB/cm/MHz attenuation. The ARF excitation was input to a cylindrical LS-DYNA finite element model (FEM) of tissue (2 kPa stiffness) containing an ellipsoidal soft plaque (270 Pa) at a range of 1 mm.

Results/Discussion

The prototype transducer tracked an average maximum displacement of 19.6 µm (σ = 6.0 µm) at a range of 5.1 mm, indicating a sufficiently-high level of radiation force. Initial FEM results of stress field propagation suggest adequate displacement amplitude and contrast between both the soft plaque and surrounding tissue, which could be tracked with a Volcano IVUS imaging array. These results demonstrate that acoustic radiation force imaging is feasible on IVUS-sized devices.
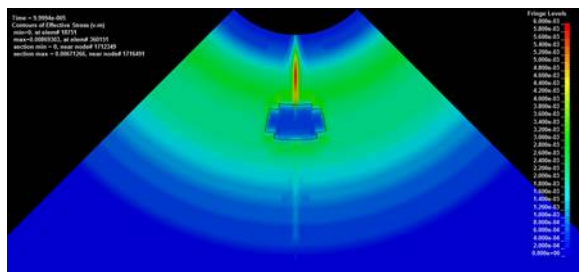
8D-4

8:45 am   Dual-element Ultrasonic Transducer for Intravascular Acoustic Radiation Force Impulse (IV-ARFI) Imaging

Teng Ma[1], Xuejun Qian[1], Mingyue Yu[1], Qifa Zhou[1], K. Kirk Shung[1]; *[1]NIH Resource Center on Medical Ultrasonic Transducer Technology Department of Biomedical Engineering, University of Southern California, Los Angeles, CA, USA*

Background, Motivation and Objective

The rupture of coronary atherosclerotic plaque is considered to be the major contributor of acute coronary syndromes such as heart attack. Knowledge of mechanical property distribution of artery wall can be used to assess the plaque vulnerability. Recently, the development of high resolution elastography techniques, such as acoustic radiation force impulse (ARFI) imaging, has opened up a new window for characterizing mechanical properties of coronary artery at the microstructural level. However, it is very challenging to implement ARFI on the traditional unfocused intravascular ultrasound (IVUS) transducer due to the limited acoustic radiation force induced at such high frequency (20-40Mz). The aim of this study is to develop a confocal dual-element ultrasonic transducer for intravascular ARFI imaging by integrating a focused low frequency (8.5 MHz) transducer for effective excitation and a high frequency (35MHz) transducer for accurate detection.

Statement of Contribution/Methods

The design schematic of dual-element transducer and photograph of the prototype were shown in Fig.1 (A-B). A mechanical focusing ring transducer (8.5 MHz) with a focal depth of 5 mm was fabricated by using modified high-Q PZT ceramics to generate detectable displacements. A flat square transducer (35 MHz) made of PMN-PT single

---

crystal was used to detect the induced displacements. The square transducer was aligned 1 mm above the bottom of the ring transducer to ensure the confocal field of view of 2 mm. ARFI imaging of side-by-side gelatin phantom was performed by linearly scanning the dual-element transducer.

Results/Discussion

The pulse echo testing results of the dual-element transducer were shown in Fig.1(C-D). The boundary of side-by-side gelatin phantom cannot be distinguished in the B-mode image [Fig. 1 (C)]. The corresponding ARFI image [Fig. 1 (D)] provides a clear visualization of the regions with different stiffness by mapping the displacements into different colors. The averaged displacements are about 2.7 μm for the left side (13kPa) and 1.1 μm for the right side (45 kPa), respectively. The preliminary results demonstrate the feasibility of using dual element transducer to perform IV-ARFI to characterize the mechanical properties of atherosclerotic plaque upon further miniaturization in the near future.
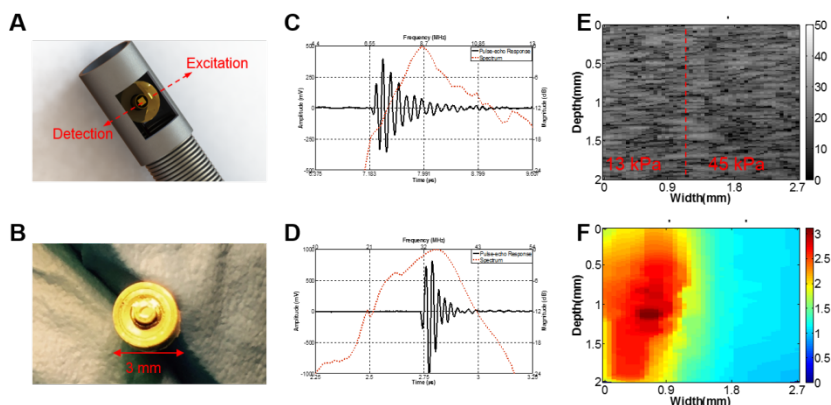
Figure 1. (A) Schematic of dual-element IV-ARFI transducer. (B) Photo of the dual-element IV-ARFI transducer prototype. (C) Pulse-echo results of ring shape excitation transducer (8.5 MHz). (D) Pulse-echo results of square detection transducer (35 MHz). (E) B-mode Image of side-by-side gelatin phantom (50dB dynamic range, estimated Young's Modulus: left-13kPa, right-45kPa). (F) ARFI image of side-by-side gelatin phantom (unit: μm).

8D-5

9:00 am   Dual frequency IVUS transducer for acoustic radiation force impulse imaging (ARFI)

Zhuochen Wang[1], Tomasz Czernuszewicz[2], Caterina Gallippi[2], Xiaoning Jiang[1]; [1]North Carolina State University, USA, [2]University of North Carolina, USA

Background, Motivation and Objective

Coronary atherosclerotic disease is the major cause of mortality in the United States. Vulnerable coronary plaques, with soft lipid/necrotic cores and fibrous caps, are directly linked to 60% to 70% of coronary events. Currently, intravascular optical coherence tomography (IV-OCT), contrast-based computed tomography (CT), and magnetic resonance imaging (MRI) are used to describe the composition and structure of plaques, but with high cost. Acoustic radiation force impulse (ARFI) ultrasound can provide an inexpensive method to achieve plaque characterization. Conventional intravascular ultrasound (IVUS) transducers with frequency of 20 MHz - 60 MHz are not optimized for high-voltage, long-duration pulses required for ARFI imaging. In this paper, a small-size, dual frequency IVUS-ARFI transducer is designed, characterized and tested.

Statement of Contribution/Methods

This dual frequency IVUS transducer consists of a lead magnesium niobate-lead titanate (PMN-PT) single crystal low frequency pushing element (6.5 MHz) and a PMN-PT single crystal high frequency tracking element (30 MHz). The dimensions of the low and high frequency pushing elements are 5 mm × 0.6 mm × 0.3 mm and 0.5 mm × 0.6 mm × 0.07 mm, respectively. A thermal barrier layer is placed between two layers to protect the high frequency tracking element when a high voltage, long duration pulse are applied to the low frequency pushing element. Following the prototyping, electrical and acoustic characterizations were conducted. Electrical impedance and phase spectrum were measured using an impedance analyzer. The acoustic pressure generated by the pushing element at a 5 V, 10-cycle burst excitation was measured by using a hydrophone (HNA-0200, ONDA, Co., Sunnyvale, CA) positioned at 5 mm axially. The impulse response of the tracking element was characterized using a pulser/receiver (Olympus 5900 PR, Olympus Corp, Newton, MA) with the setting of 1 μJ energy. An ARFI test was performed by pushing a 10 kPa phantom with a 160 V, 1000-cycle burst excitation using the low frequency pushing element. Induced displacement was tracked using the high frequency tracking element with 1 μJ energy impulse. Displacement was calculated using normalized cross-correlation between the up-sampled reference and tracking lines.

Results/Discussion

Initial test shows that the center frequency of the high frequency tracking element is 26 MHz and the bandwidth is 47 %. The peak-to-peak pressure generated by the low frequency pushing element with the 5 V, 10-cycle burst excitation was measured to be 233 kPa at 5 mm axially from the transducer surface. In ARFI testing with the 160 V, 1000-cycle burst excitation, a displacement of 40 μm was detected in the 10 kPa phantom. These results suggest that the prototype dual frequency IVUS transducer is capable of performing ARFI imaging, which may be relevant to delineating coronary atherosclerotic plaque structure and composition.

8D-6

9:15 am   Design and Fabrication of Intravascular Focused Ultrasound Transducers

Junsu Lee[1], Jihun Jang[1], Jin Ho Chang[1,2]; [1]Department of Electronic Engineering, Sogang University, Korea, Republic of, [2]Interdisciplinary Program of Integrated Biotechnology, Korea, Republic of

Background, Motivation and Objective

Intravascular Ultrasound (IVUS) transducers have a small aperture (i.e., about 0.5 mm in diameter) to easily insert it into blood vessel, so that the natural focusing occurs over imaging depth ranging from 1 to 5 mm. Therefore, geometric focusing is not effective for IVUS transducers. The small aperture hampers increasing sensitivity of IVUS transducers and thus a signal-to-noise ratio in images. Also, this causes the slice thickness of scan plane to become broader with increasing imaging depth, which results in increasing side-lobe level of a lateral beam pattern and artifacts. To overcome the limitations, we designed and fabricated an IVUS transducer focused at a certain point in elevational direction.

Statement of Contribution/Methods

The width of an IVUS transducer defined in the lateral axis should be much less than the diameter of blood vessel, but its length in elevation axis is relatively free from the restriction. The general IVUS transducer has circular or square aperture (e.g., 0.5 X 0.5 mm); its natural focal depth is about 2 mm with the center frequency of 50 MHz in both lateral and elevation directions. In contrast, the proposed IVUS transducer has oblong aperture (i.e., 0.5 X 1.5 mm); its natural focal depth in elevation direction is 18 mm, so that geometric focusing can be conducted for blood vessel imaging. Both the general and the proposed IVUS transducers were fabricated consisting of PZT-5H, two

---

matching layers (2-3 silver epoxy and parylene), backing (E-solder 3022). The press focusing technique was used for the elevational focus at 3 mm. The performances were evaluated through pulse-echo test and 25-¥im wire phantom experiments.

Results/Discussion

Fig. 1(a) shows photographs of the fabricated general and proposed IVUS transducers. From the pulse-echo test, it was measured that the center frequency and -6dB bandwidth were 44.5 MHz and 45 MHz in the case of the proposed IVUS focused transducer and 53.7 MHz and 24.7 MHz in the general one. The axial and lateral resolutions were also measured from the wire phantom images (see Fig. 1(b) and (c)). The lateral beam width of the proposed transducer (i.e., the -6dB and -20 dB lateral beam widths of 0.165 mm and 0.316 mm) was narrower than that of the general one (0.181 mm and 0.486 mm) due to mainly low side-lobe level. Consequently, the elevation focusing is viable for IVUS transducers and improves the lateral resolution.

Figure 1
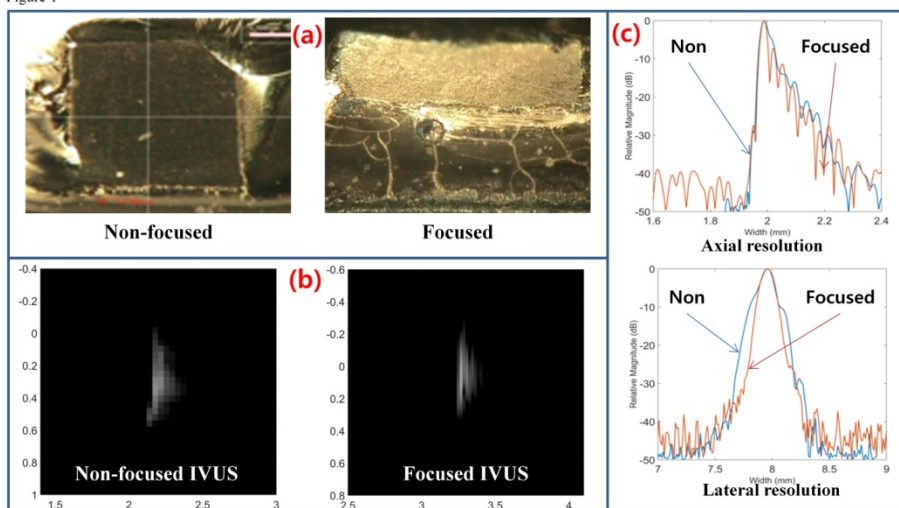
1E - Clinical Ultrasound

Plenary Hall

Friday, October 23, 2015, 10:30 am - 12:00 pm

Chair: **Pai Chi Li**
National Taiwan University

1E-1

10:30 am   Ultrasound-guided high intensity focused ultrasound: clinical experience

Jae Young Lee[1]; [1]Radiology, Seoul National University Hospital, Seoul, Korea, Republic of

Background, Motivation and Objective

In the comparison of MRI and ultrasound as guiding modality for the treatment of uterine myoma, ultrasound provides real-time guidance, higher availability, higher cost-benefit, and easiness to handle than MRI. However, lower spatial resolution, impossibility to obtain thermometry, and presence of blind spot and artifacts limit the use of ultrasound as a guiding tool. To enhance the advantages of ultrasound and to overcome the limitation of ultrasound described above, evolutionary advance is essential in ultrasound-guidance technique. Recently, a new machine with increased portability, 3D electronic steering, pretargeting, real-time cavitation monitoring, 3D image reconstruction algorithms, and interleaved image display was developed. In our preclinical study using this new HIFU system with advanced functions described above, a small discrepancy (width, 0.5-1.1 mm; length, 3.0 mm) was shown between the planning ultrasound and pathological specimens and inordinate thermal damage was not observed in the adjacent tissues and encapsulated organs. We would like to share our experience using this new HIFU system for the treatment of uterine fibroids.

Statement of Contribution/Methods

A clinical study with 28 uterine fibroids of 19 patients (age range, 33-53) was performed. All patients were treated with HIFU with 3D electronic steering. MR imaging studies were performed before HIFU, immediately after HIFU, and 1 month and 3 months after HIFU treatment. Ablation volume ratio, procedure time and complication were analyzed.

Results/Discussion

The volume of treated uterine fibroids ranged from 17.1 cm3 to 269.6 cm3 (mean, 86.8 cm3; SD, 67.6 cm3). Ablation volume ratio on immediate post-HIFU MR imaging ranged from 28.3% to 100% (mean, 78.6%; SD, 21.1%). Time taken to ablate a fibroid was less than 30 minutes in most of tumors. Minimal signal intensity changes in rectus muscle were noted in four patients without any associated significant symptom and signs. Skin burns were not noted. Therefore, this newly developed portable HIFU machines with 3D electronic steering may be very promising for the treatment of uterine fibroids in terms of cost-benefit and time saving.
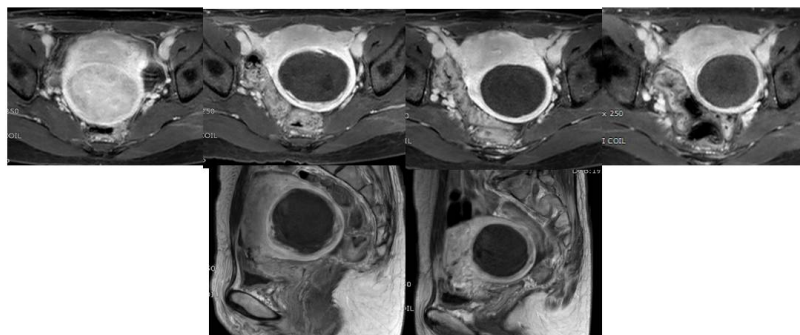
1E-2

11:00 am   Clinical Application of Liver Elastography

Yi-Hong Chou[1], Hsin-Kai Wang[1]; [1]Taipei Veterans General Hospital, Taiwan

Ultrasound elastography is an emerging imaging technique that enables evaluation of liver stiffness noninvasively. There are two types of commercially available ultrasound elastography systems: compression elastography and shear wave elastography. Compression elastography basically provides qualitative assessment of liver stiffness, whereas shear wave elastography provides quantitative data of liver stiffness, either expressed as kilopascal (kPa) meter/sec (m/sec) or m/sec. During the development of liver cirrhosis, the liver tissue became stiffer due to deposition of the collagen fiber. Liver stiffness thus can be used as a parameter for the diagnosis of liver cirrhosis. Studies have shown that liver stiffness is a reliable indicator in the assessment of liver cirrhosis, and potentially a useful biomarker for the assessment of other liver diseases. Measurement of liver stiffness may facilitate the diagnosis of liver cirrhosis, monitoring the treatment response, predict the prognosis / complication of liver cirrhosis, and assessment of the hepatic tumor. Despite its wide potential application, liver elastography sustains several limitations: several factors result in variability at measuring liver stiffness. These can be categorized into factors related to the underlying of cause of liver disease, physiological status, ultrasound machine, or operator. In addition to cirrhosis, necroinflammatory activity, cholestasis, venous congestion lead to elevation of liver stiffness. Liver stiffness is different between fasting and non-fasting status, especially in cirrhotic patient. Right hepatic lobe liver provides more reliable and consistent stiffness measurement than left lobe. As a result, a consistent protocol in an experienced hand is necessary for reliable measurement of liver stiffness. Despite these limitations, the degree of liver stiffness obtained from elastography can be well correlated with the liver fibrosis / cirrhosis. Liver elastography may become a useful tool for clinical assessment of liver fibrosis.

1E-3

11:30 am   Ultrasound Fusion Imaging of Liver Tumor: Recent Progress and Clinical Relevance

Masatoshi Kudo MD,PhD, Department of Gastroenterology and Hepatology, *Kinki University School of Medicine*

With advances in technology, imaging techniques that entail fusion of sonographic and CT or MRI have been introduced in clinical practice. Ultrasound fusion imaging provides CT or MR cross-sectional multiplanar images that correspond to the sonographic images, and fusion imaging of B-mode sonography and CT or MRI can be displayed simultaneously and in real-time according to the angle of the transducer. Ultrasound fusion imaging helps us to understand the 3-dimensional relationship between the liver vasculature and tumors, and can detect small liver tumors with poor conspicuity. This fusion imaging is attracting the attention of operators who perform radiofrequency ablation (RFA) for the treatment of hepatic malignancies because this real-time, multimodality comparison can increase monitoring and targeting confidence during the procedure. When RFA with fusion imaging was performed on small hepatocellular carcinomas (HCCs) with poor conspicuity, it was reported that the rates of technical success and local tumor progression were 94.4–100% and 0–8.3%. However, there have been no studies comparing fusion imaging guidance and contrast-enhanced sonography, CT or MRI guidance in ablation, fusion imaging–guided RFA has proved to be effective for HCC that are poorly defined on not only conventional B-mode sonography but also contrast-enhanced sonography. In addition, fusion imaging could be useful to assess treatment response of RFA because of 3-dimensional information. Here, we give an overview of the current status of ultrasound fusion imaging for clinical application in the liver.

Another important progress of US technology is a virtual US imaging device, SYNAPSE VINCENT, as a tool to assist novice sonographers. A prospective blinded pilot study was conducted involving patients with liver lesions. Two sonographers and two medical doctors with less than 5 years of experience performed US examinations. Detecting time on US and the success rate for detecting liver lesions with/without using the virtual US imaging device, before US examination were evaluated.

A total of 32 patients with 42 liver cancers were included. The maximal diameter of these lesions ranged from 0.3 to 1.5 cm. The average time for detecting liver lesions on US was 47.8 seconds with VINCENT and 112.9 seconds without VINCENT before US examination. There were significant differences in the duration of US examination with/without VINCENT (p = 0.0002, Student's t-test). The rates for accurately detecting liver lesions were 100% and 76.2% (16/21) in US beginner with/without VINCENT respectively. Significantly higher detection rates in the US beginners were compared to without VINCENT (p = 0.047).

Before US examination, a reference with VINCENT could contribute to the successful detection of liver lesions and time-saving for US beginners.

FRIDAY ORAL

2E - MEL: Characterizing Vascular Disease

VIP

Friday, October 23, 2015, 10:30 am - 12:00 pm

Chair: **Chris de Korte**
            Radboud university medical center

10:30 am   Evaluating Arterial and Plaque Elasticity with Shear Wave Elastography in an *ex vivo* Porcine Model

Erik Widman[1,2], Elira Maksuti[1], Carolina Amador Carrascal[3], Matthew W. Urban[3], Matilda Larsson[1]; [1]*KTH Royal Institute of Technology, Stockholm, Sweden, [2]Department of Molecular Medicine and Surgery, Karolinska Institutet, Stockholm, Sweden, [3]Department of Physiology and Biomedical Engineering, Mayo Clinic College of Medicine, Rochester, MN, USA*

Background, Motivation and Objective

Visual assessment of carotid duplex scanning and angiography is the current clinical standard for determining plaque vulnerability and quantitative tools are needed. Quantifying plaque elasticity using shear wave elastography (SWE) has been proposed as elastic properties of plaques have shown to correlate with plaque vulnerability. Previously, plaque characterization via SWE has been successfully validated by mechanical testing in a carotid artery phantom. The objective of this study is to apply the validated algorithm in an *ex vivo* plaque model as a step towards an *in vivo* implementation.

Statement of Contribution/Methods

Five porcine aortas from small Swedish Yorkshire pigs (weight 36 ± 2 kg, 3 male, 2 female) were used as a model for a human carotid artery as they were of similar dimensions (wall thickness 1.3 ± 0.1 mm, lumen diameter 8.5 ± 0.2 cm). Simulated calcified plaques were induced by soaking sections of the arteries in 36% formaldehyde solution for 20 minutes. The arteries were attached to a fixture, connected to a water column, placed in a saline bath, as the pressure was varied from 20 to 120 mmHg in 20 mmHg increments. Acoustic radiation force (center frequency 4.09 MHz, push length 100 μs) and plane wave imaging (10 kHz) was performed using a Verasonics acquisition system with a linear L7-4 probe in the anterior arterial wall and calcified plaque. The shear waves were tracked using a 2D auto-correlation followed by Fourier analysis to calculate phase velocity as a function of frequency. The arterial wall and plaque shear modulus (μ) was obtained by fitting the phase velocity curve to a model of a Lamb wave propagating through a thin, elastic plate.

Results/Discussion

The experimental setup and preliminary results of shear moduli estimates with respect to pressure for the arterial wall (blue line) and plaque (red line) can be seen in Figs. 1A and B respectively. The results show a clear difference in elasticity estimates between the plaque and wall, which are in an appropriate range when compared to the literature. Moreover, the results show an approximate linear stiffness for realistic *in vivo* pressures between 60 and 120 mmHg. The results demonstrate the feasibility of SWE for quantitative plaque characterization in biological tissues in addition to the applicably of SWE for the detection of early onset atherosclerosis.
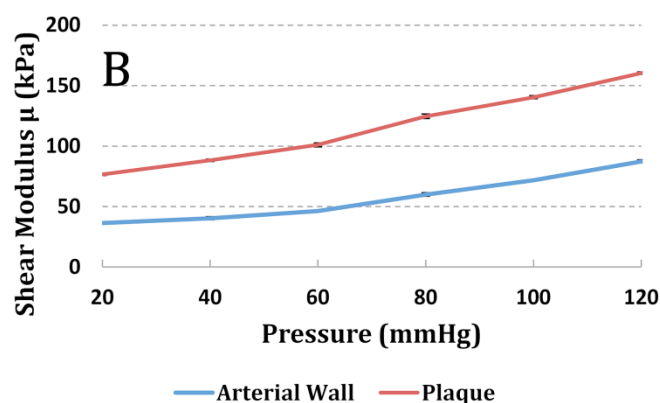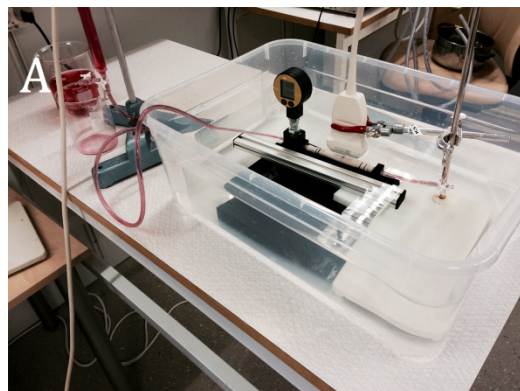
Fig. 1a) Porcine artery attached to a fixture, placed in a saline bath, and connected to a water column. The ultrasound probe was fixed 1 cm above the artery. b) Sample shear moduli estimates (kPa) with respect to lumen pressure (mmHg) in one of the arteries for the arterial wall (blue line) and plaque (red line).

10:45 am   2D versus 3D cross-correlation-based radial and circumferential strain imaging in a 3D atherosclerotic carotid artery model using ultrafast plane wave ultrasound

Stein Fekkes[1], Abigail E.S. Swillens[2], Hendrik H.G. Hansen[1], Anne E.C.M. Saris[1], Maartje M. Nillesen[1], Francesco Iannaccone[2], Patrick Segers[2], Chris L. de Korte[1]; [1]*Medical UltraSound Imaging Center (MUSIC), Department of Radiology and Nuclear Medicine, Radboud university medical center, Nijmegen, Netherlands, [2]Department of Electronics and Information Systems, Ghent University, Belgium*

Background, Motivation and Objective

Vascular strain estimation in 3D might improve the detection of rupture prone plaques in carotid arteries. This study assesses the performance of radial and circumferential strain imaging derived from 2D and 3D displacement estimations using a 3D model of an atherosclerotic carotid artery (CA).

Statement of Contribution/Methods

A 3D finite element model of a patient-specific, pulsating atherosclerotic CA (pulse pressure 60 mmHg) surrounded by tissue was generated using Abaqus. Global cyclic longitudinal movement as reported by Cinthio et al. 2006 was superimposed to the model. Radiofrequency (RF) element data without attenuation and a SNR of 30 dB were simulated in Field II by moving point scatterers according to the model over one cardiac cycle. A linear array transducer (fc = 9 MHz, pitch = 198 μm, 192 elements) was simulated, transmitting plane waves at 3 sequentially alternating angles (0°, -19.5°, 19.5°) at a frequency of 10 kHz. Transmissions were simulated at a frame rate of 50 Hz (systole) and 10 Hz (diastole) to ensure an inter-frame (IF) strain range of <2%. Acquisitions were performed for 191 equally spaced (0.1 mm) transversal positions of the internal CA distal from the bifurcation. After delay-and-sum beamforming, IF displacements were estimated using a normalized cross-correlation-based algorithm, using either 2D or 3D kernels. The 0° axial displacement was used as vertical displacement component. Horizontal displacements were obtained by projection of the +19.5° and

19.5° axial displacements. After tracking, the vertical and horizontal displacements were converted to radial and circumferential displacements. Least squares 2D-strain estimation was performed to derive radial and circumferential strain. The 2D and 3D method were compared by determining the absolute error of the strain with respect to the ground truth strain derived from the model.

Results/Discussion

The overall median radial strain error significantly reduced from 0.82% in 2D to 0.62% (P<0.01) using the 3D technique. For the circumferential strain, a decrease of 0.46% to 0.41% (P<0.01) was found. Figure 1 shows the progression of the strain error during 1 cardiac cycle. A clear deviation between the 2D and 3D method can be seen at 0.2 seconds, where a ~0.4 mm longitudinal shift is present. Overall these results show that the 3D technique improves radial and circumferential strain estimates.
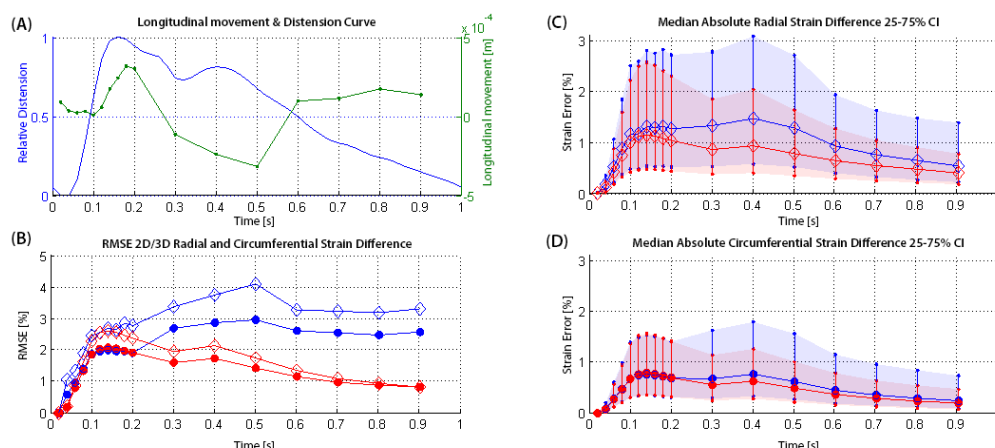
Figure 1. Strain error of 2D and 3D radial and circumferential strain estimates with respect to ground truth strain.
A: Distension curve of one cardiac cycle and the longitudinal cyclic movement of the carotid artery show a overall movement range of ~± 0.3mm.
B: RMSE of the ground truth strain - estimate strain for both methods.
C: Radial strain error progression along the cardiac cycle indicating a clear 2D vs 3D error increase at 0.2 s.
D: Circumferential strain error progression along the cardiac cycle.

2E-3

11:00 am   A novel intravascular ultrasound (IVUS) elastography based on high resolution acoustic radiation force impulse (ARFI) imaging for assessing the elastic properties of atherosclerosis

Cho-Chiang Shih[1], Pei-Yu Chen[1], Lei Sun[2], Chih-Chung Huang[1]; *[1]Department of biomedical engineering, National Cheng Kung University, Taiwan, [2]Interdisciplinary division of biomedical engineering, The Hong Kong Polytechnic University, Hong Kong*

Background, Motivation and Objective

It is well known that vulnerability of plaque is influenced by the mechanical properties of both vessel wall and plaque itself. Therefore, measurements of the elastic properties of plaque and vessel have a great significance in clinical diagnosis of atherosclerosis. The conventional intravascular ultrasound (IVUS) can only visualize the anatomical structure of epicardial vessels and plaque without providing the viscoelastic information of them. In order to measure the elastic properties of soft tissue, ultrasound elastographs have been proposed for noninvasive examination, such as acoustic radiation force impulse (ARFI) imaging . However, most of these elastographs are not suitable for visualizing the plaque and epicardial vessels due to imaging resolution. In order to overcome this problem, a system of combining the IVUS and high resolution ARFI imaging by using a novel dual-elements transducer was proposed for intravascular elastography in present study.

Statement of Contribution/Methods

An IVUS transducer with dual elements was fabricated in the study. The pushing element with 12 MHz frequency was used to generate acoustic radiation force to induce the localized tissue displacements, and the displacements can be detected by the detecting element of 42 -MHz, as shown in Fig 1(a). The transducer was attached on the motor system to perform rotating scan. Experiments were carried out by scanning the artificial-atherosclerotic phantom which manufactured by different concentrations of gelatin.

Results/Discussion

Fig. 1(b) shows the displacement curves from gelatin phantoms which were induced by the 12 MHz pushing element and detected by 42 MHz element. The maximum displacements of 2% and 7% gelatin phantom were 4.6 and 1.5 µm, respectively. Softer phantom exhibits larger displacement. Figure 1(c) shows the conventional IVUS echogenic image and its corresponding high resolution ARFI-IVUS image from artificial-atherosclerotic phantom, respectively. Both the location and dimension of plaque were observed obviously using ARFI imaging, however, it is difficult to distinguish each of them in the echogenic image. The ARFI-IVUS system was successfully developed in the study. In the future, the system will be further verified by scanning in vitro and in vivo atherosclerotic arteries of animal to demonstrate the feasibility for clinical applications.

FRIDAY ORAL

(a)

(b)

(c)

B-mode

ARFI
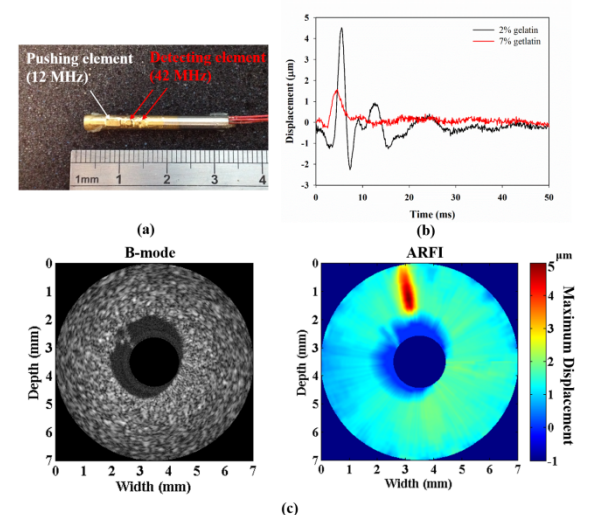
11:15 am   A 1D model-based inverse problem for recovery of spatially varying vessel stiffness for Pulse Wave Imaging

Matthew Mcgarry[1], Ronny Li[1], Iason Apostolakis[1], Elisa Konofagou[1,2]; [1]*Biomedical Engineering, Columbia University, New York, New York, USA, [2]Radiology, Columbia University, New York, NY, USA*

Background, Motivation and Objective

Many vessel pathologies of interest (such as plaques and aneurysms) cause focal changes in the wall properties. Therefore, a method to accurately estimate spatially varying mechanical properties is required. Pulse wave imaging (PWI) images the propagation of intrinsic pulse waves along the vessel wall. Modeling can predict reflections and changes in the waveform caused by inhomogeneities; a full 3D fluid-solid interaction model including both blood flow and vessel wall motion comes at a prohibitive computational cost, but in many cases a 1D approximation is reasonable as the blood velocity along the vessel is much larger than the radial components. This work presents a 1D pulse-wave inverse problem, where a set of spatially discretized unknown properties and boundary conditions of the governing 1D partial differential equations are found which provide the most accurate match between the model and the spatiotemporal vessel wall displacements measured by PWI.

Statement of Contribution/Methods

A finite difference model of the 1D pulse-wave equations was developed where the unknown quantities are parameterized as a set of discretized wall moduli values and a number of discrete cosine transform components of the inlet pressure boundary conditions. Starting from an initial guess, the quasi-Newton method was used to iteratively determine the set of unknown parameters which minimize the mismatch between the model and the experimental measurements.

Results/Discussion

Inversions of simulated pulse-wave data showed that the algorithm is capable of recovering accurate property distributions and boundary conditions with measurement noise up to 50%. Typical inversion time is around 5 minutes. PWI data collected from a PVA gel vessel phantom driven by a peristaltic pump was used to validate the method in an experimental setting. A comparison of Young's modulus estimates produced by the inverse problem, piecewise pulse-wave velocity estimation and static inflation is given in figure 1, along with the recovered inlet pressure and match between the model and measurements. The stiffness estimates of the three methods are consistent, and the spatial profile is consistent with variation in circumferential pre-strain due to axial pre-stretch applied during phantom fabrication. This work was supported in part by NIH R01-HL098830.
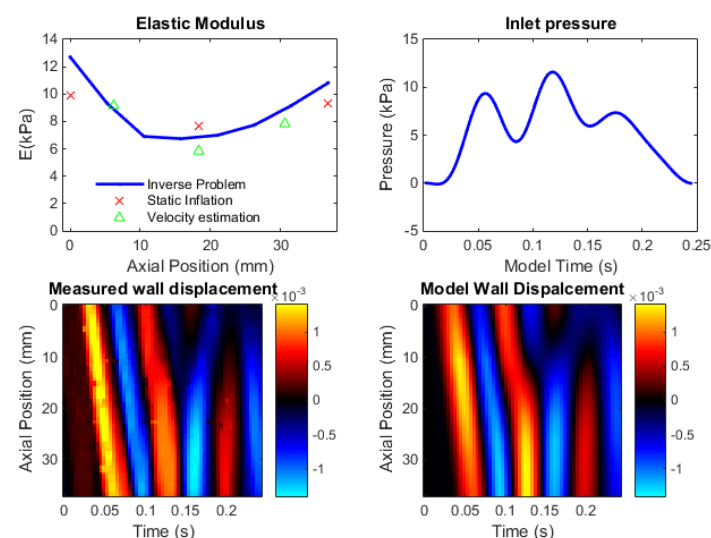
11:30 am   Mechanical Characterization of Abdominal Aortic Aneurysms using 4D Ultrasound

E.M.J. van Disseldorp[1,2], N.J. Petterson[1], F.N. van de Vosse[1], M.R. van Sambeek[2], R.G.P. Lopata[1]; [1]*Cardiovascular Biomechanics Group, Department of Biomedical Engineering, Eindhoven University of Technology, Eindhoven, Netherlands,* [2]*Department of Vascular Surgery, Catharina Hospital Eindhoven, Netherlands*

Background, Motivation and Objective

Rupture of abdominal aortic aneurysms (AAAs) is a major cause of death in the Western world. The current criteria for intervention, maximum diameter ($\geq$ 55 mm) or large growth ($\geq$ 5 mm / 6 months) have proven to be inadequate. The mechanical properties of the AAA and stresses in the wall could be a better predictor for rupture risk, since rupture will occur when the wall stress exceed local wall strength. The aim of this study is to characterize the mechanical behaviour of AAAs using 4D ultrasound (US).

Statement of Contribution/Methods

In this study, 13 patients in the age of 60 - 82 years with a AAA of 32 – 53 mm were imaged preoperatively using a Philips iU22 equipped with a 3D X6-1 probe (f_c = 3.5 MHz). Volume data were acquired for 5 seconds (volume rate = 5-8 Hz) during breath-hold. The brachial pressure was measured using an arm cuff during the US acquisition.

The US data were segmented manually, after which smoothing was performed to reduce irregularities. The patient-specific geometry was tracked over time using a 3D coarse-to-fine block matching algorithm (2.0 by 2.0 by 1.5 mm kernelsize) to estimate the 3D displacement fields of the vessel wall. The diastolic geometry was converted into a quadratic tetrahedral element mesh (wall thickness = 2mm). Finite element analysis (FEA) was performed assuming a neo-Hookean material model. The initial stresses at diastolic pressure were reconstructed using a backward incremental method after which the systolic pressure measured was applied. The model was optimized by iteratively adapting the material property (shear modulus) until the model output matched the in vivo displacements of the AAA found by the 3D speckle tracking algorithm. The resulting patient-specific incremental shear modulus (G_{FEA}) was compared to a direct elastographic estimate, G_{ELASTO}, which is based on the 3D deformation data and LaPlace's law.

Results/Discussion

Good agreement was found between the moduli determined with the elastographic approach and FEA: G_{ELASTO} = 1.2 ± 0.6 MPa and G_{FEA} = 1.3 ± 0.6 MPa (Fig. 1A-B). The resulting patient-specific wall-stresses ranged from 100 to 300 kPa (Fig. 1C), which are in accordance with literature. The advantage of the FEA is the ability to analyse wall stress using both patient-specific geometry and material properties. In future research, this approach could be improved using automatic segmentation and a more complex material model.
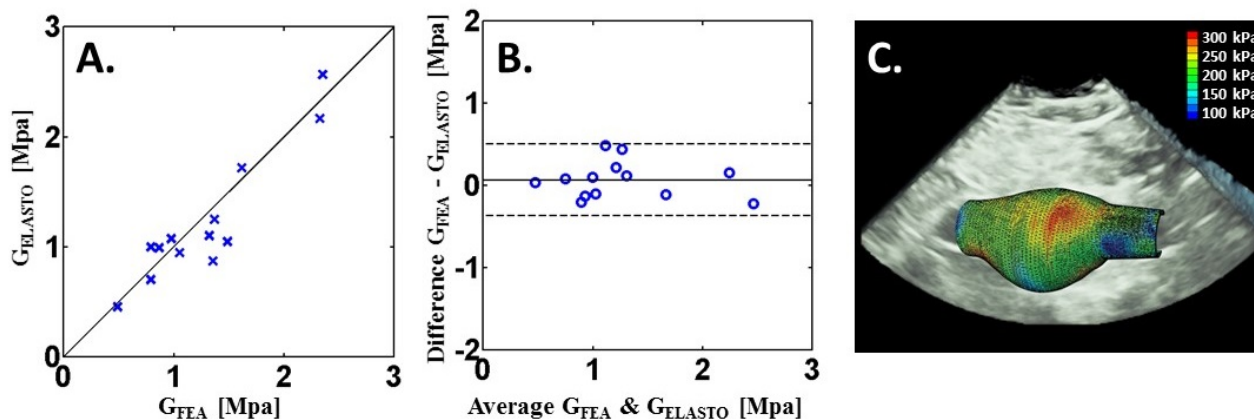
Figure 1:

A. Incremental shear modulus determined with the elastographic approach (G_{ELASTO}) vs finite element analysis (G_{FEA}) for all patients. **B.** Bland-Altman plot of G_{ELASTO} and G_{FEA}. **C.** Example of ultrasound based patient-specific AAA geometry and wall stress.

11:45 am   Detection of Coronary Artery Disease with Myocardial Elastography with validation against myocardial perfusion imaging and coronary angiography

Julien Grondin[1], Marc Waase[2], Vincent Sayseng[1], Elisa E Konofagou[1,3]; [1]*Department of Biomedical Engineering, Columbia University, New York, NY, USA,* [2]*Department of Medicine, Columbia University, New York, NY, USA,* [3]*Department of Radiology, Columbia University, New York, NY, USA*

Background, Motivation and Objective

Myocardial Elastography (ME) is a radiofrequency (RF)-based technique that can image 2-D cardiac strains in vivo. Prior studies have shown that ME with conventional beamforming can detect abnormal function of coronary artery disease (CAD) patients and identify the territories affected by occluded arteries. Early detection of CAD can prevent patients from undergoing invasive catheterization or ionizing procedures. The objective of this study was to evaluate the performance of ME in detecting and characterizing abnormal myocardial perfusion, infarct scars or coronary occlusion in patients using ME with diverging wave imaging.

Statement of Contribution/Methods

In this study, two set of patients were investigated: patients scheduled for a nuclear stress test (N = 36) and patients scheduled for a coronary angiography (N = 23). All patients recruited for this study were imaged with ME prior to and on the same day as their nuclear stress test or their coronary angiography. Diverging wave imaging was used to acquire transthoracic images in short-axis view using a Verasonics system and a 2.5 MHz center frequency probe. Channel RF data were acquired at 2kHz and ECG was acquired synchronously. Incremental axial and lateral displacements were estimated using normalized 1-D cross-correlation (window size: 5.9 mm, 90% overlap) in a 2-D search and then accumulated during systole. Axial and lateral cumulative strains were computed by applying a least-squares estimator on the axial and lateral cumulative displacements (kernel size: 6.6mm) before converting to radial and circumferential cumulative strains. The radial strain were computed in the total cross-section of the myocardium and in each region perfused by the LAD, the LCX and the RCA.

Results/Discussion

For patients who had the nuclear stress test, the average radial end-systolic cumulative strain in the total cross-section of the myocardium was significantly higher in the normal patients (18.3±12.1%) than in the patients with abnormal perfusion or scar (6.1±9.1%, p < 0.05). In the LCX territory, the average radial end-systolic cumulative strain was higher in normal patients (14.1±16.4%) than in patients with abnormal perfusion or scar (-2.6±5.9 %, p < 0.05). For patients who had the coronary angiography, the average radial end-systolic cumulative strain in the total cross-section of the myocardium was significantly higher in the normal patients (11.2±8.9%) than in the patients

with obstructive CAD (1.0±8.6%, p < 0.05). In the LAD territory, the average radial end-systolic cumulative strain was higher in normal patients (14.3±11.5%) than in patients with obstructed LAD (-0.9±6.2 %, p < 0.05). These preliminary clinical findings indicate the potential of ME to noninvasively differentiate patients with a normal myocardial perfusion or coronaries from patients with a perfusion defect, a scar or an obstructed coronary with the highest significance in the LCX and LAD territory.

3E - MTH: Bubbles and HIFU

201BC

Friday, October 23, 2015, 10:30 am - 12:00 pm

Chair:　　**Emad Ebbini**
　　　　　Univ. of Minnesota

3E-1

10:30 am　**Large diameter microbubbles produced by a catheter-based microfluidic device for sonothrombolysis applications**

Adam Dixon[1], Brian Shin[1], Vamsi Meka[1], Joseph Kilroy[1], Alexander Klibanov[1], John Hossack[1]; [1]*Biomedical Engineering, University of Virginia, Charlottesville, VA, USA*

Background, Motivation and Objective

Sonothrombolysis clinical trials have utilized microbubble (MB) formulations with MB diameters between 1–4 μm. The restriction on MB size is due to a risk of gas emboli formation and caused MBs outside of this diameter range to be unexplored for thrombolysis. However, large MBs confer increased bioeffects when excited acoustically, as has been shown in sonoporation and blood brain barrier disruption studies. In this work, we demonstrate that MBs in the 10-30 μm diameter range increase sonothrombolysis rates by up to 4.5X when compared to small MBs of ~2 μm diameter.

Statement of Contribution/Methods

We fabricated a catheter-sized microfluidic device (1 mm diameter) that has the potential to be advanced intravascularly to the site of thrombosis and produce MBs to enhance sonothrombolysis. The MBs are comprised of nitrogen gas and an albumin shell, which limits MB lifetimes to less than 120 s and reduces the risk of gas embolism. We evaluated in vitro sonothrombolysis rates and varied MB, ultrasound, and tPA parameters to optimize clot lysis. We also evaluated in vivo safety of large diameter MB administration in a rat stroke model.

Results/Discussion

In vitro clot lysis studies produced two key results: (1) at a clinical tPA dose of 1 μg/ml, 15 μm diameter MBs enhanced clot lysis by 4.5X relative to ~2 μm diameter MBs, and (2) 15 μm diameter MBs with reduced dose tPa (0.1 μg/ml) achieved a 2X increase in lysis relative to 2 μm diameter MBs at full tPa dose. The results indicate large MBs may accelerate thrombolysis at reduced tPA dose. Significantly, improved performance at reduced tPA dose may enable usage in patients contraindicated for the conventional dose of tPA.

In vivo administration of 15 μm diameter MBs to the rat brain produced no signs of infarction or ischemia at MB production rates below 150,000 MB/s.
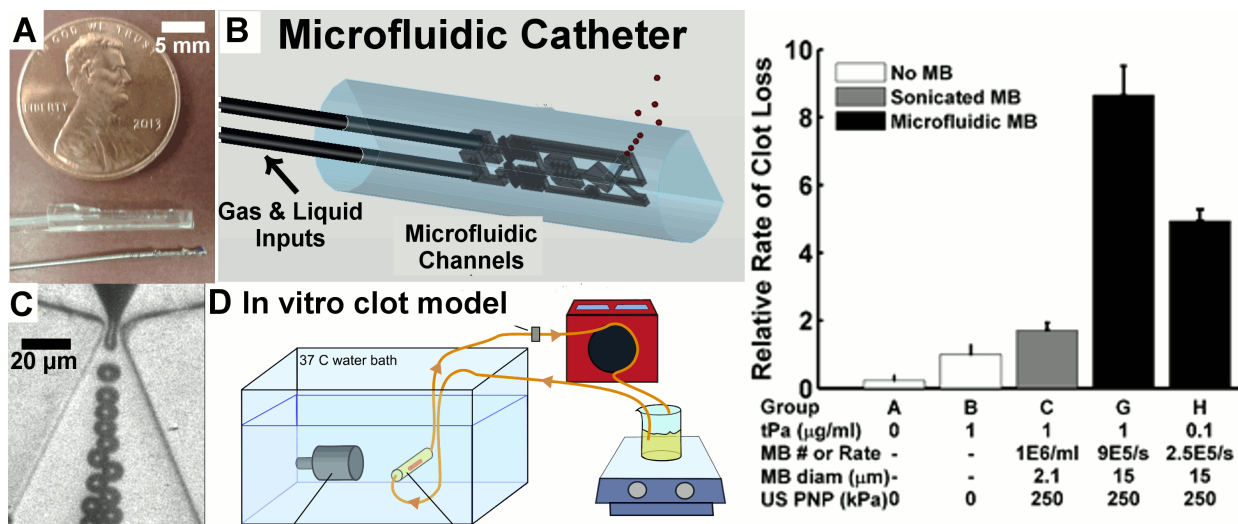
3E-2

10:45 am　**High Pulse Reputation Frequency Crushing Model Renal Calculi Using Cavitation Bubbles Induced by Dual-Frequency Ultrasound Pulses**

Masamizu Osuga[1], Jun Yasuda[1], Hayato Jinbo[1], Shin Yoshizawa[1], Shin-ichiro Umemura[1]; [1]*Tohoku University, Japan*

Background, Motivation and Objective

When cavitation bubbles collapse, strong shock waves and jets cause cavitation erosion. Ikeda, et al. found that renal calculi can be crushed into small fragments using high-intensity focused ultrasound (HIFU) via cavitation erosion. [1] However, the crushing rate of this method is much slower than conventional methods such as shock wave lithotripsy (SWL). The control of cavitation bubble behavior is an important factor to improve erosion rate because excessive generation of cavitation bubbles blocks ultrasound propagation to the stone and reduces the erosion rate. In this study, the peak-positive enhanced (PPE) and peak-negative enhanced (PNE) waves are generated by superimposing the second harmonic to fundamental to control cavitation bubbles.

[1] T. Ikeda, et al., Ultrasound Med. Biol., vol. 32, pp. 1383–1397, Sep. 2006.

Statement of Contribution/Methods

A model stone made from cement and tap water was set in a tank containing degassed water. HIFU was generated from a 256-channel array transducer (Imasonic) with both outer diameter and geometrical focal length of 120 mm. The focused dual-frequency ultrasound pulses at a maximum intensity of 24 kW/cm^2 were sequentially scanned at each apex of a 6 mm wide regular hexagon in the geometrical focal plane. The irradiation time at one apex was 20 μs. The sequence was repeated for 2 minutes at a pulse reputation frequency (PRF) of 0.2, 0.5, 1, 2 and 3 kHz.

Results/Discussion

Fig.1 shows high speed images of the PNE and PPE waves near the model stone. With the PPE waves a cloud of cavitation bubbles was expanded toward the transducer. With the PNE waves, cavitation bubbles were generated only on the stone surface. Fig.2 shows the stone erosion rate plotted as a function of PRF. From 2 to 3 kHz, the erosion rate decreased in the case of PPE waves but increased in the case of PNE waves. This was because ultrasound propagation in the case of PNE waves was not blocked by generated cavitation bubbles unlike the case of PPE waves.

(a) PNE-waves   (a) PPE-waves
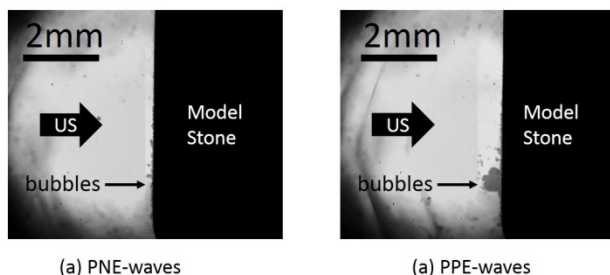
Fig. 1 High speed images of the PNE and PPE-waves near the model stone
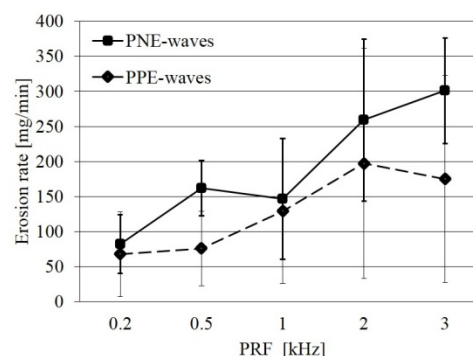
Fig. 2 Stone erosion rate plotted as a function of PRF

3E-3

11:00 am The accumulation and behaviour of ultrasound stimulated bubbles on a compliant surface: implications for sonothrombolysis

Ben Leung[1], Christopher Acconcia[1,2], Kullervo Hynynen[1,2], David Goertz[1,2]; [1]*Physical Sciences Platform, Sunnybrook Research Institute, Toronto, Ontario, Canada,* [2]*Medical Biophysics, University of Toronto, Canada*

Background, Motivation and Objective

We previously examined micro-scale interactions of ultrasound stimulated microbubbles (USMBs) with fibrin clots, gaining direct evidence of the ability of MBs to enter clots and, depending on MB size and exposure condition, damage the fibrin network and promote fluid uptake [Acconcia *et al* APL 2013; UMB 2014]. This work also illustrated the role of radiation forces, namely translation of MBs toward the clot, their possible coalescence, and interactions at the surface of and within clots. While current mechanistic theories focus on the effect of exposure schemes on MB-clot interactions, here we hypothesize that a key aspect of an exposure scheme is its impact on how MBs are brought to the clot boundary and their subsequent interactions.

Statement of Contribution/Methods

A novel experimental approach was developed in this study using a ring transducer (1.1 MHz) mounted to a microscope lens such that US propagated coaxial to the optical axis (Fig 1a). Pressures of 0.1, 0.4, and 1 MPa were applied in pulses (10^3 cycles, 15% duty cycle). A phantom with a flow channel was made of Mylar® on top and either agarose gel or fibrin clot on the bottom. The phantom was positioned so that US passed through the channel (orthogonal to flow of Definity® MBs) and the lower channel surface was in optical and acoustic focus. High speed video (up to 10^4 fps) observed the arrival of MBs at the boundary and their subsequent interactions. This approach is distinct from other studies that have floated MBs to a surface.

Results/Discussion

After exposure began, MBs accumulated on the lower surface. At 0.1 MPa (Fig 1b), more US pulses were needed to push MBs to the surface compared to 0.4 MPa. At both pressures, some MBs remained at the boundary and stably oscillated (expansions > 2x resting size at 0.4 MPa). Then, smaller MBs were observed to coalesce with the larger stable MBs via secondary radiation force (Fig 1c). The spatial distribution of MBs at the boundary exhibited a degree of uniformity, which is likely linked to a balance of secondary forces (Fig 1d). Notably, MBs that stayed at the boundary were typically in the range of 3-6 μm, which differs from the size distribution of native Definity® within the channel. These results therefore reveal complex MB behaviors indicating the pulsing scheme must be considered not only from a MB-clot interaction perspective but also in its impact on MB accrual and distribution at the boundary.
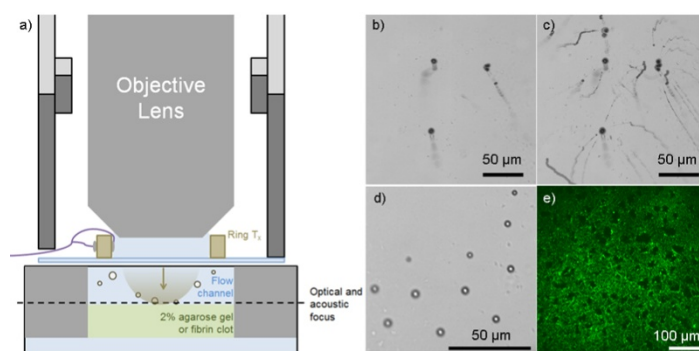
Fig. 1: a) Schematic diagram of ring transducer coaxial with microscope objective. Ultrasound propagation downward as indicated by arrow. Flow of microbubble suspension is into the page. b) Minimum Intensity Projection (MIP) of high speed video (5000 fps) of the first 40 pulses of ultrasound (0.1 MPa, 1000 cycles/pulse, 15% duty cycle) showing three microbubbles pushed and coming into focus at the channel-agarose boundary. c) After 200 pulses, the MIP shows many smaller bubbles converging onto and coalescing with the three original and larger bubbles, in addition to translation of bubbles along the boundary. d) A single frame captured between a sequence of 0.4 MPa pulses (1000 cycles/pulse, 15% duty cycle) showing bubbles at rest and in focus (mostly 4-5 μm in diameter) on the agarose boundary with a roughly uniform spatial distribution. e) Two-photon microscope image of fluorescently tagged fibrin in a whole blood clot after microbubble mediated sonothrombolysis treatment in the same orientation as b) - d). Note the regular presence of circular voids indicative of patent tunnels, which may have correlation to the way microbubbles arrive at the boundary before being pushed into the clot.

3E-4

11:15 am　A Theoretical Model for Acoustic Microstreaming Generated by Two Interacting Contrast Microbubbles

Alexander Doinikov[1], **Ayache Bouakaz**[1]; *[1]Inserm U930, Université François-Rabelais, Tours, France*

Background, Motivation and Objective

Stationary vortical flows generated by acoustically induced bubbles, which are known as acoustic microstreaming, are used in many technical applications such as ultrasonic cleaning and intensification of heat and mass exchange. This effect is thought to play an important role in medical ultrasound techniques such as sonoporation. Available theoretical studies of acoustic microstreaming are restricted to the case of a single bubble, whereas in practice one has to deal with a cloud of bubbles. The aim of our work is to develop a theoretical model for the calculation of acoustic microstreaming generated by two interacting bubbles and to study the effect of bubble interactions on the characteristics of acoustic microstreaming.

Statement of Contribution/Methods

The derivation of the model is based on the mathematical methods of fluid dynamics which are applied to two interacting bubbles undergoing small radial and translational oscillations in a viscous liquid. Linear solutions to the equations of bubble motion are first found and then used to calculate time-averaged second-order solutions, which describe acoustic microstreaming around the bubbles. To compare the microstreaming characteristics at different parameters, numerical simulations are performed for bubble pairs with diameters $1 - 5$ µm, driven at frequencies $1 - 10$ MHz and separation distances between the bubbles $10 - 1000$ µm.

Results/Discussion

It is shown that the interaction of the bubbles leads to a considerable increase in the intensity of the velocity and stress fields of acoustic microstreaming when the bubbles are driven near resonance frequencies that they have in the presence of each other. Patterns of streamlines for different situations are provided. As an example, the left part of the presented figure shows the streamlines of acoustic microstreaming for two equal bubbles with the equilibrium diameter $D_0 = 3$ µm at separation distance $5D_0 = 15$ µm and the driving frequency 2.74 MHz, which is the resonance frequency at this distance. For comparison, the right part of the figure shows streamlines for a single bubble under the same conditions. It is also demonstrated that the developed theory can be applied to the case of a bubble near a rigid wall.
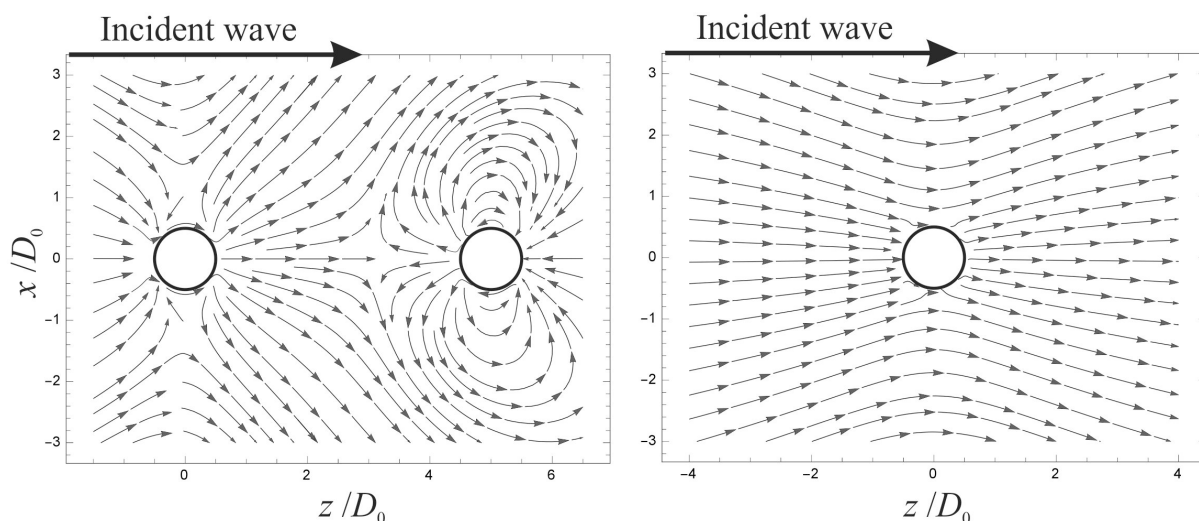
3E-5

11:30 am　High IntensityFocused Ultrasound applied to the placental unit: First results of an in vivo study in monkeys

David Melodelima[1], Jonathan Caloone[1,2], Anthony Kocot[1], Jeremy Vincenot[1], Cyril Huissoud[2]; *[1]LabTAU - U1032, INSERM, France, [2]Hopital de la Croix Rousse, France*

Background, Motivation and Objective

This work was conducted in order to demonstrate the feasibility of high intensity focused ultrasound (HIFU) to treat extracorporally the placental unit using a toroidal-shaped transducer with possible application to the treatment of the twin-to-twin transfusion syndrome using a monkey pregnant model.

Statement of Contribution/Methods

A toroidal HIFU transducer working at 2.5 MHz and composed of 32 ring-shaped emitters was used. An ultrasound imaging probe working at 7.5 MHz was placed in the center of the HIFU transducer. The acoustic parameters used during HIFU exposures were selected according to preliminary simulations taking into account the attenuation coefficient of placentas that were measured previously. Ex vivo experiments were performed using an animal abdominal wall simulating the maternal wall and placed at the top of placentas. Single and juxtaposed HIFU lesions were created. A pregnant monkey (gestational age: 63 days) was included and HIFU treatment was performed using acoustic parameters determine from ex vivo trials. A single HIFU lesion was performed after maternal anesthesia, and monitoring of maternal and fetal parameters (subcutaneous and amniotic fluid temperature, maternal and fetal heart rate). The resulting HIFU lesion was studied on sonogram, macroscopically and microscopically.

Results/Discussion

Attenuation coefficients of 12 human placentas were measured in vitro and ranged from 0.07 to 0.10 $Np.cm^{-1}.MHz^{-1}$ according to the gestational age (17 to 40 weeks). Thirty-three human placentas (from 17 to 40 weeks) were included and exposed to HIFU. 25 single HIFU lesions were obtained, with an average diameter and depth of 7.1 ± 3.2 mm, and 8.2 ± 3.1mm respectively. Eight placentas were used for juxtaposing 6 HIFU lesions. The average diameter of these HIFU lesions was 23 ± 5 mm and the average depth was 11 ± 5 mm. The average thickness of the abdominal wall was 10.5 ± 1.8 mm. No lesions or damage were observed in intervening tissues. In-vivo, a single HIFU lesion has been created in the placenta with a diameter of 10 mm and a depth of 5 mm. No lesions or damage were observed in intervening tissues nor in the fetus. These findings were confirmed by histological analyses. Ultrasound examination revealed a hyperechoïc HIFU lesion in the placenta. The diameter and the depth of the HIFU lesion measured in ultrasound images were 10.0 and 4.4 mm respectively. During the HIFU exposure, no significant variation of maternal and fetal parameters was observed. The subcutaneous and intra-amniotic fluid temperature were 25°C (24.9-26) and 34°C(33.4-34.5) respectively. The fetal heart rate was 124 (122-125). This study demonstrates the feasibility, the reproducibility, the harmlessness and the effectiveness of HIFU applied to the placental unit within an in vivo model using a toroidal transducer. These results remain to be confirmed using a significant population of pregnant monkeys.

3E-6

11:45 am   3D focusing of high intensity ultrasound pulses using a time reversal cavity

Justine Robin[1], Bastien Arnal[1], Mathias Fink[1], Mickael Tanter[1], Mathieu Pernot[1]; *[1]Institut Langevin, France*

Background, Motivation and Objective

Ultrasound pulse therapy such as histotripsy or lithotripsy requires focusing very high pressures to mechanically fragment and liquefy tissues. Large spherical transducers are commonly used to achieve these pressures at the focal spot. Mechanical steering is required to treat large regions. Electronic steering is highly limited by the number of elements that cannot exceed several hundreds for reasons of cost and complexity. In this study, we have developed a 3-dimentional time reversal cavity (3D-TRC) to focus high intensity pulses over a large volume only using electronic steering, and keeping the number of elements to a minimum.

Statement of Contribution/Methods

We built a 3D-TRC by enclosing a 3D-multiple scattering medium (MSM) in a reverberating cavity. The MSM was made of 3 successive metal grids (wire diameter 0.8mm, size of cell 5 mm), and the cavity was 15x13x20 cm. We used 2 linear transducers (128-elements, 1 MHz, Imasonics, Besançon, France), placed orthogonally at the back of the cavity, sonicating the MSM with an angle of 60 degrees. The probes were driven by custom multi-channel electronics (Correlec, France). 40 µs US pulses emitted through the cavity were temporally spread to up to 1 ms, picked up by a HGL 200 hydrophone (Onda, Sunnyvale, CA) and stored. Time reversal focusing (TRF) by compressing these signals in space and time then allowed us to reach the needed high negative pressures. Steering the focal spot over a large volume was achieved by moving the hydrophone. We reemitted the reversed signal at a pulse repetition frequency (PRF) of 260 Hz to form a bubble cloud, which was observed using an ultrasound scanner (Supersonic Imagine, Aix-en-Provence, France).

Results/Discussion

Hydrophone measurements confirmed the spatio-temporal focalisation of the signal. Observations in a plane 10 cm away from the cavity showed a 1.2 x 1.2 mm focal spot, with a temporal peak less than 2 cycles long. The peak pressure obtained at the focus was about 40 MPa (linearly extrapolated value). These observations were consistent over a large area (- 3 dB area 10x6 cm). The negative pressure obtained was sufficient to achieve cavitation. It was even possible to generate bubble clouds in various spots at the same time by emitting the stored signals corresponding to several locations successively at a PRF of 313 Hz between the different signals and between 16 and 260 Hz overall. We also succeeded in creating lesions in a slice of ham using this cavity for histotripsy.

4E - MBB: Beamforming III

201DE

Friday, October 23, 2015, 10:30 am - 12:00 pm

Chair: **Jørgen Jensen**
                Technical University of Denmark

4E-1

10:30 am   An automatic method for determining the anatomical relevant space for fast volumetric cardiac imaging

Alejandra Ortega[1], Brecht Heyde[1], João Pedrosa[1], Ling Tong[2], Jan D'hooge[1]; *[1]Department of Cardiovascular Sciences, KU Leuven, Leuven, Belgium, [2]Department of Biomedical Engineering, Tsinghua University, Beijing, China, People's Republic of*

Background, Motivation and Objective

Fast volumetric cardiac imaging requires to reduce the number of transmit events within a single volume. One way of achieving this is by limiting the field-of-view (FOV) of the recording to the anatomically relevant domain only (e.g. the myocardium when investigating cardiac mechanics). Although fully automatic solutions towards myocardial segmentation exist, translating that information in a fast ultrasound scan sequence is not trivial. The aim of this study was therefore to develop a methodology to automatically define the FOV from a volumetric mesh in the context of anatomical scanning.

Statement of Contribution/Methods

In order to define the anatomical relevant space, a fully automatic real-time segmentation of the left ventricular myocardium in a volumetric ultrasound recording was used (i.e. BEAS). The extracted meshes were employed to define a binary mask identifying myocardial voxels only. Using these binary images, a 'coverage function' was defined which expresses the percentage of pixels along a given image line that belong to the myocardium. In order to find a spatially continuous FOV that covers 'T' percentage of the myocardium, a ring-shaped template matching was used, whereby the amount of myocardial coverage could be expressed as a function of the inner radius of the ring template (Ri) and its thickness (dR). From all combinations of the Ri and dR that provided the T% myocardial coverage, the one with minimal dR was chosen.

To test this approach, 10 volumetric ultrasound datasets were acquired in patients with suspicion of chronic ischemia that were enrolled in a multi-center FP7-funded study (DOPPLER-CIP). A T = 85‰ was chosen.

Results/Discussion

The figure shows an example of the coverage function and the template matching for one of the patients. The mean of the initial opening angle for a conical scan was 18.7±10.7° while the mean 'thickness' of the cone was 33.93±3.7°.

Anatomical scanning in combination with new beam forming techniques can increase frame rate significantly while keeping information of the relevant structures for functional imaging. In this study, a reduction of 57.7‰ in the number of transmit events was achieved, for a frame rate gain factor of 2.36. Future work will include other templates matching shapes to allow for better myocardial coverage using a smaller FOV and combining this reduced FOV with fast imaging strategies.
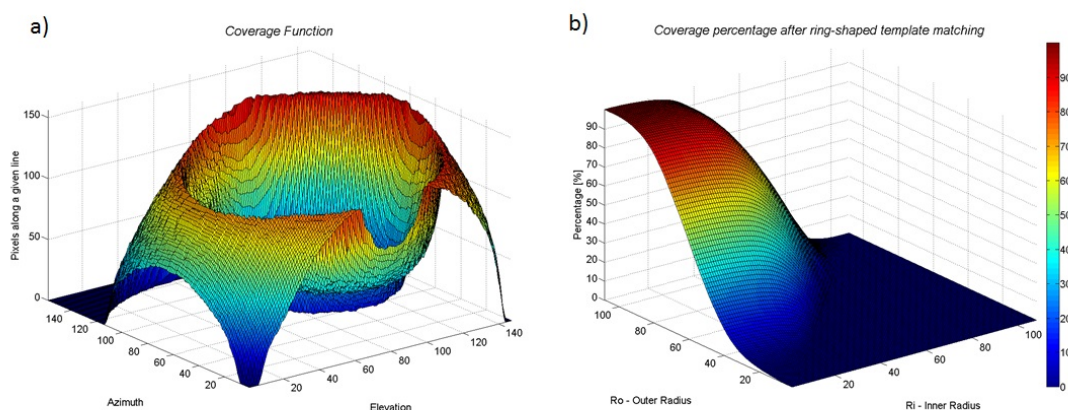
Figure. a) Coverage function expressing the percentage of pixels along a given image line that belong to the myocardium, b) Amount of myocardial coverage as a function of the inner radius (R_i) and the outer radius (R_o) of the ring-shaped template matching.

4E-2

10:45 am   Coded Excitation Reconstruction by Impulse Response Estimation and Retrospective Acquisition: Application to B-mode Imaging

John Flynn[1], Lauren Pflugrath[1], Peter Kaczkowski[1], Ron Daigle[1]; *[1]Verasonics, Inc, Kirkland, WA, USA*

Background, Motivation and Objective

Coded excitation (CE) imaging enables transmission of large time-bandwidth waveforms [1]. Since such waveforms are typically pulse-compressed by matched filtering, much research investigates schemes for reducing auto- and cross-correlation sidelobes to decrease clutter with distributed targets. The goal of this presentation is to harmonize CE transmission with the image quality of Synthetic Transmit Aperture (STA) imaging at high frame rates. We propose a two-step process that estimates medium impulse responses (IR), then retrospectively images using the IR set. In this way, the probing code sequence is used optimally yet is decoupled from the imaging step, circumventing the sidelobe problem.

Statement of Contribution/Methods

The method first estimates transmit-receive (TR) pair impulse responses (IR) of the acoustic medium, using space-time-IID random codes transmitted simultaneously across channels and acquisition intervals. This gives a joint convolution model for TR channel pairs. Linear model theory solves for unbiased estimates of the IR set. In the second step, retrospective STA imaging excites the estimated IR set, using it as a simulation of the medium. Retrospective transmit signals and apodizing can differ at each pixel. Using Gauss-Markov theory we show the resulting beamformed pixels are unbiased estimates of STA pixels, and that time diversity in codes greatly improves precision over

static codes. To address tissue motion, the model is extended to polynomial and Fourier basis. We also demonstrate retrospective transmission of a transducer-compensated Gaussian pulse in the retrospective imaging step, eliminating the encoding required in limited precision transmitter HW.

Results/Discussion

Transmitting code lengths up to 48 cycles, we evaluate resolution and contrast using a commercial research ultrasound system and phantoms with linear and phased-array probes at 5 and 15 MHz. The figure below shows a carotid artery imaged by the method using a linear 5MHz probe. Significant improvement in frame-rate and image quality is typically achieved over dynamic receive-focus at equivalent frame energy.

[1] Misaridis, Thanassis, and Jørgen Arendt Jensen. "Use of modulated excitation signals in medical ultrasound. Part III: high frame rate imaging." Ultrasonics, Ferroelectrics, and Frequency Control, IEEE Transactions on 52.2 (2005): 208-219.

Coded Excitation Imaging (Philips L7-4)
24 cycles on 26 elements with 48 transmissions at 15.4 Volts
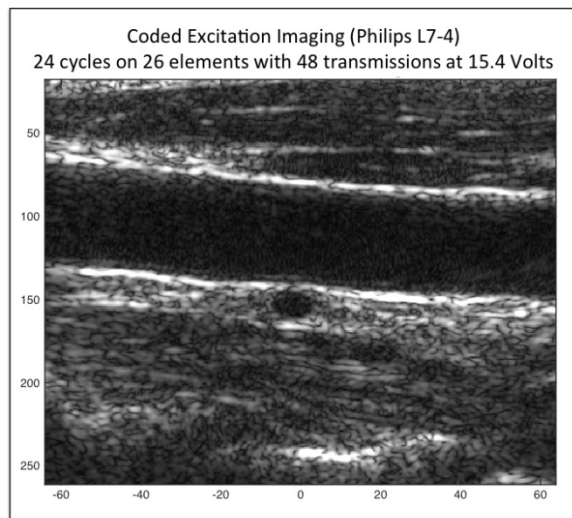
4E-3

11:00 am   Image quality degradation from transmit delay profile quantization

Matthias Bo Stuart[1], Jørgen Arendt Jensen[1]; [1]CFU - Technical University of Denmark, Kgs. Lyngby, Denmark

Background, Motivation and Objective

The receive beamforming in digital ultrasound scanners employs interpolation to avoid quantization effects in the receive field. This is however not generally possible in the transmit field. In this work, the effects of transmit delay profile quantization on image quality is shown. It is also shown that exciting each transducer element with an individually phase-shifted excitation restores the image quality.

Statement of Contribution/Methods

A 7 MHz, linear, $\lambda/2$ pitch transducer array is simulated in Field II. Steered, unfocused beams (plane waves) are emitted, and the resulting images are summed in the RF domain. Steering angles from -9 to +9 degrees in steps of 2 degrees are used. By default, Field II interpolates in transmit, which is used to make a reference (unquantized) simulation. The simulation is also done for quantized (fs=70 MHz) transmit delay profiles, as well as for quantized profiles with per-element phase-shifted excitation waveforms. The phase-shift is set to cancel the phase errors introduced by the delay quantization. Spline interpolation is used in receive such that the observed effects stem from the transmit setup only. The resulting point-spread functions are compared.

Results/Discussion

The figure shows the PSFs at 10 mm depth. On the left, the reference (no delay quantization) PSF is shown. In the middle, the transmit delay profiles have been quantized, while on the right, quantized delay profiles are used together with individually phase-shifted excitations per element. The full-width at half-maximum is unaffected by both the quantization and the phase-shifted excitations. However, a large degree of clutter (up to 30 dB below the peak value) is produced behind the point target when the delay profiles are quantized. This clutter lowers the contrast in B-mode images and can negatively impact blood velocity estimators. It is seen that using phase-shifted excitations restores the reference PSF and thereby the image quality.
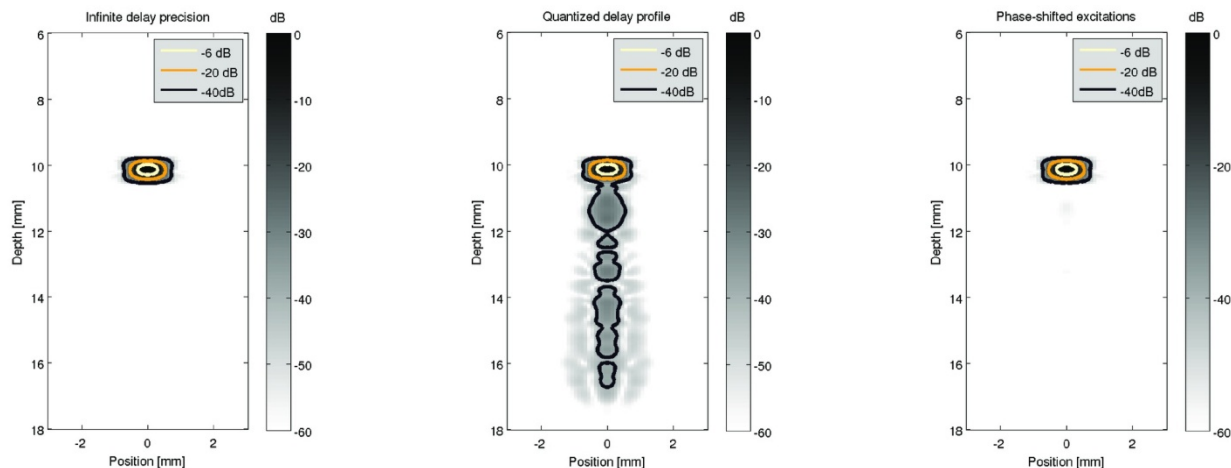
4E-4

11:15 am   Enhancement of specular reflection using Directional Spatial Coherence with 2D Phased Array

Raja Sekhar Bandaru[1,2], Anders Sornes[1], Margot Pasternak[1,2], Eigil Samset[1,3], Jan D'hooge[2]; [1]*GE Vingmed Ultrasound, Oslo, Norway*, [2]*Cardiovascular Imaging and Dynamics, KU Leuven, Leuven, Belgium*, [3]*Department of Informatics, University of Oslo, Oslo, Norway*

Background, Motivation and Objective

Ultrasound based image guidance during catheter based interventions could be highly desired due to its advantages over X-ray fluoroscopy. Methods like Spatial coherence has been used extensively in many researches to improve the Contrast to Noise Ratio (CNR) of tissue. Also it was recently used in detection of fiber orientation. Here we propose a new beamforming method based on Directional Spatial Coherence (DSC) to improve the CNR of specular reflecting objects like needles, catheters or guide wires, by detecting their orientation from the channel data. We observed a CNR improvement of 4 times compared to traditional beamforming.

Statement of Contribution/Methods

The beam pattern of the wire produced on the aperture has a line like signature (top row of Fig 1) which represents the cylindrical cross section of the wire surface. Hence we introduced a modified spatial coherence method which also considers direction of the spatial coherence. This was calculated by multiplying the axial samples at a given time in the direction orthogonal to the wire. But in order to get the direction of the wire we first calculate the DSC from 0° to 180°. Finally Specular B-mode image was reconstructed by using delay and DSC (at θ with maximum DSC value) . The method was evaluated using the channel data from the real data acquired with a Vivid E9 and a 4V sector probe, 3MHz (GE, Horten, Norway) on a Gammex 403GS as shown in the figure. CNR was calculated as the ratio of the intensity of wire to the intensity of tissue.

Results/Discussion

DSC was calculated for angles from 0° to 180°; and it was found to be high at an angle orthogonal to the wire orientation (2nd row of Fig 2). Subsequently beamformed images shows improved gray scale contrast of the wire by reducing all non-specular intensities in the image (last row of Fig 1). CNR of traditional delay and sum was observed to be -23dB, -31dB and -26dB respectively for a), b) and c) in the figure. Whereas for the B-mode images with delay and DSC was found to be -96dB, -127dB and -101dB. Our method was primarily based on the coherent specular echo from the cylindrical surface of a wire with diameter greater than the wavelength. It was demonstrated in the results that our methods works well on SAP data. The specular beamformed image we obtained can also be fused with the traditional delay and sum image to see the anatomic information.
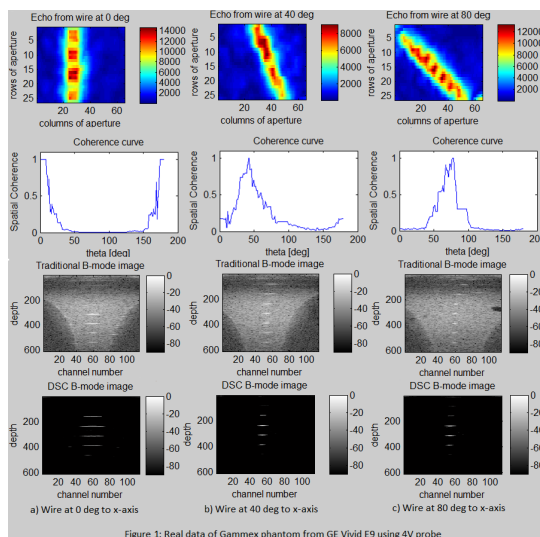
Figure 1: Real data of Gammex phantom from GE Vivid E9 using 4V probe

4E-5

11:30 am   2D Wire Orientation using Directional Spatial Coherence with 2D Phased Array

Raja Sekhar Bandaru[1,2], Anders Sornes[1], Eigil Samset[1,3], Jan D'hooge[2]; [1]*GE Vingmed Ultrasound, Oslo, Norway*, [2]*Cardiovascular Imaging and Dynamics, KU Leuven, Leuven, Belgium*, [3]*Department of Informatics, University of Oslo, Oslo, Norway*

Background, Motivation and Objective

Fiber imaging based on the spatial coherence across a 2D matrix array was recently demonstrated using plane-wave transmits. Hereto, an ellipse was fit to the instantaneous signal amplitudes across the array where the long axis of the ellipse identifies the orientation of the respective fiber. The aim of this study was bi-fold: i) to verify whether regular focused transmits could equally define fiber angles, and ii) to propose an alternative approach towards automatically defining the directivity of the spatial coherence across the aperture.

Statement of Contribution/Methods

A synthetic fiber model was created by filling a 6mm diameter cylinder with a combination of regular and random scatterers at high density (7500 scatterers/mm3). This fiber was positioned within a diffuse scattering environment (1 scatterer/mm3) (Fig 1a). The phantom was scanned using Field II simulation tool assuming a 2D phased array (11x21 elements with 10x10 sub elements, 9MHz) transmitting conventional beams focused on the fiber located at a distance of 2 cm. Channel data was acquired for different orientations of the fiber. In order to extract the orientation of the spatial coherence, a Directional Spatial Coherence (DSC) function was defined expressing the total instantaneous spatial coherence across the aperture as a function of the direction θ (after applying delays for receive focusing). Hereto, the instantaneous (delayed) amplitudes in direction θ were multiplied and summed (Fig 1b). The direction in which the maximal total coherence was found (θ₀) represents the direction orthogonal to the coherent scattering object for focused transmits beams.

Results/Discussion

The synthetic channel data clearly showed a directive spatial coherence orthogonal to the direction of the fiber being imaged (Fig 1c-d). Detecting the direction for which the DCS function reached its maximum could clearly identify the fiber orientation (Fig 1e-f). For all fiber angles tested, the DCS function automatically detected the correct fiber angle (Fig 1g). Elaborate experimental validation of the proposed method is ongoing.

a) Specular reflection of wire cross section

b) Directional Spatial Coherence

c) Transmit Field, Field II simulation of 2D array

d) Simulated wire phantom

e) Detected angles of wire simulated phantom, by rotating the wire

f) Directional Coherence functions of wire at 0 and 50 degrees inside simulated phantom.
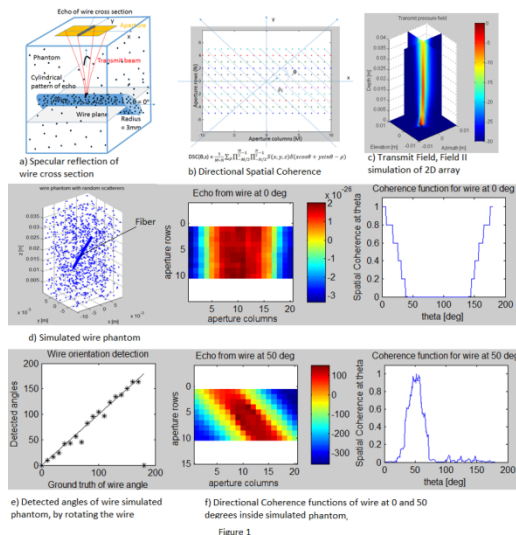
Figure 1

4E-6

11:45 am   Frequency Domain Beamforming for Coherent Plane-Wave Compounding

Tanya Chernyakova[1], Regev Cohen[1], Yael Sde-Chen[1], Christophe Fraschini[2], Jeremy Bercoff[2], Yonina Eldar[1]; *[1]EE, The Technion, IIT, Haifa, Israel, [2]SuperSonic Imagine, France*

Background, Motivation and Objective

Ultrafast imaging based on coherent plane-wave compounding is one of the most important recent developments in medical ultrasound. It significantly improves image quality and allows for much faster image acquisition. This method, however, is limited by severe computational loads that create a bottleneck for its implementation in commercial systems. To overcome this limitation we translate the beamforming, the basic processing step, to the frequency domain. Here the computations can be carried out much more efficiently and from less data samples.

Statement of Contribution/Methods

In this work we extend the frequency domain beamforming (FDBF) framework developed recently for the focused imaging mode to plane-wave modality. We show that the core of FDBF, the relationship between the beam and the detected signals in the frequency domain, holds and can be implemented efficiently by introducing an appropriate approximation. We also show that dynamic aperture and apodization, crucial for image quality improvement, can be applied directly in frequency as a part of FDBF. Translation of beamforming into the frequency domain allows for data rate reduction by eliminating oversampling, required by digital implementation of beamforming in time. As a result the signals are sampled and processed at their effective Nyquist rate, leading to 4-fold reduction in the number of samples.

Results/Discussion

The proposed method is applied on data obtained by an Aixplorer scanner. The equivalence of time domain is shown both for a single beam corresponding to an image line and for the entire image after compounding. To compare the 1D signal the normalized root-mean-square error (NRMSE) is calculated. The similarity of the resulting images is measured by the structural similarity (SSIM) index. Figure 1 (a) shows an image obtained by standard focused mode. Figures 1 (b) and (c) show the plane-wave images obtained by time-domain and low-rate frequency domain processing together with corresponding values of NRMSE and SSIM. These values verify the extreme similarity of both 1D signals and the resulting image.

FDBF applied to coherent plane-wave compounding imaging mode allows sampling and processing the signals at their effective Nyquist rate, leading to reduction in computational burden while retaining optimal image quality, solving the major bottleneck of plane wave coherent compound.

(a)   (b)   (c)
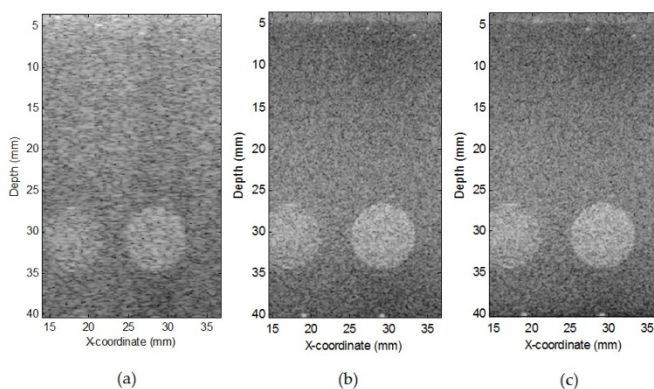
Fig.1 Image (a) is obtained by standard focused mode. Images (b) and (c) are obtained by coherent plane-wave compounding, (b) by time-domain beamforming and (c) by frequency domain beamforming with 4-fold reduction in data rate. The values of NRMSE and SSIM between (b) and (c) are 0.07 and 0.95 respectively.

5E - Signal Processing

103

Friday, October 23, 2015, 10:30 am - 12:00 pm

Chair: **Jafar Saniie**
              Illinois Institute of Technology

5E-1

10:30 am   Sparse Inversion SVD for Multichannel Ultrasonic Guided Waves Analysis in Cortical Bone

Kailiang Xu[1,2], Jean-Gabriel Minonzio[2], Dean Ta[1], Bo Hu[1], Weiqi Wang[1], Pascal Laugier[2]; [1]*Department of Electronic Engineering, Fudan University, Shanghai, China, People's Republic of,* [2]*Laboratoire d'Imagerie Biomedicine, UMR CNRS 7371 - INSERM U1146 - UPMC, Paris, France*

Background, Motivation and Objective

The singular value decomposition (SVD) has been applied to analyze the dispersion of propagating multimode signals in cortical bone (Minonzio et al., JASA, 127(5), 2913-19, 2010). The method involves a spatio-temporal Fourier transform, in which a SVD denoising step is added, of the temporal waveforms recorded by an array transducer with 5 emitters and 24 receivers (the response matrix). The strategy of the SVD-based noise reduction technique is to apply a SVD to the frequency response matrix and to discard small singular values and the corresponding singular vectors which mainly represent noise. The limited spatial sampling with a few tens of receiving points at the best, results in a poor resolution on the wavenumber k-axis, which prevents a clear identification of dispersion curves.

Statement of Contribution/Methods

In this study, a sparse inverse SVD (SI-SVD) technique, which combines SVD and a least-squares sparse inverse method, is presented to overcome the above mentioned limits. The assumption is that the classical SVD method enables obtaining stable singular values which are not highly correlated to the noise, so that the SVD procedure can be iteratively optimized using the sparse penalty of the (f, k) spectrum.

Results/Discussion

Two sparse penalty terms, the L2-norm and the revised Cauchy-norm, were compared, the results being presented using a 2-D projection (f, k) of the mode maxima associated to the wavenumber dispersion curves (Fig.1). The technique was first tested by processing synthetic signals corrupted by additive Gaussian noise (signal-to-noise ratio of 20dB) simulating the propagation of wideband dispersive guided waves (Fig.1(a-c)). Then, the technique was used to measure the dispersion curves of Lamb waves on a 1.8-mm-thick bone-mimicking plate (Fig.1(d-f)) and on a 1.6-mm-thick ex-vivo human radius specimen (Fig.1(g-i)). The analysis of the results suggests that the SI-SVD method using the revised Cauchy-norm has potential to significantly enhance the k-axis resolution for improving the extraction of the dispersion curves.
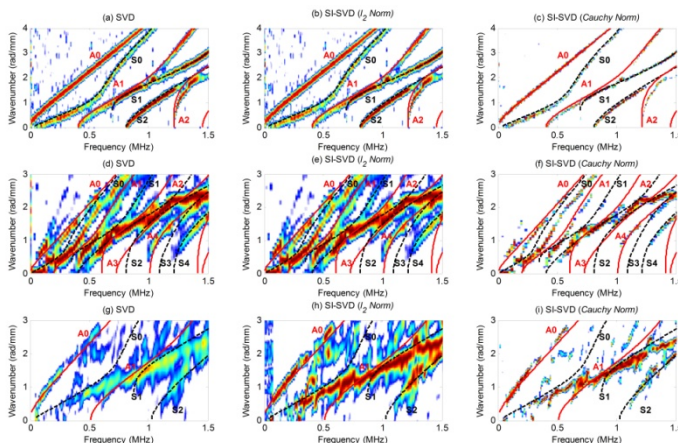
Fig. 1 The SVD, SI-SVD (l2 Norm) and SI-SVD (Cauchy Norm) results of the synthetic signals of wideband dispersive guided waves (a-c), the experimental signals of the 1.8-mm-thick bone-mimicking plate (d-f) and the 1.6-mm-thick *ex-vivo* human radius specimen (g-i).

5E-2

10:45 am   Ultrasonic Flaw Detection using Support Vector Machine Classification

Kushal Virupakshappa[1], Erdal Oruklu[1]; [1]*ECE Department, Illinois Institute of Technology, Chicago, Illinois, USA*

Background, Motivation and Objective

Ultrasonic flaw detection in NDE applications is a challenging problem due to suppression of flaw echoes within the high scattering noise (clutter) echoes. Advanced signal processing techniques are necessary in order to enhance the visibility of the flaws and increase the flaw-to-clutter echo ratio. In this work, a Support Vector Machine (SVM) classifier is introduced for flaw detection based on features extracted from the output of the subband decomposition filters, (i.e. split-spectrum processing). SVM is a machine learning method used for classification and regression analysis of complex real-world problems that may be difficult to analyze theoretically. Typically, SVM has been used for pattern recognition but recently it has been applied to financial market analysis, electric utility forecasting and also ultrasonic NDE. Previous ultrasound SVM applications used A-scan data itself or ultrasonic signal parameters such as time-of-arrival, center frequency and bandwidth as feature vectors. In contrast, we use subband filter outputs as feature vectors for the SVM in order to exploit the frequency diversity among the flaw and clutter echoes.

Statement of Contribution/Methods

In SVM, using training data, a maximum margin decision boundary is constructed which divides the data into two classes (i.e., flaw or no flaw). In complex problems, the boundary separating the two classes can be nonlinear. In order to perform classification, input space is transformed (using a kernel function) into a new higher-dimensional space where a linear classification can be now carried out. In the proposed work, A-scan data (1024 sample points) are decomposed with 8 subband filters and resulting subband channels are concatenated to form the feature vector of size 8192 to be used in SVM. A data set constituting feature vectors of signals containing flaw and no flaw, is created in order to train and test the SVM. A k-fold cross validation technique is then performed to choose the best parameters. For transformation, Radial Basis Function

---

(RBF) kernel is chosen since the dimensionality is very high. LIBSVM-3.20 tool library has been used to train and obtain the final SVM model for performance evaluation and real-time implementation.

Results/Discussion

A-scan data measurements from a steel block (type 1018, with defect) are acquired using an ultrasonic pulse-echo system with a 5 MHz broadband transducer. 140 A-scan data are used for training and another set of 140 A-scan measurements are used for testing the SVM classifier. 10-fold cross validation was implemented and the best parameters were found to be C=32 (penalty parameter of the error term) and γ =0.005, (γ is the RBF parameter), with accuracy of 92% for the cross validation. Preliminary results show that classification accuracy of 94% sensitivity and 96% specificity is achieved with the proposed SVM classifier. Robust performance of the classifier is due to proper selection of feature vectors and successful training.

5E-3

11:00 am   Simultaneous Multi-Mode Analysis of Surface Acoustic Wave Device Temperature Stability using Time-Frequency Methods

Christopher J. Harrison[1], Samuel J. Ippolito[1,2], K. M. Mohibul Kabir[2], Glenn I. Matthews[1]; [1]*School of Electrical and Computer Engineering (SECE), RMIT University, Melbourne, Victoria, Australia,* [2]*Centre for Advanced Materials and Industrial Chemistry (CAMIC), School of Applied Sciences, RMIT University, Melbourne, Victoria, Australia*

Background, Motivation and Objective

Perturbations in the boundary conditions of Surface Acoustic Wave (SAW) devices are typically quantified through the use of frequency-domain methods, where the device is incorporated as the feedback element in a closed-loop oscillator. While simple in implementation the closed-loop method is inherently limited to tracking a single acoustic mode and discards useful information from the time-domain. This work considers an alternative approach using transient analysis with time-frequency methods to track multiple acoustic modes simultaneously and provide additional metrics for analysis which may be significantly advantageous for many chemical sensing applications.

Statement of Contribution/Methods

The proposed method was applied to an XY-cut LiNbO$_3$ SAW device shown in Figure 1a, subjected to cycling operating temperatures. Exciting the input transducer with a fast rising edge transient effectively causes all acoustic modes to be stimulated simultaneously. The resultant signal at the output transducer is then captured and digitally band-pass filtered to isolate the response from the individual acoustic modes. A time-frequency transform such as Wigner-Ville is then applied to generate distributions for analysis. For comparison the device was incorporated into a conventional closed-loop topology and was also monitored with a Vector Network Analyzer (VNA).

Results/Discussion

Preliminary experimentation was performed using Wigner-Ville time-frequency transform with 512 frequency bins, the resulting distribution is shown in Figure 1b and Figure 1c. The advantages of the proposed method are demonstrated with the position in time and frequency of multiple acoustic modes monitored simultaneously. Metrics such as peak shape, area and relative locations show distinct changes as the operating temperature of the SAW device is varied, making them good candidates for analysis. Tracking the position of the main acoustic mode in the frequency domain shows excellent agreement with data from both the closed-loop and VNA methods.
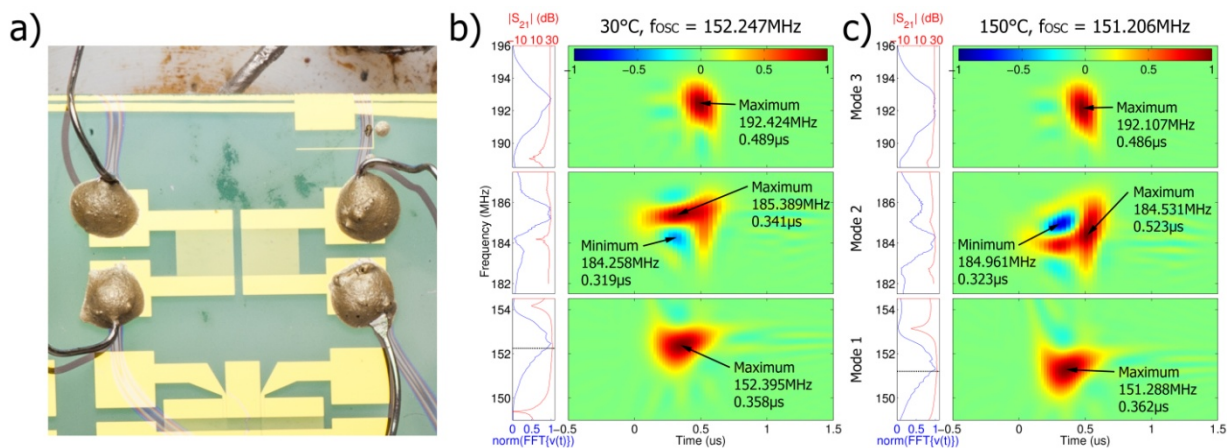
Figure 1. a) XY-cut LiNbO$_3$ SAW device, b) Normalised Wigner-Ville time-frequency distribution at 30°C with acoustic modes indicated, closed-loop frequency (f$_{osc}$, black), VNA S$_{21}$ (red) and FFT (blue), c) distribution at 150°C

5E-4

11:15 am   A clustering-based damage segmentation for ultrasonic C-Scans of CFRP plates

Antonio Rodriguez[1,2], Angel M. Gomez[2], Nicolas Bochud[3], **Juan M. Soto**[2], Antonio M. Peinado[2]; [1]*Depto. de Teoría de la Señal y Comunicaciones, Universidad Carlos III de Madrid, Leganés, Madrid, Spain,* [2]*Depto. de Teoría de la Señal, Telemática y Comunicaciones and CITIC-UGR, Universidad de Granada, Granada, Spain,* [3]*Depto. de Mecánica de Estructuras e Ingeniería Hidráulica, Universidad de Granada, Granada, Spain*

Background, Motivation and Objective

Non-destructive evaluation (NDE) combined with signal processing techniques helps to evaluate complex damage patterns in materials, especially when they remain invisible from the surface. In this work, we propose a novel procedure for the generation of clear and consistent damage maps of a carbon fiber-reinforced polymers (CFRP) plate from ultrasonic signals obtained under C-Scan mode, by applying an underlying sparse signal model and unsupervised clustering techniques.

Statement of Contribution/Methods

In this work, a CFRP plate subjected to impact damage is evaluated using C-Scan mode under a through transmission configuration. Our proposal is based on a sparse all-pole signal model, which has been shown to retain the most representative information from the ultrasonic signal, improving the discrimination process between damage levels. Then, we perform a cepstral transformation of the model parameters that allows us to compare the response signals in an Euclidean space. By applying cesptral distances as distortion criterion, five different unsupervised clustering-based approaches are tested: K-means, K-medoids, Linkage, DBSCAN and Leader-Follower algorithm.

Results/Discussion

The all-pole modeling with sparse coefficients plays an essential role within this framework. Indeed, the higher the damage energy is, the larger the amount of coefficients necessary to model the response signals is required. Over-fitting problems related with high-order models are overcome thanks to our sparse-based proposal, which retains only the most representative information.

Institute of Electrical and Electronics Engineers

Different damage maps were obtained depending on the applied clustering technique, achieving the best results with the Linkage and DBSCAN algorithms. The latter technique generates the less noisy and most mechanically consistent damage patterns, as depicted in Figure 1 where a wave velocity map and K-means results are also shown as a reference. K-means and K-medoids algorithms provided precise results, but delivered more noisy maps around the impacted area, while the leader-Follower algorithm provided inconsistent results.
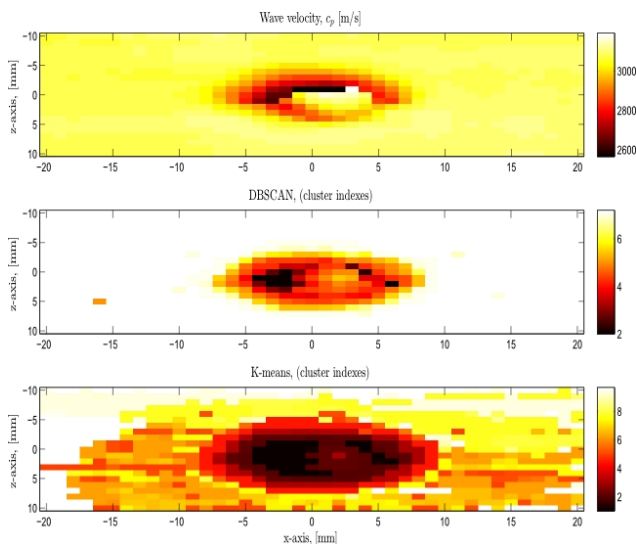
5E-5

11:30 am   A new methodology to reduce the activation sequence in SAFT techniques

Javier Villazon-Terrazas[1], David Romero-Laorden[1], Alberto Ibañez[1], Oscar Martinez-Graullera[1], Montserrat Parrilla[1]; *[1]Instituto de Tecnologías Físicas y de la Información Leonardo Torres Quevedo, Consejo Superior de Investigaciones Científicas, Madrid, Spain*

Background, Motivation and Objective

Currently, volumetric ultrasound imaging in real-time is a powerful medical diagnostic technique, as well as, in NDT applications. A volume scanning is performed by a 2-D array that greatly speeds up the data acquisition and provides uniform resolution in both azimuthal and elevation directions. However, the large number of elements required, the complexity of the involved hardware and the need to produce high frame rates for a correct inspection, are some major difficulties which have limited the feasibility to generate a non-expensive volumetric ultrasound imaging system. In this regard, Synthetic Aperture techniques "SAFT" can help to reduce hardware requirements and to accelerate information capture. In addition, general-purpose computing on graphics processing unit techniques "GPGPU" provide the necessary computing power to process the very large volume of data involved in image conformation.

This work presents a new methodology, based on genetic algorithms, which is applied to search for emission-reception activation sequences of the array elements that produce minimum-redundancy coarrays when are used in SAFT.

Statement of Contribution/Methods

Different configurations of minimum-redundancy coarrays for synthetic aperture techniques exist in the literature; most of them have been designed for standard ultrasonic matrix or linear arrays. Currently new ultrasonic arrays with complex distribution of its elements to improve its performance for imaging are being developed. In this sense, we propose to use an optimization technique based on evolutionary computing to find quasi-optimal activation sequences in arbitrary arrays that can be used to perform SAFT in a graphics processing unit. A systematic approach to formulate the problem of designing ultrasonic arrays as multiobjective evolutionary optimization problems is presented. So codification schemas, genetic operators and some guides for selecting fitness functions are presented. Finally, the proposed methodology is applied to find activation sequences for a segmented annular rings array with 64 elements distributed along 3 rings. In order to reduce the amount of data to be transmitted from the ultrasonic frontend to the GPU used for the beamforming.

Results/Discussion

Two different sequence activations are presented. The best of them reduce the number of signals more than 60%, which is acceptable to be acquired in a non-expensive electronic system. With this configuration we were able to produce a volumetric image beamformer in a graphics processing unit. That yields a frame rate of 30 volumes per second for a volume size of 64*64*64 pixels.

The proposed methodology is able to use low hardware requirements, and maintaining a good compromise between image resolution and frame rate. Furthermore, it is possible to adapt for any dimension ultrasonic array.

5E-6

11:45 am   On the Use of Parametric Models for Cancelling Reverberations in Imaging of Thin Materials

Miguel Castaño Arranz[1], Johan E. Carlson[1], Biao Jiang[1], Philip Lindblad[1]; *[1]Div. of Signals and Systems, Department of Computer Science, Electrical and Space Engineering, Luleå University of Technology, Luleå, Sweden*

Background, Motivation and Objective

Ultrasound imaging in thin materials is hindered by the overlapping wavefronts due to shorter time-of-flight inside the media than the time support of the emitted signal. Whilst increasing the transducer frequency and decreasing the pulse width may prevent these overlaps, this approach is limited by effects like too short propagation distances or high-frequency attenuation and absorption.

In this paper, parametric models are used to describe the pattern of reverberations based on prior information of the tested material. This allows the suppression of reverberating echoes prior to the use of conventional imaging techniques.

Statement of Contribution/Methods

The subject of study is thin materials under pulse-echo immersion test. The cancellation of the reverberations is performed through a calibration model based on time-of-flight, attenuation and reflection coefficients. The used parametric model is a particularization of a general model for multi-layered media which assumes normal incidence of planar waveforms with unfocused transducer.

A Maximum Likelihood Estimation scheme in the frequency domain is used to characterize the response of the material for the cancellation of the echoes.

Results/Discussion

Reverberation suppression for imaging of thin materials has successfully been achieved in simulations performed with the k-wave toolbox. This toolbox uses a full-wave model based on the k-space pseudospectral, which can account for the propagation of nonlinear ultrasound waves in generally heterogeneous media.

Reverberation suppression and imaging of flaws have been achieved in both plane and spherical wave scenarios. The use of spherical waves violates the model assumptions, introducing distortions due to unmodeled dynamics and affecting the estimation of the model parameters.

The figure (left) illustrates a k-wave simulation of a measurement on a 2mm material with a Side Drilled Hole (SDH) using a 5MHz transducer. This simulation is depicted together with the estimation of the reverberation pattern. The difference between these signals (right) estimates the flaw response, which is compared with a simulation of the separated flaw response. The substantial difference between the flaw response and the first top-layer echo hinders the estimation of the flaw response. Additional averaging during imaging using TFM allows successful flaw imaging.
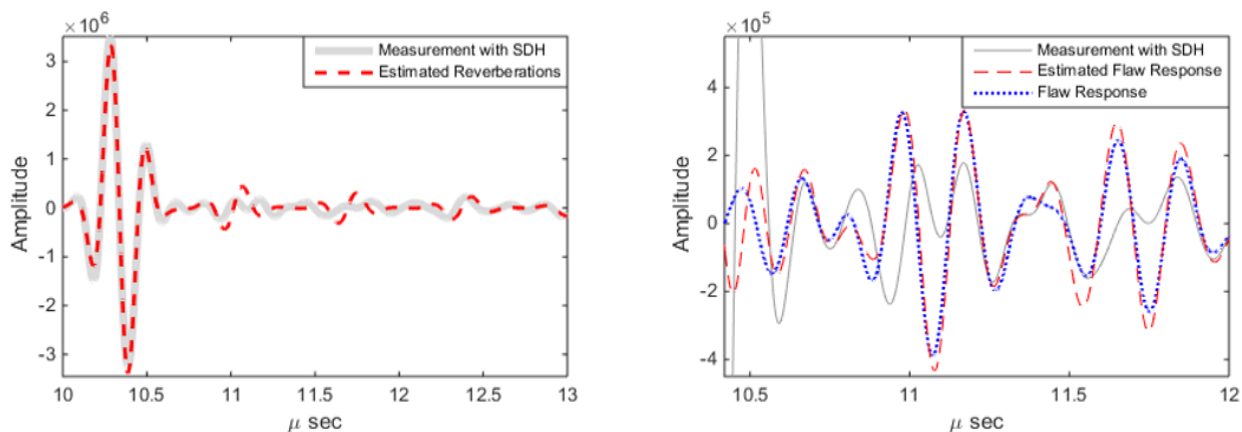
6E - General Physical Acoustics & Ultrasonic Motors & Actuators

201AF

Friday, October 23, 2015, 10:30 am - 12:00 pm

Chair: **Andreas Mayer**
           HS Offenburg

6E-1 _____

10:30 am   Four ways to justify temporal memory operators in the lossy wave equation

Sverre Holm[1]; *[1]Informatics, University of Oslo, Oslo, Norway*

Background, Motivation and Objective

Attenuation of ultrasound often follows near power laws which cannot be modeled with conventional viscous or relaxation wave equations. More general temporal memory operators in the wave equation can be made to fit such measurements. This paper discusses ways such loss operators can be interpreted.

Statement of Contribution/Methods

Temporary memory operators can be justied in four ways: 1.) Via power laws for attenuation with exponents other than two which correspond to the use of convolution operators with a temporal memory kernel. This kernel is a temporal power law. 2.) The corresponding constitutive equation is also a convolution. 3.) It is also equivalent to an infinite set of relaxation processes which can be formulated via the complex compressibility. 4.) The constitutive equation can also be expressed with higher order derivatives.

The two last ones are the ones which are least understood.

Results/Discussion

The justification for the four cases is: 1.) If the measured attenuation follows a power law, the memory operator can be shown to be a convolution with a temporal power law. For convenience this can also be expressed as a fractional derivative (see e.g. chap 4 in [1]) opening up for a host of useful properties from mathematics. 2.) These wave equations can be derived from more basic principles that include constitutive equations which also include a convolution with a temporal power law. For some materials, such laws can be verified by time domain measurements, [2] 3.) A common method for simulation of power law attenuation is to use a few relaxation processes as the loss term. This is not as ad hoc as it may look as it can be shown that a temporal power law loss operator is equivalent to an infinite sum of exponential time domain operators weighted in a particular way [3]. Simulation with a few such processes is therefore equivalent to a truncation of a sum of relaxation processes, e.g. to fit a limited frequency range as is commonly done in simulations. 4.) The equivalence with a sum of relaxation processes opens up for modeling the constitutive equation alternatively with higher order derivatives. The viscous constitutive equation requires only first order derivatives, but in general second, third, and higher order derivatives may describe more general loss relations in the constitutive equation.

All of these four descriptions are equivalent and bring new perspectives to the interpretation and justification of temporal memory operators in the wave equation.

1. T L Szabo, Diagnostic ultrasound imaging: inside out, 2nd ed, Academic Press, 2014.

2. S Holm and S P Näsholm,"A causal and fractional all-frequency wave equation for lossy media", Journ. Acoust. Soc. Am, Oct. 2011.

3. S. P. Näsholm and S. Holm, "Linking multiple relaxation, power-law attenuation, and fractional wave equations," Journ. Acoust. Soc. Am, Nov. 2011.

6E-2 _____

10:45 am   LONGITUDINAL SHEAR WAVE AND TRANSVERSE COMPRESSIONAL WAVE IN ELASTIC SOLIDS

Stefan Catheline[1], Nicolas Benech[2], Ali Zorgani[3]; *[1]INSERM, University of Lyon, Lyon, France, [2]Physics institute, University of Montevideo, Montevideo, Uruguay, [3]University of Lyon, France*

Background, Motivation and Objective

What general definition can one give to elastic P-wave and S-wave, especially when they are transversely and longitudinally polarized respectively? This question is the main motivation of the analysis of the Green's function in elastic solids reported in this letter.

Statement of Contribution/Methods

The anomalous polarization of S-wave was observed in seismology [1] in non-destructive testing [2] and medical imaging [3]. It is in this latter field called elastography, that this special wave has been systematically studied [4,5] and even commercialized [6] for fibrosis diagnostic. In this paper, it is shown that this latter longitudinal S-wave has a symmetrical counterpart: the transverse P-wave.

Results/Discussion

These unexpected waves are shown to be special parts of the solution of the wave equation known as coupling terms. Similarly to surface water wave, they are divergence and rotational free. Their special motion is carefully described and illustrated. Some practical applications of this work could consist in using a longitudinal transducer or a laser to measure both P-wave and S-wave arrivals from a point source. Equivalently a transverse transducer is able to detect both waves if placed in the correct direction. Thus one measurement only can supply elastic properties of solids.

References

1) K. Aki and P. Richards, "Quantitative seismology: Theory and methods" 2nd Edition, University Science Books, chapter 4 "Elastic waves from a point dislocation source", 63-121, (2002).

2) P.Gendreu, M.Fink, D.Royer "Optical imaging of transient acoustic fields generated by piezocomposite transducers", IEEE Trans.Ultrason. Ferroelec.Freq.Contr., 42, pp. 135-143 (1995).

3) Y. Yamakoshi, J. Sato, and T. Sato, ''Ultrasonic imaging of internal vibration of soft tissue under forced vibration,'' IEEE Trans. Ultrason. Ferroelectr. Freq. Control UFFC-37, 45–53 (1990)

4) S.Catheline, F. Wu, and M. Fink, "A solution to diffraction biases in sonoelasticity: The acoustic impulse technique," J. Acoust. Soc. Am., vol. 105, no. 5, pp. 2941–2950 (1999).

5) S. Catheline, J. L. Thomas, F.Wu, and M. Fink, ''Diffraction field of a low frequency vibrator in soft tissues using transient elastography,'' IEEE Trans. Ultrason. Ferroelectr. Freq. Control 46, 1013–1019 (1999).

6) L. Sandrin, S. Catheline, M. Tanter, X. Hennequin and M. Fink, Ultrasonic Imaging 21, 259 (1999)

FRIDAY ORAL
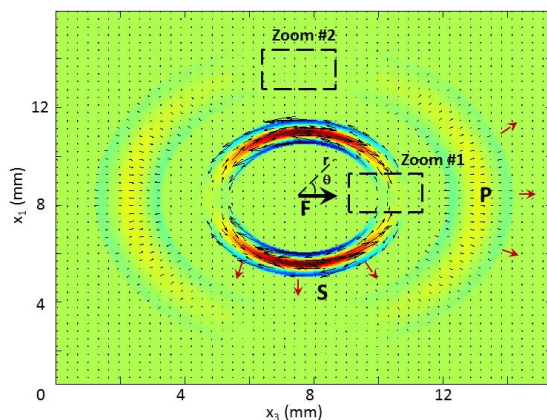
Fig.1 Elastic Green's function. The P and the S wave are clearly visible at θ=0 and θ=π/2. The longitudinal S-wave and the transverse P-wave are located inside dashed boxes called Zoom #1 and #2.

6E-3

11:00 am   Ultrasound bonding characterization of a bi-layer metal/epoxy with different chemical and mechanical interface treatments.

Camille GAUTHIER[1], Damien LEDUC[1], Jocelyne Galy[2], **Mounsif ECHCHERIF ELKETTANI[1]**, Jean-Louis IZBICKI[1]; *[1]LOMC CNRS 6294, University of Le Havre, Le Havre, France, [2]IMP CNRS 5223, INSA of Lyon, France*

Background, Motivation and Objective

Structural bonding are widely used in advanced industries, due to their well known properties of lightness and distribution of stresses on the whole structure.Ultrasounds are one of the most used methods to evaluate the quality of the bonding. This work is a collaboration between physical-chemists and acousticians and deals with ultrasounds characterization of the adhesive bonding in a bi-layer metal/epoxy. The cure level of the epoxy is taken into consideration. To improve the quality of the bonding, different mechanical and chemical treatments are achieved on the metal surface. The aim is to discriminate acoustically each bi-layer, using guided Lamb waves.

Statement of Contribution/Methods

The considered bi-layer is an Aluminum plate of 5 mm thick bonded to an epoxy film of 0.5 mm thick. The epoxy is based on Diglicidyl Ether of Bisphenol A (DGEBA, DER 331, Dow Chemicals) cross-linked with an aliphatic diamine (Jeffamine, D230, Aldrich). The conversion of the mixture is measured by Differential Scanning Calorimetry, and leads to a total cross-linked of the epoxy networks. The theoretical dispersion curves of lamb modes are obtained in the perfect contact assumption. Experimentally, to gradually improve the quality of the adhesion to the epoxy, different treatments are achieved on the Aluminum surface in contact with the epoxy: degreasing using alcoholic solution (sample called D), adhesion promoter using Silane (sample called Si), sandblasting that leads to 10 μm and 30 μm RMS roughness heights (samples called Rq10 and Rq30), and finally sandblasting followed by a deposit of Silane (samples called SiRq10 and SiRq30). The aim is to link the acoustic behaviour of these samples to the different treatments, using Lamb modes of high order. The experimental study is performed using a contact transducer of 1 MHz central frequency for the excitation, and a laser vibrometer to measure the time dependent normal displacement of the propagating waves on the Aluminum surface. A double time-space FFT is applied to determine the experimental dispersion curves in the wavenumber-frequency domain.

Results/Discussion

Results show that for a given mode and in the same frequency range, the dispersion curves are less or more shifted by the variations of the wavenumber, depending on the mode sensitivity to the interface. The samples SiRq30, SiRq10, Rq30 and Si are clearly discriminated by a significant shift of the wavenumber to increasing values. The samples Si and Rq30 are also clearly discriminated from the sample D which corresponds to an elementary treatment. Results show also that even if the samples Rq10 and Rq30 are slightly different, the addition of Silane to roughness in samples SiRq10 and SiRq30 highlights this difference. The next step is to quantify the attenuation introduced by each interface treatment on the propagating Lamb waves. This work will be extended to a three layer metal/adhesive/metal.

6E-4

11:15 am   Study on Micro Ultrasonic Motor using a Preload Mechanism

Tomoaki Mashimo[1]; *[1]Toyohashi University of Technology, Japan*

Background, Motivation and Objective

Piezoelectric ultrasonic motors are well-known as the most prominent micromotors for actuating miniature devices that can help minimally invasive diagnoses and treatments, such as endoscopes and catheters. They have two advantages for miniaturization: high energy densities with high torques at low speeds and simple structures using simple components. We have built a micro ultrasonic motor stator with a volume of approximately one cubic millimeter and succeeded in spinning the rotor. An advantage of this motor is the use of a vibration mode that generates three waves around the circumference of the hole in the stator. This mode generates a certain magnitude of vibration amplitude, even if the size is reduced to as little as 1 mm. Next goal of this study is to improve the motor torque and combine the rotor into the stator with micro mechanism.

Statement of Contribution/Methods

We discuss how to improve the torque of the micro ultrasonic motor for practical use. (The desired specification for practical use is the torque over 2 μNm as well as a torque generated in watch's ultrasonic motor.) Key parameter for motor torque improvement is the preload between the stator and rotor. A prototype micro ultrasonic motor and preload mechanism are built and its performances are measured by varying the preload. Another important subject for this study is the miniaturization of the motor components, such as rotor and preload mechanisms. We build the preload mechanism with a micro coil less than 1 mm in diameter.

Results/Discussion

The angular velocity of the prototype motor reaches a steady-state at approximately 10 ms and the peak angular velocity is more than 2000 rpm at the applied voltages of 80 V_{p-p} and 1040 kHz. The motor torque more than 10 μNm (1 gmm) is calculated from the product of the moment of inertia and the angular acceleration. Figure shows the prototype motor comprising of one cubic millimeter stator, the rotor, and the preload mechanism. All components in the prototype motor are fabricated by ordinary machining processes. We have examined the motor output values such as torque and angular velocity by varying the amplitude and frequency of the applied voltages.
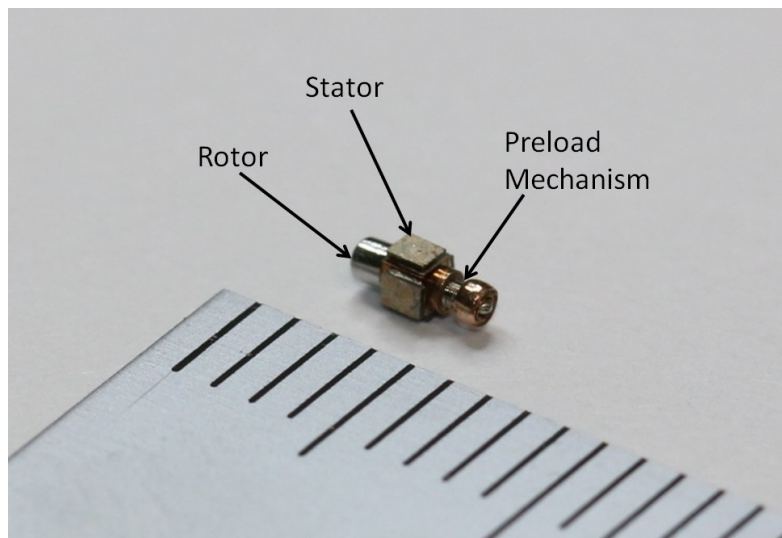
6E-5

11:30 am **Small Size Pneumatic Valve for Smooth Flow Control using PZT vibrator**

Daisuke HIROOKA[1], Tomomi YAMAGUCHI[1], Naomichi FURUSHIRO[1], Koichi SUZUMORI[2], Takefumi KANDA[3]; *[1]Kansai University, Japan, [2]Tokyo Institute of Technology, Japan, [3]Okayama University, Japan*

Background, Motivation and Objective

Pneumatic actuators have potential to downsize because they have simple structure. However many control devices that can control pneumatic actuators continuously are large volume and weight. We have designed the flow control valve driven by PZT vibrator. This control valve is small volume and light weight and it can control air flow smoothly. This valve fit to control small pneumatic actuators.

Statement of Contribution/Methods

The flow control valve that we proposed uses resonance vibration with a PZT vibrator. The valve consists of an orifice plate, a PZT vibrator and iron particles worked the poppet. The orifice plate was made stainless steel and it has 9 orifices. The orifice aperture diameter is 0.5 mm. The PZT vibrator consists of two PZTs that are 10 mm in external diameter, 8.2 mm in inner diameter and 0.2 mm in thick. The PZT transducer fixed orifice plate using nut. The flow control valve is 10 mm in diameter and 9 mm height. The mass of the valve is only 2.5 g. The control valve normally closes because iron particles put a stopper on orifices. When the voltage are applied PZT, the orifice plate excitation by the PZT vibrator works to make the particles away from the orifice plate. As a result, the space is generated between the particles and orifices, and air flows through the orifice. The intensity of the excitation controls flow rate. Therefor flow rate can be controlled by supplying voltage to PZT vibrator.

Results/Discussion

From experiment of flowing quantity evaluation, this control valve succeeds to control air flow smoothly with low hysteresis at large flow rate. In addition, this flow control valve achieves a maximum flow rate of 65 L/min under air pressure of 0.70 MPa. The results show that the valve has high controllability.
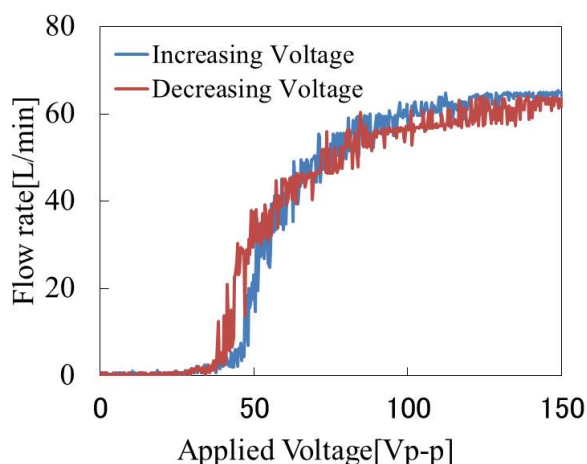
6E-6

11:45 am **Low flow rate spraying using a torsional ultrasonic transducer**

Shunsuke Tsuyuki[1], Takefumi Kanda[1], Koichi Suzumori[2], Shin-ichiro Kawasaki[3], Shoki Ofuji[1]; *[1]Okayama University, Okayama, Japan, [2]Tokyo Institute of Technology, Tokyo, Japan, [3]National Institute of Advanced Industrial Science and Technology, Miyagi, Japan*

Background, Motivation and Objective

In many industrial fields, a spraying of coating materials with a low flow rate is expected for the coating quality improvement. When the flow rate of the spraying is low, the pressure applied to coating materials have to be diminished. An ultrasonic vibration can effectively assist to enlarge a spray angle and atomize of materials even if the pressure is low. In this research, we propose the ultrasonic atomization by using a torsional vibration mode transducer. We have evaluated on the low flow rate spraying by using a bolt-clamped transducer.

Statement of Contribution/Methods

Figure 1 shows a schema of ultrasonic transducer for the spraying. This transducer can oscillate the tip of nozzle in perpendicular to the flow direction. Generally, the atomization condition is dominated by Weber number. From the macroscopic view the surface tension is changed when the nozzle is oscillated. Therefore we can control the atomization of the liquid by changing the Weber number. In this research, we have fabricated the torsional transducer to evaluate the effect of the atomization. We have observed the spray angle and atomization condition at the low flow rate. Additionally, the results of have been compared with those by using a longitudinal transducer.

Results/Discussion

Figure 2 shows the relationship between flow rates and spray angle when water was sprayed. In the case of torsional vibration mode, when the driving frequency, the applied voltage, and the flow rate were 18.3 kHz, 60 Vp-p, and 15 ml/min, the water has been successfully atomized. In addition, although the ethylene glycol has higher viscosity, we have succeeded in atomizing ethylene glycol effectively. As a result, the torsional vibration has generated a stable atomizing condition than the longitudinal vibrational mode in a low flow rate spraying.

Fig. 2 Relationship between flow rates and spray angle when water was sprayed

Fig. 1 Structure of bolt-camped transducer for spraying

7E - Emerging Technologies

105

Friday, October 23, 2015, 10:30 am - 12:00 pm

Chair: **Jan Kuypers**
            Qorvo Inc.

7E-1

10:30 am   Heterogenous integration technology using wafer-to-wafer transfer

Shuji Tanaka[1]; [1]*Department of Bioengineering and Robotics, Tohoku University, Sendai, Japan*

Background, Motivation and Objective

Frequency control, which is one of the most fundamental functions for communication as well as signal processing, is governed by piezoelectric devices. One of promising future direction of device technology is the wafer-level integration of heterogeneous components including piezoelectric devices, CMOS and so on. In general, integration is helpful to reduce the size and parasitics of devices. However, the integration of heterogeneous components is often difficult due to a variety of "mismatch" in terms of process temperature, the coefficient of thermal expansion, the cross-contamination of materials, die size etc.

Statement of Contribution/Methods

To overcome such "mismatch" problems, low-temperature wafer-bonding-based integration is useful, because two different components can be separately fabricated in suitable manners for each on different wafers. What is presented in this paper is our technology to transfer components or materials from one wafer to another for heterogeneous integration. A PZT-actuated MEMS switch was monolithically integrated with a CMOS circuit by polymer-based transfer process. A one-chip tunable SAW filter integrated with BST varactors was fabricated by laser-assisted film transfer process. One-chip FBAR oscillator was also fabricated by selective die transfer process.

Results/Discussion

A PZT-actuated MEMS switch was monolithically integrated with a CMOS circuit by polymer-based transfer process. PZT was deposited by sol-gel method at 600°C on a Si wafer, and then patterned into cantilevers. The PZT cantilevers were transfered to a CMOS wafer by polymer bonding and Si lost wafer etching. The cantilevers and the CMOS were mechanically and electrically conencted by Au electroplating, and finally the bonding polymer was removed.

Laser-assisted film transfer was adopted for a tunable SAW filter with BST varactors. BST was deposited and patterned on a sapphire wafer, and then irradiated with third harmonic Nd:VO$_3$ laser from the backside. The patterned BST film was bonded with a LiTaO$_3$ SAW wafer via Au films, and then transferred to the SAW wafer. The prototyped tunable SAW filter was installed and successfully worked in a cognitive wireless LAN demo system based on the draft of IEEE 801.11af.

One-chip BAW and SAW oscillators were fabricated by selective die transfer processes, which is useful when two dies to be integrated are much different in size. The interconnection was done by low temperature Au-Au diffusion bonding following Ar plasma activation. The backside of the dies on a glass support wafer was irradiated with third harmonic Nd:VO$_3$ laser for separation, and the dies were selectively transferred to the target wafer. An AlN-based FBAR with a die size of 1 mm × 1 mm and a BiCMOS-sustaining amplifier with a die size of 2 mm × 2 mm were integrated and simultaneously packaged at wafer level. The integrated device worked as a chip-size-packaged 2 GHz timing oscillator.

7E-2

11:00 am   Transverse modes in STW resonators on quartz

Victor Plessky[1], Ventsislav Yantchev[2], Weibiao Wang[3], Michael Yang[4], Bob Hsiao[4]; [1]*GVR Trade SA, Switzerland,* [2]*Uppsala University, Sweden,* [3]*Nanjin Electronic Devices Institute, China, People's Republic of,* [4]*Tai-SAW Technology Ltd., Taiwan*

Background, Motivation and Objective

Surface transverse wave (STW) resonators on quartz provide excellent Q-factors and low loss in 2GHz frequency range [1]. Meanwhile, the transverse modes were observed unusually situated on the left side from the main resonance, which was explained by concave form of the slowness curve in plane of substrate [2]. Moreover, propagation along the busbars can, probably, radically change the acoustic field distribution across the aperture and introduce additional perturbation in 2-port resonator/filter performance [2]. These effects can manifest themselves as notches and other perturbations of the narrow band 2-port resonator performance, which can be unacceptable for the device applications [3]. In this presentation we analyze, using COMSOL simulations, the dependences of transverse modes on aperture, electrode's metal thickness and metallization and compare the results to experimental data.

Statement of Contribution/Methods

The presence of transverse modes in STW resonators on quartz on the left side from the resonance [2] is confirmed by numeric simulations and by experimental data. We have modelled STW resonances in periodic electrode structure of Al electrodes (h/λ=2%, 4%) on 36° rotated cut STW direction with finite aperture (W=10λ, 20λ, 40λ) using COMSOL software. The transverse modes were found in most of structures and the table of modes will be presented. It was also found that the busbars play essential role and even in the main resonance a part of STW energy is concentrated in the busbars. Further, dummy fingers are used to concentrate STW energy in the active part of the electrode structure. The influence of the waveguiding conditions on the transversal STW modes is specifically addressed.

Results/Discussion

Figure 1a,b below shows real part of admittance as a function of frequency. The narrow aperture structure with W=10λ has only one transverse mode at about 6 MHz below the main resonance. The structure with W=40λ has at least 4 transverse modes separated quasi periodically about every 2 MHz below main resonance. Comparison with experimental data will be presented.

[1] C. U. Kim et. al., "High Q-factor STW-Resonators on AT-Cut of Quartz.", Proc. Int. Ultrason. Symp., p. 2582, 2007

[2] M. Mayer et. al., "Transversal Mode Orthogonality in SAW waveguides with transversally varying slowness anisotropy", Proc. Int. Ultrason. Symp., p. 337, 2011

[3] V.Plessky and V. Yantchev, "Two Resonances of different Nature in STW Resonators with Aperture Weighted Metallisation", IEEE TUFFC, April, 2015

W=10Lam

(a)

W=40Lam, Re(Adm)

(b)
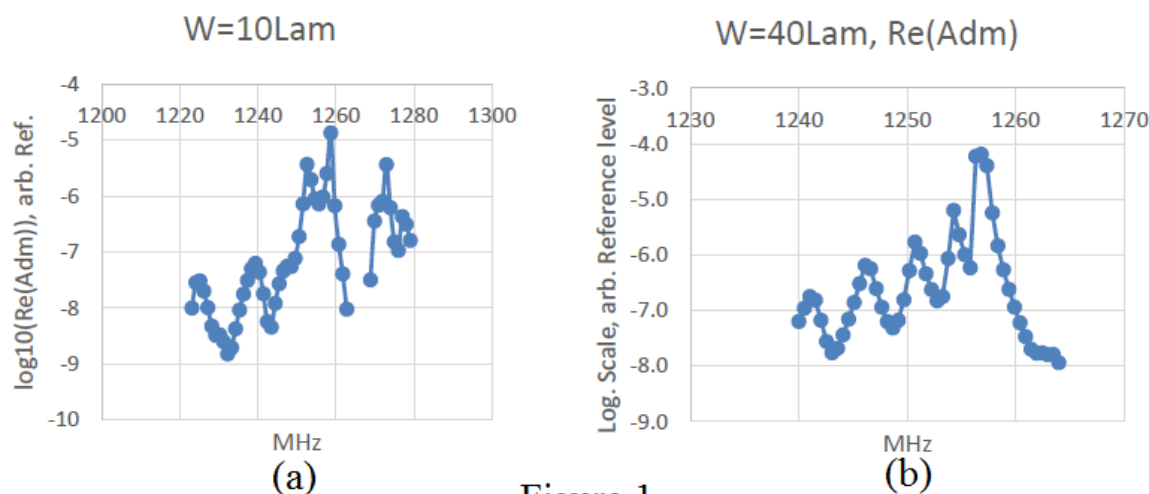
Figure 1

11:15 am   Characterization of Thin ScAlN Film based Natural Single-Phase Unidirectional SAW Transducers using Sagnac Interferometer

Abhay Kochhar[1], Yasuo Yamamoto[2], Akihiko Teshigahara[2], Ken-ya Hashimoto[3], Shuji Tanaka[1], Masayoshi Esashi[1]; *[1]Tohoku University, Japan, [2]DENSO CORPORATION, Japan, [3]Chiba University, Japan*

Background, Motivation and Objective

Natural single-phase unidirectional SAW transducers were reported previously for oriented quartz, LiNbO$_3$, LiTaO$_3$, La$_3$Ga$_5$SiO$_{14}$ substrates, etc. The reason behind the directionality is in the shift in the transduction and reflection coefficient. These substrates observed 15-20 dB of directivity. However, the directionality in the thin piezoelectric films hasn't been reported elsewhere till recently by our group. The motivation to utilize the directionality in thin piezoelectric films was to improve the transducer's return loss effectively such that it can be utilized in integrated sensor applications. For characterization of directionality, in this paper we utilized Sagnac interferometer. More rigorous study and characterization with the different wave propagation direction and film's c-axis tilt is in progress.

Statement of Contribution/Methods

Figure 1 (a) shows the IDT pattern used for comparison. The Split IDT is used, as it is bidirectional on any crystalline orientation. The Normal IDT pattern has λ = 4 μm, aperture = 40 λ, finger pairs = 40 and spacing of 50 λ between Split IDTs is fabricated. In Split IDT, the transducer employs split-finger electrodes with the finger width and space of 0.5 μm each. The number of finger pairs is 10 and aperture of 40 λ. For this reported abstract, the 4.5° c-axis tilted ScAlN thin film is used and confirmed by 2D XRD system. The c-axis tilt in ScAlN is in the wave propagation direction of 90°. SAW IDT is patterned by EB lithography on ScAlN/Sapphire (0001) and metallized with Au electrode (lift-off process).

Results/Discussion

We compared the forward and backward acoustic signals for propagation direction (i) parallel to the c-axis tilt as shown in Figure 1 (b) and (ii) perpendicular to the c-axis tilt as shown in Figure 1 (c) using network analyzer and Sagnac interferometer. In Figure 1 (b), higher acoustic signals is seen on the backward direction as compared to the forward one because of orientation being in that direction. The difference (or directivity) in forward and backward direction is 11.3 dB. But if the wave propagation is perpendicular to c-axis tilt (Figure 1(c)), the acoustic signals in either direction produce same power (no directivity). Such level of directionality in SAW devices due to the lower c-axis tilted thin film enables improvisation in insertion and return loss hence making it useful for integrated sensor applications.

Fig. 1 (a) Directionality pattern:
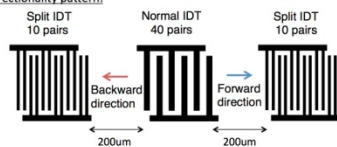
Fig. 1 (b) Wave propagation parallel to the c-axis tilt
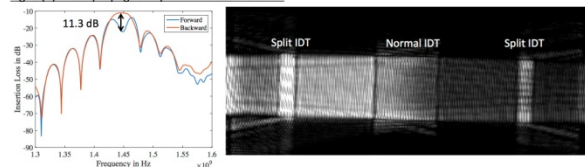
Fig. 1 (c) Wave propagation perpendicular to the c-axis tilt
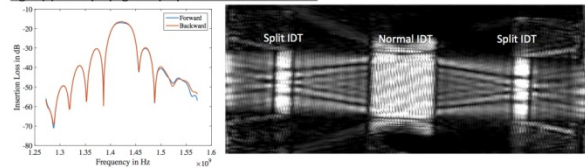
7E-4

11:30 am   Evaluation of Acoustic Properties of CaTiO₃-(K,Na)NbO₃ Film Using Microfabricated Structure

Ryosuke Kaneko[1], Michio Kadota[1], Yuji Ohashi[2], Jun-ichi Kushibiki[1], Shinsuke Ikeuchi[3], Shuji Tanaka[1]; [1]*Graduate school, Tohoku University, Sendai, Miyagi, Japan,* [2]*Institute for Material Research, Tohoku University, Sendai, Miyagi, Japan,* [3]*Devices Development, Murata Manufacturing Co., Ltd., Nagaokakyo, Kyoto, Japan*

Background, Motivation and Objective

Pb(Zr,Ti)O₃ (PZT) is the most widely used for piezoelectric devices, because it has high piezoelectric constants over a wide range of temperature. However, it contains lead at high concentration. Nowadays, lead-free piezoelectric films have been widely studied for the next-generation piezoelectric devices. (K,Na)NbO₃ (KNN) is one of the candidates of the replacement, because its d_{31} is around 100 pm/V, which is equivalent to that of PZT. However, the material constants and acoustic properties of the KNN film have not been measured yet. In this research, we develop a method to measure the acoustic properties of a (001)-oriented KNN film deposited on a blanket platinum film.

Statement of Contribution/Methods

We used a 1.7 μm thick CaTiO₃-doped KNN film on Si (500 μm)/SiO2 (150 nm)/Ti (10 nm)/Pt (100 nm) [1]. First, we fabricated piezoelectric resonators on the KNN film by microfabrication technology. Fig. 1 shows length extension mode and radial/longitudinal thickness modes resonators. The radial and longitudinal thickness modes are generated on the same resonator. The resonance and antiresonance frequencies of each mode are measured using a network analyzer. The velocity of leaky Lamb wave in a KNN diaphragm of 2 mm diameter covered with 200 nm thick Al is measured using an acoustic microscope.

Results/Discussion

The following material constants were extracted from measured results of the resonators; $s_{11}^E = 9.27 \times 10^{-12}$ /Pa, $s_{12}^E = -3.06 \times 10^{-12}$ /Pa, $s_{66}^E = 24.7 \times 10^{-12}$ /Pa, $k_{31}^2 = 0.06\%$, $k_t^2 = 13.5\%$, $d_{31} = -119$ pC/N, Poison ratio $\sigma_{12}^E = 0.33$, $\varepsilon_{33}^T/\varepsilon_0 = 1{,}226$. The phase velocity of length extension mode is 4,905 m/s. The phase velocity of A₀ and S₀ mode of Lamb waves in the KNN diaphragm of 0.2-0.3λ thickness were measured by ultrasonic microscopy as 1,491 m/s and 5,370-5,180 m/s, respectively, as shown in Fig. 2. The developed method can be basically applicable to any piezoelectric blanket films unlike our previous study [2], where ScAlN was deposited on a patterned platinum layer.

[1] S. Ikeuchi et al., "Preparation of (K,Na)NbO₃-CaTiO₃ film by RF magnetron sputtering", IEEE Ultrason. Symp. 2014, pp. 1578-1581.

[2] Akira Konno et al., "Determination of Full Material Constants of ScAlN Thin Film from Bulk and Leaky Lamb Waves in MEMS-based Samples", IEEE Ultrason. Symp. 2014, pp. 273-276.

(a) Length Expander mode resonator: *l* = 200~600 μm

(b) Radial/Longitudinal thickness modes resonator: *d* = 30~200 μm

Fig. 1 Fabricated piezoelectric transducers.

Fig. 2 Measured phase velocity of leaky Lamb wave on KNN diaphragm as a function of KNN thickness.

7E-5

11:45 am   Dry Deagglomeration and Alignment of Carbon Nanotubes using the Acoustic and Electric Fields of SAW

Morteza Miansarigavzan[1,2], **James Friend**[2]; [1]*Mechanical and Aerospace Engineering, Monash University, Clayton, VIC, Australia,* [2]*Center for Medical Devices, Dept of Mech and Aero Engineering, University of California, San Diego, La Jolla, CA, USA*

Background, Motivation and Objective

Carbon nanotubes (CNTs) immediately agglomerate after production into microscale bundles with mechanical and electrical properties far inferior to the spectacular capabilities of individually separated and aligned CNTs attractive for composites and conductive surfaces. To extract CNTs from bundles, aqueous suspension with contaminating surfactants and damaging ultrasonic treatments is required, and these CNTs often rebundle soon after. This problem has plagued researchers for so long that most have moved on to consider graphene and other materials. Our objective was to solve this problem in carbon nanotube use: debundle and align dry carbon nanotubes.

Statement of Contribution/Methods

Using 30 MHz, X-axis surface acoustic waves propagating upon bare, 127.86° Y-rotated lithium niobate (LN) we accomplished our objective. Naturally occurring in ~100 μm bundles, the nanotubes were placed onto the piezoelectric substrate with a glass coverslip cover pressed against them with a known force. The bundles were exposed to SAW to deliver individual CNTs through bundle breakdown. Alignment was performed through shear by translation of the coverslip. Through careful experimentation over hundreds of runs the complex physical mechanism responsible for SAW nanotube extraction has been elucidated. Substantial image processing of scanning electron microscopy photos was performed to quantify the number of extracted nanotubes, the bundle volumes, and quality of alignment. Raman spectroscopy of the G band was used to assess the carbon nanotubes' molecular structure.

Results/Discussion

The CNT bundles were found to reduce in size to ~5 μm due to impact from the extremely large (~10 Mm/s²) SAW substrate acceleration. At this point, the van der Waals force overcomes inertial forces to adhere the bundles to the substrate. The bundles experience rapid electric field reversals due to the SAW. The CNTs within are Coulombically ejected through electrostatics: all of the CNTs possess the same charge polarity. Over a few seconds, this completely depletes the bundle to leave nanotubes strewn across the substrate. Dragging the coverslip across the CNTs aligns ~90% within ±10° of the sliding direction, and completely independent of the SAW propagation direction. Raman spectroscopy confirmed the CNTs remained intact, without worm-eaten damage typical of past methods.
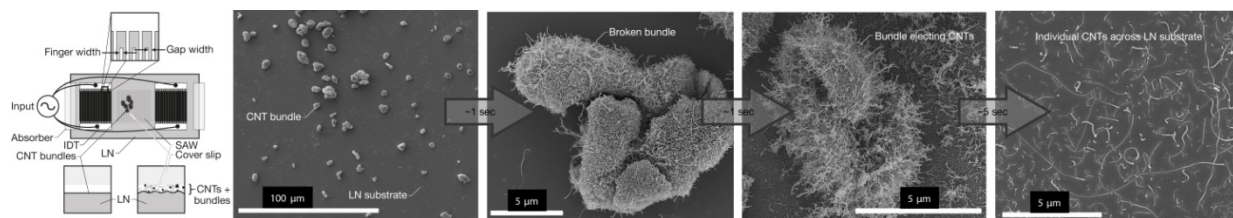
8E - Front-End and Integrated Electronics

102

Friday, October 23, 2015, 10:30 am - 12:00 pm

Chair: **David Cowell**
           University of Leeds

8E-1

10:30 am   Development of a Hybrid Custom / Commercial Multi-Channel, High-Frequency Transmit Pulser and Beamformer System

Holly Lay[1], Romans Poltarjonoks[1], Florence Ndum[1], David Lines[2], Geoffrey Lockwood[3], Sandy Cochran[1]; [1]*University of Dundee, Dundee, United Kingdom,* [2]*Diagnostic Sonar Ltd, Livingston, United Kingdom,* [3]*Queen's University (deceased), Kingston, Canada*

Background, Motivation and Objective

Microultrasound imaging above 25 MHz is a rich field of research, with applications in intravascular, endoscopic, ocular and skin imaging amongst many. However, there has been some lag in the development of electronics required to drive and focus ultrasound arrays at these frequencies, with commercial solutions often suffering bandwidth, power or channel count restrictions. To address this, we have developed a series of low-cost, expandable channel-count circuits to drive microultrasound transducer arrays at frequencies up to 50 MHz and voltages up to 100 Vpp.

Statement of Contribution/Methods

In this paper, the progressive development of a custom series of transmit circuitry is presented. This includes both benchtop supply and electrical mains powered system development with expandable channel count and also includes the integration with the multi-channel FI Toolbox commercial product (Diagnostic Sonar, Livingston, UK). These systems have the advantage of being easily expanded to the required channel count for a given target device whilst requiring only low-cost components. They are also highly tuneable in both frequency and voltage. A series of discrete focusing delay chips with variable delay steps allow them to be programmed either serially or in parallel. This allows the system to be operated in isolation or in conjunction with commercial generic hardware platforms.

Results/Discussion

To address the core issue of expandability, a preliminary system design was selected with a central power and trigger backplane and a grid of expandable card slots for individual transmit channels. The single channel circuit design was based on THS3001 (Texas Instruments, USA) op-amps and ZXMP10A13F and ZXMN10A07Z MOSFETs (Diodes Inc, USA) and simulated in pSPICE. To allow a separate channel-dependent beamforming delay on each board, a set of three pulse-width modulation (PWM) chips (DS1023, Maxim Inc, USA) were added to the circuit input both to adjust the width of the transmit pulses and add relative delays. Once manufactured and connected to benchtop power supplies, the system produced 90 Vpp pulses at 50 MHz with 65% duty cycle (55% simulated). Based on this design, a second system was developed with a custom power backplane to convert 220 VAC mains to 5 V, +/- 12 V and an adjustable 5 - 75 V supply. By implementing mains input, the system becomes far more portable, allowing it to be used in labs without additional power equipment. The single channel boards were also simplified into a mono-polar design to give better frequency control.

To allow multi-channel acquisition and beamforming, the system was interfaced with the FI Toolbox, a 32 - 128 channel transmit/receive beamformer operating up to 20 MHz natively. The previous transmit board was modified to allow direct control from the FI Toolbox and a 250 MS/s digitizer (PXIe-5170R, National Instruments, USA) was added. The resulting system can transmit and acquire up to 32 channels at 50 MHz with 100 Vpk transmit.

8E-2

10:45 am   A Mixed-Signal Multiplexing System for Cable-Count Reduction in Ultrasound Probes

Qilong Liu[1], Chao Chen[1], Zu-yao Chang[1], Christian Prins[2], Michiel A. P. Pertijs[1]; [1]*Electronic Instrumentation Laboratory, Delft University of Technology, Delft, Netherlands,* [2]*Oldelft Ultrasound, Delft, Netherlands*

Background, Motivation and Objective

A significant challenge in the realization of endoscope- and catheter-based 3D ultrasound probes is the electrical connection between the imaging system and the transducer elements. Since the number of elements needed for real-time 3D imaging readily exceeds the number of cables that can be accommodated, in-probe integrated circuits (ICs) are required to reduce the number cables. Solutions based on in-probe switches and sub-array beamformers have been reported. In this work, we present a compact and low-power IC that combines multiple RF receive signals on a single micro-coaxial cable. We show that digitization and equalization on the system side, where the associated complexity and power are acceptable, allow reconstruction of the individual RF signals in spite of cable non-idealities.

Statement of Contribution/Methods

We propose an in-probe IC that converts the sampled-and-held input signals of four analog receive front-ends (AFEs) to currents that are alternately driven onto a micro-coaxial cable (Fig. 1a). The resulting time-multiplexed current is sensed by a trans-impedance amplifier (TIA) on the far end of the cable and digitized by an ADC. Due to reflections, attenuation and dispersion of the cable, the signals associated with the four inputs get mixed up. This crosstalk is repaired by means of digital equalization on the system side, which can be calibrated in-system by recording the pulse response of the individual channels. Thus a multiplexing solution is obtained that can be implemented within the size and power constraints of the targeted probes.

Results/Discussion

The multiplexing chip has been fabricated in a 0.18 μm CMOS process (Fig. 1b), has an active area of 0.16 mm^2 occupied by the multiplexer, and consumes 1.9 mA from a 1.8 V supply. The chip samples its 4 inputs at 25 MHz and drives a time-multiplexed signal onto a 3m micro-coaxial cable, connected to a TIA implemented on PCB. The TIA's output is digitized using an oscilloscope and equalized and demultiplexed in Matlab. Non-overlapping Gaussian-shaped 6 MHz pulses applied to the four inputs can be accurately recovered at the outputs, with equalization effectively suppressing channel-to-channel crosstalk (Fig. 1c,d).The measured performance (Fig. 1e) shows that this is a promising approach for cable reduction in future miniature ultrasound probes.

FRIDAY ORAL
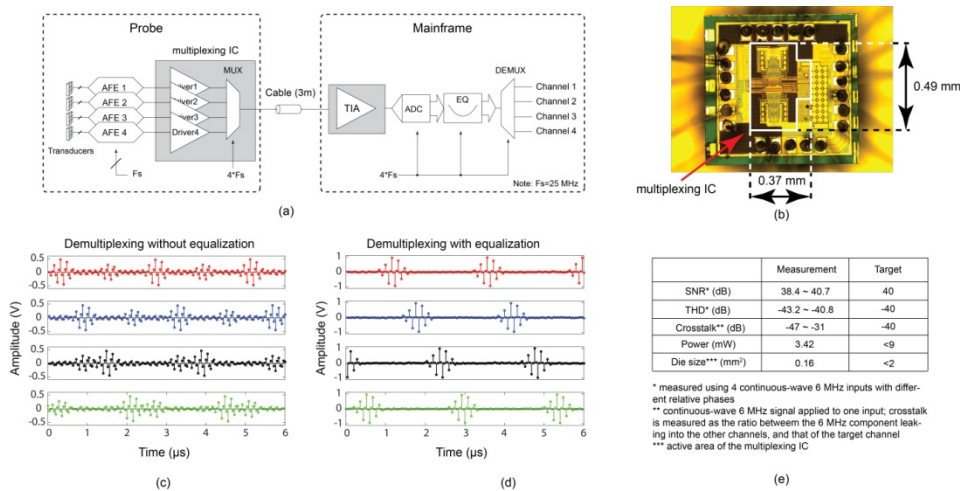
Fig. 1: (a) Block diagram of the multiplexing system; (b) photograph of the prototype multiplexing IC; (c) digitized outputs for non-overlapping Gaussian-shaped inputs without equalization, showing crosstalk; (d) with equalization, showing strongly reduced crosstalk; (e) performance summary.

8E-3

11:00 am   A Single-Cable PVDF Transducer Readout IC for Intravascular Photoacoustic Imaging

Chao Chen[1], Verya Daeichin[2], Qing Ding[1], Gijs van Soest[2], Geert Springeling[2], Ton van der Steen[2,3], Michiel Pertijs[1], Nico de Jong[2,3]; [1]*Electronic Instrumentation Lab, Delft University of Technology, Delft, Netherlands,* [2]*Dept. of Biomedical Engineering, Erasmus MC, Rotterdam, Netherlands,* [3]*Lab of Acoustical Wavefield Imaging, Delft University of Technology, Delft, Netherlands*

Background, Motivation and Objective

Intravascular photoacoustic (IVPA) imaging can visualize the coronary atherosclerotic plaque composition on the basis of the optical absorption contrast. Our ex vivo experimental finding shows that more than 80% of the PA energy of human coronary plaque lipids lies in the frequency band below 15 MHz. In order to cover such low frequency band with an IVPA catheter, a broadband low-frequency PVDF transducer (0.6 × 0.6 mm, 52 μm thick) has been manufactured in house to receive the PA signal. To match the impedance between such a small PVDF element (>> 1 kΩ) and the connecting cable (50 Ω), we have designed a readout integrated circuit (IC) to be connected directly behind the PVDF, as depicted in Figure (a). The capability of the readout IC to work with a single cable will reduce the rigidity of the IPVA catheter. The acoustic performance of a prototype PVDF transducer co-integrated with the proposed IC has been evaluated.

Statement of Contribution/Methods

The readout IC, fabricated in a standard 0.18 μm CMOS process, consists of a trans-impedance amplifier (TIA) that converts the current generated by the PVDF element to voltage, and a source follower (SF) that provides a low output impedance matched with the 50 Ω cable (see Figure (b)). Both circuit blocks are powered by an external bias current source via a single micro-coaxial cable, which also carries the signal current drawn by the SF. The bias current is divided between the TIA and the SF by means of an on-chip current mirror with a low-pass filter. The ground reference of the IC is provided by the shield of the 1 m micro-coaxial cable, which is also connected to the top electrode of the PVDF element. The bottom electrode of the PVDF element is directly glued to the input bondpads of the IC, as shown in Figure (c). Our PVDF probe was acoustically compared with a 1 mm calibrated needle hydrophone (calibrated for 0.25-20 MHz). As a source a calibrated 2 MHz unfocused PZT transducer transmitting a 2-cycle pulse was used.

Results/Discussion

Electrical measurements show that the readout IC provides a 50 Ω output impedance across the frequency range of 2-20 MHz with a 6 mA external current supply. Acoustical results (see Figure (d)) show a signal to noise ratio of 47.4 dB for our probe vs. 29.0 dB for the commercial hydrophone (up to 20 MHz). Moreover, it is possible to measure an acoustical signal as low as 25 Pa at 2 MHz with our PVDF probe.
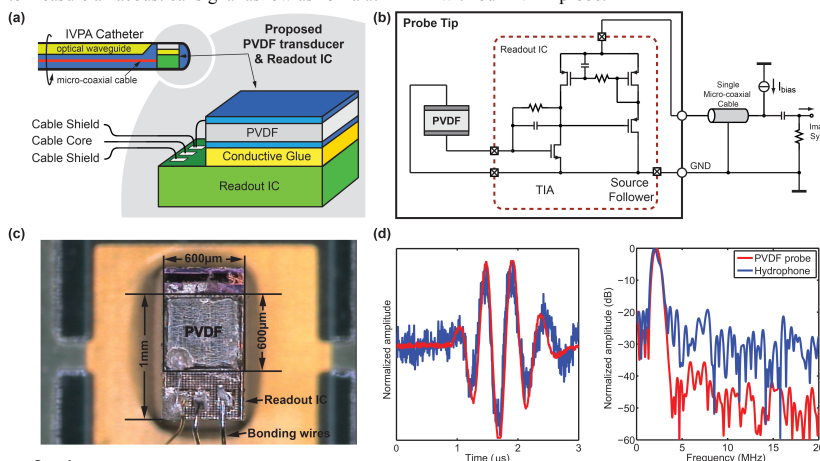
Captions:
(a) Architecture of the IVPA catheter and the proposed PVDF transducer & readout IC;
(b) Schematic diagram of the proposed single-cable PVDF transducer readout IC;
(c) Micro-photograph of the readout IC with co-integrated PVDF transducer;
(d) Acoustic measurement results in comparison with a 1mm calibrated commercial hydrophone (Precision Acoustics, SN:1875)

8E-4

11:15 am   A Row-Column Addressed CMUT Probe with Integrated Electronics for Volumetric Imaging

Thomas Lehrmann Christiansen[1], **Mathias Engholm**[1], Christopher Beers[2], Michael Berkheimer[2], Lars Nordahl Moesner[3], Jan Peter Bagge[3], Matthias Bo Stuart[4], Anders Lei[1], Søren Elmin Diederichsen[1], Jørgen Arendt Jensen[4], Erik Vilain Thomsen[1]; [1]*Department of Micro- and Nanotechnology, Technical University of Denmark, Kgs. Lyngby, Denmark,* [2]*Sound Technology,*

State College, PA, USA, [3]BK Medical, Herlev, Denmark, [4]Center for Fast Ultrasound Imaging, Department of Electrical Engineering, Technical University of Denmark, Kgs. Lyngby, Denmark

Background, Motivation and Objective

The number of transmit and receive channels needed to perform real-time 3-D ultrasound imaging can be greatly reduced if row-column addressed 2-D transducer arrays are used. So far, a fully assembled hand-held row-column probe for volumetric imaging has not been demonstrated.

This work presents results from the development of such a probe. The probe is designed to be used on a commercial bk3000 scanner from BK Medical (Herlev, Denmark).

Statement of Contribution/Methods

A 3 MHz, $\lambda/2$-pitch 62+62 channel row-column addressed 2-D capacitive micromachined ultrasonic transducer (CMUT) array with a footprint of 26 mm x 26 mm is fabricated using a LOCOS (LOCal Oxidation of Silicon) process with 4 lithography steps. The array employs integrated apodization to avoid ghost echoes in the image. It is mounted and wire-bonded on a flexible printed circuit board (PCB), which is connected to two rigid PCBs with pre-amplifiers for driving the cable to the scanner. The array and PCBs are encapsulated in a 3-D printed handle, and a grounded shielding layer and silicone coating is applied to the front-side of the array for physical and electrical isolation. The handle is assembled together with a 128-channel coaxial cable that connects it to the ultrasound scanner, which supplies the probe with a 190 V DC bias voltage and an AC excitation voltage of 150 V_{pp}. The electronics are designed to allow all elements to be used interchangeably as either transmitters or receivers.

Results/Discussion

The image shows the probe components before assembly. The array is seen on the flexible PCB, which connects to the in-handle electronics PCBs driving the cable to the scanner. The probe handle itself is composed of three parts. The square acoustic window for the transducer array is seen in the nose piece, which is to be sealed off with a grounded shielding layer and a silicone coating. The shielding layer is measured to give a noise performance equivalent to a commercial 8812 transducer (BK Medical, Herlev, Denmark). The array elements are measured prior to mounting and exhibit stable performance with no significant change in resonance frequency or coupling coefficient over 10 hours of continuous use.
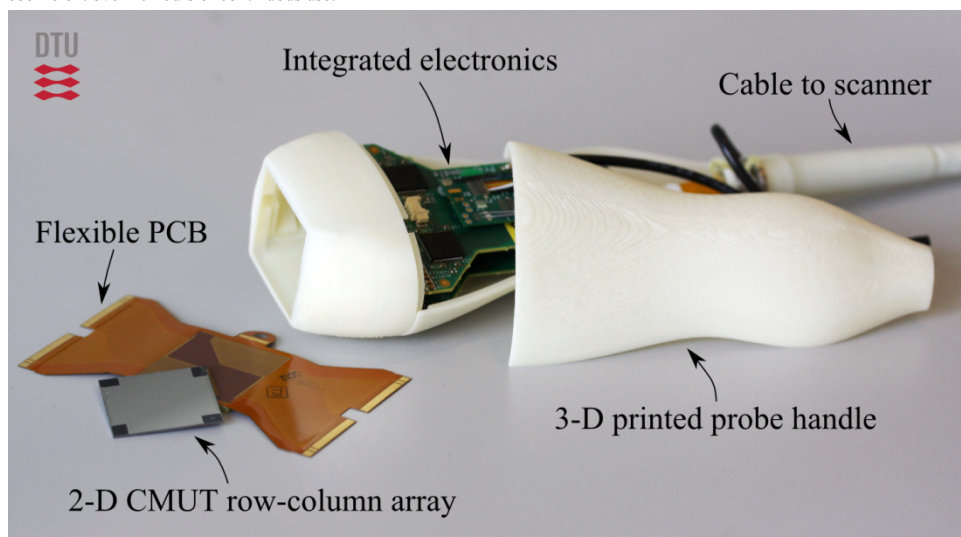
8E-5

11:30 am   Front end circuit simulation for CMUT systems based on an accurate nonlinear CMUT array model

Jaemyung Lim[1], Gwangrok Jung[1], Evren Fatih Arkan[2], F. Levent Degertekin[2], Maysam Ghovanloo[1]; [1]School of Electrical and Computer Engineering, Georgia Institute of Technology, Atlanta, Georgia, USA, [2]G.W. Woodruff School of Mechanical Engineering, Georgia Institute of Technology, Atlanta, Georgia, USA

Background, Motivation and Objective

Simple equivalent circuits for CMUTs are not adequate especially when the devices are part of a large imaging array with crosstalk. Although accurate large signal models are available for CMUTs and electrical impedances can be extracted from them, they are not suitable for direct use with circuit simulators such as SPICE and Spectre. An accurate equivalent circuit representation incorporating nonlinearities and bias dependence is needed for fast simulations to determine noise performance, transient response, and stability of CMUT front end circuits.

Statement of Contribution/Methods

We obtained the bias dependent electrical impedance, transformer ratio, and static capacitance (C0) from the model in [1]. First we de-embedded C0 from the CMUT impedance using MATLAB, extracted remaining series impedance terms Z_rad and Z_mem in Touchstone file format, imported the impedance data to Agilent ADS, and modeled local maxima with series and parallel RLC circuits that were determined by ADS. We optimized the equivalent circuits at different bias voltages up to 95% of the collapse voltage. To verify this equivalent model, we compared the results of this equivalent circuit with short-circuit result from the full MATLAB CMUT simulator [1]. We then incorporated it with a typical TIA design in Cadence to demonstrate that we can use the circuit model for front-end design.

Results/Discussion

We modeled a 12 element CMUT array for guidewire IVUS with center frequency of 40 MHz, and bandwidth of 20 MHz. Each element is made of 40-membranes with of 20 μm $\times$ 20 μm size and the array has 25 μm pitch. We also ran a transient simulation and showed that the equivalent circuit presents comparable results to the full MATLAB simulation for short circuit conditions verifying the model for time domain simulations. Example simulation results are shown for 85% and 95% of collapse voltage biasing along with the same resistive feedback TIA. The CMUT array with higher bias is predicted to have higher gain, higher noise, lower resonant frequency but overall 3.5 dB better SNR.
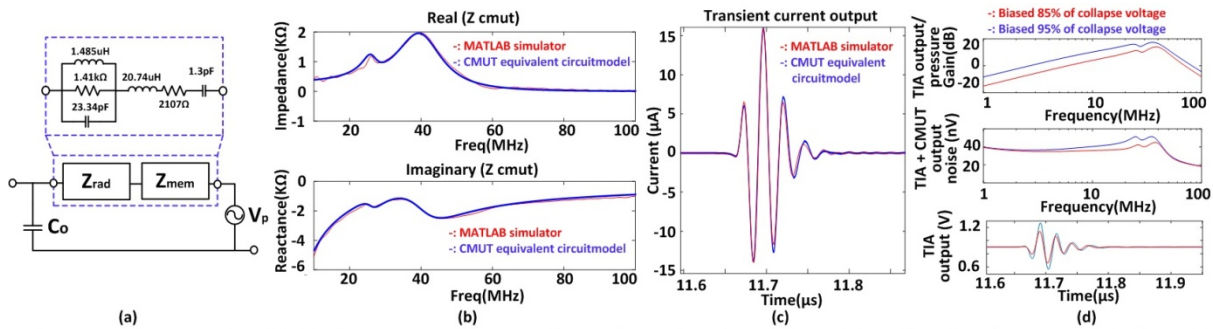
Figure 1. (a) Equivalent circuit model of the CMUT array element at 95% of 47-V collapse voltage, (b) comparison of Electrcal impedance from MATLAB simulator and the CMUT Equivalent circuit model, (c) current output from the simulator and the model when CMUT shorted, and (d) Cadence simulation results for two different bias voltages
[1] S. Satir, J. Zahorian, F.L. Degertekin, "A large-signal model for CMUT arrays with arbitrary membrane geometry operating in non-collapsed mode," IEEE Trans. Ultrason. Ferroelectr. Freq. Control , vol. 60, no. 11, pp 2426-2439, Nov. 2013.

8E-6

11:45 am   Development of High-Sensitive and Wideband FET-Based Ultrasound Receiver Directly Driven by Piezoelectric Effect

Hiroki Makino[1], Jing Zhu[1], Tsuyoshi Okubo[1,2], Yhisin Ho[1], Norio Tagawa[1], Ming Yang[1]; *[1]Graduate School of System Design, Tokyo Metropolitan University, Tokyo, Japan, [2]Konica Minolta, Inc., Japan*

Background, Motivation and Objective

For high performance piezoelectrics, few technology options are currently available. Recent study projected a novel sound pressure sensor using a ferroelectrics-gated FET [1], but few were reported with an evident observation. In this study, we propose a structure possessing direct coupling of a PZT to a gate of a MOS-FET (PZT-FET), which is characterized by direct control of a semiconductor channel with charges generated by piezoelectric effect and enables ultrasound receiving with high sensitivity and wide bandwidth. This sensor is promising for application to a medical diagnosis and an NDT requiring higher resolution and deeper imaging. We measure its acoustic properties.

Statement of Contribution/Methods

We prepared the equivalent circuit of PZT-FET by wiring a PZT′s anode and a gate of an NMOS-FET. The size and the dielectric constant of the PZT critical to the observation were tuned to be optimized. The resonant frequency of the transmitter is 15 MHz, and its transmitted power is regulated by tuning excitation voltages to be constant over all frequency range measured. Continuous waves were transmitted to observe nearly single frequency response of the PZT-FET. The frequency of transmitted ultrasounds ranges from 10 MHz to 20 MHz. The output of the PZT-FET is recorded by a drain voltage determined by I-V conversion of a source-drain current with a 10 MΩ resistor.

Results/Discussion

The receiving performance of the PZT-FET was evaluated in terms of a minimum detectable sound pressure, a linear dynamic range and a -6 dB-ranged bandwidth, those which were observed to be 8 Pa, 63 dB and 20%, respectively. The former two are highly improved against the current typical medical ultrasound transducer having 2000 Pa and 40 dB, respectively. These findings are attributable to a sensitivity of piezoelectrics linearly varying charges and the channel conductivity. The bandwidth still stays at low due to a dominancy of PZT resonance at the frequency, f_R (18 MHz). The possible solution to increase it is to design an array of plural number of PZT-FET MUTs, each having different f_R. As an example, the structure having square diaphragm as a gate of the PZT-FET was simulated, whose f_R is at almost 20 MHz. The PZT-FET MUT ranging its f_R from 10 MHz to 30 MHz can be obtained by dimensional control of the diaphragm.

[1] Y. Q. Chen *et al.*, Electron Device Letters, 33(1), 110, 2011.

Experimental setup

Output vs. pressure property

Frequency property

Schematic diagram of PZT-FET

FEM analysis of f_R for designed MUT diaphragm
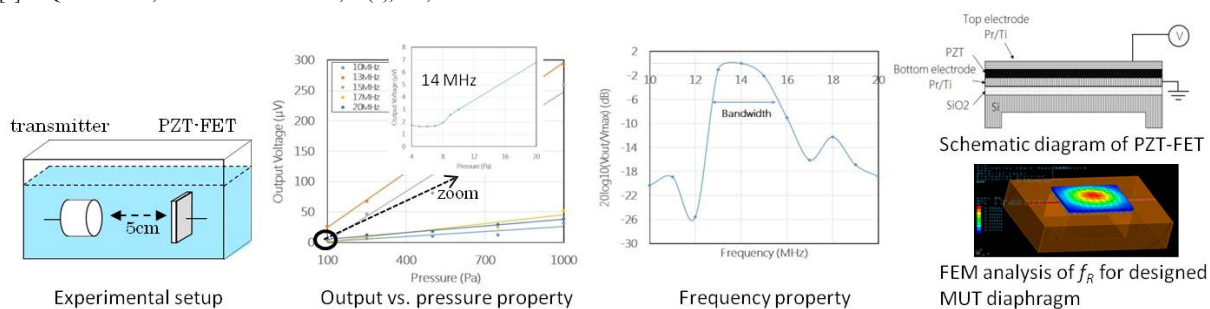
1F - MSD: Novel Imaging Systems

201AF

Friday, October 23, 2015, 01:00 pm - 02:30 pm

Chair: **Piero Tortoli**
Università di Firenze

1F-1

1:00 pm **A Live Color Encoded Speckle Imaging Platform: Towards Bedside Visualization of Complex Flow Patterns**

Alfred C. H. Yu[1], Billy Y. S. Yiu[1], Marcin Lewandowski[2], Mateusz Walczak[2], Damien Garcia[3]; *[1]Medical Engineering Program, University of Hong Kong, Pokfulam, Hong Kong, [2]Department of Ultrasound, Polish Academy of Sciences Institute of Fundamental Technological Research, Warsaw, Poland, [3]Department of Radiology, University of Montreal, Montreal, Canada*

Background, Motivation and Objective

Previously, we have devised a new high-frame-rate flow imaging paradigm called color encoded speckle imaging (CESI) that offers, at sub-ms time resolution, duplex rendering of complex flow dynamics via parallel visualization of flow trajectory (flow speckle motion) and flow velocity (Doppler color coding). Although this new method can provide a more intuitive depiction of vascular hemodynamics as compared to color Doppler, its initial demonstration was merely based on offline processing of pre-beamformed data acquired from plane wave Tx events, and aliasing is still a nuisance factor to be addressed. In this work, we have sought to pursue system and algorithmic innovations that can enable the live use of CESI with alias-free visualization, so as to translate CESI towards clinical use.

Statement of Contribution/Methods

Expanding upon a programmable Tx pulser (SonixTouch), we have reworked the Rx module by incorporating: 1) a new 128-channel parallel acquisition hardware with PCI-e enabled data streaming (RX-DAQ; IPPT, Poland), 2) a CUDA/OpenGL-interoperability enabled GPU platform for high-speed CESI computing and live display (GTX-980). To achieve consistent Doppler estimation, the Posada-Garcia dealiasing algorithm (based on PRF staggering) was adopted by periodically swapping the Tx PRF between 2.25 and 3 kHz through a programmable external trigger. During operation, plane wave pulses were sent at the two PRFs, and channel-domain data were streamed to the GPU at 6 GB/s throughput. Beamforming, CESI processing, and dealiasing were executed on the GPU via CUDA-based parallel computing. Results were streamed to the display live through an OpenGL codec (with 60 fps live refresh rate), and a slow-motion playback function was created to replay buffered high-frame-rate cineloops with no frame drops.

Results/Discussion

Using carotid bifurcation imaging as a demo case, we have achieved live CESI rendering of complex flow dynamics, and can readily replay time-resolved CESI cineloops (2000 fps frame rate) at slow motion to visualize stenotic flow jets and recirculation zones. Also, with the inclusion of Doppler dealiasing in the processing chain, the color coding of CESI cineloops at the stenosis site was resilient against spurious artifacts due to fast flow beyond the Doppler sampling limit (see figure). This platform will next be used in bedside vascular diagnosis.
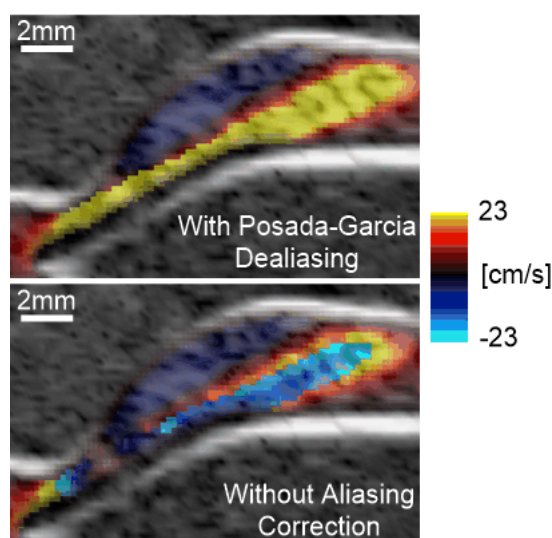
1F-2

1:15 pm **ULA-OP 256: a portable high-performance research scanner**

Enrico Boni[1], Luca Bassi[1], Alessandro Dallai[1], Gabriele Giannini[1], Francesco Guidi[1], Valentino Meacci[1], Riccardo Matera[1], Alessandro Ramalli[1], Monica Scaringella[1], Jacopo Viti[1], Stefano Ricci[1], Piero Tortoli[1]; *[1]Dipartimento di Ingegneria dell'Informazione, Università degli studi di Firenze, Firenze, Italy*

Background, Motivation and Objective

Open scanners have rapidly advanced in the past few years to offer a variety of solutions to ultrasound researchers. Each system presents specific performance in terms of flexibility, number of channels, processing power and raw data storage capability. This paper describes a 256-channel ULtrasound Advanced Open Platform (ULA-OP 256), designed to provide high performance in a small (portable) size.

Statement of Contribution/Methods

ULA-OP 256 is designed to be capable of controlling standard and matrix arrays as well as larger probes with integrated microbeamformers. A modular approach is adopted, which allows the system to host from 1 to 8 front-end (FE) boards interconnected one to each other by 16 SerialRapidIO (SRIO) lanes running at 5Gbit/s each. Every FE board integrates all of the electronics to manage transmit (TX), receive (RX), beamforming and processing for 32 channels. A single FPGA generates 32 independent TX signals, and beamforms the received ultrasound echoes, sampled at 80Msps, according to programmable strategies. The board hosts two 8-cores DSPs (TMS320C6678, by

Texas Instruments) in charge of receiving beamformed data and applying coherent demodulation, filtering, and custom elaboration modules. The cumulative processing power of the installed DSPs is 5000GMAC or 2500GFLOP. A total of 64GB of DDR3 memory (expandable up to 128 GB) are available to store channels raw data, post beamformed data or the signals from any other point of the RX chain. Fast connection to a host PC is guaranteed by a USB 3.0 SuperSpeed link. Probe connection is done through an interchangeable adapter, thus enabling the use of probes with different pin-outs and number of elements. Both channels number and functionalities can be expanded thanks to the modular design and the expansion connectors hosted on the system.

Results/Discussion

A first prototype system has been completed in our laboratory. Up to 256 elements can be independently controlled by an equal number of sigma-delta arbitrary waveform generators and linear power amplifiers producing analog excitation signals up to 150Vpp. Arbitrary groups of active elements can be selected both in TX and in RX. A massive parallel multi-line beamformer was implemented in order to speed up the elaboration in high frame rate imaging techniques. Inside each FPGA, eight beamformers sustain an output rate of 1.8Gsps, enabling up to 4000 fps, depending on the frame size. Sample movies obtained at kHz frame rate will be presented. The system is currently tested with both standard 192- and 256-element probes.

Following the positive experience made with ULA-OP, which is currently used worldwide, we aim sharing this new system with the ultrasound research community. For this reason, we took care of keeping its dimensions (34x30x26 cm) compatible with the system portability.

1F-3

1:30 pm   Implementation of real-time duplex synthetic aperture ultrasonography

Martin Christian Hemmsen[1], Thomas Kjeldsen[2], Lee Lassen[2], Jesper Mosegaard[2], Jørgen Arendt Jensen[1]; [1]*Electrical Engineering, Technical University of Denmark, Lyngby, Denmark,* [2]*Computer Graphics Lab, Alexandra Institute, Aarhus, Denmark*

Background, Motivation and Objective

This paper presents an implementation of a real-time duplex synthetic aperture imaging system on a commercially available hand-held device. The implementation includes real-time wireless reception of ultrasound signals and GPU processing for B-mode and Color Flow Imaging (CFM) imaging. The objective of the work is to investigate the implementation complexity and processing demands for CFM using the principle of Synthetic Aperture Sequential Beamforming (SASB) and a time shift estimator. The overall goal is to include flow imaging capabilities into a synthetic aperture scanner connected to a wireless probe.

Statement of Contribution/Methods

It has previously been shown that 802.11ac technology satisfies the required bandwidth for real-time data transfer for B-mode imaging. In this work the shot sequence is extended to include eight flow emissions transmitted sequentially and repeated 16 times after each block of 183 B-mode emissions. The frame rate is 34 frames/s, imaging a 5 x 6 cm region. The required data throughput is 36.1 MB/s. For prof-of-concept, a wireless probe is emulated using a BK Medical BK3000 ultrasound scanner and a BK Medical 10L2W linear array probe. The scanner is configured to beamform the received echo signals using a fixed receive profile and modulate data to baseband. Data is transferred using Wi-Fi to a Samsung Nexus 9 for refocusing and image processing for both B-mode and CFM imaging. The GPU is instructed to do general purpose computations using the high level API OpenGL ES 3.1.

Results/Discussion

To evaluate the implementation, a laminar flow with a parabolic profile was generated by a flow rig system. Data were acquired and stored for processing in Matlab and on the tablet. Fig. 1a shows the result of the CFM processing. Benchmarking the processing performance for B-mode and CFM imaging showed a total processing time of 58 ms (17 frames/s), which is higher than the acquisition time (29.4 ms). The required data rate for 17 frames/s is 18.1 MB/s which was measured to comply with the data throughput of the Wi-Fi ac link (28.8 MB/s). Fig. 1b shows a screen dump from the real-time processing on the Nexus 9.

In conclusion, an implementation of a real-time duplex synthetic aperture imaging system on a commercially available hand-held device was presented. The implementation demonstrates that SASB can be used for both B-mode and CFM real-time ultrasound imaging.
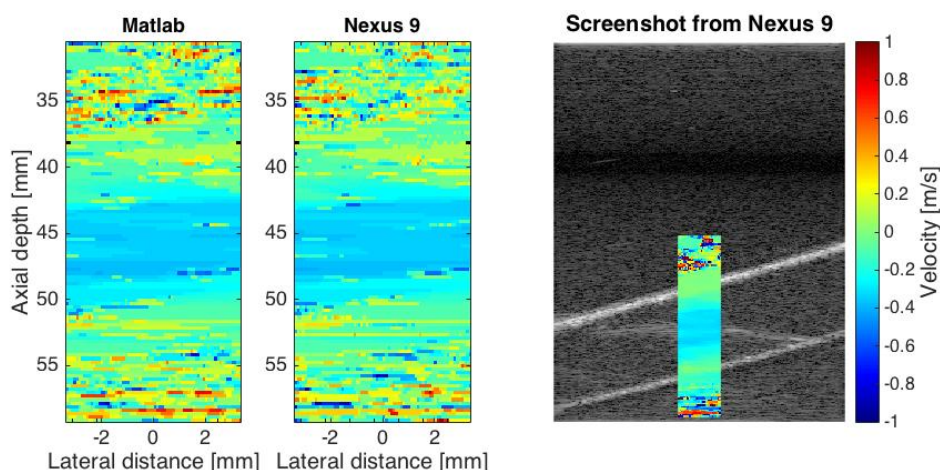
Fig. 1a

Fig. 1b

1F-4

1:45 pm   A New Wireless Hand-held Ultrasound System with Smartphone, Tablet for Mobile Healthcare

Dong-Ki Ahn[1], Suyeol Lee[1], Sung-Hyun Kim[1], **Jeongwon Ryu**[1,2]; [1]*Advanced Medical Technology Laboratory, Healcerion Co., Ltd., Seoul, Korea, Republic of,* [2]*Clinical Neuroscience & Development Lab, Korea Advanced Institute of Science and Technology, Daejeon, Korea, Republic of*

Background, Motivation and Objective

This paper introduces a new wireless hand-held ultrasound device and software applications of iOS and Android for mobile healthcare and point of care diagnosis. Based on concept of alternative of legacy stethoscope, this wireless hand-held Ultrasound system (SONON 300C, Healcerion) can be carried in your pocket with extreme portability.

Statement of Contribution/Methods

The wireless hand-held device is embedded with Front-end and Back-end part, CPU, Wi-Fi module. These functions perform to make final B-mode image though ultrasound signal and image processing then, to transmit these images using Wi-Fi. The application on smartphone and tablet has the functions of ultrasound image viewer and controller of hand-held device.

This paper describes the design method of wireless hand-held ultrasound system in hardware aspect. A hand-held sized ultrasound can create the problems such as hardware noise and temperature rising. Hardware noise should be resolved in various ways such as optimizing of analog circuit design, allocating and partitioning the source of noises, and applying the filter technologies.

Because of an extreme compact structure and power consumption of Front-end part the device generates massive heat. The complex thermal management system is applied to reduce the temperature of device into medical device certification range.

Results/Discussion

The Developed system has the following specifications 78(W) x 219(L) x 38(H) mm3, weight 390g with battery, wireless communication Wi-Fi IEEE 802.11b/g/n, Soft AP (2.4Ghz), Mobile App OS Compatibility iOS and Android, Convex transducer, frequency 3.5Mhz, view depth 4~20cm.

At last, the result of images from actual fabricated application will be showed for evaluating this system.
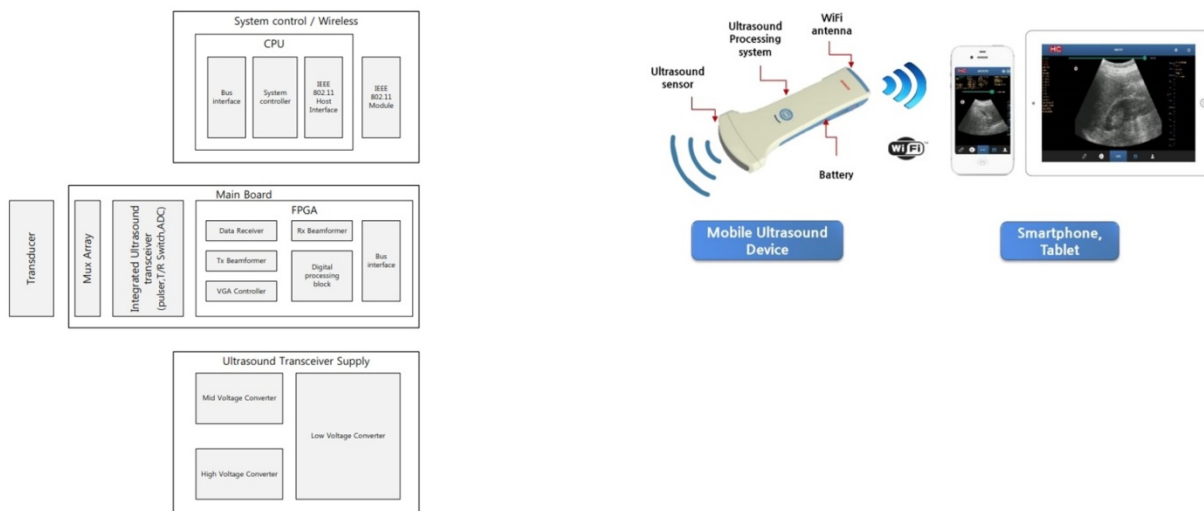
1F-5

2:00 pm   Fast ultrasound signal and image processing on a tablet device

Gabriel Kiss[1], Naiad Hossain Khan[1], Eva Tegnander[2,3], Sturla H. Eik-Nes[2,3], Hans Torp[1]; *[1]Department of Circulation and Medical Imaging and MI Lab, Norwegian University of Science and Technology, Trondheim, Norway, [2]National Center for Fetal Medicine, St. Olavs Hospital, Trondheim, Norway, [3]Department of Laboratory Medicine, Children's and Women's Health, Norwegian University of Science and Technology, Trondheim, Norway*

Background, Motivation and Objective

During the last decade, portable ultrasound devices have been proven beneficial in a variety of situations (e.g. OB/GYN, point of care and cardiovascular applications). The aim of this work is to investigate the feasibility of implementing standard signal and image processing algorithms on a tablet device, instead of the scanner's backend unit. Furthermore the additional benefit of using the tablet's graphical processing unit to offload the CPU intensive tasks and balance the battery consumption was tested.

Statement of Contribution/Methods

Standard tissue and color-flow scan conversion methods were implemented using a combination of vertex/fragment shaders in OpenGL ES 2.0 and displayed using VES-VTK (Kitware Inc.). For each frame the ultrasound data is transferred to the GPU and stored in texture memory, a rectangular window defines the region of interest on the display. With the introduction of OpenGL ES 3.1 in Android 5.0 it has become possible to further optimize the rendering pipeline by using compute shaders. Scan conversion is performed to an intermediate texture with a predefined resolution matching the one of the ultrasound data and smaller than the native display resolution and updates occur when new data arrives from the scanner. Additionally, Doppler spectrum (sliding Hamming window and FFT) and audio (Parks-McClellan FIR-filtering, frequency up mixing and Hann windowing) generation are implemented on the tablet device.

Results/Discussion

A plugin for streaming of raw tissue, color flow and Doppler data over a wired or wireless TCP/IP connection from a VividQ scanner (GE Vingmed Ultrasound) was implemented and data sent to a Nexus 10 (Samsung) tablet device, with native display resolution of 2560x1600. The tissue/color FPS was set to 20 whereas the display FPS was 60. The figure shows battery usages for 2 hours of continuous scanning at different resolutions. A resolution of 512x512 was deemed sufficient for our purposes. For Doppler processing the size of the FFT was set to 256. The overall system delay was measured to be between 60 and 110ms, including TCP-IP transfer times.

Conclusively, most of the backend components of an ultrasound scanner can be implemented on a tablet's GPU. Computer shaders have a significant impact on battery consumption which can be reduced by a factor of up to 3 and as such significantly extend the scanning time of a portable system.
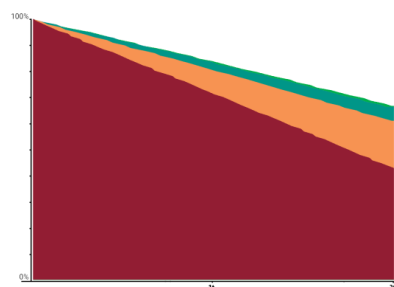
Resolution	Render type	Battery scan convert	Battery display	Battery overall
2560x1600	Continuous	10%	28%	56%
1024x1024	On demand	4%	28%	39%
512x512	On demand	3%	27%	34%
256x256	On demand	3%	26%	34%

1F-6

2:15 pm   Miniature Single-Supply Ultrasonic Imager for Personal Fitness Tracking

Hao-Yen Tang[1], Dongjin Seo[1], Michel M. Maharbiz[1], Bernhard E. Boser[1]; *[1]EECS, UC Berkeley, Berkeley, CA, USA*

Background, Motivation and Objective

Ultrasonic imaging can enable personal fitness tracking by directly measuring both fat and muscle thicknesses. Unlike the traditional bioelectrical impedance analysis, ultrasound can image and identify individual tissue and therefore provide a significantly more fitness relevant data. However, ultrasound transducers must be driven by high-voltage to meet the SNR target, and most high-voltage supplies are too bulky for portable devices.

Instead, we propose an imager that integrates all high-voltage generation and thus achieving small size amendable for consumer electronics. The performance of the system is demonstrated with a series of fat-muscle measurements *in-vivo*.

Statement of Contribution/Methods

In our previous work [1] we demonstrated an ultrasonic interface ASIC with integrated 1.8-to-32V charge-pump for high-voltage generation. Based on the ASIC, we developed an ultrasonic imager, shown in the figure, which consists of the ASIC, off-chip buffer amplifiers, ADC, and a commercially available 4mm × 4mm × 0.8mm PZT transducer. The transducer is encapsulated in PDMS and placed in contact with a human arm. Ultrasonic gel is used to increase coupling during the measurement. Finally an FPGA is used as a digital controller and data capturer. The imager is able to perform pulse-echo measurement with single 1.8V supply.

[1] H. Tang, et. al., "11.8 Integrated Ultrasonic Imaging System for Measuring Body-Fat Composition," *Solid-State Circuits Conference Digest of Technical Papers (ISSCC), 2015 IEEE International*, pp.210,211, 22-26 Feb. 2015.

Results/Discussion

The transducer is driven with 5 pulses of 32V wave at its resonance frequency of 2.8MHz to emit a 170kPa ultrasonic pulse into human tissue. The measured 1-D time-amplitude compensated sonograph of a human arm is shown in the figure. The two peaks representing boundaries between fat, muscle, and bone can be clearly identified, resulting in approximately 6mm and 37mm of fat and muscle thickness, respectively. The entire measurement cycle takes 68μs to image human tissue as deep as 50mm.

In conclusion, we present an ultrasonic imager that is capable of quantifying pulse-echo response and performing measurements *in-vivo* with minimal effort. The overall size of the system is significantly smaller than the traditional ultrasonic imaging system, thanks to a custom ASIC that integrates high-voltage generation.

System Architecture
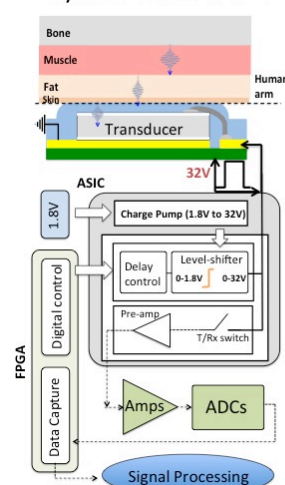
Fat-Muscle measurement
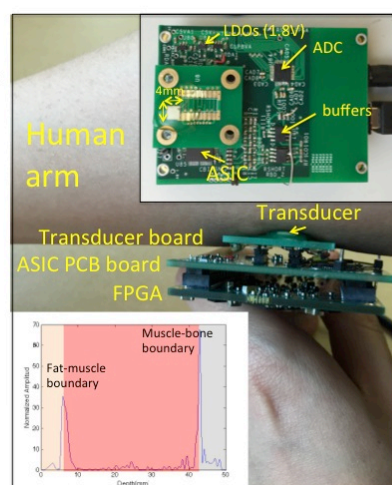
2F-1 - Ultrasonics in Biometrics

VIP

Friday, October 23, 2015, 01:00 pm - 02:30 pm

Chair: **Manfred Weihnacht**
                Leibniz Institute for Solid State and Materials Research

2F-1 _____

1:00 pm   Acoustic-property maps of cornea for improved high-frequency ultrasound corneal biometric accuracy

Daniel Rohrbach[1], Harriet O. Lloyd[2], Ronald H. Silverman[2], Raksha Urs[2], Jonathan Mamou[1]; *[1]Lizzi Center for Biomedical Engineering, Riverside Research, New York, NY, USA, [2]Department of Ophthalmology, Columbia University Medical Center, New York, New York, USA*

Background, Motivation and Objective

Early diagnosis of keratoconus, a progressive disease characterized by corneal thinning and bulging, is important for avoiding corneal refractive surgery and for treatment planning. Current gold-standard procedures rely on surface topography and corneal-thickness measurements using high-frequency ultrasound (HFU) or optical coherence tomography (OCT). In a previous study of 20 normal corneas, OCT measurements of epithelial thickness were systematically thinner than those obtained from 40-MHz HFU measurements (Fig 1 a). In the present study, acoustic impedance (Z), attenuation (a) and speed of sound (c) of the corneal epithelium and stroma were independently measured using a scanning acoustic microscope (SAM) to investigate the discrepancy in thickness estimates.

Statement of Contribution/Methods

Corneas of two pigs were snap-frozen and 12-μm thick sections were scanned using a custom-built SAM with an F-1.16, 250-MHz transducer (160-MHz bandwidth). Radio frequency (RF) signals were digitized at 2.5 GHz using a 12-bit oscilloscope. A frequency-domain, model-based approach was used to process RF signals and derive 2D maps of c, Z and a, with a spatial resolution of 7 μm. These maps were used to model HFU propagation *in silico* and to provide more-accurate estimates of corneal and epithelial thicknesses

Results/Discussion

HFU significantly overestimated epithelial thickness by 1.2 to 2.2 μm (Fig 1a, p < 0.01, paired t-Test) because a single value of c (1640 m/s) was used to estimate thickness for all corneal layers. SAM showed that the value of c (Fig 1 b) in the epithelium is substantially lower (i.e., 1539 ± 18 m/s) than the value of c in the stroma (i.e., 1591 ± 28 m/s), which constitutes 90% of corneal thickness (c values were increased by 30 m/s to account for room versus body temperature). Z and a values for epithelium and stroma were found to be $Z_E = 1.59 \pm 0.04$ Mrayl, $Z_S = 1.58 \pm 0.07$ Mrayl, $a_E = 1.88 \pm 0.8$ dB/MHz/cm and $a_S = 3.86 \pm 2.1$ dB/MHz/cm, respectively. After using the SAM-based c values, no significant difference between HFU and OCT thickness determinations could be found (Fig 1a) corroborating that assumption of a constant value of c for all layers is incorrect. SAM permitted obtaining reliable thickness measurements because it provides accurate acoustic–property estimates at fine resolution.
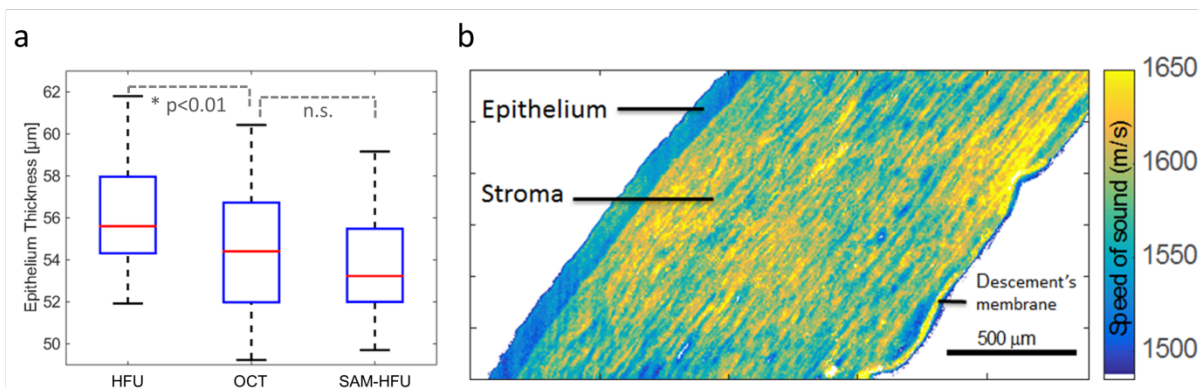
Figure 1 (a) Boxplot with epithelium thickness for HFU, OCT and SAM based corrected HFU (SAM-HFU) measurement. Difference in thickness between HFU and OCT was significant. (b) 250 MHz scanning acoustic microscope (SAM) image of 12-μm cryosection of unfixed pig cornea. Pixel colors represent speed of sound.

FRIDAY ORAL

1:15 pm   Theory and Experimental Analysis of Scratch Resistant Coating for Ultrasonic Fingerprint Sensors

Stephanie Fung[1], Yipeng Lu[1], Hao-Yen Tang[2], Julius M. Tsai[3], Michael Daneman[3], Bernhard E. Boser[2], David A. Horsley[1]; *[1]Department of Mechanical and Aerospace Engineering, University of California, Davis, CA, USA, [2]Department of Electrical Engineering and Computer Sciences, University of California, Berkeley, CA, USA, [3]Invensense, San Jose, CA, USA*

Background, Motivation and Objective

Ultrasonic imaging for fingerprint applications is on the rise due to better tolerance of external conditions and high spatial resolution compared to typical optical and solid state sensors respectively. Similar to current fingerprint sensors, the performance of such ultrasonic imagers is sensitive to physical damage. Typical single-chip fingerprint sensors use a soft thin-film protective layer which is susceptible to scratches and deformation under normal use. Harder and thicker materials may also be used to protect the sensor, but many of these hard coatings would reflect most if not all of the ultrasound signal due to the difference in acoustic impedance of the material. However, with a sufficiently thin layer of the protective material coated on coupling material, it is possible to transmit and receive ultrasound while protecting the fingerprint sensor from performance degrading physical damage. Therefore it is important to understand the theory behind transmission effects of protective coating for ultrasonic fingerprint sensors.

Statement of Contribution/Methods

In this work, we present the analytical theory behind effects of transmitting ultrasound through a thin film of scratch resistant material. When this film is adequately thin, the transmission coefficient of the interface stack is dominated by impedance values from other interface layers. This is supported by finite element method (FEM) simulation and experimental results. Nominal 1 um layer of Al_2O_3 was deposited on polyimide adhesive substrate, which was subsequently adhered to a thin layer of PDMS. This stack was submerged into inert fluid and placed on top of a piezoelectric micromachined ultrasound transducer (PMUT) array pulsed at 20MHz while a needle hydrophone was used to measure transmitted pressure through the medium. This model emulates a thin protective coating with high acoustic impedance mismatch.

Results/Discussion

Experimental results indicate transmission through 1 μm thick Al_2O_3 measured to be 96% of transmission without, which matches both theory and FEM simulation well. This is depicted in the included figure. Consequently, feasibility is demonstrated of ultrasonic transmission through acoustic impedance mismatched material when sufficiently thin. This provides a guide for designing sensor protection when using materials of vastly different acoustic impedance values.
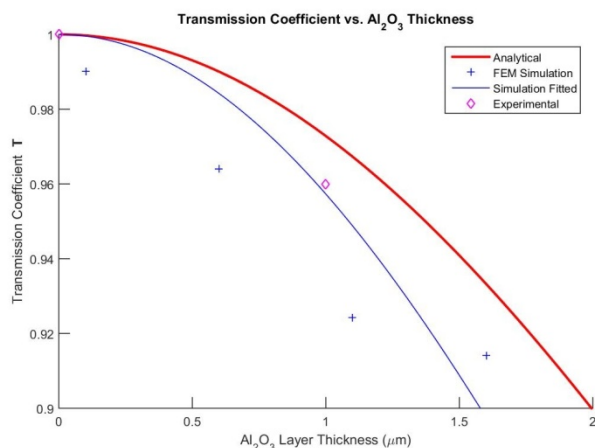
2F-3 _____

1:30 pm Ultrasonics and Biometrics: 130 years past Galton

James. L. Wayman, Ph.D., FIEEE, IEEE Distinguished Lecture, Office of Research, *San José State University, USA, 95192-0025*

Sir Francis Galton can be considered the original nexus of ultrasonics and biometrics as he both discovered the dog whistle and founded the journal Biometrika.   In the intervening 130+ years, both fields have diversified widely, with the addition of imaging technologies to ultrasonics and automated human recognition technologies to biometrics.   Current applications of ultrasonics to automated human recognition are limited to contact-based finger imaging (fingerprinting), principles of which will be described in this talk.   More general "biometric" technologies are now used widely in government applications, raising some very interesting fundamental questions involving persons, bodies, identities, and privacy, which will also be discussed.   We will close by suggesting some areas in which ultrasonics might make a strong contribution to the future of biometrics.

2F-4 _____

2:00 pm   Towards Spoof Proof Fingertip Biometrics using Ultrasound

Rainer M Schmitt[1], Devin Delong[1], Andrea C Casanova[1], Joe Zeichman[1], Yanli Xie[1], Heng Zhao[1], Chen-Wei Wei[1], *[1]R & D, Sonavation Inc.*

Fingerprinting is the oldest, most simple and widely used method for human identification. Implemented in mobile devices, fingerprints are utilized to enable financial transactions at an unprecedented scale. However, fingerprints can be spoofed as demonstrated recently by e.g. the Chaos Computer Club [1]. Over the last decade, Sonavation has developed an ultrasound-based, two-step concept utilizing both fingerprinting and subcutaneous imaging of fingertip tissue anatomy and morphology for identification. The final sensor combines acoustic impediography for fingerprinting and phased array pulse echo (P/E) imaging to relate fingertip anatomy such as vasculature and bone shape to the fingerprint map.

The sensor is based on 1-3 piezo-composite (50 µm) in which each piezo-element in the rectangular matrix is utilized as an individual sensor, which is addressed by a connecting scheme of rows (top electrodes) and columns (bottom electrodes) to the electronic control and data acquisition hardware. As outlined previously[2,3] for fingerprinting, the sensor is driven at the serial pillar resonance in which the current through the pillar reflects the acoustic load (ridge or valley) providing a fingerprint of 500 dpi resolution. Combining 64 electrodes into a transmit aperture and up to 64 electrodes into a receive aperture, an effective pulse- echo aperture is created by the intersection of the orthogonal apertures which can be 2D shifted across the available sensor matrix for pulse echo RF data acquisition. Doppler, as well as backscatter imaging, is implemented to extract subcutaneous information.

Active sensor matrices of 384 x 256 (256 x 256) have been manufactured and being implemented for acoustic impediography. Figure 1. Subcutaneous imaging is under test with the Verasonic 256 channel Vantage system (128 xmit, 128 rcv channels), fig 2 presents a first image of a metal wire in gelatin. A full scale R&D system implements both impediography and P/E imaging is in its final stage of testing. Hardware is co-designed with FEM, from which the imaging system performance is predicted: using a 5 V single sinus burst of 16.4 MHz focused at 4.5 mm depth, peak pressure P_{sptp} of ~ 700 KPa is achieved with a azimuthal 6dB beam width of 185 µm and an elevation beam width of 3 mm.

"CCC | Chaos Computer Club Breaks Apple TouchID." *CCC | Chaos Computer Club*. N.p., n.d. Web. <http://www.ccc.de/en/updates/2013/ccc-breaks-apple-touchid>.

Impediography: Imaging Surface Acoustic Impedance Using 1-3 Piezo-Composite for Integrated fingerprinting.
RM Schmitt, J. Owen
IEEE ECTC-2011 Symp Proc p 1296-1300.

Model Based Development of a Commercial, Acoustic Fingerprint Sensor.
Rainer M Schmitt (Invited speaker), Joseph Zeichman, Andrea C. Casanova and Devin Delong
IEEE International Ultrasonics Symposium, Oct 7-10, 2012, Dresden, Germany

FRIDAY ORAL
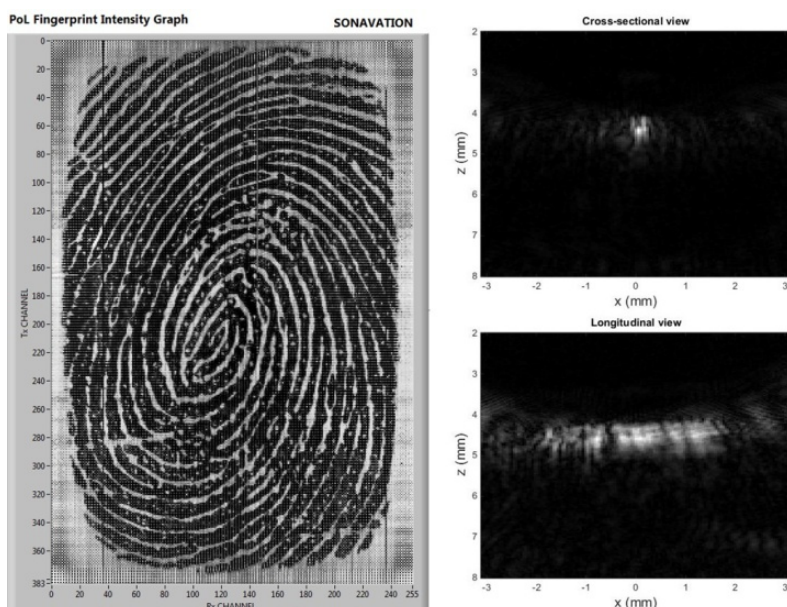
3F - MEL: Mechanical Characterization of the Heart

201BC

Friday, October 23, 2015, 01:00 pm - 02:30 pm

Chair: **Elisa Konofagou**
Columbia University

3F-1

1:00 pm   Semi-3D strain imaging in normal and LVAD supported *ex vivo* beating hearts

N.J. Petterson[1], K.A.M.A. Pennings[1], S. van Tuijl[2], M.C.M. Rutten[1], F.N. van de Vosse[1], R.G.P. Lopata[1]; *[1]Biomedical Engineering, Eindhoven University of Technology, Eindhoven, Netherlands, [2]LifeTec Group, Eindhoven, Netherlands*

Background, Motivation and Objective

End stage heart failure is often treated with a left ventricular assist device (LVAD), when donor hearts are unavailable. Monitoring function of these patients is challenging due to the lack of suitable imaging techniques. Cardiac strain imaging (CSI) is a powerful technique which is able to quantify and localize cardiac defects, however, validation and reproducibility remain major issues. Simulations and phantoms are often not realistic, whereas *in vivo* measurements lack the ground truth and crucial information on governing parameters like pressures and flow, both related to the strains measured.

In this study, semi-3D CSI was performed in normal and LVAD supported *ex vivo* porcine hearts. The platform was used to quantify the reproducibility of CSI and examine the feasibility of non-invasive assessment of cardiac function in LVAD patients.

Statement of Contribution/Methods

A state-of-the-art platform was used, in which *ex vivo* beating porcine hearts were attached to a mock loop (LifeTec Group, NL). The setup was water-immersed to enable ultrasound imaging. Five normal hearts were examined as well as three hearts supported by an LVAD at varying pump speeds. A Mylab 70 scanner (ESAOTE Europe, NL), equipped with a curved array transducer (fc = 2.7 MHz) and a radio frequency (RF) interface was used to image the left ventricle. Multiple heartbeats were acquired for five short axis views, ranging from apex to mitral valve. The cardiac wall was segmented and a coarse-to-fine strain imaging algorithm was used on the RF data to acquire 2D displacement fields, which were converted into radial and circumferential strain (rate) images of the left ventricular wall. For each heart, a total of five 3D strain images of the left ventricle were reconstructed using the short-axis slices.

Results/Discussion

Strain analysis of multiple heartbeats was highly reproducible, see figure. However, differences were found between hearts, due to biological variation and condition of the hearts. LVAD-supported hearts showed a decrease in strain and strain rate with higher pump speeds. The images revealed very dyssynchronous patterns, possibly due to implantation trauma. Future work should include translation of the measured parameters into quantitative assessment of cardiac function of the supported heart, and validation in a long-term patient study.
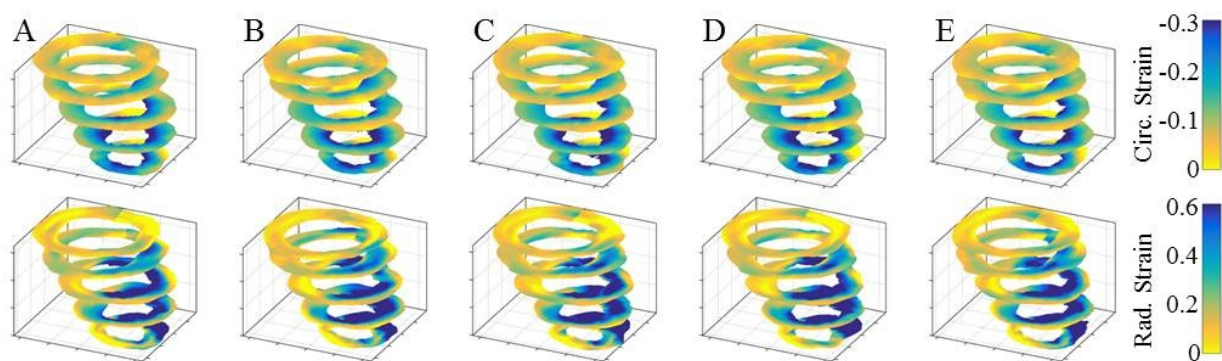
Figure: 3D reconstructions showing circumferential (upper row) and radial (lower row) strain at end systole of five different heartbeats (A-E) of the same heart.

3F-2

1:15 pm   Myocardial passive shear wave detection

Hendrik Vos[1,2], Bas van Dalen[3], Johannes Bosch[1], Antonius van der Steen[1,2], Nico de Jong[1,2]; *[1]Biomedical Engineering, Erasmus MC, Rotterdam, Netherlands, [2]Acoustical Wavefield imaging, Delft university of Technology, Netherlands, [3]Cardiology, Erasmus MC, Rotterdam, Netherlands*

Background, Motivation and Objective

Accurate echocardiographic diagnosis of diastolic dysfunction is needed to guide heart failure treatment. Despite expected correlation between diastolic dysfunction and myocardial stiffness, only few studies have addressed shear waves to measure the myocardial stiffness non-invasively. We explore the naturally-occurring shear waves in the porcine septal wall caused by aortic and mitral valve closure with high frame rate recordings and subsequent shear wave imaging [Kanai, IEEE TUFFC 2005; Brekke et al., UMB 2014]. The aim is to estimate their propagation velocity.

Statement of Contribution/Methods

We examined 34 Goettingen minipigs (37±7 kg), of which 18 were a model for diastolic heart failure by induced diabetes mellitus, and 16 controls. Each pig was in principle examined at baseline (1 yr age), midpoint (+ 3 months), and before sacrifice (+ 6 months). In total we recorded 72 useable datasets. Each dataset contained 2 to 4 heart beats in a trans-thoracic parasternal long-axis view. Raw data were acquired with a research scanner (SonixTOUCH, Ultrasonix/Analogic Ultrasound) and DAQ module for offline data processing. The transmission was a 2.5 MHz, 1.5 cycle pulse in a diverging beam. A full frame was constructed from each transmit, yielding a frame rate of 4,000/s. Local tissue Doppler velocity (TDI) was obtained with an IQ-based autocorrelation technique. Wave phenomena in the TDI were displayed in a 2D map as function of time and distance (fig 1). Manual tracking, cross-correlation, and the Radon transform were tested to extract the wave propagation velocity. Wave dispersion was investigated through a 2D Fourier transform method.

FRIDAY ORAL

Results/Discussion

The waves after mitral valve closure had a median velocity of 1.8 m/s (90% interval: 1.5 - 3.0 m/s) , while the waves after aortic valve closure had a median velocity of 3.7 m/s (2.2 - 6.1 m/s; fig 2). This is close to values reported earlier with radiation-force based intra-cardiac shear wave measurements in healthy pigs (1.4 m/s and 4.1 m/s, respectively [Hollender et al., UMB 2012]). The 2D Fourier transform method generally showed an increasing phase speed with shear wave frequency. Such dispersion is expected from asymmetric Lamb waves in the septal wall, but the propagation velocities found were larger than expected from the Lamb wave model when inserting viscoelastic values from literature [Nenadic et al., PMB 2011].
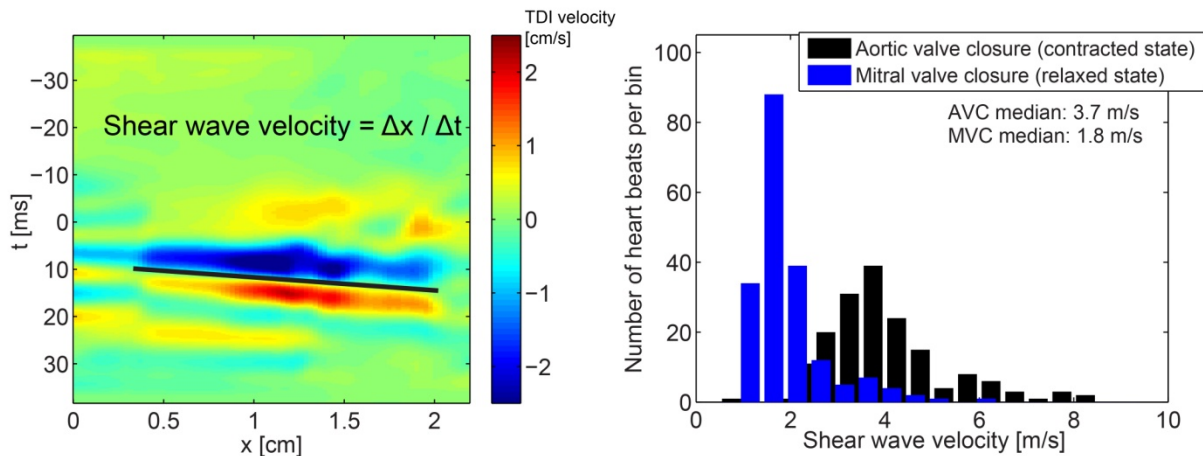
3F-3

1:30 pm   A Systematic Investigation of Feasible Acoustic Windows and the Impact of Myocardial Anisotropy for In Vivo Human Cardiac Shear Wave Elastography

Pengfei Song[1], Xiaojun Bi[2,3], Daniel C. Mellema[1], Armando Manduca[1], Matthew W. Urban[1], James F. Greenleaf[1], Shigao Chen[1]; *[1]Department of Physiology and Biomedical Engineering, Mayo Clinic College of Medicine, Rochester, Minnesota, USA, [2]Department of Cardiovascular Diseases, Mayo Clinic College of Medicine, Rochester, Minnesota, USA, [3]Department of Medical Ultrasound, Tongji Hospital Medical College, Wuhan, Hubei, China, People's Republic of*

Background, Motivation and Objective

Direct and quantitative assessment of left ventricular end-diastolic stiffness (LVEDS) with ultrasound shear wave elastography (SWE) provides a potential tool for diagnosis of diastolic heart failure (DHF). Recent improvements of shear wave detection techniques with pulse-inversion harmonic imaging (PIHI, Song, IEEE TMI, 32(12), 2013) realized *in vivo* transthoracic measurement of human LVEDS. This study aimed at systematically investigating the feasible echocardiography acoustic windows for *in vivo* cardiac SWE and studying the impact of myocardial anisotropy on shear wave speed (SWS) when imaging different LV segments from different views.

Statement of Contribution/Methods

Ten healthy volunteers were recruited and scanned 3 times on 3 different days. Cardiac SWE with PIHI shear wave detection was implemented on a Verasonics Vantage system and a cardiac transducer P4-2 (Philips Healthcare). The LV wall could be positioned orthogonally to the push beam under the parasternal short-axis and long-axis views. The base, mid, and apex segments of the LV anterior wall were measured using both short-axis and long-axis views; the posterior LV wall was only measurable with short-axis apical view. A B-scan sequence and a SWE sequence were ECG-gated to fast capture a reference B-mode image and LVEDS during end-diastole. Five repeated measurements were acquired for each view/segment combination. Two-dimensional (2D) SWS maps of the myocardium were reconstructed and used to measure LVEDS.

Results/Discussion

The success rates (defined by at least 2 successful SWS measurements out of 5 trials) of LVEDS measurements were 77%, 67%, 73%, 57%, 40%, 43%, and 80% for base short-axis, base long-axis, mid short-axis, mid long-axis, apex short-axis, apex long-axis, and apex posterior wall short-axis, respectively. The SWS measurements are summarized in Fig. 1(a). Figure 1(b) shows example 2D SWS maps. The median SWS were 1.8, 1.24, 1.72, 1.31, 1.93, 1.6, and 1.7 m/s for the 7 views. Student's t-tests showed that the short-axis LVEDS were all significantly different from the long-axis measurements due to myocardial anisotropy. The differences between long-axis and short-axis SWS are in good agreement with a previous open-chest sheep heart study (Couade, IEEE TMI, 30(2), 2011). These results provide important guidance for future clinical studies of using cardiac SWE for DHF diagnosis.
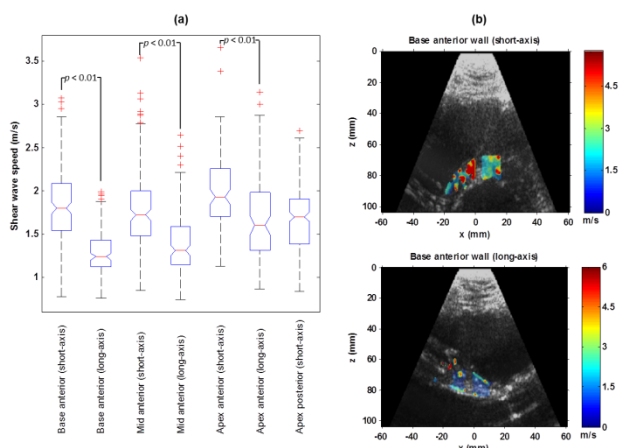
Figure 1. (a) Standard boxplots of SWS measurements of LVEDS at different LV segments from different scan acoustic windows. (b) Example 2D SWS maps overlaid on B-mode images of the LV base anterior wall from one healthy volunteer. The short-axis view (upper panel) imaged the same segment of the LV wall as the long-axis view (lower panel) with a 90° transducer rotation, yet the myocardium appears to be stiffer in the short-axis view. This reveals the impact of myocardial anisotropy on SWS measurements when imaging from different acoustic windows.

3F-4

1:45 pm   **Investigation of the effects of myocardial anisotropy for shear wave elastography at different frequencies using acoustic radiation force and harmonic vibration**

Matthew Urban[1], Bo Qiang[1], Pengfei Song[1], Ivan Nenadic[1], Shigao Chen[1], James Greenleaf[1]; *[1]Physiology and Biomedical Engineering, Mayo Clinic College of Medicine, Rochester, Minnesota, USA*

Background, Motivation and Objective

Shear wave elastography with acoustic radiation force (ARF) or harmonic vibration (HV) has been applied in animals and humans to evaluate myocardial material properties. The anisotropic myocardial structure presents a unique challenge to wave propagation methods because the fiber direction changes through the wall thickness.

Statement of Contribution/Methods

We constructed systolic and diastolic finite element models (FEMs) and performed an experiment on an *ex vivo* porcine heart. Both models were constructed with multiple elastic, transverse isotropic layers with a shear wave velocity (SWV) along and across the fibers where each layer has 1 mm thickness. The orientation of the muscle fibers was changed for each layer ranging from -50° to 80° from top to bottom. The systolic FEM had 20 layers and SWV along and across the fibers of 5.0 and 2.5 m/s, respectively. The diastolic FEM had 10 layers and SWV along and across the fibers of 2.0 and 1.0 m/s, respectively. Harmonic excitations at 30, 50, 100, and 200 Hz and an impulsive force were used.

An *ex vivo* porcine heart was tested using ARF excitations with a transesophogeal probe driven with a Verasonics ultrasound system applied directly to the left ventricular wall. The motion data was analyzed using a two-dimensional Fourier transform to evaluate the SWV at 50, 100, 200, and 300 Hz.

Results/Discussion

We evaluated the measured orientation of the fibers in each layer by evaluating the angle with the highest SWV. The 30 and 50 Hz results showed little or no variation in the measured orientation angle in the layers. The 100 and 200 Hz results showed some variation of the orientation with respect to the layer. The impulse simulation results showed good agreement with the true orientations except near the top and bottom boundaries. The values of SWV were found to have different levels of bias depending on the excitation. The experimental results in the *ex vivo* heart showed similar trends as the FEM model results where the waves at lower frequencies had lower sensitivity to fiber direction (Fig. 1).

This multi-layered anisotropic model demonstrates how to resolve different anisotropic layers in the myocardium using ARF or HV while also revealing that using lower frequencies results in measurements that are less sensitive to anisotropy variation through the thickness of the myocardial wall.
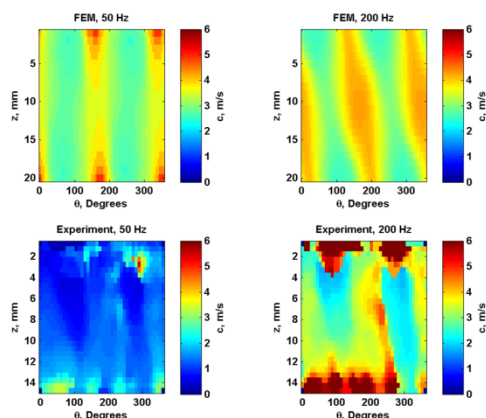
Figure 1. Comparison of systolic FEM results at 50 and 200 Hz and experimental results from the ARF excitation in the porcine heart at 50 and 200 Hz. At 50 Hz there is minimal sensitivity to the fiber direction changing through the thickness of the sample, while at 200 Hz, there is a variation of the fiber direction that can be observed in the FEM and experimental results.

3F-5

2:00 pm   **Repeatability of Systolic-to-Diastolic Displacement Ratios in Transthoracic Cardiac ARFI Imaging**

Vaibhav Kakkad[1], Lily Kuo[1], David Bradway[1], Joseph Sivak[2], Joseph Kisslo[2], Gregg Trahey[1]; *[1]Biomedical Engineering, Duke University, Durham, North Carolina, USA, [2]Cardiology, Duke University Hospital, Durham, North Carolina, USA*

Background, Motivation and Objective

Transthoracic echocardiography is widely used to assess anatomical and physiological features of the heart. However, acoustic radiation force based methods such as ARFI, SWEI are yet to be clinically established for cardiac applications. We have previously shown the feasibility and safety of transthoracic cardiac ARFI on a research scanner but have been limited due to cardiac motion, depth of penetration and poor tracking SNR. This work aims to address these challenges on a commercial US system, validate the robustness of TTE ARFI and translate this technique into clinical practice.

Statement of Contribution/Methods

M-mode ARFI data was acquired, within FDA limits, on a 4V1c phased array using the Siemens Acuson SC2000. Following IRB approval, data was acquired on 5 healthy volunteers and 2 post heart transplant in parasternal long (PLAX) and short axis (PSAX) views. Displacement measurements in the inter ventricular septum were made at 20 Hz over the cardiac cycle and registered to ECG. Harmonic tracking and motion filtering were employed. Displacement data and the ECG were used to calculate systolic-to-diastolic ratios. In an ongoing study we are comparing this ratio between healthy volunteers and subjects who are several years post heart transplant.

Results/Discussion

The stability of displacement estimates was quantified using the standard deviation of displacements (over the cardiac cycle) for repeated acquisitions. This mean value of this metric was found to be 0.58 µm.

Systolic-to-diastolic displacement ratios were computed for the 5 healthy volunteers and were measured to be 2.22±0.33 (n=34) in the PLAX view and 2.05±0.31 (n=28) in the PSAX view. These results demonstrate the potential of transthoracic cardiac ARFI as a robust tool for non-invasive assessment of cardiac elasticity.
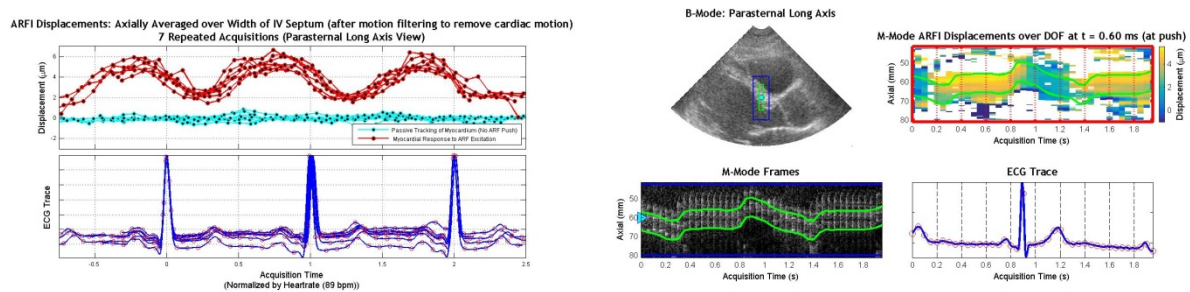
3F-6

2:15 pm   SNRe Improvements in Two-Dimensional Cardiac Strain Estimation using Coherent Compounding *in silico* and *in vivo*

Ethan Bunting[1], Julien Grondin[1], Clement Papadacci[1], Elisa Konofagou[1,2]; [1]*Department of Biomedical Engineering, Columbia University, New York, New York, USA,* [2]*Department of Radiology, Columbia University, New York, New York, USA*

Background, Motivation and Objective

Myocardial elastography has been shown capable of estimating and imaging radial and circumferential strains for the detection and localization of abnormal myocardial contraction resulting from ischemia and/or arrhythmia. Estimation in the transverse (lateral) direction is inherently hindered by the lack of usable phase information that exists between reconstructed radiofrequency (RF) signals. Diverging beam transmissions have been developed to increase frame-rate and decrease frame-to-frame decorrelation at the cost of spatial resolution. Recently, coherent compounding has been proposed as a technique to increase the spatial resolution of diverging beam sequences with only a moderate tradeoff in frame-rate. To date, there has been no investigation that has studied the effect of compounding on two-dimensional cardiac strain estimation *in vivo*.

Statement of Contribution/Methods

Both simulations and *in vivo* studies were performed to determine the effect of coherent compounding on the precision of two-dimensional cardiac strain estimation. Simulations were performed using *FieldII* of a circular myocardial structure under uniform radial contraction. *In vivo* data was collected using a Verasonics V-1 system in both open chest canines (n=3) and in healthy, human volunteers (n=3). A 5-angle compounding sequence and single transmit diverging sequence were used to acquire *in vivo* RF signals at 500 Hz for the duration of the systolic phase. 2-D inter-frame displacements were estimated with a normalized cross-correlation function using a 1-D window in a 2-D search. 2-D cumulative strains were then obtained from the inter-frame displacements by tracking the myocardial points through time and computing the Lagrangian strain tensor. Quantitative analysis was performed on the basis of the conditional expected value of the elastographic signal-to-noise ratio, $E(SNRe|\varepsilon)$, which was obtained by calculating the SNRe of each strain estimation at every point in the myocardium at end-systole.

Results/Discussion

Results from both simulations and in vivo acquisitions indicated increased precision in strain estimation using the 5-angle compounding compared to a single diverging transmission, especially for lateral strain estimation. Improvement in lateral strain estimation precision was also more variable compared to axial strain estimation. Peak $E(SNRe|\varepsilon)$ increased by 1.0-11% for axial strains and by 5.8-89% for lateral strains. Furthermore, qualitative analysis of end-systolic strain images revealed more physiological strain distributions, i.e. uniform radial thickening, were obtained in healthy subjects using the compounding sequence. This initial study demonstrates the important role of compounding for increasing SNRe of high frame-rate, 2-D cardiac strain estimation without a significant tradeoff in frame-rate. This work was supported in part by NIH R01-EB006042 and R01-HL114358.

FRIDAY ORAL

4F - MSP: Compressive Sensing and Image Reconstruction

201DE

Friday, October 23, 2015, 01:00 pm - 02:30 pm

Chair: **Svetoslav Nikolov**
          BK Medical

4F-1

1:00 pm   Joint compressive sampling and deconvolution in ultrasound medical imaging

Zhouye Chen[1], Adrian Basarab, Denis Kouamé[1]; [1]*IRIT, UMR CNRS 5505, University of Toulouse, France*

Background, Motivation and Objective

Compressive Sampling (CS) and ultrasound (US) image deconvolution are two research tracks explored in the literature. CS seeks to reduce the volume of acquired data, but an image quality degradation of the restored images from a low number of samples was observed in practice. Deconvolution aims at improving the quality (spatial resolution, contrast, SNR) of US images. Combining these two frameworks (Compressive Deconvolution (CD)) is an interesting alternative for high quality CS reconstructions. The benefit of CD is the joint volume reduction of the acquired data and the image quality improvement. We propose herein a novel scheme of CD and its application to US imaging.

Statement of Contribution/Methods

The model of CD is given in eq. (1) (top of Fig 1), where **y** is the RF image, **x** is the tissue reflectivity function (TRF) to be estimated, **H** is a matrix representing the PSF, **Φ** is a rectangular random matrix commonly used in CS and **n** is a Gaussian noise. To solve (1), we reformulate it as the optimization problem in (2): the first term represents the data fidelity, the second enforces the sparsity of RF data in wavelet domain **ψ** [Liebgott, Ultrasonics'11] and the third imposes a Laplacian prior on the TRF [Michailovich, IEEE TIP'07]. The resulting restoration problem is far more difficult than those addressed in CS or deconvolution separately.

To solve (2), we propose a novel numerical scheme based on the alternating direction method of multipliers that allows us to split the three terms in (2) into three sub-problems and to solve them separately.

Results/Discussion

We compare our method with the only existing approach on CD [Amizic, IEEE TIP'13] **on simulated data**. The results (Fig 1 and Table 1) show that our method performs better in terms of PSNR and Structure SIMilarity for different data reduction ratios. Our method was then applied to **in vivo data** showing a mouse bladder acquired with a 20 MHz single-element probe (Fig 2). The PSF was previously estimated following [Michailovich, IEEE TMI'05]. Despite the data reduction, we remark that our method is able to restore images with better contrast (CNR is computed between the two red blocks in Fig 2) than the native B-mode image.

Future work will explore different priors on the TRF (e.g. generalized Gaussian [Alessandrini, IEEE UFFC'11]), compressive blind deconvolution (joint TRF and PSF estimation) and validation on further experimental data.

Equations

$$y = \Phi H x + n \qquad (1)$$
$$\hat{x} = \arg\min_x \left[\|y - \Phi H x\|_2^2 + \alpha \|\Psi H x\|_1 + \beta \|x\|_1 \right] \qquad (2)$$

Fig.1 Comparison results
(SNR=40dB, CS ratio=80%)

Table. 1 Quatitative comparison results
(Average metrics for 10 experiments for each CS ratio)

Fig.2 Results on in-vivo data

		CSratio	20%	40%	60%	80%			CSratio	20%	40%	60%	80%
[Amizic, IEEE,TIP'13]	SSIM		17.79	48.67	67.35	74.35	Proposed	SSIM		23.98	56.53	70.86	77.92
	PSNR		19.80	21.57	22.39	22.89		PSNR		21.09	22.97	23.79	24.45

4F-2

1:15 pm   Compressed sensing reconstruction of line-wise sub-sampled 3D echographic images based on dictionary learning: an experimental study

Oana Lorintiu[1], Hervé Liebgott[1], Adeline Berndard[1], Olivier Bernard[1], Denis Friboulet[1]; [1]*Université de Lyon, CREATIS ; CNRS UMR5220 ; Inserm U1044 ; INSA-Lyon ; Université Lyon 1, Lyon, France*

Background, Motivation and Objective

In 3D US imaging, the number of RF lines that must be acquired to sweep the whole volume can be extremely high, thus leading to low frame rate. In this context, the recently introduced compressed sensing (CS) theory offers the perspective of reducing the amount of data acquired.

The objective of this study is to investigate the feasibility of compressive sensing on 3D ultrasound experimental data using a learned overcomplete dictionary and a line-wise subsampling scheme.

Statement of Contribution/Methods

Successful CS reconstruction implies the data should have a sparse decomposition in a basis, frame or dictionary. Thus, we use learned overcomplete data-driven dictionaries that have proven to optimally represent the US images.

Conventional CS reconstruction uses random point-wise sampling. However, due to the physical constraints of the US instrumentation, this point-wise sampling is not achievable in practice. Thus, we focused on a strategy that consists in randomly skipping the acquisition of several RF lines. The main interest of this strategy relies on the fact that it is easily implementable in practice and offers the perspective of increasing the frame.

Results/Discussion

For the acquisition of the volumes we use the Ultrasonix MDP research platform equipped with the 4DC7-3/40 Convex 4D transducer. The central frequency of the probe was of 5 MHz and the signals were collected using a 40 MHz sampling rate. Using this system we imaged the ex vivo organs purchased from the store: 3 pig brains and 3 sheep hearts.

CS reconstruction was performed on a sub-sampled dataset by removing 20 to 80% of the original samples using the proposed line-wise subsampling and a point-wise sub-sampling scheme.

The figure shows the reconstruction NRMSE errors as a function of the number of removed samples for the ex vivo brain and heart US volumes. The error associated to the line-wise sampling is larger but close to the one corresponding to the point wise sampling. The K-SVD dictionary yields the smallest error, whatever the subsampling rate.

This study thus demonstrates that CS using overcomplete learned dictionaries can be applied to experimental 3D ultrasound imaging to reduce the volume of data needed and speed up the acquisitions. High quality reconstruction can be obtained using only 50% of the initial data, potentially leading to a frame rate two times higher than the standard.
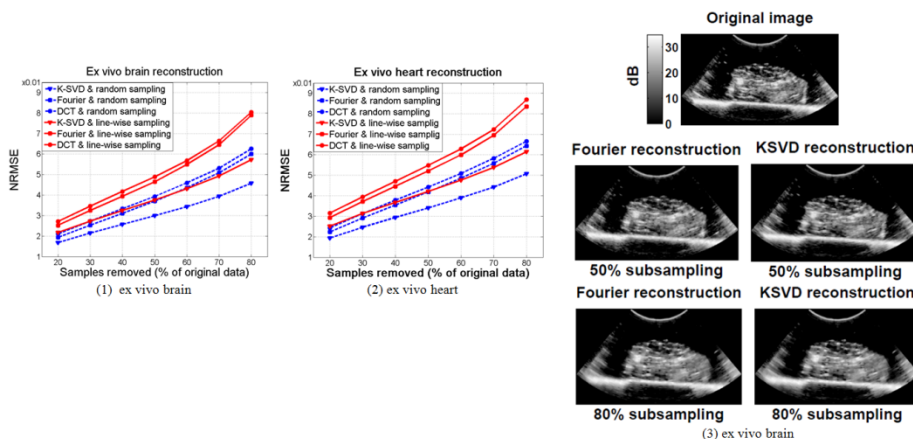
Figure: (1) and (2) NRMSE as a function of the number of removed samples using the point-wise and line-wise sampling masks. The error is computed for the CS reconstruction of the ex vivo: (1) brain and (2) heart using organ-dependent K-SVD dictionary, Fourier basis and DCT. (3) Visualization of 3D CS reconstructions of an ex vivo brain using the line-wise sub-sampling mask. Log envelopes of original data, Fourier and K-SVD reconstructions at 50% and 80% subsampling rates.

4F-3

1:30 pm **Compressed Sensing for Beamformed Ultrasound Computed Tomography**

Ruud van Sloun[1], Ashish Pandharipande[2], Massimo Mischi[1], Libertario Demi[1]; [1]*Electrical Engineering, Eindhoven University of Technology, Eindhoven, Netherlands*, [2]*Philips Research, Eindhoven, Netherlands*

Background, Motivation and Objective

Ultrasound computed tomography (UCT) allows reconstruction of quantitative tissue characteristics and is commonly used for breast cancer localization. In this application, a typical arrangement is one where the breast is enclosed by a circular array of ultrasound elements, sequentially transmitting and receiving the scattered wave fields at all elements. Lowering the acquisition time would be beneficial; however, this is limited by the time of flight and the number of transmission events. Moreover, corruption of the measurements by noise may cause inverse scattering reconstruction methods such as the Born Iterative Method (BIM) to converge to a wrong solution. Beamforming using multiple elements to obtain a narrow beam has the potential to mitigate the effects of noise; however, spatial coverage per transmission event reduces in this case. To excite the full domain, more transmissions are required and hence acquisition time increases even further. In this study, we propose a Compressed Sensing (CS) solution with beamforming for narrow beam inverse scattering UCT.

Statement of Contribution/Methods

By combining multiple consecutive elements, we narrow the beam in an effort to reduce the influence of noise. To reduce acquisition time, we consider compressive acquisitions based on parallel randomized transmissions from the circular array. The transducers simultaneously transmit pressure waves with random amplitudes that are Gaussian distributed. Relying on the assumption that the object is compressible, we combine the BIM with sparse reconstruction to obtain the estimated image. For compressive reconstruction, we adopt a Total Variation (TV) based penalty with l_1 heuristic.

Results/Discussion

Scattering measurements from a 48x48 numerical phantom having 4% wavenumber contrast were obtained using a 96 element transducer and a transmission frequency of 1 MHz. In Figure 1, a comparison is given between the reconstruction results when using standard uniform undersampling of transmissions and the proposed CS scheme. In both cases a compression factor of 12 is used, and narrow beams are obtained by combining 5 consecutive elements with unity beamforming weights. The measurements are corrupted by -40dB/-34dB Gaussian noise. The results indicate that CS outperforms uniform undersampling at preserving the object's features and can be applied effectively to UCT.
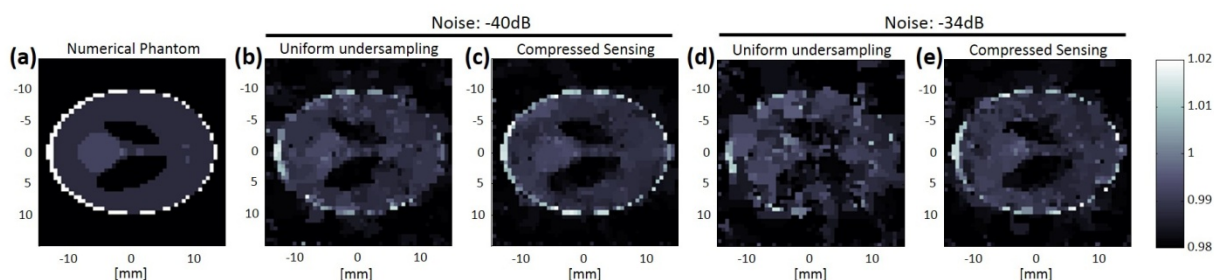
Figure 1. In (a), the numerical phantom is given. Plots (b,c) and (d,e) show the reconstructions for uniform undersampling and Compressed Sensing, when considering -40dB and -34dB noise, respectively. The colormap indicates the wavenumber contrast, given in percentage.

1:45 pm   **Extension of FM-Chirp Super Resolution Imaging for Ultrasound Synthetic Aperture System**

Takayuki Wada[1], Yihsin Ho[1], Norio Tagawa[1], Kan Okubo[1]; *[1]Graduate School of System Design, Tokyo Metropolitan University, Tokyo, Japan*

Background, Motivation and Objective

We have proposed a method for super resolution ultrasound imaging called the Super resolution FM-Chirp correlation Method (SCM) [1], which uses phase information of carrier waves. The method transmits a focused FM-chirp pulse multiple times each having slightly different frequency for generating each line in an image. To reduce the total number of transmission and as a result, to improve a frame rate of imaging, it is effective to extend the SCM as a synthetic aperture (SA) version called the SA-SCM in the following. To obtain an image consisting of M lines by the SCM using N-times of transmission for each line, $M \times N$ pulses are totally required to be transmitted, but the SA-SCM needs only N-times of transmission to generate the corresponding image, in principle.

Statement of Contribution/Methods

It is expected that the SA-SCM is inferior at the following two points for the conventional SCM, although it is advantageous with the aspect of imaging efficiency. Firstly, the image degradation compared with the SCM is concerned, because the phase of carrier waves would corrupt by a delay-and-sum processing. Another is that the SNR would lower because of the decrease of total penetration energy. In this study, after confirming the operating property of the SA-SCM, we evaluate the degree of the former defect through FEM simulations.

Results/Discussion

In the simulations, a linear array transducer consists of 64 elements with an aperture size of 9 mm. Transmitted pulses emitted towards a wide range region are formed by the partial array consisting of 8 elements, while moving in turn among 64 elements, and an echo for each transmission is received respectively by each of 64 elements. The reference FM-chirp pulse has a center frequency of 5 MHz, a bandwidth of 2 MHz and time duration of 5 μs. 30 pulses were transmitted with randomly varying the center frequency from 4 MHz to 6 MHz. A target object was located 10 mm away from the transducer in the area filled with water. We generated 2-D images by the SA-SCM and the SCM respectively. The range resolution of the SA-SCM deteriorates to approximately 2 times as compared with the SCM, but is sufficiently superior to the simple pulse compression image. In the future, azimuth resolution, which has not been taken into consideration on the SCM, should be examined by making use of a merit of the SA scheme validly.

[1] M. Fujiwara *et al.*, IEEE Int. Ultrasonics Symp., 2390 (2009).

Amplitude profile obtained by simulations
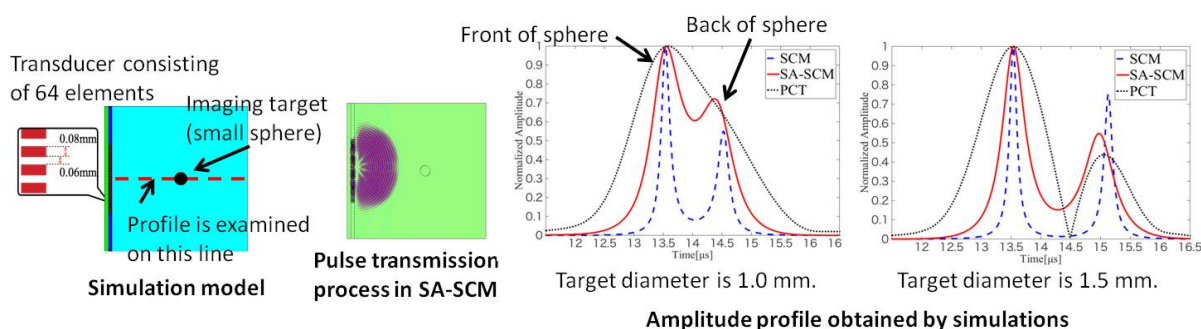
2:00 pm   **Spatiotemporal clutter filtering of Ultrafast ultrasound data highly increases Doppler and fUltrasound sensitivity**

Charlie Demené[1], Thomas Deffieux[1], Mathieu Pernot[1], Olivier Baud[2], Mickael Tanter[1]; *[1]Institut Langevin, ESPCI ParisTech, CNRS UMR7587, Inserm U979, Paris, France, [2]INSERM U1141 and Neonatal Intensive Care Unit, Paris Diderot University, Children's hospital Robert, Paris, France*

Background, Motivation and Objective

The use of compounded plane or diverging wave transmissions to increase the frame rate of ultrasound imaging completely changed the paradigm of Doppler imaging, by providing large synchronous datasets. However, to date, clutter filtering has not been optimized to this new framework, being restricted to a temporal tissue/blood discrimination. Here we propose a Spatiotemporal Clutter (STC) filter based on singular value decomposition to outperform classical temporal clutter filter.

Statement of Contribution/Methods

The STC filter is based on the formation of a Casorati matrix, whose dimensions are space and time, from Ultrafast ultrasound data. Performing singular value decomposition on this matrix turns it into a weighted, ordered sum of separable matrices (separable meaning written as the outer product of a spatial and a temporal vector). Tissue signal and blood signal having different spatiotemporal statistics, clutter filtering is performed by recombining only the separable matrix containing blood flow information. A flow phantom study with various blood and tissue speeds has been conducted to quantify precisely the Contrast to Noise Ratio (CNR) improvement of STC filtering of Ultrafast Doppler data compared to standard methods (butterworth and down-mixing filtering). STC filter efficiency has also been verified in various clinical settings, such as liver, kidney, cardiac and neonate brain imaging.

Results/Discussion

The phantom study clearly showed a strong increase in CNR while using the STC filter instead of standard approaches (see Fig. (a)), especially in the presence of strong tissue motion and slow blood flow speeds. For strong tissue motion (>8mm/s), butterworth and down-mixing CNR stay below 2 for blood speeds up to 15.5 mm/s, whereas STC filter CNR values ranged from 2.8 to 6.1 for blood speeds from 2.6 mm/s to 15.5 mm/s. In clinical setting, STC filtering showed systematic improvement with smaller vessels detection and substantially better motion artefact suppression (see Fig. (b)).

STC filtering will become mandatory for Ultrafast Doppler in both context of cerebral imaging and microcirculation clinical imaging. It enables the discrimination of blood flow slower than tissue motion, which is impossible with a temporal-solely clutter filtering. Its original spatiotemporal formulation makes it immediately transposable for 4D Ultrafast Imaging.
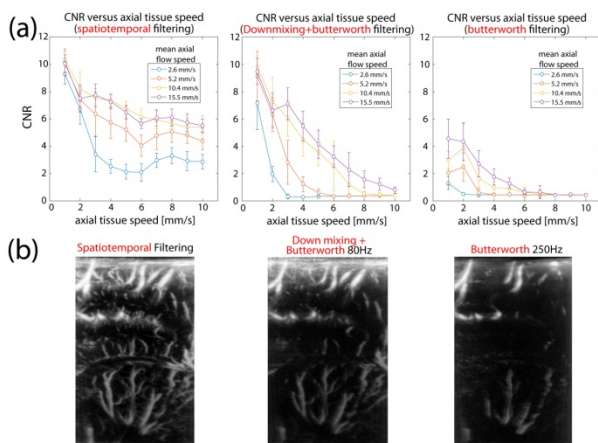
Figure: *(a) Phantom study: quantification of the contrast to noise ratio for different blood et tissue velocities for the spatiotemporal filter compared to the standard butterworth high pass filter and downmixing+high pass filter. (b) In a clinical setting: imaging of the neonate brain vascularisation in a parasagittal section through the fontanel in the presence of tissue motion.*

4F-6 _____

2:15 pm   Contrast-Enhanced Ultrasound Imaging with Chirps: Signal Processing and Pulse Compression

Sevan Harput[1], James McLaughlan[1], David Cowell[1], Steven Freear[1]; *[1]School of Electronic and Electrical Engineering, University of Leeds, Leeds, United Kingdom*

Background, Motivation and Objective

Contrast-enhanced ultrasound imaging creates a challenging signal processing scenario due to frequency dependent attenuation, high level of harmonic generation, phase variations due to resonance behavior of microbubbles, and increased broadband noise by microbubble destruction. When microbubbles are insonified around their resonance frequency, both the phase and amplitude response will be significantly different than that of tissue. Signal processing techniques become less efficient because of this resonance behavior of a microbubble population, which causes unpredictable phase variations and frequency shifts in the scattered pressure field. This study addresses the following question "Is it possible to perform signal processing, such as pulse compression, filtering, and averaging, in the existence of resonant microbubbles, and why?".

Statement of Contribution/Methods

In diagnostic imaging, chirp excitation increases the scattering from polydisperse microbubbles and a matched filter improves the SNR by compressing the scattered energy with a certain chirp rate into a single pulse. Therefore, it is of interest to analyze the phase of radiated pressure waveforms from microbubbles. Simulations and experimental measurements were performed by studying the scattering response of Definity-like microbubbles (f_0 = 3.8 MHz, R = 1 ± 0.5 μm) for various chirp excitation waveforms between 100-500 kPa peak negative pressures. A 128 element medical ultrasound transducer was used to replicate ultrasound imaging conditions. Scatter pressure waveforms were captured by a needle hydrophone and averaging, filtering and pulse compression were performed in Matlab.

Results/Discussion

Findings of this study showed that the scattered pressure from a microbubble population excited by a chirp waveform preserves its chirp rate even for harmonic frequencies. The chirp rate was verified by using the time-frequency distribution of the scattered ultrasonic energy from microbubbles as shown in the figure. The red dashed lines show the theoretical center frequency and chirp rate of the fundamental and second harmonic components that are in good agreement with the experimental measurements. The conservation of the chirp rate makes the pulse compression, filtering and averaging possible.

FRIDAY ORAL
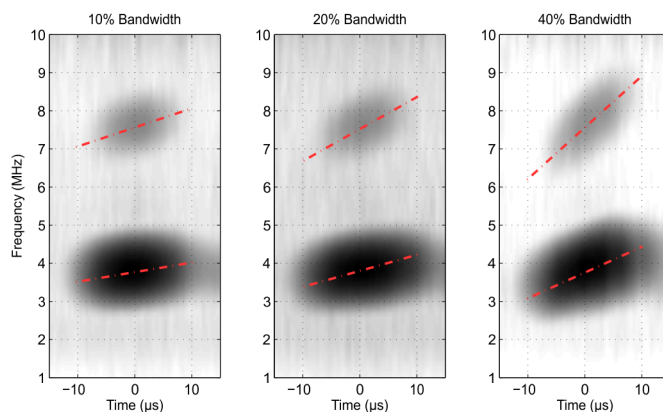
5F - Industrial Applications

103

Friday, October 23, 2015, 01:00 pm - 02:30 pm

Chair: **Kentaro Nakamura**
Tokyo Institute of Technology

5F-1

1:00 pm   Blind Component Separation Analysis for Highly Corrupted Ultrasonic Signals in Real-Time Spot Weld Inspection
Aryaz Baradarani[1], Andriy M. Chertov[1], Waldo Perez Regalado[1], Roman Maev[1]; [1]*Institute for Diagnostic Imaging Research, University of Windsor, Windsor, Canada*

Background, Motivation and Objective

The harsh environment surrounding the inspection system generates multiple sources of noise. Bubbles in the cooling water stream, temperature variations around transducer, electromagnetic noise from power electronics, transformers and servo motors corrupt the received A-scans. This paper introduces an efficient technique that has been developed to analyze the ultrasonic signals obtained in the process of nondestructive testing of resistance spot welds.

Statement of Contribution/Methods

The ultrasonic transducer integrated inside a water-cooled welding electrode sends multiple impulses into the welded metal sheets in reflection mode. As welding progresses, the proposed processing technique is capable of monitoring the dynamics of the key parameters of spot weld growth and the presence of the liquid nugget within welded sheets. The method describes how to separate signal components from the corrupted A-scans in order to extract the desired features indicating the reflections from multiple interfaces of spot weld structure. The technique is mainly based on blind component analysis of signals where possible features are initially marked and then the so-called contrast of data is increased to magnify the features.

Results/Discussion

Several experiments were carried out using the welding system available at the institute as well as the real data received from the leading auto makers in the North America and Europe. Fig.1. shows a sample before the use of the proposed technique. As it can be seen in Fig.1. (b), we are able to clearly show what was behind the strong disturbance presented in Fig.1. (a). Experimental setup is shown in Fig.1. (c).
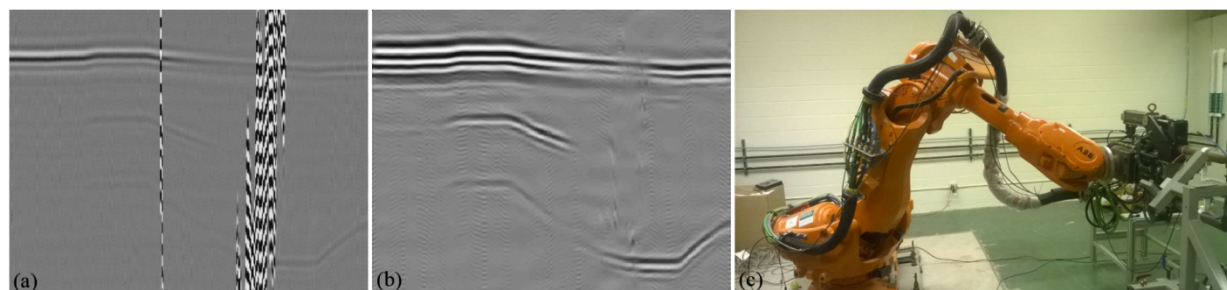
Figure 1. (a) A sample before the use of the proposed technique contaminated by strong noise; (b) After applying the proposed technique; (c) Experimental setup showing the welding robot, transducer, scanner and processing units.

5F-2

1:15 pm   Ultrasonic Welding Using a Long and Thin Complex Transverse Vibration Welding Tip with Vibration Detector and Static Pressure Controller
Jiromaru Tsujino[1,2], Eiichi Sugimoto[3]; [1]*Kanagawa University, Yokohama, Japan, [2]R & D Center, Asahi EMS Co. Ltd, Yokohama, Kanagawa, Japan, [3]Asahi EMS Co. Ltd, Tokyo, Japan*

Background, Motivation and Objective

Ultrasonic welding could not been applied for deep and narrow parts positioned at long distance from the vibration system. Usually, electric resistance or laser welding was used to weld such part, but there are possible fatal defect caused by sparked metal particles. To join such deep area, ultrasonic complex vibration system using small diameter long welding tip were developed. Using ultrasonic complex vibration with circular to elliptical vibration locus, required vibration amplitude, and static pressure decreased significantly due to two-dimensional vibration stress. To improve welding characteristics furthermore, complex vibration velocity detector of welding tip and static pressure control system were developed.

Statement of Contribution/Methods

27 kHz and 19.5 kHz ultrasonic complex vibration systems using 2.0- and 3.0-mm-diameter, 75- to 100-mm-length hard metal welding tip were developed for joining deep and narrow welding part. The welding tip was installed a longitudinal to torsional complex vibration converter with diagonal slit part. Fig. 1 shows 19.5 kHz complex vibration system with a 3.0-mm-diameter hard metal welding tip installed a complex vibration velocity detector. The detector consists of a ferrite ring magnet and two detecting coils and detect only circular vibration locus.

To weld several terminals to inner bottom of Li-ion-battery case, larger static clamping force is required to suppress initial deformation of battery case bottom and fix several terminal first and drive the weld area under static force required for ultrasonic welding. Static clamping force during welding must be maintained constant using metal spring actuator. Fig. 2 shows welded conditions of two nickel-clad copper terminals.

Results/Discussion

Using developed 19.5 and 27 kHz ultrasonic complex vibration welding systems, various specimens including nickel-clad copper terminals and nickel coated steel case Li-ion battery and capacitors were successfully welded with strength near to material. Weld strength of nickel-clad copper terminal was over 150 N using a 3.0-mm-diameter welding tip.

To weld lapped many aluminum and copper foil electrodes of battery, same static pressure control system is essential. Fig. 3 shows successfully welded conditions of 30 lapped 0.02-mm-thick copper and aluminum foils using 10-mm-wide complex vibration welding tip.
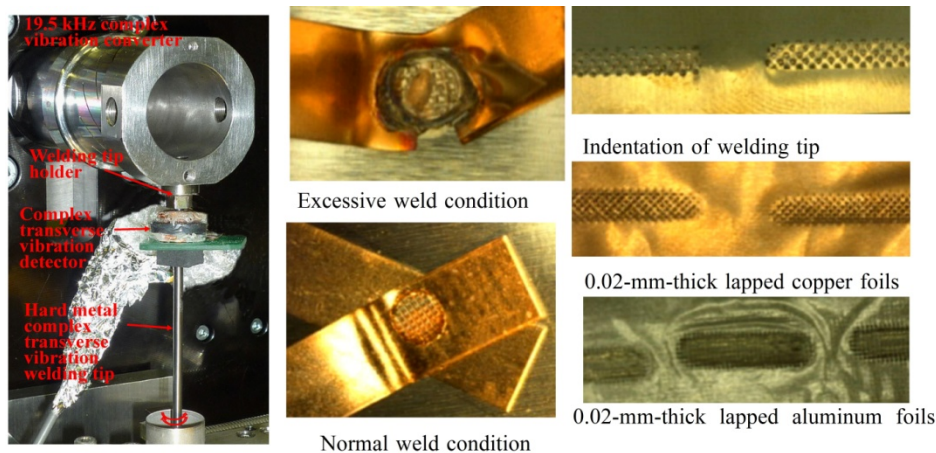
Fig.1 19.5 kHz welding system with 3.0-mm-diameter complex vibration welding tip.

Fig. 2 Welded conditions of two nickel clad tabs on nickel coated steel

Fig. 3 Welded conditions of 30 lapped 0.02-mm-thick copper and aluminum foils for battery.

5F-3 _____

1:30 pm   Novel real-time diagnostic of injection molding process at nozzle by high-temperature ultrasonic transducer

Che-Hue Yang[1], Chin-Chi Cheng[2], Makiko Kobayashi[3], **Yi_Lin Wu[1]**; *[1]Graduate Institute of Mechanical and Electrical Engineering, National Taipei University of Technology, Taiwan, [2]Dept. of Energy and Refrigerating Air-Conditioning Engineering, National Taipei University of Technology, Taipei, Taiwan, [3]Dept. of Computer Science and Electrical Engineering, Kumamoto University, Japan*

Background, Motivation and Objective

The key process condition parameters of conventional injection molding (IM) process include temperature of barrel and mold, screw back-pressure and rotation speed of plasticizing unit, etc. The process monitoring at mold side has been well discussed. However, the resin flow characteristics at barrel, especially at nozzle, are still under investigation. The most utilized sensors for IM process monitoring are temperature and pressure sensors. These sensors may have some limitations for application, such as limited machine space, direct contact with the substrate, operation environment of room temperature, etc.

Statement of Contribution/Methods

This study attempts to apply ultrasonic techniques for real-time diagnosis of conventional IM process at nozzle side. In this study, a high temperature ultrasonic transducer (HTUT) is to be integrated onto the designed extension nozzle of an IM machine by using a sol-gel spray technique. The resin flow characteristics at nozzle, including dynamic flow speed and static density of polymer melt, would be monitored real-time.

Results/Discussion

The cross section schematic drawing of the designed extension nozzle is shown in Fig. 1. According to the designed extension nozzle of IM machine, the dimensions of the sensor probe are 12.5mm-in-radius and 32mm-in-length, as shown in Fig. 2. The radius of central channel for resin flow is 8mm-in-radius. It could operate at temperature higher than 400¢XC without ultrasonic couplant, and use an ultrasonic pulse-transfer technique. The center frequency of the ultrasonic echo was 2 MHz and the 3 dB bandwidth was 5 MHz. During the IM process, the dynamic flow speed and static density of polymer melt at nozzle would be monitored and compared with the product characteristics and quality for process optimization.

5F-4
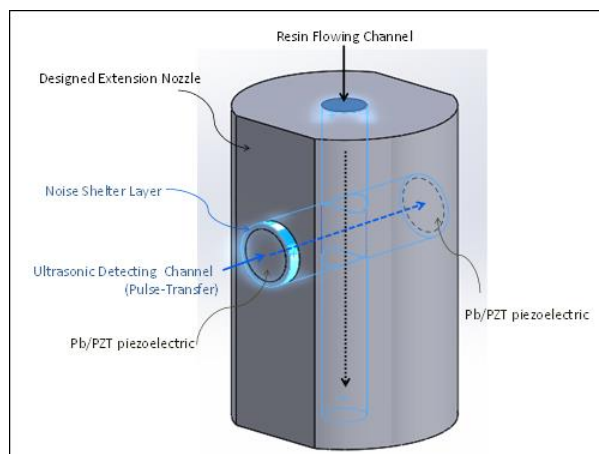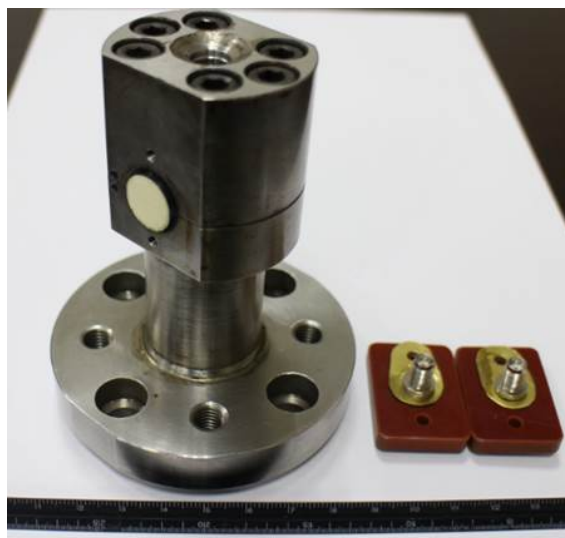
1:45 pm   High temperature performance of PbTiO₃/PZT ultrasonic transducer above 400°C

Taiga Kibe[1], Tsukasa Kaneko[1], Makiko Kobayashi[1]; *[1]Kumamoto University, Japan*

Background, Motivation and Objective

In recent years, there is a growing demand of non-destructive testing (NDT) chemical plant safety assurance. NDT by ultrasound is usually carried out during operation shut down period. It is difficult to increase the operation shutdown frequency due to economic loss, thus it is desired to perform ultrasound NDT with operation condition. Some chemical plant temperature during operation can reach relatively high temperature such as 500°C or even higher, even though it is very challenging conditions for ultrasonic transducers for NDT applications. In past experiments, performance of the PbTiO₃ (PT)/ Pb(Zr,Ti)O₃ (PZT) sol-gel composite ultrasonic transducers showed high sensitivity from room temperature to 400°C hot plate heating though the maximum operation temperature was not determined yet.

Statement of Contribution/Methods

High temperature test was carried out for 100μm thick PT/PZT sample fabricated onto 3mm thickness titanium substrate to investigate the maximum operation temperature. The sample of PT/PZT by spray coating was set onto a hot plate with 550°C maximum operation temperature, and the temperature was changed every 50°C up to 550°C. After 3 min holding time, ultrasonic waveform in pulse-echo mode was recorded by a digital oscilloscope at each temperature.

Results/Discussion

Measurement result at 550°C is shown in Fig. 1. Multiple reflected echoes from the bottom surface of 3 mm thick titanium substrate were confirmed with reasonable signal to noise ratio for thickness monitoring, though signal amplitude was dropped by ~40dB above 500°C hot plate temperature due to depoling. From 50°C to 450°C of hot plate temperature, the signal amplitude was almost constant. From this result, it was confirmed that the PT/PZT ultrasonic transducer had good potential for high temperature applications. Further investigation will be carried out to determine maximum longterm operation temperature and performance comparison with other sol-gel composite materials.

5F-5
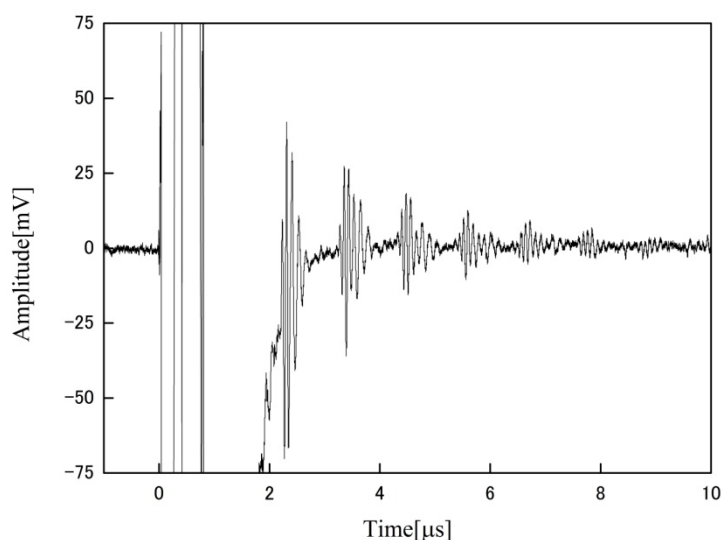
2:00 pm   Non-contact Measurement of Elastic Property of Fruits by using Parabolic-Reflector Airborne Ultrasonic Transducer

Marie Tabaru[1], Kentaro Nakamura[1]; *[1]Precision and Intelligence Laboratory, Tokyo Institute of Technology, Yokohama, Kanagawa, Japan*

Background, Motivation and Objective

In the field of agriculture, there is increasing demand for automatic decision system of harvest season of farm product. Elastic property is one of the important factors for the decision. Especially, non-contact test is required to minimize damage of fruits. In this paper, we develop a non-contact measurement system, which evaluates elastic property of fruits by using airborne ultrasonic transducer. Displacement characteristics of fruits were measured as a fundamental study.

Statement of Contribution/Methods

Fig.1(a) shows the developed system. First, a pulsed plane-wave was exposed by a high-power airborne ultrasound transducer (NCG100-D50, Ultran) (diameter: 50 mm, center freq.: 100 kHz). The exposed wave was focused on a fruit surface by using a parabolic-reflector, which was made by a 3D printer. Measured focal widths were 3.7 and 4.4 mm, and maximum pressure was 1440 Pa (@ 14 V_{0p}). Acoustic radiation force, which was produced by the pulsed focused wave, caused mechanical low-frequency vibration on the surface. The vibration velocity was measured by a laser Doppler velocimeter (LDV) (LPF: 5 kHz, range: 10^{-2} m/s /V). A laser window (diameter: 3 mm) was made to the reflector so that the LDV could detect the vibration.

Bananas (fresh, old), strawberry, orange, and apple were used as specimens. Burst waves (70 V_{0p}, 100 kHz, exposure time: 0.5, 1, 2, 3 ms) were inputted to the transducer, and velocities were measured and stored to a PC. Here, we considered the maximum displacements relate to elastic property. Displacements were calculated as follows. First, the velocity waveforms were transformed from the time- into the frequency-domain by FFT. Then, velocities were divided by jω to get displacement. Finally, displacements waveforms were calculated by i-FFT.

Results/Discussion

Fig.1(b) shows the resulted displacement waveform for old banana. The maximum value was 18 nm for the exposure time of 3 ms. Fig.1(b) also summarizes the maximum displacements. The displacements of hard fruits (apple, orange) tended to be smaller values as expected. In addition, the displacements increased for longer exposure time for all the fruits. On the other hand, the incremental quantities of the displacements for exposure time were different for freshness and the type of fruits. From the results, we expect that the developed system can be applied to test the elastic property of fruits.

Fig. 1(a)

Fig. 1(b)
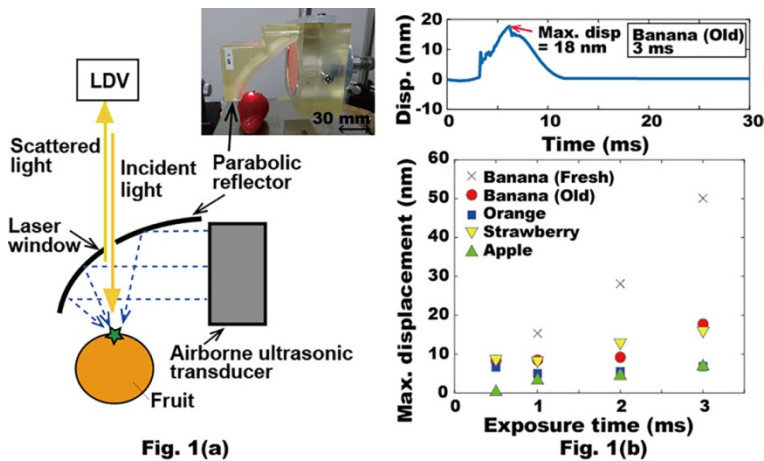
2:15 pm   **Development of a real-time acoustic backscatter system for solids concentration measurement during nuclear waste cleanup**

David Cowell[1], Hugh Rice[2], Tim Hunter[2], Derrick Njobuenwu[2], Jeff Peakall[3], Michael Fairweather[2], Geoff Randall[4], Steven Freear[1]; *[1]School of Electronic and Electrical Engineering, University of Leeds, Leeds, United Kingdom, [2]School of Chemical and Process Engineering, University of Leeds, Leeds, United Kingdom, [3]School of Earth and Environment, University of Leeds, Leeds, United Kingdom, [4]Sellafield Ltd, United Kingdom*

Background, Motivation and Objective

The UK civil nuclear industry has a large, diverse waste inventory that requires processing and disposal. This work aims to address the lack of suitable online measurement systems for real time characterization of suspended solids in sludges and slurries to aid the development of new nuclear waste processing procedures, with additional applicability to process control in the chemical, mining, minerals and waste water engineering industries.

Statement of Contribution/Methods

A 16-channel instrumentation system (a) has been developed for online measurement within an active nuclear environment. The instrument is capable of arbitrary and coded excitation to improve SNR, allows transducer connection by long coaxial cables, operates from a low-voltage supply, and communicates via optical fiber to allow remote deployment and resilience to electromagnetic interference. Initial real-time suspended solids concentration measurements were obtained through the application of a marine acoustic backscatter model. A pilot-scale horizontal settler of volume $9m^3$ has been constructed (b) to allow thorough evaluation of the instrumentation and comparison of particle concentrations computed via acoustic data with theory and physical samples.

Results/Discussion

The acoustic system has undergone initial evaluation using 41 µm spherical glass particles suspended in water at concentrations from 2 to 32 kg/m^3 in a custom mixing vessel. Range corrected backscatter amplitude G for each concentration M was measured (c) at each measurement frequency. The gradient of G vs concentration M at 1.75, 2.25 and 2.75 MHz shows the frequency-dependent behavior of the backscatter method (d). This data demonstrates the success of the method and acts as calibration curves for real-time concentration measurement.
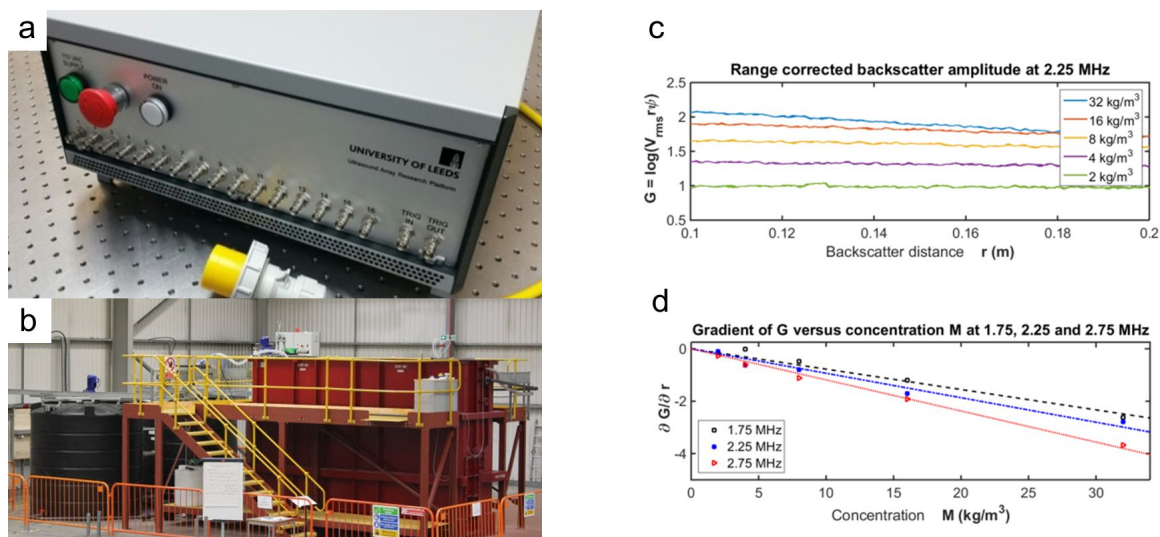
8F - Applications of CMUTs

102

Friday, October 23, 2015, 01:00 pm - 02:30 pm

Chair: **Omer Oralkan**
North Carolina State University

8F-1

1:00 pm **Reliability measurements of CMUT arrays of a semiconductor manufacturer**

Christophe Antoine[1], Erik Tarvin[1], Sushil Bharatan[1], Urvi Shah[1], Rob O'Reilly[1], Michael Judy[1]; [1]*Analog Devices Inc., Wilmington, MA, USA*

Background, Motivation and Objective

Capacitive Micromachined Ultrasonic Transducer (CMUT) technology has been developed both in academia and industry for two decades. Manufacturers of medical ultrasound imagers have been facing two issues preventing a wider CMUT adoption: unreliable performance across manufacturing variations and, for a single device, its poor performance over time. This submission addresses both of these shortcomings.

Statement of Contribution/Methods

A CMUT fabrication process based on sacrificial release of polysilicon membranes was developed and two generations of CMUT single-element and 1D arrays were manufactured. To address performance across manufacturing variations, wafers were manufactured and probed to evaluate electrical performance characteristics. Measurement of resonant frequency at zero bias as well as under various biases helped assess variations while the devices are operated near their collapse voltage.

An accelerated life test was created to emulate standard use of ultrasound imager in a radiology clinic. This included storing the devices at a temperature of 80 degrees Celsius for 10 days. As dielectric charging had been identified by many groups as a source of drift over time, the devices were biased 35% above their collapse voltage during the experiment, i.e. the movable membrane was in physical contact with the underlying substrate, only separated by a few hundred nanometers of a dielectric film.

Results/Discussion

Over one hundred wafers were manufactured and measured in an automated setting to gather frequency variations across wafer and between wafers. After several iterations, the process was controlled to a tighter degree and results will be shown at the conference.

The device stress test proved that the second generation of devices exhibited significantly less drift than the initial demonstration. Most drift was observed in the first three days of the experiment. Over 10 days at high temperature and high bias field, a change of 0.25% of the zero-bias capacitance was measured.

This work focused on setting a reference for the level of process control and reliability that can be achieved by a semiconductor manufacturer and thus clarifies where further innovation would be needed to broaden market adoption of CMUTs.

8F-2

1:30 pm **Dual-Mode Integrated Circuit for Imaging and HIFU With 2-D CMUT Arrays**

Ji Hoon Jang[1], Anshuman Bhuyan[1], Hyo-Seon Yoon[1], Jung Woo Choe[1], Amin Nikoozadeh[1], Douglas Stephens[2], Butrus Khuri-Yakub[1]; [1]*Electrical Engineering, Stanford University, Stanford, California, USA,* [2]*Biomedical Engineering, University of California, Davis, Davis, California, USA*

Background, Motivation and Objective

For successful high intensity focused ultrasound (HIFU) operation, it is important to have a reliable guidance and monitoring method such as magnetic resonance imaging (MRI) and ultrasound imaging. However, MR-guided HIFU systems are typically bulky, and the imaging-guided HIFU systems use separate ultrasound transducers and electronics. In this paper, we present a dual-mode integrated circuit (IC) that can perform both ultrasound imaging and HIFU with a single 2D capacitive micromachined ultrasonic transducer (CMUT) array.

Statement of Contribution/Methods

The dual-mode IC consists of pulsers, transmit beamforming circuitry, and low-noise amplifiers for imaging mode and switches for HIFU mode. In the imaging mode, only the 64 diagonal CMUT elements are used as receivers without significant loss of image quality, and the other 960 elements transmit the ultrasound beam. In the HIFU mode, each of the 1024 CMUT elements is assigned to one of the eight HIFU channels based on the phase delay from it to the desired focal point using a dedicated high-voltage switch. The eight HIFU channels are connected to an eight-channel phase generating system for a fixed focal point in front of the CMUT array. We can alternate between the imaging and HIFU modes on demand by turning the switch network on and off (Fig. 1).

Results/Discussion

The dual-mode IC was fabricated in the 0.18-μm, high-voltage process. We previously fabricated a 250-μm-pitch, 32×32-element CMUT array that has a center frequency of 5 MHz using the sacrificial release process, and flip-chip bonded this CMUT array to the IC. The integrated assembly is connected to a custom-designed printed circuit board (PCB) to interface the IC to an 8-channel phase generating system, an image reconstruction system, and a field-programmable gate array (FPGA). The phase generating system consists of digital synthesizers and power amplifiers to drive eight HIFU channels. The imaging system processes the data received by the 64 receive channels to reconstruct real-time ultrasound images. The FPGA sends the beam patterns to the IC and control signals to switch the modes. We have successfully demonstrated the functionality of all the individual components. We are currently working on demonstrating interleaved imaging and HIFU using a single 2D CMUT array. This work was supported by the National Institutes of Health (NIH) under grant R01HL117740

8F-3

1:45 pm   A dual-mode CMUT array optimized for tissue harmonic imaging

Søren Elmin Diederichsen[1], Mathias Johannes Grøndahl Mølgaard[1], Anders Lei[1], Matthias Bo Stuart[2], Jørgen Arendt Jensen[2], Erik Vilain Thomsen[1]; *[1]Department of Micro- and Nanotechnology, Technical University of Denmark, Kgs. Lyngby, Denmark, [2]Center for Fast Ultrasound Imaging, Department of Electrical Engineering, Technical University of Denmark, Kgs. Lyngby, Denmark*

Background, Motivation and Objective

Tissue Harmonic Imaging (THI) is a widespread technique in medical ultrasonography. However, current commercial piezoelectric transducers for THI are designed to have a center frequency between the excitation frequency and the generated second harmonics, resulting in a bandwidth-limited signal. The Capacitive Micromachined Ultrasonic Transducer (CMUT) facilitates the possibility of separate transmit and receive optimization. In order to generate harmonics, CMUTs must be able to transmit a high pressure. The objective is therefore to fabricate CMUTs optimized for THI with different transmit and receive cells, using Ni-electroplating to add mass to the transmit cells. This decreases the center frequency and increases the output pressure of the transmit cells.

Statement of Contribution/Methods

We present a $3/4\lambda$-pitch, 192-element 1-D linear dual-mode (3 MHz/6 MHz) CMUT array. The design is optimized using finite element analysis (COMSOL Multiphysics 4.4), resulting in an insulation gap of 259 nm and a pull-in voltage of 238 V for all cells. The array is composed of a 2 µm thick plate with 6 mm x 196 µm elements having alternating rows of 90.4 µm x 90.4 µm transmit cells and 43.3 µm x 43.3 µm receive cells. The CMUTs are fabricated using fusion bonding and standard silicon micromachining. Electroplating is used to add 6 µm Ni on top of each transmit cell.

Results/Discussion

Compared to a 4.5 MHz single-mode CMUT in immersion, simulation results scaled to the element area show a 6 dB decrease in receive sensitivity and 9 dB increase in transmit pressure. This substantiates the advantage of a dual-mode CMUT. The pull-in voltage of the transmit cells is measured to >255 V and for the receive cells it varies from 145-175 V. The discrepancy between measured and simulated results is related to fabrication issues, including deviation in Ni mass height and plate thickness. This deviation results in immersion center frequencies of approx. 1.5 MHz and 3 MHz for transmit and receive cells, respectively. Therefore acoustical measurements in immersion are performed with a 1.5 MHz, 10-period sinusoid, 32-element focused emission to evaluate the pressure. The figure shows the resulting energy of the second harmonic to fundamental ratio as function of distance from the transducer. The ratio increases with distance, which demonstrates the generation of second harmonics.

SEM micrograph of electroplated nickel mass added on the transmit cells.
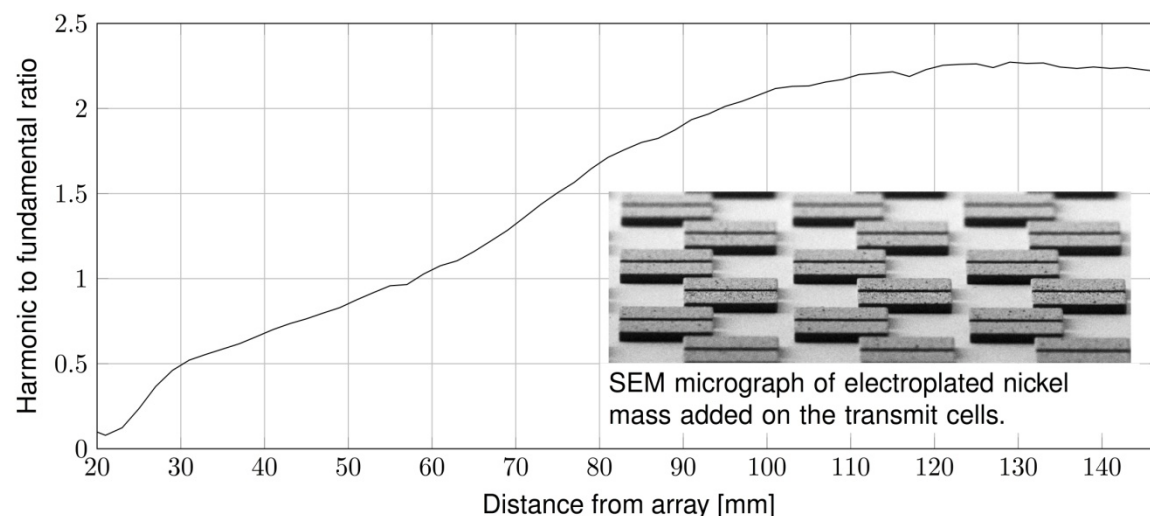
2:00 pm   A High-Frequency (~30-MHz), Broadband (FBW>100%) 1-D Linear CMUT Array Fabricated by Anodic Bonding

Xiao Zhang[1], F. Yalcin Yamaner[2], Omer Oralkan[1]; *[1]Department of Electrical and Computer Engineering, NCSU, Raleigh, North Carolina, USA, [2]Department of Electrical and Electronics Engineering, Istanbul Medipol University, Istanbul, Turkey*

Background, Motivation and Objective

High-frequency (>20 MHz) ultrasound is desired for various applications including dermatology, ophthalmology, and small animal studies. The major technology hurdle for making high-frequency arrays is associated with the conventional piezoelectric transducer fabrication techniques. The thickness of the piezoelectric crystal and the pitch of the array need to be tens of microns which is difficult to achieve using conventional fabrication techniques. Furthermore, small element size results in high electrical impedance and makes it difficult to drive the elements using external electronics. Capacitive micromachined ultrasonic transducers (CMUT) have demonstrated great promise for the implementation of high-frequency arrays because of the precise dimension control and ease of integration with electronics. However, the fractional bandwidth of the early high-frequency CMUT designs was limited (<80%) mainly because of the low fill factors. In this work, we successfully demonstrated that we can design and fabricate high-frequency broadband arrays on a glass substrate using anodic bonding.

Statement of Contribution/Methods

We designed, fabricated, and characterized a 256-element, 65-um-pitch, 1-D linear array operating at ~30-MHz center frequency with 105% fractional bandwidth. The cells are densely packed to achieve a relatively high fill factor (~60%). The gap of the device is defined by BOE etching and metal deposition. The 1.5-μm SOI device layer with 200-nm silicon nitride insulation was transferred on to the cavities by anodic bonding. The trapped gas inside the cavities was evacuated after bonding and the cavities were then sealed with PECVD silicon nitride. As a last step, silicon nitride on bottom pads and top electrode contacts was removed and metal was deposited and patterned.

Results/Discussion

The optical images show the fabricated high-frequency linear array. The SEM image shows the cross section of a CMUT cell. The gap height is measured as 50 nm. The shallow gap is desired for high-frequency designs to reduce the collapse voltage and improve the efficiency. A single element (63 μm × 1800 μm) was biased at 50-V DC and excited by a 15-ns, 65-V unipolar pulse. A hydrophone measurement at 2.5-mm shows the center frequency is 28.5 MHz and the fractional bandwidth is 105% after correcting for the pulse spectrum.
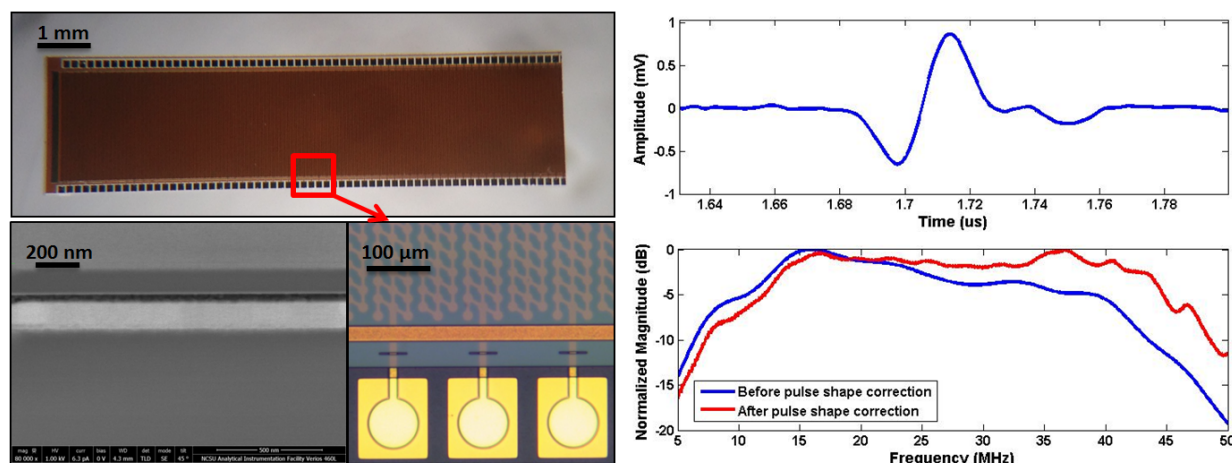
2:15 pm   Capsule Ultrasound (CUS) Device

Farah Memon[1], Gerard Touma[1], Amin Nikoozadeh[1], Jung Woo Choe[1], Amin Arbabian[1], Eric W. Olcott[2,3], R. Brooke Jeffrey[2], Butrus (Pierre) T. Khuri-Yakub[1]; *[1]Stanford University, Stanford, California, USA, [2]Stanford University School of Medicine, Stanford, California, USA, [3]Palo Alto Veterans Affairs Health Care System, Palo Alto, California, USA*

Background, Motivation and Objective

We are developing a capsule ultrasound (CUS) device to serve as a wireless and portable pill for investigating the multiple layers of the complete gastrointestinal (GI) tract, in particular, the small intestine, using ultrasound. The CUS device seeks to surpass the limitations of capsule endoscopes that rely on optics and only examine the outer-most layer of the GI tract. The CUS device will consist of a cylindrically-shaped capacitive micromachined ultrasonic transducer (CMUT) array, wrapped around its body, to acquire B-mode images with 360° field-of-view (FOV) and a larger penetration depth than those acquired using capsule endoscopes. In addition, the CUS device will include an application-specific integrated circuit (ASIC) and a transceiver, as displayed in Figure 1, to wirelessly transmit image-data to an external recorder.

Statement of Contribution/Methods

This project involves fabrication of the CMUT array, design of an ASIC and a transceiver, and system-level integration of these multiple components. In order to fabricate the array, we performed simulations using FOCUS to find design specifications and created test devices to derive a fabrication technique for wrapping the CMUT arrays around the capsule. We also developed a detailed fabrication plan which incorporates the wafer-bonding technology with the process used to create test devices. In addition, we have designed most of the components of the ASIC while maintaining the total power below 20 mW.

Results/Discussion

A cylindrical transducer with a center frequency of 5 MHz, 128 total elements, 16 active elements, and a fixed focus using an $F_\#$ of 4 provides decent resolution up to a penetration depth of 5 cm and reduces image quality degradation due to grating lobes, as indicated by the continuous wave (CW) pressure profile in Figure 2. In addition, we successfully fabricated test devices, wrapped them around cylindrical rods, and are currently in the process of fabricating the cylindrical CMUT arrays. Furthermore, we have designed the transmit, receive, and power management units of the ASIC, generated the specifications for the transceiver, and are working on developing the interface between the two components. The power calculations indicate the CUS device to be active for 8 hours, enough to traverse the entire GI tract, while providing 2 - 4 frames/second.

CUS System Level Diagram
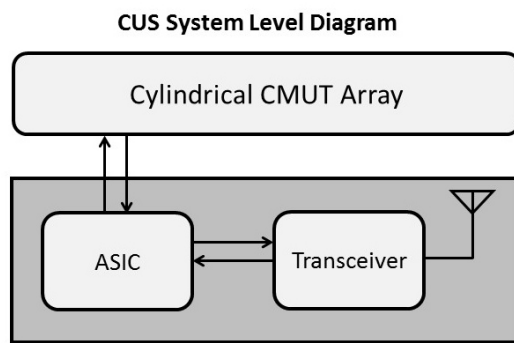
Figure 1: CUS System Level Diagram.
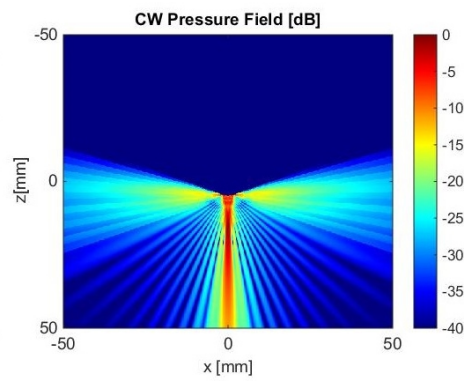
Figure 2: CW pressure field response of the cylindrical CMUT array using an $F_\#$ of 4. Simulation performed using FOCUS (R. J. McGough, J. Acoust. Soc. Am, 2004).

FRIDAY ORAL

1G - MTC: High Frequency Tissue Characterization

103

Friday, October 23, 2015, 03:30 pm - 05:00 pm

Chair: **Michael Oelze**
Univ. of Illinois

1G-1

3:30 pm   **Fine resolution elastic property maps of myopic sclera by means of acoustic microscopy**

Daniel Rohrbach[1], Quan Wen[2], Quan Hoang[2], Sally McFadden[3], Ronald H. Silverman[2], Jonathan Mamou[1]; *[1]Lizzi Center for Biomedical Engineering, Riverside Research, USA, [2]Department of Ophthalmology, Columbia University Medical Center, USA, [3]Vision Sciences Group, Faculty of Science and IT, School of Psychology, University of Newcastle, NSW, Australia*

Background, Motivation and Objective

Myopia is caused by excessive axial eye length, which results in images short-focused in front of the retina. Myopia affects > 2.3 billion persons and pathologic myopia can lead to irreversible vision loss. The anatomic change underlying excessive eye elongation likely occurs in the eye wall (sclera), which is more flexible in myopic than in non-myopic eyes. In the present study, we employed a form-deprivation (FD), guinea-pig myopia model and a scanning acoustic microscope (SAM) to study distributions of bulk modulus (K) and mass density (ρ) in the sclera at microscopic levels.

Statement of Contribution/Methods

Sclera from 3 animals with different levels of induced myopia were cryosectioned into 12-μm thicknesses and measured using a custom-built SAM. The SAM was equipped with an F-1.16, 250-MHz transducer (160-MHz bandwidth) and 7-μm lateral beam width. The amplified radio frequency signals were digitized at 2.5 GHz using a 12-bit oscilloscope. Maps of speed of sound (c), acoustic impedance (Z), attenuation (a), and K and ρ were derived from the frequency-domain representation of each recorded signal using a model-based approach. To induce myopia, each animal wore a translucent diffuser in front of the right eye from 4-12 days of age. After 7 days, refractive error was measured in myopic eyes, and eye length was measured using high-frequency ultrasound. The differences between the FD eyes and the control eyes were -5.08, -3.38 and -0.35 diopters for animals 1, 2 and 3, respectively.

Results/Discussion

In animal 1, K was 0.4 GPa higher (p<0.001, n-way ANOVA) for the control eye (3.0 ± 0.3 GPa, Fig. 1a) compared to the myopic eye (2.6 ± 0.1 GPa, Fig. 1b). Z and c also were significantly different for the myopic eye (Z = 1.62 ± 0.04 Mrayl, c = 1605 ± 61 m/s) compared to the control eye (Z = 1.77 ± 0.07 Mrayl, c = 1702 ± 85 m/s). No significant difference in acoustical properties existed between myopic and control eyes for the less-myopic animals 2 and 3. SAM is capable of providing fine-resolution quantitative images which may be invaluable in the investigation of the biomechanical properties of ocular tissues in diseases where tissue elasticity is believed to play an important role such as high myopia, and glaucoma. Supported by NIH grants R21EB016117 and K08EY023595 and an unrestricted and career-development grant from Research to Prevent Blindness.
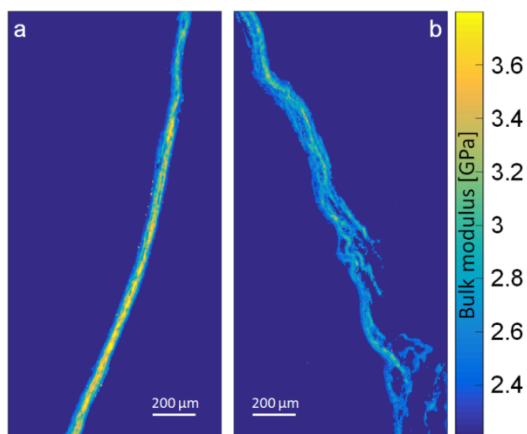
Figure 1 bulk modulus (K) image of 12-μm cryosection of unfixed guinea pig sclera. (a) Normal eye and (b) myopic eye from same animal.

1G-2

3:45 pm   **Ultrasonic Characterization of Extra-Cellular Matrix in Decellularized Murine Kidney and Liver**

Lauren A. Wirtzfeld[1], Elizabeth S. L. Berndl[1], Michael C. Kolios[1]; *[1]Ryerson University, Canada*

Background, Motivation and Objective

Three-dimensional scaffolds are essential to the field of tissue engineering. While novel synthetic structures are being developed, there is still a great interest in exploring natural scaffolds in tissue, the extra-cellular matrix (ECM). A recently developed technique known as "decellularizing" allows for the removal of cells from intact tissue while preserving the ECM structure. In order to exploit the uniqueness of the native ECM, a structure which varies significantly between organs, it first needs to be well studied.

This study outlines the use of quantitative ultrasound as a non-destructive method to characterize the extracellular matrix of excised murine kidneys and livers. This allows for the study of both natural tissue scaffolds, as well as the contributions of the cellular and extra-cellular components to ultrasound backscatter.

Statement of Contribution/Methods

In this study, excised murine livers and kidneys were imaged with a Vevo2100 (VisualSonics Inc, Toronto) using nominal 40 MHz linear-array transducer, after being maintained in PBS. Subsequently the organs were decellularized by washing the tissue in sodium dodecyl sulfate (SDS) for 24 hours, followed by washing with Triton-X for

24 hours and finally washing and storing in PBS. In this process, the ECM of the tissue is isolated from its inhabiting cells, leaving an ECM scaffold of the tissue. The remaining extra-cellular matrix structures were reimaged.

Raw RF data was acquired and normalized by a reference phantom. Linear fits to the normalized power spectra allow for the estimation and comparison of the spectral slope and midband fit.

Results/Discussion

After decellularization, the organs were significantly smaller in volume with increased backscatter. The average spectral slope decreased from 0.12 dB/MHz to 0.04 dB/MHz for the kidney, compared to from 0.23 dB/MHz to 0.09 dB/MHz for the liver. The heterogeneous structure of the kidney was apparent in parametric images (see Figure), with the spectral slope and midband fit higher in the central medulla region.

The ability to compare backscatter from the extracellular matrix with and without cells allows for a detailed analysis of the contribution of individual cells to the ultrasound backscatter and could be employed to evaluate scaffold structures and progress of growth on these scaffolds.
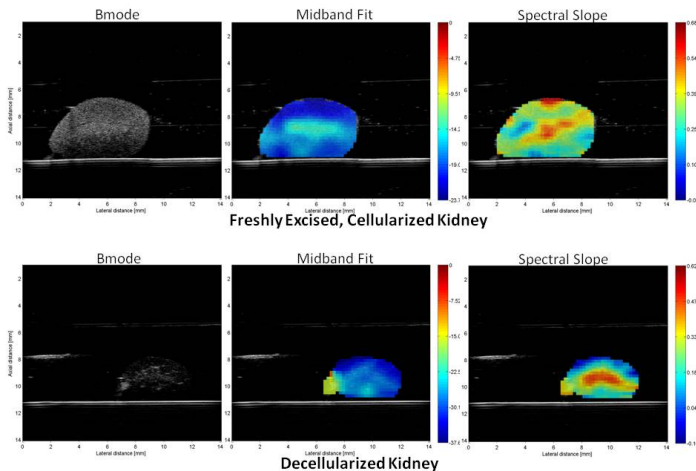
Figure: Columns show the Bmode image and parametric midband fit (dB) and spectral slope (dB/MHz) images of an excised murine kidney after excision (top) and after decellularizing (bottom). Axis dimensions are identical and images are of the same kidney to show relative change in size. Colorbars are scaled to the observed parameter ranges.

1G-3

4:00 pm   Structure Function: Relating Ultrasonic Measurement to Theory and Histology

Aiguo Han[1], William D. O'Brien, Jr. [1]; *[1]Department of Electrical and Computer Engineering, University of Illinois at Urbana-Champaign, Urbana, IL, USA*

Background, Motivation and Objective

Ultrasonic scattering is determined by the properties of individual scatterers and the correlation among scatterer positions. The role of scatterer spatial correlation is significant for dense medium, but has not been fully understood. The effect of scatterer spatial correlation may be modeled by structure function (three-dimensional Fourier transform of the scatterer positions) as a frequency-dependent factor in the backscatter coefficient (BSC) expression. The objectives are to estimate the structure function acoustically and relate the structure function to theory and histology for improved tissue scattering modeling.

Statement of Contribution/Methods

The study has several contributions. First, we developed the cell pellet biophantom technique to isolate experimentally the structure function effect from the BSC, as opposed to incorporating the structure function into BSC models to interpret the experimental BSC as a whole. Second, we establish evidence to support that the structure function observed acoustically is correlated with the scatterer positions determined histologically. Third, the modeling of structure function is extended to polydisperse scatterer sizes.

Biophantoms were constructed by placing live cells of known concentration into coagulation media to form a clot. Three cell lines [Chinese Hamster Ovary (CHO; ATCC #CCL-61); 13762 MAT B III (ATCC #CRL-1666); 4T1 (ATCC #CRL-2539)] were used with multiple realizations for each cell line. The BSCs of the biophantoms were estimated over the frequency range 11 – 105 MHz. The structure function for a high-concentration (tissue-like) biophantom was isolated by comparing the BSC of the high-concentration biophantom with the BSC of a low-concentration biophantom for the same cell line (the low-concentration biophantom structure function was assumed to be unity). This acoustically determined structure function was then compared with the proposed model.

The histologically determined structure function was obtained as follows. The ultrasonically scanned biophantoms were histologically processed. H&E stained sections were digitized using the digital camera in sync with a light microscope (Olympus BX–51) at a magnification of 40 X. The positions of cell nuclei were recorded from the digital image and Fourier transformed to yield the structure function.

Results/Discussion

Acoustically determined, histologically determined, and model predicted structure functions showed agreement with each other. Fitting the model to the experimental data yielded cell radius estimates that were consistent with direct light microscope measures. The results demonstrate the role of scatterer position correlation on dense media scattering, and establish the correlation between acoustically determined structure function and histology.

1G-4

4:15 pm   Viscoelastic Imaging Using Acoustic Impedance Microscope and Its Application to Biological Tissue

Naohiro Hozumi[1], Shota Kajima[1], Agus Indra Gunawan[1], Sachiko Yoshida[1], Kazuto Kobayashi[2], Yoshifumi Saijo[3], Seiji Yamamoto[4]; *[1]Toyohashi University of Technology, Japan, [2]Honda Electronics Co., Ltd., Japan, [3]Tohoku University, Japan, [4]Hamamatsu Univ Sch Med, Japan*

Background, Motivation and Objective

Acoustic microscope is a powerful tool for tissue observation. As it can skip staining process, the observation can be finished in very short time. We have proposed the acoustic microscope for viscoelastic imaging by utilizing both pressure and shear waves focused on the target. This presentation deals with viscoelastic observation of cancerous liver.

Statement of Contribution/Methods

The specimen was placed on an acrylic plaque substrate with thickness of 0.5 mm. Pulsed pressure and shear waves with frequency range of 40 - 120 MHz were sequentially produced in the substrate and focused on the top surface of the substrate where the specimen was attached. The shear wave was produced when the pressure wave in water comes into the substrate with oblique incidence. Reflections were received by the same transducer and interpreted into bulk modulus, shear modulus and viscosity by means of frequency domain analysis. Mechanical scan made it possible to acquire 2D profiles of these three parameters.

Results/Discussion

Bulk modulus was estimated by pressure wave response. Shear modulus and viscosity were estimated by shear wave response, considering its frequency dependence. As a preliminary experiment, cancerous liver of rat was quantitatively observed. 2D profiles of bulk modulus, shear modulus and viscosity were displayed. Among these three profiles viscosity profile successfully highlighted the cancerous region as shown in Fig. 1. A good agreement with optical image was seen after staining with antibody.

Fig. 1 Cross sectional micro-images of a cancerous liver of rat, (left) elasticity image indicated in GPa and (right) viscosity image indicated in Pa·s. Displayed in color scale.
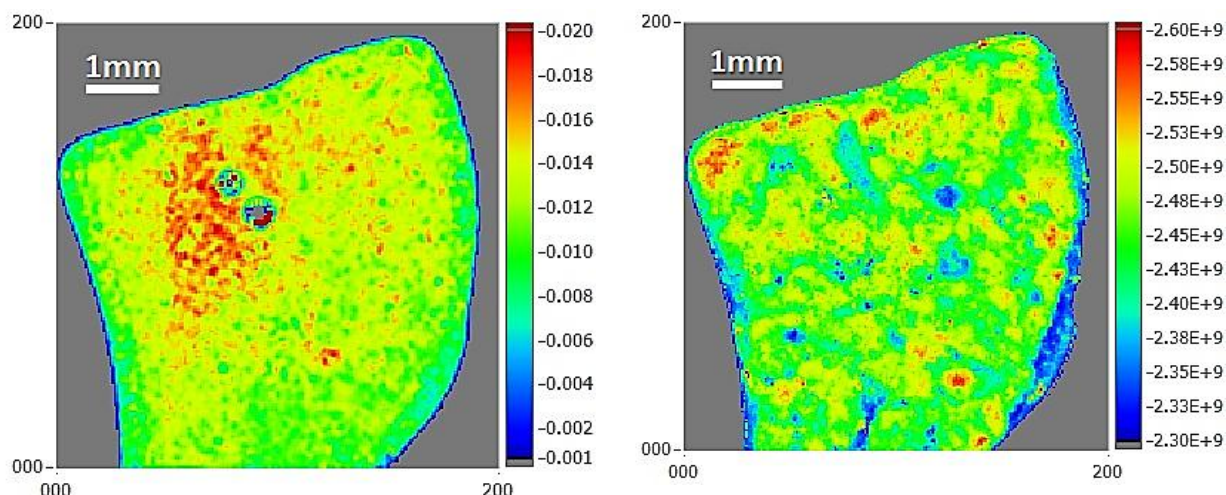
1G-5

4:30 pm **Ultrasound-scattering models based on quantitative acoustic microscopy of fresh samples and unstained fixed sections from cancerous human lymph nodes**

Jonathan Mamou[1], Daniel Rohrbach[1], Emi Saegusa-Beecroft[2], Eugene Yanagihara[2], Junji Machi[2], Ernest J. Feleppa[1]; *[1]F. L. Lizzi Center for Biomedical Engineering, Riverside Research, USA, [2]Department of General Surgery, University of Hawaii and Kuakini Medical Center, USA*

Background, Motivation and Objective

Quantitative ultrasound (QUS) methods were developed to detect metastatic regions in freshly excised sentinel lymph nodes from breast-cancer patients using a 26-MHz transducer. These QUS methods use a Gaussian form factor to model ultrasound scattering. In this study, quantitative acoustic microscopy (QAM) at 250 MHz was performed to obtain 2D maps of speed of sound (c), attenuation (A) and acoustic impedance (Z) of nodal tissue microstructure with a spatial resolution of 7 μm. These maps were used to develop new ultrasound-scattering models to enhance the sensitivity and specificity of QUS methods.

Statement of Contribution/Methods

QAM was performed on 12 fixed and three fresh lymph-node samples. 12-μm sections of deparaffinized, fixed tissue and fresh half nodes were scanned using a custom-built QAM system based on an F-1.16, 250-MHz transducer (160-MHz bandwidth). Radio-frequency (RF) signals were digitized at 2.5 GHz with 12-bit accuracy, and 2D QAM maps of Z (Fig. 1a), A, and c were generated using custom-developed signal-processing algorithms. Scanned samples were stained using hematoxylin and eosin and imaged by light microscopy (Fig. 1b). Z maps were then processed to yield a novel lymph-node-specific scattering model (i.e., form factor), which then was compared to the currently used Gaussian model (Fig. 1c). The new model was obtained by optimizing an exponential model fit to the Fourier transform of the autocorrelation of the 2D Z maps that assumed isotropy.

Results/Discussion

The spatial resolution and contrast of QAM maps were sufficient to distinguish among tissue regions consisting of lymphocytes, fat cells, and fibrous tissue (Figs. 1a and 1b). Average properties for lymphocyte-dominated tissue were 1577 ± 13 m/s for c, 4.3 ± 0.7 dB/MHz/cm for A, and 1.65 ± 0.04 Mrayl for Z. For the sample of Fig. 1, we found a significant increase ($p < 0.05$) of 29 ± 1 m/s for c and 2.1 ± 0.1 dB/MHz/cm for A in fibrous connective tissue compared to lymphocyte-dominated tissue. The study also demonstrates that fine-resolution maps of acoustic properties of lymph nodes can be used to improve the model of ultrasound scattering at 26 MHz. The new lymph-node-specific, ultrasound-scattering model is expected to improve current QUS approaches for detecting metastatic regions in freshly excised sentinel lymph nodes from breast-cancer patients.
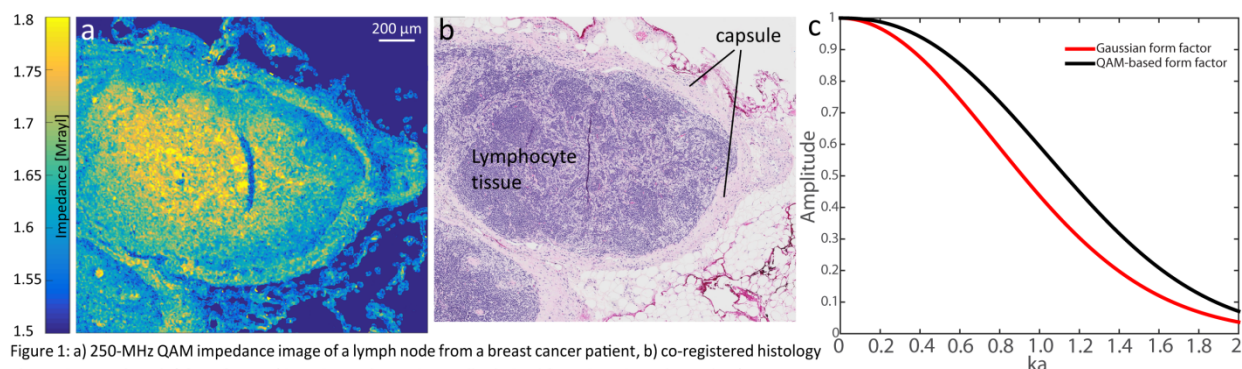
Figure 1: a) 250-MHz QAM impedance image of a lymph node from a breast cancer patient, b) co-registered histology photomicrograph and c) form factors (Gaussian and experimentally-derived from QAM impedance data).

4:45 pm **Plaque characterization using integrated electrochemical spectrum and intravascular ultrasound sensors**

Rongsong Li[1], Xiaoxiao Zhang[2], Teng Ma[3], Nelson Jen[1], Tyler Beebe[1], **Jianguo Ma[1]**, K. Kirk Shung[3], Qifa Zhou[3], Yu-Chong Tai[2], Tzung Hsiai[1]; [1]*Department of Medicine, University of California, Los Angeles, Los Angeles, California, USA,* [2]*Department of Electrical EngineeringEngineering and Applied Science Division, California Institute of Technology, Pasadena, California, USA,* [3]*Department of Biomedical Engineering, University of Southern California, Los Angeles, California, USA*

Background, Motivation and Objective

Vulnerable plaque rupture is the leading cause of death in the developed world. Growing evidence suggests that thin-cap fibroatheromas rich in macrophage/foam cells and oxidized low density lipoprotein (oxLDL) are prone to destabilization. However, it is challenging to characterize the vulnerable plaques with individual detection methods. We developed an integrated sensor composed of an electrochemical spectrum (EIS) sensor to measure plaque laden with oxLDL and a broadband intravascular ultrasound (IVUS) transducer to acquire plaque morphology. Correlation analysis of EIS and IVUS results would lead to improved characterization of the vulnerable plaques *in vivo*.

Statement of Contribution/Methods

The integrated sensor was fabricated on an acoustic-transparent ethylene-vinyl acetate (EVA) tube. The IVUS transducer with a center frequency of 15 MHz was mounted at the tip of torque coil and fitted inside the tube. The EIS sensor was attached on a balloon mounted on the outer surface of the EVA tube (see Fig. (a)). In the experiment, the chirp signal was used to excite the IVUS transducer and pulse compression algorithm was used to improve the imaging quality. Then the EIS sensor was positioned to areas of plaques and the EIS was acquired with the balloon inflated.

Results/Discussion

The integrated sensors were deployed in 7 rabbits: 4 control rabbits fed on normal chow, 3 rabbits fed on a high-fat diet to develop atherosclerotic plaques. The EIS results (Fig. (b)) indicate > 15% differences on the impedance magnitude at > 100 kHz and > 11% differences on the phase at 15 -- 100 kHz between the high fat diet and the control group. The IVUS imaging result (Fig. (c)) reveals the plaques inside the lumen, which were validated by histology. In the imaging position, the plaques cover about 40% of the lumen. The current iteration of the sensor does not account for the relative orientation of the EIS and IVUS sensors. As a result, the EIS sensor may not be positioned directly on the plaques of interest, leading to a relatively large standard deviation (up to 17%). An alignment mechanism will be included in the next design and further correlation of the results will be analyzed.

(a) (b) (c)
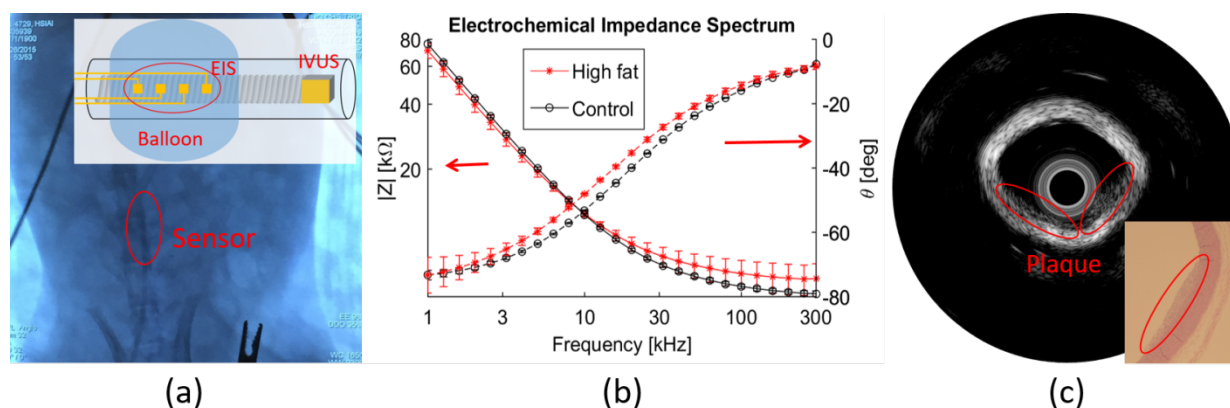
2G - MBB: Beamforming IV

VIP

Friday, October 23, 2015, 03:30 pm - 05:00 pm

Chair: **Jan D'hooge**
Catholic University of Leuven

2G-1

3:30 pm   Nonlinear beamforming of aperture domain signals

Brett Byram[1]; [1]*Biomedical Engineering, Vanderbilt University, TN, USA*

Background, Motivation and Objective

Despite the advances in ultrasound system hardware and transducers, ultrasound image quality continues to be a challenge. Despite ultrasound's high potential image quality, the variability in realized image-quality is extremely large. In some patients, ultrasound produces pristine images that rival any modality, but in others, ultrasound fails to be useful. There are a number of causes of image degradation; however, growing evidence suggests that image quality may be substantially improved just by correcting for reverberation. Reverberation can be suppressed using non-linear beamforming strategies, which includes our aperture domain model image reconstruction (ADMIRE) method.

Statement of Contribution/Methods

In order to address both reverberation and off-axis scattering, we introduced ADMIRE. ADMIRE linearizes the problem of reverberation by only considering the final scattering event after energy is scattered multiple times. Using this insight, we create a linear model matrix where each column is a model of the wavefront from a given spatial origin. The model matrix is used to decompose a set of channel data, but the problem is ill-posed since we may have 10's to 100's of thousands of predictors in our matrix. In the past we implemented a form of forward selection regression with a continuous model space. Currently, we decompose a discrete model-space with an elastic-net regularization constraint. Elastic-net combines properties of L1 and L2-type constraints. We apply this technique to various types of data including non-linear and pseudo non-linear simulations, as well as *in vivo* data.

Results/Discussion

First, we apply our algorithm to linear Field II simulations. In this case, with no added clutter, ADMIRE should reproduce delay and sum beamforming exactly. We find that delay and sum and ADMIRE differ by 0.5±1.1 dB on lesions ranging from anechoic to +20dB contrast. When adding simulated reverberation and off-axis clutter to the linear Field II simulations and then applying ADMIRE, we see average contrast improvements of 4.0, 8.7, 15, and 12 dB for signal to clutter ratios of 20, 10, 0 and -10 dB. On *ex vivo* reverberation measurements we see 15 dB of clutter suppression. We also applied our algorithm to *in vivo* data. With our newest realization of ADMIRE we find 15±7.0dB improvement in contrast. Two *in vivo* examples are shown below.
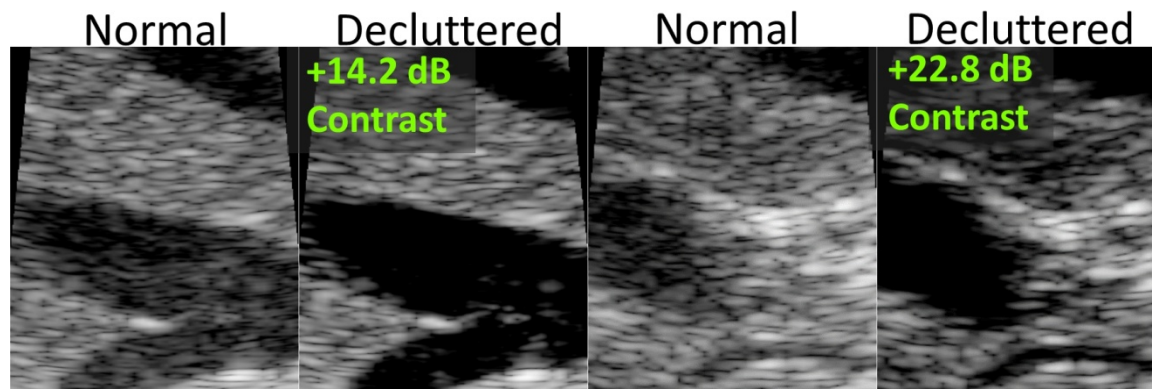
2G-2

4:00 pm   Improved array beam steering capability by compensation of inter-element cross-talk

Alessandro Ramalli[1], Alessandro Stuart Savoia[2], Giosuè Caliano[2], Piero Tortoli[1]; [1]*Information Engineering Department, University of Florence, Firenze, Italy*, [2]*Department of Engineering, Università degli Studi Roma Tre Roma, Rome, Italy*

Background, Motivation and Objective

When steered one-way beams of ultrasound linear/convex array probes are experimentally detected, distortions like those visible in Fig.1A may be observed. These beam deformations, and in particular the reduced steering, can have detrimental effects, especially in Doppler applications. In this paper, it is hypothesized that such effects are due to the cross-talk between neighbor elements, causing an apparent widening of the transmitting elements, which increases the equivalent directivity. A simple cross-talk model is introduced and its validity is tested through Field II simulations that are compared to measurements. Furthermore, a suitable element apodization, based on the above hypothesis, is proposed and shown able to reduce the beam distortions.

Statement of Contribution/Methods

The simplified model assumes that the cross-talk significantly affects only the two elements adjacent to the transmitting one. The model adds to the signal transmitted by each element a certain percentage (X) of the signals transmitted by the nearest neighbor elements.

One-way fields like that in Fig.1A were measured by using two different scanners coupled to 1 convex and 4 linear arrays produced by different manufacturers. For each probe, we collected measurements with different settings in terms of active aperture, focal depth, steering angle, apodization, and central frequency. With the same settings, we conducted simulations by sweeping the variable X in 5%-step. Using the measured fields as reference, X was then indirectly estimated as the value that minimized the average relative error (ε) of the resulting one-way field in the region delimited by the -12dB isoline.

Since the effect of constructive or destructive interference on neighbor elements may be seen as equivalent to an undesired apodization over the active aperture, predictable for each estimated X value, a proper apodization function may be applied to compensate the above effects.

Results/Discussion

For the 5 probes, one-way measurements were made and for each of them X was estimated (maximum value: 35%). The relative error between simulations and measurements is reduced from more than 20% to less than 6% (Fig. 1A-B) by introducing the cross-talk model. The proposed apodization function demonstrated to be effective in correcting the steering direction both in simulations and measurements (Fig. 1C-D) ($\varepsilon = 10\%$).
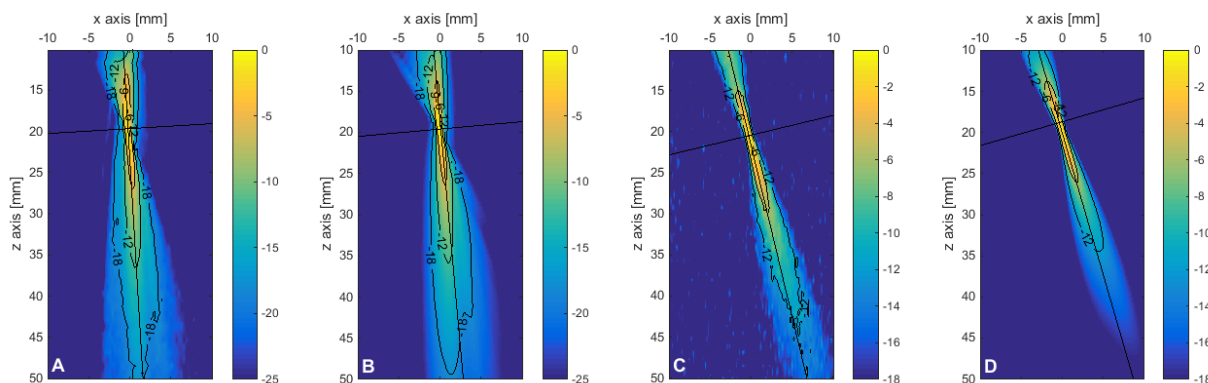
Fig. 1 Measured (A) and simulated (B) distorted one-way fields (nominal steering: 18°). The focal position (0, 20) mm is correct, while the steering is significantly reduced. Measured (C) and simulated (D) one-way fields, both obtained with an apodization function designed to compensate a 35% cross-talk.

2G-3

4:15 pm   Time domain compressive beamforming: application to *in-vivo* echocardiography

Guillaume David[1], Jean-luc Robert[2], Bo Zhang[3], Andrew Laine[1]; [1]*Biomedical Engineering, Columbia University, New York City, New York, USA,* [2]*Philips Research North America, USA,* [3]*Medisys, Philips Research France, France*

Background, Motivation and Objective

Over the past few years, Compressive Sensing (CS) has gained interest from the beamforming community as it allows the reconstruction of images from less measurements than conventional techniques such as Delay-and-Sum (DAS). Whereas the beamforming of medical ultrasound images is typically done in the time domain, CS was previously implemented in the frequency domain. The authors developed a time domain compressive beamforming (t-CBF) technique based on expressing beamforming as a matrix multiplication. Images of bubbles in water at a very high frame rate (about 5 kHz) were demonstrated, as well as hyper-resolution of point scatterers. In this paper, we propose to study how t-CBF performs on images displaying a speckle pattern and *in-vivo* data using a single diverging wave as the excitation pulse.

Statement of Contribution/Methods

In order to apply t-CBF to *in-vivo* data, two important refinements are introduced here. First, we apply the Hilbert transform to the pre-beamformed signal to reduce the sampling frequency. This allows us to compute wide field-of-view images, and to decrease the computational cost. Then, we use wavelet transforms. Indeed, whereas images of point scatterers in a homogeneous medium are naturally sparse, images displaying speckle are not. The wavelet transform sparsifies them. Different wavelet bases are studied (Haar, Daubechie, Battle-Lemarie) as well as decimated/non-decimated transforms. The technique was tested on Field II simulated phantoms. A phased array was modeled, emitting a single diverging wave at 2.6 MHz with a 0.6 fractional bandwidth. Then, it was applied to *in-vivo* cardiac data acquired with a hardware-modified Philips iU33 and a S5-1 sector probe.

Results/Discussion

On the simulated phantom, we found that with only one transmit we were able to reconstruct an image (figure 1.a) with resolution and side-lobe level much better that 1 Tx DAS images (figure 1.b) and comparable to conventional 80 Tx DAS. The contrast in the cysts is close to 60dB. The use of the Hilbert transform allowed us to reduce the number of time samples up to 15-fold without noticeably affecting the IQ. The non-decimated wavelet transform introduced more redundancy and improved the general robustness of the technique (figure 1.a-c), while moderately increasing the computational cost. A comparison of DAS and t-CBF on an *in-vivo* cardiac image is shown in figure 1.d-e.
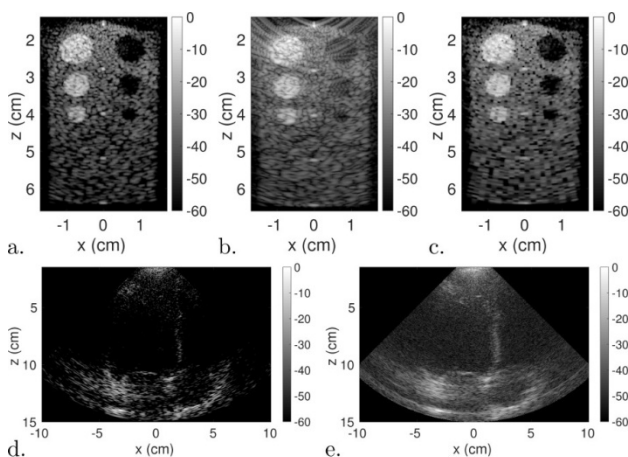
Figure 1: cyst phantom a. non-decimated Haar wavelets, t-CBF; b. DAS, 1 Tx; c. Haar wavelets, t-CBF and in-vivo cardiac d. non-decimated Haar wavelets, t-CBF; e. DAS, 1 Tx. We can perceive the left wall of the heart in the t-CBF image whereas it is completely masked by noise in the DAS image.

FRIDAY ORAL

4:30 pm **Multi-line transmit beamforming for high frame rate wide field-of-view tissue Doppler imaging: in-vivo validation and initial clinical findings**

Ling Tong[1,2], Alessandro Ramalli[3], Giuseppe Fradella[4], Sabina Caciolli[4], Piero Tortoli[3], Jianwen Luo[1], Jan D'hooge[2]; *[1]Department of Biomedical Engineering, Tsinghua University, Beijing, China, People's Republic of, [2]Department of Cardiovascular Sciences, KU Leuven, Leuven, Belgium, [3]Department of Information Engineering, Università degli Studi di Firenze, Florence, Italy, [4]Cardiology Unit, Careggi Hospital, Florence, Italy*

Background, Motivation and Objective

Tissue Doppler imaging (TDI) is widely used in clinical routine to assess regional myocardial motion/deformation. Typically, a high frame rate (HFR) can be achieved by narrowing down the field of view (FOV) to ~30° (only covering 1 cardiac wall). However, a wide FOV is required in some clinical applications to image the whole left ventricle (LV), reducing the frame rate. We previously proposed to use multi-line transmit beamforming (MLT) achieving HFR TDI and preserving a wide FOV (i.e. 90°sector) (MLT-TDI), thus avoiding any compromise. The aim of this study was to validate the MLT-TDI technique in-vivo and to investigate its performance in a clinical setting.

Statement of Contribution/Methods

Two different TDI sequences were implemented and interleaved on the ULA-OP research scanner: a conventional TDI sequence covering a 22.5° sector and a 4MLT-TDI sequence over a 90°sector. In both cases the achieved frame rate was 208 Hz. Using this setup, the septal wall of 8 healthy volunteers was imaged and the velocity was extracted using a standard autocorrelation estimator. For both TDI methods, the similarity of the extracted velocity curves was measured through their correlation coefficients and the peak systolic, early, late diastolic velocities (S', E', and A') were compared by linear regression and Bland-Altman analysis. Finally, this setup was also used to determine the basal septal-lateral wall time delay in a patient with LV dyssynchrony.

Results/Discussion

For both TDI methods, the velocity curves were very similar, with a mean correlation coefficient of 0.93 over all healthy subjects. Moreover, strong correlation and good agreement were found between the peak velocities obtained using both TDI methods (Figure (a)-(f)). Finally, for the patient, a time delay of 110 ms (> 65 ms, LV dyssynchrony marker) between the basal septal and lateral wall was estimated for both TDI methods. It may be outlined that a single recording was used to detect this time delay using 4MLT-TDI, whereas 2 recordings were required for the conventional TDI. Overall, our results demonstrate the suitability of MLT for wide FOV HFR TDI. This may open the opportunity of simultaneously assessing the regional myocardial function of the whole LV at HFR.
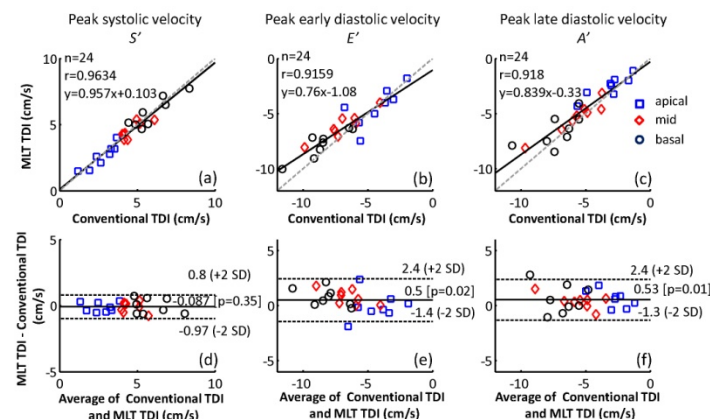
Figure. (a)-(c) The correlation and (c)-(f) Bland-Altman plots of peak velocities obtained by conventional-TDI and MLT-TDI. The mean difference (middle line) and the 95% limits of agreement are indicated (dashed lines) in the Bland-Altman plots.

4:45 pm **Optimum beamformer strategy for detecting signals in clutter noise**

Hans Torp[1], Alfonso Rodriguez-Molares[1], Lasse Lovstakken[1]; *[1]Circulation and Medical Imaging, Norwegian University of Science and Technology, Norway*

Background, Motivation and Objective

Several approaches to enhance image contrast between signal and clutter have been proposed based on the coherence between the array element signals. However, the performance of said methods is often difficult to assess, as it is dependent on the grayscale mapping. In this work, classical detection theory is used to find an optimum beamformer algorithm, and compare detection performance and spatial resolution with two other methods; standard beamsum and Short Lag Spatial Coherence (SLSC).

Statement of Contribution/Methods

We apply the Neyman-Pearson (NP) test to obtain optimum detection of a region with fully developed speckle in clutter noise. NP-test gives maximum detection probability, with a given clutter level. Assuming Gaussian signals with known covariance matrix for signal and noise, a sufficient statistics is found as a quadratic form of the element signals, with weight-matrix given by the signal and noise covariance matrices. Several beamforming methods, including standard beamsum (BS), and short lag spatial coherence (SLSC) can be expressed in the same way as a quadratic form, with different weight–matrices.

By eigenvalue decomposition of the weight-matrix, the beamformer output can be written as a square sum of several standard beamsum terms, with the eigenfunctions as apodization windows. The receive beamprofile can therefore be calculated as the square sum of the Fourier transform of the eigenfunctions. In this way the weight-matrix can be optimized both for detection and spatial resolution/side lobe level.

Results/Discussion

A simulation experiment, using Field II, was performed: a circular-shaped uniform speckle region was set in band-pass filtered white noise, with SNR= 9 dB. The left panel shows the receiver operating characteristic (ROC) curves for the 3 beamformer methods NP, BS, and SLSC with Q=5.2%(fraction of transmit aperture), and corresponding binary images where the threshold is set for a 5 % false positive detection in all images. The right panel shows the point spread functions and the 2-way beam profiles. The B-mode images has 22 dB dynamic range.

The NP-test showed the best detection performance, but slightly higher sidelobe level than BS. SLSC showed poorer detection performance than the two other methods, as well as higher sidelobes. For higher SNR (>18 dB) the detection performance of SLSC becomes better than BS but it is still inferior to NP
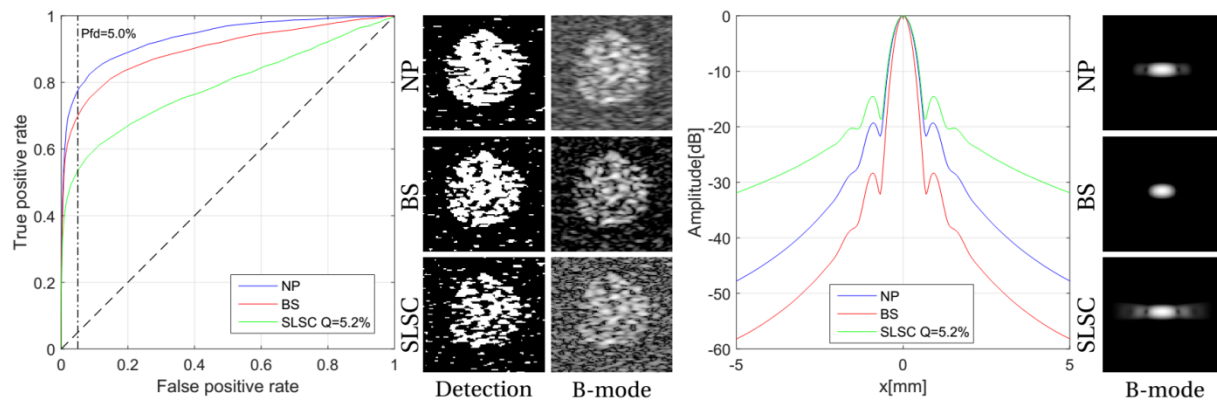
3G - MEL: New Applications of Elasticity Imaging

201BC

Friday, October 23, 2015, 03:30 pm - 05:00 pm

Chair: **Caterina Gallippi**
UNC Chapel Hill and NCSU

3G-1

3:30 pm   **Ultrasound Strain Relaxation Time Ratio: A Quantitative Marker for Assessment of Cortical Inflammation/edema in Renal Allografts**

Jing Gao[1], Robert Min[1], Keith Hentel[1], Jonathan Rubin[2]*; [1]Radiology, Weill Cornell Medical College, New York, New York, USA, [2]Radiology, University of Michigan, Ann Arbor, Michigan, USA*

Background, Motivation and Objective

A significant challenge in managing renal transplant recipients is how to detect subclinical allograft inflammation. Ultrasound elasticity imaging (UEI) has been used to assess soft tissue mechanical property changes following pathological damage. Renal cortical edema caused by rejection and inflammation is a dominant pathology following renal transplantation. We assessed the ability of ultrasound strain zero crossing ratio, as the ratio of strain relaxation time of cortex to reference soft tissue in quantifying cortical inflammation/edema in renal allografts.

Statement of Contribution/Methods

IRB approved the study and all subjects provided informed consent. We prospectively performed freehand UEI on 16 patients who underwent ultrasound guided transplanted kidney biopsy as standard of care. Strain relaxation time is estimated with ultrasound strain zero crossing measurement technique that is the time point of renal cortex (reference abdominal soft tissue) return to its initial status during tissue relaxation in decompression. Tissue strain was produced by freehand external compression with an ultrasound transducer and was estimated with 2-D speckle tracking software (EchoInsight). We used 3-second cycle single compression technique in the study. We analyzed the relationship between strain relaxation time ratio that is defined as the time of the cortical strain return to zero divided by the time of reference strain return to zero and grade of the cortical inflammation using Banff score as reference standard.

Results/Discussion

A statistically significant difference in the strain relaxation time ratio was found between the recipients with ≤25% (n=8) and >26% (n=8) renal cortical inflammation/edema (0.92±0.08 vs 1.15±0.10, P= 0.0002) based on t test. The strain relaxation time ratio also has high reliability, reproducibility, and accuracy. Using 1 as the best cutoff value, both sensitivity and specificity of the strain relaxation time ratio in determining >26% cortical inflammation/edema was 100%. The time of strain relaxation returning to its initial state is closely correlated with the severity of cortical inflammation in renal allografts. The strain relaxation time ratio is greater than 1 when cortical inflammation/edema is >26% whereas it is less than 1 when cortical inflammation/edema is ≤ 25%. Our results suggest that the strain relaxation time ratio of cortex/reference soft tissue can be used as a quantitative marker for monitoring cortical inflammation in renal allograft. Further study in variable grade of cortical inflammation in a large of subjects is warranted.

Main references:

1. Gao J and Rubin JM. Ultrasound Strain Zero-crossing Elasticity Measurement in Assessment of Renal Allograft Cortical Hardness: A Preliminary Observation. UMB 2014;40:2048-57.

2. Berry GP, et al. The spatio- temporal strain response of oedematous and nonoedematous tissue to sustained compression in vivo. UMB 2008; 34:617-29.

3G-2

3:45 pm   **Ex vivo measurement of shear wave speed dispersion in placenta using Transient Elastography.**

Samuel CALLE[1], Emmanuel SIMON[1,2], Marie-Coline DUMOUX[1], Emmanuel NICOLAS[1], Franck PERROTIN[1,2], Jean-Pierre REMENIERAS[1]*; [1]INSERM U930 - F. Rabelais University, TOURS, France, [2]Department of obstetrics, gynecology and fetal medicine, University Hospital Center of Tours, TOURS, France*

Background, Motivation and Objective

Obstetric pathologies associated with placental dysfunction correspond to an important public health issue. In the case of intrauterine growth retardation (IUGR), significant changes in the villous architecture of IUGR placentas compared to normal placentas are observed, most likely changing the absolute value of viscoelasticity, but also its relationship with frequency. To this day, there have been a few studies of the placenta's biomechanical properties, but no clinical device provides information about its elasticity or architecture. The frequency behaviour of tissue mechanical parameters may be modeled as a power law, in which case the exponent parameter represents a mechanical property inherent to a given material. In this context, the feasibility of measuring shear wave dispersion in placentas is tested *ex vivo*.

Statement of Contribution/Methods

The proposed Transient Elastography (TE) method is based on the propagation of a plane shear wave generated by a plate fixed to a low-frequency electromechanical actuator and measured using an ultrafast US scanner (Aixplorer). IQ demodulated complex data are acquired at 2.8 MHz with a PRF of 5 kHz. The particle velocity Vz is computed using extended autocorrelation method. Calculating the spatial FFTs of $Vz(x,\omega)$, the shear wave speed dispersion curve $Cs(\omega)$ is obtained between 20 Hz and 60 Hz. Previously validated on calibrated elasticity phantoms, this method is applied on 8 healthy delivered placentas (<12h after delivery). TE measurements are performed 3 times with repositioning (central and peripheral regions) and compared with ShearWave Elastography (SWE) measurements.

Results/Discussion

In agreement with literature, elasticity measured at a fixed frequency by SWE and TE is in the same order of magnitude for both regions. Moreover, a low inter-individual variation is found: in the peripheral region, Cs measured with SWE is 1.83±0.18 m/s, and 1.80±0.24 m/s with TE (at 50 Hz). TE measurements show high reproducibility: for example, Cs measured at 50 Hz in placenta 3 is 2.05±0.10 m/s. The experimental data obtained with TE (between 20Hz and 60Hz) is fitted with a classical Voigt model and a fractional rheological model $(G^*(i\omega)=G_e+K.[i\omega]^n)$. One result is that 2 placentas with similar elastic modulus values can present different exponent parameter n. For example, the values of placentas 1 and 8 are, respectively: Cs from SWE method: 1.76±0.09 m/s and 1.70±0.16 m/s; Cs at 50 Hz from TE method: 1.87±0.19 m/s and 1.86±0.23 m/s; linear constitutive parameter n from the fractional rheological model: n=1.10±0.05 and n=1.35±0.07. These preliminary results suggest the added-value of the elasticity frequency analysis for placental exploration. *Ex vivo* measurements comparing healthy and IUGR placentas using an optimized system dedicated for *in vivo* application are in progress.

4:00 pm   3D Ultrasound Strain Imaging of Skeletal Muscle Deformation

Kaj Gijsbertse[1], André Sprengers[2], Nico Verdonschot[2,3], Chris de Korte[1]; *[1]Medical UltraSound Imaging Center (MUSIC), Department of Radiology and Nuclear Medicine, Radboud university medical center, Netherlands, [2]Orthopaedic Research Laboratory, Department of Orthopaedics, Radboud university medical center, Netherlands, [3]Department of Biomechanical Engineering, University of Twente, Netherlands*

Background, Motivation and Objective

The aetiology of many musculoskeletal diseases is related to the biomechanical condition of the affected muscle. Muscle contraction is characterized by large deformation and translation, which requires a multi-dimensional imaging modality to reveal its deformation. We developed a full 3D ultrasound technique for a comprehensive mapping of the 3D muscle contraction whereas previous work was limited to 2D and bi-plane techniques.

Statement of Contribution/Methods

A phantom (10x10x10cm), constructed from a homogeneous 10% gelatin and 1% silica scattering particles solution, was compressed 3% vertically using an automated plate compressor. Pre- and post-compression, full volume radio frequency (RF) ultrasound data were acquired using a Philips iE33 system, equipped with an X7-2 matrix array. A cross-correlation based algorithm using 2D and 3D kernels was applied to obtain the displacements estimates. These estimates were converted to Cartesian space and subsequently, strain was derived using a Least Squares Strain Estimator. The 3D results were compared with the 2D results and the theoretically predicted displacement and strain. Comparison between 2D and 3D kernels was performed on data from a plane with a large tilt angle to study the influence of out-of-plane motion on the two techniques. To demonstrate the in vivo feasibility, 3D strain was calculated from live 3D data, acquired during a 2 second isometric contraction and relaxation of the quadriceps muscle in a healthy volunteer.

Results/Discussion

The phantom study showed good agreement between estimated displacements and the theoretically predicted displacements. Root Mean Squared Errors (RMSE) were 0.16, 0.17 and 0.13 mm in x-, y- and z-direction respectively. The RMSE for the 3D strain values were 0.94, 1.2 and 0.41 % in x-, y- and z-direction respectively. The 2D method performed worse, with 3 (x-direction) to 6 (z-direction) times higher RMSE values. The 3D technique provided high quality in vivo strain images over the contraction and relaxation cycle (Figure 1). The strain curves show the anisotropic behavior of the muscle.

In conclusion, the use of 3D kernels improves 3D displacement estimation and allows muscle deformation estimation using real-time 3D ultrasound RF-data. Future work will focus on investigating local differences of strain in muscles and its clinical relevance.
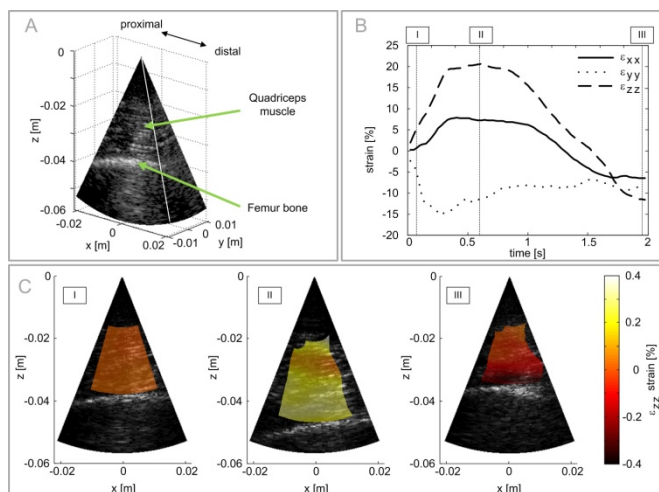
Figure 1. A) 3D ultrasound image of the quadriceps muscle. B) Mean strain curves as a function of time, and C) the strain in z-direction visualized at the middle plane for the three annotated time points in panel B: point I, at starting of the contraction, point II, at maximum contraction and point III, at total relaxation of the muscle.

4:15 pm   Prostate Vibro-Elastography: Multi-frequency 1D over 3D Steady-State Shear Wave Imaging for Quantitative Elastic Modulus Measurement

Julio Lobo[1], Ali Baghani[1], Hani Eskandari[1], Sara Mahdavi[2], Robert Rohling[1], Larry Goldenberg[3], William James Morris[4], Septimiu Salcudean[1]; *[1]Electrical and Computer Engineering, University of British Columbia, Vancouver, BC, Canada, [2]British Columbia Cancer Agency, Vancouver, BC, Canada, [3]Department of Urologic Sciences, Vancouver General Hospital, Vancouver, BC, Canada, [4]Department of Oncology, British Columbia Cancer Agency, Vancouver, BC, Canada*

Background, Motivation and Objective

This article describes a state of the art ultrasound system that is used to quantify tissue elasticity of the prostate.

Statement of Contribution/Methods

The system involves the measurement of the steady-state multi-frequency response of tissue to transperineal excitation while imaging the gland using the sagittal array of the BK Medical 8848 trans-rectal ultrasound transducer. A roll motor rotates the transducer in discrete steps to create a volume sector of images. GPU Processing of raw in-phase/quadrature data streamed from the ultrasound machine is used to measure the axial (radial) spatial distribution of tissue motion and compute displacement phasors. Bandpass sampling is used to perform the reconstruction since the sampling frequency is below the Nyquist rate. Finally, a local frequency estimator is used to compute the Young's Modulus from the three dimensional local spatial wavelengths of the shear wave that is created at each of the excitation frequencies.

The system is not constrained by displacement amplitude restrictions and also allows for continual repeated measurement.

Results/Discussion

The system has been used in several clinical studies but its design and function has not been published before. Some of the study results have been published and include an area under receiver operating characteristic curve of 0.82±0.01 with regards to prostate cancer identification in the peripheral zone.

The accuracy of the elastic modulus measurement was validated using a CIRS elastography phantom. Numerical and visual correlations between our elasticity measurements and pathology results (see figures) demonstrate its clinical potential. The system has been expanded to a generic platform that can be used to provide real-time quantitative elasticity measurements in other organs.

A comparison of absolute elasticity maps to pathology results for one patient.
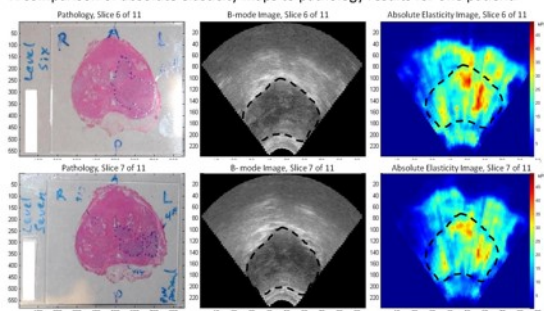
A comparison of absolute elasticity maps to mapping biopsy results for one patient.
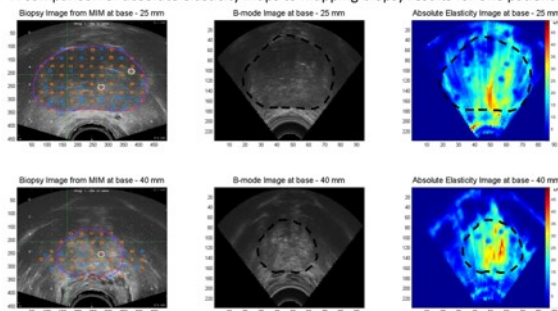
3G-5

4:30 pm   Spleen Ultrasound Shear Wave Elastography in Monitoring Transjugular Intrahepatic Portosystemic Shunt Function

Yuan-Yi Zheng[1], Xiao Zheng[1], Hai-Tao Ran[1], Zhi-Gang Wang[1], **Jing Gao**[2]; [1]*Ultrasound, Chongqing Medical University, Chongqing, China, People's Republic of,* [2]*Radiology, Weill Cornell Medical College, New York, New York, USA*

Background, Motivation and Objective

The creation of transjugular intrahepatic portosystemic shunt (TIPS) has been used in the management of the severe consequences of portal hypertension (PHTN) to control refractory acute variceal hemorrhage and intractable ascites in late stage liver diseases. It is important to monitor TIPS function in effectively decompressing portal vein pressure after TIPS placement. Therefore, non-invasive techniques for evaluating TIPS function are preferred since portosystemic pressure gradient (PPG) is too invasive. The aim of this study was to assess the ability of spleen ultrasound shear wave elastography in monitoring TIPS function following TIPS placement.

Statement of Contribution/Methods

Local ethical committee approved this study and all subjects provided written informed consents. We prospectively measured spleen ultrasound shear wave velocity (SWV, m/s) in 33 patients one day before TIPS procedure, then 3-6 days, 3 months, 6 months, and 12 months after TIPS placement. We also measured spleen SWV in 10 of 33 cases one day before and 3-6 days after TIPS revision. The differences in PPG and spleen SWV before and after primary TIPS placement and TIPS revision were examined with a paired t-test. The difference in spleen SWV before and at different time points following TIPS placement was tested with repeated-measures ANOVA. The correlation between PPG and spleen SWV was analyzed with Pearson's correlation coefficient. The diagnostic accuracy of spleen SWV in determining TIPS dysfunction was tested by ROC curve analysis.

Results/Discussion

During 12 months following up after TIPS placement, 23 patients had patent TIPS and 10 patients developed TIPS dysfunction. The PPG and spleen SWV decreased after TIPS placement and TIPS revision. The SWV increased when TIPS occluded. differences in PPG and SWV were found pre and post the primary TIPS placement and TIPS revision (all p<0.001). The best SWV value was observed in the third month of TIPS placement. A moderate positive correlation was found between PPG and spleen SWV (R2 =0.70). Area under ROC curve was 0.814. Using 3.6 m/s as the optimal cutoff value, the sensitivity and specificity of SWV in determining TIPS dysfunction was o.58 and 0.96, respectively. Our results suggest that spleen SWV can be used as a non-invasive quantitative marker in monitoring TIPS function.
Reference:

Gao J, et al. Clinical Imaging 2012
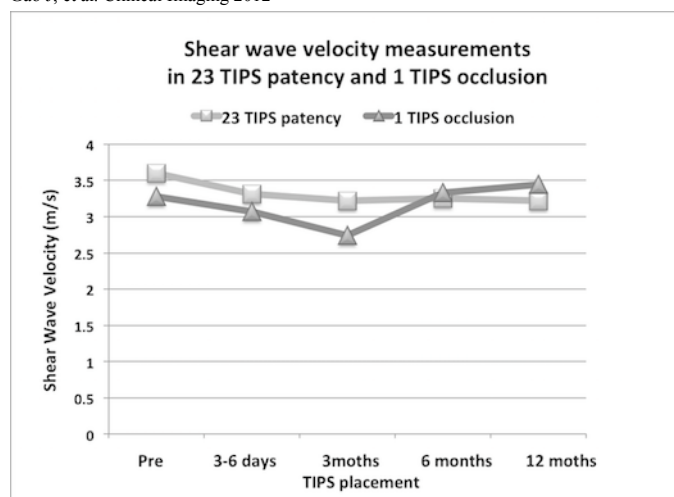
3G-6

4:45 pm   Local Lung Ventilation Estimation Using Ultrasound Strain Measurements

Jonathan Rubin[1], Jeffrey Horowitz[2], Thomas Sisson[3], Kang Kim[4], Luis Ortiz[5], James Hamilton[6]; [1]*Radiology, University of Michigan, Ann Arbor, Michigan, USA,* [2]*Internal Medicine, University of Michigan, USA,* [3]*University of Michigan, USA,* [4]*University of Pittsburgh, USA,* [5]*University of Pttsburgh, USA,* [6]*Epsilon Imaging, USA*

Background, Motivation and Objective

Estimating local lung ventilation would have major clinical consequences, however, such measurements are presently nearly impossible. Yet if possible, applications for such a method would include mechanical ventilator monitoring, assessments of chronic obstructive lung disease, pulmonary edema, and acute pneumonias. We hypothesized that ultrasound strain measurements from the moving lung surface during ventilation could provide such information.

Statement of Contribution/Methods

The surfaces of the right lungs in two human volunteers and the lungs in 7 mice, 2 controls and 5 mice with pulmonary fibrosis experimentally induced by either transtracheal bleomycin injection or intraperitoneal diphtheria toxin (DTR:DR) injection in a transgenetic mouse model. The human scans were done for demonstration purposes as part of an IRB approved protocol and were performed with a 6 MHz linear array (Epsilon Imaging, Ann Arbor, MI).

The mouse lung surfaces were scanned with a Visualsonics 2100 ultrasound scanner (FujiFilm, Visualsonic, Toronto, CA) at 40 MHz using a 55 MHz linear array. The mice were scanned in the prone position, and the lung surface motion was acquired in the longitudinal orientation. Lagrangian strains were estimated for both the humans and mice between two user defined regions of interest on the lung surface. The lateral strains were tracked using a commercial software package (EchoInsight, Epsilon Imaging, Ann Arbor, MI). Real-time radiofrequency (rf) signals were downloaded to the tracking program. In the mouse, an average peak-to-trough strain estimate was made for each acquisition. These averages were then combined to calculate mean strains for the controls and the treated mice. A hydroxyproline assay was used to assess pulmonary fibrosis. The groups of mice were compared using two-tailed t-test with $p < 0.05$ being considered significant.

Results/Discussion

The mean strain differences between the control mice and the two groups of treated mice are statistically significant (control vs DTR:DR, $p < 0.03$; control vs bleomycin, $p < 0.03$). Hydroxyproline concentrations were statistically significant or nearly statistically significant between the groups (control vs DTR:DR, $p<0.002$; control vs bleomycin, $p<0.06$). The human scans demonstrated strain estimates consistent with measurements in the literature.

Our preliminary results suggest that local lung strain estimates can be made in real-time using ultrasound speckle tracking of the lung surface during breathing. In mice, it was possible to distinguish normal lungs for those with pulmonary fibrosis. In humans, it appears that normal lung ventilation can be assessed. These results imply that local lung ventilation estimation could be evaluated with ultrasound, and methods similar to this could lead to a completely new application of ultrasound in clinical medicine, i.e. assessment of pulmonary function.

FRIDAY ORAL

4G - MIM: Medical Imaging I

201DE

Friday, October 23, 2015, 03:30 pm - 05:00 pm

Chair: **John Hossack**
Univ. of Virginia

4G-1

3:30 pm **Evaluation of directional reflectivity characteristics as new modality for 3D Ultrasound Computer Tomography**

Ernst Kretzek[1], Patrick Hucker[1], Nicole Ruiter[1]; *[1]Karlsruhe Institute of Technology (KIT), Institute for Data Processing and Electronics (IPE), Eggenstein-Leopoldshafen, Germany*

Background, Motivation and Objective

3D Ultrasound Computer Tomography (3D USCT) promises reproducible high-resolution images for early detection of breast tumors. Our prototype provides three different modalities: reflectivity, speed of sound, and attenuation. For reflectivity reconstruction a 3D synthetic aperture focusing technique (SAFT) is used which calculates one reflectivity value for each voxel from about 10 million A-scans. Due to this averaging the directional information of the reflection is lost. The aim of this work was to generate directional reflection characteristics for each voxel in the volume and to evaluate the results.

Statement of Contribution/Methods

Reflectivity characteristics were generated by extending the standard SAFT algorithm. Instead of averaging all A-scan values, the values are mapped to different directions, exploiting the advantage of the aperture, which records A-scans by transducers surrounding the measured breast in 3D. For the mapping different platonic solids and spherical grids with varying number of surfaces are used (see Fig 1. a)). Different post-processing methods were applied to extract new information about the measured breast based on the directivity data (see Fig 1. b)-e)). Evaluation was done with in-vivo experiments. Due to the high demands on performance and memory a GTX TITAN GPU is used, based on Kepler architecture with 6 GB global memory.

Results/Discussion

Using the reflectivity characteristics more information about different reflecting tissues inside the breast was made available. E.g. the local normals were approximated using the main direction of the reflections (see Fig 1. d)). Post-processing using the maximum of the reflectivity characteristic increased the contrast of the image by 32% (see Fig 1.c)) compared to the standard SAFT (see Fig 1. b)). Furthermore, the new data shows potential to be used for tissue classification by comparing features of their reflectivity characteristics (see Fig 1. e)). Regardless of calculating twelve-times more data for the simplest case, a performance of 46% of the standard SAFT algorithm on GPUs could be reached.
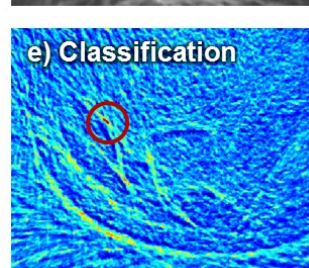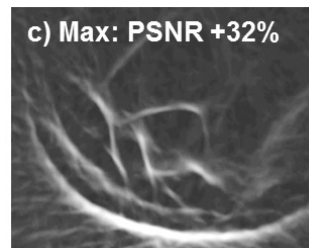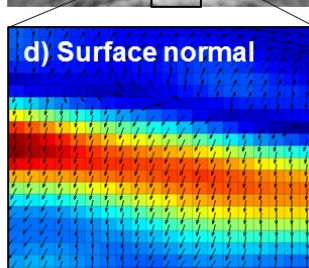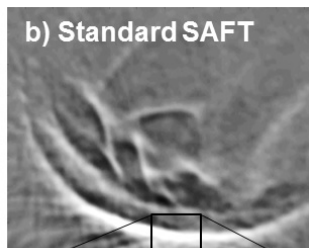
4G-2

3:45 pm **Quantitative imaging of speed of sound in echo ultrasonography**

Michael Jaeger[1], Martin Frenz[1]; *[1]University of Bern, Switzerland*

Background, Motivation and Objective

Imaging speed of sound (SOS) using ultrasound (US) is promising as a diagnostic modality. Computed ultrasound tomography in echo mode (CUTE) allows imaging SOS spatially resolved using pulse-echo US, based on the changing echo phase with changing angle of US transmission. Volunteer results demonstrate the potential of translating SOS-based diagnosis from through-transmission imaging to handheld echo US where it could help diagnose diseases of the abdomen. Apart from providing contrast, an absolute SOS value is highly desirable which would allow a user-independent quantitative diagnosis of e.g. liver disease progression. However, previous results strongly depended on the choice of the reference SOS (see Fig. a) and b): Same phantom, reference SOS was 1500 and 1460 m/s, respectively). The goal of this study was the further development of the technique towards the demonstration of quantitative CUTE.

Statement of Contribution/Methods

Thorough simulations allowed the identification of various data inconsistencies that led to a distortion of the baseline of the SOS image: i) A spatially varying centre frequency that affected the echo phase shift measurement. ii) Refraction of the transmit pulse at the probe aperture that led to an angle-dependent phase offset close to the image edges. iii) Missing echoes close to the image edges when transmitting at an angle different from zero. iv) A disadvantageous regularisation strategy.

By solving the inverse problem of CUTE in the space domain as opposed to frequency-domain, edge effects could be reduced. In combination with an improved regularisation strategy and a calibration of the local echo centre frequency, a strongly improved CUTE image could be obtained.

Results/Discussion

Simulation results suggest that with the above modifications, an accurate reconstruction of absolute SOS is possible. The modified technique was experimentally tested on layered phantoms. Distortions of the baseline of the SOS could be strongly reduced, and the SOS could be consistently reconstructed independent of the initial choice of the reference SOS (see Fig. c) and d): Same as (a) and (b) but using the modified technique). These results suggest that CUTE allows a quantitative diagnosis of tissue composition. In preparation for a pilot study of liver disease staging, preliminary volunteer results of SOS measurement of the liver will be presented.
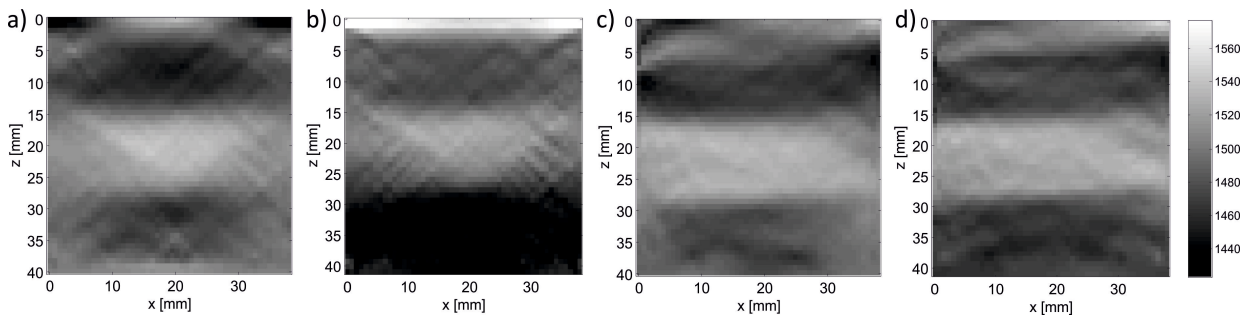
4G-3

4:00 pm   Needle detection by Image Source Localization

Alfonso Rodriguez-Molares[1], Lasse Lovstakken[1], Ingvild Kinn Ekroll[1], Hans Torp[1]; *[1]Circulation and Medical Imaging, Norwegian University of Science and Technology, Trondheim, Norway*

Background, Motivation and Objective

In conventional B-mode images, needles are poorly visualized due to the directivity of specular reflectors. A correct localization of needles is important for a number of ultrasound-guided clinical procedures, such as biopsies, regional anesthesia and fetal blood transfusion.

Statement of Contribution/Methods

We present a method for needle detection based on image source localization (ISL). The image source principle states that, if a sound source is placed in front of a planar reflector, the reflected sound field would be as if it were generated by an image source. The ISL method utilizes this interpretation in the following manner: a virtual source is generated in front of the reflecting plane by focusing the beam at a desired location, the image source location is estimated from channel-data with a state-of-the-art sound source localization algorithm based on statistical region contraction, finally the location and orientation of a section of the needle is resolved from the position of both sources. This procedure, illustrated in the left panel, is repeated iteratively to cover the full length of the needle and to refine the detection by optimization of the virtual source location.

Results/Discussion

The accuracy of the ISL method has been studied numerically using the k-wave simulation program. As shown in the central panel, the positional error stays below 30 μm for orientations respect to the transducer plane of up to 50°. The method also shows a notable robustness against thermal (SNR=-5dB) and speckle (SNR=5dB) noise that makes it possible to localize needles even when they are not visible in B-mode images.

The proposed method has also been tested experimentally with a Verasonics Vantage research scanner and a L12-3v probe. An Agar phantom (10 g/l) with scattering agent (Sephadex G-25 1 g/l) is used as background and a 20G cannula (Mediplast 0.9 x 150 mm) as target. One of the tests is shown in the right panel, for a needle orientation of 38.5°.
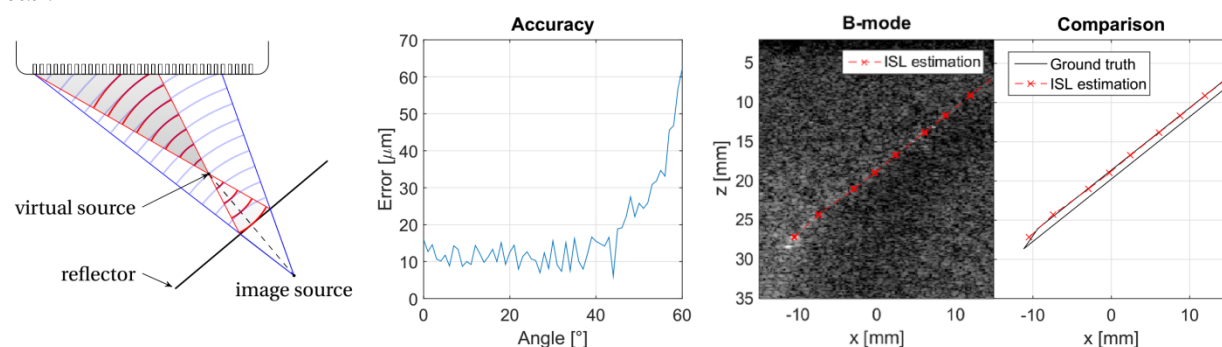
4G-4

4:15 pm   A sparse regularization approach for ultrafast ultrasound imaging

Rafael Carrillo[1], Adrien Besson[1], Miaomiao Zhang[2], Denis Friboulet[2], Yves Wiaux[3], Jean-Philippe Thiran[1], Olivier Bernard[2]; *[1]LTS5, Swiss Federal Institute of Technology, Lausanne, Switzerland, [2]CREATIS, CNRS UMR5220, Inserm U630, University of Lyon, INSA-Lyon, University of Lyon1, Villeurbanne, France, [3]Institute of Sensors, Signals and Systems, Heriot-Watt University, Edinburgh, United Kingdom*

Background, Motivation and Objective

Ultrafast imaging based on plane-wave (PW) insonification is an active area of research due to its capability of reaching high frame rates. Several approaches have been proposed based on either Fourier-domain reconstruction [Lu et al., IEEE UFFC97], [Garcia et al., IEEE UFFC13], [Bernard et al., IEEE IUS14], or delay-and-sum (DAS) reconstruction [Montaldo et al., IEEE UFFC09]. Using a single PW, these techniques achieve low quality, in terms of contrast, compared to the DAS method with focused beams. To overcome this drawback, compounding of several steered PWs is needed, which decreases the high frame rate limit. Based on a compressed sensing (CS) framework [Candès et al., IEEE SPM09], we propose a new method that allows reconstruction of high quality ultrasound (US) images from only 3 PW at the expense of augmenting the computational complexity at the reconstruction.

Statement of Contribution/Methods

Our method is based on transmitting PW steered at different angles. From each received echo, the technique uses Fourier slice theory to recover incomplete Fourier information of the object [Bernard et al., IEEE IUS14]. The spectrum derived from the different echoes are then averaged to create a synthetic spectrum which is modeled as

follows: y=Φx + n, where x is the desired image, Φ is the partial Fourier matrix and n is the model inaccuracy. Retrieving the USimage from the incomplete spectrum is an ill-posed problem, well studied in the CS framework. Assuming x has a sparse representation in a basis or in a redundant frame [Friboulet et al., IEEE IUS10], i.e. x=Ψu where Ψ is the sparsifying basis and u is a sparse vector, we use an L1-minimization algorithm [Carrillo et al., IEEE SPL13] to reconstruct a high quality image.

Results/Discussion

Contrast to Noise Ratio (CNR) has been computed from a numerical phantom of size 2x2cm with an echo-free inclusion of 1cm diameter in its center, positioned at 3cm depth from a linear-array probe. Raw signals were generated using Field II. The selected sparsifying transform is the Undecimated Wavelet Transform with Daubechies 4 function. The CNR results(Figure 1) were compared with 4 state-of-the-art PW imaging methods, and the DAS method based on focused beams. The proposed method outperforms all existing PW imaging methods. Using only 3 PW, it reaches same quality as Montaldo method with 13 PW and as the DAS method with 83 focused beams.
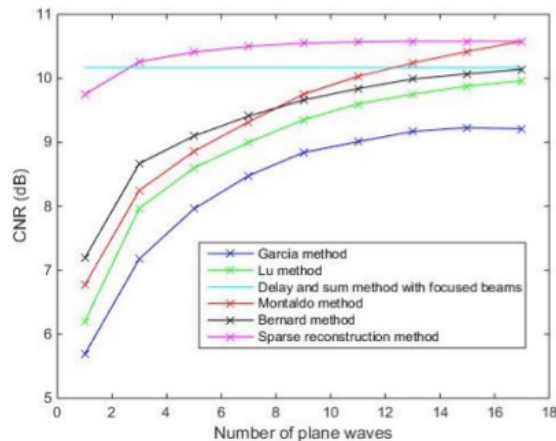
Figure 1. CNR comparison between the proposed method (magenta) and state-of-the-art methods.

4G-5

4:30 pm   Extension of Ultrasound Fourier Slice Imaging Theory to Sectorial Acquisition

Miaomiao Zhang[1], Adrien Besson[2], Rafael E. Carrillo[2,3], François Varray[1], Hervé Liebgott[1], Jean-Philippe Thiran[2,3], Denis Friboulet[1], Olivier Bernard[1]; [1]*CREATIS, CNRS UMR5220; Inserm U630;University of Lyon; INSA-Lyon; University of Lyon1, Villeurbanne, France,* [2]*Signal Processing Laboratory (LTS5), Ecole polytechnique fédérale de Lausanne (EPFL), Lausanne, Switzerland,* [3]*Department of Radiology, University Hospital Center (CHUV) and University of Lausanne (UNIL), Lausanne, Switzerland*

Background, Motivation and Objective

Ultrafast imaging based on diverging wave (DW) is an active area of research in ultrasound sectorial acquisition because of its capacity of reaching high frame rate. The current state-of-the-art technique is based on DW transmission and a reconstruction strategy using delay and sum (DW/DAS) [Hasegawa et al., J Med Ultrasonics11][Papadacci et al., IEEE UFFC14]. Recently, we have introduced the Ultrasound Fourier Slice Imaging theory [Bernard et al., IEEE IUS14] for the reconstruction of ultrafast imaging from linear acquisition using a single plane wave (PW). In this study, we extend this formalism to sectorial acquisition by using DW transmission and by developing a framework which allows projecting the PW reconstruction into a dedicated space.

Statement of Contribution/Methods

The key idea is to express the problem of sectorial image reconstruction in an equivalent formalism as the PW imaging theory we developed. Starting from the time-traveling equations involved when either a DW or a PW is emitted, we derived an explicit and invertible spatial transformation which allows deforming the referential Cartesian space into a dedicated one where the modified medium can be considered as being excited by a PW. We show that the use of ultrasound Fourier slice theory from the received raw data along with the application of the proposed inverse spatial transform allows reconstructing the insonified medium in the Cartesian space.

Results/Discussion

Contrast to noise ratio (CNR) has been computed from numerical phantoms of size 2x2cm with an echo-free inclusion of 1cm of diameter located at different depths and for different lateral positions (Fig.1-a,b). Each given value corresponds to a mean and standard deviation measurement computed from 50 phantoms, each of them being generated using a distinct random scatterers set. The RF signals were simulated using Field II with one DW transmission. The ultrasound images were reconstructed from the raw data using our approach and DW/DAS. The two algorithms exhibit similar performances in axial direction, whereas our approach obtains slightly higher CNR scores in lateral direction. This aspect is further reinforced by the better quality of the reconstructed PSFs using our method (Fig.1-c,d). These results show the ability of the proposed approach in recovering higher quality ultrafast images from sectorial acquisition compared to DW/DAS.
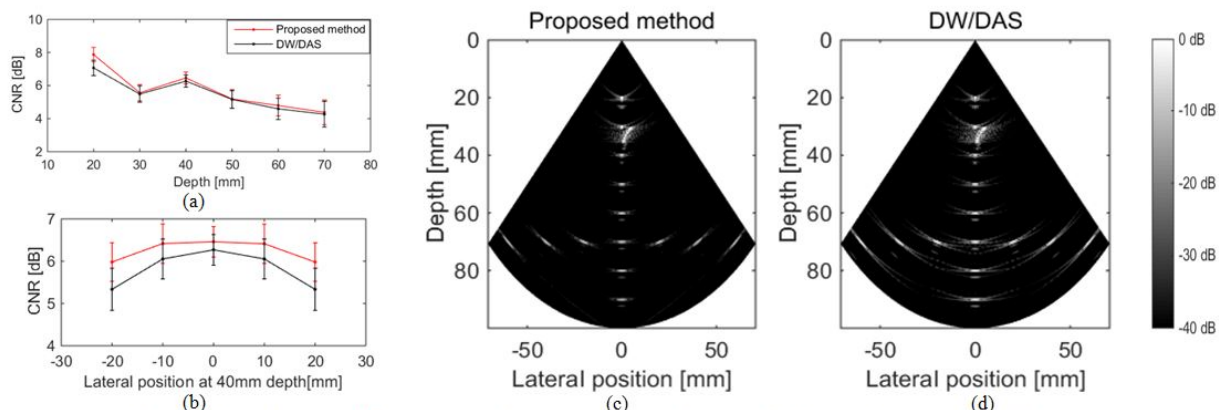
Figure1. Mean and standard deviation of CNR measurements as a function of axial depth a) and lateral positions b).
Reconstructed Bmode images using the proposed method (c) and the DW/DAS method d)

Institute of Electrical and Electronics Engineers

4G-6

4:45 pm **3D Post-processing of pre-beamformed RF Data in the Frequency-wavenumber Domain**

Hendrik Vos[1,2], Paul van Neer[3], Martin Verweij[2], Nico de Jong[1,2], Arno Volker[3]; *[1]Biomedical Engineering, Erasmus MC, Rotterdam, Netherlands, [2]Acoustical Wavefield imaging, Delft university of Technology, Netherlands, [3]TNO, Netherlands*

Background, Motivation and Objective

Lately, 3D ultrasound has become increasingly important. However, the image quality is generally lower than that of conventional 2D ultrasound. This is largely caused by the data reduction methods needed to transport the large amount of data produced by the matrix probe to the mainframe. Therefore, methods need to be developed to cope with such amount of data in an efficient and cost-effective way. We propose a two-step imaging method based on the virtual-source concept [Kortbek et al., Ultrasonics 2013] and efficient and cost-effective 3D Fourier transforms, and show the application of the imaging step on 3D experimental and numerical data sets.

Statement of Contribution/Methods

Conceptually, the first step is the production of scan lines having a single focal depth in transmit and receive. This provides a considerable data reduction because the data from many elements is combined into single line RF data. The resulting data is transferred to the back end of the system at relatively low rates. The second step is an additional imaging step, performed efficiently in the frequency-wavenumber domain based on 3D Fast Fourier transforms and an interpolation step (Stolt migration). The result is a volume image having an optimal lateral resolution over the entire depth. The experimental dataset was obtained by scanning a single transducer over a pin diffractor in water with a xyz stage. The 1 MHz transducer had a diameter of 3.8 cm and a focal distance of 7.6 cm. A simulated dataset was created using the Field II numerical simulation package with geometries equal to the experiments.

Results/Discussion

Both the experiments and simulations showed a significant improvement in lateral resolution, see Fig 1 for slices from the 3D volume and a quantitative analysis. The -6dB lateral point spread functions (PSF) were reduced by a factor of about 5 and 4 in the near-field (35mm) and far-field (135mm), respectively. This improvement was obtained in both lateral directions. The focal resolution was maintained. The SNR was increased by about 20dB, caused by the coherent combination of traces in the processing method.
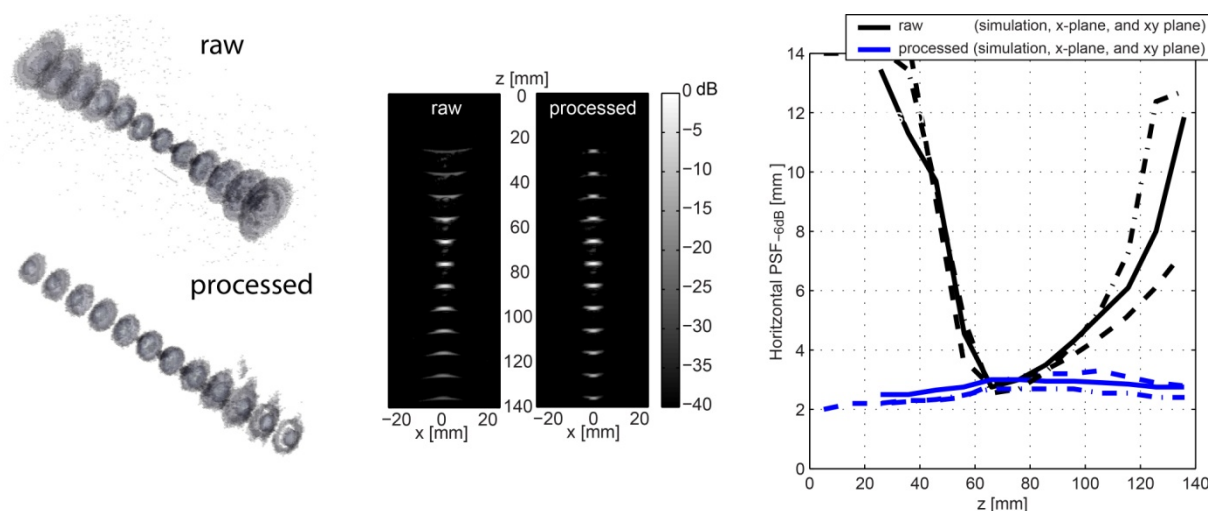
6G - Physics of Thin-Film Resonators

201AF

Friday, October 23, 2015, 03:30 pm - 05:00 pm

Chair: **Vincent Laude**
FEMTO-ST / CNRS

6G-1

3:30 pm **Finite element analysis of BAW devices: principles and perspectives**

Robert Thalhammer[1], John Larson[2]; [1]*Avago Technologies, Munich, Germany,* [2]*Avago Technologies, San Jose, CA, USA*

Background, Motivation and Objective

Numerical simulations by Finite Element Modeling (FEM) methods are an indispensable part of today's R&D work. This work illustrates the model setup and the computer implementation of FEM acoustic models. Due to advances in model sophistication and computing power, FEM simulations are now capable of supporting product design, improving our understanding of the underlying physics, and exploring novel device concepts at reasonable time and cost levels.

Statement of Contribution/Methods

While the governing equations are straight forward, boundary conditions for typical RF acoustic devices are tricky. We will discuss representing electrodes by equipotential surfaces versus implementing Ohmic conductivity. To make practical size models, the FEM discretized equations require absorbing boundaries, another challenging aspect. In particular for dispersion type II resonators, with evanescent and propagating modes present simultaneously, numerical techniques and test strategies for verifying their functionality will be demonstrated. As computation time is governed by model complexity, we will discuss discretization aspects in relation to dispersion, address parallel computing, and compare 2D and 3D FEM models, particularly illustrating that a variety of important aspects can be tackled by 2D models.

Results/Discussion

As affordable computing power and the efficiency of numerical techniques keep increasing, simulations get ever more appealing. Today, 2D FEM is in the ballpark where 1D models were in the beginning of FBAR technology. Though 2D simulations don't cover effects like apodization, major features of acoustic devices, such as spurious mode suppression or enhanced energy confinement by frames, are properly reflected. Combining a FEM simulator and optimization tools will be discussed.

For understanding the fundamentals, FEM can illustrate the internal distribution of any physical quantity on a much higher resolution than any experimental technique. More information is gained by post processing the results, e.g. Fourier analysis reveals which modes are excited. We will demonstrate how to extract any type of mode, even if propagating, evanescent, and complex modes are present simultaneously.

As an example for novel concepts, BAW filters based on interdigital transducers have been proposed. Their operating modes are beyond 1D, but 2D FEM has been successfully employed for exploring the pass band and identifying spurious modes. For standard FBAR devices, frames for Q-value improvement are not perfectly understood theoretically, but optimum design is well predicted by FEM simulations. Even more complex structures for enhanced energy confinement have been proposed. FEM is a valuable tool to pioneer the way into novel technologies, as it can be flexibly tailored to any R&D need - ranging from fast and efficient models addressing particular aspects, up to large-scale models reflecting the comprehensive physics of complex devices.

6G-2

4:00 pm **Laterally Coupled FBAR resonator filters**

Kun Wang[1], Robert Thalhammer[2], Steven Martin[3], Uli Koelle[1], John D Larson III[1]; [1]*Avagotech, San Jose, USA,* [2]*Avagotech, Munich, Germany,* [3]*Avagotech, Fort Collins, USA*

Background, Motivation and Objective

Thin film bulk acoustic resonator (FBAR) filters are an indispensable technology for many RF applications. While mainstream FBAR technology is based on ladder topology, acoustically-coupled resonator filters (CRF) are able to provide wider bandwidth and more configuration options.

A very attractive CRF concept is to couple FBAR resonators laterally. However, as the lateral coupling between FBAR resonators is very weak, laterally coupled resonator pairs are formed as an interdigital configuration. Both narrow electrode width and multiple coupled pairs enhance lateral acoustical coupling to form a wider passband.Since the central frequency is determined by vertical dimension, it is very easy to realize filters in GHz range without using high precision photolithography as in SAW filter.

Statement of Contribution/Methods

This paper explores the design and fabrication of laterally coupled FBAR resonator filters using an interdigital configuration. It is found that the lateral dimensions such as resonator width and the space between the resonators play important roles in passband formation. A detailed study of different resonator geometries is conducted. A comprehensive analysis of the device physics is accomplished by 2D Finite-Element simulations solving the coupled system of electrostatic, mechanical, and piezoelectric constitutive equations. An illustrative overview of LCRF modes for comparing different structures will be introduced. The modeling is suitable for guiding geometric optimization.

Results/Discussion

The most important factors impacting the fundamental modes are finger width and gap width. Plotting resonance frequencies versus a design parameter illustrates that various modes form branches of symmetric and antisymmetric modes. Any mode creates a peak in the transmission characteristics. Typical passbands are formed by coupling a symmetric and an antisymmetric mode.

First experimental results are very encouraging. A 5.4% 3dB bandwidth at 900MHz (Band 8) and a minimum insertion loss of 0.7dB in the center of the pass band was demonstrated experimentally (see figure 1). Filters at higher frequencies (Band 1) were investigated as well. These filters exhibited with 3dB-bandwidth as high as 8.7%, and as low as 2%, at 2100MHz. Experimental and FEM simulation results will be given in the presentation.

FRIDAY ORAL

Figure 1 Measured characteristics of A LCRF filter

m1
freq=893.0MHz
dB(S(2,1))=-3.021

m2
freq=943.3MHz
dB(S(2,1))=-3.044

m3
freq=917.8MHz
dB(S(2,1))=-0.699
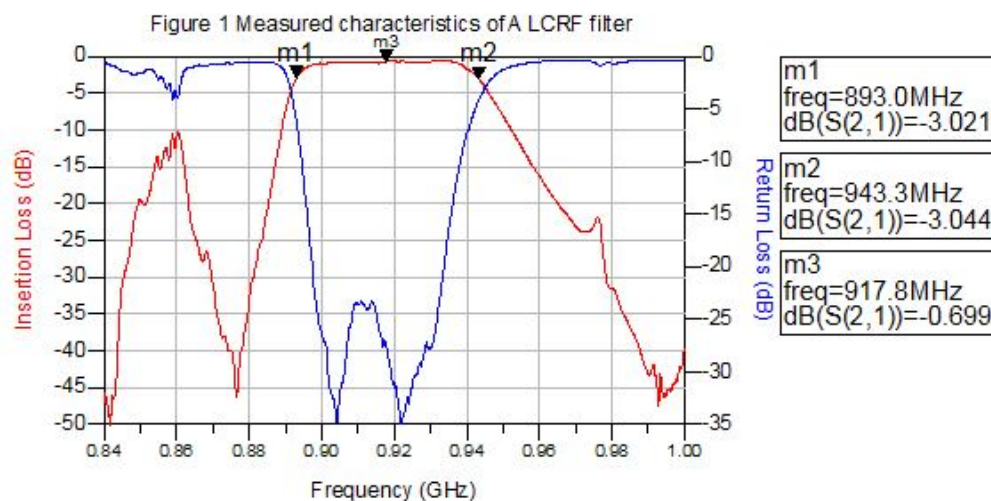
6G-3

4:15 pm   High order mode polarity inverted Al-polar (0001) ScAlN/O-polar (000-1) ZnO film resonator

Takeshi Mori[1], Takahiko Yanagitani[2], Masashi Suzuki[1]; *[1]Nagoya Institute of Technology, Japan, [2]Waseda University, Tokyo, Japan*

Background, Motivation and Objective

Polarization-inverted multi-layer resonators are attractive for high order mode excitation and high power operation. In the ultrasonic microscope applications, *n*-fold low capacitance of *n*th polarization-inverted multi-layer enables *n*-fold increase of emission area in the transducer without sacrificing impedance matching between the transducer and 50Ω measurement system. Large emission area leads to a concentration of the ultrasonic. Previously, we reported the control of the polarity in ScAlN and ZnO films by ion beam irradiation during film growth, and we found that the usual ScAlN and ZnO films grown by a standard planar sputtering possess (0001) Al-polarity and (000-1) O-polarity, respectively [1,2]. In this study, we considered that the polarization-inverted (0001)/(000-1) multi-layer can be easily obtained by depositing usual (0001) Al-polar ScAlN film on usual (000-1) O-polar ZnO film. To check this assumption, we fabricated two layer (0001) ScAlN/(000-1) ZnO film resonator by a conventional magnetron sputtering.

[1] M. Suzuki et al., APL 104 172905 (2014)

[2] R. Hashimoto et al., IUS 2013, IUS3-H-6.

Statement of Contribution/Methods

c-axis oriented ZnO films (approximately 4.2 μm) were grown on (0001) Ti films/silica glass substrate by off-axis deposition geometry. c-axis oriented ScAlN films (approximately 3.9 μm) was grown on the ZnO films by on-axis deposition geometry. The polarities of the layers were determined by a press test using an oscilloscope. We also investigated longitudinal wave conversion loss of the ScAlN/ZnO film HBARs to determine the resonance mode.

Results/Discussion

As shown in Fig. 1, positive response indicating O-polarity, was observed in the first layer ZnO film when the compressive stress was applied, whereas the, negative response, indicating Al-polarity, was observed in the second layer ScAlN film.

As shown in Fig. 2, two layered (0001) ScAlN/(000-1) ZnO film excited the 2nd mode resonance at 0.72 GHz with suppression of the 1st mode resonance at 0.27 GHz. The experimental conversion loss curve agreed well with the theoretical one calculated by Mason's model including the effects of polarity inversion. This indicates that the polarization direction of the second layer and the first layer are perfectly inverted. Minimum conversion loss of 1.8 dB is smaller than that of typical single layer ScAlN film HBAR.

Fig. 1 Opposite piezoelectric responses of the usual ScAlN and usual ZnO films when compressive stress is applied

Fig. 2 Longitudinal wave conversion loss curves of the ScAlN/ZnO HBAR, showing perfect polarity inversion

6G-4

4:30 pm   **Elastic constant c_{ij}^E tensors of (0001) $Sc_xAl_{1-x}N$ films (x=0-0.63)**

Takahiko Yanagitani[1,2], Hayato Ichihashi[3], Masashi Suzuki[2], Shinji Takayanagi[3], Mami Matsukawa[3]; *[1]Faculty of Science and Engineering, Waseda University, Tokyo, Japan, [2]Nagoya Institute of Technology, Nagoya, Aichi, Japan, [3]Doshisha University, Kyotanabe, Kyoto, Japan*

Background, Motivation and Objective

Large piezoelectricity in ScAlN film has received increasing interest in recent years. Elastic constant tensors of ScAlN films are required to design the SAW and BAW devices. Last year, Tanaka's group presented the full tensors of elastic, dielectric, and piezoelectric constants of the ScAlN films (x=0.4) where the electromechanical coupling k_t reaches maximum [1]. However, for the filter application, the range x<20% is important because mechanical Q and TCF degrade by increasing x. In this study, we determined the elastic constant tensors (except c_{13}) of ScAlN films in the wide concentration range of x=0-0.63.

[1] A. Konno, et al., Proc. IUS. pp. 273-276, (2014).

Statement of Contribution/Methods

In-plane longitudinal and shear BAW velocities (V_{11}^E and V_{66}^E) in c-axis oriented (0001) ScAlN were measured by a Brillouin scattering method with RIΘA geometry. The out-of plane BAW velocities (V_{33}^D and V_{44}^E) and k_t in the (0001) films were extracted from the minimum point of the longitudinal wave and shear wave conversion loss curves in the HBAR, respectively. c_{12} can be calculated from c_{11} and c_{66}. Thus c_{ij}^E tensor except c_{13} can be determined independently from the one (0001) film using only BAWs. c-Axis oriented thirteen (0001) ScAlN films with x=0-0.63 were prepared. These samples are the same as those used in Ref. [2]. Fabrication procedure and crystallographic properties of the films were also described in Ref. [2]. Thicknesses of the films were 5-6 μm. Mass density of the film was estimated in the separately-prepared three 14 μm thick ScAlN films by using Archimedes method (ρ =3638 kg/m³).

[2] T. Yanagitani and M. Suzuki, Appl. Phys. Lett., 105, 122907 (2014).

Results/Discussion

The resulting c_{ij}^E were summarized in Table I. Resulting c_{ij}^E were somewhat higher than the values predicted by the *ab initio* calculation [3]. The change rate of each c_{ij}^E with x in the present experiment (Fig. 1 (a)) is almost the same as those obtained in the calculation (Fig. 1 (b)).

[3] S. Zhang, W. Y. Fu, D. Holec, C. J. Humphreys, and M. A. Moram., J. Appl. Phys., 114, 243516 (2013).

Table I Elastic constants (in GPa) of (0001) $Sc_xAl_{1-x}N$ films (x=0-0.63)

Sc (x)	c_{11}^E	c_{12}^E	c_{33}^E	c_{44}^E	c_{66}^E	k_t^2 (%)
0.00	428	145	438	148	141	3.8
0.06	405	147	413	147	129	4.8
0.11	392	148	378	146	122	5.8
0.14	374	148	359	142	113	5.7
0.21	357	150	324	129	104	6.4
0.28	335	150	296	122	92	7.4
0.34	305	146	257	123	79	8.9
0.37	303	152	241	120	75	10.1
0.37	295	142	235	105	77	10.1
0.41	279	146	206	103	67	11.9
0.47	269	146	219	86	61	3.5
0.52	323	203	281	111	60	0.4
0.63	364	204	312	–	80	0.0
0.40 [1]	234.5	101.4	267.4	39.6	66.6	
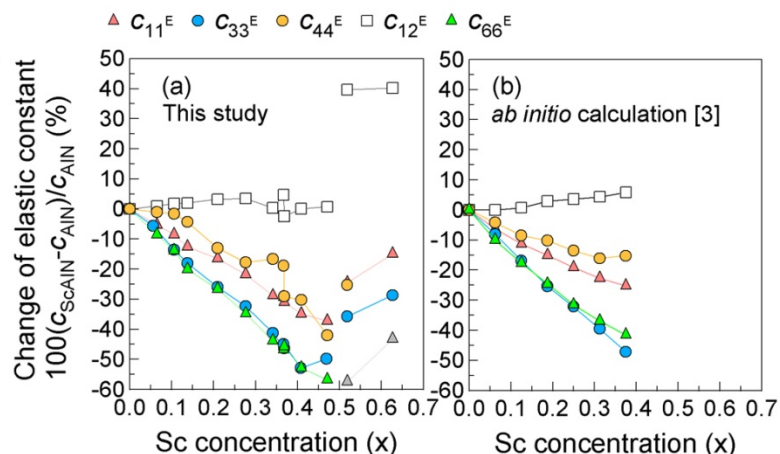
Fig. 1 A comparison of the change rate of elastic constants with x for (a) the present experiment and (b) the reported *ab initio* calculation [3]

6G-5

4:45 pm   **Quasi-shear mode electromechanical coupling k'_{15} and shear wave velocity in c-axis tilted $Sc_xAl_{1-x}N$ films**

Masashi Suzuki[1], Takahiko Yanagitani[2]; *[1]Nagoya Institute of Technology, Japan, [2]Waseda University, Japan*

Background, Motivation and Objective

ScAlN has been attracted as a potential piezoelectric material for BAW and SAW resonators. The k_t^2 of the ScAlN film near the phase boundary was approximately 200 % of that of pure AlN single crystal [1]. Shear mode resonators are suitable for liquid sensor and bio-sensor applications. In IUS 2010, we reported that the quasi-shear mode electromechanical coupling k'_{15} of c-axis tilted ScAlN films near the phase boundary is larger than that of pure AlN single crystal [2]. In this study, the relationship between the k'_{15}^2 and the c-axis tilt angle in ScAlN film were investigated. The effect of Sc concentration in c-axis tilted ScAlN film on the k'_{15}^2 and quasi-shear wave velocity V'_{44} were also estimated.

[1] M. Suzuki, et al., IUS2013, IUS4-G-1. [2] T. Yanagitani, et al., IUS2010 Proc., 2095.

Statement of Contribution/Methods

$Sc_{0.3}Al_{0.7}N$ films with various c-axis tilt angles (3°, 11°, 31°, 43°) were prepared by a glancing angle sputter deposition. The c-axis tilt angle of the $Sc_{0.3}Al_{0.7}N$ films was controlled by adjusting the substrate angle to the Al-Sc target surface plane. Moreover, c-axis tilted $Sc_xAl_{1-x}N$ films with various Sc concentration (0<x<0.6) were also prepared. The c-axis tilt angle of these $Sc_xAl_{1-x}N$ samples was determined to be 21-41° by an XRD pole figure. k'_{15}^2 and V'_{44} were estimated from the conversion loss of c-axis tilted ScAlN film HBARs.

Results/Discussion

As shown in Fig. 1 (a), the k'_{15}^2 of the c-axis tilted $Sc_{0.3}Al_{0.7}N$ films were higher than that of AlN single crystal (solid line) in all c-axis tilt angles. The k'_{15}^2 increased with increasing c-axis tilt angle from 2.6° to 31°. On the other hand, the k'_{15}^2 for c-axis tilt angle of 43° was smaller than the maximum k'_{15}^2 for c-axis tilt angle of 31°. This tendency is similar to the curve of the pure AlN single crystal (solid line).

As shown in Fig. 1 (b), the k'_{15}^2 of c-axis tilted $Sc_xAl_{1-x}N$ films increased with increasing Sc concentration from x=0 to 0.41. The k'_{15}^2 reaches maximum of 16.4 % at x=0.41. The significant decrease of the k'_{15}^2 value was observed for x > 0.48. This may be due to the phase transition from a piezoelectric wurtzite to a non-piezoelectric cubic. The V'_{44} of c-axis tilted $Sc_xAl_{1-x}N$ film decreased with the increase of Sc concentration. The k'_{15}^2 of 16.4 % and the V'_{44} of 3851 m/s in c-axis tilted $Sc_{0.41}Al_{0.59}N$ film near the phase boundary was approximately 320 % and 60 % of that of the AlN single crystal, respectively.
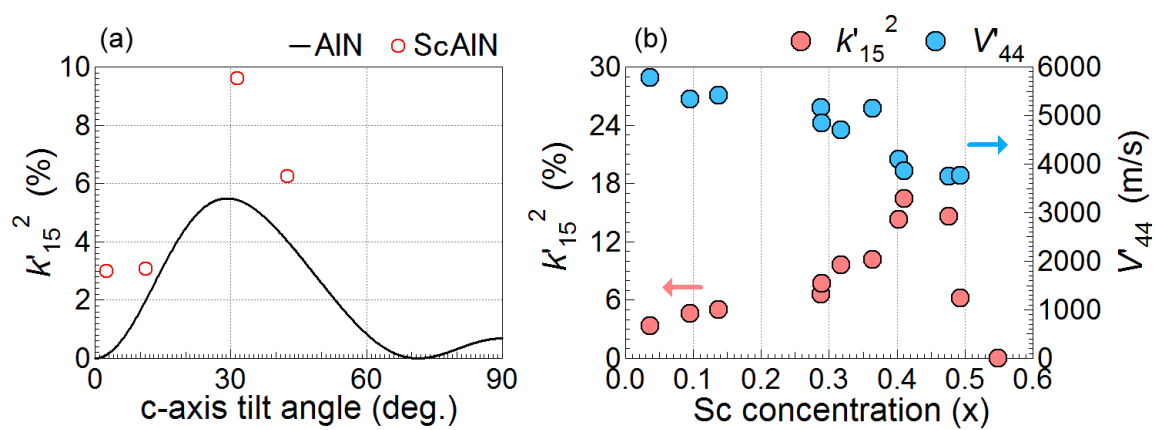
Fig. 1 (a) The relationship between k'^2_{15} and c-axis tilt angle in $Sc_{0.3}Al_{0.7}N$ films. (b) k'^2_{15} and V'_{44} of c-axis tilted $Sc_xAl_{1-x}N$ films (x=0-0.6) vs Sc concentration (x)

FRIDAY ORAL

8G - Transducers for Therapy

102

Friday, October 23, 2015, 03:30 pm - 05:00 pm

Chair: **Anne-Christine HLADKY**
           IEMN

FRIDAY ORAL

8G-1

3:30 pm   Capsule-based Ultrasound-mediated Targeted Gastrointestinal Drug Delivery

Fraser Stewart[1], Antonella Verbeni[2], Yongqiang Qiu[1], Benjamin Cox[1], Jan Vorstius[1], Sandy Cochran[1]; *[1]Institute for Medical Science and Technology, University of Dundee, United Kingdom, [2]The BioRobotics Institute, Scuola Superiore Sant'Anna, Italy, [3]School of Engineering, Mathematics and Physics, University of Dundee, United Kingdom*

Background, Motivation and Objective

Focused Ultrasound (FUS) has a variety of potential uses, including therapeutic treatment of the gastrointestinal (GI) tract. Capsule endoscopy is already a key interest for researchers for the diagnosis of GI conditions such as inflammation, Crohn's disease and neoplasms and has the potential to be developed for treatment by incorporating a FUS transducer and associated drug delivery (DD). This paper describes a tethered capsule for targeted drug delivery (TDD) of GI conditions. We also compare piezo-ceramic (PZ) materials for the transducer to be housed in the capsule.

Statement of Contribution/Methods

Miniature bowls made with PZ54 and PZ26 (Meggitt Sensing Systems, Kvistgaard, Denmark) with frequencies of 4 MHz and 3.5 MHz respectively were selected and characterised to find the most suitable candidate for TDD. Both bowls have an outer diameter of 5 mm and focal distance of 15 mm, making them ideal to be embedded in a therapeutic capsule made with rapid prototyping and also including CMOS camera, LED illumination and DD channel (Fig. 1a). The DD channel pathway beyond the capsule is confocal with the transducer (Fig. 1a) with the intention to deliver drugs and increase cell membrane permeability through sonoporation. Functional tests included running microbubbles (MB) through the DD channel and monitoring the behaviour at the ultrasound (US) focus.

Results/Discussion

The PZ54 transducer provided an acoustic pressure P_{ac} = 125 kPa (PZ54 pressure mapping shown in Fig. 1b)and mechanical index MI = 0.063 with a beam diameter BD = 0.75 mm at the focus and the corresponding figures for the PZ26 transducer were P_{ac} = 157 kPa, MI = 0.084 and BD = 1.35 mm, both transducers were driven at 4 V_{pp}. Values for P_{ac} in the range $50 < P_{ac} < 300$ kPa ($0.05 < MI < 0.3$) are suitable for reversible sonoporation [1], and both PZ26 and PZ54 transducers fall in this range. The PZ54 transducer was selected due to its BD allowing a smaller area to be sonicated; PZ54 is also more suitable for FUS purposes because it has a higher permittivity than PZ26, which is better for electrical impedance matching. Functional tests showed that the MB egress was heavily influenced by the FUS, with their course of travel redirected due to acoustic radiation force. This suggests that a capsule configured as we have has potential in biomedical and DD applications.

[1] Qiu et al (2012) J. of Bio. Mech. 45(8) 10.1016

Figure 1(a)

Figure 1(b)

Peak to Peak Pressure [kPa]

8G-2

3:45 pm   Capacitive Micro-machined Ultrasound Transducers for High Intensity Ultrasound Applications

W. Apoutou N'DJIN[1], Bjoern GEROLD[1], Michael CANNEY[2], Nicolas SENEGOND[3], Mathieu ROY[3], Alexandre CARPENTIER[2], Jean-Yves CHAPELON[1]; *[1]LabTau, Inserm, U1032; Université de Lyon, Lyon, France, [2]CarThera, Paris, Ile-de-France, France, [3]Vermon SA, Tours, Centre, France*

Background, Motivation and Objective

For the development of image-guided high intensity ultrasound therapies, Capacitive Micro-machined Ultrasound Transducers (CMUTs) exhibit several advantages, such as ease of miniaturization (cell size: micron size), inherently broad bandwidth (>several MHz), good MR compatibility and low fabrication costs. Although cMUTs have been mostly developed for imaging purposes, this technology also has a potential for high electro-acoustic efficiency (low mechanical loss in the material thickness). To date however, the use of CMUTs for high intensity ultrasound applications has only been shown in a few preliminary studies, since the development of specific cell structures and driving strategies remains challenging. Here, the performances of CMUTs designed for high intensity ultrasound applications were evaluated in the continuous wave mode operation regime. The feasibility of generating directional ultrasound-induced heating and thermal damage in biological tissues was studied in the context of interstitial thermal ablation.

Statement of Contribution/Methods

The CMUT prototypes were 12-element 1D linear-arrays (element size: 2.7 mm x 0.8 mm). Electrical impedance and interferometry measurements were performed to detect manufacturing defects, confirm correct electrical matching, identify the collapse voltage and determine the active working density. Preliminary numerical simulations guided the experimental investigations by identifying a range of surface ultrasound intensities (Iac) suitable for inducing thermal ablation in biological tissue with this CMUT design (Iac > 10 W/cm2). The influence of varying the bias voltage (VDC) and driving voltage (VAC) on the acoustic output was studied to reach the thresholds required for

therapy. Ultrasound exposures were performed in tissue-mimicking gel phantoms under infrared (IR) or magnetic resonance (MR) thermometry monitoring. A cylindrical catheter combining multiple 1D linear-arrays was tested for multi-directional targeting.

Results/Discussion

Acoustic intensities compatible with thermal ablation were obtained with MR-compatible LC matching-circuits tuned for driving CMUTs in the collapse-mode operation (Iac >30 W/cm2). Hysteresis in the acoustic power outputs were observed with varying VDC. IR- and MR-thermometry monitoring showed directional ultrasound-induced heating patterns in tissue-mimicking phantoms (frequency: 6-8 MHz, exposure time: 60-120s) extending over >2 cm from the CMUT element. Irreversible thermal damage in tissues was achieved in turkey breast samples (ΔTmax>40°C). First trials with the CMUT catheter confirmed the feasibility for MR-monitored multi-directional HICU heating. Further investigations are ongoing to improve the robustness of the CMUT devices. This project was supported by the French National Research Agency (ANR, 2010) and the French Single Interministerial Fund (FUI, 2013).

8G-3

4:00 pm   Development and acoustic characterization of lead-free high intensity focused ultrasound transducers

Elaheh Taghaddos[1], Teng Ma[2], Mehdi Hejazi[1], Qifa Zhou[2], Hui Zhong[3], Ming Xi Wan[4], Ahmad Safari[1]; [1]*Materials Science and Engineering, Rutgers University, Piscataway, NJ, USA,* [2]*Biomedical Engineering, University of southern california, USA,* [3]*Xi'an Jiaotong University, China, People's Republic of,* [4]*Biomedical Engineering, Xi'an Jiaotong University, China, People's Republic of*

Background, Motivation and Objective

High intensity focused ultrasound (HIFU) transducers have been widely utilized for noninvasive therapeutic procedures. Piezoelectric ceramics with high depolarization temperature, high mechanical quality factor, low dielectric loss, and relatively high coercive field are required for high power devices such as HIFU transducers. Until now, only lead-based piezoelectric compositions such a PZT4 have been employed as active element of HIFU transducers. Lead is a toxic element which can cause severe health issues for human beings. As a result, researchers have been motivated to develop and characterize hard lead-free piezoceramics for high power applications. It is reported that BNT-based ceramics with rhombohedral structure exhibit promising performance under high drive conditions. In this research, firstly, the electrocmechanical and high power properties of hard BNT-based ceramics were studied and then HIFU transducers with different center frequencies of 1, 5, and 8 MHz were fabricated and characterized.

Statement of Contribution/Methods

The electromechanical and high power properties of 0.88[Bi0.5Na0.5TiO3]-0.08[Bi0.5K0.5TiO3]-0.04[Bi0.5Li0.5TiO3] (abbreviated to BNKLT88) ceramics doped with 1.5 mol.% Mn was studied. For the first time, plain circular HIFU transducers with center frequencies of 1, 5, and 8 MHz were designed and fabricated using 1.5 mol.% Mn doped–BNKLT88 piezoelectric as the active element. The multiscan system with PRP 4000 (pulse/receiver) and Precision Acoustics Ltd, Dorchester, UK hydrophone with 0.5 mm diameter has been utilized to characterize the acoustic performance of the transducers.

Results/Discussion

It has been demonstrated that BNKLT88 ceramics doped with 1.5 mol.% Mn show outstanding high power performance. Manganese doping significantly increased the vibration velocity and suppressed the heat dissipation under high drive condition. Hard lead-free piezoceramics with a maximum vibration velocity of 0.6 m/s exhibited superior high power performance compared to PZT4 and PZT8 which are commonly used in fabrication of high-intensity focused ultrasound transducers. The outer diameter of 1, 5, and 8 MHz transducers were 23.5, 12.5, and 10.9 mm, respectively. The acoustic properties of the transducers such as the frequency spectrum and acoustic pressure field were characterized. Unfocused 5, and 8 MHz transducers showed linear response up to 140, and 135 V in which maximum peak acoustic pressures of 6.5, and 1.8 MPa were achieved, respectively. The 1 MHz transducer did not demonstrate any non-linearity up to 200 V, which was the maximum voltage of characterization. The result of this research showed that hard lead-free BNT-based piezoelectrics can be regarded as promising alternatives for lead-based materials used in HIFU transducers.

8G-4

4:15 pm   Broadband Dual-Mode HIFU Array used for Therapy and Therapy Monitoring

Kyle Morrison[1], George Keilman[1], Peter Kaczkowski[2]; [1]*Sonic Concepts, Inc., Bothell, Washington, USA,* [2]*Verasonics, Inc., Kirkland, Washington, USA*

Background, Motivation and Objective

To accurately monitor HIFU therapy and three-dimensional target motion estimation using a broadband spherically focused HIFU array transducer with a Verasonics platform. The described series of dual-mode HIFU array transducers use a single Archimedean spiral close packed element arrangement. Earlier work has shown this arrangement to adequately reduce grating lobes and unwanted therapy outside of the intended focus. This paper shows parallel advantages in reducing grating lobes and maximizing therapy monitoring accuracy.

Statement of Contribution/Methods

Several configurations within the series have been characterized from frequencies 1 thru 4 MHz and number of elements 128 thru 512 to evaluate and compare results. Using the single Archimedean spiral, elements are sized to maximize a fixed surface area of a spherical annular ring with a defined geometry of 15 cm x f/1. The resulting element size is used to approximate the therapeutic steering range down -3 dB and monitoring range down -6 dB.

The broadband dual-mode HIFU array transducer under test is 128 elements and operates with a center frequency of 2 MHz. The HIFU array is used to generate heat or radiation force at the intended focus within the steering range and interleaves with imaging sequencing to monitor and track the focus at a PRF > 10 Hz.

Results/Discussion

Target motion is performed in 3D using pulse-echo measurements of three small 7-elements clusters widely distributed about the array. These 3 clusters produce respective A-lines and cross-correlation of the RF data over time provides displacements in 3 independent directions. Combined vectorially, the displacement is in agreement to the known imposed displacement of the target.

HIFU heating detection is proven to be similar to target motion estimations, but interleaves HIFU exposure between monitoring measurements. The RF distortion is mapped in 3D to provide a heating strain map and is in agreement with thermocouple readings at the intended target.

Further stiffness monitoring experiments are performed in interleaving radiation force within the steering range and monitoring a medium's maximum displacement and its rebound vs. time. These experiments provided reasonable stiffness and attenuation results.

Measurements confirm simulation in that a reduction in one-way transmit grating lobes offers parallel advantages in monitoring accuracy using the single Archimedean spiral.

8G-5

4:30 pm **Double-Focusing Ultrasound Transducer for Skin Disease Treatment**

Jihun Jang[1], Jin Ho Chang[1,2]; [1]*Department of Electronic Engineering, Sogang University, Seoul, Korea, Republic of,* [2]*Interdisciplinary Program of Integrated Biotechnology, Sogang University, Seoul, Korea, Republic of*

Background, Motivation and Objective

For the treatment of skin wrinkles and cancers such as melanoma, high-intensity ultrasound should be focused at a small focal area (on the order of a few millimeters in diameter) placed in shallow depth (from the surface down to 1-4 mm). At a given frequency, the tight focusing can be achieved when a transducer has a small F-number. Since F-number should be larger than unity in clinical practice, the aperture diameter of the transducer needs to be smaller than 4 mm for the skin disease treatment. With such aperture, however, it is difficult to produce ultrasound intensity high enough to induce tissue coagulation. Therefore, the focal depth of the general therapeutic transducers for skin diseases is much deeper than the treatment depth to secure a large enough aperture; an additional medium such as water is placed in between the transducer and skin surface to locate the focal depth at the treatment area. As a remedy for the problem, we propose a double-focusing ultrasound transducer.

Statement of Contribution/Methods

For the proposed double-focusing transducer, the piezoelectric material is geometrically focused and the acoustic lens is used to further focus ultrasound on a target depth (see Fig. 1(a) and (b)). In fact, the double-focusing structure makes it possible for the F-number of the transducer to be less than unity. A key design parameter here is the radius of lens curvature with which ultrasound from the edge and the center of the piezoelectric material simultaneously arrives at the desired focal depth. The performances of the proposed method were verified after fabricating the transducer; the aperture and the press-focal depth of a 7-MHz transducer were 10 mm and 15 mm, respectively, the lens material was Epoxy, the radius of lens curvature was 6 mm. Therefore, the final focal depth was designed to 4 mm (F-number of about 1).

Results/Discussion

The focal depth, depth of focus and lateral beam width of the fabricated double-focusing ultrasound transducer were, respectively, measured to 9.35 mm, 1.15 mm, and 0.15 mm (see Fig. 1(d)) by using a hydrophone, which fairly agreed with the PZFlex simulation results, i.e., 9.57 mm, 0.803 mm, 0.095 mm (see Fig. 1(c)). The results demonstrated that the proposed double-focusing method can be used to change the F-number from the original value of 1.5 to 0.935 without reducing the aperture of 10 mm.

8G-6
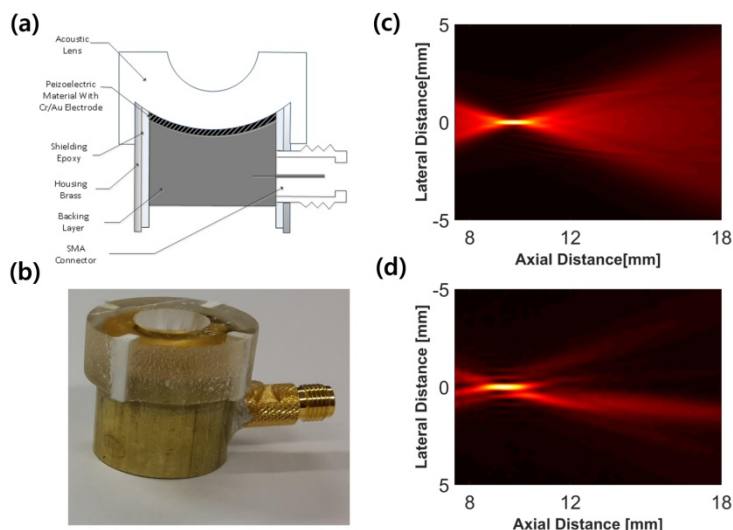
4:45 pm **Non-linear generation of harmonic content within high intensity ultrasound signals using granular chains**

Sevan Harput[1], James McLaughlan[1], Steven Freear[1], Pierre Gelat[2], Nader Saffari[2], Jia Yang[3], Omololu Akanji[3], Peter Thomas[3], David Hutchins[3]; [1]*School of Electronic and Electrical Engineering, University of Leeds, Leeds, United Kingdom,* [2]*Department of Mechanical Engineering, University College London, London, United Kingdom,* [3]*School of Engineering, University of Warwick, Coventry, United Kingdom*

Background, Motivation and Objective

Applications such as High Intensity Focused Ultrasound (HIFU) conventionally use narrowband signals of high amplitude, which are then focused to a known point within the body. It would be advantageous to able to broaden the bandwidth, as this could lead to a more spatially-concentrated focal region. One way of increasing the bandwidth is to generate harmonics. The eventual aim of this study is to generate wideband ultrasonic signals with high amplitudes, primarily for therapeutic ultrasound and drug delivery applications. In this paper, a new ultrasonic transducer technology using a one-dimensional chain of spheres is presented to achieve this.

Statement of Contribution/Methods

An ultrasonic process horn with a fundamental frequency of 40 kHz was used to generate narrowband signals for input into the chain of spheres. A sinusoidal tone burst with varying durations between 5 and 50 cycles was used for excitation at fundamental, 2nd, 3rd, and 6th harmonic frequencies of the ultrasonic horn. The driving signals were generated by a linear power amplifier, so a displacement of 5 µm can be achieved at the horn tip. The chain consisted of 6, 7, or 8 stainless steel spheres with a diameter of 1 mm, held vertically under gravity loading to apply a small static force between each sphere. The end of the chain was terminated with different matching layers, such as glass, acrylic, or carbon, to increase the coupling into the water. The system as shown in the figure was partially submersed and the output was measured in water using a membrane hydrophone.

Results/Discussion

The Hertzian contact between adjacent spheres caused the nonlinearity of the system to increase as the signal traveled along the chain. After propagating in the chain, the narrowband sinusoidal excitation waveform was thus transformed into a signal with a greatly-extended bandwidth. The figure shows the input and output spectra using the 6th harmonic from the ultrasonic horn as the excitation frequency. It can be seen that the output signal accommodates higher order harmonics that extended to frequencies above 1 MHz due to the nonlinearity in the chain. The results are consistent with theoretical predictions for such a system under small static loading. Extension to wider bandwidth signals will be discussed, by using smaller diameter spheres, so as to generate high frequency ultrasound waves in water at biomedical ultrasound range.

Institute of Electrical and Electronics Engineers

FRIDAY ORAL
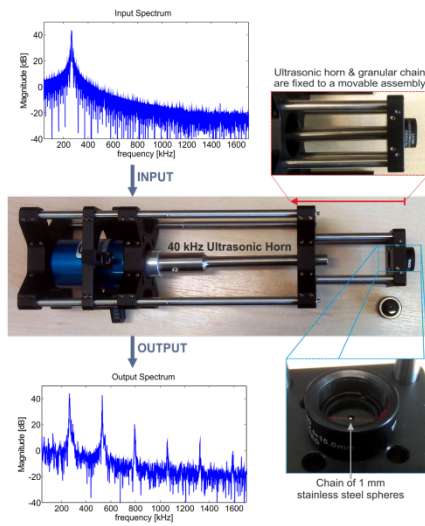
P1B1 - Elasticity Imaging Methods

4th floor

Friday, October 23, 2015, Posters displayed 08:00 am - 05:00 pm. Authors must be present at their poster from 9:30 - 10:30am (odd number posters) and 14:30 – 15:30pm (even number posters).

Chair: **Hendrik Hansen**
Radboud university medical center

P1B1-1 _____

8:00 am   Regularized, Weighted Temporal Multiresolution Speckle Tracking of Small Displacements in Ultrasound

Peter Hollender[1], Vignesh Vudatha[1], Gregg Trahey[1,2]; *[1]Biomedical Engineering, Duke University, Durham, North Carolina, USA, [2]Radiology, Duke University Medical Center, Durham, North Carolina, USA*

Background, Motivation and Objective

Estimating the motion of tissue in ultrasound is of paramount importance to elasticity imaging. There are a number of estimators available to estimate the local axial displacement between two ultrasound A-lines, which use phase or pattern matching methods, including normalized cross-correlation. When estimating the motion through an M-mode, two reference schema are typically used: anchored, where the motion between the first frame and every other frame are estimated directly, and progressive, where the motion between each sequential pair of frames is estimated and summed to provide the total displacement. Anchored referencing fails in the presence of decorrelation due to motion, while progressive estimation is prone to error accumulation. We demonstrate here a multiresolution method which uses all combinations of frames to form a single, robust estimate.

Statement of Contribution/Methods

For each frame pair in the ensemble, the motion at each depth u_{ij} is estimated by normalized cross-correlation. To from a consistent set, the individual estimates u_{ij} must obey three rules: 1. $u_{ii} = 0$, 2. $u_{ij} = -u_{ji}$, and 3. $u_{ij} + u_{jk} = u_{ik}$. #1 is automatic by autocorrelation properties. #2 is enforced by shifting both the i and jth signals equally in opposing directions when checking candidate lags. #3 is used to combine the estimates in a least squares sense, by setting up an over-determined system of equations AU = u, where U are the final progressive displacement estimates. Introducing Tikhonov regularization on the first difference of U, and using the peak correlation coefficient to weight each estimate, we solve for U using

$U = (A'WA + \lambda G'G)^{-1}A'Wu.$

We test the algorithm on simulated, phantom and *in vivo* data, varying the weighting scheme and regularization parameter.

Results/Discussion

Using regularized weighted least squares, the estimates at multiple temporal resolutions combine to provide a single profile with reduced jitter. The figure shows an example from *in vivo* intracardiac data, with an ARFI push superimposed on downward wall motion. Multiresultion tracking preserves the absolute estimate (top) while reducing noise between time steps (bottom). Weighting provides resistance to decorrelation and makes the estimator handle the corrupted push frame without *a priori* knowledge of its location. This algorithm provides scalable flexibility for a variety of *in vivo* applications.
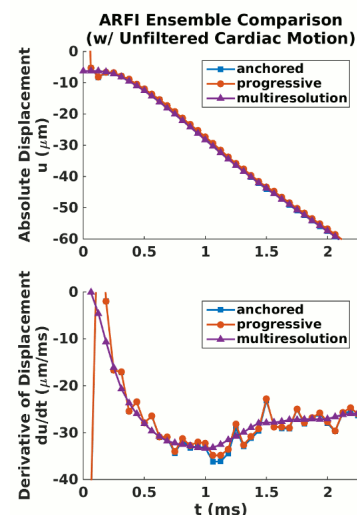
P1B1-2 _____

8:00 am   On-Axis Radiation-Force-based quantitative stiffness estimation with a Bayesian displacement estimator

Kristy Walsh[1], Douglas Dumont[1], Mark Palmeri[2], Brett Byram[1]; *[1]Biomedical Engineering, Vanderbilt University, Nashville, TN, USA, [2]Biomedical Engineering, Duke University, Durham, NC, USA*

Background, Motivation and Objective

In traditional shear wave elasticity imaging (SWEI), shear wave velocity is measured away from the acoustic radiation force (ARF) axis. Instead, we measure the time-to-peak displacement of tissue directly along the ARF axis (see blue arrows in figure below). Measuring displacements along this axis rather than off-axis simplifies hardware required for quantifying tissue stiffness. Previously this method has been demonstrated, but the variance was too high for practical feasibility. To reduce stiffness estimation error, we apply our Bayesian displacement estimator.

Statement of Contribution/Methods

To evaluate the Bayesian estimator, we use 3D finite element analysis to model soft tissue response to the acoustic radiation force and Field II to simulate the radio-frequency data of the tissue response. The Bayesian displacement estimator is applied to RF data to improve tissue displacement estimates, which then improves time-to-peak

displacement estimates and the subsequent stiffness estimate. Time-to-peak displacement is proportional to shear wave speed if we assume the medium is linear, elastic, and isotropic. Here, shear wave speed is directly related to shear stiffness, and we create look-up tables to estimate stiffness using time-to-peak displacement as a function of depth. We modeled an L12-5 50 mm linear transducer with a transmit frequency of 7.8 MHz, 2 cm focus, and F/2.5. The average displacement data from 20 speckle realizations of each tissue stiffness (Young's Modulus of 3, 6, 9, 12, 15 kPa, attenuation of 0.7 dB/cm/MHz) were used to generate the stiffness look-up tables.

Results/Discussion

Test cases were simulated at a Young's modulus of 8 kPa. Our Bayesian displacement estimator has lower mean square error (MSE) than traditional Normalized Cross-Correlation (NCC) estimator, shown in the figure below. Near the focal depth (1.75-2.5 cm), Bayesian MSE ranges from 0.24 - 3.53 kPa^2 with a mean of 1.37 kPa^2 and NCC ranges from 1.02 - 352.52 kPa^2 with a mean of 12.76 kPa^2. We also studied the effect of using the look-up table with an attenuation of 0.7 dB/cm/MHz on data with an attenuation of 0.5 dB/cm/MHz. At depths of 1.75-2.5 cm, the lower attenuation results were biased by a mean of -2.63 kPa while data with the same attenuation as the look-up table had a mean bias of 0.25 kPa. We analytically computed the theoretical upper limit of Young's modulus to be 1110 kPa at 2 cm depth.
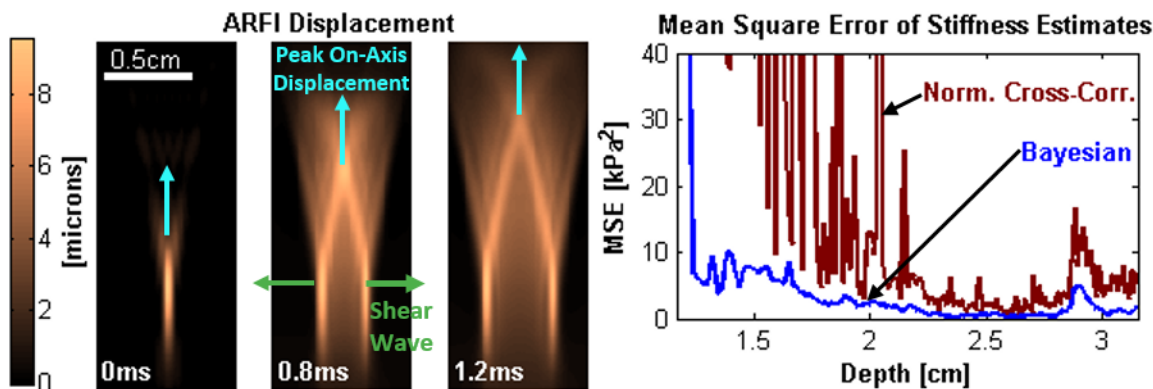
P1B1-3

8:00 am   **Crawling Waves Shear Wave Speed Estimation using Null Space Pursuit and AM-FM demodulation**

Renán Rojas[1], Juvenal Ormachea[2], Kevin Parker[2], **Benjamin Castañeda[1]**; *[1]Departamento de Ingeniería, Sección Electricidad y Electrónica, Pontificia Universidad Católica del Perú, Lima, Peru, [2]Department of Electrical & Computer Engineering, University of Rochester, Rochester, New York, USA*

Background, Motivation and Objective

Crawling waves sonoelastography (CWS) allows measuring viscoelastical properties in soft tissue at regions of interest. Recently, the Dominant Component Analysis AM-FM method (DCA-AMFM) was proposed for modeling non-stationary patterns in CWS to locally estimate their shear wave speed (SWS).

Although DCA-AMFM evaluations show coherent results for homogeneous and inhomogeneous phantoms, high noise levels and few available data samples forbid a rigorous spectral analysis by filtering approaches.

We propose a novel method to isolate AM-FM components based on the Null Space Pursuit algorithm that alleviates such limitation. Preliminary results for the proposed method (NSP-AMFM) for homogeneous and inhomogeneous phantoms, and a contrast against alternative methods are presented.

Statement of Contribution/Methods

Each spatio-temporal plane from the data is vectorized and stacked into a matrix. Then, its low-rank component is computed to preserve small variations representing the shear wave spatial frequency changes, and to reject large variations which are inconsistent with the CWS model. AM-FM components are then iteratively separated via the null space pursuit algorithm and subsequently demodulated.

Gelatin-based phantoms are excited by a vibration field (140 Hz - 360 Hz) generated by two mechanical sources. SWS maps are computed by the NSP-AMFM method and compared against the Phase Derivation (CWS-PD) and DCA-AMFM methods. Statistical properties are also compared against mechanical measurements (MM) obtained by stress relaxation tests and fitting the relaxation curve to the Kelvin-Voigt Fractional Derivative model.

Results/Discussion

For the homogeneous case, NSP-AMFM SWS estimates are coherent with MM values. Fig. 1a shows their mean and Std. Dev. along with MM values. The SWS mean has its largest error at 160 Hz and its shortest at 220 Hz. The SWS Std. Dev. has its largest value at 160 Hz, its shortest at 360 Hz, and shows a low precision for tests below 220 Hz (large wavelengths).

Figs. 1b-1d show the SWS maps for CWS-PD, DCA-AMFM, and NSP-AMFM, respectively, for the inhomogeneous case. Overall, NSP-AMFM obtains better contrast with fewer artifacts. Further research is required for dealing with low spatial frequencies and shadowing artifacts.

FRIDAY POSTER
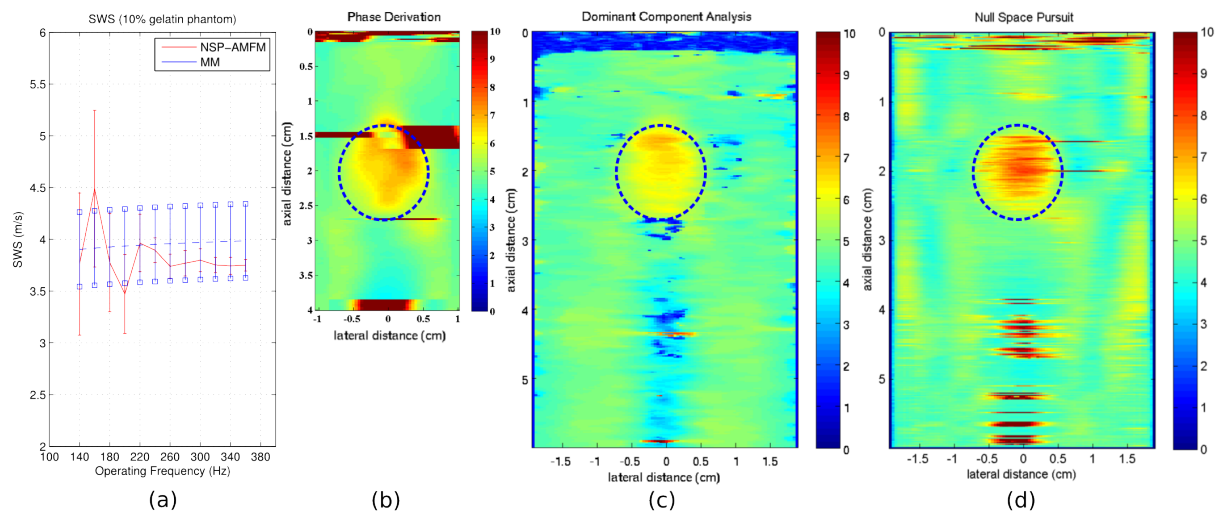
Figure 1

P1B1-4

8:00 am   Near Field Shear Wave Elasticity Imaging with High Frequency Single Element Transducers

Nien-Ching Ho[1], Pai-Chi Li[2]; *[1]Biomedical Electronics and Bioinformatics, National Taiwan University, Taipei, Taiwan, [2]Electrical Engineering, National Taiwan University, Taipei, Taipei, Taiwan, Taiwan*

Background, Motivation and Objective

Shear wave elasticity imaging (SWEI) has emerged as a promising technique for tissue stiffness quantification by measuring shear wave speed (SWS) propagating within tissue. High frequency (≥40MHz) ultrasound imaging, which provides higher spatial resolution and better sensitivity for detecting shear wave (SW) displacements, is suitable for pre-clinical small animal studies. In our previous setup, the region of interest (ROI) is imaged through mechanical scanning single element transducers. In this case, the push transducer is fixed while the imaging transducer performs scanning. Due to attenuation and diffraction, the SNR and accuracy decrease with distance, as shown in Fig. (a), where shear wave propagation by the previous setup is shown. The speed calculation map tends to be incorrect for large ROI. Thus, we hypothesize that by adopting near field SWEI (i.e., detection transducer and imaging transducer are kept close to each other), SWEI resolution and accuracy can be improved.

Statement of Contribution/Methods

The imaging system consists of two single element transducers: a 20MHz push transducer for generating acoustic radiation force and inducing shear wave, and a 40MHz transducer for imaging shear wave propagation. The two transducers are fixed by a setup shown in Fig. (b), where the lateral distance between the focal points of the two transducers is 0.5 mm. Thus, SWS is calculated as the SW propagation distance divided by the SW arriving time.

Results/Discussion

The B-mode image of a gelatin phantom (with concentration of 4% and 8% for the background and a 2 mm inclusion, respectively) is shown in Fig. (c). The corresponding SWS maps, which superimpose with the B-mode image of the phantom, are shown in Figs. (d) (previous) and (e) (near field). The contrast-to-noise ratio, defined as $|(I_{inclusion}-I_{background})/(\sigma_{inclusion}+\sigma_{background})|$, is 1.57 for the B-mode image, 1.67 for the previous setup, and 2.88 for near field setup, is here. The cross-sectional slices of the B-mode (green solid line), the near field setup (red dashed line) and the previous setup (blue dotted line) are shown in Fig. (f). Results from an in vivo study of a tumor bearing mouse will be presented in the full report.
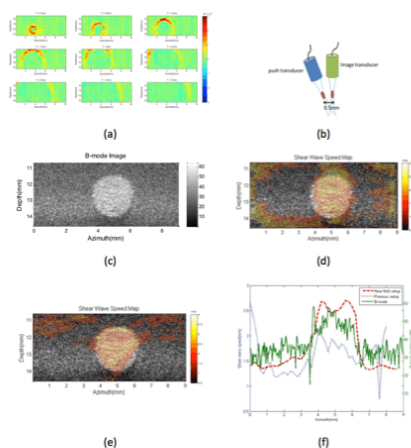
Fig. (a) Shear wave propagation plot by the previous setup (b) Experiment setup (c) B-mode image of the gelatin phantom (d) SWS map by the near field setup (e) SWS map by the previous setup (f) Cross-sectional slices of B-mode (green solid line), near field setup (red dashed line) and previous setup (blue dotted line).

8:00 am   Effects of Aberration in Crawling Wave Sonoelastography

Gabriela Torres[1], Kevin Parker[2], Roberto Lavarello[1], **Benjamin Castaneda[1]**; *[1]Electrical Engineering, Pontificia Universidad Catolica del Peru, Lima, Lima, Peru, [2]Electrical and Computer Engineering, University of Rochester, Rochester, USA*

Background, Motivation and Objective

Crawling Wave (CrW) Sonoelastography is a technique that allows the estimation of elastic parameters through the calculation of the shear wave speed (SWS) in tissues using pulsed wave Doppler techniques to monitor the shear waves produced by external mechanical vibrators. However, the usefulness of CrW may be compromised for in vivo applications due to aberration effects, i.e., the degradation of the ultrasonic wavefront when propagating in inhomogeneous media. In this work, a preliminary experimental evaluation of the effects of aberration when estimating SWS from homogeneous phantoms was performed.

Statement of Contribution/Methods

A Logiq 9 Ultrasound System (General Electric Healthcare) was used for conducting experiments at room temperature ($20°C\pm1°C$). A homogeneous phantom was prepared with a 10% gelatin concentration and layers of beef brisket with thicknesses of 10.21 mm (L1) and 15.32 mm (L2) were used for producing the aberration. Two mechanical vibration sources (Brüel & Kjaer 4810) were located in opposite sides of the phantom to generate sinusoidal vibrations with frequencies ranging between 200 Hz and 300 Hz. SWS maps were generated for each vibration frequency, and the effects of aberration in the SWS estimates were quantified by calculating the mean and standard deviation of the reconstructed elastograms.

Results/Discussion

The estimated SWS values as a function of the vibration frequency are shown in Figure 1 for the non-aberrated and aberrated cases. The estimated mean SWS values in the presence of the L1 aberrator were nearly identical to the ones obtained in the non-aberrated case. The use of the thicker L2 aberrator resulted in only a slight bias (i.e., less than 5% increment in the mean value for a given frequency) and a reduced precision (i.e., a maximum increase of 100% in the standard deviation) in the estimation of the SWS. These experimental results suggest that CrW sonoelastography may not be significantly affected by aberration effects.

(a)   (b)   (c)
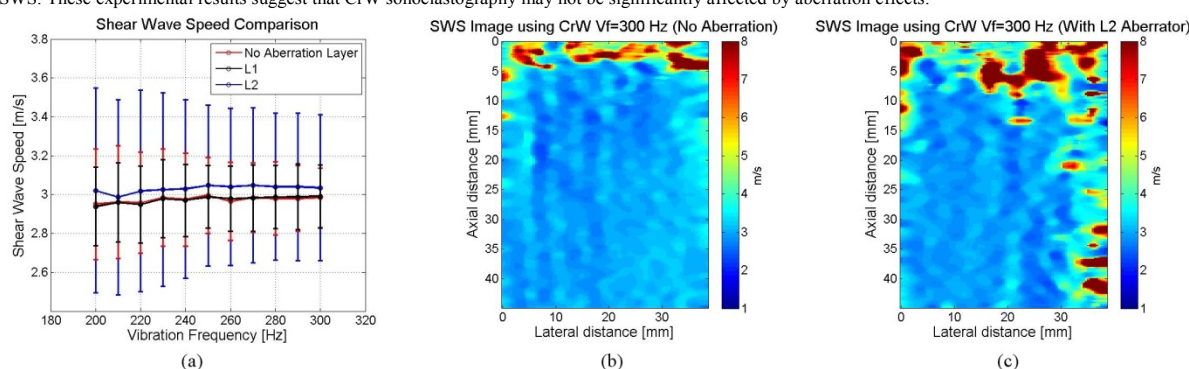
8:00 am   Acoustic particle palpation – a feasibility study on a novel stress source for elasticity imaging

Hasan Koruk[1,2], **Ahmed El Ghamrawy[1]**, Mengxing Tang[1], James Choi[1]; *[1]Department of Bioengineering, Imperial College London, London, United Kingdom, [2]Mechanical Engineering Department, MEF University, Istanbul, Turkey*

Background, Motivation and Objective

Changes in stiffness occur in nearly every disorder ranging from cardiovascular diseases to cancer and neurodegeneration and occur across scales from the molecular to tissue level. Current ultrasound (US) palpation techniques use acoustic radiation force (ARF) as a stress source to deform the tissue and is the basis for a diverse range of US elasticity imaging technologies including acoustic radiation force impulse (ARFI) imaging and supersonic shear wave elasticity imaging. Yet ARF-based palpation methods can diagnose only a few diseases due to limitations of the stress source size, distribution, and depth. We propose a novel stress source that uses acoustic particles (e.g., microbubbles) driven by ultrasound to push against tissue surfaces deep in our body. This acoustic particle palpation (APP) method could reduce the stress source size, improve the distribution of stress, and enable deeper palpations.

Statement of Contribution/Methods

In this study, we administered lipid-shelled microbubbles (mean diameter: 1.32 ± 0.76 µm) into a wall-less 0.8-mm-in-diameter tunnel of a tissue-mimicking material (1.2% Gelatin) so that they were compartmentally separate from the surrounding tissue. US pulses (fc: 5 MHz) forced the microbubbles against the tissue wall to cause a transient deformation, which was observed with high-speed optical microscopy. A wide range of acoustic parameters were evaluated for different concentrations of microbubbles while optical observations were recorded before, during, and after sonication with and without microbubbles present.

Results/Discussion

Without the presence of microbubbles in the tunnel, no tissue deformation was observed. However, when microbubbles were administered, a net displacement of microbubbles were observed in the direction of wave propagation (left to right in the figure), which ultimately caused the tissue to deform in the same direction. The deformation magnitude was shown to increase with peak-rarefactional pressure and microbubble concentration. Our results are the first demonstration of APP using clinically-relevant acoustic particles. Thus APP is a novel stress source that could measure elasticity in new tissue environments.

FRIDAY POSTER
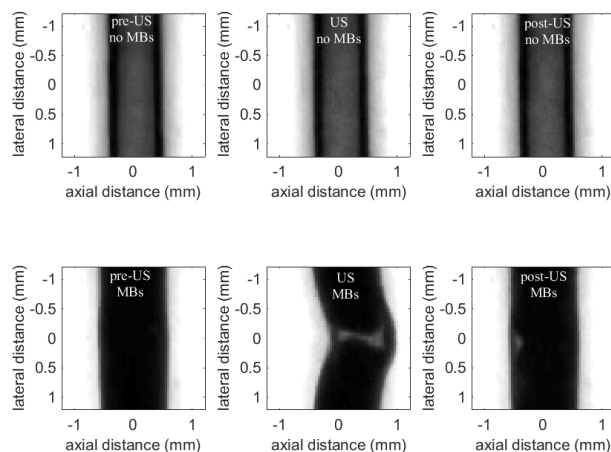
P1B1-7

8:00 am **Novel imaging method of continuous shear wave by ultrasonic color flow imaging**

Yoshiki Yamakoshi[1], Atsushi Yamamoto[2], Yasushi Yuminaka[1], Naoki Sunaguchi[1]; [1]*Grad. School of Science and Technology, Gunma University, Kiryu, Japan,* [2]*Department of Orthopaedic Surgery, Graduate School of Medicine, Gunma University, Maebashi, Japan*

Background, Motivation and Objective

Shear wave velocity measurement which uses continuous shear wave excited by a vibrator is an effective method to evaluate the stiffness of tissue near skin, such as skeletal muscle and breast. A problem of this method is that the shear wave does not always propagate to the correct direction, for example the direction to muscle fiber, due to the diffraction and the refraction at tissue boundary. However, if the propagation of shear wave is visualized in real-time, the accuracy of velocity measurement improves dramatically, because the required wavefront is produced on ROI by adjusting the position of vibrator and the shape of vibration head which is attached to the tissue surface. This paper proposes a novel real-time imaging method of continuous shear wave which propagates in soft tissue.

Statement of Contribution/Methods

In this method, shear wave's wavefront is reconstructed directly using a complex-value signal processing unit which is equipped in conventional ultrasonic color flow imaging (CFI) without adding any function to the CFI system. The shear wave's wavefront is displayed on CFI as a binary pattern which consists of zero and the maximum flow velocities. Two conditions are needed to obtain the shear wave map. Shear wave frequency condition defines the available frequencies of shear wave. The frequency is set to n/4 times of the pulse repetition frequency of CFI, where n is an odd number. Shear wave displacement amplitude condition defines the range of shear wave displacement amplitude. However, these two conditions are not severe restrictions in actual applications, because the shear wave frequency is chosen from several frequencies which are suitable for shear wave imaging and the minimum displacement amplitude of the shear wave is a few tens micron for the ultrasonic wave frequency of 6.5 MHz. Quantitative shear wave maps, such as shear wave velocity map and the propagation direction map, are reconstructed from the observed shear wave's wavefront map by applying the Fourier analysis followed by wave-number vector estimation.

Results/Discussion

Experiments were carried out under the approval of IRB. Small type linear vibration actuator (35 mm in length) with a vibration head made by an acrylic hemisphere (10 mm in diameter) was adopted to excite a continuous shear wave. Ultrasonic color flow imaging system (Hitachi, EUB-7500, Japan) with 6.5 MHz linear probe was used in order to observe the shear wave's wavefront in trapezius muscle. The shear wave frequency was set to 273.6 Hz, which was n=3 in the shear wave frequency condition. By observing the shear wave's wavefront in real-time, the position of vibrator was adjusted so that the shear wave propagated along the muscle fiber. The shear wave velocity of trapezius muscle was 4.3 ± 0.4 m/s for 10 healthy volunteers in their twenties and thirties. This value was

consistent with the shear wave velocity which was calculated from shear elastic modulus measured by ARFI method.

P1B1-8

8:00 am **Spatial Variance Induced by Tissue Compression in Ultrasound Shear Wave Imaging**

Hideki Yoshikawa[1], Teruyuki Sonoyama[2], Noriaki Inoue[2], Ken-ichi Kawabata[1]; [1]*Hitachi, Ltd., Tokyo, Japan,* [2]*Engineering R&D Department 1, Hitachi Aloka Medical,Ltd., Tokyo, Japan*

Background, Motivation and Objective

Ultrasound shear wave imaging (SWI), in which elasticity is estimated by measuring wave velocity, has great potential for characteristic cancer diagnoses. On applying SWI, a tissue is compressed by diagnostic probe, which causes velocity dispersion in accordance with an acousto-elasticity theory. In this study, the effect of the degree of compression on the probability of errors was investigated. Furthermore, the effect of directional filtering (DF), which detects a wave with specific propagation direction among waves, on reducing errors was studied.

Statement of Contribution/Methods

The experimental setup is shown in Fig. 1. A phantom (Background: 19 kPa, Mass: 37 kPa) was set between a transducer and a diagnostic probe. A shear wave was generated by acoustic radiation force by the transducer, and the wave velocity of the specimen was measured with the probe. The velocity measurement was taken in the whole imaging area of the set probe, and an elasticity image was constructed. The phantom was uniaxially and statically compressed along the y-axis. With this setup, the shear wave velocity under statically compressed conditions was measured with various strain ratios from 0 to 30%. Errors in the elasticity image were analyzed in a region set in the mass area, and a comparison between the coefficient of variation in the presence and absence of DF was made.

Results/Discussion

Fig. 2 (a-1) and (a-2) are images without DF, and Fig. 2 (b-1) and (b-2) are images with DF. Comparing Fig. 2 (a-1) to (a-2) with strain ratios of 0% and 20%, elasticity in both background and mass has increased as expected. A spot artifact with high elasticity (50 kPa) appeared in both images Fig. 2 (a-1) and (a-2), and spatial variance of elasticity is larger in the compressed image (a-2). Additionally, elasticity in the peripheral part of the mass area is greater in compressed image Fig. 2 (a-2) due to stress concentration. The spatial variance is clearly improved by DF as shown in Fig. 2 (b-1) and (b-2) because an error of velocity measurement due to refraction is effectively reduced. The coefficient of variation is reduced by 27% on average (Fig. 2 (c)). The obtained results reveal that compression is one of the dominant causes of spatial variance

---

of elasticity, and DF is effective in reducing the artifact. We will perform further studies in vivo to improve the accuracy of shear wave imaging with complex heterogeneous tissue.
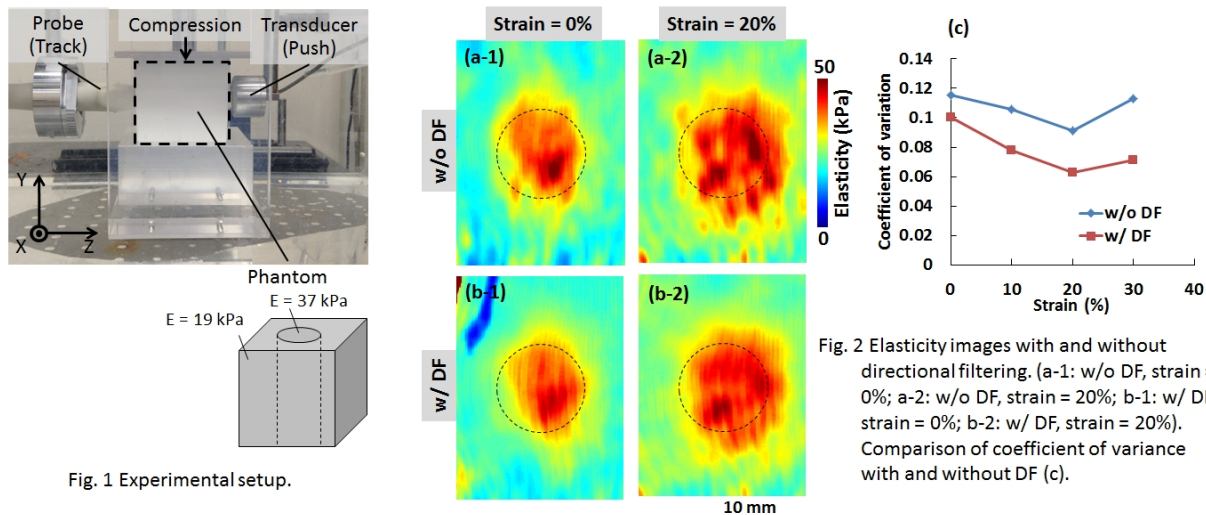
Fig. 1 Experimental setup.

Fig. 2 Elasticity images with and without directional filtering. (a-1: w/o DF, strain = 0%; a-2: w/o DF, strain = 20%; b-1: w/ DF, strain = 0%; b-2: w/ DF, strain = 20%). Comparison of coefficient of variance with and without DF (c).

P1B1-9 _____

8:00 am   A reliability index of shear wave speed measurement for shear wave elastgraphy

Kiwan Choi[1], Junho Park[1], Donggoen Kong[1], Hyoung-Ki Lee[1]; *[1]Ultrasound R&D Group, Samsung Electronics, Seoul, Korea, Republic of*

Background, Motivation and Objective

Recently, shear wave elastography is widely used for the noninvasive measurement of the tissue stiffness. Especially, assessing the liver fibrosis by measuring the shear wave propagation speed is gaining popularity. However, it has a shortcoming that an unreliable measure occurs sometimes and it can confuse the assessment of liver fibrosis. In this paper, we propose a method to assess the reliability of shear wave speed calculation.

Statement of Contribution/Methods

For the quantification of the reliability of shear wave speed measurement, we propose an index named ″Reliable Measurement Index (RMI)″ which is calculated by the weighted sum of two factors: one is the residual of the wave equation and the other is the magnitude of the shear wave. The residual of the wave equation that calculated from the equation in Fig. 2 indicates how well the measured shear wave propagation satisfies the wave equation. The residual becomes bigger as it has more errors, such as measurement noises, motion artifacts and other artifacts. The residual had better be normalized with the spatial Laplacian or the second time derivative. The normalization helps a threshold of the residual remain constant. As for the second factor, the max amplitude of shear wave is used to reflect the SNR of shear wave, but it is less important than the residual.

Results/Discussion

The proposed approach has been successfully implemented on the commercial diagnostic ultrasound system (RS-80A with Prestige, Samsung Medison, Korea). In phantom studies, RMI reaches the maximum values of one. Initial in-vivo studies show that large RMI values are correlated with the reproducible measurements. As a result, the proposed index can be utilized to filter out unreliable measurements and results in increasing the performance of shear wave elastography.

$$res_n = \frac{\sum \left| \frac{\partial^2 u}{\partial t^2} - c^2 \nabla^2 u \right|^2}{\sum \left| \nabla^2 u \right|^2}$$

Fig. 2. Normalized residual of the wave equation.
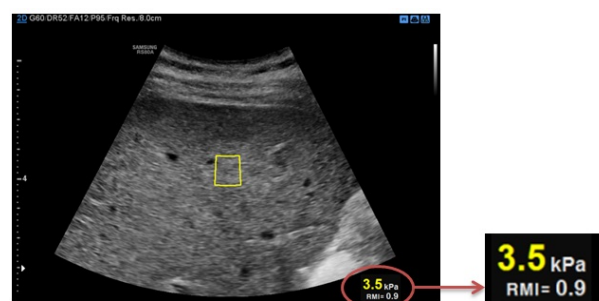
Fig. 1. Young's modulus was measured in the ROI of a human liver. RMI = 0.9 indicates this measurement is reliable.

P1B1-10 _____

8:00 am   Pixel-based ultrasound image reconstruction: impact of grid size on signal frequency content

Mahdi Bayat[1], Alireza Nabavizadeh[1,2], Azra Alizad[1,3], **Mostafa Fatemi**[1]; *[1]Physiology and Biomedical Engineering, Mayo Clinic, Rochester, MN, USA, [2]Biomedical Informatics and Computational Biology, University of Minnesota, Rochester, MN, USA, [3]Department of Internal Medicine, Mayo Clinic, Rochester, MN, USA*

Backgroud, Motivation and Objective

High speed imaging via single transmit imaging such as plane wave imaging is becoming a requirement for many of the new ultrasound applications such as shear wave elastography. While pixel-based image reconstruction algorithms allow for selecting the grid size in both axial and lateral directions independent of received channel data sampling rate, lower than the Nyquist rate sampling can result in simultaneous down sampling and down conversion of the beamformed signal. When using narrow band techniques, such as autocorrelation method for displacement tracking,this can lead to an estimation bias due to inaccuracy in center frequency estimation. Here we present the effect of image reconstruction grid size on the frequency content of the beamformed data using simulation and experimental data when using plane wave imaging.

Statement of Contribution/Methods

Plane wave images of a uniform scattering phantom with an anechoic inclusion was simulated using Field II. Images were reconstructed at different grid sizes and the analytic signal in time and frequency were compared in terms of B-mode appearance and frequency spectrum. To investigate the impact of frequency content on ultrasound speckle tracking, a simple experiment based on uniform translational motion test was also performed. Sequential images were acquired from a homogenous tissue mimicking phantom immersed in water while transducer was moved at a constant speed. In all cases, images were reconstructed using a grid size based on the wavelength λ equivalent to that of transducer's center frequency. Two-dimensional autocorrelation technique was used for displacement estimation.

Results/Discussion

Figure (a) shows the frequency spectrum of the beamformed data from a uniform region inside the simulated image. As it can be seen the signal center frequency and spectrum is highly affected by the grid size. Figure (b) shows the result of displacement tracking from the translational motion for two different grid sizes. It is seen that the finely sampled image results in a more uniform displacement map with values close to the true displacement (10 mm) while coarsely sampled data has resulted in wrong displacement variations within the phantom. The results of this study highlight the importance of appropriate grid size selection to preserve the bandpass features of the beamformed ultrasound signals.

(a) (b)
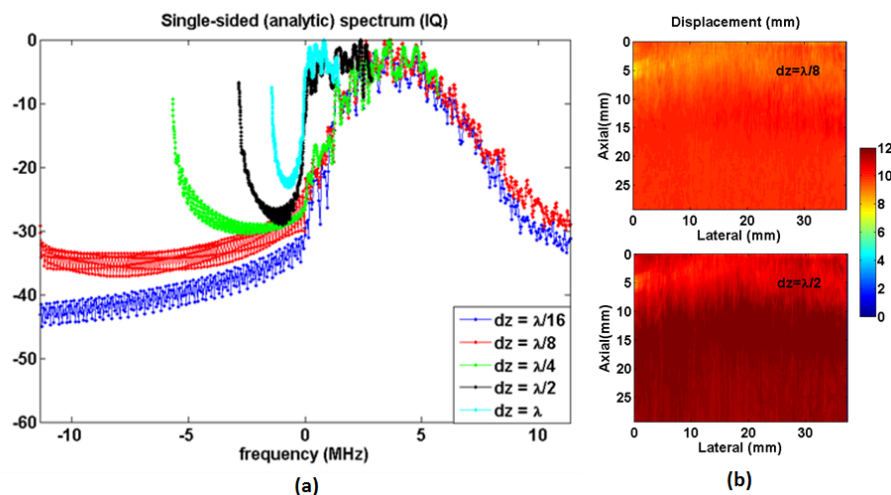
P1B1-11 _____

8:00 am   A Shear Wave Propagation Tracking Method Based on Modal Assurance Criterion in Acoustic Radiation Force Impulse Imaging

Yang Jiao[1], Jie Xu[1], Yongjia Xiang[1], Tianming Gu[1], Yaoyao Cui[1]; *[1]Suzhou Institute of Biomedical Engineering and Technology,CAS, Suzhou, Jiangsu, China, People's Republic of*

Background, Motivation and Objective

Shear wave elasticity imaging (SWEI) can measure tissue stiffness, which contribute to the assessment of various diseases. The key challenge of SWEI is the shear wave tracking algorithm, where normally the Loupas 2D autocorrelator is used. The Modal Assurance Criterion (MAC) is a statistical quality assurance indicator which is essential to recognize the similarity of varied modal vectors and most sensitive to the largest difference between the comparative values. In this paper, we applied MAC method to track the propagation of the shear wave, which is effective and stable. And we also will use GPU to accelerate (e.g. CUDA) our algorithm in the near future.

Statement of Contribution/Methods

To verify the effectiveness of this velocity tracking approach with MAC, a 5ms ARFI excitation was applied to a FEM model, and displacements perpendicular to wave travel were observed in the next 100ms and 128 lines of the radio frequency (RF) data was obtained. The MAC matrix of the discrete echo signals could be calculated with equivalent formulation as fig. 1 (c), where φ_i and φ_{Xi} represent the i-th element of an n-dimensional referenced signal and measured signal, respectively. Then A homogeneous phantom composited of high elastic modulus was tested by the SonixTouch and DAQ system with a probe L14-5. After a shear wave generated by the HIFU, the probe was used to measure the pre-beamformed radio frequency (RF) data, which is sampled and stored in buffer. Finally, an image can be reconstructed from the delays and amplitudes of the echoes.

Results/Discussion

Fig.1 (a) represents the propagation velocity is about 0.9 m•s^{-1} in the soft tissue and 1.9 m•s-1 in the hard inclusion. Fig. 1 (b) shows the 2-D results of shear wave tracking by MAC matrix. It is bounded between 0 and 1, with 1 (red) indicating no displacements in the tissue and value near 0 (blue) indicates to the contrary. The MAC matrix shows the propagation process of shear wave which provided values for velocities as 1.323±0.060 m•s^{-1}. These results demonstrate that the method based on MAC was capable of detecting the shear wave velocities. And with the effectiveness and stability of the proposed method, it has the superiority of speeding up the shear wave tracking process with the GPU acceleration. Experimental tests with a tissue-mimicking phantom have also proved this conclusion.
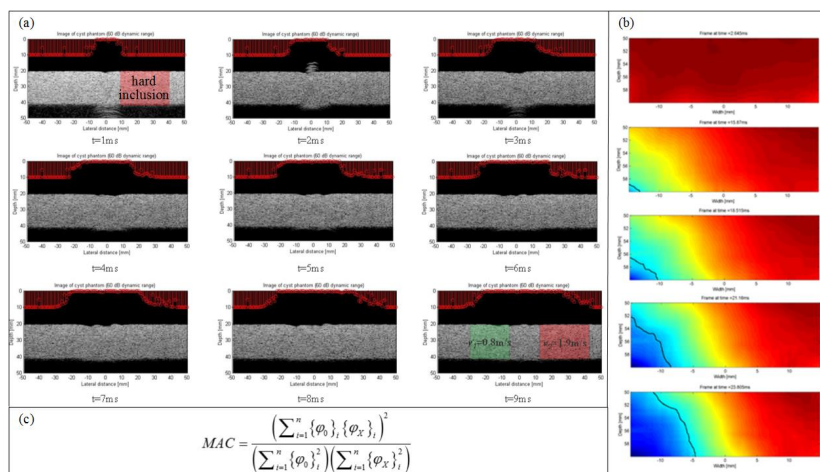
Fig. 1. *(a) The* MAC *values (the 128 red lines above) of a single slice of the phantom, where 0 indicating the shear wave propagation has been tracked in this line and 1 representing the opposite; (b) The experimental results of shear wave tracking with* MAC; *(c) The general expression of the* MAC *matrix calculated for* SWEI.

P1B2 - MCA: Microbubbles and Nanodroplets

4th floor

Friday, October 23, 2015, Posters displayed 08:00 am - 05:00 pm. Authors must be present at their poster from 9:30 - 10:30am (odd number posters) and 14:30 – 15:30pm (even number posters).

Chair: **Lori Bridal**
Univ. Pierre and Marie Curie

P1B2-1

8:00 am **Cosolvent-infused precursor bubbles and droplets for production of ultra-small, ultrasound-activatable, nanoscale perfluorcarbon agents**

Minseok Seo[1], Siqi Zhu[1], Ross Williams[1], Naomi Matsuura[2]; *[1]Sunnybrook Research Institute, Canada, [2]University of Toronto, Canada*

Background, Motivation and Objective

The development of perfluorocarbon nanodroplets (PFC NDs) as *in situ* microbubble precursors for ultrasound imaging and therapy is an active area of research. For applications in cancer, the NDs size, ranging from ~200 to 400 nm in diameter, means that, unlike larger, less stable microbubbles that are purely intravascular, long-circulating PFC NDs can leak from blood vessels into the interstitial space in solid tumours. After accumulation into tumours, these PFC NDs can be activated by ultrasound or light, to undergo phase change in situ to form echogenic bubbles. Despite early promising preclinical results, it is clear that the successful translation of these PFC NDs into clinical use will require substantial improvements in the controlled synthesis of PFC NDs of specific sizes for predictable tumour accumulation and efficient conversion into bubbles. In this study, we evaluate the feasibility of adapting current microfluidic methods to engineer highly size-controlled PFC NDs for the practical design of future, clinically-translatable PFC NDs for cancer therapy.

Statement of Contribution/Methods

Size-controlled, ultrasound-activable PFC NDs were prepared using a standard microfluidic device. Diethyl ether (DEE)-infused PFCs were heated above their boiling temperatures before emulsification to generate precursor bubbles in water. DEE was removed through evaporation and dissolution. Nanodroplets were converted to microbubbles *in vitro* using ultrasound. Size characterization was done by microscopy as well as dynamic light scattering.

Results/Discussion

Using microfluidics in combination with a dissolvable cosolvent, highly size-controlled PFC NDs, ranging from 240 to 470 nm, were produced. A key finding here was that the use of the cosolvent enabled the production of droplets that are much smaller than the orifice of the device: specifically, ~24 times smaller than the smallest droplet that could be directly produced using the microfluidic device. In vitro experiments confirmed that the monodisperse PFC NDs produced using this new synthesis method were converted into echogenic and monodisperse microbubbles. In the future, since DEE can also permit the direct loading of hydrophobic NPs and dyes into hydrophobic PFCs, this new method may also be used to permit PFC NDs to perform as a highly controlled delivery vehicle for anticancer, hydrophobic drugs.
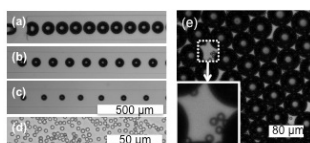
Figure: Microscope images of the size reduction of DEE-infused PFC bubbles (a-c) (φ_{PFC}=0.014) to form the final PFC droplets (d) (D_f = 4.2 μm, CV = 3.9 %). The size reduction is a result of combined condensation and DEE dissolution. a) DEE-infused PFC bubbles (D_i = 99.1 μm, CV = 2.4 %) at the MFD orifice immediately after generation (T_{MFD}=80 °C); (b) 9 mm downstream from the orifice; and (c) 20 mm downstream from the orifice. e) microscope images of PFC droplets and bubbles (D_{bubble} = 52.4 μm, CV = 3.5 %) embedded in PAA gel after exposure to high-pressure ultrasound. The diameter increase due to the vapourization of the droplet to the bubble (D_{bubble}/D_f) is 7.9.

P1B2-2

8:00 am **Influence of the surrounding media on the acoustic behavior of gas vesicle nanostructures at high ultrasound frequencies**

Emmanuel Cherin[1], Raymond W. Bourdeau[2], Melissa Yin[1], Mikhail G. Shapiro[2], F. Stuart Foster[1]; *[1]Imaging Research, Sunnybrook Research Institute, Toronto, Ontario, Canada, [2]Division of Chemistry and Chemical Engineering, California Institute of Technology, Pasadena, California, USA*

Background, Motivation and Objective

Gas vesicles (GVs) are gas-filled nanostructures generated by species of archaea and bacteria as a means to regulate buoyancy. A preliminary study showed that GVs embedded in an Agar matrix exhibit a non linear behavior when exposed to ultrasound in the 12.5-27.5 MHz frequency range, and a collapse pressure around 500 kPa. This collapse pressure is more than twice higher than the collapse pressure of Halo GVs in solution in hydrostatic conditions reported in the literature (50-200 kPa). The present study investigates the influence of the surrounding media on GVs collapse pressure and acoustic behavior.

Statement of Contribution/Methods

The acoustic behavior of GVs from Halobacterium NRC-1, and their collapse pressure, were investigated in vitro with a Vevo770 (VisualSonics), at F0=20 MHz (6 cycle pulses), with pressures from 0.2 to over 1.2 MPa. GVs were embedded in Agar phantoms by mixing 300μL of OD 2.4 solutions of GVs with a 900μL of 0.5 and 1% (w/w) Agar solution at 40°C. The mixture solidified in a 0.4(W) x 0.7 (D) x 4 (L) cm³ cast. The phantom was scanned in 4x1mm ROIs (1 per pressure), separated by a 1-mm gap (no exposure). In each ROI, one pulse was transmitted at each probe location (5μm step), with the focus positioned just below the surface. The phantoms were then imaged

FRIDAY POSTER

along their length (L) at the lowest pressure, and ROIs where collapse occurred identified (Fig.1). A third scan was performed at a pressure just below collapse pressure, in ROIs with intact GVs. Signals corresponding to the -1dB focal zone were collected, the average power spectrum was computed, corrected for background noise and transducer sensitivity. The average fundamental and second harmonic powers were estimated over a 30% relative bandwidth centered on F0 and 2F0, respectively.

Results/Discussion

The collapse pressure was between 513 and 576 kPa, and between 645 and 696 kPa for the 0.5% and 1% Agar concentration, respectively. The second harmonic to fundamental ratio was 9 dB higher for the 0.5% (-5 dB, at 454 kPa) than for the 1% Agar concentration (-14 dB, at 576 kPa). These results indicate that damping of GVs oscillations increases with Agar concentration. It suggests that the behavior of GVs in vivo might be affected by the viscoelastic properties of the surrounding (blood, vessel wall, etc.). Modeling suggests that collapse pressure will also increases with surrounding liquid viscosity.
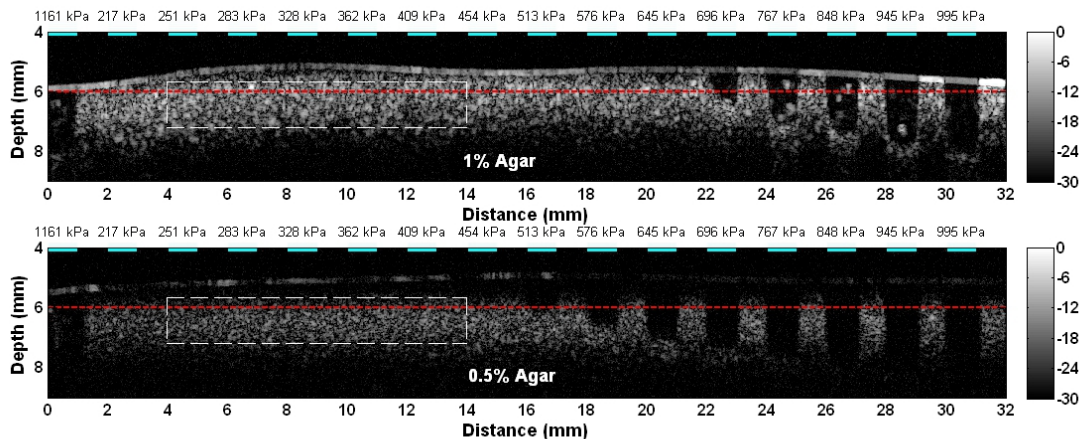
Fig. 1: B-scans of Agar phantoms containing GVs, after exposure to 20 MHz 6-cycle ultrasound pulse at peak positive pressures ranging from 217 to 1161 kPa. ROIs are delineated by cyan lines with corresponding acoustic pressures above. ROIs where GVs collapsed appear anechoic. The red line represents the focus of the probe. The signals used for the estimation of the second-harmonic to fundamental ratio are delineated in white.

P1B2-3

8:00 am   **Nonlinear Acoustic Properties Characterization of Nano Size Gas Vesicles**

Yaoheng Yang[1], Yongmin Huang[1], Zhihai Qiu[1], Cheng Liu[1], Jiyan Dai[2], Lei Sun[1]; *[1]Interdisciplinary Division of Biomedical Engineering, The Hong Kong Polytechnic University, Hong Kong, [2]Department of Applied Physics, The Hong Kong Polytechnic University, Hong Kong*

Background, Motivation and Objective

Microbubble is a widely used ultrasound contrast agent, whose structure is a spherical shell encapsulating inertial gas. However, due to the micrometer size, microbubbles are limited within blood circulation, so they are mainly used for mapping blood vessels. Recently, biogenetic nano gas vesicles at the size of ~250nm were reported [1], and they become possible to travel across the endothelial layer and reach targeted cells beyond. The objective of this study is to investigate the nonlinear acoustic property of these gas vesicles, and understand its potential in contrast enhanced ultrasound imaging. Specifically, we would like to identify its resonance frequency and examine the harmonic response by ultrasound stimulation.

Statement of Contribution/Methods

Nano gas vesicles were isolated from anabaena flos-aquae by lysing and centrifuge method. Concentration and size distribution were measured using optical density and dynamic light scattering method. The gas vesicle resonance frequency was measured using pulse-echo attenuation method. Short pulse of acoustic signal was transmitted to a stainless steel flat reflector, and received by the same transducer through gas vesicle suspended solution. The same measurement was performed on water as a reference. Fourier transform was performed on averaged gas vesicle signals, and normalized against the reference signal from water. The experiments were repeated by three customized high frequency transducers with center frequencies of 22 MHz, 38 MHz and 46 MHz. Next, the backscattered intensities of the gas vesicles were measured at the harmonic frequencies using a receiving transducer. The incident intensity levels were selected as 0.25MPa, 0.5MPa, 0.75MPa and 1MPa by a transmitting transducer at the resonance frequency. These two transducers were placed at a 90o angles.

Results/Discussion

The size of the gas vesicles is normally distributed with an average diameter of 309 nm and a polydispersity index of 0.206. The resonance frequency is found to be 48 MHz. The gas vesicle demonstrates substantial sub- and second harmonic signals, especially under higher intensity levels. The gas vesicles claps at 1MPa.

[1]   Shapiro et al., (2014) Nature Nanotechnology 9(4) 311-316.

P1B2-4

8:00 am   **Ultrasound-enhanced extravasation of dual-modality multifunctional nanodroplets**

Yujin Zong[1], Xinru Zou[1], Rongrong Wang[1], Yi Feng[1], Xuan Du[1], Mingxi Wan[1]; *[1]The Key Laboratory of Biomedical Information Engineering of Ministry of Education, Xi'an Jiaotong University, Xi'an, Shaanxi, China, People's Republic of*

Background, Motivation and Objective

Poorly organized vascular architecture of tumor tissue allows extravasation of drug-loaded nanoparticles through the large interendothelial gaps. Extravasated perfluorocarbon (PFC) nanodroplets can convert into microbubbles under ultra¬sound irradiation to imaging or deliver drug for tumor treatment. However an increased interstitial fluid pressure in tumor tissue hinders convectional transport of drug carriers across blood vessel walls, thus extravasation of sufficient amounts of droplets remains a major challenge. We propose an ultrasound(US)-enhanced extravasation strategy using synergetic effect of acoustic radiation force and cavitation enhanced penetration. And we prepared a dual-modality multifunctional nanodroplet that combine properties of US triggered drug carriers and fluorescence probe to monitor the extrasavation.

Statement of Contribution/Methods

DiI was incorporated into PFC droplets to get dual-modality nanodroplets that allow monitoring the extravasation of droplets by fluorescence observation. 0.6% agrose gel vessel phantom that has a pore size range of 500-1000 nm was prepared to mimic the leaky tumor vascular. A two-element annular transducer was utilized to carry out the extravasation strategy. Lower intensity and continuous US wave (CW) was emitted from the outer 1.1MHz transducer to generate acoustic radiation force. While higher intensity and shorter pulse (10 cycles) was repeatedly emitted from the inner 5MHz transducer to active the droplets near vessel wall. The vessel phantom was observed under inverted fluorescence microscope to determine the extravasation of nanodroplets. Then B-mode US imaging is performed to verify the acoustic vaporization of nandroplets in the vessel wall under focused US irradiation.

FRIDAY POSTER

Results/Discussion

Using only either CW or pulsed US exposure, there is no obvious fluorescence observed in the area out of the vessel wall, only on the vessel wall (Fig1a and 1b), indicated no obvious extravastion of nanodroplets. While the synergetic strategy enhanced nanodroplet penetration through the vessel wall (Fig 1c). The extravasation of nanodroplets was also verified by contrast enhancement within the area out of vessel in the US image. The combined action of radiation force of CW and high intensity pulse US induced cavitation could be responsible for US-enhanced vessel permeability.

(a) 1.1 MHz CW US

(b) 5MHz pulsed US (10cycles, PRF=200)

(c) 1.1 MHz CW US + 5MHz pulsed US (10cycles, PRF=200)
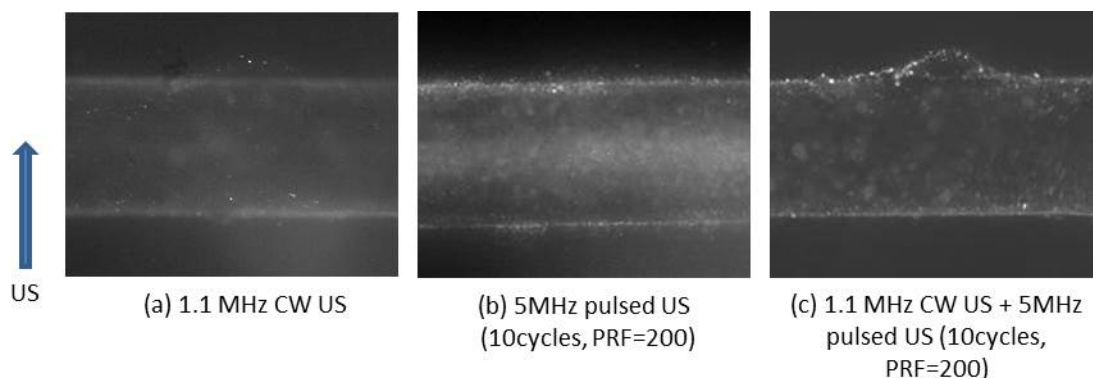
Fig.1 Fluorescence micrographs of vessel phantom after 1min US exposure

P1B2-5

8:00 am   Evaluation the potential of the hair growth enhancements with ultrasound-mediated minoxidil loaded microbubbles cavitation

Ai-ho Liao[1], Ying-jui Lu[1]; [1]*National Taiwan University of Science and Technology, Taiwan*

Background, Motivation and Objective

A first commercially available formulation of minoxidil improves its poor water solubility and increase permeability by chemical enhancement methods (ethanol, propylene glycol). The commercially products require to treat at least two times a day to ensure its pharmacological effect, because the products is made of chemical formulations (ethanol, propylene glycol) to increase the ability of transdermal drug delivery so it will often occur atopic dermatitis for long-term use. In this study, a new ultrasound contrast agent, minoxidil loaded microbubbles (MBs) were created and combined with US energy in water-phase to enhance hair growth and reduce the side effects of skin.

Statement of Contribution/Methods

The MBs which are layer by layer (LbL) assembly of chitosan oligosaccharide lactate (COL) shell which absorbed minoxidil on this cationic carriers. The zeta potential and size distribution of the minoxidil loaded MBs in suspension were measured by DLS. The in vitro and in vivo experimental parameters will be randomly divided into four groups (n=5 animals per group): (1) only penetrating minoxidil (2) US combines with minoxidil (3) US combines with MBs in minoxidil solution (4) US combines with minoxidil loaded COL-MBs (minoxidil-COL-MBs).

Results/Discussion

The cationic MBs were modified by chitosan. The mean diameters of MBs, MBs coated with COL, and minoxidil-COL-MBs were 1.48, 4.15, 4.50 μm. The loading effciency of minoxidil on cationic MBs was 14.5% (n=5). The zeta potentials of MBs coated with COL and minoxidil-COL-MBs were 24.13±0.44 and 11.78 ±1.24 mV, respectively. The release kinetics of minoxidil from minoxidil-COL-MBs were determined by dynamic dialysis method. After US treatment, the released rate increased 33% at 2 hour. For the in vivo experiments, the minoxidil-COL-MBs would be promoted hair growth rapidly, reduced the treatment dose and side effects.
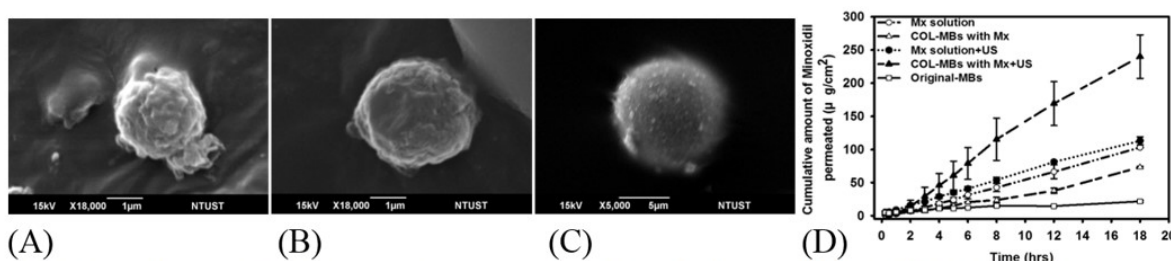
Fig. 1 SEM images of (A) MBs, (B) MBs coated with COL, and (C) minoxidil loaded COL-MBs. (D) *In vitro* drug penetration from the different experimental groups through pigskin in Franz diffusion cell at 37°C ± 0.5°C.

P1B2-6

8:00 am   Quantification of endothelial αvβ3 expression with high frequency ultrasound and targeted microbubbles: in vitro and in vivo studies

Verya Daeichin[1], Ilya Skachkov[1], Judith C. Sluimer[2], Johan G. Bosch[1], Klazina Kooiman[1], Andrew Needles[3], Ben Janssen[4], Mat J.A.P. Daemen[5], Antonius van der Steen[1,6], Nico de Jong[1,6]; [1]*Thoraxcenter Biomedical Engineering, Erasmus MC, Rotterdam, Netherlands*, [2]*Pathology, CARIM, Maastricht University, Netherlands*, [3]*FUJIFILM VisualSonics, Inc., Canada*, [4]*Pharmacology, CARIM, Maastricht University, Netherlands*, [5]*Pathology, AMC, Netherlands*, [6]*Technical University Delft, Netherlands*

Background, Motivation and Objective

Angiogenesis is a critical feature of plaque development in atherosclerosis and might play a key role in the eventual rupture of plaques. The precursory molecular or cellular events that initiate plaque growth and that ultimately contribute to plaque instability, however, cannot be detected directly with any current diagnostic modality. This study is designed to investigate the feasibility for molecular imaging of endothelial αvβ3 expression in vitro and in vivo using the αvβ3-targeted ultrasound contrast agents (UCA).

Statement of Contribution/Methods

In the in vitro study, $\alpha v\beta 3$ expression was confirmed by Western blotting in murine SVEC cells and tracked by using the targeted UCA and imaged a Vevo 2100 ultrasound imaging system at 18 MHz transmit frequency. In the in vivo study in animal models of atherosclerosis, in apolipoprotein E-deficient (ApoE-/-) mice, expression of endothelial $\alpha v\beta 3$ integrin in carotid artery vessels and salivary glands were quantified using targeted microbubble (tMB) and high-frequency ultrasound (n= 7).

Results/Discussion

Applying our previously described tMB quantification method [1], our results showed that endothelial $\alpha v\beta 3$ expression was 4.2 times higher in the carotid wall artery containing atherosclerosis lesions compared with parts without any lesions (p <0.01) (Fig.1. d vs h). The ratio of the quantified molecular signals for the tMB vs control MB (cMB) in the plaque area was 4.8 (p<0.01, Fig.1. d vs c) and 3.9 in the salivary gland (p<0.01, Fig.1. f vs g).This results also showed that the salivary gland can be used as an internal positive control for successful binding of tMB to $\alpha v\beta 3$ integrin. Moreover, during live contrast enhanced ultrasonography of one of the animals (a 50-week old ApoE-/- male mouse), symptoms suggesting plaque disruption in the right brachiocephalic artery were observed.

In conclusion, $\alpha v\beta 3$-targeted UCA allows noninvasive assessment of the expression levels of $\alpha v\beta 3$ on the vascular endothelium and may provide potential insights into early atherosclerotic plaque detection and treatment monitoring.

Reference:

[1]V Daeichin et al. IEEE International, pp.1825,1828, 21-25 July 2013 doi: 10.1109/ULTSYM.2013.0465

Microscopic photo and Molecular sonogram of carotid artery vessels and salivary gland of a ApoE$^{-/-}$ mouse: a) Anatomical structure of the right carotid and presence of atherosclerosis lesions in the aortic arch, brachiocephalic trunk and carotid bifurcations and the absence of lesions in the common carotid; b) Bmode image of the right carotid and right salivary gland with region of interest in the salivary gland, around the plaque at the carotid bifurcation and around the common carotid artery where there is no plaque present; c) Nonlinear contrast mode image (maximum intensity projection over 100 frames) of the right carotid and salivary gland after injecting the ultrasound contrast agent (UCA); d) Detected bound UCA in the plaque region of interest for the targeted microbubbles (tMBs) injection; e) Detected bound UCA in the plaque region of interest for the control microbubbles (cMBs) injection; f) Detected bound UCA in the salivary gland region of interest for the tMBs injection; g) Detected bound UCA in the salivary gland region of interest for the cMBs injection; h) Detected bound UCA in the region of interest around the common carotid artery wall where there is no plaque present for the tMBs injection; i) Detected bound UCA in the region of interest around the common carotid artery wall where there is no plaque present for the cMBs injection.
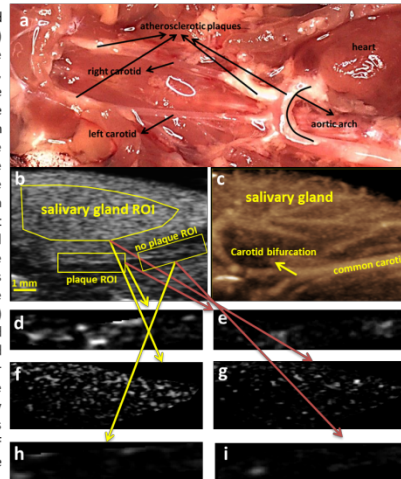
P1B2-7 _____

8:00 am **Subharmonic Threshold for Chirp Excitations of High Frequency Contrast Agents**

John Allen[1], Rintaro Hayashi[1], Parag Chitnis[2], Jonathan Mamou[3], Jeffrey Ketterling[3]; *[1]Mechanical Engineering, University of Hawaii, Honolulu, Hawaii, USA, [2]Department of Bioengineering, George Mason University, Fairfax, Virginia, USA, [3]Riverside Research Institute, New York CIty, New York, USA*

Background, Motivation and Objective

Ultrasound contrast agents (UCA) driven at a sufficient pressure amplitude can produce a scattered subharmonic response lower in frequency than the fundamental. Less attenuation occurs at a lower frequency so increased penetration depth can be achieved in tissue, particularly for high-frequency applications. Moreover, tissues do not exhibit a subharmonic response. Chirped excitation signals have been shown to enhance the subharmonic. This provides a methodology for enhanced amplitude response and axial penetration; however, a pressure excitation beyond the threshold may result in undesired UCA destruction. Typically, theoretical predictions for the threshold have been restricted to single-frequency, narrow band, forcing. Experimental and numerical studies have implemented threshold definitions based on the ratio of the spectral amplitudes of the subharmonic to the fundamental. We propose a robust, time domain based method for analysis of subharmonic signals appropriate for chirp excitations.

Statement of Contribution/Methods

We investigated chirp and single frequency subharmonic responses with numerical simulations and experimental comparisons for polymer UCAs driven at 30-50 MHz. Adaptive, nonlinear signal processing methods based on the Empirical Mode Decomposition (EMD) were used to characterize the scattered signals and develop an appropriate subharmonic threshold criteria. The instantaneous frequencies were obtained from the respective Intrinsic Mode Functions (IMFs). These are an orthogonal set of components based on inherent oscillations symmetric to a local mean defined within the signal's envelope. The subharmonics were determined from instantaneous frequency ratios and phase differences.

Results/Discussion

A time domain definition based on the energy ratio of the respective IMFs of the fundamental and subharmonic was established for the subharmonic threshold. This result had excellent agreement with the spectral amplitude definition for single-frequency forcing over many cycles. However, by comparison for chirp excitations the spectral method had limited applicability. Figure 1 is a scattered signal and the IMFs of fundamental (IMF 1) and subharmonic (IMF 2). The subharmonic is obscured in the spectra. However, the onset of the subharmonic at 1.0 microseconds agrees with phase locking, a constant phase difference.
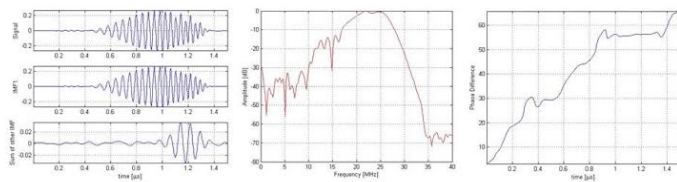
P1B3 - MIM: Cardiovascular Imaging and Mechanics

4th floor

Friday, October 23, 2015, Posters displayed 08:00 am - 05:00 pm. Authors must be present at their poster from 9:30 - 10:30am (odd number posters) and 14:30 – 15:30pm (even number posters).

Chair: **Richard Lopata**
               Technical University Eindhoven

P1B3-1

8:00 am   **Full-cycle left ventricular segmentation and tracking in 3D echocardiography using active appearance models**

Marijn van Stralen[1], Alexander Haak[2], Esther Leung[3], Gerard van Burken[2], Clemens Bosch[1], Johan Bosch[2]; *[1]Imaging Division, UMC Utrecht, Utrecht, Netherlands, [2]Biomedical Engineering, Erasmus MC Rotterdam, Rotterdam, Netherlands, [3]Albert Schweitzer Hospital, Dordrecht, Netherlands*

Background, Motivation and Objective

Fully automatic segmentation of the left ventricle in 3D echocardiography is a challenging task due to its low contrast-to-noise compared to other cardiac imaging modalities, its typical artifacts and the grainy appearance due to speckle. A recent challenge on this topic [1] showed that state-of-the-art technology is approaching interobserver variabilities, but there is still room for further improvement.

Statement of Contribution/Methods

We previously demonstrated the use of active appearance models (AAM) for segmentation of the end-diastolic (ED) and end-systolic phases of the cardiac cycle, which results in a competitive performance with respect to state-of-the-art methods. In this work we propose an extension of the 3D AAM segmentation with tracking of the left ventricle (LV) over the entire cardiac cycle. To this end we build a single generative model for ED and ES LV shape and appearance and perform tracking by initializing the AAM in the next frame from the AAM parameters found in the previous frame. We investigate the added value of tracking from ED to ES to improve ES detection, as well as repetitive full cycle tracking to improve both ED and ES estimates.

We test and evaluate the methodology in the framework of the CETUS challenge [1] on data of 30 patients with varying pathology, imaged with varying ultrasound equipment at three centers. The training set consisted of the 15 training patients from the CETUS data set and 25 patients from our own center.

Results/Discussion

Detections in ED result in mean absolute surface distances of 2.0 ± 0.6 mm. The results confirm that tracking the endocardium from the initial detection in ED improves the detection of ES, as surface distances for ES drop from 2.8 ± 1.5 mm to 2.5 ± 0.8 mm. Furthermore, tracking the full cycle twice renders stable detections for ED and ES, resulting in further improvement in ED surface distances (1.9 ± 0.8 mm), see Fig. 1, and an estimation of the clinically relevant ejection fraction (limits of agreement [-6.7; 23.5%], r = 0.75) that competes with the currently best performing (semi-)automatic methods.

Our results show that tracking improves overall segmentation results and prediction of clinical parameters. Segmentation and tracking based on AAMs might be a solid base for future hybrid solutions where locally refined detection is added by different methodology.
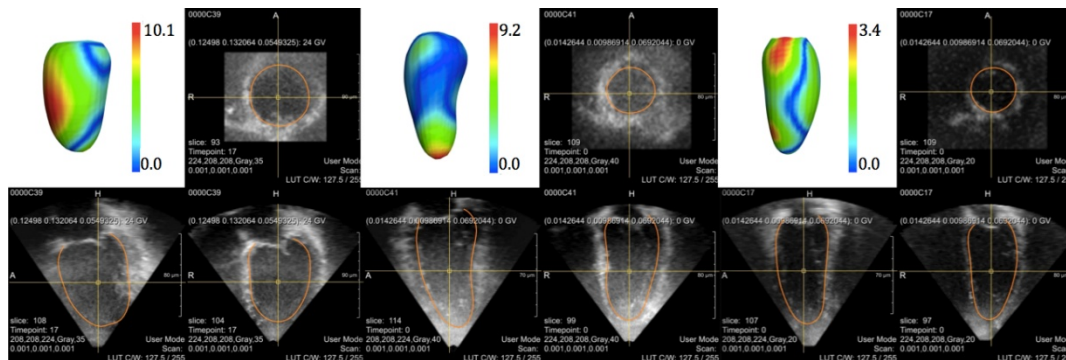
Fig. 1. The worst (*left*, #39 ES), median (*center*, #41 ED) and best (*right*, #17 ED) segmentation results after tracking. Note the different scaling of the colored error bars.

[1] Van Stralen et al., Segmentation of multi-center 3D left ventricular echocardiograms by active appearance models, Proc MICCAI challenge CETUS 2014, 73-80

P1B3-2

8:00 am   **Optimization-based speckle tracking algorithm for LV strain estimation**

Hanan Khamis[1], Nahum Smirin[1], Zvi Friedman[2], Dan Adam[1]; *[1]Department of Biomedical Engineering, Technion-Israel Institute of Technology, Haifa, Israel, [2]GE Ultrasound, Tirat Hacarmel, Israel*

Background, Motivation and Objective

Two dimensional (2D) speckle tracking echocardiography (STE) has emerged as a promising imaging modality that allows left ventricular (LV) function estimation by calculating global and regional strains. The accuracy of this modality is affected by speckle decorrelation noise, which is usually addressed by a post-processing regularization or smoothing. Moreover, the software products offered by the various vendors produce different results for the same clip/patient. These issues limit the clinical acceptance of 2D STE. Here a new algorithm is proposed, termed "error-dependent weighted speckle tracking algorithm" (EWST), which allows a more accurate estimation of strain values by solving an optimization problem, to improve tracking of tissue speckles.

Statement of Contribution/Methods

The algorithm automatically defines the LV borders, then a block matching technique is used to locate all possible displacements, and an optimization problem is solved to find the best solution that guarantees optimal smoothness in local displacements while a similarity metric and a local uniformity index are maximized.

A validation study was performed using 36 clips generated by a software-based phantom, modeling the LV myocardial cross-section shape, and simulating different clinical cases and noise levels. Also, clips of 410 healthy subjects were processed, and the results compared to a commercial product. In both studies, peak global longitudinal systolic strain (PGLSS) values at full wall-width (FWW) and at the sub-endocardium (SE) were measured, in addition to other clinical parameters. All parameters were compared to a commercial product 2D Strain (EchoPAC PC, BT13, GE Healthcare Inc.).

Results/Discussion

The software-based phantom clips were analyzed by the EWST and compared to the 'ground-true' values: the PGLSS had bias of -0.03±0.05 and -0.05±0.07 at FWW and SE, respectively. 2D Strain had a significantly higher bias for the SE (-0.2±0.13, P<0.01), and a non-significant difference for FWW (0.018±0.071, P=0.18). The apex-to-base strain ratios were 1.16±0.2 (EWST) and 1.8±0.3 (2D Strain). The SE-to-FWW strain ratios were: 1.39±0.12 vs. 1.39±0.11, (EWST vs. ground true, P=0.55) and 1.22±0.07 vs. 1.39±0.11, (2D strain vs. ground true, P<<0. 01).

Analysis of the healthy subjects by the 2 methods had significantly different PGLSS values: -18.21±2.4% and -21.4±2.81% (EWST) at FWW and SE, respectively, and -21.33±2.86% and -24.49±3.22% (2D Strain); (P<<0.01). Apex-to-base ratios were different (1.18±0.09 (EWST) vs. 1.15±0.04 (2D Strain), P<<0.01).The SE-to-FWW strain ratios were also significantly different (1.26±0.69 vs. 1.62±0.56, P<<0.01).

It is evident that optimizing a similarity metric while forcing uniform and smooth displacements produces a significant enhancement of the accuracy of strain estimation versus a leading commercial product.

P1B3-3 _____

8:00 am   **Tracking quality in plane-wave versus conventional cardiac ultrasound: a preliminary evaluation in-silico based on a state of the art simulation pipeline**

Martino Alessandrini[1], Brecht Heyde[1], Ling Tong[1,2], Olivier Bernard[3], Jan D'hooge[1]; [1]*Cardiovascular Imaging and Dynamics, KU Leuven, Leuven, Belgium,* [2]*Center for Biomedical Imaging Research, Dept. of Biomedical Engineering, Tsinghua University, China, People's Republic of,* [3]*CNRS UMR 5220; INSERM U1044; Université Lyon 1; INSA Lyon, Lyon, France*

Background, Motivation and Objective

Fast cardiac ultrasound (US) imaging based on plane wave (PW) transmits is fostering significant research efforts. Coupled with a technique for deformation imaging, the new modality allows a more thorough assessment of cardiac function due to its higher temporal resolution. However, although the higher frame rate eases the tracking problem by enforcing speckle coherency, the loss in spatial resolution makes it harder. Moreover, at higher frame rate, a bias in the motion estimator will accumulate faster. It thus remains unclear whether myocardial tracking on PW recordings outperforms tracking on conventional images or vice versa. The aim of this study was therefore to directly contrast the intrinsic tracking quality of both acquisition schemes using a testing environment recently proposed by our lab.

Statement of Contribution/Methods

The testing environment combines a state-of-the-art mechanical cardiac model with ultrasound simulation techniques. As such, we simulated 3 apical 4 chamber recordings ($\theta = 66°$, 160 lines) of a healthy heart from the same ground truth deformation model using FieldII: 1) 80 focused transmit beams with 2 multi-line acquisition (MLA) representative of a standard setup; 2) 40 PW with 4MLA; 3) 20 PW with 8MLA resulting in a frame rate of 62, 125 and 250 frames/s respectively as no compounding was used to keep maximal frame rate. An optic flow (OF) technique previously described by the author was applied on the reconstructed B-mode images in order to track a set of test points distributed along the LV. To assess the tracking accuracy the distance between the ground truth and the tracked positions was calculated. For each acquisition scheme, the OF parameters were optimized to have the smallest mean least squares error.

Results/Discussion

Fig. 1(a,b) illustrates the tracking error over time. The error's coefficient of variation was $CV_{STANDARD} = 0.8$, $CV_{PW40} = 0.65$ and $CV_{PW20} = 0.71$. Fig. 1(c) displays end systolic error maps. Overall, in both PW cases the gain in frame rate counterbalanced the loss in spatial resolution. In particular the error dispersion decreased (cf. Fig. 1(b)). In the 8MLA case, due to more pronounced block-like artifacts, the error increased at late diastole when tracking lateral displacements of the free wall. Direct comparison with other acquisition schemes (i.e. diverging waves and multi-line transmit) is the topic of ongoing work.
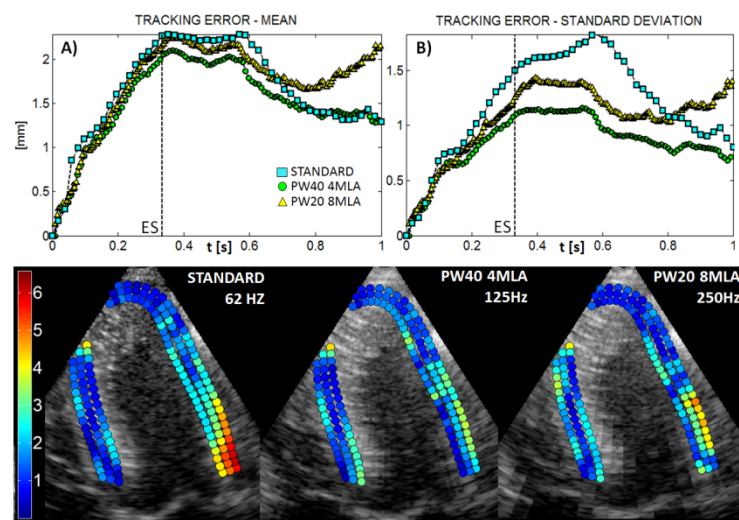
(C) *End systolic error mapped on the ground truth positions.*

P1B3-4 _____

8:00 am   **Effects of coherent compounding on Pulse Wave Imaging (PWI) in phantoms and *in vivo***

Iason Zacharias Apostolakis[1], Ronny Li[1], Matthew McGarry[1], Ethan Bunting[1], Elisa Konofagou[1,2]; [1]*Biomedical Engineering, Columbia University, New York, New York, USA,* [2]*Radiology, Columbia University, New York, New York, USA*

Background, Motivation and Objective

Pulse wave imaging (PWI) is a noninvasive technique developed by our group for tracking the propagation of pulse waves along the arterial wall at high spatial and temporal resolution. In order to achieve high frame-rates without relying on stroboscopic techniques (ECG-gating), plane wave acquisitions were implemented. However, single plane-wave transmission results to lower SNR and higher side-lobe levels that further challenge the motion estimation techniques. Coherent compounding is known to significantly improve displacement estimation at the cost of lower frame-rate. The objective of this study was to use a variety of metrics in order to investigate the PWI performance in tracking the pulse waves with and without compounding.

Statement of Contribution/Methods

A phantom and the right carotid arteries of six healthy subjects (n=6) were scanned using 1-, 3-, 5-, 9- and 12-plane wave acquisitions. The frame-rate of the acquisitions ranged from 8333 Hz (1 plane wave) down to 694 Hz (12 plane waves). Axial wall displacements (AWD) were depicted over time to generate spatiotemporal maps of the pulse propagation. In each case, the regional Pulse Wave Velocity (PWV) and associated coefficient of determination (r^2) were calculated by performing linear regression on the 50%-upstroke markers of the pulse-wave-induced AWDs. The percentage of 50%-upstroke markers that occur at the same time-point (temporal resolution misses) was also estimated. Finally, the SNR of the AWD of the constructed spatiotemporal maps was calculated within 2D windows (0.2 mm × 7 ms) and a stochastic metric of precision (E(SNR|awd)) was computed.

Results/Discussion

The PWV values were highly reproducible in the same subject over different plane-wave sequences. Furthermore, as shown in Fig. 1, there was excellent agreement between the phantom and in vivo findings showing significant increase in both the mean SNR and r^2 with the number of transmitted plane waves, thus indicating higher quality and reliability of the measurements. However, this was at the expense of temporal resolution, preventing further localization of PWV measurements, which is critical for focal arterial disease. Finally, the proposed stochastic metric may aid in optimizing the acquisition sequence for the given wall displacement amplitudes. Analysis will also be performed on atherosclerotic patient datasets.

Figure 1
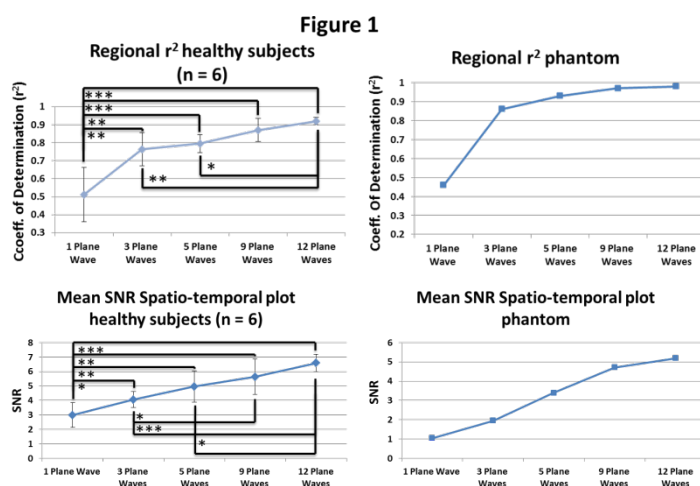
- This work was supported in part by NIH R01-HL098830

P1B3-5

8:00 am   Atlas-based mosaicing of 3D transesophageal echocardiography images of the left atrium

Harriët W. Mulder[1], Josien P.W. Pluim[1], Ben Ren[2], Alexander Haak[3], Max A. Viergever[1], Johan G. Bosch[3], Marijn van Stralen[1]; *[1]Imaging Division, UMC Utrecht, Utrecht, Netherlands, [2]Cardiology, Erasmus MC Rotterdam, Rotterdam, Netherlands, [3]Biomedical Engineering, Erasmus MC Rotterdam, Rotterdam, Netherlands*

Background, Motivation and Objective

3D transesophageal echocardiography (TEE) is a promising non-invasive imaging modality for planning and guidance of cardiac interventions. However, it offers a limited field-of-view and thus stitching of multiple images is often necessary to provide a complete view of a cardiac region of interest, e.g. the left atrium (LA). We propose atlas-based mosaicing as a method for fusion of different views of the LA.

Statement of Contribution/Methods

Previously, we developed an imaging protocol, consisting of the acquisition of six partly overlapping views covering the LA. We propose the use of fused TEE data of other patients as atlases for registering the views in a novel method, denoted atlas-based mosaicing (ABM). In this method, each TEE view is rigidly registered to a fused TEE atlas image of another patient, using the transformations between the different views in the atlas image as prior knowledge. This is followed by pairwise registration of neighboring TEE views. The method was compared with pairwise mosaicing, initialized with mean transformations derived from previous acquisitions or without any initialization. Normalized cross-correlation was used as a metric for all registrations, using data from 10 patients and 5 atlases. Registration results were evaluated against manual registration. A fictive spherical LA (diameter of 50 mm, positioned in the near field of the fused image) was transformed with the manual or automatic transformations and the resulting surface distance was calculated.

Results/Discussion

As an example Figure 1 shows the cross-sections of a fused 3D TEE data set after registration. Without initialization the surface distance was 26 ± 20 mm (mean +/- sd) after registration (Figure 1A). Using the average transformation as initialization, this was reduced to 10 ± 11 mm (Figure 1B). ABM outperformed the other two approaches with a surface distance of 8 ± 6 mm for the best atlas image (Figure 1C). The strength of this method is the prospect to combine the intermediate results from multiple atlases to improve registration results further, similar to atlas-based segmentation approaches. Evaluation on a larger cohort and automatic atlas selection are subject of ongoing research. ABM shows great promise for 3D TEE stitching in the case of TEE views with little overlap, which might overcome one of the major limitations of TEE for treatment planning and guidance.

FRIDAY POSTER
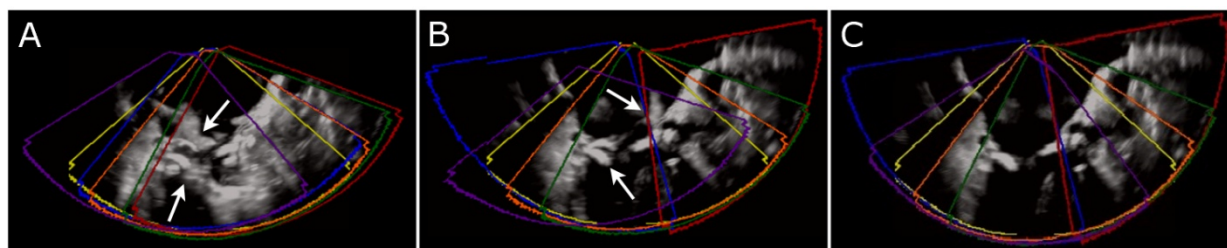
Figure 1: Cross-sections of a fused 3D TEE data set. The six different views are outlined in the different colors. The arrows indicate some parts of the image that are not correctly aligned. **A:** Registration without initialization. Three views are not correctly registered. **B:** Registration using the average transformation as initialization (note the mis-registration of the purple view). **C:** Atlas-based mosaicing using the best atlas image.

P1B3-6

8:00 am   **Estimation of Flow Mediated Vasodilatation of the radial artery**

Andrzej Nowicki[1], Robert Olszewski[2], Wojciech Secomski[1], Marcin Lewandowski[1], Michal Byra[1]; *[1]Ultrasound, Institute of Fundamental Technological Research, Warsaw, Poland, [2]Cardiology and Internal Medicine, Military Institute of Medicine, Warsaw, Poland*

Background, Motivation and Objective

Preceding atherosclerosis is dysfunction of the endothelial dysfunction. There is therefore interest in the application of non-invasive clinical tools to assess endothelial function. There are commercially available ultrasound scanners to measure flow-mediated vasodilatation (FMD) of the brachial artery using 10-12 MHz linear array probes, however the attainable precision in estimating the changes in artery dilation does not exceeds 0.2 mm, far beyond the required one. The higher the probe frequency, the greater is the axial resolution. Our aim was to introduce a high frequency; both 25-35MHz encoded (Golay) wobbling type (uScan developed in our lab) and linear array 30 MHz ultrasound (Ultrasonix) to exam the radial artery dilation.

Statement of Contribution/Methods

FMD of radial artery was examined in 22 healthy young volunteers (25-35 years) men and 6 volunteers after minor cardiac incidents. The FMD results obtained using linear array probe were next normalized to the mean blood flow.

The examined radial artery was visualized in B-mode in a longitudinal plane and recording several seconds of the artery pulsation after switching the scanner to the M-mode, both, with the probe at rest and after reactive hyperemia induced by forearm cuff occlusion.

The Radial Artery Reactive Response (RARR) was induced by a five minutes artery ischemia through the inflated tourniquet on the arm or forearm - Restoration of blood flow in the artery is strongly promoted the release of nitric oxide. The measured initial internal radial artery diameter was in range of 1.59-2.25 mm; the maximum diameter 2.01-2.60 mm was observed 2-3 min after tourniquet deflation.

Results/Discussion

The application of high frequency ultrasonic scanning to examining radial artery opened a new window for imaging of endothelial function.

In the pilot study, on the model of the brachial artery ultrasound demonstrated that ultrasound head high frequency we are able to precisely register an increase in the diameter dimension of the radial artery ultrasound model already by 5%. RARR in healthy volunteers, using a transient ischemic calling stimulation have shown changes from 30 to 40 %, while in the four volunteers after cardiac incidents, these changes did not exceed 10 %.

If such a big difference in FMD of RARR will be confirmed in the larger cohorts, it may allow for introduce a method as a widely available test of estimation the endothelial function.

P1B3-7

8:00 am   **Electromechanical Eave Imaging of atrial tachycardia and myocardial infarct in vivo: a feasibility study**

Alexandre Costet[1], Ethan Bunting[2], Elaine Wan[3], Elisa Konofagou[2,4]; *[1]Biomedical Engineering, Columbia University, New York, New York, USA, [2]Biomedical Engineering, Columbia University, New York, NY, USA, [3]Medicine Cardiology, Columbia University Medical Center, New York, New York, USA, [4]Radiology, Columbia University, New York, NY, USA*

Background, Motivation and Objective

The burden of cardiovascular diseases remains high and represented about 31% of all death in the US in 2012. Atrial tachycardia (AT) can be treated in the clinic by ablation of the trigger but there is currently no non-invasive way to detect such region. Myocardial Infarct (MI) increases the risk of stroke and can lead to a heart attack. Electromechanical Wave Imaging (EWI) is a direct imaging technique that can map the transmural electromechanical activation in all four chambers in vivo. In this study, we use EWI to image and localize triggers of AT as well as the location of MI in the ventricle in vivo.

Statement of Contribution/Methods

A Verasonics system (Verasonics, Redmond, WA) with a 2.5-MHz phased array was used to perform EWI in six open-chest canines (n=6): four during pacing from the left atrium (LA) at 150 beats per minute (within range of AT rate), and two after generation of a MI by ligation of the left anterior descending artery and a waiting period of 4 days. An unfocused beam sequence at 2000 frames/s in the standard apical views was used and axial incremental displacements and strains were estimated using RF-based cross-correlation with a window size of 6.2mm and a window shift of 0.62 mm, and a least square kernel size of 5.0 mm, respectively. The myocardium was segmented and pseudo-3D isochrones of the electromechanical activation were generated from four different apical views.

Results/Discussion

EWI during AT produced isochrones showing early electromechanical activation originating in the LA at the site of pacing which then spread out to the rest of the atria within 150 ms (Fig 1 B). EWI of MI in the ventricles produced isochrones showing a delayed activation in the left side at the expected location of the MI and shows regions of the myocardium not activating (Fig 1 A). The isochrones showed a clear difference in activation patterns between the normal right ventricle and the infarcted left ventricle.

This study showed that EWI was feasible during atrial tachycardia and in the presence of an infarct. EWI can localize early and late activation sites as well as regions which did not electromechanically activate. This suggests EWI could be used as an imaging modality before treatment to non-invasively localize treatment sites and reduce treatment duration while increasing safety by limiting radiation exposure during fluoroscopy.
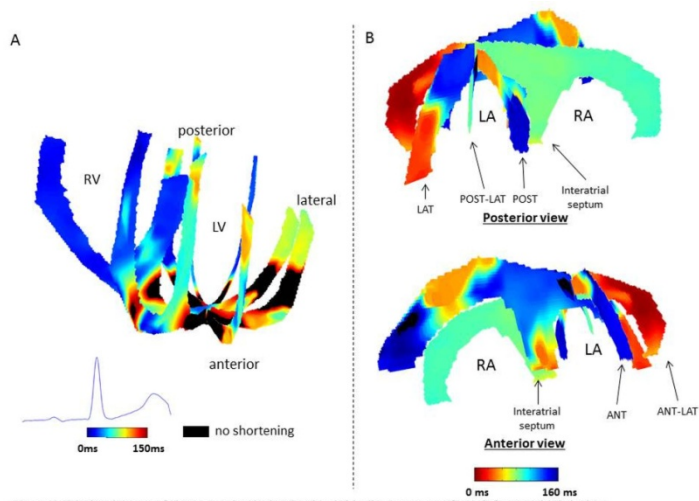
Figure 1: EWI isochrones of electromechanical activation (A) in the presence of a LV infarct and (B) during pacing-induced atrial tachycardia. LV = left ventricle, RV = right ventricle, LA = left atrium, RA = right atrium.

P1B4 - MPA: Photoacoustics

4th floor

Friday, October 23, 2015, Posters displayed 08:00 am - 05:00 pm. Authors must be present at their poster from 9:30 - 10:30am (odd number posters) and 14:30 – 15:30pm (even number posters).

Chair: **Richard Lopata**
            Technical University Eindhoven

P1B4-1 _____

8:00 am   Optimizing Simultaneous Multispectral Emission Photoacoustics

Martin F Beckmann[1], Hans-Martin Schwab[1], Georg Schmitz[1]; *[1]Chair for Medical Engineering, Ruhr-Universität Bochum, Bochum, Germany*

Background, Motivation and Objective

Several multispectral photoacoustic imaging methods employ systems that allow for simultaneous use of multiple wavelengths, for example laser diode systems with multiple diodes or white light approaches used e.g. in photoacoustic microscopy. By emitting multiple wavelengths at once, it is possible to form a higher SNR fused image, e.g. for orientation and morphological imaging, together with extracting single wavelength information. For a given set of combined acquisitions an optimal SNR reconstruction was derived in [1]. However, it is still necessary to optimize the acquisition strategy itself to gain optimal SNR, which we discuss in this contribution.

Statement of Contribution/Methods

Reconstruction with arbitrary wavelength combination acquisitions yielded a linear least squares result for the optimal weighting of the acquisitions. This can be used in the inverse optimization problem to find the best wavelength combinations for given wavelengths and a given problem. The optimization depends on the desired outcome, the desired SNR ratios (i.e. SNR of 1 wavelength in relation to all other wavelengths, SNR of the fused image in relation to all wavelengths etc.) are therefore a necessary optimization parameter. Further, the optimization is restricted by the total available imaging time or total amount of pulse energy that can be invested. Additionally, wavelength-dependent energies and safety restrictions have to be taken into account. We demonstrate that the optimization is equivalent to a multiobjective nonlinear Knapsack problem.

Results/Discussion

The Knapsack problem can be analytically solved for special cases, such as applying all single wavelengths identically. In this case, arbitrary combinations of wavelengths using identical total energy, such as combining groups of n-2 or n-1 wavelengths in the case of n wavelengths will all end up on the same SNR tradeoff curve between single wavelength and fused data (see figure). Thus, an arbitrary combination can be chosen for the tradeoff and no other combination will achieve a better tradeoff. In addition an algorithm was developed to solve the problem for arbitrary desired SNR ratios, allowing for custom optimization for the problem at hand.

[1] M.F. Beckmann et al.: "Optimized SNR simultaneous multispectral photoacoustic imaging with laser diodes", Opt. Express 23, 2015
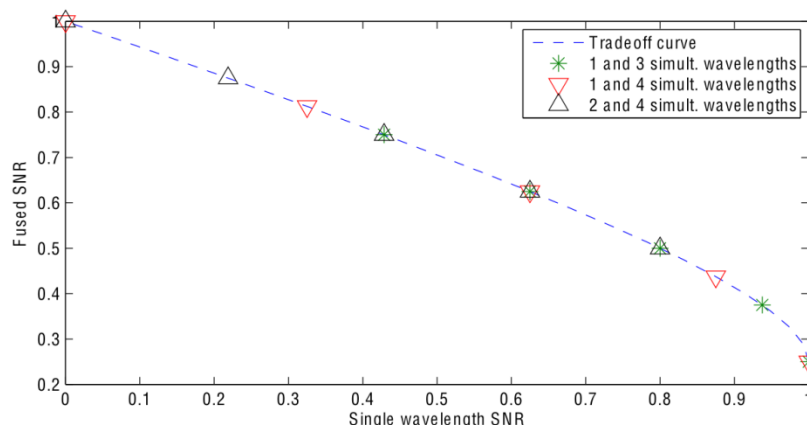
Markers show steps of 25% trade between the indicated number of simultaneously emitted wavelengths for the example of four total wavelengths. The fraction of the second number of wavelengths increases from bottom right to top left.

P1B4-2 _____

8:00 am   Dual-modal photoacoutic ocular imaging

Changhui Li[1], Ning Wu[2], Xiaoyi Zhu[2]; *[1]Biomedical Engineering, Peking University, China, People's Republic of, [2]Peking University, China, People's Republic of*

Background, Motivation and Objective

Various kinds of ophthalmic diseases have imposed a serious impact on human health, especially for the elder people. Accurate and early diagnosis plays a pivotal role for treating ophthalmic diseases. Relying on the tissue scattering properties, ophthalmoscope and optical coherence tomography (OCT), have been successfully implemented for clinical ophthalmic fundus imaging. Tissue absorption characteristic also contains important biological information. Recently, photoacoustic ocular imaging that relies on the tissue optical absorption has gained increasing progress in ocular imaging.

Statement of Contribution/Methods

In this work, we have developed a photoacoustic ocular imaging system. It employs a reflection mode configuration, where the light source and the ultrasonic detection are set in the same side of the sample. The irradiation laser pulses (532 nm) generated by a pulsed laser system was coupled into a single-mode fiber, then focused by an objective lens. A novel reflector was used to reflect the ultrasonic wave, without affecting light focusing. This system can perform photoacoustic imaging and pulse-echo based ultrasound imaging.

Results/Discussion

By using this system, we have successfully imaged mouse eye non-invasively and in vivo, from its iris to the retina region. Our results showed the 3D structure of the iris and fundus region. In addition. both ultrasound and photoacoustic ocular imaging were performed and co-registered with high spatial resolution. Based on tissue absorption, this system could provide important complementary information for other clinical ocular imaging systems.
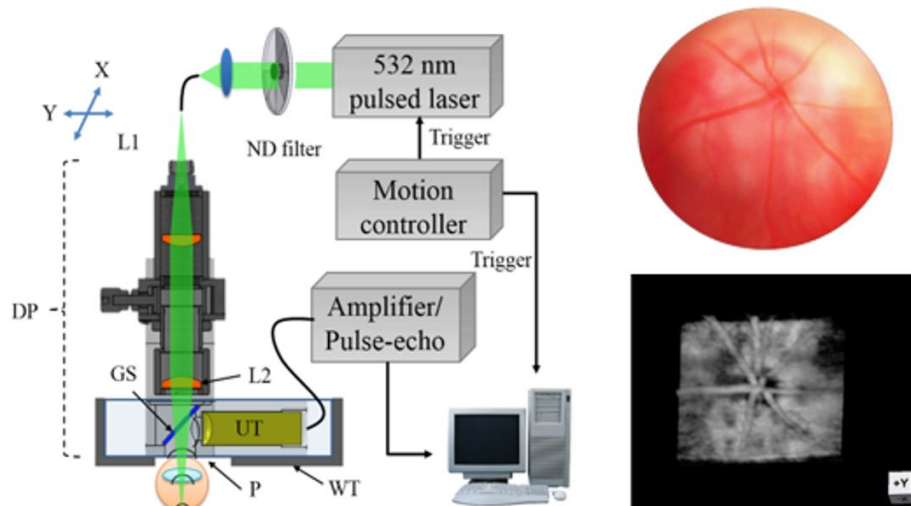
P1B4-3

8:00 am   Photoacoustic imaging of human inflammatory arthritis

Xueding Wang[1], Janggun Jo[2], Guan Xu[3], Sheeja Francis[3], April Marquardt[3], Jie Yuan[4], Gandikota Girish[3]; *[1]Biomedical Engineering, University of Michigan, Ann Arbor, Michigan, USA, [2]Radiology, University of Michigan, USA, [3]University of Michigan, USA, [4]Nanjing University, USA*

Background, Motivation and Objective

Synovial angiogenesis is an important characteristic feature in the development and perpetuation of inflammatory arthritis such as rheumatoid arthritis. The presence of hypervascularized synovial tissue is associated directly to disease activity. Due to the strong electromagnetic absorption of hemoglobin in the visible to near-infrared spectrum, the optical contrast presented by photoacoustic imaging (PAI) is intrinsically sensitive to the hemodynamic changes in synovial tissues, such as neoangiogenesis, hyperemia and hypoxia, and may shed new light in objective characterization of the chemical and physiological markers of synovitis.

Statement of Contribution/Methods

To explore the value of PAI in future rheumatology clinic, in this work a newly developed PAI and ultrasound (US) dual-modality system facilitating real-time B-scan imaging was examined for its performance in mapping the enhanced synovial flow in human peripheral joints affected by inflammatory arthritis. The patients involved in this study were men and women over 18 years old, with clinically diagnosed inflammatory arthritis. All patients have active synovitis and enhanced blood flow in their peripheral joints, as confirmed by Doppler US.

Results/Discussion

Photoacoustic (PA) images of metacarpophalangeal (MCP) joints were acquired at 580-nm wavelength that provides a desired balance between optical absorption of blood and attenuation in background tissue. The increased flow in the affected joints can be displayed successfully in PA images, and the difference between the arthritis group and the control group can be recognized. The results from eleven patients and eleven normal volunteers demonstrated the satisfactory sensitivity of PAI in assessing the physiological changes in the joints, specifically enhanced blood flow as a result of active synovitis. This study suggests that PAI, by revealing vascular features suggestive of joint inflammation, could be a valuable supplement to musculoskeletal US for rheumatology clinic.
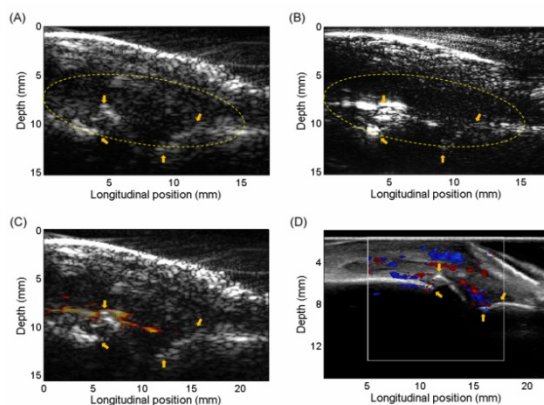
Fig. 1. Photoacoustic (PA) and ultrasound (US) dual imaging of a metacarpophalangeal (MCP) joint of a patient affected by inflammatory arthritis. (A) Gray scale B-mode US image. (B) Gray scale PA image of the same imaging plane. (C) Pseudocolor PA image super-imposed on the gray scale US image, demonstrating the active vascularity in the joint. (D) US Doppler image acquired by a commercial US unit confirming the active synovitis in the studied joint.

8:00 am   Copolymer-in-oil phantoms for photoacoustic imaging

Luciana Cabrelli[1], Diego Sampaio[1], Joao Uliana[1], Alessandro Deana[2], Antonio Carneiro[1], **Theo Pavan[1]**; *[1]Department of Physics, University of Sao Paulo, Ribeirão Preto, Brazil, [2]Department of Biophotonics, Universidade Nove de Julho, Sao Paulo, Brazil*

Background, Motivation and Objective

Photoacoustic is an imaging modality where ultrasound waves are generated from the interaction between laser pulses and tissue. Therefore, in photoacoustic the image contrast is based on optical absorption properties of tissues. A useful approach to characterizing and "optimizing" methodologies for studying photoacoustic imaging methods is through tissue-mimicking phantom experiments. Water-based materials are commonly used in phantoms for this image modality. However, these materials have disadvantages such as easy degradation and low temporal stability. In this paper, copolymer-in-oil phantoms are presented for ultrasound and photoacoustic techniques, with the advantage of presenting low temporal degradation.

Statement of Contribution/Methods

Styrene-Ethylene/Butylene-Styrene (SEBS) copolymer-in-mineral-oil gel samples were made varying the SEBS concentration between 5%-15%, and low-density polyethylene (LDPE) between 0% - 9%. Speed of sound and acoustic attenuation coefficient were obtained by the substitution technique with frequencies ranging from 2.25MHz to 10 MHz. To characterize the optical properties, the reflectance of the surface was measured, along with the absorption, scattering and Albedo coefficients ranging from 400 nm to 1200 nm. A cubic phantom made with a proportion of 7% SEBS/5% PEBD containing a 11 mm-diameter spherical inclusion made with the same material, but adding annatto, which was obtained by dissolving the seeds of the tropical tree *Bixa orellana* in mineral oil, to act as optical absorber. Photoacoustic spectroscopic images of the phantom were acquired using a Nd:YAG laser (pulses of 5 ns) operating between 532 nm and 1064 nm, and acoustic signals were acquired with a linear ultrasound transducer. For consistency, we used the same optical fluence for all wavelengths.

Results/Discussion

Phantom material acoustic and optical properties were controlled varying SEBS and LDPE concentration; speed of sound from 1445 m/s to 1480 m/s, and acoustic attenuation from 0.55 to 1.0 dB/cm/MHz were obtained. Optical absorption coefficient μ_a from 0.1 cm^{-1} to 2.6 cm^{-1} at 532 nm, and 0.1 cm^{-1} to 1.8 cm^{-1} at 1064 nm, and optical scattering coefficient μ_s from 0.2 cm^{-1} to 4.0 cm^{-1} at 532 nm, and 0.2 cm^{-1} to 3.2 cm^{-1} at 1064 nm were observed. Photoacoustic signal from the inclusion showed the highest intensities at 532 nm with consistent variation for other wavelengths according to the measured absorption spectrum. In this case, the absorption spectrum acquired for the material containing anatto showed band between 350-550 nm. Therefore, the results suggest the phantoms of SEBS and LDPE are promising for photoacoustic imaging.

8:00 am   NIR Photoacoustic Spectroscopy for Continuous Non-Invasive Glucose Monitoring

Praful Pai[1], Pradyut Sanki[1], Arijit De[1], Swapna Banerjee[1]; *[1]Department of Electronics and Electrical Communication Engineering, Indian Institute of Technology Kharagpur, Kharagpur, West Bengal, India*

Background, Motivation and Objective

This paper describes the use of near infra red (NIR) photoacoustic spectroscopy (PAS) for continuous non-invasive glucose monitoring. PAS was selected as it is unaffected by optical scattering due to tissues in comparison to conventional optical methods.

The generated PA signal depends upon sample optical and physical properties, which are influenced by the glucose concentration, and we can estimate the same by selecting excitation wavelengths specifically absorbed by glucose. An apparatus for making PA measurement is described along with a set of features extracted from the PA measurements for calibration of the system. The validity of the technique is tested in vitro and in vivo, and a calibration method is proposed for calibrating PA measurements to obtain the glucose concentration.

Statement of Contribution/Methods

A PA measurement apparatus with pulsed laser diodes, a piezoelectric transducer, and associated signal conditioning is used. Fundamental glucose absorption bands in the mid infra red are impractical for use on tissues due to high absorption by water in the region. Hence, overtone bands at 939 and 1536 nm in the NIR are selected for use, with sources at 905 and 1550 nm being used for PA generation.

Features of the PA response were used to predict the glucose concentration. Features such as the maximum, minimum, and peak-to-peak amplitude were measured along with area under the positive and negative peaks and total area of the PA waveform. In addition, frequency domain features such as the maximum coefficient and area under the spectrum were also taken.

The technique was initially verified on glucose solutions in the physiological glucose range (0-500 mg/dl). PA measurements were made at multiple pulse powers and pulse widths, and changes in features with glucose concentration were observed. This was followed by measurements on whole blood samples at different glucose concentrations. Following this, in vivo PA measurements were taken on human volunteers with capillary glucose measurements to check whether PA measurements followed glucose concentration over time. The PA measurements were calibrated and compared to reference glucose measurements.

Results/Discussion

The PA features were proportional to glucose concentration, increasing non-linearly and saturating at high glucose concentrations. The saturation was less prominent in PA measurements at 1550 nm. A similar variation was observed on PA measurements made on whole blood and on measurements made on human subjects.

A Clarke Error Grid used to compare calibrated and reference glucose values showed 196 measurements over 30 subjects, with 87.24% and 12.76% measurements being in acceptable zones A and B of the grid, and a mean absolute difference of 12.57 mg/dl and mean absolute relative difference of 9.61%. This is an improvement over previous results using PAS and other non-invasive measurement methods, and validates use of NIR-PAS for non-invasive glucose monitoring.

8:00 am   *In Vivo* Assessment of Protease Activity in Colorectal Cancer by Using Activatable Molecular Photoacoustic Imaging

Cheng LIU[1], Qijin HE[1], Yaoheng YANG[1], Zhihai QIU[1], Yongmin HUANG[1], Thomas Ming-Hung LEE[1], Lei SUN[1]; *[1]Interdisciplinary Division of Biomedical Engineering, Faculty of Engineering, The Hong Kong Polytechnic University, HONG KONG, China, People's Republic of*

Background, Motivation and Objective

Matrix metalloproteinases (MMPs), a family of zinc-dependent proteases, have been recognized as a significant biomarker associated with tumor microenvironment. MMPs has been shown to enhance the expression of pro-angiogenic growth factors, such as VEGF and bFGF in colorectal cancer. A non-invasive imaging method that could enable MMPs assessment *in vivo* would enhance the understanding of the MMPs activity in tumor micro-environments. In this report, photoacoustic (PA) imaging was used for non-invasive assessment of the MMPs activity *in vivo*, employing activatable gold nanorods (GNRs) as contrast agent.

Statement of Contribution/Methods

All procedures using laboratory animals were approved by the Department of Health, The Government of the Hong Kong Special Administrative Region and the Hong Kong Polytechnic University Animal Subjects Ethics Sub-committee. GNRs and organic dye BHQ3, which exhibit strong PA signals at the wavelength of 930 nm and 650 nm, respectively, were conjugated via a MMPs specific cleavable peptide according to standard synthesis protocol [1]. The PA signal intensity of the GNRs-peptide-BHQ3 (GPB) compound, GNRs, and BHQ3 were tested individually with human fibrosarcoma HT1080 cells (positively expressing MMPs) and human mammary adenocarcinoma BT20 cells (negatively expressing MMPs) using a PA system (Vevo 2100 LAZR, VisualSonics Inc.) at 930 nm and 650 nm. During *in vivo* experiments, a subcutaneous COLO 201 xenograft nude mice model was produced and used. The mice (n = 15) were divided into three groups according to tumor size, small (< 2 mm^3), medium (2 mm^3 - 5mm^3) and large (> 5 mm^3). Each group of mice were intra-tumorally injected with GPB (100 μl, 0.7 mg/ml) and imaged at different time points (3 min, 1 h, 2 h, 6 h and 24 h) post injection. Then, the PA intensity ratios between 930 nm and 650 nm were calculated. Finally, correlation test was conducted between *in vivo* PA intensity ratios and *ex vivo* MMPs immunohistochemical results.

Results/Discussion

The cell experiments showed that the GPB exhibited strong PA intensity at the wavelengths of 930 nm and 650 nm before cleavage by MMPs, owing to the absorption of GNRs and BHQ3, respectively. The PA intensity ratio was highly correlated with *ex vivo* immunohistochemical results. After the MMPs expressed in tumor cells, GPB released free BHQ3 which were rapidly washed out from tumor cells as small molecules, leaving GNRs retaining inside the tumor cells for much longer period of time. Thus, the recorded PA signal ratios at wavelengths 930 nm over 650 nm, were remarkably decreased accordingly. Therefore, PA with the aid of activatable contrast agent is potentially valuable for non-invasive assessment of protease activity in colorectal cancer *in vivo*.

Reference

1. Nikoobakht, B., & El-Sayed, M. A. (2003). Preparation and growth mechanism of gold nanorods (NRs) using seed-mediated growth method. Chemistry of Materials, 15(10), 1957-1962.

P1B4-7

8:00 am **Optical-resolution photoacoustic endoscope**

Ruimin Chen[1], Joon-Mo Yang[2], Chiye Li[2], Bin Rao[2], Junjie Yao[2], Cheng-Hung Yeh[2], Amos Danielli[2], Konstantin Maslov[2], K. Kirk Shung[1], Qifa Zhou[1], Lihong V. Wang[2]; *[1]Ultrasonic Transducer Resource Center, Department of Biomedical Engineering, University of Southern California, Los Angeles, California, USA, [2]Optical Imaging Laboratory, Department of Biomedical Engineering, Washington University in St. Louis, St. Louis, Missouri, USA*

Background, Motivation and Objective

Optical-resolution photoacoustic microscopy (OR-PAM) has attracted more attention as an important experimental tool of photoacoustic tomography with unique imaging capabilities for various biological applications. However, conventional OR-PAM systems are all table-top embodiments, which preclude their use in internal organs. In this study, by applying the OR-PAM concept to our recently developed photoacoustic endoscopy (PAE) technique, we developed the first fully-encapsulated optical-resolution photoacoustic endoscopy (OR-PAE) system, which enables internal organ imaging with a much finer resolution than conventional acoustic-resolution PAE systems.

Statement of Contribution/Methods

To achieve optical-resolution photoacoustic (PA) imaging, we combined a gradient index (GRIN) lens-based optical illumination with a high-frequency self-focused ring-shape ultrasonic transducer-based acoustic detection unit, and installed them in a miniaturized imaging probe (schematic shown in Figure A) with a mechanical scanning mechanism. The probe encapsulation and acoustic matching requirements were solved by adopting a related strategy utilized in our previous works.

Results/Discussion

By imaging 3-μm diameter microspheres illuminated by a 500-nJ pulse energy in a beam of 9.2 μm in diameter, we quantified the transverse resolution and the signal-to-noise ratio of the OR-PAE system to be 10 μm and 29 dB, respectively. We demonstrated the *in vivo* animal imaging capability of the OR-PAEM probe by imaging the descending colon of rat. The image (Figure B) shows that our OR-PAE probe provides a high-resolution vasculature image of the colorectum over a large area, covering a 270° angular region and a ~3.3 cm long pullback section. This system can be utilized in small animals and can also potentially accommodate many other multi-functional molecular probes. Thus, it could be a useful tool in many biological experiments, such as tumor and metabolic disease studies.
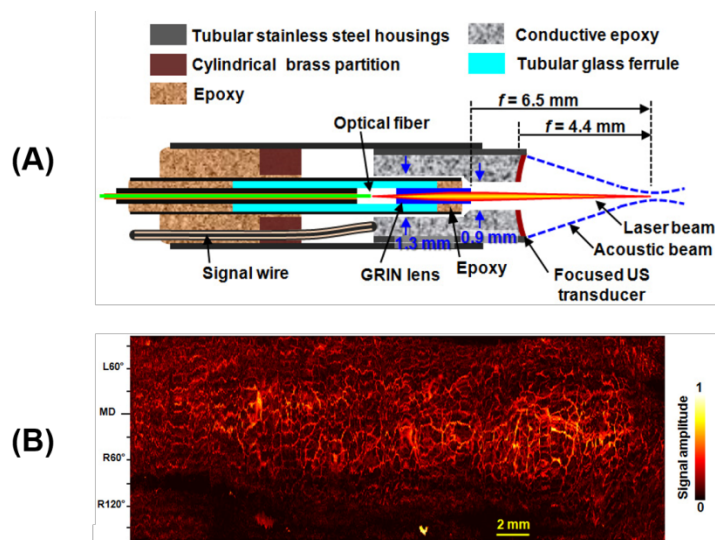
P1B4-8

8:00 am **Low power continuous wave photoacoustic microscope for bioimaging applications**

Sathiyamoorthy Krishnan[1], Michael Kolios[1]; *[1]Department of physics, Ryerson university, Toronto, Ontario, Canada*

Background, Motivation and Objective

Photoacoustic (PA) spectroscopy is a very powerful analytical tool for examining the optical absorption properties of solids as it measures directly the energy absorbed by the material upon light exposure. It can used to study many samples such as powder and samples that are opaque, highly scattering, transparent, etc.

FRIDAY POSTER

PA spectroscopy uses low power light that includes incandescent lamp or low power continuous wave (CW) laser as excitation source and uses a less expensive acoustic detection system. The measurement is based on a non-contact technique via an ambient air medium.

The main object of this study is to employ this photoacoustic spectroscopic principle for microscope imaging applications as it can be integrated to existing conventional optical microscopy system; moreover the implementation is also cost effective.

Statement of Contribution/Methods

A dual modal imaging system containing optical microscope and photoacoustic system was developed. The optical system exhibits the same configuration as conventional optical microscope system whereas PA system uses a photoacoustic chamber that contains main sample chamber which is connected to acoustic microphone through a resonant tunnel. The diameter and length of main and resonant chambers are 8 mm and 3 mm, and 1 and 20 mm, respectively. A Helium neon laser (633 nm) of beam diameter 2 mm and power of 3 mW is used. The sample is periodically exposed using intensity modulated CW light obtained using optical chopper (SR540) operated at 150 Hz. The generated PA signal due to periodic thermal expansion is measured using microphone (B&K) and lock-in amplifier (SE850) system. The system employs 10 X and 40 X objectives.

Results/Discussion

The developed system was calibrated using USAF 1951 chart from Thorlabs. The system exhibited lateral resolution of 228 lp/mm. The performance of the PA system was investigated by imaging methaemoglobin aggregates on glass substrate. Bloodstain pattern analysis (BPA) is one of several techniques used in forensic science. Blood stains contain increased levels of methemoglobin. The developed PA microscope has potential biomedical applications and in the forensic sciences. The developed system is cost effective as it uses less expensive laser sources and a microphone.

PA Image of (a) group-3 element-2 of USAF 1951 chart and (b) methemoglobin aggregates
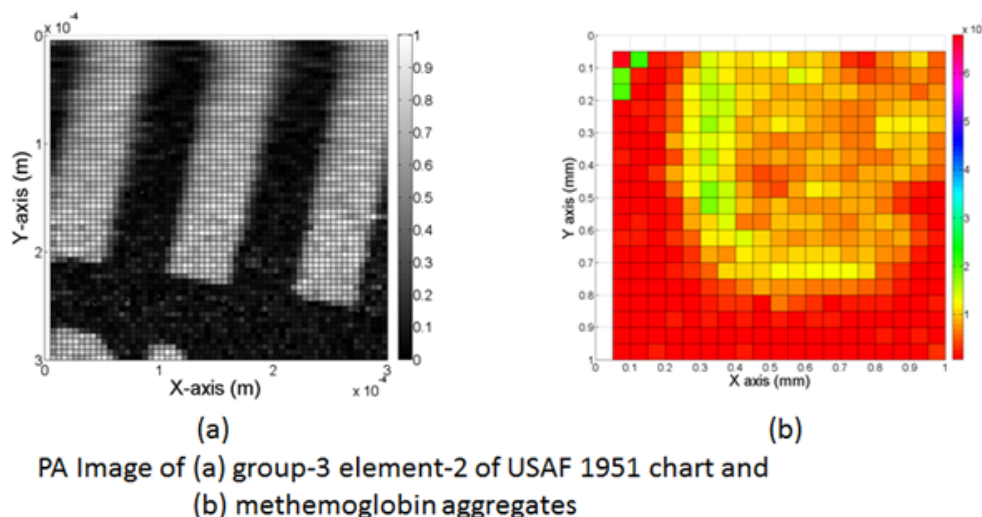
P1B4-9

8:00 am **Optical and Acoustic Observation of Photodisruption in Two Liquid Perfluorocarbons Induced by Nanosecond Laser**

Yi Feng[1], Dui Qin[1], Yujing Zong[1], Mingxi Wan[1]; [1]*The Key Laboratory of Biomedical Information Engineering of Ministry of Education, Department of Biomedical Engineering,School of Life Science and Technology,Xi'an Jiaotong University, Xi'an, Shaanxi, China, People's Republic of*

Background, Motivation and Objective

Photodisruption can be used to generate microbubble/microbubbles *in vivo*, thus has potential as an important tool in theranostics. However, high laser intensity and extremely short pulse length in femtosecond, and thus the high cost limit its wide applications. In the study photodisruption induced by nanosecond laser pulse in two liquid perfluorocarbons (PFCs), perfluoropentane (PFP) and perfluorohexane (PFH), were realized and detected in optical and acoustic way to reveal the effective parameters for photodisruption.

Statement of Contribution/Methods

A confocal microscopic system was performed to record the bubble dynamics by high speed photography, and simultaneously the acoustic signal emitted during photodisruption. A 532 nm laser, with pulse duration of 3 ns and average power of 50 μJ, was focused to the cellulose tube where the laser, acoustic detection and microscopic imaging were aligned and PFCs were injected. Passive acoustic detection (PCD) was realized by a 1 mm needle hydrophone connected via a receiver amplifier to a high speed digitizer. The spectrum analysis and time-frequency analysis were used to show the acoustic characteristics of photodisruption in liquid PFCs. Then, the laser energy thresholds of photodisruption and the influences of ambient temperature on photodisruption were revealed.

Results/Discussion

The bubble behavior mainly followed three patterns in PFP but two patterns in PFH. The difference among patterns was closely related with the ambient temperature. In acoustic detection, significant signals were recorded by PCD once photodisruption occurred in either PFP or PFH. The PCD signals of PFP and PFH showed difference in time-domain. However, their frequency spectrums were mainly distributed between 0-1.5 MHz and seemed without significant difference. The time-frequency analysis verified their difference in time-domain. The physical process of photodisruption was closely associated with both laser parameters and liquid properties. It was indicated that the thresholds for PFP and PFH were 43.33 μJ and 45 μJ, respectively. But the increasing ambient temperature was helpful to photodisruption in both PFP and PFH.
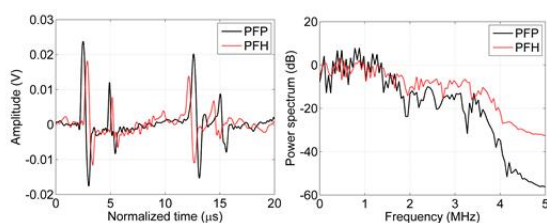
Fig. 1 Original passive acoustic signals and spectrum analysis of photodisruption in two PFCs
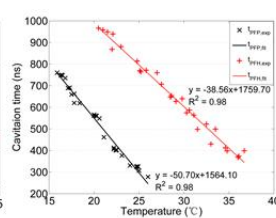
Fig. 3 Time for photodisruption vs ambient temeprature
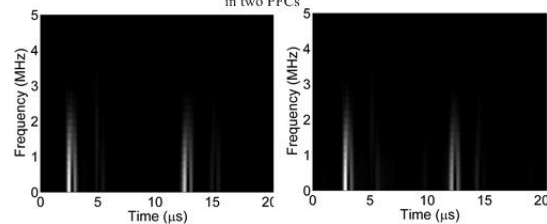
Fig. 2 Time-frequency diagram of photodisruption signals
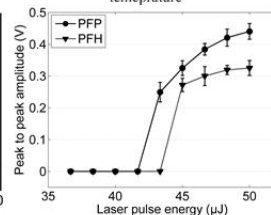
Fig. 4 Thresholds for photodisruption in PFCs

P1B4-10 _____

8:00 am   **X-ray acoustic imaging for external beam radiation therapy dosimetry using a commercial ultrasound scanner**

Diego Sampaio[1], Joao Uliana[1], Juliana Pavoni[1], Leandro Borges[2], Antonio Carneiro[1], **Theo Pavan[1]**; *[1]Department of Physics, University of Sao Paulo, Ribeirão Preto, Brazil, [2]Radiotherapy Service, University of Sao Paulo, Ribeirão Preto, Brazil*

Background, Motivation and Objective

Photoacoustic (PA) imaging has been used for numerous applications in clinical medicine and preclinical studies. Usually, nanosecond laser pulses in the visible and near-infrared (NIR) regions are used to generate PA signals. Optical scattering in soft tissues degrades spatial resolution of optical imaging significantly with depth. On the other hand, in laser-based PA, images of biological tissues have their contrast based on optical absorption and ultrasound propagation. Since ultrasound is much less scattered than light, PA images can be obtained at greater depths. However, only a small number of studies reported PA using x-ray photons, i.e. x-ray acoustic (XA) imaging. As x-ray shows higher penetration than visible and NIR photons, the number of clinical applications could be potentially increased. It has already been shown that modern linear accelerators can provide polychromatic x-ray with sufficient power density to produce microseconds x-ray pulses capable of inducing ultrasonic waves in the material. Based on this concept, the x-ray acoustic computer tomography (XACT) was proposed to generate images by combining x-ray excitation and ultrasonic detection. In XACT an ultrasonic single element transducer with central frequency of 500 kHz was moved 360º around the sample. The present study proposes the use of x-ray photons to generate XA imaging using commercial ultrasound system, where a linear ultrasound probe was used to acquire XA signals during external beam radiation therapy.

Statement of Contribution/Methods

To evaluate the system, we used spherical absorbers (diameter of 5 mm) made of lead and copolymer-in-oil tissue-mimicking material. The spherical samples were positioned inside a water tank. X-ray pulses (15 MeV) were generated using a linear accelerator (Primus, Siemens), and an ultrasonic linear probe, with operating frequency between 5 MHz and 14 MHz (Sonix RP, Ultrasonix), was used to acquire the induced XA signal. The distance between gantry and sample was chosen to provide dose-rate from 1 to 10 Gy/min. Raw XA data were acquired synchronized with x-ray emission. For each x-ray emission, one scanline was obtained and then by using delay and sum beamforming, XA images were generated with commercial ultrasound machine.

Results/Discussion

Broadband XA signals (bandwidth of 5 MHz) were detected in all cases. XA signal amplitude linearly increased with dose-rate. For the experiments with lead sphere, the signal-to-noise ratio (SNR) varied between 5.0 dB and 16.4 dB for dose-rates from 1 to 10 Gy/min. XA signals with acceptable SNR were also detected for the tissue-mimicking material; therefore, XA images, for all spheres of different materials, could be reconstructed. These results demonstrate the feasibility of generating XA images for different materials, providing dosimetric information during external beam radiation therapy using linear accelerator and commercial ultrasound system.

FRIDAY POSTER

P1B5 - MTH: Ultrasound-Mediated Agent Delivery

4th floor

Friday, October 23, 2015, Posters displayed 08:00 am - 05:00 pm. Authors must be present at their poster from 9:30 - 10:30am (odd number posters) and 14:30 – 15:30pm (even number posters).

Chair: **John Hossack**
Univ. of Virginia

8:00 am **PET and fluorescence imaging demonstrate nanoparticle delivery and accumulation in a mouse breast tumor model using microbubbles-mediated ultrasound treatment**

Josquin Foiret[1], Hua Zhang[1], Lisa M. Mahakian[1], Sara M. Tam[1], Jai Woong Seo[1], Katherine W. Ferrara[1]; *[1]Department of Biomedical Engineering, University of California, Davis, USA*

Background, Motivation and Objective

Previous studies performed in our lab in a mouse model of cancer have shown that microbubble-mediated ultrasound therapy (MB-US) can enhance the accumulation of nanoparticles by changing the permeability of tumor blood vessels. This noninvasive therapy could lead to potential applications in targeted drug delivery studies. The objective was here to quantify nanoparticle accumulation following MB-US therapy using alternative imaging methods in a mouse model of breast cancer (Neu deletion mutant (NDL)). Ultrasound parameters were first validated using fluorescence imaging (FI) with long circulating liposomes (LCL) encapsulating a near infrared dye. Quantification was then assessed with positron emission tomography (PET) using radiolabelled LCL.

Statement of Contribution/Methods

NDL breast tumors were implanted in the mammary fat pads of 33 mice (26 for FI, 7 for PET; studies approved by the UC Davis Institutional Animal Committee on Use and Care). The protocol consisted of injecting LCL in the mouse tail vein and starting the MB-US treatment immediately afterwards. Non-targeted lipid-shelled MB (median diameter: 1.3 μm; concentration: 6.6×10^8 MB/mL) were continuously injected in the tail vein (150 μL/mouse). Simultaneously, a modified US system driving a custom dual-frequency array probe [1] was used to insonify one tumor with 2 s-US bursts of 1.2 MPa at 1.5 MHz each 17 s for a treatment time of 5 minutes. For FI, LCL encapsulating a near infrared dye (Em/Ex = 754/789 nm) were used and mice were sacrificed at 1, 2 and 4 hours after insonation. Excised tumors were imaged on an IVIS Spectrum (Perkin Elmer, MA). For PET imaging, Cu-64 (t1/2 = 12.7 h) was labeled on the surface of LCL preformed with 6-BAT lipid [2]. Mice were then imaged at 0, 3, 6 and 24 hours post therapy.

Results/Discussion

Enhanced accumulation of nanoparticles was found in the US-treated tumor up to 6 hours after sonication for both fluorescence and PET imaging. PET revealed increased activity in the US-treated tumor with an enhancement of up to 34 ± 32 % right after therapy (Fig. 1 a-b). The increase in fluorescence intensity in US-treated as compared to contra-lateral tumors was significant at 1, 2 and 4 hours after the treatment with a maximum enhancement of 40 ± 24 % 1 hour post therapy (Fig. 1 c-d).

Acknowledgment: NIHCA134659 and NIHCA103838

[1] Kruse et al., IEEE TBE, 57(1), 2010

[2] Seo et al., Bioconj. Chem., 2008
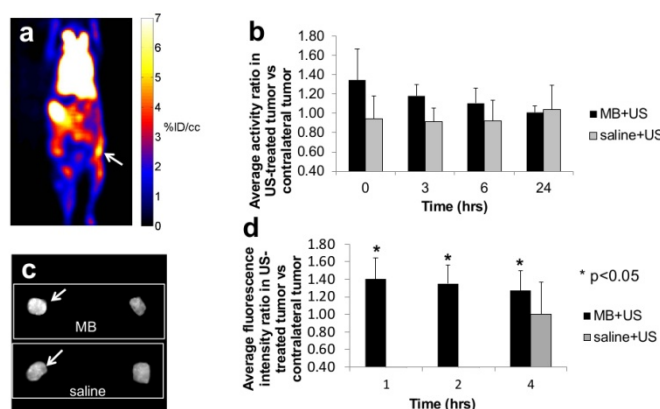
PET and fluorescence imaging demonstrates nanoparticles accumulation enhancement in tumor after microbubble-mediated ultrasound therapy.

a) PET imaging at 0 hr after injection of radiolabelled nanoparticles followed by US+MB therapy (expressed in % injected dose per cubic centimeter, arrow indicates insonified tumor). b) Average ratio in radioactivity in US treated tumor compared to contra-lateral control tumor (%ID/cc vs %ID/cc). c) Fluorescence imaging of *ex vivo* tumors 4 hrs after injection of fluorescent nanoparticles followed by US+MB therapy (arrow indicates insonified tumor). d) Average increase in fluorescence intensity in US treated tumor compared to contra-lateral control tumor obtained on *ex vivo* images.

8:00 am **Feasibility of Ultrasound Assisted Drug Delivery (UADD) via Noninvasive High Frequency Intense Therapy Ultrasound**

Michael Slayton[1], Paul Jaeger[2]; *[1]Guided Therapy Systems, Mesa, AZ, USA, [2]Ardent Sound, Inc., Mesa, AZ, USA*

Background, Motivation and Objective

Non-invasive transdermal delivery of drugs offers a number of advantages over conventional delivery methods. For the past twenty years considerable attention was paid to ultrasound assisted delivery at relatively low frequency (20 KHz-3 MHz) and low acoustic intensity (<3w/cm²) requiring minutes to several hours to enhance delivery. The purported mechanism of action is associated with cavitation increasing drug diffusion through the stratum corneum and epidermis.

We propose to show a feasibility of delivering clinically useful substances through stratum corneum into skin by utilizing Intense Therapy Ultrasound (ITU) high frequency (2.9-10 MHz), high intensity (>1,000 w/cm²). Purported mechanism of action would include inertial cavitation and high pressure (>1MPa).

Statement of Contribution/Methods

The experiments with ex-vivo pig skin were done with 2.9 MHz transducer creating a line of high intensity (4760 w/cm²) pulses at 100 msec and 10 w average acoustic power.

For ex-vivo pig skin color-coded Glycerin (viscosity of 612 Centipoise) was applied to the surface. After ultrasound exposures cross-sections of the skin along the beam propagation were excised, photographed and measured.

ITU transducers with 7.5 MHz and 10 MHz frequencies were used to create closely spaced (1.5 mm) of lesions in human skin in-vivo. Energy levels of up to 1J were used for 10 MHz and 7.5 MHz at depths of 1.5 mm (10 MHz) and 3mm (7.5 MHz) into skin.

For human skin in-vivo a topical solution of 5% lidocaine cream with negligible acoustic attenuation (1db/cm/MHz) was applied to the skin serving as coupling agent. Exposures were compared side-by-side with control exposures using regular acoustic coupling gel.

Results/Discussion

Ex-vivo pig skin showed penetration of color-coded Glycerin through the skin commensurate with series of exposures of 2.9 MHz pulses indicating the solution driven into the skin up to 1.5 mm.

Comparison between applied ITU lines for topical lidocaine covered skin and controls show absence of inflamed "welts" on the skin compared to "welts" raised in controlled exposures in three different volunteers (skin type I-II) in 10 MHz, 1.5 mm depth lines. 7.5 MHz, 3 mm depth similar exposures yielded customary "welt" raised even with the application of topical lidocaine.

Discomfort level for the volunteers during the 10 MHz exposures dropped approximately 2 points on the 10-point scale.

Active and passive cavitation detection was applied to set of ITU parameter and frequencies: water, gel and tissue. The results showed broadband spectra initiated during ITU exposures typically associated with inertial cavitation.

Feasibility of enhancing penetration through the skin of Glycerin and topical lidocaine solutions was shown in time ranging from 1 to 10 sec.

While the results and ranges of the applied ITU must be expanded and optimized it is also important to further investigate inertial cavitation mechanism of action for fast transdermal delivery of medicants.

P1B5-3 _____

8:00 am   Efficient generation of reactive oxygen species sonochemically generated by cavitation bubbles

Jun Yasuda[1], Shin Yoshizawa[1], Shin-ichiro Umemura[2]; *[1]Department of Communications Engineering, Tohoku.Univ., Sendai, Japan, [2]Department of Biomedical Engineering, Tohoku.Univ., Sendai, Japan*

Background, Motivation and Objective

Sonodynamic treatment (SDT) is a non-thermal high-intensity focused ultrasound (HIFU) treatment method by reactive oxygen species (ROS) which can induce irreversible changes to the tissue generated by ultrasonic cavitation bubbles and a sonosensitizer. Rose Bengal (RB) is one of such sonosensitizers.

In our previous studies, it has been demonstrated that triggered HIFU sequence, which consists of an high intensity short pulse (triggered pulse) for cavitation cloud inception immediately followed by a moderate intensity long burst (sustaining waves) for sustaining bubbles by volume oscillation, can generate ROS efficiently.

In this study, to clarify the primary factor of efficient generation of ROS, the correlation among the amount of cavitation cloud, sustained cavitation bubbles, and generated ROS was investigated.

Statement of Contribution/Methods

A focused ultrasound transducer and a sealed chamber were placed in a water tank. Solutions were sealed in the chamber contained either 0, 1.0 mg/L of RB and 1 mol/L of potassium iodide (KI). Cavitation cloud was captured by high-speed camera and sustained cavitation bubbles was detected by ultrasound imaging as sensitivity for bubbles was higher than high-speed camera.

The intensity and exposure duration of the trigger pulse were 40 kW/cm^2 and 100 µs, while those of the sustaining waves were 1 kW/cm^2 and 100 ms, respectively. The ultrasound frequency was 1.25 MHz. This sequence was exposed repeatedly for 1 hour at the PRF of 5 Hz.

The amount of ROS can be quantified by comparing the absorbance at 355 nm before and after ultrasound exposure because ROS oxidize iodine ion generated by KI and the absorbance at 355 nm is changed.

Results/Discussion

Figure shows captured pictures of cavitation cloud, the amount of sustained cavitation bubbles during sustaining waves exposure calculated by ultrasound images (Bar graph), and the amount of estimated ROS (Line graph). Absorbance indicates the amount of ROS.

In the result, it was found that RB concentration did not affect on the cavitation cloud inception. In contrast, the amount of sustained bubbles and generated ROS correlated with the RB concentration.

In this way, it was demonstrated that RB affects on the amount of sustained cavitation bubbles and it was the primary factor of efficient generation of ROS.

Figure :
High-speed camera pictures of cavitation cloud and
The correlation between the amount of sustained
cavitation bubbles and generated ROS
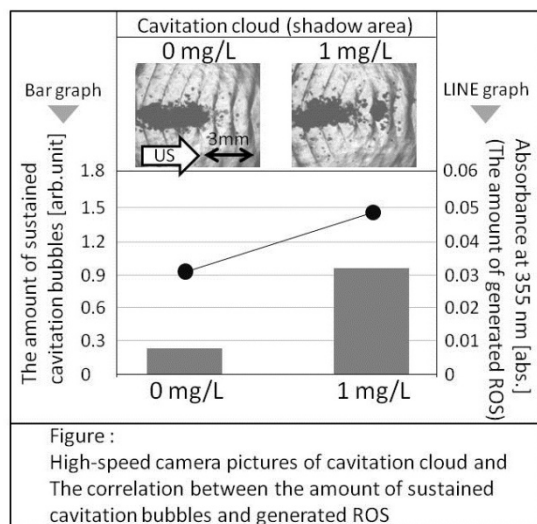
8:00 am   **Uptake and Cellular Recovery Mechanisms in Microbubble-enhanced Ultrasound Delivery of Nanoparticles for Cancer Therapy**

Lee Terron[1], Maria De Scrilli[1,2], Julien Reboud[1], Catherine Berry[3], Helen Mulvana[1]; [1]*School of Engineering, University of Glasgow, Glasgow, United Kingdom,* [2]*Department of Mechanical and Aerospace Engineering, Politecnico di Torino, Turin, Piedmont, Italy,* [3]*Centre for Cell Engineering, University of Glasgow, Glasgow, United Kingdom*

Background, Motivation and Objective

Functionalised nanoparticles (NP) have been shown to enable delivery of small silencing RNA molecules (siRNA) to cancer cells, disabling proliferation and providing a route to therapy. However the approach can be restricted to specific cell lines, limiting translation potential to in vivo treatment [1]. Here, we investigate delivery of NP to human breast cancer cell lines (MCF7), previously proven problematic in this regard, using ultrasound (US) and microbubbles (MB). In particular we examine potential mechanisms of NP delivery, opportunities for optimisation and offer insight to cellular recovery post treatment.

Statement of Contribution/Methods

MCF7 cells were cultured, grown to near confluence in OptiCells (Thermo Scientific) and treated with US in the presence of MB (SonoVue) and NP. US was 1 minute at 1MHz and 3.5MHz (20 cycles, 20% duty cycle) and matched mechanical index (MI) 0.15-0.45. SonoVue (Bracco Suisse) dose was 30 mL/L. NPs were magnetite (Chemicell, Germany) (200 nm, 2.2×10^{14} NP/L). Cell viability was assessed via Live/Dead assay, cellular uptake via TEM imaging and energy dispersive x-ray spectroscopy (EDX), and surface alterations via SEM.

Results/Discussion

Treatment did not affect cell viability. TEM and EDX confirmed delivery of NPs to MCF7 cells and suggested two uptake routes: 1. At low MI vesicular confinement (Fig 1a) of NPs dominated indicative of endocytosis, 2. At higher MI both confined and free NP were observed in the cytoplasm (Fig 1b) suggesting pore entry [2]. In addition the presence of larger NP clusters at high MI suggests pinocytosis. Membrane pores observed via SEM support our hypothesis. Again two populations existed, large (approx. 1-2 μm) and much more prevalent small pores (approx. 20–100 nm) (Fig 1c). All small pores appeared close to membrane 'blebs' (inset 1c) indicating the recently reported sonoporation recovery mechanism [3] may also underpin cellular preservation following minor insult at lower MI. No relationship between delivery route and frequency was observed. Since the therapeutic effect of NP is strongly influenced by their delivery, MI could be a critical efficiency parameter. Work continues to determine influence of delivery route on breast cancer treatment.

1. Conde et al. ACS Nano 6 (9) p8316–8324 2012

2. De Cock et al. J. Control. Release 197 p20-28 2015

3. Leow et al. J. R. Soc. Interface 12 (105) p1-10 2015
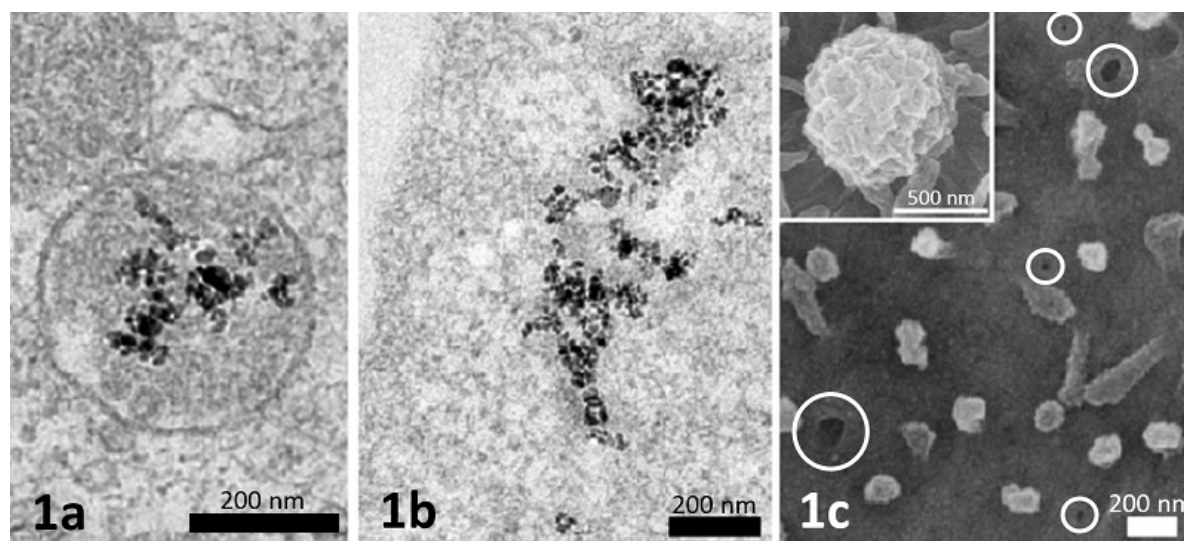
8:00 am   **Enhanced transdermal drug delivery with low frequency, low intensity (20 kHz, 100 mW/cm2) ultrasound exposure: In vivo feasibility study**

Gadi Cohen[1], Hiba Natsheh[1], Philip Lazarovici[1], Elka Touitou[1], Christopher Bawiec[2], Youhan Sunny[2], Melissa A. Lerman[3], Michael Neidrauer[2], Leonid Zubkov[2], W. Andrew Berger[4], Peter A. Lewin[2]; [1]*Hebrew University Jerusalem, Israel,* [2]*Drexel University, USA,* [3]*Children's Hospital of Pennsylvania, USA,* [4]*University of Scranton, USA*

Background, Motivation and Objective

The purpose of this work was to investigate whether low frequency, low intensity (LFLI, 20 kHz, <100 mW/cm2, spatial peak, temporal peak) ultrasound (US), delivered by a light-weight (<100g), tether-free, fully wearable, battery powered applicator has a potential as a tool for noninvasive, transdermal drug delivery. Such delivery is of interest because oral intake of a variety of drugs might be impeded due to side-effects such as decreased white blood cell counts, increased risk of infections, fatigue, oral ulcers, hair loss, nausea, and diarrhea, and liver toxicity.

Statement of Contribution/Methods

The pre-clinical evaluation was performed using a mouse model of rheumatoid arthritis (RA). RA was chosen because it is often encountered in children and juveniles. To minimize the side effects pediatric rheumathology treatment usually requires drugs to be injected, which is painful. Also, many children develop such psychological aversion to these injections that they vomit prior to drug administration. Moreover, invasiveness of delivery increases health care costs and reduces compliance, especially in early stage disease. Briefly, in in vivo animal experiments, 40 mice in 4 (n=10) groups (ultrasound combined with anti-inflammatory formulation (AIF), anti-inflammatory formulation only, ultrasound only, sham (no treatment) were treated. The applicator was intentionally designed to operate at the energy levels that excluded inertial cavitation- and thermally induced side effects. The experiments were Sγrepeated 4 to 6 times.

Results/Discussion

The outcome of the experiments indicated that the combination of ultrasound (US) exposure with topical application of 0.1% w/w betamethasone gel, exhibited statistically significant ($p < 0.05$) enhanced anti-inflammatory properties in comparison with the drug or US treatment alone. The present study confirms the potential benefits of LFLI US assisted drug delivery, but also stresses the need for a carefully designed study of the physical and chemical mechanisms involved and efficacy of delivery. The long-term goal is to explore the feasibility of using this technology to safe and painless vaccine delivery – an issue of global interest. Support: NIH R01EB009670 and NSF 1064802.

P1B5-6

8:00 am　　**Echogenic liposome as a carrier of siRNA for sonoporation: an alternative microbubble for sonoporation**

Jingam Park[1], Donghee Park[2], Unchul Shin[1], Jungwoo Son[1], Jinho Kim[1], Ohrum Cha[1], Yunsun Lee[1], Sangwoo Lee[1], Chul-woo Kim[2], Jongbum Seo[1]; [1]*Department of Biomedical engineering, Univ. Yonsei, Wonju, Gangwon, Korea, Republic of,* [2]*Seoul National University College of Medicine, Korea, Republic of*

Background, Motivation and Objective

Ultrasound contrast agents (UCAs) have been recently studied for drug delivery applications, since cavitation can increase the temporary permeability of nearby cells. However, the internal volume of UCA is generally filled with gas, hence loading drug molecules into UCAs is limited. In this study, a type of echogenic liposome having a liquid and gas core is proposed as an alternative carrier of genetic material for ultrasound-mediated drug delivery.

Statement of Contribution/Methods

We synthesized an echogenic liposome using liquid phase perfluorobutane and the structure of echogenic liposome was analyzed with TEM. The possibility of encapsulating siRNA into the proposed echogenic liposome was validated using confocal microscopy. Also, the protection of siRNA by the echogenic liposome from RNase was verified via electrophoresis experiment. Lastly, we evaluated the gene expression efficiency in HeLa cells using FAM-NC siRNA and echogenic liposome.

Results/Discussion

Under the confocal microscopy, approximately 88% of total FAM-NC siRNA signal sites overlap with liposome sites. Therefore, the possibility of siRNA encapsulation by echogenic liposomes is strongly indicated. The protection effect on siRNA provided by echogenic liposomes was verified through electrophoresis after exposure to RNase. The results indicate that at least 20% of the total siRNA used in experiment was successfully protected by the proposed echogenic liposome. Additionally, the results of transfection efficiency showed that ultrasound sonication on siRNA prior to transfection experiments contributed around 10% increase to the transfection efficiency of siRNA into HeLa cells. Despite further research regarding the controlled release of a gene into the target position in-vivo, the proposed liposome is expected to be efficient gene delivery carrier for sonoporation.
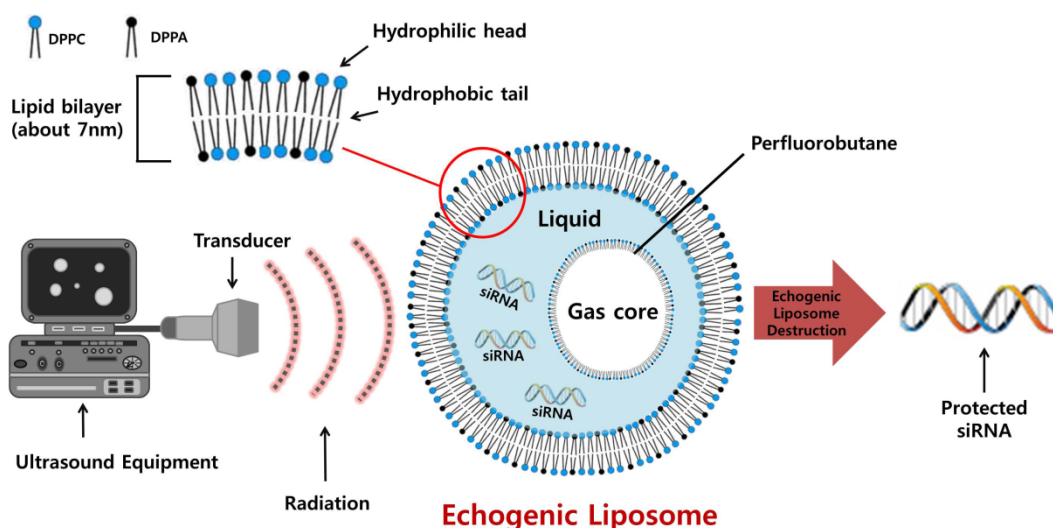
P1B5-7

8:00 am　　**Passive delivery of liposomes with different sizes to the mouse brain after blood brain barrier opening induced by focused ultrasound with microbubbles**

Jinxuan Guo[1], Gaoshu Chen[1], Jian Chen[2], Chien Ting Chin[1], Yanyan Suo[3], **Yuanyuan Shen**[1]; [1]*Department of Biomedical Engineering, Shenzhen University, Shenzhen, Guang Dong, China, People's Republic of,* [2]*School of pharmacy, Shanghai Jiaotong University, Shanghai, China, People's Republic of,* [3]*Shenzhen Entry-Exit Inspection and Quarantine Bureau, Shenzhen, China, People's Republic of*

Background, Motivation and Objective

Focused ultrasound (FUS) combined with microbubbles is an attractive method to deliver therapeutic agents to brain tissue noninvasively, transiently and locally. Recent studies showed successful delivery of liposomal drugs to animal brain. The objective of this study is to investigate the delivery outcome of liposomes with different mean diameters after ultrasound mediated blood brain barrier (BBB) disruption.

Statement of Contribution/Methods

Sonication (frequency: 1.282MHz, pulse length: 10 ms, PRF: 1 Hz, time: 60s, acoustic power: 1.1W) was applied to nine female Balb/c mice (20±2 g) after lipid-shelled microbubbles (mean Ø 1.34 μm, conc.: 2.0×10^9/mL) were injected (0.1 μL/g) intravenously via the tail vein. Immediately after sonication, two preparations of rhodamine-labeled liposomes (lipid conc.: 10 mg/mL) (mean Ø 55 nm, n=4; and mean Ø 120 nm, n=3) were administered at a dose of 0.1 mL. Undelivered liposomes were washed away from the circulation by cardiac perfusion 4 hours later. The cerebrums were harvested and sectioned using a cryostat into 10-μm-thick slides for fluorescence imaging and staining with hemotoxilin and eosin (H&E).

Results/Discussion

Scattered spots of fluorescent signals were detected. The distribution pattern of the extravasated liposomes was heterogenous rather than homogeneous. Although the area of 55 nm liposomes across BBB was statistically larger than 120 nm liposomes, the areas of fluorescence were confined, accounting for 9.7% and 2.9% respectively. The H&E staining showed no neuronal damage and necrosis. However, small areas of microhemorrhage were observed.

The work suggested that passive delivery of liposomes larger than 50 nm after FUS induced BBB disruption in normal mice could be achieved. However the distribution of liposomes penetrating from vasculature was nonuniform and confined.
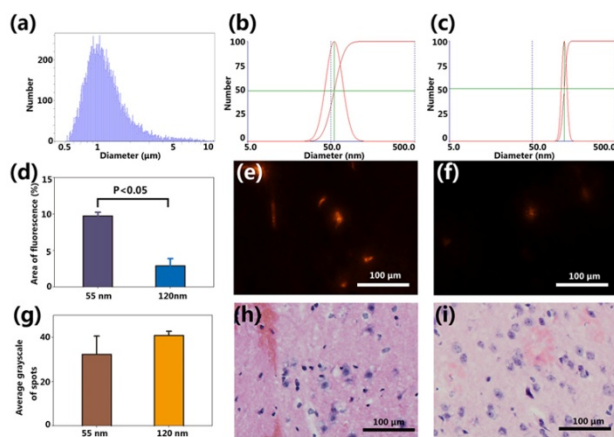
Figure 1. The size distribution of prepared microbubbles (a), 55 nm liposomes (b) and 120 nm liposomes (c); Area of fluorescence (d) and average grayscale of spots (g) of 55 nm and 120 nm liposomes across BBB; Representative microscopic images of 55 nm (e) and 120 nm (f) liposomes across BBB and corresponding H&E staining images (h-i).

P1B5-8

8:00 am   &#65533; The study of targeted delivery of microbubbles binding GDNF through the blood-brain barrier by MRI-guided focused ultrasound on treatment of addiction

Feng Wang[1], Xiaojian Jia[2], Yu Shi[3], Li Liu[3], Azhen Hu[1], Yun Chen[3]; *[1]Biomedical Research Institute,Shenzhen PKU-HKUST Medical Center, China, People's Republic of, [2]1Biomedical Research Institute,Shenzhen PKU-HKUST Medical Center, China, People's Republic of, [3]Department of Ultrasound, Peking University Shenzhen Hospital, China, People's Republic of*

Background, Motivation and Objective

Drug addiction is a chronic disease of brain, which has a trend to recur. Animal experiments showed that gliacyte derived neurotrophic factor (GDNF) had an ideal therapeutic efficacy for drug addiction, but the clinical application of GDNF was limited because of its deficincy permeability in Blood Brain Barrier(BBB). Low frequency focused ultrasound combine with microbubble can produce an non-invasive targeted BBB opening locally. To demonstrate MBs that bind GDNF combined with MRI-guided focused ultrasound may be an effective way of delivering neurotrophic factors directly into the CNS. The method described herein provides a potential means of treating patients with CNS diseases.

Statement of Contribution/Methods

In our study, the character of ultrasound combine with microbubble was utilized to investigate the time-effect parameters of Low-Freqence focused ultrasound associated with microbubble distrution on opening BBB firstly. And then we investigated the targeted delivery of GDNF MBs through the BBB by magnetic resonance imaging (MRI)-guided focused ultrasound. Evans Blue extravasation and histological examination were used to determine the optimum focused ultrasound parameters. Enzyme-linked immunosorbent assay was performed to verify the effects of GDNF bound on MBs using a biotin–avidin bridging chemistry method to promote GDNF delivery into the brain. Lastly, evaluate the effects of GDNF in rats with CPP (conditioned place preference) and acute withdrawal symptoms through the behavioral observation after the BBB is opened locally. The content of catecholaminergic neurotransmitter, the expression of TH (tyrosine hydroxylase) in brain were detected.

Results/Discussion

The results showed that GDNF can be delivered locally and noninvasively into the CNS through the BBB using MRI-guided focused ultrasound combined with MBs under optimum parameters. After sonication and a 0.5 ml bolus injection of MBs, the amount of GDNF in the target tissue increased to 5.07¡lg/g. Focused ultrasound combined with microbubbles binding GDNF can open BBB locally and increased the content of GDNF in brain. The increased GDNF disrupted the reconsolidation of morphine CPP and inhibited morphine- withdrawal signs.The change decreased significantly the content of norepinephrine and dopamine($p<0.05$);and had no effect on serotonin.In summary, our study firstly demonstrated MBs that bind GDNF combined with MRI-guided focused ultrasound may be an effective way of delivering neurotrophic factors directly into the CNS and a potential means of treating patients with drug addiction.

FRIDAY POSTER

P1B6 - MTC: Soft Tissue Characterization

4th floor

Friday, October 23, 2015, Posters displayed 08:00 am - 05:00 pm. Authors must be present at their poster from 9:30 - 10:30am (odd number posters) and 14:30 – 15:30pm (even number posters).

Chair: **Lori Bridal**
Univ. Pierre and Marie Curie

P1B6-1

8:00 am **Evaluation of ultrasound B-mode images of liver fibrosis using fibrotic probability image based on multi-Rayleigh model**

Shohei Mori[1], Shinnosuke Hirata[1], Tadashi Yamaguchi[2], Hiroyuki Hachiya[1]; *[1]Tokyo Institute of Technology, Tokyo, Japan, [2]Chiba University, Chiba, Japan*

Background, Motivation and Objective

A quantitative diagnostic method for liver fibrosis using ultrasound echo signal is highly required. A probability density function (PDF) of echo amplitudes from a normal liver can be approximated by a Rayleigh distribution; however, the PDF of echo amplitudes from liver fibrosis deviates from the Rayleigh distribution. We proposed a multi-Rayleigh model as a model of the PDF of echo amplitudes from liver fibrosis, and a fibrotic probability imaging method based on the multi-Rayleigh model. In this study, we evaluated ultrasound images of liver fibrosis using the fibrotic probability image based on the multi-Rayleigh model.

Statement of Contribution/Methods

The multi-Rayleigh model with three components is composed of hypoechoic, normal and fibrotic tissues respectively. From the multi-Rayleigh model, we can independently extract the information about each component. By comparing the each component′s information, a clinical ultrasound image can be converted to the fibrotic probability image. To evaluate ultrasound images of liver fibrosis quantitatively using the multi-Rayleigh model, a selection of a region of interest (ROI) is important because the data such as an abdominal wall and a blood vessel wall are erroneously judged as the fibrotic tissue in the multi-Rayleigh model. In this study, the ROI was automatically determined by removing the data which could not be expressed by the multi-Rayleigh model, and evaluated ultrasound images of liver fibrosis quantitatively using the fibrotic probability image.

Results/Discussion

Figures (i)(a)-(d) show clinical ultrasound images classified into (a) F0 (normal liver), (b) F1 (early-stage hepatitis), (c) F2 (moderate hepatitis) and (d) F3 (late hepatitis) in accordance with a new Inuyama classification. The yellow lines in Figs. (i)(a)-(d) show ROIs determined automatically. Figures (ii)(a)-(d) show fibrotic probability images calculated for Figs. (i)(a)-(d). The ROI was adequately determined to include only the liver tissue and pixels which have high fibrotic probabilities increased as a progress of liver fibrosis. It was concluded that the progress of liver fibrosis could be evaluated quantitatively by using the fibrotic probability image based on the multi-Rayleigh model.
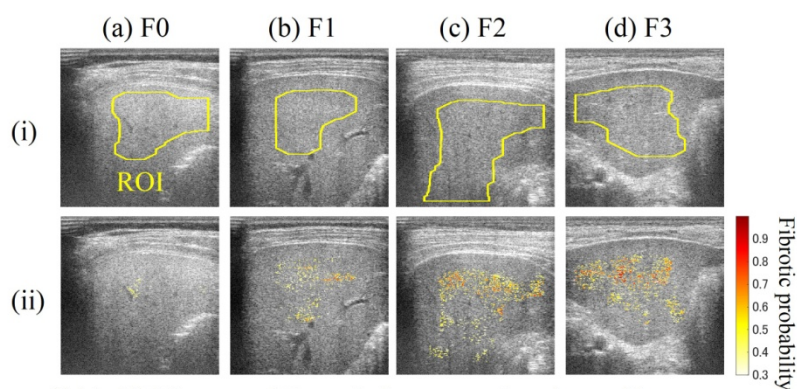
(i)(a)-(d) Ultrasound B-mode images and regions of interest (ROIs) determined automatically. (ii)(a)-(d) Fibrotic probability images in ROIs of Figs. (i)(a)-(d). Stages of liver fibrosis are (a) F0, (b) F1, (c) F2 and (d) F3.

P1B6-2

8:00 am **Backscatter coefficient estimation from human thyroids in vivo**

Tony Cueva[1], Julien Rouyer[1], Alberto Portal[2], Tamy Yamamoto[2], **Roberto Lavarello**[1]; *[1]Departamento de Ingeniería, Pontificia Universidad Católica del Perú, San Miguel, Lima, Peru, [2]Departamento de Radiología, Clínica Centenario Peruano Japonesa, Pueblo Libre, Lima, Peru*

Background, Motivation and Objective

Thyroid cancer management is a complicated clinical problem due to the high prevalence of thyroid nodules in the general population and the relatively low prevalence of cancer in this gland. Fine-needle aspiration biopsy remains the current gold standard for the diagnosis of thyroid cancer, and therefore there is a need to develop non-invasive tools that aid in the identification of malignant thyroid tissues. Quantitative ultrasound imaging using backscatter coefficients (BSCs) has shown potential to characterize thyroid tissues in rodent models ex vivo. As an initial step towards the goal of thyroid cancer diagnosis on a clinical setting, in this study the estimation of BSCs from healthy human thyroids in vivo was performed.

Statement of Contribution/Methods

Healthy subjects with no reported personal or family history of thyroid diseases, no palpable thyroid nodules, no smoking habits and body mass index less than 30 Kg/m2 were recruited for this study. Echographic examinations were conducted using a scanner equipped with a 9-MHz linear array. Data from ten volunteers (age: 22±4 years old, gender: five females, five males) were processed for this preliminary study. Backscatter coefficients were estimated using the reference phantom method and considering data blocks of 4.5 mm by 4.5 mm. The mean BSC (mBSC) between 3 and 8 MHz was computed for each data block. An agar-based phantom with speed of sound of 1540

m/s and attenuation coefficient slope of 0.5 dB/cm/MHz was used as reference media for BSC estimation. Attenuation compensation was performed considering the presence of sub-cutaneous fat, muscle, and thyroid tissues.

Results/Discussion

An mBSC image of a thyroid and the average BSC curves derived from each of the ten volunteers are shown in the left and right panels of the figure, respectively. The average mBSC was 0.036±0.009 1/(sr.cm) considering all data blocks from all subjects in the study, which resulted on a coefficient of variation of less than 12% when the mBSC was expressed in decibel scale. Furthermore, the minimum and maximum coefficients of variation of the mBSC in decibel scale for a given volunteer were 9.7% and 26.1%, respectively. Moreover, all BSC curves exhibited similar variations as a function of frequency. These results suggest that BSCs from healthy thyroids can be reliably and consistently estimated in vivo.
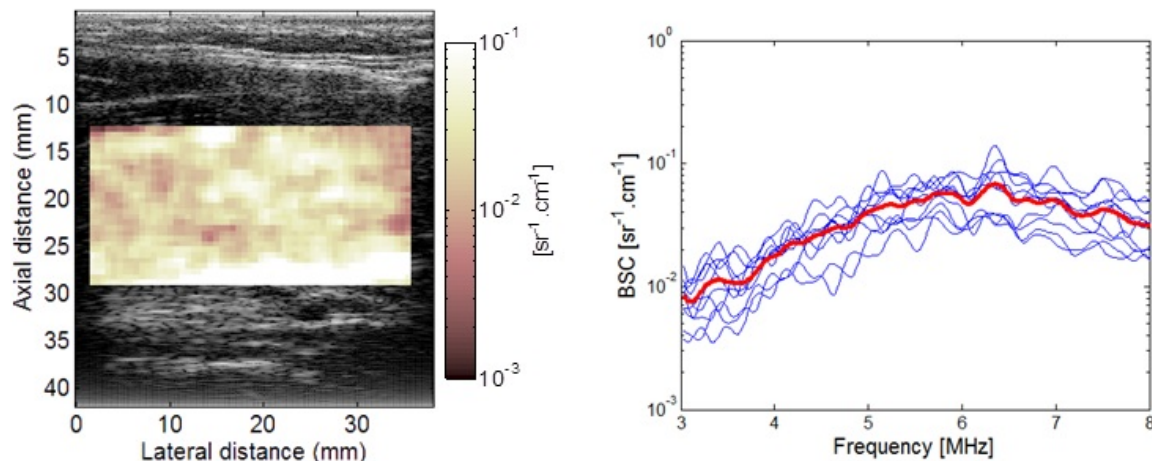
P1B6-3

8:00 am **Correcting the influence of tissue attenuation on Nakagami distribution shape parameter estimation**

Michal Byra[1], Andrzej Nowicki[1], Hanna Piotrzkowska-Wroblewska[1], Katarzyna Dobruch-Sobczak[1,2], Jerzy Litniewski[1]; *[1]Ultrasound Department, Institute of Fundamental Technological Research PAS, Warsaw, Poland, [2]Maria Sklodowska-Curie Memorial Cancer Centre and Institute of Oncology, Poland*

Background, Motivation and Objective

Nakagami distribution is used to model the statistical properties of backscatted echoes in tissue. The proper estimate requires the compensation of attenuation along each scanning line. Attenuation of the wave results in decreasing of the Nakagami scale parameter Ω (mean intensity) with depth; this phenomenon violates the assumption that samples' amplitudes within ROI are identically distributed. In this paper the impact of attenuation on estimation of Nakagami shape parameter m, used for lesion characterization, will be discussed. Three different methods are proposed to solve this issue.

Statement of Contribution/Methods

Radiofrequency (RF) data for various scattering models resulting in varying m parameter were simulated with different tissue absorption, next uncompressed B-mode images were reconstructed. Four estimators of m parameter, the Maximum Likehood, moments, Greenwood and Lorenz were compared with our three methods in case of not attenuated and attenuated media for different ROI size and absorption coefficients.

In the first method (Met1) samples are considered to be a mixture of many Nakagami distributions sharing the same shape parameter m, but with varying Ω parameter. In the second method (Met2), ROI is decomposed into smaller regions and attenuation influence in every region is considered as a scalling of amplitude by a constant factor which can be removed by division of individual samples' amplitude by the sample mean. In the next step the samples from various regions are collected and shape parameter is estimated for the entire ROI. In the third method (Met3) the division by the average is omitted, instead m parameter is estimated for every small region and shape parameter for the entire ROI appears as a mean of these values. All three above methods are then tested on RF data from a breast cancer tissue.

Results/Discussion

We have found that all proposed methods (Met1-3) considerably improved the precision of m parameter estimation. As can be seen in fig. 1. the overall error for different ROI area is not exceeding 5% while for the standard moment based estimator this error increases linearly with ROI size up to 60% for ROI of 15mm^2. In general m parameter calculation in breast lesions is strongly dependent on absorption and ROI size. It will be shown that the proposed novel algorithms result in almost attenuation independent estimation.
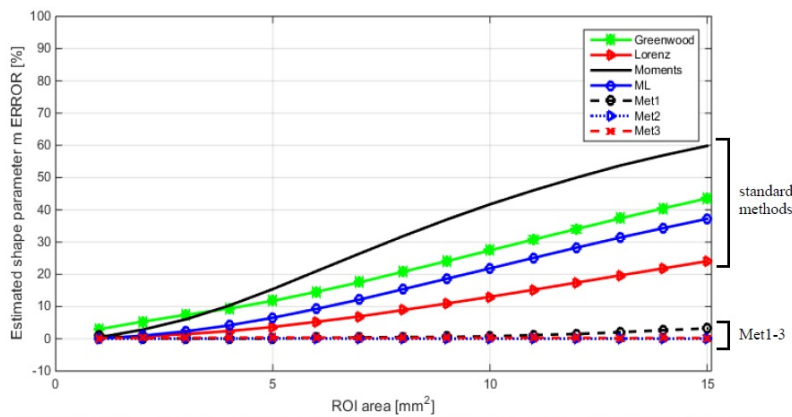
Fig. 1. Error of *m* estimation as function of ROI area. Result for *m*=1, center pulse frequency of 5MHz, absorption coefficient 0.5dB/cmMHz and ROI centered at 4cm.

P1B6-4 _____

8:00 am   Variation of longitudinal strain along the arterial wall adjacent to the asymptomatic carotid plaque

Spyretta Golemati[1], Symeon Lehareas[1], Aimilia Gastounioti[2], Konstantina Nikita[2], Achilles Chatziioannou[1], Despina Perrea[1]; [1]Medical School, National Kapodistrian University of Athens, Athens, Greece, [2]Electrical and Computer Engineering, National Technical University of Athens, Athens, Greece

Background, Motivation and Objective

The motion, and resulting strain, of the arterial wall nearby an atheromatous plaque is believed to be affected by the plaque and therefore may carry important information about disease status. Strain of the arterial wall in the longitudinal direction, i.e. along its length, has recently gained attention as determinant of cardiovascular risk (Gastounioti et al. Phys Med Biol, 2013). In this work, longitudinal strain (LS) was estimated along the wall adjacent to asymptomatic carotid plaque, in an attempt to highlight the significance of arterial wall kinematics in atherosclerotic subjects without cerebrovascular events.

Statement of Contribution/Methods

Twenty five atheromatous carotid arteries of elderly adults (59-81 y.o.) were imaged in longitudinal sections, and videos of B-mode images were analysed using a previously developed method based on optical flow. The analysis consisted in the estimation of the longitudinal positions of three regions of interest (ROIs) on the posterior wall (A, B, and C in Figure 1a). LS was subsequently defined as the normalised difference of the longitudinal positions between two ROIs, and was assessed at two locations along the wall (Figure 1a). A longitudinal strain index (LSI) was then calculated as the average of the amplitudes of the LS curves over 2-3 cardiac cycles.

Results/Discussion

Figure 1b shows examples of LS curves at the two interrogated locations for one subject. LSIs at location 1 were significantly higher than at location 2 (4.74±1.66 vs. 2.54±1.08, p-value=1.25E-06). This indicates that the wall closer to the plaque undergoes higher strain than the wall farther from it, and may be due to the effect of the presence and motion of the nearby lesion; an effect, which seems to be extended to the area around it. These findings show promise toward better understanding the complex mechanical phenomena taking place not only within the plaque but also in the neighbouring tissues.
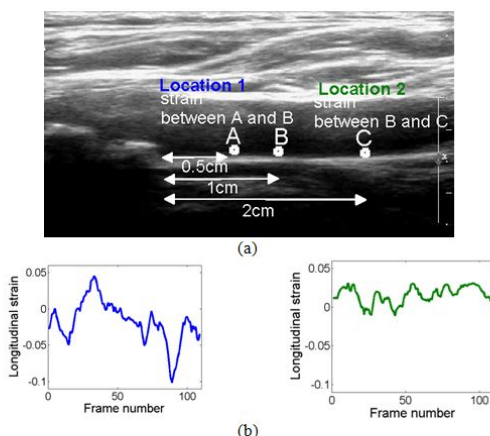
Figure 1. (a) Example of B-mode ultrasound image of arterial wall adjacent to plaque with ROIs where measurements were made (A, B, C). Arrows show distances from the plaque edge; (b) Examples of longitudinal strain curves at locations 1 (left side) and 2 (right side).

P1B6-5 _____

8:00 am   Assessment of Transmural Myocardial Orientation Using Nakagami Imaging in a Phased Array Configuration

Xue Yu[1], Wei-Ning Lee[1,2]; [1]Electrical and Electronic Engineering, University of Hong Kong, Hong Kong, [2]Medical Engineering Programme, University of Hong Kong, Hong Kong

Background, Motivation and Objective

The complex myocardial fiber architecture is associated with cardiac electromechanics and alters in diseased conditions, so its evaluation is important for the detection of the disease. Our pilot study (Yu and Lee. IEEE IUS 2014) showed that Nakagami imaging could depict the structural differences between short- and long-axis views of the left ventricle (LV) with a linear array. Routine echocardiography, however, is performed in a phased array configuration, which is challenging for kernel-based speckle analysis,

FRIDAY POSTER

like Nakagami imaging (NI), due to the non-uniform spatial resolution. This study thus aims to further investigate the feasibility of NI to find the transmural fiber orientation in myocardium with a phased array.

Statement of Contribution/Methods

The porcine LV anterior wall was embedded in a gelatin (5.5%)-agar (3%) phantom. Skeletal muscle and homogeneous gelatin-agar phantoms with glass beads (32 scatterers/mm3) were made for comparison. Phantoms were secured on a rotation device (Newport, USA) and co-axial with the probe, rotating from -90° to 90° at a 10° increment, where 0° was the fiber plane in skeletal muscle and the short axis in the myocardium. In-phase and Quadrature (IQ) data were acquired by a programmable ultrasound system (Verasonics, USA) with a 5MHz linear and a 2.5MHz phased array. Nakagami *m* parameters were computed from signal envelopes using a kernel size of 3 times the resolution cell. To achieve uniform spatial resolution in the entire field of view, coherent plane wave (64 angles) and diverging wave (43 waves) compounding techniques were used in linear and phased arrays, respectively.

Results/Discussion

Figure 1a shows gradual increase in mean *m* values (inside the ROI) when the probe became aligned (0°) with the local fiber directions in the skeletal muscle. Such *m* value variation as a function of the probe angle was not exhibited in the homogeneous phantom (fig 1b). In the LV anterior wall (fig 1e-h), estimated *m* values differed among the subepicardium, midwall, and subendocardium. The largest *m* value in each wall depth, indicated by an arrow, shows the local dominant fiber direction, in concordance with the literature (Lee et al. PMB 2012). Although NI may have the potential to depict transmural fiber orientation with a phased array, influences of SNR on the *m* value will be further studied and validation with the gold standard will be performed.
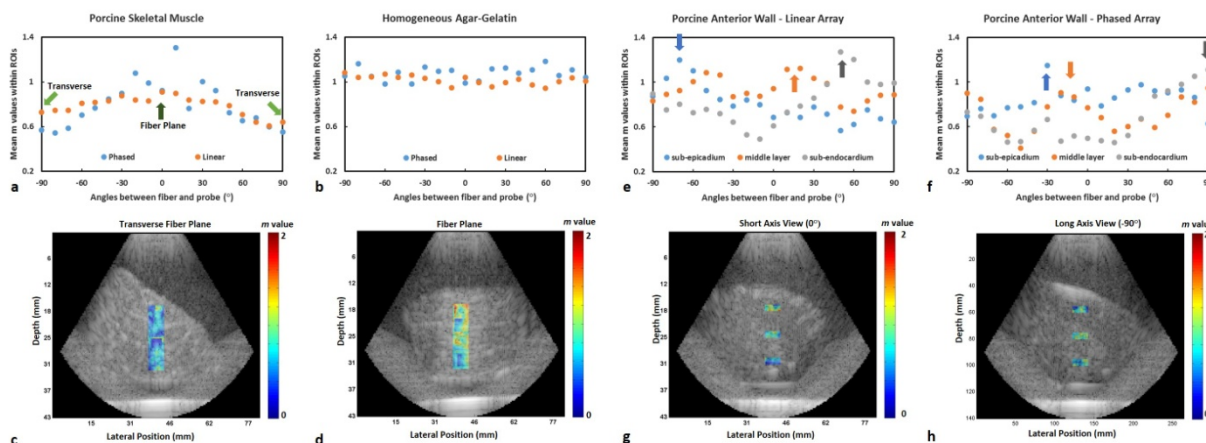
Fig 1. **a-d** Variation of *m* values with probe angle in the skeletal muscle, a homogeneous phantom, **e-h** and the anterior wall. Three 1.5x3.4 mm² ROIs were placed in the subepi-, subendocardium and midwall.

P1B6-6 _____

8:00 am **Experimental estimation of effective scatterer diameters from physical phantoms using autoregressive spectral analysis**

Julius Diestra[1], Roberto Lavarello[1]; *[1]Departamento de Ingeniería, Pontificia Universidad Católica del Perú, San Miguel, Lima, Peru*

Background, Motivation and Objective

One of the limitations of tissue characterization using backscatter coefficients (BSCs) is the relatively low spatial resolution of the technique. Although short gate lengths (Δz) can be used in order to improve the axial resolution, this approach may result in the distortion of the estimated BSC curves when using the discrete Fourier transform (DFT) for spectral estimation. Previous experimental reports suggest that autoregressive (AR) methods can improve the quality of average BSC (ABSC) estimation when using low Δz values. In this study, the estimation of effective scatterer diameters (ESDs) from a calibrated physical phantom using AR spectral analysis was experimentally assessed.

Statement of Contribution/Methods

Backscatter data was obtained from an agar-based phantom with embedded 41 ± 4 µm glass spheres using single-element focused transducers with 7.5 MHz and 10 MHz nominal center frequencies. BSCs were estimated using both DFT and AR methods from 21 analysis regions containing 21 scan lines and Δz values between 0.5 and 18 wavelengths (λ). The ABSC and ESD values were derived from the BSCs using both the -6 and -12 dB bandwidths of each transducer. ESDs were estimated from the BSC curves by using a solid sphere model. AR estimation was performed using Burg's method and the AR order was selected to optimize the fit between the estimated and theoretical BSC curves.

Results/Discussion

For illustration, the ABSC vs. Δz and ESD vs. Δz curves when using the 10-MHz transducer are shown in the figure. When using the -6 dB bandwidth, AR modeling outperformed DFT when estimating ABSCs for $\Delta z \leq \lambda$ (i.e., nearly 40% improvement for $\Delta z = 0.5\lambda$ for both transducers). However, no consistent improvements were observed when estimating ESDs with AR modeling instead of DFT. In contrast, when using the -12 dB bandwidth both the ABSC and ESD estimates were consistently improved when using AR modeling instead of DFT for $\Delta z \leq \lambda$ (i.e., up to 54% and 30% ABSC estimation error reduction and 31% and 64% ESD estimation error reduction for $\Delta z = 0.5 \lambda$ when using the 7.5 MHz and 10 MHz transducers, respectively). These results suggest that improvements in ESD estimation when using AR analysis are dependent on the ka value and the analysis bandwidth, and may not necessarily correlate with improvements in ABSC estimation.
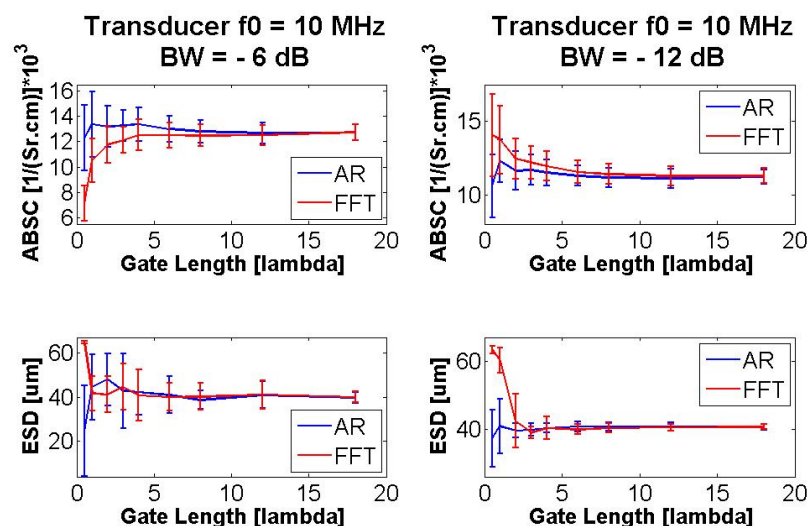
P1B6-7

8:00 am   A Technique for Mapping Shear Wave Velocity and Attenuation from the Two-Dimensional Fourier Space

Ivan Nenadic[1], Bo Qiang[1], Matthew Urban[1], James Greenleaf[1]; *[1]Mayo Clinic, USA*

Background, Motivation and Objective

Attenuation Measuring Ultrasound Shearwave Elastography (AMUSE) method independently measures shear wave velocity and attenuation due to a propagated shear wave without a need of a rheological model. AMUSE has been shown to produce biopsy like measurements of velocity and attenuation in various tissues in vivo. In this study, the feasibly of recovering maps of shear wave velocity and attenuation without a model were investigated.

Statement of Contribution/Methods

Plane wave harmonic excitation technique was used to propagate shear waves in the frequency range 100 – 500 Hz in a finite element model (FEM), gelatin phantom and excised porcine liver. A finite element model of an infinite viscoelastic medium with the density of 1000 kg/m3 and mechanical properties defined in terms of the Voigt model where the elasticity ($\mu1$) and viscosity ($\mu2$) were $\mu1 = 4$ kPa and $\mu2 = 4$ Pa·s, respectively. A plane surface inside the FEM model was used to excite harmonic waves and the motion was saved and used for analysis. In case of the gelatin and liver phantom, a glass plate was used to excite harmonic waves. A programmable ultrasound-imaging platform (Verasonics, Inc. Redmond, WA, USA) operating an L7-4 transducer (center frequency of 5 MHz and made by Philips Healthcare, Andover, MA) was used to track the motion at a pulse repetition frequency of 4 kHz. The shear wave velocity and attenuation at several frequencies were calculated by performing a two-dimensional (2D) Fourier Transform to obtain the k-space. The k-space peak at the given frequency was used to calculate the velocity using the c = f/kx formula, and the attenuation by using α = FWHM x ($\pi/\sqrt{3}$), where FWHM is the full-width-at-half-maximum. Correction factors due to cylindrical wave propagation were used to account for changes in the shape of the wave front. Corrections due to windowing errors caused by the sample size were also applied. Shear wave velocity and attenuation mapping was explored due to various impulse excitations approaches. Velocity and attenuation mapping studies were performed in phantoms containing inclusions using harmonic and impulse excitation. The results were compared to the gold standard measurements of velocity and attenuation.

Results/Discussion

The results show that the k-space method can be used to recover the shear wave velocity and attenuation due to harmonic motion within 10% of the true value of velocity and attenuation. The results in inclusion phantoms are accurate within 20% of the true values.

P1B6-8

8:00 am   Feasibility of acoustic evaluation of thermal lesions at bone-soft tissue interface of an ex vivo bovine bone exposed to high-intensity focused ultrasound

Siyuan Zhang[1], Zhiwei Cui[1], Lei Zhang[1], Xingguang Zhu[1], Tianqi Xu[1], Supin Wang[1], Mingxi Wan[1]; *[1]Department of Biomedical Engineering, Xi'an Jiaotong University, Xi'an, China, People's Republic of*

Background, Motivation and Objective

High-intensity focused ultrasound (HIFU) is a rapidly emerging non-invasive technique to selectively and locally produce thermal ablation of tumors located in various tissues, which could produce thermal lesions in periosteal structures for the thermal treatment of bone metastases that has been approved by FDA. In this work we characterized the surface vibration of an ex vivo bovine bone exposed to HIFU and explored the feasibility of using acoustic parameters to evaluate the thermal lesions at bone-soft tissue interface.

Statement of Contribution/Methods

The vibration of the bone surface was measured using a laser vibrometer when exposed to HIFU under acoustic pulse excitation and continuous sinusoidal excitation. Thermal lesions were formed at normal and oblique acoustic incidence of HIFU to the surface of the bone. 2-D RF data backscattered from the ablated region were captured by a modified diagnostic ultrasound scanner to construct the ultrasonic B-mode ultrasound images, Nakagami images and differential integrated backscatter (DIBS) images simultaneously, as well as the changes of acoustic apparent integrated backscattering (AIB) and integrated reflection coefficient (IRC) due to the thermal lesions on the bone surface.

Results/Discussion

At oblique incidence of HIFU, the amplitudes of the nano-vibration of the bone surface were higher in the opposite direction. The thermal lesion was 20 mm in width and extended along the front surface of the bone to the right of the HIFU focus. The thermal lesions in the soft tissue were visualized as hyperechoic regions in ultrasonic B-mode images, Nakagami images and DIBS images simultaneously. The mean value of AIB in the region of surface thermal lesions was increased by about 35% compared with the normal level in the control groups and the value of IRC was decreased by about 70% on average. This preliminary study suggested that the presence of bone would directionally change the spatial distribution of surface vibration and thermal effects at bone-soft tissue interface for oblique incidence of HIFU, and the ultrasonic parameters IRC may have more potential than AIB in evaluating the characteristics of thermal lesions on the bone surface.

FRIDAY POSTER
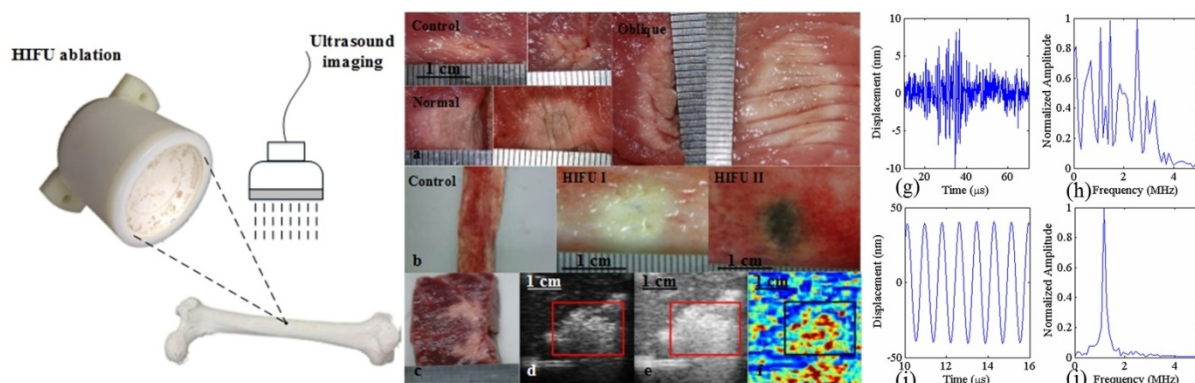
Thermal lesions (a) in the soft tissue and (b) on the surface of the bone exposed to HIFU, and (c) section plane, (d) B-mode ultrasound image, (e) DIBS image and (f) Nakagami parameter image of thermal lesions. Typical (g), (i) temporal waveforms and (h), (j) corresponding frequency spectra (all normalized to the their own maxima) of the bone surface vibration at normal incidence upon the bone under pulse excitation (upper row) and continuous sinusoidal excitation (lower row).

P1B6-9

8:00 am   High-Resolution Strain and Strain Rate Imaging of Adult Zebrafish Myocardium

Chen Ho-Chiang[1], Chih-Chung Huang[1]; [1]*Department of Biomedical Engineering, National Cheng Kung University, Taiwan*

Background, Motivation and Objective

The adult zebrafish (Danio rerio) has recently become an important small-animal model for studying human pathologies in many fields of preclinical research and translational medicine, particularly those related to cardiovascular diseases. The human heart cannot regenerate after injury, whereas the adult zebrafish can fully regenerate its heart even after 20% of the ventricle is amputated. Many studies have begun to reveal the cellular and molecular mechanisms underlying this regenerative process, which have exciting implications for human cardiac diseases. However, the dynamic functions of the zebrafish heart during regeneration are not yet understood. This study established a high-resolution echocardiography for strain and strain rate imaging of the zebrafish heart in order to explore the cardiac functions during different regeneration phases.

Statement of Contribution/Methods

Experiments were carried out using healthy AB-line adult zebrafish aged 4¡V5 months. The zebrafish was anesthetized with ethyl 3-aminobenzoate methanesulfonate salt. Figure 1(a) shows the block diagram of a 65 MHz high frequency electrocardiogram-gated echocardiography system. Figure 1(b) shows the typical B-mode image of zebrafish cardiac anatomy, including ventricle, bulbus arteriosus (BA), and atrium. In order to obtain strain and strain rate imaging, the tissue velocities from two different locations of myocardium were measured by autocorrelation velocity estimation algorithm firstly. Subsequently, the strain and strain rate imaging were obtained to evaluate the deformation of myocardium.

Results/Discussion

Strain and strain rate images of zebrafish myocardium can be derived by calculating tissue velocity at two different locations we selected. Fig.1 (c) shows the strain rate and strain image of ventricular tissue of zebrafish within one cardiac cycle, respectively. The result indicated that the deformation of myocardium segment is up to 45% over time during one cardiac cycle. This new technique is simple, rapid, widely available, and relatively inexpensive for the further study of the cardiac function of adult zebrafish
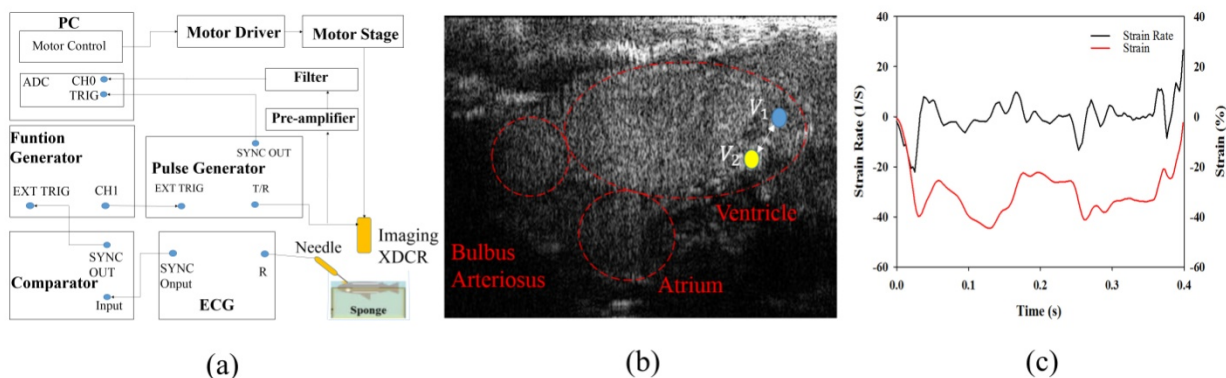
Fig.1

P1B6-10

8:00 am   Relation between Speed of Sound Measured by Using Ultrasound and Magnetic Resonance Images and Elasticity in Tissue-Engineered Cartilage

Naotaka Nitta[1], Masaki Misawa[1], Koji Hyodo[1], Yoshio Shirasaki[1], Kazuhiko Hayashi[1], Kazuhiro Homma[1], Tomokazu Numano[2]; [1]*National Institute of Advanced Industrial Science and Technology (AIST), Japan*, [2]*Tokyo Metropolitan University, Japan*

Background, Motivation and Objective

It is important to evaluate the elasticity of tissue-engineered cartilage, for evaluating its structural strength. However, in vivo evaluation of tissue-engineered cartilage elasticity has not been established. Although the elastography is the one of promising technique for evaluating tissue elasticity, it might be difficult to apply to the tissue-engineered cartilage because its size is small and internal echo from normal cartilage is weak. On the other hand, the speed of sound (SOS) is available for elasticity evaluation. We have proposed in vivo measurement method of SOS using ultrasound and MR images. This method determines the SOS based on the thickness measurement using the MR image and the time-of-flight (TOF) measurement using the ultrasound. In this study, this method was applied to the SOS measurement of tissue-engineered cartilage.

Statement of Contribution/Methods

All animal procedures were approved by the Animal Care and Use Committee of our institution. 12- and 18-week-old male F344/NJcl-rnu/rnu rats were used. Anesthesia was induced with intraperitoneal injection of a mixture of ketamine (87mg/kg), xylazine (13mg/kg) and 0.05ml of atropine. After induction, the rats were ventilated through a facemask with 1 to 5 % isoflurane in the air, and the subcutaneously-implanted tissue-engineered cartilage in the back of rat was imaged by MRI and ultrasound devices, respectively. The rats after in vivo measurements were euthanized, and then the tissue-engineered cartilage was extracted from the back. The extracted tissue-engineered cartilage was used for the mechanical compression test and in vitro measurement.

Results/Discussion

Fig.1 shows an example of comparison between SOS values obtained by in vivo and in vitro measurements for 8 weeks of implantation. Here, five different tissue-engineered cartilages (#1 to 5, n = 6 for each type) were made and measured. Since both SOS values showed a good correlation, in vivo measurement of SOS is effective. Fig.2 shows an example of comparison between SOS values obtained by in vivo measurement and Young's moduli measured by the mechanical compression test. As the result, relations between SOS values and Young's moduli also showed a good correlation. These results revealed that in vivo evaluation of tissue-engineered cartilage elasticity is available through the SOS measurement.
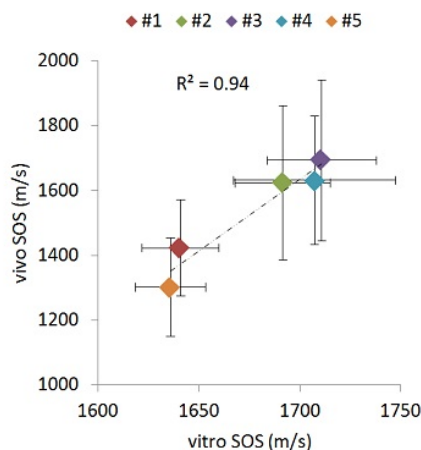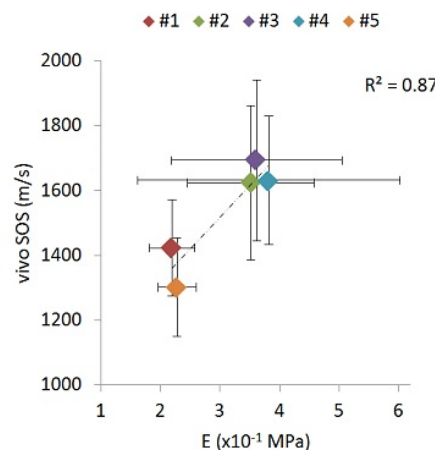
Fig. 1   Fig. 2

P1B6-11

8:00 am   Activation of Mechanosensitve Transcription Factors in murine C2C12 myoblasts by Focused Low-Intensity Pulsed Ultrasound (FLIPUS).

Regina Puts[1], Paul Rikeit[2], Karen Ruschke[2], Soyoung Hwang[3], Petra Knaus[1,2], Kay Raum[1]; [1]*Berlin-Brandenburg School for Regenerative Therapies, Charite Universitaet Berlin, Berlin, Germany*, [2]*Biochemistry, Freie Universitaet Berlin, Berlin, Germany*, [3]*Department of Biotechnology, Technische Universitaet Berlin, Berlin, Germany*

Background, Motivation and Objective

Quantitative Ultrasound (QUS) is a promising technique for bone tissue evaluation. Highly focused transducers, used for QUS, have also a capability to be applied for tissue-regenerative purposes and can provide geometrically controlled deposition of an accurate acoustic dose. This allows for overcoming of unwanted artifacts, i.e. standing waves, ring interferences, temperature elevations, cross-stimulation of adjacent wells, which often lead to irreproducible biological results, associated with existing Low-Intensity Pulsed Ultrasound (LIPUS) in-vitro set-ups. Focused LIPUS (FLIPUS) is a novel reliable tool, which is not prone to the aforementioned artifacts. This study aimed at the analysis of mechanical response in murine C2C12 myoblastic cells, possessing osteogenic-lineage differentiation potential, upon exposure to well controlled FLIPUS dose.

Statement of Contribution/Methods

The biological response of C2C12s was evaluated via measurement of activity of mechanosensitive transcription factors activator protein 1 (AP-1), specific protein 1 (Sp1) and TEA domain (TEAD) by luciferase reporter gene assay. In order to establish possible physiological function of the transcription factors, proliferation of C2C12 was assessed by BrdU assay. The cells in the set-up were stimulated by the defocused far field of the transducer from the bottom of the well plate, placed in the degased 37 ºC temperature-controlled water-bath, assuring homogenous distribution of intensity across the well. The 3.6 MHz frequency, selected for the stimulation, provided the most optimal sound transmission through the polystyrene well plate. The ultrasound was pulsed at 100 Hz PRF with 28% duty cycle. The calibrated output intensity was ISATA = 29.5 mW/cm2. No temperature change by the ultrasound exposure was observed in the well-plate.

Results/Discussion

As a result of our experiments the optimized acoustic dose induced 2 fold increase in AP-1 activity already after 5-minute exposure. The Sp1 activity was enhanced by about 40 % (p < 0.05) after the 5-min FLIPUS stimulation and the trend persisted for 30 min (p < 0.01) and 1 hour (p < 0.01) stimulation times. Activation of TEAD-binding sequences to about 2.3 fold (p < 0.01) was observed after the 5 min treatment. The proliferation of the C2C12 cells was up-regulated on day 1 and 3 of the everyday short-term FLIPUS-treatments. These results imply the pro-proliferative nature of the selected FLIPUS-dose in C2C12s, with potential functional role of the described transcription factors. Further investigation of the mechanism needs to be carried out. The well-accepted 20-minute LIPUS-stimulation, used in clinic, could be compared to

shorter stimulation time (i.e. 5 to 10 minutes) and optimized accordingly. The use of FLIPUS as a visualization and regenerative technique can be further applied in clinic as a device providing monitoring and healing of the damaged tissue.

P1B6-12 _____

8:00 am   The measurement of acoustic impedance of the cells cultured with five kinds of the fatty acid

Kazuyo Ito[1], Kenji Yoshida[2], So Irie[1], Jonathan Mamou[3], Hitoshi Maruyama[4], Tadashi Yamaguchi[2]; [1]*Graduate School of Engineering, Chiba University, Chiba, Japan,* [2]*Center for Frontier Medical Engineering, Chiba University, Chiba, Japan,* [3]*Lizzi Center for Biomedical Engineering, Riverside Research, New York, NY, USA,* [4]*Graduate School of Medicine, Chiba University, Chiba, Japan*

Background, Motivation and Objective

Accurate discrimination of non-alcoholic steatohepatitis (NASH) from simple fatty liver is a critical issue in current clinical practice because NASH may progress to cirrhosis or even liver cancer. Although the precise mechanisms of NASH progression remain unclear, some reports have shown differences in the content of free fatty acid (FFA) between controls and patients with NASH. Thus, an ultrasound-based diagnostic tool of NASH could be developed by assessing the acoustical properties of FFA. As a first step, this study aimed to evaluate the significance of acoustic impedance measurements using scanning acoustic microscopy (SAM) in order to investigate how FFA content affects the acoustic properties of liver cells at microscopic level.

Statement of Contribution/Methods

Five kinds of typical FFA were evaluated by SAM (i.e., palmitate (PA), oleate (OA), palmitoleate (PAOA), linolate (LA) and α linolenic acid (alpha)) and two sets of experiments were conducted. The FFAs were evaluated first in solution and then in cultured cells. A SAM system (modified AMS-50SI, Honda Electronics Co., Ltd, Japan) equipped with an 80-MHz center-frequency transducer was employed for measurement. The spatial resolution of the resulting images was 20-μm. The sample was located on a polystyrene plate and radio-frequency echo signals were acquired from the sample-polystyrene interface. The acoustic impedance was calculated based on relating the echo amplitude to the pressure-reflection coefficient. The 2-D map of acoustic impedance in a 2.4 * 2.4 mm^2 area was obtained by scanning the transducer in 16-μm steps. Three independent measurements of each sample were performed and the mean and standard deviation of the acoustic-impedance value were computed.

Results/Discussion

The results show that, in solution, all FFAs except PAOA have nearly the same acoustic impedance (Fig. 1a). The cultured-cell results revealed significant difference of acoustic-impedance (p < 0.01) except for PA and LA (Fig. 1b). Therefore, this study suggests FFAs had an effect on the properties of cells because they significantly affect acoustic impedance values. In addition, OA could be differentiated easily from all the other FFAs using acoustic-impedance measurements. Future work will focus on SAM studies at finer resolutions as well as using these results to develop an *in vivo* ultrasound method for NASH diagnosis.
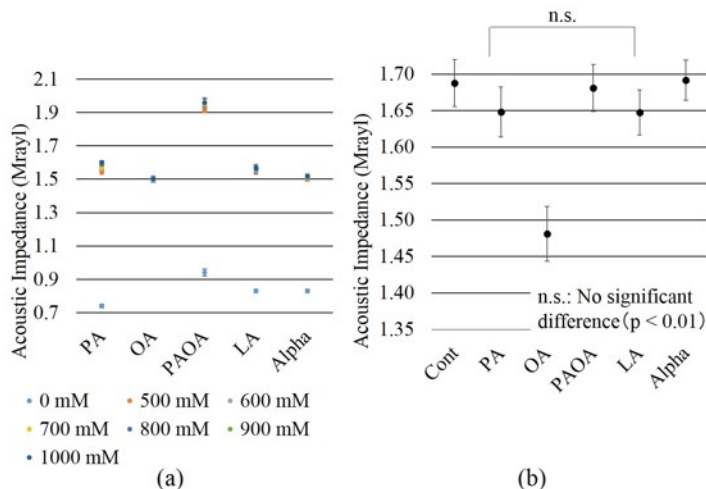
Figure 1: a) Acoustic impedance of types of FFA in solution. b) Acoustic impedance of five types of FFA in cultured cells. All measurements were performed using scanning acoustic microscopy at 80 MHz. (0 mM means solvent only and Cont means cultured cells only.)

P1B6-13 _____

8:00 am   Correction of scatterer-diameter and acoustic-concentration estimates in saturated high-frequency ultrasound signals acquired from cancerous human lymph nodes

Kazuki Tamura[1], Jonathan Mamou[2], Alain Coron[3], Kenji Yoshida[4], Tadashi Yamaguchi[4], Ernest Feleppa[2]; [1]*Graduate School of Engineering, Chiba University, Japan,* [2]*Lizzi Center for Biomedical Engineering, Riverside Research, USA,* [3]*Laboratoire d Imagerie Biomedicale, Sorbonne Unive* [4]*Center for Frontier Medical Engineering, Chiba University, Japan*

Background, Motivation and Objective

Choosing an appropriate dynamic range for acquiring radio-frequency (RF) data from a high-frequency ultrasound (HFU) system is challenging because signals can vary greatly in amplitude as a result of focusing and attenuation effects. In addition, quantitative ultrasound (QUS) methods are sensitive to saturated data. This study quantified saturation effects on effective scatterer diameter (*ESD*) and effective acoustic concentration (*EAC*). A representative dataset consisting of 82 dissected human lymph nodes included 22 metastatic lymph nodes was used and 3D RF data were acquired from these lymph nodes using a single-element transducer operating at a center frequency of 26 MHz.

Statement of Contribution/Methods

A raw unsaturated RF signal (x) was artificially saturated (x_{Sat}) and saturation was quantified by Saturate-SNR(SSNR=$20\log(\|x\|_2/\|x-x_{Sat}\|_2$) where $\|x\|_2$ is the l^2- norm of x). ESD_{Sat} and EAC_{Sat} were estimated from x_{Sat} for a wide range of SSNR values. Correction of EAC_{Sat} was performed by taking advantage of a linear relationship between EAC_{Sat} and S_x (l^1- norm of x).The slope of this linear relation was estimated by artificially saturating x_{Sat} to various degrees and plotting the computed value of EAC_{sat} vs. S_x for each SSNR value.The estimated EAC (EAC_{Est}) value was obtained at the intersection point of plotted line (Fig. 1a, red line), and value of S_x computed from desaturated RF signals using smoothing splines (Fig.1a, back line).

Results/Discussion

Saturation had no statistically significant effect on *ESD*; the average change in *ESD* value caused by saturation was less than 0.5 μm for each node (i.e., < 1.7 %). Fig. 1a illustrates the linear relationship between EAC_{Sat} and S_x as SSNR varies; EAC_{Est} was obtained after applying our correction algorithm. Fig. 1b displays how *EAC* changed before correction, after correction, and without any saturation for two illustrative nodes (cancer-free and metastatic). Fig.1c shows the relationship between SSNR and *EAC* error. The errors in corrected *EAC* values were near 0 dB/mm^3 for a wide range of SSNR values. The maximum mean error in EAC_{Est} was -0.60 dB/mm^3 when SSNR was

---

6.56 dB. Statistically-significant differences were found between corrected *EAC* values of metastatic and cancer-free nodes, which indicates that our correction method is applicable for tissue classification in the presence of echo-signal saturation.

Fig.1 :
(a) Linear relationship between S_x (l^1- norm of x) and *EAC*.
(b) Comparison of EAC values in cancer-free and metastatic nodes before and after correction.
(c) Relationship between SSNR and *EAC* error.
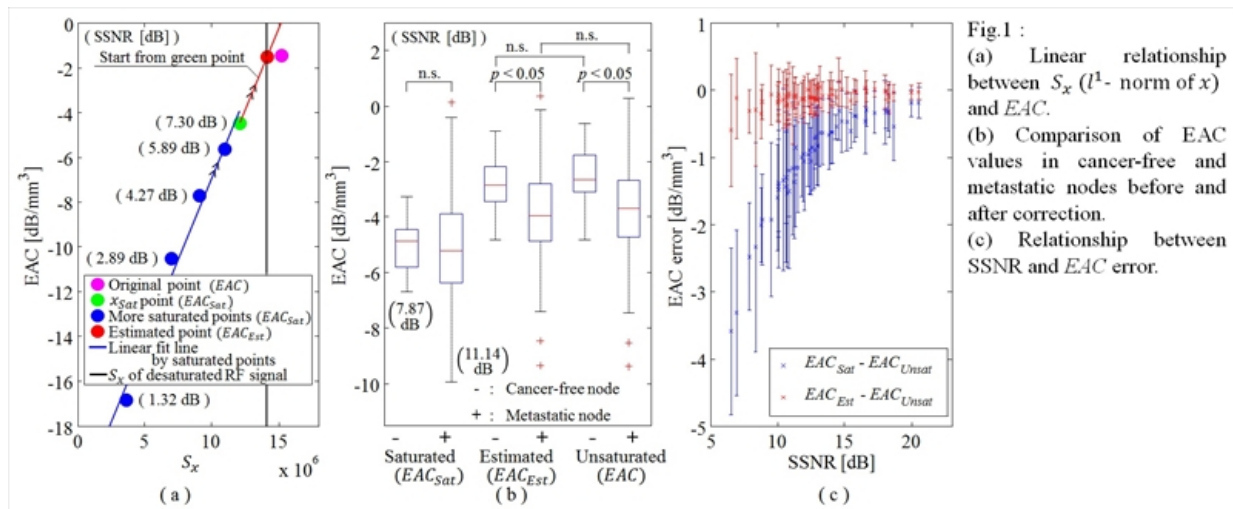
P1B6-14

8:00 am   A New Tissue-mimicking Material for Phantoms

Kazuishi Sato[1], Tomoji Yoshida[1], Toshio Kondo[1], Masahiko Taniguchi[2], Kazuhiro Yasukawa[2]; *[1]Tokushima Bunri University, Sanuki, Kagawa, Japan, [2]Takiron Co., Ltd., Kobe, Japan*

Background, Motivation and Objective

Various phantoms have been developed for the quality assurance testing and clinical calibration of ultrasound systems. Existing phantoms are composed of hydrogels. The phantoms using the gels for tissue-mimicking material (TMM) conform the IEC standard[1], but they lack long-term stability. Therefore, we developed swollen Segmented Polyurethane Gel[2] (S-SPUG) with long-term stability, but the gel had the problem that the acoustic velocity and density were not satisfied the IEC standard. In order to solve the problem, we have intended to develop a new gel with any desired acoustic velocity and very little attenuation.

Statement of Contribution/Methods

In the phantom developed previously, the S-SPUG dispersed poly(methyl methacrylate) (PMMA) particles has been used to achieve the desired acoustic velocity and density. Our experimental results have indicated that the acoustic velocity of the S-SPUG with a density of 1.05×10^3 kg/m^3 is lower than 1570 m/s. As a result the S-SPUG cannot meet the IEC standard. To achieve complete conformance of a TMM to the IEC standard, we proposed that 1-Butyl-3-methylimdazlium thiocyanate ([BMIM]$^+$ [SCN]$^-$)[3] of ionic liquid(IL) is adopted to the S-SPUG. The acoustic velocity and density of the S-SPUG without PMMA particles are 1423 m/s and 1.03×10^3 kg/m^3, respectively and those of [BMIM]$^+$ [SCN]$^-$ are 1779 m/s and 1.07×10^3 kg/m^3, respectively. In the S-SPUG, liquid exists among S-SPUG networks as dispersion media. As results, the S-SPUG with an appropriate mixing ratio of [BMIM]$^+$ [SCN]$^-$ and PMMA particles in the liquid may have the same acoustic velocity and density defined in the IEC standard. The vapor pressure of IL is zero and the property serves to long-term stability of the S-SPUG. As the dynamic viscosity of [BMIM]$^+$ [SCN]$^-$ is a low value of 59.8 mPa·s, it has little effect on the attenuation of the gel. The experimental relationship between acoustic velocities, densities and concentrations of [BMIM]$^+$ [SCN]$^-$ in the S-SPUG without PMMA particles have been obtained. The optimum concentration of PMMA particles in the S-SPUG have been calculated on Urick′s model[4]. On these results we have derived the optimum equation for concentration of [BMIM]$^+$ [SCN]$^-$ and PMMA particles in the S-SPUG of the TMM conformed the IEC standard.

Results/Discussion

We have developed a new gel with any desired acoustic velocity and very little attenuation. The TMM using the gel dispersed PMMA particles conforms to acoustic velocity and density defined the IEC standard.

References

1. IEC 61685 (2001)

2. K. Yasukawa et al.:2007 IEEE Ultrasonics Sympsium 2501.

3. S. Singh et al.: J. Molecular Liquid, (2014).

4. R. J. Urick: J. Appl. Phys. 18(1947) 893.

P1B6-15

8:00 am   Differentiation of normal tissue and tissue lesions using statistical properties of backscattered ultrasound in breast

Andrzej Nowicki[1], Hanna Piotrzkowska-Wroblewska[1], Katarzyna Dobruch-Sobczak[2], Jerzy Litniewski[1], Barbara Gambin[1], Michal Byra[1], Eleonora Kruglenko[1]; *[1]Ultrasound, Institute of Fundamental Technological Research, Warsaw, Poland, [2]Maria Sklodowska-Curie Memorial, Cancer Center and Institute of Oncology, Warsaw, Poland*

Background, Motivation and Objective

The scattering is the fundamental phenomena used for US imaging of specific organs. In this study the method searching for best fitted statistical distribution (moments, fractional moments and Lorentz estimator for Nakagami)) of the acquired echoes from the breast tissue is discussed, especially addressing the ''effective'' number of scatterers. The aim of the study was finding the relationship between Birads classification combined with envelope K and Nakagami statistics of the echoes backscattered in the breast tissue in vivo and the histological data for normal tissue and the pathological lesions.

Statement of Contribution/Methods

129 patients with 191 suspicious breast lesions (BIRADS 3, 4a, b, c, 5) were examined. The analysis method

was based on the parametric imaging representing a map of local statistical properties of the scattering of ultrasound waves

in normal and pathological tissues. Both, the RF echo-signal and B-mode images from the lesions and surrounding tissue were recorded. The statistics of backscattered speckle-like echoes envelopes were modeled using K and Nakagami distributions. For all lesions the set of sub-ROIs covering full lesion was chosen. The statistical analysis was done for every sub-ROI separately after normalizing the sub-ROIs envelopes against their average amplitude. For each patient the statistics of the surrounding ''normal'' tissue was also calculated.

FRIDAY POSTER

Results/Discussion

The evaluation of all 191 breasts lesions revealed 83 malignant and 108 benign lesions. Typically both; K and Nakagami shape parameters for malignant lesions were statistically larger than for surrounding tissue. On the other hand, the benign lesions revealed much larger variance of the parameters comparing to the surrounding and malignant tissue. The sensitivity and specificity of B-mode imaging with the cut-off points BIRADS-4b/4c were 86,4% and 93%, respectively. For K distribution the sensitivity and specificity were 68,75% and 84% while for Nakagami statistics the sensitivity and specificity were 68, % and 92%, respectively. Combine K and Birads resulted in better sensitivity of 90,63% and specificity of 96%. Finally, the combined statistics Birads plus Nakagami statistics showed an even better sensitivity of 94,5% with unchanged (comparing to K+Birads) specificity of 96%. The quantitative measurements of the breast tissue backscattering statistical properties combined with the Birads 4b/4c cut-off improve by 8% the specificity and can be helpful in the differentiation the character of the breast lesions - malignant or benign.

P1B7 - MBF: Flow Estimation Strategies: From 1D to 3D

4th floor

Friday, October 23, 2015, Posters displayed 08:00 am - 05:00 pm. Authors must be present at their poster from 9:30 - 10:30am (odd number posters) and 14:30 – 15:30pm (even number posters).

Chair: **Jørgen Jensen**
             Technical University of Denmark

P1B7-1 _____

8:00 am   Real-time pulse compression in multigate spectral Doppler imaging

Alessandro Ramalli[1], Alessandro Dallai[1], Enrico Boni[1], Francesco Guidi[1], Stefano Ricci[1], Piero Tortoli[1]; *[1]Information Engineering Department, University of Florence, Firenze, Italy*

Background, Motivation and Objective

The quality of Doppler ultrasound blood flow investigations is often limited by a low signal-to-noise ratio (SNR) due to the weak energy backscattered by erythrocytes. Pulse compression methods based on the transmission of coded pulses can improve the penetration depth while preserving the axial resolution. However, the high computational cost and the mismatch that tissue frequency-dependent attenuation produces on the receiver filter, has so far limited its real-time application. Pulse compression implementation in a real-time Doppler imaging system is here presented. Experiments show that significant improvement in multigate spectral Doppler (MSD) imaging is obtained both in vitro and in vivo.

Statement of Contribution/Methods

The arbitrary waveform generators of the ULA-OP research scanner coupled to the linear array probe LA533 (Esaote, Italy) are programmed to transmit 5μs-long linear chirps tapered by a 10% Tukey window. The chirp bandwidth (B) is programmed between 1 and 6 MHz in steps of 1 MHz. For each pulse repetition interval, the echo-signals received by 64 array elements from a selected scan line are dynamically beamformed, quadrature demodulated and down-sampled to cover a depth range of 35 mm. These samples are Fourier transformed by the on-board DSP through an efficient 1024-point FFT. The corresponding complex spectrum is multiplied by the coefficients of a suitable chirp filter and finally inverse-transformed to the time domain. The slow-time Doppler data from 512 consecutive depths are further elaborated by the DSP to extract the complex spectra modules that are formatted in MSD frames. The performance of the compression is evaluated by comparing the MSD frames obtained by the interleaved transmission of standard and chirp pulses having the same amplitude.

Results/Discussion

Experiments on a flow phantom allowed evaluating the effects of B on axial resolution and SNR. The former, as expected, improves with increasing bandwidth, while the SNR gain decreases showing a maximum of 13 dB for B=1 MHz. A possible justification of this behavior in terms of selective tissue attenuation will be discussed.

Examples of in-vivo applications like in Fig.1, confirming a significant SNR increase, will also be presented. These results show that chirp-based pulse compression is an effective means to improve SNR in spectral Doppler applications.
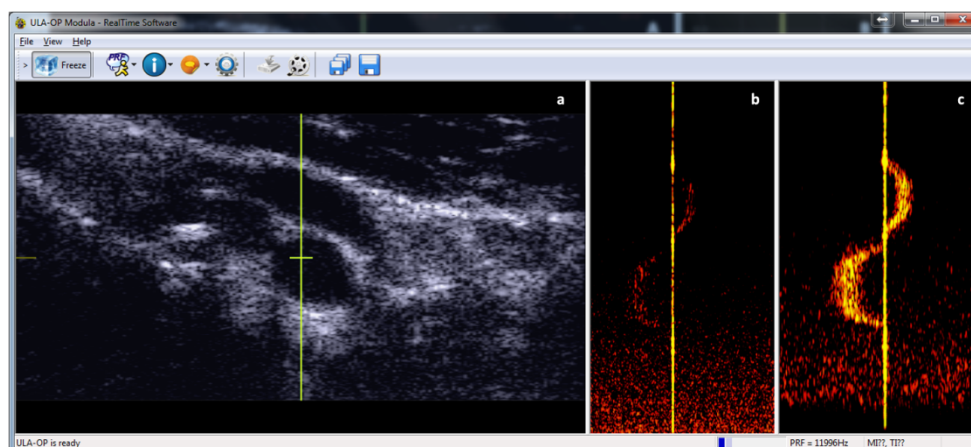
Fig. 1 ULA-OP real-time display. B-mode image of the jugular vein and carotid artery of a healthy volunteer (a); the yellow line highlights the MSD scan line. Spectral profiles obtained by transmitting a 5-cycle sine burst (b) and a 5μs-long linear chirp with 3 MHz bandwidth (c), both at 1.9 V transmission amplitude and 8 MHz center frequency.

P1B7-2 _____

8:00 am   A robust spectral envelope detection algorithm for automated blood flow measurements

Aditi Kathpalia[1,2], Yücel Karabiyik[2], Bente Simensen[3], Eva Tegnander[3,4], Sturla Eik-Nes[3,4], Hans Torp[2], Ingvild Kinn Ekroll[2,5], Gabriel Kiss[2]; *[1]School of Biomedical Engineering, Indian Institute of Technology (BHU), Varanasi, India, [2]Department of Circulation and Medical Imaging, Norwegian University of Science and Technology, Trondheim, Norway, [3]National Center for Fetal Medicine (NCFM), St. Olavs Hospital, Trondheim, Norway, [4]Department of Laboratory Medicine, Children's and Women's Health (LBK), NTNU, Trondheim, Norway, [5]St. Olavs Hospital, Trondheim, Norway*

Background, Motivation and Objective

Maximum velocity (MV) estimation in a Doppler Sonogram is of clinical interest as it indicates severity of stenosis. It is also used in obstetrics to calculate Doppler indices for monitoring placental function, fetal growth retardation and detecting pregnant women at risk for preeclampsia. The aim of this work is to develop an automated and robust technique for accurate maximum velocity envelope estimation which works for a broad range of SNRs.

Statement of Contribution/Methods

Two existing approaches to maximum velocity estimation, the Geometric method (GM) (Marasek, 1994) and the Signal Noise Slope Intersection (SNSI) method (Steinman, 2000) are combined in the new approach. Further, a data adaptive validity check is introduced that makes the proposed technique independent of user defined parameters. In the new algorithm, the decision of including a temporal bin to the envelope estimate is automatically decided based on a power threshold, calculated as the 90th percentile of

the noise power distribution. If the mean power of the temporal bin lies above this threshold, the maximum frequency is calculated based on steps from GM and SNSI, illustrated in panel A). An interpolated and smoothened version of the envelope is then further used to automatically calculate the pulsatility index (PI) as well as the (fetal) heart rate, where the latter is based on autocorrelation of the envelope data. Beam-formed IQ data was acquired from a commercial ultrasound system (Vivid E9, GE Vingmed, Norway).

Results/Discussion

Panels B) and C) show envelope traces obtained by the proposed method from the uterine and umbilical artery of a healthy pregnant volunteer. In both cases the SNR was relatively high (22 and 29 dB), and the method gives seemingly good traces of the maximum velocity envelope. The PI was also calculated in the case of the umbilical recording, with a value of 1.01, corresponding well with the value found during the routine examination. The robustness of the method to low SNR conditions was examined using a recording of flow from the subclavian artery of a healthy volunteer. The examples shown in panels D) - F) have an estimated SNR of 3.5 dB. D) and E) show envelope traces without and with the automatic thresholding, whereas F) shows the spectrum and velocity trace as it appeared on the display of the commercial system.
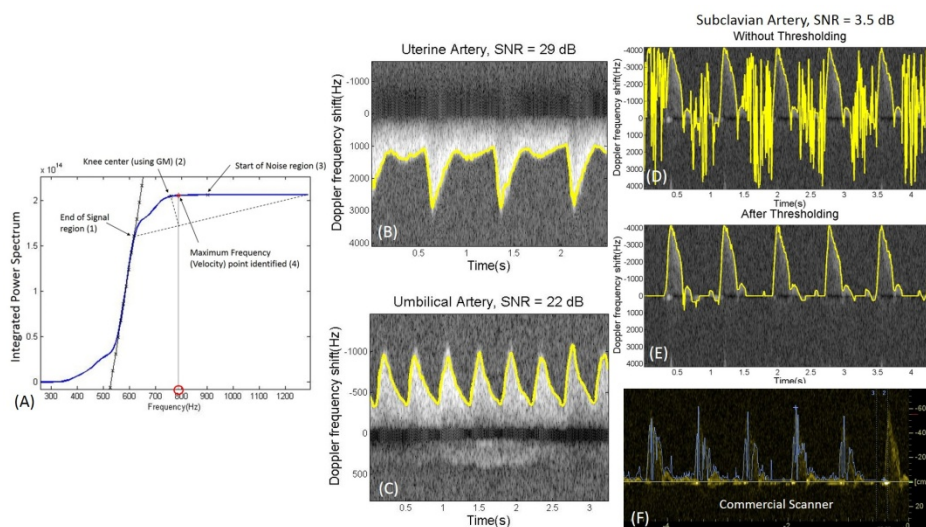
8:00 am   **Contrast-based Transient Flow Vector Distribution in Arterial Stenosis based on Plane Wave Bubble Wavelet Imaging and Modified Optical Flow Method**

Diya Wang[1], Bowen Jing[1], Jinjin Wan[1], Yingjie Jia[1], Yu Zhang[1], Mingxi Wan[1]; [1]*The Key Laboratory of Biomedical Information Engineering of Ministry of Education, Department of Biomedical Engineering,School of Life Science and Technology,Xi`an Jiaotong University, Xi`an, Shaanxi, China, People's Republic of*

Background, Motivation and Objective

Contrast-based arterial flow vector distribution (FVD) has been deeply studied to underpin insight into cardiovascular disease diagnosis, particularly in arterial stenosis. However, discontinuous microbubble (MB) flow in the imaging plane is difficult to be accurately tracked by conventional optical flow method because of the disordered and rapid motions of MBs and their non-real-time captured echoes. Although such echoes can be real-time acquired by ultrasound contrast plane wave imaging (UCPI), it is limited by low contrast-to-tissue ratio (CTR) and detection sensitivity of MBs, especially, near arterial wall. The objective of this study was to accurately obtain the transient FVD of MBs in arterial stenosis by modified optical flow method based on UCPI images with high CTR and sensitivity.

Statement of Contribution/Methods

A bolus injection experiment was performed in an arterial stenosis flow phantom using inverted plane waves at 400Hz frame rate controlled by Sonix-Touch. The CTR of UCPI images and detection sensitivity of MBs was then improved by pulse inversion bubble wavelet imaging (PIWI) technique based on a pair of inverted MB wavelet constructed according to the modified Herring equation (Diya Wang et al., 2014 IEEE Ultrason. Symp. Pro., pp. 1762-1765). Transient displacement and FVD of MBs among a set of UCPI images with high CTR and sensitivity were obtained by a modified optical flow method, which added a discontinuity preserving spatio-temporal smoothness constraint, to accurately mark and evaluate the hemodynamic feature in the stenosis.

Results/Discussion

FVD of MBs in the arterial stenosis was depicted clearly by PIWI-based UCPI. CTR of UCPI in the stenosis and detection sensitivity of MBs near arterial wall were improved respectively by up to 10.09 ± 2.77 dB and 4.54 dB, compared to those obtained using pulse inversion harmonic imaging. Axial MB velocity in the stenosis was 28.45 ± 3.05 mm/s; it was in accordance with the set value. Moreover, compared with results obtained by the conventional Brox and Lucas Kanade optical flow methods, an anticlockwise vortex of MBs in the distal was described more accurately by the transient FVD obtained using the modified optical flow method. It indicated that contrast-based transient FVD in the arterial stenosis can be acquired accurately by PIWI-based UCPI combined with modified optical flow method.
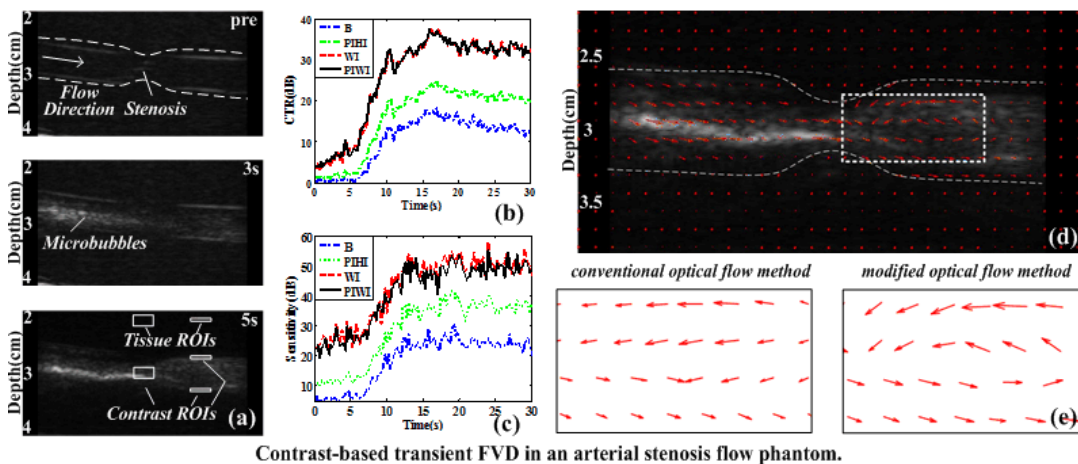
Contrast-based transient FVD in an arterial stenosis flow phantom.

(a) Typical PIWI-based UCPI images; (b) CTR in the stenosis and (c)detection sensitivity of MBs near arterial wall based on B mode, pulse inversion harmonic imaging (PIHI), bubble wavelet imaging (WI) and PIWI; (d) transient FVD of MBs obtained by modified optical flow method, compared with the conventional method (e). The dynamic range of such images is 48 dB and their gray scale range is [0,1].

P1B7-4

8:00 am　Robust blood velocity estimation using point-spread-function-based beamforming and multi-step speckle tracking

Anne E.C.M. Saris[1], Maartje M. Nillesen[1], Stein Fekkes[1], Hendrik H.G. Hansen[1], Chris L. de Korte[1]; [1]*Medical UltraSound Imaging Center (MUSIC), Department of Radiology and Nuclear Medicine, Radboud university medical center, Nijmegen, Netherlands*

Background, Motivation and Objective

Speckle tracking enables 2D blood velocity estimation. Since speckle quickly decorrelates due to high velocity gradients, high frame rate imaging is crucial for capturing high velocity blood flow. This however, hinders estimation of low velocities since interframe displacements drop below the data sampling resolution. To capture subsample motion, often 1D parabolic fitting of the peak of the cross-correlation function (CCF) is performed. We propose to capture the CCF peak in a standardized way, by beamforming according to the dimensions of the point-spread-function (PSF), followed by 2D cubic interpolation of the peak. This ensures an optimal match between the peak and the interpolation method and we expect this to increase the robustness and accuracy of speckle tracking for a larger range of velocities.

Statement of Contribution/Methods

Parabolic flow (v_{max} = 1.5 m/s) was generated in a phantom with a lumen diameter of 0.6 cm, centered at 2 cm depth. A linear array transducer (f_c = 9 MHz, 198 µm pitch, 192 elements) transmitting plane waves was simulated using FIELD II to generate ultrasound element data (f_s = 36 MHz) for a range of pulse repetition frequencies (PRF) (2.5 - 15 kHz) and beam-to-flow angles (70° – 110°). Radiofrequency (RF) data were beamformed on a PSF-based grid and a conventionally spaced grid (dx = pitch, dy = 1540/2fs). Velocities were first estimated using large windows of envelope data and next refined using smaller windows of RF data. Use of the PSF-based sampled data resulted in better defined circular CCFs for both steps (Fig. 1A). Both 2D cubic and 1D parabolic interpolation were compared for subsample motion estimation. *In vivo* data from a healthy common carotid artery were obtained using a Verasonics V1 equipped with an L12-5 transducer (PRF = 7.5 kHz) to further investigate the performance of the method.

Results/Discussion

Simulations show highest accuracy, i.e., lowest RMSEs, for the PSF-based method combined with 2D cubic interpolation to estimate the lateral and axial velocity component for all beam-to-flow angles and PRFs. Median and percentile (5-95%) RMSE scores obtained for an angle of 84° are shown in Fig. 1B. The findings are corroborated by *in vivo* results (Fig. 1C) showing the most consistent flow using the PSF-based method. PSF-based, multi-step speckle tracking thus allows for robust vector velocity estimation over a large range of velocities.
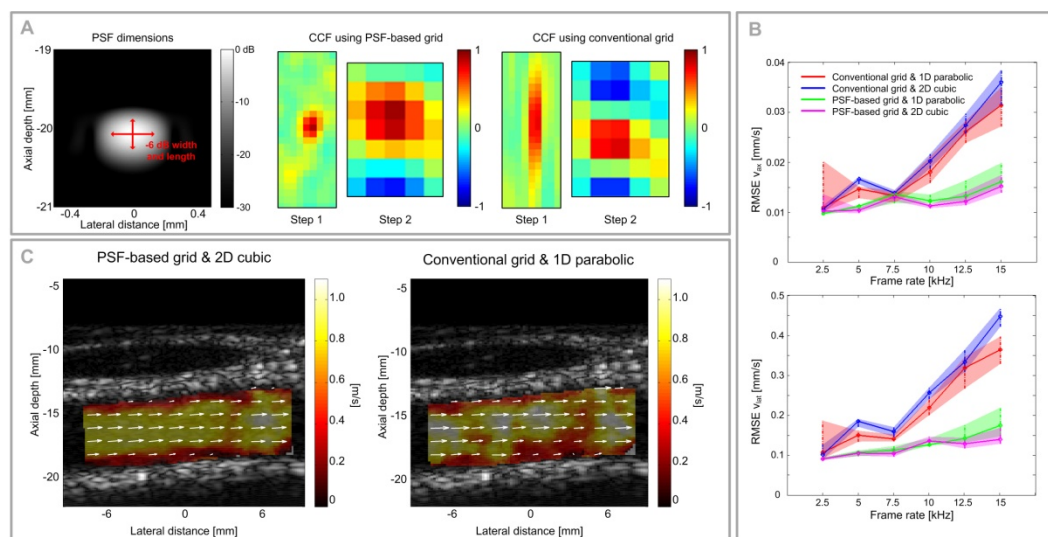
8:00 am   Two Dimensional Blood Velocity Estimation Using High Frame Rate Echocardiography with Transverse Oscillation Approach

Hiroki Takahashi[1], Hideyuki Hasegawa[1]; [1]*Graduate School of Science and Engineering for Research, University of Toyama, Toyama-shi, Toyama, Japan*

Background, Motivation and Objective

Two-dimensional (2D) blood velocity imaging inside the cardiac cavity with transthoracic echocardiography is of value in the evaluation of cardiac pumping function. Echoes from blood cells under fast flow could be measured at high temporal resolution by transmission of diverging beam and parallel beamforming (DB-PBF). Speckle tracking applied to echoes from blood cells can estimate 2D blood velocity. However, the accuracy in estimation of the transverse velocity by speckle tracking is decreased due to a low spatial frequency in the lateral direction caused by unfocused transmission and a small aperture of a phased array. In this study, the effect of the transverse oscillation (TO) method [J. A. Jensen and P. Munk, IEEE Trans. UFFC, 1998] with DB-PBF for 2D blood velocity estimation was examined.

Statement of Contribution/Methods

Echoes from the cardiac cavity were measured at a high frame rate of 6024 Hz by transmission of a single diverging ultrasound in the forward direction and receive PBF. A symmetric apodization with two separate amplitude peaks based on the Hann window was used during receive beamforming to create TO. 2D blood velocities were estimated using speckle tracking based on the beamformed signals after clutter suppression filtering. For a stable estimation of blood flow velocity, a 2D correlation function between two consecutive frames was temporally averaged for 12 times (frames) corresponding to about 2 ms. A steady flow measurement of blood mimicking fluid in a tissue mimicking phantom was implemented to compare the accuracy of speckle tracking coupled with and without the TO method.

Results/Discussion

Figure (a) shows errors in direction of velocity estimates under tubular flow at a beam-to-flow angle of 34 degree. Fast flows with higher mean velocities of 0.4 and 0.6 m/s were simulated by changing twice and triple of the frame intervals of the original echo data to keep the Reynolds number of 950. The experimental result revealed that the directional error was reduced from 21.2% to 10.3% by the TO method under a mean flow velocity of 0.6 m/s. It was found that speckle tracking with DB-PBF for measurement of 2D blood velocity could be improved using the TO method. Furthermore, the diastolic vortex flow in the left ventricle was visualized by 2D velocity vectors obtained with the TO method in an in vivo experiment of a healthy human heart as shown in Fig. (b).
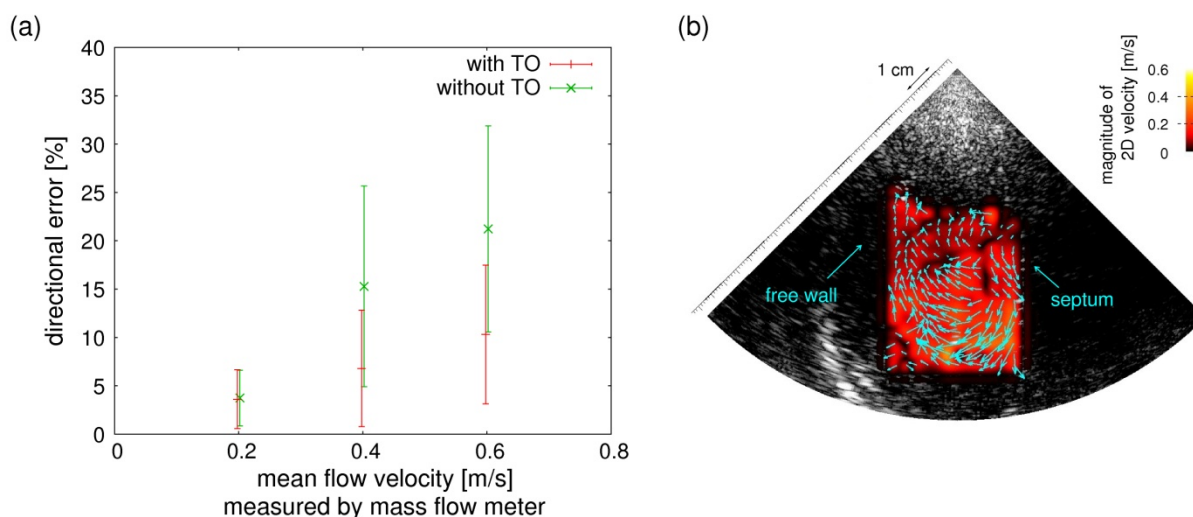
8:00 am   High Frame Rate Vector Velocity Estimation using Plane Waves and Transverse Oscillation

Jonas Jensen[1], Matthias Bo Stuart[1], Jørgen Arendt Jensen[1]; [1]*Dept. of Elect. Eng, Technical University of Denmark, Kgs. Lyngby, Denmark*

Background, Motivation and Objective

Transverse oscillation (TO) vector velocity estimation visualizes blood flow patterns in the human body without the need for angle correction. Currently, the method employs focused beams and suffers from a frame rate, which is too low for capturing the complex flow phenomena and full flow dynamics. The objective of this paper is to show the feasibility of TO implemented in a very fast imaging sequence using plane waves to obtain flow estimates for a large field of view. The performance of the method is demonstrated in measurements.

Statement of Contribution/Methods

A 5 MHz BK8812 linear array transducer is connected to the experimental SARUS scanner. All 128 elements are excited simultaneously to emit a plane wave, and the elements are used with a Tukey window in transmit to reduce the artifacts from edge waves. Parabolic flow in a 6 mm radius tube in a flow rig system is scanned and the volume flow is measured by a magnetic flow meter for reference. The vessel is at a depth of 34 mm and an emission sequence is made with a pulse repetition frequency of 6 kHz. Flow with three different peak velocities (0.1, 0.3 and 0.5 m/s) are measured at beam-to-flow angles of 90, 75 and 60 degrees. A dynamic apodization in receive creates a transverse oscillating field with constant lateral wavelength in the region of interest. Beamformed signals are then used with a standard fourth order estimator to employ velocity estimates in the axial and lateral directions.

Results/Discussion

The performance of the vector velocity estimation is assessed through the relative mean bias and standard deviation (std.) when using 128 emissions per estimate. A bias of -9.4% is obtained at 90 deg. for the lateral velocity component along with a std. of 8.3%. A vector flow image (VFI) for a measurement at 75 deg. beam-to-flow angle is shown to the left in the figure, and the velocity profile at the center line is shown to the right. The bias is -3.22% for the measurement and the angle is estimated to 75.4 +/- 1.8 degrees. The method provides continuous data and 2-D velocity estimates for a VFI of 10 mm width and at a frame rate of 6 kHz, which makes it applicable for, e.g., both slow and fast flow estimation.

Mean bias is -3.22 %, mean std. is 7.99 %
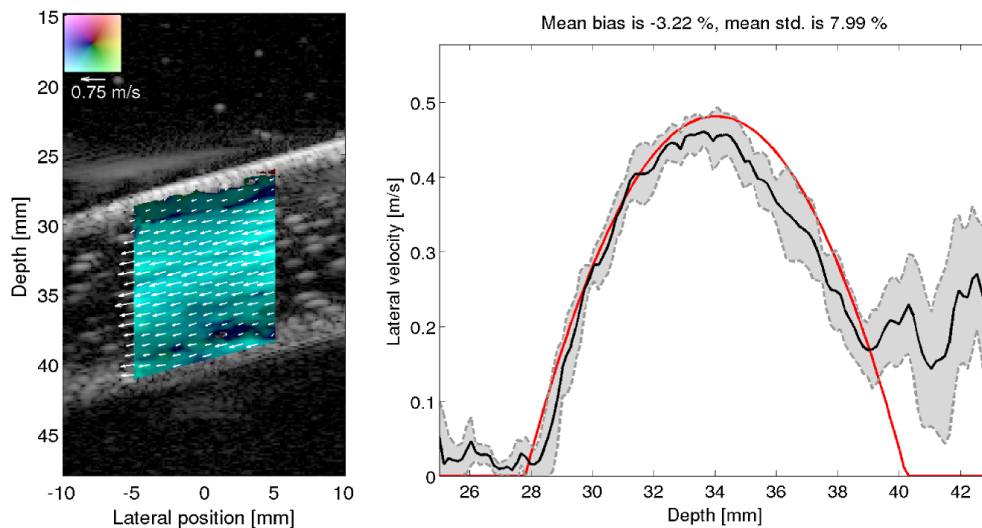
P1B7-7

8:00 am   Multi-angle imaging for robust vector Doppler and coherent compounding

Ingvild Kinn Ekroll[1,2], Jørgen Avdal[1], Abigail Swillens[3], Hans Torp[1], Lasse Løvstakken[1]; [1]*Norwegian University of Science and Technology, Norway*, [2]*St Olav's Hospital, Norway*, [3]*Ghent University, Belgium*

Background, Motivation and Objective

Multi-angle plane-wave imaging provides new opportunities for high frame rate vector-Doppler imaging, as well as improved low flow imaging by providing longer temporal ensembles and the possibility of coherent compounding. However, to achieve robust vector-Doppler estimates and a significant effect of the coherent compounding process a high number of angled plane waves is desired. This comes at the expense of aliasing in vector-Doppler (lowered PRF) and motion artifacts (SNR loss, blood velocity bias) in the compounding process (Ekroll et al., "On the accuracy of coherent compounding in Doppler imaging", Proc. IUS, 2014).

Statement of Contribution/Methods

In this work we investigate how to increase the robustness of both these approaches by using a weighted least-squares vector-Doppler (VD) approach to 1) avoid aliasing in general and 2) to compensate for motion artifacts in coherent plane wave compounding. The VD technique was implemented using linear regression of N Doppler estimates per image pixel. Least squares errors were weighted with spatial correlation in the compounded image to resolve aliasing ambiguities. The VD estimates were further used for 2D motion correction in the coherent compounding image formation. The method was tested using simulations of complex flow conditions (N = 5, $\theta_{max}=\pm15°$) using a patient specific model of the carotid artery bifurcation and further tested on data from the common carotid artery of a healthy volunteer.

Results/Discussion

The carotid bifurcation simulations showed that the proposed VD technique was able to correctly resolve ambiguities in aliased regions. This is illustrated in panels a)-c) in the Figure, showing peak systolic color flow and vector velocity fields. The normalized RMS errors for the Vx and Vz component were 10% and 5% of the respective velocity ranges when including estimates from the whole image region. Panels in the second row show *in vivo* PW Doppler spectra and mean velocity (autocorrelation) traces d)-f) and finally mean velocity estimate statistics g) from a healthy volunteer. Single plane wave estimates are used for reference. The figures demonstrate how motion correction based on the proposed VD estimation technique can be used to 1) avoid SNR loss in spectral Doppler due to incoherent summation, and 2) substantially decrease mean velocity bias, especially in the presence of high flow speeds (systole).
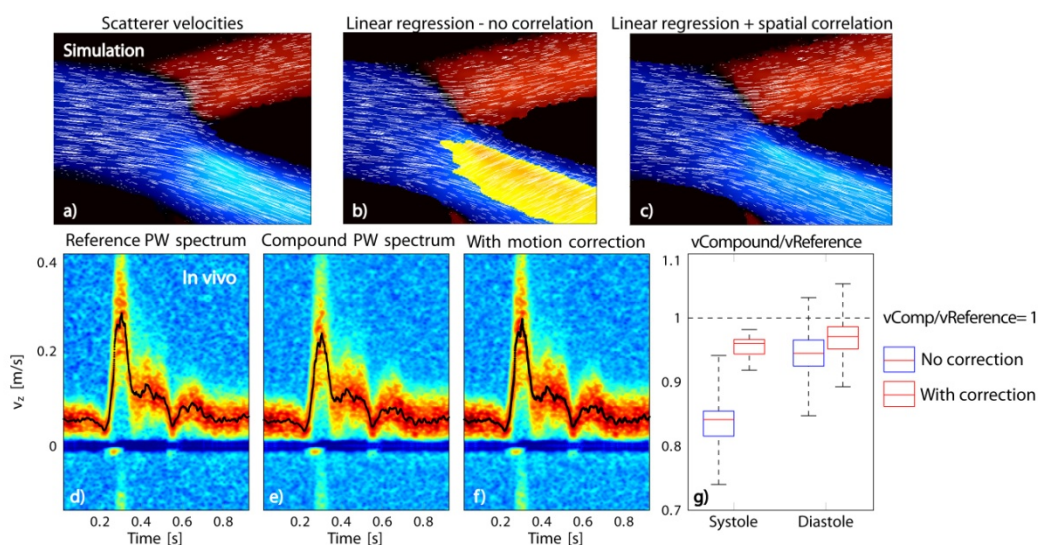
P1B7-8

8:00 am   *In-vivo* **High Dynamic Range Vector Flow Imaging**

Carlos Armando Villagómez Hoyos[1], Matthias Bo Stuart[1], Jørgen Arendt Jensen[1]; *[1]Technical University of Denmark, Denmark*

Background, Motivation and Objective

Studying hemodynamic patterns is highly relevant for evaluating the physiological state of the cardiovascular system. In current ultrasound systems, a limited range of 2-D vector flow velocities are detectable during a cardiac cycle. In today's clinic, ultrasound devices are configured either to measure during the systolic or the diastolic phase. Thus, limiting the dynamic range of the velocity estimates. In this work, a high frame rate 2-D vector velocity estimator which make use of an adaptive lag and echo-canceling filter to obtain a high dynamic range is presented.

Statement of Contribution/Methods

In-vivo datasets with a continuous data sequence are acquired using the SARUS scanner and a BK Medical 8670 linear transducer. The system pulse repetition frequency (PRF) is set to 15 KHz. Defocused waves are emitted and the received signals are directionally beamformed and cross-correlated to pre-estimate 2-D vector velocities. An independent lag and echo-canceling filter is adaptively selected at each estimation point. Synthetic aperture is then used to generate high-resolution images, which are directionally beamformed at the pre-estimated flow direction and cross-correlated at the selected lag to produce the high dynamic range 2-D vector velocities estimates. The acoustic output of the sequence was measured to be I_{spta} = 144.3 mW/cm^2 and a MI = 0.91, both within the FDA limits.

Results/Discussion

A single frame from an *in-vivo* measurement performed on the jugular vein and carotid artery of a 27 year old healthy male individual is shown. The vector flow imaging (VFI) map on the left shows the flow in the jugular vein passing through a valve during the diastolic phase of the cardiac cycle. Venous flow is detected through all the mapped vessel during the whole cardiac cycle. The carotid artery is also shown on the VFI map. On the right a single point from the VFI map is selected and plotted for the vein and artery. Is shown that the flow is detected during the whole cardiac cycle for both vessels, effectively expanding the dynamic range of 2-D vector velocity estimation.
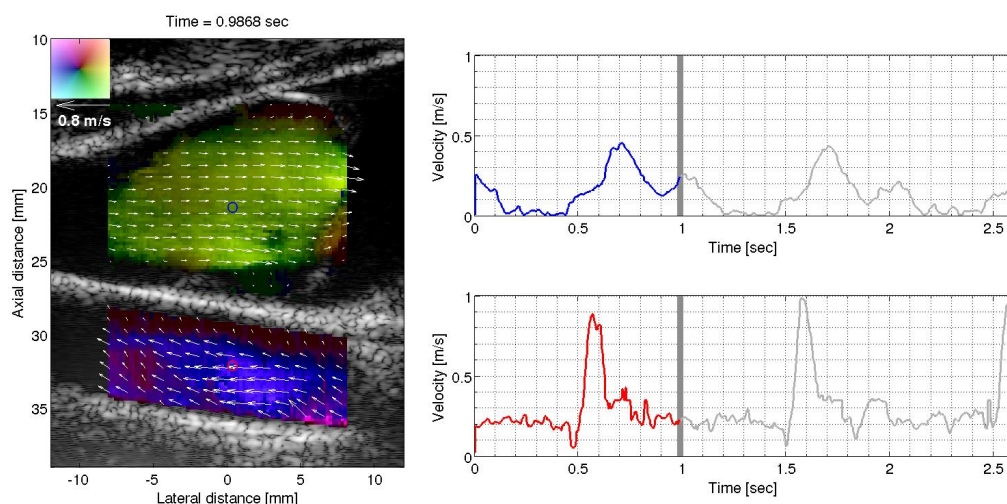
P1B7-9

8:00 am   **3-D Vector Flow Estimation with Row-Column Addressed Arrays**

Simon Holbek[1], Thomas Lehrmann Christiansen[2], Morten Fischer Rasmussen[1], Matthias Bo Stuart[1], Erik Vilain Thomsen[2], Jørgen Arendt Jensen[1]; *[1]Department of Electrical Engineering, Technical University of Denmark, Lyngby, Denmark, [2]Department of Micro- and Nanotechnology, Technical University of Denmark, Lyngby, Denmark*

Background, Motivation and Objective

For real-time ultrasonic 3-D volumetric imaging and velocity estimation a 2-D array transducer is needed. The complexity associated with fabricating 2-D matrix arrays with a large number of channels have led to the development of row-column (RC) addressed transducer arrays. The number of individual connections to the array is thereby reduced from N^2 to 2N. So far, only the imaging properties of such arrays have been investigated. It is here demonstrated that RC arrays can also be used to estimate 3-D vector flow using the Transverse Oscillation (TO) method.

Statement of Contribution/Methods

A 3 MHz, λ/2 pitch 2-D array with 64 rows and 64 columns was simulated in Field II. Velocities were estimated from a simulated cylendrical blood vessel (Ø = 12 mm) located at 3 cm depth with parabolic flow, a peak velocity of 1 m/s and a 90 degree beam-to-flow angle. To obtain RF data for estimation of all three velocity components, the emission sequence was alternating between emitting on the rows and recieving on the columns and vice versa. At a PRF of 3.2 kHz, 2x32 focused emissions were emitted one line at a time to sweep across 11 different directions within a plane perpendicular to the vessel, see Fig 1. Beamformation was performed with an in-house-developed RC-beamformer, and velocities were estimated by using the TO method. Estimates from 10 frames were scan converted, interpolated, and averaged to get the mean 3-D vector flow estimate.

Results/Discussion

A colormap of the estimated 3-D vector flow is seen in Fig. 2. Projections of the mean velocity component along the flow direction (v_x) are illustrated as shadowed areas, the standard deviations as dashed lines and the expected values as red lines. On the right side the velocity profile for a line through the center of the vessel in the *z*-direction is shown, and the left side shows the corresponding velocity profile in the *y*-direction. Relative mean bias for the velocities through the center of the vessel in the z-direction was (-8.6%, -0.6%, -0.1%) for (v_x, v_y, v_z) respectively. Peak velocity found from the 3-D vector flow image was 1.02 m/s which was 2% higher than expected. The results shows for the first time, that 3-D vector flow can be estimated with RC-arrays, despite their reduced number of channels.

Simulation Setup

Fig. 1

3-D Vector Flow
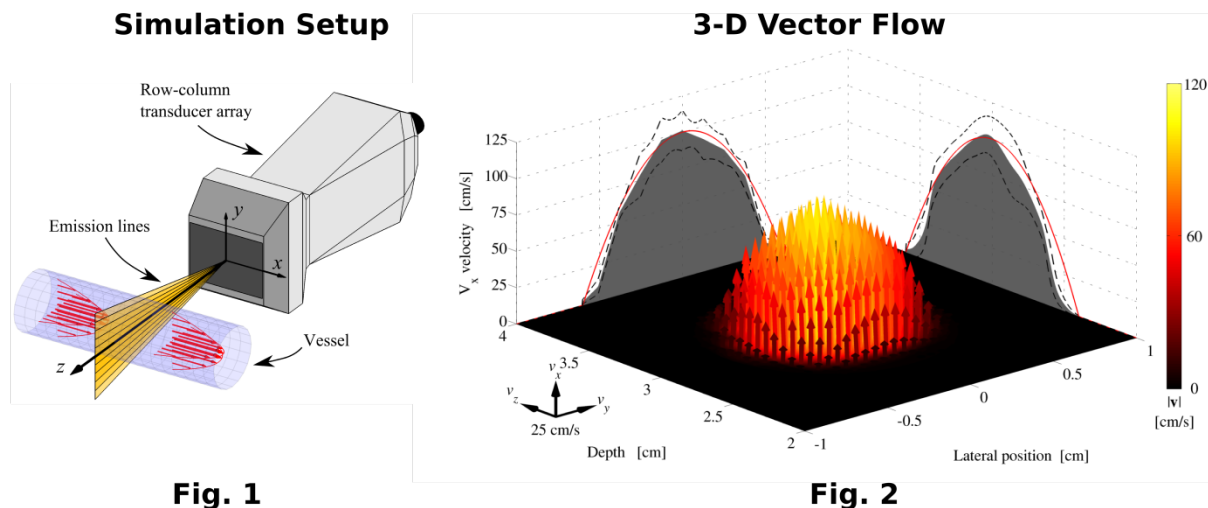
Fig. 2

P1B7-10

8:00 am   Velocity vector in three dimensions using a high-frame-rate dual-array setup

Pieter Kruizinga[1,2], Hendrik J Vos[1,2], Johannes G Bosch[1], Antonius FW van der Steen[1,2], Nico de Jong[1,2]; *[1]Thorax Center - Biomedical Engineering, Erasmus Medical Center, Rotterdam, Netherlands, [2]Faculty of Applied Sciences - Acoustical Wavefield Imaging, Delft University of Technology, Delft, Netherlands*

Background, Motivation and Objective

High frame rate ultrasound imaging (HFRI) has great potential to improve conventional Doppler imaging because high ensemble acquisitions are available for every pixel in an image. Additionally it allows deriving the lateral motion using angled plane-wave beams [1]. Despite its clinical success, conventional Doppler techniques remain limited due to the inability to measure out-of-plane flow. In this paper we present a solution for measuring all flow directions by using two linear array transducers with overlapping beams. By triangulation of the 2D Doppler signals derived for the individual imaging planes we derive the full 3D velocity vector. We show experimental proof that this imaging setup allows to extract the 3D velocity vector of blood in a human carotid artery (CA).

Statement of Contribution/Methods

We verified our method on the CA of a healthy volunteer. Two linear array transducers (ATL L7-4) were connected to a research ultrasound system (Vantage 256Tx/256Rx, Verasonics). A custom made holder kept the transducers at a 45 degree angle. The interleaved Doppler acquisitions for both transducers involved an ensemble length of 150, three angled beams (-7, 0, + 7 degree) and a Doppler pulse-repetition-rate of 2.5kHz at a 5MHz transmission frequency. After clutter rejection the velocity signal was derived for the three angled beams of each transducer with the first lag autocorrelation. The lateral and axial flow components were derived by triangulation as described in [1]. In the overlap region of two transducer beams the signal can be further processed by an additional triangulation step in the out-of-plane axis, which results in a quantification of 3D flow

Results/Discussion

In Fig. 1 the B-mode images of the two angled transducers are shown. The superimposed vector cones indicate the flow velocity in all three dimensions with (v = -31±1 // 725±34 // -299±8 mm/s) in axial, lateral and out-of-plane direction in the lumen centre. These values yield an absolute flow velocity of 785±53 mm/s which is mainly oriented in the lateral (x) direction.

[1]   Ekroll I.K. et al., "Simultaneous quantification of flow and tissue velocities based on multi-angle plane wave imaging," IEEE TUFFC, vol.60, no.4, 2013
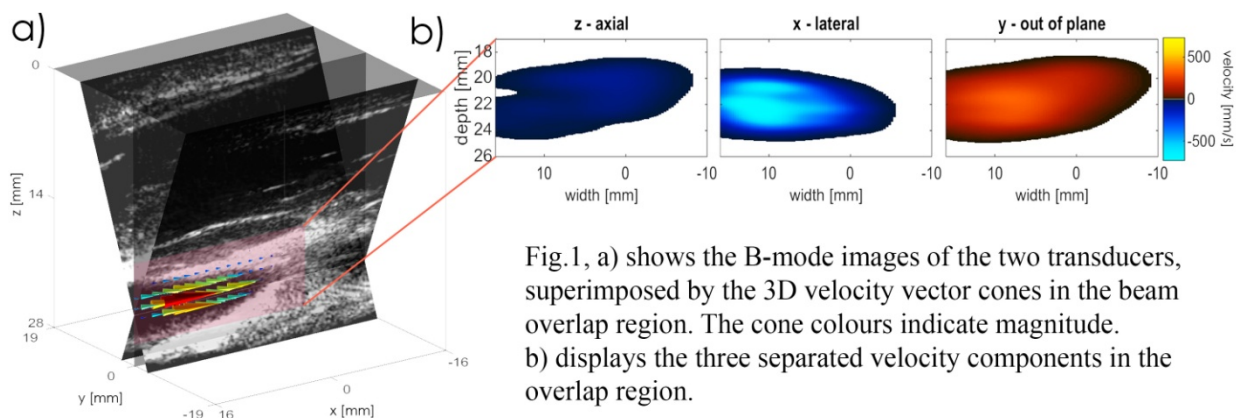
Fig.1, a) shows the B-mode images of the two transducers, superimposed by the 3D velocity vector cones in the beam overlap region. The cone colours indicate magnitude.
b) displays the three separated velocity components in the overlap region.

P1B7-11

8:00 am   3D Ultrafast Vector Doppler Imaging for in vivo Complex Flow Quantification

Mafalda Correia[1], Jean Provost[1], Mickaël Tanter[1], Mathieu Pernot[1]; *[1]Institut Langevin, ESPCI ParisTech, CNRS UMR 7587, INSERM U979, Université Paris 7, Paris, France*

Background, Motivation and Objective

2D Vector Doppler imaging has been developed for visualization and accurate quantification of complex blood flow velocity measurements. Recently, accurate estimation of 3D vector velocity along a line (M-mode) was shown using a 2D matrix transducer [J. A. Jensen, IEEE UFFC, 2014]. In this study, we developed a novel 3D Ultrafast

Vector Doppler Imaging approach for full estimation of blood flow velocity components over a large volume, based on 3D steered plane wave emissions and multi-angle cross-beam Doppler study, and we demonstrated its clinical feasibility in vivo in a healthy human subject.

Statement of Contribution/Methods

Acquisitions were performed using a 2D matrix phased array probe (3-MHz, 32x32 elements, Vermon) connected to a customized, programmable, 1024-channel ultrasound system designed to perform 3D Ultrafast Imaging.

The technique was first evaluated in an image-based 3D printed carotid bifurcation flow phantom, using five 2D steered plane waves emissions (-7°, 0°, +7° in each lateral orientation) with different flow speeds (up to 20 cm/s). The RF backscattered signals received by each transducer elements were beamformed in a multi-angle delay-and-sum approach. For each emission angle, 5 receive angles were used (-7°, 0°, +7° in each lateral orientation) with a f/D ratio of 5 at 30-mm depth, and a 3D flow vector estimated for each volume.

For in vivo feasibility, two different volumes of the carotid artery were insonified, one within the common carotid artery (CCA) and one within the bifurcation of the CCA and external and internal carotid arteries (ECA and ICA, respectively) at 1000 volumes/s.

Results/Discussion

The carotid bifurcation phantom results showed that the technique could derive 3D flow vector components, in magnitude (20 ± 1 cm/s maximum flow speed measured) and direction, consistent with the theoretical profile of the motion in the vessels. The in vivo human carotid measurements, presented in figure A and B, also showed good agreement with the theoretical flow profile in systole (50 cm/s of peak flow speed) and in diastole (20 cm/s of peak flow speed). This study demonstrates the feasibility and potential of 3D Ultrafast Vector Doppler Imaging to map complex flow dynamics in vivo in humans at a high-frame-rate.
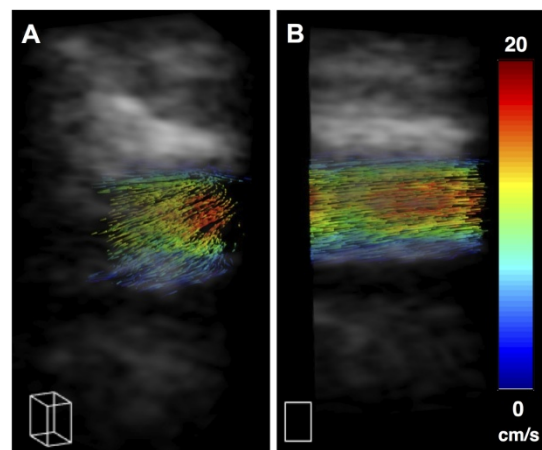
3D Ultrafast Vector Doppler Imaging
A) In vivo human carotid volume
B) In vivo human carotid volume projection

P1B7-12

8:00 am   **High frame rate 3D blood speckle tracking of intracardiac flows**

Morten Wigen[1], Jakob Høgenes[1], Joris van Cauwenberge[2], Sten Roar Snare[3], Patrick Segers[2], Solveig Fadnes[1], Abigail Swillens[2], Lasse Løvstakken[1]; *[1]Norwegian University of Science and Technology, Norway, [2]Ghent University, Belgium, [3]University of Oslo, Norway*

Background, Motivation and Objective

3D blood flow imaging may improve the knowledge and diagnosis of cardiac disease; however, the complex intracardiac flow patterns cannot be fully captured by the existing Doppler modalities. We investigate the potential of 3D blood speckle tracking (3D-BST) without contrast agent for this purpose, based on a high frame rate imaging setup enabling rapid sampling of the blood speckle movement, thereby limiting speckle decorrelation. The speckle movement in this setting will to a large extent be subsample relative to the image resolution. This necessitates either data interpolation which significantly increases processing time, or an efficient and accurate subsample interpolator. The objective of this work is to evaluate the accuracy and trade-offs of 3D-BST using parabolic fitting (PF) and Lukas-Kanade optical flow (LK) subsampling.

Statement of Contribution/Methods

Time-varying 3D flow fields obtained from an in silico CFD model of a (neonatal) left ventricle was fed into the fast simulation framework FUSK resulting in 3D IQ-data for one cardiac cycle. A 5MHz 2D matrix array transducer was modelled (1.9 / 1.6 cm in az. / el.), and plane (unfocused) transmit pulses were fired at PRF = 5000Hz in a packet acquisition scan sequence (Np = 15). The 3D ST velocity estimates were averaged over each packet, and in a 2x2x2 mm spatial region. Lukas-Kanade OF was done for one iteration, and marginal data interpolation factors were used for the SSD block matching. RMS errors for 3D-BST were calculated for varying conditions such as different noise levels, and with and without clutter filtering (cutoff = 6.4 cm/s).

Results/Discussion

Under normal SNR conditions (15dB) and without clutter filtering, 3D-BST gave acceptable global errors, demonstrating the potential of the approach. LK and PF subsampling then showed similar RMS errors, on average around 5 cm/s. For lower SNR (5 dB), LK subsampling gave significantly larger deviations (see Figure). Clutter filtering had a major impact, and although regions affected would typically not be used in practice, it was observed that LK was more sensitive to clutter filtering artifacts. Based on the current results we found that PF provided similar or better subsampling performance at lower computational cost compared to LK. Further work will include in vitro validation and an in vivo feasibility study of 3D-BST using a commercial 3D ultrasound system.

3D blood speckle tracking

RMS error of velocity magnitude
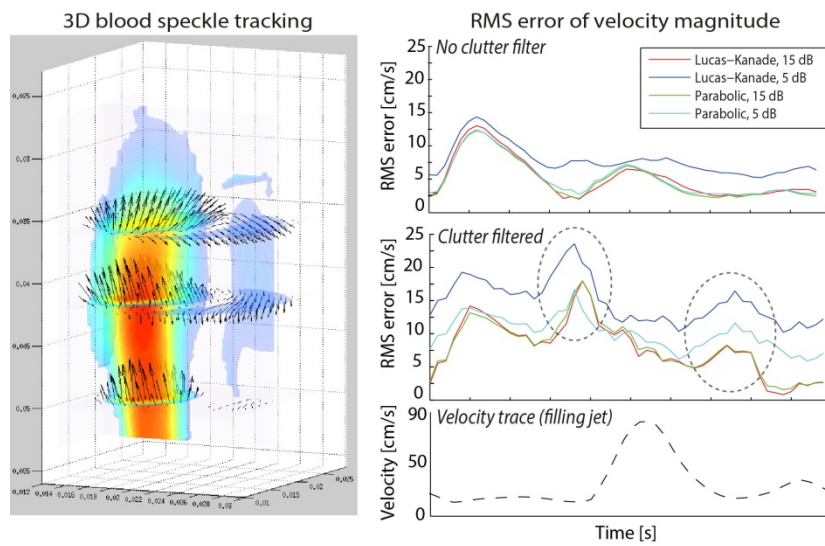
P1B8 - MSD: Implementation of Novel Ultrasound Methods

4th floor

Friday, October 23, 2015, Posters displayed 08:00 am - 05:00 pm. Authors must be present at their poster from 9:30 - 10:30am (odd number posters) and 14:30 – 15:30pm (even number posters).

Chair: **Massimo Mischi**
Eindhoven University of Technology

P1B8-1 _____

8:00 am   **Real-time dynamic scheduling based adaptive ultrasound sequence programming for research and rapid prototyping**

Richard Tobias[1], Gary Yi Hou[1], Ashish Parikh[1]; *[1]Cephasonics, Santa Clara, California, USA*

Background, Motivation and Objective

Over the past decade, a wide range of ultrasound-based diagnostic and therapeutic applications have been developed based on the emergence of user-friendly, open-ended ultrasound research systems. Open-ended research ultrasound platforms (Kaczkowski and Daigle, 2011)(Cheung et al., 2012) provide users with both the ability to access channel or beamformed RF data, as well as an interface for implementing post-processing sequences for algorithm and prototype development. Nevertheless, previous platforms relied on static list-based scheduling, which limited the user from adjusting scan parameters in real-time. The objective of this study is to demonstrate an innovative ultrasound engine and Application Programming Interface (API) equipped with a real-time dynamic hardware scheduler that allows for flexible and adaptive sequence design.

Statement of Contribution/Methods

A 64-channel research platform has been used in conjunction with a 7.5 MHz linear array transducer (Tobias, IUS 2014). The FPGA sequencer of the research platform has been equipped with a real-time dynamic scheduling algorithm (Tobias, SPIE 2014) capable of add, remove, and modify the scan instructions. Here, a C++-based API has been developed to allow users to dynamically define, operate, and integrate multiple custom sequences. An example of real-time dynamic sequence has been designed and implemented, where the delay time for implementing changes in imaging depth, beam density, and Pulse Repetition Frequency (PRF) were compared between static and dynamic scheduling modes.

Results/Discussion

Successful implementation of the custom sequences has been programmed while the delay times for adjustment of each scan parameter were recorded over 9 repeated scanning. Significant improvements were measured under real-time dynamic over static scheduling, where the system delay for adjusting imaging depth, beam density, and PRF were improved by 98.0±0.005% , 99.3±0.0002%, and 98.0±0.0007%.

A real-time dynamic scheduling-based ultrasound engine capable of performing adaptive parameter based scanning has been presented. A custom sequence has been successfully implemented, where an improvement of over 98% in system delay time was observed for adjusting various scan parameters using real-time dynamic scheduling compared to static scheduling. The presented platform and API therefore can lead to a wide range of algorithm and prototype development.

P1B8-2 _____

8:00 am   **Newton's Method based Self Calibration for a 3D Ultrasound Tomography System**

Wei Yap Tan[1], Till Steiner[2], Nicole Ruiter[1]; *[1]Institute for Data Processing and Electronics, Karlsruhe Institute of Technology, Eggenstein-Leopoldshafen, Germany, [2]Pepperl+Fuchs GmbH, Mannheim, Germany*

Background, Motivation and Objective

Our 3D ultrasound computer tomography (3D USCT) system aims at high-resolution images for early breast cancer detection. The current system consists of 2041 ultrasound transducers.

Positioned on a semi-ellipsoid, the quality of the produced images is highly sensitive to the system calibration. Parameters for calibration are: the position of ultrasound transducers, temperature distribution in the medium and the electronics' system response. A calibration accuracy better than one quarter of the wavelength is targeted for optimal image quality.

Statement of Contribution/Methods

This work proposes a self-calibration method for arbitrary ultrasound transducer systems including 3D USCT based on time-of-arrival (TOA) measurements. It is assumed that the position of each transducer is known to a certain accuracy, and the medium is not necessary homogenous, so that speed of sound changes along the signal path are possible. Lastly, transmission and reception delays in the electronics maybe present.

The problem is addressed with the following TOA equation:$\| s_i - m_j \| = c_{ij} \cdot (t_{ij} + \tau_{si} + \tau_{mj})$

with vectors s_i and m_j as position of emitter i and receiver j in 3D. c_{ij} is the mean speed of sound. The time of flight is given by t_{ij} and the transmission and reception delays with τ_{si} and τ_{mj}.

The method separates the problem into three main parts according to their magnitude ranking: position calibration, temperature calibration and delay calibration with good a priori knowledge of the system as stated above, which are individually modeled as a nonlinear equation system $f(x_0)$ of unknown vector x with custom boundary conditions. By neglecting higher-order terms in the linearization of such equation system, the problem is solved iteratively with the Newton's method: $x_1 = x_0 - (J(x_0))^{-1} f(x_0)$

Results/Discussion

The calibration method showed promising results both in simulated and real life data. We could achieve position calibration accuracy of 15 µm (2.5% λ) limited by the sample rate at 100 MHz of simulated data, the temperature gradient with a precision up to 0.3 °C and electronics delay in nanosecond range. The method was able to recognize a delay of 1.16 µs when implemented on real USCT data, which agrees with the empirically obtained value of 1 µs. Future work will be the investigation of the limitation of the calibration accuracy with linearization of non-linear equation system.

Position Error Distribution Before Calibration
mu = -1.6237e-17, sigma = 0.00042479

Position Error Distribution After Calibration
mu = -4.9873e-18, sigma = 1.5205e-05
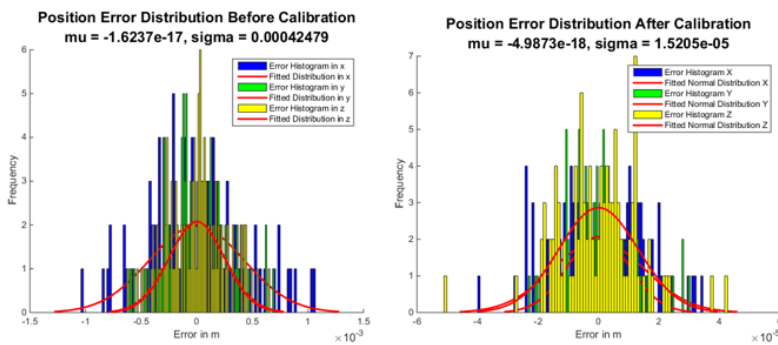
Simulation setup:
- *50 transducers on a spherical distribution of radius 12 cm with center frequency of 2.5 MHz*
- *Temperature gradient of 5 °C around 21 °C (SOS ≈ 1500 m/s)*
- *Electronics' delay up to 1 μs*

Position error:
- *before calibration: ≈ 0.4 mm*
- *after calibration: ≈ 15 μm (2.5% λ)*

P1B8-3

8:00 am　A Study of the Driving Circuit for Array Transducer Considering the Impedance Properties

Hayato JIMBO[1], Kota GOTO[1], Shin YOSHIZAWA[1], Shinnichiro UMEMURA[1]; [1]*Tohoku university, Sendai, Miyagi, Japan*

Background, Motivation and Objective

High-intensity focused ultrasound (HIFU) is a noninvasive method for cancer treatments. A multi-channel array transducer can enlarge the HIFU treatment volume by generating and scanning multiple foci. Class D switching amplifiers with LC resonant circuits to drive such transducer are not only limiting the compactness but also the freedom to choose the frequency. To solve this problem, we have developed a driving circuit generating staircase waves without major harmonic components. In order to achieve the desired voltage waveform in driving an array transducer element with either capacitive or inductive impedance, further improvement was found to be necessary.

Statement of Contribution/Methods

In our previous design of the staircase-wave driving circuit, only P-MOSFETs and N-MOSFETs were used for positive and negative voltage levels, respectively, implicitly assuming that the impedance of the transducer element is almost real. When a capacitive transducer element is driven by this circuit, the P-MOSFET cannot discharge and the N-MOSFET cannot charge the element as shown by the red curve in figure 1-(a) where the blue curve is the desired drive voltage waveform. This problem can be solved by using both P-MOSFET and N-MOSFET for each intermediate voltage level.

Results/Discussion

The desired drive voltage waveform was achieved by our newly improved circuit design. The third and fifth harmonics of focal pressure were reduced approximately by 18 and 39 dB, respectively. Since the new circuit prohibited undesired voltage jumps, it also reduced the heat generation of the circuit. This was because most of the energy consumption by a switching circuit occurs during the switching time. In this study, the impedance of the transducer were already known as capacitive, but the new circuit, using both P and N-MOSFET for each voltage level, can achieve a desired drive voltage waveform even when it is unknown whether capacitive or inductive.

(a)Output Voltage

(b)Harmonics of Focal Point
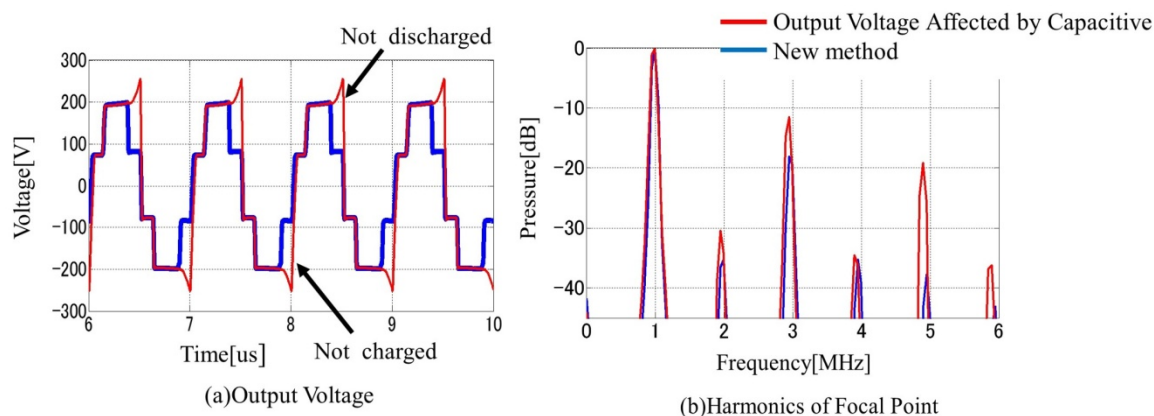
P1B8-4

8:00 am　Method for Generating Cell Aggregates using Ultrasonic Standing Wave Trapping in a Disposable Capsule

Yuta Kurashina[1], Kenjiro Takemura[1], Shogo Miyata[1], James Friend[2]; [1]*Mechanical Engineering, Keio University, Yokohama, Kanagawa, Japan,* [2]*Mechanical and Aerospace Engineering, University of California-San Diego, San Diego, California, USA*

Background, Motivation and Objective

Ultrasonic standing wave trapping (USWT) is a promising method for generating cell aggregates. However, USWT requires a complicated apparatus not suitable for sterilization for repetitive use. To solve this problem, this study proposes a novel cell aggregate generation method using USWT in a disposable capsule.

FRIDAY POSTER

Statement of Contribution/Methods

Figure 1 shows a proposed apparatus to generate cell aggregates by using USWT in a polyvinyl chloride (PVC) capsule, in which culture medium is contained. Since PVC is permeable to acoustic waves generated by a vibrator, the wave may travel through the capsule. A standing wave is generated between the surfaces of the vibrator and medium, trapping cells to the nodal position of the standing wave. The capsule is disposable, and sterilization is not required.

Results/Discussion

Figure 2 shows the image of calf chondrocytes aggregates generated with a developed apparatus after 2-hour excitation of acoustic wave. It is obvious that cell aggregates can be generated by the proposed method. It is also found that the size of cell aggregates depends on the duration of USWT treatment.
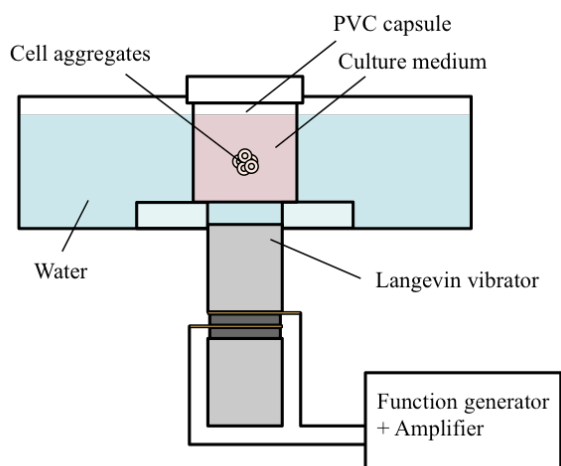
Fig. 1 Generation of cell aggregates using USWT in a capsule
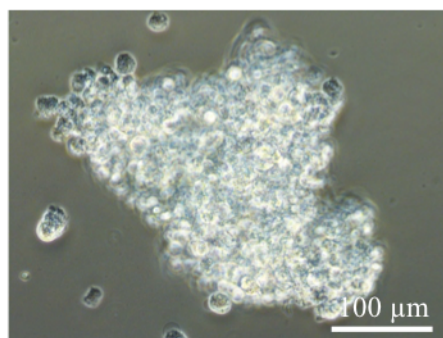
Fig. 2 Phase microscope image of calf chondrocytes aggregate generated by 2-hrs USWT treatment.

P1B8-5

8:00 am   **Cell manipulation by using natural vibration of a cell culture substrate**

Chikahiro Imashiro[1], Yuta Kurashina[1], Kenjiro Takemura[1], Shogo Miyata[1], Jun Komotori[1]; *[1]Mechanical engineering, Keio University, Yokohama, Kanagawa, Japan*

Background, Motivation and Objective

In tissue engineering, it is required to maintain functionality of cells in culturing process to generate organs.Although a scaffold is used in previous studies to generate organs, the scaffold possibly harms a human when it is inserted into patient's body with generated organs. Instead of using scaffolds, this study proposes to use natural vibration of culture substrate to manipulate cells aiming to generate organs

Statement of Contribution/Methods

A novel cell manipulation method proposed in this study manipulates cells to the node of a natural vibration of a metal cell culture substrate whose diameter is 36 mm, i.e., the cells are collected at the node of natural vibration excited. Natural vibration modes are analyzed with finite element analysis software, ANSYS 15.0. Selecting an out-of-plane vibration mode with a nodal circle shown in Fig. 1 as a representative vibration mode of circular disk, we designed and fabricated a cell culture device and evaluated its mode by a laser Doppler vibrometer. We used this cell culture device for the experiment of cell manipulation. The target cell is a calf chondrocyte. In the experiment, we changed the initial number of cells and the amplitude of vibration to acquire relation between cell distributions and experiment conditions. Note that the duration of exciting natural vibration is 120 min.

Results/Discussion

Figure 2 shows the cell distribution when the initial number of cells is 2.5×10^5 and the maximum amplitude of the vibration is 4.5 µm. With this condition, we confirmed that cells tend to be collected on the nodal circle. However, with different conditions we could not confirm this trend. This means that the number of cells and the amplitude of the vibration have appropriate values for cell manipulation.
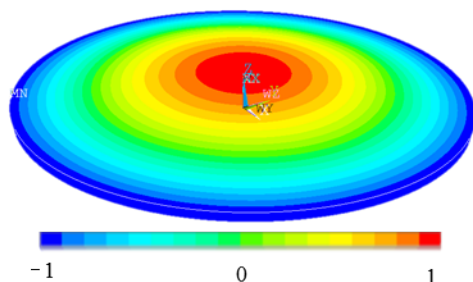
Fig. 1 Natural vibration mode of a circular disk with a single nodal circle. Color indicates the normalized amplitude.
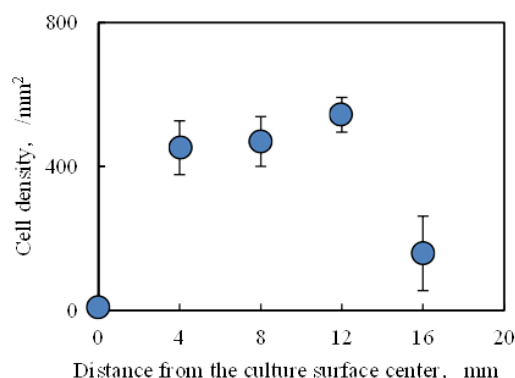
Fig. 2 Cell distribution

P1B8-6

8:00 am   A Real-time Realization of the Automatic B-mode Image Optimization on a Smart Mobile Device for Point-of-Care Ultrasound Imaging

JeeHoo Kim[1], Kwanghyun Park[1], Ilseob Song[1], Yangmo Yoo[1,2]; [1]*Electronic Engineering, Sogang University, Seoul, Korea, Republic of,* [2]*Interdisciplinary Program of Integrated Biotechnology, Sogang University, Korea, Republic of*

Background, Motivation and Objective

Dynamic range (DR) and time-gain compensation (TGC) are the prime parameters that affect image quality in ultrasound B-mode imaging. Previously, we proposed the automatic B-mode image optimization technique where DR and TGC are changed without user interaction and showed a substantial improvement in image quality. In this paper, the automatic B-mode image optimization method (i.e., Auto DR + TGC) was realized on a mobile device for point-of-care ultrasound imaging where less user independency is critical.

Statement of Contribution/Methods

For effectively implementing the proposed automatic image optimization method, a mobile graphics processing unit (GPU) inside a mobile device was utilized as a general purpose GPU (GPGPU) with the OpenGL ES. As shown in Fig. 1(a), multiple pipelines are sequentially processed to accelerate performance of the proposed optimization method in parallel. To evaluate the proposed method, 100 frames of *in-vivo* abdominal data were captured with a 3.5-MHz convex array transducer connected to a commercial ultrasound scanner with a research package (Accuvix V10, Samsung Medison, Seoul, Korea).

Results/Discussion

The performance of the Auto DR + TGC algorithm was evaluated by calculating the correlation coefficient (CC) with the reference image and measuring the frame rates on the smart mobile device. As shown as Fig. 1(b), the image of the Auto DR + TGC method showed higher similarities with the reference than other methods. The CC values of the conventional with a fixed DR value (i.e., 60 dB), Auto DR, Auto TGC and Auto DR + TGC methods with the reference image were 0.55 ± 0.36 vs. 0.92 ± 0.13 vs. 0.39 ± 0.26 vs. 0.98 ± 0.01, respectively. In addition, the frame rates of the four methods on the smart mobile device were 64.53 ± 13.25 vs. 52.37 ± 11.47 vs. 51.58 ± 7.08 vs. 47.99 ± 14.01, respectively. In conclusion, the automatic B-mode image optimization method with Auto DR + TGC can provide the enhanced similarity between the reference and input images for less user interaction in point-of-care applications.
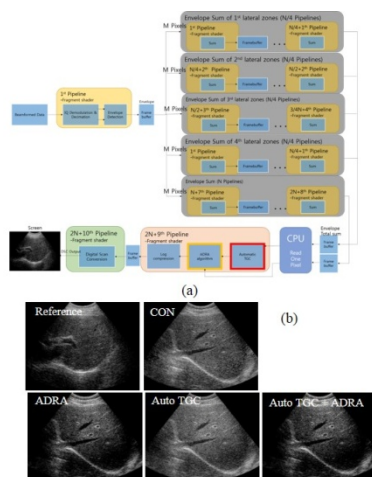
Figure 1. (a) Block diagram of the implementation on the smart mobile device
(b) The B-mode images of reference, conventional, ADRA, auto TGC, and auto TGC + ADRA

P1B8-7

8:00 am   Speed-up of acoustic simulation techniques for 2D sparse array optimization by simulated annealing

Emmanuel Roux[1,2], Alessandro Ramalli[2], Piero Tortoli[2], Christian Cachard[1], Marc Robini[1], Hervé Liebgott[1]; [1]*CREATIS, Université de Lyon, CNRS UMR 5220, INSERM U1044, Université Claude Bernard Lyon 1, INSA-Lyon, Villeurbanne, France,* [2]*Ingenieria dell'informazione, Università degli studi di Firenze, Firenze, Italy*

Background, Motivation and Objective

The design of sparse arrays is usually linked to optimization algorithms, based on simulated annealing (SA), to find the set of active elements yielding the best-achievable beam pattern. The computational load of such algorithms is high and, according to SA theory, the quality of the results increases with the number of iterations. Considering 2D array optimization, an acceptable solution is generally reached after several thousand iterations. Besides, realistic acoustic simulations improve the probe design but make the computation time even longer (up to a few days). In this work, we propose to speed-up the optimization process by 1) introducing a fast pressure field (PF) update algorithm, and 2) a method to reduce the number of pressure measurement points (PMPs).

Statement of Contribution/Methods

1) Realistic acoustic simulations are performed by FIELD II. Assuming linear propagation conditions, the superposition of individual elements contribution can be exploited for fast PF computation. Only the new PF contribution PFe_{n+1} of the perturbed element, e, is updated. The initial PF_0 is first computed and then updated as $PF_{n+1} = PF_n + PFe_{n+1} - PFe_n$ for the following iterations. In order to facilitate calculation and avoid matrix dimension variations during the optimization process, two PMPs are added above every element which guarantee the same individual signals duration and phase.

2) To analyze the beam pattern of the probe, thousands of PMPs (>50000) are located on a half-sphere of radius R. Usually the spherical coordinates are discretized and the i-th PMP is located at (R, θ_i, φ_i), which results in a non-uniform density and periodic distribution of the PMPs. To compute the beam pattern faster without losing precision, the elements placement strategy used in [Viganó, 2009] was transposed in 3D and applied to the PMPs placement with a uniform density law.

Results/Discussion

The execution time ratio between the entire probe PF update and the fast PF update defines a first speed-up gain:

$g_1 (N_e) = 1 + (42/1000) \times N_e$ where N_e is the number of active elements.

Moreover the uniform and aperiodic coverage of the half-sphere surface permits to reduce the number of the PMPs while maintaining satisfying beam pattern analysis. The PMPs reduction yields a second speed-up gain:

$g_2 (q) = 102/(q + 0.74)$ where $q = N_{PMPs}/N_{REF} \times 100$ and N_{REF} is the reference amount of PMPs from which only N_{PMPs} are maintained.

The two acceleration techniques were combined to achieve the optimization of a 256-element 7MHz probe of radius r = 6 mm ≈ 30λ with focus at 25 mm on z-axis. 10000 PMPs were located on the half-sphere of radius R = 25 mm resulting in a space sampling resolution smaller than 3λ. The total speed-up gain was g_t = 75. With the same number of PMPs, the optimization of a 1024 element probe would be accelerated 280 times.

P1B8-8

8:00 am   **Development of an Acoustic Based Sensing System for Medical Ultrasound Image Simulator**

Bo-Heng Chen[1], Kai-Sheng Heish[2], Chih-Chung Huang[1]; *[1]Department of Biomedical Engineering, National Cheng Kung University, Taiwan, [2]Kaoshiung Chang Geng Memorial Hopital, Taiwan*

Background, Motivation and Objective

Ultrasound examination highly depends on the skill of the operator. Recently, the ultrasound image simulator has been proposed to assist training procedure in hospital and medical school. As operator is moving the ultrasound probe on the manikin, simulators can provide virtual images for real examination environments which allow users to practice their skill before clinical diagnosis. A large number of clinical ultrasound data can be stored in simulator as a database for training purpose, particularly for rare disorders. The sensing system is the most crucial part of simulator because a high sensitivity sensing provides a higher performance for displaying the real image. Currently, several commercial ultrasound simulators are available based on different sensors, such as electromagnetic, optical, and RFID sensors. In present study, ultrasound sensors were used as a primary sensing system for developing an ultrasound simulator. System verification was performed by in vitro porcine heart imaging.

Statement of Contribution/Methods

Figure 1 (a) shows the photo of air-coupled ultrasound sensors which one for transmitting signal and the other one for receiving signal. The diameter of the sensor is 8.4 mm and the operational frequency is 40 kHz. Five transmitting sensors were arranged in 1-D array to transmit the ultrasound signal and 25 receiving sensors were arranged into 5 by 5 2-D array to receive the signal, as shown in Fig 1(b). Since the sequences of receiving signal were changed due to the motion of transmitting 1-D array, the position and orientation of the sham probe can be detected precisely by this acoustic sensing system. The block diagram of whole simulator is shown in Fig. 1(c). After the sham probe was positioned, the corresponding ultrasound image was displayed frame by frame according to the real examination environments. The database of image is pre-captured using a commercial ultrasound system.

Results/Discussion

Figure. 1(d) shows the user interface of this simulation system. Both sequence of receiving signal and its corresponding image are displayed on the monitor. The lateral and axial resolution of this acoustic sensing system are about 0.7 mm/frame and the rotation is about 0.5 degree/frame. The in vitro porcine heart experiments showed that the simulator can display the heart structure precisely confirmed by a well training operator.
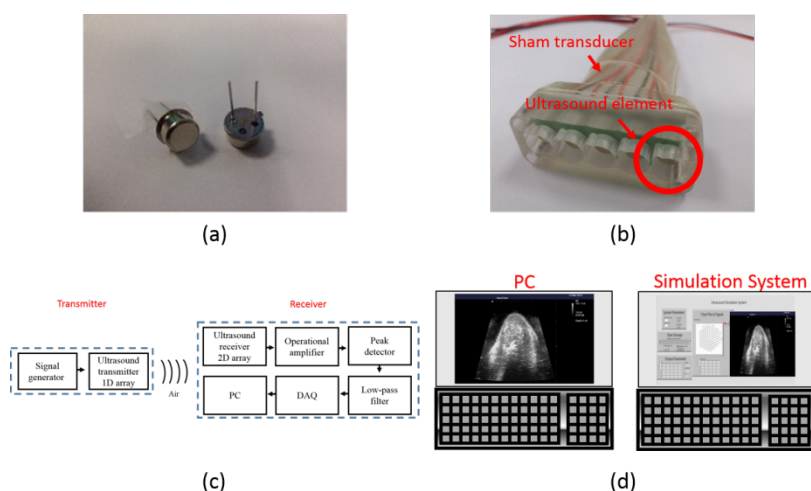
Fig.1

P1B8-9

8:00 am   **A New 2D Shear Wave Imaging System for Ultrasound Elastography**

Weibao Qiu[1], Congzhi Wang[1], Yang Xiao[1], Ming Qian[1], Hairong Zheng[1]; *[1]Shenzhen Institutes of Advanced Technology, Chinese Academy of Sciences, China, People's Republic of*

Background, Motivation and Objective

Ultrasound elastography has been a widely accepted clinical examination technique, which is able to provide a non-invasive measurement of tissue elasticity properties. Shear wave imaging (SWI) technique is a quantitative method for tissue stiffness assessment. It has been proved to be less operator dependent than the quasi-static elastography, and has the ability to acquire quantitative elasticity information in contrast with ARFI imaging. In this study, a scanning-mode 2D shear wave imaging system is proposed and evaluated. Detailed delineation of hardware and image processing algorithms are presented.

Statement of Contribution/Methods

A new SWI method is proposed in this paper to provide 2D elasticity mapping. An elasticity map is drawn ahead of the transducer targeted at the area-of-interest. The size of the map can be adjusted according to the number of elasticity pixels. Acoustic radiation force is generated by transducer to induce a shear wave propagation inside the tissue, where the shear modulus is derived by the shear wave propagation speed acquired by four beams with known equal distance. The speed is calculated from dividing the distance between each acquisition beam by flying time from one beam to another beam. An average process is applied to achieve an accurate measurement. The system scans the mapping area pixel by pixel to generate a 2D image. The 2D elasticity map acquired by the proposed system composed of group of elasticity pixels, where each pixel represents the shear modulus in the map area. The algorithms to acquire the shear modulus can be roughly divided into two steps: estimation of tissue displacement and shear wave velocity determination.

Results/Discussion

Fig. 1(a) shows the prototype of the proposed ultrasound elastography system. Programmable FPGA is employed to do the image processing in the local part, and GPU is used for fast computation of the elastography algorithms in the computer part. The *in vitro* test was achieved by imaging an excised porcine liver. Fig. 1(b) shows the B-mode image which presents the structural information of the targeted tissue but lack of elasticity properties. Fig. 1(c) shows the elasticity measurement. The stiffness range of these measurements is 4-8kPa. The value can be calculated and displayed with 2D map, which is also correlated well with the published works.
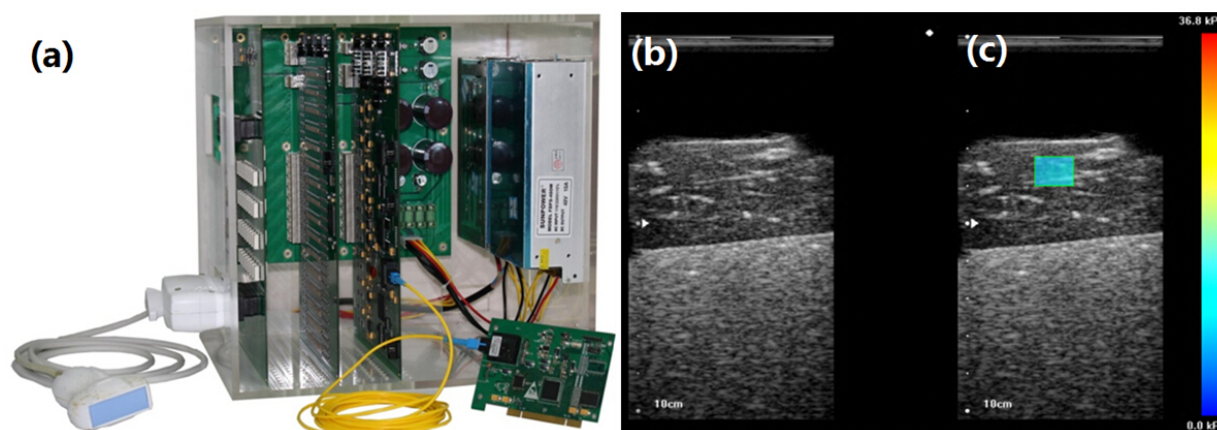
Fig. 1. (a) The prototype of the proposed ultrasound elastography system. (b) Traditional B-mode ultrasound image of an excised porcine liver. (c) The proposed s2D-SWI mode image.

P1B8-10

8:00 am   **Assessment of the performance of an ultrasonic biopsy needle**

Andrew Mathieson[1], Robert Wallace[2], Rebecca Cleary[1], Hamish Simpson[2], Margaret Lucas[1]; *[1]School of Engineering, University of Glasgow, United Kingdom, [2]School of Clinical Sciences, University of Edinburgh, United Kingdom*

Background, Motivation and Objective

This study investigates the performance of a novel power ultrasonic bone biopsy needle by assessing damage induced during the penetration of the resonant device into bone tissue. Bone biopsy is a relatively simple but crude medical procedure which performs the removal of a small bone or bone marrow sample during the diagnosis of medical conditions such as primary and secondary bone tumours, leukemia, multiple myeloma or Paget's disease. However, to penetrate bone tissue, the surgeon has to apply a large force through the needle, which can cause damage to soft tissue surrounding the biopsy site and induce bone fractures. By utilizing micrometric vibrations developed by the ultrasonic device, the force required to penetrate bone tissue is significantly reduced and there is less damage to tissue.

Statement of Contribution/Methods

The power ultrasonic bone biopsy needle, tuned to longitudinal mode resonance at 25 kHz, has been characterized using experimental modal analysis (EMA) and its modal parameters have been identified. A Skycan 1172 Micro-CT, scanning at a resolution of 3µm per voxel, was used to assess the mechanical damage induced by the vibrating biopsy needle, while histology was completed to identify thermal damage.

Results/Discussion

EMA confirmed the predicted modal parameters and illustrated that the longitudinal mode did not contain parasitic flexural vibrations. Figure (a) illustrates a biopsy site in a femur bone from a 3 month Wistar rat, while Figure (b) is a micro-CT representation of the cut site of the same femur. The micro-CT revealed a small amount of micro-damage around the hole but no large cracks. This indicates that the ultrasonic device can penetrate bone without inducing severe mechanical damage. It is therefore concluded that an ultrasonic device could be utilized in biopsy procedures which involve delicate bone structures, such as in pediatrics or from osteoporotic bones. In addition, the significantly reduced applied force required to penetrate the bone removes the risk of the biopsy needle 'punching through'. This could allow the ultrasonic needle to take biopsies in areas such as the spine.

(a)   (b)
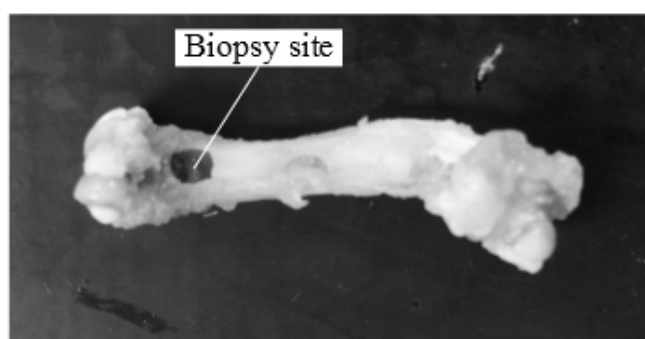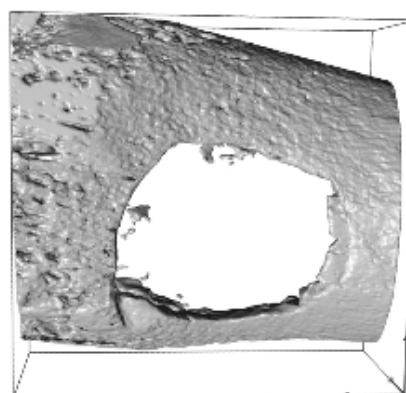
FRIDAY POSTER

P2B1 - Signal Processing NDE Methods

4th floor

Friday, October 23, 2015, Posters displayed 08:00 am - 05:00 pm. Authors must be present at their poster from 9:30 - 10:30am (odd number posters) and 14:30 – 15:30pm (even number posters).

Chair: **Erdal Oruklu**
Illinois Institute of Technology

P2B1-1

8:00 am   **A pulse compression procedure for the measurement and characterization of Non-linear systems based on Exponential Chirp signals.**

Pietro Burrascano[1], Stefano Laureti[1,2], David Hutchins[2], **Marco Ricci[1]**, Luca Senni[1]; *[1]Department of Engineering, Università degli studi di Perugia, Polo Scientifico Didattico di Terni, Italy, [2]University of Warwick, United Kingdom*

Background, Motivation and Objective

The capability of identifying the non-linear behavior of ultrasonic transducers and samples under test can be extremely useful in various ultrasonic diagnostic and non-destructive evaluation applications. Several defect detection strategies as well as imaging procedures have been recently proposed relying on the non-linear behavior of defects that produces second or higher-order harmonics [1]. At the same time, innovative methods for the generation of broadband signals exploit non-linear phenomena such as for the case of solitary waves [2]. The aim of the present work is to apply a pulse-compression procedure based on exponential chirp excitation to the characterization of non-linear behavior of various ultrasonic systems.

Statement of Contribution/Methods

A measurement procedure able to characterize a special class of non-linear systems that can be represented by a cascade of Hammerstein models has been developed, see Fig1-a. The procedure exploits a peculiar feature of exponential chirps in terms of pulse compression: it can be seen that the matched filter of an exponential chirp is capable to "compress" not only the original signal but also any n-th harmonic of it introducing a different time delay for each harmonic, see Fig. 1-b. With a proper choice of the input signal parameters, this allows the identification of the impulse responses, and hence of the transfer functions, associated at different non-linear terms in a single shot. Then, once characterized the non-linear system for a given input signal amplitude, the response of the system to a generic input signal with equal or smaller amplitude can be predicted.

Results/Discussion

In this paper, we review the method highlighting peculiar pulse-compression properties of the exponential chip and introduce an optimization procedure for lowering the sidelobes of the pulse-compression output. Moreover the extension of the method to deal with sub-harmonic generation is presented.

1.Antonaci, P., Bruno, C. L. E., Gliozzi, A. S., & Scalerandi, M. (2010). Monitoring evolution of compressive damage in concrete with linear and nonlinear ultrasonic methods. Cement and Concrete Research, 40(7), 1106-1113.

2.Akanji, O., Hutchins, D. A., Davis, L. A., & Leigh, S. J. (2013). Micromachined structures for nonlinear ultrasonic transduction. In 2013 IEEE International Ultrasonics Symposium (IUS) (pp. 1117-1120). IEEE.
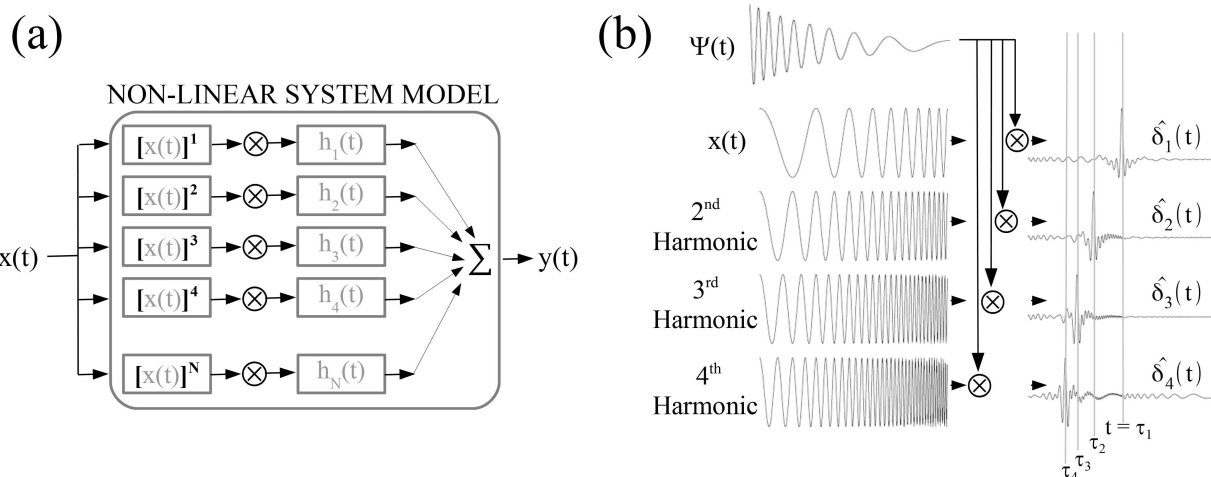
P2B1-2

8:00 am   **Visualization of Defects in Steel Billet using Back Propagation of Scattered Waves**

Koichi Kakuma[1], Koichi Mizutani[2], Naoto Wakatsuki[2]; *[1]College of Engineering Systems, School of Science and Engineering, University of Tsukuba, Tsukuba, Ibaraki, Japan, [2]Faculty of Engineering, Information and Systems, University of Tsukuba, Tsukuba, Ibaraki, Japan*

Background, Motivation and Objective

Steel billet includes some defects such as inclusions or gases. There are several ultrasonic inspection methods for the billet: the pulse-echo method, the computerized tomography method using time-of-flight, or the inspection method using back propagation. The first method is utilized actually, but the inspection accuracy is not enough. The second methods are currently under research and can visualize defects, but many paths are required. We have researched the third method to visualize defects as an alternative method of the second. In our previous research, the third method was proposed and evaluated by an experiment using a specimen of duralumin. However, the method should be improved and evaluated by using a specimen of steel. It is because steel billet is high-attenuation and it could become difficult to visualize defects. Our purpose is to improve the inspection method using back propagation and visualize defects in steel billet.

Statement of Contribution/Methods

The flow of our previous method is following:

(1) pulses are transmitted in measurement and reference planes

(2) received signals are obtained and pulse-compressed

(3) the envelopes of the reference signals are detected

(4) the reciprocals of the envelopes are calculated and windows are obtained

(5) the windows are applied to the measurement signals and scattered waves from defects are obtained

(6) the scattered waves are time reversed and back propagated on computer

(7) energy distribution is obtained and defects are visualized

In addition to the above, we consider about the following:

(i) raised amplitudes of the envelopes of measurement and reference signals

(ii) absolute values of the difference between raised amplitudes of measurement and reference signals are calculated

(iii) the windows of (ii) are applied to the scattered waves of (5)

Results/Discussion

Uploaded figure shows the summary of our research. From this figure, it is observed that visualized image of defects become clearer. These images are going to be evaluated by energy histograms or F-measure rate.
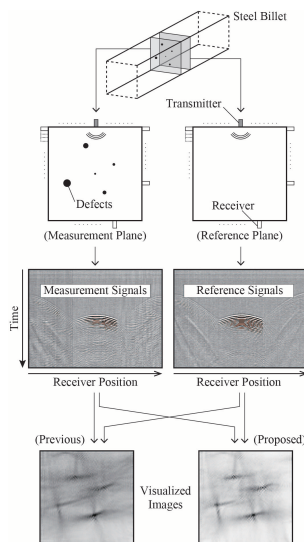
P2B1-3

8:00 am   Feature extraction for robust impact damage classification of CFRP plates using ultrasonic signals

Juan M. Soto[1], Antonio M. Peinado[1], Ángel M. Gómez [1], Nicolas Bochud[1]; *[1]Teoría de la Señal, Telemática y Comunicaciones, University of Granada, Granada, Spain*

Background, Motivation and Objective

Carbon fiber-reinforced polymers (CFRP) are widely used in industry thanks to their high-performance mechanical properties. Nevertheless, during CFRP's manufacturing, service or maintenance flaws may occur and reduce the strength of the material while remaining invisible from the surface. This work presents an ultrasonic signal classification system that discriminates between different impact damage energies. The proposed system, which is based on a sparse modeling of the ultrasonic propagation into the CFRP plate combined with dimensionality reduction techniques, achieves a 0% misclassification rate.

Statement of Contribution/Methods

A cross-ply CFRP laminate with a stacking sequence of [0/90]° was excited by an ultrasonic sine-burst at a central frequency of 5 MHz and 5 Vpp amplitude. The response signals were sampled with a 100 MHz A/D converter after a 40 dB pre-amplification stage and preprocessed using Hamming windowing. This measurement procedure was repeated 40 times for each of 6 impact damage locations in order to generate a relevant data set that accounts for the uncertainties due to the variability of the transducers alignment with respect to the impacted location. We propose a classification system where Principal Component Analysis (PCA), Factor Analysis (FA) and Stochastic Proximity Embedding (SPE) are tested over a DCT/cepstral signal representation in order to map the original high dimensional feature vectors into a lower M-dimensional space. Then, a damage level classification is performed with both Linear and Quadratic Discriminant Analysis (LDA/QDA).

Results/Discussion

To evaluate our classification system, the training/test is performed using the leaving-one-out method to make an optimal use of the training dataset (6x40 signals). The results are summarized in Table 1, which shows a significant reduction of the misclassification rate thanks to our proposal that prevents from using irrelevant and noisy information in the discriminant analysis stage. Generally, QDA results are slightly better but more parameters need to be estimated compared to LDA.

Parametrization Method	Discriminant Analysis	Dimensionality Reduction	M-preserved components in output space							
			3	4	5	6	7	8	9	10
DCT	LDA	PCA	3.75	1.25	**0.55**	2.64	7.91	11.38	12.77	12.22
		FA	**3.19**	**0.55**	**0.55**	3.19	10.13	10.83	10.00	8.19
		SPE	3.33	1.66	0.97	2.50	11.94	12.64	11.25	14.44
	QDA	PCA	3.61	1.11	1.11	0.41	0.97	0.27	0.41	0.41
		FA	5.00	1.80	0.41	**0.27**	0.41	0.27	0.13	0.13
		SPE	5.27	1.94	**0.55**	0.55	**0.27**	0.13	0.13	**0.00**
Cepstrum	LDA	PCA	6.11	4.30	3.47	0.55	2.36	6.80	8.47	13.61
		FA	5.41	5.00	2.36	2.36	4.86	11.11	14.02	16.66
		SPE	4.3	4.16	3.88	7.77	12.91	43.05	44.30	53.88
	QDA	PCA	5.41	4.48	1.94	**0.27**	0.55	**0.00**	**0.00**	**0.00**
		FA	5.55	4.02	1.38	1.11	0.83	0.69	0.13	0.13
		SPE	5.00	3.33	2.91	1.80	1.11	0.41	0.13	**0.00**

Table 1. Error ($w_{err}[\%]$) resulting from misclassification of DCT and cepstral feature vectors into damage classes after discriminant analysis (LDA or QDA) and dimensionality reduction (PCA, FA or SPE).

P2B1-4

8:00 am   Ultrasonic Chirplet Echo Parameter Estimation using Time-Frequency Distributions

Pramod Govindan[1], Alireza Kasaeifard[1], **Jafar Saniie[1]**; [1]*Electrical and Computer Engineering, Illinois Institute of Technology, Chicago, Illinois, USA*

Background, Motivation and Objective

Chirp signals are frequently encountered in ultrasonic non-destructive testing (NDT) and imaging applications. Chirplet echo parameters signify valuable information such as size, shape and orientation of the reflectors as well as the physical properties of propagation path in ultrasonic NDT applications. In most cases, detected echoes are overlapped due to microstructure scattering, and minimal spacing of reflectors. This imposes challenges in decomposing the echoes and extracting the echo parameters accurately. Hence, it is very important to develop a methodology to efficiently and accurately estimate the chirplet echo parameters.

Statement of Contribution/Methods

This study uses 2 different time-frequency (TF) representations of ultrasonic signal to sequentially estimate the chirplet echo parameters: (i) Wigner-Ville Distribution (WVD), and (ii) Short Time Fourier Transform (STFT). WVD provides high resolution, however suffers from cross term interference. STFT does not produce cross-terms, however suffer from poor resolution. Both WVD and STFT of a chirplet signal have the form of concentric ellipses in TF plane. Thus, this study utilizes the ellipse fitting method to locate chirp echoes within elliptical shape in the TF plane. TF distributions result in a number of elliptical contours with different axial lengths corresponding to different TF amplitudes. Ellipses with larger axial lengths correspond to smaller amplitude, which suffers from noise interference, thus the SNR will be low. These ellipses can more accurately estimate the parameters due to the availability of more data points. Ellipses with smaller axial lengths correspond to higher amplitude. These contours have higher SNR; and low estimation accuracy. Therefore, average of estimates from multiple ellipses corresponding to different amplitudes is considered for parameter estimation.

Results/Discussion

TF representation of the chirplet signal is analytically examined and transformed into the form of general ellipse equation. Parameters of this ellipse are compared with the parameters of the estimated ellipse from the experimental signal, to determine the chirplet echo parameters. This algorithm accurately estimates the ellipse even from an incomplete set of data points. Furthermore, the effect of window kernel being used for the estimation is analyzed, and the performance of estimation algorithm is evaluated using both simulated and experimental data. In this study, echo parameters of a simulated chirplet representing data from a 5 MHz broadband transducer and a sampling frequency of 100 MHz are examined. This chirplet echo is perturbed with different noise levels. The echo detection process is repeated 50 times with different noise patterns. The low variance values of the estimated parameters indicate that the algorithm is able to accurately estimate the echo parameters in the presence of noise. This observation is also confirmed using experimental data.

P2B1-5

8:00 am   Sparse Deconvolution of Ultrasound NDE Echoes Accounting for Pulse Variance

Ramazan Demirli[1], Pramod Govindan[2], **Jafar Saniie[2]**; [1]*Center for Advanced Communications, Villanova University, Villanova, Pennsylvania, USA,* [2]*Electrical and Computer Engineering, Illinois Institute of Technology, Chicago, Illinois, USA*

Background, Motivation and Objective

Ultrasound NDE data is comprised of a sequence of echoes backscattered from the reflectors situated along the transducers focused beam. These backscattered echoes contain valuable information pertaining to the acoustic impedance, geometric shape, and size of the reflectors. The ultimate objective of ultrasound imaging systems is to display this information termed as reflectivity function (RF). However, the backscattered echoes convey only the convolved version of the RF by the bandlimited transducer pulse. Various deconvolution techniques have been proposed over the years to restore the RF by inverting this convolution process. More recently, a new class of deconvolution algorithms is emerged in the compressive sensing (CS) field to exploit the sparsity of RF. In contrast to classical inversion based methods, these sparse deconvolution methods (SDMs) directly estimate the RF and provide significant resolution gains. However, SDMs generally assume the ultrasound pulse is invariant throughout the propagation path. While convenient, this assumption is not realistic in ultrasound NDE due to the frequency dependent absorption and scattering. As such, pulse variance severely compromises the performance of SDMs and leads to inaccurate estimations of the RF. The goal of this study is to develop a restoration technique that is sparse while accounting for pulse variance.

Statement of Contribution/Methods

We propose a new formulation of the RF recovery based on an ultrasound measurement model in which the ultrasound signal is expressed as a sequence of parametric model echoes whose shapes are allowed to vary in accordance with the spectral characteristics of the measuring transducer. We then utilize a Maximum a Posteriori Estimation (MAPE) method to estimate concurrently the reflectivity and spectral parameters of the echo from the local data. We tested our approach in comparison with an SDM (l1-regularized Least Squares Deconvolution, l1 -LSD) via series of computer simulated ultrasound data that contains varying pulses. The restored RFs are compared against the ground truths using the correlation match index (CMI) metric.

Results/Discussion

MAPE and l1-LSD have been tested on ultrasound NDE data measured from a specimen with closely spaced reflectors. Then, the RFs of the medium were restored using l1-LSD and MAPE algorithms. MAPE not only provides accurate RFs of closely spaced reflectors but also reveals the echo frequency characteristic as evident in the pulse spectrum. The l1-LSD, however, due to its inflexibility with varying pulses, fails to resolve the true reflectors. Further, compared to l1-LSD, the MAPE provides on average 20% improvement in CMI and is about 10 times computationally faster.

P2B1-6

8:00 am   Singular spectrum analysis for trend extraction in ultrasonic backscattered echoes

Yufeng Lu[1], **Jafar Saniie**[2]; [1]*Electrical and Computer Engineering, Bradley University, Peoria, USA,* [2]*Electrical and Computer Engineering, Illinois Institute of Technology, Chicago, USA*

Background, Motivation and Objective

In ultrasonic NDE applications, backscattered echoes are commonly used to characterize important physical information along the propagation path. These echoes are highly overlapped due to microstructure scattering noise resulting from the discontinuities with random locations, orientations and sizes. There have been many signal processing algorithms, parametric or non-parametric, time domain or joint time-frequency domain, that are applied to unravel and analyze ultrasonic echoes. Due to the complexity and non-stationary nature of ultrasonic signal, it still remains as a challenging problem to extract the desired signal information for nondestructive testing, quality control, material characterization and structural health monitoring.

Statement of Contribution/Methods

Unlike transform-based algorithms, singular spectrum analysis (SSA) is a time series analysis algorithm. This algorithm has been used to analyze non-stationary data in numerous applications such as biomedical, speech, geophysical, meteorology, etc. In this investigation, SSA is explored to decompose and analyze ultrasonic signals in NDE application. It is implemented as follows: First a trajectory matrix is obtained from ultrasonic signal, then singular vector decomposition (SVD) is performed on the trajectory matrix to obtain its eigenvalue and eigenvectors, where eigenvalues are sorted and regrouped. Finally, diagonal averaging is applied to reconstruct time series components corresponding to different groups of eigenvalues. As a result, the ultrasonic signal is decomposed through the four step processing (i.e., embedding, SVD, grouping and diagonal averaging). The decomposition result can be used to characterize ultrasonic signals for the nondestructive evaluation of materials.

Results/Discussion

In this paper, the application of singular spectrum analysis is demonstrated in ultrasonic signal processing. Simulation and experimental results show that singular spectrum analysis reveals signal trend related to defects and grain scatters. The performance of the algorithm is also compared with other algorithms of ultrasonic signal decomposition for signal analysis and feature extraction. Numerical and analytical results demonstrate that singular spectrum analysis is effective in ultrasonic signal analysis. Especially the data-driven nature makes singular spectrum analysis unique for signal analysis. This algorithm can be utilized for flaw detection, signal classification, and pattern recognition in NDE applications.

P2B1-7

8:00 am   Fast total focusing method for ultrasonic imaging

Ewen Carcreff[1], Dominique Braconnier[1], Gavin Dao[2]; [1]*The phased array company, West Chester, Ohio, USA,* [2]*AOS NDT, Cincinnati, Ohio, USA*

Background, Motivation and Objective

The total focusing method (TFM) is an efficient approach to perform ultrasonic imaging of industrial components. It consists in focusing at each point of a reconstruction area by applying coherent summations. The main issue of this method is the computation time which makes real-time imaging difficult for large images.

Statement of Contribution/Methods

In this paper, we propose to develop a migration technique working in the wavenumber domain and which accelerates the processing. The contribution of this paper is the fast implementation of the method using graphics processing unit (GPU) for real-time imaging applications. Moreover, we perform a comparison with the conventional approaches, also accelerated with GPU.

Results/Discussion

With real data, we show that this approach is much faster than conventional techniques, and that the signal to noise ratio is highly increased. Those results demonstrate the potential of the method in real-time imaging applications.
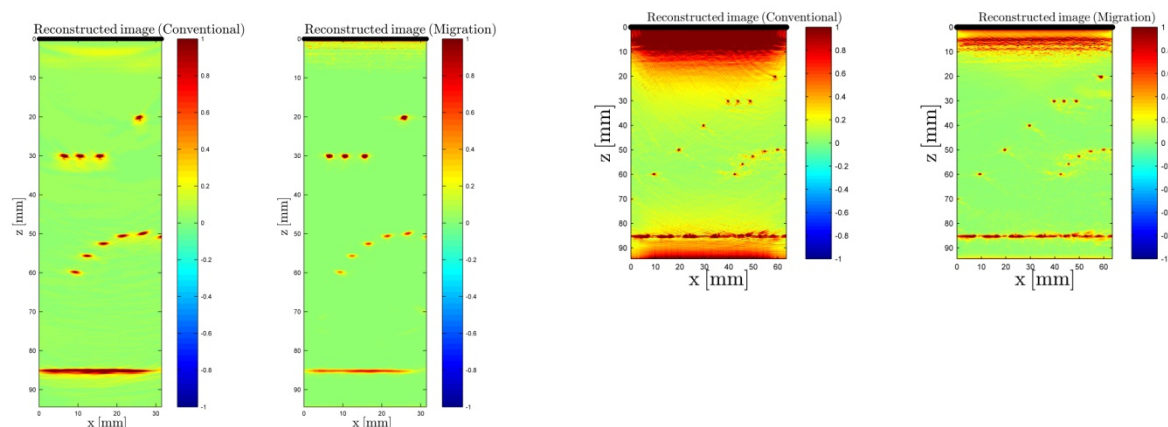
P2B2 - Wave Propagation Modeling

4th floor

Friday, October 23, 2015, Posters displayed 08:00 am - 05:00 pm. Authors must be present at their poster from 9:30 - 10:30am (odd number posters) and 14:30 – 15:30pm (even number posters).

Chair: **Walter Arnold**
Saarland University

P2B2-1

8:00 am **Acoustic Imaging of the Circular Wedge-like Acoustic Waveguides**

Tai-Ho Yu[1]; [1]*National United University, Taiwan*

Background, Motivation and Objective

This proposal investigated the propagation of flexural waves along the outer edge of a circular cylindrical wedge, as well as phase velocities and the corresponding mode displacement. Thus far, only approximate solu-tions to these problems have been derived because of the complexity of boundary-value problems. In this study, the dispersion curves were determined using the bi-dimensional finite element method (Bi-d FEM), as derived through the separation of variables and the Hamilton principle. According to a calculation of modal displacement, the maximum deformation appeared at the outer edge of the wedge tip.

Statement of Contribution/Methods

Additionally, the acoustic images were measured using a laser-induced guided wave experiment, in which a knife-edge measurement scheme and a two-dimensional fast Fourier transform (2D-FFT) method were used. According to the 2D-FFT calculation results of B-scan data from the laser-generated flexural waves at the circular cylindrical wedge tip, most of the measured signals belonged to the first and second modes.

Results/Discussion

The reliability of numerical solutions was confirmed, and the necessity of numerical solutions in the design and application of wedge-like acoustic waveguides was subsequently validated. Regarding the design of circular cylindrical wedge wave ultrasonic motors, a flexural wave with a low mode number N and high wavenumber k was selected as the driving mode.
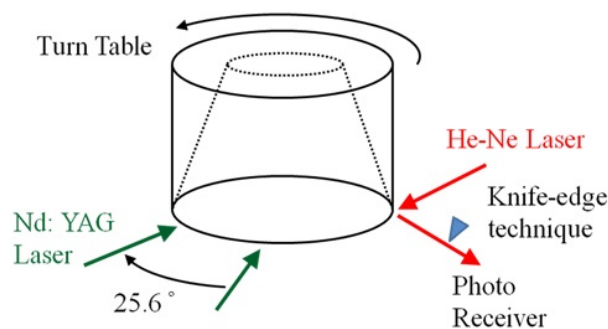
Fig. 1: Schematic of measurement process.
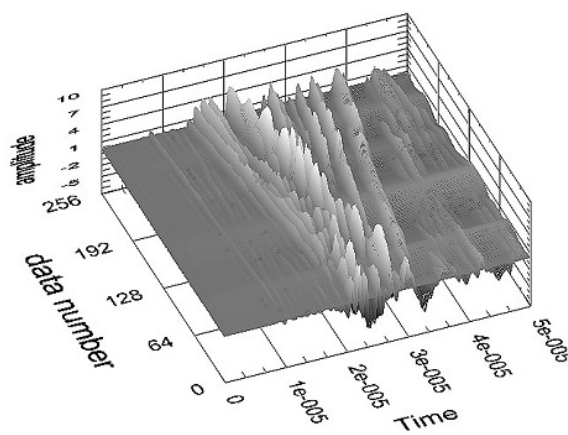
Fig. 2. Scanned image of a circular wedge

P2B2-2

8:00 am **Hybrid MM-MOC-based Numerical Simulation of Acoustic Wave Propagation with Non-uniform Grid and Perfectly Matched Layer Absorbing Boundaries**

Yuta Matsumura[1], Kan Okubo[1], Norio Tagawa[1], Takao Tsuchiya[2], Takashi Ishizuka[3]; [1]*Tokyo Metropolitan University, Japan*, [2]*Doshisha University, Japan*, [3]*Shimizu Corporation, Japan*

Background, Motivation and Objective

In recent years, time domain-numerical analysis for sound wave propagation has been investigated widely as a result of advances in computer technology. The development of accurate numerical schemes is an important issue. A method of characteristics (MOC) is used as a time domain numerical analysis method, examples of which are the constrained interpolation profile (CIP) method, and the QUICKEST method. However, new grid systems are required for the numerical simulation of large-scale simulations of wave propagation. To overcome these problems, we introduce the non-uniform grid system for the scheme combining multi-moment-MOCs, the Hybrid MM-MOC, with perfectly matched layer (PML) technique.

Statement of Contribution/Methods

In this study, we introduced the non-uniform grid for the MM-MOCs. This technique as well as sub-grid technique has an advantage of using a small amount of memory. Additionally the acoustic numerical analysis by MOCs, including CIP method, requires setting the absorbing-boundary condition (ABC); consequently, we introduce the PML technique into the non-uniform grid system for hybrid MM-MOC simulations of wave propagation.

Results/Discussion

We show that the use of a suitable non-uniform grid reduces the time and memory necessary for calculation. Figure 1 shows the sound pressure distribution obtained by hybrid MM-MOC analysis with non-uniform grids. We can ascertain the propagation behavior including the non-uniform grid region and find little reflection waves from PML boundaries. This reveals that PML technique can work efficiently for non-uniform grids of MOCs. Figure 2 shows the calculation time and memory used of conventional CIP method and hybrid MM-MOC method. From the numerical results, the use of a suitable non-uniform grid reduces the time and memory.
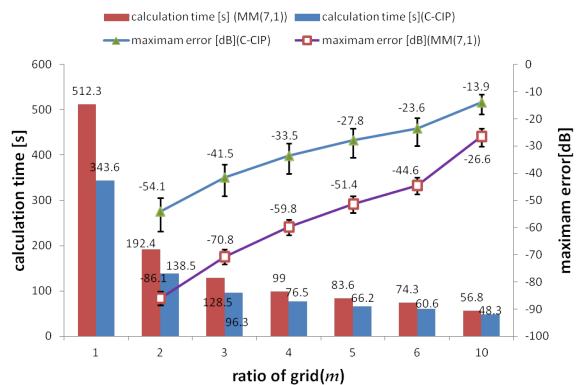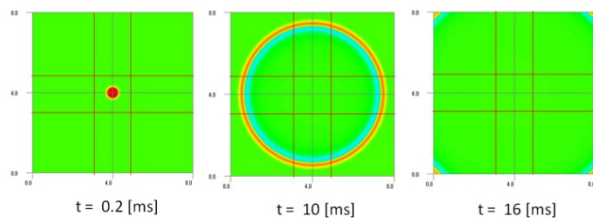
P2B2-3

8:00 am   Backward guided modes with double zero-group-velocity points in liquid-filled pipes

Weijun lin[1], Hanyin Cui[1]; [1]*State Key Laboratory of Acoustics, Institute of Acoustics Chinese Academy of Sciences, beijing, China, China, People's Republic of*

Background, Motivation and Objective

Liquid-filled pipes used in the industry need to be inspected regularly to ascertain their safety and reliability. Recently, a non-contact technique based on zero-group-velocity (ZGV) Lamb modes has been developed to measure elastic constants and geometry integrity of hollow cylinders. The objective of this paper is to study the influence of liquid loading on ZGV modes, so that to investigate whether ZGV technique can be used for online inspection of pipelines that are carrying liquid.

Statement of Contribution/Methods

This study provides theoretical and numerical analyses of dispersion and excitation characteristics of backward guided modes with double-ZGV points in liquid-filled pipes. The dispersion equation of longitudinal guided modes is derived, and then simplified to obtain its approximation form for mode coupling analyses. Then, a point source model is considered at the origin of the cylindrical coordinates, amplitude spectra and dispersion curves of ZGV modes are numerically simulated and analyzed.

Results/Discussion

Typical results are presented. Fig. 1 shows dispersion curves of three longitudinal modes in a thin-walled pipe filled with water. In Fig.1, the slope of each curve changes its sign for twice, i.e., each backward propagating mode with negative slope (dotted line) has two ZGV points. The six ZGV modes correspond to finite phase velocity and vanishing group velocity. This type of backward mode with double-ZGVs has not been found in a hollow pipe, while it is not rare in a liquid-filled pipe.

Generally, for a thin-walled pipe, the water loading could dramatically affect the backward and ZGV modes. The strong mode coupling causes two types of backward modes with single- or double- ZGV points, so that to greatly increase the number of ZGV modes. From the analysis of excitability, it is concluded that all the ZGVs are in the highly excitable condition by the point source. And those ZGV frequencies usually shift from the original ZGV frequency in the hollow pipe. It means that, next to the original ZGV frequency, it is expectable to see a number of ZGV resonances. The group of ZGV resonances may greatly increase the intensity of the ZGV signal. It implies that ZGV modes have the potential to be applied for pipeline inspections.
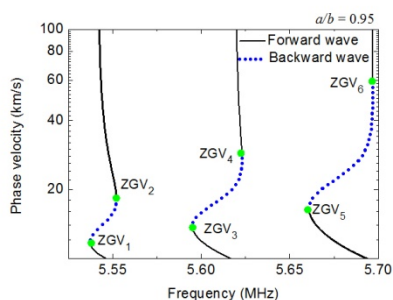
P2B2-4

8:00 am   An Optimized Guided Waves' Focus Method to Eliminate the Effect of Dispersion: Theoretical and Experimental Research

FuLi Xie[1], Shouguo Yan[1], Mingfei Cai[1], Han Dong[1], Bixing Zhang[1], Junjie Gong[1]; [1]*State Key Laboratory of Acoustics, Institute of Acoustics, Chinese Academy of Sciences, Beijing, China, People's Republic of*

Background, Motivation and Objective

Guided waves have always been an important means of non-destructive testing and evaluation (NDT&E), especially in the NDT&E of waveguide structural materials, for the guided wave is more suitable than the traditional bulk waves here. In the waveguide structure, the guided waves have energy flow mainly along the direction of the guiding configuration, so the guided waves can stably propagate longer in waveguide structural materials than bulk waves. Hence, using guided waves make the inspection of a large area of waveguide structural materials possible without moving the excited transducer.

However, the guided waves are usually dispersive and multi-mode, which causes it is hard to collect and identify. In this paper, we propose a method to eliminate the effect of dispersion of guided waves. All phases of the guided wave excited by the designed excited signal arrive at the desired target simultaneously. Not only for the amplitude gain, also the waveform is narrow down in time domain and concentrates in space domain.

Statement of Contribution/Methods

Consider a suitable structure in which acoustic guided waves can propagate. As a given wave-guide structure, the frequency dependent velocity of the guided waves is convenient to calculate by mathematical means. Therefore, if every frequency component of the guided waves has a corresponding excited delay, all phases of the guided waves can arrive at the target simultaneously. For achieving this goal, we propose an algorithm to process the excited signal. First, the time delay of every frequency component of the guided waves is obtained by solving the dispersion function. Then, add these time delays into the frequency domain function of the guided waves. Finally, the excited signal of the optimized focus method can be get by conducting the Fourier transform on the frequency function of the guided waves with time delays. Loading this signal to the excited transducer, the received waveform should be temporally and spatially focused.

Results/Discussion

We choose the Rayleigh wave propagated in a three-layer media to do the numerical simulation and experimental research, in order to investigate the feasibility and focus effect of the optimized focus method. The media consists of aluminum, Plexiglas and steel. The dispersion curves and time domain waveform of the Rayleigh wave can be calculated by transfer matrix method conveniently. The simulated results show that this method can focus the dispersive Rayleigh wave. The received waveform has high amplitude gain, and the side lobes of the waveform are efficiently suppressed. Compared with the results of time reversal method, the energy of received waveform of this optimized focus method is more concentrated, most energy concentrates on the main lobe and the amplitudes of the side lobes are lower. Furthermore, the experimental results approve the availability of the optimized focus method, which perfectly match the theoretical deduction.

P2B2-5 _____

8:00 am   **Anomalous dispersion of Stoneley waves in fluid-filled boreholes**

Weijun lin[1], Hanyin Cui[1]; [1]*State Key Laboratory of Acoustics, Institute of Acoustics Chinese Academy of Sciences, beijing, China, China, People's Republic of*

Background, Motivation and Objective

For acoustic logging, the estimation of rock properties from Stoneley waves is of considerable importance. Stoneley wave is the interfacial wave propagating on the interface between the borehole liquid and the formation. In the majority of cases in physics, phase velocity decreases with frequency, so that this type of dispersion is referred to as normal dispersion. On the other hand, phase velocity increases with frequency. It happens less frequently in physics, and it is referred to as anomalous dispersion. However, anomalous dispersions are commonly encountered for borehole Stoneley waves. We studied influences of formation properties on the existence of anomalous dispersion of Stoneley waves, to investigate the correlations.

Statement of Contribution/Methods

Dispersion properties of Stoneley waves in boreholes are investigated. The oil well model is a cylindrical fluid-filled borehole located in an infinite extended solid media. Assuming a point source is positioned at the origin, only the axisymmetric longitudinal modes are propagating in the borehole. Phase and group velocity dispersion curves are numerically calculated using the bisection technique to resolve the roots of dispersion equation. Both fast and slow formation models are considered, here the fast formation model means that shear velocity of formation is faster than sound velocity of the borehole liquid.

Results/Discussion

From literatures, in the case of fast formation, Stoneley waves hold anomalous dispersions in the whole frequency range. However, it was found that certain Stoneley waves exhibit both normal and anomalous dispersions. Typical results of phase and group velocity dispersion curves of a Stoneley wave in a fast formation model are given in Fig.1. Fig.1 suggests the existence of distinct regions where the phase velocity is larger than the group velocity-normal dispersion; and the converse-anomalous dispersion. As shown in Fig.1, these anomalous dispersions of the Stoneley wave exist in two distinct frequency bands $0.8 < f < 14.4$ kHz and $f > 82.8$ kHz.

It was also found that the appearance of anomalous dispersion is sensitive to the shear velocity of the formation, which suggests that anomalous dispersion of borehole Stoneley wave could be related to the formation properties.
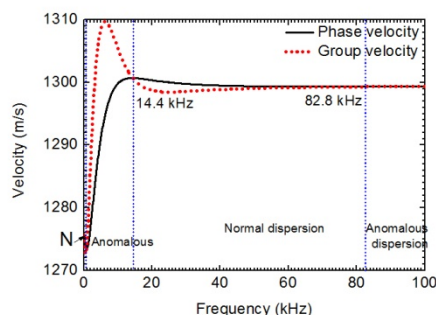
P3B1 - Acoustic Tweezers and Particle Manipulation II

4th floor

Friday, October 23, 2015, Posters displayed 08:00 am - 05:00 pm. Authors must be present at their poster from 9:30 - 10:30am (odd number posters) and 14:30 – 15:30pm (even number posters).

Chair: **Anne Bernassau**
Heriot-Watt University

P3B1-1 _____

8:00 am **Tangential Streaming Analysis on Ultrasonically Levitated Droplet through the Boundary Layer Approximation with Moving Particle Semi-implicit and Distributed Point Source Method**

Yuji Wada[1], Kohei Yuge[1], Hiroki Tanaka[2], Kentaro Nakamura[2]*; [1]Faculty of Science and Technology, Seikei University, Musashino, Japan, [2]Precision and Intelligence Laboratory, Tokyo Institute of Technology, Yokohama, Japan*

Background, Motivation and Objective

Ultrasonic levitation has recently been drawing attention as a way of non-contact transportation of small objects, such as liquid droplets, in bioengineering and manufacturing industry. The small objects in the finite amplitude sound field have been known to be trapped near the pressure node of the standing wave with the effect of acoustic radiation force. The levitated droplet is reported to turn its shape from sphere to spheroid, and to drive an internal streaming on its surface when they are exposed in the intense sound pressure field. Several analytical reports have mentioned this phenomenon, however, almost no report carried out dynamical simulation on the shape change or internal streaming of the droplet.

Statement of Contribution/Methods

The levitated droplet shape and streaming is simulated by coupling two gridless analysis methods, the one is distributed point source method (DPSM) and the other is moving particle semi-implicit (MPS) method. The acoustic radiation stress including Reynolds stress is calculated using the result of DPSM acoustic analysis. This static stress drives the droplet deformation and the streaming on MPS fluid dynamic analysis. The renewed acoustic reflection by the droplet shape and position is considered in the next step of the acoustic analysis. Because Reynolds stress on the droplet surface depends on the viscosity of air, acoustic DPSM is extended to handle the boundary layer approximation to calculate the steep change of particle velocity within the layer.

Results/Discussion

When a cylinder suspended in the acoustically vibrating field, a typical Schlichting acoustic streaming is known to be generated as a result of Reynolds stress. Fig. 1 shows the driving forces distribution within the boundary layer near the cylinder, when the cylinder is exposed in plain standing wave along the vertical (z) direction. The field is calculated by the suggested DPSM routine with boundary layer approximation. This vector field corresponds to theoretically-derived streaming function result in literature.
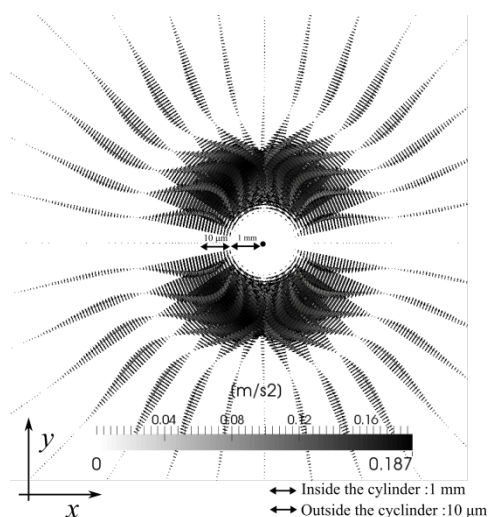
Fig.1 Driving force distribution just above the droplet surface

P3B1-2 _____

8:00 am **Controllable generation of acoustical vortices with sparse sources**

Haixiang Zheng[1], Qingyu Ma[1], Dong Zhang[2]*; [1]School of Physics and Technology, Nanjing Normal University, Nanjing, Jiangsu, China, People's Republic of, [2]Institute of Acoustics, Nanjing University, Nanjing, Jiangsu, China, People's Republic of*

Background, Motivation and Objective

Acoustical vortices are formed by helical waves rotating around the vortex core in a given direction due to the phase singularity. Based on the calculation of the acoustic intensity, it is demonstrated that the angular momentum of the acoustical vortices could be transferred to matter, which has potentials for the applications in alignment and manipulation of small object. Angular momentum transfer was determined by the ratio of the beam's topological charge to its angular frequency. In previous study, big number element matrix transducer array with the phase increment of pi/4 or pi/2 are often employed to generate acoustical vortices with high topological charge. However, the relationship among source number, phase difference and topological charge has not been investigated. How to produce controllable distributions of pressure and phase with sparse sources in simple configuration is still an important topic.

Statement of Contribution/Methods

A phase coded approach is proposed to generate controllable acoustical vortices with sparse sources. Based on the radiation theory of point and directional sources with coded initial phases, the physical mechanism of acoustical vortices is theoretically investigated with explicit formulae. Numerical simulations of axial and radial distributions

of pressure and phase are conducted for different parameters using N sources. The proposed method is also verified by the measurements of annular pressure distribution, linear phase distribution and axial null using a 16-source experimental system.

Results/Discussion

It is demonstrated that with proper design of source phases, acoustical vortices can be generated in homogeneous medium as a helical beam with annular pressure distribution and axial null. Spiral acoustic wavefront with linear circular phase distribution is also achieved with a controllable topological charge, which has a maximal value of Fix[(N-1)/2]. The measured distributions of pressure and phase of acoustical vortices and the corresponding variations caused by different topological charges have good agreements with the simulation results. Angular momentum transfer of acoustical vortices is also demonstrated by the stable rotation of a hanging plate. The favorable results confirm the feasibility of controllable generation of acoustical vortices with sparse sources and suggest the application potential in object alignment or particle manipulation.

P3B1-3

8:00 am   Transverse Manipulation of Microbubbles using Acoustic-Vortex Tweezers

Wei Chen Lo[1], Shih Tsung Kang[1], Chih Kuang Yeh[1]; *[1]Department of Biomedical Engineering and Environmental Sciences, National Tsing Hua University, Hsinchu, Taiwan*

Background, Motivation and Objective

The feasibility of particle trapping in an acoustic vortex has been theoretically validated. The low frequency, long working distance, and single-beam configuration provide superior usefulness compared with those of conventional standing-wave acoustic tweezers particularly in drug delivery applications. This study experimentally validated the feasibility of acoustic-vortex trap for manipulation of microbubbles (MBs) that are used as ultrasound contrast agents and drug delivery carriers. The trapping characteristics may be useful to increase the efficiency of MBs accumulation at targeted disease areas.

Statement of Contribution/Methods

The acoustic vortex was created by producing a phase dislocation from 0 to 2π along the beam axis using a 4-element homemade 2-MHz ultrasound transducer. The transducer transmitted 5000-cycle sinusoidal bursts with an equal phase difference of $\pi/2$ applied to the adjacent elements (Fig. 1(a)). The transverse structure of the acoustic vortex produced a steep pressure gradient (Fig. 1(b)), which was assumed to behave as a series of potential wells, especially at one fourth the Rayleigh distance (RD/4) of 10.47 cm from the transducer. The trapping of MBs was tested in an agar phantom exposed to the acoustic vortex at different distances with the peak pressure normalized to 270 kPa. The behaviors of MBs (Fig. 1(c)) were monitored using a commercial ultrasound image system.

Results/Discussion

Significant transverse trapping effect of MBs was observed at only RD/4 but not at other distances, since the pressure gradient near the beam axis was 8.25 kPa/mm, which was at least five times higher than that in the outer area. The steep pressure gradient produced inward trapping forces driving MBs to move toward the center and finally confine in the beam width of 1.1 mm. It was able to move the trapped MBs cluster along a square path with a width of 15 mm at a speed of 0.0017 m/s without loss of control (Fig. 2). Increasing the duty cycle of transmitted pulses was found to increase the stability of the manipulation. The results confirmed the trapping properties of an acoustic vortex are feasible for MBs, which is useful for spatiotemporal manipulation. The effects of varying ultrasound parameters and distances on trapping stability will be discussed.
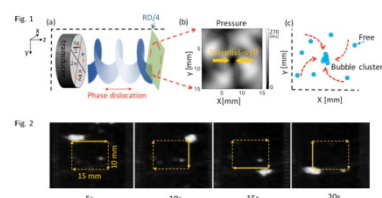
P3B1-4

8:00 am   Spatial selective trapping of microparticles using a quasi-periodic phononic crystal plate

Chen Wang[1,2], Feiyan Cai[2], Li Fei[2], Long Meng[2], Yan Kang[1], Hairong Zheng[2]; *[1]Sino-Dutch Biomedical and Information Engineering, Northeastern University, China, People's Republic of, [2]Shenzhen Institutes of Advanced Technology Chinese Academy of Sciences, China, People's Republic of*

Background, Motivation and Objective

Selective and tunable manipulation of microparticles is required to meet the demands for high-throughput and location specific analysis in lab-on-chip applications. Different types of microchannels combined with flow hydrodynamics have been widely used for the passive selective manipulation of microparticles in microchips. However, the complexity of channel structure obstructs the performance of the microchip. Recently we have demonstrated that a phononic crystal plate (PCP) with a flat surface can actively manipulate a large number of particles in a tunable manner. Here, we will further investigate spatial selective trapping of microparticles using a quasi-periodic PCP (QP-PCP). This system may have potential applications in acoustofluidics for spatial selective manipulation of microparticles with non-structural channel.

Statement of Contribution/Methods

As shown in Fig. 1(a), the QP-PCP consists of a brass plate patterned with three groups of periodical arrays (period P1, P2 and P3) of brass gratings beneath the brass plate. Each group contains 17 periodical units and therefore the total sample covers 51 periodical units. Three cylindrical brass particles (radius 0.5mm) are placed on top of the QP-PCP with a separation distance of 0.1mm and situated in the middle of each periodical array, respectively. The entire system is immersed in water. The finite element method (COMSOL) combined with momentum-flux tensor is applied to obtain the transmission spectrum of the system and the acoustic radiation force (ARF) for each particle. An acoustic Gaussian beam is normally incident from the bottom boundary.

Results/Discussion

As shown in Fig. 1(b), the transmission spectrum of the system shows three pronounced peaks with frequencies of 0.917MHz, 0.981MHz and 1.054MHz, which originate from the resonant excitation of nonleaky A0 Lamb modes by the aforementioned three groups of periodical arrays, respectively. While around these resonant frequencies, the particles on the periodical arrays experience maximum negative ARFs respectively. It is indicated that the ARFs of particles on the surface of QP-PCP are dependent on their individual positions and frequencies. Thus, this system may have potential application in spatial selective trapping of microparticles.
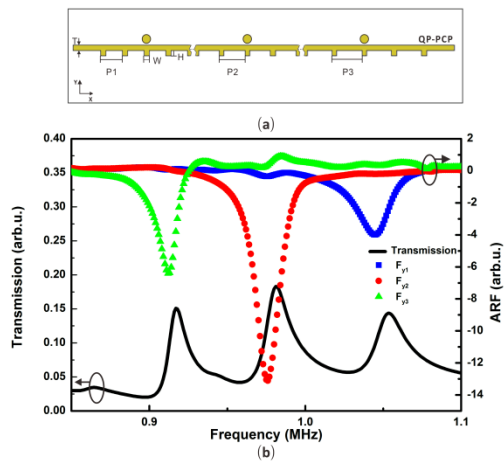
Figure 1 (a) Schematic view of the calculated system (Thickness T=0.27mm, Width W=0.23mm, Height H=0.23mm and Period P1=1.05mm, P2=1.1mm, P3=1.15mm). (b) Numerical results of transmission spetrum of the QP-PCP (black line). The ARFs (Fy₁,Fy₂,Fy₃) in the Y-direction on three particles near the surface of the QP-PCP (color dots).

P3B2 - Phononics II

4th floor

Friday, October 23, 2015, Posters displayed 08:00 am - 05:00 pm. Authors must be present at their poster from 9:30 - 10:30am (odd number posters) and 14:30 – 15:30pm (even number posters).

Chair: **Anne Bernassau**
Heriot-Watt University

P3B2-1 _____

8:00 am **Coupling and quality factor estimation of pillar resonators on a surface**

Vincent Laude[1], Lyes Djoumi[1], Sarah Benchabane[1]; *[1]FEMTO-ST / CNRS, Besancon, France*

Background, Motivation and Objective

The band gaps of phononic crystals result either from Bragg diffraction at crystal planes or from the existence of local resonances within the unit cell of the crystal. Pillar-based phononic crystals, in particular, have drawn attention recently since they display frequency band gaps extending deep inside the sound cone for surface elastic waves. As a consequence, they theoretically support radiation-less propagation of surface waves, assuming perfect periodicity. The existence of locally-resonant band gaps has also been shown experimentally not to require strictly periodicity. In this work, we examine the resonances of single pillars on a surface and how they couple via evanescent waves in the substrate when they are placed in a sequence.

Statement of Contribution/Methods

We investigate the elastic resonances of single metallic pillar resonators placed on a semi-infinite substrate. Our finite element model includes a perfectly matched layer (PML) to terminate the computational domain and estimate radiation losses. In order to estimate the quality factor of resonances, two methods are implemented. First, a spatially random time-harmonic body force is applied to the pillar and the forced response of the system is obtained as a function of frequency. Second, the complex eigenvalues of the elastodynamic problem are obtained, with the imaginary part of the frequency accounting for radiation losses. In order to investigate the coupling of neighboring pillars, the same two computation techniques can be used. In particular, the response to a force applied to one pillar and measured at another pillar is used to infer an effective coupling coefficient.

Results/Discussion

For a single pillar, the response to a random force is used to obtained a phononic power spectral density. This spectrum is composed of a sequence of Lorentzian functions, each corresponding to a resonance of the pillar connected to the substrate. The width of the Lorentzian directly measures the quality factor of the resonance. The eigenvalue computation with PML concurrently gives a sequence of complex eigenfrequencies, from which the resonance frequency and the quality factor can be directly obtained. We show that the estimated resonance frequencies and quality factors are the same with both methods. Observation of the distribution of eigenmode displacements also informs about radiation to the bulk from the vibrating pillar.

When two or more pillars are placed in proximity on the surface, we observe a splitting of the resonance frequencies, corresponding for instance to symmetric and anti-symmetric coupled eigenmodes in the case of two identical pillars. The effective coupling coefficient is estimated either via the frequency splitting effect or via the relative response of the pillars when a force is applied to one of them. With these information about coupling, we intend to find conditions for the propagation of vibrations along a chain of pillars on a surface.

P3B2-2 _____

8:00 am **Focalization of surface acoustic waves through a gradient index lens**

Bernard Bonello[1], Jinfeng Zhao[2], Olga Boyko[2]; *[1]INSP, CNRS / Paris University, Paris, France, [2]INSP, Paris University, Paris, France*

Background, Motivation and Objective

In contrast with conventional PCs whose focusing properties rely on the folding of some dispersion curves, Gradient-index (GRIN) phononic crystals (PCs) are 2D hererostructures designed to be efficient at low frequencies, where the elastic wavelength is much larger than the period of the PC. To date, most of the works dealing with these systems are considering the focusing of zero-order Lamb waves propagating in thin plates. In view of the importance of the surface acoustic waves for micro-electronics applications, we have been studying the case of Rayleigh waves propagating on the surface of PC's consisting of air holes drilled in a silicon substrate, with a diameter varying along the transverse direction of the lens. Our objective was to experimentally show that subwavelength focusing can be observed with this design of GRIN lens.

Statement of Contribution/Methods

The GRIN PCs we considered in this work were designed to focus Rayleigh waves on the silicon background in the near field behind the lens. The GRIN PCs were formed by piercing air holes in a silicon substrate. The lattice of air holes had the squared symmetry with the lattice parameter being of a few tens of μm for operations in the MHz range. The diameters of the holes, and therefore the refractive index, were varying along one direction of the lens according to a hyperbolic secant law. The ray trajectories within the lens were calculated using a formalism that accounts for the anisotropy along each line of inclusions. We then used a laser-based experimental setup to measure the normal displacements associated to the Rayleigh wave. The data were then compared to FEM simulations.

Results/Discussion

We show in Fig. 1a the GRIN lens and a snapshot of the out-of-plane displacement u_z measured on the on the Si substrate. The white lines are for the acoustic trajectories. The maximum amplitude (20 pm) is found to appear in the near field, at $x=17.5a$ and is more than twice as large as the amplitude of the incident wave (9 pm). The position of this maximum is in very good agreement with both the computed trajectories and the FEM simulations. The FWHM normalized to the wavelength in the background ($\lambda_B=4.91\ a$) was $0.58\ \lambda_B$, very close to the diffraction limit (Fig. 1b).
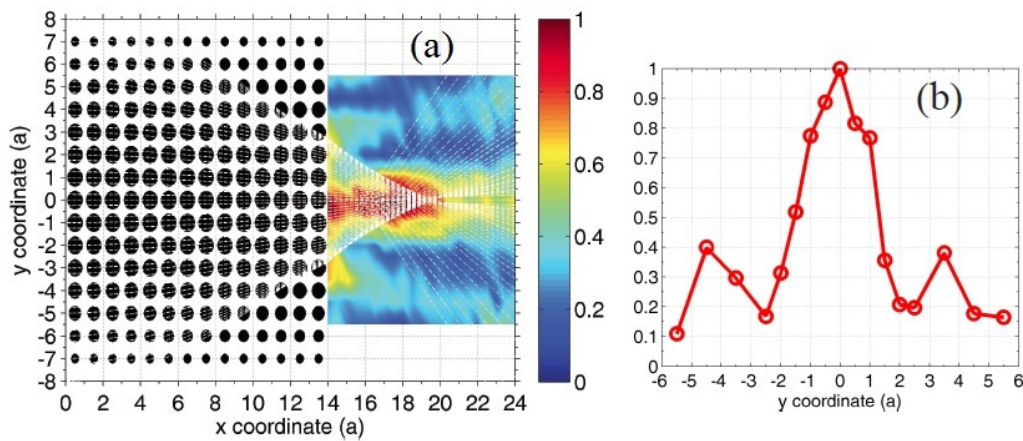
Figure 1: (a) GRIN lens (left part), ray trajectories (white lines) and normal displacement associated to the Rayleigh wave measured using an interferometric technique. The maximum displacement was measured to be ~20 pm. (b) Transverse profile at the focus, measured along *y* axis.

P3B2-3

8:00 am   Molecular dynamics simulation of nonlinear waves in granular media

Jia Yang[1], David Hutchins[1], Lolu Akanji[1], Peter Thomas[1], Lee Davis[1], Steven Freear[2], Sevan Harput[2], Nader Saffari[3], Pierre Gelat[3]; *[1]School of Engineering, The University of Warwick, Coventry, West Midlands, United Kingdom, [2]The University of Leeds, United Kingdom, [3]University College London, United Kingdom*

Background, Motivation and Objective

A train of solitary pulses has been generated experimentally in nonlinear granular chains (Hertzian chains) by a narrow frequency ultrasound excitation in our recent research [1]. The solitary pulses which exhibit a broad bandwidth with both sub-harmonic and higher-order harmonic content are of interest in biomedical ultrasound applications. The prediction of solitary pulses based on the scale, periodicity, and material properties of the chain structure is of fundamental importance to the design of new nonlinear ultrasound transducers. A molecular dynamics approach was thus studied as an effective solution to numerically simulate propagation of nonlinear waves in the discrete chain structure.

[1] D. A. Hutchins, J. Yang, O. Akanji, P. J. Thomas, L. A. J. Davies, S. Freear, S. Harput, N. Saffari and P. Gelat, "Evolution of ultrasonic impulses in chains of spheres using resonant excitation", Europhys. Lett., 109 (2015) 54002

Statement of Contribution/Methods

The discrete dynamic equations of particles in granular chains based on Hertz law were developed so as to simulate the experimental system. The contact dynamics involving both compression and separation between spheres was modelled. A Velocity Verlet Algorithm on molecular dynamics simulation was developed to solve the equations. The numerical results were compared with the experimental results and good agreement between them was obtained. Furthermore a robust simulation system was built to predict the expected output signals for a given forced resonance input and chain structure.

Results/Discussion

The simulation results indicate that the resultant waves are very sensitive to the initial conditions. The strongly nonlinear solitary pulses can be created in a certain chain structures once the excitation amplitude attains a specified threshold value. As shown in Figure, for a chain of 10 spheres with 1mm diameter, the solitary pulses gradually evolve with the voltage increase of the input sinusoidal wave for the given 73 kHz frequency. The distribution of the frequency spectrum of an output signal, after propagation along a chain of spheres, is shown to be a function of particle material, size, the length of the chain and the material of the boundaries forming the reflection at each end. An optimal chain structure can be designed by the simulation system based on the bandwidth and frequencies which are required within the output pulses.
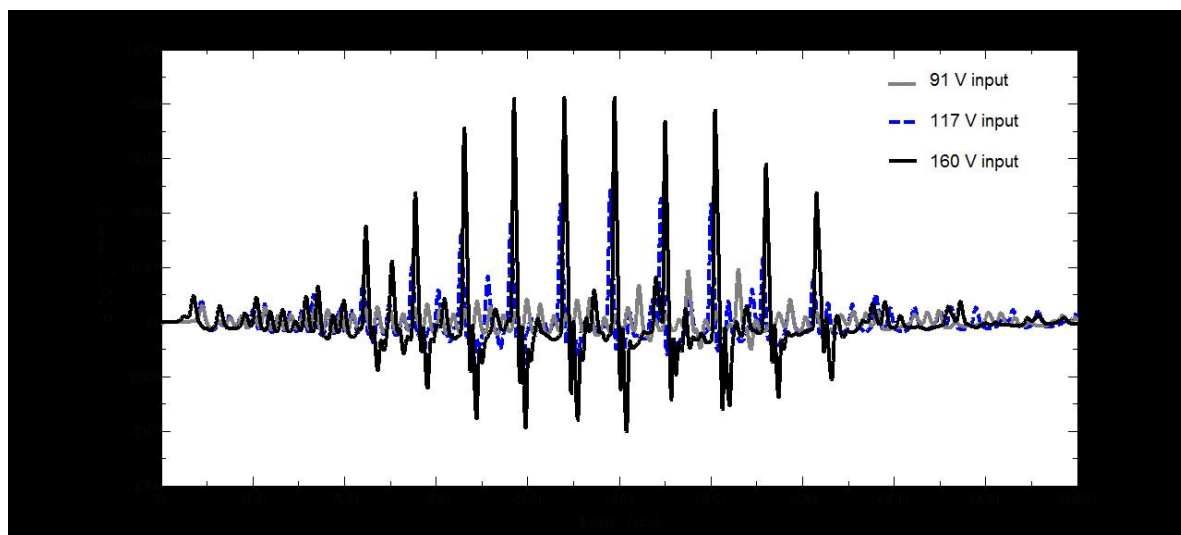
8:00 am   Effect of periodic patterned ZnO sensing film on a CO SAW resonator sensor

Tsung-Tsong Wu[1], Jia-Wei Luo[1], Lu-Chung Kuo[1]; *[1]Institute of Applied Mechanics, National Taiwan University, Taiwan*

Background, Motivation and Objective

Carbon monoxide (CO) is odourless, but highly toxic to humans and animals. In a conventional SAW sensor for CO detection, a selective film must be deposited and operate at an elevated temperature. In this paper, effect of periodic patterned sensing film on enhancing the sensitivity of the SAW resonator sensor will be studied both numerically and experimentally.

Statement of Contribution/Methods

The sensing film is an Au coated ZnO nanrods thin layer which can be operated at room temperature. To eliminate external environmental fluctuations, a dual delay line configuration[1] was adopted. The two-port SAW resonator sensor was based on a 128°YX LiNbO3 piezoelectric substrate. The resonant cavity was formed by two sets of 20 pairs of IDT and 50 reflective gratings on each side and the cavity length was 160 wavelengths. The operating frequency of the resonator was designed as 145 MHz. In the numerical calculations, the concentration of the CO gas was simulated by putting different conductivity on the ZnO sensing film. Two different configurations of the sensing film were studied, one is periodic patterned strips and the other is a full covered rectangular region. In the periodic one, the centerlines of the strips were aligned with the peak amplitudes of the waves inside the cavity (antinodes) and the width of the strip was set at one quarter wavelength.

In fabricating the Au coated ZnO nanrods thin layer, a ZnO film (50 nm thick) was deposited on the delay line as a seed layer by sputtering firstly. Lift-off process was adopted for periodically patterning the selective film width, namely $\lambda/4$ at the antinodes. Then, the ZnO nanorods were synthesized by an aqueous solution method. The gold nanoparticles were synthesized as a catalyst by immersing the SAW resonator in the aqueous solution of gold chloride trihydrate and sodium citrate tribasic dihydrate.

Results/Discussion

In the numerical simulations, the ZnO sensing layer with different conductivities were studied, i.e., 0., $0.1c_sv_0$, $0.15 c_sv_0$, $0.2c_sv_0$ and $0.25 c_sv_0$, where v_0 is the phase velocity and c_s is the sum of the dielectric constants of the substrate and air. The results showed that the resonant frequency and the insertion loss of the SAW resonator decrease as the conductivity increases. The comparison of resonant frequency shits showed that the frequency shift of the periodic patterned sensing film is approximately 20% larger than that of the full covered configuration and this in turn means the enhancement of the measurement sensitivity of the CO concentration sensing. On the experimental side, the measurement results well confirmed the numerical predictions, i.e., the sensing film with periodic patterned configuration achieves better sensitivity than that of the full covered pattern.

[1] F.-C. Huang, Y.-Y. Chen and T.-T. Wu, Nanotech. 20, 065501, 2009.

8:00 am   Design and characterization of 3D printed phononic crystals for sub-MHz ultrasound manipulation

Stefano Laureti[1,2], Omololu Akanji[1], Lee Davis[1], Marco Ricci[2], Simon Leigh[1], David Hutchins[1]; *[1]University of Warwick, United Kingdom, [2]Università degli studi di Perugia, Italy*

Background, Motivation and Objective

Phononic materials are engineered structures usually consisting of solid inclusions embedded in a matrix. Their exotic features, such as the presence of band gaps, wave bending and negative refractive index, have attracted much interest since their discovery [1]. However, there is still a need to broaden the working bandwidth of these crystals in order to increase their application to diagnostic ultrasound and non-destructive evaluation.

Statement of Contribution/Methods

The recent progresses achieved in both acoustic particle manipulation and 3D printing has opened the way to realizing more complex structures than those reported previously. Additive manufacturing has been used to construct materials in a new way, allowing different effects to be analyzed. The high acoustic impedance mismatch between the two materials used to realize our novel design assures the presence of band gaps where super-resolution can be achieved. The new structures have been used in combination with coded signals, thus exploring the possibility of using chirp signals to characterize the transfer function of the phononic crystal [2].

Results/Discussion

The specimens produced via additive manufacturing consisted of arrays of chrome-steel spheres embedded in a polymer matrix. As shown in Fig.1(a), it is possible to create columns of spheres (which can introduce non-linearity), as well as the more traditional regular array (Fig. 1(b)). These samples were placed in a water tank and excited by using a standard impulse signal and a broad-band chirp from 100kHz to 1MHz. The output signal was recorded by means of a small hydrophone held on a 2D scanning stage. The results achieved by both designs have been analyzed. We conclude that is possible to realize 3D-printed phononic crystals which can be used with coded signals. Furthermore, the careful choice of the geometrical arrangement of spheres can lead to novel effects.

[1] S. Yang, J. Page, Z. Liu, M. Cowan, C. Chan, and P. Sheng, "Focusing of Sound in a 3D Phononic Crystal," Phys. Rev. Lett., vol. 93, no. 2, p. 024301, Jul. 2004.

[2] Novak, A., Simon, L., Kadlec, F., & Lotton, P. (2010). Nonlinear system identification using exponential swept-sine signal. Instrumentation and Measurement, IEEE Transactions on, 59(8), 2220-2229.
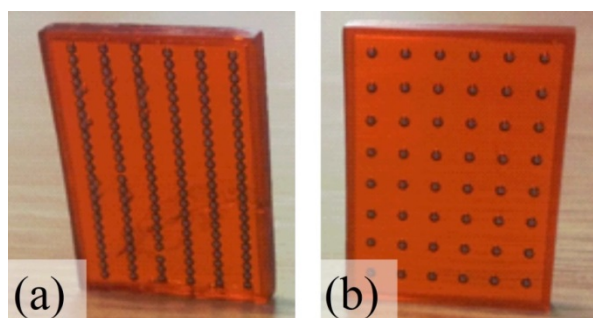
8:00 am   Anchor loss reduction of quartz resonators utilizing phononic crystals

Yung-Yu Chen[1], Yan-Ruei Lin[1], Tsung-Tsong Wu[2], Shih-Yung Pao[3]; *[1]Department of Mechanical Engineering, Tatung University, Taiwan, [2]Institute of Applied Mechanics, National Taiwan University, Taiwan, [3]TXC Corporation, Taiwan*

Background, Motivation and Objective

AT-cut quartz resonators utilizing the thickness shear mode (TSM) are used widely as frequency reference in an electronic system. The boundary condition of a quartz plate affects tremendously the TSM characteristics. For example, the unwanted flexure and loss would be induced by the anchors, which attach the quartz plate to the substrate. To improve the attachment effects, a quartz plate with beveled edge was proposed. The literatures show the steeper the bevel slope, the better the confinement of the TSM energy. However, more beveling makes the excitation weaker and cost larger. Phononic crystals are synthetic structures with periodic variation of elastic property and may give rise to acoustic band gaps. A phononic crystal with band gaps forbids any acoustic wave propagation within the frequency ranges of the band gaps. In this paper, phononic crystals are utilized for trapping acoustic energy and reducing anchor loss in AT-cut quartz resonators.

Statement of Contribution/Methods

Finite element analyses of the AT-cut quartz resonators with phononic crystals and the lossy epoxy attachments are presented herein. The resonance response of an AT-cut quartz resonator with no phononic crystal was first calculated. Four kinds of phononic crystal structures of square lattice in quartz substrate, like through hole, one-side hollow, both-side hollow, and wolfram pillar, were analyzed and designed to have a complete band gap covering the quartz resonator's resonance frequency. Finally, the mode shape and impedance of the quartz resonators with/without three rows of phononic crystals were simulated to evaluate the isolation performance of the phononic crystals.

Results/Discussion

The quartz resonator with no phononic crystal has a resonance frequency of around 16.42 MHz when the AT-cut quartz substrate is 0.1 mm thick. The phononic crystals with the designed lattice constant and filling ratio have complete band gaps covering the quartz resonator's resonance frequency. Further results show the quartz resonator with the through-hole phononic crystals exhibits a better energy confinement inside electrode area and smaller impedance than other resonators. Accordingly, the phononic crystal is verified to be capable of reducing anchor loss in quartz resonators.
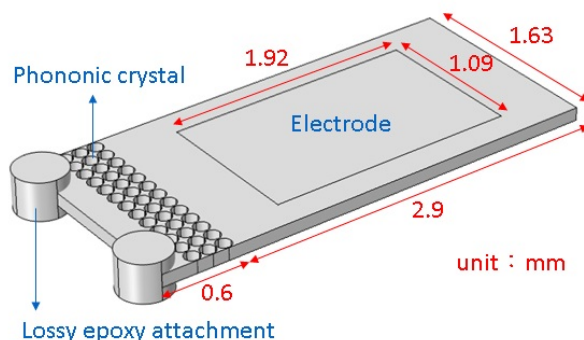
8:00 am   Lowering diffraction of surface acoustic waves by phononic crystals

Jia-Hong Sun[1], Yuan-Hai Yu[1]; *[1]Department of Mechanical Engineering, Chang Gung University, Tao-Yuan, Taiwan*

Background, Motivation and Objective

Surface acoustic wave (SAW) devices consisting of inter-digital transducer (IDT) and reflective gratings on a piezoelectric substrate were widely used today. SAW devices were suitable to be applied as filters, sensors, and wireless RFID tags. In the cases which SAW has to propagate a long distance, the noticeable diffraction of surface waves limited the performance of SAW devices. Phononic crystal (PnC) consisting of periodic media is a new acoustic metamaterial. PnC structures perform anisotropic propagation and acoustic band gaps for SAW were observed. Applications based on the band gaps were proposed for acoustic-electronic components, such as filters, reflective gratings, waveguide, and some other phononic SAW devices [1-3]. In this paper, the anisotropic propagation of SAW in PnCs was analyzed further and applied to lowering the diffraction of surface waves.

Statement of Contribution/Methods

Square lattice PnCs formed by periodic cylindrical tungsten film on the $LiNbO_3$ substrate were studied. Finite element method was used to analyze the surface acoustic waves in the PnCs. A unit cell was defined to calculate the acoustic dispersion firstly. Periodic boundary conditions (PBC) based on Bloch theorem were set around the unit cell. Wave vector in PBC was then varied in the range of the first Brillouin zone to present waves with different wavelength toward all directions. Then eigenmodes inside the unit cell were calculated to form dispersion surfaces. According to the polarization of eigenmodes, Rayleigh waves, shear-horizontal modes and high-order general SAWs in PnCs were indentified. Then equal frequency contours (EFC), equivalent to the slowness curves, were calculated at selected frequencies.

Results/Discussion

The studied PnC has a 4 μm lattice constant, 1.2 μm cylinder radius, and 0.4 μm cylinder height, and its ΓM direction aligned with X direction of the 128° rotated Y-cut $LiNbO_3$ substrate. The Rayleigh wave has a partial gap of 395-447 MHz at ΓX direction and 473-703 MHz at ΓM direction. Then the 430 MHz EFC of Rayleigh mode showed a near straight line normal to ΓM direction while the gap existed at ΓX direction. Thus this PnC can be designed in the delay line of SAW devices to bend the Rayleigh waves. Further simulation showed the phononic delay line can lower diffraction of Rayleigh waves effectively.

Reference:

[1] T.-T. Wu, W.-S. Wang, J.-H. Sun, J.-C. Hsu, and Y.-Y. Chen, Appl. Phys. Lett., vol. 94, no. 101913, 2009.

[2] M. Solal, J. Gratier, and T. Kook, IEEE Trans. Ultrason. Ferroelectr. Freq. Control, vol. 57, p. 30, 2010.

[3] V. Yantchev, Appl. Phys. Lett., vol. 104, no. 103503, 2014.

P4B1 - Acoustic Simulation & Modeling

4th floor

Friday, October 23, 2015, Posters displayed 08:00 am - 05:00 pm. Authors must be present at their poster from 9:30 - 10:30am (odd number posters) and 14:30 – 15:30pm (even number posters).

Chair: **Karl Wagner**
TDK Corporation

8:00 am **Numerical-analytical calculation of the maximum excitation current of precision quartz resonators.**

Alaxandr Lepetaev[1], **Anatoly Kosykh[1]**; *[1] Redioelectronic, Omsk State Technical University, Omsk, Russian Federation*

Background, Motivation and Objective

One of the major parameters of oscillators is a level of output signal noise. It is well known, the noise power spectral density of quartz oscillator output signal close to carrier can be estimated by semi-empirical Leeson formula [1]:

$L(\Delta f) = 10\log\{(2F \cdot k \cdot T/P) \cdot [1+(f_0/(2Q \cdot \Delta f))^2]\}$,

where P is resonator driving power.

As follow from this formula, the higher excitation power, the lower output signal noise level. However it is clear that for the real resonator excitation power cannot be made unlimited high as this can lead to mechanical damage of resonator. Some fundamental limits of frequency stability were described in [2], however in this paper there are no instructions about maximum excitation power.

According to [3], as the maximum tensile stress, you can use the value of $\sigma_{max} = 100$ MPa. This raises the question of what current

and excitation power of the resonator are limiting and how these parameters are related to the design parameters of the resonator, such

as the frequency of oscillation, the curvature of the lens surface of piezoelectric elements, the size of the electrode, mechanical

harmonic number, the type of cut. The purpose of this paper is deriving of expressions for assessing the minimum achievable own crystal oscillator noise for precision quartz resonators.

Statement of Contribution/Methods

The calculation was performed by the method described in [4] using the special program. For calculated main harmonic shape we detrmine the maximum drive power and excitation current, with maximum main stress equal σ_{max}. Calculations include the hamnonic number, curvative radius, electrode radiu and main frequency.

Results/Discussion

The results of maximum xtal excitation current (Imax) and driving power (Pmax) obtaned for resonators of AT and SC cuts under different constructive parameters of quatz plate. This result for large electode diameters was approximated with simple expressions, included harmonic number n, xtal frequency f_0, and surface curvative radius Rc:

$P_{max} = K1 \cdot n \cdot \sqrt{(Rc \cdot n/f_0)}$, $I_{max} = K2 \cdot \sqrt{(Rc/(n \cdot f_0))}$.

For AT-cut: K1=9.8, K2=284.

For SC-cut: K1=5.8, K2=111.

The proposed technique allows defining as much as possible excitation power for resonator of concrete type that has a practical importance at designing of oscillators with extremely low level of noise.

References

1. D.B. Leeson. "A Simple Model of Feedback Oscillators Noise Spectrum," Proceedeings of the IEEE. Vol. 54, NO 2, February, 1966, pp. 329 – 330.

2. F.L. Walls, J.R. Vig. "Fundamental Limits on the Frequency Stabilities of Crystal Oscillators". Procedings of the IEEE. Vol. 42, NO. 4, July 1995.

3. Sosman R.B. "The properties of Silica". New York, 1927, 856p.

4. A.N. Lepetaev, A.V. Kosykh, I.V. Khomenko. "An Analysis of Thickness-Shear Modes of Quartz Resonators By Numerically-Analytical Modeling." Ultrasonics Symposium (IUS), 2010 IEEE. Issue Date: 11-14 Oct. 2010 On page(s): 1254 – 1257. Location: San Diego, CA, USA, ISSN: 1948-5719, Print ISBN: 978-1-4577-0382-9

8:00 am **Optimization of Modified Hanma-Hunsinger Cell Geometry for the Design of High Performance SAW Filters**

Pierre Dufilie[1], Pascal Ventura[2], Frederic Hecht[3]; *[1] Phonon Corp, Simsbury, CT, USA, [2] Laboratoire LEM3, Université de Lorraine, Metz, France, [3] Laboratoire Jacques Louis Lions, Universite Pierre et Marie Curie, Paris, France, Metropolitan*

Background, Motivation and Objective

The design of high performance SAW filters requires accurate prediction of second order effects such as diffraction, electroacoustic coupling, electrical parasitics, and bulk mode signals. Filters comprised of bidirectional transducers having 3 or 4 strips per wavelength can be designed to achieve passband ripples of < 0.1dB-pp and <0.5deg-pp (with triple transit removed), and close-in rejection better than 60dBc. The drawback of these structures is the triple transit time spurious which degrades the passband ripples, increasing with lower insertion loss. The triple transit can be reduced by 15dB or more by adding mechanical reflectors in the transducers at the expense of reduced accuracy of the analysis.

Statement of Contribution/Methods

The reflectors can be added to the transducers by replacing groups of strips or cells with modified Hanma-Hunsinger cells. However care must be taken to ensure that the localized electroacoustic coupling and phase delay through the cells are not changed. Small changes in these parameters can severely degrade the filter's characteristics. Analysis of diffraction effects of transducers with mechanical reflection is not straightforward and not as accurate as for bidirectional transducers.

The goal of this study is to find the optimum geometry of modified Hanma-Hunsinger cells which will have nearly identical electroacoustic coupling in the forward direction and phase delay through the cell. These two conditions will allow the filter design to be optimized with bidirectional transducer analysis tools. A final analysis can then be made of the modified transducers to determine the reduction in triple transit.

Results/Discussion

The optimum geometry for the cells is determined from analysis using the original coupled FEM/BIE numerical model of P. Ventura presented at the 2013 IEEE Ultrasonics Symposium. Comparison of key cell parameters for bidirectional cells and modified Hanma-Hunsinger cells will be presented. The impact of partially buried electrodes

(transverse mode suppression) and raised electrodes (frequency trimming) on the design will also be examined. Measurements on a filter designed with the above method will be compared with analysis.

P4B1-3

8:00 am **Temperature compensation of the AlN Lamb Wave Resonators utilizing the S1 mode**

Jie Zou[1], Albert P. Pisano[2]; [1]*Mechanical Engineering, University of California, Berkeley, CA, USA,* [2]*University of California, San Diego, CA, USA*

Background, Motivation and Objective

The ability of high f_s is a crucial request for MEMS resonators since the high operating frequency can increase the data rate for electronics and enhance the sensitivity for sensors. The conventional AlN Lamb wave resonator employs the fundamental symmetric mode (S_0 mode) for its low phase velocity dispersion and medium electromechanical coupling coefficient (k^2). However, they can hardly achieve frequencies above 1.2 GHz due to lithographic limitation. In fact, the first symmetric mode (S_1 mode) which have a much larger phase velocity, exhibits only slightly lower Q than S_0 mode and larger or comparable k^2. So the Lamb wave resonators utilizing the S_1 mode show great potential in enabling the next-generation high-f_s devices. However, the first-order TCF of the S_1 mode in AlN is around -26 ppm/C°, so an improvement in its thermal stability is highly desirable to further enable low-drift and stable filters, sensors and oscillators.

Statement of Contribution/Methods

By adding a compensating layer of SiO_2 with an appropriate thickness, a Lamb wave resonator based on a stack of AlN and SiO_2 layers can achieve a zero first-order TCF. By calculation the electromechanical coupling coefficient and the group velocity at of the S_1 Lamb wave mode, a relatively thin AlN and SiO_2 thickness combination can be chosen that offers a low-TCF, large k^2 and a positive group velocity simultaneously. This new SiO_2/AlN structure utilizing the S_1 Lamb wave mode simultaneously offers superior temperature stability, high f_s, large k^2, and low spurious mode level.

Results/Discussion

Fig. 1 shows the phase velocity and electromechanical coupling coefficient for the first eight Lamb wave modes as functions of the AlN thickness normalized to the wavelength (h_{AlN}/λ). The k^2 for the S_1 mode tends to be large when the normalized piezoelectric layer thickness h_{AlN}/λ less than 0.4. Considering the dispersion of the S_1 mode is too strong when h_{AlN}/λ less than 0.15, which can make the fabrication tolerance too small and thus difficult to control the frequency, the h_{AlN}/λ is can be chosen between 0.2 and 0.3, so that the S_1 mode offers large phase velocity, low velocity dispersion, and large k^2 at the same time. Fig. 2 shows the first-order TCF and k^2 at different AlN and SiO_2 thickness combinations. By designing the SiO_2/AlN thickness ratio a near-zero TCF at room temperature can be obtained. For example, for $h_{AlN}/\lambda \sim$ 0.2, a thickness for SiO_2 of $h_{SiO2}/\lambda \sim 0.04$ can be chosen. What's more, from Fig. (b), the electrode configuration C, which has a top IDT on the AlN layer and an electrode at the interface, offers large k^2 at the preferred AlN and SiO_2 thickness combination and also a simple fabrication process, since the IDT electrode is not in the interface. These simulation results lay the foundation for temperature-compensated, high-f_s and k^2 SiO_2/AlN Lamb wave resonators utilizing the S_1 mode. The Lamb wave devices are under fabrication and will be presented in the full paper.
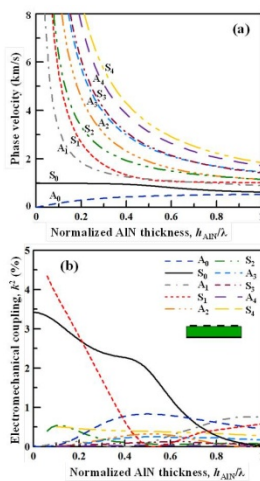
Figure 1. Simulated (a) phase velocity and (b) electromechanical coupling strength of the first 8 Lamb wave modes in AlN membrane.
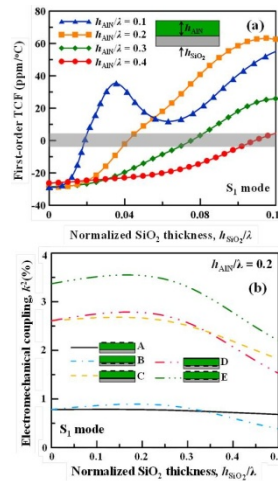
Figure 2. Simulated (a) first-order TCF and (b) electromechanical coupling strength of the S_1 mode in AlN/SiO_2 composite plates.

P4B1-4

8:00 am **Thin Plate Model for Transverse Mode Analysis of Surface Acoustic Wave Devices**

Gongbin Tang[1,2], Tao Han[1], Jing Chen[1], Tatsuya Omori[2], Ken-ya Hashimoto[2]; [1]*School of Electronic Information and Electrical Engineering, Shanghai Jiao Tong University, Shanghai, Shanghai, China, People's Republic of,* [2]*Graduate School of Engineering, Chiba University, Chiba, Chiba, Japan*

Background, Motivation and Objective

For the analysis of in-plane surface acoustic wave (SAW) propagation, the scalar potential (SP) theory has been widely used for long years. Due to the simplicity, the SP theory can be integrated into the coupling-of-mode (COM) theory and the p-matrix theory to take the SAW excitation and reflection into consideration. However, the SP theory does not seem an appropriate platform for further extension.

Statement of Contribution/Methods

This paper proposes a physical model mostly equivalent to the SP theory. The model only concerns the shear-vertical (SV) wave on an infinitesimally thin piezoelectric plate where the interdigital transducer (IDT) is placed on the top surface while the back surface is fully metallized. The SAW reflection is included by giving periodic variation of the substrate mass density while the elastic constants are set uniform throughout the structure. Lateral electric field is zero in this configuration, and excitation terms appearing in the wave equation are non-zero only at electrode edges. Then the electrical excitation can be treated in the boundary condition. Furthermore, charges induced to the IDT can be calculated from the SV wave field. Thus electric fields associating with SV wave propagation are not necessary to be calculated.

As a simulation platform, we choose the partial differential equation mode of the FEM software COMSOL. This choice allows us to analyze various complex electrode geometries without pre-calculations and software modifications.

Parameters appearing in the model can be derived from the one-dimensional COM model.

Results/Discussion

Transverse mode spectra were analyzed for the fully periodic IDT structure shown in Fig. 1. Fig. 2 shows how the spectra change with the aperture length. The simulation agrees well with the experiment.
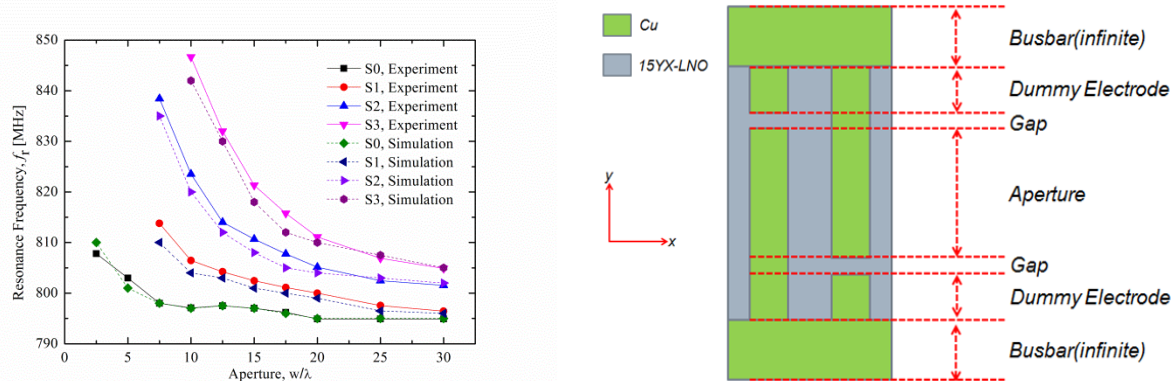
P4B1-5

8:00 am   Simulation of First Shear Horizontal Mode Plate Wave in LiNbO3 Showing 20 km/s Phase Velocity

Michio Kadota[1], Shuji Tanaka[1], Tetsuya Kimura[2]; [1]*Graduate School of Engineering, Tohoku University, Sendai, Miyagi, Japan*, [2]*Telecommunication Devision, Murata Manufacturing Co. Ltd., Yasu, Shiga, Japan*

Background, Motivation and Objective

Currently, cognitive radio using a white space of digital TV (DTV) channels is receiving a lot of attention. One of the key devices is a tunable filter capable of adjusting frequency and bandwidth throughout DTV band. The authors developed an ultra-wideband filter covering all DTV channels using 0th shear horizontal mode plate wave (SH_0) in a (0°, 120°, 0°) $LiNbO_3$ (LN) plate. However, the filter is fabricated on a self-suspended ultra-thin LN plate of only 0.5-0.6 μm in thickness, which is mechanically fragile and difficult to fabricate at high yield. A much higher phase velocity than that of SH_0 is required to make the plate practically thicker. The objective of this study is to explore a different mode of plate wave showing much higher phase velocity by FEM simulation.

Statement of Contribution/Methods

The authors found that 1st SH plate wave (SH_1) in LN showed a phase velocity of about 20 km/s as well as a large bandwidth over 20%. The phase velocity and bandwidth were systematically calculated as functions of Euler angle, assuming different structures of interdigital transducer (IDT). The results were compared with the reported characteristics of SH_0.

Results/Discussion

Figs. 1 and 2 show the phase velocity and bandwidth of SH_1, respectively, together with SH_0 as a function of Euler angle. The LN plate thickness is 0.1λ, where λ is wavelength. Single side interdigital transducer (IDT) with backside short metal and double side anti-phase IDT are assumed for SH_1, while single side IDT and double side in-phase IDT are assumed for SH_0. SH_1 shows a weakly-dispersed phase velocity of about 20 km/s, which is 4-5 times higher than that of SH_0.

The bandwidth clearly shows the maximum at a certain Euler angle, (0°, 85°, 0°) for SH_1 and (0°, 120°, 0°) for SH_0. The maximum bandwidth of SH_1 (22%) is smaller than that of SH_0 (32%), but it must be noted that the difference is practically smaller, because the double side IDT, which gives the maximum bandwidth for SH_0, is difficult to fabricate. The maximum bandwidth of the SH_0 resonator using the single side IDT is 28%, which is 6% larger than that of SH_1. In addition, 22% bandwidth of SH_1 is still attractive for tunable filter application. In conclusion, the SH_1 resonator is promising for the tunable filter used in DTV cognitive radio handsets, because a large bandwidth over 20% is obtained using a relatively thick LN plate, which is about 2 μm in thickness for DTV band.
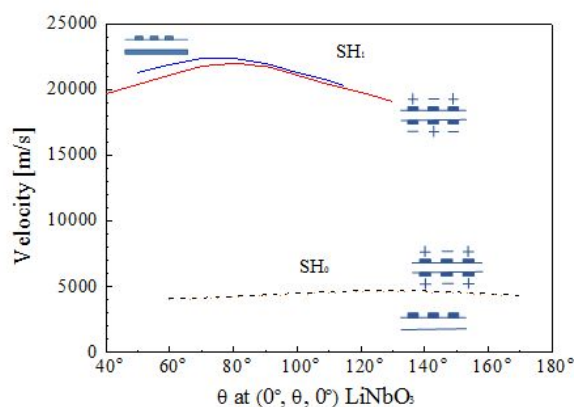
Fig1. Velocities of SH_1 and SH_0 at various structures as a function of Euler angle.
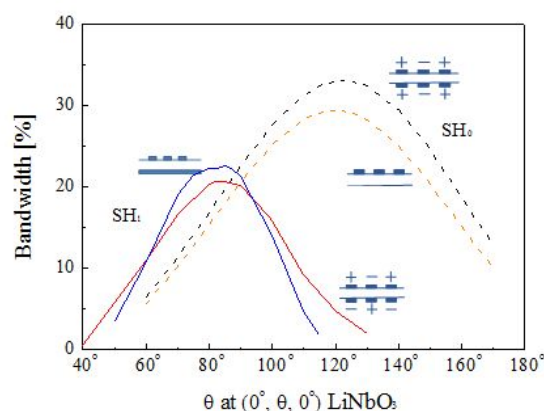
Fig. 2 Bandwidth of SH_1 and SH_0 at various structures as a function of Euler angle.

P4B2 - Sensors & Applications II

4th floor

Friday, October 23, 2015, Posters displayed 08:00 am - 05:00 pm. Authors must be present at their poster from 9:30 - 10:30am (odd number posters) and 14:30 – 15:30pm (even number posters).

Chair:　　**Natalya Naumenko**
　　　　　　National University of Science and Technology

8:00 am　　**Measurement of vibrating frequency of a cantilever using low frequency impedance-loaded SAW sensor**

Hiromitsu Hamashima[1], **Jun Kondoh**[1]; *[1]Shizuoka University, Hamamatsu-shi, Japan*

Background, Motivation and Objective

A wireless surface acoustic wave (SAW) sensor is very attractive application. Many applications, such as measurements of strain, pressure, and temperature, have been reported. For those wireless SAW sensors, changes of the SAW due to an external cause are measured. An impedance-loaded SAW sensor is also proposed. For the impedance-loaded SAW sensor, an external sensor is connected to a reflector on the SAW device. Whereas the impedance-loaded SAW sensor has also an effective method like the conventional wireless SAW sensor, the applications of it are many. An external sensor commercialized operates in DC or very low frequency. If those sensors operate at a frequency of larger than VHF range, change of impedance decreases. However, these sensors have excellent property and low cost. In this paper, to make the most of those characteristics, a SAW device with low frequency of 13.5 MHz is used. As distance between a reader unit and impedance-loaded SAW sensor is short, an ID-tag is not necessary. The impedance-loaded SAW sensor was applied for detecting the vibrating frequency of a cantilever. First, fundamental characteristics of the SAW device at 13.5 MHz were measured. Then, two external sensors for measuring the vibrating frequency were connected to the reflector on the SAW device.

Statement of Contribution/Methods

The SAW device of 13.5 MHz, which has an interdigital transducer (IDT) and a reflector, was fabricated on $128YX\text{-}LiNbO_3$ substrate. For detecting the vibration frequency, a condenser type vibration sensor and a pressure sensor (FSR406) were used. The condenser type sensor was consisted of two thin copper plates and manufactured in our lab. One plate was held on the vibrating cantilever. As the capacitance was varied due to the vibration, the vibrating frequency was measured. The pressure sensor was commercialized to use strain measurement. It is normally used in DC and its resistance is changed due to pressure. However, at 13.5 MHz range, capacitance change is dominant. Burst signal from a function generator was fed to the IDT. Reflected signal from the impedance-loaded SAW sensor was monitored using an oscilloscope with a segmented memory. The time responses were recorded at 5 ms intervals. Then maximum amplitude of the time response, which corresponds to the reflected signal from the reflector, was plotted and analyzed by the FFT.

Results/Discussion

The size of the cantilever was 130 x 195 x 0.7 mm^3. One electrode of the handmade condenser was pasted tip of the cantilever. The pressure sensor was held on the base area of it. The vibrating frequency obtained for the condenser was 3.32 Hz. Those for the pressure sensor were 3.32 and 6.64 Hz. The frequency of 6.64 Hz was 2nd harmonic. It depends on the position held on the cantilever. Therefore, the condenser type vibration sensor is suitable for the purpose. The results indicate that the impedance-loaded SAW sensor can be applied to not only vibration sensor of a structure, but also music instruments.

8:00 am　　**Continuous Temperature Monitoring Algorithm for SAW Sensors**

Mykhaylo Yudytskiy[1,2], René Fachberger[1]; *[1]sensideon GmbH, Wels, Austria, [2]Johann Radon Institute for Computational and Applied Mathematics (RICAM), Linz, Austria*

Background, Motivation and Objective

Wireless temperature identification in hazardous environments is a common problem in industrial applications. Challenges such as measuring at high temperatures or on rotating components suggest the use of surface acoustic wave (SAW) sensors. Contamination of the measurement data by noise, an unavoidable effect in these types of applications, leads to a loss of accuracy in the temperature evaluation. In the case of high measurement noise, the error in the computed temperature may be unacceptably large.

Many software-based techniques are applied to counteract the degrading effects of measurement noise on the performance of SAW sensors. Recently research tended towards SAW sensor-specific algorithms to stabilize the temperature evaluation of a single noisy measurement. In a continuous regime of operation, e.g., in continuous monitoring, data is collected at regular time intervals. The goal of our paper is to present a novel algorithm that exploits the continuity of the measurement process to validate the current measurement. The algorithm may be applied in combination with existing correction techniques.

Statement of Contribution/Methods

In this paper we present an innovative temperature monitoring algorithm for SAW sensors that utilizes a series of measurements observed over time to assert the validity of the current temperature evaluation. The algorithm is based on the assumption that the temperature of the measured object is a continuous function of time. This reasoning permits a polynomial approximation of the temperature on a bounded time domain.

The main idea of the algorithm is based on fitting a polynomial to the computed temperature data over time. For the algorithm we examined three types of data fit: a least squares fit, a sparsity promoting fit and a least squares fit with limited data, where the last two approaches help remove outliers (i.e., unrealistic jumps in temperature). Consequently, the temperature value computed from the current measurement is considered valid if the value is in the vicinity of the polynomial at the current time step and erroneous otherwise.

Results/Discussion

We examined the qualitative performance of our algorithm using experimental data from the lab. The data was collected from a series of tests, where the temperature of the sensor varied from room temperature to 350 degrees Celsius. To simulate the different noise levels we varied the distance of the radar to the sensor antenna. For these tests, we compared the three types of polynomial fitting discussed above with the control case, in which the algorithm was not applied.

These experiments allowed us to conclude that the sparse fit and the least squares fit with limited data produce the best results in quality. However, only the least squares based approach is computationally suitable. We found that the algorithm is appropriate for applications with gradually changing temperature and is useful as long as the noise level is not excessively large.

P4B2-3

8:00 am **Sensitivity improvement of a room-temperature SAW methane sensor incorporating Cryptophane-A film**

Wen Wang[1], Haoliang Hu[1], **Shitang He[1]**, Yong Pan[2], Caihong Zhang[3], Chuan Dong[3]; *[1]Chinese Academy of Sciences, Institute of Acoustics, Beijing, China, People's Republic of, [2]Research Institute of Chemical Defense, China, People's Republic of, [3]Shanxi University, Shanxi, China, People's Republic of*

Background, Motivation and Objective

Accurately measurement and monitor on methane concentration is an urgent problem to be solved in the purpose of safety and process control in homes, industries and mines. Compared with traditional methane sensors, surface acoustic wave (SAW) based sensor exhibits many advantages as simplicity, small size, high sensitivity and working at room temperature. The SAW based methane sensor developed in this contribution was composed of a differential resonator-oscillator, and a supermolecular cryptophane-A thin film coated onto the sensing device. The differential oscillation frequency was picked for sensor performance evaluation.

Statement of Contribution/Methods

The purpose of this paper is to improve the performance of a CrypA-coated SAW methane sensor by optimizing coating methods. The 300MHz two-port SAW resonators with low insertion loss (~2dB) and high Q value (~3000) were designed as the feedback element of the differential oscillator. CrypA was deposited on the SAW resonators via drop-coating and spin-coating, respectively. Experiments were conducted to analyze the sensor response towards 5% methane by using the developed SAW sensor.

Results/Discussion

the sensor responses of the developed SAW based methane sensor by using different coating methods towards 5% methane were tested. Higher sensor response over 1 kHz and fast response were observed from the sensor developed by drop-coating as shown in Fig. 1, which is higher than the sensor developed by spin-coating (~200 Hz in Fig. 2). The phenomenon is explaned by using the AFM surface topography, it means that drop-coating films provides rougher surfaces than spin-coating, indicating that surface roughness shows significant influences on the sensor response.
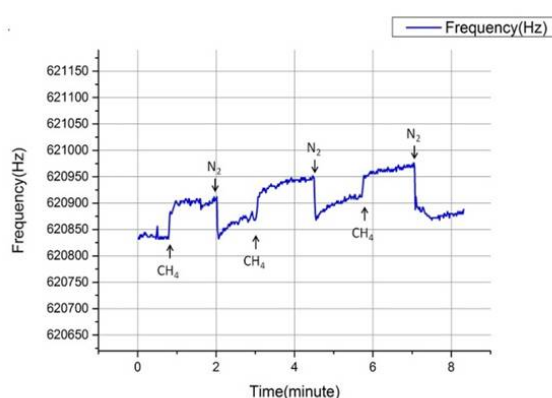
Fig. 2 Frequency response of the sensor developed by spinning-coating
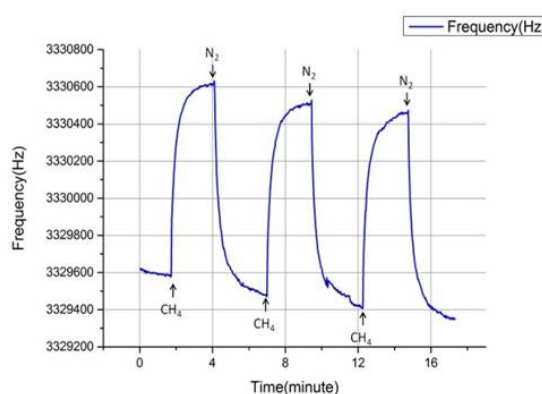
Fig. 1 Frequency response of the sensor developed by drop-coating

P4B2-4

8:00 am **Surface Acoustic Wave Accelerometer for High-G Applications**

Dmitry Lukyanov[1], Sergey Shevchenko[1], **Alexander Kukaev[1]**, Khivrich Maria[1]; *[1]Laser Measurement and Navigation Systems, St.Petersburg Electrotechnical University, St. Petersburg, Russian Federation*

Background, Motivation and Objective

Different sensors such as accelerometers, gyroscopes, pressure sensors and others are developed using MEMS technology. Review of technical characteristics and principles of construction of modern micromechanical accelerometers (MMA) showed that developed MMA do not have sufficient vibration and shock resistance due to the presence in their design moving inertial masses and elastic suspensions. To apply microaccelerometers in the areas related to the highly dynamic mobile objects, MMA must have a high shock resistance (up to 65 000 g), wide dynamic range and small size. These features are not yet available for most of microaccelerometers.

Therefore, in recent years interest in solid microaccelerometers on surface acoustic waves (SAW) has increased significantly. 2D planar technology is used for the fabrication of such type of MMA. The main elements of microsensors on SAW are delay lines or resonators, whose properties depend on the measured motion parameters. Exceptional simplicity of electrical scheme and high level of constructive integration create the preconditions for increasing of the accuracy characteristics, reducing of the overall size and substantial reduction of the total cost of their production.

Compared with traditional microaccelerometers, SAW-based ones possess a number of significant advantages, such as high resistance to vibration and shock, low cost and simplicity of production.

Statement of Contribution/Methods

Traditional SAW-based accelerometers are well known. Their sensing element consists of a console, which is clamped from one side and is loaded with an inertial mass from the other. Each side of the console possess a SAW-resonator. Under the action of acceleration the console bends and SAW resonators obtain a differential frequency shifts $\pm\Delta f$. A proper electrical scheme mixes the output signals to form the differential frequency $f_{dif} = 2\Delta f$, which is proportional to an applied acceleration. Disadvantage of this sensing element is that it brakes under high-G loads. We propose a modified sensing element with additional clamping and without inertial mass to survive shocks up to 65 000 g. To obtain the measurement range and sensitivity parameters of this sensing element a FEM-modeling was performed in OOFELIE::Multiphysics software.

Results/Discussion

Using FEM-modeling we obtained that the measurement range of a proposed sensor would be 50 - 65 000 g with good linearity. Sensitivity is about 3,57 kHz/g and cross-sensitivity is less then 0.1%. These parameters might be adjusted for the exact application by optimizing the console geometry. Validity of obtained results is provided by a number of experimental data.

P4B2-5

8:00 am   SAW force sensor based on reflective delay line quasi-mirror topology

Ivan Antcev[1], **Sergei Bogoslovsky[1]**, Gennadiy Sapozhnikov[1], Sergei Zhgoon[2]; *[1]Joint Stock Company "NPP "Radar mms", Russian Federation, [2]National Research University Moscow Power Engineering Institute, Moscow, Russian Federation*

Background, Motivation and Objective

Passive SAW sensors systems have small working distance. The wide bandwidth required for simultaneous operation of multiple sensors restricts the acceptable maximum reflection and the spectral power density of the interrogating signal. For example, the approach using a single port reflective delay line topology divided into segments with unique frequencies operates up to about 3 meters [1]. When the simultaneous operation is not required and the available bandwidth is limited, different design principles are required. We present an example of a temperature self-compensated sensitive element design for a force sensor and of an interrogation algorithm that helps increasing working distance while satisfying limited bandwidth requirement.

Statement of Contribution/Methods

Fig. 1 illustrates the SAW sensitive element installation in the Roberval parallelogram based force sensor (left) and the SAW sensitive element design (right) together with schematic strain and deformation distributions. The sensitive element design is based on a single-port reflective delay line with reflectors arranged on both sides of the IDT. Each reflector consists of several segments with 10 groves in each segment and the distances between the IDT and the reflectors ensure that the reflections from the left reflector segments fall in the middle of the gap between the reflections of the right reflector segments. The impulse response consists of a series of responses from all the segments, followed by a triple transit tail. When temperature changes, the impulse response shape remains unchanged, while when a force is applied, the opposite stress in the left and right sides of the delay line determines the intersection of the pulses from the left side with the pulses from the right side. If a relatively long (1.8 µs) interrogation RF burst is applied the device output response amplitude decreases with force increase.

Results/Discussion

Fabricated devices with central frequency 433 MHz have confirmed modeled characteristics and operation principles. The working distance with 10 mW interrogation signal reached 30 m. The paper will discuss the benefits and the drawbacks as well as the studies of other types of sensors based on this approach.

1.   N. Kozlovski, D. Malocha, A. Weeks. A 915 MHz SAW Sensor Correlator System. IEEE SENSORS JOURNAL, V. 11, N. 12, 2011, pp. 3426-3432
2.
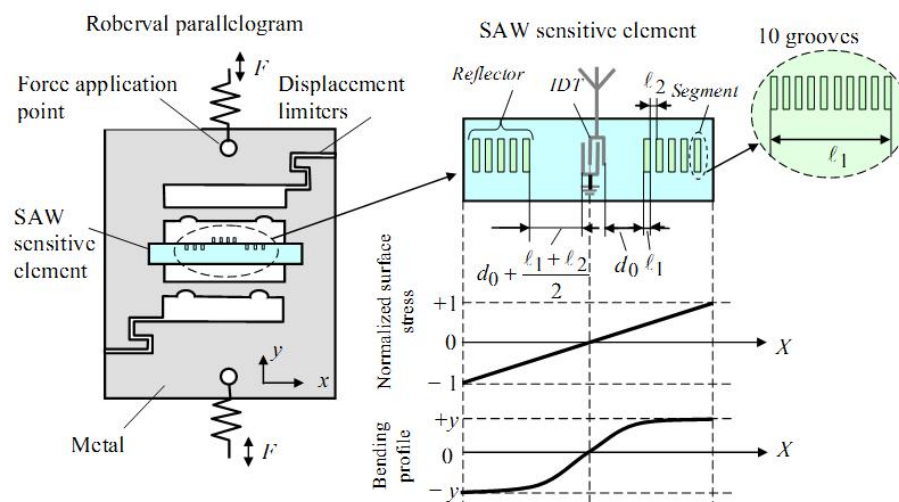
FRIDAY POSTER

P5B1 - CMUT Modeling and Design

4th floor

Friday, October 23, 2015, Posters displayed 08:00 am - 05:00 pm. Authors must be present at their poster from 9:30 - 10:30am (odd number posters) and 14:30 – 15:30pm (even number posters).

Chair: **Michael Fink**
             University Erlangen-Nürnberg

P5B1-1

8:00 am   **Accurate performance evaluation of high frequency CMUT arrays using a nonlinear model**

Evren F. Arkan[1], Sarp Satir[1], **F. Levent Degertekin[1]**; *[1]G.W. Woodruff School of Mechanical Engineering, Georgia Institute of Technology, Atlanta, Georgia, USA*

Background, Motivation and Objective

The need for high frequency (30-60MHz) ultrasound arrays increases as applications such as small animal imaging, photoacoustic imaging and intravascular imaging advance. CMUTs are especially suitable for such applications as they can be batch fabricated with small pitch (~12-25µm) required for phased array operation and can be integrated with electronics. The performance of CMUTs is improved when they are driven close to their operating limits in both transmit and receive. This highlights the importance of nonlinearity and crosstalk effects, and requires accurate predictions for high performance design. Here an accurate nonlinear CMUT array model is used on high frequency CMUT arrays for this purpose.

Statement of Contribution/Methods

The model proposed by Satir et.al. [1] is utilized for performance evaluation of high frequency CMUT arrays. The model can incorporate the large signal transmit behavior of the CMUTs, the crosstalk effect in the array, and pulse-echo response with different electrical impedance terminations can be calculated. The thermo-mechanical noise of the CMUT element can be extracted from the model through electrical impedance simulation. Therefore, the model is suitable for evaluating ultimate performance of CMUT arrays given voltage, vacuum gap, array geometry and transmit pulse generation limitations. As an example, a 40MHz CMUT array for guidewire IVUS application is analyzed for CMUT thermo-mechanical noise limited operation. The 40MHz array consists of 12 elements each comprising 40 20µm square Si3N4 membranes with 75% electrode coverage and 25µm pitch. The vacuum gap is 40nm with 100nm HfO2 isolation layer and 90% of collapse voltage is assumed on receive for high sensitivity while the same element is used both as transmitter and receiver.

Results/Discussion

The achievable SNR for a perfect planar reflector 1 cm away from the CMUT array immersed in water was used as the basis for comparison with 50V max voltage IC process. When CMUT is biased at 43V and driven by a unipolar pulse decreasing the DC bias 43V to ground a maximum SNR of 44dB is obtained for a single Tx-Rx pulse echo with 47% fractional bandwidth around 35MHz (Fig. 1). Using a bipolar pulse with 50V peak and 0V minimum around the bias, SNR is improved to 50dB and the fractional bandwidth is 55%, both suitable for IVUS imaging using a 12 element 1-D phased array.
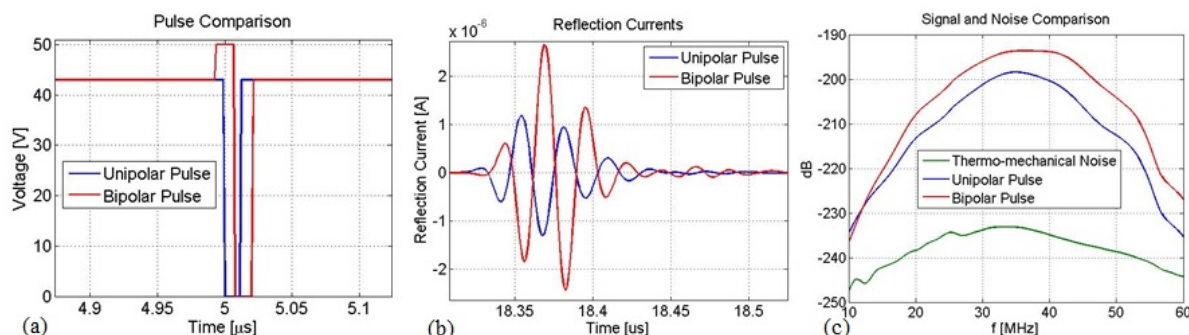
Figure 1: (a) Comparison of the unipolar and bipolar pulse, (b) Comparison of the reflection currents obtained from unipolar and bipolar pulse, (c) Comparison of the FFTs of the signals obtained from the unipolar and bipolar pulses and the thermo-mechanical noise.

[1]: S. Satir and F.L. Degertekin, "A computationally efficient nonlinear system model for CMUT arrays", Ultrasonics Symposium (IUS), 2014 IEEE International, Page(s): 313 - 316

P5B1-2

8:00 am   **Mutual Radiation Impedance for Modeling of Multi-Frequency CMUT Arrays**

Mohammad Maadi[1], Ryan Chee[1], Roger Zemp[1]; *[1]Electrical and Computer Engineering, University of Alberta, Edmonton, Alberta, Canada*

Background, Motivation and Objective

Closely packed interlaced CMUTs with different membrane sizes are designed to create multi-frequency arrays with applications to imaging-therapy, contrast imaging and photoacoustic imaging. An accurate model including the effects of the mutual acoustic interactions between CMUT cells for simulating the multi-frequency arrays is necessary. The mutual radiation impedance affects the resonance frequency of the CMUTs by shifting them to higher or lower frequencies. The main goal of this work is finding a computationally tractable expression and approximation for mutual acoustic impedance between dissimilar cells, and the implementation of a coupled membrane dynamic equivalent circuit model, along with model validation using experimental data.

Statement of Contribution/Methods

Chan found an expression for mutual acoustic impedance extending the work of Porter and Pritchard to the case of differing sizes of circular disks which only agreed with same-sized membrane expression results for the case of pistons but not flexural disks while our new comprehensive expressions are valid for pistons and flexural disks vibrating with the same phase. MATLAB simulations were used to compare the approximate expressions with new full expression and with Porter's results when membranes are of the same sizes. An equivalent circuit model of two differing membranes was developed and expanded to model multi-frequency interlaced CMUT arrays. Models were compared with experimental vibrometer measurements of 82 and 36 µm membranes interlaced in multi-frequency CMUT arrays.

FRIDAY POSTER

Results/Discussion

The obtained expression for mutual acoustic impedance between membranes of different sizes was implemented in an equivalent circuit model of multi-frequency CMUTs. Model predictions of resonance frequencies and displacements (Figure 1-a) closely matched experimental vibrometer measurements of multi-frequency CMUT arrays (Figure 1-b). Besides, vibrometer measurements were done for low and high frequency CMUTs (Figure 1-c and 1-d). Models for the mutual acoustic impedance between membranes of different sizes was validated against previous piston results but extended to flexural disks (Figure 1-e).

Figure 1-a : Multi-frequency CMUT modeling and simulation in ADS (matched with experimental results).
Figure 1-b: Matched experimental vibrometer measurements of multi-frequency CMUT arrays.
Figure 1-c and 1-d : 3D experimental vibrometer measurements of multi-frequency CMUT arrays.
Figure 1-e: Validation of obtained normalized mutual radiation impedance as a function of relative separation for ka =1.

P5B1-3 _____

8:00 am   Electrical Impedance Matching of CMUT Cells

Mohammad Maadi[1], Roger Zemp[1]; [1]*Electrical and Computer Engineering, University of Alberta, Edmonton, Alberta, Canada*

Background, Motivation and Objective

Maximizing acoustic power output from CMUTs is of major importance to ensure competitive signal-to-noise. CMUTs have a significant reactive component to the input impedance which may result in non-optimal real power dissipated as acoustic energy when transmitting. Impedance matching networks can counteract undesired reactances within specific frequency bands to permit more real power delivery. However, it is unclear how advantageous such matching networks may be if one simply has the option of using a higher transmit level. We performed simulations and experiments to demonstrate important advantages of impedance matching.

Statement of Contribution/Methods

Electrical impedance matching of the small and large signal models of the CMUT cells were studied in detail. ADS validated models are used to predict device performance before and after using impedance matching networks. Membrane velocity and displacement of a single 2.7 MHz CMUT cell, a 2 by 10 and 6 by 6 CMUT arrays were measured and compared with and without matching networks. For a given bias voltage, we found the maximum possible AC drive-level we could apply without collapsing the membrane, then found the mean membrane velocity at this signal drive-level in the cases where a matching network was present or absent.

Results/Discussion

The best-possible rms velocities associated with maximum pre-collapse drive-signals were significantly higher when a matching network was present (Figure 1-a). Thus even if we have the option of driving CMUTs with an arbitrarily high drive-signal we cannot achieve outputs as high as when we use appropriate matching networks. The output power with a matching network was enhanced ~25x compared to the case when no matching network was used in this case. Also the required AC drive voltage to obtain this maximum output power was only a few volts compared to the hundreds of volts needed without a matching network. The membrane velocity spectrum and pressure outputs also showed considerable improvements when matching was applied (Figures 1-b and 1-c). Experiments were performed by constructing matching networks to arrays of CMUTs on a 7x7mm die. Power output enhancement of several times was obtained with matching.

Figure 1-a : Impedance matching effect on membrane average velocity at pre-collapse drive-signals for a 2 by 20 CMUT array.
Figure 1-b: Impedance matching effect on a single membrane rms velocity.
Figure 1-c : Impedance matching effect on acoustic pressure for a 6 by 6 square CMUT array.
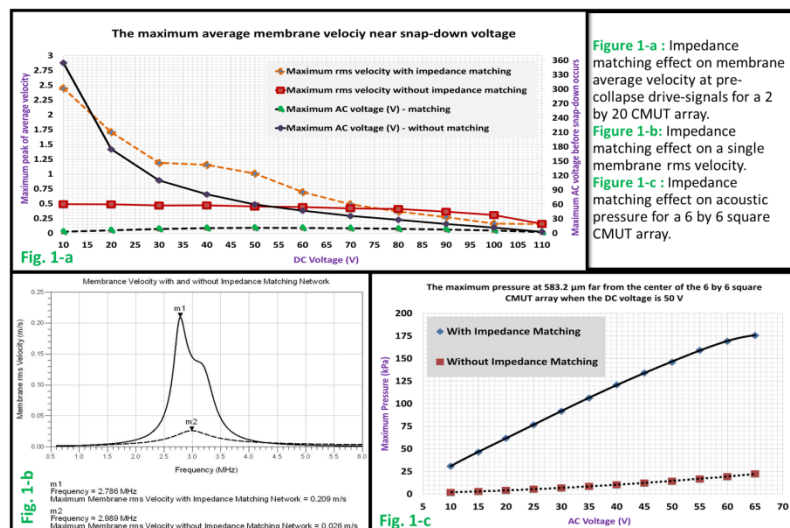
8:00 am   Nonlinear Model with Lumped Parameters for Asymmetric CMUTs

Carlos Gerardo[1], Edmond Cretu[1], Robert Rohling[1]; *[1]Electrical and Computer Engineering, University of British Columbia, Vancouver, British Columbia, Canada*

Background, Motivation and Objective

Capacitive Micromachined Ultrasonic Transducers (CMUT) offer certain advantages over piezoelectric transducers, such as their small size, wider operational bandwidth, and easier integration with electronics.

A way to analyze CMUTs is by using reduced order circuit models, in which the electro-mechano-acoustic interactions are captured by electrical elements and simulated in SPICE simulators. Many authors have followed Mason's theory to get small-signal models, where the electrical and mechanical domains are coupled by a linear transformer that has the DC bias voltage component as one of its parameters, limiting the validity of the model around a fixed operational point.

Other lumped-modeling approaches can generate valid large-signal models; capturing the nonlinearities associated with the normal operation of CMUTs in a more accurate way, such as the spring softening effect. All such current models only account for the first vibration mode of CMUTs; the description of multiple vibration modes in CMUTs using macromodels has not been considered before.

Statement of Contribution/Methods

A new type of CMUT was developed in our research group, in which a CMUT membrane is driven by two bottom electrodes. When only one of these electrodes is excited (hence the name asymmetric CMUT) the second vibration mode of the membrane becomes much more evident. Potential applications and simulation results of asymmetric CMUTs have been published by former members in our research group, including physical steering and focusing of ultrasound beams and super resolution imaging. Nevertheless, an accurate equivalent circuit model for them is still needed.

We have developed a nonlinear macromodel using lumped elements; this model remains valid under any kind of excitation voltage. The model has three input ports on the electrical side, representing the membrane and the two bottom electrodes; it has two output ports on the mechanical side, capturing the first and second vibration modes of the membrane.

Results/Discussion

When excited symmetrically (equal voltage applied on both bottom electrodes), the model behaves as many other macromodels in the literature, capturing the overdamped behaviour of the first vibration mode when immersed in water. When excited asymmetrically (voltage applied on one bottom electrode) the model still predicts the overdamped response of the first vibration mode and captures the resonant behaviour of the second mode.

The proposed model is capable to predict the pull-in voltage as well as the amount of deflection for each vibration mode when driven asymmetrically. The circuit also predicts the amount of current generated in the CMUT when pressure waves impinge on the surface at different angles. The frequency response was validated against FEM simulations and experimental measurements in air from a laser Doppler Vibrometer; getting a 0.87% prediction error for the second vibration mode and 2.44% error for the first vibration mode.

8:00 am   Efficient driving conditions of CMUT arrays for conventional and harmonic imaging

Anders Lei[1], Søren Elmin Diederichsen[1], Matthias Bo Stuart[2], Jørgen Arendt Jensen[2], Erik Vilain Thomsen[1]; *[1]Department of Micro- and Nanotechnology, Technical University of Denmark, Denmark, [2]Center for Fast Ultrasound Imaging, Department of Electrical Engineering, Technical University of Denmark, Denmark*

Background, Motivation and Objective

The low mechanical impedance of Capacitive Micromachined Ultrasonic Transducers (CMUTs) results in a high bandwidth and receive sensitivity (RX), but consequently also a low output pressure (TX). This is particularly inhibiting for harmonic imaging where high pressure is needed to generate sufficient harmonics. The electrostatic force of the CMUT is proportional to the sum of the bias (V_{DC}) and excitation voltages (V_{AC}) squared, hence maximizing TX can be achieved by increasing both voltage levels. Applying a V_{DC} close to pull-in increases the risk of collapsing the cells, but also for encountering potential intrinsic charging effects within the CMUT. Increasing V_{AC} will, due to the nonlinear driving term, inherently increase the unwanted intrinsic generation of second harmonics of the CMUT. The optimal voltage levels for driving a CMUT are ultimately a compromise between TX, RX, and intrinsic harmonic generation.

Statement of Contribution/Methods

This contribution presents a comprehensive acoustic characterisation of our latest 128 element 5 MHz λ-pitch 1-D CMUT array for examining efficient driving conditions. The CMUT is fabricated using wafer-bonding and LOCOS (LOCal Oxidation of Silicon). The circular CMUT cells have a plate thickness of 2.2 μm, radius of 24.3 μm, and effective gap height of 356 nm resulting in a pull-in voltage of 240 V. The cells are hexagonal closed packed in elements with elevation of 5 mm.

Results/Discussion

The left figure shows the measured peak pressure of a plane wave emission of 16 elements in water 10 mm from the array as function of V_{AC} for four different V_{DC} levels. A narrow-band 16 period 5 MHz sine wave was used as excitation and repeated 10 times for noise reduction. The right figure shows the resulting intrinsic Harmonic to Fundamental Ratio (HFR) which is evaluated at the transducer surface to assess the harmonic generation of the CMUT itself. The effect of increasing the V_{DC} level is unambiguous: the peak pressure increases with 0.08 dB/V_{DC}, while the HFR is decreased at the same time since the generated intrinsic harmonics is only related to V_{AC}. Higher V_{DC} levels furthermore increases RX (not shown here). Increasing the V_{AC} level results in an increase in peak pressure of 0.13 dB/V_{AC}, but also results in an increase in HFR. Efficient V_{AC} level for a CMUT therefore highly depends on whether the application is conventional or harmonic imaging.

FRIDAY POSTER
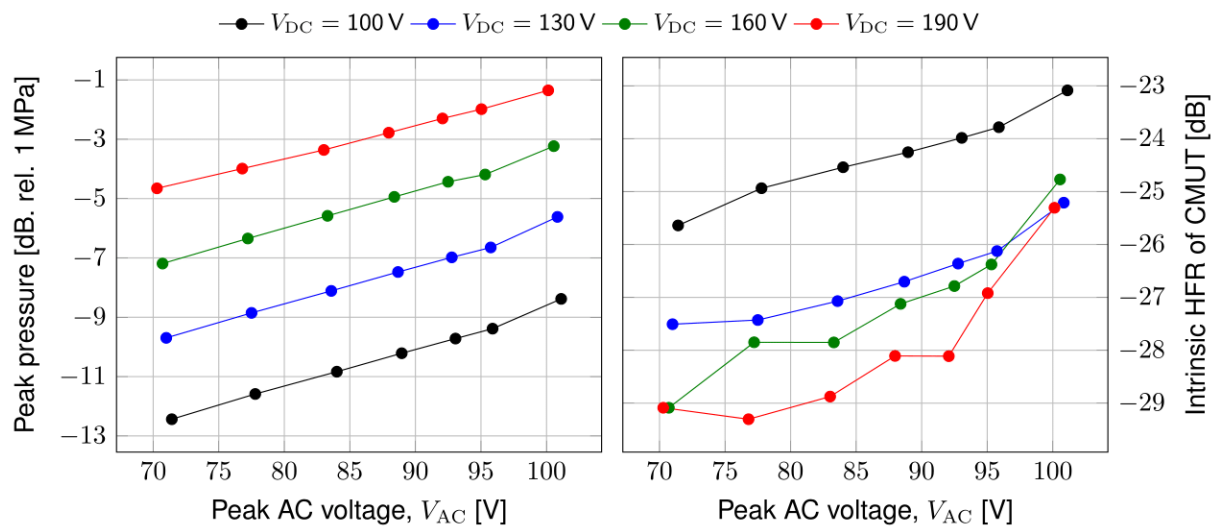
P5B1-6

8:00 am   **Optimization of the Backside Structures with Wideband Reflectivity Reduction for a CMUT**

Akifumi Sako[1], Hiroki Tanaka[1,2], Yasuhiro Yoshimura[2], Masahiro Sato[1], Tatsuya Nagata[1]; *[1]Hitachi Aloka Medical,Ltd., Japan, [2]Hitachi, Ltd., Japan*

Background, Motivation and Objective

A typical CMUT probe has a large number of fine cells placed side by side, where each membrane is mechanically coupled to neighboring supporting rims. When CMUTs receive echo signals from test objects, some part of ultrasound are converted into the electric energy. On the other hand, because of the CMUT structures, the rest of them propagate into the backside of the CMUT cells through the rims. Those should cause an unnecessary acoustic reverberation which degrades the quality of diagnostic ultrasound images. In our study, optimized CMUT models have been investigated by one-dimensional transmission line simulation for ideal backside structures.

Statement of Contribution/Methods

In order to decrease the acoustic noise, it is important to reduce the reflectivity in a frequency band lower than the CMUT resonance frequency, because the vibrating energy of the membrane transferred into the backside of CMUT behaves like transmission line. Reflectivity on CMUTs was calculated by one-dimensional transmission line simulation, where acoustic and physical properties of the backing materials and the substrate were set as the input parameters. Then, based on the simulation results, prototype backing structure with anisotropic composite material including carbon fiber was evaluated in consideration of the feasibility for a CMUT.

Results/Discussion

The results of one-dimensional transmission line analysis showed that the reflectivity varies depending on both the wavenumbers in the substrate and the acoustic properties of backing materials. Since wideband reduction in reflectivity is necessary for maintaining broadband characteristic on CMUT, the results also suggested that a combination of small thickness of the substrate and small mechanical impedance of the backing material is one of the effective ways for wideband reflectivity reduction.

Secondly, based on the results, optimum backing material which was made of polyamide resin, carbon fiber and inorganic filler by injection molding process was developed. It was found that, in a direction perpendicular to the fiber oriented direction, the backing had relatively low acoustic impedance, ranging from 3 to 5 MRayls, similar to that of general plastics, and also in a fiber oriented direction, it had good mechanical properties, e.g. high rigidity, low coefficient of linear thermal expansion, ranging from 2 to 5 x 10^{-6}/K, similar to silicon, and heat resisting property. Resultantly, this approach with anisotropic material suggested the high possibility on producing the proper backing material for a CMUT, which has low reflectivity in desired frequency bands.

P5B1-7

8:00 am   **Nonlinear Lumped Modelling of Large-Scale CMUT TOBE Architectures**

Christopher Ceroici[1], Ryan Chee[1], Roger Zemp[1]; *[1]Electrical & Computer Engineering, University of Alberta, Edmonton, Canada*

Background, Motivation and Objective

In order to reduce the wiring congestion of large two-dimensional arrays, Top-Orthogonal-to-Bottom Electrode (TOBE) CMUT architectures have been proposed where rows and columns are connected along the top and bottom, respectively [Sampaleanu et al., IEEE UFFC 2014]. In the past there had been no method of simulating a CMUT TOBE array with integrated electronics. Doing so would allow for electronics-end design accounting for the complex dynamics of CMUTs.

Statement of Contribution/Methods

Using a nonlinear lumped-model of the CMUTs electromechanical characteristics, a simulation of a 2D TOBE CMUT array is constructed based on the model from Koymen et al. [IEEE UFFC 59(8), 2012] shown in figure 1a. Our additional work includes organizing CMUT membranes into 2D arrays with multiple membranes per element and top electrode strips connecting element rows which are orthogonal to bottom electrode columns, illustrated in figure 1b. We compared model predictions to fabricated device performance in the case of dominant element actuation experiments and novel modulation-encoding schemes.

Results/Discussion

We modelled TOBE 5x5 CMUT array with 3x3 circular membranes within each element. Membranes had a radius of 40 um with a 4um thickness and an immersion center frequency of 5MHz. Simulations were compared with experimental measurements of square membrane TOBE arrays created using a sacrificial release process.

Dominant element sensitivity is achieved by biasing a column and transmitting or receiving along a row. Dominant element actuation was achieved in both simulations and experiments with sacrificial release TOBE CMUT arrays similar to our work in Sampaleanu et al., IEEE UFFC 2014. Predicted nearest-neighbor crosstalk was 19.2 dB compared to the experimentally measured crosstalk of 20.1 dB. The simulated and measured dynamic displacements are compared in figure 1c and 1d.

The model was also used for simulating modulation-encoded TOBE CMUT operating schemes where columns were modulated with high frequencies and frequency encoded signals from all elements were read-out from rows. By introducing an isolation amplifier in between each element top contact and row connection, the demodulated output signals contained 35.6 dB less crosstalk.

a)

b)

c) Simulated

d) Measured
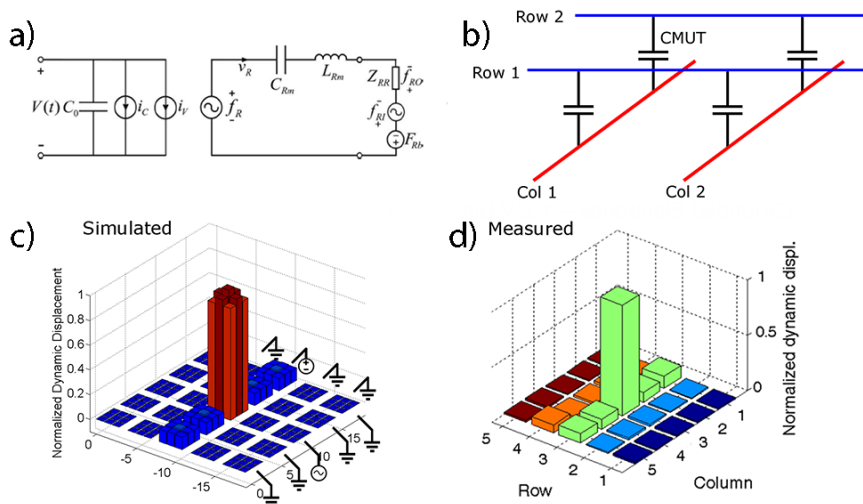
P5B1-8

8:00 am   Signal-to-Noise-Ratio Optimization For a CMUT based Medical Ultrasound Imaging System

Reza Pakdaman Zangabad[1], Ayhan Bozkurt[2], Göksenin Yaralıoğlu[3]; *[1]Biomedical Engineering, Erasmus MC, Rotterdam, Netherlands, [2]Electronics Engineering, Sabanci University, Istanbul, Turkey, [3]Electronics Engineering, Ozyegin University, Istanbul, Turkey*

Background, Motivation and Objective

CMUTs offers key performance benefits compared to their piezoelectric counterparts. However, commercial ultrasound imaging systems based on CMUTs have been limited due to low signal to noise ratio (SNR) in the obtained images [1].

Tunable parameters of the CMUT include the membrane material, radius, thickness, gap height, electrode size, and bias voltage. The aim of this work is to optimize these parameters to provide a solution for low SNR problem of CMUTs. In medical imaging, the device will be used in pulse echo mode for which both good receive sensitivity and high output pressure is required. Optimizing these performance metrics will end up in conflicting design parameters, such as a high gap for large pressure output whereas a small gap for better receive sensitivity. In this work, we develop a methodology for the investigation of the round-trip behavior of the transducer and try to co-optimize transmit and receive characteristics of the device to maximize the SNR of the received signal by tuning the bias voltage.

Statement of Contribution/Methods

An existing equivalent circuit model of the immersed CMUT array is used [2]. Analyses are carried out for two different CMUTs with membrane radii of 15 µm and 20 µm, which have collapse voltages of 180 V and 205 V, respectively. The gap height is chosen as 100 nm and other parameters are calculated so that both devices have a center frequency of 20 MHz. For the optimization of the return signal SNR in pulse echo operation, transducers are loaded with lumped circuit element model for the radiation impedance of CMUTs in an infinite field of cells. The noise source in this analysis is considered to be the thermal noise of the immersion medium and SNR values are found by measuring the output noise current power at the receive section of the model. Other device parameters being fixed, DC bias values for maximum pulse-echo output amplitude and the corresponding SNR values are determined.

Results/Discussion

Figure 1 depicts Signal-to-Noise Ratio. As bias voltage acts oppositely on output pressure and input sensitivity, an optimal value for the pulse-echo response was anticipated. The result shows that there is indeed such an optimal point and proves that maximum SNR is achieved at DC bias values of 75% of the collapse voltage.

References

[1] Mills, D.M., et. Al. IUS 2003, pp. 568 - 571 vol.1

[2] H. Koymen, et. Al. , IEEE Trans. UFFC. vol. 59, pp. 1791-1799, 2012
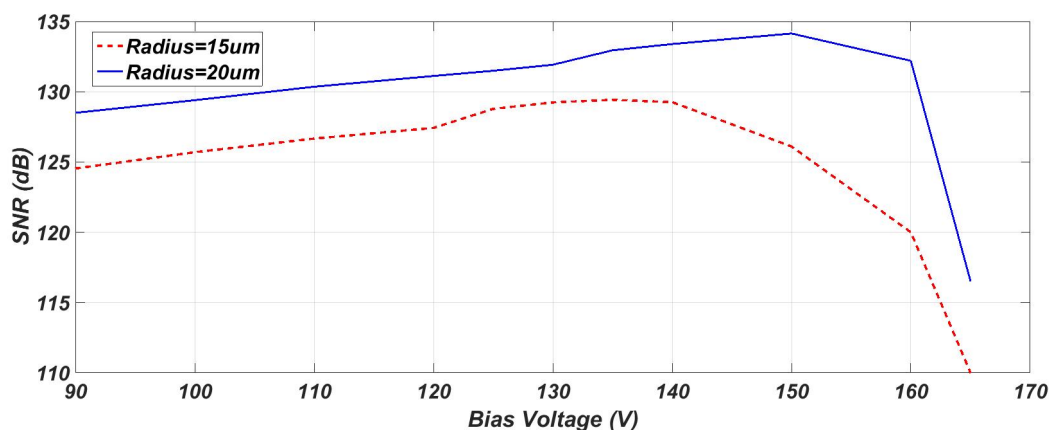
P5B1-9

8:00 am   Performance comparison of acoustic lens materials for Capacitive Micromachined Ultrasonic Transducers: simulation study

Jin Ho Chang[1,2], **Sung Ho Kim[1]**; *[1]Interdisciplinary Program of Integrated Biotechnology, Sogang University, Seoul, Korea, Republic of, [2]Electronic Engineering, Sogang University, Seoul, Korea, Republic of*

Background, Motivation and Objective

Acoustic lens for capacitive micromachined ultrasonic transducers (cMUT) is responsible for not only elevation focusing but also insulation from a high DC bias voltage. Since ultrasound signals are transmitted and received through acoustic lens, its acoustic characteristics are crucial to achieve the full performance of a cMUT. The acoustic characteristics of lens materials such as attenuation coefficient and viscosity affect signal strength, center frequency, and bandwidth. Although polydimethylsiloxane (PDMS) and room temperature vulcanization (RTV) silicone have been used as an acoustic lens for cMUTs, no performance comparison between those materials has been conducted. The objective of this study is to seek an optimal acoustic lens material for cMUTs through finite element method using PZFlex software; the candidate materials are PDMS, RTV, and urethane generally used for piezoelectric transducers.

Statement of Contribution/Methods

A single cMUT membrane covered by each lens material was modeled in PZFlex and pulse-echo simulation was performed. Water was used as a propagation medium. The acoustic impedance and attenuation coefficient were, respectively, 1.13 MRayl and 2.311 dB/MHz1.38-cm in the case of PDMS, 1.32 MRayl and 4.08 dB/MHz-cm in RTV, and 1.59 MRayl and 25 dB/MHz-cm in urethane. Also, three different thicknesses of each acoustic lens material were used in the pulse-echo simulation: 0.4, 0.8, and 1.2 mm. The pulse-echo signals obtained in each case were used to ascertain signal amplitude, center frequency, and bandwidth.

Results/Discussion

Echo amplitude of PDMS was similar to that of RTV but its low frequency component was reduced more than that of RTV. Therefore, the center frequency of PDMS was higher than that of RTV. This was possibly due to higher viscosity of PDMS (153 Pa-s vs. 290 Pa-s). Also, acoustic impedance mismatch between PDMS and water resulted in the secondary echo as shown in Fig. 1(c). The high attenuation coefficient of urethane led to severely reducing the echo amplitude and its highest viscosity (i.e., 640 Pa-s) caused considerably decreasing low frequency component. As expected, the echo amplitude, the center frequency, and -6dB bandwidth were lowered as the thickness increased; among them, urethane had the highest decrease rate. Based on the simulation results, RTV may be the best choice as an acoustic lens material for cMUT.
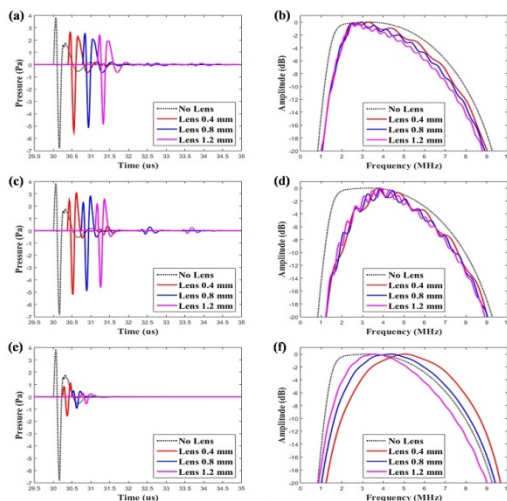
Fig. 1. Pulse echo of (a) RTV, (c) PDMS, (e) urethane and its frequency spectrum of (b) RTV, (d) PDMS, (f) urethane

P5B1-10

8:00 am   Comparison of Simulation Models for Electrical Characteristics of CMUT

Markus Klemm[1], Anartz Unamuno[1]; *[1]Fraunhofer IPMS, Germany*

Background, Motivation and Objective

One main advantage of CMUT (Capacitive Micromachined Ultrasonic Transducers) is the ability of integrating them with driving and readout circuits on CMOS. The electrical design of such frontends requires accurate simulation models, describing the electrical input characteristics of the CMUT. This allows the optimization of the electronics design and maximizing energy transfer between electrical and acoustic fields.

Lumped element models (e.g. Mason's model) or equivalent circuits like Butterworth Van Dyke (BVD) [1] are used to model electrical behavior of CMUTs. They represent a passive capacitive oscillator, but do not cover the dynamically changing capacity of the CMUT.

Statement of Contribution/Methods

Three different approaches to model the electrical behavior of a CMUT will be compared: The BVD equivalent circuit (linear, frequency domain) [1], a novel analytical description of the impedance of a CMUT (linear, time domain) [2] as shown in fig. 1 and the results of a FEM based analysis (nonlinear, time domain) [3]. The results are verified by impedance measurements on different CMUT designs.

Results/Discussion

Measured electrical impedance curves from different CMUTs will be compared to the three models discussed. The appropriateness of each model for the design of the different sections of the electronics (send pulse, receive) needed will be analyzed in terms of accuracy, time and hardware required.

[1] Lee et Al. "The effect of parallelism of CMUT cells on phase noise for chem/bio sensor applications", IUS 2008

[2] Klemm et Al, "Analytical Model for Electrical Impedance of CMUT including Dynamic Changing Capacity", to be presented at ICU 2015, Metz, France.

[3] Klemm et Al, "Simulation model for CMUT with rapid structure fluid interaction in time domain" IUS 2014

Fig 1: Measured electrical impedance and fitted analytical time domain model
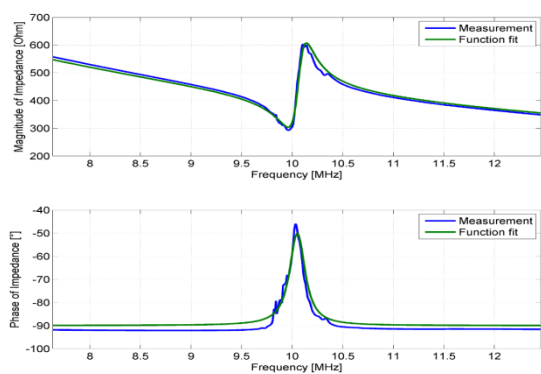
P5B2 - Applications of CMUTs

4th floor

Friday, October 23, 2015, Posters displayed 08:00 am - 05:00 pm. Authors must be present at their poster from 9:30 - 10:30am (odd number posters) and 14:30 – 15:30pm (even number posters).

Chair: **Michael Fink**
          University Erlangen-Nürnberg

P5B2-1 _____

8:00 am   cMUT technology applied to galvanic isolation : theory and experiments

Jacques Heller[1], Audren Boulmé[1], Daniel Alquier[1], Sophie Ngo[1], Marie Perroteau[1], Dominique Certon[1]; *[1]UMR CNRS 7437 - GREMAN, Université François Rabelais, TOURS, France*

Background, Motivation and Objective

Galvanic isolation is a key function of power electronic. Recently, the first prototype of an ultrasound-based isolator using cMUT technology was successfully fabricated [1]. The operating principle consists of transmitting a triggering signal using the thickness mode resonance of a substrate covered on each side of a cMUTs array. One of the two arrays is the primary circuit of the galvanic isolator; the other is the secondary circuit. The present study focuses on modeling and characterizations of these devices in order to identify design rules to optimize the power transmitted from primary circuit to secondary circuit.

[1] S.Ngo et al., "Galvanically-Isolated Data Transmission Device", US Patent 20130135970A1

Statement of Contribution/Methods

A complete model of the cMUT-based galvanic isolator was developed using the commercially available Comsol Finite Element Code. Thanks to symmetry conditions, modeling one cMUT placed on both sides of a silicon block was sufficient to solve the problem. In addition, double-sided device prototypes having a surface of 100mm2 were fabricated using square cMUTs of 22x22μm². The substrate thickness was chosen to ensure that its thickness mode resonance was as close as possible to that of the membrane. Laser interferometry and electrical measurements were undertaken to characterize the fabricated devices.

Results/Discussion

The developed model allows predicting the electrical and mechanical response of cMUTs by taking into account the mechanical coupling with substrate. It will be shown that one can accurately define, and so compute, an electromechanical coupling factor of the substrate's thickness mode like for the cMUT resonance. The FE model was also used to compute the four elements of the galvanic isolator transfer matrix and to predict the power efficiency of the device.

Experimental and computational investigations have so far yielded promising results. In particular, relevance of the model was demonstrated by comparing measurements with simulations. A method to measure the electromechanical coupling coefficient of the substrate's resonance from electrical impedances curves was implemented. High values were measured with a maximum of 40%. Theoretical investigations indicated that this maximum is obtained when the resonance frequency of the membrane falls to a value just below that of the substrate. First measurements of power efficiency were also performed in two different ways in order to ensure reproducibility and relevancy of the experimental results. Several galvanic isolator prototypes were compared, showing good and homogeneous performances. For all devices, the power efficiency was comprised between 15 % and 20 %. Comparison with simulations shows that these first results may still be improved with future prototypes.

P5B2-2 _____

8:00 am   On-Chip Piezoelectric Polymer Ultrasonic Transceivers for Point-of-Care Testing

Chien-Chong Hong[1], Kuan-Wen Chen[1]; *[1]Department of Power Mechanical Engineering, National Tsing Hua University, Hsinchu, Taiwan*

Background, Motivation and Objective

Traditional biochemical instruments require large fluidic samples, complex and lengthy procedures, and professional operators. In recent years, biomedical microinstruments have applied lab-on-a-chip technologies with biosensors to speed up detection and improve accuracy compared with traditional instruments. The main concept of lab-on-a-chip is to integrate all devices and procedures on a chip. Acoustic sensors are one of the most promising devices for achieving sensing with ultrahigh sensitivity. However, it¡¦s difficult to minimize and integrate on a chip for most of acoustic sensors. For point-of-care testing, this causes a loss of fluidic samples, increases contamination, prevents minimization, decrease sensitivity, and decreases portability. On-chip ultrasonic sources and receivers are the keys to develop fully integrated ultrasonic sensing biochips for point-of-care microfluidic testing.

Statement of Contribution/Methods

This study presents a method to realize ultrasonic transceivers on a chip based on piezoelectric polymer, poly (vinylidene difluoride-co-trifluoroethylene (P(VDF-TrFE)). Also, this research studies the surface topography and piezoelectricity of electrodeposited piezoelectric polymer film for optimization of the fabrication parameters. In this work, several parameters have been investigated, such as thickness, piezoelectricity, deposition duration, and deposition temperature.

Results/Discussion

Finally, the circular interdigitated ultrasonic transceiver array has been realized and integrated on a chhip. The device size of one single ultrasonic transmitter or receiver is 680 um. The ultrasonic transceiver array is tested in a 30 um microfluidic channel filled with deionized water at room temperature. NI PXI 100 MHz high frequency function generator and 100 MS/s, 14 bit high speed scope are used to trigger the transceiver and capture the signal. From the experimental results, our developed ultrasonic transceivers can reach 3.61 V/watt at 100 kHz.
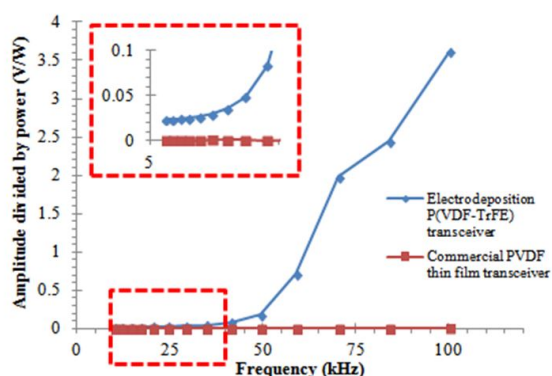
Figure 2. Comparisons of our developed ultrasound transceivers with the commercial thin films
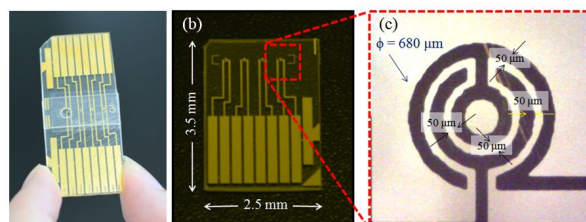
Figure 1. Pictures of on-chip ultrasonic transceivers for point-of-care testing. (a) microfluidic chip with on-chip ultrasonic transceivers, (b) ultrasonic transducer array, and (c) single ultrasonic transducer.

P5B2-3

8:00 am   CMUT for high sensitivity greenhouse gas sensing

Dovydas Barauskas[1], Donatas Pelenis[1], Gvidas Sergalis[1], Gailius Vanagas[1], Marius Mikolajunas[1], Darius Virzonis[1], Jonas Baltrusaitis[2]; *[1]Panevezys Faculty of Technologies and Business, Kaunas University of Technology, Panevezys, Lithuania, [2]Chemical and Biomolecular Engineering, Lehigh University, Bethlehem, USA*

Background, Motivation and Objective

With the emergence of the shale gas the problem of reliable and cost-effective sensing of both carbon dioxide (CO_2) and methane (CH_4) is especially accentuated. In our work we aim to design the CMUT based sensor platform, which would have the cross-selectivity and high sensitivity for CH_4, CO_2 and other gases. We selected capacitive micromachined ultrasound transducers (CMUT) approach, because they are well known for their ability to sense the mass loading of the transducer structure. For this purpose we designed, fabricated, assembled and tested surface micromachined CMUTs, which have necessary structure for required cross-selectivity due the different functional reagents. In this report we present the results of testing the polyethylenimine-modified CMUTs for CO_2 sensing.

Statement of Contribution/Methods

Devices were fabricated by surface micromachining technologies on highly doped silicon wafer. Silicon nitride acted as CMUTs structural material and chromium as the sacrificial material. The fabricated CMUTs were modified by a thin layer of PEI (Polyethylenimine) which was used for CO_2 absorbtion. Devices were placed in a closed, dry nitrogen gas filled chamber of 2 cubic decimeters volume. The mass loading was measured by using the CMUT structure as electromechanical resonator in the Colpitts type resonator circuit. The change in frequency was tracked in the real time when different flow of CO_2 gas was introduced into the chamber, keeping the pressure and temperature of the gas mixture constant. The flow of the CO_2 was controlled by the precision mass flow controller.

Results/Discussion

In the picture we present the change of the oscillator frequency after introduction of different CO_2 flows, namely 15, 20 and 30 standard cubic centimeters per minute. Different significant frequency shift can be observed for different target gas flow rates. This confirms the viability of selected approach. The noise can be removed from the signal by improving the CMUT resonance quality and minimizing the electrical noise to the oscillator.
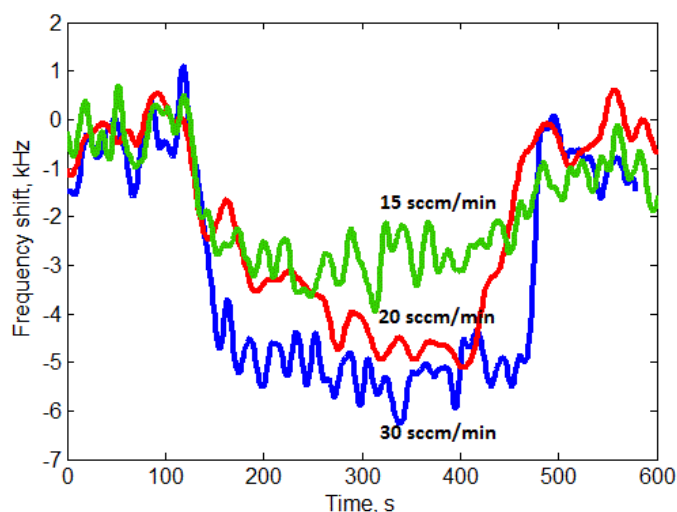
1H - MSP: Medical Signal Processing

201AF

Saturday, October 24, 2015, 08:00 am - 09:30 am

Chair: **Svetoslav Nikolov**
BK Medical

1H-1

8:00 am **Robust Sound Speed Estimation for Hepatic Steatosis Assessment**

Marion Imbault[1], Alex Faccinetto[2], Bruno-Félix Osmanski[1], Mathias Fink[1], Jean-Luc Gennisson[1], Valérie Vilgrain[2], Mickaël Tanter[1]; [1]*Institut Langevin, ESPCI ParisTech, PSL Research University, CNRS UMR 7587, INSERM U979, Paris, France*, [2]*Department of Radiology, Beaujon Hospital, Paris, France*

Background, Motivation and Objective

Hepatic steatosis is a common condition, the prevalence of which is increasing along with non-alcoholic fatty liver disease (NAFLD). Currently, the most accurate noninvasive imaging method for diagnosing and quantifying hepatic steatosis is MRI, which estimates the Proton-Density Fat Fraction (PDFF) as a measure of fractional fat content (Leporq, 2013). However MRI has several limitations including cost, contra-indications and poor availability that could be overcome by using ultrasound. Although conventional ultrasound is widely used by radiologists for hepatic steatosis assessment, it remains qualitative. It is well known that speed of sound within soft tissues varies slightly with fat content. The objective of this study is to assess the accuracy for steatosis detection and staging of a specific ultrasonic sequence for sound speed estimation (SSE). A preliminary clinical trial was undertaken, with PDFF measurement as a gold standard, to test this new sequence based on the assessment of spatio-temporal properties of the local speckle noise for SSE.

Statement of Contribution/Methods

Prospectively, 10 patients underwent MRI (3T Philips Ingenia), conventional ultrasound examination and specific ultrasound sequence acquisition; the later two using an abdominal curved probe (SC6-1, Supersonic Imagine (SI)) driven by an ultrafast ultrasound scanner (Aixplorer, SI). We implemented a new ultrasonic sequence for SSE based on time reversal processing of local speckle noise and focusing criterion (Montaldo, 2011). As steatosis can be considered as a homogeneous diffuse disease, only one single region of interest at 6 cm depth in the right liver was required for each patient. Fat and muscle layers thickness were measured with conventional ultrasound and were integrated in the calculation of the final SSE in the liver.

Results/Discussion

Our approach enables an accurate estimate of the ultrasonic sound speed in the liver with a standard deviation below 2.4 %. We obtained SSE ranging from 1.43 ± 0.01 mm/μs to 1.56 ± 0.01 mm/μs for patients with PDFF from 28.17% to 0.18% respectively. Strong correlation for quantification of hepatic steatosis was observed between the decrease of SSE and the increase of PDFF ($R^2 = 0.92$) (Fig. 1). In conclusion, this first pilot study demonstrates the feasibility of hepatic steatosis detection and staging with SSE in patients with NAFLD.

Fig. 1: Correlation between sound speed estimation (SSE) and proton density fat fraction (PDFF) for ten patients. Patients without steatosis are characterized by PDFF<2.5%. We observe that speed of sound in liver decreases when fat fraction increases.

1H-2

8:15 am **Monitoring and Delivery of Transcranial Therapies Using Dual-mode Ultrasound Arrays**

Alyona Haritonova[1], Dalong Liu[2], Emad Ebbini[2]; [1]*Biomedical Engineering, University of Minnesota, Minneapolis, MN, USA*, [2]*Electrical and Computer Engineering, University of Minnesota, USA*

Background, Motivation and Objective

We have previously shown that dual-mode ultrasound arrays (DMUAs) are capable of delivering therapeutic and sub therapeutic (subThx) HIFU transcranially in a rat model *in vivo*. We have also shown that echo data from DMUA imaging allowed for monitoring temperature changes due to the transcranial focused ultrasound (tFUS) beams. In this study, we investigate the spatial accuracy of the transcranial DMUA-based temperature imaging.

Statement of Contribution/Methods

A 3.5MHz DMUA with a focal point of 40mm was used for guidance, monitoring and delivery of FUS subThx treatment. Temperature imaging derived from high-frame rate (400fps) single transmit focus rf-data enabled visualization of subThx heating. *In vivo* subThx heating was performed in eight Sprague Dawley rats; the rats were sedated and secured inside a stereotaxic frame during the procedure. Three days after the procedure animals were sacrificed and the skullcap removed and formalin-fixed. We then performed characterization studies on the skull to corroborate feedback received during *in vivo* therapy. First, transmission study was done utilizing two single element transducers (Tx & Rx). Second, spatial hydrophone maps at two different frequencies (1.8MHz and 3.2MHz) were measured in water and through skull. Third, the skullcap

was encapsulated inside phantom material and DMUA subtherapy protocol was repeated. A diagnostic imaging probe was used to image the temperature in a plane perpendicular to the DMUA tFUS beam.

Results/Discussion

Figure 1A depicts a typical result of an *in vivo* axial-temporal temperature profile. As seen from the image the dominant heating spot is visualized approximately ~2mm above the intended focus. The result of the hydrophone test, through skull (Figure 1B) have confirmed apparent shift of the focus towards the array, consistent with *in vivo* observations. Transmission maps revealed better and more uniform penetration at lower frequencies and indicated the need of refocusing at higher frequencies. However, the higher frequencies resulted in more localized heating in the axial direction. A 3.2 MHz tFUS frequency provided the best compromise within the available bandwidth. In conclusion, the *in vitro* characterization confirmed that the DMUA provided spatially-accurate temperature feedback in the presence of skull aberration.

A **B**

1H-3

8:30 am   Automatic Mouse Embryo Brain Ventricle Segmentation, Gestation Stage Estimation, and Mutant Detection from 3D 40-MHz Ultrasound Data

Jen-wei Kuo[1], Yao Wang[1], Orlando Aristizabal[2,3], Daniel H. Turnbull[3], Jeffrey A. Ketterling[2], Jonathan Mamou[2]; *[1]Electronics and Computer Engineering, Polytechnic School of Engineering, New York University, Brooklyn, USA, [2]F. L. Lizzi Center for Biomedical Engineering, Riverside Research, New York, USA, [3]Skirball Institute of Biomolecular Medicine, New York University School of Medicine, New York, USA*

Background, Motivation and Objective

Volumetric analysis of brain ventricles (BVs) is important to the study of normal and abnormal development of the central nervous system (CNS) of mouse embryos. High-frequency ultrasound (HFU) is frequently used to image embryos because HFU is real-time, non-invasive, and provides fine-resolution images. However, manual segmentation of BVs from 3D HFU volumes remains challenging and time consuming. Therefore, automatic segmentation, staging, and brain phenotypes detection algorithms are needed for studies with large embryo counts.

Statement of Contribution/Methods

Volumetric ultrasound data were acquired in utero and in vivo from pregnant mice using a 5-element, 40-MHz annular array. A 5-channel pulser was used to consecutively excite each array element. The 25 resulting transmit/receive signals processed using delay-and-sum beamforming which yielded a depth of field sufficient to cover the entire head of the embryo. An automatic segmentation algorithm called nested graph cut (NGC) was developed to segment the BVs, head, amniotic fluid, and uterus. To define the missing boundary between objects (e.g., head and uterus), NGC only applied predefined structural information and, thus, did not require any training. After segmentation, it is possible to stage embryos or detect mutants with a BV phenotype based on the volume ratio between the BVs and head (Fig. 1a) and BV morphology (Fig. 1b). Mutations caused by the loss of midbrain tissue (Fig. 1b) were automatically detected by extracting and quantifying the skeleton geometry of the third and fourth BV.

Results/Discussion

The NGC algorithm was applied to 40 wild type embryos spanning from days E10.5 to E14.5 and the Dice similarity coefficient (DSC) was used to quantitatively compare automatic and manual segmentations. The average DSC was 89±5% for BV segmentation and 90±3% for head segmentation. The NGC algorithm also showed better performance than region growing, active shape model (ASM), and our previous work, which refines the ASM result by shape-constrained region growing. In addition, NGC permitted to automatically detect mutants from stage-matched wild-type embryos. Therefore, our NGC-based framework could be invaluable in streamlining development biology studies requiring quantitative CNS assessment, staging, and mutant detection.

SATURDAY ORAL

Fig. 1: (a) BVs-Head volume ratio automatically computed from NGC-based segmentation can be used to stage embryos. (b) Mid-sagittal section of E12.5 embryos showing the expected loss of mid-brain tissue (arrows) in an Engrailed 1 (En1) mutant compared to a wild-type littermate. 3D renderings generated from NGC segmentation results also reveals an increase in BV volume for the EN1 mutant due to loss of midbrain tissue.

1H-4

8:45 am   Use of B-splines in fast dynamic ultrasound RF simulations

Sigurd Storve[1], Hans Torp[1]; [1]*Department of Circulation and Medical Imaging, Norwegian University of Science and Technology, Trondheim, Norway*

Background, Motivation and Objective

Synthetic ultrasound data is invaluable for applications such as tuning image segmentation algorithms. Unfortunately, simulation time can become prohibitive for phantoms consisting of a large number of point scatterers. In such cases, simplified simulation algorithms can trade accuracy for speed. Storage of dynamic scatterer phantoms requires vast amounts of disk space when the number of time steps is large. We propose (1) a spline-based approach for efficient handling of dynamic scatterer phantoms with arbitrary time resolution, and (2) a fast and open source C++ implementation of a previously published convolution-based technique (COLE by Gao et al.) using our spline-based approach.

Statement of Contribution/Methods

We propose to represent the complete trajectory of individual scatterers as B-splines of arbitrary degree, all sharing the same knot vector, as illustrated in the figure. This is very computationally efficient as the B-spline basis functions only need to be evaluated once at each time step. Multiple scan lines are simulated concurrently by using OpenMP. We recorded the time for simulating the RF data for both a 2D B-mode scan of a 3D left ventricle phantom (128 scan lines and 4.7 million scatterers) and a PW tissue Doppler scan of a deforming tissue scatterer phantom (157007 scatterers and 10000 Doppler beams). In both cases a laptop computer with a quad-core 2.7GHz Intel i7 processor and an analytic Gaussian beam profile with a standard deviation of 0.5mm and 1.0mm in the lateral and elevational direction was used. The C++ source code is available on Github (project OpenBCSim).

Results/Discussion

The simulation time for the LV phantom was 10 seconds, while simulating the RF data for the PW tissue Doppler example took 65 seconds. The resulting images are shown in the figure. We believe that our spline-based approach is a useful technique in general for applications involving large amounts of dynamic scatterers, and also that it will enable an efficient GPU implementation, since the complete trajectory of all scatterers can be kept in GPU memory, which avoids expensive memory transfers between the CPU and the GPU at each time step. We conclude that our spline-based technique for representing scatterers is both storage-effective and permits fast simulation of synthetic RF data. Both CUDA source code and results from a GPU implementation will be ready for the conference.

a) Example of a spline representation of a complex 3D scatterer trajectory. A single scatterer from a rotating cube phantom is shown with its control polygon in black. The red dots indicate the motion from t=0.8s to t=0.9s.

b) Simulated 2D B-mode scan through a 3D LV phantom consisting of 4.7 million cubic scatterer splines.

c) Simulated PW tissue Doppler scan of a dynamic tissue phantom consisting of 157007 cubic catterer splines.

1H-5

9:00 am   Evaluation of a Huffman Sequence Based Mismatched Filter for the Bandwidth Limited 3D USCT system

Shreyank Gupta[1,2], Michael Zapf[1], Herbert Krauß[2], Nicole V. Ruiter[1]; [1]*Institute of Data Processing and Electronics, Karlsruhe Institute of Technology, Germany, [2]Electrical Engineering and Information Technology, University of Applied Sciences Darmstadt, Germany*

Background, Motivation and Objective

A 3D Ultrasound Computer Tomography (USCT) system for early detection of breast cancer was developed at KIT. The system was optimized for Synthetic Aperture Focusing Technique using unfocused ultrasound transducers. Due to low SNR of the data, a signal chain with Coded Excitation (CE) and a offline filtering step with an

matched filter (MF) is applied. For complex objects the measured A-scans consist of multiple superimposed reflections. The separability of reflections is mainly limited by the system's limited bandwidth and the resulting side lobe artifacts in the signal. Non-separable reflections limit the resolution and contrast of the resulting images.

The contained energy of the applied CE defines the SNR in the measured data. Also, with well-defined CEs, like Huffman Sequences (HS), side lobe suppression can be achieved but on compromised SNR. The objective of this work is to overcome this trade-off in CE selection.

Statement of Contribution/Methods

The basic idea is separation of concerns in the signal processing chain: specializing the CE for maximum energy in the measured A-scans and use case specific adaptive offline filtering for side lobe suppression. A simpler and for maximum energy specialized CE can be used, e.g. a linear chirp with a bandwidth and energy preserving damping window (LCH). Due to this separation the filter is a mismatched filter (MMF). The proposed filter, called HSD-MMF, is designed under use of a HS to result in suppressed side lobes.

Results/Discussion

The approach was evaluated by a A-scan simulation of multiple superimposed normally distributed reflections with equal amplitudes. Realistic USCT parameters as given in Table A were used for comparing HSD-MMF to the standard MF filter performance.

The shifting metric shows shifts of the detected pulse positions in time. The detectability metric measures how many multiple superimposed reflections were separated.

For single reflection: Analysis showed 118% suppression of peak side lobe compared to standard MF while compromising 11% on ME.

For multiple superimposed reflections: Analysis showed mean detection of 9% using MMF and also 16% less localization error compared to standard MF, see Table B.

This approach gets rid of the trade-off between SNR and side lobe suppression. It is concluded that using MMF improves the overall capability of the system to separate more reflections compared to MF.

Table A: Simulation parameters		Table B: Evaluation results							
		First part- single reflection			Second part- superimposed reflections				
					Shifts (localization errors)		Detectability		
	Filters	MSR (Main lobe to peak side lobe ratio) $\frac{|f(n)|_{n=0}}{max|f(n)|_{n\neq0}}$	ME (Main lobe energy) $|f(n)|^2_{n=0}$	ISL (Integrated side lobe energy) $\sum_{n=1}^{N} f(n)^2$	Mean	Standard deviation	Mean	Standard deviation
Bandwidth: 1.7 MHz									
Center frequency: 2.4 MHz									
Sampling frequency: 10 MHz									
Total number of reflections: 1000									
CE type: LCH									
CE length: 100 µs	MF	1.38	19.05	26.76	4.38 µs	1.62 µs	50.05%	20.43%
Filter length: 300 µs	HSD-MMF	3.02	17.12	15.88	3.76 µs	1.33 µs	59.20%	19.97%

Table 1: Shows comparison of MF and MMF for a single and superimposed reflections. f (n) = Filtered output, N= Total length in samples

1H-6

9:15 am   Towards Sub-Nyquist Doppler Ultrasound Imaging Using Non-Uniformly Spaced Stream of Pulses

Avinoam Bar-Zion[1], Martino Alessandrini[2], Jan D'hooge[2], Dan Adam[1], Yonina Eldar[3]; *[1]Department of Biomedical Engineering, Technion - Israel Institute of Technology, Haifa, Israel, [2]Cardiovascular Imaging & Dynamics, Department of Cardiovascular Sciences, KU Leuven, Leuven, Belgium, [3]Department of Electrical Engineering, Technion - Israel Institute of Technology, Haifa, Israel*

Background, Motivation and Objective

Tissue Doppler ultrasound imaging (TDI) enables the estimation of cardiac function by transmitting streams of pulses in a certain direction and estimating the velocity of the tissue from the phase shifts of the returning echoes. The duration of time needed for a single velocity estimation is the coherent processing interval (CPI). In order to estimate the velocity of the tissue precisely and separate slow tissue movement from dominant clutter, a large number of pulses has to be transmitted in the same direction. The number of transmitted pulses per unit of time is limited by the speed of sound and the desired imaging depth, therefore there is an inherent tradeoff between spectral and spatial resolution. This limitation impedes TDI usage to a few measurements through the LV wall. Compressed sensing (CS) is a signal processing framework that allows the reconstruction of signals sampled at a sub-Nyquist rate using priors on the sparsity of the signal. This work aims to facilitate reduced time per velocity estimation by transmitting non-uniformly spaced pulses in each direction and processing the signal within the CS framework.

Statement of Contribution/Methods

A parametric model describing the TDI data in both fast-time (a-line) and slow-time (between pulses) is proposed. This model has been extended to the case in which only a non-uniformly spaced subset of the received pulse-echo transmissions are processed while preserving the overall CPI. The received signals are processed using the matrix form of the fast iterative shrinkage threshold algorithm (FISTA). Doppler estimations using subsets of 20%-50% of the received pulse-echo transmissions were compared to the estimations based on 100% of the data set in a series of simulated phantoms including clutter and various velocities.

Results/Discussion

The correlation coefficient between the estimated velocities calculated from 50% of the pulses and those calculated from the entire dataset is 0.92. When fewer pulses are used, this correlation gradually decreases (Figure 1). The compressed sensing framework for TDI presented in this work reduces the number of pulses needed for velocity estimation at a given spectral resolution, changing the tradeoff between spectral and spatial resolution. The resulting time between pulses in each direction can be used for scanning in different directions during the same CPI.
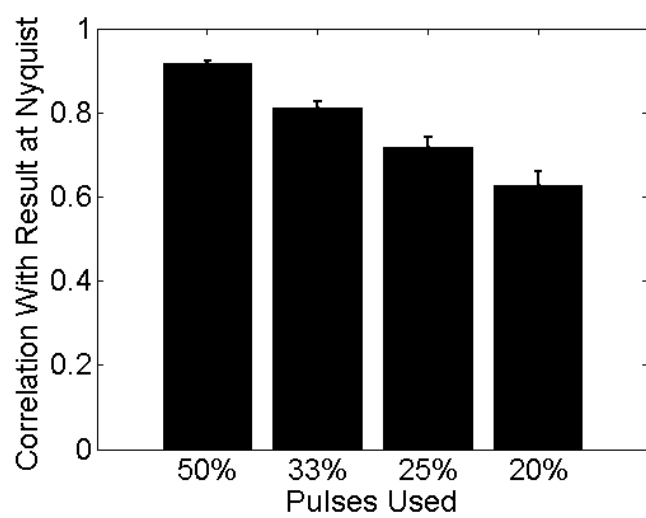
SATURDAY ORAL

2H - MBB: Beamforming V

VIP

Saturday, October 24, 2015, 08:00 am - 09:30 am

Chair: **Herve Liebgott**
           CREATIS

2H-1

8:00 am   High Frame Rate 3D Tissue Velocity Imaging Using Sub-Aperture Beam Forming

Pedro Santos[1,2], Lasse Lovstakken[2,3], Eigil Samset[2,4], Jan D'hooge[1,3]; [1]*Department of Cardiovascular Sciences, KU Leuven, Leuven, Belgium, [2]GE Vingmed Ultrasound AS, Horten, Norway, [3]Department of Circulation and Medical Imaging, NTNU, Trondheim, Norway, [4]Center for Cardiological Innovation, Oslo, Norway*

Background, Motivation and Objective

High frame rate (HFR) 3D tissue Doppler imaging (TDI) using diverging waves (DW) has been demonstrated on experimental systems, with fully wired matrix arrays. However, current clinical systems have a limited number of channels (e.g. ~128 cables) and require sub-aperture (SAP) beam forming. The first stage beam forming is performed in the probe and typically limited to static focusing (i.e. pre-fixed direction and depth).

Motivated by intraoperative monitoring of electrophysiology procedures, this study aims at translating HFR 3D TDI to a SAP beam forming system.

Statement of Contribution/Methods

A TEE matrix array (48x48 elements; 9.6x9.6 mm^2) with 3 different SAP geometries (1x1, 4x4 and 6x6 elements per SAP) transmitting a 2.5 MHz pulse was simulated in Field II. To study the effect of SAP directivity due to static receive focusing and the reduced penetration due to a broad transmit, 3 scan sequences were designed: i) 1 DW, f = -2mm; ii) 2x2 DW, f = -6mm; iii) 3x3 DW, f = -9mm; all covering a field of view of 70° by 70°.

Static receive focusing (foci at the centre of each sub-sector) was applied in the first stage, whereas dynamic focusing was applied in the second stage.

TDI was computed for a rotating sphere (ω = 2 rad/s on azimuth-depth plane, r = 4 cm) using the autocorrelation method on beam formed IQ data, followed by spatial smoothing. The configuration without SAP beam forming (i.e. 1x1) was used as benchmark.

Results/Discussion

Static receive focusing in the first stage SAP beam forming led to grating lobes (Fig - left) and thus, biased velocities (Fig - middle, mainly the 6x6 SAP). The bias increased for larger SAPs due to their higher directivity (Fig - right). Similarly, velocity errors increased towards the edges of the DWs (Fig - middle), as receive steering became larger and the magnitude of grating lobes approached (or surpassed) the one of the main lobe.

The 1 DW sequence showed very limited penetration and severe grating lobes for SAP configurations, thus seeming impracticable. Interestingly, 2x2 and 3x3 DW sequences showed comparable results for SAPs and fully wired probe configurations, while still providing HFR (1375 and 611 fps).

As such, preliminary results indicate that HFR 3D TDI may be translated to clinical systems, considerably improving current temporal resolution. Future work will include *in vitro* validation of our findings and an *in vivo* feasibility study of HFR 3D TDI.
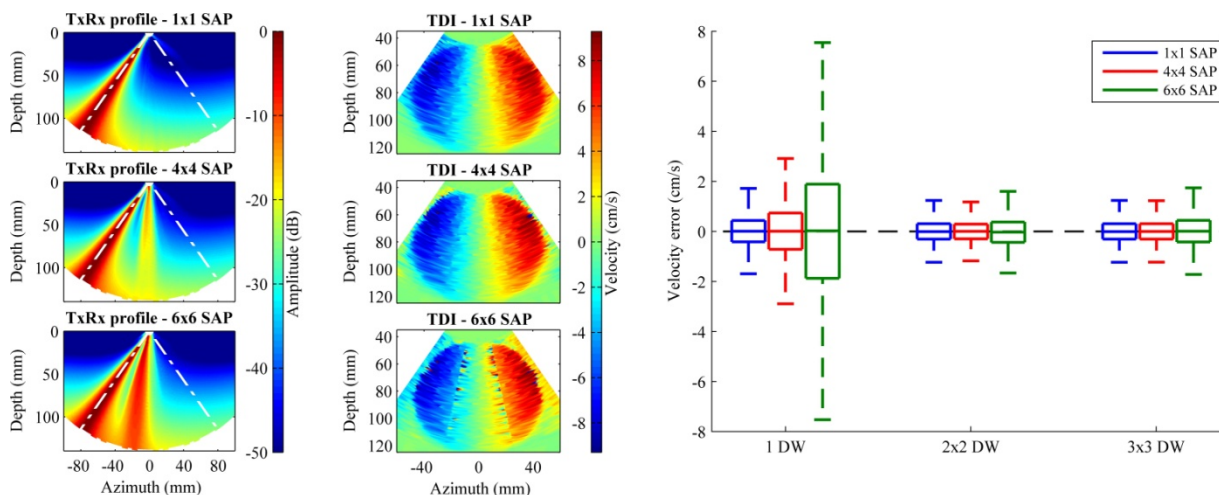
Fig – Two-way beam profiles (left) and TDI maps (middle) for 1x1, 4x4 and 6x6 SAP configurations using a 3x3 DW scan sequence; distribution of the velocity error (right) for all the configurations tested.

2H-2

8:15 am   A 50 MHz Phased Array Beamformer Using a Novel 'One Sample per Pixel' Variable Sampling Technique

Christopher Samson[1], Jeff Leadbetter[1], Jeremy Brown[1]; [1]*Biomedical Engineering, Dalhousie University, Halifax, Nova Scotia, Canada*

Background, Motivation and Objective

In comparison to conventional low-frequency beamformers, high-frequency phased array beamforming requires high analog-to-digital (A/D) sampling and data capture rates in order to adequately align the received echoes. Delay alignment accuracy of approximately ±1ns is required at 50MHz (~20 samples per wavelength) to avoid quantization error between channels. Studies have shown that using a variable sampling rate for each channel independently, the data capture rates can be reduced. To determine the pattern of sampling, the round trip time of flight for each element to image pixel is pre-calculated and used to trigger the A/D converters. Unfortunately, this technique requires an in-phase (I) and quadrature (Q) sample separated by ¼λ for each pixel in order to detect the envelope, meaning that high frequency A/D converters are still required. We have developed a new method of variable sampling in which only one sample is required per pixel, significantly reducing the required sampling and data rates.

Statement of Contribution/Methods

With this technique, the pixels in the image are spaced at exactly ¾λ, and the variable sampling method of receive beamforming is implemented with ±1ns accuracy. The reason that we only require one sample per pixel is that the envelope detection is approximated by samples spaced at ¾λ instead of ¼λ. By spacing the pixels this way and demodulating with ¾λ, each successive sample (pixel) is used as both the 'Q' sample for the current pixel and the 'I' for the next pixel. This relaxes our sampling rate to 3/4λ or 67MHz. Prototype 64 channel FPGA-based transmit and receive beamformers have been developed and the delay accuracy characterized. Images were generated comparing the ¼ and ¾ λ variable sampling methods using an in house fabricated 50MHz phased array endoscope with 55% bandwidth.

Results/Discussion

The transmit beamformer timing accuracy has been measured to be ±125ps and the timing accuracy for the dynamically varied A/D encode clocks on the receive beamformer was measured to be ±1ns. The dynamically variable clocks were generated for 64 channels, 512 pixels per line, and 64 image lines. Figure 1 shows a comparison image using the phased array endoscope by demodulating with ¼ and ¾λ sample spacing. There is no noticeable difference between the quality of the two images and for a 55% bandwidth probe the worst theoretical envelope error is only -1.3dB.
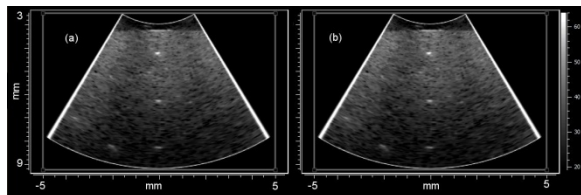
2H-3

8:30 am   Busting the ghost in coherent plane-wave imaging

Alfonso Rodriguez-Molares[1], Lasse Lovstakken[1], Bastien Denarie[2], Hans Torp[1]; [1]*Circulation and Medical Imaging, Norwegian University of Science and Technology, Trondheim, Norway,* [2]*GE Healthcare, Norway*

Background, Motivation and Objective

In recent years coherent plane-wave imaging (CPWI) has become one of the most popular methods in ultrasound beamforming as it provides equivalent resolution to optimal multifocus imaging using a reduced number of plane wave transmissions (N). It has been described in the literature that the decimation of the angle sequence results on the introduction of grating lobes and the reduction of the contrast ratio (CR). The effect of edge waves is however less documented. Edge waves result on a ghost artifact that lags behind the point spread function (PSF) and impacts both the images CR and axial resolution.

Statement of Contribution/Methods

Even though the amplitude of the ghost tends roughly to decrease for increasing N, both our simulated and experimental data show that its variation is not monotonically decreasing. On the contrary, in some cases increasing N leads to a reduction in the CR.

The intensity of the ghost can be reduced by transmitting apodized plane waves. Tukey windows have proved useful to reduce the influence of the edge waves, however fluctuations in the CR are still observed.

We propose an angle dependent transmit apodization that eliminates the CPWI ghost and increases the convergence of the CR to the theoretical maximum, given by an idealized synthetic transmit aperture imaging (STAI) scheme. The proposed apodization scheme is calculated based only on the scan geometry. It assigns a different apodization to each of the transmitted plane waves that weights down the portion of the aperture that does not contribute to image formation. The proposed scheme can be applied without increasing the complexity of the imaging system.

Results/Discussion

Two sets of experiments were conducted: an in silico experiment (left panel), and an in vitro experiment (right panel). Three transmit apodization schemes were compared: Flat, 25% roll Tukey window, and the proposed angle dependent apodization. The panels show how CR varies with N for the three schemes. In all cases the angle span was [-23.87°,23.87°].

In silico data was computed with Field-II and features a single scatterer. It shows the ghost and the fluctuations in the CR. The Tukey 25% mitigates the fluctuations only partially whilst the proposed scheme removes them. It also accelerates significantly the convergence of the CR to the one of STAI.

In vitro data was obtained with a Verasonics Vantage research scanner, a L12-3v probe, and a multipurpose ultrasound phantom (CIRS) and it features an anechoic cyst. Fluctuations are observed both with the Flat and Tukey 25% apodizations, but not with the proposed scheme. An improvement of up to 9 dB is obtained compared to the other two apodization schemes.

SATURDAY ORAL
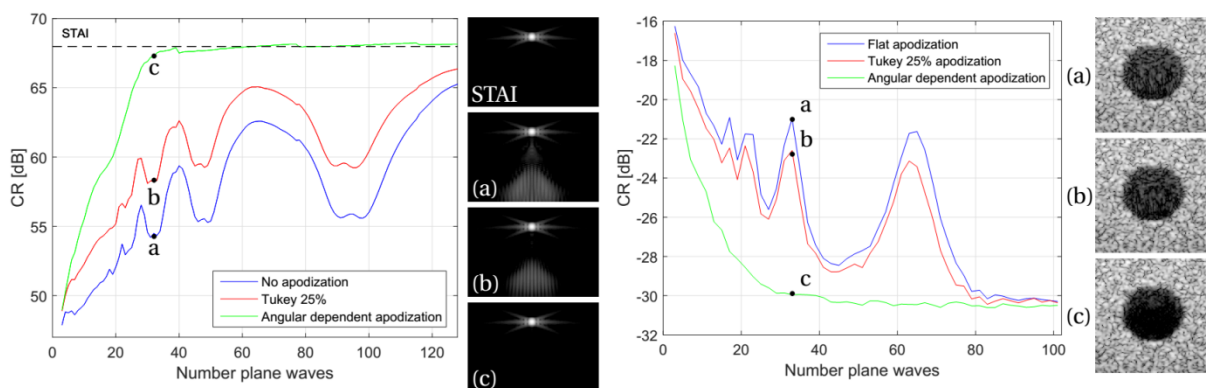
8:45 am   Coded excitation for crosstalk suppression during multi-line transmit beamforming: a simulation study

Ling Tong[1,2], Alejandra Ortega[2], Jianwen Luo[1], Jan D'hooge[2]; *[1]Department of Biomedical Engineering, Tsinghua University, Beijing, Beijing, China, People's Republic of, [2]Department of Cardiovascular Sciences, KU Leuven, Leuven, Belgium*

Background, Motivation and Objective

Multi-line transmit (MLT) beamforming was recently proposed to increase frame rate. Although crosstalk between MLT beams could induce artifacts, we recently demonstrated that a Tukey-Tukey (TT) transmit-receive apodization can largely – but not completely – suppress this crosstalk. As coded excitation has been proposed to suppress crosstalk for synthetic aperture imaging, the aim of this study was to investigate whether it could be an alternative and/or to further suppress MLT crosstalk.

Statement of Contribution/Methods

A typical 64-element cardiac probe (2.5MHz; bandwidth 60%) transmitting 2-, 4-, and 6-MLT beams over a 90° sector respectively, was simulated in Field II. To avoid significant impact on frame rate only two sets of orthogonal Golay codes with their two complementary codes were encoded to neighbouring MLT beams for every MLT system. Similarly, two orthogonal linear frequency modulated chirps were tested. These coded systems were investigated with and without TT apodization and contrasted against non-coded MLT with TT apodization. To quantify the crosstalk of the different MLT implementations, their point spread functions (PSF) were simulated and quantitatively compared to a single line transmit (SLT) system.

Results/Discussion

As summarized in the figure, without apodization, for a 2MLT system, the crosstalk was removed completely using Golay codes, whereas it was suppressed under ~-50 dB using chirps. For a coded 4- and 6-MLT system without apodization, high crosstalk level (Golay: ~ -39dB, Chirp: ~-30dB) was observed as a result of using only 2 sets of orthogonal codes. Adding Tukey (α=0.5) apodization, a Golay coded 4MLT, 6MLT, and Chirp coded 4MLT showed slightly lower crosstalk level with respect to the corresponding non-coded apodized MLT systems. Note that the effective gain in frame rate of Golay coded MLT systems was compromised by a number of 2 as a result of transmitting complementary codes. In terms of spatial resolution and SNR, the coded MLT systems were very competitive compared to the SLT system. Overall, our results demonstrated that coded excitation can be used to suppress MLT crosstalk but that apodization is still required when the number of MLT beams is larger than the number of orthogonal codes. Furthermore, adding coded excitation to TT-apodized MLT setup can further suppress crosstalk, although the benefit remained limited.
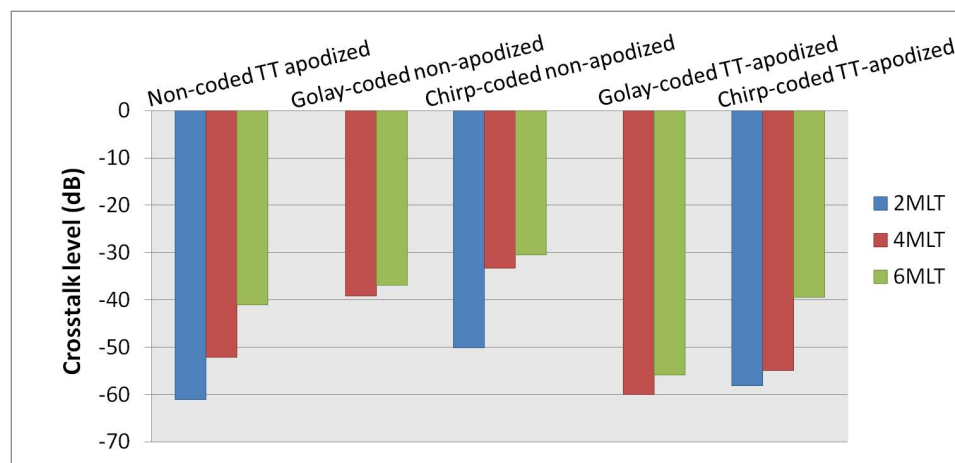
Figure. Crosstalk level of different MLT imaging systems.
(TT: Tukey apodization on transmit and receive)

9:00 am   Filtered Spatial Compounding (FSC) in Synthetic Transmit Aperture Imaging

Ping Gong[1], Michael C. Kolios[1], Yuan Xu[1]; *[1]Biomedical Physics, Ryerson University, Toronto, Canada*

Background, Motivation and Objective

Ultrasound speckle usually reduces contrast-noise-ratio (CNR) and detectability (lesion signal to noise ratio (lSNR)) of targets. Sidelobes and clutter caused by undesired signals arising from off-axis targets also lower the image CNR.

Typically, CNR can be improved by spatial or frequency compounding, but at the expense of temporal or spatial resolutions. Here we propose a filtered spatial compounding (FSC) technique that implements a 3-dimentional (3D) spatial filter for spatial compounding on synthetic transmit aperture (STA) imaging data. The technique suppresses the speckle pattern and reduces the effect of the off-axis signals, improving spatial resolution, image CNR and lSNR.

Statement of Contribution/Methods

The received channel RF data are presented as a 3D data matrix (i.e. time×receive×transmit). First, delays are applied to each receive channel (R) under each transmission (T) while focusing at one image point. Once the RF signals are aligned (post-aligned), they are summed coherently (conventional delay-and-sum (DAS)) or incoherently (conventional spatial compounding (CSC)) to produce the value of the corresponding image point. In FSC, before summation, we apply a 3D spatial filter to the post-aligned RF data in which the off-axis signals are displayed as high spatial frequencies in both T and R directions. The spatial filter is designed as an all-pass filter along the time direction and a low-pass filter (hanning window function) along both the T and R directions (i.e. all×low×low). Afterwards, spatial compounding is applied to the filtered RF data to further improve the image CNR and lSNR.

FSC was tested with Field II simulations (experimental test is in progress). A 64-element 2-cm-wide 5 MHz linear array was placed 15 mm above a 5×20 mm^2 tissue mimicking phantom. The phantom contained a 4-mm-diameter hyper- (left) and a hypo- (right) inclusion (almost invisible in the DAS image), and a point inclusion at the center. STA RF data were processed by DAS, CSC and FSC and displayed as log-enveloped images.

Results/Discussion

Fig. 1 shows beamformed DAS (a), CSC (b) and FSC (c) images. The axial resolution in FSC (as assessed by the point target indicated by the arrow), was improved by 18% and 45% over that in DAS and CSC, respectively. CNR and lSNR values (as assessed by the inclusions) were also significantly enhanced (183% maximum) in the FSC image.

(a) DAS   (b) CSC   (c) FSC
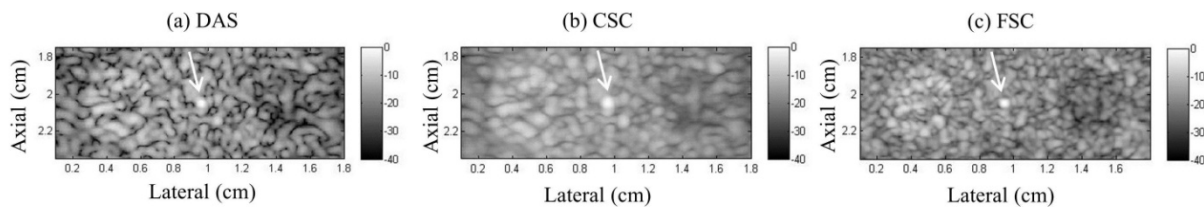
2H-6_____

9:15 am   Improving lateral resolution in ultrasonic imaging by utilizing nulls in the beam pattern

Jonathan Reeg[1], **Michael L. Oelze[1]**; *[1] Electrical and Computer Engineering, University of Illinois at Urbana-Champaign, USA*

Background, Motivation and Objective

Reduction of lateral sidelobes results in improved ultrasonic imaging. In general, apodization is used to lower sidelobes in exchange for increasing the width of the mainlobe and thus decreasing lateral resolution. Null Subtraction Imaging (NSI) is a technique that uses different on-receive apodizations on copies of the same image data to reduce sidelobe levels while also improving lateral resolution.

Statement of Contribution/Methods

In the NSI technique, several apodization functions are applied on receive. The first apodization weight is applied having a zero mean when summed across the aperture. This places a null at the center of the receive pattern. The second apodization is the same as the first apodization except that a constant DC offset is applied (non-zero mean). The third apodization is the transpose of the second. The intensity image created with the zero-mean apodization is then subtracted from the mean of the images created with the second and third apodizations.

To evaluate the performance of this technique, experiments were performed with an ATS539 phantom containing wire targets to assess lateral resolution and cylinder targets to assess contrast. For imaging, a 9L4 array (center frequency of 5 MHz) connected to an Ultrasonix RP system having a SonixDAQ was used. Plane waves were emitted from the array and received by each array element. Image reconstruction involved synthetic aperture focusing using Stolt f-k migration with the different apodization schemes applied on banks of 32 elements corresponding to a receive aperture size of 9.5 mm. Images were constructed using NSI and compared with rectangular and Hamming apodizations. Image quality was assessed by estimation of lateral resolution (-3-dB receive beamwidth), the mainlobe to sidelobe ratio (MSR) in dB and estimation of the contrast-to-noise ratio (CNR).

Results/Discussion

Table I lists the -3-dB receive beamwidth values estimated from the small wire targets located at different depths. The NSI scheme provided lateral resolution better than half that of rectangular apodization (e.g., for an f-number of 1, the lateral resolution was better than $\lambda/2$). The MSR for the novel apodization scheme was 6 to 10 dB lower than rectangular apodization. Only small changes in CNR were observed between the NSI apodization and rectangular apodization (1.25 and 0.86, respectively).

	Apodization					
	Rectangular			NSI		
Wire Depth (cm)	-3-dB width (mm)	-3-dB width (λ)	MSR (dB)	-3-dB width (mm)	-3-dB width (λ)	MSR (dB)
1	0.37	1.25	-20	0.12	0.42	-26
2	0.65	2.20	-15	0.26	0.88	-24
3	0.97	3.29	-16	0.41	1.40	-22
4	1.48	5.01	-13	0.55	1.87	-23

SATURDAY ORAL

3H - MEL: Methods for Elasticity Imaging

201BC

Saturday, October 24, 2015, 08:00 am - 09:30 am

Chair: **Timothy Hall**
           University of Wisconsin

3H-1

8:00 am   **Measurement of the frequency dependent phase velocity and attenuation from the Fourier description of shear wave propagation: addressing geometric spreading arising from spatially asymmetric Gaussian excitations**

Ned Rouze[1], **Mark Palmeri[1]**, Kathryn Nightingale[1]; *[1]Biomedical Engineering, Duke University, Durham, North Carolina, USA*

Background, Motivation and Objective

Viscoelastic (VE) properties of materials can be determined by observing shear wave propagation following an impulsive excitation and measuring the frequency dependent phase velocity $c(f)$ and attenuation $\alpha(f)$. Nenadic, et al. [2014 IEEE-IUS proceedings] have described a method to measure $c(f)$ and $\alpha(f)$ from the two dimensional Fourier transform (2DFT) of a spatial-temporal shear wave signal. This procedure assumes the shear wave is described as either a plane wave or as the asymptotic form of a cylindrically expanding wave and does not take into account the size and shape of the excitation source or observation of the shear wave at non-asymptotic locations near the source.

Statement of Contribution/Methods

The equation of motion describing shear wave propagation in a VE material is derived in the Fourier domain and solved analytically for the case of an asymmetric Gaussian source. This solution is used to evaluate the 2DFT analysis method by constructing the 2DFT signal describing shear wave propagation in a VE material (3-parameter solid) and comparing the analysis results with the true $c(f)$ and $\alpha(f)$ calculated using the model parameters.

Results/Discussion

The figure shows analytically computed 2DFT results for shear wave propagation following an asymmetric Gaussian excitation with a source aspect ratio of 2 ($\sigma_x = 1$ mm and $\sigma_y = 2$ mm) in a material described by a 3-parameter VE model of liver. Figures (b) and (c) show $c(f)$ and $\alpha(f)$ obtained using the 2DFT analysis (black) as compared to the true analytic values (red). We observe that the 2DFT analysis gives biased results for both $c(f)$ and $\alpha(f)$. Also, the dispersion slope is biased by 47% which is consistent with the biases observed by Nightingale, et al. [IEEE-TUFFC 62, 165-175, 2015]. These biases can be reduced by weighting the spatial-temporal shear wave signal by the factor x^p to address the impact of geometric spreading. Figure (d) shows the optimal power p that minimizes the combined biases in $c(f)$ and $\alpha(f)$ as a function of source aspect ratio. Figures (b) and (c) show results obtained using $p = 0.42$.
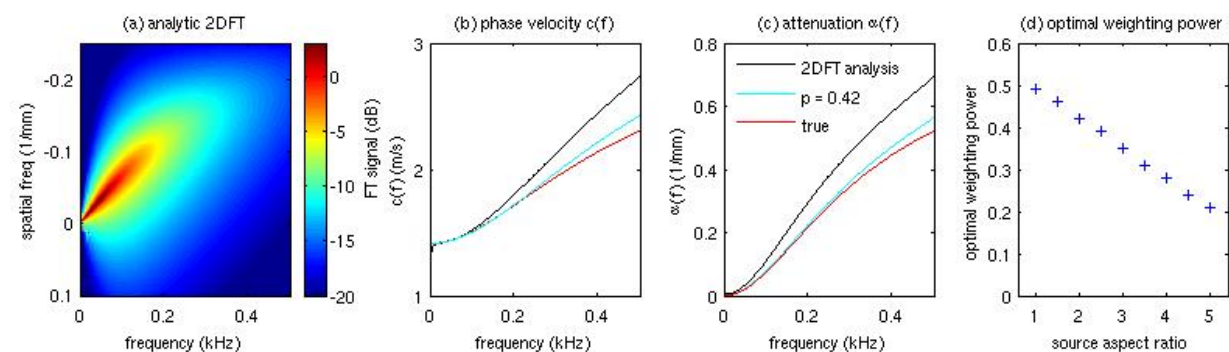
3H-2

8:15 am   **Quantitative poroelastic property imaging combining shear wave and strain elastography**

Maria Theodorou[1,2], Jérémie Fromageau[1,2], Nandita deSouza[2,3], Jeffrey C. Bamber[1,2]; *[1]Joint Department of Physics, Sutton, London, United Kingdom, [2]Cancer Research UK Cancer Imaging Centre, Sutton, London, United Kingdom, [3]Department of Diagnostic Radiology, Royal Marsden NHS Foundation Trust, Sutton, London, United Kingdom*

Background, Motivation and Objective

Soft tissue contains mobile fluid that creates a time-dependent and spatially-varying internal strain field under sustained compression [1], which may be imaged dynamically by repeated scanning with ultrasound (US). The resulting technique, known as poroelastography [2], allows the measurement of the product of the tissue's aggregate modulus and permeability, $H_A k$, and its Poisson's ratio, ν [1]. The aim of this study was to evaluate the potential of simultaneous dynamic imaging with shear wave elastography and strain elastography to separate the components of $H_A k$, and therefore recover the k, independently of ν and Young's modulus, E.

Statement of Contribution/Methods

Poroelastic phantom experiments were performed using an Aixplorer® US scanner (SuperSonic Imagine) and a linear array US transducer (SL15-4) with central frequency 7.5 MHz. Cylindrical samples made of 1.5 % (w/v) agarose gel (type I-B, Sigma-Aldrich) were subjected to a sustained axial compression (Instron 3342®) under computer control. The fluid-rich gels were scanned with the US beam aligned along their radial direction. Initial global axial strains of either 3 % or 7 % were applied over a time interval of 1 s. A frame rate of 1 transmit-focused radiofrequency (RF) echo image per second was used to capture the early and rapidly changing part of the relaxation. The frame rate was then decreased to 1 image every 30 s, for a total data acquisition time of 60 min. Two-dimensional cross-correlation RF echo-tracking was performed between the last pre-compression frame and all subsequent frames, followed by linear least-squares strain estimation, providing strain relative to the instant before compression. Images of ν and the product $H_A k$ were produced by fitting the time-dependent strain data to a poroelastic model. The supersonic shear imaging (SSI) [3] mode of the scanner was used to monitor the E of the sample by acquiring elasticity maps interleaved between the echo images.

Results/Discussion

By combining the mean pixel values of the $H_A k$, ν and E maps, the permeability of agarose was extracted with an estimated uncertainty of ± 5.8 %. The E of the sample was observed to decrease during the 1 hour of relaxation from an initial value of 111.5 to a final value of 107 ± 24 KPa and from 119.4 to 107.1 ± 14 KPa, for the 3 % and 7 % applied strain respectively. These changes could be due to the nonlinear response of agarose, pore size variation and/or the absence of perfect slip boundary conditions.

Institute of Electrical and Electronics Engineers

Nevertheless, they are negligible relative to a 72.3 % change in radial strain that was observed over the same time period and was associated with the poroelastic response. With further development, this quantitative technique could enable a more complete characterization of the poroelastic behavior of soft tissue for tumour diagnosis, treatment stratification and monitoring response.

[1] GP Berry et al, Ultra Med Biol, 32, 2006b

[2] E Konofagou et al, Ultra Med Biol, 27, 2001

[3] M Tanter et al, Ultra Med Biol, 34, 2008

3H-3_____

8:30 am   3D Elastic Tensor Imaging (ETI): characterization of soft tissues elastic anisotropy

Mafalda Correia[1], Jean Provost[1], Clément Papadacci[1], Thomas Deffieux[1], Jean-Luc Gennisson[1], Mickaël Tanter[1], Mathieu Pernot[1]; [1]*Institut Langevin, ESPCI ParisTech, CNRS UMR 7587, INSERM U979, Université Paris 7, Paris, France*

Background, Motivation and Objective

Assessing elastic anisotropy could aid the quantification and visualization of myocardial fiber architecture in order to evaluate myocardial disease. 2D ETI, based on ultrafast shear wave imaging (SWI) with an elastic-tensor-based approach, has shown potential for both fiber angle and elastic-tensor estimation [Lee W.N., et al., PMB, 2014]. However, this technique was limited by the need of a mechanical rotation of 1D probe to estimate the elastic-tensor and fiber orientation along the rotation axis. Recently, 3D Ultrafast SWI was developed, allowing the tracking of tissues' elastic properties changing in an entire volume. In this study, we investigated the applicability of ultrasound ETI to map fiber architecture through a tensor-based approach of anisotropic mediums in a 3D volume.

Statement of Contribution/Methods

Acquisitions were performed in isotropic and anisotropic phantoms as well as in vivo on open-chest sheep myocardium, using a customized, programmable, 1024-channel ultrasound system designed to perform 3D ultrafast SWI and 3D coherent plane-wave compounding (up to 4 2D tilted plane-waves, at 5000 volume/s). A 32x32, 3 MHz matrix phased array (Vermon, France), was used to induce 3D plane-shear-waves (10 plane shear waves steered every 36° in the transverse plane) in the medium by acoustic radiation force. In receive, a conventional delay-and-sum 3D beamforming was applied on the 1024 elements of the array and 3D tissue velocity volumes were reconstructed using local multiscale cross correlation of shear wave profiles in the three main directions. Shear wave speed at all propagation directions was estimated, and fiber angle orientation was derived from eigendecomposition of the shear velocities at each location. ETI Fractional anisotropy (FA) for each volume was calculated from the elastic tensor.

Results/Discussion

The propagation of 10 successive steered plane shear waves was imaged in the phantoms. The shear wave velocity was estimated for the 10 propagation directions, along with the fiber orientation and the shear velocity eigenvalues that were successively determined at each voxel of the entire volume. The FA was found to be consistent with the elastic properties of both isotropic (FA = 0.1 ± 0.05) and anisotropic (FA = 0.45 ± 0.1) phantoms. In the in vivo experiment, only 5 successive steered plane shear waves were used which allowed us to increase frame-rate imaging and decrease the acquisition time for shear wave tracking. Fiber orientation and shear velocities were successively derived. 3D ETI can be used to determine tissue elasticity, and simultaneously, to track fiber angles orientation of anisotropic tissues at high frame-rate.

3H-4_____

8:45 am   Vibro-Elastography: Absolute Elasticity from Motorized 3D Ultrasound Measurements of Harmonic Motion Vectors

Jeffrey Abeysekera[1], Robert Rohling[1,2], Septimiu Salcudean[2]; [1]*Mechanical Engineering, University of British Columbia, Vancouver, British Columbia, Canada, [2]Electrical and Computer Engineering, University of British Columbia, Vancouver, British Columbia, Canada*

Background, Motivation and Objective

Absolute elasticity images have been successfully generated by measuring harmonic motion vectors over a volume with MRI elastography (MRE). This work aims to apply the same method using motorized 3D ultrasound (US).

Previous studies have demonstrated tracking 3D motion components over US volumes by extending block matching methods to 3D. Most of these studies measure static compression motion to generate strain images. In comparison, dynamic motion is a challenge as each US beam line must be collected at a common motion state to allow for block matching in 3D. In a 3D cardiac strain imaging study, a matrix array was triggered to collect sub-volumes synchronized with an ECG, resulting in a high frame rate relative to the heart rate. This work applies a similar approach by triggering each beam line with a function generator applying harmonic excitation. For successive frames, the phase of the excitation signal is shifted such that each frame measures a different phase of the motion. This approach creates volumes of US data at common motion states.

Statement of Contribution/Methods

Images of a CIRS Model 049 elastography phantom were acquired with a 4DL14-5 motorized US transducer connected to an Ultrasonix SonixTouch scanner. Each beam line was synchronized with an exciter applying 200 Hz vibrations before reprogramming the exciter to a total of 25 phases distributed evenly across the excitation period.

Block matching results have large variance in two of the three measurement directions, causing problems in elasticity estimation. Most soft tissues are nearly incompressible so we expect a divergence close to zero. Applying this constraint to the block matching results generates a smoothed field with lower variance.

Elasticity is computed from the average of local frequency estimates for each direction of the harmonic wave as in MRE.

Results/Discussion

The figure below from left to right shows the measured motion in the x, y, and z directions and the resulting elasticity showing a stiff inclusion in a homogenous background. Values of elasticity correspond to manufacturer values.

This study has demonstrated measurement of 3D harmonic motion over a volume by adding a synchronization step to previous tracking techniques. After smoothing the motion vectors via a physical constraint consistent with soft tissues, a high-quality elasticity volume, similar to MRE results, is generated.

SATURDAY ORAL
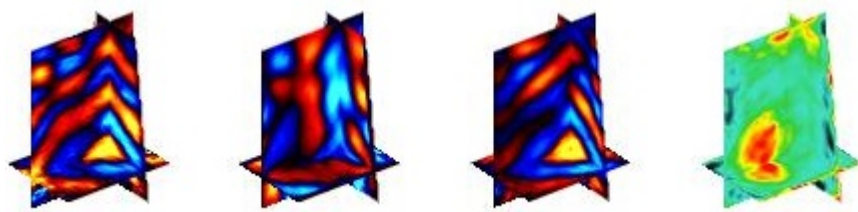
9:00 am   **Three-Dimensional Shear Wave Imaging Based on Full-Field Optical-Sectioned Laser Speckle Contrast Imaging**

Pei-Yu Chao[1], Pai-Chi Li[2]; *[1]Biomedical Electronics and Bioinformatics, National Taiwan University, Taipei, Taiwan, [2]Electrical Engineering, National Taiwan University, Taipei, Taipei, Taiwan, Taiwan*

Background, Motivation and Objective

A non-scanning 2D shear wave (SW) imaging method based on laser speckle contrast imaging (LSCI) was previously developed, where a SW velocity estimation error of less than 4% was achieved on homogeneous phantoms. In this report, the method is extended with a wide field microscope that both 3D structural and SW imaging can be performed. We hypothesize that 3D SW imaging based on optical-sectioned LSCI can achieve sub-millimeter resolution for samples with thickness less than 3mm. This method is suitable for applications in 3D cell culture analysis. The composition and biomechanical properties of the extracellular matrix contribute to the structural support and the regulatory functions of the cell microenvironment. Studies have shown that ECM stiffening may promote cancer cell invasion and migration. Thus, in vitro analysis of the topology and the stiffness of the 3D matrix can provide information about the dynamics of the cell and its microenvironment during tissue development and pathogenesis.

Statement of Contribution/Methods

Local disturbance within a diffused object induced by the propagation of SW causes the phase of the transmitted optical wave to change. Consequently, blurring in the time-integrated speckle pattern is observed. The speckle contrast $K=\sigma/[I]$ is computed to display the local blurring caused by SW propagation, where σ and $[I]$ are the standard deviation and mean intensity of pixels in a image region of 156×156 μm. The setup of the system enables SW propagating in X- and Y-direction to be imaged simultaneously. The axial resolution (dz) of the developed system is defined as $dz=4\lambda n/(NA)^2$, where λ is the laser wavelength, NA is the numerical aperture of the objective, and n is the refractive index. The dz is estimated to be 55 μm.

Results/Discussion

The camera image and the SW velocity map of an agar phantom with a stiff inclusion are shown in Fig. (a) and Fig. (b). The estimated SW velocity for region 1 and 2 in Fig. (b) were 1.51 m/s and 1.93 m/s, respectively, with an error of less than 3%. The cross-sections of the SW velocity map were extracted. The spatial resolution of the SW imaging achieved is evaluated by calculating the full width half maximum of the derivative of the cross-sectional waveform, as shown in Fig. (c). The estimated spatial resolution for SW imaging is 350 μm. A 3-D SW imaging reconstruction of a layered phantom will be presented in the full report.
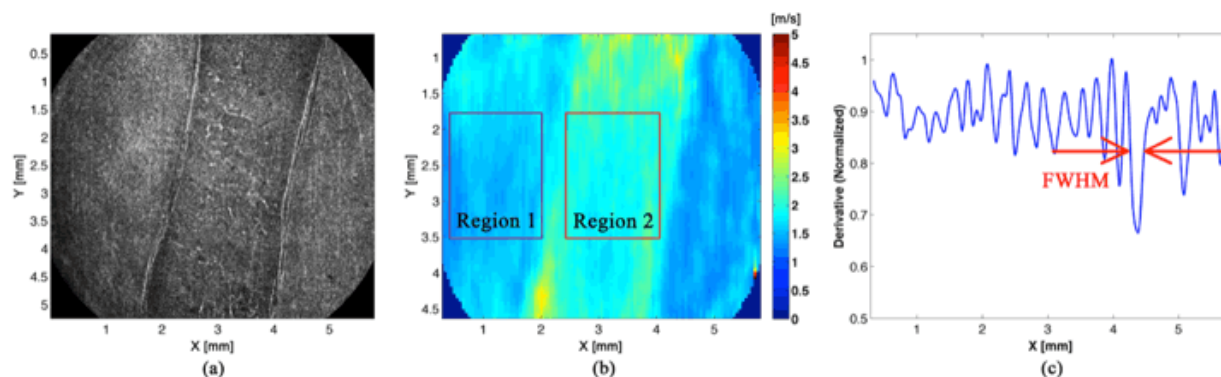
Fig. (a) The camera image, and (b) the shear wave velocity map of a heterogeneous phantom with a stiff inclusion. (c) Derivative of the cross-sectional waveform of the SW velocity map shown in (b).

9:15 am   **A High Frame-rate and Low-cost Elastography System by Generating Shear Waves through Continuous Vibration of the Ultrasound Transducer**

Daniel C. Mellema[1], Pengfei Song[1], Armando Manduca[1], Matthew W. Urban[1], Randall R. Kinnick[1], James F. Greenleaf[1], Shigao Chen[1]; *[1]Department of Physiology and Biomedical Engineering, Mayo Clinic College of Medicine, Rochester, MN, USA*

Background, Motivation and Objective

Acoustic-radiation-force (ARF) based shear wave elastography (SWE) techniques have proven to be clinically useful. Due to hardware demands, ARF-based SWE is typically limited to high-end ultrasound scanners. The frame rate of ARF-based SWE is also limited (~1 Hz) by push pulses due to probe/tissue heating. It is of interest to develop a low-cost and high frame-rate method to translate SWE to mid/low-tier systems and broaden the clinical impact of SWE. This study investigates the use of continuous wave (CW) motion generated by vibrating the transducer to simultaneously generate and detect shear waves (SW) for SWE.

Statement of Contribution/Methods

An in-house vibration system was designed by mounting a voice coil actuator in-line with a L11-4v transducer (Verasonics Inc.); this was held single-handedly while a 250 Hz CW signal was applied to the voice coil to generate motion (Fig. 1a). During vibration, the L11-4v was driven by a Verasonics Vantage system to detect the SW motion with plane waves transmitted at a 2.5 kHz PRF for 20 ms. A spatial high pass filter was designed to decouple the SW from transducer motion artifact. Two-dimensional (2D) SW speed (SWS) maps were reconstructed using a fine-tuned local frequency estimation approach (LFE). Three homogenous CIRS liver fibrosis phantoms were tested with five repeated measurement. A CIRS 049A inclusion phantom was also tested using the proposed technique.

Results/Discussion

The SWS of the liver fibrosis phantoms were 1.64, 2.58, and 3.68 m/s, and showed excellent repeatability (Fig. 1b) and are in good agreement with the Aixplorer (SuperSonic Imagine): 1.65, 2.49, 3.56 m/s. Figure 1c shows 2D SWS maps from the inclusion phantom. A 9.8% and 25.9% underestimation bias was found for the 20 and 6.5 mm inclusion, as compared to a 9.5% and 12.5% underestimation bias from the Aixplorer. The larger bias of the 6.5 mm inclusion may be resolved by increasing the vibration frequency which generates SW with better spatial resolution. This system has potential for real-time SWE as each 2D SWS map requires 20 ms of detection and no cooling time is needed between consecutive SWS maps. While this study used plane wave imaging, the periodicity of the CW SW will allow conventional line-by-line scanning for SW detection. These advantages show great promises of realization of 2D real-time SWE on mid/low-tier ultrasound systems with the proposed technique.
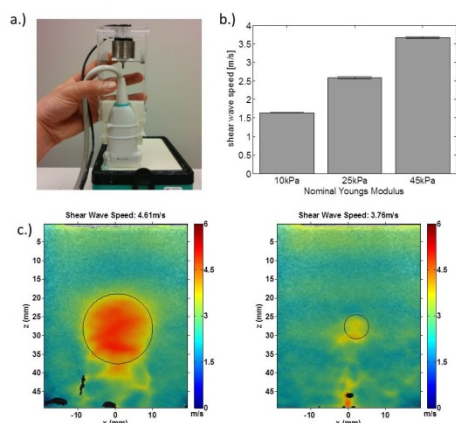
Figure 1. (a) The vibration system consisting of a voice coil actuator and L11-4v transducer able to be used in one hand. (b) Bar plots showing the mean and standard deviation of SWS measurements obtained from the three CIRS liver fibrosis phantoms. The nominal Young's moduli are 10, 25, and 45 kPa. (c) Examples of the 2D SWS maps overlaid on B-mode images for a 20 mm and 6.4 mm inclusion phantom (CIRS 049 A, Type IV, ROI depicts inclusion edge). The SWS is 4.61 m/s and 3.76 m/s for the two inclusions, respectively.

SATURDAY ORAL

4H - MTH: Ultrasound-Mediated Agent Delivery

201DE

Saturday, October 24, 2015, 08:00 am - 09:30 am

Chair: **Katherine Ferrara**
UC Davis

4H-1

8:00 am Ultrasound-triggered and targeted gene delivery by using cationic microbubbles to enhance GDNF gene transfection in a rat Parkinson's disease model

Ching-Hsiang Fan[1], Chien-Yu Ting[1], En-Ling Chang[1], Hao-Li Liu[2], Hong-Lin Chan[3], You-Yin Chen[4], Chih-Kuang Yeh[1]; *[1]Department of Biomedical Engineering and Environmental Sciences, National Tsing Hua University, Taiwan, [2]Department of Electrical Engineering, Chang-Gung University, Taiwan, [3]Department of Medical Science and Institute of Bioinformatics and Structural Biology, National Tsing Hua University, Taiwan, [4]Department of Biomedical Engineering, National Yang Ming University, Taiwan*

Background, Motivation and Objective

Glial cell line-derived neurotrophic factor (GDNF) is a potent agent for treating Parkinson's disease (PD). Microbubbles (MBs) have been exploited as a carrier for GDNF delivery with focused ultrasound (FUS) destruction. However, GDNF supplementation only relieves PD symptoms rather than cure it. Thus, design of an endogenous GDNF generative mechanism is an urgent concern for novel PD treatment. Here, we synthesized a cationic MBs (CMBs) with high DNA binding to achieve blood-brain barrier disruption (BBBD) with FUS, and currently enhance the GDNF-gene transfection for PD therapy.

Statement of Contribution/Methods

CMBs composed of phospholipid and C_3F_8, with GDNF-gene (GCMBs) binding by electrostatic interactions. The mean concentration and size of GCMB were (33.06 ± 7.18) $\times 10^9$/ mL and 0.97 ± 0.37 μm, respectively. DNA binding onto CMBs was evaluated by propidine iodide stain. PD lesions were established by implanting 6-hydroxydopamine into left medial forebrain bundle of Sprague-Dawley rats (N = 36). A 1-MHz FUS (0.7 MPa, duty factor = 5 %, PRF = 1 Hz, sonication = 90 s) was sonicated at striatum and substantia nigra to open BBB and release gene after GCMBs injection (500 μg/ 10^8 CMBs, 0.5 mL). Sites of BBBD and gene transfection were confirmed by Evans Blue and firefly luciferase gene-loaded CMBs (LCMBs) with bioluminescence imaging, individually. GDNF Expression were determined by Western blot and ELISA tests. Apomorphine-induced rotations, climb test, and in vivo microdialysis with electrochemical detector were applied weekly to trace the motor asymmetry, akinesia phenomenon and dopamine (DA) levels, separately.

Results/Discussion

The positively charge of CMBs (+39.48 $\pm$ 9.28 mV) made them significant for DNA binding (Fig. A). GCMBs with FUS provided sufficient BBBD area for enhanced gene transfection in PD lesion (Fig. B). Bioluminescence data showed that the released Luc-gene transfected at 54 h after treatment (5.5-fold higher than right brain; Fig. C). The GDNF level of PD rats restored following the combing treatment (66.6 % of recovery) (Fig. D-E). The treatment reduced rotations by 92.2 $\pm$ 5.7%, reduced climbing behaviors by 88.9 $\pm$ 10.8%, and improved of DA levels by 164.9 $\pm$ 1.23% (Fig. F-H).

We verified that GCMBs with FUS provides a novel strategy for local gene therapy in PD rats. Future works include long-term follow of side-effects after gene transfection.
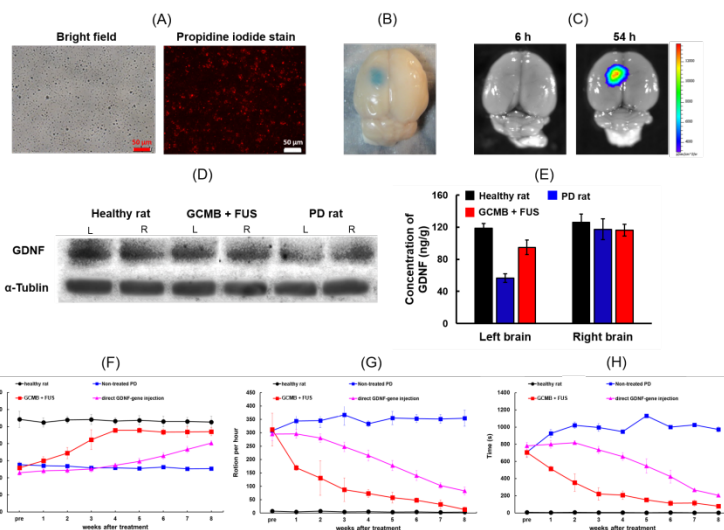
4H-2

8:15 am In situ Activation of Doxorubicin using Ultrasound-Triggered Release of Composite Droplets

Marine Bezagu[1,2], Stellios Arseniyadis[2], Olivier Couture[3], Fabrice Monti[1], Patrick Tabeling[1], Janine Cossy[2], Mickael Tanter[3], Jonathan Clarhaut[4,5], Sebastien Papot[4]; *[1]MMN (ESPCI, CNRS, UPMC), Paris, France, [2]LCO (ESPCI, CNRS, UPMC), Paris, France, [3]Institut Langevin (ESPCI, CNRS, INSERM), Paris, France, [4]IC2MP (Université de Poitiers, CNRS), Poitiers, France, [5]CHU Poitiers, Poitiers, France*

Background, Motivation and Objective

We previously established that composite droplets comprised of a nanoemulsion of water loaded with fluorescein and encapsulated in a perfluorohexane matrix (4 μm in diameter) could release their content by acoustic vaporization (Couture et al. *Medical Physics*, **2011** and **2012**). As two-third of the droplets is payload, large doses of active agents could thus be potentially delivered. However, like other conventional delivery strategies, the carriers also accumulate in healthy organs and tend to release their content in a non-specific manner. For this reason, we recently introduced the concept of chemistry in-situ, whereby an active agent would be created at the ultrasound focus by inducing a chemical reaction after the release of the droplets' content (Bezagu et al. *J. Am. Chem. Soc.*, **2014**). Such targeted chemistry could be applied to the localized in-vivo activation of a drug that would be either too toxic or unstable to be directly injected. In this perspective, we studied the in vitro localized release of a doxorubicin prodrug and its subsequent activation by a specific enzyme, the β-glucuronidase, leading to the localized production of doxorubicin.

Statement of Contribution/Methods

The demonstration was achieved by encapsulating a solution of HMR1826 (doxorubicin's glucuronide prodrug) at 4.5 mM into composite droplets of perfluorohexane, and releasing their content in a 96-well plate containing adherent KB cancer cells. The β-glucuronidase, an endogenous enzyme specifically localized in the tumor extracellular microenvironment, was used in solution in the culture medium to activate the released prodrug. Four acoustic pulses of five cycles at 1.5 MHz were focused in each well using a single-element transducer. Cell proliferation was recorded after a 72 h incubation time using a XTT colorimetric assay.

Results/Discussion

In the presence of the β-glucuronidase enzyme, in the following 72 h upon the release of the droplets, cell proliferation was as low as 38% when compared to the non-treated cells. In comparison, cell proliferation was comparable (>90%) to non-treated cells when HMR1826 was released in the absence of the enzyme, thus confirming the specific production of the cytotoxic doxorubicin drug when both reactants are allowed to be in contact. Moreover, it is worth noting that a 25% gain of cytotoxicity is observed when applying the acoustic pulses compared to the sole effect of the leakage where the same droplets are left in contact with both the cells and the enzyme for 72 h. In summary, we managed to 1) initiate the in vitro conversion of a doxorubicin prodrug to the active drug by locally releasing it in a medium containing the β-glucuronidase, and 2) induce a significant toxicity on KB cancer cells. We expect that such targeted chemistry will lead to a new approach to chemotherapy.

4H-3

8:30 am   Red Blood Cells as Therapeutic Ultrasound Agents

Johnny Chen[1], Ali Dhanaliwala[1], Justin Farry[1], John Hossack[1,2], Alexander Klibanov[1,2]; [1]*Department of Biomedical Engineering, University of Virginia, Charlottesville, Virginia, USA,* [2]*Robert M. Berne Cardiovascular Research Center, Charlottesville, Virginia, USA*

Background, Motivation and Objective

Acoustically active microbubbles and nanodroplets are investigated as drug delivery vehicles because drug release can be precisely controlled by ultrasound. However, their drug loading capacity is somewhat limited, requiring further studies to improve drug payload. Concurrently, red blood cells (RBCs) have been extensively investigated as carriers of therapeutics since the 1970s. Unfortunately, it is difficult to control the spatiotemporal release of these long-circulating RBC carriers (a.k.a ghosts, resealed erythrocytes) [1]. We combine drug loaded RBCs and acoustically active ultrasound agents to create acoustically active RBCs (aaRBCs), a biocompatible agent capable of improved ultrasound-mediated drug delivery.

Statement of Contribution/Methods

Calcein, a green fluorophore, was used as a model drug and loaded into RBCs using a hypotonic lysis method. Perfluorocarbon (PFC) lipid-stabilized droplets were labeled with DiI, a red fluorophore, and attached to the RBC surface via electrostatic adhesion; the aaRBCs were analyzed via fluorescence microscopy. Using a single element 10 MHz transducer with single bursts at peak negative pressures (PNP) of 6-11MPa, activation of aaRBCs were recorded at 30 fps. Calcein release, as a function of PNP and pulse duration, was investigated by measuring fluorescence of the supernatant after ultrasound treatment and RBC sedimentation.

Results/Discussion

PFC droplets were attached to calcein-loaded RBCs, enabling ultrasound-mediated disruption of RBC membranes by vaporization of liquid PFC droplets and subsequent release of calcein (Fig 1). Significant calcein release (p < 0.05, vs. without ultrasound) was measured at mechanical indices of 0.95 – 3.16. A maximum calcein release of $75.7 \pm 23.8\%$ was achieved at 10 MPa, with pulse duration of 100 μs and pulse repetition frequency of 5 Hz. These results demonstrate the first instance of acoustically triggered release of a model drug from RBC carriers. By selectively localizing drug delivery and achieving high local concentrations, lower concentrations of cytotoxic drugs may be administered, thereby reducing side effects. Additionally, aaRBCs may increase the circulation time of encapsulated agents, as native human RBCs have a lifetime of approximately 120 days.

[1] Magnani, Mauro, ed. Erythrocyte engineering for drug delivery and targeting. Vol. 6. Springer, 2003.
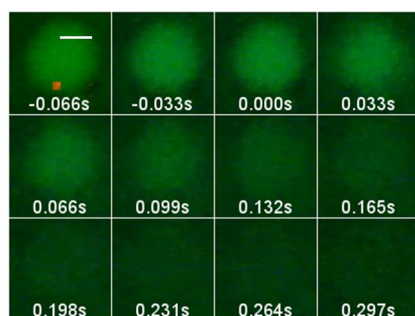
Fig 1. Twelve consecutive fluorescent image frames captured at 30 fps. Ultrasound is triggered between 0.000s and 0.033s. Lysis of aaRBC and loss of calcein occurs following ultrasound. First frame shows overlay of calcein (green) encapsulated in an aaRBC and a DiI perfluorocarbon droplet (red) attached to the membrane. Scale bar = 2 μm.

SATURDAY ORAL

4H-4

8:45 am   Combining the antiangiogenic drug Sorafenib with the antivascular action of microbubbles for the treatment of hepatocellular carcinoma

Niroo Sivapalan[1], Ben Leung[1], **David Goertz**[1,2]; [1]*Sunnybrook Research Institute, Toronto, Ontario, Canada,* [2]*Medical Biophysics, University of Toronto, Canada*

Background, Motivation and Objective

Hepatocellular carcinoma (HCC) is a leading cause of cancer related deaths worldwide. For advanced HCC the standard medical treatment is Sorafenib, a molecularly targeted agent with a primary mode of action exerted through antiangiogenic effects. However, survival prolongation with this treatment is very modest (~3 months). Thus, a clear need exists for more effective HCC treatments. There is growing interest in using ultrasound stimulated microbubbles (USMBs) to potentiate the uptake of anticancer agent into tumors. We recently demonstrated a novel concept for drug potentiation which was not to enhance drug delivery, but rather induce vascular damage with microbubbles (MBs) coupled with antiangiogenic strategy (Todorova et al, Int J Cancer 2013). This is effectively vascular targeting rather than a drug delivery approach. It is

conceptually analogous to coupling small molecule vascular disrupting agents with antiangiogenic agents, with the latter inhibiting the pro-angiogenic 'rebound' that follows the acute vascular collapse induced by VDAs. In the present study we investigate the feasibility of enhancing the ability of Sorafenib to treat HCC by coupling it with antivascular USMB exposures.

Statement of Contribution/Methods

Heb3B HCC tumors were initiated subcutaneously in the legs of BalbC mice. USMB treatments were conducted at 1 MHz employing short bursts (0.00024 duty cycle) at 1.4 MPa combined with an experimental lipid encapsulated agent (Artenga Inc). Longitudinal experiments were conducted with control (CN), drug only (SF), USMB-only, and combined USMB+drug (USMB-SF) groups (n=6-8/group). In drug groups, animals received Sorafenib at 30mg/kg through daily oral gavage. USMB treatments were performed for 2 consecutive weeks, starting 2days after drug treatments began. Size was monitored with 3D high frequency US and vascular effects were observed with US contrast imaging. Acute experiments were also conducted where animals were sacrificed, after the injection of a perfusion stain (DiOC7) at baseline, 1 hr or 4 days post-treatment with tissue excised for analysis.

Results/Discussion

USMB treatments induced an acute reduction of tumor blood flow as confirmed with US contrast imaging and perfusion staining. Longitudinal experiments demonstrated both the USMB and SF groups had non-significant trends of reduced sizes relative to the CN group for time points >=11 days. The USMB-SF group was significantly smaller than the CN group for days >=11 (p<0.01) and for the SF and USMB groups at days >=14 (p<0.01 to p<0.02). The growth delay (time to reach 5x initial size) for the combined group was 9.4, 8.3 and 8.5 days longer than CN, SF and USMB groups respectively. These results indicate the preclinical feasibility of potentiating Sorafenib with antivascular USMB effects to treat HCC tumors. Notably, this approach employs exposure levels that are low relative to ablative treatments which would facilitate the exposure of larger tumor volumes.

4H-5

9:00 am   Focused ultrasound facilitated adenoviral delivery for optogenetic stimulation

Shutao Wang[1], Amanda Buch[1], Camilo Acosta[1], Oluyemi Olumolade[1], Elisa Konofagou[1,2]; *[1]Biomedical Engineering, Columbia University, New York, New York, USA, [2]Radiology, Columbia University, New York, New York, USA*

Background, Motivation and Objective

Optogenetics is a recently developed technique that has been widely implemented in the field of neuroscience. Channelrhodopsins (ChR), i.e., proteins that function as optically-activated ion channels, are introduced into neurons either by viral transduction or transgenic manipulations. Traditional viral transduction involves invasive direct infusion procedures which may pose unnecessary brain damage. Recent advances in focused ultrasound (FUS) offer an alternative, non-invasive approach to carrying out viral transduction in the brain as shown by our group and others. In the presence of microbubbles, the blood-brain barrier (BBB) can be temporarily opened, and we have demonstrated the feasibility of non-invasive AAV-GFP delivery to the targeted brain region. Taking advantage of the FUS-mediated BBB opening, we propose a FUS-based, non-invasive adenoviral delivery scheme suitable for optogenetic applications.

Statement of Contribution/Methods

Wild-type mice were used in this study, and each animal was sonicated using a single-element FUS transducer (center frequency 1.5 MHz). The acoustic parameters used for each sonication are: peak-rarefactional pressure 0.45 MPa, pulse length 10 ms, pulse repetition frequency 5 Hz, and a duration of 120 s. Both AAV1 and AAV9 vectors were constructed with synapsin promotor and YFP marker. In-house manufactured polydisperse microbubbles were mixed with AAV-syn-YFP-ChR vectors and injected immediately prior to sonications via the tail veil. The targeted regions investigated here included the caudate putamen and the hippocampus. Animals were survived for 12 days after sonication and sacrificed via transcardial perfusion. Brain tissue was collected and sectioned at 30 m in thickness. Confocal microscopy was performed to visualize the transduced brain region and compared to that resulted from direct infusions.

Results/Discussion

Fluorescence images revealed that AAV-syn-YFP-ChR vectors were successfully delivered to the targeted regions with FUS. Mice injected with AAV9 vectors showed higher levels of transduction compared to mice that received AAV1 vectors. Under the control of synapsin promoters, transduction occurred almost exclusively in neurons, which was verified via immunostaining. In AAV9-injected mice, YFP enhancement in the caudate-putamen was quantified as 1.54 mm^2 for the sonicated side, while the contralateral side showed virtually null transduction. Results from this study revealed that AAV9 is superior to AAV1 vectors to achieve larger transduction volume via the FUS-mediated BBB opening and findings with FUS were comparable to those with direct injection. Therefore, the successful non-invasive AAV delivery can provide an alternate and safer route for Channelrhodopsin neuronal transduction for optogenetic stimulation. Funding sources: NIH R01EB009041, NIH R01AG038961, and Kinetics Foundation.

4H-6

9:15 am   Local and targeted delivery of a therapeutic monoclonal antibody in a colorectal cancer model: in-vivo proof of concept

Thomas Barré[1], Emilie Dalloneau[2], Thierry Lecomte[3,4], Valérie Gouilleux-Gruart5[3,5], Nathalie Heuzé-Vourc'h[2], **Ayache Bouakaz[1]**; *[1]UMR Inserm U930, Université François-Rabelais, TOURS, France, [2]Inserm, Centre d'Etude des Pathologies Respiratoires, UMR 1100, Université François Rabelais, TOURS, France, [3]CNRS, GICC UMR 7292, Université François Rabelais, France, [4]Service Hépato-Gastro-Onco-Entérologie – CHRU, Tours, France, [5]CHRU de TOURS, laboratoire d'immunologie, TOURS, France*

Background, Motivation and Objective

Monoclonal antibodies are used as therapeutic agents for the treatment of diseases including cancer. However, their therapeutic efficiency for solid tumors remains modest, likely due to a limited intratumoral distribution of these macromolecules after systemic administration. Sonoporation is an innovative approach using ultrasound and gas microbubbles leading to increased permeability of endothelial wall, thus facilitating the passage of molecules. The objective of this study is to optimize the bioavailability of a therapeutic antibody Cetuximab into the tumor after sonoporation.

Statement of Contribution/Methods

HT29 cells were inoculated subcutaneously with matrigel in nude mice and the tumor growth was monitored every two days using a VEVO2100 imaging system. Ultrasound B-scans were used to calculate tumor volume. Contrast-Enhanced Ultrasound Imaging (CEUS) was performed once a week after retro orbital administration of microbubbles (MM1 Bracco ®). Both tumor vasculature growth and tumor perfusion were assessed using VevoCQ® software. The antibody Cetuximab (anti-EGFR antibody indicated in the treatment of metastatic colorectal cancer) was conjugated to AlexaFluor-750 (Cetux-AF750, 30 µg) and administered systemically in animals bearing tumors of ± 153 mm3 with or without sonoporation. Sonoporation was applied using three different ultrasound settings: (i) exposure time of 3 minutes with a repetition period (RP) of 100µs, a 40% duty cycle (DC) and a acoustic pressure of 600 kPa; (ii) 5 min, 10ms RP, 20% DC, and 500 kPa; (iii) 15 min, 1s RP, 5% duty cycle, and 350 kPa. Quantitative tumor uptake of Cetuximab AF 750 was carried out by fluorescence imaging in the near infrared. The uptake of the antibody was measured at different times post sonoporation up to 6 hours. Its intratumor distribution was determined by immunohistochemistry. Tumor volume was measured up to 3 weeks post sonoporation. To evaluate the effectiveness on tumor growth of Cetuximab delivery assisted by microbubbles and ultrasound, the treatment (100µg of cetuximab) was performed twice per week.

Results/Discussion

Based on fluorescence data, the results showed that Cetux-AF750 uptake was increased up to 3 folds within the tumor depending on the applied US settings and the fluorescence signal persisted significantly longer after sonoporation compared to control. These results indicate that cetuximab accumulated more efficiently and durably in the tumor after sonoporation. In addition, the bioavaliability of the Cetux-AF750 was only slightly different between the 3 groups of sonoporated animals. Tumor volume analysis showed that the animals of group 1 (sonoporation + Cetux-AF750) had a significantly slow tumor growth in comparison to the two other sonoporated groups and to

the Cetux alone group. This study demonstrates the high efficiency of sonoporation in increasing the bioavailability and improving the delivery therapeutic antibody in the targeted tumor site.

SATURDAY ORAL

5H - Microfluidics

103

Saturday, October 24, 2015, 08:00 am - 09:30 am

Chair: **Pierre Khuri-Yakub**
Stanford University

5H-1

8:00 am **SAW synthesis with inverse filter and IDT Arrays for microfluidic and biological applications: one ring to rule them all**

Michaël Baudoin[1], Antoine Riaud[1,2], Jean-Louis Thomas[2], Adrien Bussonière[1], Olivier Bou Matar[1]; [1]*IEMN, University of Lille, EC Lille, CNRS, France*, [2]*INSP, CNRS, Paris, France*

Background, Motivation and Objective

In the past 20 years, it has been shown that Surface Acoustic Waves (SAW) actuators are versatile tools for the manipulation of fluids at micrometric scales. A non-exhaustive list of operations that can be performed with SAW include sessile droplet displacement, atomization, division and merging but also the actuation of fluids embedded in microchannels or the manipulation of suspended particles. In the field of biology, it has also been shown that these waves can be used to perform fundamental operations such as cells characterization and sorting according to relevant biological properties.

However, each of the aforementioned operations requires a specific design of the wave generation system, the so-called interdigitated transducers (IDTs). Depending on the application, it might indeed be necessary to generate focused or plane, propagating or standing, aligned or shifted waves. Furthermore, the possibilities offered by more complex wave fields such as Bessel beams for particle tweezing and liquid twisting cannot be explored with classical IDTs. The objective of this presentation is to show that inverse filter technique coupled with interdigitated transducers arrays (IDTA) not only enables to perform all the classical operations with a single platform but also provides an elegant solution to unsolved fundamental issues.

Statement of Contribution/Methods

In the first part of the presentation, we will review the possibilities offered by SAW for fluid actuation at microscales and biological applications. Then we will introduce the principle of inverse filter and discuss the constraints on the design of IDTA for proper SAW synthesis in anisotropic materials. Finally, we will illustrate the possibilities offered by such a platform and in particular original wave field synthesis such as Bessel beams for acoustical twisting and tweezing.

Results/Discussion

Indeed, Bessel beams are helical waves possessing a pseudo-orbital angular momentum and a phase singularity on their axis. These specificities can be used to trap particles by using acoustic radiation pressure or to create controlled "cyclone-like" flows. In this work, we will show that the use of anisotropic material such as Niobate Lithium to synthesize these wave fields, while requiring some refinements in the theory, offers some new possibilities for the design of acoustical tweezers.

5H-2

8:30 am **Ultrasound Image-based Absolute Concentration Measurement Technique for Materials with Low Scatterer Concentration**

John H. Lee[1], Javier Jimenez[2], Xiang Zhang[1], Duane S. Boning[1], Brian W. Anthony[1]; [1]*Massachusetts Institute of Technology, Cambridge, MA, USA*, [2]*Madrid-MIT M+Vision Consortium, Massachusetts Institute of Technology, Cambridge, MA, USA*

Background, Motivation and Objective

Ultrasound-based measurement of absolute concentration of scatterers has a wide range of potential applications such as in microbiology, cell culture, and blood work. When the material is dilute and the scatterer size is similar to the wavelength of ultrasound, individual scatterers can be distinguished in the image. While the number of scatterers in the image can be counted, quantifying the image volume is challenging since the exact slice thickness is unknown. We propose a method for estimating the volume of image of a dilute monodispersed sample acquired with a mechanically scanned single element transducer. The method does not require prior characterization of the transducer or the setup.

Statement of Contribution/Methods

For a disk transducer the beam shape is the same in the azimuth and elevation directions due to radial symmetry. Therefore, the resulting beam of a mechanically scanned disk transducer will have a slice profile identical to the azimuthal beam shape. The azimuthal beam width can be estimated from the spreading of an individual scatterer, which depends on the point spread function and properties of the scatterer.

Images are acquired with a linearly scanned 75-MHz spherically focused transducer. The samples consist of 10-µm polystyrene particles in distilled water with concentration ranging from 5 - 50 particles/µL. After envelope detection, the particle echoes are detected (Fig. 1a) and characterized by fitting to a 2D Gaussian. From the population of

---

Institute of Electrical and Electronics Engineers

particles, beam widths are mapped as a function of axial position and used to estimate the image volume. Concentration is calculated for each frame and combined to produce the final measurement.

Results/Discussion

Fig. 1b shows a plot of beam width vs. axial position. Slice thickness is estimated from the upper boundary in the plot, which represents the maximum observable beam width at a given axial position. This method is compared to hemocytometer measurements. While the means show good agreement, the proposed ultrasound method shows smaller variance (Fig. 1c).

The proposed method enables the measurement of absolute concentration of dilute sample using only ultrasound image data with significantly better performance than the widely accepted hemocytometer method. Currently, this method is limited to mechanically scanned single element imaging, but work to extend the method to array imaging is ongoing.

Figure 1. (a) B-mode image showing the detected particles (yellow). (b) Scatter plot of extracted beam width vs. axial position. (c) Comparison of absolute concentration measurement between the proposed method and the hemocytometer.

5H-3

8:45 am   Particle separation using bulk acoustic waves in a tilted angle microfluidic channel

Erin Dauson[1], **David Greve**[2], Kelvin Gregory[1], Irving Oppenheim[1], Gregory Healy[1]; *[1]Civil and Environmental Engineering, Carnegie Mellon University, Pittsburgh, PA, USA, [2]Department of Electrical and Computer Engineering, Carnegie Mellon University, Pittsburgh, PA, USA*

Background, Motivation and Objective

In prior research, separation of particles or biological cells in liquids has been accomplished using a balance of ultrasonic forces and viscous drag forces, which depends on particle size and acoustic contrast. Recent work by two groups has exploited surface acoustic waves launched into tilted microfluidic channels for particle or cell separation. While this approach has been effective there is significant fabrication complexity. Here we demonstrate a similar tilted-channel approach using machined channels in PMMA (poly (methyl methacrylate)) and PZT (lead zirconate titanate) wafer excitation.

Statement of Contribution/Methods

Channels in PMMA have been fabricated by machining a slot 300 μm deep on the surface of a flat sheet using a 0.05 in end mill. The channel is oriented at a 30 degree tilt with respect to standing waves produced by PZT wafers. The wafers are backed with tungsten-filled polymer and inserted in slots in the PMMA sheet. A closed channel is formed by bonding a second PMMA sheet with matching PZT slots.

Separation of 2 μm and 15 μm polymer spheres suspended in water was accomplished by driving the PZT wafers with 33 V amplitude at 6.8 MHz. Large polymer spheres experience stronger acoustic force relative to the drag force and follow the tilted node lines. The trajectories followed by spheres with different size have been visualized by forming a composite of multiple frames recorded by a CCD camera. The larger spheres depart from the main flow at different locations, suggesting that they may be traveling at different heights in the channel. Simulations performed using COMSOL 4.3 are in general agreement with the observed behavior and yield insight into the location and strength of nodes.

Results/Discussion

We have developed and demonstrated an alternative geometry for particle separation in a tilted channel. Our approach using machined channels in PMMA does not require microelectronic fabrication techniques and yields a structure that is expected to be cheaper and more robust.

SATURDAY ORAL
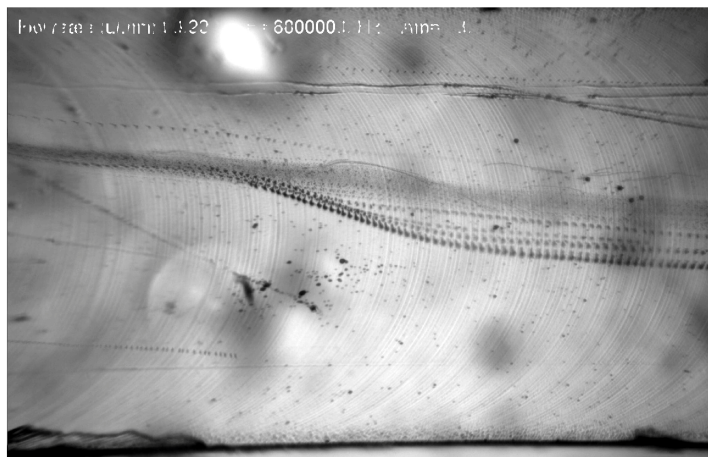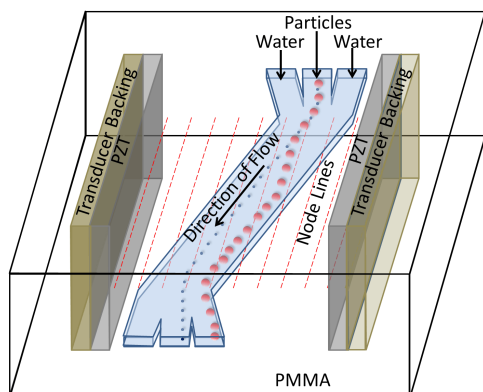
9:00 am   **On-chip ultrasonic manipulation of micro-particles using flexural vibration of a glass substrate**

Ryota Yamamoto[1,2], Daisuke Koyama[2,3], Mami Matsukawa[2,3]; [1]*Faculty of Life and Medical Sciences, Doshisha University, Japan,* [2]*Wave Electronics Research Center, Doshisha University, Japan,* [3]*Faculty of Science and Engineering, Doshisha University, Japan*

Background, Motivation and Objective

In recent years, with the development of gene therapy and biochemical analysis, manipulation and separation techniques of small particles such as cells and DNA are required in the field of life sciences. While noncontact ultrasound manipulation techniques enable position control of micro-particles without damage by using acoustic standing-wave fields in the MHz range, the transportation distance and the degree of freedom of the motion are limited within the ultrasound-wave field. In this report, an on-chip ultrasound manipulation technique of micro-particles in a micro-channel is discussed.

Statement of Contribution/Methods

The chip consists of a rectangular glass substrate ($26.0 \times 26.0 \times 2.0$ mm^3) having a cross-shaped channel (cross-section: 4.0×1.0 mm^2) and four ultrasound PZT transducers ($10.0 \times 10.0 \times 1.0$ mm^3) attached on the reverse side of the glass substrate. The channel is filled with degassed water, and silicon carbide micro-particles with an average diameter of 50 μm were immersed in water. The configuration of the glass substrate and the transducers were determined by the finite element analysis to generate the flexural vibration mode on the chip efficiently. When the phase difference of the input voltages to the transducers was changed, the particles can be trapped at the nodal lines of a standing wave in the channel generated by the flexural vibration. By changing the input voltage 90V$_{pp}$ to four transducers, the vibrational distribution of the chip can be changed and the trapped particles can be manipulated.

Results/Discussion

The flexural vibration mode with the wavelength of 9.0 mm was excited along the channel at 232 kHz. By controlling the driving phase difference between two pairs of the transducersθ, the flexural vibration of the glass substrate could be moved and the acoustic standing-wave field in water could be shifted along the channels, which enabled the noncontact manipulation of the micro-particles in the same direction with an accuracy of 92 μm/deg (Fig. 1). When the driving phase difference was changed from 150 to 200°, the moving distance of small particles was approximately 4.6 mm, which corresponds with half the wavelength of the flexural vibration on the glass substrate.
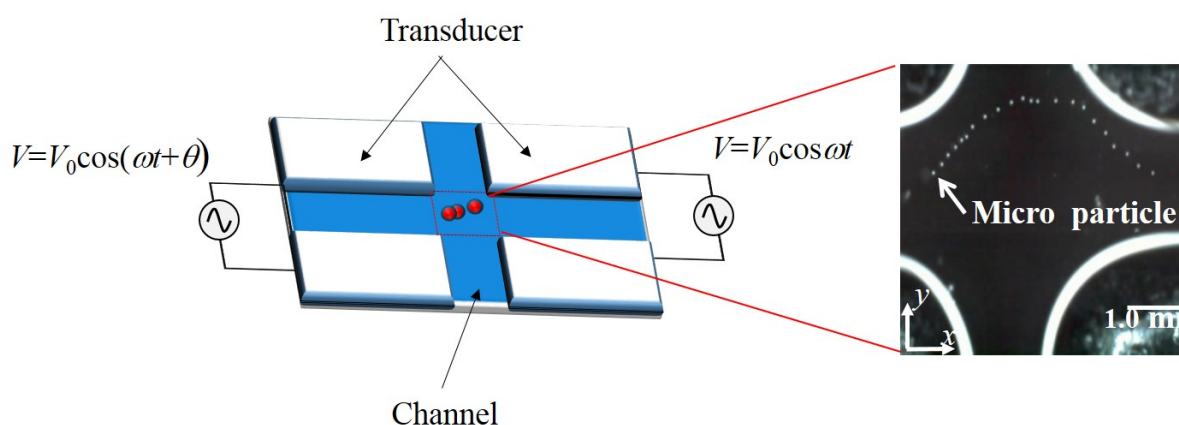
9:15 am   **Splitting Drops using Surface Acoustic Waves**

Sean Collingon[1], **James Friend**[1]; [1]*Department of Mechanical and Aerospace Engineering, University of California, San Diego, La Jolla, CA, USA*

Background, Motivation and Objective

Open droplet microfluidic platforms offer attractive alternatives to closed microchannel devices, including lower fabrication cost and complexity, significantly smaller sample and reagent volumes, reduced surface contact and adsorption, as well as drop scalability, reconfigurability, and individual addressability. For these platforms to be effective, however, they require efficient schemes for planar drop transport and manipulation. While there are many methods that have been reported for drop transport, it is far more difficult to carry out other drop operations such as dispensing, merging and splitting.

Statement of Contribution/Methods

We introduce a novel alternative to merge and, more crucially, split drops using 20 MHz laterally-offset modulated surface acoustic waves (SAW) propagated on 128[deg] lithium niobate (LN). The energy delivery into the drop was divided into two components: a small modulation amplitude excitation to initiate weak rotational flow within the drop followed by a short burst in energy to induce it to stretch. Upon removal of the SAW energy, capillary forces at the center of the elongated drop cause the liquid in this capillary bridge region to drain towards both ends of the drop, resulting in its collapse and therefore the splitting of the drop.

Results/Discussion

Splitting of the drop occurred only below a critical Ohnesorge number, which is a balance between the viscous forces that retard the drainage and the sufficiently large capillary forces that cause the liquid bridge to pinch. We show the possibility of reliably splitting drops into two equal sized droplets with an average deviation in their volumes of only around 4% and no greater than 10%, which is comparable to the less than 7% splitting efficiencies associated with electrowetting drop splitting techniques. In addition, we also show that it is possible to split the drop asymmetrically to controllably and reliably produce droplets of different volumes. Such potential as well as the flexibility in tuning the device to operate on drops of different sizes without requiring electrode reconfiguration, i.e., the use of different devices, as is required in electrowetting – therefore makes the present method an attractive alternative to electrowetting schemes.

8H - Transducer Applications

102
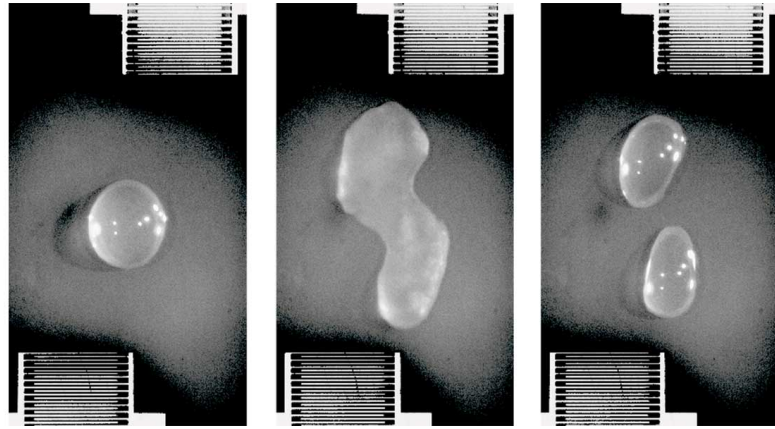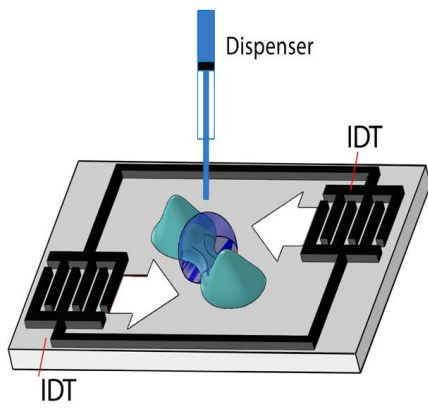
Saturday, October 24, 2015, 08:00 am - 09:30 am

Chair: **Scott Smith**
GE Global Research

8H-1

8:00 am   Perpetual-operation Frequency Response and Equivalent Circuit Modelling of Piezoelectric Ultrasonic Atomizer Devices

Xinyi Zhong[1], **Sang Lam[1]**; [1]*Department of Electrical & Electronic Engineering, Xi'an Jiaotong-Liverpool University, Suzhou, Jiangsu Province, China, People's Republic of*

Background, Motivation and Objective

Piezoelectric ultrasonic atomizer devices find applications from inhalation drug therapy to humidification of living environments. Through the piezoelectric action of a vibrating multi-pinhole membrane, liquid droplets can be discharged easily using simple driving circuits. For perpetual operation of the atomizer devices in droplet formation, the device characteristics may change over time thus weakening the atomization performance with fixed circuit settings. Equivalent-circuit modelling of the ultrasonic devices with prolonged atomization is desirable for performance prediction, circuit design optimization and reliability checking.

Statement of Contribution/Methods

A multi-pinhole piezoelectric ceramic plate is driven by a pure sinusoidal signal with $V_{pp} = 20$ V. The signal frequency is varied from below the resonance frequency f_r to a few 10 kHz above. The impedance Z of the atomizer device is determined by measuring the voltage (both magnitude and phase) across the water-loaded device with continuous atomization. Small-signal impedance measurements were also performed to determine the electrical circuit elements of the atomizer device.

Results/Discussion

Fig. 1 shows the measured Z of a water-loaded atomizer device in prolonged operation. Slight drift in the frequency response curves is observed at higher frequencies while f_r for atomization remains almost unchanged at about 112 kHz. Using the Butterworth-Van Dyke model, the mechanical-equivalent C_m and L_m are determined and found to decrease and increase respectively after prolonged atomization. The mechanical-equivalent R_m increases from 89 Ω gradually to 100 Ω. Such changes needed to be considered in developing atomizer systems by proper design of the driving circuit. More comparative results will be available.
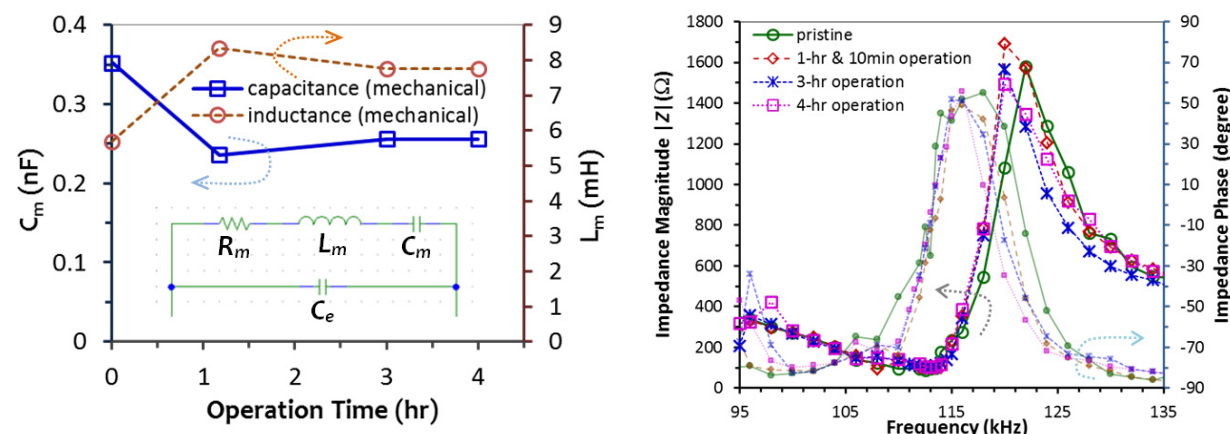
8H-2

8:15 am   Sol-Gel Composite Materials for Continuous Monitoring at 550°C

YUSUKE INADA[1], Makiko Kobayashi[1], Hajime Nagata[2], Tadashi Takenaka[2]; [1]*Kumamoto University, Japan,* [2]*Tokyo University of Science, Japan*

Background, Motivation and Objective

Thermal power generation increased its share up to ~88% in 2013 Japan due to shutdown of nuclear power plants so that maintenance of thermal power plants becomes the critical issues since unexpected shutdown could cause huge economical loss. On-line monitoring during operation has been desired since it can reduce risk of unexpected shutdown and periodical shutdown time for maintenance. Ultrasonic testing is mainly used because it can detect internal defects however, on-line monitoring for thermal power generation is difficult due to high temperatures such as 550°C. Sol-gel composite ultrasonic transducers can operate high temperatures and Mn-doped $CaBi_4Ti_4O_{15}$ (CBT)/$Pb(Zr,Ti)O_3$ (PZT) sol-gel composites has been developed for nondestructive testing above 500°C to improve sensitivity and signal-to-noise ratio high temperatures and it demonstrated comparable performance with $Bi_4Ti_3O_{12}$ (BiT)/PZT at 550°C, though long-term monitoring test is necessarily to evaluate on-line monitoring capability.

Statement of Contribution/Methods

50-μm-thick films of Mn-doped CBT/PZT and BiT/PZT were fabricated onto 3-mm-thick titanium substrates for comparison purpose. All sol-gel composites were manufactured by spray coating. After poling, high temperature paste top electrodes were fabricated for long-term high temperature test. The samples were put into a furnace and high temperature electrical cables were contact with a top electrode and titanium substrate (ground) through holes of the furnace. The cables were connected with coaxial cable which was outside of the furnace and connected with Pulser/Receiver machine. Pulser/Receiver machine was connected with a digital oscilloscope. Ultrasonic responses in pulse echo mode were recorded first at room temperature and at 550°C continuously.

Results/Discussion

At room temperature, both samples, Mn-doped CBT/PZT and BiT/PZT showed equivalent performance. When the temperature increased up to 550°C, signal amplitude of Mn-doped CBT/PZT was dropped by ~20 dB, though the signal amplitude was stable for 36 h and signal to noise ratio (SNR) was sufficient to detect multiple reflected echoes from 3-mm thick titanium substrate. On contrast, for BiT/PZT, the SNR became too low to detect any reflected echo. As a result, Mn-doped CBT/PZT was more suitable than BiT/PZT for long-term monitoring at 550°C. Further new material evaluation will be proceed.

8H-3_____

8:30 am   Ultrasonic biopsy needle based on the class IV flextensional configuration

Andrew Mathieson[1], Andrew Tweedie[2], Andrew Feeney[1], Margaret Lucas[1]; [1]*School of Engineering, University of Glasgow, United Kingdom,* [2]*Weidlinger Assoc. Ltd., Glasgow, United Kingdom*

Background, Motivation and Objective

This study builds on previous research to investigate the adaption of a miniaturized class IV transducer configuration, which has a needle end-effector attached, for use in bone biopsy. The transducer has been optimized to maximize needle displacement, with the objective of controlled penetration through bone tissue. Flextensional transducers typically comprise of a transduction material sandwiched between two metal shells. These devices have been utilized in SONAR applications, but more recently a class V configuration has been successfully miniaturized for use in bone cutting procedures. Initial research on the optimization of a miniaturized class IV flextensional transducer has demonstrated that the class IV configuration exhibits a higher level of performance for the same piezoceramic volume in comparison with a miniaturized class V configuration.

Statement of Contribution/Methods

A comprehensive parametric design study, utilizing the finite element analysis software PZFlex, has been conducted to identify the optimal design of the class IV flextensional device which contains a non-resonant needle end-effector. This approach equips the designer with a full set of performance data for each candidate design. Experimental vibration characterization of the selected device was performed using electrical impedance measurement and laser Doppler vibrometry, with experimental modal analysis conducted to investigate the modal behavior.

Results/Discussion

The miniaturized class IV transducer, combined with a non-resonant needle, was tuned to be resonant at 30 kHz. The predicted electrical impedance and modal characteristics of the optimized configuration, which possesses a PZ26 bar that has an aspect ratio of 5 to 1, has been shown to closely match experimental data. Furthermore, it has also been illustrated that a high uniformity across the output face of the transducer has been achieved. Additionally, the influence of flexural motions, which affect the longitudinal motion of the needle end-effector, have been minimized. Finally, it has been demonstrated that the needle end-effector can successfully penetrate the bone mimic, Sawbones. These results show that there is great potential for class IV flextensional transducers to be applied in minimally-invasive surgical procedures, such as biopsies.

8H-4_____

8:45 am   Development of Air–Coupled Low Frequency Ultrasonic Transducers and Arrays with PMN-32%PT Piezoelectric Crystals

Rymantas Jonas Kazys[1], Reimondas Sliteris[1], Justina Sestoke[1]; [1]*Ultrasound Institute of Kaunas University of Technology, Lithuania*

Background, Motivation and Objective

Nowadays air-coupled ultrasonic techniques are increasingly used for non-destructive evaluation. The biggest problem is big losses of ultrasonic signals mainly due mismatch of acoustic impedances of ultrasonic transducers and air. One of the ways to solve this problem is application of novel more efficient piezoelectric materials like PMN-PT type crystals. The objective of this research was development of air-coupled ultrasonic transducers and arrays with PMN–32% PT crystals.

Statement of Contribution/Methods

For air-coupled applications the operation frequency usually is $f \leq 100$ kHz. In order to obtain such low frequencies the main transverse extension mode of piezoelectric plates has been selected. For radiation and reception of ultrasonic waves the edge of piezoelectric element is used. For this mode the electromechanical coupling factor k_{32} may reach $(0.84 \sim 0.97)$. The high electromechanical factor of the transverse extension mode helps to achieve a good performance of air-coupled transducers.

Results/Discussion

In order to get an uniform distribution of displacements on the active surface of the piezoelectric elements strips with dimensions $(15 \times 5 \times 1)$ mm^3 and the [011] poled direction were selected. For improvement of performance special acoustic matching elements made of low impedance plastics were bonded to the edge of the crystal. The ultrasonic array was assembled from individual piezoelectric strips separated by insulating elements. In this case a bigger rectangular aperture of the transducers is obtained. As a result a 47 kHz 8-elements air–coupled ultrasonic transducer with PMN-32%PT crystals was developed simulated and tested. Vibrations of piezoelectric single crystals and ultrasonic array were investigated both theoretically and experimentally. Operation of the transducer with matching elements was simulated by the finite element method using ANSYS Mechanical APDL software. Spatial distributions of displacements at the resonance frequency were measured by the laser interferometer Polytec OFV-5000. Measurements of the acoustic pressure fields were performed by the Bruel&Kjaer wide band 1/8" microphone. Performance of the developed transducer was a few times better than of the air-coupled PZ-29 composite ultrasonic transducer of similar dimensions.

8H-5_____

9:00 am   Red blood cell manipulation using ultrasound microbeam

Kwok Ho Lam[1], Ying Li[2], Qifa Zhou[2], Kirk K Shung[2]; [1]*Department of Electrical Engineering, The Hong Kong Polytechnic University, Hong Kong,* [2]*NIH Transducer Resource Center and Department of Biomedical Engineering, University of Southern California, USA*

Background, Motivation and Objective

Devices for microparticle and cell manipulation have been developed for many biophysical applications. Similar to optical tweezers, tightly focused ultrasound microbeam (acoustic tweezer) has been reported to be capable of manipulating a single microbead. Although previous results suggested that the microbeam device is capable of manipulating particles at the cellular level, it had difficulty in manipulating cells especially non-spherical ones. It is mainly attributed to the gentle intensity gradient around the focus of the microbeam. In order to trap single cells, the f-number (f# = focal length / aperture size) of the device must be further reduced in order to allow the microbeam to form the steeper intensity gradient, resulting in much stronger trapping capability. The goal of this research is to develop an acoustic tweezer that can manipulate a single red blood cell (RBC) which is an oval and flexible biconcave disk in ~7 μm diameter. This is for the first time that the utilization of acoustic microbeam for manipulating non-spherical cells is re-ported.

Statement of Contribution/Methods

A 60-MHz lithium niobate single crystal single-element ultrasonic transducer with an f# of 0.6 was developed for cell manipulation. The f# of the transducer is the smallest ever reported on the study of acoustic tweezers. The transducer design was modeled with PiezoCAD in which the single crystal was ~45 μm thick with an aperture size of 1.6 mm. In fabrication, the transducer was press-focused at a focal length of 1.0 mm to obtain the designated f#. Pulse-echo measurement was employed to evaluate the basic transducer performance. Cell trapping experiment was performed in Alsever's solution in which the blood used was drawn from a healthy donor. The motions of RBC were recorded via a CMOS camera combined with a microscope.

Results/Discussion

Although the f# fabricated approaches the physical limit, the microbeam device exhibits high sensitivity in pulse-echo results. The measured centre frequency of the transducer was found to be ~60 MHz. The measured -6 dB bandwidth of the transducer was ~50 %, which agrees quite well with the simulation. RBC trapping experiment

SATURDAY ORAL

demonstrated that the microbeam device can manipulate a single RBC within the range of tens of micrometers as shown in Fig. 1. This preliminary result proves that the small f# microbeam could be used for cell manipulation.
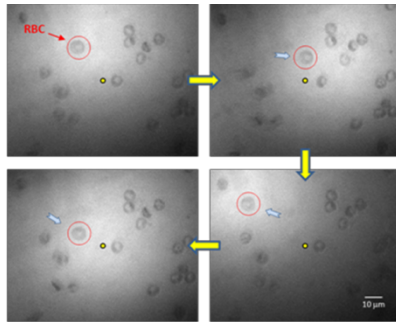
Fig. 1: Example of RBC manipulation. A single RBC (a red circle) was manipulated along the movement of the 60-MHz press-focused transducer. The bright circular shape is the projection of the transducer. A yellow dot is given as a reference point to show the location change of the RBC. (The capturing frame rate was 10 frames/second.)

8H-6

9:15 am   Design of High-Efficiency, Miniaturized Ultrasonic Receivers for Powering Medical Implants with Reconfigurable Power Levels

Ting Chia Chang[1], Marcus Weber[1], Jayant Charthad[1], Amin Nikoozadeh[1], Butrus T. Khuri-Yakub[1], Amin Arbabian[1]; *[1]Electrical Engineering, Stanford University, Stanford, CA, USA*

Background, Motivation and Objective

Millimeter and sub-mm sized implantable medical devices with high available power are attractive for many novel therapeutic applications. Ultrasonic power delivery can be used to shrink down the dimensions of an implant and eliminate the need for batteries and wires, while achieving high power levels (> 1 mW) for great depths in the body. Compared to RF wireless powering, ultrasonic energy transfer has several advantages: high acoustic-electrical power conversion efficiency (PCE), lower losses through tissue, superior energy focusing, and favorable impedance to interface with integrated circuits. To design for desired impedance and high PCE, we investigate ultrasonic receivers with different piezoelectric materials; and we propose an electrical matching technique in the operating region to optimize efficiency over various load power from different operation modes of an implant.

Statement of Contribution/Methods

Ultrasonic receivers are made with PZT4, PZT5H, and $BaTiO_3$ and sized to 1.5 mm thick and 1.1 mm wide on the sides. Air backing is utilized to increase the harvesting efficiency. We do not use acoustic matching layers for the ease of implementation and because a large instantaneous bandwidth is not required for the design of receiver. To study the energy harvesting capability for typical loads of active circuits (1 kΩ to 100 kΩ), impedance and PCE are measured and simulated using the 3-D finite element method. Mineral oil is used to imitate acoustic impedance of tissue in the measurement.

Results/Discussion

The receivers exhibit inductive impedance between the fundamental series and parallel resonances; moreover, the real part mimics typical implant loads, allowing for efficient overall impedance matching with capacitors. When the receiver's electrical matching is appropriately adapted, high PCE of 40% - 60% is achieved over a wide band (~300 kHz) for both PZT4 and PZT5H; and PCE of 40% - 50% is predicted for $BaTiO_3$ in simulation. The receiver can be designed to operate for a given implant load, and we can also program switched-capacitor network (without bulky inductors) to match to varying load powers. As a result, the proposed system can harvest acoustic power efficiently over large dynamic range of loads to enable miniaturized and complex medical implants.

Fig. 1. Measured (solid) and simulated (dash) real impedance and PCE of the receiver with (a) PZT4 (b) PZT5H. The impedance is inductive in the shaded region. (c) Proposed system diagram with tunable switched capacitor network.

1I - MTC: Tissue Characterization

201AF

Saturday, October 24, 2015, 10:30 am - 12:00 pm

Chair: **Pascal Laugier**
Université Pierre et Marie Curie

1I-1

10:30 am   **In vivo biopsy by photoacoustic based tissue characterization**

Xueding Wang[1], Guan Xu[2], Zhuo-xian Meng[2], Jian-Die Lin[2], Cheri Deng[2], Paul Carson[2], Brian Fowlkes[2]; [1]*Biomedical Engineering, University of Michigan, Ann Arbor, Michigan, USA,* [2]*University of Michigan, USA*

Background, Motivation and Objective

Majority of current studies on photoacoustic (PA) imaging are focused on the total signal magnitudes as the reflection of the macroscopic optical absorption by specific chemical contents at single or multiple optical wavelengths. Our recent research has demonstrated that the frequency domain power distribution of radio-frequency (RF) PA signals contains the microscopic information of the optically absorbing materials in the sample. In this research, we were seeking for the best method of systematically analyzing the PA measurement from biological tissues and the feasibility of quantifying tissue chemical and microstructural features for potential tissue characterization.

Statement of Contribution/Methods

By performing PA scan over a broad spectrum covering the optical fingerprints of specific relevant chemical components, and then transforming the radio-frequency signals into the frequency domain, a 2D spectrogram, namely physio-chemical spectrogram (PCS) can be generated. The PCS presents the "optical signature" and the "ultrasonic signature" of tissue simultaneously in one 2D spectrogram, thus contains rich diagnostic information allowing quantification of not only contents but also histological microfeatures of various chemical components in tissue. Comprehensive analysis of PCS, namely photoacoustic physio-chemical analysis (PAPCA), could reveal the histopathology information in tissue and hold the potential to achieve comprehensive and accurate tissue characterization.

Results/Discussion

The experiment on human prostate tissues with Gleason grades confirmed by histopathology has validated the capability of photoacoustic spectral analysis in characterizing the Gleason patterns. Another experiment on non-alcoholic fatty liver disease (NAFLD) mouse models has demonstrated that, by quantifying the PCS at the optical absorption peaks of major chromophores in liver tissue including hemoglobin, lipid and collagen, PAPCA can non-invasively characterize the pathological changes correlated to steatosis and fibrosis in liver, two of the leading medical problems in the United States. All the findings support our hypothesis that the PA measurement holds the promise to provide histopathology information comparable to gold standard biopsy and pathology.
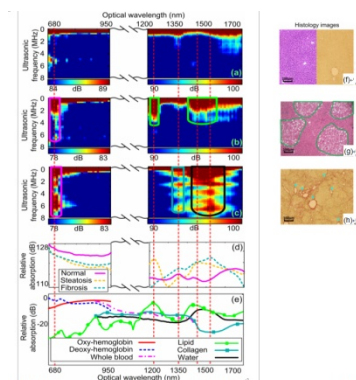
Fig. 1. Photoacoustic physio-chemical analysis (PAPCA) of liver tissues from non-alcoholic fatty liver disease (NAFLD) mouse models. Example physio-chemical spectrogram (PCS) of (a) normal, (b) extreme steatosis, and (c) extreme fibrotic livers. The optical spectrum of 680-950nm & 1200-1700nm covers the strong optical absorption (i.e. optical fingerprints) of hemoglobin, lipid, collagen and water which are marked respectively by the magenta, green, blue and black contours in the PCS. For each chemical component, its concentration in the tissue is reflected by the magnitude of its PCS fingerprint, as shown by the color scale; while its heterogeneous distribution is reflected by the extension of its fingerprint along the axis of ultrasonic frequency. (d) Example photoacoustic spectra of normal, extreme steatosis, and extreme fibrotic livers. (e) The relative optical absorption spectra of major relevant chemical components in liver tissues. Example histology photographs of (f) normal, (g) extreme steatosis, and (h) extreme fibrotic livers. As shown in the H&E stained histology pictures in panels (**f, left**) and (**g**), and in the Sirius Red stained histology pictures in panels (**f, right**) and (**h**), abnormal liver conditions involve changes in both chemical contents and histological microstructures. The steatosis regions containing scattered lipid clusters are outlined in green. The spatially distributed fiber collagen (stained in red) are marked by blue arrows.

1I-2

10:45 am   **In-Plane Anisotropy Method for the Characterization of the Elastic Properties of Anisotropic Materials**

Sara Aristizabal[1], Ivan Z. Nenadic[1], Bo Qiang[1], Carolina Amador[1], James F. Greenleaf[1], Matthew W. Urban[1]; [1]*Physiology and Biomedical Engineering, Mayo Clinic College of Medicine, Rochester, MN, USA*

Background, Motivation and Objective

Currently, the mechanical properties of anisotropic tissues such as skeletal muscle are evaluated by assuming the media to be transversely isotropic (TI) and estimating the shear wave group velocity (c_g) as a function of the angle between the tissue fibers and the direction of shear wave propagation in the range -180° to +180°. Here, we propose a simplified method, called In-Plane Anisotropy (IPA), to estimate the TI shear moduli by measuring the shear waves directed at different angles with respect to the main axis of the muscle fibers, defined as 0°, in a single B-mode imaging plane. By measuring c_g at angles centered around 0°, we can fit a TI model to these values to estimate the complete TI behavior. To investigate the IPA method, we used a finite element model (FEM) of the shear wave propagation in an elastic TI media, and we evaluated the properties of a TI phantom.

Statement of Contribution/Methods

The FEM consisted of a square block with fibers oriented along the x-direction. The value of c_g along (0°) and across (90°) the fibers was set to 5 and 3 m/s respectively. The block was excited using a line displacement source generating shear waves around the 0° location from 0-40°. The particle velocity in the z-direction of the data plane was extracted and processed for the estimation of c_g.

SATURDAY ORAL

Measurements were made in the TI phantom in the plane where the transducer was aligned with the fiber orientation (0°) then by steering the push beam and measuring the shear waves generated around the 0° location from -40° to +40°. Reference measurements to define the TI behavior were made at 0° and 90°. Shear waves were generated and measured with a phased array transducer and a Verasonics ultrasound system.

A 3D Fourier method was used to isolate the shear wave propagation along the angles of interest where c_g was calculated as the ratio of frequency (f) and the wavenumber (k).

Results/Discussion

Motion for the FEM (Figs. 1(a)-(c)) and phantom experiment (Figs 1(e)-(g)) are shown for different excitation angles. The estimated c_g behavior from the FEM and the phantom, obtained with the IPA method, and the correct c_g values associated with the material are displayed in Figs. 1(d) and 1(h), respectively. These results demonstrate that by steering the excitation beam with the IPA method, we can obtain accurate estimates of the true wave speed in a TI material. This method could be extended for use in anisotropic tissues.
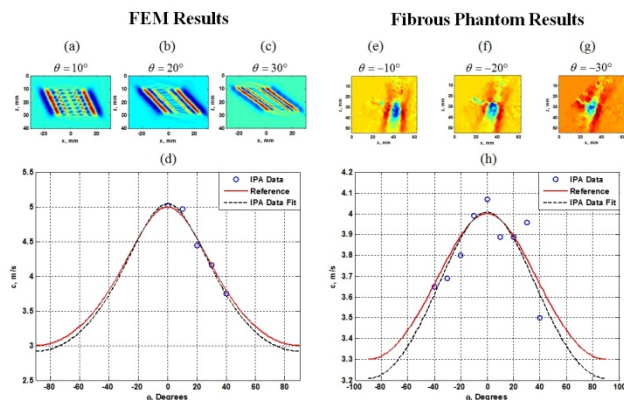
Figure 1: FEM generated shear wave propagation in a TI material at **(a)** 10°, **(b)** 20°, **(c)** 30°. The shear wave speed as a function of angle for the TI material is shown in **(d)**, where the red curve (Target curve) corresponds to the TI fit of the correct shear wave speeds along (5 m/s) and across (3 m/s) the fibers. The black dashed curve corresponds to the estimated shear wave velocity behavior obtained with the IPA method by fitting the TI model to the speed values obtained in the range 0° to +40° (blue circles). The error in the shear wave speed estimation along and across the fibers was about 0.4% and 2.8% respectively.
Shear wave propagation in the fibrous phantom at **(e)** -10°, **(f)** -20°, **(g)** -30°. The shear wave velocities as a function of angle for the phantom are shown in **(h)**, where the red curve (Target curve) corresponds to the TI fit of the correct shear wave speeds along (4 m/s) and across the fibers (3.3 m/s). The black dashed curve corresponds to the estimated shear wave velocity behavior obtained with the IPA method by fitting the transverse isotropic model to the speed values obtained in the range -40° to +40° (blue circles). The error in the shear wave speed estimation along and across the fibers was about 1.7% and 2.8% respectively.

1I-3

11:00 am   Measurements of the Shear wave Velocity and Attenuation of the Pancreas in Volunteers

Ivan Nenadic[1], Benjamin Wood[1], Carolina Amador Carrascal[1], James Greenleaf[1], Matthew Urban[1]; [1]Mayo Clinic, USA

Background, Motivation and Objective

Pancreatic cancer is the fourth most common cause of cancer-related deaths in the United States with no well-established biomarkers for the disease. We have been investigating the use of shear wave elastography methods to quantify mechanical properties of the pancreas. We performed in vivo transabdominal measurements of shear wave velocity and attenuation of the pancreas in healthy volunteers. The goal of this study is to show the feasibility of measuring mechanical properties of the pancreas in humans in vivo and establish the range of values in healthy volunteers.

Statement of Contribution/Methods

Ultrasound radiation force was used to excite shear waves in the pancreas and pulse-echo ultrasound was used to track the motion of the tissue. Autocorrelation was used to calculate tissue displacement as a function of time and propagation distance, u(x,t). A two-dimensional fast Fourier transform (2D FFT) of u(x,t) yielded the k-space whose coordinates are the spatial wavenumber (k) and temporal frequency (f). Shear wave velocity (c) and attenuation (α) at multiple frequencies were calculated from the k-space. A fully programmable ultrasound system (Vantage, Verasonics, Inc. Kirkland, WA, USA) operating a phased array probe (P4-2 Philips Healthcare, Andover, MA) was used to excite 900 μs impulse in the pancreases and track the motion by sector imaging at 3.906 kHz. The study protocol for the healthy volunteer studies was approved by the Mayo Clinic Institutional Review Board. Shear wave measurements were made in the tail, body and head of the pancreas.

Results/Discussion

The average group velocity (cg), phase velocity (cp) and attenuation (αp) at 100 Hz in the head of pancreas were cg = 1.01 m/s, cp = 1.32 m/s and αp = 149 Np/m. In the body of pancreas, the values were cg = 1.83 m/s, cp = 1.54 m/s and αp = 118 Np/m. In the tail of pancreas, the values were cg = 1.67 m/s, cp = 1.49 m/s and αp = 132 Np/m. The values of shear wave velocity in healthy volunteers were in agreement with the previously reported MRE studies, where the average shear wave velocity in the head, body and tail of the pancreas were 1.02, 2.18 and 2.19 m/s, respectively. These results demonstrate the feasibility of using shear wave elastography to assess elastic and viscoelastic mechanical properties of the pancreas.

1I-4

11:15 am   Attenuation Measuring Ultrasound Shearwave Elastography (AMUSE) for Measuring Shear Wave Velocity and Attenuation: Application in 15 Post-Transplant Liver Patients and Comparison with Biopsy Findings

Ivan Nenadic[1], Matthew Urban[1], William Sanchez[1], James Greenleaf[1], Shigao Chen[1]; [1]Mayo Clinic, USA

Background, Motivation and Objective

Attenuation Measuring Ultrasound Shearwave Elastography (AMUSE) is a technique for measuring shear wave velocity and attenuation without a rheological model. AMUSE was used to produce biopsy like measurements of velocity and attenuation in 15 post-transplant liver patients and the results were compared to biopsy findings.

Statement of Contribution/Methods

AMUSE uses a two-dimensional (2D) Fourier Transform of the shear wave motion to obtain the k-space whose coordinates are the frequency (f) and the wave number (k). The shear wave velocity (c) at the given frequency is equal to f0/k0, where f0 and k0 are the coordinates of the peak at the given frequency. The shear wave attenuation is calculated using $\alpha = (\pi/\sqrt{3}) \times FWHM$, where FWHM is the full-width at half maximum of the peak along the wave number axis. Measurements of shear wave velocity and attenuation were made at 100, 200 and 300 Hz in 15 patients with transplanted livers that were being evaluated for potential acute cellular rejection, and the results were compared to clinical diagnoses made by liver biopsy in a blind study.

Results/Discussion

At 100 Hz, the mean and standard deviation for the shear wave velocity and attenuation for patients without acute rejection were $c = 1.68 \pm 0.14$ m/s and $\alpha = 120.37 \pm 8.10$ Np/m, and for patients with acute rejection were $c = 2.36 \pm 0.31$ m/s and $\alpha = 94.05 \pm 6.94$ Np/m. At 200 Hz, the mean and standard deviation for the shear wave velocity and attenuation for patients without acute rejection were $c = 1.86 \pm 0.24$ m/s and $\alpha = 156.01 \pm 13.58$ Np/m, and for patients with acute rejection were $c = 2.56 \pm 0.42$ m/s and $\alpha = 113.25 \pm 15.17$ Np/m. At 300 Hz, the mean and standard deviation for the shear wave velocity and attenuation for patients without acute rejection were $c = 2.02 \pm 0.25$ m/s and $\alpha = 176.44 \pm 27.68$ Np/m, and for patients with acute rejection were $c = 2.76 \pm 0.52$ m/s and $\alpha = 135.34 \pm 28.41$ Np/m. The Hotelling trace criterion assessing the ability of parameters to differentiate between groups was 2.4 for the velocity, 3.6 for the attenuation, and 5.1 for velocity and attenuation combined at 100 Hz. At 200 Hz, the Hotelling trace criterion was 1.2 for the velocity, 2.6 for the attenuation, and 2.7 for velocity and attenuation. At 300 Hz, the Hotelling trace criterion was 1.0 for the velocity, 0.6 for the attenuation, and 1.1 for velocity and attenuation. The results suggest that using both the shear wave velocity and attenuation improves the ability to differentiate between two groups of patients.

1I-5

11:30 am   Ultrasonic guided waves to predict fracture risk in post-menopausal women: Clinical findings

Jean-Gabriel Minonzio[1], Quentin Vallet[1], Nicolas Bochud[1], Adrien Etcheto[2], Sami Kolta[2], Christian Roux[2], Pascal laugier[1]; *[1]Laboratoire d'Imagerie Biomedicale, Sorbonne Universites, UPMC Univ Paris 06, INSERM, CNRS, Paris, France, [2]Service de Rhumatologie Centre d'Evaluation des Maladies Osseuses Hopital Cochin, Paris, France*

Background, Motivation and Objective

Structural decay of bone is not fully assessed by current X-ray methods, and there is an unmet need in identifying women at risk of fracture who should receive a treatment. The last decade has seen the emergence of ultrasound axial transmission (AT) techniques to assess cortical bone, known for its key role in the mechanical strength of bone. Recent AT techniques exploit the multimode waveguide response of long bones (Vallet et al. IEEE IUS 2014). Applied to long bones such as the radius or tibia, guided waves-based approaches would be expected to provide estimates of important bone quality factors, such as cortical thickness and porosity, which cannot easily be captured by X-ray densitometry techniques (DXA). The objective of this cross sectional study was to evaluate if a new guided waves-based AT prototype can discriminate between fractured and non fractured postmenopausal women.

Statement of Contribution/Methods

Fifty nine post menopausal women aged 50-94 years were included in the study ; 26 patients were fractured (F) and 33 were non-fractured (NF). Measurements were performed at the distal radius using our AT prototype device (Azalée, Paris, France) consisting in a multi-transmitter multi-receiver probe. In addition to the fundamental flexural wave (FW) velocity, the cortical thickness (C.Th) and the apparent porosity (App.Por) were estimated by fitting a homogenized free plate model to the experimental dispersion curves measured in the 0.5-1.5 MHz frequency bandwidth. The areal bone mineral density (aBMD) was obtained using DXA at the proximal femur (TF) and at the lumbar spine (LS).

Results/Discussion

The best discriminating parameters are the cortical thickness C.Th (NF: 2.5 ± 0.6, F: 2.1 ± 0.5 mm, $p = 0.03$) and BMD TF (NF: 0.81 ± 0.09, F: 0.71 ± 0.09 g.cm2, $p<0.01$). Odds ratios (OR) and area under the Receiver Operating Characteristic curve (AUC), are reported in Table 1. FW velocity and C.Th are the best ultrasonic predictive variables, with an OR equal to 2.5 and 1.7 ($p = 0.03$) and an AUC of 0.67 and 0.71, respectively. The best predictive model is obtained with a combination of App.Por (OR = 2.1) and C.Th (OR = 2.3) and an AUC of 0.75 similar to that of aBMD TF. These preliminary results suggest the potential of ultrasonic guided modes to predict fracture risk in postmenopausal women. The study will be completed in the next future by the inclusion of a larger population.

Table 1. Odds ratios (OR) and areas under the curve (AUC) for ultrasound and DXA measurements

	OR [95 % CI]	*p*-values	AUC [95 % CI]	NF	F	*nm*
Ultrasound						
FW	2.52 [1.11 - 5.75]	0.03	0.67 [0.50 - 0.79]	32	25	2
App.Por	1.75 [1.13 - 3.45]	0.10	0.65 [0.48 - 0.78]	28	23	8
C.Th	2.06 [1.08 - 3.95]	0.03	0.71 [0.55 - 0.84]	28	23	8
combination of ultrasonic measurements (App.Por and C.Th)						
App.Por	2.08 [1.01 – 4.36]	0.05	0.75 [0.60 - 0.87]	28	23	8
C.Th	2.34 [1.17 – 4.71]	0.02				
DXA						
aBMD LS	*ns*	*ns*	0.53 [0.36 - 0.66]	33	25	1
aBMD TF	2.91 [1.47 - 5.76]	< 0.01	0.76 [0.62 - 0.87]	33	25	1

Reference category is nonfractured, CI confidence interval, *ns* not significant, *nm* not measured

---

1I-6

11:45 am   Estimation of bone quality on scoliotic subjects using ultrasound reflection imaging method – a preliminary study

Rui Zheng[1], Lawrence H Le[2], Doug Hill[1,3], Edmond Lou[1,3]; *[1]Department of Surgery, University of Alberta, Edmonton, Alberta, Canada, [2]Department of Radiology and Diagnostic Imaging, University of Alberta, Canada, [3]Glenrose Rehabilitation Hospital, Alberta Health Services, Canada*

Background, Motivation and Objective

Adolescent idiopathic scoliosis (AIS) is a three-dimensional deformity of the spine. Researches have indicated that osteopenia is a common phenomenon in scoliotic patients. Quantitative ultrasound (QUS) has been used to assess skeletal status, and the results demonstrate a good correlation with bone mineral density (BMD) using DXA method. Recently ultrasound imaging using reflection signals from vertebra has been applied to measure the severity of spinal curvature in AIS children, and the results show consistency with the measurements from radiography. The objectives of this study are to develop a method which can extract parameters from ultrasound signals to determine bone quality of vertebra and to investigate if the severity of spinal curvatures can be differentiated by the derived parameters.

Statement of Contribution/Methods

Eighteen consented AIS subjects were divided into two groups (9/9) based on the severity of the spinal curvature: mild curve (12-24°) and moderate to severe curve (27-52°). Their ultrasound spinal images were captured, and a single B-frame image located in the area at the thoracic level between T7-T9 was selected based on the clearness of echoes from the vertebral surface. The original radio frequency (RF) data of the frame were exported. Each frame contained 128 signal records, and approximately 54-88

SATURDAY ORAL

records with distinguishable echoes from the selected vertebra were chosen for analysis. For each signal, three types of amplitudes including time amplitude, envelope time amplitude and spectral amplitude were measured, and the reflection index (RI) indicating the reflection coefficient of vertebra cortex and soft-tissue interface was calculated. The average and linear regression methods were applied to estimate the mean RI along the vertebral-cortex/soft-tissue interface, respectively. A total of 6 mean RI values (3 amplitudes x 2 methods) were calculated and compared between the two groups.

Results/Discussion

Of all three amplitude configurations, the time methods showed inconsistency and the average of RI value illustrated little changes (ranged 0.45-0.58). The spectral amplitude method with linear regression approach presented the most reliable and consistent results. The RI of moderate-severe curve group was 0.47 which showed 36% lower than the group with mild curvatures (0.74). It demonstrates a potential in using ultrasound imaging method to assess bone quality of scoliotic patients and to distinguish the curve severity.

SATURDAY ORAL

2I - MIM: Advances in Vascular and Flow Imaging

VIP

Saturday, October 24, 2015, 10:30 am - 12:00 pm

Chair: **Lasse Løvstakken**
         NTNU

2I-1

10:30 am   Ultrafast vector flow imaging
Damien Garcia[1]; [1]*University of Montreal, Canada*

Background, Motivation and Objective

Medical ultrasound imaging has long been used for real-time visualization of blood flow dynamics through the use of color Doppler. Conventional color Doppler only provides one-dimensional velocity components parallel to the transmit beam axes. Another limitation of clinical color flow imaging is the relatively low frame rate often limited to a few tens frames per second. With the advent of high-speed data stream processing in ultrasound imaging, there has been a recent revival of interest in vector blood flow imaging. Vector blood flow ultrasound imaging at high frame rates is expected to be of significant clinical relevance since it could enable comprehensive time-resolved investigation of transient hemodynamic events.

-

Statement of Contribution/Methods

To get vector blood velocities at high temporal resolution, ultrasound imaging has been combined with mainly three established approaches: **1)** multi-beam transmits and/or receipts, **2)** speckle tracking (also known as echo-PIV when contrast agents are used), and **3)** transverse oscillations (TO).

1) Historically, the multi-beam method has been the first strategy in ultrasound vector flow imaging. It trigonometrically combines at least two non-parallel Doppler measures to deduce the velocity vector components.

2) Speckle tracking, with or without contrast agent, refers to the application of cross-correlation-based optical flow methods to ultrasonic speckle images. Tracking is performed on the RF or envelope ultrasound images through spatial cross-correlation or phase-correlation.

3) The TO method produces oscillations in cross-beam directions which allow estimation of velocity components perpendicular to the ultrasound beam axes.

These three approaches have all been adapted to high-frame-rate ultrasound imaging. High-frame-rate ultrasound imaging is commonly performed by generating wide unfocused ultrasound wavefronts illuminating the medium of interest. Pros and cons of vector flow methods pertaining to the abovementioned families will be discussed in the context of high-frame-rate ultrasound imaging. Other emerging techniques will be also introduced.

-

Results/Discussion

Recent *in vitro* and *in vivo* studies suggest that it is becoming possible to obtain precise and accurate vector velocity mapping at high temporal resolution in the great arteries. Intracardiac vector flow imaging yet remains challenging. Although it is recognized that wall shear rates, vortex flow patterns and recirculation zones might play a key role in several cardiovascular diseases, clinical relevance and patient impact of high-frame-rate vector flow imaging are still to be demonstrated.

-

2I-2

11:00 am   In-vivo Ultrafast Doppler Volumetric Imaging using Undersampled 2D Array
Martin Flesch[1,2], Thomas Deffieux[1], Jean Provost[1], Guillaume Ferin[2], An Nguyen-Dinh[2], Mathieu Pernot[1], Mickael Tanter[1]; [1]*Institut Langevin, ESPCI ParisTech, PSL Reaserch University, CNRS UMR7587, INSERM U979, Paris VII, Paris, France,* [2]*Vermon, Tours, France*

Background, Motivation and Objective

Ultrafast Volumetric Doppler imaging was recently shown to be achievable with a 2D fully populated matrix (Provost & al 2014). However, clinical applications of this technology are limited today by the large number of matrix transducer elements which require costly and complex electronics to be driven.

As a consequence, our investigation focuses on implementing a new beamforming strategy for ultrafast imaging with an undersampled matrix using a Row-Column Addressing matrix (RCA) technology (Seo and Yen & al 2009).

Statement of Contribution/Methods

The dedicated beamforming strategy is based on coherent compounding of plane wave transmissions with receive beamforming along the orthogonal direction and a coherent recombination of complementary orthogonal sequences. This approach was studied theoretically, numerically and validated experimentally in vitro in phantoms and in vivo on the carotid of human volunteer using ultrafast Doppler.

The experiment results are based on a matrix-array probe, centered at 3MHz, composed of 32x32 elements connected to a customized ultrafast scanner of 1024 independent channels. Thanks to this architecture, an RCA array, with the same dimension, composed of 32+32 elements, was emulated by an implementation of flat delays along a line or a column and benchmarked with the optimal fully sampled matrix configuration.

Results/Discussion

The first experiment was conducted on a CIRS phantom made up of anechoic cysts and echogenic wires. Using two sequences with an identical number of transmissions (16 plane waves, 2 degrees steering pitch) the performances of both the RCA and 2D matrix arrays have been quantified at a 4 cm depth with a F-Number value set at 3.

	2D matrix	RCA	
Resolution:	1.2mm	2mm	(−6 dB width)
Contrast:	23dB	16dB	(tissue-to-cyst B-mode amplitude ratio)

In vivo results confirmed that Doppler imaging is achievable with slightly reduced performances compared to the fully populated matrix (due to applied element density reduction factor of 16). Volumetric anatomic Doppler rendering and voxel based PW Doppler quantification are shown in the figure.

SATURDAY ORAL

Our solution can easily be implemented on marketed GPU-based scanners with a wide range of clinical and preclinical applications for various imaging frequencies (from 2.75MHz to 15MHz) at reasonable costs.
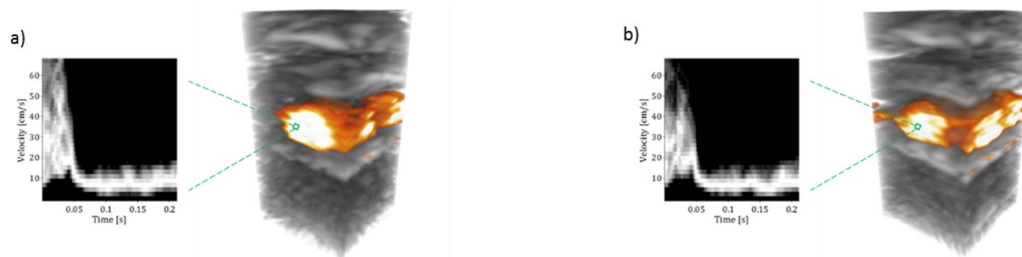
In vivo power and PW Doppler on a volunteer human carotid using 2D matrix (a) and RCA matrix (b)

2I-3

11:15 am   Super-Resolution Velocity Estimation in Microvessels using Multiple Hypothesis Tracking

Dimitri Ackermann[1], Georg Schmitz[1]; [1]*Chair for Medical Engineering, Ruhr-Universität Bochum, Bochum, Germany*

Background, Motivation and Objective

Imaging of blood flow in microvasculature is of particular interest, e.g. in cancer research. High frequency (>20 MHz) ultrasound with an image resolution of ~50 µm and ~200 µm in axial and lateral direction, respectively, is not capable to image the smallest microvessels, which have a diameter of ~8 µm. Thus, Doppler or speckle-tracking methods cannot image the blood flow in microvasculature in high resolution.

Statement of Contribution/Methods

We present an approach to image microvessels and blood flow at super-resolution by tracking the paths of multiple microbubbles (MBs) in contrast enhanced B-mode images. For this, the images are first separated in a static background and a moving foreground. The background images are calculated by temporal median filtering of B-mode frames. The difference of B-mode and background images are the foreground images. The positions of single MBs will be determned as local maxima from the foreground images. The number of MBs to be tracked is unknown as well as the association of the positions to the MB's tracks. This NP-hard combinatorial problem is known by the radar community as multiple target tracking. Here, we implemented the well-proven MHT algorithm according to [1] for this task.

We simulated MBs flowing through a vessel tree (see fig.) at a speed of 1 mm/s and a concentration of 150x10e6 MB/ml. The center vessels had a diameter of 17 µm and an inter vessel distance of 100 µm in lateral direction. The Field2 software was used to simulate the receive data from an ultrasound array (64 elements, 30 MHz center frequency) at 30 frames per second. The 1440 images were reconstructed by a SAFT algorithm.

Results/Discussion

The axial and lateral resolution was 35 µm and 195 µm, respectively. From these images, the MB's positions were localized and the MHT algorithm yielded estimates position and velocity for every MB. The mean velocity of all MBs was 1.04±0.08 mm/s. Figure 1 shows an overlay of the mean flow speed calculated from MB's velocities and a maximum intensity projection (MIP) image. The center vessels cannot be distinguished in the MIP image. In contrast, the mean flow speed is shown over the vessel tree and shows the center vessels separated.

[1]R. Danchick and G. E. Newnam, "Reformulating Reid's MHT method with generalised Murty K-best ranked linear assignment algorithm," IEE Proceedings - Radar, Sonar and Navigation, vol. 153, no. 1. p. 13, 2006.
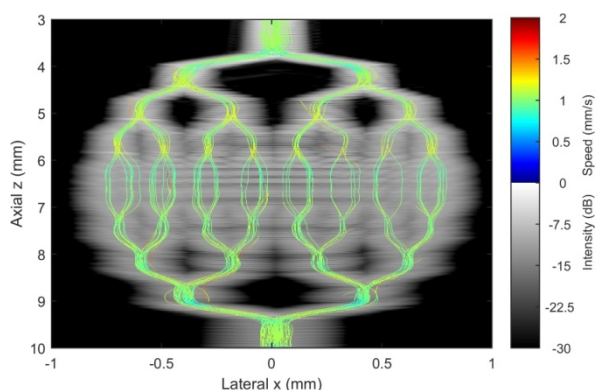
2I-4

11:30 am   Cerebral monitoring of neuroprotective ultrafast cooling post cardiac arrest via multiparametric ultrafast ultrasound Imaging

Charlie Demené[1], **David Maresca**[1], Matthias Kohlhauer[2], Fanny Lidouren[2], Bijan Ghaleh[2], Renaud Tissier[2], Mathieu Pernot[1], Mickaël Tanter[1]; [1]*Institut Langevin, ESPCI ParisTech, CNRS UMR7587, Inserm U979, Paris, France,* [2]*Inserm U955 Equipe 03, Université Paris Est Créteil et Ecole Nationale Vétérinaire d'Alfort, Maison Alfort, France*

Background, Motivation and Objective

Ultrafast cooling by total liquid ventilation (TLV) is a novel therapeutic hypothermia technique that improves outcome in brain tissues after asphyxial cardiac arrest. However, the neuroprotective mechanism of ultrafast cooling and its effect on cerebral microcirculation remain largely unknown. Here, we report multiparametric ultrafast cerebral imaging of ultrafast cooling in rabbits to monitor the spatiotemporal post arrest hemodynamics with and without TLV neuroprotection.

Statement of Contribution/Methods

4 rabbits were anesthetized, immobilized, curarized and underwent a craniotomy while mechanically ventilated. Arterial blood pressure and body temperature were recorded. An ultrasonic probe (128 elements, 0.2mm pitch, 6 MHz) was positioned to image a coronal section of the rabbit brain. Every 10 s, an Ultrafast Doppler (4 tilted plane wave emissions, PRF 8 kHz) and an elastography acquisition were performed. After 10 min of baseline, ventilation was stopped during 13 min to induce cardiac arrest. The rabbits were resuscitated via cardiac massage and monitored during 1h. In a TLV group, ventilation switched to oxygenized cold perfluorocarbon to decrease body temperature

---

SATURDAY ORAL

(40°C to 32°C in 15 min), whereas control rabbits were kept with conventional ventilation. For each time point, parametric maps of relative blood volume and resistivity index were computed from Ultrafast Doppler data and shear wave speed was extracted from elastographic data. In additional rabbits, blood brain barrier (BBB) permeability was assessed within 2h after cardiac arrest using Evans blue dye leakage method.

Results/Discussion

In the control group, large hyperemia was observed 5 min after resuscitation and lasted 20 min, with local variations (70% cerebral blood volume (CBV) increase in the cortex, 100% in the thalamus, 150% in the hippocampus). Brain areas presenting the most severe hyperemia were also exhibiting the most severe BBB dysfunction. In the TLV group, hyperemia was shortened (5 min) and attenuated over the entire brain (+20% in the hippocampus, +35% in the cortex and thalamus). Hypothermia was also protective regarding the BBB dysfunction. In the control group the resistivity index dropped by up to 0.22 during hyperemia vs. baseline, whereas in the TLV group it did not change significantly. Shear wave speed increased from 1.5 m/s at baseline to 2.5m/s during hyperemia in the control group and to 3m/s in the TLV group. In the control group, this increase is mostly due to the CBV increase whereas in the TLV group it appears to be driven by temperature.

Multiparametric ultrafast imaging enabled to track hyperemia in control and TLV rabbits, unveiling regional and temporal variations of blood volume/resistivity index in the brain. The fast CBV increase after resuscitation may explain why hours-long conventional cooling provides weaker neurological outcome than TLV. The tremendous regional CBV increase may explain local damages caused to the BBB.

2I-5 _____

11:45 am   Cardiac Motion Estimation based on Transverse Oscillation and Ultrafast Circular Wave Imaging

Philippe JOOS[1], Sebastien Salles[1], Didier Vray[1], Barbara Nicolas[1], Hervé Liebgott[1]; *[1]CREATIS, Villeurbanne, Rhône, France*

Background, Motivation and Objective

Ultrafast imaging using plane waves (PW) has demonstrated its potential in assessing complicated motion patterns in the blood or in the tissue. On the other hand, the introduction of transverse oscillations (TO) combined with Phase Based vector Motion estimation algorithms (PBM) has shown to be very precise. Cardiac imaging could greatly benefit of a combination of ultrafast TO and PBM.

Unfortunately, due to the presence of the ribs, cardiac imaging has to be done with a phased array. Consequently ultrafast imaging of the heart is usually performed with diverging waves (DW) instead of PW.

In this paper, the objective is to extend to ultrafast imaging of the heart using DW our previously developed ultrafast PW TO technique.

Statement of Contribution/Methods

A DW is generated with all the elements of the probe assuming a virtual source behind the probe. From one DW transmission, a polar image is built with a specific delay and sum beamforming considering the virtual source instead of the probe centre as the origin of the [R-θ] coordinate system. This beamforming aims at avoiding the "sheared appearance" of the PSF in the images and keeping the characteristic transverse patterns, thus preserving the efficiency of the PBM.

The beamformed images are then filtered in the [nu_R nu_θ] Fourier domain to generate TO following the method proposed for linear geometry in [Salles et al. IEEE TUFFC 2015].

The PBM [Alessandrini et al. TMI 2014] is applied on polar filtered images to estimate the motion along the R and θ directions.

Results/Discussion

The method is validated with FIELD II simulations. The realistic cardiac sequence from [Alessandrini et al. ICIP 2012] is used. The frame rate of the initial sequence was 45 FPS. Only the scatterrers composing the myocardium are kept and their positions are interpolated to increase the frame rate up to 4400 FPS. The virtual source is 17.6 mm behind the probe and the sector is Pi/2. We generate TO images with a radial and angular wavelengths equal to 0.257 mm and 0.0338 rd, respectively. Several points of the myocardium are tracked using our PBM method and the error of estimation is calculated for each pair of consecutive frames and for each tracked point. The figure shows a polar TO filtered image and the lateral trajectory and error for one point. The errors (mean +/- std) in milli-pixels in angular and radial directions are equal to 6.6+/-68.5 and 1.1+/-95.2, respectively.
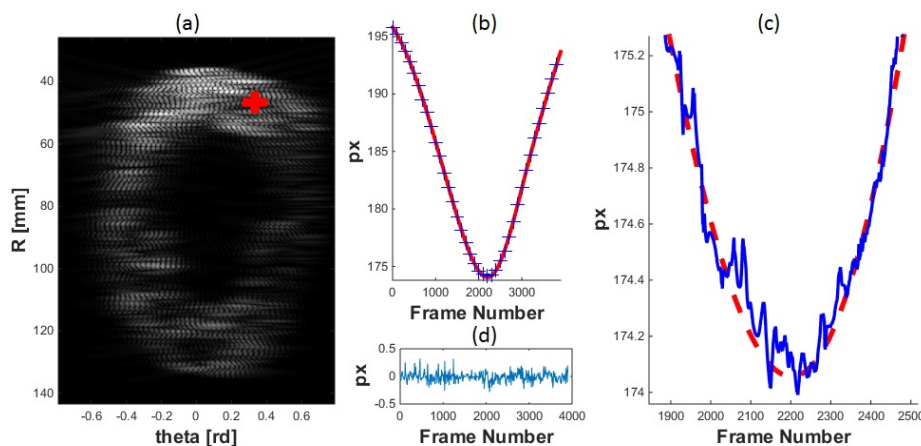
Fig : (a) polar beamformed image and point studied ➕ , (b) lateral real ━━ and estimated ✛ trajectories on 4000 frames, (c) zoom : lateral real ━ ━ and estimated ━━━ trajectories on 700 frames , (d) lateral errors in pixels on 4000 frames

3I - MEL: Towards Clincial Application of Elasticity Imaging

201BC

Saturday, October 24, 2015, 10:30 am - 12:00 pm

Chair: **Mark Palmeri**
           Duke University

3I-1

10:30 am   Sonic Estimation of Elasticity via Resonance (SEER): Initial Results from a New Method of Assessing Hemostasis

William Walker[1], F. Scott Corey[2]; [1]*HemoSonics, Charlottesville, Virginia, USA,* [2]*Key Technologies, Inc., Baltimore, Maryland, USA*

Background, Motivation and Objective

Hemostasis is the physiological process that stops bleeding. While individual hemostatic components can be tested biochemically, the most clinically relevant tests quantify the evolving mechanical properties of whole blood as it clots. Existing tests are difficult to operate and interpret.

This paper describes SEER sonrheometry, a next-generation sonorheometry method for ultrasound quantification of shear modulus and the assessment of hemostasis. This method forms the basis of a new in vitro Point-of-Care diagnostic instrument, the HemoSonics Quantra DX, designed to assess hemostasis in the operating room, intensive care unit, and trauma center.

Statement of Contribution/Methods

Sonic Estimation of Elasticity via Resonance (SEER) builds upon our prior method, sonorheometry, by enabling quantitative modulus measurement without knowledge of the applied radiation force magnitude. SEER uses a high-energy pulse to apply acoustic radiation force; exciting a shear wave that resonates within a rigid test chamber. Low energy pulses measure resultant displacements. For simple geometries, the resonant period is related to sample modulus through an analytical model. For more complicated geometries, the time-displacement (TD) is related to modulus through a Finite Difference Time Domain (FDTD) model.

Results/Discussion

Figure 1 shows experimental TD curves. Figure 2 shows evolving modulus during coagulation in a 330 ul whole blood sample. Modulus was estimated by comparing each experimental TD curve to 1,167 TD curves predicted by an axisymmetric FDTD model with varying moduli. The model with the best fit (typically > 0.98) indicated the modulus estimate. Simultaneous measurements of the same sample in four test channels showed a coefficient of variation at peak modulus of 2.2%.
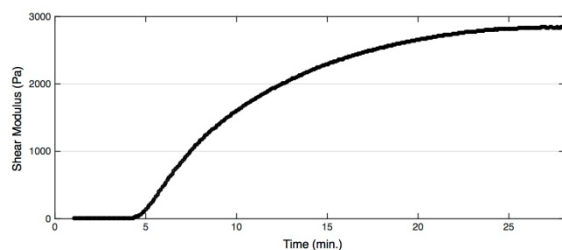
Figure 2
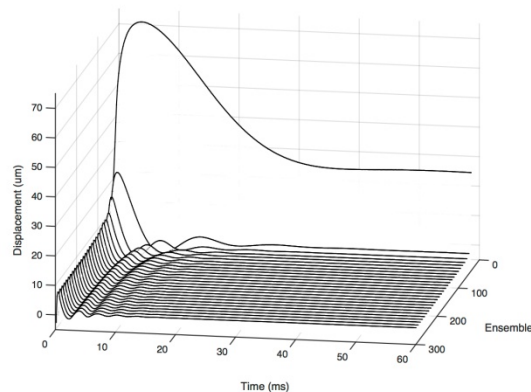
Figure 1

3I-2

10:45 am   Myocardial stiffness assessment in children using Shear Wave Imaging: an in-vitro and in-silico study

Annette Caenen[1], Darya Shcherbakova[1], Clément Papadacci[2], Mathieu Pernot[2], Patrick Segers[1], Abigaïl Swillens[1]; [1]*IBiTech-bioMMeda, Ghent University, Ghent, Belgium,* [2]*Institut Langevin, ESPCI ParisTech, Paris, France*

Background, Motivation and Objective

Shear wave elastography (SWE) is a potential tool to support diagnosis and surgical decision making in children with cardiac disorders. However, SWE in this particular setting is challenged by dispersion and 3D shear wave (SW) propagation paths, caused by the relatively thin and curved left ventricle (LV) with its anisotropic material properties, ultimately complicating the link between SW propagation and tissue stiffness. To study these complex SW phenomena, we used a combined experimental and numerical approach.

Statement of Contribution/Methods

Experimental: A phantom representative of the child's LV (see fig. A for dimensions) in the age-group 10-15 years was created using a 10% polyvinyl alcohol solution (freeze-thawed once). SWE-acquisitions were performed at 10 mm depth by submerging the phantom in water, mimicking invasive imaging. A cross-sectional (90°) and longitudinal (0°) plane were imaged (fig. A) using a push frequency of 8 MHz and PRF of 6.9 kHz. Group and phase velocity analysis allowed shear modulus μ estimation, which was compared to the actual stiffness determined via uniaxial mechanical tensile testing.

Numerical: To get insight into the full 3D SW physics, a corresponding numerical model was created in the finite element software Abaqus. The experimentally applied acoustic radiation force (ARF) was computed in the Field II software and imposed as a body force. The ventricle was modeled with an elastic material law based on the mechanical testing.

Results/Discussion

Analysis of the experimental tissue velocities shows clear dispersion in fig. B due to the ventricular geometry. Consequently, the derived shear modulus underestimates the actual stiffness μmech by 40.7% and 7.2% for the group (blue) and phase (red) speed analysis in the 0°-plane, respectively. A 58.9% and 0.7% underestimation is present for the 90°-plane (fig. B). This demonstrates that group speed analysis is challenged by SW dispersion, whereas phase speed analysis improves μ-estimation. Hence, we will

look for additional insights into the complex SW mechanics via modeling, to ultimately improve these material characterization techniques. Initial simulation results show a full 3D view of the SW propagation, corresponding well with the experiment in the imaging plane (fig. C).
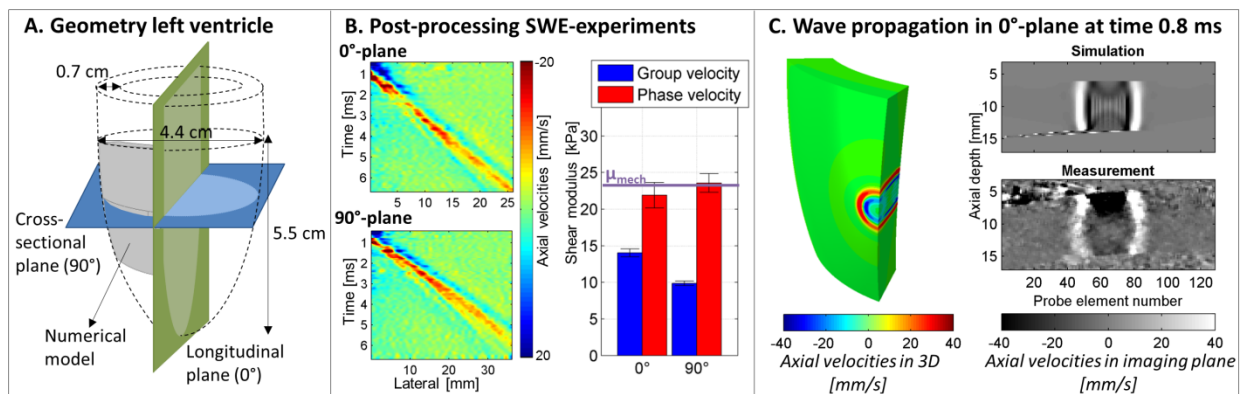
3I-3

11:00 am   3-D ultrasound elastography of the breast: first steps towards ABVS implementation

Gijs A.G.M. Hendriks[1], Branislav Holländer[1], Jan J.M. Menssen[1], Hendrik H.G. Hansen[1], Chris L. de Korte[1]; [1]*Medical UltraSound Imaging Center (MUSIC), Department of Radiology and Nuclear Medicine, Radboud university medical center, Nijmegen, Netherlands*

Background, Motivation and Objective

Mammography is the gold standard for breast cancer screening but less suitable for women with dense breasts. Therefore, ultrasound automated breast volume scanner (ABVS) was introduced as an alternative. Although clinical studies showed high sensitivity of ABVS to detect breast cancer, specificity and long acquisition times (>1 minute) remain an issue. Since specificity can be improved using elastography, the aim of this study was to develop 3-D strain imaging for ABVS scanning while also reducing acquisition times by plane-wave imaging.

Statement of Contribution/Methods

To mimic the ABVS, an ATL L12-5 50mm transducer was attached to a motorised XZ-translational setup (Fig. 1a) and connected to a Verasonics V1 ultrasound system. The aim was to obtain 150 equidistant (0.5 mm) 2-D strain images (60×25 mm^2) of a breast phantom (model 059, CIRS) containing multiple inclusions. To obtain these images, beamformed ultrasound radiofrequency (RF) data were acquired before and after deformation of the breast, followed by coarse-to-fine 2-D cross-correlation and 1-D least-squares strain estimation. The performance of strain estimation was compared for two transmission schemes at two frame rates of 2 Hz and 16 Hz (one breath hold) by calculating elastographic contrast-to-noise ratios (CNRe) and signal-to-noise ratios (SNRe). In transmission scheme 1 pre- and post-deformation RF data were acquired per position, whereas in scheme 2 (ABVS-like acquisition) RF data were acquired for all positions per state of deformation (Fig. 1b).

Results/Discussion

All methods provided similar strain images upon visual inspection (Fig. 1c/d) for most positions, although first and last 15 strain images (corresponding to rounder parts of the breast) resulted in reduced quality (SNRe 0±6 dB; CNRe 15±0 dB) in scheme 2 compared to scheme 1 (SNRe 16±1 dB; CNRe 28±4 dB). For the other 120 images, the two methods were similar (CNRe 33±1 dB; SNRe 15±1 dB). The frame rates did not seem to affect the CNRe and SNRe in both methods. In summary, scheme 1 performed similarly to the ABVS-like scheme 2 in the central part of the breast. Thus we might conclude that implementation of strain imaging in ABVS is feasible, although the reduced quality at the borders of the breast has to be improved. Moreover, plane-wave imaging will enable high frame rates and lateral compounding and allow 3-D elastography within one breath hold.
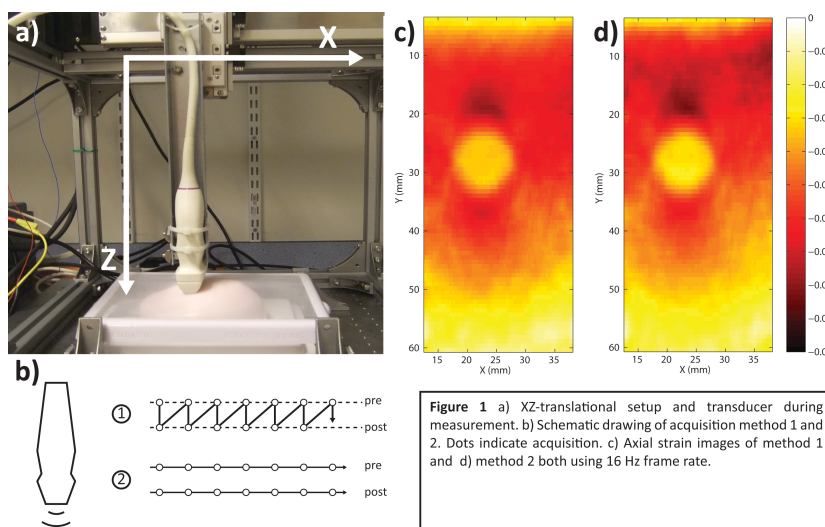
Figure 1 a) XZ-translational setup and transducer during measurement. b) Schematic drawing of acquisition method 1 and 2. Dots indicate acquisition. c) Axial strain images of method 1 and d) method 2 both using 16 Hz frame rate.

3I-4

11:15 am   In vivo liver shear wave motion detection and shear wave speed comparison between fundamental and harmonic imaging

Carolina Amador[1], Pengfei Song[1], Duane Meixner[2], Shigao Chen[1], Matthew Urban[1]; [1]Department of Physiology and Biomedical Engeenering, Mayo Clinic College of Medicine, Rochester, Minnesota, USA, [2]Department of Radiology, Mayo Clinic College of Medicine, Rochester, Minnesota, USA

Background, Motivation and Objective

A major application of shear wave elasticity imaging (SWEI) is to non-invasively quantify liver elasticity, which has shown correlation with chronic liver disease. SWEI measurements can be highly affected by phase aberration and clutter. Usually, SWEI measurements use fundamental imaging. Recently, it has been shown that harmonic imaging can significantly improve SWEI. The purpose of this study was to evaluate liver shear wave motion detection with fundamental and harmonic imaging.

Statement of Contribution/Methods

Fourteen healthy volunteers were recruited. The protocol was approved by the Mayo Clinic Institutional Review Board and written informed consent was obtained prior to scanning. A Vantage ultrasound system (Verasonics, Inc., Kirkland, WA) equipped with a curved array transducer (C5-2v, Verasonics, Inc., Kirkland, WA) was used. A focused ultrasound beam with duration of 600 μs was used for shear wave generation. The detection beams were transmitted with a frequency of 2 MHz which produced a second harmonic signal around 4 MHz. During receive the RF signals from 2 steering angles were compounded, giving an effective PRF of 2.77 kHz. Then a finite-impulse response (FIR) filter was used to extract the fundamental and second harmonic components of the RF signal separately. The axial particle displacement (Uz) was then calculated from both components using autocorrelation method. The shear wave maximum displacement (Max. Uz) and shear wave speed (SWS) with RANSAC algorithm (inlier ratio higher than 0.5) were estimated. Measurements with the interquartile range (IQR) to median ratio more than 30% were considered failures. Five measurements in two acoustic windows (8th and 7th intercostal spaces) and two depths (1 and 2.5 cm from the liver capsule) were taken for each subject.

Results/Discussion

The shear wave motion from of one volunteer is shown in Figs. 1(a)-(b). The mean and standard deviation of maximum displacement, SWS and success ratios of 14 volunteers are summarized in Fig. 1(c). With harmonic imaging higher displacements were detected, SWS values and success ratios were lower and with higher precision. These results indicate that harmonic imaging can decrease the shear wave elasticity measurements variability in liver. [This study was supported in part by NIH grants DK092255 and DK106957]

	Max. Uz, μm		SWS, m/s		Success ratio, %	
	Fundamental	Harmonic	Fundamental	Harmonic	Fundamental	Harmonic
7th space, Depth 1	1.08 ± 0.84	2.75 ± 1.89	1.75 ± 0.78	1.54 ± 0.25	52.86	69.29
7th space, Depth 2	1.03 ± 0.39	2.57 ± 1.28	1.54 ± 0.35	1.48 ± 0.19	63.57	86.43
8th space, Depth 1	1.23 ± 0.61	3.84 ± 1.89	1.71 ± 0.59	1.59 ± 0.50	80.71	75.00
8th space, Depth 2	0.98 ± 0.45	2.88 ± 1.48	1.60 ± 0.48	1.50 ± 0.40	57.14	69.29
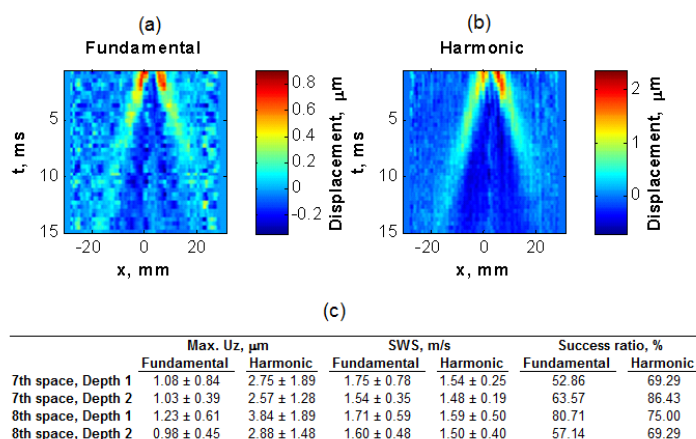
Figure 1. Shear wave propagation with (a) fundamental and (b) harmonic detection of one volunteer. (c) Summary of results of 14 volunteers.

3I-5

11:30 am   Validation of Electromechanical Wave Imaging in canine left ventricles against electrography

Julien Grondin[1], Alexandre Costet[1], Ethan Bunting[1], Alok Gambhir[2], Elaine Wan[2], Elisa E Konofagou[1,3]; [1]Department of Biomedical Engineering, Columbia University, New York, NY, USA, [2]Department of Medicine, Columbia University, New York, NY, USA, [3]Department of Radiology, Columbia University, New York, NY, USA

Background, Motivation and Objective

Electromechanical Wave Imaging (EWI) is a technique that can image the transient deformation in the myocardium resulting from electrical activation. This technique can be used as a surrogate for the measurement of the electrical activation of the heart. EWI has been shown capable of detecting and characterizing ventricular pacing, left bundle branch block (LBBB) and atrial flutter. A previous study has shown good agreement between electromechanical and electrical activation in a canine. However, this technique has not been fully validated in vivo. The objective of this study is to investigate the relationship between electromechanical and electrical activation.

Statement of Contribution/Methods

In this study, six canines were investigated. The canines were anesthetized and their chest was opened by lateral thoracotomy. A 64-electrode basket catheter was inserted through the apex of the left ventricle. Two external electrodes were sutured onto the epicardial surface of the left ventricle in the anterior and lateral regions. A suture was attached to one spline of the basket catheter as a landmark to determine the location of the splines. Ultrasound channel data were acquired at 2000 Hz using a 2.5 MHz center frequency operated by a Verasonics system. Four different apical views were acquired: the standard 4-, 2- and 3-chamber views as well as the 3.5-chamber view which is located between the 4- and the 2-chamber views. Axial motion was estimated using normalized 1-D cross-correlation with a window length of 6.2 mm and 90 % overlap. Axial strain was computed from axial displacement using a least-squares estimator with a kernel of 5 mm. Channel data, ECG and endocardial potential were acquired synchronously during sinus rhythm, pacing from the sutured electrodes or pacing from one electrode of the basket catheter. Electromechanical activation timing at a given location was defined as the first zero-crossing of the EWI strain curve after the onset of the Q-wave and electrical activation timing was defined as the time of maximum amplitude of the depolarization wave.

Results/Discussion

A linear regression was performed between electromechanical and electrical activation timings and the mean correlation coefficient (R) and intercept (i) were computed across all six animals. The mean correlation coefficient and intercept for sinus rhythm were R = 0.56 and i = 41 ms respectively, for pacing from the sutured electrodes we obtained R = 0.74 and i = 33 ms and for pacing from one electrode of the basket we obtained R = 0.62 and i = 35 ms. The suboptimal alignment between the basket splines and the image planes due to lack of simultaneous CT imaging may have impacted the correlation.

Despite these shortcomings, the relatively good correlation between EWI and electrography further support our initial findings that EWI-based electromechanical activation is linearly related to electrography-based electrical activation.

3I-6

11:45 am Viscoelastic Response (VisR) Assessment of Longitudinal Dystrophic Degeneration in Clinical Duchenne Muscular Dystrophy

Christopher Moore[1], Mallory Selzo[2], Melissa Caughey[3], James Howard, Jr[4], Caterina Gallippi[1,2]; *[1]Department of Electrical and Computer Engineering, North Carolina State University, Chapel-Hill, NC, USA, [2]Joint Department of Biomedical Engineering, University of North Carolina and North Carolina State University, Chapel Hill, NC, USA, [3]Department of Medicine, University of North Carolina at Chapel Hill, Chapel Hill, NC, USA, [4]Department of Neurology, University of North Carolina at Chapel Hill, Chapel Hill, NC, USA*

Background, Motivation and Objective

Duchenne muscular dystrophy (DMD) is a lethal genetic disorder primarily occurring in males, which causes progressive muscle degeneration through necrosis and replacement of muscle fibers with fat and fibrosis. Current metrics for measurement of disease state, such as physical testing, are insufficient for properly tracking the progression of the disease. The aim of this work is to develop an improved metric for monitoring disease state with Viscoelastic Response (VisR) ultrasound. VisR ultrasound is an acoustic radiation force (ARF)-based imaging method that delineates tissue viscoelasticity by fitting displacements induced by successive, co-located ARF impulses to a mechanical model.

Statement of Contribution/Methods

In a longitudinal clinical study, VisR imaging was performed serially (every 4 months) in the right leg of a boy with DMD aged 5.4 to 7.8 yrs. Images of the Vastus Intermedius (VI) and Gastrocnemius Medial (GM) muscles were acquired at the midpoint between the iliac crest and the tibial plateau. The data were captured using a Siemens Acuson Antares with a custom VisR beam sequence consisting of two ARF impulses delivered to the same region of excitation and separated in time by 0.4 ms. The ARF impulses , were centered at 4.21 MHz, with F/3.0 focal configuration. Two-cycle tracking pulses, centered at 6.15 MHz with an F/1.5 focal configuration, were used to measure the ARF-induced displacements. This beam sequence was delivered at 40 locations across a 20-mm lateral field of view. Measured displacements were fit to the solution of the Mass-Spring-Damper model to calculate the ratio of viscosity to elasticity (τ), and parametric VisR τ images with VI and GM muscles manually segmented from B-Modes were rendered.

Results/Discussion

In the τ images of the GM (A), a region of high τ value at the bottom of the muscle at 6.2 yrs grows progressively until 7.4 yrs, and the fraction of the muscle with $\tau \geq 1.2$ ms increases from 12.0 to 62.7% over the 1.2 year period. In the VI (B), an area of high τ value at 5.4 yrs progressively decreases in size until 6.6 yrs, and the fraction of the muscle with $\tau \geq 1.2$ ms decreases from 57.2 to 22.2%. These results suggest that VisR outcomes are consistent with the natural history of DMD, involving phenotypic variation between the GM (progressive necrosis and/or fatty infiltration) and VI (early fatty infiltration progressively replaced by fibrosis).
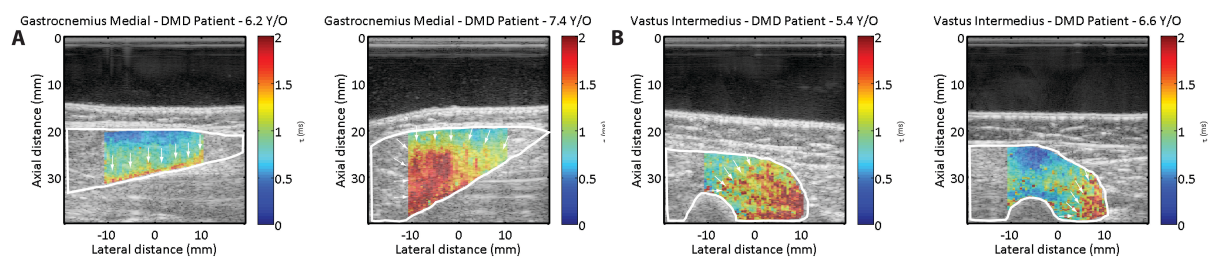
Figure: Images of τ, the ratio of viscosity by elasticity, in a patient with Duchenne muscular dystrophy in the A) Gastrocnemius Medial muscle at 6.2 Y/O and 7.4 Y/O and B) Vastus Intermedius muscle at 5.4 Y/O and 6.6 Y/O. The area of high τ increases in the Gastrocnemius, indicating progressive fatty infiltration, and decreases in the Vastus Intermedius, indicating progressive replacement of fatty tissue with fibrosis.

SATURDAY ORAL

4I - MTH: Histotripsy, Shockwaves and Liquefaction

201DE

Saturday, October 24, 2015, 10:30 am - 12:00 pm

Chair: **Jean-Yves Chapelon**
INSERM

10:30 am   Histotripsy Cardiac Therapy for Non Invasive Chordal Cutting

Olivier Villemain[1], Wojciech Kwiecinski[1], Justine Robin[1], Bastien Arnal[1], Alain Bel[2], Mickael Tanter[1], Emmanuel Messas[2], Mathieu Pernot[1]; *[1]Institut Langevin, France, [2]Hopital Européen Georges Pompidou, France*

Background, Motivation and Objective

Chordal cutting is a technique that has been developed recently to improve the efficacy of ischemic mitral regurgitation (MR) surgery. The technique relies on the surgical section of one type of mitral chordae and is achieved during open chest procedure with the heart stopped and extracorporeal circulation (ECC). In this study we investigated the feasibility of using histotripsy for non-invasive chordal cutting on ex vivo chordae samples and in vivo beating hearts in a model of large animal.

Statement of Contribution/Methods

Experiments were performed in vitro in explanted sheep heart (N=10) and in vivo in sheep beating heart (N=5, 40+/-4 kg). In vitro, the mitral valve basal chordae was removed, fixed on a holder in a water tank. The ultrasound pulses were emitted from the therapeutic device (1-MHz focused transducer, pulses of 8µs duration, peak negative pressure of 17 MPa, repetition frequency of 100Hz) placed at a distance of 64 mm. A confocal ultrasound imaging probe was used to monitor the procedure. In vivo, we performed sternotomy and the device was applied on the thorax cavity filled out with degassed water. We analyzed MV coaptation and chordae by real time 3D echocardiography (Philips IE33, X5-1 probe Xmatrix) before and after chordal cutting. The animals were sacrificed at the end of the procedure, for postmortem anatomical and histological exploration to confirm the section of the basal chordae and the integrity of the remaining marginal chordae.

Results/Discussion

In vitro, all the basal chordae were completely cut. The mean procedure time was 5.5 (+/-3) minutes. The thickness of the chordae was the main criteria affecting the duration of procedure. In the sheep, central basal chordae of anterior leaflet were completely cut. The mean procedure time was 20.8 (+/-5) minutes. The sectioned chordae was visible on the ultrasound images. All the postmortem anatomical exploration of hearts confirmed the section of the basal chordea. No additional macroscopic lesions were found. There was no histological evidence for inflammation or thrombosis in the sites of the lesion. It was non argument for the presence of tissue fragment with risk of embolus.

Noninvasive ultrasound histotripsy succeed to cut mitral valve basal chordae in vitro and in vivo in beating heart. Future investigation will be needed to test this noninvasive technique on its ability to decrease ischemic or functional MR. If positive, this will open the door of completely noninvasive technique for mitral valve repair especially in case of functional MR.

10:45 am   Non-invasive Thrombolysis using Histotripsy beyond the "Intrinsic" Threshold (Microtripsy)

Xi Zhang[1], Cabe Owens[2], Hitinder Gurm[3], Yu Ding[1], Charles Cain[1], **Zhen Xu**[1]; *[1]Department of Biomedical Engineering, University of Michigan, Ann Arbor, Ann Arbor, USA, [2]Department of Pediatrics and Communicable Diseases, University of Michigan, Ann Arbor, Ann Arbor, USA, [3]Department of Internal Medicine, University of Michigan, Ann Arbor, Ann Arbor, USA*

Background, Motivation and Objective

Histotripsy has been investigated as a non-invasive, drug-free, and image-guided thrombolysis method that fractionates blood clots using acoustic cavitation alone. In previous histotripsy thrombolysis studies, cavitation clouds were generated using multi-cycle pulses. The cavitation bubbles tended to form on vessel walls where weak nuclei reside, potentially subjecting the vessel walls to high stress. To avoid damage to vessel wall, a new histotripsy approach, termed Microtripsy, has been recently discovered where cavitation is generated via an intrinsic-threshold mechanism using a 1.5-cycle pulse. We hypothesize that, using Microtripsy, the cavitation cloud can be generated reliably and entirely within the vessel lumen, without contacting or damaging the vessel wall. To test our hypothesis, Microtripsy was investigated for precise clot removal in an in vitro flow model.

Statement of Contribution/Methods

Clots made from bovine blood were formed inside a vessel phantom (6.5 mm inner diameter) connected to a flow system with a pressure of 3.7 mm Hg applied. Guided by ultrasound imaging, Microtripsy was applied by a 1 MHz transducer at a pulse repetition frequency (PRF) of 50 Hz and P- of 30 MPa or 36 MPa. To create a flow channel through a 2-cm clot, the therapy focus was scanned through the clot at intervals of 0.3 or 0.7 mm, with 300 or 1000 pulses applied at each scan location, respectively. The treated clots were 3D-scanned to quantify the size of the flow channels generated by Microtripsy. Restored flow rates were measured and clot debris particles were analyzed.

Results/Discussion

In all treatments, cavitation clouds were consistently generated in the center of the vessel lumen, with no cavitation observed on the vessel wall (Fig. 1a). A flow channel was successfully generated through the clot after each Microtripsy treatment, and was completely confined inside the clot (Fig. 1b-d). The channel created by Microtripsy treatments had a diameter up to 60 % of the vessel diameter and restored flow up to 500 mL/min. The debris particles generated by Microtripsy were small with over 99.9% of the particles being smaller than 10 µm and the largest particle at 153 µm. Each clot was recanalized within 7 minutes. The results show the potential of this new Microtripsy thrombolysis method for fast, precise, and effective clot recanalization, minimizing risks of vessel damage and embolism.
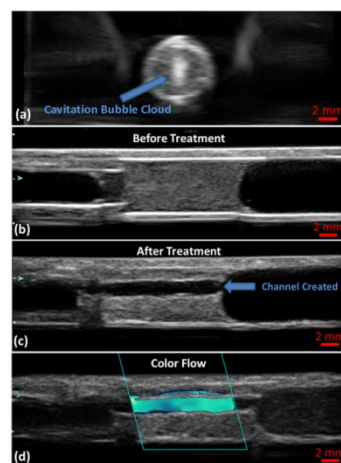
Figure 1: Representative ultrasound images of clot in vessel-mimicking phantom. **a)** Cavitation bubble cloud in vessel lumen during treatment. **b)** Before treatment. **c)** After treatment with flow channel present. **d)** After treatment with Color Doppler flow.

4I-3 _____

11:00 am   Transcranial aberration correction using histotripsy pulse backscatter from the bubble clouds they create

Jonathan Sukovich[1], Timothy Hall[1], Zhen Xu[1], **Charles Cain[1]**; [1]*Biomedical Engineering, University of Michigan, Ann Arbor, MI, USA*

Background, Motivation and Objective

Transcranial ultrasound therapies can be compromised by acoustic aberrations introduced by the skull resulting in significant reduction in pressure amplitude and distortion of the ultrasound focus in the target region. Complex schemes have been used to correct for the aberrations, requiring expensive MRI and CT scans of the brain. We seek to demonstrate a new very rapid aberration correction method for transcranial histotripsy therapy. First, cavitation is generated transcranially without aberration correction using a single one-cycle histotripsy pulse with a phased array histotripsy transducer. Second, the ultrasound signals of the histotripsy pulse backscattered from the small localized cavitation cloud are received with the phased array elements and used to perform aberration correction. The feasibility of this new aberration correction method was demonstrated with excised human skullcaps using a 256-element phased array histotripsy transducer. Histotripsy can generate clean bubble clouds without aberration correction which allows for this approach to work. The subsequent aberration correction greatly increases transducer headroom allowing for more effective phased array scanning.

Statement of Contribution/Methods

Cavitation clouds were first generated through an excised human skullcap by applying histotripsy pulses without aberration correction using a custom 500 kHz, 256-element phased array transducer, which was capable of generating estimated peak negative pressures in excess of 30 MPa without aberration correction. Single measurements of the backscattered signals from individual bubble clouds were then taken using 8-element sub-apertures of the histotripsy array, and repeated 32 times such that backscattered signals from all 256 elements of the array were collected. The relative phase delays of the elements of the array were then calculated in order to perform aberration correction. To assess the effectiveness of aberration correction, histotripsy pulses were then applied through the skullcap to agarose phantoms embedded with a layer of redblood-cells (RBC) and the resulting cavitation bubbles and lesions generated were imaged via high-speed camera. These results were then compared to lesions generate in RBC phantoms treated using histotripsy with 'perfect' aberration correction from hydrophone measurements.

Results/Discussion

Using the backscattered signal from single bubble clouds generated through the skullcap without aberration correction, we were able to effectively perform aberration correction. Lesions generated with this correction method had radii equivalent to those generated using "perfect" correction (1.1mm) with the hydrophone measurement. Hydrophone measurements at the focus indicated that pressure amplitudes achieved in this way were up to 90% of those using "perfect" aberration correction, compared to only 60% with no aberration correction.

4I-4 _____

11:15 am   Transcranial Histotripsy Therapy to Treat Hemorrhagic Stroke

Jonathan Sukovich[1], Yohan Kim[1], Aditya Pandey[2], Timothy Hall[1], Charles Cain[1], **Zhen Xu[1]**; [1]*Biomedical Engineering, University of Michigan, Ann Arbor, MI, USA*, [2]*Neurological Surgery, University of Michigan, Ann Arbor, MI, USA*

Background, Motivation and Objective

Intracerebral hemorrhage (ICH) accounts for 10-15% of all stroke and is characterized by the bleeding and clotting in the brain caused by the rupture of blood vessels. Current treatment options include surgery and medication, both with high mortality and morbidity rate. MR-guided focused ultrasound (MRgFUS) is currently being investigated to improve ICH therapy. With MRgFUS applied outside the skull, the clot in the brain can be liquefied and aspirated with a needle, providing a faster minimally invasive treatment. Treatment times can be extensive (3 hours to drain ≤40 mL clot) and cannot treat clot volumes larger than 40mL. Tissue within 2 cm of the skullcap cannot be treated. Transcranial histotripsy can overcome all these limitations, In addition. this study evaluated the effect of frequency on transcranial histotripsy ICH treatment efficiency.

Statement of Contribution/Methods

Fresh clots (78mL) were prepared using whole bovine blood. Histotripsy pulses of 1.5 cycles were delivered to the clots through excised human skullcaps using custom 250 kHz and 500 kHz, 256-element phased array transducers, producing an estimated peak negative pressure over 30MPa at the geometric focus of the transducer. During clot treatments, the therapy focus of the histotripsy transducer was steered electronically throughout a 2cm radius spherical region within the clot, with a treatment site density of 120 treatment sites/cc for the 500 kHz array, and 30 treatment sites/cc for the 250 kHz array. Using the 500 kHz array, treatments were delivered at pulse repetition frequencies (PRF) of 100-200 Hz, and each treatment site was treated for 50-100 pulses, resulting in total treatment times of 16- 34 minutes. Using the 250 kHz array, treatments were delivered at PRFs of 50-100 Hz, and each treatment site was treated for 50-100 pulses, resulting in total treatment times of 8-16 minutes. After treatment, a catheter was inserted into the clots to drain the liquefied clot volume for measurement. The effectiveness of the treatments was quantified as the volume liquefied divided by the total duration of treatment.

Results/Discussion

Using the 500 kHz array, histotripsy liquefied up to 45 mL of clot in 30 minutes through the skullcap, yielding peak liquefaction rates of 2 mL/min. Using the 250 kHz array, histotripsy liquefied up to 20 mL of clot in 9 minutes, yielding peak liquefaction rates of 2.2 mL/min. Histotripsy treated clots within 5 mm of the skullcap. These data

---

demonstrate that histotripsy can liquefy clots at a speed an order of magnitude faster and cover a wider spatial extent compared to MRgFUS. Treatments using the 250 kHz transducers were faster than when the 500 kHz transducer was used. More work is needed for optimization, safety investigation, and in vivo feasibility.

4I-5

11:30 am   Rapid HIFU-aided liquefaction for fine-needle aspiration of large extravascular hematomas: feasibility study

Tatiana Khokhlova[1], Wayne Monsky[2], Yasser Haider[3], Yak-Nam Wang[4], Thomas Matula[4]*; [1]Medicine, University of Washington, Seattle, WA, USA, [2]Radiology, University of Washington, Seattle, WA, USA, [3]Urology, University of Washington, Seattle, WA, USA, [4]Applied Physics Lab, University of Washington, Seattle, WA, USA*

Background, Motivation and Objective

Intra- and extra- muscular hematomas result from repetitive injury as well as sharp and blunt limb trauma. The clinical consequences can be serious including debilitating pain, functional deficit and limb threatening extremity compartment syndrome. Due to gelatinous nature, hematomas can only be drained surgically, which can be disfiguring and is associated with significant morbidity. The goal of this work was to evaluate the feasibility of HIFU-based technique termed histotripsy for rapid (within clinically relevant timeframe of 15-20 minutes) liquefaction of large volume (up to 30 cc's) extra-vascular hematomas for subsequent fine-needle aspiration. Two different histotripsy methods have been developed, cavitation histotripsy (CH) and boiling histotripsy (BH). Both methods utilize very short (microsecond-millisecond) HIFU pulses at a low duty factor. Each pulse induces violent bubble activity at the focus, which leads to tissue lysis into subcellular debris without broad thermal effects. The induced bubbles are highly echogenic and allow for precise targeting and treatment monitoring.

Statement of Contribution/Methods

Experiments were performed using in vitro extravascular hematoma phantoms - fresh bovine blood was poured into 50 ml molds and allowed to clot. The resulting phantoms were treated by BH, CH or the combination in a degassed water tank under ultrasound guidance. Series of individual lesions using different CH and BH parameters were first created in the phantoms to find the most rapid liquefaction procedure. Two different transducers operating at 1 MHz and 1.5 MHz with f-number=1 were used with duty cycles of 1-2% for BH and 0.3-0.5% for CH, pulse durations 10 ms for BH and 3.3-5 us for CH, treatment duration 5-60 s and peak focal pressures of $p+$=70-100 MPa, $p-$=15-25 MPa. Next, the focus was translated within the sample in a 2D rectangular grid with 2-5 cm dimensions in 2-5 mm steps while the optimized CH or BH pulsing protocol was applied at each location. The contents of the lysate were analyzed by histology and by sizing in a Coulter counter.

Results/Discussion

The peak instantaneous power to achieve BH was lower (at 1.5 MHz) or equal to (1 MHz) that required to initiate CH. Under the same exposure duration, BH lesions were 1.5-2 times larger than the CH lesions, which indicate that BH is more appropriate for the large-scale debulking of the hematoma. The lysates contained minute amount of debris larger than 70 um and 99% of particulates were smaller than 10 um. The contents of the large-scale voids produced by BH were successfully aspirated using 18-21 gauge needles, yielding 8 cc (for 1.5 MHz treatment) to 20 cc (for 1 MHz) of lysate in only 10 minutes of treatment. CH-aided liquefaction was slower, but the voids were more regularly shaped, facilitating easier aspiration. It is thus concluded that a combination of BH and CH may be most optimal for liquification of large extravascular hematomas.

4I-6

11:45 am   Preclinical evaluation of an MR-guided thermal HIFU ablation strategy using shockwaves and millisecond boiling in an in-vivo porcine liver model

Pascal Ramaekers[1], Martijn de Greef[1], Johanna van Breugel[1], Chrit Moonen[1], Mario Ries[1]*; [1]Imaging Division, UMC Utrecht, Utrecht, Netherlands*

Background, Motivation and Objective

A potential application of High Intensity Focused Ultrasound (HIFU), guided by either diagnostic ultrasound or MRI, is the ablation of tumor cells in abdominal organs. A major challenge for this particular application is that the volumetric ablation rate, using current clinical equipment and sonication protocols operating below the stable cavitation pressure regime, is generally low in these high-perfused organs. Sonication strategies making use of shockwaves, millisecond boiling, and cavitation have been evaluated pre-clinically to enhance the energy uptake in the target area. However, the complex nature of these mechanisms has so far limited their application in clinical practice. The goal of this study was to investigate, under MR guidance and clinical conditions, whether a thermal ablation protocol using shockwaves and millisecond boiling can be used to enhance the energy uptake in the treatment area and ablate a confluent region in a highly perfused organ (porcine liver).

Statement of Contribution/Methods

A Philips Sonalleve HIFU system integrated in a 1.5 T Achieva MRI scanner was used to sonicate pre-defined treatment cells (4x4x8 mm) in the livers of 4 pigs (50-55 kg) under general anesthesia. Sonications using a modified, pulsed protocol (P_{ac} = 1000 W, PRF = 40 Hz, pulse length = 10500 cycles, t = 10 s, E_{tot} = 3500 J) were compared to those using an energy-equivalent continuous wave (CW) protocol (P_{ac} = 350 W, t = 10 s). Treatment cells were planned using MRI and energy delivery was monitored in real-time using MR thermometry. Additionally, MRI was used to compensate for respiratory motion by employing a gated energy delivery based on motion tracking of the diaphragm (dc 65-70%). Non-perfused volumes (NPV) were segmented based on contrast-enhanced MR images. Histopathological evaluation was performed to reconfirm the non-viability of the ablated region. In a complementary ex vivo experiment, passive cavitation detection was employed during both sonication protocols to investigate the mechanism of energy uptake enhancement.

Results/Discussion

The pulsed sonication protocol was able to ablate confluent lesions in the porcine liver, as confirmed by NPV segmentation and histopathology. The pulsed protocol potentially allows for an ablation rate of ~4ml / h in liver tissue without adverse effects in (sub)cutaneous tissue layers intersecting with the beam cone.
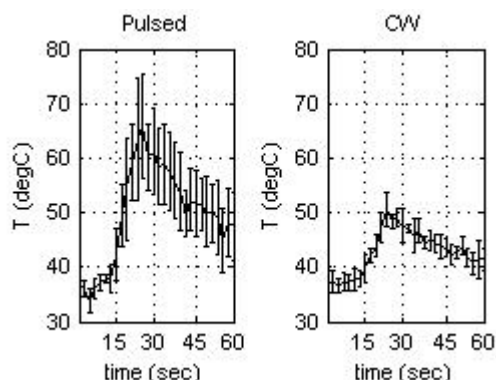
5I - MBE: Bioeffects and Dosimetry

103

Saturday, October 24, 2015, 10:30 am - 12:00 pm

Chair: **Jeff Ketterling**
Riverside Research

10:30 am **Local cavitation induced vessel wall injury of artery and its potential application in animal model of atherosclerosis**

Yujin Zong[1], Rongrong Wang[1], Xinru Zou[1], Lei Zhang[1], Yi Feng[1], Gang Liu[1], Mingxi Wan[1]; *[1]The Key Laboratory of Biomedical Information Engineering of Ministry of Education, Xi'an Jiaotong University, Xi'an, Shaanxi, China, People's Republic of*

Background, Motivation and Objective

According to the postulated "response to injury theory", atherosclerosis develops as a result of repetitive injury and ongoing inflammatory process of the inner arterial wall of large and medium-size arteries. Mechanical arterial balloon injury combined with hypercholesterolemia is one of the most widely employed methods to induce atherosclerosis in animal models. However, the balloon injury operation is complicated and the plaque site is unpredictable and difficult to control. It is reported that some application of ultrasound (US) to microvessels that contained microbubbles can result in endothelial cells damage and arteries injury. Thus we propose that microbubble enhanced US cavitation would induce controllable local artery wall injury and then could be an alternative method to the balloon injury for inducing a localized eccentric vulnerable plaque at desired specific site.

Statement of Contribution/Methods

A clear vessel-mimicking polyacrylamide gel phantom with a Young Modulus similar to the artery wall was used to visually observe the vessel wall damage that is generated by flowing microbubble (MCA) and phase-changed contrast agent (PCCA) separately under 1.2MHz focused US exposure. The flow velocity was set to about 60cm/s similar to actual rabbit abdominal aorta blood flow velocity. Passive cavitation detection was made using a 5 MHz confocal transducer mounted in the central hole of the 1.2MHz transducer. Additionally, the rabbit abdominal aorta was processed by balloon and cavitation separately using US image guidance. After 24h, the aorta was isolated and fixed, and then slices of the aorta were stained with hematoxylin and eosin (H&E) for routine microscopic evaluation.

Results/Discussion

For a flowing vessel phantom of 4mm in diameter, the damage usually occurred on the proximal wall in the direction of US propagation (Fig. 1a). Many tunnels were formed from the proximal wall toward the transducer (Fig. 1b). The area of vessel wall damage increases with the increase in US intensity. And the area of damages induced by PCCAs was larger than that induced by MCAs (Fig. 1c). Both inertial and stable cavitation contributed to the wall damage. In the animal experiment, it is found that the lesion occurred only within the US exposure area in the cavitation group, while the site of wall injury occurred at random in the balloon group.

(a) Front view of vessel wall (b) Top view of vessel wall

(c) The diameter of damage induced by PCCAs and MCAs
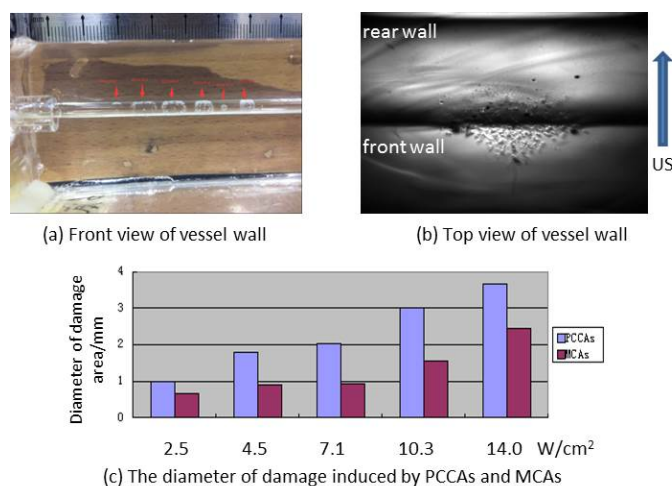
Fig.1

10:45 am **Understanding the Biophysical Origin of Protrusive Blisters in Sonoporated Cells: Actin Network Disruption and Membrane Blebbing**

Ruen Shan Leow[1], Jennifer M. F. Wan[2], **Alfred C. H. Yu**[1]; *[1]Medical Engineering Program, University of Hong Kong, Pokfulam, Hong Kong, [2]School of Biological Sciences, University of Hong Kong, Pokfulam, Hong Kong*

Background, Motivation and Objective

Protrusive membrane blisters have often been observed on the surface of sonoporated cells that were subjected to acoustic cavitation exposure. Alas, why these blisters would emerge remain unknown, and providing answers would be important to understand how cells may strive to restore plasma membrane integrity in a sonoporation episode. Such a research topic is especially relevant to sonoporation episodes that were triggered locally by targeted microbubbles bordering the plasma membrane, because resulting cavitational impact would be discharged firsthand to the cell. Here, we seek to test the hypothesis that the blisters are membrane blebs that arise due to acute disruption of cytoskeleton during sonoporation, and that this phenomenon is part of the sonoporated cell's anti-stress machinery.

Statement of Contribution/Methods

Central to our investigation is the use of a previously established confocal imaging protocol that allowed us to track the in situ position of sonoporation sites. The three key aspects of the protocol are: 1) single shot ultrasound exposure (1 MHz frequency, 0.45 MPa peak negative pressure, 30 cycle duration); 2) the use of one targeted microbubble per cell (1-5 um diameter; specific to VEGF receptors; fabricated in-house using avidin-biotin conjugation); 3) live confocal imaging of membrane periphery (labeled with CellMask), actin cytoskeleton (labeled with CellLight Actin-GFP), and cytoplasmic Ca2+ (labeled with Fluo4-AM). Note that propidium iodide or Cytox-

SATURDAY ORAL

Green were used as sonoporation tracers during experiments. The actin dynamics of ZR-75-30 breast carcinoma cells were first imaged live over a 1 h period from the onset of sonoporation. Next, the membrane periphery was monitored to gain insight into its bleb dynamics over the course of sonoporation; statistical analysis over multiple trials were performed to quantify possible relationship between bleb features (size) and sonoporation parameters (microbubble diameter). Third, blebbing was concurrently imaged with Ca2+ dynamics to explore the functional implication of the latter.

Results/Discussion

Immediate rupturing of the actin network was evident at the sonoporation site. The phenomenon was found to propagate to elsewhere in the cell, and the entire actin network progressively vanished over 60 min. The extent of actin disruption was more substantial in cells with higher uptake of sonoporation tracer. In line with these findings, blebbing was found to occur at a recovering sonoporation site after its resealing and elsewhere along the membrane periphery. 99% of blebbing cases at sonoporation sites were inflicted by microbubbles larger than 1.5 um (N=124). Blebs were not observed at irreversible sonporation sites or when sonoporation site repair was inhibited via Ca2+ chelation. Functionally, the bleb volume was found to serve as a buffer compartment to accommodate the cytoplasmic Ca2+ excess brought about by Ca2+ influx during sonoporation.

5I-3

11:00 am   Drug Delivery Is Promoted by Low-Intensity Ultrasound Due to an Increase in Clathrin-Mediated Endocytosis.

Sophie Tardoski[1], Evelyne Gineyts[2], Jacqueline Ngo[1], Anthony Kocot[1], Philippe Clézardin[2], **David Melodelima[1]**; [1]*INSERM UMR 1032, France*, [2]*INSERM UMR 1033, France*

Background, Motivation and Objective

Ultrasound (US) mediated drug delivery is a field with promising results although the exact mechanisms behind intracellular delivery of drugs remain to be elucidated. Most of the studies used drug carriers and cavitation to enhance drug uptake in tumor cells. However, cavitation could induce cell lysis and remain difficult to control and predict in vivo. In this study, low intensity ultrasound with proper sonication parameters were used to induce clathrin-mediated endocytosis and to force the penetration of a bisphosphonate (Zoledronic acid: ZOL) into tumor cells.

Statement of Contribution/Methods

Flat transducers working at a resonance frequency of 2.9 MHz (C-US) and 1.2 MHz (LIPUS) were used. C-US was used to induce and maintain mild hyperthermia (temperature increase of 5°C) as well as to create mechanical effects but no cavitation. This was achieved by adjusting the acoustic power between 8 and 13 W as a function of time and temperature (maximal peak negative-pressure: 0.29 MPa). Pure mechanical effects were created using LIPUS. Pulse length was 200 μs at 40 mW/cm2 (SATA) and repeated every 1 ms. Both treatments lasted 30 minutes. MCF-7 human breast cancer cells and a surrogate marker (isopentenyl pyrophosphate, IPP) of ZOL penetration were used to evaluate ultrasound effects on drug uptake. Transmission electronic microscopy was used to quantify accumulation of endocytosis vesicles in cells cytoplasm. Immunogold staining was used to assess the localization of clathrin in cells cytoplasm.

Results/Discussion

Intracellular accumulation of IPP in tumor cells was observed with ZOL alone (498 ± 79 pmol/mg) due to non-specific endocytosis. If ZOL treatment was combined with LIPUS, the intracellular accumulation of IPP in tumor cells was significantly higher when compared with ZOL alone (1097 ± 246 pmol/mg; p < 0.01). Combining temperature increase and mechanical stress (C-US groups) was demonstrated to be more efficient in drug penetration (accumulation of IPP: 1746 ± 448 pmol/mg) when compared to all other groups.

Immunogold staining demonstrated a statistically significant increase of endocytosis vesicle only in ultrasound-treated cells. C-US produced a 3-fold increase in immunogold staining compared with ZOL-treated cells (P<0.001) and twice more endocytosis vesicle when compared with LIPUS (P<0.01). Only ultrasound treatments impact clathrin-mediated endocytosis.

In conclusion, low intensity ultrasound can induce bisphosphonate uptake in cancer cells via clathrin-mediated endocytosis. Unlike other studies in ultrasound mediated drug delivery the parameters we used do not create cavitation and no microbubbles, such as contrast agents, were used. Low intensity ultrasound create mechanical stress that forces the penetration of ZOL inside cells. If the temperature was slightly increase a further accumulation of ZOL was noticed due to increased cell membrane permeability.

5I-4

11:15 am   Silicon Horn Transducer Based Ultrasonically Enhanced Nerve Firing

Tiffany St. Bernard[1], Po-Cheng Chen[2], Jason Hoople[2], Bruce Johnson[3], Amit Lal[2]; [1]*Biomedical Engineering, Cornell University, Ithaca, NY, USA*, [2]*Electrical and Computer Engineering, Cornell University, Ithaca, NY, USA*, [3]*Neurobiology and Behavior, Cornell University, Ithaca, NY, USA*

Background, Motivation and Objective

Post Traumatic Stress Disorder (PTSD) effects 7-8% of Americans at some point in their lives. When pharmacological methods are ineffective, vagus nerve stimulation (VNS) may be a viable option. The vagus nerve is part of the autonomic nervous system which oversees involuntary control, such as heart hate. However, current method are invasive and expensive, and is done through surgical implantation of a commercially available programmable pulse generator device. Prior research has shown that brain neurons can be stimulated via transcranial pulsed ultrasound transducer at various frequencies. This work addresses the need for low frequency approaches to trigger nerve responses by external ultrasound. These transducers are designed to focus sound to achieve high amplitudes in small end-effector cross-sectional areas of <1mm to that we can target specific nerves in the near-field zone of the transducer. The transducers operate at low voltages of 1-10Vpp, at frequencies ranging from 50-150kHz.

Statement of Contribution/Methods

Initial experiments investigate the effects of ultrasound from a silicon horn transducers on the crayfish abdominal nerve cord at the resonance frequency of 105.6 kHz as a function of drive voltage. Transducer dimensions 40mm length, and shank to tip area ratio of 10/1 was fabricated and driven by an adhesively bonded PZT plate. Integrated Wheatstone bridges can be used to drive the transducers at a fixed tip velocity and ultrasonic power level. An extracellular suction electrode was used to measure the nerve firing rate before and during exposure to US. The temperature of the horn tip was measured using an IR camera.

Results/Discussion

Action potential (AP) firing rates were used to verify whether sufficient acoustic pressure wave is applied to the nerve for stimulation. An increase of AP firing rate by 5.055%, 7.622%, and 10.649% with respect to stimulation and non-stimulation under different conditions was observed. Additionally, we saw an average increase of 0.03V in the average AP amplitude during US stimulation. These results suggest that at low 1.57 V, a CMOS compatible voltage range, the nerve can be stimulated. Temperature measurements indicated that an average increase of temperature of ~ 1 degree is possible. At present we are modeling the effect ultrasound on the action potential by changes in the ion-channel activation and resting potentials.

SATURDAY ORAL
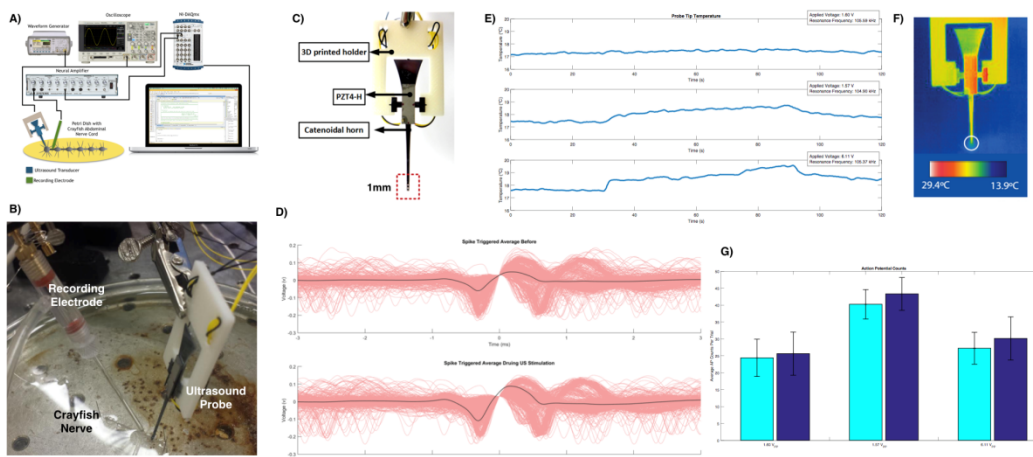
Figure: A) Equipment setup schematic; B) experiment setup; C) US Probe; D) n=30 overlapping (in red) and average (in black) for APs before and during US stimulation when driven at 1.60 Vpp demonstrating an increase in AP firing and amplitude; E) Probe tip temperature increase in chilled crayfish saline at different voltages; and G) IR image of transducer with tip placed in chilled crayfish saline; and F) IR image of probe.

5I-5

11:30 am   Quantitative Measurement of Pulsed Ultrasound Pressure Field Using Optical Phase Contrast

Seiji Oyama[1], Mohd Syahid[1], Jun Yasuda[1], Shin Yoshizawa[1], Shin-ichiro Umemura[2]; [1]*Communication Engineering, Tohoku University, Sendai, Japan,* [2]*Biomedical Engineering, Tohoku University, Sendai, Japan*

Background, Motivation and Objective

In recent years, the research and development of ultrasound applications in medicine has progressed especially for diagnostic purpose. Establishment of fast and accurate measurement of ultrasound pressure field accelerates the development of ultrasound application in medicine. The most common method to measure ultrasound pressure field is a hydrophone scan which requires a long scanning time and may disturb the acoustic field. In this study, we proposed an optical phase contrast (PC) method for the measurement which enables a fast and noninterfering measurement.

Statement of Contribution/Methods

In a PC method, the ultrasonically diffracted component of light interferes with the spatial DC component, whose phase is advanced by a phase plate. This way, its phase modulation is converted to amplitude modulation. A computed tomography algorithm was then applied to reconstruct the three-dimensional ultrasound pressure field. In addition, a filter in the spatial frequency domain was used to improve the signal-to-noise ratio (SNR). The filter combining rectangular and gauss windows was carefully tuned by taking the bandwidth of the ultrasonic pulse into account.

Results/Discussion

The pressure field of pulsed ultrasound was measured, and its normalized distribution is mapped in Figure 1(a). The cross-sectional waveform in the axial and lateral direction is shown in Figure 1(b) and (c), respectively. The result of the proposed optical measurement agreed well with that of hydrophone while. The measurement time was shorter by orders of magnitude as shown in Table 1.
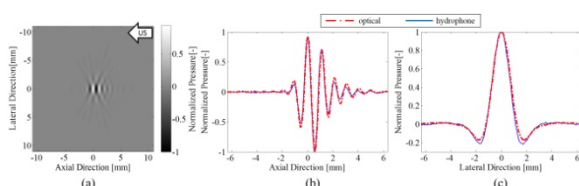
Figure 1 (a) Normalized ultrasound pressure field reconstructed from optical method . Comparison between optical method and hydrophone: (b) axial direction and (c) lateral direction.

Table 1   Measurement time

	Optical method	Hydrophone
Measurement range	$50 \times 50 \times 50$ mm	20×20 mm (40,000 points)
Acquisition time	3 minutes／Space	60hours／Plane
Analysis time	5 minutes／Space (Depend on PC)	10 minutes／Plane (Depend on PC)
Spatial resolution	50 μm (Depend on camera)	100 μm

5I-6

11:45 am   Rapid spatial mapping of the acoustic pressure in high intensity focused ultrasound fields at clinical intensities using a novel planar Fabry-Peròt interferometer

Elly Martin[1], Edward Zhang[1], Paul Beard[1], Bradley Treeby[1]; [1]*Medical Physics and Biomedical Engineering, University College London, London, United Kingdom*

Background, Motivation and Objective

The measurement of high intensity focused ultrasound (HIFU) fields is critical in monitoring the stability of clinical ultrasound therapy systems, validating models of ultrasound propagation, and understanding these complex acoustic fields and their bioeffects. To fully characterise clinical therapeutic ultrasound fields, they must be measured at clinical levels where extremely high pressures are generated in the focal region. At present there are no suitable methods for fully mapping focused ultrasound fields under these conditions. Most currently available equipment, piezoelectric hydrophones for example, will be destroyed by the high pressures and temperatures generated at clinical levels. Extrapolating from low level measurements is possible but can introduce large errors in the magnitude and position of pressure maxima. While there is one type of fibre-optic hydrophone, based on a bare cleaved fibre tip, which is able to withstand these conditions, its high noise equivalent pressure (>0.5 MPa) renders it unsuitable for mapping regions of lower pressure. Here, a novel planar Fabry-Peròt interferometer, capable of withstanding these conditions while maintaining high signal to noise ratio was used to spatially map focused ultrasound fields at clinically relevant levels.

Statement of Contribution/Methods

The acoustic pressure field generated by a single element spherically focused ultrasound transducer driven at both 1.1 MHz and 3.3 MHz was measured using a planar Fabry-Perot interferometer placed at the surface of a temperature controlled water bath. The interferometer was formed of a glass substrate with sputtered hard dielectric (silicon oxide) mirrors and 3 μm thick spacer. The sensor had a -3dB bandwidth of 600 MHz with a noise equivalent pressure of approximately 20 kPa. The element size was 25 μm, optically defined by the spot size of the interrogating laser raster scanned over the sensor surface. To maintain the sensitivity and linearity of the device, the wavelength of the laser was tuned to the maximum gradient of the interferometer transfer function (ITF).

SATURDAY ORAL

The acoustic field was mapped over a 25 mm x 25 mm area with a 75 µm step size. Eight measurement planes were acquired over the prefocal, focal and post focal regions of the field. Each measurement plane took approximately 30 minutes to acquire. The temperature rise generated in the acoustic field was also measured by tracking the shift in the ITF over time.

Results/Discussion

Measurements were acquired at unprecedented fidelity up to 20 MPa peak positive pressure. The low pressure pre and post focal regions were mapped accurately with low noise levels. Measurements in these areas agreed well with measurements made with a PVDF needle hydrophone. High pressure measurements also compared well with simulations of the non-linear ultrasound field performed using the k-Wave Matlab toolbox. This technique represents a critical improvement in measurement capability for HIFU fields.

SATURDAY ORAL

8I - CMUTs and Signal Processing

102

Saturday, October 24, 2015, 10:30 am - 12:00 pm

Chair: **Jian Yuan**
Philips Shanghai Apex

8I-1

10:30 am   Phase Modulated Pulse Sequences for Nonlinear Imaging with CMUTs

Sarp Satir[1], Levent Degertekin[1]; *[1]Georgia Institute of Technology, USA*

Background, Motivation and Objective

The inherent nonlinearity of CMUTs presents a problem for nonlinear imaging, especially when these devices are driven with large signals to achieve the desired pressure levels. A nonlinear imaging method especially for contrast agent imaging with CMUTs utilizing phase modulated pulse sequences is presented. The method is based on the assumption that the output pressure of the CMUT can be expressed as a power series of the input voltage for both small and large signals at any DC bias level. It is shown through modeling and experiments that any number of particular harmonic components in the received signal due to CMUT nonlinearity can be suppressed using proper number of transmit firings with inter-pulse phase modulation. More importantly this can be achieved without any CMUT membrane displacement limitations.

Statement of Contribution/Methods

To verify that CMUT dynamics obey the postulated power series relationship we used an accurate large signal model. For small signal operation the pressure output is a second order function of the input voltage as expected. When the CMUT is simulated for large membrane displacements, it is observed that the power series relation still holds albeit requiring more terms than the commonly used second order approximation. As the power series relationship is validated, the phase modulated pulse sequence is implemented using an example CMUT with a collapse voltage of 40V. The proposed method is validated by experiments where pressure signals transmitted by a CMUT is measured with a hydrophone and the resulting signals from phase modulated pulse sequences are combined to quantify the suppression of CMUT nonlinearity in the received signal.

Results/Discussion

The power series obtained for an arbitrary CMUT shows that by using a 4 pulse sequence with respective phases of $0, \pi/2, \pi, 3\pi/4$, the contributions from the CMUT up to the 3rd harmonic can be eliminated. Experimental results demonstrate that even in the most dramatic large displacement case, during collapse-snapback operation, the fundamental, second and third harmonics are reduced by 55dB, 40dB and 32dB (Fig. 1), respectively using this particular 4 pulse phase modulated sequence. The results indicate that with the proposed method, CMUTs can be used for nonlinear contrast imaging effectively without compromising its output pressure level.
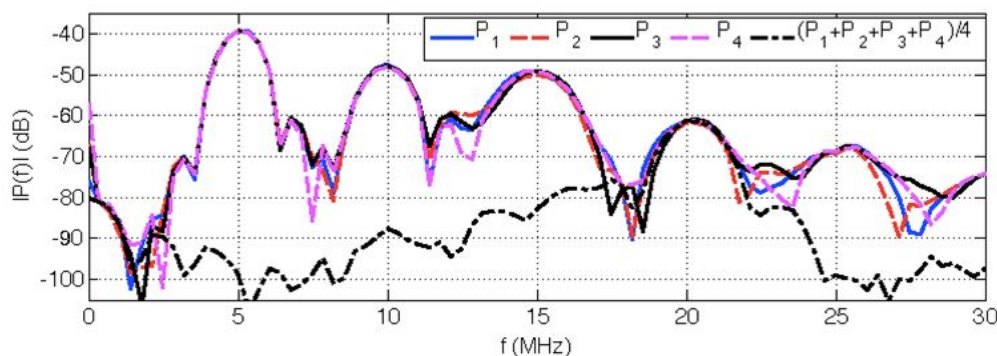
Fig. 1–(a) Measured pressure signals for $V_{DC} = 36V$, $V_{AC} = 30V$, $\varphi_1 = 0$, $\varphi_2 = \pi/2$ (b) Measured pressure signals for $V_{DC} = 36V$, $V_{AC} = 30V$, $\varphi_1 = \pi$, $\varphi_2 = 3\pi/2$ (c) Amplitude spectra of the four phase modulated pressure output signals and The sum signal $\left(p_1(t) + p_2(t) + p_3(t) + p_4(t)\right)/4$

8I-2

10:45 am   Second-Harmonic Reduction in CMUTs Using Unipolar Pulsers

Alessandro Stuart Savoia[1], Giuseppe Scaglione[1], Marco Sautto[2], Andrea Mazzanti[2], Fabio Quaglia[3], Giosuè Caliano[1]; *[1]Dipartimento di Ingegneria, Università degli Studi Roma Tre, Roma, Italy, [2]Dipartimento di Ingegneria Industriale e dell'Informazione, Università degli Studi di Pavia, Pavia, Italy, [3]STMicroelectronics, Cornaredo, Italy*

Background, Motivation and Objective

Linear behavior of ultrasonic transducers is a stringent requirement in nonlinear ultrasound imaging. In addition to linearity, high transmit pressure capability is necessary to successfully address tissue harmonic imaging. High-voltage-driven Capacitive Micromachined Ultrasonic Transducers (CMUTs) behave nonlinearly, due to the nonlinear relation between the applied voltage and the generated electrostatic force. A possible linearization approach, extensively investigated in literature, consists in applying pre-distorted analog excitation signals with a spectral content such as to compensate the harmonic distortion introduced by CMUTs. This method requires the use of high-voltage linear transmitters, limiting its possible implementation only in high-end imaging systems.

In this paper, we investigate the use of a similar approach applied to digital pulse excitation signals where the pre-distortion is achieved by acting on the amplitude (A), duty cycle (D), and slope of the rising (S_r) and falling (S_f) edges of the pulses. This kind of signals can be generated using high-voltage pulser topologies similar to those used in any current imaging system.

Statement of Contribution/Methods

For a certain operating condition, i.e. center frequency and number of cycles of the excitation signal, we generate the pre-distorted analog waveform using a synthesis method already developed and tested by us, and compute its spectrum. Then, we derive the analytical expression of the spectrum of a trapezoidal pulse with the same center

frequency as a function of the aforementioned parameters A, D, S_r, and S_f. We successively find the values of the trapezoidal pulse parameters by equating the two spectra at the fundamental and second-harmonic frequencies.

The described pulse generation method is implemented using Matlab while the large-signal behavior of an immersed CMUT is modeled using PSPICE. A set of pre-distorted trapezoidal pulses at different frequencies within the bandwidth of the modeled CMUT are generated. Simulations are carried out to assess the performance of the proposed method in terms of harmonic distortion by analyzing the CMUT transmit pressure. The results are compared with those obtainable by using pre-distorted analog waveforms and undistorted sinusoidal and square-wave signals.

The numerical results are experimentally validated by performing transmit pressure measurements with a CMUT in immersion operation driven using a high-voltage unipolar pulser with rising and falling edge slope control capability.

Results/Discussion

Simulation results show that the total suppression of the second-harmonic distortion introduced by the CMUT may be obtained using high-voltage pre-distorted trapezoidal pulses. Experimental results demonstrate a significant reduction of the second-harmonic distortion, estimated to be lower than -30 dB, resulting in good linearization for typical nonlinear imaging operation.

8I-3

11:00 am   Revised amplitude modulation for contrast-enhanced ultrasound imaging with a cMUT array.

Damien Fouan[1,2], Ayache Bouakaz[1,2]; [1]*Inserm U930, Imagerie et Cerveau, Tours, France,* [2]*Université François Rabelais de Tours, France*

Background, Motivation and Objective

Over the past 15 years, capacitive micro-machined ultrasonic transducers (cMUT) have been developed as a promising alternative to standard PZT transducer. A large bandwidth and a reduction in self-heating are among the main advantages of this high potential technology but suffers from a high intrinsic nonlinearity [1]. This behavior could lead to misclassification of tissue in ultrasound contrast-enhanced imaging. Classical sequences, such as Pulse Inversion (PI) or Amplitude Modulation (AM) are no longer suitable and the only solution seems to be the compensation of the cMUT nonlinearity by sending a pre-compensated waveform [2]. In this work, we show that an alternative sequence to amplitude modulation mode (already used with PZT arrays) can be successfully applied with a cMUT probe without any limitation due to the nonlinearity of the transmitter and without any compensation.

Statement of Contribution/Methods

Alternate Amplitude Modulation (AAM) is performed using a three-pulse sequence. A first sequence is transmitted with the odd elements alternately with a second sequence transmitted with the even elements. Then, a third sequence is transmitted with all the probe elements. The applied voltages are the same for all the elements (sequences). AAM is performed by subtracting the echoes of the third sequence from the sum of echoes of the two first sequences. The proposed approach is compared to classical contrast-enhanced sequences (PI, AM) using two equivalent probes (128 elements), one based on a cMUT technology and the other on a PZT technology. The evaluation and validation of the method is performed with an open scanner with 128 analog transmitters. Plane wave transmit (7 angles from -10° to 10°) at 3 MHz is used with acoustic amplitudes ranging from 50 to 250 kPa. In-vitro validation is performed on a linear reflector and by imaging a tissue mimicking phantom with flowing Sonovue contrast microbubbles. Contrast to Noise Ratio (CNR) and Contrast to Tissue Ratio (CTR) estimations allow a quantitative comparison.

Results/Discussion

As expected, classical sequences (AM and PI) showed a poor contrast detection when applied with a cMUT probe in comparison with the PZT probe. However, the three-pulse sequence as proposed here showed to perform equally on both cMUT and PZT probes (CTR of 34 dB and 32 dB respectively). Since no priori hypothesis on the linearity of the probe is made in the three-pulse sequence, the nonlinearity of the cMUT has no impact. In conclusion, nonlinear contrast imaging using alternate AM mode is feasible with cMUTs without a need for compensation or cancellation of the transducer nonlinearity.

[1] Oralkan et al. 2002, IEEE Trans. UFFC, Vol. 49, pp. 1596-1610.
[2] Novell et al. 2009, IEEE Trans. UFFC, Vol. 56, pp. 2733-2743.

8I-4

11:15 am   Feasibility of Interlaced Multi-Band CMUTs for Photoacoustic Imaging

Ryan Chee[1], Roger Zemp[1]; [1]*University of Alberta, Canada*

Background, Motivation and Objective

The photoacoustic signal frequency of an optical absorber depends on the absorber size. In many molecular imaging applications we are interested in imaging distributions of optical dyes or genetically-encoded reporters. Often these distributions have slowly-varying spatial profiles and will hence produce very low photoacoustic frequencies undetectable by high-frequency transducers often used to visualize microvascular networks. We propose multi-band CMUTs for multi-wavelength photoacoustic imaging to render dye concentration estimates with low resolution but high sensitivity, overlaid on high-resolution hemoglobin images.

Statement of Contribution/Methods

To demonstrate the feasibility of imaging diffuse concentrations using multi-band CMUTs, we use two targets (methylene blue-dyed 1mm floss and 100um hair) of significant size difference. Photoacoustic images were obtained at 615nm and 665nm wavelengths. A single linear multi-band CMUT (Fig 1a&b) element of interlaced 82- and 36um membranes was linearly scanned using a 3-axis motor for 99 steps with a step size of 250um to simulate a larger array. The relative absorption coefficients were found using peak image intensity of the methylene blue and hair in the 615nm and 665nm images. Spectral de-mixing was done using Matlab. The concentration image of the methylene blue obtained from the 82um devices is shown overlaid on the higher resolution concentration image of the hair obtained from the 36um devices.

Results/Discussion

Fig. 1c is a graph showing the relative peak intensity of the larger methylene blue floss over the hair for the 82um and 36um devices. It demonstrates that the low-frequency 82um devices are more sensitive to the larger-sized optical absorbers than the high-frequency 36um devices. Fig. 1d illustrates a low-frequency higher intensity image of methylene blue concentration overlaid on a high-frequency higher resolution image of the hair mimicking microvessels. Multi-band CMUTs offer a new paradigm for molecular imaging.

(a)

(b)

(c)

(d)
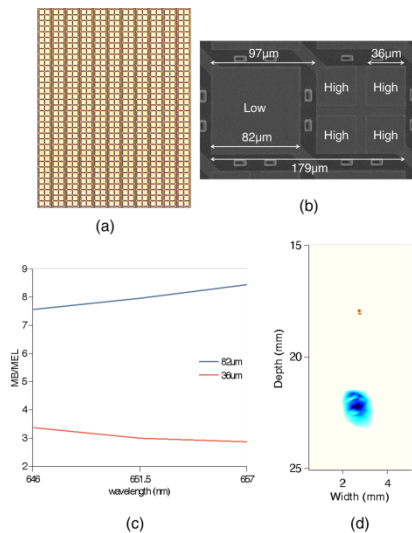
8I-5

11:30 am   Multi-frequency imaging with collapse-mode CMUT

Martin Pekar[1,2], Wendy Dittmer[1], Nenad Mihajlovic[1]; [1]*In-Body Systems, Philips Research, Eindhoven, Netherlands,* [2]*Department of Biomedical Engineering, Thorax Center, Erasmus MC, Rotterdam, Netherlands*

Background, Motivation and Objective

In a clinical examination it is beneficial to perform ultrasound imaging at multiple frequencies. This is difficult to achieve with conventional piezoelectric transducers. In this study we investigate frequency agility of a collapse-mode capacitive micromachined ultrasound transducer (CMUT) with respect to imaging.

Statement of Contribution/Methods

The collapse-mode CMUT device was at first characterized in transmission. It was found that the maximum acoustic output for every given sine-burst frequency is reached only when appropriate bias voltage is applied.

Pulse-echo (PE) measurement was used to evaluate the CMUT performance in transmission and reception. The CMUT was connected as a single element to one channel of a custom imaging system having -6 dB bandwidth of 4.8 MHz – 50.3 MHz.

Optimal bias voltage and driving pulse settings as obtained from the hydrophone and the PE measurements were used in a subsequent motion-based imaging experiment. The CMUT was connected to the same PE imaging system and moved with a motor at constant speed of 4 mm/s across a surface of a phantom. Subsequently, motion-based images at different driving pulse lengths and bias voltages were acquired.

Results/Discussion

Our CMUT exhibits a peak transmit sensitivity of 40 kPa/V at a center frequency of 11.0 MHz when a bias voltage of -120 V is applied. This center frequency is observed to further decrease or increase at the cost of the transmit sensitivity. 3 dB decrease in the transmit sensitivity occurs at a center frequency of 5.9 MHz and 15.5 MHz at bias voltage of -96 V and -135 V, respectively.

PE impulse response showed peak transmit-receive sensitivity at a center frequency of 11.6 MHz when a bias voltage of -120 V is applied. At this setting the -6 dB relative fractional bandwidth was 73 %. By modifying the bias voltage of the CMUT, the center frequency was either decreased or increased to 9.1 MHz and 12.9 MHz, at which point the transmit-receive sensitivity decreased by 6 dB and the bandwidth was 83 % and 71 %, respectively. The total pulse-echo performance was further optimized by using different pulse widths and various number of pulse cycles which allowed the center frequency to be swept from 6.7 MHz to 13.9 MHz or from 5.4 MHz to 15.6 MHz when 1 or 2 cycles of the driving pulse were employed, respectively.

Penetration depth of 19.1 mm and 10.9 mm was reached in a tissue mimicking phantom for the long (100 ns, bias voltage -90 V) and short (25 ns, bias voltage -145 V) pulse scenarios, respectively. Axial resolution at these two settings was evaluated in a PE experiment in terms of search-in-pulse length, which was measured to be 0.480 μs and 0.210 μs for the long and short pulse settings, respectively.

This study shows that a collapse-mode CMUT can operate efficiently at multiple center frequencies when the driving pulse and the bias voltage are optimized. First imaging results with a single collapse-mode CMUT operated at the center frequency of 6.7 MHz and 13.9 MHz are presented.

8I-6

11:45 am   Practical S-Sequence Aperture Coding Schemes for Volumetric Imaging with Top Orthogonal to Bottom Electrode (TOBE) Arrays

Roger Zemp[1], Tyler Harrison[1]; [1]*Electrical & Computer Engineering, University of Alberta, Edmonton, Alberta, Canada*

Background, Motivation and Objective

Recently we introduced top orthogonal to bottom electrode 2D CMUT arrays with novel bias-sensitive 3D imaging capabilities. Two imaging schemes were presented using such arrays: Scheme 1 involved transmitting on a column and receiving along all rows in parallel. Rectilinear retrospective beamforming produces a volumetric image with one-way x-focusing and one-way y-focusing. Scheme 2 involved biasing a column to effectively create dominant element sensitivity on one linear array which could then be scanned by switching the biasing pattern. Retrospective beamforming produced one-way focusing in the x-z plane, yet with 2-way (transmit-and-receive) focusing in the y-z plane. Scheme 1 has considerable practical significance due to fast imaging speeds but may be SNR-limited owing to limited transmitting area for each transmit event. Scheme 2 likewise has limited dominant element transmitting area and hence limited SNR. We introduce new aperture encoding schemes that improve SNR over Scheme 1 and 2 without any frame-rate degradation.

Statement of Contribution/Methods

To enhance Scheme 1 we fire on multiple columns simultaneously, such that the on-elements are selected from rows of a Hadamard or S-Matrix. Signals are read-out from rows simultaneously. Channel data is then subject to transmitter-decoupling by applying an inverse of the Hadamard- or S-Matrix.

To enhance Scheme 2 we bias multiple columns simultaneously instead of only 1. Column biasing patterns are chosen from rows or columns of a Hadamard or S-Matrix. When transmitting on rows, large signals are used such that even unbiased cells act as strong transmitters. However, on receive, only biased cells offer dominant sensitivity. Thus transmitting elements are effectively entire rows while receiving elements are only elements along rows which are biased. After collecting the complete set of data associated with all S-sequence biasing patterns, data is decoded and subject to retrospective beamforming.

Field II simulations demonstrate ideal capabilities. The schemes are also practically implemented using double-SOI wafer-bonded CMUTs connected via a pre-amp board to a programmable Verasonic imaging platform.

Results/Discussion

Aperture-encoded Scheme 1 decoded data is then subject to rectilinear beamforming to give resolution similar to Scheme 1 and with the same frame-rate (requiring N transmit events) but with enhanced SNR. Even this simple imaging scheme is demonstrated to have superior resolution and SNR compared to Explososcan 3D imaging for a given channel count. Pulse-width modulation on transmit and signal-weighting on receive is used to implement electronic apodization to reduce edge-wave artifacts.

Aperture-encoded Scheme 2 data is also decoded and beamformed to produce images offering resolution similar to Scheme 2, and with the same frame-rate (requiring N^2 transmit events), but with enhanced SNR.

1J - MBF: 3D Imaging and Flow Simulations

201AF

Saturday, October 24, 2015, 01:00 pm - 02:30 pm

Chair: **Alfred C. H. Yu**
University of Hong Kong

1J-1 _____

1:00 pm **Patient-specific flow simulation of the left ventricle from 4D echocardiography – feasibility and robustness evaluation**

David Larsson[1], Jeannette H Spühler[2], Tim Nordenfur[1], Johan Hoffman[2], Massimiliano Colarieti-Tosti[1], Hang Gao[3], Matilda Larsson[1]; *[1]Medical Engineering, KTH Royal Institute of Technology, Stockholm, Sweden, [2]Computational Technology Laboratory, High Performance Computing and Visualization, KTH Royal Institute of Technology, Stockholm, Sweden, [3]Lab on Cardiovascular Imaging and Dynamics, KU Leuven - University of Leuven, Leuven, Belgium*

Background, Motivation and Objective

For cardiovascular diagnostics, anatomically accurate *in-silico* models in combination with complex computational fluid dynamics-solvers have given insight into important regional blood flow pattern. However, so far most models have been based on either generic geometries or high-spatial resolution modalities such as MRI or CT, unable to capture temporally transient flows. Models based on ultrasonic acquisition would then be advisable. Therefore, the aim of this study is to present a pathway from routine 4D echocardiography to a patient-specific left ventricular flow simulation, evaluating its feasibility and robustness.

Statement of Contribution/Methods

4D echocardiography from a single healthy subject was acquired using a GE Vivid E9 (4VD, 45 fps, 1.7MHz/3.3MHz). The endocardial surface was segmented 3 times using EchoPac 4D Auto-LVQ by a trained cardiologist (Fig 1a), with mitral and aortic valve regions additionally identified. A tetrahedral volume mesh was generated from the segmented volume and imported into Unicorn of the FEniCS project, to solve the incompressible Navier-Stokes equations of the simulated flow (1b). Spherical regions of 5 mm spread between apex and base were used to assess the calculated flow velocities, evaluated with respect to repeated segmentation and mitral and aortic valve positioning. Flow velocities over the ventricular valves were compared with clinical Doppler measurements and, as a proof-of-concept, ultrasound images were simulated using COLE (KU Leuven) on point scatters moving in the simulated velocity field.

Results/Discussion

The evaluated regional mean velocities did not change considerably with changing input parameters (max. rel. difference ±25% at basal (±0.6m/s) and ±24% at apical (±0.05m/s) position with repeated segmentation), indicating the robustness of the proposed method. Showing similar behavior to clinical Doppler measurements (1c), the technique serves as a promising tool for patient-specific flow modelling based solely on 4D ultrasound images. Additionally, the ability of simulating ultrasound images from the calculated data (1d) illustrates promising research and clinical usability features in the future. With the present pilot study performed on a single subject, a large-scale validation of the proposed technique will be performed, investigating the general applicability of the method.
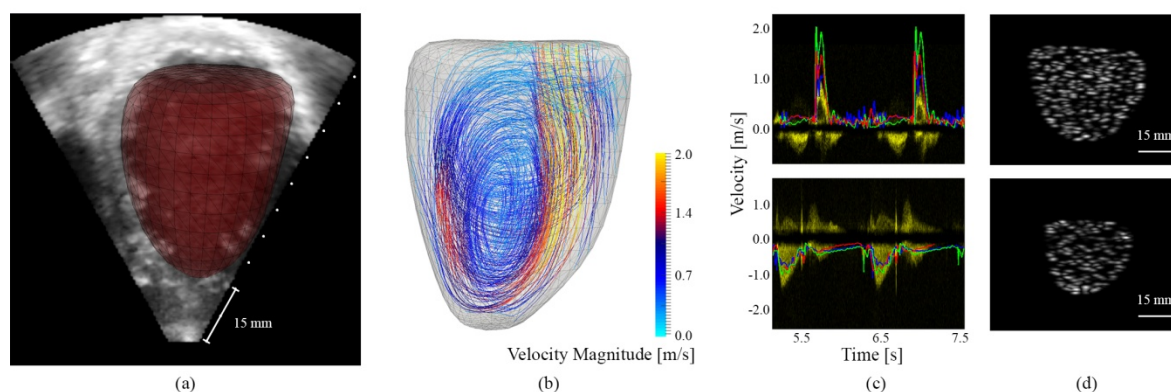
Figure 1: Illustration of presented patient-specific pathway, from left to right: (a) Segmented left ventricle from 4D echocardiography, (b) Simulated blood flow (late diastole), (c) Comparison with clinical Doppler at mitral (upper) and aortic valve (lower), presented for the three segmentations (red, blue, green) and, (d) Simulated Ultrasound 2D long-axis images from the simulated flow at end diastole (upper) and end systole (lower).

1J-2 _____

1:15 pm **Three-dimensional intra-cardiac flow estimation using multi-planar echo particle image velocimetry: A feasibility study**

Hang Gao[1], Qiong He[2], Jianwen Luo[2], Jan D'hooge[1]; *[1]Lab. on Cardiovascular Imaging & Dynamics, Dept. of Cardiovascular Sciences, KU Leuven, Belgium, [2]Center for Bio-Medical Imaging Research, Dept. of Biomedical Engineering, Tsinghua University, China, People's Republic of*

Background, Motivation and Objective

Estimating three-dimensional (3D) intra-cardiac vector flow by volumetric echocardiography is expected to be of benefit but remains technically challenging as blood within the left ventricle can move at relatively high velocities (e.g. 1 m/s) while acquisition rates remain moderate (~25-30 Hz). In order to overcome this limitation, we propose to estimate the 3D left ventricular (LV) flow field by reconstructing it from multiple 2D acquisitions at high frame rate. The aim of this study was to test this approach in silico.

Statement of Contribution/Methods

A dynamic LV volume change profile and a typical inflow velocity profile together with a 3D anatomical model of the left ventricle were used to build a realistic computational fluid dynamics (CFD) vector flow field (Fluent 12.1, ANSYS). Multiple two-dimensional (2D) B-mode sequences (opening angle 50 degrees, frame rate 113 Hz) were simulated from an apical position by rotating the probe (4.5 MHz, bandwidth 65%) around its axis (in steps of 10 degrees) between subsequent heartbeats. Hereto, virtual contrast bubbles were placed in the 3D flow field and their instantaneous position used as input to a fast ultrasound simulator (COLE). To estimate the 2D flow fields in the acquisition planes, a previously developed 2D speckle tracking approach using a dynamic kernel size (initial kernel 0.6×1.7 mm2 growing by 0.18×0.18 mm2; search

region 4.3×4.0 mm2, axial/lateral overlap 40%/90%). The resulting planar flow velocity vectors were subsequently reconstructed in 3D and regularized using the modified 3D Navier-Stokes equations of an incompressible Newtonian fluid. To compensate for the loss of high velocities in the speckle tracking process, the diastolic inflow velocities were also introduced in the regularization approach using the hybrid PISO-SIMPLE (PIMPLE) algorithm.

Results/Discussion

The figure shows one example of the estimated 3D flow field during diastasis (Regu) in a short and long-axis plane together with the CFD reference (Truth), the multi-planar speckle tracking velocity field (Track) and the point-wise velocity vector errors (Error). The averaged point-wise errors in velocity magnitude normalized to the maximum reference values were 21.32±3.32% during E wave, 17.15±4.03% during A wave and 8.49±1.1% during ejection. The experimental validation of this approach is ongoing.
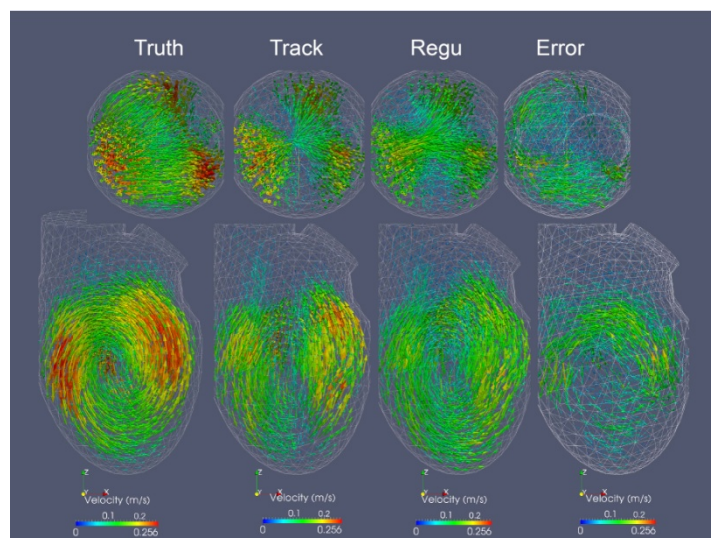
1J-3

1:30 pm **An in-vitro and numerical study of ultrafast vector flow imaging in the neonatal heart.**

Joris Van Cauwenberge[1], Solveig Fadnes[2], Ingvild Kinn Ekroll[2,3], Lasse Løvstakken[2], Jan Vierendeels[4], Patrick Segers[1], Abigail Swillens[1]; *[1]IBiTech - bioMMeda, Ghent University, iMinds Medical IT, Gent, Belgium, [2]Department of Circulation and Medical Imaging, Norwegian University of Science and Technology, Trondheim, Norway, [3]St Olav's University Hospital, Trondheim, Norway, [4]Department of Flow, heat and combustion mechanics, Ghent University, Gent, Belgium*

Background, Motivation and Objective

Ultrafast and 2D intracardiac blood flow imaging could enhance the diagnosis of congenital heart disorders in newborn patients since current clinical ultrasound modalities are hampered by aliasing, beam-to-flow angle dependency and low frame rates. Hence, we investigated, using in-vitro data and multiphysics simulations, how 2D speckle tracking (ST) might overcome these limitations when performed in a high frame rate setting realized by diverging waves.

Statement of Contribution/Methods

Simulations: Synthetic images were acquired with the Field II software, by moving point scatterers according to complex 3D intraventricular flow patterns. Such flow patterns were obtained from computational fluid dynamics (CFD) performed in a generic neonatal left ventricular model (fig. 1A). A 1D cardiac phased array probe (6 MHz) was implemented and diverging waves were emitted with an opening angle of 60° at a PRF of 9 kHz. Channel data were received on 128 lines in parallel (SNR of 20 dB), and were subsequently IQ-demodulated, beamformed and clutter filtered (4th order polynomial regression filter) before ST-analysis. ST-performance and potential artifacts were assessed by comparison to the CFD ground-truth.

In-vitro: The numerical findings observed during diastolic inflow were validated with ST-data obtained in a jet-flow phantom (fig. 1B) using an open research scanner (Verasonics Vantage platform). A similar flow magnitude as observed during the diastolic phase of the simulations (0.8-1 m/s) was assured.

Results/Discussion

Full spatial performance analysis showed a median deviation in magnitude and phase of respectively 15.6% and 7.8° at the end of the diastolic early-wave, still clearly tracking the intraventricular vortex (fig. 1C compared to 1D). Decreased performance was noticed at the start of diastole (deviations of 62.5% and 52°) due to the very low flow. The most prominent artifact is depicted in fig. 1D and was noticed during the diastolic early wave. The incoming jet portrays apparent lateral flow at the edges of the jet in zones of high axial velocity gradients. In-vitro tests with a similar jet flow clearly displayed the same artifact at the edges of the jet (fig. 1E).

Despite this artifact, we demonstrated that high frame rate vector flow imaging with diverging waves has an acceptable to very reliable performance in the neonatal heart depending on the cardiac phase.

A: CFD setup

B: In-vitro setup

C: CFD Flow

D: ST Flow

E: In-vitro result
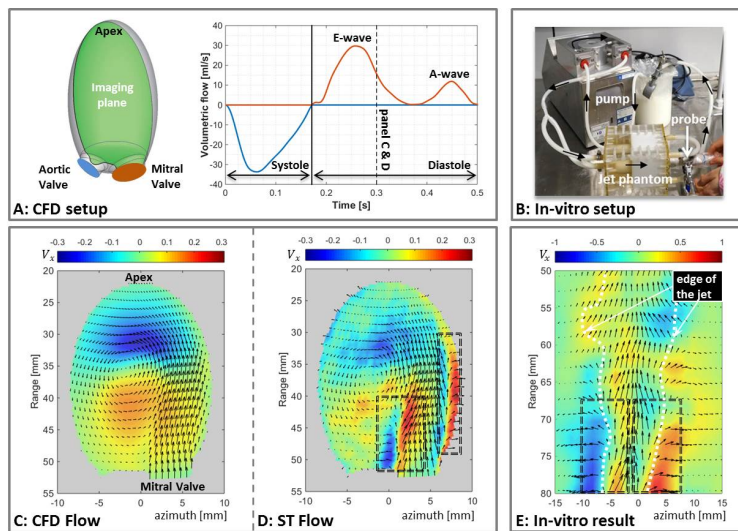
1J-4

1:45 pm   Reconstruction of 3D vector flow fields from sparse measurements using B-spline regularization

Solveig Fadnes[1], Alberto Gomez[2], Morten S Wigen[1], Jakob Høgenes[1], Joris van Cauwenberge[3], Patrick Segers[3], Abigail Swillens[3], **Lasse Lovstakken[1]**; [1]Department of Circulation and Medical Imaging, Norwegian University of Science and Technology, TRONDHEIM, Norway, [2]Department of Biomedical Engineering, King's College London, United Kingdom, [3]Ghent University, Belgium

Background, Motivation and Objective

Three-dimensional intracardiac blood velocities contain valuable clinical information but are currently of limited availability due to the angle-dependency of Doppler methods. This limitation can be overcome using broad transmit beams for high-frame-rate imaging and 3D blood speckle tracking (ST) for estimating 3D angle-independent blood velocities. However, processing time for 3D ST is substantial, and in the pursuit of a real-time modality our aim in this work is to investigate the possibility of using a sparse set of ST measurements, while reconstructing sufficiently accurate and dense 3D vector field based on a fast B-spline interpolation framework.

Statement of Contribution/Methods

A B-spline least-squares fitting approach was used to smooth noisy data and to reconstruct a dense 3D velocity field from sparse measurements. Regularization was introduced by penalizing non-zero divergence following incompressible flow assumptions to increase accuracy in presence of noise, outliers, and dropouts due to clutter filtering. A CFD simulation model of neonatal ventricular flow was used as input to a fast ultrasound simulation tool (FUSK). Sparse measurement grids for ST were used with and without the B-spline framework and compared with the CFD ground truth in terms of RMS error over the cardiac cycle for varying measurement grids, SNR, and B-spline grid spacing and amount of regularization (weighted 0 to 1). The reference ST measurements were spatially smoothed $2 \times 2 \times 2 mm^3$.

Results/Discussion

The study showed that a down-sampling factor of 15 ($8 \times 8 \times 22 = 1408$ measurements) compared to the original resolution in the image was sufficient to reproduce the 3D flow field with reasonable accuracy over the cardiac cycle, which significantly reduced processing time. For the flow fields given, a coarse B-spline grid (e.g. $4 \times 4 \times 10 = 160$ nodes) could be used with smoothing benefits due to the added regularization constraint (lambda = 0.3). In the Figure, the 3D model with ground truth, sparse ST measurements, B-spline reconstruction, and RMS error plots are shown left to right. The RMS error was reduced for the regularized measurements throughout the cardiac cycle for SNRs of 15 and 5 dB. Accuracy was particularly improved for regions of low blood velocities partly affected by the clutter filter. Further in vivo studies will reveal the potential of this method in a clinical setting.

Ground truth   ST measurements   B-spline reconstruction   Root-mean-square error

1 cm
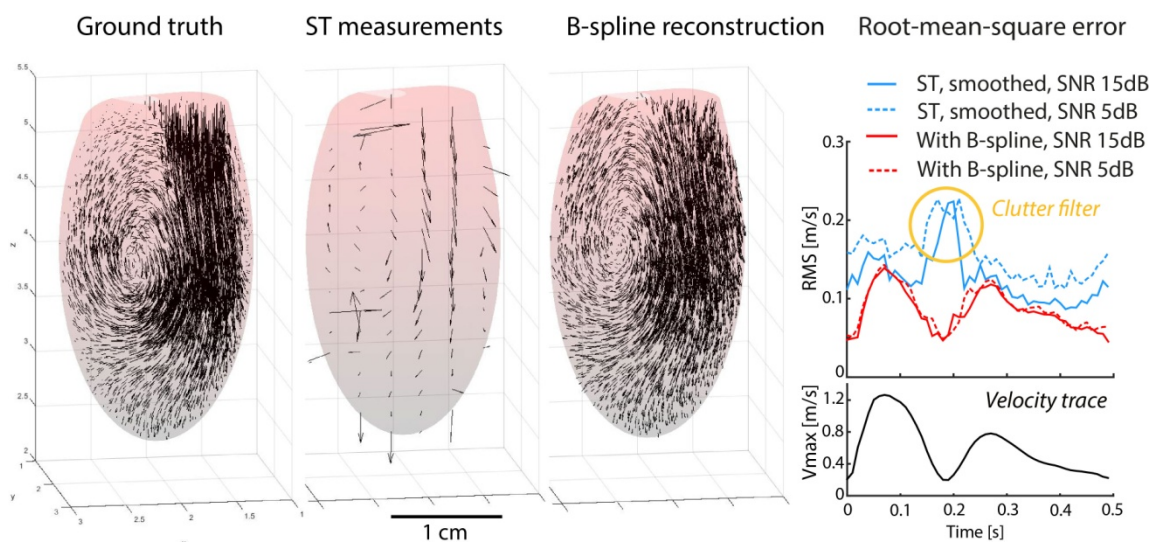
2:00 pm *In vivo* **3-D Vector Flow Estimation with Continuous Data**

Simon Holbek[1], Michael Johannes Pihl[1], Caroline Ewertsen[2], Michael Bachmann Nielsen[2], Jørgen Arendt Jensen[1]; *[1]Department of Electrical Engineering, Technical University of Denmark, Lyngby, Denmark, [2]Department of Radiology, Copenhagen University Hospital, Copenhagen, Denmark*

Background, Motivation and Objective

The cardiovascular blood flow is very complex as it propagates in all three dimensions, where short-lived vortices can arise and vanish within 100-200 ms. Thus, to provide the true dynamics of the blood flow, 3-D vector flow imaging at a high frame rate is a necessity. However, current methods for velocity estimations are restricted to 1-D or 2-D methods. To solve these problems, a method for estimating 3-D vector flow *in vivo* at 2100 fps is presented.

Statement of Contribution/Methods

An interleaved sequence was designed where the time between flow emissions along the same direction was the same throughout the data acquisition, thereby providing continuous data. At a PRF of 12.6 kHz, intensities and MI were measured for the sequence to ensure compliance with current FDA regulations. The experimental ultrasound scanner SARUS was used along with a Vermon 3.5 MHz, 32x32 element 2-D phased array transducer. A transverse scan on the common carotid artery of a healthy 27-year old female was performed by an experienced radiologist and data for three heart cycles were acquired. Data were processed off-line on a Linux cluster to estimate 3-D vector flow using the Transverse Oscillation method. The results were compared with spectral Doppler measurements obtained with a BK Medical Pro Focus scanner.

Results/Discussion

Velocity estimates from three recorded heart cycles showed peak out-of-plane velocities (v_x) of 83 cm/s, 87 cm/s and 90 cm/s in agreement with the 92 cm/s found with spectral Doppler. The figure shows the 3-D vector flow averaged over the three heart cycles at end-diastole (A) and at peak-systole (B). This shows that both slow and fast flow can be detected with the presented method. Mean flow rate, based on the out-of-plane velocity component v_x and the cross-sectional vessel area was 257±15 ml/min. In the literature the corresponding flow rate found with a 1-D technique for a healthy person is 334±103 ml/min [1]. These results show that accurate 3-D vector flow at a high frame rate of 2100 fps can be obtained from which the true dynamics of the blood flow can be examined. Furthermore, the presented method reduces operator dependency for peak velocity and flow rate estimations, thereby increasing measurement accuracy and consistency.

[1] P. Likittanasombut *et al* , Journal of Neuroimaging, vol. 16, 2006.
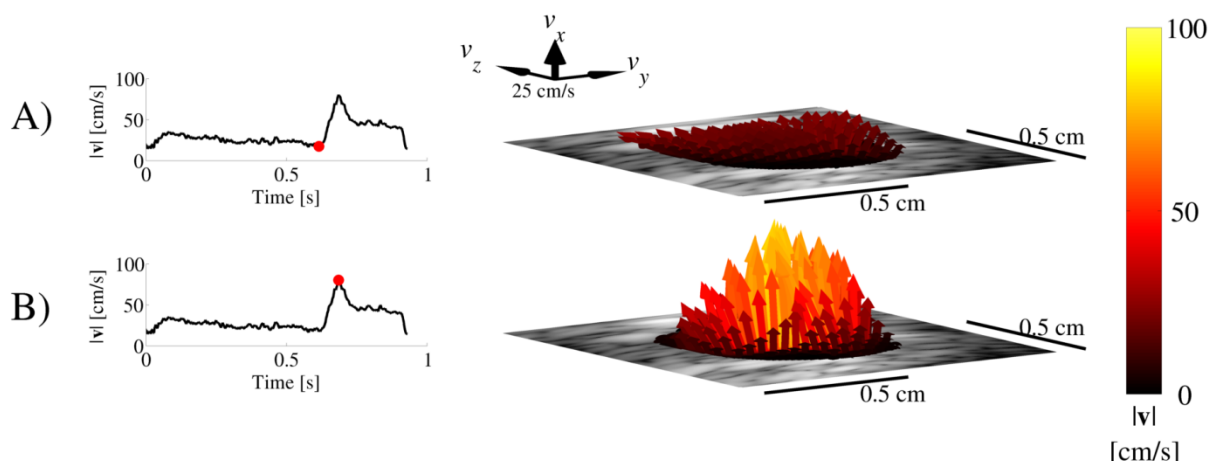
2:15 pm **Improved quality of freehand 3-D ultrasound color flow imaging by multi-angle compounding**

Daniel Høyer Iversen[1,2], Frank Lindseth[3,4], Geirmund Unsgaard[5], Hans Torp[1], Lasse Lovstakken[1]; *[1]Department of Circulation and Medical Imaging, Norwegian University of Science and Technology, Trondheim, Norway, [2]St.Olavs University Hospital, Trondheim, Norway, [3]Department of Computer and Information Science, Norwegian University of Science and Technology, Trondheim, Norway, [4]Department of Medical Technology, Sintef, Trondheim, Norway, [5]Department of Neurosurgery, St.Olavs University Hospital, Trondheim, Norway*

Background, Motivation and Objective

3-D imaging of blood flow based on 2-D ultrasound scanning and position sensor information can be used to portray clinical information not currently available in vascular and peripheral imaging. For instance, 3-D intraoperative ultrasound flow imaging has proven useful in this respect to identify and avoid damage to important vessels during surgery. However, due to Doppler angle-dependencies and complexity of the vascular architecture, the generated 3-D image of blood vessels often have dropouts in the vessel structure.

Statement of Contribution/Methods

In this work we aim to reduce dropouts in the 3-D blood flow images by combining 2-D flow images with different transmit angles. The compounded 2-D images are further reconstructed to a 3-D flow image based on information from an accurate position sensor system.

To validate the method, an *in vitro* model was constructed to mimic a small blood vessel. For the *in vitro* trials the method was implemented on an Ultrasonix MDP research ultrasound scanner for real-time processing of the data.

We further evaluated the potential of the approach in the intraoperative context of neurovascular surgery, where both the presence of blood flow and the flow direction and velocity are of interest. For *in vivo* trials a clinical approved high-end scanner was used, and the data were processed offline.

Results/Discussion

The *in vitro* trials showed promising results. The localization of the the dropout is shown for three different transmit angles in Fig. 1A-C, and by combining these frames the dropout will be removed.

An arteriovenous malformation (AVM) is an abnormal connection between the arteries and veins in the brain, bypassing the capillary vessel network. The 3-D volume of the AVM, shown in Fig. 1D, had a very complex structure. The red-colored volume is the result without compounding, and the yellow-colored volume shows the extra information obtained by compounding of three different transmit angles. As can be observed, compounding significantly improves the final 3-D volume. At point I in Fig. 1 one of the smaller feeding vessels is in fact only visible after compounding of the different transmit angles. The dropout marked with II in Fig. 1D was identified as a blood

vessel going out of the 2-D plane. The presented method is limited to reduce dropouts in the azimuth plane. By doing two acquisitions in orthogonal directions the number of dropouts can be reduced even more.
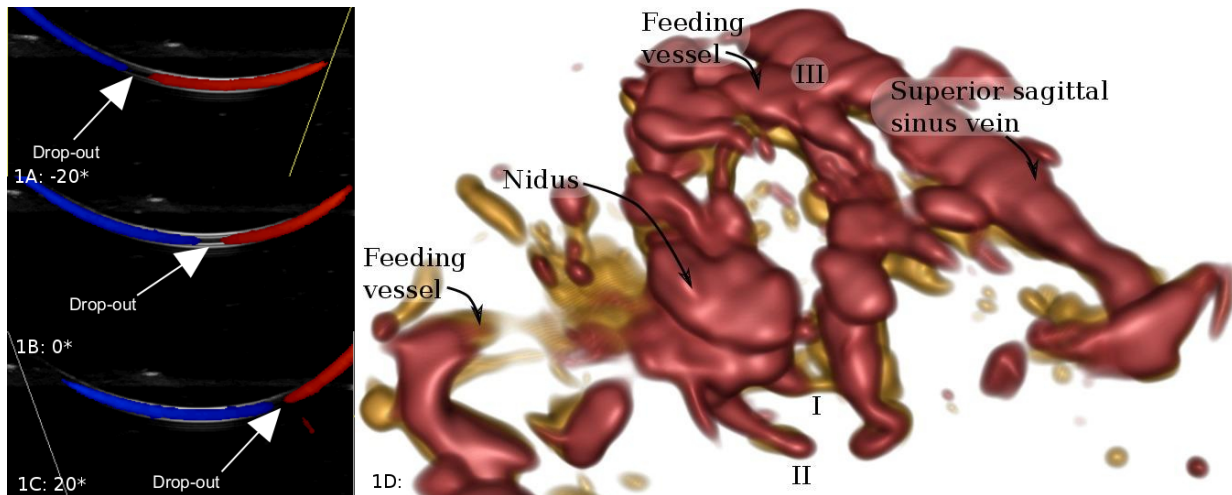
2J - MPA: Photoacoustic Imaging and Reconstruction

VIP

Saturday, October 24, 2015, 01:00 pm - 02:30 pm

Chair: **Michael Kolios**
Ryerson University

2J-1

1:00 pm   Photoacoustic Clutter Reduction using Plane Wave Ultrasound and a Linear Scatter Estimation Approach
Hans-Martin Schwab[1], Martin F. Beckmann[1], Georg Schmitz[1]; *[1]Chair for Medical Engineering, Ruhr-Universität Bochum, Bochum, NRW, Germany*

Background, Motivation and Objective

In clinical photoacoustic imaging, strong light absorption in the skin and the resulting acoustic backscatter from inside the tissue are a major challenge. In the reconstructed image, these reflections, referred to as clutter, can hardly be distinguished from actual photoacoustic sources. It has been shown that especially in setups, where the strong skin absorption is within the field of view, clutter amplitudes are very strong. In this contribution, we focus on such setups with all absorbers and scatterers inside the imaging plane. Our approach uses additional plane wave ultrasound measurements from various angles that are processed according to linear scatter theory in order to approximate the reflections in the photoacoustic measurement. Using this information, the corresponding artifacts can be reduced.

Statement of Contribution/Methods

We assume the measured photoacoustic wave PM to be a superposition of a desired photoacoustic wave PH generated in an acoustically homogeneous medium and an unwanted clutter wave PC, which is generated by PH and scattered once at the acoustic inhomogeneities. By applying a plane wave decomposition, PC can be expressed as a function of PH and a superposition of plane wave ultrasound measurements from various angles. This relation could be used for a direct inversion approach yielding PH. However, we use a computationally less demanding approximation, which works well in the practically relevant case when the strongest signals in the image reconstructed from PM are photoacoustic sources. By this, we are able to estimate PC and reconstruct an image that shows only the reflected clutter. Subtracting this image from the original reconstruction of PM returns a clutter compensated image with enhanced photoacoustic contrast.

Results/Discussion

In a verification setup based on simulations, a mean-squared-error of the reconstruction was calculated using a simulation in a homogeneous medium for reference. By applying the clutter reduction method, the mean-squared-error was decreased by 11 dB. Additionally, experimental data was acquired using a handheld photoacoustic diode laser prototype (FULLPHASE). After clutter reduction, the contrast between a photoacoustic source and a clutter artifact was increased by 4.4 dB. The algorithm can be parallelized in the frequency domain and thus is a good candidate for real-time clutter reduction.
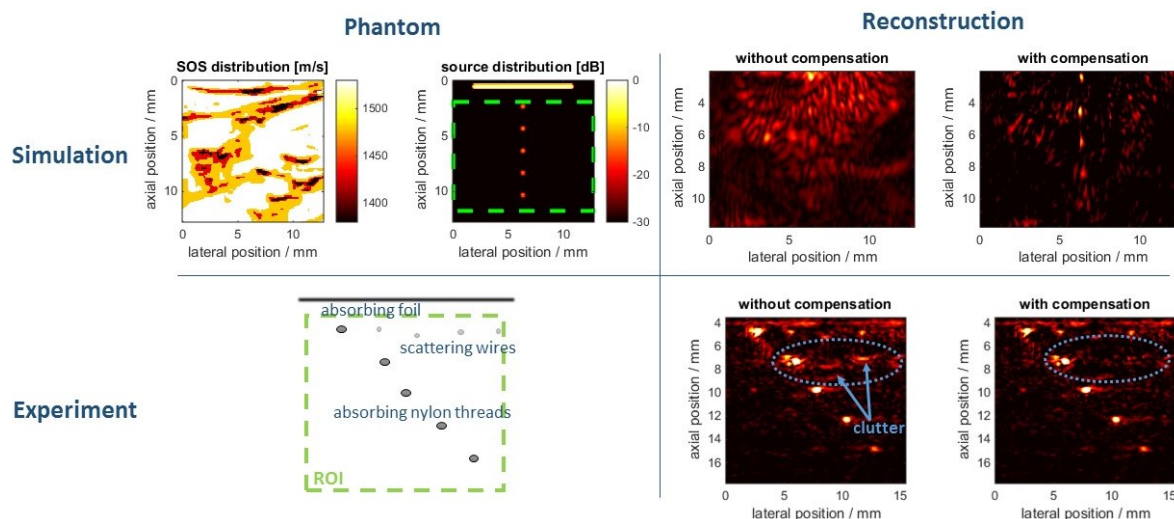
2J-2

1:15 pm   Volumetric optoacoustic and pulse echo imaging by elaborating a weigthed synthetic aperture technique
Mohammad Azizian Kalkhoran[1], François Varray[1], Didier VRAY[1]; *[1]Université de Lyon, CREATIS ; CNRS UMR5220 ; Inserm U1044 ; INSA-Lyon ; Université Lyon 1, France., Villeurbanne, France*

Background, Motivation and Objective

Integrating the optoacoustic (OA) and pulse-echo (PE) ultrasound images is essential to characterize the optical and acoustic properties of the tissue and lesion. The coupling is optimum when the transducer design accommodates the laser beam inherently, such as annular array. Yet, this synergistic approach suffers from the low depth resolution, relatively high level of side lobe, off axis contributions and phase distortion (S.Park et al. 2008). Indeed, it is challenging to tackle all of these elements simultaneously. A weighted dynamic focusing based reconstruction technique namely, weighted synthetic aperture (WSA), has been developed to address the aforementioned defects. In this work, we probe the efficiency of WSA method in 3D reconstruction of simulated phantom.

Statement of Contribution/Methods

In order to provide a 3D image of the medium in both OA and PE modes, a virtual annular array with inner diameter of 1cm is designed. The proposed array is composed of 64 transceiver elements with the central frequency of 3 MHz, radially arranged surrounding the laser beam. We elaborate WSA to estimate the spatial location, size, acoustic reflectivity function and optical absorption coefficient of the insonified/illuminated simulated targets for both imaging modalities. The phase distortion introduced by the interference between received acoustic waves is addressed with an adaptive weighting factor that combines coherence factor (CF), phase coherence factor (PCF) (Camacho et al. 2009) and spatial impulse response (SIR).

Results/Discussion

In this study, WSA performance is validated for enhancing the dynamic ratio and modulate the grating lobe using numerical phantom. A faster volumetric PE imaging is achieved due to low number of elements, but this property introduces the orientation based artifacts in PA images since the detecting surface is smaller than the physical aperture. Quantitative evaluation of simulated images is performed to establish the advantages of weighting factor. At the depth of 2.5 cm the main lobe width (-6dB) is improved by a factor of ~1.6 and a dynamic range up to 60 dB in PE is achieved. The side lobe is also suppressed by ~24 dB. As presented in the figure, our simulation results demonstrate that incorporating SIR into the weighting factor ensures the isotropic sensitivity while CF and PCF are suppressing the artifacts for both OA and PE images.
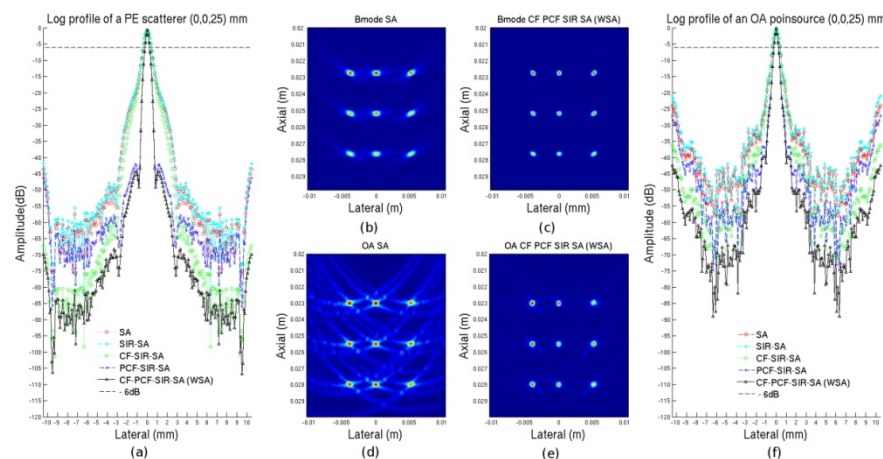
Figure 1. (a) Lateral profile of an individual PE scatterer located at the center of the transducer (1cm dia.) at 26 mm depth, (b) Original PE Bmode Image, (c) processed PE image (WSA), (d) Original OA Image, (e) processed OA image (WSA), (f) Lateral profile of an individual OA point source located at the center of the transducer at 26 mm depth.

2J-3 _____

1:30 pm   Differential phase photoacoustic imaging for high-resolution position sensing

Sophinese Iskander-Rizk[1], Pieter Kruizinga[1], Antonius FW Van der Steen[1,2], Gijs Van Soest[1]; *[1]Thorax center, Erasmus MC, Rotterdam, Netherlands, [2]Delft University of Technology, Delft, Netherlands*

Background, Motivation and Objective

Analysis of the phase difference between ultrasound signals received by pairs of transducer elements yields a robust estimate of lateral and axial displacements between frames [1]. This technique has been used to estimate motion with submicron resolution. In this study, we apply this principle to distinguishing two closely spaced photoacoustic (PA) sources with spectral (optical) contrast. If the separation between two sources is smaller than the point spread function (PSF) width of the imaging system, they will appear as a single object at different wavelengths. The RF phase difference acquired at two spectral acquisitions provides the means to localize multiple sources below the resolution limit of the system.

Statement of Contribution/Methods

We chose two imaging wavelengths that maximize absorption contrast between pink and green cotton threads of approximately 270 µm diameter, laterally separated by roughly 360 µm, which is below the system resolution. We extracted the PA signal delays, by taking the difference in phase, between the RF data sets obtained at those two wavelengths for all channels. Every pair of channels provides a unique estimate of the distance between the two absorbers; we used the median of all estimates to measure this distance. A pilot experiment was performed to prove the concept. An ultrasound machine (SonixTouch with SonixDAQ, Ultrasonix medical corporation) recorded the signals received by a phased array transducer (SA4-2/24, 2-4 MHz -6dB bandwidth, 254µm pitch). A tunable laser (Vibrant B-355II, Opotek) illuminated the test object with 5 ns pulses at 538 nm and 688 nm.

Results/Discussion

B-mode PA imaging, with a lateral PSF width of 800 µm, does not resolve the two absorbers (Fig 1a), but the slope in the phase difference between the two PA signals shows the presence of two nearby absorbers that are laterally separated (Fig 1b). In Figure 1c, the calculated distance between the sources is represented by arrows, pointing out a green absorber located to the left of the pink absorber, at a distance of ~350 µm.. Source size and relative PA signal strength at the two imaging wavelengths also affects the phase which may influence the position estimate. Applied to biological systems, this technique could improve imaging of microvasculature by e.g. resolving arteriole/venule pairs.
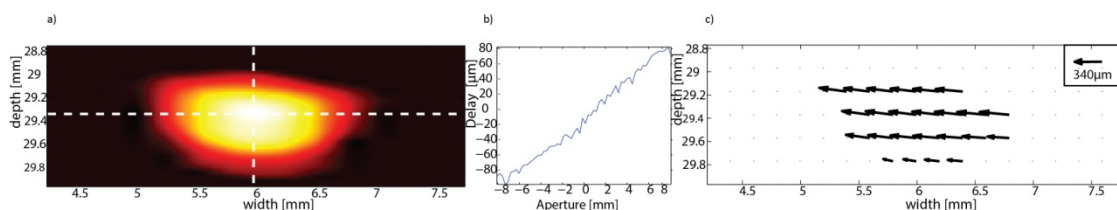
Figure 1.
a) Photoacoustic signal at 538nm from two ~270µm threads separated by ~360µm.
b) Delay in µm for the pixel at the intersection in a). The delays are obtained by calculating the difference in phase between two RF photoacoustic signals (two wavelengths) . The phase difference is delayed and not summed for each individual pixel , giving a delay for each aperture point.
c) Unresolved absorber relative position. Each arrow represents the absorber's true pixel position with respect to the main absorber (the one giving stronger PA signal).

References
[1] Kruizinga, Pieter, et al. "High frame rate ultrasound displacement vector imaging." IEEE Ultrasonics Symposium (IUS) , 2014

2J-4

1:45 pm   Photoacoustic properties of plasmonic-nanoparticle coated microbubbles

Adam Dixon[1], Song Hu[1], Alexander Klibanov[1], John Hossack[1]; [1]*Biomedical Engineering, University of Virginia, Charlottesville, Virginia, USA*

Background, Motivation and Objective

We present the design of a multimodality contrast agent for photoacoustic and ultrasound imaging comprising microbubbles coated with optically absorbing gold nanorods (AuMBs). We hypothesized that coupling nanorods to the microbubble shell would drive thermal expansion of the microbubble's gaseous core and result in an amplified photoacoustic emission following excitation by 5 nanosecond pulsed laser irradiation (λ=750 nm). Results of both in vitro and in vivo ultrasound/photoacoustic dual-modality imaging are presented.

Statement of Contribution/Methods

Gold nanorods were covalently attached to the microbubble shell using a gold-thiol bond. The behavior of single AuMBs following excitation by a single nanosecond-duration laser pulse was characterized by high-speed video microscopy, analysis of the photoacoustic emission, and finite element numerical modeling.

Results/Discussion

We identified two-distinct AuMB responses to pulsed laser excitation. At low laser fluence (below 5 mJ/cm2), microbubble wall motion was not detectable via high speed microscopy and photoacoustic emissions were relatively weak. At higher laser fluence, the microbubble diameter expanded by several hundred nanometers and photoacoustic emissions were over 10-fold greater than photoacoustic emissions from comparable concentrations of freely dispersed gold nanorods. Rapid microbubble expansion was hypothesized to result from water vapor formation at the gold nanorod-water interface. Thermal modeling of the gold nanorod/water/microbubble system confirmed that temperatures sufficient for water vaporization were reached at the nanorod surface (above 600 K). Finally, we demonstrated 9 dB photoacoustic contrast enhancement derived from the presence of AuMBs in the murine kidney.

(a): Geometry and results of finite-element simulations of heat transfer from a single gold nanorod to the microbubble gas core. Note temperatures rise above the critical point of water. (b) Top: temperature of the gas core. Bottom: radial oscillations of the microbubble.

2J-5

2:00 pm   Ratiometric Photoacoustic Imaging of Acidic pH

Richard Bouchard[1], Samit Guha[2], Trevor Mitcham[1], Gillian Shaw[2], Bradley Smith[2]; [1]*Imaging Physics, University of Texas MD Anderson Cancer Center, USA*, [2]*Department of Chemistry and Biochemistry, University of Notre Dame, USA*

Background, Motivation and Objective

As a result of the Warburg effect, dysregulated cellular pH is considered an emerging hallmark of cancer. Thus, The ability to noninvasively probe acidity at a cellular level could prove valuable in the early detection of cancer and sensing of cellular dynamics (e.g., endocytosis) given that cancer cells are known to have a significantly higher intracellular than extracellular pH. To this end, we have developed a biocompatible pH-sensitive dye that is able to noninvasively measure cellular acidity through ratiometric analysis of multi-wavelength NIR photoacoustic (PA) imaging data. We demonstrate in vitro feasibility of ratiometric PA imaging of acidic pH of this novel liposome-encapsulated dye.

Statement of Contribution/Methods

The imaging probe was formulated with a croconaine dye that was trapped within a tetralactam marocycle, generating an interlocked croconaine roxtaxane (CrocRot; Fig. a). This construct was then encapsulated within a biocompatible liposome membrane (CrocRot-SL). Optical absorption characterization of the probe was achieved with a PerkinElmer Lambda-25 spectrometer at pH 2.0-7.4 (Fig. b). PA spectral scans (Fig. c) and images were acquired using phantoms consisting of narrow vinyl tubes suspended in 0.7% milk fat; phantoms contained solutions of CrocRot-SL in buffer at pH 7.4 or pH 5.0 (concentration ~15 µM). PA imaging was performed on a Vevo LAZR imaging system (680-970 nm). Ratiometric PA images (pH 5.0 and 7.4; Fig. d) were generated by applying a noise-elimination threshold to each single-wavelength image and then dividing pixel-wise an 812 nm thresholded image by a 690 nm thresholded image.

Results/Discussion

Based on its optical absorption spectra, the CrocRot-SL probe presents two local absorption maxima, the amplitudes of which depend on environmental pH. Multi-wavelength PA imaging results present a similar phenomenon, which permits ratiometric PA-based estimation at the aforementioned absorption peaks to obtain a quantitative estimate of acidity (Fig. d). Such a probe coupled with multi-wavelength PA imaging in the NIR range allows for robust and dynamic/reversible (unlike insertion-peptide-based probes) estimates of local pH to provide a potentially diagnostic microenvironment biomarker, which avoids problems due to the heterogeneity of protein biomarkers and allows for exciting therapy-monitoring opportunities.
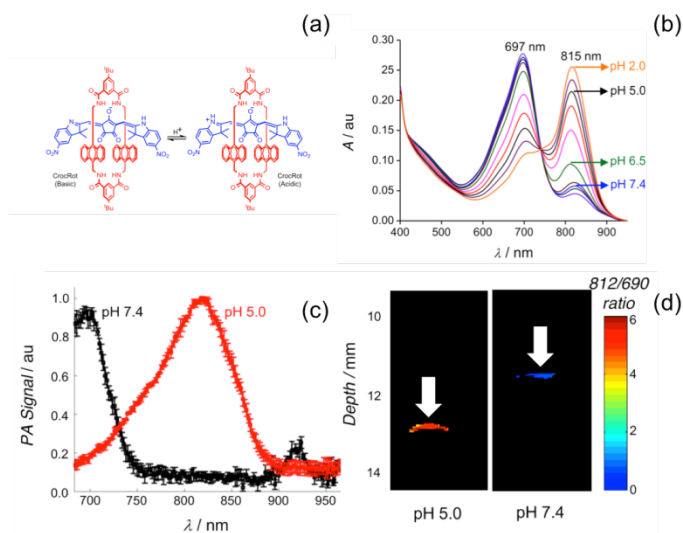
2J-6 _____

2:15 pm   Broadband detection of dynamic acoustic emission process induced by 6 MV therapeutic X-ray beam from a clinical linear accelerator

Xianfen Diao[1], Jing Zhu[1], Weihao Li[2], Nan Deng[1], Chien Ting Chin[1], Xinyu Zhang[1], Xin Chen[1], Xianming Li[2], Yu Kuang[3]; *[1]Shenzhen University, China, People's Republic of, [2]Shenzhen People¡¯s Hospital, China, People's Republic of, [3]Dept. of Medical Physics, University of Nevada, Las Vegas, Las Vegas, USA*

Background, Motivation and Objective

Acoustic waves induced by megavoltage photon beam from a clinical linear accelerator (Linac) could provide location and dosimetric information of actual delivered radiation during the course of therapy. A different dynamic acoustic emission process induced by X-ray from Linac could represent a longitudinal and/or heterogeneous response to the treatment. However, to improve the signal to noise ratio (SNR) in X-ray acoustic signal detection, previous studies averaged the whole acoustic signals triggered by X-ray pulses, thus compromising diagnostic accuracy in personalized treatment efficacy. In this study, we investigated, for the first time, the technical feasibility of detecting the dynamic acoustic emission process induced by Linac with high SNR.

Statement of Contribution/Methods

As a proof of concept, a 6 MV pulsed X-ray beam (200 MU/min dose rate, 30X30 mm^2 field size at 100 cm SSD) produced by a Linac was used to excite the X-ray acoustic signals from two cylindrical phantoms with a diameter of 8 cm and a height of 2 cm. The induced acoustic signals were collected with a circular plane piston, immersion hydrophone in the frequency range 100 kHz to 1 MHz perpendicular to the incident X-ray beam direction. The signals were amplified using a preamplifier with a bandwidth of 50 KHz-5 MHz at 34 dB and sampled by a high-speed 14-Bit 100 MS/s data acquisition card. A trigger circuit was designed to synchronize the process of incident pulsed X-ray generation and emitted acoustic signal acquisition.

Results/Discussion

The dynamic X-ray acoustic emission process were consecutively detected from Phantoms A and B (Fig 1) with high SNR. The peak amplitude shows a marked increase in the phase of X-ray irradiation and then a rapid fall-off with different dynamic acoustic signal profiles in both phantoms, suggesting the different processes of accumulation and the absorption of the X-ray energy in different phantom properties. X-ray acoustic waves detected with high SNR may be used to verify the dose distribution during radiation therapy. Moreover, it may open the opportunity of using X-ray acoustic signals emitted from the tumor to evaluate the radiation treatment efficacy.
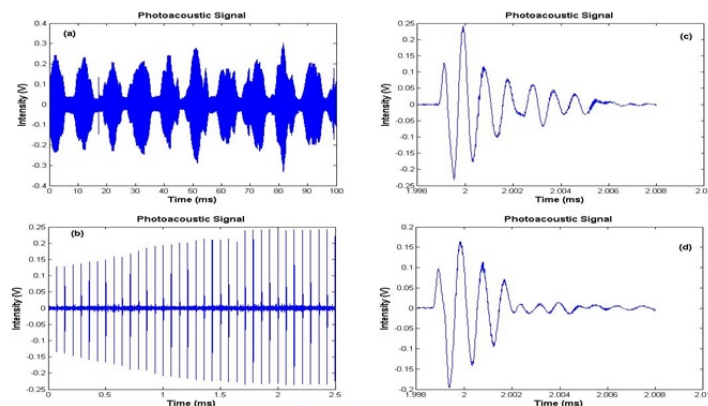
Fig 1. Phantom A was mixed with 2% cellulose, 10% gelatin, 88% water and Phantom B was mixed with 15% gelatin, 85% water. (a):X-ray acoustic signals emitted from Phantom A with a recording time of 100 ms; (b) and (c):detailed waveforms recorded in (a); (d):X-ray acoustic signals with different peak amplitude and fall-off rate emitted from Phantom B.

3J - MTC: Cardiovascular Tissue Characterization

201BC

Saturday, October 24, 2015, 01:00 pm - 02:30 pm

Chair: **James G. Miller**
            Washington University

3J-1

1:00 pm   3D Ultrasound Backscatter Tensor Imaging (BTI) in vivo: assessment of the myocardial fiber orientation dynamic

Clement Papadacci[1], Jean Provost[1], Olivier Villemain[1], Jean Luc Gennisson[1], Mickael Tanter[1], Mathias Fink[1], Mathieu Pernot[1]; *[1]Institut Langevin, CNRS, INSERM, ESPCI, Paris 7, Paris, France*

Background, Motivation and Objective

Fiber architecture is of major interest in the cardiac function. Recently, Backscatter Tensor Imaging (BTI), a new imaging technique enabled the detection of fiber organization in ex vivo myocardial samples using spatial coherence measurement on a linear array. In this study, 3D BTI was developed on a 2D matrix probe to calculate 2D coherence function (CF) to retrieve the 3D fiber architecture dynamic in vivo on a beating heart of an open-chest sheep during an entire cardiac cycle. Moreover, we validated the fiber orientations derived with 3D BTI against histology.

Statement of Contribution/Methods

Acquisitions were performed using a 2D matrix array (3MHz, 1024 elements, 0.3 mm pitch, Vermon) connected to a prototype of programmable ultrasonic scanner, with 1024 channels. The 3D BTI sequence consisted in: the emission of 98 2D tilted plane waves, the coherent compounding of the RF backscattered signals received by each transducer elements, the autocorrelation of the compounded RF signals performed by pairs of elements to compute the 2D CF at each point of the beamformed volume, an elliptic fit applied on the 2D CF to retrieve fiber angle by assessing the major axis orientation of the ellipse. Finally a fiber tracking algorithm (Amira, Visualization Sciences Group, Burlington, MA) was applied to display the fiber orientations in 3D. Fiber orientation was evaluated on n=5 ex vivo porcine myocardial samples and validated against histology. The probe was placed at 15mm from the left ventricular wall of the beating heart of an open-chest sheep immersed in saline water. The fiber architecture dynamic during an entire cardiac cycle was assessed in vivo using the 100 3D BTI images acquired at a volume rate of 89.5 volumes/s during 1.2 s.

Results/Discussion

The fiber angles were successfully derived from 3D BTI and histology for the n=5 myocardial ex vivo samples. A good agreement was found between the two techniques (MDV= 2.7° ± 10.6°). The transmural orientation was found to vary continuously through the wall with an average difference of 123°± 18° between the epicardium and the endocardium. The fiber architecture was also assessed successfully in vivo in 3D on the beating heart during the entire cardiac cycle and its complete dynamic was analyzed. 3D BTI could become a major tool for the mapping of fiber directions in real time in the human heart for the early detection of myocardial diseases.
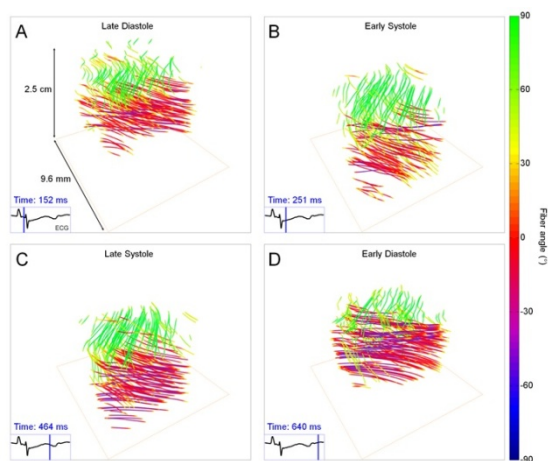
In vivo 3D representation of fibers in the left ventricle of an open-chest sheep at four different moments of the cardiac cycle (i.e. A Late Diastole, B Early Systole, C Late Systole, D Early Diastole).

3J-2

1:15 pm   Scatter size estimation using time domain phase of ultrasound radio frequency data

Tobias Erlöv[1], Tomas Jansson[2,3], Hans W Persson[1], Magnus Cinthio[1]; *[1]Department of Biomedical Engineering, Lund University, Sweden, [2]Department of Clinical Sciences Lund, Biomedical Engineering, Lund University, Sweden, [3]Medical Services, Skåne University Hospital, Sweden*

Background, Motivation and Objective

We have recently performed a study where what we term the average phase derivative (APD) of the RF data was successfully used to assess carotid plaque vulnerability. The APD is a time domain measure of the backscattered central frequency but without any trade off in time-frequency resolution like the FFT, which enables a more accurate estimation. The fact that scatter properties affect the frequency content of the backscattered data has been confirmed both theoretically and practically by several groups using spectrum analysis. However since the APD is a measure of the center frequency only, the effect of scatter properties in the tissue is unclear. In this study we investigated the relationship between APD and scatter size.

Statement of Contribution/Methods

Five agar phantoms with different well defined sizes of glass beads (10-22µm, 27-32µm, 38-45µm, 45-53µm and 53-63µm) were made with a concentration of 20 beads/mm3. The phantoms were placed in water and imaged using two different transducers with variable transmit center frequencies using the ULA-OP scanner. The time domain phase of the RF data was calculated using the Hilbert transform. The phase was unwrapped, differentiated and averaged using a 3x3 mm kernel. The result was then compensated for frequency attenuation. The APD of the four phantoms with larger scatter sizes were normalized to the APD of the first phantom which was assumed to

---

approximate Rayleigh scattering. Both transducers were used with three different transmit frequencies (8-12MHz) to reflect several different k*a values, where k is the wavenumber and a is the radius of the glass beads.

Results/Discussion

The figure shows the mean and standard deviation of the normalized APD as a function of k*a. Each value is based on 1000 calculations from different positions and depths within the phantom. Our results show that scatter size can be well estimated using only the center frequency obtained with APD. Normalization to Rayleigh scattering, which has a uniform frequency response, seems to effectively remove the frequency dependence resulting from the use of finite receive and transmit apertures and transmission frequency. The result could therefore be used to derive the first form factor describing the central frequency response of different scatter sizes. This shows the potential for APD to be used for scatter size estimation and tissue characterization.
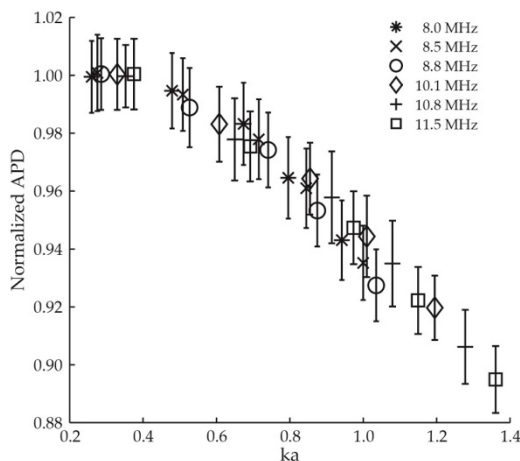
3J-3

1:30 pm **Noninvasive assessment of age-related arterial changes using the carotid stress-strain relationship in vivo**

Spyretta Golemati[1], Marianna Tzortzi[1], Ronny Li[2], Cesare Russo[3], Elisa Konofagou[2,4]; [1]*Medical School, National Kapodistrian University of Athens, Athens, Greece,* [2]*Biomedical Engineering, Columbia University, New York, NY, USA,* [3]*Medicine, Columbia University, New York, NY, USA,* [4]*Radiology, Columbia University, New York, NY, USA*

Background, Motivation and Objective

The feasibility of noninvasively measuring regional carotid artery stiffness by way of the stress-strain relationship was recently demonstrated in young normal adults *in vivo* (Khamdaeng et al. Ultrasonics, 2012). In this paper, similar methods were used to assess the stress-strain curve and derive the Young's moduli in young and older subjects to evaluate the sensitivity of this approach in assessing age-related wall changes.

Statement of Contribution/Methods

Two types of recordings were performed on the common carotid arteries of 3 young and 2 older subjects: (a) RF signals acquired at 505-642 Hz using a Sonix RP system, and (b) the pulse pressure signal using a customized applanation tonometry system (Millar instruments). Subsequently, (a) arterial strain was calculated from the diameter waveform obtained using the radial displacements estimated by a 1D cross-correlation technique on the RF signals, and (b) arterial stress was estimated using the pressure (tonometry) signal, the diameter, and the wall thickness measured on the B-mode. The strain and stress signals were combined to produce the stress-strain curve. Using bilinear curve fitting, the Young's modulus of the elastin-collagen fibers (E_2), as well as the moduli for elastin (E_1) and collagen (E_3), separately, were estimated, under the assumption of a linear elastic two-parallel spring model.

Results/Discussion

Figure 1 shows examples of stress-strain curves and derived Young's moduli from the carotid of two normal subjects of different ages. Table 1 shows the Young's moduli values for all subjects. E_1 and E_2 were significantly larger in the older subjects, indicating stiffer tissues probably due to reduced elastin, which is in agreement with the related literature. No differences in E_3 were noted between young and older subjects.
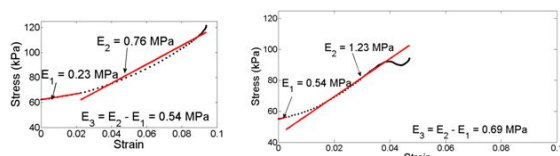
Figure 1. Examples of stress-strain curves and corresponding curve fitting, along with derived Young's moduli (E_1, E_2, E_3), for two normals, (left, 23 y.o., Male) and (right, 37 y.o., Male). Straight red lines correspond to bilinear fitting.

Table 1. Average±std values of Young's moduli over four different recordings and at five locations along the wall for 3 young and 2 elderly subjects.

Subject	E_1, MPa	E_2, MPa	E_3, MPa
Male, 23 y.o.	0.20±0.03	0.63±0.10	0.43±0.07
Male, 24 y.o.	0.37±0.06	0.89±0.18	0.52±0.15
Female, 26 y.o.	0.42±0.08	0.87±0.23	0.45±0.17
Male, 37 y.o.	0.68±0.21	1.20±0.21	0.52±0.26
Female, 43 y.o.	0.70±0.23	1.02±0.38	0.31±0.38

3J-4

1:45 pm **Imaging the Ultrasonic Coefficient of Nonlinearity**

Ruud van Sloun[1], Libertario Demi[1], Caifeng Shan[2], Massimo Mischi[1]; [1]*Electrical Engineering, Eindhoven University of Technology, Eindhoven, Netherlands,* [2]*Philips Research, Netherlands*

Background, Motivation and Objective

Cardiac ablation is increasingly used to treat atrial fibrillation. Although it is effective, the nonuniform thickness of the left atrial wall and the variable thickness of the fatty layer between the wall and the esophagus are risk factors. The potential ability of distinguishing fat and muscle tissue types with an intra cardiac ultrasound probe would allow risk assessment with respect to esophageal injury. The acoustical coefficient of nonlinearity β is a particularly suitable feature for discriminating the tissues relevant to this application, since fatty tissues are known to have a high coefficient of nonlinearity. However, β imaging in echo mode is a challenging task. In particular, previous methods fail to address spatially varying backscattering coefficient and absorption and/or the methods require a special measurement setup or transducer, posing serious limitations for translation into clinical applications.

SATURDAY ORAL

Statement of Contribution/Methods

Starting from an 1D inhomogeneous generalized lossy nonlinear Westervelt equation, we derived an analytical solution for β, which is then further adapted to work in echo mode. By considering the ratio between the harmonic and fundamental fields, the influence of spatial variations in backscatter coefficient is addressed, and spatial absorption variations are mitigated. The method's ability to discriminate muscle, cardiac and fat tissue is first evaluated *in silico*. Using the 3D Iterative Nonlinear Contrast Source simulator, pressure fields as obtained from a 52 element linear array scan are produced. For each line, 13 elements are simultaneously excited and a β estimate is obtained within the beam. The β image is then formed by translating the active aperture along the array. The method was also tested *in vitro*, where the ULA-OP system and an Esaote LA332 probe were used to image an phantom consisting of 2 layers obtained as a mixture of oil, gelatin and water. By varying the percentage of oil (which has a β similar to fat), a contrast in β is obtained.

Results/Discussion

Fig. 1(a) and 1(b) show the *in silico* results, and the *in vitro* results are given in Fig. 1(c) and (d). Although the initial results are promising, further testing is required to evaluate the use of the presented method for clinical imaging. Particular attention will be given to the position of the focal point(s) and achievable spatial resolution.
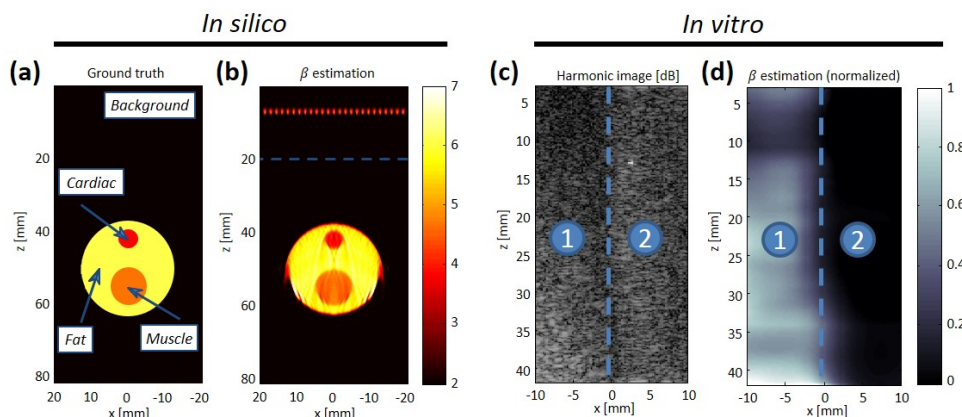
Figure 1. Plot (a) shows the numerical phantom where the color scale indicates the coefficient of nonlinearity β . Three tissue types are considered, being cardiac, muscle and fat. (b) shows the obtained β images for the *in silico* linear array scan. Plots (c) and (d) show the 2nd harmonic image and the resulting β map, respectively, as obtained *in vitro*. The two phantom layers are annotated by '1' and '2'.

3J-5

2:00 pm **Determining carotid plaque vulnerability using the average phase derivative of ultrasound radio frequency data – first ex vivo and in vivo results**

Tobias Erlöv[1], Isabel Goncalves[2,3], Andreas Edsfeldt[2], Simon Segstedt[1], Nuno Dias[4], Jan Nilsson[2], Magnus Cinthio[1]; *[1]Department of Biomedical Engineering, Faculty of Engineering LTH, Lund University, Sweden, [2]Department of Clinical Sciences Malmö, Lund University, Sweden, [3]Department of Cardiology, Skåne University Hospital, Sweden, [4]Vascular Center, Skåne University Hospital, Sweden*

Background, Motivation and Objective

Rupture-prone vulnerable plaques are characterized by a core of necrotic debris and lipids, accumulation of inflammatory cells and a reduced content of fibrous tissue and smooth muscle cells. Identification and treatment of vulnerable plaques before they give rise to acute events represents a great challenge in cardiovascular medicine today. In this study we have evaluated a new method to detect vulnerable carotid plaques using non-invasive ultrasound against histology.

Statement of Contribution/Methods

We have developed a method based on what we term the average phase derivative (APD) of the radio frequency data. This is a time-domain parameter which reflects the local average frequency of the RF data. The frequency content of the backscattered signal is dependent on scatter characteristics, e.g. scatter size, and the APD is therefore tissue dependent. The RF data, obtained using the ULA-OP scanner with a 9 MHz transducer, was first demodulated with the center frequency and then compensated for frequency attenuation. The sample-wise phase obtained with demodulation was then differentiated and averaged within the manually outlined plaque. The method was first validated *ex vivo* on 157 fragments obtained from 18 human atherosclerotic plaques. The method was then further validated *in vivo* where we analyzed 49 fragments from 39 patients 1-day prior to carotid plaque removal. The result from both the ex vivo and in vivo measurements were then compared to histology.

Results/Discussion

The APD correlated with a plaque vulnerability index based on histological areas stained for lipids, macrophages, haemorrhage, smooth muscle cells and collagen (r=0.637, P<0.0001). Plaques with APD above median had larger cores, more macrophages and were more lipid-rich in agreement with the definition of rupture-prone plaques. The accuracy of UPSA to detect plaques with high vulnerability index was 76% with sensitivity 77% and specificity 74%. The figure shows three human carotid plaques with vulnerable (two top rows) and stable (bottom row) phenotypes assessed with B-mode (left), APD (middle) and histology stained for lipids (right). Our method is the first that applies APD to characterize atherosclerotic plaque components that affect plaque vulnerability. This could improve preventive strategies, risk stratification and monitoring of interventions.
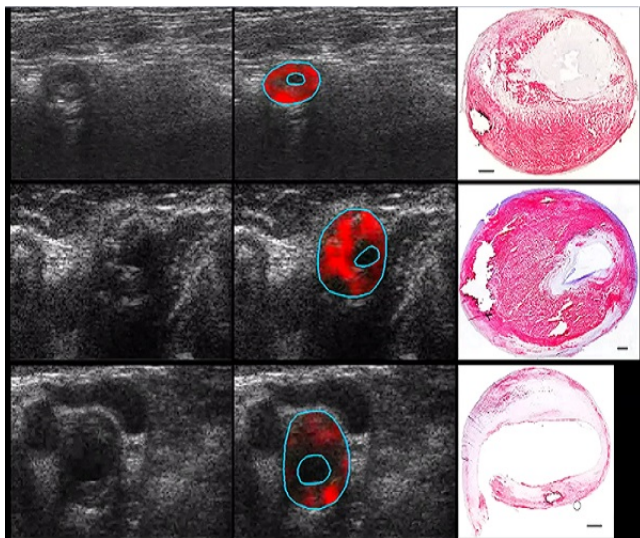
3J-6

2:15 pm   Diffraction independent estimation of the ultrasound attenuation coefficient

Natalia Ilyina[1,2], Jeroen Hermans[3], Emiliano D'Agostino[3], Koen Van Den Abeele[4], Jan D'hooge[1]; [1]*Dept. of Cardiovascular Sciences, KU Leuven, Belgium,* [2]*Belgian Nuclear Research Centre, SCK•CEN, Belgium,* [3]*DoseVue NV, Belgium,* [4]*Dept. Of Physics, KU Leuven Kulak, Belgium*

Background, Motivation and Objective

Estimation of the acoustic attenuation (α) has several imaging as well as clinical applications. To obtain an accurate α estimate diffraction effects have to be considered. This is usually done by means of a reference phantom technique which is not practical in the clinical setting. Previously we proposed an iterative attenuation reconstruction technique under the assumption of plane wave propagation. In this method, the local α is estimated by iteratively solving the forward wave propagation problem and matching the simulated signals to measured ones. The aim of the present study was to extend this methodology by including diffraction effects.

Statement of Contribution/Methods

Forward wave propagation was modeled in the frequency domain, applying the effects of attenuation and diffraction. Attenuation was described using a power law, while diffraction was simulated using the angular spectrum approach. Scattering was modeled by propagating the signal received at the scattering site back to the source including the above effects. The parameters of this model can be iteratively changed to approximate the experimentally observed signals. In order to test this methodology, RF signals were recorded from 3 homogeneous tissue-mimicking phantoms (gelatin-graphite; 5.5 cm long; 3.5 cm diameter), the reference α of which were determined using an insertion-substitution method. 20 recordings were made for each phantom when positioned in the focus and in the far field of a single-element ultrasound transducer (5 MHz, focus = 7.5 cm). The proposed method was used to estimate α both with and without diffraction compensation. As an optimization criterion, the sum-of-squared-differences between the averaged spectra of the experimentally observed and the simulated signals were calculated using a sliding window of 4 mm with 50% overlap.

Results/Discussion

As expected, when neglecting diffraction effects, α estimates were acceptable near the focal zone of the transducer but were overestimated in the far field (Figure; reference value shown as a horizontal line). Taking diffraction into account reduced the far field estimates bringing them closer to the reference values. These preliminary data show that the proposed methodology might provide an attenuation estimate independent of diffraction effects. A more elaborate evaluation of the proposed method is the topic of ongoing work.
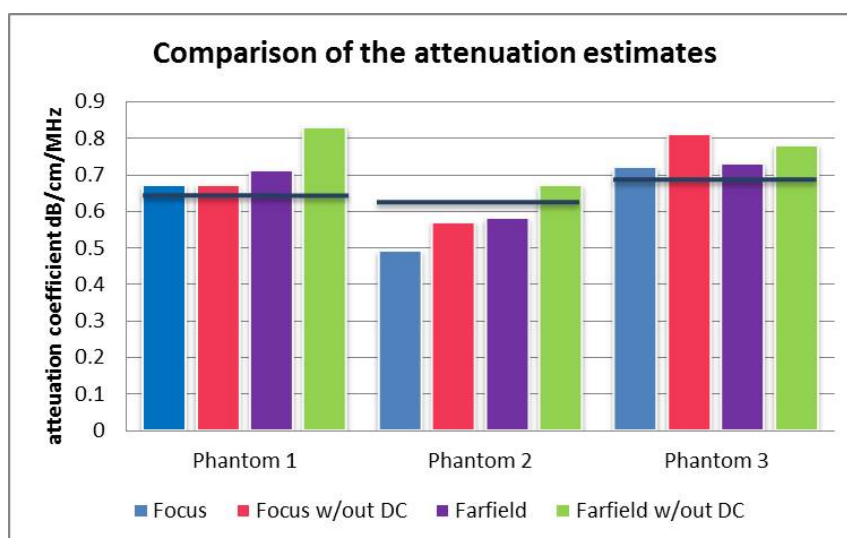
4J - MTH: Taming Cancer, Tumors, and Bacteria

201DE

Saturday, October 24, 2015, 01:00 pm - 02:30 pm

Chair: **Tom Matula**
University of Washington

4J-1

1:00 pm   Intra-operative toroidal HIFU transducer for the treatment of colorectal liver metastases: Results of a Phase I-II clinical study in 20 patients

David Melodelima[1], Aurelien Dupre[1,2], Yao Chen[2], Jeremy Vincenot[1], David Perol[2], Jean-Yves Chapelon[1], Michel Rivoire[1,2]; [1]LabTAU - U1032, INSERM, France, [2]Centre Leon Berard, France

Background, Motivation and Objective

Surgery is the only curative treatment in patients with colorectal liver metastases (CLM), but only 10–20% of patients are eligible. High Intensity Focused Ultrasound (HIFU) technology is of proven value in several indications, notably prostate cancer. Intra-operative use of HIFU in patients with CLM has not previously been studied. Preclinical work suggested the safety and feasibility of an intra-operative toroidal HIFU device capable of ablating liver volumes of up to 50 cm^3 in a few seconds.

Statement of Contribution/Methods

The transducer has a toroidal shape with a diameter of 70 mm and was divided into 32 ring-shaped emitters of 86 mm^2 each. The radius of curvature was 70 mm to enable treatment of the deepest regions of the liver. The operating frequency was 2.5 MHz. A 7.5 MHz ultrasound imaging probe was placed in the center of the device to guide the treatment. The imaging plane was aligned with the HIFU focal zone. A prospective, single-centre phase I-II trial was conducted in 24 patients. HIFU was delivered immediately before scheduled hepatectomy. In order to demonstrate the safety and efficacy of rapidly ablating liver metastases, ablations were performed first on healthy tissue (Phase I-IIa) and then on liver metastases (Phase IIb) within the areas scheduled for resection.

Results/Discussion

In Phase I-IIa, 30 ablations were carried out in 15 patients. These ablations were all generated within 40 seconds and on average measured 27.5mm x 21.0mm. The phase I study (n = 6) showed that use of the toroidal HIFU device was feasible and safe and did not damage neighboring tissue. The phase IIa study (n = 9) showed both that the area of ablation could be precisely targeted on a previously implanted metallic mark (used to represent a major anatomical structure) and that ablations could be undertaken deliberately to avoid such a mark. Ablations were achieved with a precision of 1–2mm.

In Phase IIb, 5 ablations were created in 5 patients. Nine liver metastases were treated. HIFU ablations were generated within 40 seconds for metastases of 10 mm in diameter (n=2). Using electronic focusing it was possible to increase the coagulated volume. Liver metastases of 20 mm in diameter (n=3) were treated in 370 seconds. On average the dimensions of ablations created in 370 seconds were 65.6 mm x 44.5 mm. In all cases liver metastases were treated with safety margins (>3 mm) in all direction and this was confirmed histologically.

Intra-Operative use of a HIFU toroidal transducer was feasible, safe and effective in ablating areas of liver scheduled for resection. The first results obtained on liver metastases are promising but need to be confirmed. It is planned to treat 27 liver metastases in Phase IIb.

4J-2

1:15 pm   Coincident light/ultrasound therapy to treat bacterial biofilms

Mark Schafer[1], Tessie McNeely[1]; [1]PhotoSonix Medical, Inc., Ambler, Pennsylvania, USA

Background, Motivation and Objective

Bacteria preferentially grow as colonies surrounded by a complex matrix, together called a biofilm. According to the NIH over 80% of microbial infections in the human body consist of biofilms. Biofilms are highly resistant to antibiotics and the immune system, making them difficult to treat at best, and nearly impossible to eradicate at worst. We propose to treat bacterial biofilms by simultaneous exposure to low energy, non-focused ultrasound, combined with blue/violet light (i.e. CLENS™: Coincident Light Energy and Non-focused ultraSound). Low intensity ultrasound has previously been explored for anti-biofilm activity, however it has generally been applied in conjunction with an antibiotic. Similarly, blue/violet light has been explored as a bactericidal agent for planktonic bacteria. We hypothesized that the simultaneous application of blue/violet light with ultrasound would synergize the beneficial properties of each, and successfully provide a technologically new method to attack biofilms.

Statement of Contribution/Methods

A prototype laboratory device was built to deliver simultaneous ultrasound and light energy to bacterial biofilm grown in-vitro. Light emitting diodes (405nm) were used to generate 30mW/cm^2; and a coincident ultrasound source (450kHz) created a pressure field at less than 100mW/cm^2. Staphylococcus epidermidis, S. aureus, and P. acnes were grown on hanging inserts (i.e. transwells) at 37°C for up to 72 hours before exposure. Following CLENS exposure, bacteria killing was quantified by serial dilution and plating on media agar. After an appropriate growth time on agar, Colony Forming Units (CFUs) were counted.

Results/Discussion

Killing was dose dependent on exposure time, and could be optimized with tuning of either the light or ultrasound energy. There was >1 log_{10} reduction after 5 min and >3 log_{10} reduction after 30 min treatment (p<0.05). In comparison, 24 hr exposure to erythromycin reduced biofilm CFU by less than 1 log_{10} (p<0.05). While a 30 min CLENS treatment induced significant bacterial death, the die off continued to 24 hr after exposure with an additional 2 log_{10} reduction (p<0.05). Biofilm regrowth started at 48 hr, but after 4 additional days of growth, the biofilm had not returned to the original CFU levels (p<0.05). Importantly, the two energies must be delivered coincidentally for optimal effect. These initial results validate that the basic CLENS mechanism is effective on relevant biofilm-producing bacteria: low intensity ultrasound "activates" the bacteria within the biofilm such that they become susceptible to the antimicrobial effects of blue light.

4J-3

1:30 pm   Improvement of Drug Penetration in Solid Tumors by Vascular Disruption with Acoustic Nanodroplet Vaporization

Yi Ju Ho[1], Chih Kuang Yeh[1]; [1]Department of Biomedical Engineering and Environmental Sciences, National Tsing Hua University, Hsinchu, Taiwan

Background, Motivation and Objective

Tumor microenvironments play an important role on drug penetration within solid tumor. Although anticancer drugs can extravasate into tissue via enhanced permeability and retention effect, the extravascular diffusion is still restricted by the higher interstitial fluid pressure. Recent studies have demonstrated that ultrasound sonication can vaporize perfluorocarbon droplets into the gaseous phase. The so-called acoustic droplet vaporization (ADV) can reportedly be used to liberate encapsulated anticancer drugs in droplets for tumor treatments. In this study, we investigated the improvement of drug penetration via disrupting tumor vasculature induced by ADV.

Statement of Contribution/Methods

Perfluorocarbon nanodroplets (337±80 nm) stabilized with a monolayer of phosphatidylcholine and PEG were prepared in house. DiI-liposomes (139±45 nm) were fabricated to emulate drugs and also provided fluorescence signature in vivo. A skinfold chamber tumor-bearing mouse model was integrated with acousto-optical system for the intravital microscopic investigation of dynamic fluorescence changes under the focused ultrasound insonations (2-MHz with 3-cycle, single pulse and 10 MPa). Focused ultrasound triggered ADV at time points of 1, 10, 30, 60, 120, and 180 min after nanodroplets/ DiI-liposomes injection, respectively. The extravascular diffusion areas in intravital images were quantified. The histological experiments of solid tumors w/ and w/o ultrasound sonications were also introduced to observe the locations of tissue hemorrhage (H&E stain), vessel pattern (CD31 stain) and DiI-liposomes.

Results/Discussion

The acoustic nanodroplets with focused ultrasound causing vascular endothelium destruction provided the increased DiI-liposomes penetration over time in vivo (Fig. A). The cumulative diffusion area still increased at 180 min and the results showed 1.48 folds compared to the case at 1 min (Fig. B). In histological images, the extensive DiI-liposomes distribution and tissue hemorrhage were observed in sonicated tumors (Fig. C). The proposed strategy might induce direct tumor cell killing by ADV mechanical effect and inflammation responses leading to the accumulation and activation of leukocytes providing antitumor effect. Future works include delivering encapsulated drugs droplets into solid tumor and evaluating treatment efficacy.
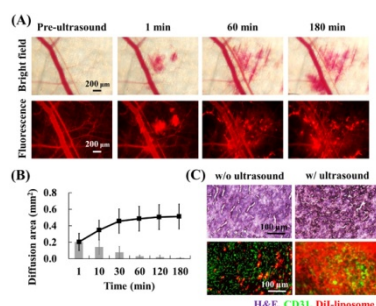
4J-4

1:45 pm   Achieving a durable response by combining chemotherapy with focused ultrasound in mouse models of cancer

Andrew Wong[1], Azadeh Kheirolomoom[1], Yu Liu[1], Josquin Foiret[1], Brett Fite[1], Elizabeth Ingham[1], Katherine Ferrara[1]; *[1]Biomedical Engineering, UC Davis, Davis, CA, USA*

Background, Motivation and Objective

Our ultimate goal is to use focused ultrasound within curative protocols in the mouse and in human medicine. Curing mice with ultrasound is challenging as highly absorptive skin and critical organs such as intestine are in close proximity to the tumor. Thus, the mouse is a useful model for evaluating strategies to augment ablation with drug delivery near sensitive structures. In this model, ablation alone not only enhances therapeutic T cells, but also can increase T-regulatory cells associated with the immunosuppressive environment. We have previously shown that within 8 treatments, hyperthermia and temperature sensitive doxorubicin liposomes are curative for this local cancer. However, identifying strategies that incorporate ablation to debulk larger tumors and induce a systemic immune response is also attractive.

Statement of Contribution/Methods

All studies were approved by the UC Davis Institutional Animal Committee on Use and Care. Tumors were generated in 45 FVB/n mice expressing an activated form of ErbB2/neu. These tumors were then transplanted into the mammary fat pads of wild type FVB/n mice. For ablation, we used 3 MHz ultrasound with a 16 element annular array that is mechanically scanned to treat a region of interest, with MR guidance and temperature monitoring. Ablation protocols were designed to induce temperatures >65°C and a CEM43>5000, e.g. 20-second application of 3.1 MPa PNP at a single point or 60-second application of 3.1 MPa PNP in a circular pattern. Twenty-five minute hyperthermia (42°C) was delivered using a 256-element transducer with 128 therapeutic elements operated with a center frequency of 1.5 MHz, with US guidance and a needle thermocouple for temperature monitoring. We have developed temperature-sensitive and long-circulating doxorubicin liposomal formulations (Dox-TSL and Dox-LCL, respectively). Each is geared to treat a region without toxicity to surrounding tissues by encapsulating non-bioactive copper-doxorubicin crystals which dissociate in the low pH of the tumor microenvironment.

Results/Discussion

Delivering a small ablation focus in 4 treatments in conjunction with Dox-LCL or Dox-TSL achieved a durable response in 25% of mice treated. Increasing the volume of ablation to a sphere of ~5 mm diameter fitting within ~5-6 mm tumors did not produce a durable response. Integrating this sphere of ablation with Dox-TSL further increased the rate of durable response with 4 treatments to 75% of mice treated. Alternatively, preapplication of hyperthermia to enhance release of Dox-TSL prior to the application of the spherical region of ablation produced durable response in 100% of mice within 4 treatments.

In conclusion, initial results for the combination of hyperthermia, ablation and liposomal doxorubicin in a fully immunocompetent aggressive syngeneic model demonstrated multiple opportunities to achieve a durable response in local disease.
Acknowledgement: NIHCA103828 and NIHCA134659

4J-5

2:00 pm   Low-Intensity Ultrasound Promotes Antitumoral Effect of Bisphosphonates in Breast Cancer Xenografts and Bone Metastasis

Sophie Tardoski[1], Jacqueline Ngo[2], Evelyne Gineyts[3], Jean-Paul Roux[3], Philippe Clézardin[3], David Melodelima[2]; *[1]INSERM UMR 1032, Lyon, France, [2]INSERM UMR 1032, France, [3]INSERM UMR 1033, France*

Background, Motivation and Objective

Bisphosphonates (BP) like zoledronic acid (ZOL) have demonstrated clinical utility in the treatment of patients with bone metastases. However, ZOL exhibits antitumor effects only at high doses incompatible with a clinical use due to renal toxicity. Bisphosphonates exhibit a high affinity for bone mineral, which reduces their bioavailability for tumor cells. We examined if low intensity ultrasound could enhance the effects of a clinically relevant dose of ZOL in experimental breast cancer and bone metastasis murine models.

Statement of Contribution/Methods

A plane transducer working at a frequency of 2.9 MHz was used. The free field acoustic power was adjusted between 8 and 13 watts applied for 30 minutes in order to produce and maintain mild hyperthermia (43°C). These parameters enhance locally the temperature in mice and produce mechanical stimulation without creating cavitation. In vivo experiments were performed in a bone metastases model and on a subcutaneous tumor xenograft model. Animals were randomly assigned to different groups (vehicle, ZOL, US, ZOL+US). Clinically relevant dose of ZOL was used (100 μg/kg). Osteolytic lesions were detected by radiography. Tumor angiogenesis and tumor cells

SATURDAY ORAL

proliferation were assessed by immunohistochemistry. Unprenylated Rap1A, a surrogate marker of the penetration of ZOL into tumor cells, was observed by Western Blotting. A quantification of remaining bisphosphonate in bone after ultrasonic treatment was performed using a fluorescent bisphosphonate (FAM-RIS).

Results/Discussion

With the acoustic parameters used, no signs of cavitation were found. Temperature in tumors was $42.0 \pm 2.8°C$ during US treatment. No lesion was observed in surrounding tissues. US alone did not have any effect on bone metastasis and tumor outgrowth. In the bone metastasis model, mice treated with ZOL+US had osteolytic lesions that were 58% smaller than those of ZOL-treated animals (p<0.01). ZOL+US also significantly decreased skeletal tumor burden. In the animal model of primary tumors, ZOL+US treatment reduced by 42% the tumor volume, compared with ZOL-treated animals (p<0.01). In all cases tumor angiogenesis and tumor cell proliferation were reduced. Using a fluorescent bisphosphonate, it was demonstrated that US forced the release of bisphosphonate from the bone surface, enabling a continuous impregnation of the bone marrow. Additionally, US forced the penetration of ZOL within tumors, as demonstrated by the intratumoral accumulation of unprenylated Rap1A.

In conclusion, our results demonstrate the potential of low intensity ultrasound as an effective strategy to force bisphosphonate desorption from bone and its penetration through tumor tissue, enabling bisphosphonate antitumor activity (both in bone and outside bone). Our findings made US a promising modality in oncology to trigger anticancer therapy with bisphosphonates.

4J-6

2:15 pm **Thermal Ablation of a Confluent Lesion in the Porcine Kidney with Magnetic Resonance guided High Intensity Focused Ultrasound**

Johanna MM van Breugel[1], Martijn de Greef[1], Joost W Wijlemans[2], Gerald Schubert[3], Chrit TW Moonen[1], Maurice AAJ van den Bosch[1], Mario G Ries[1]; *[1]Center for Image Sciences, University Medical Center Utrehct, Utrecht, Netherlands, [2]University Medical Center Utrehct, Utrecht, Netherlands, [3]Philips Healthcare, Netherlands*

Background, Motivation and Objective

There is an increasing interest in non-invasive kidney sparing therapy for renal cancer, since ~1.6% of men and women will be diagnosed with kidney and renal pelvis cancer during their lifetime. Therefore, several patient studies investigated the feasibility of high intensity focused ultrasound (HIFU) for the thermal ablation of renal masses using B-mode US for guidance or a laparoscopic approach. Disadvantages are i.a. the lack of respiratory motion compensation, no means to visualize the energy deposition in real time, and the complexity of the probe positioning. Alternatively, feasibility of magnetic resonance guided HIFU (MR-HIFU) interventions on the kidney with respect to motion compensated real-time thermometry and acoustic energy delivery was established. Here, we extend this prior work to investigate if MR-HIFU can provide for a reliable confluent volumetric lesion in the renal cortex in a porcine study.

Statement of Contribution/Methods

Nine anesthetized pigs were placed on a clinical Philips Sonalleve MR-HIFU therapy system integrated with a 1.5T Achieva MRI. Both acoustic energy delivery and MR-thermometry were respiratory gated (3mm gating window, 80% duty cycle) and active surface cooling was employed to prevent near-field damage. A honeycomb pattern of 7 ablation cells (9-25s, 450W acoustic power, 4x4x10 mm3 per cell) was planned (Fig. 1). The therapeutic endpoint was evaluated non-invasively by a non-perfused volume (NPV) measurement using dynamic contrast enhanced T1-weighted MRI. Subsequently, the animal was euthanized and the necrotic volume was examined using a cellular viability staining (NADH).

Results/Discussion

Temperatures exceeding 60°C and confluent NPV and NADH volumes were obtained in 6 pigs. The false rib of pig 2 was overlooked resulting in heating of the rib. Navigator positioning in pig 4 was suboptimal resulting in residual motion, heat spread, and poor heating of the kidney. A combination of a large angle of incidence, different near field stacks in the beam cone, and suboptimal positioning of the animal led to poor heating in pig 6.

These first results indicate that current MR-guided clinical HIFU equipment might be suitable for non-invasive therapy of renal masses. Planning of the sonications and the subject based on anatomical scans is very important, as well as adequate motion compensation.
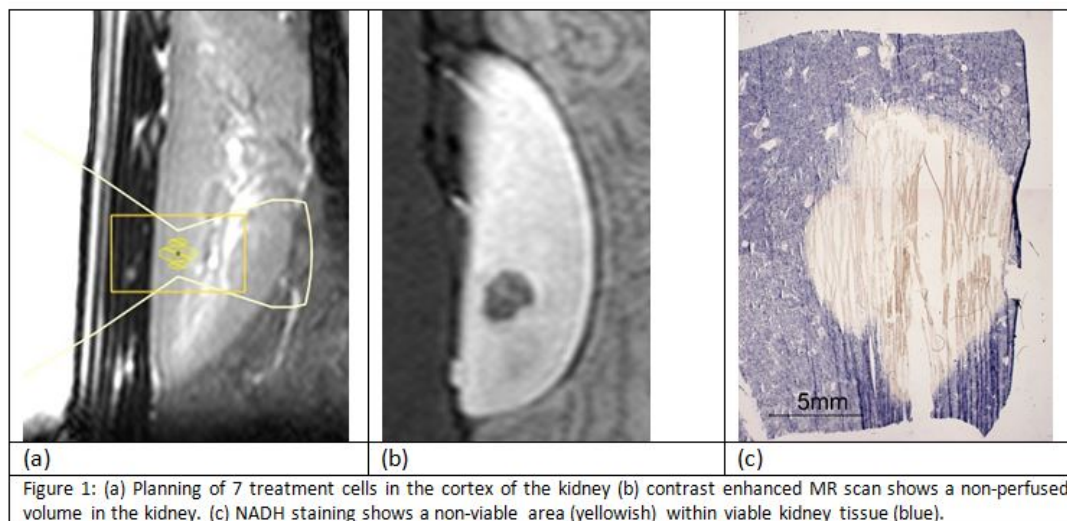
Figure 1: (a) Planning of 7 treatment cells in the cortex of the kidney (b) contrast enhanced MR scan shows a non-perfused volume in the kidney. (c) NADH staining shows a non-viable area (yellowish) within viable kidney tissue (blue).

5J - Sensors and Sensing

103

Saturday, October 24, 2015, 01:00 pm - 02:30 pm

Chair: **James Friend**
University of California, San Diego

5J-1 _____

1:00 pm   **Assessment of the nucleus to cytoplasmic ratio for tumor cell identification using high-frequency ultrasound and photoacoustics.**

Michael Moore[1], Eric Strohm[1], **Michael Kolios[1]**; *[1]Ryerson University, Canada*

Background, Motivation and Objective

The nucleus to cytoplasm ratio (N:C) is a parameter commonly used during histopathological assessment of biopsied tissues. Cells exhibiting malignant characteristics have enlarged nuclei due to their increased DNA content and thus demonstrate a larger N:C ratio than non-malignant cells. The most common method of determining the N:C ratio involves using optical microscopy to examine a sample of biopsied tissue to assess the cross sectional area of both nucleus and cytoplasm; however the stereological interpretation of the N:C ratio may be inaccurate depending on the cellular cross section being assessed. High frequency ultrasound (US) and photoacoustics (PA) may be used to determine a more accurate N:C ratio, as the diameter of cells in suspension can be directly calculated without the need for inference using 2D cross sections.

Statement of Contribution/Methods

Cultured MCF7 breast cancer and HT29 colorectal cancer cells were stained with DRAQ5, a dye which binds to DNA within the nucleus. Suspensions of both stained cell lines were examined using a photoacoustic microscope outfitted with a pulsed 532nm laser co-aligned with a transducer with a 375 MHz central frequency. Pulse-echo US signals were recorded from the cells and PA signals were recorded from the cell nuclei by focusing the laser onto the cell using an optical objective. DRAQ5 absorbs light at 532nm and facilitated the generation of photoacoustic waves from the nucleus. The power spectra of the acquired US and PA A-lines were compared to analytical solutions for a spherical scatterer and a spherical absorber to determine the cell and nuclear diameters, respectively.

Results/Discussion

A total of 20 cells were measured. The average diameters for the MCF7 and HT29 cells were found to be 15.88μm and 12.30μm respectively. The average nuclear diameter was 11.86μm for MCF7 cells, and 11.40μm for HT29 cells. Using these values the corresponding N:C ratios were found to be 1.26 for the MCF7 cells and 6.06 for the HT29 cells. This work is the first demonstration that US and PA signals can be used to calculate the nuclear and cell diameters, providing a more consistent evaluation of the N:C ratio for cells in suspension. In the future, the use of this measurement methodology will enable the evaluation of the N:C ratio for a population of cells without the need for time consuming sample preparation and analysis using optical microscopy.
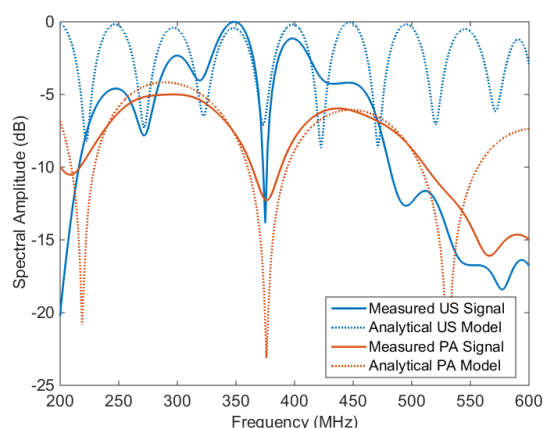
Figure 1. Measurements obtained from a single MCF7 cell. Shown in blue is the power spectrum of the backscattered US signal (solid line) as well as the analytical solution for a spherical US scatterer (dashed line). Shown in orange is the power spectrum of the measured PA signal from the cell nucleus (solid line) as well as the analytical solution for a spherical PA absorber (dashed line).

5J-2 _____

1:15 pm   **Multiparametric Ultrasonic Monitoring of Composition and Physical Properties of Liquids**

Aba Priev[1], Slava Boktov[2], Lev Ostrovsky[3]; *[1]Biochemistry and Molecular Biology, Hebrew University, Jerusalem, Israel, [2]NDT Ultrasonics Ltd., Jerusalem, Israel, [3]Zel Technologies, University of Colorado, Bouder, Colorado, USA*

Background, Motivation and Objective

Nowadays food safety and drinking water security are very much at the top of the agenda, but despite these facts, the food industry does not possess a capability to measure and check the liquid food quality in a cheap and efficient manner. Sensitivity and specificity of the ultrasonic microsensor for liquids has been improved through a multiparametric monitoring of ultrasonic parameters of a droplet of liquid and the combination of low and high intensity ultrasonic cylindrical waves. Our theoretical and experimental results demonstrate the potential use of the ultrasonic technology for monitoring the composition and quality control of dairy and other liquid food products, and also for online monitoring of impurities and bacteria in water.

Statement of Contribution/Methods

This ultrasonic analyzer uses radially oscillating PZT piezoceramic micro-tubes, and employs high-intensity standing waves for preliminary separation or aggregation of the particles by the acoustic radiation forces and low-intensity standing waves for compositional analysis. A number of ultrasonic parameters of liquids were measured: sound velocity, acoustic impedance, sound absorption, their temperature and frequency slopes, and particle aggregation rate by acoustic radiation forces. Sound velocity and acoustic impedance, as well as their temperature slopes, reflect the compressibility, density, hydrophobicity, and temperature of the sample. Sound absorption, its frequency slope, as well as particle aggregation rate are sensitive to viscosity, size of the particles, and to relaxation processes due to energy losses or conformational transitions.

SATURDAY ORAL

Results/Discussion

Preliminary testing of the analyzer was carried out on more than 500 samples of water and milk. Obtained results demonstrate a possibility of ultrasonic online monitoring and comparison of the ultrasonic data with the central certified laboratory-produced linear calibration curves for different properties or composition of the milk and water with correlation coefficients higher than 0.98. A device based on standing cylindrical waves is useful for sample pretreatment and mixing, and far superior to other instrumentation in respect to industrial requirements such as cost, precision, and ease of use in flow-through systems. The main advantages of the proposed ultrasonic method include its nondestructive nature, no need for adding reagents, rapid results, and ability to work with original, undiluted liquid food samples.

5J-3

1:30 pm   Ultrasonic Viscometer with Integrated Depth Measurement

Po-Cheng Chen[1], Amit Lal[1]; *[1]SonicMEMS, School of Electrical and Computer Engineering, Cornell University, USA*

Background, Motivation and Objective

Miniaturized liquid sensors are essential devices in online process or condition monitoring. In the cases of viscosity and density sensing, microacoustic sensors such as quartz crystal resonators or SAW devices have proved useful. The high frequency of operation limits these devices to measurement of thin liquid layers, owing to the low shear viscous depth and smaller bulk absorption depth. These parameters are often not comparable to the macroscopic parameters probed by conventional viscometers operating at 1-100 Hz in liquid. Miniaturized cantilever-based devices offer an alternative, but precise immersion depth control limits the measurement accuracy. For handheld portable viscosity measurements, such as those for biomedical sample testing, one needs to be able to measure the viscosity without the need for measuring the depth of insertion of an ultrasonic actuator. Here we present a viscometer that can measure the viscosity while keeping track of the depth of insertion.

Statement of Contribution/Methods

We report on a microfabricated silicon ultrasonic sensor with integrated holes and four sets of piezoresistive strain gauge for viscosity measurement (1A). The silicon beam is actuated at its $\lambda/2$ longitudinal resonance frequency, ~88 kHz, by one PZT plate bonded at its longitudinal mode node. The modes excited by the actuator are a combination of surface motion generating the shear strain in liquids and an out-plane motion drive bulk mode into the liquid. Two rows of 700 µm pores are used to create a step-like function in transducer amplitude (1C), which is measured by strain signals upon immersion in liquid. This step signal is caused by decreasing and increasing the sensor-liquid contact area (1B), which can provide the immersion depth and liquid viscosity information simultaneously. The microprobe was characterized in various bulk viscosities reference standards. From the vibration amplitude measured by the strain gauges, we were able to quantify the damping in the fluid which is proportional to the viscosity (1D).

Results/Discussion

In this work, we demonstrate an ultrasonic actuated silicon viscometer with integrated immersion depth sensor and strain gauges. The immersion depth and viscosity information from the liquid can be extracted simultaneously, solving a major problem of depth calibration in the portable application of ultrasonic viscometers.
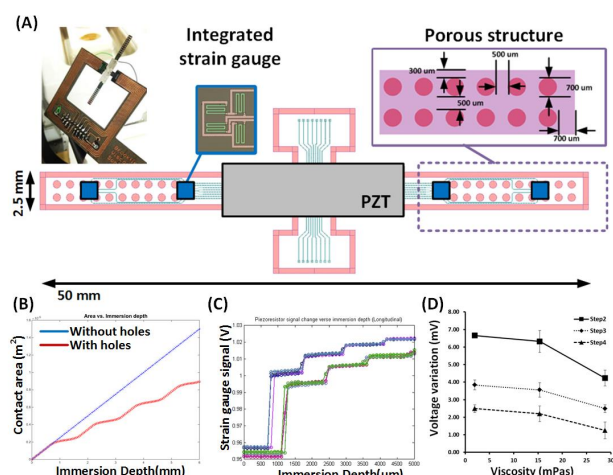
Figure 1 (A) Silicon ultrasonic viscometer with integrated strain gauge and porous structure. (B) Contact area comparison between non-porous and porous structure. (C) Strain gauge signal measured from viscous liquids. (D) Summary of voltage variation under different viscous liquid at different steps.

5J-4

1:45 pm   Design and Performance of an Active Acoustic Back Cover Based on Piezoelectric Elements

Nicola Lamberti[1], Monica La Mura[1], Giosuè Caliano[2], Alessandro Stuart Savoia[2]; *[1]DIIn, University of Salerno, Fisciano, Italy, [2]Dept. of Engineering, University Roma Tre, Rome, Italy*

Background, Motivation and Objective

In recent years, the advent of smartphones and tablet PCs, has made necessary to use multi-touch or stylus-based input devices that are more useful for mobile applications. Several solutions based on different types of optical and acoustical interactions have been presented in literature. In the IEEE IUS 2014 conference, we demonstrated that the back cover of a smartphones can be used as active input devices; in this paper we analyze its performances both by FEM and experimentally, by means of a prototype.

Statement of Contribution/Methods

The device is composed by the back cover of the smart device on which we glue two small, thin piezoelectric plates, one in the cover center and the other in a corner. The presence and position of a finger on the cover external surface is revealed by the variation of the electrical input impedance, measured by electrically connecting in parallel the two piezoelectric plates. We analyzed the device both by FEM and experimentally, in order to evaluate the resolution of the sensor varying the finger position.

Results/Discussion

In figure 1 is shown the FEM (ANSYS ®) model of the back cover, a rectangular plate (L = 12 cm, W = 7 cm, t = 1.5 mm), with two piezoelectric plates (L = W = 1 cm, t = 1 mm). The finger is simulated by a parallelepiped (L = W = 1 cm, t = 10 cm), placed on the outer cover face. Figure 2 shows the electrical input impedance amplitudes (|Zi|) computed connecting in parallel the two piezoceramics and placing the finger in the four cover corners. Varying the finger position, we obtain different curves, confirming the device usability. In the paper, we computed, and measured on a prototype, |Zi| by moving the finger along the cover surface; the obtained results demonstrates that the finger position can be located by analyzing the frequencies of all |Zi| minima and maxima in the explored frequency range.
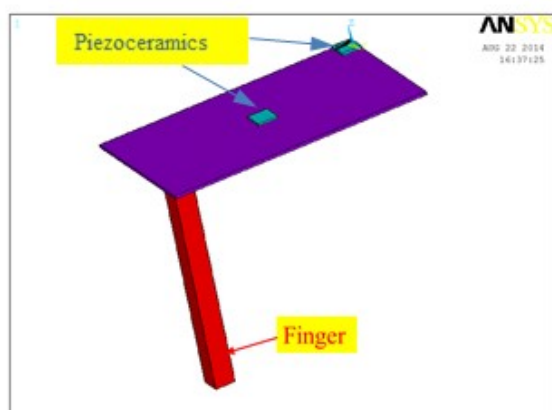
Figure 1
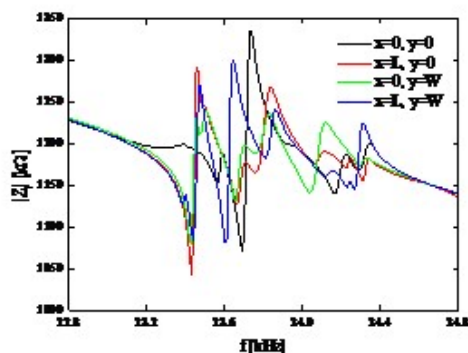
Figure 2

5J-5

2:00 pm   Experimental evaluation of ultrasonic oscillating temperature sensors (UOTS) under cyclically changing temperatures

Anas Hashmi[1], Alexander Kalashnikov[1], Roger Light[1]; [1]*Department of Electrical and Electronic Engineering, The University of Nottingham, United Kingdom*

Background, Motivation and Objective

In contrast to most conventional temperature sensors, which need to come to thermal equilibrium with the medium of interest to report its temperature, UOTS interrogate this medium based on the propagation speed of ultrasound, and will return temperature data that are "averaged" for the complete ultrasound pathway.

It has been demonstrated that UOTS can provide consistent high resolution temperature readings under steadily decreasing temperatures using inexpensive ultrasonic transducers [1] and low cost electronic instrumentation [2].

General purpose temperature sensors must also be able to operate under cyclically changing temperatures. We present experimental results showing that piezoelectric temperature hysteresis complicates interpretation of the UOTS output frequency but that this can be overcome by using sensor data fusion.

Statement of Contribution/Methods

The experimental setup included eight conventional temperature sensors (DS18S20 being the sensing element) and four pairs of inexpensive ultrasonic transducers placed inside a cylindrical vessel with an inner diameter of 100 mm, filled with tap water. Electronic instrumentation consisted of an UOTS driver, which also provided output frequency measurement, and a device for DS18S20 data collecting. Both devices reported acquired data over USB. The assembly was either left on a laboratory desk for prolonged time periods (up to several days, Fig.1) or was placed inside a thermostat controlled incubator where the temperature was ramped up and down. The recorded data were plotted versus time (Fig.1a) and against each other (Fig.1b).

Results/Discussion

Fig.1b shows the presence of ambiguity between the UOTS output frequency and temperature where the same frequency can be related to different temperatures. Moreover, the frequency-temperature relationship consists of a set of different curves each starting at a different temperature extremum. We believe that this behaviour was observed due to thermal hysteresis common to piezoelectric materials. For this reason an UOTS sensor needs to be complemented with a conventional temperature sensor, which will ensure disambiguation.

[1] S.Alzebda and A.N.Kalashnikov, IEEE Trans. UFFC, vol.57, pp.2704-2711, 2010.

[2] P.Popejoy, S.Alzebda, A.Hashmi et al, Proc.IEEE Ultr.Symp. 2012,pp.2427-2430.
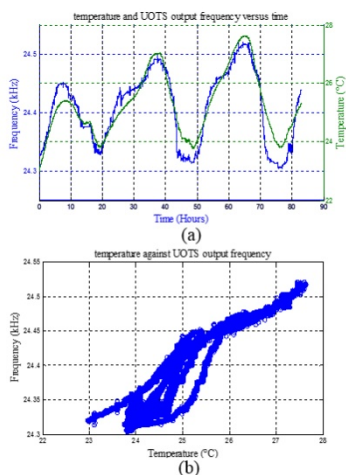
Fig.1. Experimental records of temperature and UOTS output frequency versus time (a) and against each other (b).

5J-6

2:15 pm   Smart Autonomous wireless acoustic sensors for aeronautical SHM applications

Guillaume Ferin[1], Yuvashankar Muralidharan[1], Naoufal Mesbah[1], Claire Bantignies[1], Hung Le Khanh[1], Pascal Chatain[1], Etienne Flesch[1], An Nguyen-Dinh[1]; *[1]Advanced Research Dpt., VERMON, France*

Background, Motivation and Objective

Ultrasound technologies are of great interest for aeronautical structure inspection. Mainly deployed through Phased Array (PA) ultrasonic transducer, ultrasound inspection is thought as a local examination of the structure to determine geometry, damage or composition of invisible flaws like cracks, delamination and corrosion. This approach in aeronautical structure cannot be easily automated since it requires access to area of interest with various complex geometries, along a spatial inspection sampling in agreement with the structure composition and vulnerability requiring a high degree of human interaction.

Structure Health Monitoring, namely SHM, overcomes these limitations by enabling rapid, automated, remote, and real-time monitoring of the structure to reduce operational costs and increase lifetime of structures. This inspection strategy gains its strength from the use of a large amount of individual embedded sensors with basic cognitive skills (sensing, signal processing, communicating and storing relevant data in non-volatile memories) organized in dense network, a Neural Network.

Statement of Contribution/Methods

We present in this paper the developments of a custom autonomous wireless acoustic sensor node, including a flat flexural acoustic sensor capable of working in transmit and receive, a custom vibrational piezoelectric energy harvesting device (PEH) charging a 0.5 Farad buffer supercapacitance through an off-the-shelf IC, an ARM based cortex M3 microprocessor driving digitalization, signal processing, memory storage and two ways RF communication. The main objective was to create a versatile hardware tool that can be embedded within the structure to monitor and capable of hosting different acoustic inspection strategies.

Results/Discussion

As a result, we have built an integrated autonomous wireless acoustic sensor. This unitary acoustic transducer sense guided wave at 200 kHz and can achieve basic Digital Signal Processing to shorten the information to be exchanged with closest sensor nodes. The averaged consumption of the sensor node has been measured at 100µW during a 200ms inspection mode and then turn off into a sleep mode to recharge the supercapacitance for further inspection processes. The PEH device converted a $2m.s^{-2}$ uniaxial harmonic acceleration centered at 75Hz in 50µW (rms) of electrical power. As a result, the inspection duty cycle is reasonable (<6hours) and can be multiplied with serialized energy harvesting devices.

8J - Materials Fabrication and Characterization

102

Saturday, October 24, 2015, 01:00 pm - 02:30 pm

Chair: **Wei Ren**
Xi'an Jiaotong University

8J-1

1:00 pm   **Current Status and Future Prospects of High Performance Piezoelectric Single Crystals: Bridgman Method vs. Solid-state Single Crystal Growth (SSCG) Method**

Ho-yong Lee[1]; [1]*Ceracomp Co. Ltd, Cheonan, Chungnam, Korea, Republic of*

Background, Motivation and Objective

Crystallographically engineered Relaxor-PT single crystals, specifically PMN-PT, offer much higher piezoelectric and electromechanical coupling coefficients ($d_{33} > 1,500$ pC/N, $k_{33} > 0.9$), when compared to PZT ceramics. The technique that has commonly been studied and used for fabricating PMN-PT single crystals is the Bridgman method. Commercial production of PMN-PT single crystals by the Bridgman method has been successful with good reproducibility. However, the production cost is still high and a compositional gradient is usually present in the produced crystals. And these single crystals have very limited usage range in terms of temperature, electric field, and stress because of their low T_C, T_{RT} and E_C. To overcome the high production cost and chemical inhomogeneity problem, the solid-state single crystal growth (SSCG) method has been attempted since the late 1990s. The SSCG method has several advantages over the Bridgman growth, in particular for complex systems, in terms of cost-effectiveness, easy control of chemistry, and the chemical uniformity of the product. Despite these ample advantages, however, studies on the fabrication of single crystals by the SSCG method have only been carried out by a few research groups and commercial application of the technique has been very limited.

Statement of Contribution/Methods

The dielectric and piezoelectric properties of ceramics and single crystals fabricated by various methods are summarized and compared. [001] oriented single crystals with similar compositions, regardless of their fabrication method, exhibit even higher piezoelectric properties than those of ordinary PMN-PT and [001] textured PMN-PT ceramics. The properties of single crystals fabricated at the laboratory scale exhibit considerable variations according to the fabrication method. Several companies are now producing PMN-PT, PIN-PMN-PT and PMN-PZT single crystals by the Bridgman and the SSCG method. In contrast to those of lab-scale products, the properties of the commercial products do not exhibit a considerable difference in piezoelectric properties according to the fabrication method, either the Bridgman or the SSCG method. Compared to PMN-PT single crystals, PMN-PZT single crystals newly developed by dopant engineering technique show much higher piezoelectric properties such as very high dielectric constant ($K_3^T > 10,000$), high T_C ($>200^oC$)/T_{RT} ($>150^oC$), or high Q_m ($>1,000$). These new SSCG PMN-PZT singe crystals are very promising piezoelectrics for very high performance medical ultrasound transducers (imaging and HIFU).

Results/Discussion

Considering recent technical developments in fabricating single crystals and their physical properties, newly developed piezoelectric single crystals are expected to be studied and utilized more widely for piezoelectric applications such as medical ultrasound transducer, SONAR transducer, piezoelectric sensor, and piezoelectric energy harvesting, etc.

8J-2

1:30 pm   **Functional Characterization of Piezocrystals Monitored under High Power Driving Conditions**

Xiaochun Liao[1,2], Tingyi Jiang[1], Muhammad Sadiq[2], Zhihong Huang[1], Sandy Cochran[2]; [1]*School of Engineering, Physics and Mathematics, University of Dundee, Dundee, Scotland, United Kingdom,* [2]*Institute for Medical Science and Technology (IMSaT), University of Dundee, Dundee, Scotland, United Kingdom*

Background, Motivation and Objective

Relaxor-based ferroelectric single crystals exhibit high coupling coefficient as one aspect of their piezoelectric properties. Three generations have been developed, (I) binary e.g. PMN-PT, (II) ternary, e.g. PIN-PMN-PT and (III) doped ternary e.g. Mn:PIN-PMN-PT with compositional engineering for higher rhombohedral-to-tetragonal phase transition temperature (T_{RT}), higher coercive field (E_C) and higher mechanical quality factor (Q_M). Ultrahigh piezoelectric coefficients ($d_{15} = 2190$ pC/N and $d_{36} = 1060$ pC/N) have been confirmed with domain engineering, when the single crystal was characterized under ambient conditions (Liu, Zhang et al. 2010; TRS 2014). All these improvements contribute to their potential applications in high power applications, such as therapeutic ultrasonic transduction and underwater SONAR projection. The work for this paper aimed to characterize the piezocrystals under high power driving conditions, including investigation of the electrical impedance spectroscopy curve, vibration performance and loss analysis.

Statement of Contribution/Methods

A high power characterization system was implemented integrating bespoke impedance spectroscopy, laser vibrometry and thermal imaging. Impedance analysis was realized with a 10:1 passive voltage probe (N2862B, Agilent Technologies, Santa Clara, USA) and a current probe (P6021A, Tektronix, Plano, USA). High frequency vibration response was measured with a laser vibrometer (OFV-2570 / OFV-534, Polytec Ltd, Herts, UK) and the thermal response with a thermal imaging camera (TIM 160, Micro-Epsilon Ltd, Birkenhead, UK). These components were controlled with a PXIe-1082 system (National Instruments, Newbury, UK), with high power signal generation with an RF power amplifier (31002A, Electronics & Innovation, Rochester, NY, USA). Impedance spectra and vibration performance were recorded together with the thermal response when the piezocrystal material was driven with different signal amplitudes. Loss analysis took place off-line and comparison was made between the three piezocrystal generations.

Results/Discussion

Experiments were conducted with TE-mode plates 5 x 5 x 0.5 mm3 with high driving fields, generating temperatures of 40, 60, 80, 100 and 120°C. Electrical impedance spectra were found to become unstable when the temperature increased with the increased high driving voltage. Abrupt changes were identified, with the potential indication of sometimes unexpected ferroelectric-ferroelectric phase transitions (120°C for Mn:PIN-PMN-PT, 100°C for PIN-PMN-PT and 80°C for PMN-PT). As expected, the comparison demonstrated more stable performance from Mn:PIN-PMN-PT when high electric field was applied, if the temperature was limited to 100°C.

Reference:

Liu, X., S. Zhang, et al. (2010). Applied Physics Letters 96(1): 012907.
TRS (2014). "D36 Datasheet."

SATURDAY ORAL

1:45 pm **Characterization of Elastic Properties of Ca₃TaGa₃Si₂O₁₄ at High Temperatures by Antenna Transmission Acoustic Resonance**

Hongfei Zu[1], Huiyan Wu[1], Quanming Lin[2], Yanqing Zheng[2], Qing-Ming Wang[1]; *[1]University of Pittsburgh, USA, [2]Shanghai Institute of Ceramics, China, People's Republic of*

Background, Motivation and Objective

Recently, piezoelectric Ca₃TaGa₃Si₂O₁₄ (CTGS) crystal has drawn much research interest as a promising candidate for the high-temperature sensing applications. The elastic coefficients and their temperature dependence are critical for the design and fabrication of acoustic wave sensors. Among the techniques used for the characterization of the elastic coefficients, resonant ultrasound spectroscopy (RUS) has been widely recognized. However, the RUS method is not perfectly applicable under high temperatures and harsh conditions. As an improvement for RUS, antenna transmission acoustic resonance (ATAR) method provide better approach to overcome the measurement difficulty as high-temperatures. In this work, ATAR method is employed to determine the elastic constants of CTGS up to 800°C.

Statement of Contribution/Methods

As shown in Figure 1, the CTGS bar-shaped resonator specimen is placed inside the antenna tube where temperature can be controlled. The swept sinusoidal excitation signal is applied to excite acoustic waves inside the sample, and the acoustic wave resonances would result in resonant spectrum in which the peaks correspond to the resonant frequencies of acoustic wave specimen. Subsequently, the resonance spectrum can be used to determine the elastic properties of the resonator.

Results/Discussion

Figure 2 shows the resonant spectrum of a CTGS sample measured by ATAR method at room temperature over the frequency range of 130 KHz to 900 KHz. More than 20 resonant frequencies with different amplitudes could be identified. We have systematically investigated the resonant spectrum of CTGS crystal resonators at elevated temperatures, and extracted the complete elastic coefficients of the crystal resonator. The results will be reported in this presentation.
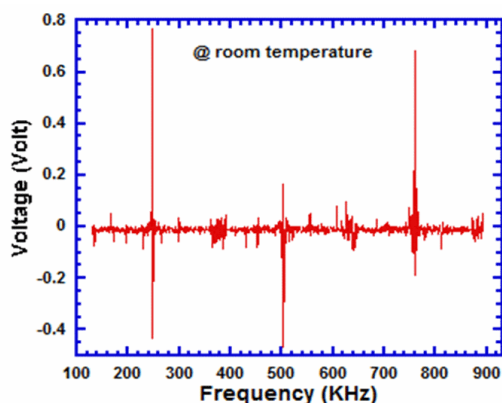
Fig. 2. Resonant spectrum of a CTGS sample measured by ATAR method
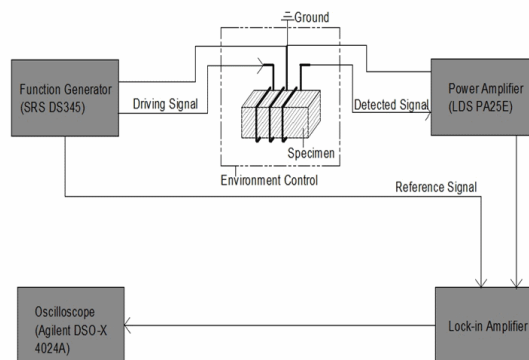
Figure 1. Block diagram for the ATAR measurement setup

2:00 pm **Characterization of lead-free alkali niobate piezoceramics by the Inverse Method**

Kenji Ogo[1], Manuel Weiß[2], Stefan Rupitsch[2], Reinhard Lerch[2], Ken-ichi Kakimoto[1]; *[1]Department of Materials science and Engineering, Nagoya Institute of Technology, Nagoya, Japan, [2]Chair of Sensor Technology, Friedrich-Alexander University Erlangen-Nürnberg, Erlangen, Germany*

Background, Motivation and Objective

Alkali niobate piezoceramics are considered as one of the most important lead-free piezoelectric materials because of their high *T*c (Curie temperature) and great piezoelectric properties. However, their temperature dependence of material parameters have not been characterized yet. Therefore, this research focuses on temperature dependence of alkali niobate piezoceramics. The material parameters were identified by the Inverse Method, which provides the material parameters by minimizing the deviation between experimental results and FE (finite elements) simulations.

Statement of Contribution/Methods

Alkali niobate piezoceramics NKN+0.25 mol%MnO (NKN-Mn) were prepared by solid reaction method. All samples were cut and polished into block shape (1.0×3.5×10.0 mm³). Gold sputtered electrodes were added to the samples and polling treatment (3 kV/mm, 30 min in silicon oil at 150 ºC) was conducted. Two types of samples have different polarization directions from each other: thickness (1.0 mm) direction and width (3.5 mm) direction. Frequency resolved electrical impedance was measured as a function of temperature ranging from 25 ºC (R.T.) to -25 ºC, up to 150 ºC and back down to 25 ºC (R.T.). Temperature dependence of the material parameters was determined by using the measurement results and the Inverse Method.

Results/Discussion

Frequency resolved electrical impedance curves shifted to low impedance and low frequency with increasing temperature. In addition, the minimum impedance range of the resonance-antiresonance pair was observed at 75 ºC. Temperature dependences of the material parameters determined by the Inverse Method are shown in Fig. 1. Although permittivity and piezoelectric coefficients increase with temperature, elasticity constants decrease as temperature increase. In particular, c^E_{44}, ε^S_{11} and e_{31} exhibit strong temperature dependences. It can be expected that the temperature dependence of NKN-Mn originates from the phase transition due to their phase transition temperature from orthorhombic to tetragonal phase around 200 ºC. The maximum loss factor all at 75 ºC causes the minimum impedance range of the resonance-antiresonance pair at the same temperature. Furthermore, a thermal hysteresis was observed in case of NKN-Mn, which indicates that irreversible domain wall motions affect the temperature dependence of this material.
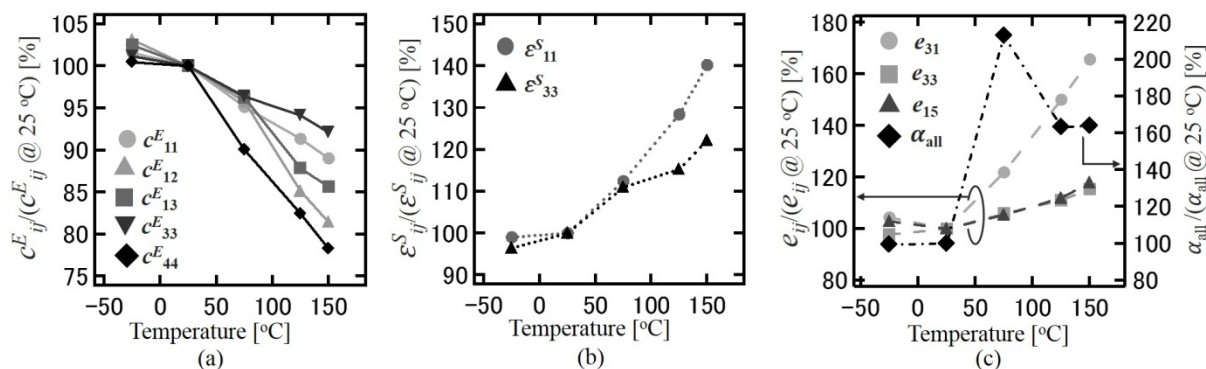
Fig. 1. Temperature dependence of material parameters was identified by using the Inverse Method:
(a) elasticity constants, (b) permittivity and (c) piezoelectric coefficients and loss factor

---

8J-5 _____

2:15 pm **Development of PZT-Based Single Crystals as High-T** and High-Performance Piezoelectric Materials
Zuo-Guang Ye[1,2], Bixia Wang[1], Yujuan Xie[1], Xiaoqing Wu[2], Wei Ren[2]; *[1]Simon Fraser University, Burnaby, BC, Canada, [2]Xi'an Jiaotong University, China, People's Republic of*

Background, Motivation and Objective

Lead zirconate-titanate solid solution, $PbZr_{1-x}Ti_xO_3$ (PZT), has been widely used in electromechanical stransducers and extensively studied for both applied and fundamental research, but almost exclusively in the forms of ceramics and thin films because of the difficulties encountered in growing PZT single crystals. On the other hand, the relaxor-based PMN-PT and PZN-PT (Generation I) and PIN-PMN-PT (Generation II) single crystals exhibit excellent piezoelectric properties, but suffer from a low Curie temperature and a small coercive field which make them unsuitable for high-temperature and high-power applications. Therefore, it is of particular interest to grow large single crystals of PZT for thorough characterization of the anisotropic properties, and also for potential applications. The objective of this work is to synthesize the PZT-based single crystals and to characterize their piezo-/ferroelectric properties, domain structures, phase transitions, and micro polar structures in order to understand the structure-property relations.

Statement of Contribution/Methods

In this work, the $PbZr_{1-x}Ti_xO_3$ single crystals of composition across the MPB range, as well as the donor- and acceptor-doped PZT single crystals, are grown by a top-seeded solution growth (TSSG) technique. We demonstrate that PZT single crystals exhibit superior piezo- and ferroelectric performance over the PZT ceramics, and a higher T_C and a higher coercive field (E_c) than the relaxor-based PMN-PT and PZN-PT single crystals, making them a pormising material for a broad range of advanced applications. The systematic characterization of the grown PZT single crystals by a variety of techniques, such as dielectric and piezo-/ferroelectric measurements, polarized light microscopy, piezoresponse force microscopy and transmission electron microscopy, has allowed us to discover a series of new physical phenomena.

Results/Discussion

The crystal growth conditions are optimized in terms of the chemical, thermodynamic and kinetic parameters. The growth temperature is found to be a key factor for controlling the composition of the grown crystals. The crystals of MPB composition, x = 0.46, exhibit the best properties, with a piezoelectric coefficient d_{33} = 1223 pC/N, an electromechanical coupling factor k_{33} = 0.8, a large coercive field Ec= 7 kV/cm and a high Curie temperature TC = 386 ¡ãC, making them a unique class of high-TC and high-performance piezoelectric materials useful for high temperature and high power electromechanical transducer applications.

In the tetragonal crystal of x = 0.54, microscopic polar domains are observed in the form of islands which can be switched using piezoresponse force microscopy. Donor (Bi^{3+} or La^{3+})-doped PZT crystals exhibt high polarization, while acceptor (Mg^{2+} or Mn^{2+})-doped PZT crystals are found to be hardened with an increased coercive field. The doping effects on the structure and properties of PZT single crystals are discussed.

SATURDAY ORAL

1K - MSD: Novel High-Frequency Systems

201AF

Saturday, October 24, 2015, 03:30 pm - 05:00 pm

Chair: **Alfred C. H. Yu**
University of Hong Kong

1K-1

3:30 pm **Real-time ophthalmic imaging with a hand-held, 20-MHz annular array**

Jeffrey A. Ketterling[1], Daniel Gross[1], Ronald H. Silverman[1,2]; [1]*Lizzi Center for Biomedical Engineering, Riverside Research, New York, NY, USA,* [2]*Department of Ophthalmology, Columbia University Medical Center, New York, NY, USA*

Background, Motivation and Objective

Ophthalmic ultrasound is almost exclusively performed using single-element, hand-held transducers. Linear-array systems are not feasible for ophthalmology for the foreseeable future, but annular arrays permit image quality of a linear array without the system complexity and cost. Here, an annular-array transducer previously demonstrated using a cumbersome immersion-scan technique (i.e., water bath coupled to eye) was integrated into a hand-held probe that permitted contact scanning of the human eye.

Statement of Contribution/Methods

A custom, 5-element, 20-MHz annular array based on a 25-µm, P(VDF-TrFE) membrane was packaged in a stainless steel shell and mounted in a commercial, hand-held, mechanical probe specifically designed for clinical ophthalmic imaging. The array had a focal length of 25.8 mm and an aperture of 9 mm with 100-µm gaps between array elements. The array was excited with a 5-channel pulser/receiver (Daxsonics) and a 4-channel, PCIe digitizer (Alazartech) recorded the echo signals for real-time image formation. The array was characterized using a 25-µm wire, an anechoic-sphere phantom and a calibrated hydrophone. After establishing the acoustic parameters were within safety limits, human subjects were imaged. Human subject scanning was accomplished by filling the tip of the probe with water, capping with a fluid pouch and then placing the pouch directly in contact with the sclera.

Results/Discussion

The array was used in a 3-transmit, 4-receive configuration such that all five elements were used in some form. This configuration was chosen to achieve the fastest possible frame rate (4.1 fps) without sacrificing image quality. This frame rate was limited by the hand-held probe. Beamwidth measured with the wire target ranged from about 0.16 mm at 16 mm to 0.42 mm at 45 mm (Fig 1a). Images of the anechoic phantom revealed spheres down to ~ 300 µm diameter could be clearly resolved. Human subject scans revealed images of the full globe (Fig 1b), something not possible with current ophthalmic systems.
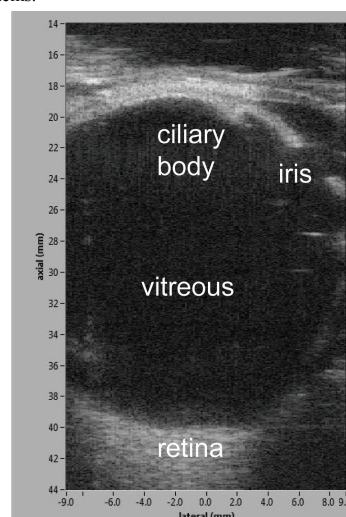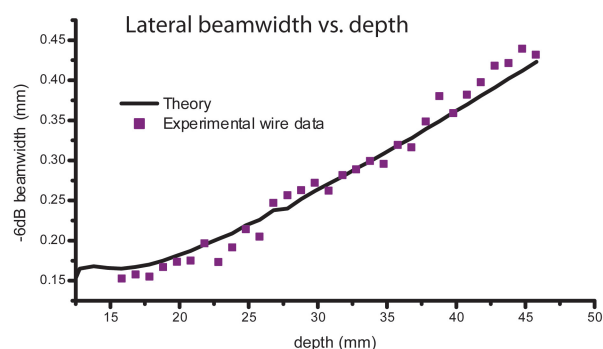
1K-2

3:45 pm **Ultrahigh Frame Rate High-Frequency Array Imaging System for Time-Resolved Monitoring of Cardiac Dynamics in Spontaneous Hypertensive Rats**

Billy Y. S. Yiu[1], Aung Moe Zaw[2], Erwan Filoux[3], Adrian J. Y. Chee[1], Leo T. O. Lee[2], Alfred C. H. Yu[1]; [1]*Medical Engineering Program, University of Hong Kong, Pokfulam, Hong Kong,* [2]*School of Biological Sciences, University of Hong Kong, Pokfulam, Hong Kong,* [3]*Vermon SA, Tours, France*

Background, Motivation and Objective

With the advent of high-frequency arrays, achieving micro-resolution ultrasound imaging at real-time frame rates is nowadays readily feasible. However, in using this tool to image cardiovascular dynamics in small animals, the time resolution remains inadequate because data acquisition was typically done via scanline-based beam sweeping. This issue is further aggravated by the fact that the heart rate of rats (up to 400 beats/min) is typically 4-6 times higher than that of humans. To overcome this technical bottleneck, here we aim to establish a new high-frequency array platform with achievable frame rate well above 1000 fps as realized through plane wave compounding.

Statement of Contribution/Methods

Our platform hardware is a composite system that consists of four components: 1) an L20/128 high-frequency array (Vermon SA; 0.1 mm pitch, 8 mm elevation focus); 2) a software-programmable transmit pulser (SonixTouch front-end); 3) a 128-channel pre-beamformed data acquisition tool (80 MHz sampling rate, 10 bit resolution, 16 GB buffer); 4) a GPU beamformer (array of three GTX-590 devices). The transmit pulser was configured such that each transmit event would fire a plane wave pulse (1 cycle duration) from a particular steering angle (from -10 to + 10 deg, in +1 deg increments). With a 10 kHz PRF, channel data frames can be consecutively acquired over 3s for a 2cm depth. This platform was used to study cardiac contraction dynamics in spontaneous hypertensive rats (400 g, 20 week old male, normal rodent diet). When acquiring image data, the rats were anesthetized, and the array was positioned to image the cardiac cross-section. Raw channel data were streamed using a USB link to the GPU beamformer to derive: 1) plane-wave compounded images at real-time throughputs; 2) M-mode traces at different radial angles.

Institute of Electrical and Electronics Engineers

Results/Discussion

With a 2500 fps nominal frame rate (with 4-frame sliding window steps), cardiac contraction dynamics can be rendered consistently throughout the entire cardiac cycle [Figs (a) & (b): frames during diastole and systole, 40 um pixel resolution]. Also, parallel M-mode monitoring from different angles shows how radial cardiac contraction may vary in hypertensive rats [Fig (c): M-mode traces for three angles marked in (b)]. These functionalities show that our platform can offer time-resolved monitoring of cardiac dynamics in rat models of heart diseases.
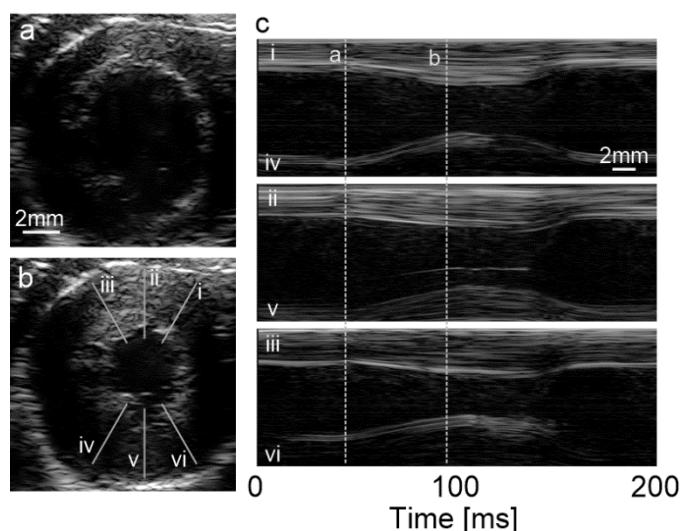
1K-3

4:00 pm   Very high frequency ultrasound beamformer for biomedical applications and non-destructive testing

Christoph Risser[1], Hans Joachim Welsch[1], Heinrich Fonfara[1], **Holger Hewener[1]**, Steffen Weber[1], Steffen Tretbar[1]; *[1]Ultrasound, Fraunhofer IBMT, Sankt Ingbert, Germany*

Background, Motivation and Objective

There are different research platforms available for the development of ultrasound applications and algorithm designs but they are all limited by its digitalization frequency ranging up to 80 MHz for standard medical imaging. Using transducers with mid frequencies above 20 MHz for high resolution (bio-)medical imaging, small animal imaging, skin imaging or non-destructive material testing requires ultrasound devices with higher sampling rates. Usually these systems are based on single channel electronics combined with multiplexing electronics for array transducers or mechanical movement of single element transducers. High speed imaging using modern beamforming like plane wave compounding and improved measurement resolution require higher ultrasound frequencies and multiple channels electronic.

Statement of Contribution/Methods

Based on the existing highly scalable and flexible ultrasound research platform "DiPhAS" that can be used to develop new technologies and integrate them to real life applications based on its cost efficient system design we now realized the high frequency version of the beamformer. The innovation in this version is the digitalization rate of up to 480 MHz with 12 bit resolution at all 128 channels in parallel. Based on a Virtex-6 FPGA and MicroBlaze soft processors the system features 16 application specific front ends set up on the common modular mainboard and power supply. Each front end includes digital and analog circuits for each of the 8 channels per board individually because commercially available integrated circuits are not available for such a high digitalization rate. Transmission can be done with pre-flashed but customizable excitation sequences with voltage up to 20 Vpp. The received data can be accessed as single element channel data of all 128 channels in parallel and transferred to a PC via Gigabit Ethernet or PCI-Express where beamforming can be done on a massive parallel computing graphics processor (GPU). Plane wave imaging is implemented for visualization beside channel data analysis. Online and offline software packages including closed loop control and filtering interfaces for Matlab and C# are used to process, analyze and visualize the data to characterize the beamformer.

Results/Discussion

The system was set up successfully and evaluated and characterized for biomedical imaging methods with three 128 element ultrasound arrays (all designed by Fraunhofer IBMT) with center frequencies at 35 MHz, 56 MHz and 80 MHz. The applications demonstrate the performance of the system to meet real time and signal quality demands for high frequency ultrasound imaging.

1K-4

4:15 pm   An All-Digital Transmit-Beamforming ASIC for High-Frequency and Portable Ultrasound Imaging Systems

Duo Sheng[1], Chih-Chung Huang[2], Zong-Ru Yang[1], Yi-Shang Wang[1]; *[1]Department of Electrical Engineering, Fu Jen Catholic University, New Taipei City, Taiwan, [2]Department of Biomedical Engineering, National Cheng Kung University, Tainan City, Taiwan*

Background, Motivation and Objective

High-frequency ultrasound (HFUS) imaging has been desired in many clinical applications, such as dermatology, ophthalmology, and intravascular imaging of the coronary arteries, which require higher image resolution. Transmit-beamformers of conventional ultrasound imaging system are typically implemented via field programmable gate arrays (FPGAs). However, owing to the limitations of FPGAs, the delay resolution of the chip is not good enough for meeting the requirements of HFUS imaging systems because the beamformer of HFUS imaging needs very small delay time for transmitting each scan line in real time. In addition, the size of the beamformer chip and the number of interconnection cables must be reduced for a small agile probe or portable ultrasound imaging system. Therefore, the purpose of this study is to design an all digital transmit-beamforming application-specific integrated circuit (ASIC) for achieving a high resolution delay time of array elements which can be directly integrated with the high-voltage pulser integrated circuit (IC) for HFUS imaging and portable ultrasound imaging system applications.

Statement of Contribution/Methods

The proposed transmit beamformer comprises an all-digital delay-locked loop (ADDLL) and a beamforming delay line (BDL). The digitally-controlled delay cells (DCDC) in the ADDLL and the BDL have the same circuit structure. After the ADDLL is locked, the digital control code is sent to the BDL, and thereby generates an accurate delay for beamforming. The digital control signal is robust when it has long path propagation. The proposed DCDC comprises a ladder-shaped delay stage (LSDS) and an interpolation delay stage (IDS), which extends the delay range and improves the delay resolution, respectively. The framework of ASIC is shown in Figure (left). In addition, the proposed ASIC can be implemented with all-digital design manner, making it easily be ported to different processes and very suitable for system-level integration.

SATURDAY ORAL

Results/Discussion

The proposed transmit beamformer ASIC is implemented in 0.18 µm CMOS technology and integrated with a 30-MHz high-frequency linear array. The simulation results show that each channel can be programmed to achieve a maximum time delay of 439 ns at a resolution of 441 ps. In addition, the lateral resolution at 5, 7.5, and 10 mm is 39.2, 43.4, and 60.1 µm, as shown in Figure (right).
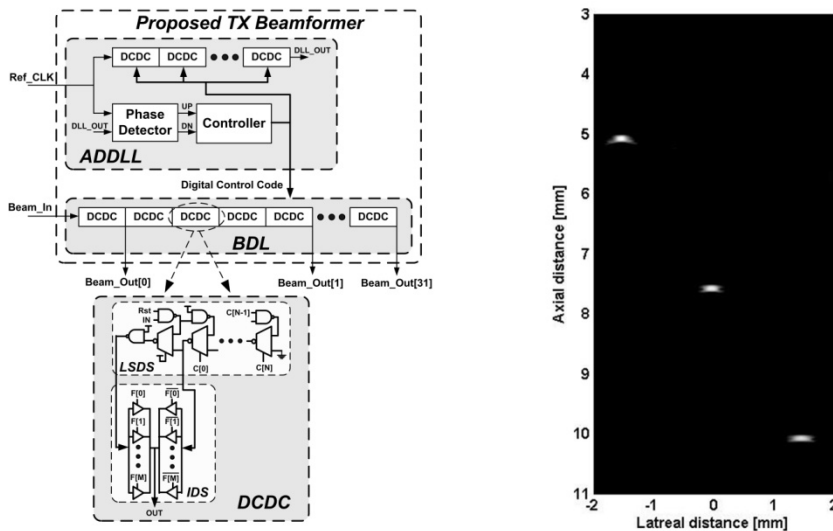
1K-5

4:30 pm   Distortion Reduction for a Dental HFUS Microscanning Device

Thorsten Vollborn[1], Christoph Schorn[1], Daniel Habor[1], Fabrice Chuembou Pekam[1], Klaus Radermacher[1]; *[1]Chair of Medical Engineering, RWTH Aachen, Germany*

Background, Motivation and Objective

Silicone impression-taking of teeth is an established but inefficient technique for CAD/CAM of dental prosthetics. Hence, intra-oral scanners based on optical technologies have been developed to optimize the process of impressioning and to enable a complete chairside workflow. However, during the scan, critical model defects can result from the presence of blood or saliva and sub-gingival areas still must be invasively exposed for scanning.

We introduced high frequency ultrasound (HFUS) as a new method of scanning dental structures. Ultrasound is less sensitive to oral fluids and is inherently able to penetrate gingiva non-invasively. HFUS-based intra-oral microscanning (USM) of teeth requires both a high spatial resolution and mechanical precision to finally achieve an optimal impression detail (<50µm).

Statement of Contribution/Methods

We designed a microscanner based on a direct drive mechanism with 2 degrees of freedom to move an HFUS probe (f=50MHz) along a scan field of 15x15mm² (Fig. 1). In a preliminary study we tested the system's distortion by scanning a ball grid array as a reference body (RB) in tempered water. The ball grid's accuracy was measured by an optical reference scanner (OS) to ±20µm. The Euclidean distance (ED) between ball centers of the RB and the USM were calculated. The maximum ED was measured at 5Hz oscillation rate (OR) up to 295µm (SD 24.8µm). Hence, we implemented a distortion reduction method (DRM) based on a multivariate polynomial. The scaling factors (coefficients of the compensation matrix) were calculated by a regression analysis on the EDs. Finally, the system's precision was evaluated by scanning the occlusal surface of a molar tooth with the USM (OR 5 Hz, trigger distance 60µm) and applying the DRM. The acquired model was aligned and compared to a scan of the OS by using a best-fit algorithm.

Results/Discussion

Fig. 1 shows the resulting deviation of the USM from the OS surface. Without using the DRM we measured a mean deviation of 14.8µm (positive) and 21.2µm (negative) (SD 22.7µm). After the application of the DRM we achieved a mean deviation of 7.6µm (positive) and 19.9µm (negative) (SD 16.9µm). The scan quality of the USM was improved by the developed DRM and thus reached the anticipated precision range for intra-oral impressioning. The integration of the USM into an intra-oral device as well as in-vivo evaluation is part of our ongoing work.
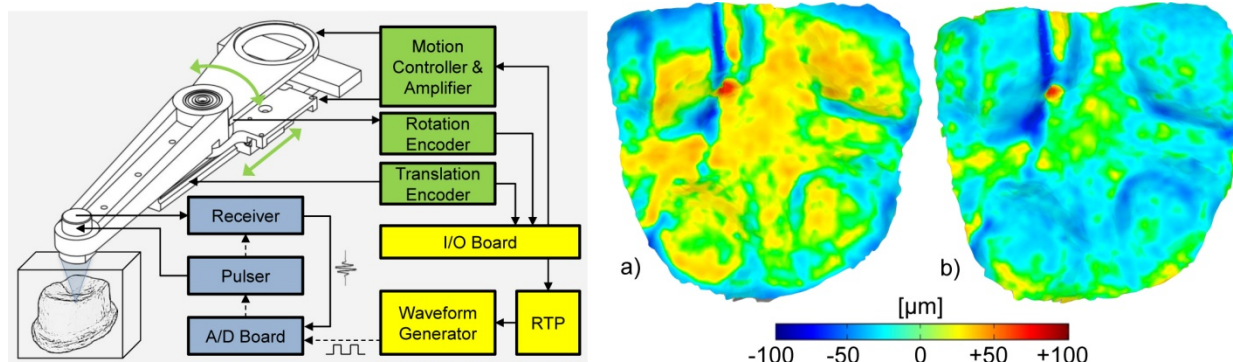
Fig.1: Ultrasonic microscanner based on direct drive mechanism (left); Occlusal tooth surface from ultrasonic scan in comparison to optical reference without (a) and after (b) application of distortion correction (right).

1K-6

4:45 pm   A Graphic Processing Unit based Intravascular Ultrasound(IVUS)

Yongjia Xiang[1], Tiejun Lv[1], Zhile Han[1], Jie Xu[1], Tianming Gu[1], Yaoyao Cui[1]; *[1]Suzhou Institute of Bio-medical Engineering and Technology,CAS, China, People's Republic of*

Background, Motivation and Objective

Intravascular ultrasound (IVUS) plays an important role in the diagnosis of coronary heart disease and intervention therapy. Increasing frequency of IVUS catheter helps to improve the resolution as well as the volume of data expanded to be a serious issue to imaging system. An approach of processing the data in real time and keeping most of the details that original echo signals conveyed is introduced in this study.

Statement of Contribution/Methods

A complete IVUS imaging system was built to work compliance with 60MHz IVUS catheters, which can achieve an axial resolution of 60¦Ìm. There is a handheld module in the system integrated with a motor controller to drive the imaging core of the catheter turning under a speed of 1800 RPM, this module also include a high frequency pulse generator to stimulate the transducer at the distal end of the catheter. Since the catheter is keep rotating, the high voltage pulses are send forward and the echo signal goes back through a wide band contactless magnetic coupler. The radio frequency data captured from the catheter's echo signal with a sample rate of 220MHz is kept untouched into data packages, those packages then be transfer back through PCI Express bus to the data processing platform frame by frame, with graphic processing units (GPU), B mode image can be reconstructed in real time. The best of all, most of the details are accessible by software, so there will be an outlet for the algorithm to do multi-kinds of analysis.

Results/Discussion

A basic PDMS material phantom was utilized to test the functionality of the machine. The testing result is illustrated in figure 1 (b). The picture of system and its critical parts are given in figure 1(a). A resolution phantom with target thread diameter of 10um is assembled to test the axial and lateral resolution of the system. The minimum gap that the system can tell apart in axial and lateral directions are 60um and 300um respectively.

(a)   (b)
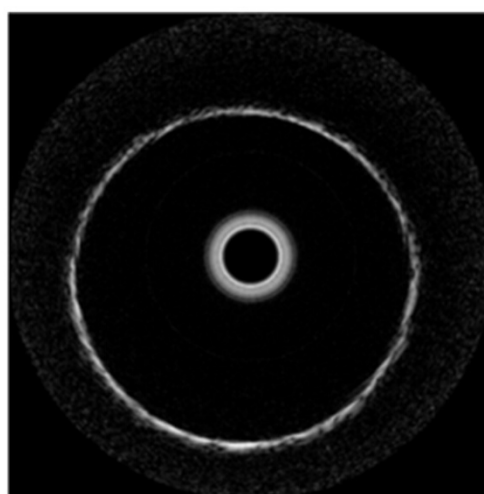
SATURDAY ORAL

2K - MIM: Medical Imaging II

VIP

Saturday, October 24, 2015, 03:30 pm - 05:00 pm

Chair: **Matthew O'Donnell**
University of Washington

2K-1

3:30 pm   High Speed Imaging and Measurement of Laryngeal Vibration during Phonation Using Ultrafast Ultrasonography: a Preliminary Study

Bowen Jing[1], Shanshan Tang[1], Liang Wu[1], Supin Wang[1], Mingxi Wan[1]; [1]*The Key Laboratory of Biomedical Information Engineering of Ministry of Education, Department of Biomedical Engineering,School of Life Science and Technology,Xi`an Jiaotong University, Xi'an, Shaanxi, China, People's Republic of*

Background, Motivation and Objective

Observation and measurement of laryngeal vibration during phonation is essential for study of voice production. Due to the advantages in noninvasiveness and penetration, conventional B mode ultrasonography has been introduced in our previous studies of laryngeal tissue vibration. However, its main drawbacks are the insufficient frame rate, drastically narrowed field of view(FOV) and line to line acquisition lag. Thus, ultrafast ultrasonography that offers a much wider FOV and ultrahigh frame rate is introduced in the present study for observation and measurement of laryngeal vibration.

Statement of Contribution/Methods

Ultrafast ultrasonography is achieved by emitting an 8MHz plane wave using the full aperture of a linear array transducer on a scanner(SonixTouch, Ultrasonix, Canada) and then applying beamforming on received raw RF data. The FOV($25 \times 38mm^2$) covers the whole glottis as well as sub and supra glottal structures of the larynx. Non-stationary laryngeal vibration are recorded at 5k fps when subjects start voicing vowel /u:/ during experiments. To measure the vibration, a RF speckle tracking algorithm based on normalized cross correlation is used. The cross correlation coefficient between the displaced and best matched reference speckle is also obtained at each point within the region of interest. The electroglottogram(EGG) is recorded as a reference indicator of vibration phase .

Results/Discussion

The vibration of the vocal fold can be easily identified and shows clear correlation with EGG waveform(Fig.1). The non-stationary process of the vibration of sub and supra glottal tissue during onset of voicing is well quantified with high temporal resolution, while the vibration of the body and cover of the vocal fold appears chaotic and against mechanical principle (Fig.2). Actually, the cross correlation coefficient at the body and cover are significant lower than that at the sub and supra glottal regions(Fig.3). Despite of the fact that measurement of vibration of the body and cover is compromised by their high deformation rate and interference of strong echo at mucosa-air interface, ultrafast ultrasonography can be used in visualization and measurement of tissue vibration and deformation of certain structures in the larynx. Thus, there is potential value of this technique being used in estimation of mechanical properties of laryngeal tissue.

Fig.1 Images of the larynx are obtained in coronal plane. Four inconsecutive frames shown here are captured at four different glottal phases as marked in EGG waveform. Regions marked by blue, red, green and magenta rectangles represent the supra-glottis, sub-glottis, body of vocal fold and cover of vocal fold respectively. FVF: false vocal fold; VF: vocal fold.

Fig.2 The cross correlation coefficient at each region varies from moment to moment during a laryneal vibration cycle. The cross correlation coefficient are shown in the form of mean with 25th and 75th percentiles of all the sample points in the region.

Fig.3 Vibration displacement of tissue at the marked point(Fig.1) in each region is shown here.

2K-2

3:45 pm   High spatial-resolution cavitation imaging of laser-triggered PFP droplets

Jaesok Yu[1,2], Nguyen Man[1], Kang Kim[1,2]; [1]*Center for Ultrasound Molecular Imaging and Therapeutics, University of Pittsburgh School of Medicine and University of Pittsburgh Medical Center, Pittsburgh, PA, USA,* [2]*Department of Bioengineering, University of Pittsburgh School of Engineering, Pittsburgh, PA, USA*

Background, Motivation and Objective

The broadband inertial cavitation signals from microbubbles (MBs) have been used for detecting and monitoring drug release. Rupturing MBs in general requires a significantly large negative peak pressure and long pulses, which both raise safety concerns and limit the spatial resolution of cavitation images. Phase transition droplets have been proposed as promising contrast agents for ultrasound (US) and photoacoustic imaging and drug delivery vehicles. In our study of laser-triggered droplets, it was found that vaporized droplets as form of bubbles cavitate and rupture in response to a relatively short acoustic pulse that allows for imaging inertial cavitation at high spatial resolution. In this study, the cavitation imaging of the laser-triggered droplets with high spatial resolution is demonstrated.

Statement of Contribution/Methods

Droplets with perfluoropentane (PFP) were synthesized. ICG was added to the core coated by BSA shell. Droplets of 0.5-5.0 µm were injected into a polyethylene tube (OD/ID: 965/580 µm) submerged in a water tank. Cavitation imaging system was implemented in a programmable US scanner. The system was synchronized with an unfocused single element transducer. (Fig 1a) To induce inertial cavitation, a 700 kPa 1 MHz single cycle excitation US pulse was insonified on the droplets in the tube before and after the droplets were vaporized by a short pulse laser with fluence of $600mJ/cm^2$. Simultaneously, a receive mode on the linear transducer was used to capture

cavitation signals, which were beamformed offline subsequently. The image was reconstructed at different frequency bands; fundamental representing signals from tube walls and broadband component representing inertia cavitation activities.

Results/Discussion

Fig. 1b shows the overlaid cavitation images of droplets before (R) and after (L) vaporization. Inertial cavitation signals were only detected from the vaporized droplets in 20dB scale. These findings were confirmed with the frequency spectra in Fig. 1c, where 4-8 MHz broad band emission was found at -27.5 dB for vaporized droplets while it was found at as low as -43.2 dB for unvaporized droplets. In summary, the optically vaporized droplets can be cavitated and ruptured using a single cycle US pulse. This allows for an inertial cavitation imaging with a high spatial resolution, which can improve the localization of drug delivery.
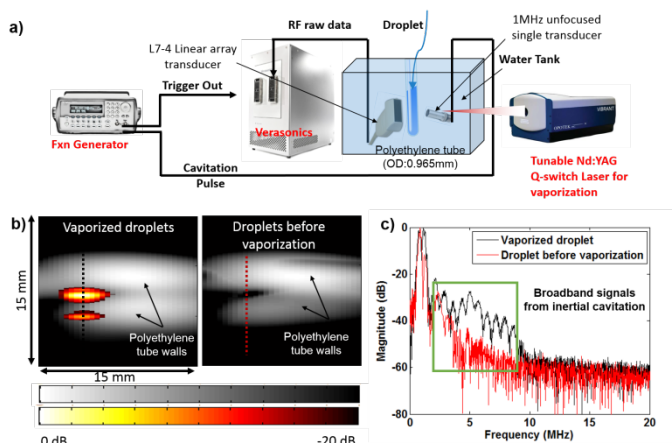
Figure 1. a) Schematic of experiment setup. **b)** Reconstructed image of broadband inertial cavitation signals from the optically vaporized droplets. The inertial cavitation was induced by applying 1 MHz single cycle ultrasound pulse with a peak pressure of 700 kPa (Left). No broadband inertial cavitation signals were recorded from the droplets before vaporization(Right). **c)** Averaged spectrum of 10 selected scanlines from the droplets before (red) and after (black) vaporization.

2K-3

4:00 pm ***In vivo* magnetomotive ultrasound imaging of rat lymphnodes – a pilot study**

Maria Evertsson[1], Magnus Cinthio[1], Pontus Kjellman[2,3], Sarah Fredriksson[2], Roger Andersson[1], Hanna Toftevall[2], Hans W Persson[1], Tomas Jansson[4,5]; *[1]Biomedical Engineering, Faculty of Engineering, LTH, Lund University, Lund, Sweden, [2]Genovis AB, Sweden, [3]Medical Radiation Physics, Clinical Sciences Lund, Lund University, Lund, Sweden, [4]5Biomedical Engineering, Clinical Sciences Lund, Lund University, Lund, Sweden, [5]Medical Services, Skåne University Hospital, Lund, Sweden*

Background, Motivation and Objective

We have previously developed a frequency and phase tracking algorithm which is able to detect superparamagnetic iron oxide nanoparticles (SPIO NPs) using magnetomotive ultrasound imaging, with our primary aim being to detect sentinel lymph nodes (SLNs) in breast cancer surgery. Recently we have shown detection of SPIO laden rat SLNs *in situ* (IEEE T-UFFC, 61:1276-1283). Here we present the feasibility of *in vivo* detection of SLNs in rats and how the signal-to-clutter-ratio is affected by magnetic coil excitation.

Statement of Contribution/Methods

Three Wistar rats were subcutaneously injected with 0.1 mL 35 nm NP solution in concentrations of 0.1, 0.2, 0.3 mg iron oxide/mL in their right hind paws. 24 hours post injection the animals were anaesthetized and scanned with a high frequency ultrasound scanner (Visualsonics VEVO 2100). For each rat the location of the popliteal lymph node, proximal to the injection site, was positioned between the transducer (center frequency 30 MHz) and a coil producing a time varying magnetic field. The AC-voltage (5 Hz) applied on the coil was varied between 5-60 V, in steps of 5 V. The RF IQ cineloops were processed offline in Matlab where our algorithm was implemented. Signal-to-Clutter-Ratios (SCR), defined as magnetomotive displacement amplitude in the lymph node divided by that in the rest of the ultrasound image, were calculated.

Results/Discussion

The SPIO-NP laden sentinel lymph nodes in all three rats were successfully imaged using MMUS and our phase-gated algorithm. Panel A shows a graph of SCR versus excitation voltage. The SCR increases with higher voltage and after 20-30 V the SCR stabilizes and only a small increase can be seen. This is primarily due to magnetic saturation of the iron core at higher voltages. The mean SCR for the three rats (conc. 0.1, 0.2 and 0.3 mg Fe/ml) were 15.7 dB, 23.5 dB and 18.2 dB respectively. This indicates inter-subject variation in SPIO-NP uptake in the sentinel lymph node and/or geometrical differences. Panel B and C show the SLN in rat 2 at 55 V. Panel B shows the total movement in the ultrasound image at all frequencies and phases and panel C shows the frequency and phase gated image obtained using our algorithm. The color represents displacement, note the different scales on the color bars. The SCR was 28.2 dB. In panel B, observe the bright area to the left of the SLN, stemming from the popliteal artery.

SATURDAY ORAL

2K-4

4:15 pm   Ultrafast Pulsed Magnetomotive Ultrasound Imaging of Sentinel Lymph Nodes: Small Animal Study

Yu-Chun Huang[1], Jieh-Yuan Houng[1], Yi-Da Kang[2], San-Yuan Chen[2], Meng-Lin Li[1,3]; [1]*Dept. of Electrical Engineering, National Tsing Hua University, Hsinchu, Taiwan, [2]Dept. of Materials Science and Engineering, National Chiao Tung University, Taiwan, [3]Institute of Photonics Technologies, National Tsing Hua University, Taiwan*

Background, Motivation and Objective

Sentinel lymph nodes (SLNs) are the first draining lymph nodes while the metastatic cancer cells are spreading. A noninvasive imaging modality for SLN identification with fine needle aspiration biopsy (FNAB) would be beneficial for staging the axillary lymph nodes without surgical intervention. Recently, photoacoustic imaging has shown its feasibility of SLN mapping. However, it is not available for clinical use yet, and involves laser safety issues. MRI has been tried with superparamagnetic iron oxide nanoparticles (SPIOs) for SLN imaging. Because of its high cost and low imaging rate, MRI is not a good solution for SLN FNAB.

Statement of Contribution/Methods

Here we propose an alternative solution – ultrafast pulsed magnetomotive ultrasound (pMMUS) for noninvasive SLN identification, which leverages the MRI SPIOs and offers real-time imaging capability for SLN FNAB. Ultrafast pMMUS is based on plane wave imaging, which frame rate is fast enough for tracking of the magneto-motion of the SPIOs induced by a magnetic pulse. Ultrafast pMMUS localizes the SPIOs drained to the SLNs and thus identify the SLNs. Experiments on rats were carried out to verify the feasibility. Each rat was injected intradermally on the hind paw pad with 0.1 ml of SPIO solution under anesthesia. Ten minutes post injection, ultrafast pMMUS with a 5-kHz frame rate and a 6-ms magnetic pulse was performed postmortem using a clinical ultrasound research platform (Prodigy, S-Sharp, Taiwan). Matched filtering with the measured magnetic pulse was applied to improve the pMMUS contrast deteriorated by false motion estimation and magnetic field inhomogeneity.

Results/Discussion

Fig. (a) showed the B-mode image of the SPIO-laden SLN and its surrounding fat tissue where the SLN was hard to be localized. Ultrafast pMMUS displacement mappings at 0- and 6.4-ms when the magnetic pulse being applied were shown in Figs. (b) and (c), respectively. The SLN was identified in Fig. (c), and was confirmed by the methylene blue assay. The dynamic response of the excited SPIOs was visualized and compared with the measured magnetic pulse (Fig. (d)). Overall, we demonstrated the feasibility of the proposed ultrafast pMMUS for noninvasive SLN identification. Proper SPIO particle size, time window of imaging, and motion-tracking algorithm will be studied to further improve the performance of the proposed method.

(a) B-mode image

(b) Ultrafast pMMUS at t=0 msec

(c) Ultrafast pMMUS at t=6.4 msec

(d) Normalized displacement curve

2K-5

4:30 pm   Sonographic Detection of Magnetic Nanoparticles in Weak Echogenic Tissue

Michael Fink[1], Helmut Ermert[1], Moritz Nüßlein[1], Stefan Lyer[2], Christoph Alexiou[2]; [1]*Chair of Sensor Technology, Friedrich-Alexander-University Erlangen-Nuremberg, Germany, [2]Section for Experimental Oncology and Nanomedicine (SEON), University Hospital Erlangen, Germany*

Background, Motivation and Objective

Magnetic Drug Targeting (MDT) is a new cancer treatment technique that enables a local chemotherapy. For this purpose chemotherapeutic drugs are bound to magnetic nanoparticles and accumulated in the tumor area by means of an external magnetic field. As visualization of nanoparticles is of vital importance for MDT, we present a special approach for a sonographic detection of magnetic nanoparticles which are not visible directly using ultrasound imaging techniques because of their weak backscattering.

Statement of Contribution/Methods

We present an evaluation algorithm in order to detect injected nanoparticles by means of ultrasound imaging techniques. Due to an external time harmonic magnetic field the nanoparticles and consequently the surrounding tissue is oscillating with twice the frequency of the magnetic field. This tissue movement offers a measurable effect.

In this contribution we analyze the received high frequency ultrasound data (rf data). Axial tissue movements lead to a shift of these rf data. The algorithm is based on the observation of the magnitude value at certain points of the ultrasound image. For each point the time-dependent chart of the magnitude value can be transformed into frequency domain using fourier transform. The amplitude spectrum depends on the magnitude value of this chart which means that the result depends on the echogenicity of the observed tissue. This problem is solved by normalizing the rf-data to its envelope. Furthermore, the amplitude spectrum depends on the phase of the rf data at the point of observation. Thus, two points of observation suffering the same shift of the rf data may differ in their amplitude spectrum. This problem is handled by weighting each point of observation concerning its exact position. We introduce a weighting factor which depends on the phase of the high frequency data.

Results/Discussion

These improvements allow to detect shifts in the ultrasound image even in areas that suffer from weak echogenicity. Figure 1 shows the experimental setup and the B-mode image of the tissue mimicking phantom. It contains a bubble in which nanoparticles are located. Because of the weak echogenicity of the tissue material and the nanoparticles only movements of the bubble shell can be made visible (figure 1 center right). The new algorithm allows to detect movements in areas of weak echogenicity, too (right).

SATURDAY ORAL
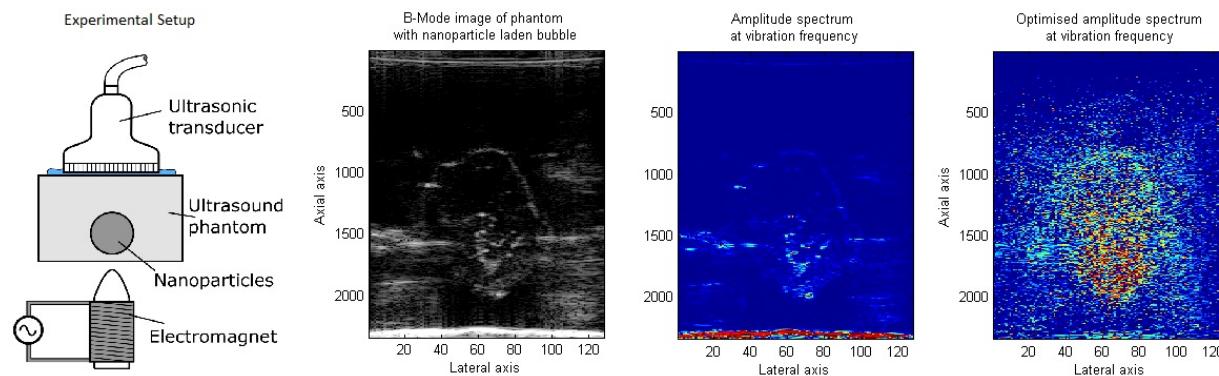
2K-6

4:45 pm   Non-Contact Thermoacoustic Imaging of Tissue with Airborne Ultrasound Detection

Kevin C. Boyle[1], Hao Nan[1], Nikhil Apte[2,3], Miaad S. Aliroteh[1], Anshuman Bhuyan[1], Amin Nikoozadeh[1,2], Butrus T. Khuri-Yakub[1,2], Amin Arbabian[1]; *[1]Electrical Engineering, Stanford University, Stanford, CA, USA, [2]Edward L. Ginzton Lab, Stanford University, Stanford, CA, USA, [3]Mechanical Engineering, Stanford University, Stanford, CA, USA*

Background, Motivation and Objective

The medical imaging field continues to require an imaging modality with tissue conductivity contrast. Tumor angiogenesis and necrotic cores create conductivity contrasts, and in the RF frequency range cell membrane structure strongly influences tissue impedance and absorption rates, illustrating medical applications of mapping dielectric properties of tissue. Furthermore, portability and ease of use considerations push imaging systems towards full non-contact operation. We propose a non-contact radio frequency (RF)/ultrasound hybrid imaging system based on the local RF energy absorption and the thermoacoustic (TA) effect. Airborne capacitive micromachined ultrasonic transducers (CMUTs) are used to create images by standoff detection of the thermoacoustic-generated pressure waves that originate from deep within tissue and propagate through the air interface.

Statement of Contribution/Methods

A detection system (Fig. 1a), leading to an imaging system, has been designed based on 1) pulsed microwave excitation that generates absorption contrast based on dielectric properties of the tissue, 2) the thermoacoustic effect that generates ultrasonic waves due to minute local expansions, and 3) high sensitivity acoustic detection with vented wideband air-CMUTs. The carefully designed vented CMUT structure provides a fractional bandwidth (FBW) of 3.5% in air by utilizing the squeeze-film damping of the air in the cavity. The flexibility in designing the squeeze film damping effect allows for tradeoff between sensitivity and bandwidth, which will be explored in extending the capabilities of this imaging system; for example, we have recently fabricated air-CMUTs with over 30% FBW.

Results/Discussion

A minimum detectable pressure at the face of the CMUT of 240 µPa (rms) was achieved. This pressure is equivalent to a minimum detectable displacement at the face of the CMUT of 1.3 pm. The system achieves a high SNR (with N_{avg}=100 and an average RF power of 13.8 W) to detect 1 cm thick layers embedded in 5 cm of high water content Agarose at a 20 cm standoff (Fig. 1b). We are currently working on the design of multi-frequency CMUTs and CMUT arrays with various center frequencies, fractional bandwidths, and sensitivities. For this paper we will be assessing detection limits for various CMUT designs in the context of the end-to-end imaging system in order to optimize performance.
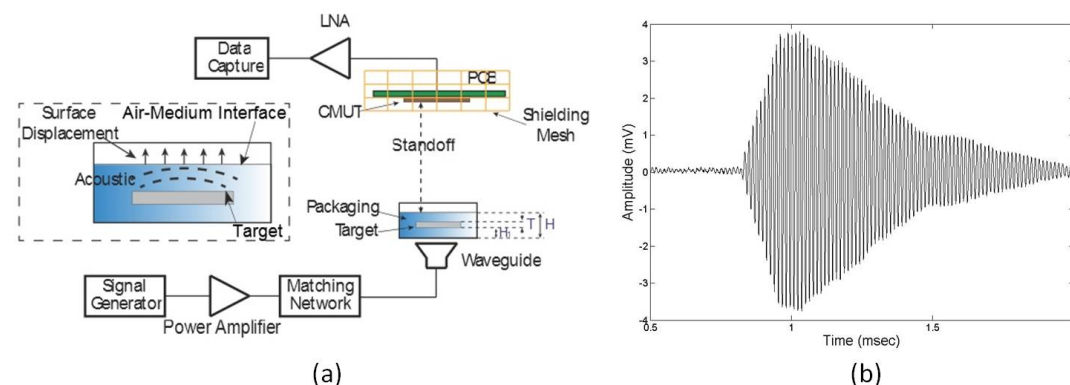
Fig. 1 (a) System diagram for the non-contact thermoacoustic detection setup. H is the thickness of packaging material (around 5 cm of Agarose). T is the thickness of embedded target (1 cm layer of 4 cm² area). (b) Measured response of airborne CMUT to thermoacoustic signal from embedded target where time 0.8 msec corresponds to the location of the target.

3K - MEL: Fundamental Elastography Studies

201BC

Saturday, October 24, 2015, 03:30 pm - 05:00 pm

Chair: **Emad Ebbini**
           Univ. of Minnesota

3:30 pm   **The effect of tissue anisotropy on ultrasound strain imaging (USI): a preliminary study**

He Li[1], Wei-Ning Lee[1]; *[1]The University of Hong Kong, Hong Kong*

Background, Motivation and Objective

The mechanical parameters and view-dependent ultrasonic backscattering of anisotropic soft tissues have been extensively demonstrated, but to our knowledge, whether and how such tissue anisotropy impacts ultrasound elastographic methods has not been substantiated. Hence, this study aims to investigate the influence of tissue anisotropy on the theoretical performance of two-dimensional (2D) ultrasound strain imaging (USI).

Statement of Contribution/Methods

A finite element (FE) isotropic model (*IS*) as a reference and a FE transversely isotropic model of a tendon (Abaqus) were simulated. A 3% axial strain was applied to deform the model, and the pre- and post-compression radio-frequency (RF) data were yielded using Field II in a linear array configuration, with the acoustic anisotropy incorporated. Three scenarios of the fiber orientations, the axial (TIS_{para}), lateral (TIS_{perp_fb}) and elevational (TIS_{perp_cfb}), were considered. Moreover, in vitro examinations were done on a porcine skeletal muscle embedded in a gelatin-agar phantom, which was compressed by 1.2 mm along the beam axis, normal to either the fiber or transverse plane. The RF data were recorded using a Verasonics® Vantage system. An improved USI technique derived from Lee et al. (IEEE-UFFC, 2007) was performed to estimate the 2D displacements between consecutive RF frames. The 2D strain tensor was then obtained from the estimated 2D displacements using a 2D least-squares strain estimator.

Results/Discussion

The lateral strains of the *IS*, TIS_{para}, TIS_{perp_fb} and TIS_{perp_cfb} cases were 1.5%, 1.6%, 0.4%, and 2.4%, respectively, and their corresponding elastographic signal-to-noise ratios (unit: dB) were 23.6, 17.8, 14.0 and 27.5, respectively. Fig. 1(a-d) shows a lower strain accuracy when the fiber was parallel to the acoustic beam (TIS_{para} vs. *IS*), and a higher strain quality in the cross-fiber plane due to the mechanical anisotropy (TIS_{perp_fb} vs. TIS_{perp_cfb}). The lateral strains depicted the anisotropy of skeletal muscle, and the low estimated axial strain quality showed the challenge of accurate strain estimation when the fiber was parallel to the beam (Fig. 1(e-h)). This preliminary study demonstrates that tissue anisotropy affected the performance of USI, and a more comprehensive theoretical study together with experimental examinations is being done to corroborate our study findings.
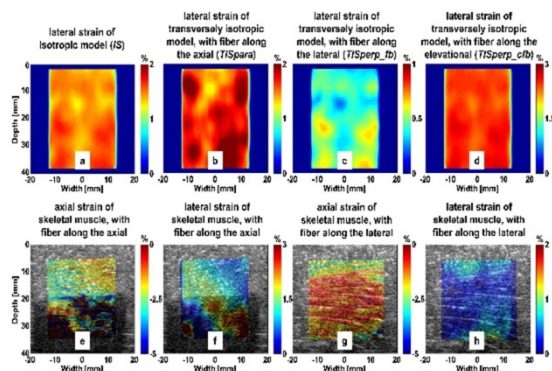
3:45 pm   **Speckle Bias as a 3D Stationary Offset of the Tracking Location for Shear Wave Imaging**

Peter Hollender[1], Gregg Trahey[1,2]; *[1]Biomedical Engineering, Duke University, Durham, North Carolina, USA, [2]Radiology, Duke University Medical Center, Durham, North Carolina, USA*

Background, Motivation and Objective

For Shear Wave Elasticity Imaging (SWEI), the local velocity of a generated shear wave is estimated using time-of-flight (TOF) methods. While a variety of TOF estimators exist, conventional methods all use beamformed ultrasound to listen to the signal at multiple tracking locations. Denoting these methods as MTL-SWEI, single track location SWEI (STL-SWEI) uses a single tracking position, and a multitude of push locations synthesize a wave. STL-SWEI generates superior estimates because push beams are not affected by speckle bias, a stationary noise source which affects the arrival time estimates in MTL-SWEI systems, and provides a fundamental limit on their resolution. This work explores the nature and properties of the speckle bias in three dimensions through simulations.

Statement of Contribution/Methods

A set of analytical point spread functions (PSF) were generated with center frequencies of 10 MHz. Sets of stationary scatters were created to create fully-developed speckle when convolved with the PSF. Motion was induced to provide a radially radiating cylindrical shear wave from a source position (xp,yp), with uniform amplitude through depth. The wavelength and frequency of the wave were chosen to provide a shear velocity of 1 m/s. Tracking lines were beamformed in a 3D grid at the locations (xt,yt) over a 2 cm x 2 cm grid, and through 1 cm of depth, with 0.4 mm spacing in x and y. Each A-line was recorded every 0.1 ms for 1.5 ms. RF cross correlation was used to estimate displacement. The simulation was repeated for the source location at each (xt,yt), making 2601 3D simulated shear wave volume movies. Arrival times were estimated from the phase of the motion, and velocities were found from the radial component of their gradient. Each push and track location generated a full MTL-SWEI or STL-SWEI movie, respectively.

Results/Discussion

The figure shows MTL-SWEI estimated arrival times for a push at (0,0), STL-SWEI arrival times for a track at (0,0), and the simulated motion. We see the speckle bias in the leftmost panel as the over- and under-estimation of the arrival time with spatial correlation. The STL-SWEI estimates are much more accurate, but are centered away
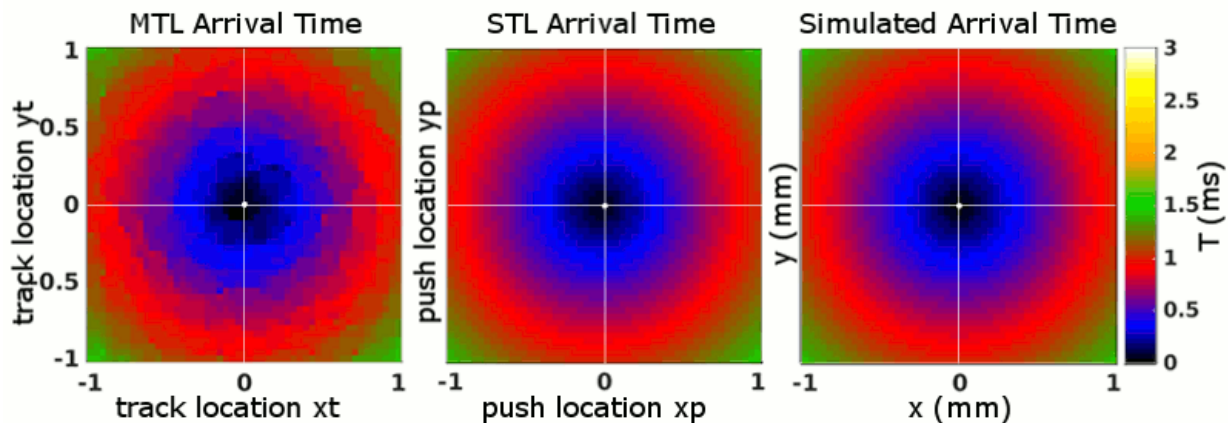
3K-3_____

4:00 pm   Towards Low-push ARFI imaging: Overcoming limitations in Displacement SNR with a Bayesian Estimator

Douglas Dumont[1], Brett Byram[1]; [1]*Biomedical Engineering, Vanderbilt University, Nashville, TN, USA*

Background, Motivation and Objective

Poor displacement signal-to-noise ratio (SNR) due to thermal noise, low displacement magnitudes, and signal decorrelation can impact acoustic radiation-force (ARF) based elasticity imaging (i.e. ARFI imaging and SWEI imaging). Poor SNR due to low displacement magnitudes in particular can be challenging to overcome due to current limitations in acoustic output. Previously, we proposed using a Bayesian estimator to improve the tracking of small-displacements induced in ARFI imaging. In this work, we examine the relationship between displacement magnitude and displacement SNR, and hypothesize that poor displacement SNR can be overcome using Bayesian estimation.

Statement of Contribution/Methods

We simulated ARFI scans of homogeneous (6.5 kPa Young's modulus, n = 25 speckle realizations) and 3mm lesion phantoms (6.5 kPa background, 32.5 kPa lesion, n = 10 speckle realizations) and then varied the ARF to generate peak displacements ranging from 0.31 to 16.51 μm (homogeneous simulations). We tracked the ARF-induced displacements using normalized cross-correlation (NCC) and a Bayesian estimator. Displacement SNR in the homogeneous data was quantified by computing the ratio of the mean and standard-deviation across 25 realizations. Lesion image quality was assessed by measuring the contrast-to-noise ratio (CNR) of the lesion (n=10) realizations.

Results/Discussion

Figure 1 (left column) shows how the displacement SNR changes as a function of peak ARF-induced displacement. The error bars shows the mean and standard deviation of the displacement SNR axially (20 mm axial field-of-view). The results show that the mean axial SNRs for the Bayesian estimator are 8.9 dB higher (range 8 - 9.8 dB) than the NCC estimator. Figure 1 (middle, right) shows ARFI lesion images (units are in μm) for low (middle) and high (right) displacement magnitudes. The Bayesian images compare favorable to the mean NCC image (n=10 realizations) whereas the NCC images show higher variability. The CNR was found to be higher for the Bayesian images (3.5±0.5 and 2.4±0.3, high and low displacement magnitude, respectively) than the NCC images (1.7±0.2 and 0.9±0.1, high and low displacement magnitude, respectively). The results show that displacement magnitude can be lowered by almost an order of magnitude when using a Bayesian estimator, while still maintaining comparable performance to NCC.
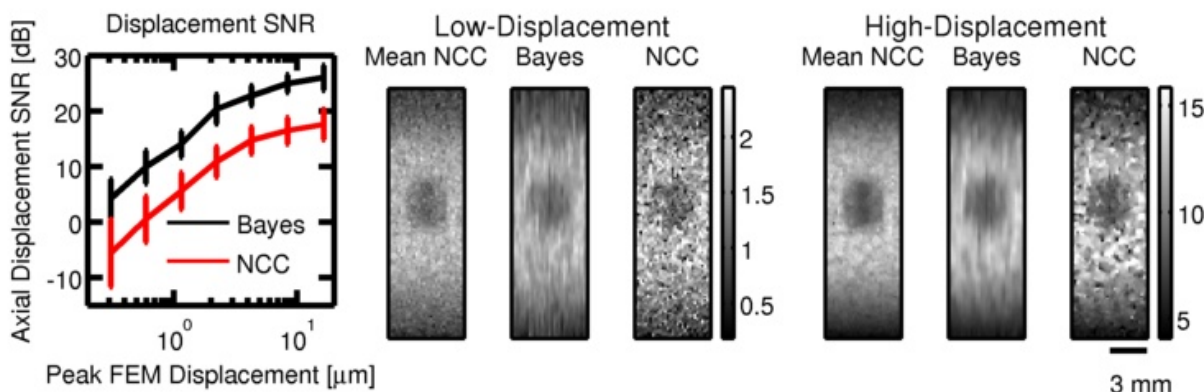
3K-4_____

4:15 pm   Spatial Resolution in Passive Elastography

Ali Zorgani[1], Rémi Souchon[1], Stefan Catheline[1]; [1]*LabTau, UMR1032 INSERM, Lyon, France*

Background, Motivation and Objective

Early cancer diagnostic is an important issue in oncology and medical imaging. The ability of the imaging systems to detect small cancer nodules depends on their spatial resolution. Shear wave elasticity imaging techniques known as elastography, have already shown their ability to locally retrieve the tissue elasticity and therefore suspicious nodules. The resolution of shear wave elastography is investigated in this presentation. Shear waves are generally generated by external sources (radiation force or mechanical shakers). In Passive Elastography, no source is used. It is based on the correlation of the physiological noise-like shear wave field induced by muscles activity, heart beating, and blood pulsatility. The spatial resolution of this technique is compared to the resolution of ultrasound on B-Mode imaging.

Statement of Contribution/Methods

The experiments were conducted on a homemade gelatin phantom. Inclusions with different elasticities imbedded in the phantom were obtained by changing the concentration of gelatin. A random shear wave field is generated in the sample with multiple magnetic shakers. In a first step, using standard speckle tracking algorithm, the displacement field is measured inside the sample at a high frame rate (1000 frames/second) using 5, 10 and 20 MHz? ultrasound probes connected to an ultrafast Verasonics® Vantage ultrasound scanner. Then with algorithms based on spatiotemporal noise correlation, local shear wave speed maps are retrieved.

Results/Discussion

Shear wave speed maps are presented (fig 1.c and d) and compared to the B-Mode images (fig 1.a and b). The contrast in the elasticity maps enables to clearly distinguish both small inclusions with a diameter of 4.5 mm and spaced with 2.5 mm from the background (fig 1.d), and a triangle edge of 2.5 mm (fig 1.c). Other results using different frequencies of ultrasound probes - which changes the spatial resolution of the imaging system were tested and will be presented. They all indicate that a resolution much smaller than the shear wavelength of ≈1.5cm is observed.

This study shows that, with an unchanged shear wave field, resolution increases with the ultrasound frequency. It demonstrates that elastography is not limited by the shear wavelength but by the resolution of the imaging system.
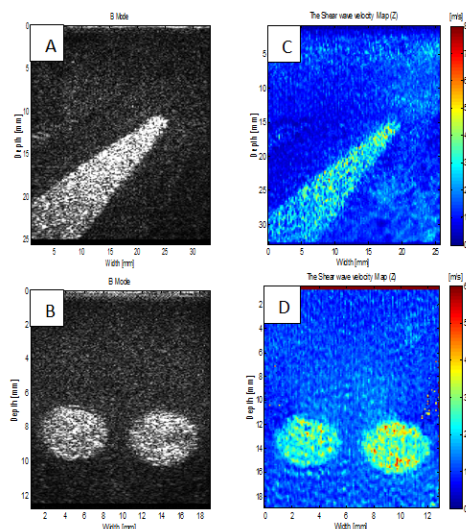
3K-5

4:30 pm   System dependent sources of error in time-of-flight shear wave speed measurements

Yufeng Deng[1], Ned Rouze[1], Mark Palmeri[1], Kathryn Nightingale[1]; [1]*Duke University, Durham, North Carolina, USA*

Background, Motivation and Objective

Several research groups have developed shear wave imaging methods to measure the speed of propagating shear waves following acoustic radiation force (ARF) excitations to reconstruct tissue elasticity. These methods estimate tissue motion from ultrasound data before and after the ARF excitation, and then reconstruct shear wave speed (SWS) from temporal-spatial tissue motion data using time-of-flight (TOF) methods. This work investigates the sources of uncertainty and bias arising from ultrasound system-dependent parameters, such as spatial location and timing, in shear wave speed measurements.

Statement of Contribution/Methods

Errors arising from both spatial and temporal sources lead to errors in TOF-SWS measurements. System-derived temporal errors include master clock jitter, pulse repetition frequency (PRF) and arrival time estimation noise. Sources of spatial errors include phase aberration, beamforming misalignment, and coupling medium sound speed mismatch. Beamforming errors include pitch errors in linear and phased arrays, as well as radius of curvature (ROC) and sector angle errors in curvilinear arrays. Each of the error sources is investigated with the aid of Field II simulations, full-wave acoustic propagation simulations and experimental validation on tissue mimicking phantoms using a Verasonics research scanner.

Results/Discussion

Beamforming errors, coupling medium sound speed mismatch, and PRF noise cause biases in SWS measurements (accuracy errors), while the other error sources cause uncertainties (variance). Phase aberration and arrival time estimation noise are the dominant sources of uncertainty, leading to an uncertainty of ≤ 3% in a typical shear wave imaging system for liver fibrosis staging. These errors can be reduced by averaging over the number of beams used in the SWS reconstruction. Incorrect transducer parameters result in beamforming errors. A 5% pitch error would lead to biases in SWS measurements of 5% in linear arrays and ≤ 5% in phased arrays. The steering effect and the parabolic delay profile in phased array focusing bias SWS measurements in opposite directions. For curvilinear arrays, a 5% error of sector angle would lead to 5% errors in SWS measurements, while a 5% error of ROC would lead to < 5% errors depending on the imaging depth. In our experience, the calibration of transducer parameters in research systems is likely to be less rigorous than in commercial systems. Calibration of these sources of error is an important step in the development of shear wave imaging systems. Spatial errors can be characterized by calibrating the lateral beam positions, which can be accomplished by imaging point targets with known lateral translations. Supported by NIH grant R01EB002132 and RSNA/QIBA studies.

3K-6

4:45 pm   Performance comparison of rigid and affine models for motion estimation using ultrasound radio-frequency signals

Xiaochang Pan[1], Lingyun Huang[2], Jing Bai[1], Jianwen Luo[1]; [1]*Department of Biomedical Engineering, Tsinghua University, Beijing, China, People's Republic of,* [2]*Philips Research China, Shanghai, China, People's Republic of*

Background, Motivation and Objective

Tissue motion estimation is widely used in many ultrasound techniques. Rigid model-based and non-rigid model-based methods are the two main groups of space-domain methods of tissue motion estimation. Affine model is one of the commonly used non-rigid models. The performances of the rigid model and affine model have not been compared on ultrasound radio-frequency (RF) signals, which obtain higher accuracy, precision and resolution compared with B-mode images. In this study, three methods, i.e., the normalized cross-correlation method with rigid model (NCC), the optical flow method with rigid model (OFRM) and optical flow method with affine model (OFAM) are compared using ultrasound RF signals.

Statement of Contribution/Methods

Finite element simulations with a stiffer circular inclusion (75 kPa, 6.5 mm diameter) embedded in a homogeneous background (25 kPa, 38×38 mm^2) were performed under applied strains between -2% to 2%. RF signals from a 6 MHz, 60% bandwidth linear array were simulated using Field II. The root-mean-square error (RMSE) of estimated axial and lateral displacements and elastographic signal-to-noise ratio (SNRe) and contrast-to-noise ratio (CNRe) of estimated axial strains were used to assess the quality of motion estimation. Experiments on a CIRS tissue-mimicking phantom (25±6 kPa) with a stiffer inclusion (80±12 kPa) were conducted under applied strains between -2.4% to 2.4%. The RF signals of the phantoms were acquired from an L9-3 linear array on a Philips iU22 system. The registration error defined as of the sum of squared differences (SSD) between the pre- and post-deformed RF signals and the SNRe and CNRe of axial strain images were utilized as the evaluation criterions. *In vivo* experiments on 5 human subjects with carotid atherosclerotic plaques were also performed. The RF signals of the plaques were acquired from an L9-3 linear array on the iU22 system. The registration error was used to evaluate the estimation performance.

Results/Discussion

The results show that the method with affine model (i.e., OFAM) obtains the lowest RMSE or registration error, and the highest SNRe and CNRe among all the methods. In the simulations, compared with NCC and OFRM, OFAM reduces the RMSE of axial displacements by up to 36.72% and 37.22%, reduces the RMSE of lateral displacements by up to 51.60% and 52.92%, increases the SNRe of axial strains by up to 3.61 dB and 1.31 dB, and increases the CNRe of axial strains by up to 3.68 dB and 2.63 dB, respectively. In the phantom experiments, OFAM reduces the registration error by up to 15.72% and 15.66%, increases the SNRe by up to 4.66 dB and 2.64 dB, and increases the CNRe by up to 9.00 dB and 5.26 dB, respectively, when compared with NCC and OFRM. In the *in vivo* experiments, compared with NCC and OFRM, OFAM reduces the registration errors by up to 28.72% and 16.25%, respectively. The affine model is shown to be superior to the rigid model and is recommended to be employed in ultrasound RF signal-based tissue motion estimation.

SATURDAY ORAL

4K - MCA: Contrast Perfusion Imaging

201DE

Saturday, October 24, 2015, 03:30 pm - 05:00 pm

Chair: **Massimo Mischi**
Eindhoven University of Technology

4K-1

3:30 pm   **Fractal dimension of tumor microvasculature by dynamic contrast-enhanced ultrasound**

Massimo Mischi[1], Carola Heneweer[2], Julian von Broich-Oppert[2], Tamerlan Saidov[1], Hessel Wijkstra[1,3]; *[1]Eindhoven University of Technology, Netherlands, [2]University Hospital Schleswig-Holstein, Germany, [3]Academic Medical Center University of Amsterdam, Netherlands*

Background, Motivation and Objective

Neo-angiogenesis, resulting in the formation of an irregular network of microvessels, plays a fundamental role in the growth of several types of cancer. Characterization of the microvascular architecture and blood flow has therefore gained increasing attention as a tool for cancer diagnosis, treatment monitoring, and test of new drugs. However, available techniques for assessment of the main features of the microvascular architecture, such as the microvascular density (MVD), require immunohistological analysis of the resected tumors. Nowadays, dynamic contrast-enhanced ultrasound imaging (DCE-US) provides new options for minimally invasive investigation of the microvasculature by analysis of ultrasound-contrast-agent (UCA) transport kinetics; features of the temporal and spatiotemporal evolution of the UCA concentration provide insight on perfusion, vascular fraction, and microvascular architecture. In this work, we propose a different method to analyze the UCA concentration that is based on the spatial distribution of blood flow.

Statement of Contribution/Methods

The well-known concept of Mandelbrot allows interpreting vascular networks as fractal objects related to the regional blood flow distribution by a specific parameter, the fractal dimension (FD). To test this hypothesis, the fractal dimension of parametric maps reflecting blood flow, such as UCA wash-in rate and peak enhancement, was derived for areas representing different microvascular architectures in dedicated models. Subcutaneous xenograft mouse models of DU-145 (5 mice) and PC-3 (8 mice) prostate-cancer lines were employed that showed marked difference in MVD spatial distribution inside the tumor. The ability of DCE-US FD analysis to differentiate between these models was therefore evaluated. For validation purposes, the method was compared with immunohistological MVD and FD assessment, as well as with UCA dispersion maps, reflecting the underlying microvascular architecture. Immunohistology was performed either by tomatolectin-FITC or by CD31 staining. Contrast-enhanced imaging was performed using a Vevo 2100 ultrasound scanner equipped with a MS-250 probe following the injection of a 0.1-mL bolus of MicroMarker Non-Targeted Contrast Agent Kit by a tail vein catheter.

Results/Discussion

The results showed a good agreement between FD and MVD assessment, with FD analysis of UCA wash-in rate and peak enhancement maps able to differentiate between the two xenograft models (p-value < 0.05). Good agreement was also obtained with the UCA dispersion maps, reflecting differences in the microvascular architecture. Simple flow maps based on either wash-in rate or peak enhancement could not differentiate between the two models. These results motivate towards further investigation of the FD by DCE-US as an additional, promising feature to discriminate between different cancer types characterized by a different degree of vascular disorder.

4K-2

3:45 pm   **Estimation of Local Perfusion Parameters from Non-uniform Contrast-Enhanced Ultrasound Temporal Samples**

Avinoam Bar-Zion[1], Melissa Yin[2], Elizabeth Kuczynski[3,4], Robert S. Kerbel[3,4], Dan Adam[1], F. Stuart Foster[2,4]; *[1]Department of Biomedical Engineering, Technion - Israel Institute of Technology, Haifa, Israel, [2]Physical Sciences, Sunnybrook Research Institute, Toronto, Ontario, Canada, [3]Biological Sciences, Sunnybrook Research Institute, Toronto, Ontario, Canada, [4]Department of Medical Biophysics, University of Toronto, Toronto, Ontario, Canada*

Background, Motivation and Objective

Dynamic contrast-enhanced ultrasound (d-CEUS) imaging enables the estimation of blood perfusion in tissue. However, in many cases respiratory movements add substantial motion artifacts to the scans. Therefore, motion compensation is important for reliable analysis of d-CEUS movies. Although B-mode based image registration can compensate for in-plane movement, frames acquired outside of the main imaging plane should be excluded. Currently due to the incompatibility of standard d-CEUS processing methods with non-uniformly sampled data, study scans containing considerable motion artifacts are discarded. This work aims to facilitate the estimation of perfusion parameters and visualization of vasculature even when a significant percentage of frames are excluded.

Statement of Contribution/Methods

Log-transformed single-pixel signals were processed in the temporal domain within the framework of reconstruction of non-uniformly sampled signals in shift-invariant (SI) spaces. An efficient iterative algorithm was used for the estimation of the SI representation coefficients. A log-normal model was fitted to the estimated signals with and without spatial averaging. The proposed method was validated in a series of numerical simulations and *in vivo* bolus injection scans. Static hind-limb LS174T tumor scans (n=6) were used to test the stability of the algorithm over different proportions of missing frames. An orthotropic mouse model of hepatocellular carcinoma (HCC, n=22) was used to test the algorithm under substantial motion artifacts.

Results/Discussion

In silico - The proposed method was able to estimate the simulated time-intensity curves with mean normalized root mean square error (NRMSE) of 0.14 at 25 frames per second. When 50% of the samples were removed, the NRMSE increased by only 0.05, to 0.19. The proposed method facilitated improved perfusion parameter estimation (P<0.001) at 50% frame removal. In the *in vivo* experimental data, local parametric curve fitting with small averaging filters (e.g. 3x3 pixels, fig. 1 A) had significantly lower MSE compared to large averaging filters ($\geq$ 10x10 pixels, fig. 1 B). The proposed method enabled high-resolution quantification of scans containing substantial motion artifacts, thus extending the usability of d-CEUS imaging.
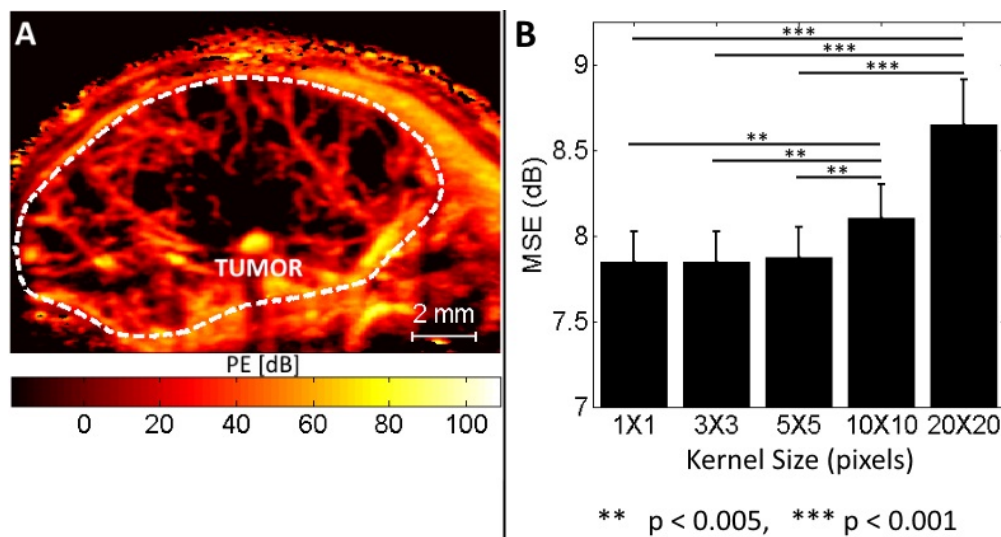
4K-3_____

4:00 pm **Ultrasound Microbubble Capture Using Bioorthogonal Coupling: An In Vivo Validation**

Melissa Yin[1], Aimen Zlitni[2], Judy Yan[1], John Valliant[2], **F. Stuart Foster[1,3]**; *[1]Sunnybrook Research Institute, Toronto, Ontario, Canada, [2]Chemistry and Chemical Biology, McMaster University, Hamilton, Ontario, Canada, [3]Medical Biophysics, University of Toronto, Toronto, Ontario, Canada*

Background, Motivation and Objective

Targeted contrast enhance ultrasound allows for the opportunity to visualize and track changes in molecular signalling pathways in relation to disease progression and response to therapy. To date, molecular ultrasound imaging using targeted microbubbles (MBs) have demonstrated selective localization to sites of angiogenesis, inflammation, and intravascular thrombus formation. However, the traditional approach has been to link biomolecules through interactions such as biotin-streptavidin noncovalent binding, which are not suitable for clinical use. Here we introduce a new strategy of MB targeting using a covalent, highly selective and rapid bioorthogonal coupling reaction: the inverse-electron-demand Diels-Alder reaction between tetrazine and trans–cyclooctene (TCO).

Statement of Contribution/Methods

The ability of TCO-conjugated anti-VEGFR2 to capture tetrazine tagged microbubbles (MBTZ) has been previously demonstrated in vitro [1]. Here we report the results of an initial in vivo imaging study of MB capture through bioorthogonal coupling using a VisualSonics Vevo 2100 scanner. Ultrasound imaging was preformed at 18MHz on xenograft tumours. Two groups of mice were used, one pre-administered with TCO-antiVEGFR2 (200µL, 0.5µg/µL) 24 hours prior to MB injection to allow antibodies to accumulate at the site of interest and clear out from non-targeted regions (n=4), and the other control (n=3). A disruption replenishment sequence was employed 4 minutes after MBTZ injection (70µL, 6.9x106 MBs/mL) and the differential targeted enhancement (dTE) signal was measured using the VevoCQ analysis software.

Results/Discussion

Parametric maps generated for each tumour showed high retention of MBTZ across all regions of the tumour in VEGFR2 targeted mice compared to control mice (see figure). Quantification of target specific contrast signal enhancement showed relatively consistent dTE values within each group, with the VEGFR2 targeted animals showing 2.5-fold higher dTE than the controls (p = 0.03, by student t-test). These initial in vivo results further validates previous in vitro observations to suggest that MB capture using bioorthogonal coupling reactions is a potential alternative for ultrasound molecular imaging, and establishes a path for their future development for specific applications.

1 Zlitni A, et al. Angewandte Chemie int. Ed. (2014)
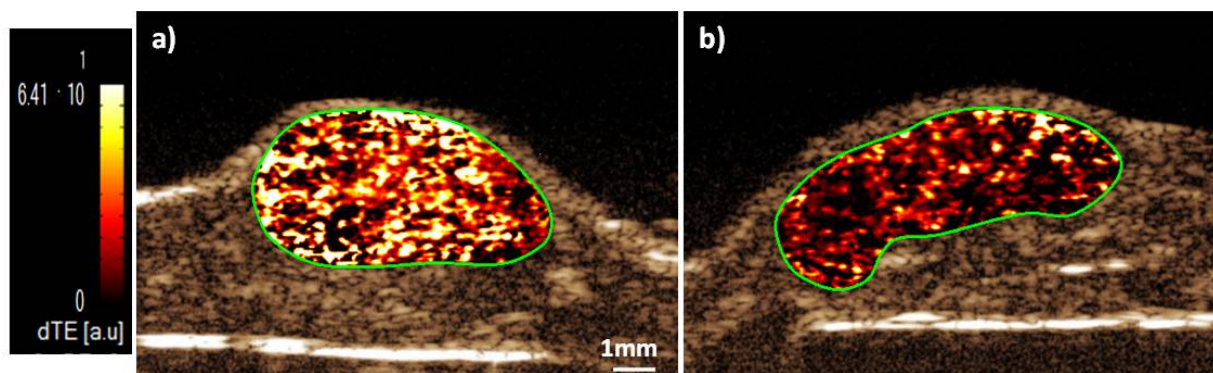
Representative parametric non-linear contrast mode ultrasound images of MB$_{TZ}$ localization in a) VEGFR2 targeted and b) control (no antibody injection) tumours. dTE = differential targeted enhancement; regions of high dTE are represented by white and yellow, whereas low dTE are represented by orange and black.

SATURDAY ORAL

4:15 pm   **Contrast-Enhanced Ultrasound Imaging with High CTR and Improved Resolution by Bubble-Echo based Deconvolution**

Hong Hu[1], Runna Liu[1], Diya Wang[1], Hui Zhong[1], Supin Wang[1], Mingxi Wan[1]; *[1]The Key Laboratory of Biomedical Information Engineering of Ministry of Education, Department of Biomedical Engineering,School of Life Science and Technology,Xi'an Jiaotong University, Xi'an, Shaanxi, China, People's Republic of*

Background, Motivation and Objective

In microvascular perfusion imaging by contrast-enhanced ultrasound (CEUS), inhibiting the strong tissue backscatters to enhance contrast-to-tissue ratio (CTR) and improving the imaging resolution to distinguish small vessels are two critical aspects. Pulse inversion bubble-wavelet imaging (PIWI) has greatly enhanced the CTR of CEUS; however, the resolution of it is limited. Deconvolution has been widely used in ultrasound imaging to improve the resolution, but rare study on deconvolution in CEUS is found. The purpose of this study is to improve CEUS images in terms of both CTR and resolution by a peculiar bubble-echo based deconvolution (BED).

Statement of Contribution/Methods

The deconvolution process consisted of the construction of point spread function (PSF) and the restoration of original echoes. A novel bubble-echo based PSF was used, where bubble-echo referred to the theoretical backscattered echo from a single bubble under the insonification. This PSF was constructed firstly using the modified Herring equation, then band-pass filtered and time-domain scaled. Afterwards, the original CEUS echoes were recovered axially using regularized inverse Wiener filtering by the above constructed PSF. Meanwhile, as comparisons, PIWI and the approved cepstrum-based deconvolution were also performed. *In vivo* rabbit kidney perfusion experiment was carried out to compare the above methods from CTR, time-intensity-curve (TIC) and resolution. All processing was implemented on the basis of pulse inversion (PI) technique.

Results/Discussion

Compared with that of PI, CTRs of PIWI and BED enhance by 6.13±1.33 dB and 8.51±2.21 dB, respectively, while that of cepstrum-based deconvolution reduces 0.83±0.57 dB; considering with the peaks of TICs, the intensity values for PIWI, cepstrum-based deconvolution and BED are 4.08 dB, 0.28 dB and 2.60 dB higher than that for PI. Meanwhile, axial resolution gains for PIWI, cepstrum-based deconvolution and BED are 0.75±0.09, 1.35±0.27 and 1.17±0.25, in contrast to PI. In short, PIWI enhances CTR but lowers the resolution; cepstrum-based deconvolution improves the resolution, but the CTR decreases; BED improves both the CTR and resolution. All results indicate that BED provides new CEUS methods with higher CTR and better resolution, which has important significance to microvascular perfusion evaluation in deep tissue.
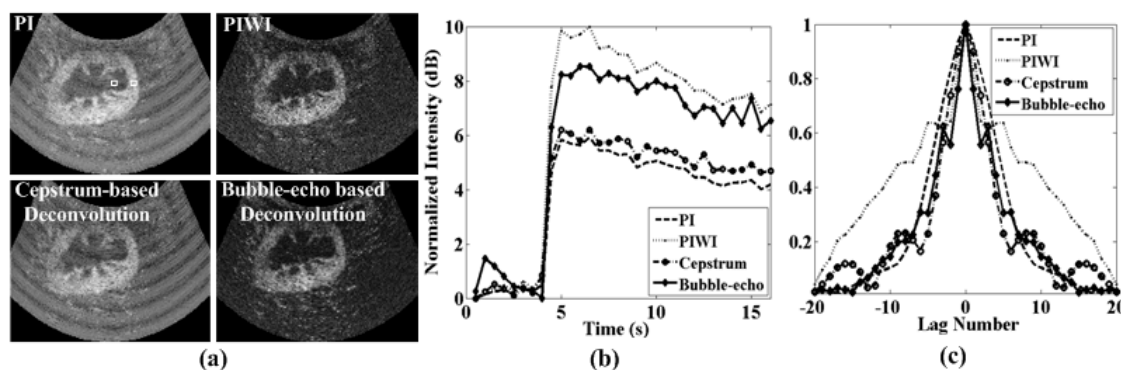
Figure: Comparison among CEUS images in *in vivo* kidney experiment. **(a)** CEUS images corresponding to PI, PIWI, cepstrum-based deconvolution and bubble-echo based deconvolution. **(b)** Time-intensity-curves relative to the baseline prior to the injection of contrast agent corresponding to CEUS images in (a). **(c)** The corresponding axial autocorrelation functions of the RF data for CEUS images in (a), which were calculated to qualify the resolution.

4:30 pm   ***In Vivo* Transcranial Imaging of Blood Perfusion in Rat Brain Using Contrast-enhanced Ultrasound**

JUAN DU[1], Dalong Liu[1], Emad Ebbini[1]; *[1]Electrical and Computer Engineering, University of Minnesota, Minneapolis, MN, USA*

Background, Motivation and Objective

Transcranial focused ultrasound (tFUS) is gaining increased attention in applications like blood brain barrier (BBB) opening, neuromodulation, and tumor ablation. Microbubble contrast agents (UCA) play an important role in many of these applications, especially due to the reduced focusing gain resulting from skull aberration. We have investigated the feasibility of in vivo high resolution imaging of blood perfusion in the rat brain tissue using a dual-mode ultrasound array (DMUA). The DMUA is capable of generating therapeutic tFUS beams as well as forming images of the target in synthetic-aperture (SA) mode. Low-MI SA frames are used to estimate the dynamic changes in perfusion, which could serve as a form of guidance, monitoring, or damage assessment.

Statement of Contribution/Methods

We have previously demonstrated the advantages of the post-beamforming third-order Volterra filter in imaging nonlinear echo components due to UCA oscillations using diagnostic probes. In this study, we decompose the beamformed transcranial DMUA SA data into its linear, quadratic, and cubic components and evaluate a temporal perfusion index (TPI) to characterize perfusion. The data collection used a 3.2-MHz, concave (40-mm roc) DMUA operating in SA mode at a frame rates of approximately 23 fps and in the low MI setting (about 0.05 to 0.11). The experiment was performed on healthy rats (250 – 300 gram). Targestar P UCA (60 µL in 140 µL of sterile saline) was injected through the animal tail vein. Images from the linear, quadratic, and cubic components were formed as B-mode, QB-mode, and CB-mode, respectively. TPI image frames were computed from each image component after limiting the dynamic range appropriately.

Results/Discussion

Fig. 1a&b shows TPI images in rat brain before and after UCA injection, respectively. The TPI was obtained from the QB-mode (120 dB) frames by maximum projection over 68 frames (3sec). The maximum TPI images clearly show numerous localized perfusion regions. Both in-plane and out-of-plane UCA motions could be discerned on movies of QB-mode and CB-mode images. Fig. 1c shows temporal profiles of the TPI at a pixel representing an active micro vessel before and after UCA injection. A clear separation of TPI values can be observed. These results demonstrate the feasibility of high-resolution estimation of blood perfusion in rat brain transcranially.

SATURDAY ORAL

(a)   (b)

(c)
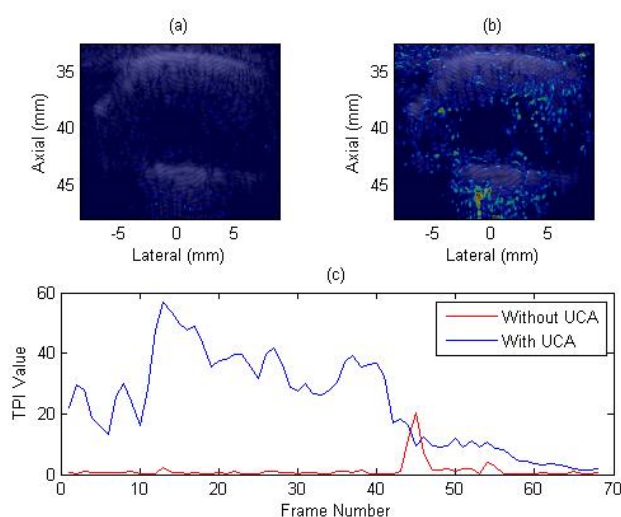
4K-6

4:45 pm   Flow Phantom for Contrast Enhanced Ultrasound Research, Device Validation, and Clinical Training

John Kucewicz[1], Barbrina Dunmire[1], Vijay Shamdasani[2], Jeffry Powers[2], **Thomas Matula[1]**; *[1]University of Washington, Seattle, WA, USA, [2]Philips Ultrasound, Bothell, WA, USA*

Background, Motivation and Objective

Phantoms are an important part of ultrasound research, instrument development, and clinical training. There are, however, no standardized research or commercial phantoms for contrast enhanced ultrasound. Reported research phantoms typically include either tubes to mimic flow in larger vessels or dialysis tubing to mimic perfusion in the capillary bed. These approaches fail to mimic the full range of flow regimes and tissue scattering observed in the body during imaging. To address these limitations, we have designed a low-cost phantom that integrates flow in both the macro and microcirculation with physiological tissue backscatter, attenuation, and sound speed, and that can be customized to simultaneously mimic flow in normal and malignant tissues.

Statement of Contribution/Methods

A variety of commercially available sponges and foams were considered. Each was evaluated in terms of acoustic properties, pore size, machinability, and ease of integration into a pump-driven flow system. Acceptable materials were fit in a custom-built flow chamber and imaged with a commercially available ultrasound system.

Results/Discussion

A polyvinyl alcohol (PVA) sponge was deemed to be the most suitable phantom material. PVA has a sound speed of 1490 m/s, and attenuation coefficient of 0.6 dB/cm/MHz with a frequency dependence of 1.6. PVA is easily machined when dry and appears similar to tissue when imaged. Pump type and salinity had minimal impact on agent longevity. Figure 1 (left) shows a contrast image of 15x7.5x2.5 cm sponge drilled from opposing sides to create overlapping flow channels. After introducing contrast agent into the flow system, the agent could be visualized rapidly entering the flow inlets, perfusing slowly through the sponge, and rapidly exiting through the flow outlets. Figure 1 (right) shows a system-generated reperfusion curve for a region between an inlet and outlet. The phantom has shown value in optimizing contrast images not only in 2D but also in 3D/4D. Additional work demonstrated that replacing portions of the PVA with other foams or sponges could locally alter flow to mimic malignant and normal tissue, as indicated by standard contrast perfusion kinetics metrics. (Funded by Philips Ultrasound and the Life Sciences Discovery Fund #3292512).
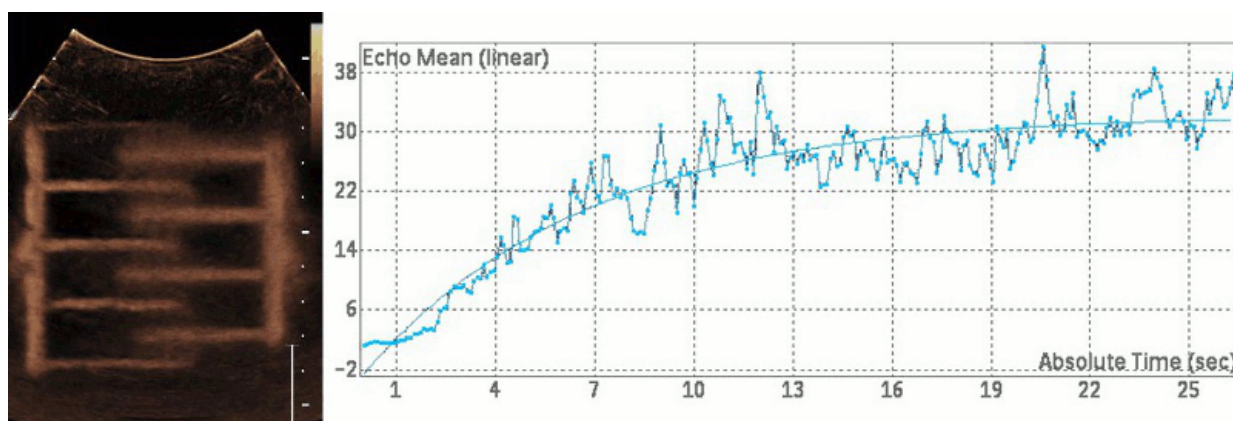
5K - Flow Measurement

103

Saturday, October 24, 2015, 03:30 pm - 05:00 pm

Chair: **Walter Arnold**
Saarland University

5K-1

3:30 pm **Effect of transducer port cavities in invasive ultrasonic transit-time gas flow meters**

Maik Hoffmann[1], Alexander Unger[2], Axel Jäger[2], Mario Kupnik[2]; [1]*BTU Cottbus-Senftenberg, Germany,* [2]*Technische Universität Darmstadt, Germany*

Background, Motivation and Objective

We investigate the effect of the ultrasonic transducer location (depth or protrusion at three different inclination angles) inside the pipe wall (transducer port cavity) of invasive ultrasonic transit-time gas flow meters with a focus on the symmetry of the acoustic sound pressure field. Basically, there are different choices in use in flow meters. The transducers can be recessed into the pipe wall; they can be flush-mounted; or they can be protruded up to full extent into the gas flow - all with different inclination angles. The motivation to flush-mount or to recess the transducers into the pipe wall is two-fold. First, the disturbance of the flow is minimized and, second, the transducer experiences better protection against the gas, its temperature and its possible contaminations. We focus on the effect of these different acoustic boundary conditions on the symmetry of the acoustic main lobe.

Statement of Contribution/Methods

By using a calibrated microphone (B&K 4138), mounted on a volumetric positioning stage [Hoffmann et al., IUS 2013], we investigate whether the assumption that the acoustic main lobe is symmetric is valid for these different acoustic boundary conditions. Three different quarter sections of a ten-inch pipe were printed, using a 3D printer. Two representative arrangements of transducer port cavities with 30 degree and 45 degree to the flow axis, and, in addition, one with 90 degree for comparison purpose. The diameter of the transducer port cavities was chosen to be 16 mm so that a test ultrasonic transducer with a resonance frequency of 40 kHz (MA408BS, Murata, Japan) fitted in smoothly. During these first measurements with stationary fluid only, the transducer was positioned at different depths, ranging from -50 mm to + 30 mm with 1 mm step size, to cover all different transducer port cavity arrangements. The zero depth location is defined as the location of the flush-mounted transducer. At each transducer location inside the port, three sets of data have been gathered: the sound pressure level at a fixed location in front of the transducer port opening; the sound pressure field at 567 locations in a plane orthogonal to the transducer front face; and the sound pressure level along a half-circle path with a resolution smaller one degree.

Results/Discussion

Depending on the depth of the transducer inside the port cavity, the sound pressure level, 12 cm in front of the port opening, varies up to 3 dB with a maximum at a depth of -36 mm. Further, we observe a main lobe that changes its form from a single symmetric lobe to multiple overlapping non-symmetric lobes. The direction is bent up to more than 12 degrees, depending on the position of the transducer. Our results prove that the transducer port cavity has significant effects on the sound pressure field and that these effects need to be taken into account when a flowmeter is supposed to be designed properly in terms of a symmetric or intentionally non-symmetric sound propagation.

5K-2

3:45 pm **Embedded System for In-line Ultrasound Velocity Profile Detection**

Stefano Ricci[1], Valentino Meacci[1], Beat Birkhofer[2], Johan Wiklund[3]; [1]*Information Engineering Dept., Università di Firenze, Florence, Italy,* [2]*Sika Services AG, Zurich, Switzerland,* [3]*SP Technical Research Institute of Sweden, Gothenburg, Sweden*

Background, Motivation and Objective

The in-line assessment of the rheological properties of fluids in chemical, cosmetic, pharmaceutical, and food industries is fundamental for process optimization and product quality. The rheology of a fluid in a process pipe can be investigated through the combination of Pressure Difference (PD) with Pulsed Ultrasound Velocimetry (PUV) methods. PUV is a non-invasive Doppler technique capable of measuring the radial velocity distribution. Till now, few PUV systems are suitable for industrial applications, and they often need cumbersome electronics or computer for data post-processing. In this work we present a compact (10x12 cm), fully programmable and low cost PUV board that embeds also all the signal-processing. The board, specifically design for industrial use, is integrated in the Flow-Viz[TM] platform (SP, Sweden).

.

Statement of Contribution/Methods

The PUV board has two separate transmit-receive stages. An Arbitrary Waveform Generator produces the transmission pulse at 100Msps with programmable amplitude (up to 80Vpp) and frequency 1-7MHz. The received echoes are amplified with a gain 7-55 dB, converted at 100 Msample/s, 16 bit and moved to a Field Programmable Gate Array (FPGA, Cyclone III, Altera). The FPGA demodulates and filters the samples. Spectral profiles (SPs) are generated by applying a block floating point FFT, module extraction and programmable averaging. A floating point processor extracts the velocity profile (VP) from the SP through a power-weighted mean. The SP, VP and raw data, buffered in a 64MB SDRAM, are downloaded to the host via a sbRIO 9606 board (National Instruments) with Ethernet interface.

.

Results/Discussion

The PUV board calculates a VP in 42 us per depth (e.g. a 512-depth VP is generated at 45 Hz rate), with no need of further processing on host. For example, the figure shows the SPs obtained in a 6 mm pipe with different averaging (left: no averaging, right: 32 frames) and the VP (cyan curve) superimposed. The error with respect to the same processing carried out in Matlab® is -100 dB.

The PUV board achieves high spatial and temporal resolution thanks to the possibility of rapidly process a large number of pulses in the FPGA. This feature, jointly to the full programmability of acquisition and processing parameters, makes the system ideal for industrial application, in particular where the attenuation of ultrasound is a major limitation.

.

SATURDAY ORAL
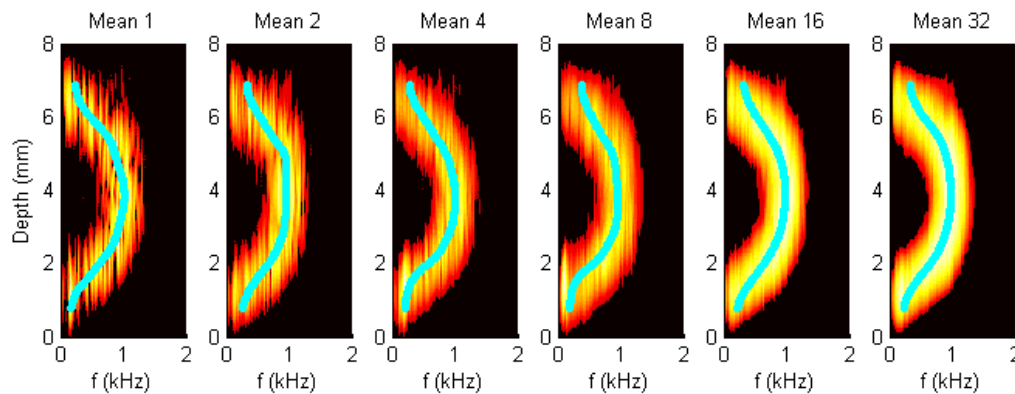
5K-3

4:00 pm   In-Situ Monitoring of Particle Velocities and Solids Concentration Variations in wet Low-Intensity Magnetic Separators

Johan E. Carlson[1], Jan F. Stener[1], Anders Sand[1], Bertil I. Pålsson[1]; *[1]Lulea University of Technology, Lulea, Sweden*

Background, Motivation and Objective

In the mining industry, magnetite particles are separated from other solid particles using wet low-intensity magnetic separators. A suspension is pumped into the separator tank, and the magnetite is extracted by use of magnetic forces. In this process it is of interest to monitor the flow patterns inside the separator structure, as well as particle build-up when applying the magnetic field. Since the suspension is essentially opaque and the solids concentration rather high, the aim of the current project has been to develop an ultrasonic technique for measurement of local particle velocity vectors and local variations in solids concentration. Previous work has presented the findings from lab-scale experiments and measurements in simple flow geometries. In this paper we demonstrate the principle on a full-scale separator, installed in the pilot plant of LKAB at Malmberget, Sweden.

Statement of Contribution/Methods

The particle velocity measurement is based on a cross-correlation principle, where two consecutive ultrasonic pulse-echo signals are correlated, piece-wise, to obtain a particle velocity estimate as a function of depth, along the axial direction of the transducer. By using two transducers, mounted at an angle, particle velocity vectors can be estimated for the volume where the sound fields overlap. Using the same backscatter signals, but instead studying how the spectral contents vary with axial distance, a qualitative measure of variations in local solids concentration can be obtained. These estimates can provide valuable information on how changing the process parameters affect the flow properties inside the separator geometry.

Results/Discussion

The experiments were conducted *in-situ*, at the LKAB pilot plant in Malmberget, Sweden, where a setup with two ultrasound transducers (2.25 MHz) were mounted at the bottom of the separator tank (Fig. A). The transducers were mounted at a relative angle of 60. The operating conditions of the separation process were then varied based on a designed experiment. The factors varied were feed solids concentration, rotational speed of the drum, the position of the concentrate weir, and the magnet assembly angle. For each of these settings, flow velocity (Fig. B) and solids concentration profiles (Fig. C) were measured.
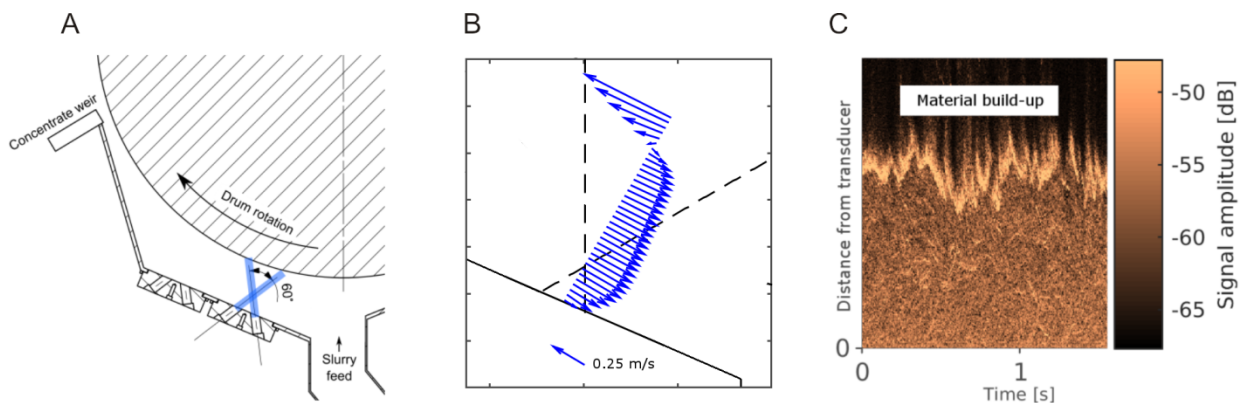
5K-4

4:15 pm   Modular Research Platform for Adaptive Flow Mapping in Liquid Metals

Richard Nauber[1], Hannes Beyer[1], Kevin Maeder[1], Arne Klass[1], Norman Thieme[1], Lars Buettner[1], Juergen Czarske[1]; *[1]MST, TU Dresden, Dresden, Saxony, Germany*

Background, Motivation and Objective

Understanding the complex interaction of conductive fluids and time-varying magnetic fields is the main goal of research in magnetohydrodynamics (MHD). Customized magnetic fields can be used to optimize the melt flow of technical and industrial processes involving liquid metals. For example the performance of batteries with replaceable liquid electrolytes, such as zinc-slurry energy storage systems, can be improved by magnetically influencing the flow of the electrolyte. However, necessary experimental studies are often limited by the performance of flow instrumentation for opaque liquids.

Statement of Contribution/Methods

We present a modular research platform for flow mapping in liquid metals, the phased array ultrasound Doppler velocimeter (PAUDV). It is based on the pulsed-wave ultrasound Doppler principle in combination with the phased array technique to provide an electrically steerable sound-field, enabling novel applications in MHD research. The ability to dynamically focus the ultrasound beam allows to resolve smaller flow structures in planar measurements compared to fixed-beam sensors. The PAUDV can be applied to flows in narrow channels and two velocity components can be measured with only one acoustical access via the cross beam technique. Fast electrical traversing of the measurement volume allows to obtain and visualize turbulence statistics. A two-point correlation function can be retrieved by interleaving velocity measurements at two focal points of varying distance (see Fig. 1). The PAUDV consists of a modular electronics unit with up to eight beamformer cards, capable of driving a total of 256

channels. Each channel can be individually configured regarding the excitation pattern (three level quantization, 64 samples) and the delay (1.6 ns resolution). Data acquisition and processing is implemented on a FPGA system, control and data visualization are performed on a PC.

Results/Discussion

We demonstrate the capabilities of the PAUDV on multi-modal measurements in the low melting alloy GaInSn at room temperature. A map of the flow induced by a rotating magnetic field is visualized in a plane with two velocity components (2d-2c), as well as two point correlation functions.
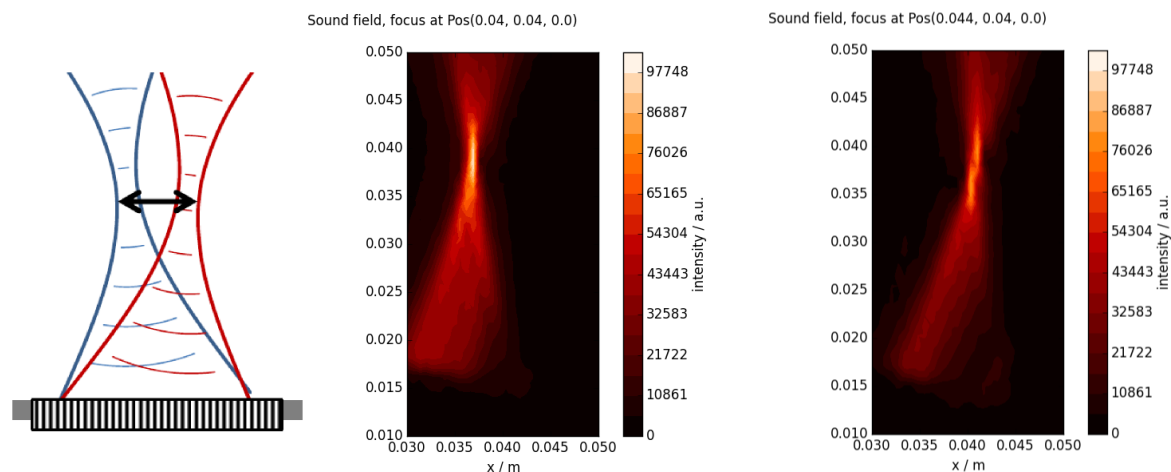
5K-5

4:30 pm   Ultrasound flow mapping for the investigation of crystal growth

Norman Thieme[1], Richard Nauber[1], Hannes Beyer[1], Hannes Radner[1], Lars Büttner[1], Paul Bönisch[2], Kaspars Dadzis[2], Lamine Sylla[2], Dagmar Meier[3], Olf Pätzold[3], Jürgen Czarske[1]; *[1]Laboratory for Measurement and Sensor System Techniques, Dresden University of Technology, Dresden, Germany, [2]SolarWorld Innovations GmbH, Freiberg, Germany, [3]Institut für Nichteisen-Metallurgie und Reinststoffe, Technische Universität Bergakademie, Freiberg, Germany*

Background, Motivation and Objective

The production of high quality solar cells requires a deep understanding of the solidification process. Especially when time-dependent magnetic fields are used to improve the material and heat transfer in the melt, the resulting flow structures are complex and unsteady. Hence, numerical simulations are used to gain an insight into the melt flow. For the calibration of the numerical simulations, model experiments at room temperature are used. This requires a comprehensive flow mapping of complex and unsteady flow phenomena. Commercial flow instrumentation systems usually utilize only one or a few single element probes that are operated strictly in sequential multiplex. This leads to low frame rates and limits their application to quasi-static flow fields.

Statement of Contribution/Methods

We present an ultrasound array Doppler velocimeter (UADV) suited for model experiments with solidification in crucibles with a 220 x 220 mm² base. The UADV is equipped with four ultrasound arrays with 42 elements each. Due to its modular set-up various arrangements of the ultrasound arrays are feasible, for example, measuring two horizontal 2d-2c flow fields. The melt flow is strongly influenced by the melt height, that constantly decreases during a solidification process. Hence, measuring the position and the shape of the solidification front is required for an understanding of the melt flow. The vertical position of the solidification front is measured with nine single US transducers which are placed on top of the melt.

The signal processing is done by a FPGA enabling long running measurements of up to one day, which is required for solidification processes. The 2d-2c flow fields are composed of two orthogonal 2d-1c flow fields. This composition requires an exact knowledge of the relative positions of the ultrasound arrays. The relative positions are determined by a novel spatial self-calibration that uses mutual time of flight measurement.

Results/Discussion

The UADV was applied to solidification experiments with gallium in a crucible with a 220 x 220 mm² base and an external magnetic field. Measurement results including the measurement of the solidification front will be shown. A comparison with numerical simulations will be provided. The figure shows an exemplary flow and solidification interface measurement with GaInSn and a mock-up solidification interface.

8K - More Medical Transducer Applications

102

Saturday, October 24, 2015, 03:30 pm - 05:00 pm

Chair: **Xiaoning Jiang**
North Carolina State University

8K-1

3:30 pm **Cost-effective linear arrays for medical imaging fabricated using PZT thick film technology**

Louise M. Borregaard[1], **Tomasz Zawada[1]**, Michele Guizzetti[1], Ruichao Xu[1], Erling Ringgaard[1], Jan P. Bagge[2], Lars N. Moesner[2]; *[1]Meggitt Sensing Systems, Kvistgaard, Denmark, [2]BK Medical, Herlev, Denmark*

Background, Motivation and Objective

Screen- and pad-printed single element ultrasonic transducers have been successfully commercialized over the recent years. Typically, PZT(Lead Zirconate Titanate) thick films are pad- or screen-printed on a curved ceramic substrate acting as integrated backing layer and providing mechanical pre-focus. Center frequency ranges between 8 MHz and 80 MHz. The devices are characterized by very good sensitivity as well as high relative bandwidth.

The main objective of the presented work has been to apply similar technology to manufacture multi-element transducers enabling novel cost-effective fabrication of imaging arrays for medical applications. It has been assumed that due to low lateral coupling of the printed PZT the elements can be defined only by the top electrode pattern leading to kerf-less design and low cross-talk between the elements.

Statement of Contribution/Methods

In this work PZT thick film technology has been applied for manufacturing of linear arrays. Linear arrays have been fabricated using InSensor(TM) TF2100 thick film. The arrays have been printed on acoustically matched ceramic blocks acting both as the backing as well as substrate for deposition. The electrodes and the TF2100 film have formed a sandwich structure deposited by screen printing. 32 element transducers have been fabricated with center frequency around 12 MHz. The pitch has been equal to about 200 micrometers with an element width of about 45% of the pitch. The devices have been packaged using flip-chip technology for easy interconnect and testing.

Results/Discussion

The arrays have been characterized at the transducer level using a pulse echo system consisting of a JSR DPR500 system and digital oscilloscope. The samples have been immersed in demineralized water with an acoustic reflector. Several arrays have been tested showing center frequencies ranging from 11 MHz to 13 MHz. In average insertion loss of -66.4 dB and a bandwidth of 53.6% have been achieved. The measured cross-talk has been equal in average to -38.2 dB. The transducers are characterized by good reproducibility of the properties. For example the capacitance variation between the elements is less than 14% in average.

The thick film arrays have been integration-tested using a commercial ultrasound scanner (BK Ultrasound – bk3000). The integration test revealed that the 32 element thick film transducers have been compatible with a commercial scanner, had a frequency range of 7.5 MHz to 12 MHz, and a TX bandwidth of 70%. Moreover the transducers support delay and sum beamforming as well as they can support phased array beamforming.

The performance of the tested linear arrays tested at the device as well at the scanner level show that printed PZT technology is highly suitable for cost effective manufacturing of high- and mid-frequency linear and phased arrays for medical imaging.

8K-2

3:45 pm **Heartbeat Interval Monitoring by PZT/PZT Flexible Piezoelectric Film Sensor**

Makiko Kobayashi[1], Takahiko Ikari[1], Shugo Kurose[1], Tomohiko Igasaki[1]; *[1]Kumamoto University, Japan*

Background, Motivation and Objective

Recently, fluctuation analysis of heartbeat interval has received a lot of attention because it relates with human stress and heath conditions and heartbeat intervals of normal condition people tend to have more fluctuation than the others. Electrocardiogram can monitor heartbeat interval precisely though measurement setup is relatively complicated and it is not suitable for daily monitoring at home. It is possible to measure heartbeat interval by arterial pulse pressure monitoring and it could be more convenient for home user. However, the sensor development with high sensitivity is required.

Statement of Contribution/Methods

Sol-gel composite flexible piezoelectric sensors was attempt for pulse monitoring, because of flexibility, relatively low dielectric constant and less ringing effect. PZT/PZT was chosen as piezoelectric material because of high piezoelectricity and high dielectric constant.150 μm thick PZT/PZT film was fabricated onto 200 μm thick stainless steel substrate as flexible piezoelectric sensors. The sensor was fixed around the human wrist by a commercial sport-type watch wristband. Voltage change caused by piezoelectric sensor was monitored and recorded by oscilloscope. The setting of oscilloscope low pass filter cut off frequency was 30 Hz. Electrocardiogram measurement was also carried out simultaneously for validation purpose.

Results/Discussion

The Typical measurement results by PZT/PZT sensor in the wrist and by electrocardiogram is shown in Fig.1. Very sharp peaks of arterial pulse pressure was obtained by PZT/PZT pirzoelectric sensor without amplifier. The intervals of positive peaks of PZT/PZT sensor showed high correlativity with those of electrocardiogram. Further data analysis and will be carried out to determine the usefulness of PZT/PZT sensor for heartbeat interval monitoring application.

SATURDAY ORAL
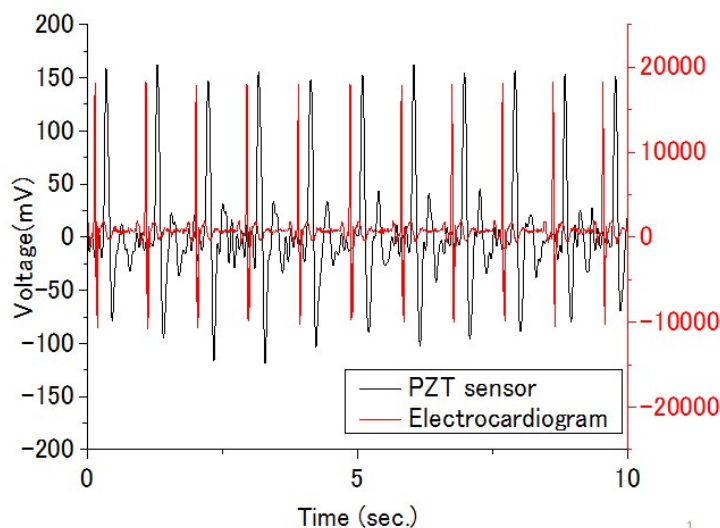
8K-3

4:00 pm An ultrasonically assisted sagittal saw for large bone surgeries

Daniel Richards[1], Andrew Mathieson[1], Margaret Lucas[1]; [1]*School of Engineering, University of Glasgow, United Kingdom*

Background, Motivation and Objective

Ultrasonic bone cutting devices are widely utilised in modern surgeries, principally for small bones in spinal, oral and maxillofacial operations, due to their higher accuracy than traditional saws and burs. The cutting of large bone, however, is still widely undertaken using tools such as sagittal saws. Previous research into ultrasonic devices for large bone cutting has largely focused on a tuned longitudinal-mode ultrasonically vibrating blade excited by a Langevin transducer. This new study describes an investigation into the capabilities of an ultrasonically assisted sagittal saw that superimposes an ultrasonic vibration on the high-speed small-angle reciprocating oscillatory motion of the saw blade.

Statement of Contribution/Methods

A number of sagittal saw blades of different geometries were modelled using Abaqus and PZFlex finite element analysis (FEA). The modelling allowed the identification of designs for a planar transducer based on current sagittal saw blades, but which coupled either a longitudinal or flexural mode of vibration with the reciprocating motion. Through this analysis, a potential benefit of creating an elliptical cutting locus by tuning the planar transducer to a combined longitudinal-flexural mode was identified. Subsequently, two of the most promising blades were manufactured, one exhibiting a longitudinal ultrasonic vibration superimposed on the reciprocating motion (LR blade) and one exhibiting a combined longitudinal-flexural mode superimposed on the reciprocating motion (LFR blade). The predicted impedance characteristics and modal parameters were validated through impedance analysis and experimental modal analysis, respectively.

Results/Discussion

The predicted electrical characteristics and modal parameters of the resonant sagittal saw blades were found to closely match those identified through experimental characterisation. The cutting performance of both blades has been demonstrated using the bone mimic, Sawbones, and it has been shown that superimposing ultrasonic vibrations onto the reciprocal motion of a sagittal saw has enhanced its performance by improving the accuracy of the cut.

8K-4

4:15 pm Arbitrary Waveform Generation based on Phase and Amplitude Synthesis for Switched Mode Excitation of Ultrasound Imaging Arrays

David Cowell[1], Sevan Harput[1], Steven Freear[1]; [1]*School of Electronic and Electrical Engineering, University of Leeds, Leeds, United Kingdom*

Background, Motivation and Objective

In ultrasound imaging, chirp, Gaussian, and n-cycle sine wave excitation are common. The ability to transmit an arbitrary ultrasound wave allows the application of advanced imaging methods; such as predistortion, pulse inversion, multi-pulse, sub-harmonic and tissue harmonic imaging.

Excitation waveforms with arbitrary amplitude and phase/frequency characteristics can be generated with low harmonic distortion by an arbitrary waveform generator (AWG) and linear amplifier. However, implementation practicalities such as power, size and cost limit the availability of true arbitrary excitation in array systems where concurrent excitation is required across hundreds of channels, and is especially applicable to miniaturized excitation circuits integrated into transducer heads and CMUTs or PMUTs.

Previous work has shown that amplitude modulated tone and linear frequency modulated waveforms, free from the third harmonic, can be generated using a 5 level switched excitation system, termed Harmonic Reduction Pulse Width Modulation (HRPWM).

The HRPWM algorithm required parameterized inputs of amplitude window, frequency, bandwidth and duration to calculate a switched excitation waveform.

This work aims to address these limitations.

Statement of Contribution/Methods

Firstly, a 3 level solution to the HRPWM arbitrary excitation algorithm is proposed through modifications to modulating waveforms. This allows implementation of arbitrary excitation on the majority of ultrasound platforms with switched excitation, in either 3 or 5 level modes as available.

Secondly, the necessity for parameterized design is removed through the implementation of a phase and amplitude synthesis algorithm. The proposed algorithm analyses the phase and amplitude of an arbitrary input waveform and synthesizes modulation waveforms plus positive and negative envelopes for the generation of 3 and 5 level excitation sequences.

Results/Discussion

A non-linear frequency modulated (NLFM) waveform was predistorted to compensate for transducer bandwidth characteristics. The waveform was processed with the proposed algorithm. The analog, 3 and 5 level excitation waveforms, spectra and transducer responses are shown below. The 3 and 5 level switched excitation waveforms show the same fundamental spectral components and have a suppressed third harmonic component.
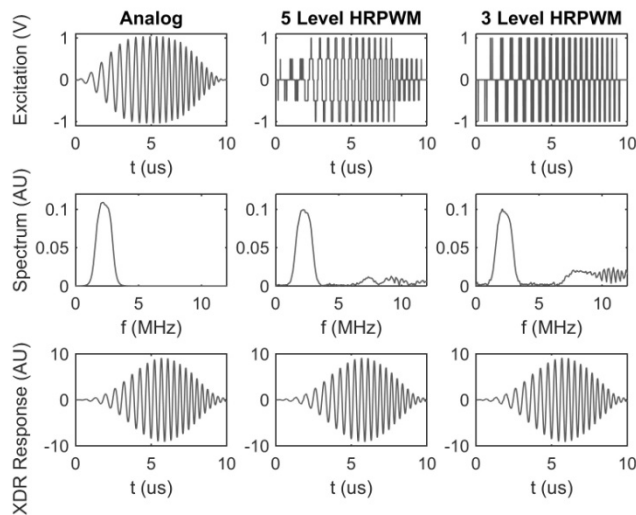
8K-5

4:30 pm   A Discrete Source Model for Simulating Bowl-Shaped Focused Ultrasound Transducers on Regular Grids: Design and Experimental Validation

Yan To Ling[1], Elly Martin[1], Bradley Treeby[1]; [1]*Medical Physics and Biomedical Engineering, University College London, London, United Kingdom*

Background, Motivation and Objective

Accurately representing source conditions is an important part of numerical simulation in ultrasound, particularly in ultrasound therapy where multi-element arrays are used. Typically, ultrasound sources are defined as boundary conditions within a 2D input plane, either measured experimentally or projected using analytical expressions. However, for arrays with multiple elements distributed over a non-planar surface, this approach is no longer sufficient and an explicit source model is required. For finite difference and pseudospectral models (the most commonly used models in ultrasound), the source geometry must be represented on a regular Cartesian grid. In this work, a novel grid-based discrete source model for single and multi-element transducers is developed, and validated against experimental data.

Statement of Contribution/Methods

The discrete source model was created by defining a distance matrix centred on the geometric focus of the transducer. For each row and column, a series of bi-directional line searches was performed to label the pair of grid points with the coordinates closest to the ideal sphere, removing grid points lying outside the desired sector angle. This leaves a symmetric and simply-connected bowl-shaped surface with a single grid point thickness. To evaluate the source model, the source geometries were used within the open-source k-Wave toolbox. Each source grid point was assigned as a monopole driven by a 1.1 MHz sinusoid. Simulations were run at three different grid resolutions, which affects the level of staircasing in the source geometry. For validation, experiments were performed in a scanning tank using Sonic Concepts H101 and H151 focused bowl transducers. A calibrated hydrophone was used to map the pressure field in a 2D plane. This was projected to other positions in the field using holography.

Results/Discussion

Simulation and experimental results were compared in both axial and lateral planes. The results show an excellent match, even at low grid resolutions (see figure). This demonstrates the source model can be used for simulating the pressure fields of curved transducers. As the model only requires the geometry and drive signal, it allows modelling of multi-element transducers where measuring an input plane is not possible. This is critical for modelling clinical therapeutic ultrasound arrays, particularly in the brain.

SATURDAY ORAL

8K-6
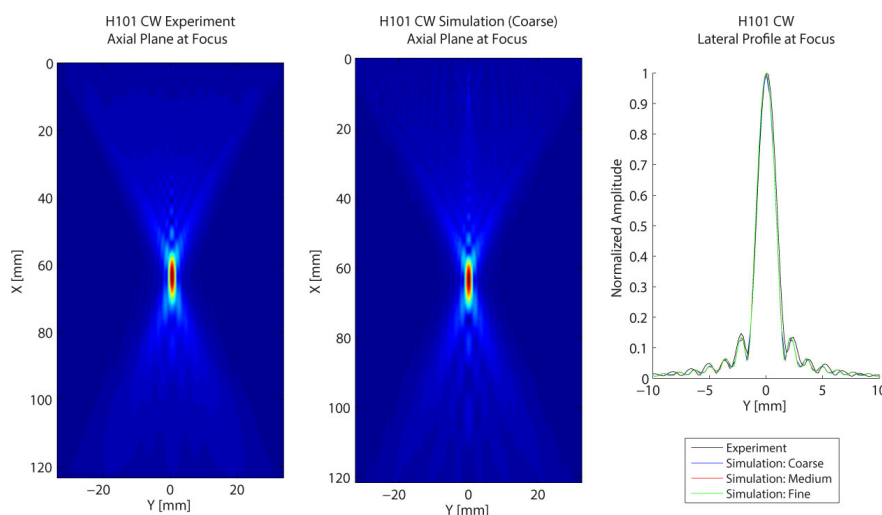
4:45 pm   Graphene Oxide Nanofabricated Ultrasonic Transducers (GO-NUTs)

Ka Hing Cheng[1], **Ching-Hsiang Cheng[1]**, Dennis Kwong Chun Lo[1]; *[1]Department of Industrial and Systems Engineering, The Hong Kong Polytechnic University, Hong Kong*

Background, Motivation and Objective

Historically, piezoelectric crystals, ceramics and polymers materials have usually been used to generate and detect ultrasound. Ultrasonic transducers can be classified as magnetostriction, piezoelectricity and electrostatics according to the physical mechanism upon the way they convert electrical energy to ultrasonic energy and vice versa. Graphene, with one atomic thickness, could be the new material for fabricating capacitive nanomachined ultrasonic transducers. Graphene fabrications enable realization of the submicron gaps between nano thickness layers that make it possible to achieve high electric fields and hence the high transduction efficient frequencies. GO-NUTs offer alternative advantages in wide bandwidth, ease of fabricating large arrays, and ability of integration with electronic circuits.

Statement of Contribution/Methods

A graphene oxide (GO) film was drop casted on DVD disc and then LASER reduced by Lightscribe DVD drive with array patterns. The reduced GO (rGO) film was fabricated to two identical graphene based electrodes with ionic liquid [BMIm]BF4 electrolyte between them. A micro thickness insulating polypropylene (PP) layer was inserted to allow ionic liquid to pass through the small hole on it and to prevent the two electrodes from contact shorting. A single transducer with many small capacitor cells connected in parallel was fabricated. 2D array could easily be patterned by organizing small capacitor elements in different geometries with Lightscribe design software. A GO-NUT is simply a device with two rGO plate electrodes bias with a DC voltage and driven with an additional AC signal to harmonically move the rGO membrane. The charged particles were grouped by the electric field at the electrode to build electrical double layers. The electrode-electrolyte interface is the PP membrane. With double layers charging/ discharging characteristic, electroacoustic effects take place in rGO electrodes and electrolyte interface. The efficiency of GO-NUT was determined by the amplitude of the response voltage and its fourier transform subjected to ultrasound in a function of bias current, frequency and device capacitance.

Results/Discussion

GO-NUTs were designed and fabricated by using rapid and scalable LASER Lightscribe annealing of GO. GO-NUTs can transmit and receive ultrasound by vibrating its membrane with electroacoustic effect. The capacitance, potential and frequency response measurement of the GO-NUT had shown the functionality of the device and suggested it was used in the high frequency range. High transduction efficiencies from kHz to MHz range frequencies are useful in practical applications. The result showed that the rGO had similar advantage as the materials used in traditional CMUT. The wide bandwidth and the potential for integration with electronic circuits are advantages associated with CMUTs. The resonant frequency of GO-NUT could further be tested and confirmed by an impedance analyzer.

P1C1 - MEL: Clinical Application of Elasticity Imaging

4th floor

Saturday, October 24, 2015, Posters displayed 08:00 am - 05:00 pm. Authors must be present at their poster from 9:30 - 10:30am (odd number posters) and 14:30 – 15:30pm (even number posters).

Chair: **Hiroshi Kanai**
            Tohoku University

P1C1-1 _____

8:00 am   VisR Ultrasound Evaluation of Dystrophic Muscle Degeneration in a Dog Cross-Section and Comparison to Histology and MRI

Mallory Selzo[1], Joe Kornegay[2], Amanda Bettis[2], Eric Snook[2], Martin Styner[3,4], Jiahui Wang[5], **Caterina Gallippi**[1,6]; [1]*Biomedical Engineering, UNC Chapel Hill, USA,* [2]*Veterinary Integrative Biosciences, Texas A&M University, USA,* [3]*Psychiatry, UNC Chapel Hlll, USA,* [4]*Computer Science, UNC Chapel Hill, USA,* [5]*Physciatry, UNC Chapel Hill, USA,* [6]*Radiology, UNC Chapel Hill, USA*

Background, Motivation and Objective

In Duchenne muscular dystrophy, absence of the protein dystrophin causes progressive degeneration of skeletal and cardiac muscle accompanied by muscle fiber necrosis, with subsequent replacement of muscle by fibrous tissue and fat. Because muscle viscoelasticity is related to composition and structure, interrogating the viscoelastic properties of muscle may be useful for stratifying degrees of muscle degeneration in DMD. Viscoelastic Response (VisR) ultrasound, a new acoustic radiation force (ARF)-based method for assessing tissue viscoelasticity, is herein applied for evaluating muscle viscoelastic properties in the Golden Retriever Muscular Dystrophy (GRMD) canine model, and VisR outcomes are compared to matched histology and MRI.

Statement of Contribution/Methods

In this cross-sectional study, in vivo VisR imaging was performed on the cranial sartorius (CS) and vastus lateralis (VL) muscles in 20 (n=10 control and 10 GRMD, age-matched pairs) dogs aged 3, 6, 12, 24, or 60 months. VisR used two 4.21 MHz, 300-cycle, F/1.5, ARF excitations administered 0.8 ms apart in time and delivered to the same region of excitation (ROE), with 6.12 MHz, 2-cycle, F/1.5 tracking pulses to measure induced 1D axial displacements in the ROE. VisR displacement profiles were fit to the Mass-Spring-Damper model to estimate the ratio of viscosity to elasticity, τ. Standard deviation (SD) of τ was measured within each muscle as a metric for heterogeneity. Following VisR, T2-weighted MRI imaging was performed, and run percentage (RP) (measuring the number of 'runs', or groups of consecutive voxels of the same intensity) was calculated to reflect heterogeneity. Finally, muscle tissue samples were acquired by open surgical biopsy, sectioned, and stained with Hemotoxylin and Eosin (H&E) and Masson's trichrome or picrosirius red for collagen. Collagen percent and fat percent were calculated from digital microscopy images for each section using Aperio ImageScope software.

Results/Discussion

In the VL, τ SD was consistently larger in GRMD versus age-matched control dogs (p=0.001, Wilcoxon two-sample test). This VisR result was consistent with higher MRI RP measures, reflecting greater GRMD muscle heterogeneity, and higher histology percent collagen. Similarly in the CS, τ SD was larger in GRMD (p=0.001), consistent with higher histology percent collagen. However MRI RP in the CS did not differentiate GRMD and control. These results suggest that VisR measures of τ SD reflect heterogeneity due to collagen deposition in dystrophic muscles. Future work will evaluate VisR measures with direct spatial correlation to histology and MRI.

P1C1-2 _____

8:00 am   Elasticity mapping of abdominal organs using Harmonic Motion Imaging

Thomas Payen[1], Carmine Palermo[2], Steve Sastra[2], Hong Chen[1], Yang Han[1], Kenneth Olive[2], Elisa Konofagou[1,3]; [1]*Biomedical Engineering, Columbia University, New York, NY, USA,* [2]*Herbert Irving Comprehensive Cancer Center, Columbia University, USA,* [3]*Department of Radiology, Columbia University, USA*

Background, Motivation and Objective

Harmonic Motion Imaging (HMI) assesses tissue viscoelasticity by inducing localized oscillation from a periodic acoustic radiation force. The amplitude of the resulting displacement is directly related to the underlying tissue stiffness. The objective of this study was to evaluate the feasibility of HMI for mapping abdominal organs in vivo based on their differences in relative stiffness. In the case of the pancreas, feasibility in a pathological case, i.e. chronic pancreatitis was also studied in vivo.

Statement of Contribution/Methods

A 4.5-MHz focused ultrasound transducer (FUS) generated an amplitude-modulated beam resulting in harmonic tissue oscillations at its focus. Axial tissue displacement was estimated using 1D cross-correlation of RF signals acquired with a 7.5MHz diagnostic transducer (P12-5, ATL) using a planewave beam sequence, confocally aligned with the FUS. Phantoms with stiff occlusions were first used to evaluate the performances of this setup in terms of resolution. Ex vivo canine liver, pancreas, spleen and kidney were assessed with HMI, and mechanical indentation was performed as a gold standard. Relative stiffness maps were obtained in vivo using HMI in mice. Ex vivo measurements were then performed in phantoms for reference.

Results/Discussion

The results showed that HMI was capable of providing reproducible relative stiffness values of the abdominal region in vivo. The phantom measurements demonstrated the high spatial resolution and sensitivity of HMI. The canine study showed good agreement between the mechanical testing and the HMI measurements. The in vivo relative 2D stiffness maps provided values similar to the ones obtained ex vivo with the hardest one first, i.e. kidney, spleen, liver, and pancreas. HMI also enabled pancreatitis detection as shown on relative 2D stiffness maps (Figure). Inflamed pancreases (Figure B) demonstrated HMI displacements on average 2.1 times lower than in the normal pancreas (Figure A) indicating higher overall stiffness. HMI was also capable of identifying the stage of disease as well as the specific location in the pancreas at the early stage when the inflammation is not systemic. This work shows that HMI can produce reliable 2D elasticity maps of the abdominal region in vivo. This work is supported by NIH grant R01EB014496.

SATURDAY POSTER

A. Normal pancreas | Bmode 7.5MHz | Overlay | Relative stiffness map

B. Pancreatitis
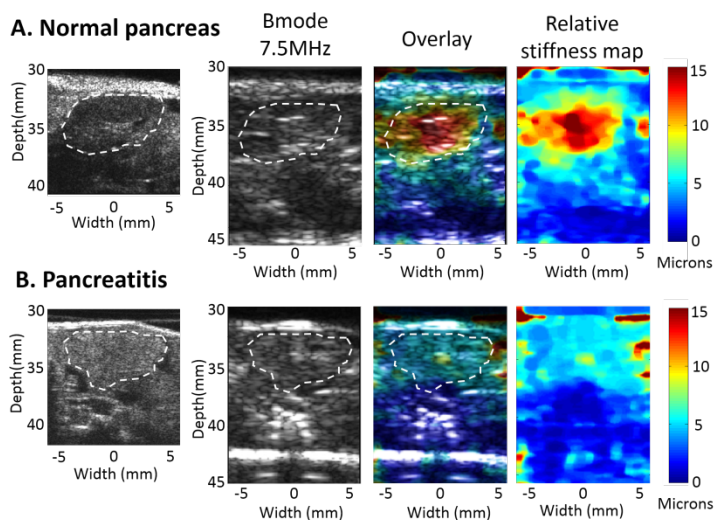
8:00 am   New Inverse problem for visco-elastic characterization of fatty liver using Vibration Controlled Transient Elastography

Jean-pierre Remenieras[1], Cecile Bastard[2], Veronique Miette[2], Jean-marc Perarnau[3], Frederic Patat[1,3]; *[1]Equipe 5, UMR INSERM U930 University of Tours, Tours, France, [2]Echosens, Paris, France, [3]INSERM CIC IT 1415, Tours, France*

Background, Motivation and Objective

Steatosis is an accumulation of fat in the liver. Fatty liver disease is divided into Alcohol-related fatty liver disease and non alcoholic fatty liver disease (NAFLD). When inflammation is present, this becomes non-alcoholic steatohepatitis (NASH), which can progress to cirrhosis and hepatocellular carcinoma. NAFLD is associated with obesity, abnormal glucose tolerance and dyslipidaemia, and has been described as the hepatic manifestation of the metabolic syndrome. In Europe prevalence of NAFLD is estimated at 20-30% in the general population.

A definitive diagnosis can only be achieved by liver biopsy and histopathological analysis. Ultrasound imaging shows a hyper-echogenic bright image and has some diagnostic accuracy in detecting steatosis but is not good at distinguishing NASH and fibrosis within NAFLD.

The objective of this work is to evaluate the feasibility of fatty liver quantification using VCTE. In addition, a correlation of these measurements with the hepatic fat percentage measured with MRI sequence was carried out.

Statement of Contribution/Methods

Initial clinical validation was carried out on two patients at Tours Hospital. We repeated 10 successive measurements using our method at the same position without displacement of the probe. Observation of transient shear-wave propagation in the liver is performed with a 1D research Fibroscan platform with different consecutive transient vibrations at the same measurement point. Transient strain rate dVz(z,t)/dz is determined using the sixteen-point least squares estimator on axial particle velocity estimates which were determined using the extended autocorrelation method. The 2D kernel of the autocorrelation is 16 temporal points at 9.3 KHz (i.e 1.7ms) and 128 pts à 50MHz (i.e 1.9mm). With a windows overloap of 75% in time and 93.75% in space, we obtain a strain rate elastogram with 0.43ms and 0.12mm temporal and axial resolutions respectively. After segmentation and Fourier transform, the shear wavelength λs is estimated in the spatial domain for each known frequencies of the transient vibration bandwidth using a new inverse problem algorithm based on a shear wave propagation model. This model is derived using the elastodynamic Green function who takes into account the strong diffraction effect in the near field of the shear wave and extra attenuation due to viscosity.

Results/Discussion

Shear wave dispersion curves in 20Hz-100Hz bandwidth are fitted by the Voigt model for shear elastic modulus μ and shear viscosity η estimation. The clinical validation showed that for the first patient who has 2% of fat in the liver (as measured using MRI sequence), we obtained a shear elastic modulus μ=1.6±0.1 kPa and a shear viscosity η=1.4±0.3 Pa.s. For the second patient with 22% of fat, we obtained μ=1.1±0.1 kPa and η=2.3±0.4 Pa.s. In conclusion, this novel method showed to be sensitive in characterizing the visco-elastic properties of fatty liver. Additional clinical validations are underway.

8:00 am   An acoustical generator to induce low amplitude shear waves in the human brain

Emmanuel Nicolas[1], Samuel Callé[1], **Jean-Pierre Remenieras**[1]; *[1]INSERM U930 - Tours University, TOURS, France*

Background, Motivation and Objective

Brain elastography using MRI has been recognized as a promising diagnostic tool. Neurodegenerative diseases evolution as well as normal aging could be precisely evaluated using quantitative elastography. Ultrasound elastography could be a cheaper, more accessible alternative. One of the challenges to overcome is the generation of the shear wave in the brain. Several methods have been developed for magnetic resonance elastography (rotating plate clamped in the patient's teeth, vibrating plate behind the skull), which we found to be unsatisfactory both for patient's comfort and ease of use. We investigate here a novel technique to induce shear waves in the brain.

Statement of Contribution/Methods

Unlike magnetic resonance elastography which uses harmonic waves, we chose to use transient excitation which allows shorter acquisitions and easier separation of shear and compression wave. The acoustical generator is made of a dynamic loudspeaker affixed with a tuned flexible hose, the other end being placed in the subject's mouth. The upper respiratory tract then acts as a resonator, making the whole cranium vibrates. By adjusting the length of the hose and the signal sent to the loudspeaker we can adjust the frequency, length and amplitude of the shear wave generated in the brain. The system was characterized with a microphone before use. The signal used is a 3 periods 80 Hz sinusoid. The excitation signal is also used to trigger an ultrafast ultrasound recorder (SSI Aixplorer), using a linear 2.8 MHz, 128 elements probe. The system was tested in a tissue mimicking phantom and in the human brain by placing the probe on the temporal window. Particle velocity is derived from the IQ data using a Doppler algorithm. A custom strain rate estimator is then used to isolate the shear wave from the compression wave.

Results/Discussion

Firstly validated on a calibrated elasticity phantom, this new wave inducing method gives the same shear wave speed value as with a plane wave experiment: 1.8±0.2 m/s. We are also able to observe the wave pattern of the theoretical Green function of the source. In the *in vivo* measurement, the shear wave speed measured is 1.3±0.4 m/s, in

---

Institute of Electrical and Electronics Engineers

accordance with the literature. Tissue displacement was measured between 10 μm and 50 μm. This technique also proved to be virtually painless for the subject, compared to existing techniques.

P1C1-5 _____

8:00 am   An Arrayed-Range-Gate Data Acquisition for Spatial Distribution Analysis of Myocardial Tissue Vibration from Stenosis in Coronary Doppler Vibrometry

Daehyeon Lee[1], Sungjoo Yoo[2], Dong-Bin Kim[3]; *[1]Department of Electrical Engineering, Pohang University of Science and Technology, Pohang, Korea, Republic of, [2]Department of Computer Science and Engineering, Seoul National University, Seoul, Korea, Republic of, [3]Division of Cardiology, College of Medicine, The Catholic University of Korea, Seoul, Korea, Republic of*

Background, Motivation and Objective

Coronary Doppler vibrometry (CDV) is a non-invasive diagnosis to detect vibrations from stenosis in coronary artery using ultrasound. Although recent CDV shows considerable sensitivity and specificity in diagnosing coronary artery disease, there still remains a serious problem that normal subjects can also have high-frequency components in vibration, which are representative symptoms of stenosis, because they have naturally such a high-frequency motion in myocardial tissue. We developed new data acquisition and analysis algorithm that focus on the spatial distribution of high-frequency vibration in myocardial tissue. Our purpose is to observe variation of vibration in myocardial tissue depending on location.

Statement of Contribution/Methods

We recruited total 33 subjects in a hospital clinical study; four are known as patients who have coronary artery stenosis (over 50 % occlusion in coronary angiography) and the other 29 subjects are normal. We used Verasonics data acquisition system with P4-2 phased array transducer to acquire focused ultrasound Doppler data at a PRF of 2400 Hz. Unlike conventional focused CDV, we use 12 range gates in a view of echocardiography (Fig. 1). Six range gates are located near stenosis (or left anterior descending (LAD) in case of normal subjects) and the other six are located at normal tissue (or right coronary artery (RCA) in case of normal subjects). After beamforming the range gate data, we calculate velocity and velocity spectrum. We define the segment vibration index (SVI) as the proportion of high-frequency component intensity (400 Hz ~ 800 Hz) to entire intensity (100 Hz ~ 800Hz) in early diastole period. In addition, we define the myocardial tissue vibration distribution index (MVDI) as the ratio of the standard deviation of SVI in stenosis (or LAD) segments to that of SVI in normal (or RCA) segments. Thus, it is expected that myocardial tissue vibrations caused by stenosis can give a spatial distribution of vibration intensity, i.e., a large MVDI.

Results/Discussion

MVDI effectively classifies normal subjects and patients with stenosis. Our proposed MVDI algorithm has a sensitivity of 75% and specificity of 83% (threshold of MVDI = 1.83). This result shows that the patients with coronary artery disease tend to have higher MVDI value than normal subjects. Therefore, our method shows a potential for feasible diagnosis application.
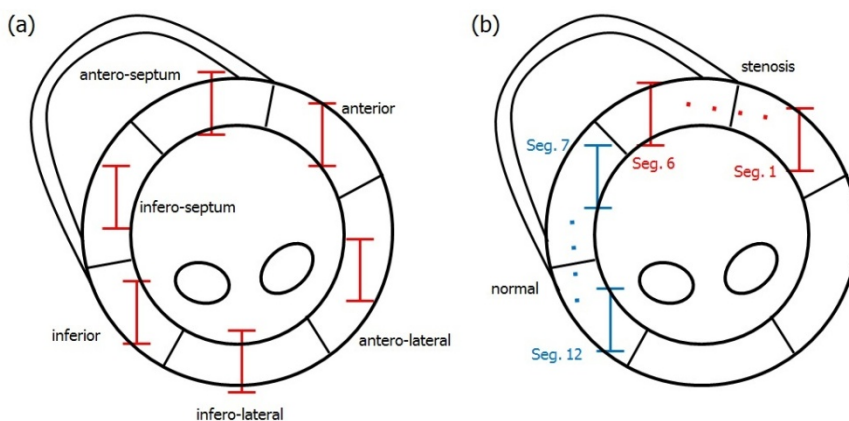
Fig. 1 Myocardial segment analysis in parasternal short axis view.
(a) Range gate set-up in conventional focused CDV.
(b) Range gate set-up in arrayed-range-gate CDV.

P1C1-6 _____

8:00 am   How Calcifications Affect Shear Wave Speed Estimations? An Experimental Study

Adriana Gregory[1], Mahdi Bayat[1], Max Denis[1], Qiang Bo[1], Mohammad Mehrmohammadi[1,2], Mostafa Fatemi[1], Azra Alizad[1]; *[1]Physiology and Biomedical Engineering, Mayo Clinic College of Medicine, Rochester, Minnesota, USA, [2]Biomedical Engineering, Wayne State University, Detroit, Michigan, USA*

Background, Motivation and Objective

OBJECTIVE: To quantify the effect generated by calcifications on shear wave elastography estimates.

Statement of Contribution/Methods

METHODS: Comb-push ultrasound shear elastography (CUSE) was used in this study. The study consists of 2 parts. The first part involved 3 phantom experiments to study the interaction of shear waves in presence of macro and microcalcifications. We used kidney stones to simulate calcifications, as they have similar chemical composition found in benign breast calcifications (CaC2O4). Seven kidney stones with sizes ranging from 2mm to 15mm were imbedded in tissue mimicking gelatin, and crushed kidney stones were used to evaluate the effect of calcifications in the form of cluster and regional-dispersed distributions on shear wave elastography (SWE) estimates. The second part of our study included a finite element method (FEM) simulation to observe closely the effect of calcifications on SWE and corroborate shear wave speed measurements with our phantom results.

Results/Discussion

RESULTS: Our phantom study results showed that elasticity measurements are directly proportional to the size of macrocalcifications and density of clustered microcalcifications. Shear wave speed values as high as 4m/s were observed for our smallest macrocalcification (2mm). Our maximum speed of the display scale (8m/s) was observed for macrocalcifications larger than 5mm. Calcifications larger than 6mm created high shear wave speed regions in the calcification shadow area generating a bias on speed measurements. A two-transducer experiment designed to determinate the source of high shear wave speeds below macrocalcifications demonstrated that they result from low signal-to-noise ratio of the detection beam, therefore are considered artifacts. Phantom elasticity estimates were to some extent higher than FEM simulation results.

SATURDAY POSTER

CONCLUSION: The results from our study demonstrate that clustered and large calcifications can induce the appearance of high stiffness regions in SWE. Considering that benign masses normally have significantly lower elasticity values than malignant tumors, such areas with high elasticity appearing due to presence of calcification in benign masses may lead to misdiagnosis. In vivo studies with various types of calcification in breast or thyroid lesions are needed to further quantify the apparent elasticity estimations.
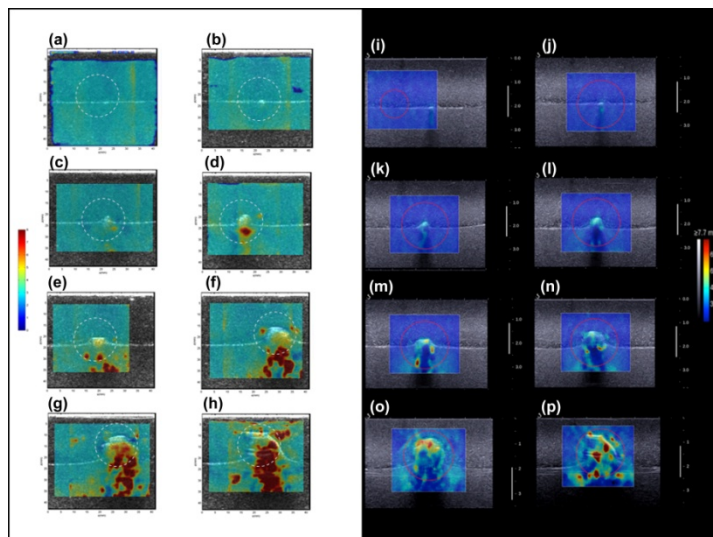
P1C1-7

8:00 am **Evaluating Hepatic Fibrosis in Rat Liver by using Ultrasound Elastography: Comparison between Model-dependent and Model-independent Approaches**

Haoming Lin[1], Xinyu Zhang[1], **Xin Chen[1]**, Yuanyuan Shen[1], Xianfen Diao[1], Chien Ting Chin[1], Yi Zheng[2], Yanrong Guo[1], Tianfu Wang[1], Siping Chen[1]*; [1]Shenzhen University, Shenzhen, China, People's Republic of, [2]St. Cloud State University, St. Cloud, MN 56301, USA*

Background, Motivation and Objective

A number of ultrasound elastography techniques, primarily based on shear wave dispersion, have been applied to measure the viscoelastic properties of the liver for the diagnosis of liver fibrosis. Most of the studies focused on the model-dependent approach which fitted the dispersive data to the biomechanical model, Voigt model for example, to solve the model parameters for staging fibrosis. By contrast, the model-independent approach directly measures the dispersive pattern such as dispersive slope without any model assumption. Although the model-independent approach is relatively simple and robust than the model-dependent approach, it has been seldom used for staging fibrosis; and the correlation and difference between the two approaches are still unclear. The objective of this study was to evaluate and compare the diagnostic accuracy of both approaches for staging liver fibrosis in a rat model.

Statement of Contribution/Methods

Liver fibrosis was induced in 37 rats using carbon tetrachloride (CCl4); 6 rats served as controls. Shear wave speed as a function of frequency, referred to as speed dispersion, was measured in vitro by using SonixRP system. For the model-dependent approach, the dispersion data was fit to Voigt model to solve for the elasticity and viscosity modulus. For the model-independent approach, the dispersion data was analyzed by linear regression to extract the slope and intercept features. The parameters obtained by both approaches were evaluated separately using a receiver operating characteristic (ROC) curve analysis; and the correlations between the two sets of parameters were analyzed.

Results/Discussion

The measured mean values of liver elasticity and viscosity ranged from 0.84 to 3.45 kPa and from 1.12 to 2.06 Pa.s for fibrosis stages F0~CF4, respectively; and the mean values of dispersion slope and intercept ranged from 1.90 to 4.61 m/s/kHz and from 0.34 to 3.36 m/s respectively. The Pearson's correlation coefficients indicated that elasticity was highly correlated with intercept ($r = 0.84$); while viscosity was poorly correlated with slope ($r = -0.15$). For diagnosis of significant fibrosis (METAVIR scores $\geq$ F2), the sorted areas under ROC curve (AUROC) values were 0.99 (intercept), 0.98 (elasticity), 0.89 (viscosity), and 0.42 (slope). These findings confirmed the hypothesis that increasing collagen content (more elastic) will increase the dispersion intercept in liver fibrosis. Compared with the nonlinear processing in the model-dependent approach, the feature extraction method used in the model-independent approach is relatively straight forward and robust. More importantly, the staging performance of the model-independent approach is better than that of the model-dependent approach. Therefore, the model-independent approach may provide an alternative method to the model-dependent approach for staging liver fibrosis.

P1C2 - MCA: Contrast Applications

4th floor

Saturday, October 24, 2015, Posters displayed 08:00 am - 05:00 pm. Authors must be present at their poster from 9:30 - 10:30am (odd number posters) and 14:30 – 15:30pm (even number posters).

Chair: **Hairong Zheng**
                Shenzhen Institutes of Advanced Technology

P1C2-1 _____

8:00 am   Imaging of the Dispersion Coefficient of Ultrasound Contrast Agents by Wiener System Identification for Prostate Cancer Localization

Ruud van Sloun[1], Libertario Demi[1], Hessel Wijkstra[1,2], Massimo Mischi[1]; *[1]Electrical Engineering, Eindhoven University of Technology, Eindhoven, Netherlands, [2]Academic Medical Center Amsterdam, Netherlands*

Background, Motivation and Objective

Prostate cancer (PCa) is the most prevalent form of cancer in Western men, however reliable tools for detection and localization are lacking. Dynamic Contrast Enhanced Ultrasound (DCE-US) is a diagnostic tool that allows analysis of vascularization, by imaging an intravenously injected microbubble bolus. The localization of angiogenic vascularization associated to the development of tumors is of particular interest. Recently, methods aiming at estimating bolus dispersion to localize angiogenesis have shown promise. However, independent estimation of dispersion was not possible due to the ambiguity between dispersive and convective processes. Therefore, in this study we propose a new method that considers the vascular network as a dynamic linear system, whose impulse response can be locally identified. To this end, model-based parameter estimation is employed, allowing extraction of the apparent dispersion coefficient (D), convective time (μ) and Péclet number (Pe) of the system.

Statement of Contribution/Methods

We model the discrete indicator dilution curve (IDC) of the ith pixel d_i in a ring kernel (inner and outer radius of 0.9 mm and 1.5 mm, respectively) as a filtered version of the IDC of the pixel x at the center. The filter coefficients w_i can then be found by solving the Wiener-Hopf equations:

$$r_{d\_i\,x} = R_{xx}w_i,$$

where $r_{d\_i\,x}$ denotes the cross correlation vector between d_i and x, and R_{xx} is the autocorrelation matrix of x. From this set of equations, the Wiener coefficients are obtained by first pre-whitening x with an autoregressive filter. The same filter is applied to d_i. As x is now approximately white, its autocorrelation matrix is close to being an identity matrix. Hence, w_i can be estimated from $r_{d\_i\,x}$ directly. Next, all non-causal impulse responses are discarded and a mean causal impulse response h is computed for the kernel. Finally, the 1D Green's function of the convection-diffusion equation is fitted to h, facilitating the extraction of D, μ, and Pe. This procedure is repeated for all pixels to produce parametric maps.

Results/Discussion

Figure 1 shows an example of the parametric images obtained by applying the proposed method to a DCE-US loop of a patient referred for radical prostatectomy, along with the corresponding histology slice. These preliminary results encourage future investigation of system identification techniques for PCa localization.
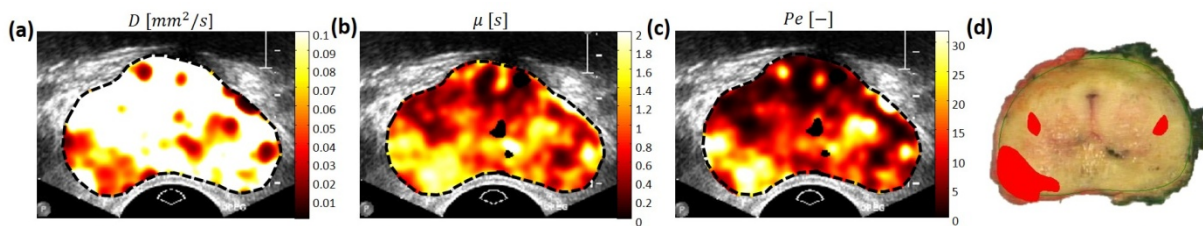
Figure 1. Plot (a), (b), and (c) show the obtained dispersion, convective time, and Péclet number parametric images, respectively. The corresponding histology slice is shown in (d).

P1C2-2 _____

8:00 am   Investigation of Membrane and Uptake Kinetics in Sonoporation Using a Giant Unilamellar Vesicle Cell Model

Ruen Shan Leow[1], Wenjing Zhong[1], Alexander L. Klibanov[2], Alfred C. H. Yu[1]; *[1]Medical Engineering Program, University of Hong Kong, Pokfulam, Hong Kong, [2]Division of Cardiovascular Medicine, University of Virginia, Charlottesville, Virginia, USA*

Background, Motivation and Objective

Sonoporation is essentially an act of acute disruption of the plasma membrane, and there is common belief that the perforation site would naturally be repaired over time. However, our earlier data has shown that post-sonoporation recovery is not a definite event, and it is not clear whether the repair process is presided by physical (membrane forces) or biological means (subcellular signal activation). To stepwise address this question, we surmise that it is essential to dedicate an investigation to study whether membrane forces exclusively play a significant role in regulating sonoporation kinetics. Accordingly, we have aimed to establish a cell model that is free of subcellular organelles to rule out the influence of biological maneuvers in sonoporation episodes, and have sought to use it to analyze possible correlation between transmbranous diffusion kinetics and the size of sonoporation sites.

Statement of Contribution/Methods

The cell model was constructed from giant unilamellar vesicles (GUV) with size that ranged between 10-30 um. Fabricated using an electroformation protocol, the GUV membrane was composed of 95:5 (molar ratio) DPPC:DPPG (with 200 mM sucrose internal buffer), and it was fluorescently tagged using CellMask. In a subset of experiments, DPPC was partly replaced with cholesterol (10, 15, or 20%) to alter the GUVs' membrane fluidity. After anchoring the GUVs on a cell plate (with 200 mM glucose external buffer and 10 uM calcein as influx tracer), a dilute microbubble solution (10e4 per mL) was added to facilitate the creation of single-site sonoporation scenarios. To improve their binding on the negatively charged GUV surface, the microbubbles were cationic charged. Microbubble-attached GUVs were then observed live using confocal microscopy (3 fps), and the onset of sonoporation was triggered through a single-pulse (30 cycles; 0.45 MPa peak negative pressure) ultrasound transmission protocol via a 1 MHz single element transducer (2.54 cm diameter; coupled to cell chamber with a waveguide). Cross-sectional gap size across the sonoporation site was measured in-situ, and the calcein influx into the GUV was tracked as a function of time to study sonoporation-related diffusion kinetics.

Results/Discussion

Successful perforation site repair was only observed in GUVs with cholesterol-enriched membranes that are more fluidic in nature (N=30). This suggests that membrane fluidity is a physical factor that influences the post-sonoporation recovery process. A strong correlation (R=0.9164; N=10) between calcein influx rate and the microbubble-

SATURDAY POSTER

to-GUV size ratio was also observed, implying that relatively larger microbubbles (with respect to cell size) would lead to larger transmembranous influx. This finding is synchronous with the positive correlation between pre-exposure microbubble diameter and pore gap size (R=0.8381; N=30).

P1C2-3

8:00 am **Feasibility of in vivo contrast-enhanced ultrasound imaging of the renal cortex during hemorrhagic shock**

Tom van Rooij[1], Alexandre Lima[2], Verya Daeichin[1], Patricia A.C. Specht[3], Bulent Ergin[4], Yasin Ince[2,4], Nico de Jong[1,5], Can Ince[2,4], Klazina Kooiman[1]; [1]*Department of Biomedical Engineering, Thorax Center, Erasmus MC, Rotterdam, Netherlands,* [2]*Department of Intensive Care Adults, Erasmus MC, Rotterdam, Netherlands,* [3]*Laboratory of Experimental Anesthesiology, Department of Anesthesiology, Erasmus MC, Netherlands,* [4]*Department of Translational Physiology, Academic Medical Center, Amsterdam, Netherlands,* [5]*Laboratory of Acoustical Wavefield Imaging, Faculty of Applied Sciences, Technical University Delft, Delft, Netherlands*

Background, Motivation and Objective

A direct and non-invasive measurement of kidney function could aid in early recognition of acute kidney injury (AKI) at bedside and may prevent severe kidney damage. This study investigates the feasibility of contrast-enhanced ultrasound (CEUS) imaging of the kidney cortex in an in vivo pig model of hemorrhagic shock. We hypothesize that the inflow-slope (SL) of the time-intensity curves (TICs) is lower as a result of decreased renal blood flow (RBF) in shock.

Statement of Contribution/Methods

Six female pigs (30.8 ± 2.6 kg) underwent surgery to expose the right kidney and hemorrhagic shock was induced by withdrawing 40% of the blood. Lactate levels, mean arterial pressure (MAP), heart rate (HR), and cardiac output (CO) were measured at baseline (t0), 15 min after blood withdrawal (t1), and 60 min later (t2). Blood flow in the renal artery (RBF) was measured using a flow probe. For the CEUS measurements a 1 mL bolus of microbubbles (C_4F_{10} gas; lipid coating in mol%: 92.4 DSPC, 7.6 DSPE-PEG2000; made by Vialmix) or Target-Ready MicroMarker (VisualSonics) was injected in the jugular vein followed by a 10 mL saline flush. We used the Vevo2100 equipped with a MS250 transducer (VisualSonics) transmitting at 18 MHz and recording 10 frames per second. Regions of interest were drawn in the cortex and TICs were obtained. After average-filtering the TICs using Matlab, the inflow-slope (SL), rise time (RT), peak-enhancement (PE), mean transit time (MTT), and area under the curve (AUC) were calculated (Fig. 1A) [1,2]. Differences between t0 and t2 were evaluated in SPSS.

Results/Discussion

Higher HR and lactate levels, and decreased CO and MAP indicated the pigs were in shock. We showed that changes in the renal cortical inflow could be measured using CEUS. The decrease of RBF from t0 to t2 (median 35%, p = 0.03) was followed by a decrease in SL in 3/6 pigs (median 70%, Fig. 1B). However, in the other 3 pigs we measured an increase in SL (median 45%).

Our results indicate a disparity in the kidney between decreased RBF and the inflow of microbubbles, i.e. SL, in the renal cortex in response to hemorrhagic shock. This opposite response could be caused by the renal autoregulation; vessels in different parts can constrict or dilate to maintain a constant RBF. Further research will focus on validating CEUS in this, and other models of AKI.

[1] Strouthos et al. IEEE IUS Proc, 2009; [2] Needles et al. Ultrasound Med & Biol, 2010
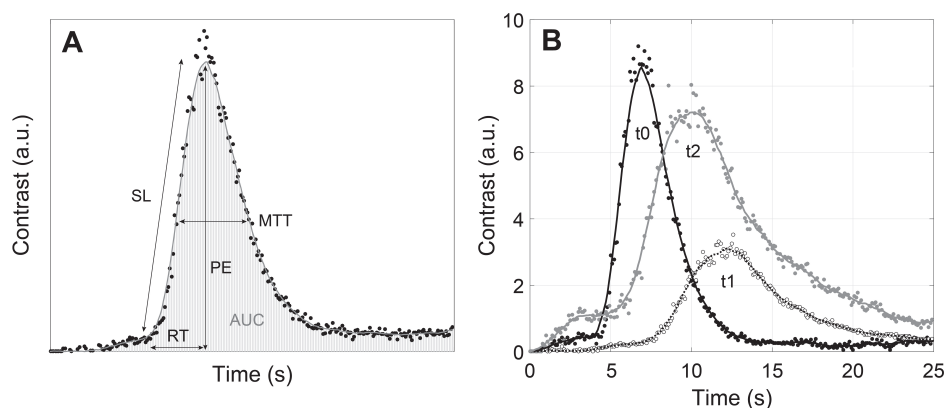
Figure 1. **A)** Definition of parameters determined from the time-intensity curves (TICs). SL = inflow-slope, RT = rise time, MTT = mean transit time, PE = peak-enhancement and AUC = area under the curve. **B)** Example of measured (dots) and filtered (lines) TICs at baseline (t0), early shock (t1) and late shock (t2) with decreasing slope following the decrease in renal blood flow (RBF).

P1C2-4

8:00 am **Molecular Ultrasound Assessment of Colorectal Tumor Angiogenesis with Endoglin-targeted Contrast Microbubbles**

Cheng LIU[1], Yaoheng YANG[1], Zhihai QIU[1], Yongmin HUANG[1], Fei YAN[2], Lei SUN[1]; [1]*Interdisciplinary Division of Biomedical Engineering, Faculty of Engineering, The Hong Kong Polytechnic University, HONG KONG, China, People's Republic of,* [2]*Paul C. Lauterbur Research Center for Biomedical Imaging, Shenzhen Institutes of Advanced Technology, Chinese Academy of Sciences, Shenzhen, China, People's Republic of*

Background, Motivation and Objective

Colorectal cancer (CRC) remains the third most popular cancer in US. CRC biopsy usually shows substantially increased angiogenesis, which is promoted by a number of pro-angiogenic growth factors. Among all these factors, the expression of endoglin has been remarkably up-regulated on actively proliferating endothelial cells of neo-vasculature. Endoglin has been an independent clinical pathological target for the tumor aggressiveness assessment. In this study, we developed endoglin-targeted microbubbles (MBs), and employed targeted microbubbles enhanced ultrasound (US) imaging to assess the endoglin expression levels in neo-vasculature for non-invasive assessment of colorectal tumor angiogenesis.

Statement of Contribution/Methods

All procedures using laboratory animals were approved by the Department of Health, The Government of the Hong Kong Special Administrative Region and the Hong Kong Polytechnic University Animal Subjects Ethics Sub-committee. Endoglin-targeted microbubbles and control microbubbles (MBs) were prepared according to standard protocol [1]. A parallel-plate flow chamber was employed, in which endoglin-targeted MBs and untargeted control MBs were tested across mouse SVR angiosarcoma cells (positive endoglin expression) and mouse 4T1 cells (negative endoglin expression) with the adhesion quantified. *In vivo* contrast enhanced US imaging (Vevo 2100; VisualSonics) was conducted using these two types of MBs at different progression stages in a subcutaneous COLO 201 xenograft model in nude mice (n=16). Finally, statistical analysis of endoglin expression levels was performed between *in vivo* molecular US signals and *ex vivo* endoglin expression levels from immunohistochemical test.

Results/Discussion

Cell attachment of endoglin-targeted MBs was significantly higher than untargeted control MBs. Endoglin-positive SVR cells bound significantly more endoglin-targeted MBs than negative control 4T1 cells, and MBs attachment significantly correlated with endoglin expression levels on cells. There was a good correlation between *in vivo* molecular US signals using endoglin-targeted MBs and *ex vivo* expression levels of endoglin from immunoblotting result. The results indicate that the molecular US is much potential for non-invasive assessment of the expression levels of endoglin in colorectal tumor angiogenesis.

Reference

1. Klibanov, A. L. (2005). Ligand-carrying gas-filled microbubbles: ultrasound contrast agents for targeted molecular imaging. Bioconjugate chemistry, 16(1), 9-17.

P1C2-5 _____

8:00 am   Evaluation of Accuracy of Bolus and Burst Method for Quantitative Ultrasound Perfusion Analysis with Various Arterial Input Function Models

Martin Mezl[1,2], Radovan Jirik[1,3], Karel Soucek[4,5], Radim Kolar[1,2]; [1]*Center for Biomedical Engineering, International Clinical Research Center, St. Anne's University Hospital Brno, Brno, Czech Republic,* [2]*Department of Biomedical Engineering, Brno University of Technology, Brno, Czech Republic,* [3]*Institute of Scientific Instruments of the ASCR, v. v. i., Brno, Czech Republic,* [4]*Department of Cytokinetics, Institute of Biophysics, Academy of Sciences of the Czech Republic, v.v.i., Brno, Czech Republic,* [5]*Center of Biomolecular and Cellular Engineering, International Clinical Research Center, St. Anne's University Hospital Brno, Brno, Czech Republic*

Background, Motivation and Objective

The aim of this study is to provide analysis of robustness and accuracy of perfusion parameter estimations obtained by the bolus and burst (B&B) method with different models of the arterial input function (AIF). The B&B method is an current and promising method for quantitative ultrasound perfusion analysis. The basic idea of the method is the combination of two common approaches for perfusion-imaging data acquisition – bolus tracking and burst replenishment. The estimation of perfusion parameters is based on a blind deconvolution of the measured tracer concentration curves. A parametric model of the AIF and the tissue residual function (TRF) is used. Estimation of the model´s parameters is a crucial factor for assessment of the perfusion parameters. Two different AIF models have been used for the bolus and burst method yet, one based on two lognormal functions (2-logn) and one based on three gamma-variate functions (3-gam). The aim of this contribution is comparison of these two models based on simulated and preclinical data.

Statement of Contribution/Methods

Simulated data were created from reference AIFs (approximating a representative measured AIF) and from a monoexponential TRF with a typical mean transit time (MTT=4 sec). The data were additionally distorted with additive zero-mean Gaussian noise to provide the same SNR as in the measured sequences. Preclinical data were recorded on a BALB/c mice with subcutaneously implanted colon tumor cells CT26. Two mice were examined using a Vevo 2100 ultrasound scanner with the MS 250 probe and using of the nonlinear contrast imaging mode with the contrast agent MicroMarker®.

The AIF models were compared on synthetic data by evaluating the achieved accuracy of the estimated AIFs with respect to the reference AIF. For evaluation on preclinical data, 10 small regions of interest with a high SNR were chosen for each of 2 animals. Variability of the estimated AIFs within each animal was estimated.

Results/Discussion

Estimated values of MTT for simulated data were 4.1±1.5 sec for 3-gam AIF model and 4.7±1.3 sec for 2-logn model. Results of the mean AIF (solid line) and the mean AIF with ±standard deviation (dashed line) for all datasets and both models are shown in the figure. Variability of the AIF estimation is lower for 3-gam AIF model in all experiments. The study will be extended to include data from more animals and to evaluate more AIF models.
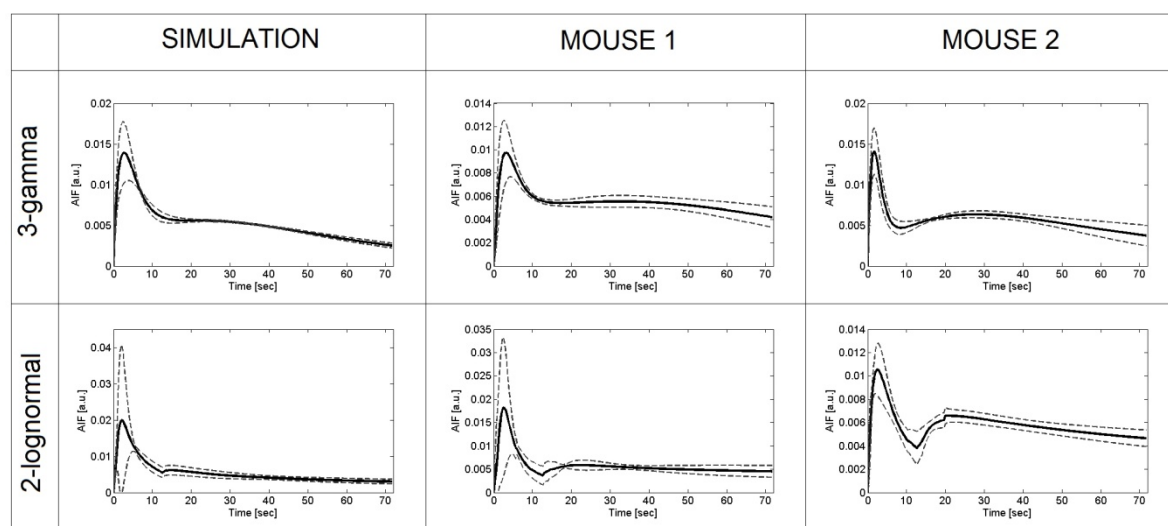
P1C2-6 _____

8:00 am   An ImageJ plugin for the sizing and counting of microbubbles

Charles SENNOGA[1], Emma Kanbar[1], Ayache Bouakaz[1]; [1]*Inserm U930, Université François-Rabelais de Tours, France*

Background, Motivation and Objective

Although the efficacy of various microbubble sizing and counting methods is now well-documented, there is no community-wide consensus regarding what method to use. A quick and accurate way of determining the size and count of microbubbles is not only important for the quality control of fabricated microbubbles but also necessary for quantifying the impact of microbubbles, in therapeutic and quantitative applications. Here we describe the development of a plugin designed to identify and analyse the dimensions, size distribution and count of microbubbles from standard output generated by ImageJ.

Statement of Contribution/Methods

SonoVue™ microbubbles (Bracco, Milano, Italy) were dispersed in saline, at a known dilution. Uncompressed 24-bit images of non-overlapping microbubbles captured by video-microscopy were uploaded and converted to 8 bit binary images, by using an automated thresholding ImageJ function which minimizes the intra-class variance of the black and white pixels. The resulting images were inverted and the holes that optically appear in the centre of bubbles filled. The algorithm then works through each row of each column in the image detecting white pixels. When a white pixel is detected a contour is traced around the cluster. The contour is compared against a circle of

corresponding mean diameter. If the least-square-error between the contour and the circle falls <10%, the bubble is counted and the algorithm steps on through the image. Otherwise, a bubble cluster or a bubble partly off the image edge is assumed, and the bubble is not counted. However, the area obscured by the bubble cluster is recorded as this is used in the algorithm to correct for clustering in the final bubble number count. The algorithm treats each image independently and outputs a list of the bubbles detected and their diameters. If enabled, batch processing accumulates the output across several images. Provided there are enough isolated bubbles, the plugin is able to adjust the final number count to remove the effects of bubble clustering. To validate our method, we determined the size and count of calibration microspheres, with NIST traceable size diameters and number counts. The size of the microspheres was comparable to microbubbles.

Results/Discussion

Images of dispersed SonoVue™ were batch processed (n=4). Mean diameters of 2.26±0.18 µm and counts of 2.2×10^8 microbubbles/mL were recorded for SonoVue™, as compared to literature mean diameters of 2.5 µm, and number count of $1–5\times10^8$ microbubbles/mL. Validation measurements conducted using calibration microspheres returned diameters of 2.96±0.03 µm and 3.07±0.07 µm; and, counts of 7.3×10^6 and 7.2×10^6 microspheres/mL for mono- and poly-disperse microspheres, in good agreement with literature and NIST traceable diameters of 3.0 µm (for both microspheres) and counts of 7.5×10^6 and 7.25×10^6 microspheres/mL, respectively. Our findings suggest that the plugin can be reliably used to size and count microbubbles.

P1C2-7

8:00 am   The evaluation system for measuring sensitivity of microbubbles to target molecules using a quartz crystal microbalance

Yasuhiro Yokoi[1], Kenji Yoshida[2], Ryosuke Shimoya[1], Yoshiaki Watanabe[1]; *[1]Doshisha University, Japan, [2]Chiba Univercity, Japan*

Background, Motivation and Objective

Targeted microbubbles (MBs) has been used in the molecular imaging and drug delivery system. Although it is important to understand the sensitivity of bubbles to the target molecules, the evaluation of the sensitivity is difficult in in-vivo experiment. Our goal is to construct an artificial system to measure quantitatively both the concentration of target molecular and the number density of specifically adsorbing MBs. Quartz crystal microbalance (QCM) as biosensor has potential to quantify the both amount. It is demonstrated that QCM can be used to evaluate the amount of target molecular on its surface. We needed to establish the method for measuring the amount of adsorbing MBs and proposed the physical model for calculating the number density of MBs on QCM [1]. This study validates the model based on the measurement of the number density of biotinylated MBs adsorbed to streptavidin on QCM.

Statement of Contribution/Methods

Biotinylated phospholipid MBs were specifically adsorbed to streptavidin as target molecular fixed on QCM surface electrode. The equivalent electrical circuit of QCM with adsorbed bubbles was described as shown in Fig.1 (a). Using a network analyzer, the motional impedance (R_b and L_b) related to bubble adsorption could be measured. The number density of MBs were calculated from R_b or L_b when the suspension (30 µL) containing MBs (average diameter of 2 µm) was deposited on QCM. Using an optical microscope, the number density of adsorbed MBs was also evaluated as reference and compared with the result of QCM measurement.

Results/Discussion

Figure 1 (b) shows the relation between motional impedance R_b and the concentration of bubbles in the bubble suspension. R_b logarithmically increased as the concentration of MBs increase. This suggests that R_b is effective parameter for describing the adsorption of MBs. Our physical model indicated that the number density of adsorbing MBs on QCM is 450 bubbles/mm² from the result of R_b=33.6±9.4 Ω at concentration of 670 bubbles/mm³. This result is roughly consistent with the reference data using optical microscope, which is 240 bubbles/mm². Thus it is supposed that the number density of bubbles on QCM could be quantitatively measured although the further examinations are needed.

Reference

[1] R. Shimoya et al., Jpn. J. Appl. Phys. (2015) (in press)
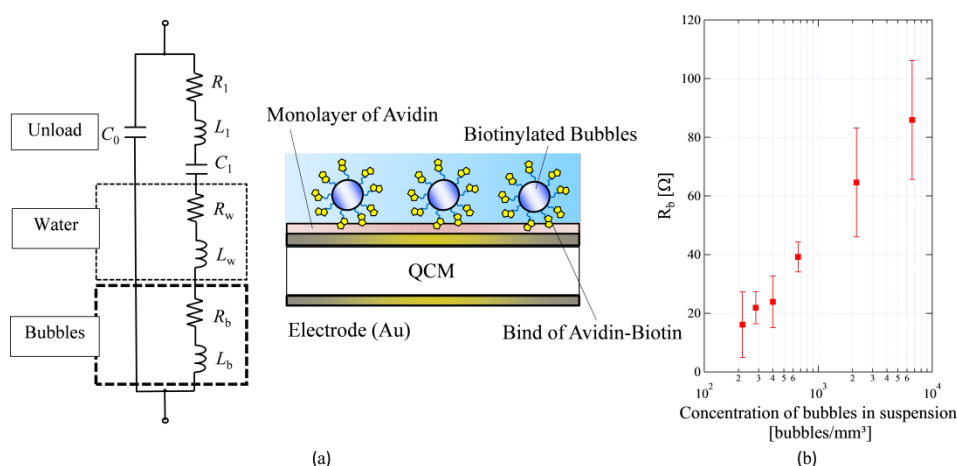
Fig.1 (a) The equivalent circuit of QCM under the condition of absorbing bubbles on the surface.
(b) Relation between Rb and concentration of bubbles in suspension.

P1C2-8

8:00 am   Optical Observation of Microbubble Behaviors to Modulated Acoustic Radiation Force in Large Vessels

Shiying Wang[1], Claudia Y Wang[1], Alexander L Klibanov[1,2], John A Hossack[1], F William Mauldin Jr[1]; *[1]Biomedical Engineering, University of Virginia, Charlottesville, Virginia, USA, [2]Division of Cardiovascular Medicine, University of Virginia, Charlottesville, Virginia, USA*

Background, Motivation and Objective

Ultrasound molecular imaging has been studied for pre-clinical applications including detection of cancer and cardiovascular disease. We recently developed a modulated Acoustic Radiation Force (ARF)-based beam sequence for detection of targeted adhesion using short imaging protocols without necessitating control measurements [1-2]. Many previous studies have performed optical verification of microbubble (MB) behavior, however, they are all limited to small vessels or with application of constant ARF. In this study, the first optical observation of adherent MB dynamic behavior in large vessels under the influence of secondary ARF and molecular force was achieved.

Statement of Contribution/Methods

Polydimethylsiloxane (PDMS) flow channels (Ø = 4 mm) were used to mimic large blood vessels. Targeted and control channels were incubated with 50 µg/mL streptavidin and 5% bovine serum albumin solution, respectively. Biotinylated lipid-perfluorobutane MB (Ø ≈ 2 µm) dispersion (5×10^5 mL^{-1}) was drawn through the channels. The PDMS channels were placed between the ultrasound transducer (L12-8 38mm) and objective lens (40×), which are coaxial and focused at the bottom channel wall. The custom modulated ARF-based beam sequence [1-2] was programmed on a Verasonics scanner. The dynamic response of adherent MBs was detected acoustically and simultaneously visualized using a video camera connected to the microscope.

Results/Discussion

Residual signal magnitudes were approximately 0% and 50% of the maximum signal magnitudes for control and targeted channels, respectively. Aggregates of adherent MBs were observed optically under the influence of ARF. Large aggregates were observed solely in control channels without targeted adhesion (b). After the cessation of ARF, aggregates dispersed immediately in control channels but remained largely intact in the targeted channels. The dispersion of aggregates led to a transient acoustic signal enhancement in control channels (referred to as "control peak"). Findings in this study provide a better understanding of MB behavior in large vessel environments with application of ARF, and could potentially guide future beam sequence designs or signal processing for enhanced ultrasound molecular imaging.

[1] Wang *et al*, Phys Med Biol, 2014; 59(2): 465-484

[2] Wang *et al*, Ultrasound Med Biol, 2015; 41(1): 222-234
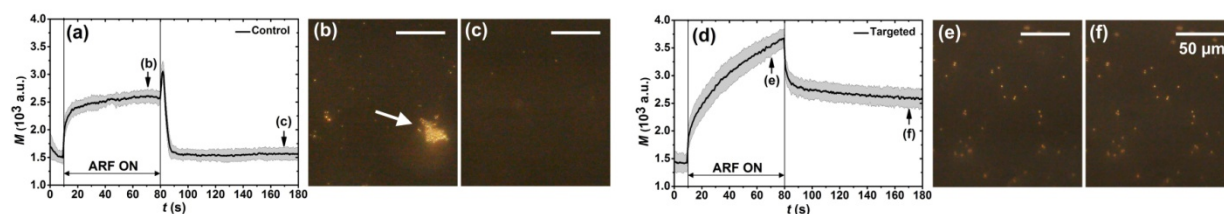
Figure. Ultrasound signal magnitude (*M*) curves of adherent microbubbles (MBs) for control (a) and targeted (b) flow channels. Solid lines indicate the mean values from ten trials. Light shadows indicate the corresponding error bars (mean ± standard deviation). Images of adherent MBs (bright dots) within the microscope field of view at different times: (b) control, *t* = 70 s; (c) control, *t* = 170 s; (e) targeted, *t* = 70 s; (f) targeted, *t* = 170 s. MB dispersion flowed from left to right (6 cm/s). Arrow (b) indicates the large aggregate of adherent MBs.

SATURDAY POSTER

P1C3 - MIM: Medical Imaging

4th floor

Saturday, October 24, 2015, Posters displayed 08:00 am - 05:00 pm. Authors must be present at their poster from 9:30 - 10:30am (odd number posters) and 14:30 – 15:30pm (even number posters).

Chair: **Kai Thomenius**
GE Corporate R&D

P1C3-1

8:00 am **Spatial mapping of electromechanical properties in bone measured through acoustically stimulated electromagnetic response**

Kakeru Watanabe[1], Shuntaro Hamazumi[1], Hisato Yamada[1], Kenji Ikushima[1], Yoshitsugu Kojima[2], Nobuo Niimi[2], Yoshihiro Hagiwara[3]; [1]*Department of Applied Physics, Tokyo University of Agriculture and Technology, Koganei, Japan, [2]Nippon Sigmax Co. Ltd., Tokyo, Japan, [3]Department of Orthopaedic Surgery, Tohoku University School of Medicine, Sendai, Japan*

Background, Motivation and Objective

Bone is a connective tissue largely composed of collagen fibers and inorganic mineral hydroxyapatite. Depending on the orientation of collagen fibers, two types of bone can be distinguished: outer cortical bone and inner trabecular bone. Bone mineral density obtained by X-ray or ultrasonic techniques is normally used as an indicator of bone conditions, but the evaluation method of collagen quality is still in development.

We here focus on acoustically stimulated electromagnetic (ASEM) response through electromechanical coupling in bone. Since the origin of electromechanical coupling is considered to be the piezoelectricity of fibrous collagen crystals, the ASEM response probes collagen crystal orientation and qualities.

Statement of Contribution/Methods

A rectangular 50 ns wide pulses are applied at a repetition rate of 1 kHz by a pulser/receiver. To distinguish ASEM response from transducer noise, a target sample is placed in a focused zone at a distance of about 60 mm from 10 MHz transducer. The signals are detected through a capacitive resonant antenna. Two-dimensional images of ASEM response are obtained by mechanically scanning the focused ultrasonic beam. The spatial mapping of ASEM signals are measured for health rat femurs and the models of osteoporosis.

Results/Discussion

We found that (1) the ASEM response is generated on the cortical bone, (2) the maximum ASEM intensity is obtained at a specific spot in the diaphysis of femur on the knee joint side for five healthy specimens, and (3) the maximum ASEM intensity is reduced for the models of osteoporosis. The ASEM response may thus provide a potential indicator for noninvasive evaluation of bone quality.
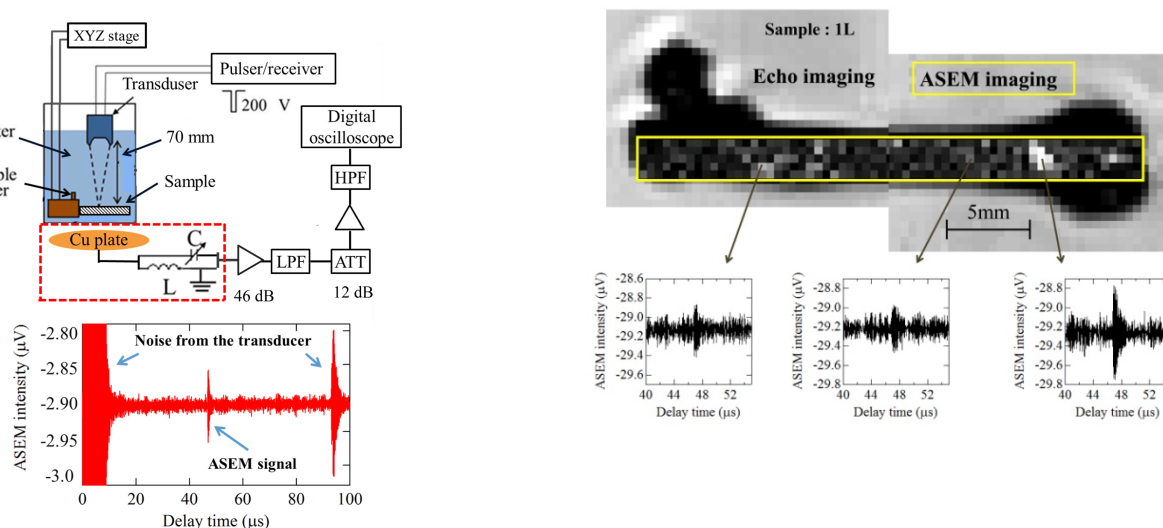
P1C3-2

8:00 am **Assessment of Scoliosis Using 3D Ultrasound Volume Projection Imaging with Automatic Detection of Spine Curvature**

Guang-Quan Zhou[1], **Yong-Ping Zheng[1]**; [1]*The Hong Kong Polytechnic University, Hong Kong*

Background, Motivation and Objective

X-ray imaging is a gold standard to diagnose scoliosis, a medical condition defined as lateral spine curvature > 10¢X, which affects 2-4% of population. However, radiation hazard restricts its application. 3D ultrasound imaging shows potential for radiation-free scoliosis assessment. Recently, ultrasound volume projection imaging (VPI) was reported to provide a coronal view of spine for manual measurement of spine curvature. An automatic method for processing VPI images is now very much desired to avoid using tedious and subjective manual procedures, especially for scoliosis mass screening.

Statement of Contribution/Methods

Figs 1a and 1b shows a typical coronal view image of spine. The spinous profile located in the midline of the image can reveal the spine deformity of a subject. The curvature of spine could be manually measured by locating two most tilt regions. In this study, an automatic method was developed to quantitatively determine the spine curvature by fitting the curve of spinous profile with image pre-processing and identifying the inflection points of curve in the coronal images. The performance was tested on the VPI images obtained from 36 subjects (Age: 30.1 ± 14.5) with different spine curvatures.

SATURDAY POSTER

Results/Discussion

A typical result of automatic spine curvature measurement is shown in Fig. 1c, with the red line indicating the curve profile detected. The curvatures obtained using the automatic method had a significant correlation with those by the manual method (r = 0.92; p < 0.001). The result of Bland-Altman plot (Fig. 2) also supported the good agreement between the results of the two methods. The proposed automatic method is capable of measuring the spine curvature on the VPI images, thus greatly facilitates the use of 3D ultrasound for scoliosis assessment.
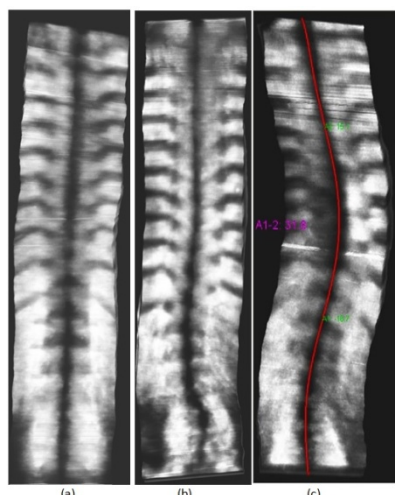
Fig. 1 Examples of VPI images (a, b), and spine curvature measurement using the automatic method (c)
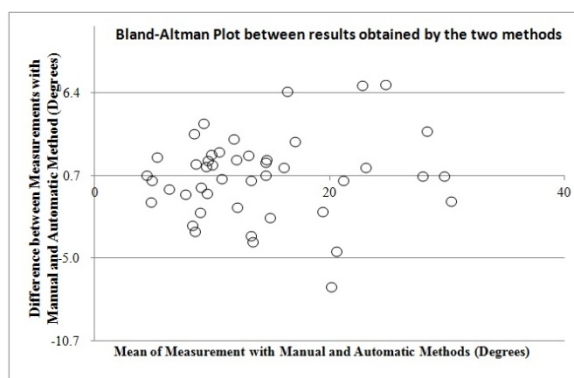
Figure. 2 The Bland-Altman plot between the measurements obtained by the automatic and manual methods

P1C3-3

8:00 am **Automatic Detection and Measurement of Fetal Femur Length using a Portable Ultrasound Device**

Naiad Hossain Khan[1], Eva Tegnander[2,3], Johan Morten Dreier[2], Sturla Eik-Nes[2,3], Hans Torp[1], Gabriel Kiss[1]; [1]ISB, MI Lab and Department of Circulation and Medical Imaging, NTNU, Trondheim, Norway, [2]National Center for Fetal Medicine (NCFM), St. Olavs Hospital, Trondheim, Norway, [3]Department of Laboratory Medicine, Children's and Women's Health (LBK), NTNU, Trondheim, Norway

Background, Motivation and Objective

A reliable estimated date of delivery (EDD) and gestational age (GA) are important to provide optimal care during pregnancy. Using ultrasound technology the biparietal diameter (BPD) and femur length (FL) of a fetus are measured to calculate these parameters. Our research group have been developing a portable and user-friendly ultrasound scanner for the inexperienced midwives in low and middle-income countries. The goal of this work is to develop an automatic method of detecting and measuring fetal femur length that can run on a tablet device to assist the health care worker during the scanning process.

Statement of Contribution/Methods

An ultrasound image containing a fetal femur is saved in the portable scanner. Colored UI elements are separated by selecting a threshold from HSV color space and the image is converted into grayscale. An adaptive binary threshold is selected by calculating the mean and standard deviation of the intensity of image pixels and a binary image is produced. Potential fetal femur contour candidates are computed from the edges between the black and white regions in the binary image. The fetal femur is detected by comparing its size, orientation and position with other femur candidates. A Hough transform is applied in the location of the detected femur to find a straight line with the highest number of supporting points to measure the length of the fetal femur. All these steps are performed by using OpenCV image processing library.

Results/Discussion

Sixty-four different femur ultrasound images have been acquired by experienced (43 images) and inexperienced midwives (21 images). The gestational age range of the fetuses was between 18 - 32 weeks. The images had different quality, intensity and zoom levels. The automatic method was able to detect femurs in 37 out of 43 images (86%) from experienced midwives, and 11 out of 21 images (52%) from inexperienced midwives. The overall detection rate was 75%. The automatic measurements were compared with the manual measurements from experienced midwives. The correlation plot and the error versus reference plot are presented. The correlation coefficient was R=0.95 and the mean error±1.96*STD was -2.35±6.41[mm]. Images containing curved femurs caused important FL underestimation, our method is currently being adapted to work on these cases. The average time of computation was 3.2 seconds in a SM-P600 tablet device.

2D ultrasound slice

Binary image with femur candidates

Correlation plot

Femur contour

Femur detection & measurement

Error vs. reference

SATURDAY POSTER
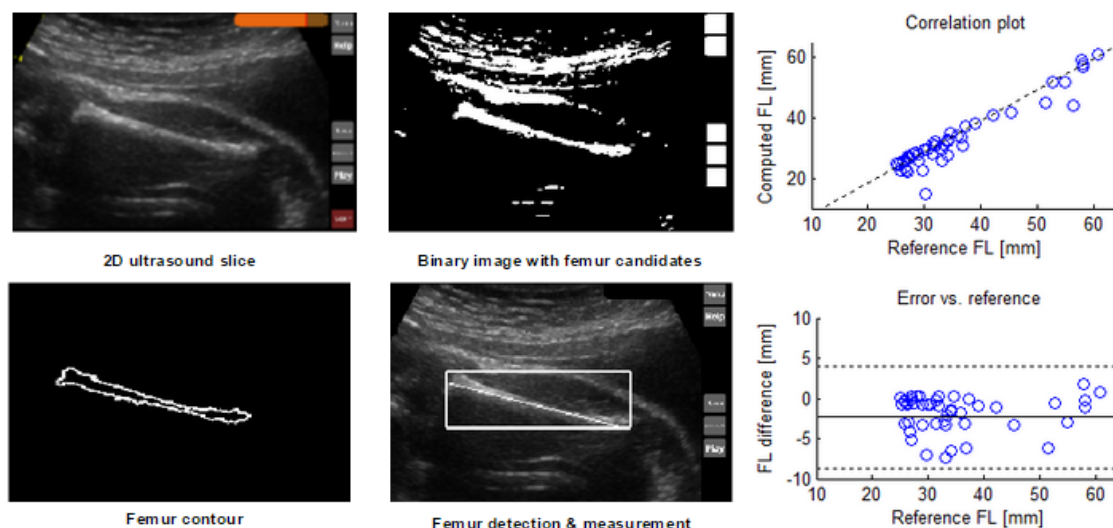
P1C3-4

8:00 am   3D printed phantom for high frequency ultrasound imaging

Jean-Rene Jacquet[1], Frederic Ossant[1,2], franck Levassort[3], Jean-Marc Gregoire[1]; *[1]Université François-Rabelais de Tours, Inserm, Imagerie et Cerveau UMR U930, Tours, France, [2]CHRU de Tours, Tours, France, France, [3]Université François-Rabelais de Tours, GREMAN, UMR 7347 CNRS, Tours, France*

Background, Motivation and Objective

In the field of high frequency ultrasound imaging i.e., > 20 MHz, there is a lack of tools for characterizing the performance of imaging systems. Indeed, for this frequency range, commercial phantoms are inadequate. The development of home-made phantoms, at the laboratory scale is often required, but hindered by the difficulty of fabricating very small structures which must be distributed with high accuracy in 3D space. We propose the use of 3D photo-polymer printing in order to make, resolution and tissue mimicking phantoms dedicated to high frequency ultrasound imaging. To this end, we have designed and manufactured several phantoms with surrounding material and inclusions. The quality and interest in these phantoms are discussed from the point of view of ultrasound parameters and imaging.

Statement of Contribution/Methods

First, density, acoustic impedance, dispersion of compressional phase velocity and attenuation of two photo-polymer materials were measured by temporal and spectral methods in a double transmission experimental set-up. Measurements were made on printed samples by using three different focused single-element transducers (20MHz, 30MHz, and 40MHz) covering a large frequency range. Then, a 3D model (Fig. 1.b, c and d) was designed and printed using our exacting printer settings (Objets30 Stratasys, Israel) knowing that the printer had a minimum inclusion size of 42x42x28 $\mu m3$. The phantoms comprised inclusions of differing shapes (spheres, cylinders and squares) and dimensions (from 100μm to several millimeters). Finally, 3D acoustic images were obtained by using a mechanically driven single element transducer.

Results/Discussion

3D printing allowed us to make phantoms adapted for high frequency and conventional ultrasound imaging with inclusions of complex geometries and surrounding (support material) with acoustics properties close to soft tissue (see Table in Fig 1.a). The SNR between inclusion and surrounding media is around 50dB (Fig 1.e). In conclusion, 3D printing can be a useful tool for directly, easily and rapidly manufacturing ultrasound mimicking phantoms for assessing ultrasound imaging systems and validating computational.

Photo-polymer material	Velocity (m/s)	Density (Kg/m³)	Attenuation (dB/cm Mhz)	Impedance (MRayl)
FullCure 705 (support)	1436-1646	1156	0.5-0.8	1.66-1.90
VeroWhite 835 (model)	2353-2376	1179	2.6-3.1	2.77-2.80
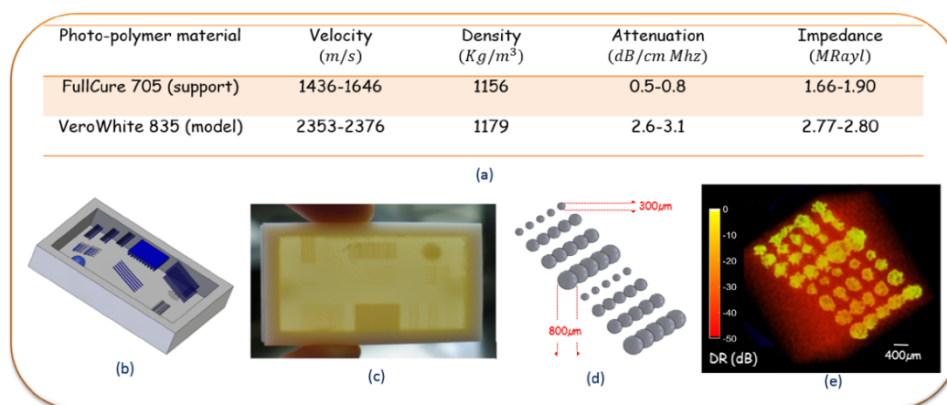
Figure 1: (a) Acoustic properties of the two photo-polymer materials, (b) 3D CAD phantom model, (c) Photography of the 3D printed phantom: white is model and translucent is support, (d) selected inclusions of 3D phantom from CAD model, (e) 3D acoustic image of selected inclusions at 25MHz.

P1C3-5

8:00 am   Mobile 3D augmented reality system for ultrasound applications

Gabriel Kiss[1], Cameron Lowell Palmer[1], Bjørn Olav Haugen[1], Eva Tegnander[2,3], Sturla H. Eik-Nes[2,3], Hans Torp[1]; *[1]Department of Circulation and Medical Imaging and MI Lab, Norwegian University of Science and Technology, Trondheim, Norway, [2]National Center for Fetal Medicine, St. Olavs Hospital, Trondheim, Norway, [3]Department of Laboratory Medicine, Children's and Women's Health, Norwegian University of Science and Technology, Trondheim, Norway*

Background, Motivation and Objective

The acquisition and interpretation of ultrasound images remains a great challenge for new users during a typical learning process which takes up to 12 months under direct expert supervision. The purpose of this work was to investigate if augmented reality can be helpful during the teaching and the acquisition process by providing a patient specific correspondence between a highly detailed anatomic model of the organ to be imaged and the ultrasound data acquired in real-time.

Statement of Contribution/Methods

An augmented view is generated by merging the image of the scene (acquired with a tablet's camera) with a virtual geometric model of the examined organ and the ultrasound image data acquired by the probe. Either the front or the back camera of a tablet is used to record the scene. In order to generate a consistent augmented view that preserves depth cues the position and orientation of both patient and ultrasound probe with regards to the tablet's camera need to be tracked in real-time. For tracking purposes the Vuforia framework (Qualcomm Technologies Inc) has been used. Two frame markers (special type of fiducial markers) are attached to the patient and the ultrasound probe and subsequently tracked if they are present in the camera image. Finally all elements are placed in a 3D scene and rendered using the OpenGL ES framework VES-Kiwi (Kitware Inc).

Results/Discussion

The augmented reality prototype was tested in two cases: echocardiography and fetal imaging. For fetal imaging a learning scenario was simulated where a midwife simulates a 18 week scan, whereas for echocardiography augmentation is performed during a live recording. Data streaming from the ultrasound scanner and heart model deformation are performed as described in our prior work. Initially the heart model is placed at a predefined location; however its relative position to the frame marker is updated when the heart is detected in the 3D ultrasound data. A frame rate of 15 was achievable for frame marker tracking when the camera image was subsampled to a resolution of 640x480 pixels. The frame rate of the 3D echo data was 10 frames per second. Figure 1 shows the two scenarios and the corresponding augmented views. No significant lag was experienced during live operation. Conclusively, the presented tool offers an augmented visualization that is beneficial for both teaching purposes and inexperienced ultrasound users.

P1C3-6

8:00 am **Feasibility of uterine speckle tracking for improved embryo implantation**

Massimo Mischi[1], Nienke Kuijsters[1,2], Chiara Rabotti[1], Benedictus Schoot[2]; *[1]Eindhoven University of Technology, Netherlands, [2]Catharina Ziekenhuis Eindhoven, Netherlands*

Background, Motivation and Objective

Boosted by the modern trend in postponing conception, the number of women facing infertility problems is considerably increasing. Many couples are therefore referred for in vitro fertilization procedures. Despite representing the most advanced option, in vitro fertilization still counts for a low success rate of about 30%. This rate drops progressively with aging up to just 8% at 40 years. There is evidence that uterine movement may play an important role influencing fertilization outcome. Until now, no objective means of measuring uterine movement is available. Therefore, in this work we present the first method for quantitative analysis of the uterine movement and strain.

Statement of Contribution/Methods

Given its widespread availability and cost effectiveness, ultrasound imaging is employed for the analysis. In particular, a speckle-tracking algorithm has been implemented that is based on block matching by normalized cross correlation. Wiener deconvolution is used to regularize the image resolution (speckle size) prior to speckle tracking (see Figure 1). The value of the cross correlation peak was considered to optimize block size and image oversampling ratio. The search area was based on the maximum observed velocity. The method feasibility was tested for its ability to distinguish between active and non-active phase of a natural menstrual cycle in eight women. An ultrasound scanner Accuvix 20 (Samsung-Medison) equipped with a transvaginal EC4-9IS probe was employed for the acquisition. Two pairs of sites were manually defined on the uterine muscle and automatically tracked over time (see Figure 1). Sites close to the fundus were chosen due to the higher activity of this region. Variance and mean frequency of the strain and distance between these sites were the features extracted and evaluated for classification.

Results/Discussion

The results are promising, showing significant class separation by paired, single-tail, Student t-test ($p<0.05$), and sensitivity and specificity both equal to 75% for the strain variance and distance mean frequency. Extensive validation is however required to confirm this result, also exploring additional features. Once fully validated, this method will be tested for quantitative evaluation of uterine movement in the context of in vitro fertilization.
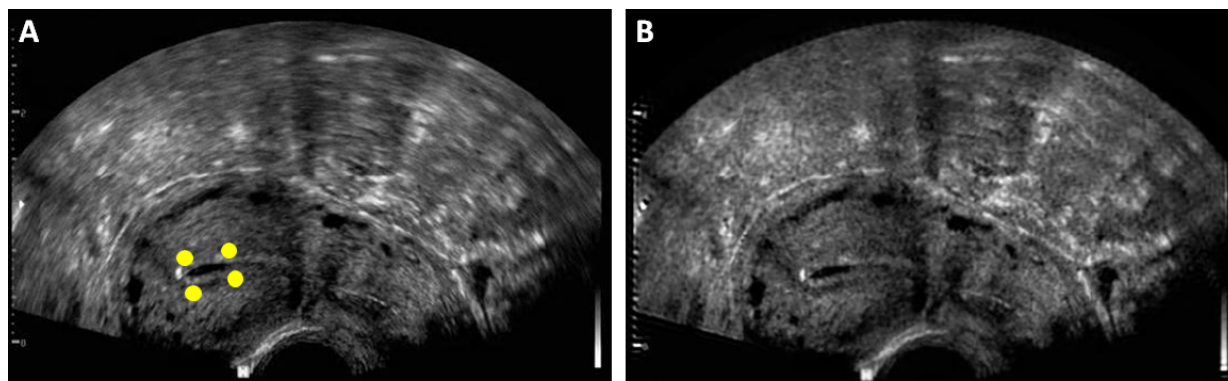
Figure 1: Ultrasound image of the uterus prior to (A) and after (B) Wiener regularization. In (A), four sites are selected near the fundus to be tracked over time.

P1C3-7

8:00 am **Sparse Constrained Born Inversion for Breast Cancer Detection**

Ana Ramirez[1], **Koen W. A. van Dongen**[2]; *[1]Department of Electrical, Electronics and Telecommunications Engineering, Universidad Industrial de Santander, Bucaramanga, Colombia, [2]Department of Imaging Physics, Delft University of Technology, Delft, Netherlands*

Background, Motivation and Objective

Ultrasound has been used successfully for detecting and characterizing small breast lesions. To improve the image quality, an imaging method known as Born Inversion (BI) in combination with compressive sensing (CS) theory has been studied. BI is an iterative method which is simple and computationally efficient. However, due to the ill-posedness of the inverse problem, the resulting image will diverge from the correct solution after several iterations. In this work, we use CS ideas to (1) regularize the inversion process and (2) reduce the number of unknowns by restricting the solution of the BI method to be sparse in a wavelet domain.

Statement of Contribution/Methods

The tested sparse BI method estimates a speed of sound image by minimizing a cost function given by the mean square error between the measured and modeled data. To regularize the inverse problem and to include sparseness, an extra penalty term is added to this cost functional. This penalty term defines the set of coefficients of the estimated image in the wavelet transform domain whose L0-norm is minimal. A solution for the sparse BI method is found by using an iterative algorithm, which at each iteration first estimates a speed of sound image using the conjugate gradient solution, then computes the wavelet transform of the estimated image and finally selects only the largest wavelet coefficients.

Results/Discussion

The sparse BI method has been tested successfully on a synthetic data set representing a tomographic scan of a cancerous breast. The obtained results are displayed below. The figure shows reconstructed speed of sound images for different number of iterations (N=8, 128, 512). The first column shows images obtained using traditional BI; the second column using sparse BI. The results confirm that the new inversion method not only remains convergent but also that the resulting image, at any iteration, yields a lower absolute error in comparison to conventional BI. For the displayed results, at iteration 512, the error in the reconstruction as compared to the ground truth, is 10% smaller for sparse BI as for conventional BI. At the same time, less than 12% of the available wavelet coefficients have been used for the reconstruction.
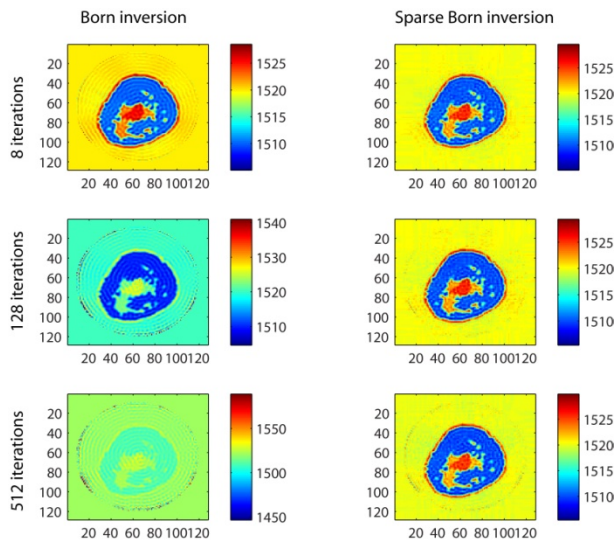
P1C3-8

8:00 am   **Monitoring imaging of lesions induced by high intensity focused ultrasound based on a matching pursuit method**

Weidong Song[1], Siyuan zhang[1], Minxi Wan[1], **Jin Wan[1]**; *[1]Department of Biomedical Engineering, School of Life Science and Technology, Xi¡¯an Jiaotong University, China, People's Republic of*

Background, Motivation and Objective

We investigated the feasibility of a monitoring imaging method to visualize and evaluate the high intensity focused ultrasound (HIFU) induced lesion in vitro during and after their formation, which was based on a modified matching pursuit algorithm (MP).

Statement of Contribution/Methods

The method is based on the concept of sparse signal approximation in an overcomplete dictionary composed of unit-norm vectors that mimic the ultrasonic pulse-echo to be estimated. Each ultrasonic echo is principally represented by a unit-norm vector and therefore has a physical interpretation. we use the MP method to analyze noisy ultrasonic echo obtained in different stages during and after HIFU treatment and decompose the noisy echo into unit-norm vectors. The approximation of the echo can be obtained by the reconstruction result with several large coefficient unit-norm vectors.

Results/Discussion

In the current research we compared lesion sizes obtained from our method, from measurement of physical lesions after exposure, ultrasonic integrated backscatter (IBS) images and from conventional B-mode images, no matter with or without hyperecho. It was found in freshly excised bovine livers that more precise definition of the treated area was obtained from the MP images than from the IBS images and the conventional B-mode images. When comparing to physical lesion sizes, there was no significant difference. We demonstrated the feasibility of our proposed MP-based method for the localization of HIFU-induced lesions immediately after HIFU treatment. Meanwhile our method can detect lesion locations even without the appearance of hyperecho.
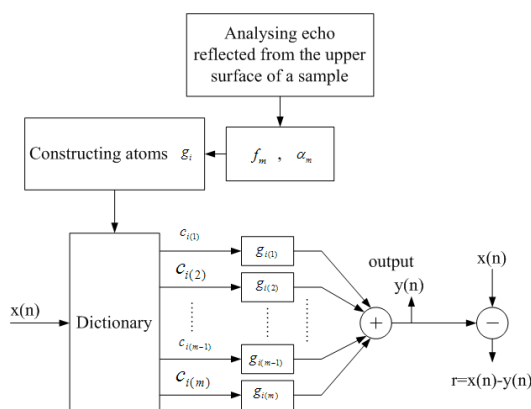
Fig. 2 Structure of the algorithm used in lesion detection. $g_{i(m)}$ is atom chosen from an overcomplete dictionary, $c_{i(m)}$ is the weight associated to the atom $g_{i(m)}$, x(n) is the measured signal, y(n) is the reconstructed signal.

Table 2. Comparison between the MP images and the differential IBS images for the error of the lesion size (mm).

Acoustic powers	Number of trials	MP images				IBS images			
		Immediately after treatment		10 min after treatment		Immediately after treatment		10 min after treatment	
		Length	Width	Length	Width	Length	Width	Length	Width
45 W	10	1.28±1.09	0.94±0.88	-2.04±0.86	-0.89±0.34	2.85±1.21	-1.71±1.32	-5.62±0.97	-2.83±1.27
55 W	10	1.32±0.56	0.61±0.81	-2.40±0.47	-0.47±0.76	1.74±0.93	-1.39±0.81	-5.10±1.39	-2.71±0.99
88 W	10	1.44±0.98	1.49±0.70	-2.96±1.09	-0.43±0.66	1.92±0.86	-2.12±0.83	-6.63±0.92	-2.80±1.11

P1C3-9

8:00 am **Adaptive learning of tissue reflectivity statistics and its application for blind deconvolution of medical ultrasound scans**

Oleg Michailovich[1], Yogesh Rathi[2]; [1]*Electrical and Computer Engineering, University of Waterloo, Waterloo, Ontario, Canada*, [2]*Harvard Medical School, USA*

Background, Motivation and Objective

A standard way to extend the spatial resolution of medical ultrasound scanners beyond their default limits is by means of image deconvolution. The latter is an inverse problem that is normally rendered ill-posed by the band-limited characteristics of the scanners. As a result, the problem of image deconvolution rarely admits a stable and unique solution, unless properly regularized via incorporation of some a priori statistical assumptions about the reflectivity properties of biological tissues under insonification. Specifically, to account for the spatially localized nature of specular reflection, it is common to use prior models promoting "sparse" reconstructions. However, while working flawlessly in vicinity of vascular and organ boundaries, such models fail to produce useful results in the areas dominated by speckle noise, where the reflectivity exhibits a more Gaussian behavior.

Statement of Contribution/Methods

Unfortunately, resolving the deficiency of stationary prior modelling by using adaptive approaches often leads to more complex numerical procedures, while rarely guaranteeing convergence to a unique optimal solution. To address this problem, we propose to model the statistical behavior of tissue reflectivity based on Huber's model (Huber, 1981), subject to concomitant scale estimation (Owen, 2006). This approach allows the prior model to vary adaptively between a Laplacian ("sparse") or a Gaussian behaviour, depending on the nature of local reflectivity. Moreover, the proposed solution is formulated in the form of a convex optimization problem that, subject to further regularization, guarantees the reconstruction to be anatomically consistent and unique.

Results/Discussion

The performance of the proposed method is demonstrated based on both phantom and in vivo data, which shows its superiority over some standard solutions. The provided figure provides a typical reconstruction example showing a small image segment of a normal liver (A), its "sparse" reconstruction (B), and the proposed solution (C). One can see that the latter improves the spatial resolution by a factor comparable to that of the "sparse" solution, while producing much more credible and physiologically meaningful reconstruction results in the areas corresponding to speckle noise.
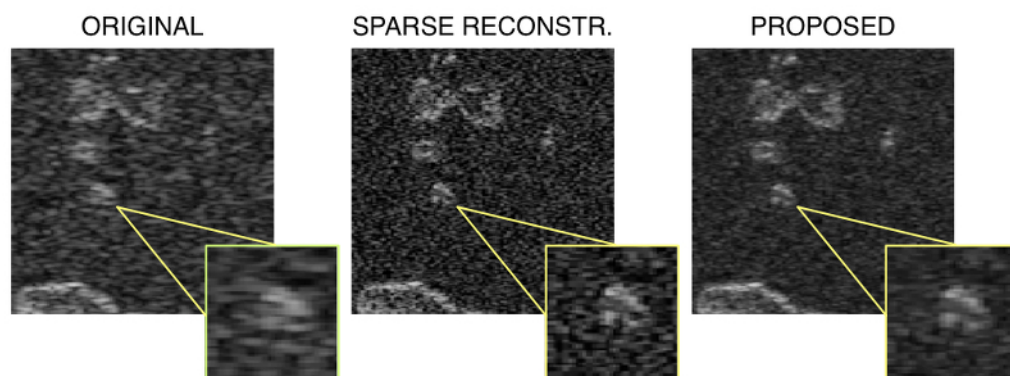
P1C3-10

8:00 am **3D Contrast Ultrasound Dispersion Imaging by Mutual Information for Prostate Cancer Localization**

Stefan Schalk[1], Libertario Demi[1], Martijn Smeenge[2], Jean de la Rosette[2], Pintong Huang[3], Hessel Wijkstra[1,2]; [1]*Biomedical Diagnostics, Eindhoven University of Technology, Eindhoven, Netherlands*, [2]*Dept. of Urology, AMC University Hospital, Amsterdam, Netherlands*, [3]*Dept. of Ultrasound, Zhejiang University School of Medicine, Zhejiang, China, People's Republic of*

Background, Motivation and Objective

Prostate cancer (PCa) is the most occurring type of cancer in the Western World. However, the most common diagnostic tool, systematic biopsy, is invasive and has low sensitivity. Recently, contrast-ultrasound dispersion imaging (CUDI) by spatiotemporal similarity analysis on contrast-enhanced ultrasound (CEUS) has been proposed as a promising alternative diagnostic tool for PCa localization. It was shown that increased mutual information (MutI) between the time-intensity curves in a block kernel and its central pixel relates to the presence of PCa. However, until now CUDI by MutI has been investigated in 2D only, requiring a separate UCA injection for each imaging plane. Moreover, out-of-plane UCA flow could not be taken into account. In this work, we implemented CUDI by MutI using 4D CEUS to overcome the aforementioned issues and tested its feasibility to perform 3D CUDI in 3 patients.

Statement of Contribution/Methods

4D CEUS recordings were made in 3 patients in 2 different hospitals using a LOGIQ E9 scanner (GE Healthcare) with an RIC9-5 probe after an intravenous injection of 2.4 mL SonoVue (Bracco). The CEUS recordings were preprocessed by a speckle regularization filter to compensate for depth-dependency and anisotropy of the spatial resolution. The block kernel used in 2D CUDI was replaced by a hollow, shell-shaped one to avoid a similarity bias caused by the intrinsic spatial resolution of the CEUS data. Furthermore, no temporal filtering was used and the time window was extended to 25 s because of the low temporal resolution (0.26-0.31 Hz) of 4D CEUS. For the same reason, the number of grey levels was reduced from 256 to 64 to avoid grey level sparsity in the kernel. To test the feasibility, the average MutI in each prostate was compared with results from 12-core systematic biopsies.

Results/Discussion

Figure 1 gives the central plane of the 3D CUDI maps for each of the three patients. The mean ± standard deviation of the MutI for the three patients was 0.26 ± 0.14, 0.61 ± 0.25, and 0.51 ± 0.17, respectively. In patient 1, only one biopsy sample was positive, whereas in both other patients more than half of the samples were positive. The difference between the mean value of the MutI for the first patient and the other two patients was significant as was determined by a two-tailed Student's t-test ($p < 0.001$), encouraging validation of the presented method in a larger patient group.

SATURDAY POSTER
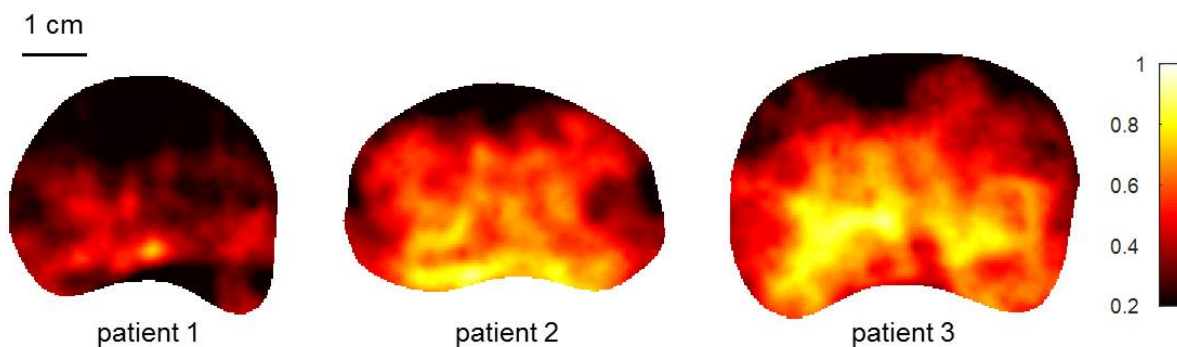
Fig. 1: Mid-plane of 3D CUDI by mutual information for three different patients. In patient 1, only 1 biopsy was positive, in patient 2 and 3, more than half of the biopsies were positive.

P1C3-11

8:00 am **Functional Transcranial Doppler and Cerebral Lateralization during Two Visuospatial Tasks**

Benjamin Hage[1], Mohammed Alwatban[1], Erin Barney[1], Mark Mills[2], Michael Dodd[2], Edward Truemper[3], **Gregory Bashford[1]**; *[1]Department of Biological Systems Engineering, University of Nebraska-Lincoln, Lincoln, NE, USA, [2]Department of Psychology, University of Nebraska-Lincoln, NE, USA, [3]Department of Pediatric Intensive Care, Children's Hospital & Medical Center, Omaha, NE, USA*

Background, Motivation and Objective

Functional transcranial Doppler ultrasound (fTCD) is a non-invasive sensing modality that measures blood flow velocities in cerebral arteries (CBFV) with high temporal resolution. CBFV change is correlated to changes in cerebral oxygen uptake, enabling fTCD to measure brain activity and lateralization with high accuracy during language and visuospatial activities. However, few studies have examined the relationship of CBFV change during visual search and memory tasks. Here we demonstrate a protocol to compare lateralization between two cognitive tasks using fTCD.

Statement of Contribution/Methods

Thirteen healthy volunteers (age 21±2 years) were shown visual scenes on a computer and performed search and memory tasks while monitored with fTCD. The fTCD transducers measured CBFV in the bilateral middle cerebral arteries. Each subject completed 40 trials, consisting of resting/baseline (25 s), calibration (variable), instruction (2.5 s), and task (20 s) epochs.

Using MATLAB, the CBFV magnitude data for each subject were filtered for noise suppression. The data for each side (right/left) were divided into 40 baseline and 40 task sections and averaged together. Lateralization ($\Delta V(t)$) was computed for each task by calculating the bilateral CBFV envelope percent change from baseline and subtracting the right side from the left side. Finally, the ensemble average $\Delta V(t)$ was computed across all subjects.

Results/Discussion

The memory task was more left-lateralized than the search task, with memory reaching ΔV of 1.4%, and search reaching ΔV of -0.5% (see Figure), agreeing with the hypothesis that search is more right lateralized (involves "holistic perception") and memory is more left lateralized (involves "analytical thought"). After the instruction epoch, a paired t-test showed a statistically significant difference ($p<0.001$) between search and memory $\Delta V(t)$ curves for all time points.

Using this method, we were able to show lateralization versus time during two cognitive tasks. This method could be used to compare cerebral activity for any related cognitive tasks (e.g., encoding and retrieval phases of memory, reading versus memorizing a text), as long as the same stimulus is used in all tasks. The protocol is straightforward and the equipment inexpensive, introducing a low-cost, high temporal resolution technique to further study lateralization of the brain.
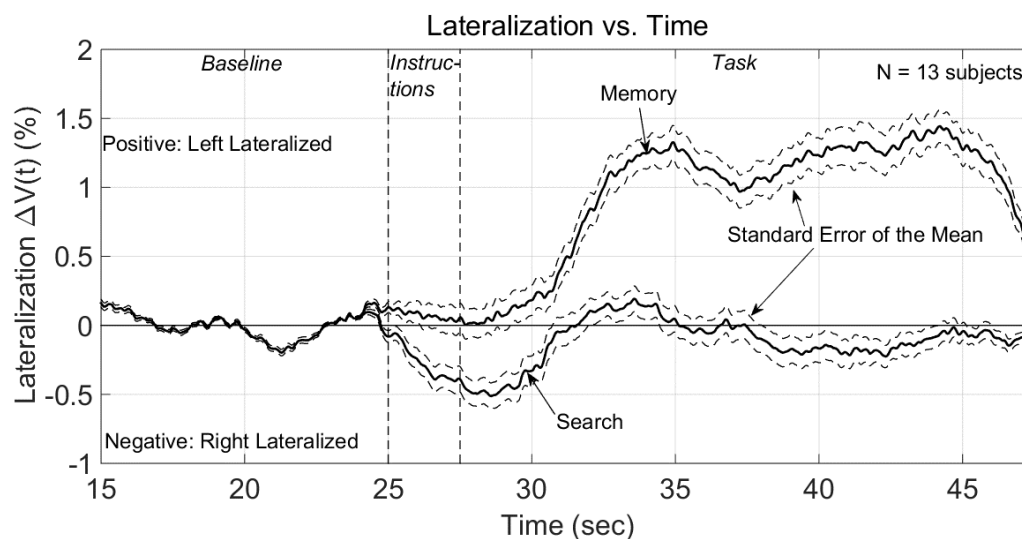
P1C4 - MBB: Beamforming II

4th floor

Saturday, October 24, 2015, Posters displayed 08:00 am - 05:00 pm. Authors must be present at their poster from 9:30 - 10:30am (odd number posters) and 14:30 – 15:30pm (even number posters).

Chair: **Mingxi Wan**
Xi'an Jiaotong University

P1C4-1

8:00 am   ***Ex vivo* evaluation of an eye-adapted beamforming for axial B-scans using a 20 MHz linear array**

Tony Matéo[1], Yassine Mofid[1], Frédéric Ossant[1,2]; *[1]Imagerie et Ultrasons, UMR Inserm U930 - Université François Rabelais de Tours, Tours, France, [2]CHRU de Tours, Tours, France*

Background, Motivation and Objective

In ophthalmic ultrasonography the crystalline lens is known to be the main source of phase aberration, as ultrasounds (US) propagate about 10% faster than in the surrounding intra-ocular medium. Consequently, it impairs significantly both spatial and contrast resolution of axial B-scans, and in addition causes important distortion, especially on the ocular fundus.

In view of the next coming of US arrays in ophthalmologic practice, which are more sensitive to phase aberration but also represent a unique way to correct them, we developed in a previous work [1] an adapted beamforming (BF) free from crystalline lens aberrations. The adapted BF lies on a two point ray tracing approach to compute focusing delays that take into account crystalline lens aberrations including refraction at the interface.

Previous *in vitro* experiments carried out on an eye phantom mimicking the *in vivo* velocity ratio between crystalline lens and surrounding humors have demonstrated the efficiency and interest of this adapted BF and motivated the current *ex vivo* study.

Statement of Contribution/Methods

Adapted BF has been performed with a custom US research scanner working with a 20 MHz linear array. The adapted BF has been extended to take into account the velocity gradient that exists in the real lens [2]. A mathematical model is proposed to determine axial and lateral velocity profile that defines the 2D velocity map inside the lens along the B-scan plane (Fig. c).

Ex vivo experiments were conducted on human eyes, first on an isolated crystalline lens set up between the array and a wire phantom that allows to quantify both image quality and spatial fidelity, and then on an entire eye to appreciate clinical interest. B-scans from adapted BF were compared with those from conventional DAS BF.

Results/Discussion

Quantitative analysis of the wires PSFs shows a 2-fold improvement of both axial and lateral resolution, a greater sensitivity (about 8 dB) and 86% decrease in spatial distortions (from 621 to 97 µm) compared to conventional BF.

Adapted B-scan of the eye (Fig. b) shows great enhancement of both the image fidelity (retina no more protruded) and quality, especially on the posterior coat where, in contrast with conventional B-scan (Fig. a), its layered structure becomes distinguishable.

Accounting for the lens heterogeneity in the adapted BF favors essentially the spatial fidelity and slightly the resolution.
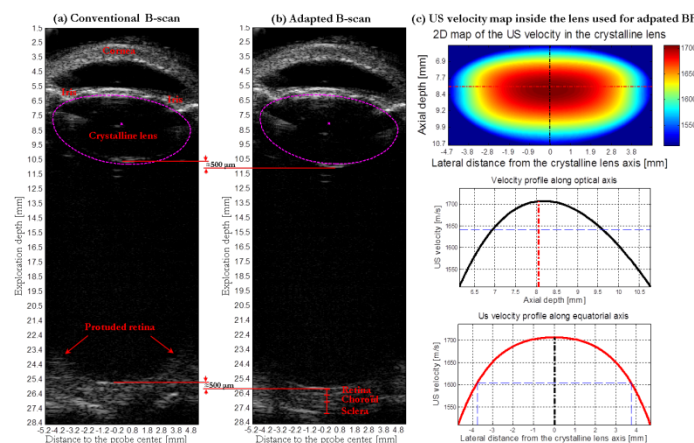
Fig. 1: B-scans of an entire human eye obtained with conventional BF (a) and adapted BF (b) using the map of the US velocity in the crystalline lens (c)

[1] Matéo, Chang, Mofid, Pisella, Ossant, *IEEE TMI*, Vol. 33, No11
[2] De Korte, Van Der Steen, Thijssen, Duindam, Otto, Puppels, *Experimental eye research*,1994, Vol. 59, No 5

P1C4-2

8:00 am   **Synthetic transmit beam steering for spatial compounding applications using continuous transmit focusing**

David Napolitano[1], Robert Steins[1], Al Gee[1], Ting-Lan Ji[2], Ching-Hua Chou[1], Glen McLaughlin[1]; *[1]Advanced Technology, Zonare Medical Systems, Mountain View, California, USA, [2]Mindray, Mountain View, California, USA*

Background, Motivation and Objective

Traditional spatial compounding in general, employs multiple distinct transmit/receive beam angles which insonify a common region, from which multiple images are formed. The individual images are detected, scan converted onto a common grid, and combined in order to produce better image quality, whose attributes are better contrast resolution, reduced speckle, reduced shadowing artifacts, and better borders. However, the increase in image quality comes at a cost in increased acoustic acquisition time, with a corresponding drop in frame rate. To minimize the perception of reduced frame rate, the individual views can be displayed in sequence as individual frames, thus maintaining the individual frame rate, with the compounding effect achieved through the use of persistence. However, motion between frame acquisitions can produce image blurring. Combination modes such as B+CD places heavy demands on acquisition time, and in order to maintain adequate frame rates, the number of B-mode spatial compounding views is reduced or eliminated when in CD-mode, reducing B-mode image quality.

Statement of Contribution/Methods

In order to provide spatial compounding while maintaining the same acoustic acquisition time, multiple steered transmit beams are synthesized from the same set of channel data acquired for the non-steered view, using the continuous transmit focusing technique developed in [1]. Forming multiple receive beams from each transmit beam, and through proper delay, phasing, weighting, and combining the same receive beam from multiple transmit beams, a continuous transmit focus is achieved throughout the image, for fundamental and harmonic imaging. This amounts to a range dependent spatial filter that effectively removes the quadratic delay/phase error inherent in a defocused transmit beam. To synthesize an image using a steered transmit beam from the same channel data, a modification to this spatial filter is made, that upon application effectively masks out the left or right half of the applied transmit aperture, in addition to removing quadratic delay/phase errors, creating a continuously focused steered transmit beam image on the same acoustic grid.

Results/Discussion

Both body (see L10-5 Figure) and phantom results are examined, demonstrating the improvement.

US Patent 8002705, Napolitano D, DeBusschere D, McLaughlin G, Mo L, Chou CH, Ji TL, Steins R
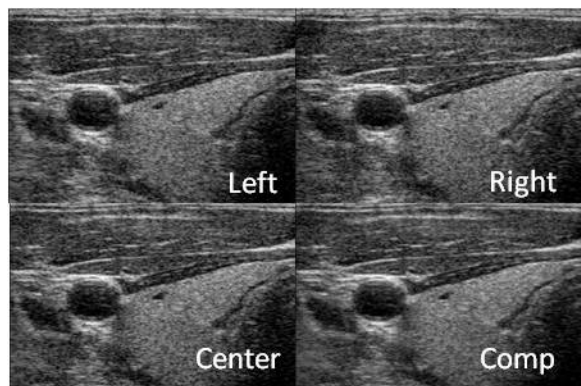
P1C4-3

8:00 am   CW-Doppler focal plane array imaging for deep intra-corporeal vascular mapping; feasibility study with 1:1 focused projection to single pixel receiver and phase continuous Fresnel lens

Seiji Matsumoto[1], Yasuhito Takeuchi[1], Hidehiro Kakizaki[1]; *[1]Renal and Urologic Surgery, Asahikawa Medical University, Asahikawa, Japan*

Background, Motivation and Objective

For Doppler examination, intra-corporeal major vascular flows are relatively easy object for duplex or CFM scanner, shallow small flows are also easy for single beam CWD system because their locations are relatively well known. Motivation and object of this study is to provide a skill-free volumetric method and means for Doppler imaging and measurement for deep intra-corporeal small flows typically in pelvic zone.

Statement of Contribution/Methods

Here we use lens-focused orthographic focal plane Doppler imager having per-pixel Doppler receiver array. The subsystem level studies are completed years of ago (1,2), the study here presented is in-water vessel feasibility verification by 1:1 focused projection to single pixel receiver using double strength full (convex-convex) version of our previously developed half version (plano-convex) phase continuous Fresnel lens (2,3). Sample target (2mm dia. flow phantom and human palm artery) is illuminated by 3MHz 2mW/cm2 CW plane wave while Doppler echo is 1:1 lens-focused to 2x2mm small single element transducer representing unit pixel of focal plane array, followed by unit CW Doppler receiver. Focal length of the lens is 10cm. f-number is 2. The figure introduces the scheme and setup.

Results/Discussion

As shown in figure, proximity reception and 1:1 lens- focused reception are compared. Their viewing solid angles are kept about equal. Signal power yields are compared to conclude lens-focused system is similar to proximity reception. Spatial resolution of this lens focused 1:1 projection system is also measured and found nearly theoretical level. The results suggests that, when the single element test probe is replaced by per-pixel focal plane CW-Doppler array, it is expected to make intra-corporeal observation focal plane CW-Doppler imaging system having reasonable sensitivity and angular resolution.

References: (1) Takeuchi, Y., 2000 IEEE IUS proceedings pp1501-1504

(2) Takeuchi, Y., 2002 IEEE IUS proceedings pp1139-1142

(3) Mori, K. et. al., JJAP vol.46, part 1, pp4990.
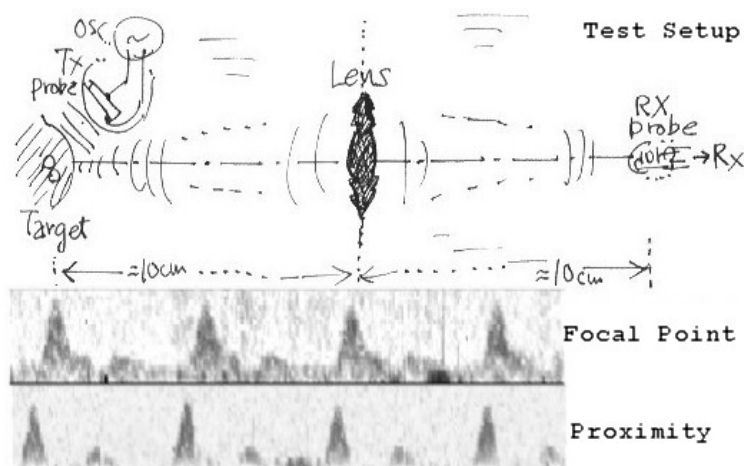
8:00 am   Volumetric Synthetic Aperture Ultrasound Imaging with Row-Column Addressed 2-D Arrays Using Spatial Matched Filter Beamforming

Hamed Bouzari[1], Morten Fischer Rasmussen[1], Matthias Bo Stuart[1], Svetoslav Ivanov Nikolov[2], Jørgen Arendt Jensen[1]; [1]*Technical University of Denmark, Lyngby, Denmark*, [2]*BK Medical ApS, Herlev, Denmark*

Background, Motivation and Objective

In a row-column (RC) addressed 2-D array, the elements are accessed by their row index in transmit and by their column index in receive, or vice versa. This effectively reduces the number of elements on an N×N 2-D array from N^2 to 2N. The large elements in a RC addressed array produce ghost echoes which are undesirable. Besides, two-way focusing similar to fully addressed arrays is not possible since the transmit and receive beams are perpendicular to each other. To remove the ghost echoes, fixed hardware apodization along the rows and columns, has to be implemented. That reduces the transmitted acoustic energy to the side views, which is undesired for volumetric imaging. Therefore, to collect the energy from the main echo and all the ghost echoes, spatial matched filtering (SMF) is used for beamforming. Furthermore, with synthetic aperture imaging technique, due to synthesizing a larger aperture behind the transducer, a better resolution has been achieved.

Statement of Contribution/Methods

All simulations are carried out using Field II. The transducer used in the simulations is a λ/2-pitch row-column addressed 128+128 elements 2-D array. The point spread function was simulated by imaging a volume containing a single point scatter. To achieve a resolution similar to a fully addressed array, the number of elements in a RC array had to get doubled, that lead to 256 virtual sources behind the array. The received data from each element were spatial match filtered and then were summed. Since the filtered data had zero phase, thereby all frequencies added constructively. The transfer function (TF) of the matched filter is a time-reversed version of the desired signal which is the pulse-echo response of the RC array.

Results/Discussion

Based on the simulation results, by using SMF beamforming, the SNR increased by 12 dB and the amplitude of the ghost echoes, decreased by 9 dB. The figures show the 2-D profiles of the 3-D point spread function (PSF) of an unapodized RC array imaged using synthetic aperture imaging (left, the axial direction; right, the azimuthal direction). The single point scatterer was located at (0,0,10)mm in front of the transducer. The RF data were beamformed with delay-and-sum (DAS) and SMF methods. The amplitude of the undesired ghost echoes, reduced below 40 dB with SMF beamforming. Using SMF beamforming, the FWHM in azimuthal plane was reduced by 32%.
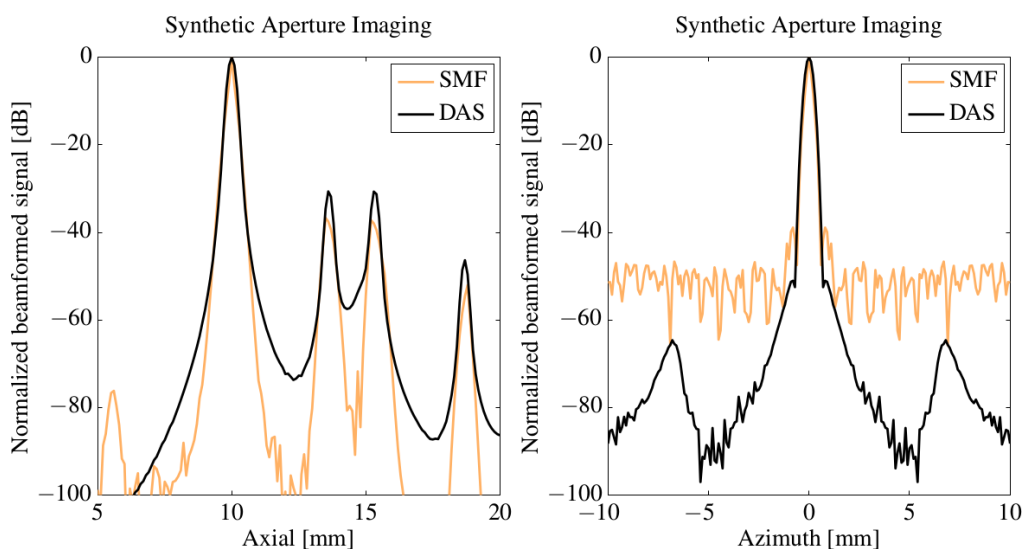
8:00 am   An Optimized Plane Wave Synthetic Focusing Imaging for High-Resolution Convex Array Imaging

Sua Bae[1], Pilsu Kim[1], Jeeun Kang[1], Tai-kyong Song[1]; [1]*Department of Electronic Engineering, Sogang University, Seoul, Korea, Republic of*

Background, Motivation and Objective

High quality ultrasound imaging is required throughout entire imaging depths for abdominal ultrasound. In general, sector scanning with a convex array transducer is performed by using a focused ultrasound beam to obtain a wide field-of-view. However, the conventional focusing (CF) method suffers from the degraded spatial resolution except for the vicinity of the focal depth due to the diffractive propagation of the focused ultrasound. Plane wave synthetic focusing (PWSF) method has been initially proposed for linear array transducer to give a solution to the diffraction problem of interrogating beam. In this paper, to our best knowledge, we present the first report on the PWSF method for B-mode convex array imaging as well as the optimization strategies for enhancing image quality.

Statement of Contribution/Methods

To generate the ultrasound beams with linear wave front (plane wave) for arbitrary steering angle θ_{PW}, propagation delay differences between elements in a convex array were compensated. As shown in Fig. 1 (a), the transmit aperture width should be limited by the directivity of elements θ_d to deactivate the elements located in different directions from θ_{PW}. From the strategy, the synthetic focusing can be conducted by coherently compounding the frames reconstructed from the PWs with different transmit angles. The validation study is performed by acquiring data from a tissue-mimicking phantom (040GSE, CIRS Inc., USA) using an ultrasonic research platform (Vantage 128, Verasonics Inc., USA) with a convex array transducer (C5-2). The CF image was reconstructed with the number of scanlines of 256, a focal depth of 70 mm, and F-number of 2.5. Otherwise, the PWSF image is synthesized using 256 PWs with the maximum transmit angle of 58.7°.

Results/Discussion

Fig. 1 (b) indicates the proposed PWSF method provides improved image quality in visual assessment. The -6 dB lateral resolutions were measured for wire targets over depths as presented in Fig. 1 (c). Consistently, the proposed PWSF method offers significantly enhanced resolution throughout the imaging depth. The PWSF method shows improvement of 13.4 dB in SNR compared to that of the CF method (79.7 dB vs. 66.3 dB). Therefore, these results indicate that the PWSF method can be successfully employed to convex array imaging and yield significantly improved image quality compared to that of CF method.

SATURDAY POSTER
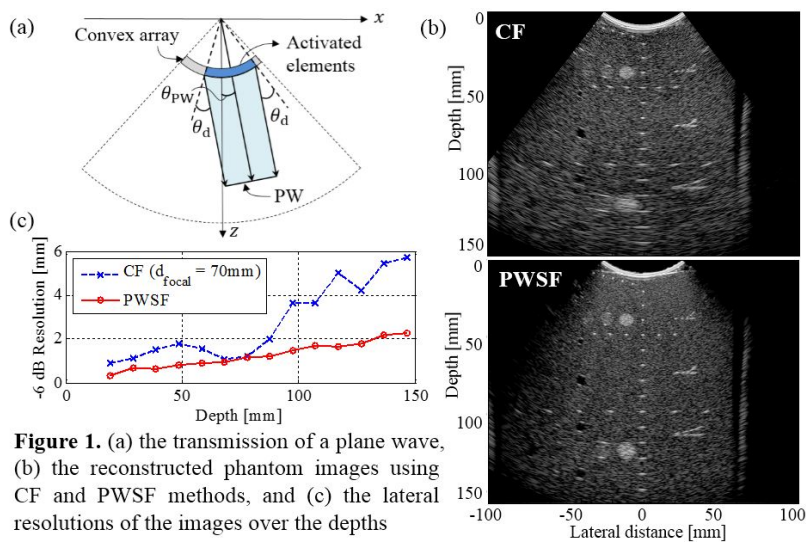
Figure 1. (a) the transmission of a plane wave, (b) the reconstructed phantom images using CF and PWSF methods, and (c) the lateral resolutions of the images over the depths

---

P1C4-6

8:00 am **Synthetic Aperture Sequential Beamforming for Phased Array Imaging**

Deep Bera[1], Johan G. Bosch[1], Nico de Jong[1], Hendrik J. Vos[1]; *[1]Erasmus MC, Rotterdam, Netherlands*

Background, Motivation and Objective

We propose a technique of utilizing Synthetic Aperture Sequential Beamforming (SASB) [Kortbek et al., Ultrasonics 2013] in phased array imaging. The motivation is to apply synthetic aperture focusing technique (SAFT) for improving lateral resolution without storing raw channel data which is immensely important for 3D/4D imaging settings with matrix transducers.

Statement of Contribution/Methods

Phased array Synthetic Aperture Sequential Beamforming (PSASB) employs two stages of beamforming. In the first stage (Low Resolution Beamforming, LRB), a single focal point for both transmit and receive are used for each line and beamformed RF line data are stored. The second stage (High Resolution Beamforming, HRB) combines information from multiple LRB RF lines and produces the final High Resolution Image (HRI) considering the transmit and receive focal points as virtual sources (VS) in SAFT. The delay profile during HRB is computed from the round trip time-of-flight of the ultrasound wave considering the geometry of phased array imaging technique shown in Fig. 1. For PSASB, the number of LRB RF lines ($N(r_{im})$) at depth r_{im} contributing to a single HRI line is determined by the opening angle (α in Fig. 1) of the transmit wave at the VS locations and can be calculated using the equation in Fig. 1, where VS is at r and angle between intermediate scanlines is $d\theta$.

Results/Discussion

The PSASB method has been examined using simulations in Field II and by off-line processing of data acquired with a Verasonics Vantage 2.8 scanner using a CIRS tissue mimicking phantom. The performance of PSASB is compared with Dynamic Receive Focusing (DRF) performed by Verasonics scanner. Lateral resolution using PSASB improves by 34±29% at -6dB over different depths (Fig. 1). PSASB outperforms DRF in terms of lateral resolution both in near and far field. Therefore, this technique is capable of yielding phased array images with better lateral resolution with limited system complexity and can be potentially useful for 3D/4D imaging.
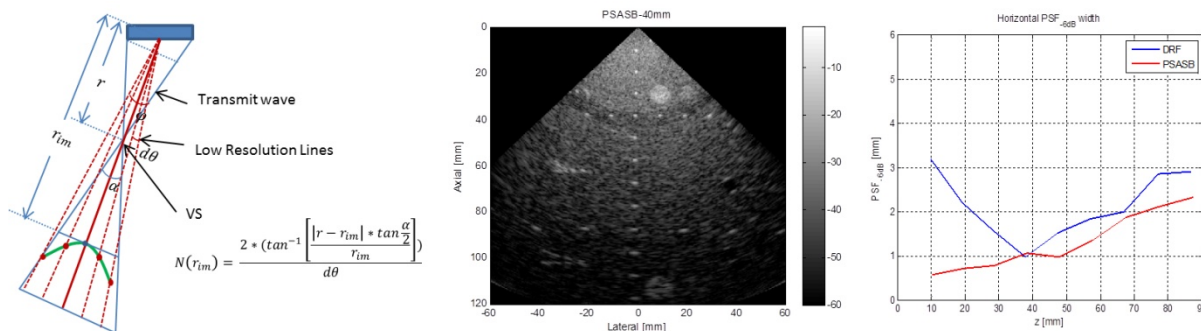
Figure 1: Geometry of LRB lines contributing to the high resolution line (left) , PSASB image with raw data acquired using Verasonics (middle) and Lateral resolution of DRF and PSASB as function of depth at -6 dB (right). For DRF transmit focal point is at 40mm. For PSASB the VS is at 40mm and with scanning angle ±45°

P1C4-7

8:00 am **A New Synthetic Aperture Imaging Method Using Virtual Elements on Both Transmit and Receive**

MooHo Bae[1], Nam Ouk Kim[1], Moon Jeong Kang[1], Sung-Jae Kwon[2]; *[1]Hallym University, Chuncheon, Korea, Republic of, [2]Daejin University, Korea, Republic of*

Background, Motivation and Objective

The synthetic aperture imaging (SAI) method in medical ultrasonic imaging is widely known for improving image quality by synthesizing the transmit focusing at all depths. As in the bidirectional pixel-based focusing (BiPBF; M. H. Bae et al., IEEE TUFFC, vol. 47, 2000), SAI can be combined with receiving dynamic focusing, or as in the synthetic aperture sequential BF (SASB; J. Kortbek et al., IUS 2008), SAI can be used with fixed-point receive focusing (FPRF). SASB has a significant advantage over BiPBF that its hardware complexity can be greatly reduced. However, since SASB utilizes FPRF and all-point transmit focusing by synthesis, the performance of SASB is

basically the same as the conventional B-mode imaging that uses dynamic receive focusing and fixed-point transmit focusing. We propose a new SAI method that can improve the image quality of SASB without requiring more hardware than SASB.

Statement of Contribution/Methods

We found that the dynamic (i.e., all-point) receiving focusing can also be done using virtual receive elements (VREs) as synthesizing transmit focusing can be done using virtual transmit sources (VTSs) in SAI. We will call this new beamforming approach, which uses both VTSs and VREs, full virtual SAI (FVSAI). A VRE can be implemented using an FPRF system. Conceptually, for best performance like BiPBF, the number of the required VREs is roughly the same as the number of the physical elements in the array. Considering that each VRE needs each FPRF system at the same time, implementing this system seems to be impractical in most cases due to the excessive complexity. This problem can be traded off with temporal resolution (i.e., frame rate). As an example, instead of operating many FPRF beamformers in parallel, we can reuse the FPRF beamformer for a VRE several times with several different transmit events. These transmit events must be repeated for different VREs. Through this trade-off, we can improve the performance of SASB with little or no hardware modification.

Results/Discussion

The efficacy of the proposed method is verified with the Field II simulation. A linear probe with 7 MHz, 128 elements, and 0.25 mm pitch is modeled. Compared to SASB, the simulation results in Fig. 1 show that the clutter level at a depth of 5 mm and lateral distance of 10 mm is suppressed by 5 dB for 8 VREs and 20 dB for 40 VREs, and that the -10 dB main lobe width is reduced to 91 % for 40 VREs.

(a)
SASB
64 VTSs
1 VRE

(b)
FVSAI
64 VTSs
8 VREs

(c)
FVSAI
64 VTSs
40 VREs

(d)
Beam profile at depth of 5mm
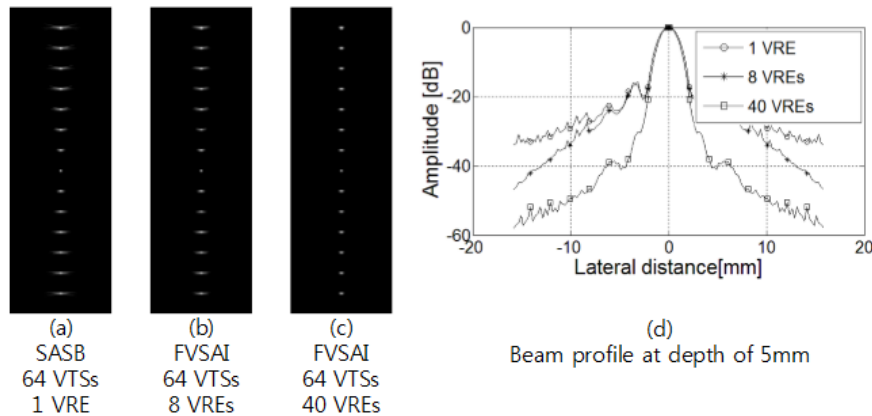
Fig. 1

P1C4-8

8:00 am   Phase Aberration Correction with Adaptive Curve Fitting for Medical Ultrasound Imaging

Yeokyeong YOON[1], Jinbum Kang[1], Ilseob SONG[1], Yangmo Yoo[1,2]; [1]*Electronic Engineering, Sogang University, Seoul, Korea, Republic of*, [2]*Interdisciplinary Program of Integrated Biotechnology, Sogang University, Korea, Republic of*

Background, Motivation and Objective

In medical ultrasound imaging, a constant sound speed (e.g., 1540 m/s) is typically used for receive beamforming. However, due to inhomogeneity in soft tissues, the propagating sound speed considerably varies, resulting in phase aberration. This phase aberration substantially degrades spatial resolution in medical ultrasound imaging. To overcome the phase aberration problem, various techniques based on cross-correlation have been proposed. However, these cross-correlation-based phase aberration methods are too sensitive to interferences from surrounding hyper-echoic targets and noise. In this paper, a new phase aberration correction method based on adaptive curve fitting is proposed.

Statement of Contribution/Methods

In the proposed adaptive curve fitting-based phase aberration correction method, phase aberration profiles are first generated with cross-correlation of radio-frequency (RF) channel data with a fixed sound speed (i.e., 1540 m/s) and then a model-based curve fitting algorithm is applied to determine optimal focusing delay for each pixel. To evaluate the performance of the proposed phase aberration correction method, RF channel data from a tissue mimicking phantom (ATS539, ATS Laboratory Inc., Brideport, CT, USA) with sound speed of 1450 m/s were captured with an ultrasound research platform (Vantage 128, Verasonics Inc., Redmond, WA, USA). The 18-dB lateral resolutions and sidelobe levels were measured for the conventional (CON), cross-correlation (CC) and proposed (PRO) methods.

Results/Discussion

Figs. 1(a)-1(c) shows ultrasound B-mode images reconstructed from the CON, CC and PRO methods. The zoom images for each method are shown in Figs. 1(d)-1(f). As shown in Figs. 1(c) and 1(f), the PRO method with adaptive curve fitting showed a substantial improvement in spatial resolution over imaging depths. These results are consistent with the measured 18-dB lateral resolution (i.e., 3.47 mm ± 1.7 mm, 2.1 mm ± 1.5 mm and 1.48 mm ± 0.61 mm for CON, CC and PRO, respectively) and sidelobe level (i.e., -20.71 dB ± 3.53 dB and -23.68 dB ± 4.55 dB for CC and PRO, respectively). In addition, the PRO method showed comparable results on speckle regions as well. In conclusion, the proposed phase aberration correction method can improve image quality by providing optimal focusing delays. The *in vivo* evaluations on the proposed method are under investigation.
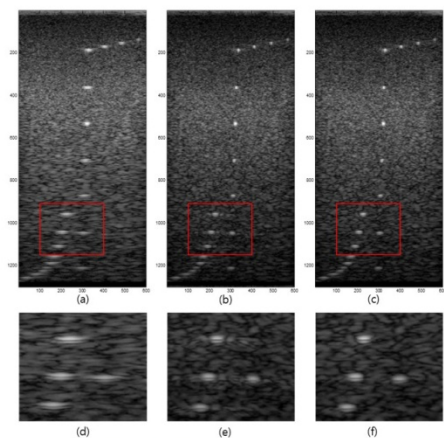
Figure 1 (a) Conventional beamforming (CON) (1540m/s) (b) Cross-correlation method (CC) (c) P roposed method (PRO) (d) Zoom image of CON method (e) Zoom image of CC method (f) Zoom i mage of PRO method

P1C4-9

8:00 am **Multi-focus tissue harmonic images obtained with parallel transmit beamforming by means of orthogonal frequency division multiplexing**

Libertario Demi[1], Gabriele Giannini[2], Alessandro Ramalli[2], Piero Tortoli[2], Massimo Mischi[1]; *[1]Biomedical Diagnostics Lab., Eindhoven University of Technology, Eindhoven, Netherlands, [2]Information Engineering Dept, Università degli Studi di Firenze, Firenze, Italy*

Background, Motivation and Objective

Parallel beamforming in transmit (PBT) by means of orthogonal frequency division multiplexing (OFDM) has recently been investigated as a means to improve the frame rate of ultrasound tissue harmonic imaging. OFDM-PBT improves the data acquisition rate by generating, for each transmission event, multiple beams that are allocated to a specific portion of the available transducer bandwidth. Improving the frame rate is not the only possible application of an increased data acquisition rate. Indeed, in this paper, OFDM-PBT is exploited as a means to perform multi-focus tissue harmonic imaging for improving the penetration depth and signal to noise ratio (SNR) without affecting the frame rate.

Statement of Contribution/Methods

The ULA-OP research scanner (University of Florence, Italy) is used in combination with the linear array probe LA533 (Esaote Spa, Italy). At each transmission event, three narrow-band (1 MHz) beams generated at different center frequencies (4.5, 5.5, and 6.5 MHz) are fired in the same direction and focused at decreasing depths (40, 30, and 20 mm). Next, the same 64-element aperture is used in receive and coherent demodulation and low-pass filters are used to discriminate between the echoes related to each beam. A line is thus obtained as the sum of the envelopes of the received echoes. Finally, a 129 lines image is formed by linearly shifting the 64 elements aperture over the linear array.

Results/Discussion

The tissue-mimicking phantom 404GSE (Gammex, WI, USA) was used as a test target. Tissue harmonic images obtained as described above were compared to standard B-mode tissue harmonic images obtained by using a 3 MHz bandwidth sine-burst centered at 5.5 MHz, and focused at 30 mm.

As shown in the figure, the results present improved penetration depth and SNR for multi-focus PBT images as compared to standard B-mode images. We estimated an improvement of 10 dB of the average SNR, (calculated as the ratio between image intensity and noise variance) and a signal gain of 11 dB (evaluated as the ratio of the average intensities from wire targets), at the expenses of a reduction of the axial resolution (0.7 vs 1.0 mm).
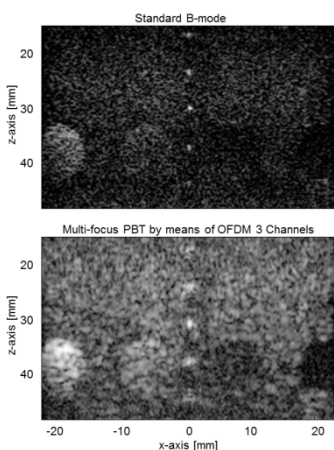
Tissue harmonic image of a gelatin phantom as obtained with (a) standard B-mode and (b) multi-focus PBT by means of OFDM. A 30 dB dynamic range is shown. Improved penetration depth and SNR can be observed for the PBT image as compared to standard B-mode.

P1C4-10

8:00 am   **Low-complexity adaptive beamforming using autocorrelation-based generalized coherence factor**

Yong-Qi Xing[1], **Shue-Han Jiang[1]**, Gency Jeng[2], Che-Chou Shen[1]; *[1]Electrical Engineering, National Taiwan University of Science and Technology, Taipei, Taiwan, [2]S-Sharp Corporation, Taiwan*

Background, Motivation and Objective

Ultrasound focusing quality can be adaptively estimated by calculating generalized coherence factor (GCF) from channel data and each image pixel is weighted by GCF to suppress sidelobe artifacts. Conventionally, Fourier Transform (FFT) is utilized to determine the full channel spectrum and thus suffers from high computation load. In this work, autocorrelation (AR)-based algorithm is utilized to provide the spectral parameters of channel data for GCF estimation with reduced complexity.

Statement of Contribution/Methods

Autocorrelation takes advantage of the phase difference among neighboring channel pairs to estimate the mean frequency and bandwidth of channel spectrum. Based on these spectral parameters, GCF weighting can be approximated by assuming normalized distribution (e.g., Gaussian) of the channel spectrum. Since the spatial frequency in channel spectrum actually corresponds to the incident angle of echoes, the spectral power ratio within the defined range of mainlobe direction can be analytically computed from the simulated spectral shape as the value of GCF weighting.

Results/Discussion

While the GCF computation complexity of a N-channel system reduces from O(NlogN) with FFT to O(N) with AR, Fig. (A) demonstrates that GCF-AR weighted image increases the image contrast by 1~3 dB compared to that with GCF-FFT. Corresponding B-mode images in Fig.(B) also indicate that the speckle background in GCF-AR image is more resistant to the shadowing artifacts in the presence of strong reflectors. Overall, GCF-AR can improve the computation efficiency of adaptive imaging while providing comparable image quality.
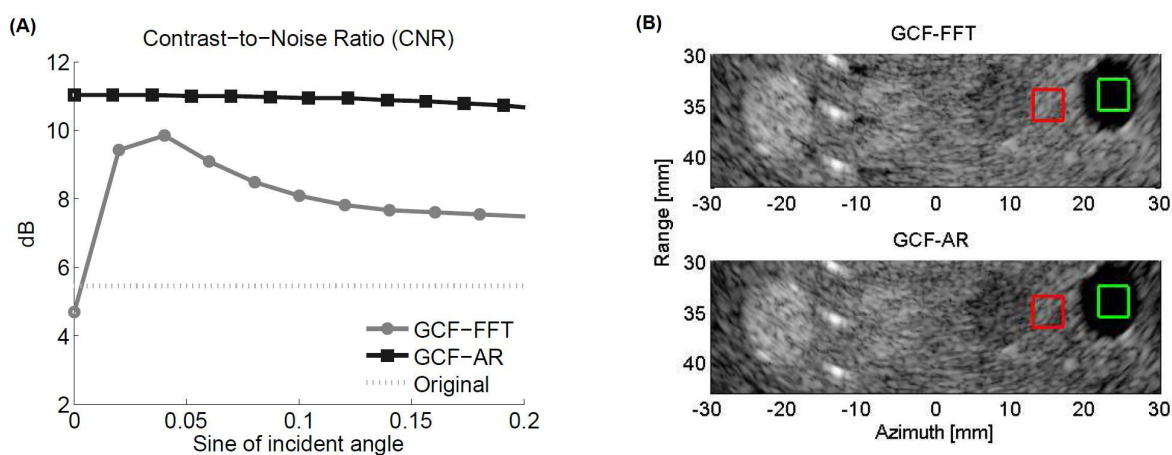
P1C4-11

8:00 am   **Study of Phase Aberration on Coherent Plane Wave Compounding**

Chang-Lin Hu[1,2], Meng-Lin Li[1,3]; *[1]Dept. of Electrical Engineering, National Tsing Hua University, Hsinchu, Taiwan, [2]Industrial Technology Research Institute, Taiwan, [3]Institute of Photonics Technologies, National Tsing Hua University, Taiwan*

Background, Motivation and Objective

High frame rate ultrasound imaging systems can implement innovative applications of real-time 3D ultrasound, elastography, and so on. The approach for reaching high frame rate consists of transmitting single plane wave because emission of a single plane wave is enough to form an image. However, due to the lack of transmit focus, the SNR, and contrast are lower than those with line-by-line scanning. Thus, coherent plane wave compounding (CPWC), which can upgrade the imaging quality, has drawn more and more attention recently.

Statement of Contribution/Methods

Here, we are interested in the effect of phase aberration, caused by inhomogeneity of sound speed, on CPWC imaging. Degradation between image quality with and without phase aberration is estimated and compared with that using line-by-line scanning and single plane wave imaging (PWI), respectively. Near-field phase screen model was used. The correlation length of the simulated phase-aberration profile was 5 mm, and the maximum phase error varied depending on specific simulation conditions. Images of a 3-mm anechoic cyst at 30-mm depth were simulated using Field II. Four beamforming schemes were considered - line-by-line scanning with transmit focusing at the 30-mm depth and dynamic receive focusing (i.e., ideal focusing), PWI, CPWC using 15 angles with 1-degree separation, and CPWC using 31 angles with 1-degree separation.

Results/Discussion

Top panels in the figure show 55-dB B-mode images of the anechoic cyst of ideal focusing, PWI, CPWC using 15 angles, and CPWC using 31 angles without phase aberration. Bottom panels show the corresponding B-mode images with maximum phase error of $\pi/2$ on both transmit and receive. The degradation in contrast and contrast-to-noise ratio from the case without phase aberration to that with a maximum phase error of $\pi/2$ was 5.29 dB and 0.58 for ideal focusing, 0.68 dB and 0.11 for PWI, 3.08 dB and 0.98 for CPWC using 15 angles, and 5.62 dB and 1.25 for CPWC using 31 angles. It is found that the effect of phase aberration on PWI is minimum among the four beamforming schemes. The overall wavefront of the transmit plane wave mitigates the phase aberration on transmit. With phase aberration, as the angles of CPWC increase, the degradation in image quality becomes greater, which is similar to the case with ideal focusing, though the image quality can be upgraded by CPWC with more steered angles.

SATURDAY POSTER
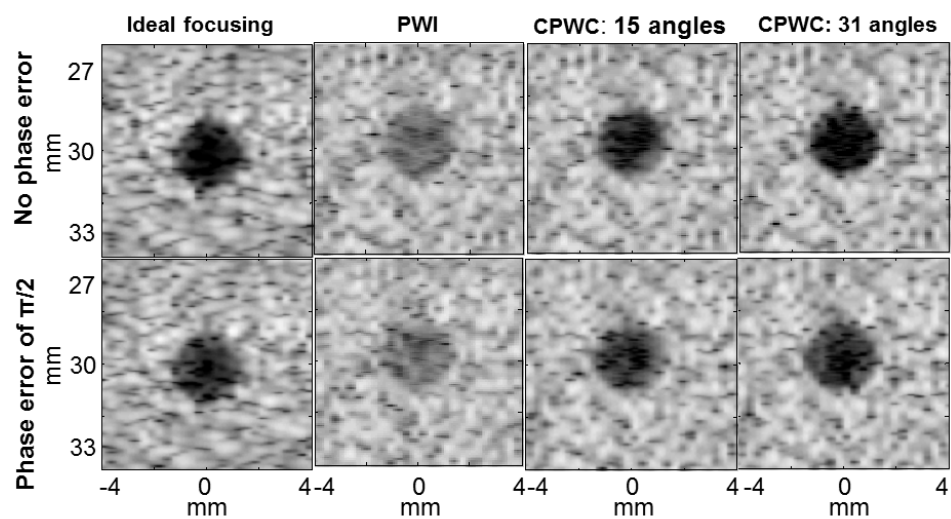
SATURDAY POSTER

P1C5 - MTH: In Vitro and in Vivo Therapeutics

4th floor

Saturday, October 24, 2015, Posters displayed 08:00 am - 05:00 pm. Authors must be present at their poster from 9:30 - 10:30am (odd number posters) and 14:30 – 15:30pm (even number posters).

Chair: **Nobuki Kudo**
            Hokkaido University

P1C5-1 _____

8:00 am   Ultrasound stimulation of carotid baroreceptors: initial canine results

Jesse Yen[1], Mike Partsch[2], Yu Chen[1], Alejandro Covalin[3]; [1]*University of Southern California, Los Angeles, CA, USA,* [2]*Accelemed, San Francisco, CA, USA,* [3]*Atidtek, CA, USA*

Background, Motivation and Objective

Hypertension affects 1 in 3 American adults and is the single largest contributor to death world-wide. Approximately 25-35% of people with hypertension cannot adequately control their hypertension with medications and lifestyle modifications. In cardiovascular physiology, the baroreflex or baroreceptor reflex is one of the body's homeostatic mechanisms for maintaining blood pressure. It provides a negative feedback loop in which an elevated blood pressure reflexively causes blood pressure to decrease. Many decades ago, researchers showed that it is possible to stimulate neurons using focused ultrasound and there has been an increased interest in recent years. The goal of this initial study is to determine if the baroreceptor neurons located at the carotid artery bifurcation can be stimulated using ultrasound.

Statement of Contribution/Methods

An Animal Care and Use Protocol (ACUP)-approved study was performed to assess the feasibility of using ultrasound energy to affect blood pressure in a canine (beagle) model. Two canines were used in this initial study, one for transcutaneous stimulation and one for invasive stimulation. The canines had been previously implanted with a DSI (Data Sciences International) Cardiovascular Implant device which measures EKG, blood pressure, and body temperature. The position of the carotid bifurcation was first located via ultrasound imaging and ultrasound stimulation was applied transcutaneously using different parameters. Intensities were estimated to range from 70-355 W/cm^2 I$_{sppa}$ and 1.53-15.5 W/cm^2 I$_{spta}$. Exposure times ranged from 30-60s. To elicit the largest possible effect, bilateral stimulation of the baroreceptors was performed using 2 custom-made, air-backed 1 MHz transducers with a focal depth of 30 mm. For invasive stimulation, both carotid arteries were exposed and water-filled coupling cones were used to direct the ultrasound at the location of the bifurcation. Blood pressure, heart rate, and body temperature were continuously monitored and recorded.

Results/Discussion

The effect of transcutaneous stimulation is compared to a baseline when the anesthetized canine can be assumed to be in steady-state. A blood pressure drop of approximately 12 and 16 mmHg can be seen relative to the baseline in two instances of transcutaneous stimulation. Stimulating the exposed carotid arteries resulted in 12 and 17 mmHg decreases. As a standard of comparison, manual non-invasive stimulation of the baroreceptors also resulted in a 12-16 mmHg decrease. A blood pressure drop was not observed for every ultrasound exposure. Limitations on this initial experiment included positioning of the ultrasound transducers and maintaining the canine at a suitable level of anesthesia. Nevertheless, the results represent a first step to show that blood pressure may be affected by ultrasound stimulation of the carotid baroreceptors.

P1C5-2 _____

8:00 am   Pulsed high-intensity focused ultrasound exposure decreases shear wave speed of rabbit¡¦s Achilles tendons

Chia-Lun Yeh[1], Pa-Chi Li[1], **Po-Ling Kuo**[2,3]; [1]*Graduate Institute of Biomedical Electronics and Bioinformatics, National Taiwan University, Taipei, Taiwan,* [2]*Department of Electrical Engineering, National Taiwan University, Taipei, Taiwan,* [3]*Department of Rehabilitation, National Taiwan University Hospital, Taipei, Taiwan*

Background, Motivation and Objective

Tightening and contracture of dense fibrous tissues including tendons and ligaments are debilitating conditions frequently encountered in clinical practice. Conservative management for loosening of the tightened tissues usually has limited effectiveness and invasive interventions are inevitable in most protracted conditions. Pulsed high-intensity focused ultrasound (HIFU) holds the promise of being an alternative nonsurgical option for releasing of the tightened tissues. In this work, we evaluated the feasibility of combining pulsed-HIFU and supersonic shear imaging (SSI) as a novel platform for loosening of tightened tissues in a controllable manner.

Statement of Contribution/Methods

An ex vivo model using fresh porcine tendons was first employed to determine the acoustic parameters set for the delivered HIFU pulses that are optimized for decrease of shear wave speed (SWS) in the tendons measured by SSI. Pulsed-HIFU insonation was then applied to the Achilles tendons of New Zealand white rabbits using the acoustic setting optimized in the ex vivo model. Tissue temperature was recorded concurrently with the HIFU application. The tendons after pulsed-HIFU exposure were harvested for histological examination.

Results/Discussion

We found that pulsed-HIFU exposure with a pulse repetition frequency of 500 Hz, a pulse cycle of 50, and an exposure duration of 1 min significantly reduced SWS of the Achilles tendons in vivo without rising of the tissue temperature. Histology exams revealed that the pulsed-HIFU treatment using the chosen acoustic setting did not bring about massive tissue damage. By contrast, application of conventional continuous-wave HIFU in the ex vivo samples markedly increased tissue SWS and temperature. These findings suggest that pulsed-HIFU may loosen the treated tissue via non-thermal mechanisms. Our results indicate that pulsed-HIFU combing SSI as a promising therapeutic alternative for contracture of dense fibrous tissues.

SATURDAY POSTER
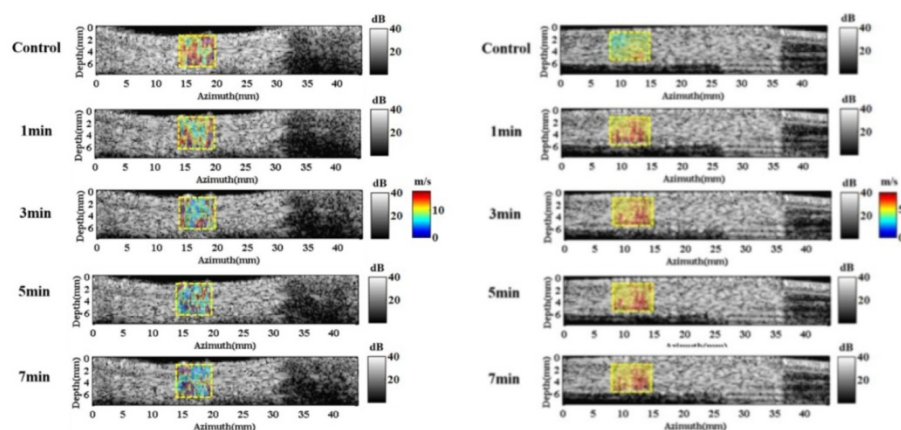
B mode images of tendon superimposed with pseudocolor map of shear wave speed at the region exposed to either (left) pulsed-HIFU or (right) continuous-wave HIFU of durations ranging from 0 (i.e., control) to 7 min. Decrease of shear wave speed is seen in region exposed to pulsed-HIFU as the exposure time increases. By contrast, continuous-wave HIFU exposure increases shear wave speed.

P1C5-3

8:00 am   Optically Transparent and Acoustically Scattering Bovine Serum Albumin Gel Phantoms for Therapeutic Ultrasound Dosimetry

Rei Asami[1], Takashi Maruoka[1], Kenichi Kawabata[1]; *[1]Hitachi, Ltd, Japan*

Background, Motivation and Objective

In the field of therapeutic ultrasound, a tissue mimicking phantom is essential for dosimetry and standardization. A bovine serum albumin (BSA) based gel phantom is widely used for these purposes as its color changes from transparent to opaque at around 70 °C[1], critical tissue denaturation temperature. However in many aspects BSA phantoms are far from actual tissues. For instance, a BSA phantom does not contain any acoustic scatterers to retain optical transparency, and therefore is acoustically lucent. It becomes an issue when realistic echo image is preferred.

This paper introduces a new gel phantom that is both optically transparent and acoustically scattering. Tumor-embedded prostate shaped phantom is fabricated to demonstrate that more versatile and realistic BSA phantom is possible when optical transparency and acoustic scattering are both achieved.

Statement of Contribution/Methods

Polyacrylamide gel was prepared with 9% BSA and various concentrations of additives such as perfluorocarbon droplets, beads and gelatin. Structural parts such as 10 mm spherically shaped mass and lengthy neurovascular bundle were made with color dye. 40 mm diameter spherical casing is used to cast gel. A gel was then placed in a water bath adjacent to a focused ultrasound transducer and a convex probe to test for tissue coagulation.

Results/Discussion

An appearance and a B-mode image of a prostate-mimicking gel are shown in fig. 1a. Optical transparency is preserved and colored structural parts are clearly seen. Scatterers are present in the mimicked prostate, and its echogenisity is significantly higher than the neurovascular bundle, which is made without the scatterers. Coagulated region is clearly visualized post HIFU irradiation in both optical and echographic images (fig.1b.). During focused ultrasound irradiation, changing to opaque by heat denaturation is observed simultaneously in gels prepared with and without acoustic scatters, indicating that the addition of scatters has no influence on denaturation of BSA, and does not interfere with the visualization of coagulated region.

The results suggest that usage of BSA phantom may readily be expanded to applications such as HIFU monitoring research or effective demonstration tools to clinicians and patients.

[1] Lafon, C., et al., Ultrasound Med. Biol., vol. 31, no.10, pp.1383-1389, 2005
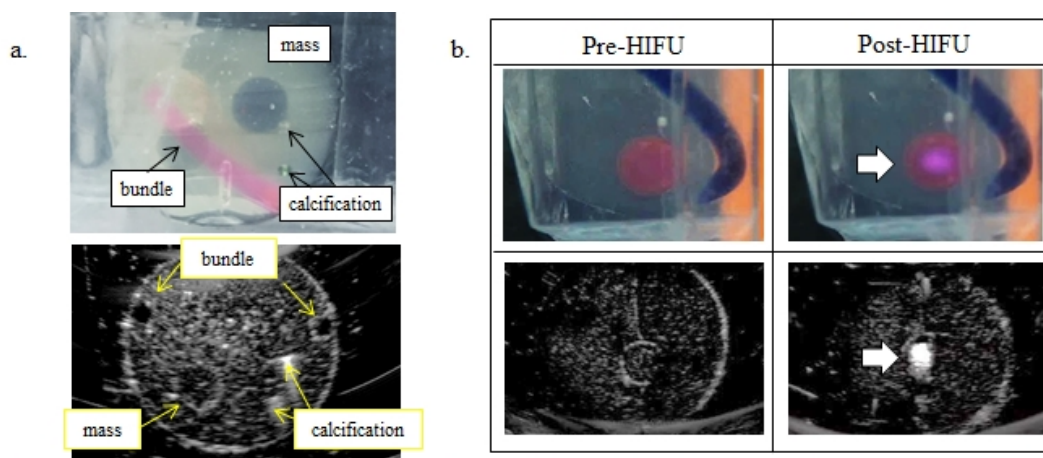
Figure 1 a. An appearance (top) and an echography image (bottom) of the phantom
b. Phantom images pre and post HIFU irradiation. Coagulation is indicated by arrows.

P1C5-4 _____

8:00 am   Ex-vivo Perfused Swine Kidney Simulating in FUS Therapy

Jiaqiu Wang[1], Xu Xiao[1], Robyn Duncan[2], Helen McLeod[3], Benjamin Cox[4], Andreas Melzer[1]; *[1]Institute for Medical Science and Technology, University of Dundee, Dundee, United Kingdom, [2]Centre for Anatomy and Human Identification, University of Dundee, Dundee, United Kingdom, [3]Division of Cardiovascular & Diabetes Medicine, University of Dundee, Dundee, United Kingdom, [4]Division of Imaging & Technology, University of Dundee, Dundee, United Kingdom*

Background, Motivation and Objective

This article illustrates the preparation of perfused Thiel swine kidney which is used for the image-guided FUS therapy on this perfused phantom to simulate the influence from blood circulation.

Statement of Contribution/Methods

The simulator consists of a pair of Thiel swine kidneys, a waterproof transparent acrylic box, connect tubes, feed-through, and a heart lung machine. To prepare the simulator, the fresh swine kidney is cleaned and washed by perfusing physiological saline water, and then perfused and soak into the Thiel fluid for 3-4 days. The Thiel swine kidneys are placed into the waterproof box, and the superior aortas are connect with the tube from the pump to inflow the physiological saline water to simulate the inflow blood, the outflow from veins and the ureters flow into box, and a tube is connect to the box to extract the saline water back to the heart lung machine to complete the blood circulation.

The simulator is placed under the image-guided FUS surgical environment. Multiple image technologies is used for the FUS therapy experiment. X-Ray, MR scan and Doppler ultrasound is used to monitoring the perfusing procedure, the swine kidney vessel. The ExAblate 2000 focused ultrasound is used to ablate the swine kidney phantom. The result will state the effect of different blood flow velocity on FUS therapy.

Results/Discussion

The early-stage experiment has been done and the result from MR temperature monitoring has shown some significant influence on the sonication therapy is caused by the blood flow. To complete the repeatability of the experiment, a new-design waterproof transparent box made of acrylic is made, taking place the previous equipment which using a sealed waterproof plastic bag, because the plastic bag is unstable to cause water leaking for repeatable experiment.
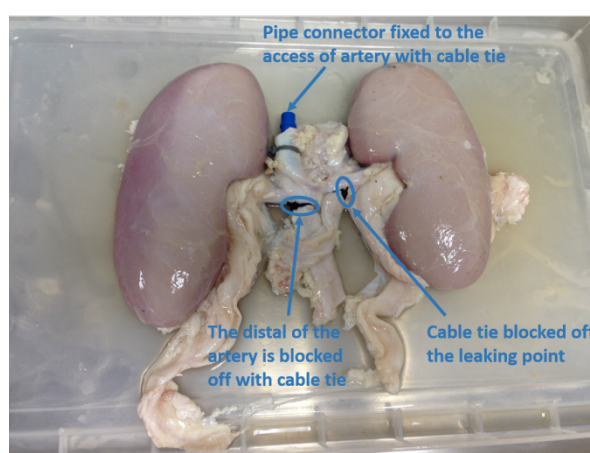
P1C5-5 _____

8:00 am   Neuronavigation-Guided Focused Ultrasound-Induced Blood-Brain Barrier Opening: Feasibility When Considering the Human Skull

Meng-Yen Tsai[1], Po-Chun Chu[1], Hong-Li Wang[2], Hao-Li Liu[1]; *[1]Department of Electrical Engineering, Chang Gung University, Tao-Yuan, Taiwan, [2]School of Information and Electronic Engineering, Zhejiang Gongshang University, Hangzhou, China, People's Republic of*

Background, Motivation and Objective

Burst-mode focused ultrasound (FUS) exposure with the presence of microbubbles has shown its promise in temporally and targeted open the blood-brain barrier (BBB), and brings potential in delivering therapeutic agents into the brain for CNS disease treatment. Previously we have demonstrated the feasibility in using neuronavigation system to successfully guide the FUS-BBB procedure in large animals, and the guidance precision has been measured to be acceptably low. However, it is still unknown whether same precision and power compensation strategy is valid when FUS beam is intend to penetrate the human skull. The purpose of this study is to verify that using neuronavigation system combined with a prior treatment plan can successfully guide FUS-BBB opening with the consideration of involvement of human skull.

Statement of Contribution/Methods

A human skull bone cadaver was employed to perform CT scan, and a treatment planning software was developed to simulate focal beam redistribution and pressure decay when transcranial FUS exposure were performed. To verify the success of BBB-opening when incorporating with the in-prior treatment plan, 24 exposure number in 12 rats dividing to 4 groups were conducted the FUS-BBB opening process, whereas during experiments the human skull cadaver was inserted between the FUS transducer and the small animal head (Group 1: free-field control experiment; Group 2: treatment plan applied, but only consider beam shifting; Group 3: treatment plan applied, but only consider pressure decay). A clinically employed neuronavigation system was incorporated to guide the animal experiment process. Evans blue dye (EB) were administered after FUS exposure and the success of brain stained by EB was employed to confirm the success and scale of FUS-BBB opening. Discrepancy of the targeted and actual BBB opened location was measured to evaluate the guidance accuracy.

Results/Discussion

Neuronavigation has been confirmed can successfully guide the FUS-BBB opening process when tested in group 1 without human skull bone been inserted (no discrepancy been measured; occurrence = 100%). Only compensating beam shifting when transcranial exposure the FUS did not successfully induce BBB-opened effect (occurrence = 0%). When compensating pressure distortion can reproduce the BBB-open effect (occurrence = 50%), but with a relatively large position discrepancy (~ 3 mm). When both considering beam shifting and pressure decay in treatment planning can optimally restore the FUS-BBB opening effect (occurrence = 87.5%; discrepancy < 1 mm).

Our results suggest that under the guidance of neuronavigation and prior treatment planning is feasible to precisely guide the FUS-BBB opening procedure, and may have potential to be applied for future clinical brain drug delivery interventions.

SATURDAY POSTER

P1C5-6

8:00 am **Ultrasonic Monitoring of Cavitation Bubbles Induced by High-Intensity Focused Ultrasound in Gel Phantom Containing Thin Layer of Graphite Gel**

Kei Taguchi[1], Ryo Takagi[1], Jun Yasuda[2], Shin Yoshizawa[2], Shin-ichiro Umemura[1]; [1]*Biomedical Engineering, Tohoku University, Sendai, Japan*, [2]*Communication Engineering, Tohoku University, Sendai, Japan*

Background, Motivation and Objective

Acoustic cavitation bubbles can accelerate therapeutic effect in high-intensity focused ultrasound (HIFU) treatments. In our previous study, it was demonstrated that such bubbles can be detected by high-speed ultrasonic imaging with unfocused transmission in spite of their short lives. Nonlinear echoes from bubbles in resonance size can be selectively detected by pulse inversion (PI) method. In this study, the behavior of cavitation bubbles during exposure at lower intensity immediately after exposure with high-intensity short pulse are investigated with and without using PI method on the objective to check the life of cavitation bubbles that can enhance HIFU treatment.

Statement of Contribution/Methods

An acrylamide gel phantom was prepared for simultaneous high-speed photography observation. It contained a 0.5% graphite powder layer with a thickness of 0.75 mm as a linear ultrasonic scatterer to characterize the scattering by cavitation bubbles. HIFU was generated by a 128-element array transducer at 1.2 MHz. The phantom was exposed to a high-intensity pulse at a maximum intensity of 60 kW/cm^2 for 100 μs for generating cavitation bubbles. Immediately after that, it was exposed to lower-intensity HIFU at a maximum intensity of 1 kW/ cm^2 for 0 to 500 ms for sustaining the bubbles. 700 μs after such HIFU exposure, plane imaging pulses with positive and negative initial polarities were transmitted from a sector probe steered at -18, 0, 18° at a repetition frequency of 5 kHz.

Results/Discussion

Fig. 1 shows the PI images, in which the HIFU propagated from left to right. Relatively high echoes are observed in the HIFU focal region, which was consistent with high-speed optical images. Fig. 2 shows the contrast ratio of mean brightness between cavitation bubbles and the background. The contrast ratio of PI image was much higher than that of linear image without PI immediately after high-intensity pulses. As the duration of lower-intensity waves increased, it dropped much faster than the linear echoes. .The relatively fast decrease of nonlinear echoes may imply that the size of bubbles have shifted from the resonance. These results suggest that the life of bubbles, which may be limited for enhancing HIFU treatment, can be monitored by high-speed ultrasonic imaging such as PI.
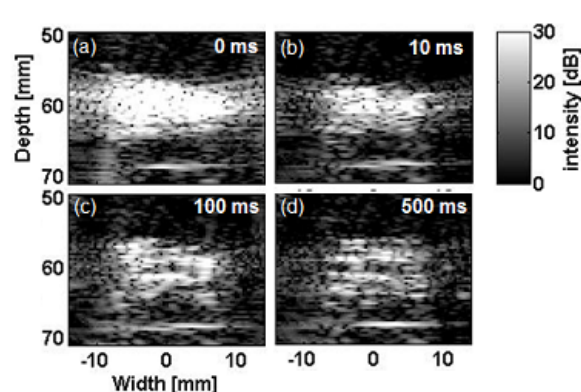
Fig. 1 PI images at 1.88 MHz
Duration of lower-intensity waves
(a)0 ms (b)10 ms (c)100 ms (d)500 ms
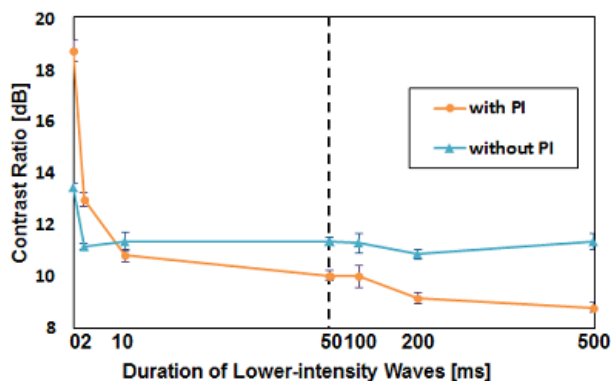
Fig. 2 Contrast ratio of mean brightness between cavitation bubbles and the background

P1C5-7

8:00 am **Histotripsy Produced by Hundreds of Microsecond Focused Ultrasound Pulses in Gels and Tissue *ex vivo***

Yubo Guan[1], Mingzhu Lu[1], Yujiao Li[1], Mingxi Wan[1]; [1]*The Key Laboratory of Biomedical Information Engineering of Ministry of Education, Department of Biomedical Engineering,School of Life Science and Technology,Xi'an Jiaotong University, Xi'an, Shaanxi, China, People's Republic of*

Background, Motivation and Objective

Histotripsy is a non-invasive, controllable and fine focused ultrasound surgery method using microsecond or millisecond pulse with peak negative pressure larger than 10 MPa. Among these methods, hundreds of microsecond pulse is never used for histotripsy. We are trying to explore the feasibility to generate histotripsy using hundreds of microsecond pulse through a different mechanism which starts with changing the mechanical properties of target tissue in focus area to make histotripsy easier to achieve. Furthermore, transducer of smaller size is considered to improve the flexibility in clinical therapy but limits the max pressure.

Statement of Contribution/Methods

There are two stages for the ultrasound pulse modes. The first stage was for alteration of tissue mechanical properties which was carried out by pulsed focused ultrasound with single-element transducer at 1.06 MHz operating frequency, 500 μs pulse duration (PD), 100 Hz pulse repetition frequency (PRF) which was 4.9% duty cycle, and approximately 4 ~ 6 MPa negative pressure within focus. The second stage was histotripsy which was through a sequence composed of 500 μs PD with 100 Hz PRF and 200 μs PD with 200 Hz PRF which was 1% duty cycle. The experiment was proceeded in polyacrylamide gel phantoms to analyze the single lesion and monitored using high-speed photography and passive cavitation detection. Another experiment is on rabbit liver *ex vivo* to perform the tissue resection through repeat therapy with 0.5 mm clearance.

Results/Discussion

The final lesion exhibited cylinder and hollow shape with a dimension of 5 mm × 1 mm (axial × lateral) in phantom with visible thermal damage around. The rabbit liver tissue was successfully cut disconnected with emulsified substance inside. Boiling bubbles in first stage, achieved by heat accumulation without shock wave, effectively turn focus area loose and yield numerous bubble nuclei which makes the inertial cavitation easier to happen in second stage. The lesion inside was mechanically eroded or emulsified by the inertial cavitation during the second stage. We uses much lower ultrasound intensity than conventional histotripsy method but yields some thermal damage. A potential use is for tissue resection in less-moving and heat-sensitive organs, such as livers.

(a) Boiling bubble with about 2 mm diameter in phantom acquired by high-speed photography.
(b) Single lesion pattern after therapy.
(c) RMS amplitude of the PCD signals in the frequency domain of therapy in phantom. The red triangle marks the time after boiling.
(d) Successive therapy in rabbit liver *ex vivo*.
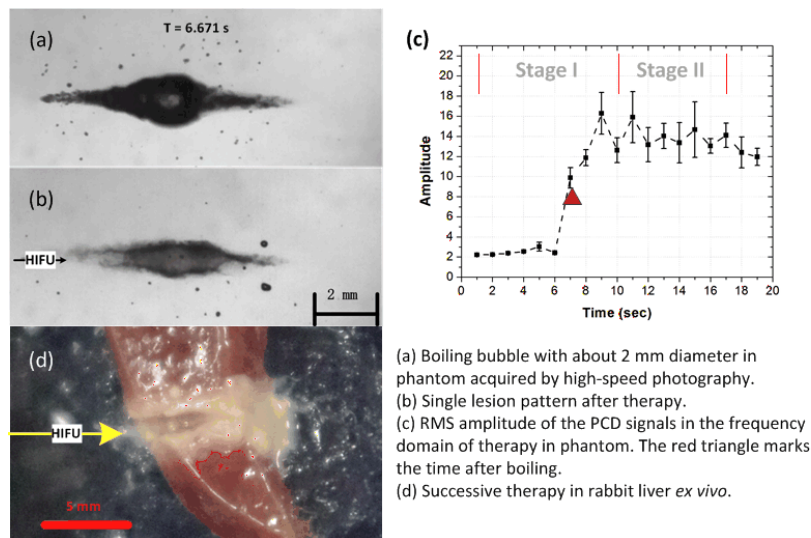
P1C5-8 _____

8:00 am   Motion-triggered Lesion Formation with Close-loop Control in Rats Liver *In Vivo*

Dalong Liu[1], Emad Ebbini[1]; [1]*Electrical and Computer Engineering, University of Minnesota, Minneapolis, Minnesota, USA*

Background, Motivation and Objective

Dual-mode ultrasound array (DMUA) systems have been shown to provide to provide closed-loop control of lesion formation *in vivo* in targets with limited motion. In this study, we address two major issues in lesion formation *in vivo*: spreading of lesion due to out of plane motion, and over-exposure due to uncertainties in dose estimation. Previously we have shown that DMUA synthetic aperture (SA) imaging is suitable for motion estimation, but lacks the sensitivity of detecting bubble activities. On the other hand, single transmit focusing (STF) imaging is more sensitive to bubble activity, but has limited field of view (FOV). Combining the two imaging modes offers a more complete solution to lesion formation *in vivo*.

Statement of Contribution/Methods

The study was performed using our custom designed DMUA system with a 32-element array described previously. The system has been extensively re-architected to enable transmission of combined beam sequence and processing of the hybrid imaging data (SA-STF). On transmitter side, we programmed the micro-sequencer to transmit 31 SA sub-frame and 1 STF frame. On the receiver side, the frontend software de-multiplexed the sub-frames into two data streams which were then delivered to our Programmable Imaging Pipeline Engine (PIPE), which supports simultaneously processing of multiple data streams with a dedicated GPU-accelerated pipeline. We configured Pipeline 1 for SA beamforming followed with motion detection and triggering, and Pipeline 2 for STF beamforming followed with bubble detection algorithm. The output of Pipeline 1 was fed into the control port of Pipeline 2 so the HIFU application and bubble detection were always under the control of motion detection output.

Results/Discussion

We present results from experiments in the liver of Sprague Dawley rats demonstrating the benefit of using motion trigger and close-loop lesion formation control. Motion-gated lesion formation has been demonstrated with great precision in rat liver tissue *in vivo*. In addition, close-loop control of bubble activity ensures lesion formation without excessive dose. Histological evaluation of the treated tissues confirms the effectiveness of the motion-triggered closed loop control algorithm. Tissue damage profiles of motion-triggered lesion formation are consistent with the HIFU beam and do not exhibit the spreading in the elevation direction due to out of plane motion. Imaging (movie) data from lesion formation experiments and corresponding histology will be presented. The results clearly demonstrate that combining motion triggers and closed-loop control produces more predictable lesions in rat liver *in vivo*.

P1C5-9 _____

8:00 am   Sonogenetics Non-invasive Brain Stimulation: Examination of thermal effect of ultrasound

Lili Niu[1], Long Meng[1], Fei Li[1], Fei Yan[1], Ming Qian[1], Yang Xiao[1], Hairong Zheng[1]; [1]*Shenzhen Institutes of Advanced Technology, Chinese Academy of Sciences, Shenzhen, China, People's Republic of*

Background, Motivation and Objective

Low Intensity, Low-Frequency Ultrasound has emerged as a non-invasive brain stimulation tool. This approach is called ″sonogenetics″. William J. Tyler, SS Yoo, HR Zheng et al. have proven that sonogenetics can deliver ultrasound pulses for both reversible excitation and suppression of neuronal activity in cell, animal, human experiments (Neuron 66, 681-694, 2010; NeuroImage 56, 1267-1275, 2011; Nature Neuroscience 17, 322-332, 2014; 2015 1st International Brain Stimulation Conference, 2015, Oral Presentation). Although most studies agree that sonogenetics does not damage tissue, thermal effect of ultrasound is unavoidable and potential safety issues. Therefore, this study examines the potential thermal effects from the sonication.

Statement of Contribution/Methods

We administered ultrasound pulses to the somatomotor area of the rat brain and measured the temperature variation using a thermocouple (Figure 1a). Ultrasound pulses were generated by a pinducer (VP-1063, valpey fisher) with a set of sonication parameters (1MHz frequency; 100 cycles; 90s sonication duration; 3.33kHz, 5kHz, 6.5kHz pulse repetition frequency; 0.27Mpa ~ 2.27Mpa peak rarefactional pressure). Some parameters have been previously shown to stimulate somatomotor areas in rats.

Results/Discussion

Figure 1 shows the temperature variation measured using the thermocouple from the sonication locus with three different duty cycles, 30% (b), 50% (c), and 70% (d). When the peak rarefactional pressure is smaller than 1 Mpa, lower than the current FDA limit, neuronal activity can be modulated and the temperature variation is $0.05^{\circ}C \pm 0.06\ ^{\circ}C$ with the duration of 90s. However, when the peak rarefactional pressure is lager than 1 MPa, the temperature of somatomotor area of the rat increase greatly. This suggests that sonogenetics provides a safe and noninvasive method for potential applications in neurotherapeutics.
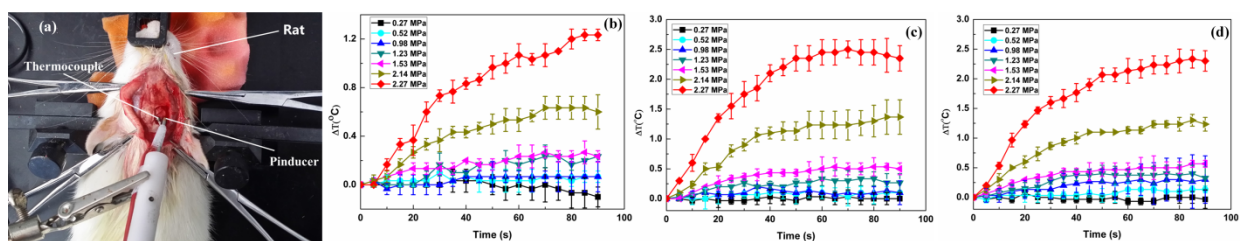
SATURDAY POSTER

Figure 1. Experimental setup (a), and rat somatomotor area temperature measured using a thermocouple (duty cycle = 30%(b), 50%(c) and 70%(d)).

P1C6 - MTC: Bone

4th floor

Saturday, October 24, 2015, Posters displayed 08:00 am - 05:00 pm. Authors must be present at their poster from 9:30 - 10:30am (odd number posters) and 14:30 – 15:30pm (even number posters).

Chair: **Mami Matsukawa**
            Doshisha University

P1C6-1 _____

8:00 am   Noninvasive Bone Assessment Using Ultrasound Radiation Force

Max Denis[1], Mostafa Fatemi[1], Azra Alizad[1,2]; *[1]Department of Physiology and Biomedical Engineering, Mayo College of Medicine, Rochester, MN, USA, [2]Department of Internal Medicine, Mayo College of Medicine, Rochester, MN, USA*

Background, Motivation and Objective

Osteopenia of prematurity (OP) is a condition found in pre-term infants and is hallmarked by radiographic evidence of decreased bone mineralization. Currently, there is no screening test that has been shown to provide both sensitive and specific evidence of developing OP over the first several weeks of life in the premature infant. The goal of this project is to develop a new type of QUS, based on a new mechanism that is compact for use on infants and allows evaluation of infant bone properties in wide range of frequencies.

Statement of Contribution/Methods

A novel noninvasive QUS bone assessment method utilizing a "nonlinear" acoustic methodology based on ultrasound radiation force (URF) is proposed. An URF remotely exerts a point force onto the bone surface, producing vibrations that generate acoustic signals that are detected with a hydrophone(Fig. 1a). Our hypothesis is that these acoustic signals can provide useful information about a bone's mechanical properties. To demonstrate the feasibility of this method, experiments were conducted on rabbit excised femurs. A B-mode ultrasound guided URF excitation was implemented on a Verasonics V1-System. Firstly, the bones were investigated in two states: intact and demineralized. In a second experiment, we embedded the entire bone in a block of gelatin. Figs. 1(b,c), shows the experimental set-up and B-mode image.

Results/Discussion

Three features were extracted from the acoustic signal: (a) In Figure 2a, the mean speed of sound (SOS) measurements demonstrate that the acoustic wave travels faster in intact bones (3150 m/s) than in demineralized bones (1734 m/s). Also, the SOS difference between the intact (2908 m/s) and demineralized (1808 m/s) bones was recoverable when the bones were embedded in gelatin. (b) In Figure 2b, the frequency response of the received acoustic wave demonstrates the low-frequency wave (200 kHz <) attenuation for a demineralized bone. The average "frequency ratio (FR)" of the low-frequency band (50-150kHz) and total band (50-500 kHz) for the intact bones (FR=0.017) and demineralized bones (FR=0.007). (c) In Figure 2c, a spectrogram analysis demonstrates the mean frequency shift due to demineralization bone with the attenuation of the low frequencies. The average mean frequencies in intact and demineralized bones were 409 and 426 kHz, respectively.
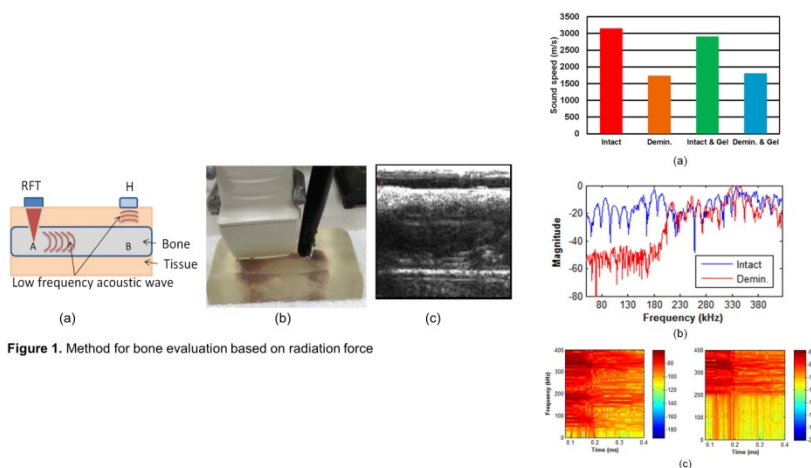
Figure 1. Method for bone evaluation based on radiation force

Figure 2. Intact and demineralized bones (a) sound of speed comparisons, (b) frequency response and (c) spectrogram of intact (left) and demineralized (right).

P1C6-2 _____

8:00 am   High-frequency backscatter measurements reveals large basic multicellular units in in cortical bone

Adeline Bourgnon[1], **Kay Raum**[1]; *[1]Charité-Universitätsmedizin Berlin, Germany*

Background, Motivation and Objective

Most bone loss occurs after age 65 at peripheral sites in cortical bone tissue. Dis-balanced intracortical remodeling leaves progressively more non-refilled basic multicellular units (BMUs), resulting in cortical thinning and the occurrence of particularly large resorption lacunae (RL) compared to the Haversian canals. Therefore, basic research on quantitative bone ultrasound has shifted towards measurements of cortical bone, e.g. dispersion analysis of low-frequency guided wave modes aims at retrieving cortical thickness and effective stiffness coefficients of the tissue (Minonzio et al. J Acoust Soc Am. 2010;127(5):2913-9). However, a-priori assumptions of the relation between cortical porosity and effective stiffness tensor (Granke et al. Bone 2011;49(5):1020-6) are necessary to estimate changes in the cortical microstructure from this measurement. The objective of this study was to prove that changes in the cortical microstructure, in particular the accumulation of RL's can be detected by high-frequency backscatter analysis.

Statement of Contribution/Methods

In this pilot study we have used of a 5-MHz broadband 2D scanning system with 2 highly focused single element transducers to i) assess the outer contour and local inclination angle, ii) separate reflected from scattered waves and iii) relate changes in spectral parameters (depth and frequency dependent amplitudes and slopes) to changes

in the cortical microstructure. Measurements were conducted in-vitro in 19 tibia mid-shafts of a representative sample cohort (19 human donors, age range: 69-94 yrs), which were previously analyzed by 50-MHz scanning acoustic microscopy (Bourgnon et al. IUS 2014). Cortical porosity varied between 3.5% and 34% and the pore size covered a broad range of values, which allowed grouping the measured backscatter properties to various microstructural features, e.g. average porosity, average individual pore area, and number of large RL's.

Results/Discussion

Each score was related to at least one of the evaluated backscatter parameters. High associations were obtained for the minimum frequency-dependent slope of the depth-dependent apparent reflection amplitude AR(f) with increasing RL-score (F=7.7) and increasing Ca.Ar (F=10.3). The results show that changes in number of BMUs and pore sizes have significant influences on the backscattered signal. Further improvements are needed to better control the angles of incidence and reception. However, this study proved the potential of ultrasound backscatter information as a diagnostic tool for bone pathologies.

P1C6-3

8:00 am **Sensitivity analysis of leaky-Lamb modes to the thickness and material properties of cortical bone with soft tissue: a semi-analytical finite-element (SAFE) based simulation study**

Tho N.H.T. Tran[1], Lawrence H. Le[1,2], Vu-Hieu Nguyen[3], Kim-Cuong T. Nguyen[1,4], Mauricio D. Sacchi[2]; *[1]Department of Radiology and Diagnostic Imaging, University of Alberta, Canada, [2]Department of Physics, University of Alberta, Canada, [3]Laboratoire Modélisation et Simulation Multi Echelle UMR 8208 CNRS, Université Paris Est, France, [4]Department of Dentistry, University of Alberta, Canada*

Background, Motivation and Objective

The fundamental ultrasonic guided modes (UGM) are consistently observed in long bones in vitro and in vivo. The responses of UGM to the changes of cortical thickness, cortical elastic parameters and thickness of the overlying soft tissues are not well understood. This study aims to investigate the sensitivity of leaky-Lamb modes to the geometry and material characteristics of layered bone model by simulation. The analysis provides opportunity to study the responses of the UGW, to identify the sensitive regimes in the frequency-phase velocity domain, and to quantify the amount of sensitivity of each mode. The study is important as it offers guidance to the parameter inversion process about the optimal selection of UGM and regions of sensitivity for better inversion results.

Statement of Contribution/Methods

A simulation framework to compute ultrasound dispersion in cortical bone with coupled soft tissue and marrow has been developed using a semi-analytical finite element (SAFE) method. Given a model, the complete set of dispersion curves can be determined by solving numerically the system of characteristic dispersion equations over a desired frequency range. In this parametric study, five material properties were studied: soft tissue thickness h_{ST}, cortical thickness h_{CB}, cortical compressional-wave velocity V_P, cortical shear-wave velocity V_S, and bone density ρ. The influence of each parameter to the dispersion characteristics was studied by varying one at a time while holding the others constant. The sensitivity of the UGM was assessed by comparing the phase velocity spectra derived from the tri-layer bone models.

Results/Discussion

We limit our analysis to the first four UGM below 1 MHz. Increasing h_{ST} from 2 to 5 mm does not have an impact on Mode 1 but reduces the phase velocities of Modes 2, 3 and 4 by at least 32% at 0.15 MHz, 0.3 MHz, and 0.4 MHz respectively. For each 1 mm h_{ST} increment, the phase speeds of Modes 2, 3, and 4 decrease by 10%. The change of h_{CB} from 2 to 7 mm leads to an increase of 37% in phase speed of Mode 1 at 0.1 MHz but a reduction of at least 37% in phase velocities of Modes 2, 3, and 4 at 0.25 MHz, 0.45 MHz, and 0.7 MHz respectively. The phase velocities of the four modes vary more than 5% for each 1 mm h_{CB} increment. When V_S increases from 1400 to 2400 m/s, the phase velocities are about 45%, 125%, 100%, and 123% faster for Modes 1, 2, 3 and 4 at 0.2 MHz, 0.1 MHz, 0.3 MHz, and 0.4 MHz respectively. The changes in V_P and ρ didn't cause any major shift to the phase velocity spectra. Based on this study, Mode 1 is insensitive to h_{ST}, V_P, and ρ and therefore is a good candidate to invert for h_{CB} and V_S. In practice, V_P can be estimated by analyzing the first arrivals of the time signals.

P1C6-4

8:00 am **Axial Transmission Measurements in Cortical Bone: A Comparison between Linear Radon Transform and SVD-based Approaches**

Kailiang Xu[1,2], Jean-Gabriel Minonzio[2], Dean Ta[1], Bo Hu[1], Weiqi Wang[1], Pascal Laugier[2]; *[1]Department of Electronic Engineering, Fudan University, Shanghai, China, People's Republic of, [2]Laboratoire d'Imagerie Biomedicine, UMR CNRS 7371 - INSERM U1146 - UPMC, Paris, France*

Background, Motivation and Objective

Quantitative ultrasonic characterization of cortical bone based on the analysis of the waveguide response of the cortical shell of long bones has been reported. However, identification of the dispersion curves of the guided modes can be complicated by the wide range of unknown cortical thickness, spanning from about 1 mm to 6 mm. Disentangling overlapping dispersion curves of guided modes by optimal signal processing could therefore lead to enhancement of cortical bone quality assessment. In this study, we compare the performance of two signal processing approaches, i.e. singular value decomposition (SVD)-based method (Minonzio et al. J Acoust Soc Am. 2010;127(5):2913-9) and linear Radon transform (LRT) (Tran et al. Ultrasound Med Biol. 2014;40(11): 2715-27), to extract dispersion curves of the guided modes.

Statement of Contribution/Methods

The current study uses a 1 MHz broadband ultrasonic array transducer with 5 emitters and 24 receivers placed in contact with the bone waveguide. SVD and LRT-based signal processing techniques are applied to the multidimensional temporal waveforms s(t,x) where x is the interdistance for a given pair of emitter-receiver. Three representative cases have been investigated: (1) low frequency thickness product f·h < 1 MHz·mm, corresponding to thin cortical bone, where only two fundamental Lamb modes S0 and A0 are observed, (2) intermediate f·h range (1 < f·h <6 MHz·mm) where multiple guided modes overlap, and (3) high f·h > 10 MHz·mm (thick cortical bone) which is in the range of body waves propagation. The techniques are applied to simulated data (case 1), to data acquired on 4-mm-thick bone-mimicking plate and a 1.6-mm-thick ex vivo human radius in which multiple guided modes propagate (case 2), and to data acquired on a 25.5-mm-thick polymethylacrylate (PMMA) plate (case 3). For each case, the experimental wavenumbers or ray paths were compared with the theoretical values computed with the known thickness and material parameters.

Results/Discussion

The analysis of case 1, for non-overlapping A0 and S0 modes, showed a better performance of the SVD-based approach compared to LRT, because of the mode maxima enhancement achieved in the last processing step. In case 2, while multiple guided modes could be separated using SVD, identification of dispersion curves could not be achieved with LRT. In case 3, although the dispersion curves of surface waves could be extract using the SVD-based method, the method failed to identify the bulk modes conversions and multipath reflections which could be successfully identified using the LRT-based method. Overall, SVD shows a better performance in cases 1 and 2 compared to LRT, specifically for noise filtering and for subsequent extraction of the weak modes. In contrast, LRT shows a good ability to extract body waves propagating along different ray paths (case 3). To conclude, signal processing strategies may be adapted depending on the frequency·thickness product being investigated.

P1C6-5

8:00 am   Numerical Analysis of Fast and Slow Waves Backscattered from Various Depths in Cancellous Bone

Atsushi Hosokawa[1]; *[1]Department of Electrical and Computer Engineering, National Institute of Technology, Akashi College, Akashi, Japan*

Background, Motivation and Objective

Ultrasound backscatter measurements in bone can be easily applicable to various skeletal sites, such as vertebra, which is advantage over through-transmission measurements. However, the backscatter measurements are intrinsically difficult because the complicated backscattering mechanism is not yet completely understood. In order to investigate the backscattering properties of the fast and slow waves in cancellous bone, the backscattered waves from various bone depths were numerically analyzed using finite-difference time-domain (FDTD) simulations with microcomputed tomographic (μCT) bone models.

Statement of Contribution/Methods

In the FDTD simulations, the μCT bone models with various thicknesses were constructed with artificial absorbing layers positioned at the back surfaces, and an ultrasound pulse wave was transmitted toward the front surfaces. The backscattered waveform from a certain range of the bone depths was calculated from the difference between two simulated waveforms obtained using the bone models with different thicknesses.

Results/Discussion

The fast and slow waves, which could propagate primarily in the solid and fluid parts, respectively, were observed in the backscattered waveforms from the deep bone depths. For each wave, the backscatter coefficient, which was defined as the amplitude ratio of the backscattered fast/slow wave to the incident fast/slow wave, was derived as a function of the bone porosity. The backscatter coefficients at the bone depths of 3.5–4.0, 4.0–4.5, 4.5–5.0 mm are shown in Figs. 1(a), 1(b), and 1(c), respectively. In all cases of the bone depths, the backscatter coefficients of the fast and slow waves tended to slightly increase and decrease with porosity, respectively. However, these values were largely scattered, and the correlations with porosity were not statistically significant ($R^2 = 0.03$–0.27, $P = 0.03$–0.43), except for the moderate correlation for the fast wave at the bone depth of 4.5–5.0 mm ($R^2 = 0.56$, $P < 0.001$). Furthermore, the dependences on the bone depth were not observed for both waves. It is therefore considered that the backscattered fast and slow waves could not significantly be affected by the porosity and the bone depth. The largely scattered data of the backscatter coefficients appear to be caused by the inhomogeneity of the trabecular microstructure.
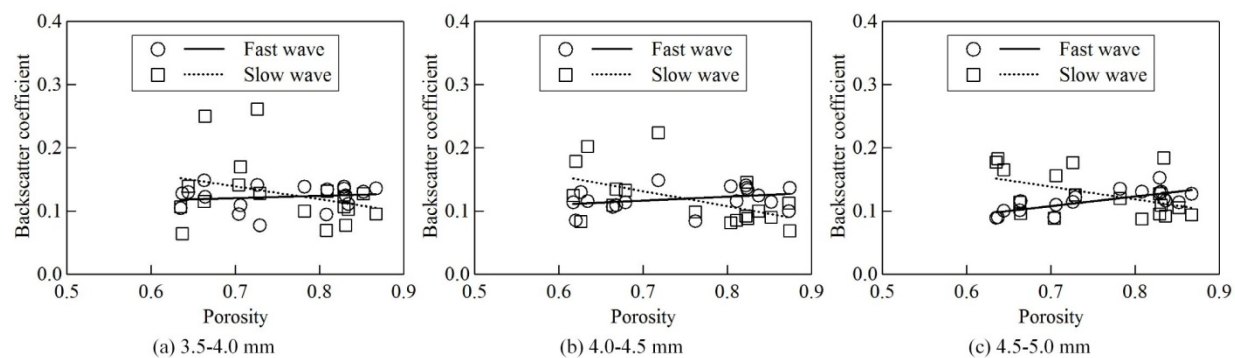
Fig. 1   Backscatter coefficients of the fast and slow waves at various depths in cancellous bone as a function of porosity.

P1C6-6

8:00 am   An anisotropic bi-layered model to estimate cortical bone properties from guided-wave measurements

Nicolas Bochud[1], Jean-Gabriel Minonzio[1], Quentin Vallet[1], Pascal Laugier[1]; *[1]Laboratoire d'Imagerie Biomedicale, Sorbonne Universites, UPMC Univ Paris 06, INSERM, CNRS, Paris, France*

Background, Motivation and Objective

Recent studies on the ultrasonic characterization of bone have reported that cortical bone behaves as a waveguide for ultrasound. Measurements of the guided modes dispersion relations, along with suitable waveguide modeling, have the potential for providing estimates of structural and material properties of cortical bone. Nonetheless, it could be observed that the presence of soft tissue may bias those estimates, especially due to the appearance of additional guided modes and coupling effects at the solid-fluid interface.

To improve our understanding of such influence, this work presents an anisotropic bi-layered model to extract unbiased estimates from cortical bone measurements. This model is first validated on a series of soft tissue-bone-mimicking phantoms using an ultrasonic probe in an axial transmission configuration. Then, the potential of this modeling is evaluated on *in-vivo* measurements at the forearm.

Statement of Contribution/Methods

The measurements were performed using a 1-MHz bi-directional multi-element probe. The full time response of the waveguide is recorded and a singular value decomposition signal processing technique is applied to extract the guided waves spectrum. The structural and material properties of the specimen can be estimated by comparing the measured dispersion curves with those predicted by the model using a model-based inverse problem procedure. This procedure is solved by making use of genetic algorithms, due to their capability of finding a global solution where the cost functional has multiple local minima.

Six soft-tissue-bone-mimicking phantoms (three bone-mimicking plates of different thicknesses (1-3 mm) coated with two layers of zerdine of different thicknesses (5 and 10 mm)) were used for validating the model, while healthy subjects were included to evaluate *in-vivo* the performance of such an approach.

Results/Discussion

Additional guided modes and coupling effects were identified in the phantoms, and our first observations suggest, that even in the presence of overlying soft tissue-mimicking layers, the modes propagating in the bone-mimicking plate can still be extracted. In addition, we also show that the anisotropic bi-layered model allows explaining experimental data from *in-vivo* measurements that were considered as outliers when using a free transverse isotropic plate model (see Fig.1).

SATURDAY POSTER
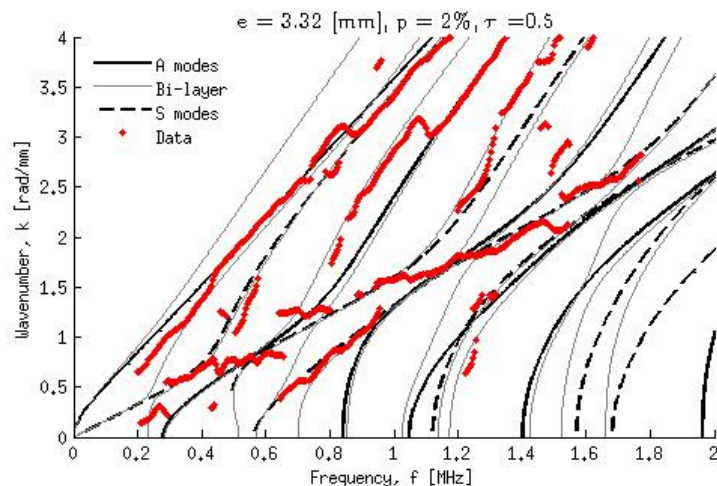
Fig. 1: Model parameters estimation using a bi-layered anisotropic model.

P1C6-7

8:00 am   Combined Estimation of Thickness and Velocities of cortical shell using reflected waves: Study on bone phantoms and samples

Jerzy Litniewski[1], Yurij Tasinkevych[1], Jerzy Podhajecki[1], Katarzyna Falinska[1]; [1]Institute of Fundamental Technological Research, Poland

Background, Motivation and Objective

BUA (Broadband Ultrasonic Attenuation) is an accepted indicator of trabecular bone status. To examine the bones lying deep in the human body one can use scattered waves to determine trabecular bone parameters, including BUA. The existence of cortical shell can substantially reduce the accuracy of measurements. Cortical bone layer acts as a band-stop filter, reducing the transmission of certain frequencies, thus changing the pulse spectrum. The accuracy of BUA values directly translates into the accuracy of diagnosis. Therefore, for reliable assessments of trabecular bone quality it is necessary to take cortical bone properties into account.

The paper presents a method that allows the thickness of a compact bone layer and longitudinal wave velocity in the bone to be determined simultaneously with the use of the reflected waves, with particular emphasis on the case of thin layers when the propagation time through the layer is shorter than the time duration of interrogating pulse.

Statement of Contribution/Methods

The proposed method estimates simultaneously the thickness of the cortical layer and acoustic wave velocity by fitting the temporal spectrum of the simulated reflected wave to the spectrum of the reflected wave measured experimentally. For the purpose of echo-simulations the model of "soft tissue - compact bone layer - cancellous bone" was developed. Next, the cost function was defined as the least square error between the measured and simulated temporal spectra. Minimization of the cost function allowed to determine the values of the parameters of the cortical bone layer which best fitted the measurements. To solve the optimization problem the simulated annealing algorithm was used.

The method was tested using acoustic data obtained at frequency of 0.6 MHz and 1MHz respectively, for a custom designed bone mimicking phantom and bovine calf femurs.

Results/Discussion

For the cortical shell of calf femur of thickness varying from 2.1 mm to 2.4 mm and velocity of 2910 m/s, the corresponding errors of measured values were 5.2 % and 3.5%, respectively. In case of artificial bone the thickness of cortical layer was equal to 1.03 mm and velocity equalled 2950 m/s. These parameters were determined with an error equalled 8.2% and 4.2%, respectively.

It was also checked that the proposed method is not sensitive to the trabecular bone impedance and attenuation of the cortical bone. Results show that the method seems to be well suited to be employed for the determination of the thickness and acoustic wave velocity of the cortical bone layer.

P1C6-8

8:00 am   Clinical study of multisite axial transmission measurements in postmenopausal women using optimized first arriving signal velocity measurements

Johannes Schneider[1], Jean-Gabriel Minonzio[2], Timo Zippelius[3], Peter Varga[1], Patrick Strube[4], Pascal Laugier[2], Kay Raum[1]; [1]BCRT, Charité Universitätsmedizin Berlin, Berlin, Germany, [2]Laboratoire d'Imagerie Biomédicale, Université Pierre et Marie Curie, Paris, France, [3]CMSC, Charité Universitätsmedizin Berlin, Germany, [4]CMSC, Charité Universitätsmedizin Berlin, Berlin, Germany

Background, Motivation and Objective

Ultrasound bidirectional axial transmission (BDAT) has been originally developed to measure the speed of sound of the first arriving signal (VFAS) in the cortex of long bones. This approach was tested in a clinical study at the distal radius of postmenopausal subjects (Talmant, UMB 35 912-919-2009). With the current measuring protocol some patients with elevated body mass index (BMI) were not accurately measured and were excluded of that study. The objective of this study was to optimize the VFAS measurement protocol to enhance its robustness in particular for patients with pronounced BMI. Results obtained with the new protocol and with the former one are compared in this pilot clinical study.

Statement of Contribution/Methods

58 postmenopausal women aged 42-89 years were included in the study. Non-fracture (N=29) and fracture (N=29) groups were defined based on the existence of at least one low-energy fracture. Ultrasound measurements were performed using a novel array transducer with 24 receivers driven with emitted broadband pulses of about 0.5-1.5 MHz. Three repetitive measurements of 20 cycles with intermediate repositioning were performed, instead of one measurement of 400 cycles (former protocol). One site at the radius and two sites at the tibia were measured: at the radius the probe was centered at one third of the bone length from the distal extremity. At the tibia the probe was centered at the medial surface (MS) and at the anterior crest (AC) at two thirds of the bone length from the proximal end. The former algorithm used a fixed number of receiver elements. An optimized automated algorithm recognized receiver elements strongly affected by soft tissue and excluded these from subsequent VFAS calculation. Areal bone mineral density (aBMD) was assessed in all subjects with dual energy x-ray absorptiometry (DXA) at the lumbar spine.

Results/Discussion

The average BMI of the whole population was 22.6±2.8. The optimized VFAS algorithm was more efficient than the former one in analyzing higher BMI cases. At the tibia AC N=0 and N=14 (BMI=21.7±3.1), at the tibia MS N=7 (BMI=25.1±2.6) and N=26 (BMI=22.9±2.6) and at the radius N=6 (BMI=24.2±0.9) and N=36 (BMI=22.9±2.3)

could not be analyzed with the new and the old protocol, respectively. At all sites the odds ratio (OR) values (ranging between 3.0 and 3.3) of the optimized VFAS measurements were significant. After adjusting for age and BMI the OR values of VFAS tibia AC (2.89; [1.08–7.75]) and VFAS radius (2.60; [1.02–6.61]) remained both significant. The highest area under the ROC curve (AUC) was found for VFAS radius (0.89; [0.76–0.95]). In comparison, the DXA values of the lumbar spine (OR=1.89; AUC=0.87) were less efficient for the fracture discrimination than the ultrasonic values. In summary, the optimized VFAS method has superior fracture discrimination performance compared to both, the conventional VFAS measurement protocol and aBMD and even can be applied in patients with pronounced BMI.

P1C6-9

8:00 am   Hypersonic wave velocity in drying collagen film with AGE crosslinks

Yuki Imoto[1], Shinji Takayanagi[1], Mitsuru Saito[2], Keishi Marumo[2], Mami Matsukawa[1]; *[1]Wave Electronics Research Center, Doshisha University, Kyotanabe Kyoto, Japan, [2]Department of Orthopaedic Surgery, Jikei University School of Medicine, Tokyo, Japan*

Background, Motivation and Objective

The abnormal collagen crosslinks called advanced glycation end products (AGEs) is expected to result in the decrease of bone quality, especially bone elasticity [1]. In thin and highly crosslinked bone samples and collagen films, micro-Brillouin (m-BR) studies showed that the hypersonic wave velocity finally decreased due to AGEs [2]. In this study, we have experimentally studied the effects of AGEs on the natural drying process in the collagen films using m-BR. The hypersonic wave velocities have been observed as a function of drying time.

Statement of Contribution/Methods

The collagen gel membrane samples (Asahi Techno Glass; Type I, thickness 20 μm in dried condition) were used. For glycation, samples were put in the mixture of Phosphate buffered saline (PBS), D-(-)-Ribose, Protease Inhibitor Cocktail Set III (without EDTA) and Penicillin-Streptomycin. The reference sample was put in the mixture of PBS and Penicillin-Streptomycin. They were kept in an incubator at 37°C for 14 days. Longitudinal wave velocities in the GHz range were measured by the m-BR system [2] (the spot diameter: 10 μm). The fully wet samples were kept in the room of relative humidity 30% at 24°C and the velocity changes during the natural drying process were measured as a function of time. The surfaces of samples were studied by a microscope (Keyence, VW-300C) and surface profile meter (Mitutoyo, SJ-400, resolution 3 μm).

Results/Discussion

Fig. 1 (a) shows the velocity changes during the drying process. The wave velocity depended on the glycation period and showed high values in the reference and initial samples, which seemed to indicate low water absorption. In all samples, the velocity gradually increased and reached the values of the dried one. However, in the samples with long glycation period (10 and 14 days), the velocity increase was not rapid, showing the slow drying. One of the possible reasons for this phenomenon is the changes of the structure. Figs. 1 (b) and (c) show the microscopic views of the samples. The smooth surface in the reference sample was lost in the glycated sample. The averaged surface roughness of the glycated sample was 0.26 μm whereas that of the reference sample was 0.16 μm. These results show the effects of collagen network on the structure and the water holding property.

[1] M. Saito, et al., *Osteoporos Int.*, **21**, p.195, 2010.

[2] Y. Imoto, et al., *Glycative Stress Research*, submitted.
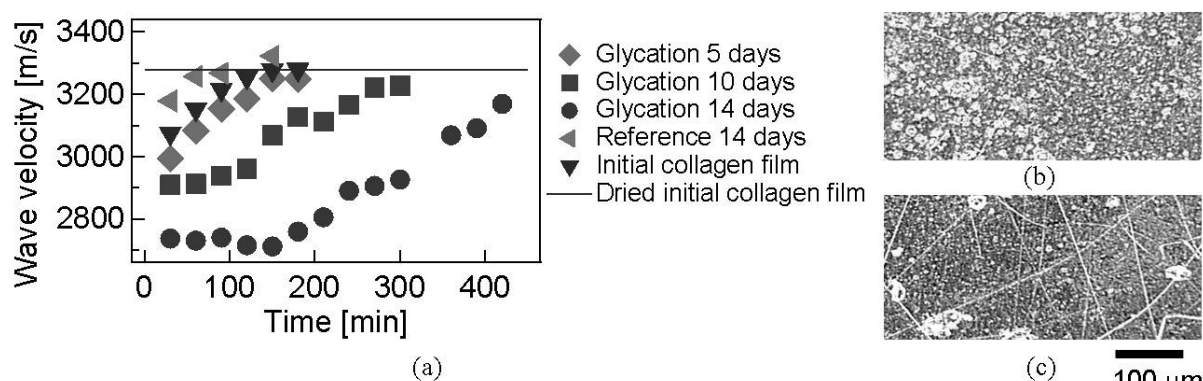
Fig. 1 Observed data of (a) wave velocity in the collagen film in the drying process, (b) the surface of the glycated collagen film and (c) the surface of the reference sample.

P1C6-10

8:00 am   Ultrasound radiation from bone transducer in the MHz range

Sayaka Matsukawa[1], Hiroko Tsuneda[1], Isao Mano[1], Katsunori Mizuno[2], Takahiko Yanagitani[3], Shinji Takayanagi[1], Mami Matsukawa[1]; *[1]Doshisha University, Japan, [2]University of Tokyo, Japan, [3]Waseda University, Japan*

Background, Motivation and Objective

Ultrasound healing is an attractive technique for bone fractures. The mechanism of ultrasonic effects on bone, however, has not been clearly understood yet. One possible effect is considered to be the piezoelectricity of bone. In order to check the piezoelectricity of bone in the MHz range, we have fabricated bone transducers, and succeeded in observing the output signals induced by ultrasound irradiation [1, 2]. In this study, to confirm the inverse piezoelectric effect, we have fabricated bone transducers as ultrasound transmitters.

Statement of Contribution/Methods

We prepared circular plate cortical bone samples (diameter; 10.0 mm, thickness; 1.00±0.01 mm) from the mid shaft of a right bovine femur. The normal direction of these plates was equal to the bone axis. Using these plates as piezoelectric materials, we fabricated air-backed bone transducers. We also fabricated two handmade PVDF transducers (diameter; 10.0 mm).

In the ultrasonic immersion experiments, the four air-backed bone transducers were used as transmitters. A burst wave with 10 sinusoidal cycles in the MHz range was amplified to 70 Vpeak-peak by a bipolar power supply (HAS 4101, NF) and applied to a transmitter. The transmitted ultrasound was received by a PVDF transducer and observed by an oscilloscope (DPO3054, Tektronix).

SATURDAY POSTER

Results/Discussion

As seen in Fig. 1 (a), a burst ultrasonic wave in the MHz range was radiated from the bone transducer. The amplitude of the observed wave was around 25 μVpeak-peak at 2.20 MHz, which was almost 0.1% of the observed wave transmitted from a PVDF transducer. The frequency characteristics of transmitting sensitivity of four bone transducers were measured by a reciprocity method (Fig. 1 (b)). The sensitivity of bone transducers increased with frequency, showing similar tendency with the PVDF transducer. Because the wave velocity in cortical bone is in the range of 3600-4400m/s [3], we can expect half-wavelength resonance mode around 2 MHz in the bone plate sample with 1 mm thickness. We could actually found the resonance peaks in the sensitivity data.

[1] M. Okino et al., Appl. Phys. Lett. 103, 103701 (2013).

[2] H. Tsuneda et al., Appl. Phys. Lett. 106, 073704 (2015).

[3] Y .Yamato et.al., Calcif Tissue Int., 82 (2008).
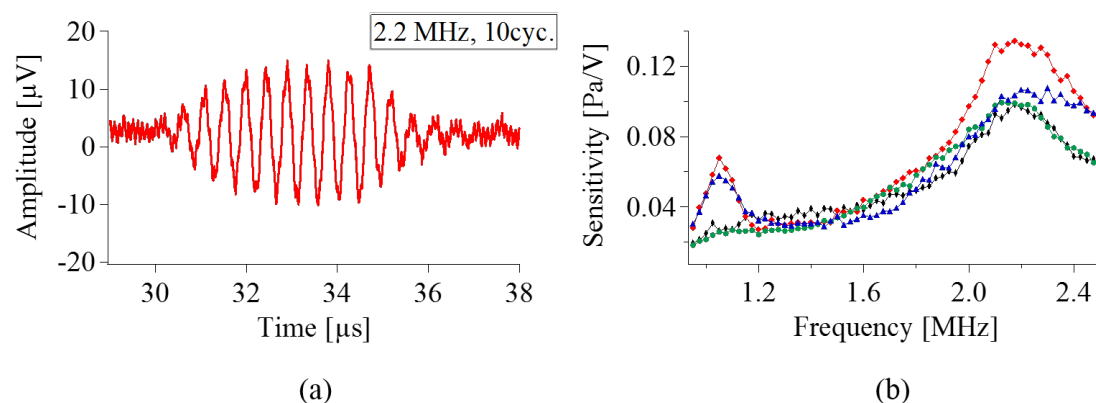
Fig. 1 (a) An observed waveform (transmitter : bone transducer, receiver : PVDF transducer), and (b) frequency characteristics of the transmitting sensitivity of four bone transducers.

P1C6-11

8:00 am   An optimization method for pairing in-vivo guided wave measurements with theoretical Rayleigh-Lamb modes

Nicolas Bochud[1], Jean-Gabriel Minonzio[1], Quentin Vallet[1], Pascal Laugier[1]; *[1]Laboratoire d'Imagerie Biomedicale, Sorbonne Universites, UPMC Univ Paris 06, INSERM, CNRS, Paris, France*

Background, Motivation and Objective

Measurements of guided modes dispersion relations, along with suitable waveguide modeling, have the potential for inferring material and structural properties of cortical bone. Such a model-based approach typically requires a complex inverse procedure for pairing the incomplete data with the model. Recent proposals solved this problem for *ex-vivo* measurements by grouping the incomplete data into *user-defined* experimental trajectories, where each trajectory was associated to a specific Lamb branch (Foiret, IEEE TUFFC, 2014). Nonetheless, this *prior* assignment is far from trivial in the case of *in-vivo* measurements.

To overcome this difficulty, the present work presents a global search approach, which enables us to estimate the properties of cortical bone, avoiding any *prior* knowledge on the experimental trajectories. This can be achieved by including an additional model parameter, which represents the number of theoretical Lamb branches that are necessary to fit the experimental trajectories. This approach is evaluated on a cohort of healthy subjects and compared to the discrete approach described in (Vallet, IEEE IUS, 2014).

Statement of Contribution/Methods

The proposed methodology consists of three elements: (1) Measured dispersion curves obtained after processing of the full time-domain response, (2) theoretical dispersion curves derived from a 2D free transverse isotropic plate model, based on homogenized elastic bone properties, and (3) a model-based inverse problem used to estimate the cortical thickness and apparent porosity, along with the optimal number of Lamb branches. These model parameters are found by a global search algorithm that minimizes the discrepancy between the measured and numerically predicted dispersion spectra. Genetic algorithms (GA's) are used as search algorithms due to their capability of finding a global solution where the cost functional has multiple local minima.

Results/Discussion

Fig. 1 shows an example of the optimal matching between measured and theoretical dispersion curves. As can be observed, the proposed algorithm (right) automatically selects the number of branches that are necessary to explain the data, which results in a smoothing of the cost functional and a maximization of its value (the true cortical thickness measured by HR-pQCT is 2.9 mm). This approach has been successfully tested on 14 healthy subjects.

$e_{opt} = 3.9$ mm, $p_{opt} = 7$ %, $c_f = 0.39$ $e_{opt} = 2.77$ mm, $p_{opt} = 3.3$ %, $c_f = 0.41$
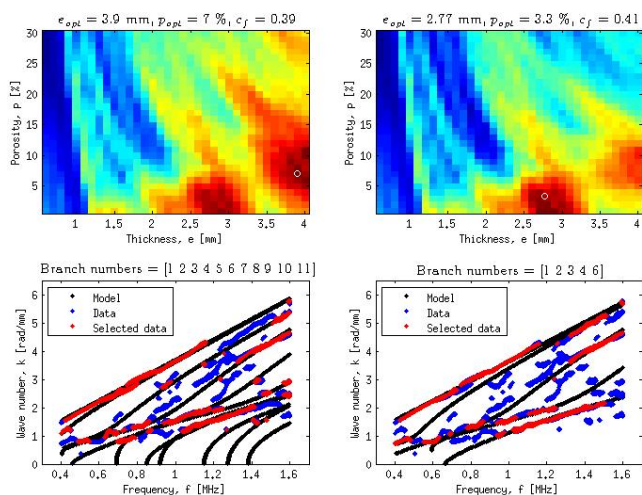
Fig. 1: Model parameters estimation using a discrete approach (left) and GAs (right).

P1C6-12

8:00 am   **Identifying novel clinical surrogates to assess the strength of human bones: An *ex vivo* study.**

Quentin Vallet[1], **Jean-Gabriel Minonzio[1]**, Nicolas Bochud[1], Yohann Bala[2], François Duboeuf[3], Rémy Gauthier[4], Edison Zapata[3,4], Hélène Follet[3], David Mitton[4], Pascal Laugier[1]; [1]*Laboratoire d'Imagerie Biomédicale, Sorbonne Universités, UPMC Univ Paris 06, INSERM, CNRS, Paris, France*, [2]*Laboratoire Vibrations Acoustique, INSA Lyon, Villeurbanne, France*, [3]*INSERM UMR 1033, Université de Lyon, Université Claude Bernard Lyon 1, Lyon, France*, [4]*IFSTTAR, UMR_T9406, LBMC, Université de Lyon, Université Claude Bernard Lyon 1, Lyon, France*

Background, Motivation and Objective

Because bone strength depends on cortical thickness and porosity that are not accurately assessed with current X-ray technologies, there is clear call for clinical surrogates to improve the assessment of bone strength. In this study, we investigated the potential of ultrasound guided waves to yield estimate of these properties and to predict bone strength.

Statement of Contribution/Methods

Five right human radius harvested from cadavers (76 to 91 years) underwent ultrasound axial transmission measurements using a 1-MHz array transducer (Azalée, Paris). A singular value decomposition signal processing technique was applied to the full time responses of all possible transmit-receive pairs to extract the guided waves frequency spectrum. Estimates of cortical thickness (Ct.Th US) and porosity (Por US) were obtained by fitting a 2-D free transverse isotropic plate waveguide model, based on homogenized elastic bone properties, to the experimental data. For comparison, reference values Ct.Th RX and Por RX were derived from X-ray micro-computed tomography (μ-CT Bruker SkyScan 1174, isotropic voxels size of 19 μm). Contralateral specimens were tested using a dynamic non-axial loading to assess the maximum load in a forward fall case.

Results/Discussion

Three representative μ-CT cross-sections are illustrated on Fig. 1: case (1) thick bone (Ct.Th RX = 2.8 mm), low porosity (Por RX = 3 %); case (2) intermediate thickness (2.3 mm), higher porosity (7 %); case (3) thin bone (1.5 mm), low porosity (3 %). Ct.Th US and Por US are in qualitative agreement with reference values. Ct.Th US showed a strong correlation with Ct.Th RX despite a systematic bias of about 0.5 mm likely caused by difficulties in reproducing the ROI between the two techniques. A strong linear relationship is observed between Ct.Th US and maximal load.

Present findings reflect the feasibility of guided wave measurements to provide estimates of cortical thickness and porosity on *ex vivo* human long bones. Assuming cortical thickness and porosity are clinically important to the ability of bone to resist fracture, our results suggest that improvement in fracture risk assessment could potentially be achieved by measurements of guided waves. This preliminary study conducted in a limited number of specimens is currently being completed by inclusion of a larger number of specimens to assess the method reliability and accuracy.
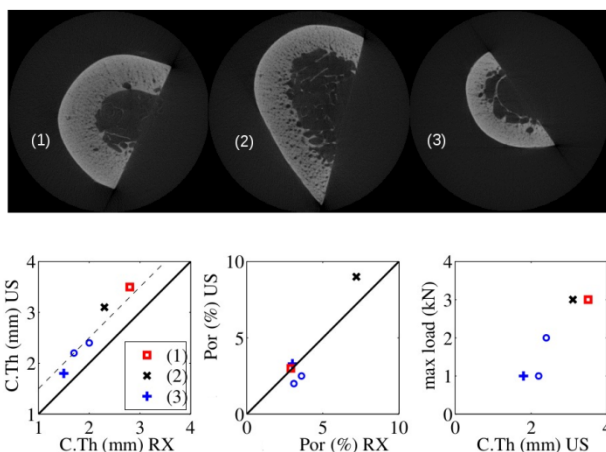
P1C7 - MSD: Novel Hardware for Ultrasound Research

4th floor

Saturday, October 24, 2015, Posters displayed 08:00 am - 05:00 pm. Authors must be present at their poster from 9:30 - 10:30am (odd number posters) and 14:30 – 15:30pm (even number posters).

Chair: **Andrzej Nowicki**
Institute of Fundamental Technological Research

P1C7-1

8:00 am **FPGA Implementation of Low-Power 3D Ultrasound Beamformer**

Richard Sampson[1], Ming Yang[2], Siyuan Wei[2], Rungroj Jintamethasawat[3], Brian Fowlkes[3], Oliver Kripfgans[3], Chaitali Chakrabarti[2], Thomas F. Wenisch[1]; *[1]Department of Electrical Engineering and Computer Science, University of Michigan, Ann Arbor, MI - Michigan, USA, [2]School of Electrical, Computer, and Energy Engineering, Arizona State University, Tempe, Arizona, USA, [3]Department of Radiology, University of Michigan, Ann Arbor, MI - Michigan, USA*

Background, Motivation and Objective

3D ultrasound is common for non-invasive medical imaging because of its accuracy, safety, and real-time ease of use. However, high bandwidth requirements and extreme computational complexity have precluded hand-held and low-power 3D systems, limiting 3D applications. In previous work, we presented Sonic Millip3De [1], a hardware design that can efficiently handle the high computational demand of 3D synthetic aperture beamforming, even in handheld and mobile applications. The design combines a custom, highly parallel hardware system with a novel delay approximation method to quickly produce high quality 3D image data within an estimated 15 W full-system power budget. Prior evaluations of the design relied on software prototypes; this work extends previous evaluations with an FPGA implementation of the beamforming accelerator, validating the results of earlier prototypes.

Statement of Contribution/Methods

We present a scaled-down FPGA implementation of a multi-channel beamforming accelerator to both demonstrate the capabilities of the design in real hardware and validate the functionality of the algorithm. In particular, we carry out image quality analyses of our beamforming architecture using simulated 3D echo data (from Field II) and 2D echo data acquired with an ultrasound system on a tissue mimicking phantom. We compare results from the FPGA implementation to an ideal software beamformer and prior software prototypes of the Sonic Millip3De design.

Results/Discussion

For 3D analysis, we generate scatter data using a 32x32 receive aperture in Field II for a cylindrical cyst in a 3D tissue volume. We compare beamformed 3D images generated using three methods: (1) exact double precision floating-point delay and sum calculation in Matlab, (2) a software implementation of Sonic Millip3De's beamforming algorithm using fixed point arithmetic, and (3) our new FPGA implementation. Visual comparison and CNR values are used to demonstrate that the FPGA design produces no distinguishable degradation from the ideal system or software prototypes.

Furthermore, we analyze 2D echo data from a tissue phantom collected via a Verasonics V1 system and an L7-4 linear array probe to provide an end-to-end demonstration of the design. Outputs of the three beamformers are compared to validate that the FPGA implementation does not introduce any degradation in image quality. We report on the hardware resources used in the FPGA design and discuss its scalability.

[1] R. Sampson, M. Yang, S. Wei, C. Chakrabarti, and T. F. Wenisch. "Sonic Millip3De: Massively Parallel 3D-Stacked Accelerator for 3D Ultrasound." Proc. of the 19th IEEE Intnl. Symp. on High Performance Computer Architecture, Feb. 2013.

P1C7-2

8:00 am **A FPGA-Based Multi-Channel Analog Front-End Device for High-Frequency Ultrasound Plane Wave Imaging System**

Po-Yang Lee[1], Hao-Li Liu[2], Chih-Chung Huang[1]; *[1]Department of Biomedical Engineering, National Cheng Kung University, Taiwan, [2]Department of Electrical Engineering, Chang Gung University, Taiwan*

Background, Motivation and Objective

Recently, ultrasound plane wave imaging has been developed for several clinical applications, such as shear wave imaging and multi-gated Doppler sonography. However, the operational frequency of these plane wave imaging systems are less than 15 MHz, which means the image resolution still can be improved in order to observe the microstructure tissues, such as eye, skin, intravascular ultrasound, and small animal imaging. Currently, the high frequency ultrasound (HFUS) image system (>35 MHz) is available for providing the high resolution ultrasound image. However, it is still working based on the conventional beamforming technology. Therefore, the purpose of this study is to develop a multi-channel analog front-end (AFE) device for HFUS plane wave imaging system. The multi-channel AFE device and simulation result of plane wave imaging are presented here.

Statement of Contribution/Methods

Simulations of HFUS plane wave image were performed using Field II which was produced by cyst phantom with a 64-element linear array working at a center frequency of 35 MHz, 55% bandwidth, pitch of 0.05 mm, and F-number is 1.55. The simulated delay time and the angles of plane wave were obtained for hardware developments. Fig 1(a) shows the block diagram of the AFE device, including FPGAs, pulser units, T/R switches, RF amplifiers, filters, ADC, and DDR3 RAM. The core unit of this system is a FPGA chip which controls the transmitting timing of each channel independently for plane wave imaging. The excitation frequency, pulse repetition frequency (PRF), and bipolar pulse cycles were controlled by the FPGA. The receiver data were fed to DDR3 RAM after a post-processing by FPGA as well. This design was used to transfer the big data from received plane wave into computer for image reconstructio

Results/Discussion

Fig. 1(b) shows the printed circuit board of this FPGA-based multi-channel ultrasound AFE device. The max excitation frequency can up to 70 MHz with a max PRF of 100 kHz, excitation voltage is 100 Vpp, gain of each amplifier is 60 dB, and sampling of each ADC is 250 MSPS. Fig. 1(c) shows the simulated result for a 35 MHz HFUS plane wave image which was obtained using 43 angles of plane wave, and the lateral resolution is 55 μm. The simulated results were used for designing the functions of FPGA. Next works of this study will focus on digital back-end (DBE) for real time high frequency ultrafast imaging.
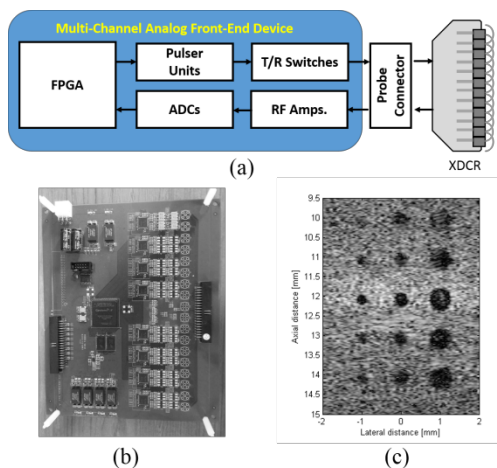
Fig 1.

8:00 am   **A FPGA-based Wearable Ultrasound Device for Monitoring Obstructive Sleep Apnea Syndrome**

Chi-Kai Weng[1], Jeng-Wen Chen[2], Chih-Chung Huang[1]; [1]*Department of Biomedical Engineering, National Cheng Kung University, Taiwan,* [2]*Department of Otolaryngology Head and Neck Surgery, Cardinal Tien Hospital, Taiwan*

Background, Motivation and Objective

Obstructive sleep apnea (OSA) defined as recurring episodes of partial or complete obstruction of the pharyngeal airway during sleeping. Some serious cases may cause complete block of upper airway and lead to suffocation or even death during sleeping. Many studies have demonstrated that the deformation of tongue plays an important role in OSA. Several medical imaging modalities have been used to record the airway changes, such as cine MRI and ultrafast CT. However, most of them are difficult to be used widely in clinical diagnosis for continuous recording the deformation of tongue in real time, particularly during sleeping. In order to overcome these problems, the purpose of this study is to develop a FPGA-based wearable ultrasound device for real time monitor of the dynamic change of the tongue base (TB). The results in present study can help physician to understand the anatomical change of TB for OSA.

Statement of Contribution/Methods

In order to achieve the wearable purpose, a custom-designed 16-channel array surface ultrasonic transducer was fabricated in this study. Fig. 1(a) shows the system block diagram of the developed wearable ultrasound device using a single FPGA chip. The 16-channel analog front-end circuit of the system includes 16-channel high-voltage pulsers and receivers. Each receiver was composed of low-noise amplifier, variable-gain amplifier, and 12-bit analog-to-digital converter running at a sampling frequency of 50 MHz. In the experiments, the transducer was placed on the submental skin for scanning the TB motion, as shown in Fig 1(b). Since the boundary between TB and airway has a huge mismatch of acoustic impedance, stronger echogenic signals can be recorded easily from each line. Consequently, the TB curve of interest can be obtained by a linear interpolation algorithm in DSP unit.

Results/Discussion

Fig. 1(c) shows the curves of TB motion during eupneic to Mueller maneuver (MM, after a forced expiration, an attempt at inspiration is made with closed mouth and nose). The blue curve represents to the state of eupneic and the red curve represents the state of MM. The dynamic variation between these two curves can be distinguished clearly by using this wearable ultrasound device. In the future, the experiments will be carried on detecting the airway situation from OSA patients for long term monitoring their anatomical change of TB during sleeping.
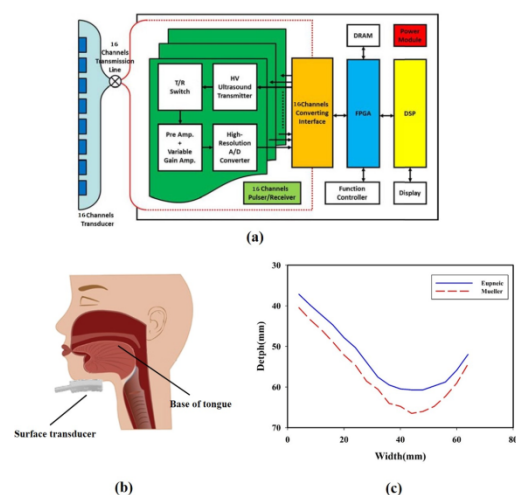
Fig. 1

8:00 am   **HD-PULSE: High channel Density Programmable ULtrasound System based on consumer Electronics**

Alejandra Ortega[1], David Lines[2], João Pedrosa[1], Bidisha Chakraborty[1], Hans Gassert[2], Jan D'hooge[1]; [1]*Department of Cardiovascular Sciences, KU Leuven, Leuven, Belgium,* [2]*Diagnostic Sonar Ltd., Livingston, United Kingdom*

Background, Motivation and Objective

The development of new beamforming techniques for volumetric (3D) ultrasound (US) imaging requires an open, flexible and fully programmable US platform. To date, such systems are scarce and required (custom-made) dedicated electronics. The aim of this report is to present a novel High channel Density Programmable ULtrasound System based on consumer Electronics (HD-PULSE).

Statement of Contribution/Methods

HD-PULSE is a modular, scalable, generic and fully programmable US platform, that allows controlling and reading-out of a 2D matrix array transducer (up to 1024 elements) for 3D imaging. The US platform is built on two National Instruments reconfigurable PXI systems (backbone data rates up to 24 Gb/s), with each chassis containing a controller, a timing module (<2ns accuracy) and 4 blocks of 4 PCI Express cards each block controlling 32 independent channels (Figure). Each of these acquisition blocks holds: 1) a tri-level high voltage pulser (+/-90V) backed-up with an FPGA allowing to define and stream arbitrary pulses by clocking out combinations of the bipolar pulsers (200MHz resolution) 2) a receiver card containing a high voltage transmit-receive protection as well as low noise pre-amplifiers (swept gain >32dB), resulting in a differential output matched to the digitizer, and 3) two NI5752 high speed AD converters that can jointly sample 64 channels at 50MS/s with 12-bit resolution out of which 2x16 channels are effectively used, permitting real-time data streaming of all channel data to disk. Both digitizer cards are supported by FPGA's allowing for onboard real-time processing. In total, the system is thus configured for 256 independent transmit-receive channels. Those are combined with 1:4 transmit and 4:1 receive programmable multiplexers. Given that all electronics is NI labeled, they can be fully programmed using a graphical user interface (i.e. LabView®). Finally, an external digitizer board can acquire physiologic signals synchronously such as blood pressure and electrocardiogram that can be used to trigger the control/read-out of the US acquisition process.

Results/Discussion

In the present report an open, flexible, scalable, tailored and fully programmable US platform was presented, HD-PULSE. This research tool will play an important role in the development of new beamforming techniques for high-frame rate and high-quality 3D cardiac US images.
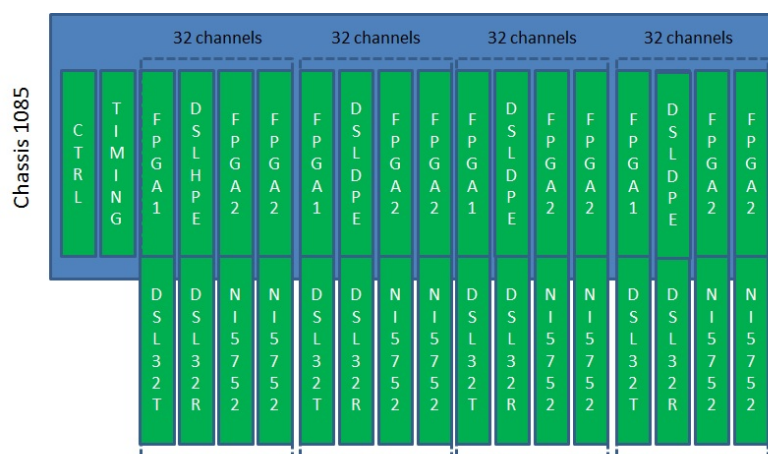
Figure. Schematic of one of the PXI systems and its 4 blocks each of them providing control over 32 independent channels.

8:00 am   **Smartphone-based Portable Ultrasound Imaging System: Prototype Implementation and Evaluation**

Sewoong Ahn[1], Jeeun Kang[1], Pilsu Kim[1], Gunho Lee[1], Eunji Jung[1], Woojin Jung[1], Minsuk Park[1], Tai-kyong Song[1]; [1]*Department of Electronic Engineering, Sogang University, Seoul, Korea, Republic of*

Background, Motivation and Objective

There have been a wide range of researches in efficient implementation of portable ultrasound (US) imaging systems to obtain portability and usability. In this paper, we present a smart US imaging system (SMUS) based on an android-OS smartphone, which can provide maximally optimized efficacy in terms of weight and size in point-of-care diagnostic applications.

Statement of Contribution/Methods

The proposed SMUS consists of the smartphone (Galaxy S5 LTE-A, Samsung., Korea) and probe system which includes analog front-end, digital core processor, and interface module. In the analog front-end, two octal high-voltage pulsers with transmit/receive switch (MAX14808, Maxim, USA) and analog-to-digital converters (AFE5808, TI, USA) composes 16-channel analog circuits for US transmission and reception. The digital core processor is implemented on a low-cost FPGA (Spartan6, Xilinx., USA) and conducts the transmit/receive beamforming and mid-processing (e.g., DC rejection, quadrature demodulation). As a result, the USB controller (3014-BZX, Cypress, USA) conveys the complex baseband signal to the smartphone through USB 3.0 protocol. Note that the probe system can be powered by battery embedded with a capacity of 2,000mAh. The smartphone performs the back-end processing (e.g., envelope detection, log compression, 2D image filtering, and digital scan conversion) and image display. To evaluate the performance of the SMUS, the phantom experiment was conducted with a custom linear array probe and tissue-mimicked phantom (Model 040GSE, CIRS, USA). In addition, usability was evaluated in terms of internal and external temperatures of SMUS with plastic shell.

Results/Discussion

Fig. 1(a) shows the appearance of the proposed SMUS; the probe system indicates the size of 40×150×30 mm³ and the weight of 180g with the power consumption of 8.16Wh. The SMUS can provide frame rate of up to 37.4 fps and battery lifetime of 1 hour with 32 effective channels. Fig. 1(b) demonstrates the reconstructed B-mode image overlaid on a GUI. In usability evaluation, the external temperature is maximally saturated at 64°C on the analog front-end of the probe system which is well under the IEC 60950-1 standard (i.e., 75°C), while the internal temperature is saturated at 78.5°C. These results indicates that the proposed SMUS can be a solution for point-of-care diagnosis with enhanced usability.
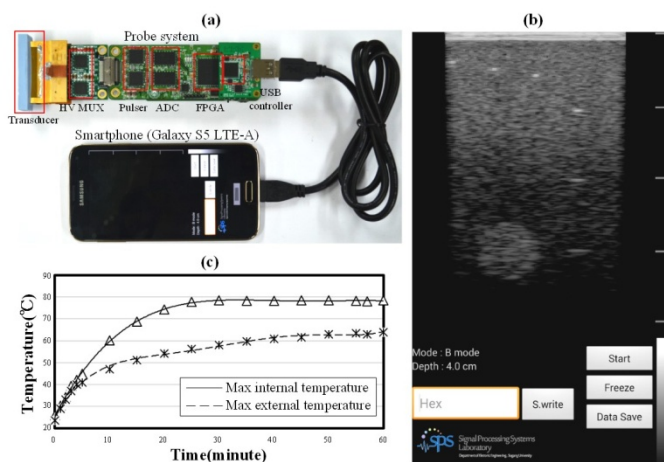
Figure 1. (a) Appearance of the smart mobile ultrasound system with the smartphone. (b) B-mode image obtained by the SMUS. (c) Maximum internal(at the ADC chipset) and external(at the plastic shell suface) temperature of the system in operation

P1C7-6

8:00 am   A Cost-effective Portable Ultrasound Imaging System with Wireless Connection

Heyuan Qiao[1], Bingjing Zhao[2]; [1]*School of Medical Engineering, Hefei University of Technology, Hefei, Anhui, China, People's Republic of,* [2]*Anhui University, Hefei, Anhui, China, People's Republic of*

Background, Motivation and Objective

Ultrasound imaging is a widely used technique in diagnosis and treatment. With the rapid development of integrated circuits and embedded systems, portable ultrasound imaging devices are seeing promising applications on first aid, point of care, bedside use or other convenient situations. With the rising popularity of smartphones and tablets, images are convenient to be viewed or saved on these friendly-used smart devices via wireless connection, and the results could be also transferred to cloud servers for further analyzing.

Statement of Contribution/Methods

In this work, a size, power and cost effective ultrasound imaging system is designed and implemented. A 16-channel linear ultrasound transducer array works as the ultrasound transmitting/receiving source, which is followed by a 16-channel analog front end for data acquisition. The acquired data is buffered in an FPGA and then processed by a DSP. Image reconstruction is performed in the DSP based on the synthetic aperture focusing technique. The reconstructed images are compressed into JPEG format and transmitted to a client application on smart devices via Wi-Fi for display, while control words are simultaneously received from it for operation. The whole system is powered by a single 3.7V Li-ion battery through a power management subsystem. With highly integrated solutions in every module, the system could simultaneously meet the demands of small size, low cost and power saving, and would be suitable for various clinical applications.

Results/Discussion

The prototype of the ultrasound imaging system is based on a four-layer printed circuit board (PCB). With a simple plastic shell, its dimension is 126×80×25(mm) and its weight is about 140g (which did not include the detachable and replaceable probe). The maximum operating current is 500mA, and a 3.7V/1100mAH Li-ion battery can provide a full-load battery life of more than 2 hours. It can be continuously reconstructing, compressing, transmitting and displaying images with 141×200 pixels at 8-9 fps. The effective imaging depth reaches 80mm and imaging angle reaches ±45°, or at least ±30°, which has met the general requirements of body imaging. The bill of materiel (BOM) cost of the system is no more than 200 USD($), and the cost of a customized single probe is around $500. The total cost is only on par with a single phone, and will be further lowered after mass production.
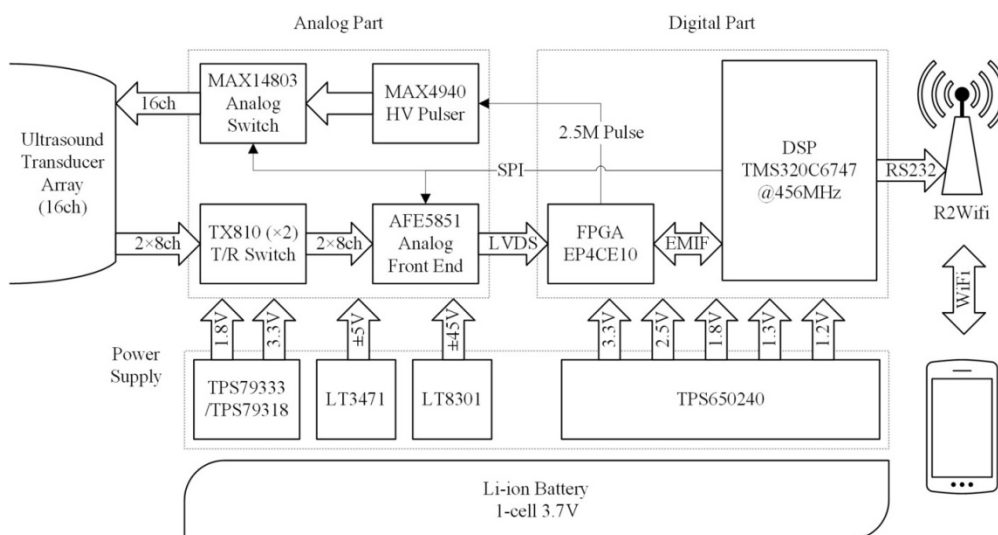
8:00 am   Color Doppler Imaging on a Smartphone-based Portable US System: Preliminary Study

Eunji Jeong[1], Sua Bae[1], Minsuk Park[1], Woojin Jung[1], Jeeun Kang[1], Tai-kyong Song[1]; *[1]Department of Electronic Engineering, Sogang University, Korea, Republic of*

Background, Motivation and Objective

There is increasing interest in the point-of-care US system using smart devices, such as a tablet PC and a smartphone, due to their high accessibility and portability. To meet this growing interest, our group recently has developed a smartphone-based portable US system but it only provided B-mode imaging. In this paper, we present the realization of the color Doppler imaging (CDI) on the aforementioned system to provide the functional information such as velocity of blood flow.

Statement of Contribution/Methods

Fig. 1(a) shows the external appearance of the smartphone-based portable US system, which consists of a smart probe with a custom 7-MHz transducer and a smartphone. In the smart probe, we redesign the transmit/receive sequences with interleaving technique on a FPGA (Spartan 6 LX150, Xilinx Inc., USA) to conduct high frame rate color Doppler and B-mode imaging as presented in Fig. 1(b). On the other hand, in the smartphone system (Galaxy S5 LTE-A SM-G906, Samsung Electronics Inc., Korea), a real-time CDI processing is implemented by OpenGL ES 3.0 to drive the embedded GPU (Adreno 420, Qualcomm Inc., USA). Overall processing blocks are divided into multiple render cycles, which optimizes the efficiency of parallel processing. The performance of the proposed CDI processing on the smartphone-based portable US system was evaluated by the phantom study with a Doppler flow phantom (Gammex 1425A LE, Gammex Inc., USA). Note that B-mode data has 128 scanlines and 1024 samples and color Doppler data has 32 scanlines, 256 samples and 12 ensembles. The maximum pulse repetition frequency (PRF) is 15 kHz for each ensemble of CDI.

Results/Discussion

For the 2-D color Doppler map overlaid on a B-mode image as shown in Fig. 1(c), a frame rate of up to 17 Hz is achieved when imaging 4-cm depth. Also, for the given condition, the proposed CDI processing satisfies the requirement of the real-time operation by providing processing time of 22 msec shorter than the data acquisition time (i.e., 34 msec). These results indicate that the smartphone-based portable US system can provide the technical feasibility on implementing the CDI processing, which will facilitate the practical use of US imaging in the point-of-care diagnosis.
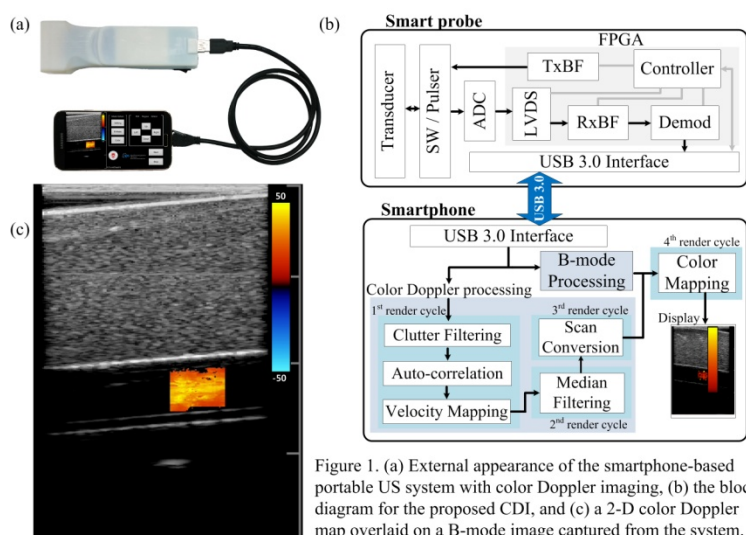
Figure 1. (a) External appearance of the smartphone-based portable US system with color Doppler imaging, (b) the block diagram for the proposed CDI, and (c) a 2-D color Doppler map overlaid on a B-mode image captured from the system.

8:00 am   A portable dual-mode ultrasound platform with multi-rail voltage power supply for adaptive diagnostic imaging and therapy sequence programming

Gary Yi Hou[1], Bob Uvacek[1], Richard Tobias[1]; *[1]Cephasonics, Santa Clara, California, USA*

Background, Motivation and Objective

Noninvasive focused ultrasound-based technologies have become a promising diagnostic and treatment strategy for a wide range of medical applications such as High Intensity Focused Ultrasound (HIFU) ablation (Al-Bataineh et al., Cancer Treat Rev 2012), lithotripsy (McClain et al., Rev Urol 2013), and acoustic radiation force (ARF) based measurement (Sarvazyan et al., UMB 2013) and therapy (Harper et al., J. Urol., 2013). Nevertheless, the designs of most present commercial therapeutic ultrasound systems are mostly large-scaled and immobilized, which limits their usage in point-of-care use cases such as emergency medicine or battlefield. The objective of this work is to present a portable ultrasound platform equipped with an adaptive, multi-rail power supply capable of dynamically switching between standard B-mode imaging, ARF-based imaging and therapy.

Statement of Contribution/Methods

A 4-rail voltage power supply has been customized inside of a portable 192-channel Analog Front End (AFE) ultrasound engine (Tobias and Schafer, SPIE 2014). The high power rail for B-mode can be adjusted between ±20V to ±100V, whereas the low power rail for Pulsed Doppler mode can be adjusted between ±3V to ±50V. Our technology provides high maximum power output (>400 W) continuously for therapeutic applications as the lower power rail has been customized by using Supercapacitors instead of the traditional capacitors. Comparable existing technologies only allow up to maximum power of 20W.

Results/Discussion

The output performance of all four voltage rails was assessed by testing a burst of 2.5 MHz Continuous Wave (CW) sequence for 50 msec with 70% duty cycle at ±50 V, and the electronic signals were monitored using an oscilloscope. Traditional capacitor-based voltage rail showed a rapid voltage droop of output power within 5 msec, whereas rails with external power source supplying equivalent maximum power as Supercapacitors (>400W) was able to maintain maximum power output during the entire 50 msec CW sequence. In addition, all rails were capable of dynamically programming and switched during a scanning procedure through an adaptive-scheduling Application Programming Interface (API).

In this work, a 4-rail voltage power supply circuitry has been designed and integrated into a portable sized ultrasound platform. The low voltage rails within the power supply circuitry were customized to support both imaging and therapy sequence. Initial feasibility has demonstrated a successful power output for a therapeutic sequence of burst transmit for 50 msec. The details of our technology and our ongoing work will also be presented.

P1C7-9 _____

8:00 am   Mobile ultrafast ultrasound imaging system based on smartphone and tablet devices

Holger Hewener[1], Steffen Tretbar[1]; [1]*Ultrasound, Fraunhofer IBMT, Sankt Ingbert, Germany*

Background, Motivation and Objective

Mobile and cost effective ultrasound devices are being used in point of care scenarios or in the drama room. To reduce the costs of such devices we already presented the possibilities of consumer devices like the Apple iPad or iPhone to compute full signal processing of raw data for ultrasound image generation. Emerging technologies like ultrafast ultrasound imaging result in new algorithms for example for shearwave elastography or vector velocity imaging but also enable the creation of a full image with only one excitation/reception event based on plane wave imaging. It is also possible to generate high quality images for diagnostic imaging using few plane wave excitations at different angles and intelligent compounding. This way acquisition times and power consumption of ultrasound imaging can be reduced for low power mobile devices based on consumer electronics realizing the transition from FPGA or ASIC based beamforming into more flexible software beamforming.

Statement of Contribution/Methods

Software based beamforming is usually performed on a GPU utilizing massive parallel processing (like CUDA or OpenCL) but with the development of modern processors (A7, A8 and A8X) for its smartphones and tablets Apple introduced parallel GPU hardware and the framework "Metal" for advanced graphics and general purpose GPU processing for the iOS platform. We use it for medical signal reconstruction in the mobile plane wave compounding beamforming and imaging on ultrasound channel data sets transmitted at different excitation angles and even defocussed beams measured with a compact version of our research systems "DiPhAS" in ultrafast imaging mode. This beamformer is controlled and read out by the mobile tablet over Wifi connection without any PC component involved.

Results/Discussion

We were able to integrate the beamforming reconstruction into our mobile ultrasound processing application on the iOS platform. The beamforming can be performed at 50 Hz providing real time imaging including the postprocessing of beamformed data into images (envelope detection and scan conversion). This solution also includes plane wave compounding to realize a high quality imaging system with Wifi transfer of measurement data to commercially available tablets or smartphones with software beamforming. Different transducer geometries and scan setups were tested and examples for linear, phased and convex scanning probes were obtained. Based on these results a compact low cost hardware is specified and currently under development that will benefit from the pure software based processing approach.

P1C7-10 _____

8:00 am   Real Time Imaging System using a 12-MHz Forward Looking Catheter with Single Chip CMUT-on-CMOS Array

Coskun Tekes[1], Thomas M. Carpenter[1], Toby Xu[1], Sebastian Bette[2], Uwe Schnakenberg[2], David Cowell[3], Steven Freear[3], Ozgur Kocaturk[4], Robert J. Lederman[4], F. Levent Degertekin[1]; [1]*G.W. Woodruff School of Mechanical Engineering, Georgia Institute of Technology, Atlanta, Georgia, USA,* [2]*Institute of Materials in Electrical Engineering, RWTH Aachen University, Aachen, Germany,* [3]*School of Electronic and Electrical Engineering, University of Leeds, Leeds, United Kingdom,* [4]*Division of Intramural Research, National Institute of Health, Bethesda, Maryland, USA*

Background, Motivation and Objective

Forward looking (FL) imaging catheters would be an important tool for several IVUS and ICE applications. Single chip CMUT-on-CMOS arrays with simplified electrical interconnect have been previously developed for highly flexible and compact catheters. Here, we present a custom built real time imaging system utilizing catheters with single chip CMUT-on-CMOS arrays and show initial imaging results.

Statement of Contribution/Methods

The real time imaging system was demonstrated on a 2.1 mm diameter single chip CMUT array with 64 Tx and 56 Rx operating at 12 MHz. The array is biased at 17 V and uses 13 external connections including 4 Rx channels. Electrical connections to micro cables in the catheter are made from the top side of the chip using anisotropic conductive epoxy on the chip and resistive welding on the custom designed flexible polyimide interconnect/cable interface (Fig.1). The device is coated with Parylene-C before final packaging of the 1 m long catheter. A braided thermoplastic catheter shaft used to support the overall catheter includes 4 grooves to house twisted micro cables. The medical grade silicon rubber was embedded into the distal shaft to secure the interconnect/cable interface and the chip at the tip. The overall catheter shaft was coated with a thin layer Pebax shaft using reflowing technique. For real time data acquisition, we developed an FPGA (Altera Stratix V) based imaging platform to generate digital control sequences for the chip and collect RF data from Rx outputs. The RF signals are amplified and digitized using an 80 MHz ADC (TI AFE5807). The incoming data is fed into the FPGA with 512 MB capacity. The data is post processed and transferred to a PC via PCI Exp. with a speed of 14 Gbps.

Results/Discussion

We performed imaging experiments using wire phantoms immersed in water to test the real time imaging system. Initial reconstructed images from the wires are shown in Fig.1-d. Due to the 12.5V pulse height limitation of integrated on-chip pulsers, the collected RF signals are averaged 16 times. However, the system has the potential to generate images at 32 fps rate with the particular catheter. We are currently working on a higher speed chip with improved SNR to test the catheter with in vivo phantoms.

We have successfully implemented a FL catheter with our single chip CMUT-on-CMOS system. The overall system is fully functional and shows promising image performance.
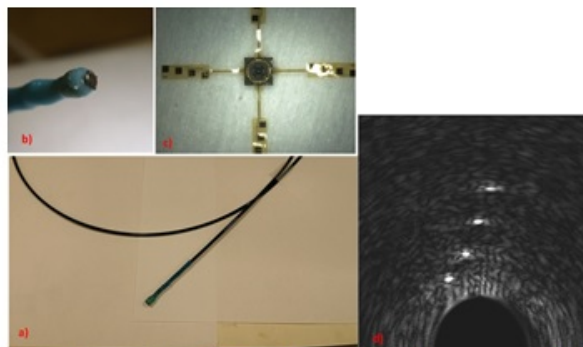
Figure 1. (a) Catheter, b) single-chip system on the tip of the catheter, c) flexible interconnect, d) 2D wire phantom image (image size = 10 mm x 10 mm)

[1] G. Gurun, C. Tekes, J. Zahorian, T. Xu, S. Satir, M. Karaman, J. Hasler, F.L. Degertekin, "Single-Chip CMUT-on-CMOS Front-End System for Real-Time Volumetric IVUS and ICE Imaging", IEEE Transactions on, Ultrasonic, Ferroelectrics and Frequency Control, Vol. 61, No. 2, February 2014.

SATURDAY POSTER

8:00 am   Characterization of the STHV748 integrated pulser for generating push sequences

Mateusz Walczak[1], Beata Witek[1], Marcin Lewandowski[1]; [1]*Institute of Fundamental Technological Research, Polish Academy of Sciences, Poland*

Background, Motivation and Objective

Push sequences are used in Acoustic Radiation Force Impulse (ARFI) imaging technique to generate acoustic radiation force. As a standard, 4 – 8 channel transmit pulsers are used in multi-channel ultrasonic scanning systems. Because of high risk of damage due to overheating, it is hard for a transmit pulser to generate a push signal whose duration is in the range of 100μs to 600μs. The aim of this work was to determine the safe range of parameters of push sequences for a high-voltage, high speed, 4-channel STHV748 (STMicroelectronics) pulser.

Statement of Contribution/Methods

Experiments were conducted on the STEVAL-IME003V1 evaluation board from STMicroelectronics, at room temperature, without any heat sink or cooling. This paper studies the feasibility of generating push sequences in the frequency range of 4MHz – 5MHz and peak-to-peak amplitude 130V – 180V. The duration of push bursts was varied from 100μs to 600μs for the pulse repetition frequency of 10Hz and 20 Hz. The impact of using ceramic capacitors (4x22μF) and electrolytic capacitors (2x141μF) on the HV supply was also examined. The reaction of the pulser was measured with three output loading conditions. The first was pure 100Ω resistance, the second was a single element of AL2442 Esaote linear probe and the third was a single element of LA510 Echo-Son probe. Push burst duration was considered as a primary parameter. It was checked which values of HV supplies and transmit frequency cause the pulser to overheat. Consequently, it was examined how often the push signal can be repeated and whether it would be necessary to decrease the HV supply voltage. The output signals, the load current and the temperature of the pulser were measured.

Results/Discussion

The STHV748 pulser is capable of generating push sequences. The ratio of the push burst duration to repetition period is a key parameter that determines the safe operating conditions of the pulser. Moreover, the current flowing through the pulser and its temperature are very much dependent on the transmit frequency and load characteristics. The measurements are presented in Table 1.

Table 1. The measured push burst duration, the duty-cycle of push sequences and the pulser temperatures for different HV supplies and frequencies.

HV supply [V_{pp}]	Frequency [MHz]	Burst duration [μs]	PRF [Hz]	Duty - cycle [%]	Measured temperature [°C]	Probe
150	5	**250**	20	0.5	48	AL2442
130	5	**300**	20	0.6	44	AL2442
150	4.5	**440**	20	0.88	64	AL2442
160	4	**500**	20	1	70	AL2442
160	4	**375**	20	0.75	76	LA510
150	5	**400**	20	0.8	76	LA510
180	4	**1000**	10	1	70	LA510
170	5	**1200**	10	1.2	75	LA510
170	4	**2000**	10	2	76	LA510

P2C1 - Microfluidics

4th floor

Saturday, October 24, 2015, Posters displayed 08:00 am - 05:00 pm. Authors must be present at their poster from 9:30 - 10:30am (odd number posters) and 14:30 – 15:30pm (even number posters).

Chair: **David Greve**
Carnegie Mellon University

P2C1-1 _____

8:00 am **Measurement of Very Low Concentration of Microparticles in Fluid by Single Particle Detection using Acoustic Radiation Force Induced Particle Motion**

John Lee[1], Javier Jimenez[2], Ian R. Butterworth[2], Carlos Castro-González[2], Shiva K. Shukla[3], Berta Marti-Fuster[2], Luis Elvira[3], Duane S. Boning[1], Brian W. Anthony[1]*; [1]Massachusetts Institute of Technology, Cambridge, MA, USA, [2]Madrid-MIT M+Vision Consortium, Massachusetts Institute of Technology, Cambridge, MA, USA, [3]Instituto de Tecnologías Físicas y de la Información (CSIC), Madrid, Spain*

Background, Motivation and Objective

The ability to measure very low concentration of scatterers suspended in fluid can be a useful technique in areas such as biotechnology, medicine and food industry. The existing backscatter coefficient (BSC) methods can quantify concentration, but when concentration is very low, BSC methods can face challenges due to the low energy of the backscatter signal. An important attribute of having scatterers suspended in fluid is that scatterer motion can be induced by the acoustic radiation force (ARF). The induced motion can enable robust detection of individual scatterers even when the signal-to-noise is low. This work proposes a method to quantify very low concentrations by single scatterer detection utilizing the motion induced by ARF.

Statement of Contribution/Methods

A 75-MHz focused single element transducer (Olympus) is used with a UT340 pulser-receiver (UTEX) and a PicoScope 5444b (Picotech) for data acquisition. The fluid phantom consists of 10-μm polystyrene microparticles (Sigma-Aldrich) and distilled water. Sample concentration ranges from 0 to 100/μL. The experimental setup is shown in Fig. 1a. A pulse repetition frequency (PRF) of 1 kHz is used and the sample is measured after transient flow patterns have dissipated. Fifty consecutive A-lines constitute a single measurement, which are repeated every 0.1 second to achieve 3000 measurements. Individual particles are detected from each measurement by detecting the trajectories observed in the resulting synthetic image.

Results/Discussion

Fig. 1b shows a synthetic image from a single measurement formed by vertically stacking fifty envelope-detected A-lines. Two slanted lines are observed (circled), which correspond to two particles moving away from the transducer. Given the low concentration, each line likely corresponds to a single particle. Cross-correlation using template matching is used to amplify the backscatter signal and a modified Hough transform is used to detect the lines (red lines in Fig. 1c). Backscatter amplitude, frequency spectrum, axial position and velocity are extracted from the detected trajectories. A linear trend is observed between the proposed method and hemocytometer measurement (Fig. 1d).
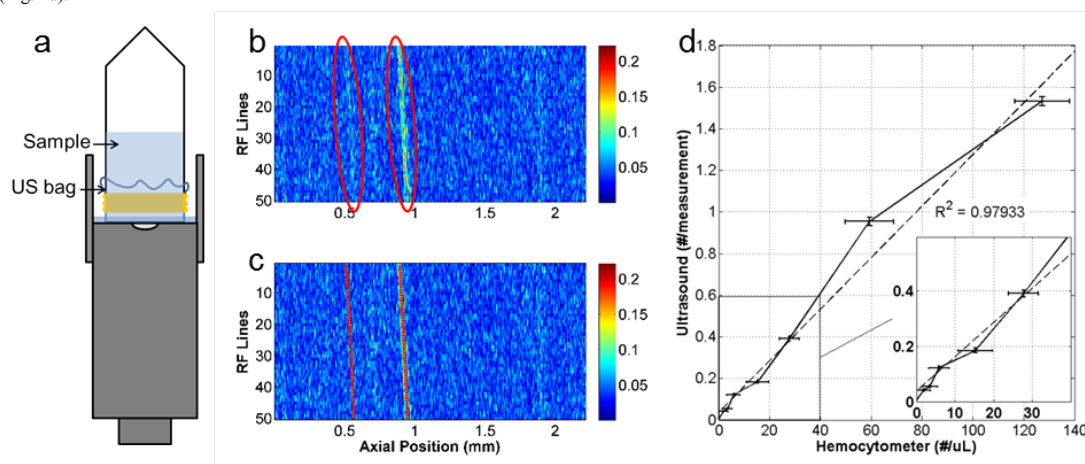
Figure 1. (a) Experimental setup. (b) Vertically stacked A-lines creating a synthetic image used for detection and (c) with detected trajectory. (d) Linear trend shown between the proposed method and the hemocytometer.

P2C1-2 _____

8:00 am **Investigation of surface-acoustic-wave atomization using Phase Doppler Anemometry**

Taiki Hiromoto[1], Motoaki Hara[1], Taku Kudo[2], Hideaki Kobayashi[2], Hiroki Kuwano[1]*; [1]Graduate school of Engineering, Tohoku University, Japan, [2]Institute of Fluid Science, Tohoku University, Japan*

Background, Motivation and Objective

Nanoparticle synthesis using an aerosol spray has excellent impact for industrial applications which are superconductors, catalyst, drug careers, luminescence devices, or ceramic capacitors. Particularly, ultrasonic based atomization gives a great solution for synthesis of bio-nanoparticle due to the unnecessary of a heating process. As a previous work, we have reported the direction-controlled atomization using a couple of arc-shaped surface acoustic wave (SAW) resonators. By applying this device to bio-nanoparticle synthesis, drastic improvement of synthesis yield is expected.

Statement of Contribution/Methods

Figure 1(a) shows the SAW based atomizer we fabricated in this study. The solvent to be atomized is poured into the reservoir, and pumped out to the trench by the burst vibration from the interdigital transducers (IDT) at the both side of reservoir. A couple of the arc-shaped IDT (AS-IDT) can be focused the SAW energy into the solvent in the trench and atomize it as shown in Fig 1 (b). For the high yield nanoparticle synthesis, monodispersity is preferable for diameter and velocity of the mist droplet in the atomization. Water and acetone, which has low and high volatility, respectively, were applied as solvents to be atomized. Behaviors of atomization were evaluated with

Phase Doppler Anemometry (PDA). In the PDA system, Ar laser (λ=514.5 nm) was used as a light source, and its theoretical resolution reaches less than 40 nm. By using the PDA system, the diameter and velocity of droplet can be measured in real time.

Results/Discussion

PDA measurement results were summarized in Fig 1(c). They showed behaviors of atomized droplets with a diameter of more than the resolution of our PDA system. In these results, dispersion of diameter indicated monodispersity, and average diameter of water and acetone mist were 8.2 μm, and 14.0 μm, respectively. Under the monitoring with a high-speed-camera, one-directional atomization has been confirmed in both solvents. However, in the PDA measurement of the water mist, most of droplets lost the initial velocity and were drifting in the air. In contrast, positive dispersion of velocity can be observed in the evaluation of acetone mist.

(a) A photoimage of developed device (b) Directional atomization with our device

(c) Summary of evaluation result with the PDA system ※*Transmit Response*
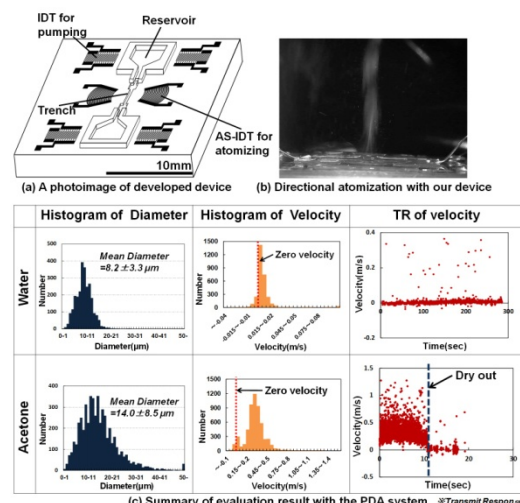
Fig.1

P2C1-3

8:00 am   The Plate Acoustic Wave Sensor for Detection of Bacterial Cells in Liquid Phase

Irina Borodina[1], Boris Zaitsev[1], Andrey Teplykh[1], Alexander Shikhabudinov[1], Iren Kuznetsova[2], Olga Guliy[3], Andrey Smirnov[4]; *[1]Saratov Branch, Kotel'nikov Institute of Radio Engineering and Electronics of RAS, Russian Federation, [2]Kotel'nikov Institute of Radio Engineering and Electronics of RAS, Russian Federation, [3]Institute of Biochemistry & Physiology of Plants & Microorganisms RAS, Russian Federation, [4]Saratov State University, Russian Federation*

Background, Motivation and Objective

At present there exists the necessity for electronic devices which are able to carry out   the multiparametric express-analysis of biological liquids of small volume, to solve the problem of detection of microbial cells and to conduct the monitoring of their interaction with antibodies, mini-antibodies and bacteriophages. The present biological sensors are not enough sensitive or weakly selective. Moreover the carrying out of the analyses may take much time from 2-3 hours up to several days. The paper describes the new method of microbial cells detection directly in liquid phase based on the registration of the interactions "bacterial cells - bacteriophages" and "bacterial cells - antibodies" with the help of sensor using plate acoustic wave.

Statement of Contribution/Methods

Acoustic sensor under study represented piezoelectric plate of thickness of 0.2 mm with two interdigital transducers for radiation and reception of plate acoustic waves with shear - horizontal polarization. The liquid container was glued on plate surface between transducers. The frequency dependencies of phase and insertion loss of output signal of sensor without suspension were measured in range 2 – 4 MHz by the meter of S – parameters. It was found that insertion loss did not exceed 24 dB and the frequency dependence of phase was linear. Then meter was switched in time regime on fixed frequency 3.3 MHz (minimum of loss) and container was filled by suspension of cells with the certain concentration. After the time interval which was enough for stabilization of the phase and amplitude of output signal the certain amount of specific bacteriophages was added in suspension. The phase and amplitude were changed and after some time achieved the stable values. The changes of phase and insertion loss were measured. Then suspension was removed and the experiment was repeated with the same cells concentration and different amount of bacteriphages.

Results/Discussion

As a result the dependencies of changes of the phase and insertion loss of output signal on the amount of bacteriophages were obtained. In control experiments with nonspecific bacteriophages the phase and amplitude of the signal did not change. Analogous experiments with specific and nonspecific antibodies revealed the same regularities. So the investigations showed the possibility of development of sensors for detection of bacterial cells directly in liquid phase by registration of the specific interaction "cells - bacteriophages" or "cells – antibodies." It has been also shown that such method allows not only qualitative analysis but also quantitative one. Such sensors may be used for recognition of the illness on the early stage and the degree of the infection of the drinking water.

P2C1-4

8:00 am   Particle Size of Non-Contact Atomization of Low Surface Tension Liquid by Powerful Aerial Ultrasonic.

Arisa Endo[1], Takuya Asami[1], Takashi Ono[1], Hikaru Miura[1]; *[1]College of Science & Technology, Nihon University, Tokyo, Japan*

Background, Motivation and Objective

Recently, there is a growing demand for atomizing techniques of chemical or production line. Current methods of atomized droplets in the air include evaporating the droplets with heat and bringing droplets into contact with an ultrasonic vibrating surface. However, these methods cause problems that the physical and chemical changes in the liquid cause by heating or contact with equipment, and contamination of the liquid by impurities and degradation can occurred. To resolve these problems, we investigated non-contact atomization by ultrasound. Because conventional devices are large, we developed a compact 28-kHz ultrasonic source based on a rectangular transverse vibrating plate, and investigated non-contact atomization of droplets in the air by ultrasonic waves emitted from this device.

The non-contact atomizer is used for atomizing part of the mass spectrometer. However, atomization characteristics have not been revealed. Therefore, it is performed a study to reveal the atomization characteristics.

Statement of Contribution/Methods

Figure 1 is the diagram of an apparatus for atomization. The distance of two vibration plates is a 1/2 wavelength of the sound pressure. The liquid was atomized in the two vibration plates. In this study, the characteristics of the atomized particle size were investigated by measuring the size of the atomized particle. Sample liquid is ethanol, and was examined the particle size of varying electric input power.

Results/Discussion

Figure 2 shows the particle size distribution of atomized ethanol droplet. The particle size of the atomization at electric input power 4 W is concentrating around 37 μm as median. And the calculated result of Lang
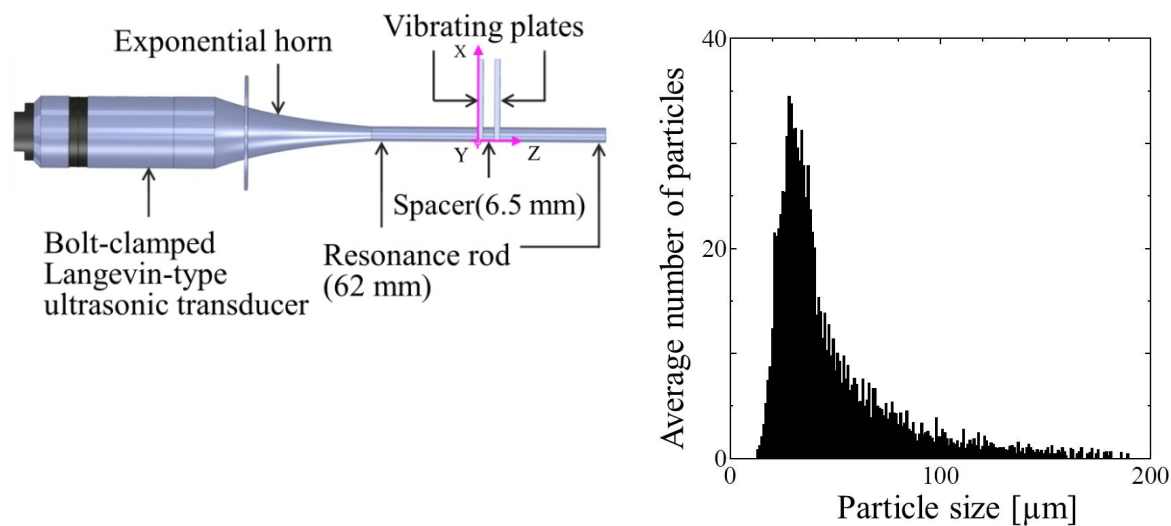
P2C2 - Transducers and Wave Generation

4th floor

Saturday, October 24, 2015, Posters displayed 08:00 am - 05:00 pm. Authors must be present at their poster from 9:30 - 10:30am (odd number posters) and 14:30 – 15:30pm (even number posters).

Chair: **Kentaro Nakamura**
Tokyo Institute of Technology

P2C2-1 _____

8:00 am   Study of ultrasonic machining using longitudinal and torsional vibration

Takuya Asami[1], Hikaru Miura[1]; *[1]College of Science & Technology, Nihon University, Chiyoda-ku, Tokyo, Japan*

Background, Motivation and Objective

Ceramic materials are used for various purposes in virtually all fields of industry. The ultrasonic machining method is a processing method using the ultrasonic vibration of the tool horn and abrasive slurry for the brittle materials as the ceramic materials. Conventional ultrasonic machining methods use only longitudinal vibration. Although, few studies have been conducted on ultrasonic machining using abrasive slurry and vibration consisted plural vibration. Accordingly, we have developed ultrasonic complex vibration machining method. The ultrasonic complex vibration consists of the longitudinal and torsional vibration. In previous studies, we found that the machining time when using a complex vibration is notably shorter as compared with that using a longitudinal vibration. In this study, we examined machining in the case of varying the displacement amplitude of the torsional vibration.

Statement of Contribution/Methods

The ultrasonic vibration source in this experiment consists of a 20-kHz bolt-clamped Langevin-type transducer, a uniform rod with a diameter of 56 mm, an exponential horn for displacement amplification (amplification factor: ≈4.6), and tool horn with the diagonal slits as a vibration converter. The diagonal slits is used to generate the complex vibration. In this experiment, the displacement amplitude of the torsional vibration was varied by the condition of the diagonal slits. The experiment was required to machine holes of 8-mm diameter and 4-mm depth for soda-lime glass. Abrasive slurry (silicon carbide #320; grain/water weight ratio, 1:10) was supplied to the machining side of the glass at approximately 1 L/min. The respective longitudinal and torsional vibration amplitudes were 10 and 0 μm_{0-p}, 10 and 11 μm_{0-p}, and were 10 and 23 μm_{0-p} at the tip of the tool horn.

Results/Discussion

Figure 1 shows the experimental results of the machining time by varying the machining pressure. The processing pressure of the shortest machining time is defined to be the optimal processing pressure. The optimal processing pressure decreased with increasing torsional vibration amplitude. The machining time at optimal processing pressure also decreased with increasing torsional vibration amplitude. From this result, we conclude that complex vibration will provide a better machining time than only longitudinal vibration.
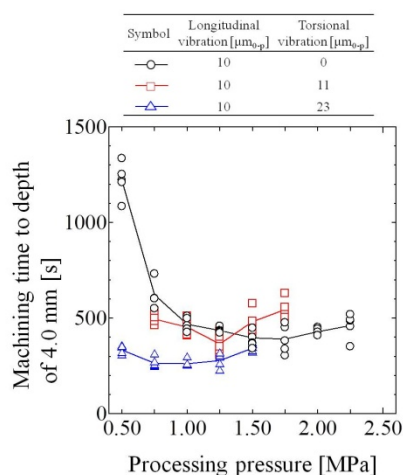
Fig. 1 Relationship between processing pressure and machining time.

P2C2-2 _____

8:00 am   ScAlN thin film transducers for ultrasonic microscopy in the VHF range

Yusuke Korai[1], Masashi Suzuki[2], Takahiko Yanagitani[2,3]; *[1]Hitachi, Ltd., Hitachi, Japan, [2]Nagoya Institute of Technology, Japan, [3]Waseda University, Japan*

Background, Motivation and Objective

Scanning acoustic tomography (SAT) has been a powerful tool to detect voids and delaminations in LSIs. To detect micron order defects, high resolution ultrasonic transducers above 100 MHz were required. Polycrystalline ZnO films have been the most commonly used for the transducers due to their low dielectric constant and easiness in obtaining c-axis orientation. However, electromechanical coupling of ZnO films (k_t =0.29) is insufficient to obtain enough signal-to-noise ratio for the micron order defect detection. Akiyama et al. recently found five-fold increase in piezoelectricity by Sc doping to AlN films and Yanagitani et al. first demonstrated the ultrasonic generation and 1.5 times increase of k_t (k_t =0.39) [1]. In this study, we demonstrated high S/N cross-sectional scan (c-scan) image observation of a trenched Si wafer specimen by using ScAlN thin film transducer.

[1] T. Yanagitani et. al., Proc. IUS 2010, 2095.

Statement of Contribution/Methods

Three types of ultrasonic transducers consisting of ZnO film/Z-cut sapphire rod, ScAlN film/Z-cut sapphire rod, and ScAlN film/silica glass rod were fabricated. Acoustic lens were fabricated at bottom surface of the rods. C-scan images of a Si wafer specimen were obtained using the focused transducers with water coupler in the SAT system

(FineSAT III Hitachi Power Solutions Co., Ltd.). The specimen with 13 types of trench patterns with widths ranging from 1 μm to 300 μm, 2 mm in length and 170 nm in depth was prepared. In the C-scan image measurements, reflection signals from trenches were measured by scanning the transducers across the trench in 0.5 μm steps in the horizontal direction.

Results/Discussion

Figure 1 shows measurement results of C-scan images and cross-sectional profiles of the Si wafer specimen. All cross-sectional profile results indicated that the reflection signals from the trench with 10 μm widths was observed with signal to noise ratio more than 2. The detectable shortest trench width is 6.5 μm in all transducer. However, signal to noise ratios of the ScAlN transducers were improved more than a factor of 4 comparing with the conventional ZnO transducer because of the capability of the use of lower digital gains.
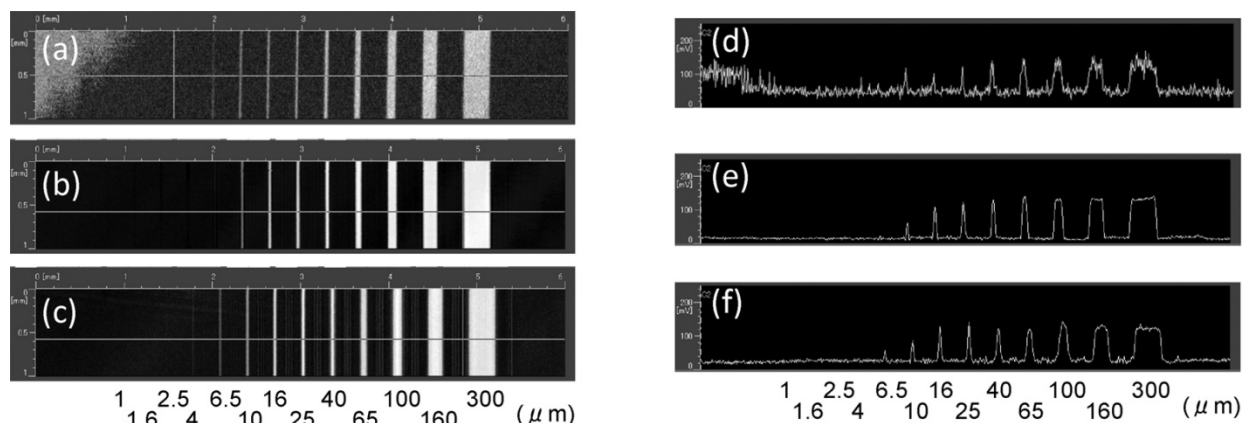
Fig. 1 C-scan images obtained by (a) ZnO/sapphire, (b) ScAlN/sapphire, and (c) ScAlN/silica glass transducers. Cross-sectional profiles of the trenched Si wafer specimen at 40 °C obtained by (d) ZnO/sapphire, (e) ScAlN/sapphire, and (f) ScAlN/silica glass transducers.

P2C2-3 _____

8:00 am   Source Location Techniques in Plate-like Structures based on Fiber Coupler Sensors

Fengmei Li[1], Yiying Liu[1], Linjie Wang[1], Zhenyu Zhao[1]; *[1]xi'an jiaotong university, China, People's Republic of*

Background, Motivation and Objective

Structural health monitoring (SHM) technologies for composite structures materials have been studied extensivel, in order to reduce the risk of mechanical failure and assess the safety of composite structures, such as aircrafts, ships and pipelines. Piezoelectric-based transducer (PZT) systems are widely used for damage monitoring in composite structures. However, some drawbacks of the PZT, such as sensitive to electromagnetic interference and cannot be embedded in equipment, constrain their deployment in specified areas. Fiber-optic sensors (FOS) with some unique merits of lightweight, immunity to electromagnetic interference, and ease of multiplexing and embedding in composite plies have been expected to be an alternative acoustic sensor in SHM. The majority of the FOS used for locating source reported to date has focused on fiber optic Bragg grating sensors.

Statement of Contribution/Methods

In this paper, the use of fiber coupler as Lamb wave sensor for source location was proposed and investigated. In order to increase the accuracy in source location, the modal analysis based on wavelet transform (WT) and fast Fourier transforms (FFT) was applied to determine the time of arrival (TOA) for two modes at certain frequency or same mode at different frequencies. Coupled with wave mode dispersion velocity and TOA method, the distance of emission source from the sensor can be obtained by only single sensor. By calculating the intersection of three circles which radius and center are source-sensor distance and sensor location, respectively, it is possible to use three sensors to find source location on two-dimensional surface. Source location experiments in carbon fiber-reinforced epoxy composite laminate and aluminum plate had been performed using pencil lead break as acoustic source.

Results/Discussion

It was found that fiber coupler sensors can easily identify propagation natures of wave modes. The performances of optical fiber coupler sensors for source location were compared to that of standard piezoelectric-based transducer . Related results show that fiber coupler sensors is better than that of the piezoelectric-based transducer in the signal acquisition and accurate source location. At last, theoretical and experimental analysis results show that optical fiber coupler sensors are suitable for identifying different modes of waves and is capable of localizing source accurately.

P2C2-4 _____

8:00 am   Research on ultrasonic detection method of fuel tank leakage

Hua Xue[1], Di Wu[1], Yongping Teng[1], Yaping Wang[1], Zhenning Zhao[1]; *[1]Beijingjiaotong University, China, People's Republic of*

Background, Motivation and Objective

At present traditional single-channel ultrasonic bubble detector based on water immersion pulse echo method was commonly used to detect the tank leakage on the production lines as figure 1 showed. The traditional method used 24 ultrasound transducers to test the leakage with one by one scanning mode. Each transducer worked 1 whole second and finished all tests in 24 seconds. It can effectively detect stable and continuously produced air bubbles, but the time interval of bubbles can not be more than 1 second. This paper aimed at detecting bubbles with longer time interval produced by smaller tank leakage(μm diameter).

Statement of Contribution/Methods

This paper proposed a new 8-channel parallel scanning detection mode, maximizing the repetition frequency of each transducer. The factors influencing the bubble detection rate in ultrasonic leak detection were analyzed first. The characteristics of ultrasonic reflection field of transducer were simulated with Helmholtz-Kirchhoff integral theorem, comparing with the experiment measurements. Then three test schemes were conducted using 8-channel parallel ultrasonic leak detector and the traditional single-channel one as followed:

Scheme1: Using traditional detector and traditional method.

Scheme2: Using traditional detector, each transducer worked one time with one by one scanning mode, and repeat scanning detection within total 24 seconds.

SATURDAY POSTER

Scheme3: Using 8-channel parallel detector, 8 equally-spaced transducers worked in parallel with three fires each time to complete work of all 24 transducers. Repeat scanning detection within total 24 seconds.

Results/Discussion

The experiment results showed the detection rates can all arrive 100% with three schemes for stable and continuously produced bubbles. For the time interval of bubble occurrence over 1 second, the detection rate was generally lower than 50% with Scheme1, but improved much with Scheme2. The detection rate of Scheme3 was significantly improved with increased repeated scanning frequency. Partial rate data of three schemes was listed as table 1. Therefore, 8-channel parallel ultrasonic testing method was more effective to detect smaller tank leakage.
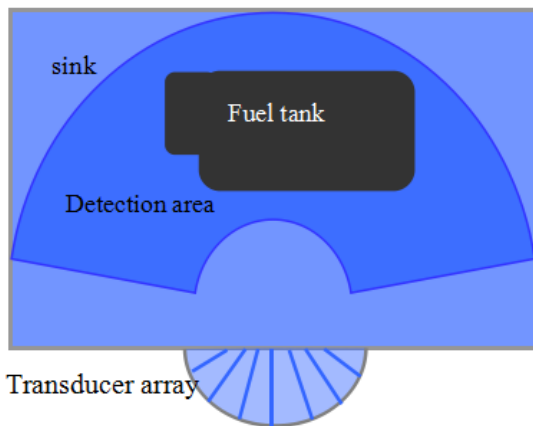
Fig.1 tank leakage detector（top view）

Number of repetitions	Time interval of bubbles(s)	Scheme1 Detection rate(%)	Scheme2 Detection rate(%)	Scheme3 Detection rate(%)
120	0.4	100	100	100
120	2	41.7	98.3	100
120	3	30.8	96.7	100
120	4	18.3	80	100
120	10	5	73.3	100
120	28	1.7	18.3	40
120	Single bubble	1.7	11.7	16.7

Table 1 Bubble detection rate comparison in three schemes

P2C2-5

8:00 am   Ultrasonic phased array on the inner surface of circular stage for detecting the circumferential flaw in a pipe

Zhongcun Guo[1], Yitao Tan[1], Fangfang Shi[1], Bixing Zhang[1], Junjie Gong[1]; *[1]State Key Laboratory of Acoustics,Institute of Acoustics,Chinese Academy of Sciences, China, People's Republic of*

Background, Motivation and Objective

The 1-D ultrasonic concave phased array plays an important role in application of pipe on-line inspection. In such inspection system, the concave phased arrays are placed in a circumference and the pipe is moved along the center axis of the phased arrays and the space between the phased arrays and the pipe is filled by water as the acoustical propagation medium. Compared with traditional ultrasonic testing technology, the mechanical rotating of the pipe can be avoided and inspection speed can be increased greatly with rapid scanning of the phased array. However, the concave phased array can detect only the axial flaws in the pipe. In fact, there are many flaws along or close to the circumferential direction. It is difficult to detect this kind of circumferential flaws by concave phased array. To increase the contact area of the incident wave beam on the circumferential flaw, the wedge is usually introduced to change the propagation direction of the incident wave beam. This method can increase the reflect coefficient of the wave beam on the flaws. However, the wedge generally decreases the signal-noise ratio of the reflect echo wave because it has more acoustical attenuation coefficient than that in water. In order to solve the problems, a new ultrasonic phased array on the inner surface of circular stage is presented and studied to increase the signal-noise ratio of the reflect echo wave without wedge.

Statement of Contribution/Methods

All elements of the new phased array are designed on the inner surface and along the generatrix of circular stage without bottom surfaces in two ends. In the detection course, the pipe is moved inside the circular stage and along the center axis. Then, the focusing characteristic of the phased array is studied. The propagation path of the acoustical wave radiated from each element of the array is complicated. The incident points on the outer surface of acoustical wave from each element to the pipe are obtained and calculated when the focal point of the beam from the phased array is designed at any position in (or on) the pipe. The field distribution and focusing characteristic of acoustical beam inside the pipe are calculated and analyzed in both continuous and pulse wave excitation modes. The effects of the parameters of the phased array on the grating lobe, main lobe and side lobe are all investigated, which is very useful for optimizing the design of the phased array.

Results/Discussion

Unlike the concave array, every element of the new phased array is not parallel and has the same angle to the central axis of the pipe. Therefore, not only the element size, the inter-element spacing and the number of effective elements, but also the angle of each element to the central axis of the pipe have an obvious effect on the field distribution. Optimal beam focus conditions are obtained. It is shown that the signal-noise ratio of the reflect echo wave can be increased greatly and the circumferential flaws can be detected easily by the new ultrasonic phased array.

P2C2-6

8:00 am   Flexible Ultrasonic Transducers for Transverse Horizontal Guided Waves in Structures

Ching-Chung Yin[1], Wei-Che Tsai[1]; *[1]Department of Mechanical Engineering, National Chiao Tung University, Hsinchu, Taiwan*

Background, Motivation and Objective

The modeling and fabrication of flexible interdigital transducers based on piezoelectric fiber composites for transverse horizontal (TH) guided wave structural health monitoring are presented. The TH modes have less attenuation in the host structures which comprise porous cores or are protected by weak-adhesive insulation. In this work, a number of parallel piezoelectric fibers embedded in epoxy resin and sandwiched between two flexible polymer sheets, instead of piezoelectric films, are used to actuate and sense the TH waves polarized parallel to the fibers. The thickness-shear or face-shear vibrations on the piezoelectric fibers are excited by the interdigital electrodes on the flexible printed circuit sheets.

Statement of Contribution/Methods

A periodic finite-element approach has been used to determine dynamic characteristics of the lowest several symmetric and anti-symmetric TH plate waves. The symmetric modes and anti-symmetric modes are related to face-shear and thickness-shear vibrations, respectively. The dispersion of layered piezoelectric fiber composite adhered on a host plate can be classified into two categories, PFC modes and plate modes. The PFC modes redistribute after layered PFC being adhered on the host plate. The PFC modes split off from their original values into the plate modes asymptotically in the vicinity of the intersections of both modes. Larger mechanical responses can be induced in the plate modes of longer wavelengths. In addition, the transducers have better sensitivity for the PFC modes in either thickness-shear or face-shear mode deformation.

Institute of Electrical and Electronics Engineers

Results/Discussion

Two flexible ultrasonic transducers were fabricated using piezoelectric fibers of diameter 250 μm. The face-shear and thickness-shear modes could be developed as the tone-burst voltage was applied to the symmetrically, or antisymmetrically aligned interdigital electrodes on the opposite polymer sheets. Performance experiments were carried out to assess the above-mentioned characteristics. The transmitting TH modes on sandwiched plates with porous cores have been verified with the delay times calculated from group velocities in time-frequency spectrograms. The experimental results are in very good agreement with simulation over the frequency range 0.5-5 MHz. The presented TH wave transducers have potential applications in guided wave structural health monitoring.

SATURDAY POSTER

P2C3 - Sensing and Energy Harvesting

4th floor

Saturday, October 24, 2015, Posters displayed 08:00 am - 05:00 pm. Authors must be present at their poster from 9:30 - 10:30am (odd number posters) and 14:30 – 15:30pm (even number posters).

Chair: **Pierre Khuri-Yakub**
Stanford University

8:00 am **Study on Movement Detection in Care Environment Using Precise Ultrasonic Distance Measurement at 40 kHz Installed in Sensor Network**

Yukari Kaneda[1], Takeo Sato[1], Mitsutaka Hikita[1]; [1]Department of GE, Kogakuin University, Tokyo, Japan

Background, Motivation and Objective

Achieving good care environment will be one of the most important issues in near future. Sensor network is considered to be a promising method to provide such services. We have proposed a novel movement detection using precise ultrasonic distance measurement for elderly and sick people without an invasion of privacy. Sensor nodes for ZigBee or Z-wave which include Tx/Rx ultrasonic transducers transmit and receive ultrasonic CWs with small amplitude. The data are sent to the center node via network, where all distance information is obtained by IFFT and stored automatically.

Statement of Contribution/Methods

Tx transmits CWs at IFFT frequencies and Rx receives them via moving reflection object (Fig. 1(a) and (b)). Data of relative amplitudes and phases are sent from sensor nodes to center node by means of ZigBee or Z-wave. In the center node, impulse responses are calculated by applying IFFT procedure. The movement information of the object is obtained by subtraction between two impulse responses at different times (Fig. 1(c)). We have proposed a new sensor node which includes function of transmitting and receiving ultrasonic CWs (Fig. 2(a)). Signals at IFFT frequencies are generated by division / multiplication of the signal from TCXO. In order to confirm our idea, we constructed experimental set up with similar performances of both sensor and center nodes (Fig. 2(b)). Lock-in amplifier provides Tx signals and X/Y components of Rx signals. PC controls frequency and executes IFFT and subtraction etc., which provides measurement data at 40 kHz.

Results/Discussion

Fundamental experiment was done using the model shown in Fig. 3(a) with variable distances between Tx and Rx at 40 kHz. Impulse responses and subtraction between two responses with 1.6- and 3.2-m distances were automatically obtained from the setup of Fig. 2(b). As shown in Fig. 3(b) and (c), we can clearly recognize not only the distances but also the movement from 1.6 to 3.2m. Therefore, when these devices will be mounted on sensor nodes, we will achieve good care environment to monitor the behaviors of elderly and sick people in near future. 1. M. Hikita, Japanese Patent (No. 5442215). 2. T. Sato, Y. Kaneda and M. Hikita in IEEE US Symp. 2014.

(a) Tx and Rx signals at IFFT frequencies

(b) Transmission and reception

(c) Impulse responses for moving object

Fig.1 Distance measurement and movement detection based on IFFT

(a) Sensor-node block diagram with ultrasonic function

(b) Experimental setup with similar performances as (a)

Fig.2 Proposed functional sensor node used in sensor network

(a) Experimental model with variable L

(b) Impulse responses with L= 1.6 and L= 3.2m

(c) Movement detection from subtraction between L= 1.6 and L= 3.2m

Fig.3 Results of fundamental experiment with automatic measurement (40kHz)

8:00 am **Research on Improving the Sensitivity of SAW/GC Gas Sensors**

Jiuling Liu[1], Minghua Liu[1], Shitang He[1]; [1]Institute of Acoustics, Chinese Academy of Sciences, Beijing, China, People's Republic of

Background, Motivation and Objective

The surface acoustic wave (SAW) gas sensors are attractive owing to their small size, low cost, high sensitivity and reliability. A typical SAW gas sensor is composed of a SAW oscillator and a sensitive coating. However, it still suffers from narrow dynamic range, poor noise rejection and detection limit. To overcome such shortcomings of current SAW gas sensors, a SAW/GC Gas Sensor was reported. Many prototypes of SAW gas sensors combined with gas chromatography(GCs) have been developed over the past several decades, and some commercial products have been applied to VOCs detection. However, to the present there is no analysis of SAW device structure influence on GC/SAW detection limit, which hinders further improvement of the sensor performance, so the purpose of this paper is to analyze the response of GC/SAW gas sensor system influenced by the structure of SAW device.

Statement of Contribution/Methods

To achieve a sufficient sensitive area, a three-transducer-structure resonator is used in GC/SAW gas sensors, as shown in Figure 1a. The displacement intensity distributions corresponding to the 1st and 3rd modes are shown in Figure 1b, which roughly illustrates the energy distribution of the resonator. And the greater the energy, the higher the sensitivity of the area of the SAW detector would be. In order to improve the detection performance of the trace gas, this paper proposes to short the resonant cavity of the SAW resonator to concentrate the energy to the central area, and then presents the experimental results.

Results/Discussion

The fabricated SAW device with a short resonator was used in GC/SAW for the detection of dimethyl methylphosphonate (DMMP). Compared with the previous structure, the new SAW resonator structure has a superior performance, as shown in Figure 2.
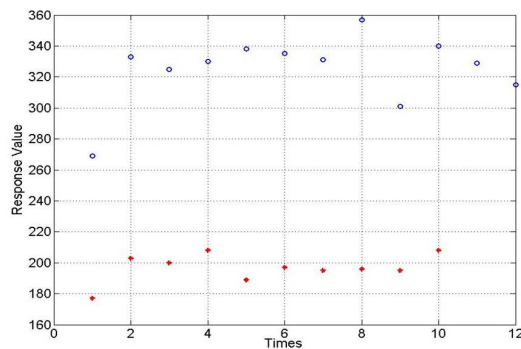
Figure 2. Sensor responses to dimethyl methylphosphonate (DMMP) corresponding to different structures of SAW devices. Circles: the new SAW resonator. Stars: the previous structure
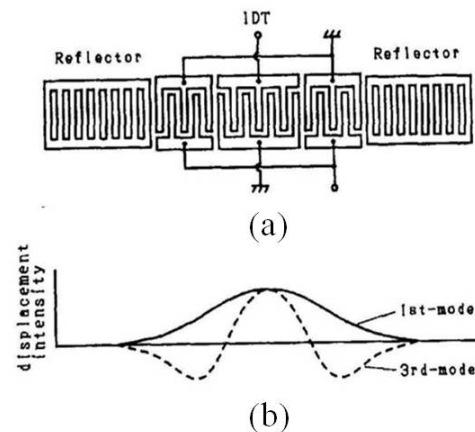
Figure 1. The SAW resonator and the displacement intensity

P2C3-3 _____

8:00 am   Powering autonomous wireless sensors with miniaturized piezoelectric based energy harvesting devices for NDT applications

Claire Bantignies[1], Thien Hoang[1], Hung Le Khanh[1], Guillaume Ferin[1], Etienne Flesch[1], An Nguyen-Dinh[1]; *[1]Advanced Research Dpt., VERMON, France*

Background, Motivation and Objective

IoT (Internet of Things) is getting a very popular research activity field sparking novel consumer applications. It has also an industrial counterpart, where thousands of sensors can be connected together into a proprietary network, i.e. into a Wireless Sensor Network (WSN). Such Industrial WSN may exhibit various shapes for different kind of applications. It can indeed be used for Structure Health Monitoring (SHM) to survey bridges, railways, Tire pressure (TPMS), avionic or automotive structures, rotating machine maintenance prediction, it can also serve security purposes like fire forest detection, frontier survey, etc.

However, the common needs for all these applications lies in the fact that the individual sensors have to be autonomous in energy to power up sensing, computing, storing and finally long or short range RF communicating tasks enabled by components requesting less and less electrical power.

Statement of Contribution/Methods

In this paper we presents the architecture of a miniaturized and low frequency piezoelectric based vibrational energy harvesting device (PEH) and its advanced manufacturing process flow. This harvesting techniques uses direct piezoelectric effect to transform mechanical vibrations in electrical power. Over the past decade, several MEMS architectures have been built and assessed to harvest such low frequency (50-75Hz) vibrations. MEMS based PEH use thin (<5µm) and thick (<50µm) piezoelectric films allowing a high degree of integration and miniaturization, but at low frequency the amount of energy harvested is less than expected and devices are not performing enough to power sensing electronics which typically consumes 100µW in average during 200ms. To overcome this limitation, we have developed and optimized an ultra-thinning process that enable us to use thinned bulk PZT material (<20µm) and propose a performant and miniaturized PEH.

Results/Discussion

We will present and detail the manufacturing process flow of an optimized thinned-bulk bimorph PEH device. This device has been fully characterized in our lab and has exhibited up to 200µW for a uniaxial harmonic vibration of 10 m.s^{-2} of acceleration at 50Hz. The packaged PEH footprint is 35 mm^2 and 3mm thick. This device can be "embedded and forget" into aeronautical structure and power wireless sensors.

P2C3-4 _____

8:00 am   3D Ultrasound Palmprint recognition system based on a mechanically tilted linear probe

Antonio Iula[1], Donatella Nardiello[1], Alessandro Ramalli[2], Francesco Guidi[2]; *[1]University of Basilicata, Potenza, Italy, [2]University of Firenze, Italy*

Background, Motivation and Objective

Biometric applications are increasing dramatically in the last years. The ultrasound technology has some unique peculiarities that allow competing with other established technologies. Fingerprint has been the most explored biometric characteristic by ultrasound research and, nowadays, first commercial devices are going to be introduced in the market.

Recently, some of the authors proposed and experimentally evaluated an ultrasound technique for extracting 3D palmprints. A volume of the human palm was acquired by exploiting a high frequency linear array, which is moved in the elevation direction by a CNC pantograph, and successively post elaborated.

With that approach the 3D profile of the human palm and also 3D information (under skin) of the main traits of the human palmprint were achieved.

In the present work, an alternative approach for achieving volumetric image of the human hand, which exploits a mechanically tilted linear probe instead of the pantograph, is experimentally evaluated.

Statement of Contribution/Methods

An in-house developed hand-holder having guidance marks on it, keeps the volunteer's hand immersed in water, the palm facing upwards. The mechanically tilted linear probe BL433 (Esaote SpA, Firenze) is positioned 30 mm far away the hand surface and is controlled by the ULA-OP research scanner, which is programmed to scan and acquire, in about 3.4 seconds, the echoes from a 3D sector volume. It is composed by 128 frames covering a 50° sector, each of them made up of 160 lines (40 mm) by 512 depths (30 mm), positioned in the center of the hand palm. During the acquisition, the system shows in real-time the central B-mode frame as well as the orthogonal one, computed from the available data-base.

SATURDAY POSTER

Results/Discussion

Examples of 3D and 2D renderings are shown in the Figure. As a first results, this new approach benefits from a simpler set-up, a shorter acquisition time, and a reduced mechanical & electromagnetic noise due to the use of a 3D probe instead of a complex CNC pantograph. The results obtained with the present approach are compared with those achieved with the previous method both qualitatively and quantitatively. The features of the two methods are highlighted and discussed.
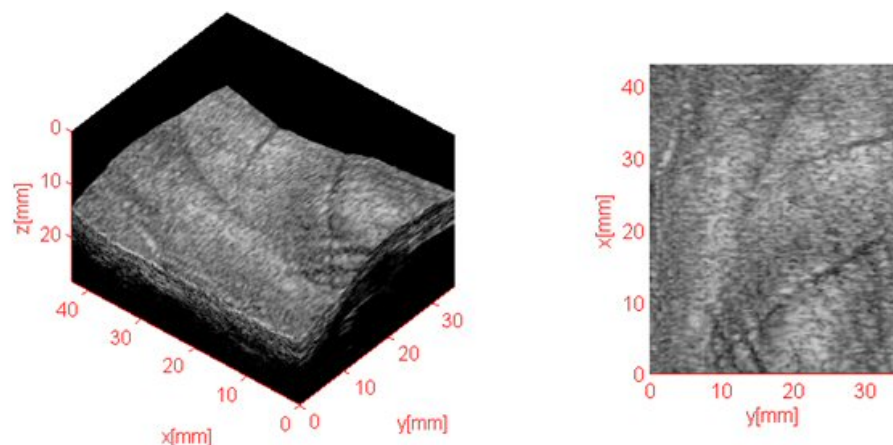
P2C3-5 _____

8:00 am   A three-dimensional, wideband vibration energy harvester using magnetostrictive/piezoelectric composite transducer

Jin Yang[1], Qiangmo Yu[2], Jiangxin Zhao[2], Nian Zhao[2], Yumei Wen[2], Ping Li[2]; *[1]Chongqing University, Shapingba, Chongqing, China, People's Republic of, [2]Chongqing University, China, People's Republic of*

Background, Motivation and Objective

There is growing interest in energy scavenging from vibration sources to power wireless devices. There has been a considerable scientific researches in vibration energy harvesting typically using piezoelectric, electromagnetic or electrostatic transducers. Despite these novel structures, there is still an obstacle facing realistic implementation, because they are deigned to harvest energy in a single vibration direction. Hence, they may not generate power effectively in the case of a motion with multiple or time-variant motion directions.

Statement of Contribution/Methods

Magnetoelectric (ME) transducers were originally intended for magnetic field sensors. Here, we report on a harvester design using ME transducer. The harvester consists of an umbrella-shaped cantilever beam system (USCBS), a ME transducer and a magnetic circuit (Fig.1). The USCBS made of three curved elastic rods is adopted as the only vibrating body. One end of the USCBS is free and can oscillate in arbitrary directions to absorb the external vibration energy. ME transducer is a sandwich of one piezoelectric layer bonded between two magnetostrictive layers. The magnetic circuit is made of a hollow cylindrical magnet within which a smaller cylindrical magnet is coaxially mounted. The external vibration will cause relative motion between the ME transducer and the magnets. In turn, the magnet circuit will produce a magnetic flux gradient through the ME transducer to generate electrical power.

Results/Discussion

Fig. 2 plots the open-circuit voltages of the harvester as a function of the in-plane excitation angles at the acceleration of 0.6 g, which showed that the harvester can scavenge the vibration with arbitrary in-plane angles, and had a bandwidth of 7.5 Hz increased by the nonlinear behavior of the magnetic forces.

P2C3-6 _____
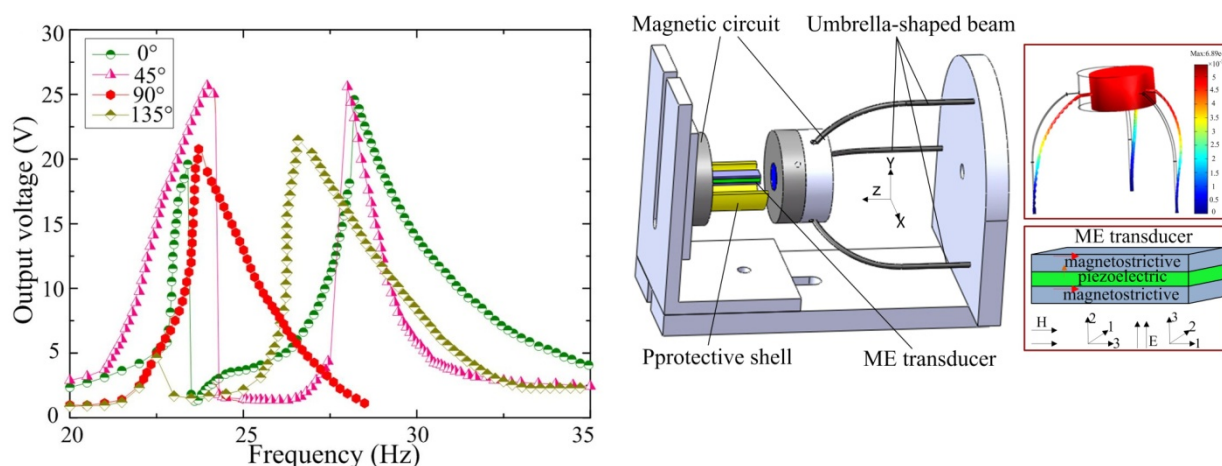
8:00 am   **A Resonant Sensor for Liquid Density Measurement Based on a Piezoelectric Bimorph**

Nicola Lamberti[1], Monica La Mura[1], Valerio Apuzzo[1], Pasquale D'Uva[1], Alessandra Casella[1], Giosuè Caliano[2], Alessandro Stuart Savoia[2]; [1]*DIIn, University of Salerno, Fisciano, Italy,* [2]*Dept. of Engineering, University Roma Tre, Rome, Italy*

Background, Motivation and Objective

Density is one of the characteristic properties of a substance, which can be used to understand other physical and chemical properties. On-line density sensors are of interest in many applications: the radioactive monitoring in waste storage tanks, in pipelines for process control in the petrochemical industry, in the production of chemical reagents, in food processing, in the production of paper and textiles, and so on. In this paper, a piezoelectric density sensor is proposed and analyzed with FE methods. The idea at the basis of the present work relies in the well-known property of piezoelectric structures to vary their resonant behavior depending on load conditions

Statement of Contribution/Methods

The active element of the proposed density sensor is a cheap piezoceramic bimorph, widely used in buzzers and telephone receivers. The bimorph is clamped all around tightening its border to the edge of a rigid open chamber in which the liquid is poured; the resonance flexural frequency of the membrane is modified by the liquid mass. The liquid volume is the volume of the chamber and therefore the membrane resonance frequency is related to the liquid mass density.

Results/Discussion

We analyzed the proposed sensor by a FEM commercial code (ANSYS ®) to test the device capability and to design the chamber in which the liquid is poured, in order to maximize the device sensitivity. Due to piezoceramic membrane (31 mm) and constrain (4 mm) diameters the inner chamber diameter is 27 mm and therefore the volume can be varied only by varying the chamber height. By the ANSYS modal analysis, we computed the sensor resonance frequency by varying the liquid density from 500 kg/m^3 to 1500 kg/m^3 for three different heights h: 2 mm, 7 mm and 25 mm. The obtained results are reported in the figure. As it can be seen, the curves with h=7 mm and h=25 mm show maximum slope, i.e. maximum sensor sensitivity. In order to reduce the device encumbrance we designed the sensor with h= 7 mm obtaining a chamber with a volume of about 4000 mm^3. In figure it also evident a good sensitivity: in the worst case, the device resonance frequency decrease of 42.3 Hz varying the liquid density from 1400 to 1500. Kg/m^3.
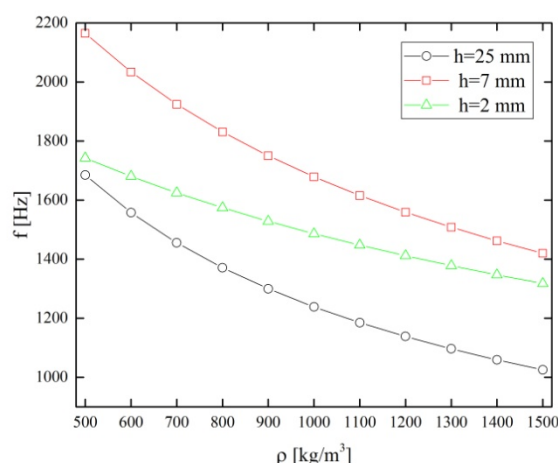
P3C1 - Thin Films

4th floor

Saturday, October 24, 2015, Posters displayed 08:00 am - 05:00 pm. Authors must be present at their poster from 9:30 - 10:30am (odd number posters) and 14:30 – 15:30pm (even number posters).

Chair: **Takahiko Yanagitani**
Waseda University

P3C1-1

8:00 am **c-axis parallel polarity inverted multilayer ZnO film resonators fabricated by grazing ion beam assisted RF magnetron sputtering**

Takeshi Mori[1], Takahiko Yanagitani[2], Masashi Suzuki[1]*; [1]Nagoya Institute of Technology, Japan, [2]Waseda University, Tokyo, Japan*

Background, Motivation and Objective

c-axis parallel ZnO film is attractive for pure shear mode resonator sensors and SH-SAW sensors operating in liquid. Polarization-inverted multi-layer makes it possible to realize high order mode excitation and high power handling. Large sensor area provides a increase of S/N ratio of the sensors. *n*-Fold low capacitance of *n*th polarization-inverted multi-layer enables *n*-fold increase of electrode area in the sensors when capacitive impedance is matched to 50Ω measurement system. In this study, we investigated the piezoelectric properties of polarity inverted multilayer c-axis parallel ZnO films fabricated by grazing ion beam assisted RF magnetron sputtering.

Statement of Contribution/Methods

Single-layered c-axis parallel ZnO film HBAR and polarization-inverted two-layered c-axis parallel ZnO film HBAR were prepared on a silica glass substrate. k_{15} of the single-layered film was determined by comparing experimental conversion loss curve with the theoretical curve simulated by Mason′s equivalent circuit model. Polarization direction of the layers was inverted by inverting the in-plane ion beam irradiation direction.

Results/Discussion

As shown in Fig. 1 (a), impulse response (which is an inverse Fourier transform of S_{11}) of the single-layered films and two-layered films excited only pure shear wave without any excitation of longitudinal wave. The experimental conversion loss curve of single layer HBARs show good agreement with the theoretical one. k_{15} of the film was determined to be 0.19 which is 73% of the single crystalline ZnO (k_{15}=0.26).

As shown in Fig. 1 (b), two-layered film layer excited the 1st mode resonance around 0.52 GHz with suppression of 2nd mode resonance, indicating that polarization direction of the second layer was not inverted to that of the first layer, although in-plane ion beam direction of first layer and second layer was 180° inverted in the film deposition. This may be due to the epitaxial effect of the first layer. To avoid the effect, SiO$_2$ buffer layer was inserted between the first and second layers. Suppression of the 1st mode resonance around 0.50 GHz and 2nd mode resonance around 1.1 GHz were clearly observed as shown in Fig. 1 (b), indicating that polarization direction of the second layer and the first layer are perfectly inverted.
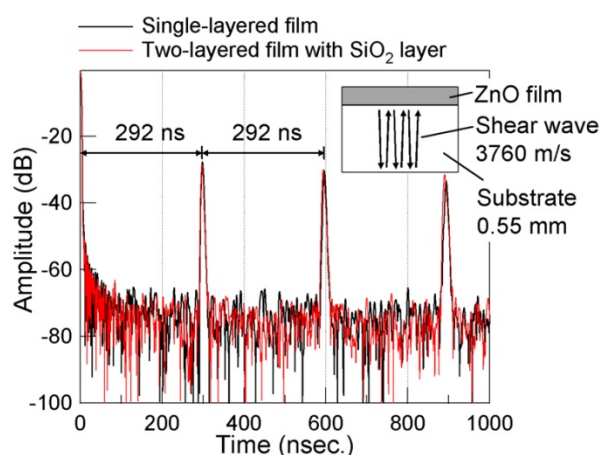
Fig. 1 (a) Impulse response of the c-axis parallel ZnO HBARs (0.55 mm × 2 mm/3760m/s=292.5 ns)
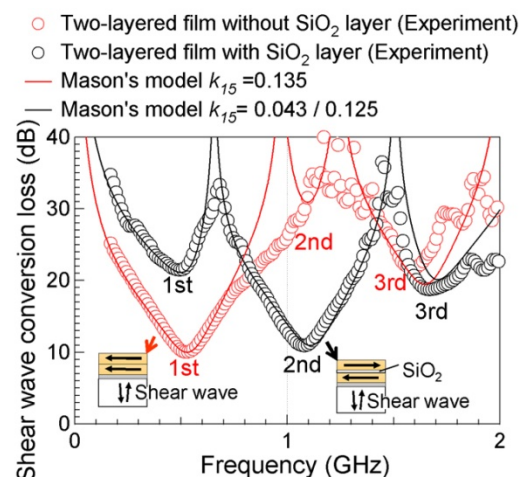
Fig. 1 (b) Shear wave conversion loss of two-layered ZnO film HBARs with and without SiO$_2$ buffer

P3C1-2

8:00 am **Shear mode properties of c-axis parallel oriented Sc$_x$Al$_{1-x}$N films grown by RF bias sputtering**

Shinji Takayanagi[1], Takahiko Yanagitani[2], Mami Matsukawa[1]*; [1]Doshisha University, Kyotanabe, Japan, [2]Waseda University, Tokyo, Japan*

Background, Motivation and Objective

Because of their high piezoelectricity, Sc heavily doped AlN films are attractive for various acoustic wave devices. In particular, c-axis parallel oriented ScAlN films are expected for use as shear mode piezoelectric devices. In previous studies, we demonstrated RF substrate bias RF magnetron sputtering method to fabricate c-axis parallel oriented AlN and ScAlN films [1]. The flux and energy of positive ions which enter the substrate were increased by the RF bias, resulting in the growth of the unusual c-axis parallel oriented films. However, the c-axis randomly oriented in the plane of the film. In this study, we discussed growth conditions of the c-axis parallel oriented ScAlN film including the in-plane c-axis alignment. In addition, piezoelectric properties of c-axis parallel oriented ScAlN films were investigated.

Statement of Contribution/Methods

ScAlN films were grown on Al/silica grass substrates. The distance from the substrate to an Al target was 20 mm. 2 MHz RF bias was supplied to the electrode on which the substrate was set. Sc ingot grains were set on the Al target for Sc doping. We prepared samples with Sc concentrations of 0, 5, 12, and 38%. The crystalline orientations were determined by XRD analyses, and the frequency responses of ScAlN film resonators were measured by a network analyzer.

Results/Discussion

AlN and Sc$_{0.05}$Al$_{0.95}$N films were preferentially oriented in (10-10) plane. An AlN(10-10) XRD peak was not observed in Sc$_{0.12}$Al$_{0.88}$N film, but an AlN(0002) pole was concentrated near ψ=74°, as shown in Fig.1. Therefore, the c-axes of these films were parallel to the substrate plane. Because the AlN(0002) pole was also concentrated near φ=18° in Fig. 1, the c-axis aligned in the in-plane direction. On the other hand, the c-axis of Sc$_{0.38}$Al$_{0.62}$N was not aligned parallel to the substrate plane. A probable reason of this crystalline degradation is oxygen gas desorption from Sc ingot grains. Fig.2 shows the frequency responses of shear mode conversion losses of the samples. The conversion loss of Sc$_{0.12}$Al$_{0.88}$N film was smaller than that of pure AlN film. Smaller conversion losses will be expected in ScAlN films with high Sc concentration if highly-crystallized ScAlN films can be obtained.

[1] S. Takayanagi, et al., presented at IEEE IUS 2012.
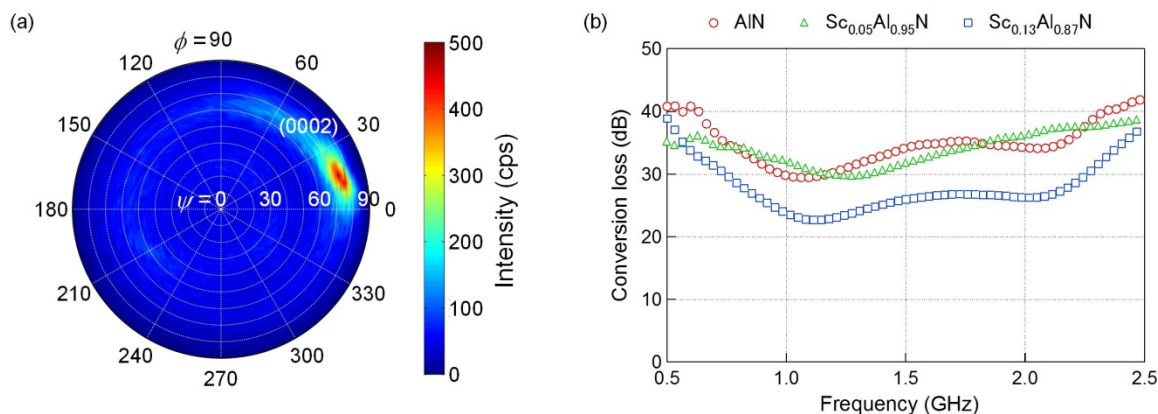
Fig. 1 (a) AlN(0002) XRD pole figure of the Sc$_{0.13}$Al$_{0.87}$N film, and (b) Frequency responses of the Shear-mode conversion losses of the AlN, Sc$_{0.05}$Al$_{0.95}$N and Sc$_{0.13}$Al$_{0.87}$N films.

P3C1-3

8:00 am   Measurement of acoustic wave velocity and refractive index in thickness direction of c-axis oriented ScAlN films by Brillouin scattering

Shota Tomita[1], Takahiko Yanagitani[2], Masashi Suzuki[2], Hayato Ichihashi[1], Shinji Takayanagi[1], Mami Matsukawa[1]*; [1]Doshisha University, Kyotanabe, Kyoto, Japan, [2]Waseda University, Okubo Shinjuku, Tokyo, Japan*

Background, Motivation and Objective

A Brillouin scattering technique (BRS) is proposed for the simultaneous measurement of acoustic wave velocities and refractive indices. This technique is nondestructive and noncontact and can be applied to uniaxial bulk and thin film materials. In this technique, wave velocities in the thickness direction and ordinary refractive index can be observed by a combination of 90R and 180° (90R+180°) scattering geometries. We experimentally confirmed the applicability of this technique to the measurement of c-axis oriented ScAlN films.

Statement of Contribution/Methods

A Tandem Fabry-Perot interferometer (JRS Instruments) and Ar ion laser (Coherent Inc., wave length: 514.5 nm, spot diameter: 50 μm, 187 mW near the sample) were used for BRS. The temperature of the sample was kept at 32±1°C. First, longitudinal wave velocities and ordinary refractive indices were estimated by the combination of 90R+180° scattering geometries. These values were obtained from the Brillouin shift frequencies (BSF) of longitudinal phonons. Next, ordinary refractive indices were again estimated with BSF measured by 90R scattering geometry and reported longitudinal wave velocity measured by HBARs[1]. Then, shear wave velocities were estimated from BSF of shear phonons by 90R scattering geometry and the ordinary refractive index. Here, the c-axis oriented Sc$_x$Al$_{(1-x)}$N films with Sc concentrations (x) of 0-0.63 (thickness ;4 to 5 μm) were used[1].

Results/Discussion

As Sc concentration increased, ordinary refractive indices increased. Fig. 1 shows dependence of longitudinal wave velocity on Sc concentration estimated by 90R+180° scattering geometries. The values of estimated velocities were similar to the reported values and decreased as the Sc concentration increased. However, the uncertainties of the measured velocities and refractive indices obtained by 90R+180° scattering geometries were large. To avoid this problem, we did not use the combination for the estimation of shear wave velocities. Shear wave velocities also decreased with the increase of Sc concentration. These results suggest that wave velocities and ordinary refractive index can be determined by the combination of 90R+180° scattering geometries. However, the large uncertainty should be improved in the next step.

[1] T. Yanagitani and M. Suzuki: Appl. Phys. Lett, 105, 122907 (2014)

SATURDAY POSTER
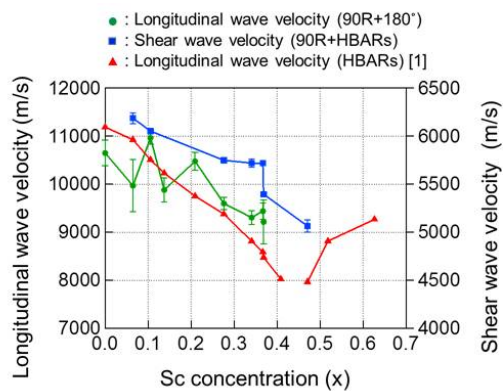
Fig.1 Sc concentration dependence of longitudinal wave velocity estimated by BSF obtained of 90R+180° scattering geometries, and shear wave velocity by BSF obtained of 90R scattering geometry and the ordinary refractive index.

P3C2 - Nonlinear Acoustics II

4th floor

Saturday, October 24, 2015, Posters displayed 08:00 am - 05:00 pm. Authors must be present at their poster from 9:30 - 10:30am (odd number posters) and 14:30 – 15:30pm (even number posters).

Chair: **Takahiko Yanagitani**
Waseda University

P3C2-1

8:00 am **Nonlinear elastic properties of the interface solid - granular unconsolidated media**

Natalia Shirgina[1], Aleksey Kokshaiskiy[1], Alexandr Korobov[1]; *[1]Department of Physics, M.V. Lomonosov Moscow State University, Moscow, Russian Federation*

Background, Motivation and Objective

A number of studies have shown that the boundary of solids has a strong elastic nonlinearity. This nonlinearity is called non-classical (structural) nonlinearity. Structural nonlinearity can be several orders of magnitude higher than the elastic nonlinearity associated with the crystal lattice anharmonicity in solids. Investigation of the interaction of elastic waves at the solid can be applied to the diagnosis of different types of discontinuities: microcracks, delamination in products made of composite materials. The paper presents the results of experimental investigations of nonlinear elastic properties of the interface between solid and granular unconsolidated media.

Statement of Contribution/Methods

The experiments were performed in a system consisting of a flat metal plate and unconsolidated granular medium. Unconsolidated granular medium modeled by a layer of steel balls 2 mm in diameter. Study of nonlinear elastic properties of the interface were carried out using surface acoustic waves (SAW). SAW were excited and detected on the surface of a metal plate by wedge transducers at frequencies of 1.25 MHz and 2.5 MHz. Experimental studies have been performed on automated ultrasonic complex RITEC RPR-5000.

We investigated the effect of the static pressure applied to the interface granular medium - solid, and the effect of amplitude of the probe SAW (frequency of 1.25 MHz) on the velocity of SAW.

Results/Discussion

SAW velocity increases when its pressure decreases at fixed amplitude. SAW velocity change depending on the amplitude and the static pressure were nonlinear.

For a fixed value of the amplitude of the probing SAW on a frequency of 1.25 MHz, we studied the effect of pressure on the efficiency of second harmonic generation of SAW on the frequency 2.5 MHz. According to results of experimental measurements of the amplitudes of the first and second harmonics of SAW at the interface granular medium - solid, we calculated nonlinear elastic parameters of the second order of SAW depending on the external pressure applied to the interface. Nonlinear parameter has features that were caused by changes in the contact elastic nonlinearity associated with changes in the external pressure applied to the interface. The obtained results were analyzed on the basis of the theory of contact acoustic nonlinearity.

This study was supported by the Russian Science Foundation (project [1]14-22-00042).

P3C2-2

8:00 am **Influence of transmission-reception characteristics of ultrasound transducers on statistics of echoes from nonhomogeneous media**

Norbert Zolek[1], Janusz Wojcik[1], Marcin Lewandowski[1]; *[1]Institute of Fundamental Technological Research, Warsaw, Poland*

Background, Motivation and Objective

Analysis of complexity of backscattered ultrasound echoes is an element of parametric characterization of nonhomogeneous media. The statistical parameters of the envelope of echoes can be used for quantitative classification of normal and pathological tissues. Such approach is very sensitive on various subjective parameters not connected with the internal structure of measured medium, e.g. on measured setup. Here we show the theoretical analysis of the influence of the size of transducers on statistics of ultrasound echoes.

Statement of Contribution/Methods

The model used here is based on generalized Helmholtz equation. Model describes insonification of the medium, the scattering in the stochastic medium and detection of echoes. Calculations were made for transducers with radius 1-15 mm as well as for plane wave and point transmission and point detection. Particularly, emitted impulse contained three cycles of 5MHz sinusoid with triangular envelope. Focal point of the transducer was set to 35mm. Two different models of stochastic medium were used. In the first case the positions of scatterers inside the ROI were generated using uniform distribution. In the cell gas model, the ROI was divided into cubic cells. The position of the scatterer in each cell was generated from uniform distribution. Scatterers representing inhomogeneities of material (sound speed and density) were simulated as balls with mean radius 0.05mm. Configuration of the described system is shown in fig.1A. The histograms calculated from envelopes of the echoes were correlated with the histograms of fourier spectra of echoes. The histograms were averaged with respect to 200 random realizations of the medium.

Results/Discussion

For both models of the scattering medium, the decreasing of the median, mean value and variance of amplitude of the signal envelope with increasing transducer size can be observed as it is shown in fig1B. Different echo synthesis methods in multichannel arrays can provide to apertures of different sizes and to different stochastic parametrization of the same medium. The examplary distributions of envelope values for various transducer sizes are shown in fig. 1b. The proposed analytical model allows for estimation of the influence of the subjective elements of the measurement setup (i.e. the transmitted pulse spectrum) on objective information about the measured medium.
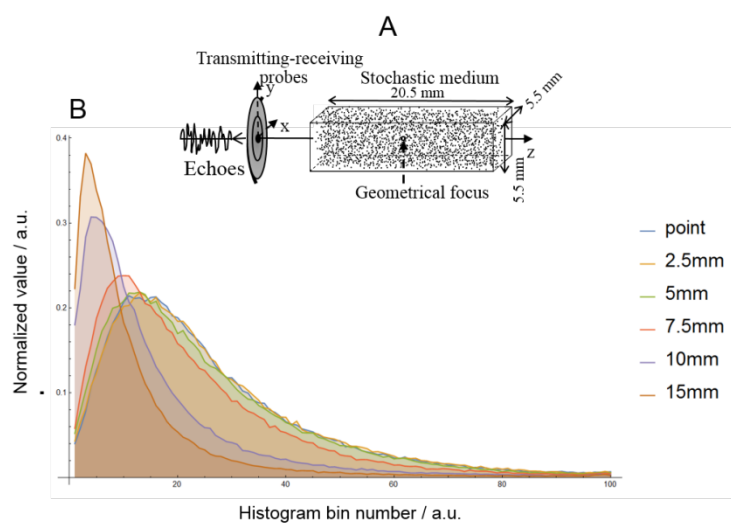
P3C3 - Ultrasonic Motors & Actuators

4th floor

Saturday, October 24, 2015, Posters displayed 08:00 am - 05:00 pm. Authors must be present at their poster from 9:30 - 10:30am (odd number posters) and 14:30 – 15:30pm (even number posters).

Chair: **Takahiko Yanagitani**
             Waseda University

P3C3-1 _____

8:00 am   **Ultra femto-liter mist generation using surface acoustic wave device for sterilization and eradication in the atmosphere**

Tatsuya Sugiyama[1], Takashi Kimura[1], Jun Kondoh[1]; *[1]Shizuoka University, Hamamatsu-shi, Japan*

Background, Motivation and Objective

In a place where a large number of people gather, such as a hospital, transportation facilities, office, and school, sterilization and eradication are important to prevent infection. Nanomaterials, such as gold, platinum, and silver, have been developed. Therefore, it is important to develop a diffusion method of those nanomaterials. Direct diffusion of the nanomaterials is difficult. If the nanomaterials are mixed in a liquid, those are diffused with the liquid, like an atomizer. Generation of mist using ultrasonics is popular and is used for humidification, aromatherapy etc. This purpose is to realize sterilization and eradication. For a medical application, the system will be used with diagnosing instruments. Typical mist diameter using a conventional ultrasonic technology is larger than 30 μm. The instruments may be damaged because of increasing the moisture. As the particle size of the nanomaterials is less than 100 nm, decrease of the mist diameter is required. The mist diameter decreases with increasing the frequency. In this paper, a surface acoustic wave (SAW) is used to generate the mist for sterilization and eradication. Frequency dependence of mist diameter and quantity of mist (mg/10 min) were experimentally investigated.

Statement of Contribution/Methods

The SAW device was fabricated on the 128YX-LiNbO₃. The frequencies of the SAW devices were 13, 50, 96, and 159 MHz. Burst signal was applied to the SAW device. The SAW device was placed on a metal plate. The plate was placed on a liquid vessel. The plate is a cover to avoid spontaneous evaporation. Two holes were bored through the plate. A U-shape filter puts the holes to supply a liquid sample due to a capillary phenomenon. The mist generated was gathered using a thin glass plate, on which silicone oil was covered. The mist gathered was observed with a microscope and the mist diameter was measured. The quantity of mist in 10 min was measured using an electronic balance.

Results/Discussion

Collection time for mist diameter measurement was 1 s. Sample was distilled water. Averages of mist diameters for 13, 50. 96, and 195 MHz SAW devices were 4.67, 3.47, 2.98, and 2.51 μm, respectively. The tendency of the diameter agrees with the Lang   frequency than those diameters for high fre which were estimated from the Lang   μ is difficult with the micros diameter less than measure with another method. Quantity of the mist, which was 16 mg for 13 MHz and 10 mg for 159 MHz, decreases with increasing frequency. This agrees with the tendency of the diameter. Moreover, gold nanoparticles were mixed and atomized. The results show that the nanoparticles were involved in the mist.

P3C3-2 _____

8:00 am   **Study on Achievement of Simultaneous X, Y Movements and Theta Rotation Using Straight-Move Ultrasonic Vibrators**

Toshiaki Sakayachi[1], Yusuke Nagira[1], Mitsutaka Hikita[1]; *[1]Department of GE, Kogakuin University, Tokyo, Japan*

Background, Motivation and Objective

High-performance machines such as optical microscope and direct drawing machine, etc. require very complicated movements to handle objects. In this paper, taking stage of optical microscope as an example (Fig. 1), we have proposed a novel ultrasonic motor to achieve both X- and Y-directional movements and theta-angle rotation simultaneously. Shapes and cut angles of piezoelectric materials and directions of driving electric fields have been investigated to design various movements and rotations in conventional ultrasonic motors. Our proposed motor has a new basic structure constructed with straight-move shafts attached to vibrators. We have also developed peripheral circuits which supply driving voltages with arbitrary amplitudes and phases. Combining above structure and the circuits, small circular / elliptic vibrations for tips of shafts were achieved, which drive the stage to move and rotate simultaneously.

Statement of Contribution/Methods

Straight-movement of back and forth can be achieved by a shaft attached to bimorph (Fig. 2(a)). One unit consists of three x-, y- and z-directional shafts connected perpendicularly to one another (Fig. 2(b)). Arbitrary circular / elliptic vibrations can be synthesized by controlling amplitudes and phases of driving voltages for bimorph vibrators. Three units are arranged at apexes of an equilateral triangle with 120 degree apart to one another (Fig. 2(b)). Discrete circuit technique is used to generate driving voltages in the experiment, because each driving voltage should be controlled independently.

Results/Discussion

Proposed motor constructed with 3 units is illustrated in Fig. 3(a), where a transparent stage is used for experimental convenience. Framework of each unit was made by 3D printer. X, Y movements of the stage were achieved by applying voltages with different amplitudes and phases to all bimorphs. As shown in Fig. 3(b), fundamental operation for movements in X and Y directions was obtained. Theta rotation of the stage was achieved by applying voltages with same amplitude and phase to all x- and y-bimorphs, while different voltages were applied to z-bimorphs. Very clear rotation of the stage was observed as shown in Fig. 3(c). These results suggest the possibility to apply the developed technology to more precise machines. 1. Y. Nagira, T. Sakayachi and M. Hikita in IEEE US Symp. 2014.

SATURDAY POSTER

Fig.1 Requirement for X, Y movements and Θ rotation (Optical microscope)

(a) Straight move of shaft by ultrasonic bimorph vibrator

(b) Fundamental motor structure (Unit: 3 shafts with bimorphs. Motor: 3 units at 120° apart to one another)

Fig.2 Principle of X, Y movements and Θ rotation for stage

(a) Proposed motor constructed with 3 units

(b) X (left), Y (right) movements

(c) Θ rotation

Fig.3 Experimental results of X, Y movements and Θ rotation with fundamental motor

P3C3-3

8:00 am   An ultrasonic motor using transmission line and horn with oblique slits driven by a Langevin transducer.

Takaaki Ishii[1], Souichiro Takehana[1], Tsuyoshi Shimizu[1]; [1]Mechatronics, University of Yamanashi, Kofu, Yamanashi, Japan

Background, Motivation and Objective

An ultrasonic micro-motor usually has small torque because of its small size of the transducer. If the micro-motor is driven by large size transducer, we can expect better motor characteristics. In this research, a Langevin transducer with 30 mm in diameter is used to drive a rotor with 5 mm in diameter.

Statement of Contribution/Methods

The driving vibration excited by the Langevin transducer is amplified by the horn (figure 1), and that vibration is transmitted through the transmission line with 2mm in diameter connected to the top of the horn. The rotor is installed at the top of the transmission line (figure 2). Since the ultrasonic motor needs elliptic locus of the vibration to drive the rotor, a part of longitudinal vibration excited by the transducer has to be converted to the torsional vibration. Six oblique slits made on the horn can convert the vibration mode. Hence the elliptic locus can be excited by the single phase Langevin transducer. The angle, width and depth of the slits are 35 degree, 4 mm and 5 mm, respectively. A radial bearing is used for the rotor and the diameter of the rotor is 5mm. The driving frequency is about 48.9 kHz and the preload by the coil spring is about 6.5 N.

Results/Discussion

Some of the fundamental motor characteristics were obtained as shown in figure 3. The weight in figure 3 refers to the mass wound by the rotor which is equivalent to the torque. The maximum revolution speed of about 102 r.p.m. at applied voltage of 50 Vp-p, the maximum torque of about 86 μNm at 50 Vp-p and 60 Vp-p, and the maximum driving efficiency of about 0.018 % at 40 Vp-p were successfully achieved for the first time.

Fig. 1   Schematic illustration of the horn with oblique slits.

Fig. 2   Picture of the ultrasonic motor using transmission line and horn with oblique slits.

(a)   Weight vs. revolution speed.

(b)   Weight vs. efficiency.
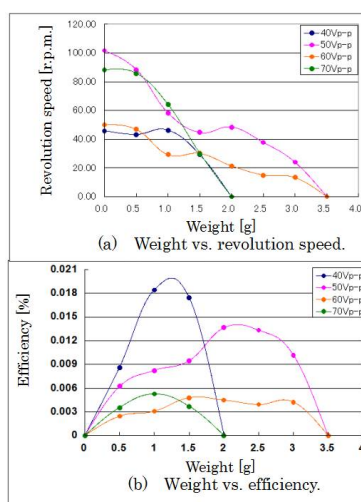
Fig. 3   Load characteristics of the proposed motor.

P3C3-4

8:00 am   An ultrasonic motor using transmission line and spiral structure driven by a Langevin transducer.

Takaaki Ishii[1], Masaki Mochizuki[1], Tsuyoshi Shimizu[1]; [1]Mechatronics, University of Yamanashi, Kofu, Yamanashi, Japan

Background, Motivation and Objective

An ultrasonic motor usually has small torque because of its small size of the transducer. If large sized transducer is used for driving small sized output part, we can expect better motor characteristics. In this research, a Langevin transducer with 30 mm in diameter was used to excite the driving vibration and its vibration was transmitted through the transmission line of 1 mm in diameter. A radial bearing is used for the rotor and its outer diameter is 5mm.

Statement of Contribution/Methods

The driving vibration excited by the Langevin transducer is amplified by the stepped horn and that vibration is travelled through the thin transmission line of 1 mm in diameter (figure 1). Since an ultrasonic motor needs elliptic motion to drive the rotor, part of the longitudinal vibration has to be converted to the torsional vibration. Spiral structure is used to convert the vibration mode as shown in figure 2. A coil spring is used for mode conversion and preload is provided by this spring at the same time. The outer diameter of the spring, line diameter of the spring and the spring coefficient are 5 mm, 0.7 mm and 6.474 N/mm. The driving frequency is about 47 kHz and the preload by the coil spring is about 13 N. The rotation of the rotor was successfully achieved.

Results/Discussion

Some motor characteristics were obtained for the first time as shown in figure 3. The maximum revolution speed was 147 r.p.m. at applied voltage of 60Vp-p, the maximum torque was 0.061 mNm at applied voltage of 60 Vp-p, and the maximum efficiency was 0.0059 % at applied voltage of 50Vp-p.
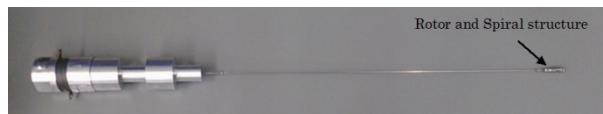
Fig. 1 Picture of the ultrasonic micro-motor with spiral structure.
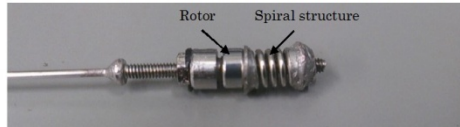
Fig. 2 Picture of the rotor and the spiral structure.
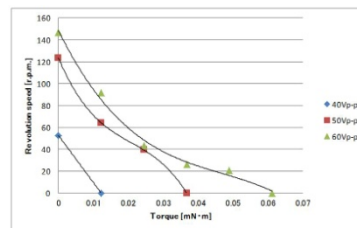
(a) Revolution speed vs. torque.
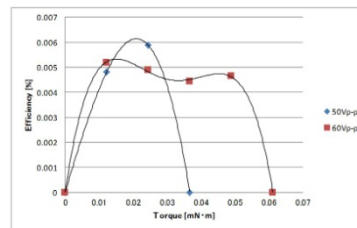
(b) Efficiency vs. torque.

Fig. 3 Load characteristics of the proposed motor.

P3C3-5

8:00 am   Precise Positioning Characteristics of Multi-Mode Ultrasonic Motor

Masaya Takasaki[1], Shuo Zhang[1], Masayuki Hara[1], Daisuke Yamaguchi[1], Yuji Ishino[1], Takeshi Mizuno[1]; *[1]Dept. Mechanical Eng., Saitama University, Saitama, Japan*

Background, Motivation and Objective

We have developed multi-mode ultrasonic motor, which consisted of coupling of two Langevin type ultrasonic transducers as a stator and a rotor. The motor requires driving voltages at different frequencies for actuation as an ultrasonic motor. Additionally, stick-slip driving mode and DC voltage driving mode are available for the motor as precise positioning function. We expected fine positioning by deformation of piezoelectric element with applied voltage. The range of the DC mode was around 50 nm with applied voltage range of -150 V - +150 V. This meant that positioning accuracy of stick-slip mode should be within the range. In our previous work, speed control of the stick-slip driving mode was succeeded with continuous saw-tooth wave form. On the other hand, positioning accuracy in stick-slip driving mode was much longer than the range, because sudden stop of the driving resulted in very rough positioning due to inertia of the rotor. Alternative positioning by stick-slip driving mode is desired to overcome this problem.

Statement of Contribution/Methods

To realize more precise positioning in the stick-slip driving mode, individual (not continuous) saw-tooth wave form was considered. In this case, much higher driving voltage should be applied, because resonance of a Langevin type transducer was involved to realize stick-slip driving in the previous work. To establish saw-tooth wave form motion at driving point, resonance of the piezoelectric actuator should be avoided. Therefore, we installed high voltage amplifier and employed individual long term saw-tooth wave form to be applied to the actuator. As a result, we can expect repeating of drive and stop of the rotor motion and precise positioning with feedback control, although it takes longer time to complete positioning.

Results/Discussion

Installing a high voltage amplifier (HVA4321), range of applied voltage was more than 3 kV. The output was connected to the Langevin transducer directly. (Previously, a transformer was installed to acquire higher voltage.) Applying 10 ms length single saw-tooth wave form at 2 kVp-p with interval of 1500 ms, rotor step motion of 126 nm in average was successfully observed. We analyzed 62 steps of the motion and obtained histogram of the step length. The length was distributed in the range from 110 nm to 145 nm. Changing amplitude of the applied wave form, the step length was reduced down to 60 nm with 1.55 kVp-p. On the other hand, displacement range of 100 nm was observed with applied DC voltage at 3 kV. This means that it is possible to position the rotor into the range of DC driving mode with stick-slip driving mode. Final positioning control with precision displacement sensor will be our future work.

P3C3-6

8:00 am   Research on a vibration induced low friction pneumatic actuator with radial-direction vibration mode

Han Gao[1], Jun Wang[2], Marius Nabuurs[2], Jun Qian[2], Gang Bao[1], Michaël De Volder[2], Dominiek Reynaerts[2]; *[1]Harbin Institute of Technology, China, People's Republic of, [2]Katholieke Universiteit Leuven, Belgium*

Background, Motivation and Objective

Pneumatic actuators are commonly used in industry. The seal rings comprised in these actuators introduce friction and affect the positioning accuracy and output force. The friction reduction effect in presence of vibration had been proved for decades, and it recently arouses an interest in pneumatic field. It is revealed that there is a good friction reduction effect when the ultrasonic vibration is introduced to pneumatic cylinders. Consequently, this research will discuss the friction reduction phenomena, generated by longitudinal vibrations of piezo stacks located circumferentially around the seal house.

Statement of Contribution/Methods

This research proposed a novel vibration mode on the friction reduction effect in pneumatic actuators. The vibration is generated by 4 tiny piezo stacks directly to the seal house part. In addition, a tribometer is developed for the tribology investigation for the prototype.

SATURDAY POSTER

Results/Discussion

On account of the vibration generated on the seal house, the friction of the pneumatic actuator has a satisfying reduction.
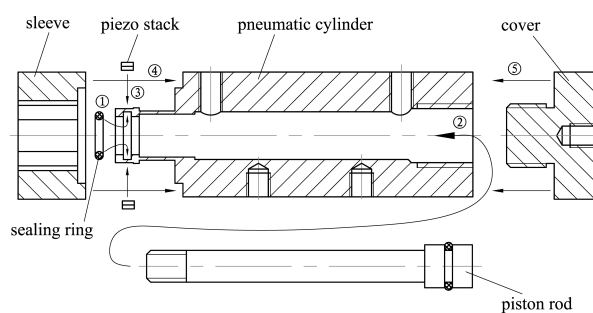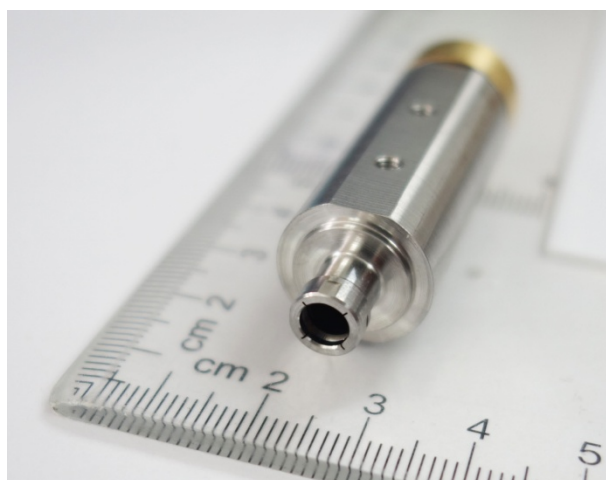
P5C1 - Front-End and Integrated Electronics

4th floor

Saturday, October 24, 2015, Posters displayed 08:00 am - 05:00 pm. Authors must be present at their poster from 9:30 - 10:30am (odd number posters) and 14:30 – 15:30pm (even number posters).

Chair: **Christine Démoré**
           University of Dundee

P5C1-1

8:00 am   A feasibility study for arbitrary waveform generator using on-off pulses and modified PWM waveforms in the front-end circuit integrated with 2D array transducer

Bae-Hyung Kim[1], Seungheun Lee[1], Kangsik Kim[1]; *[1]Ultrasound R&D Group, Samsung Electronics Co., Ltd., Seoul, Korea, Republic of*

Background, Motivation and Objective

In this paper, a feasibility study for arbitrary waveform generator (AWG) using on-off pulsers in front-end ASICs integrated with 2D array is introduced. It is a challenge to include higher performance AWG in the ASIC using digital to analog converters and linear power amplifiers due to its issue in size and power consumption. Thus we consider a modified pulse width modulation (PWM) technique using only on-off pulsers to transmit an arbitrary waveform.

Statement of Contribution/Methods

In our approach, a PWM waveform is firstly generated by modulating the pulse-width according to the amplitude of an original signal, and then a modified PWM waveform is finally generated by summing the firstly generated PWM waveform and its time-shifted waveforms. In this paper, transmission signals using uni-polar and bi-polar pulsers, and the modified PWM waveforms are theoretically analyzed and investigated in terms of the frequency characteristic, the transmission power efficiency (TPE) that shows the pulse-shaping capability of the generated waveform by defining the ratio of its output and input power through a given transducer, and the gain in signal-to-noise ratio (GSNR) that indicates an improvement in the penetration depth of an image. The simulation study are conducted to investigate the modified PWM waveform using bi-polar and uni-polar pulses which is generated from the original waveform of 3MHz sine wave with hamming window, and its frequency response. The B-mode image simulation studies using Field II are also included to see the influence of the transmission waveforms. In the experimental study, the feasibility test using ASIC simulation is shown to compare the 3MHz on-off pulsed waveform and 3MHz sine waveform generated from the modified PWM waveform using on-off pulsers.

Results/Discussion

The simulation results demonstrate the frequency characteristic of the modified PWM waveform is superior in terms of TPE and pulse-shaping capability. As shown in Fig. 1, the experimental results show that the power consumption of the modified PWM waveform is about 25% lower than classical PWM and on-off pulserd waveforms. This feasibility study demonstrates that the transmitter architecture using only on-off pulses and the modified PWM waveform is able to be adopted to reduce the size and power consumption of the front-end system.
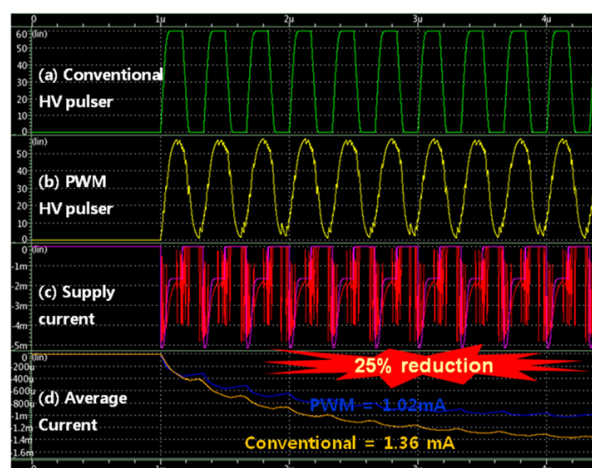
Fig. 1. ASIC test results: (a) 3MHz on-off pulsed waveform using conventional high-voltage pulser, (b) 3MHz sine waveform generated from PWM using on-off pulsers, (c) Power supply current, (d) Average current of the power supply.

P5C1-2

8:00 am   Real time autofocusing hardware for ultrasonic imaging with interfaces

Jorge F. Cruza[1], Luis Medina-Valdes[1], Carlos Fritsch[1]; *[1]Ultrasonic Systems Group, Spanish National Research Council (CSIC), Madrid, Madrid, Spain*

Background, Motivation and Objective

Imaging of arbitrarily shaped components demands a new set of focal laws for every change in the array-part geometry. The process is currently carried out off-line and requires an accurate geometric description. However, along a scan, geometry may change in an uncontrolled way and the nominal focal laws are not optimal. The main objective of this research is to find new techniques to obtain the set of focal laws adapted to unknown probe-part geometry in real-time at high frame rates (up to 500 images per second).

Statement of Contribution/Methods

Our group had previously proposed several techniques that provide automatic dynamic depth focusing (DDF) through interfaces [1-2]. But, although these procedures work well, they are not fast enough (about 2 seconds) to adapt to rapid geometric changes along a scan. In this work we propose a software-hardware approach that performs automatically all the functions required for auto-focusing with DDF at very high speed: 1) interface geometry estimation, 2) accurate focal law computing and 3) programming of DDF hardware.

SATURDAY POSTER

To this purpose, hardware design is based on High Level Synthesis (HLS) tools, which map software algorithms to synthesizable implementations in FPGAs. The adopted methodology uses time-of-flight (TOF) measurements to estimate the actual probe-part geometry, computes a virtual array operating in the second medium only and obtains the initial parameters for DDF hardware. The intermediate virtual array avoids the complications introduced by refraction at the interface, while keeping a high timing accuracy.

Results/Discussion

The proposed technique has been implemented in a SoC-FPGA platform, where software procedures (mainly geometry estimation) are combined with other implemented in hardware (virtual array computing, parameter setting and DDF execution). All processes perform in real-time, allowing up to hundreds adapted frames per second of linear scan, sectorial scan or TFM image modes. Our proposal avoids any geometric description or additional software to compute the optimal focal laws.

References:

[1] J. Cruza et al.,"New method for real-time dynamic focusing through interfaces", IEEE UFFC, 60-4, 739-751, 2013

[2] J. Camacho et al., "Automatic Dynamic depth focusing for NDT", IEEE UFFC, 61-4, 673-684, 2014
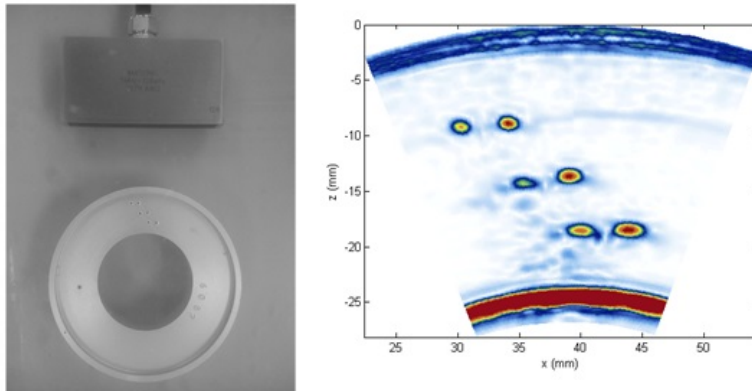
Left: Experimental arrangement, aluminum ring with 3 rows of pairs of side drilled holes. Right: Linear scan image after the auto-focusing process.

P5C2 - Transducer for Imaging and Diagnosis

4th floor

Saturday, October 24, 2015, Posters displayed 08:00 am - 05:00 pm. Authors must be present at their poster from 9:30 - 10:30am (odd number posters) and 14:30 – 15:30pm (even number posters).

Chair: **Christine Démoré**
           University of Dundee

P5C2-1 _____

8:00 am   Acoustic Characterisation of a PZT Matrix With Integrated Electronics for a 3D-TEE Probe

Shreyas Raghunathan[1], Chao Chen[2], Maysam Shabanimotlagh[1], Zhao Chen[2], Sandra Blaak[3], Zili Yu[2], Christian Prins[3], Michiel Pertijs[2], Johan Bosch[4], Nico de Jong[1,4], Martin Verweij[1,4]; [1]*Lab of Acoustic Wavefield Imaging, Delft University of Technology, Netherlands,* [2]*Electronic Instrumentation Lab., Delft University Of Technology, Netherlands,* [3]*Oldelft Ultrasound, Netherlands,* [4]*Dept. of Biomedical Engineering, Erasmus Medical Centre, Netherlands*

Background, Motivation and Objective

We evaluate the acoustic performance of a prototype PZT matrix for a miniature three-dimensional (3D) transesophageal (TEE) probe with a low-power co-integrated ASIC (Application-Specific Integrated Circuit) that would be suitable for use in neonates or for permanent transnasal use in adults.

Statement of Contribution/Methods

The prototype consists of a 9x9 PZT matrix directly mounted on an ASIC with 81 inputs, divided into 9 sub-groups of 3x3 elements each. The sub-groups are micro-beamformed, i.e. after low-noise amplification with a programmable gain, signals from 9 individual elements are properly delayed in the ASIC and coherently summed up, thus reducing the channel count by a factor of 9. The individual elements are designed for a resonant frequency around 5-6 MHz and a bandwidth of 50%. The prototype has been tested in a water tank to determine the performance of the micro-beamformer (capability to observe reflections from 0,17, and 37 degrees), the frequency response of the sub-groups, the dynamic range and the minimum detectable pressure.

Results/Discussion

Measured beam profiles of the micro-beamformer in a 3x3 sub-group, provided with appropriate delay settings, demonstrate that it can be steered to angles of 0, 17 and 37 degrees. This agrees with the analytical solution for the directivity of a 3x3 array, as shown in Figure 1(a)-1(c). On steering to an angle of 37 degrees the side-lobes become significant for a 3x3 sub-group due to the small aperture size, which is mitigated for a larger aperture. The frequency response of both a single element and a 3x3 subgroups have a central frequency of 5.5 MHz and bandwidth of 54%, see Figs. 1(d) and 1(e). The dynamic range of a sub-group, defined as the ratio between the maximum and the minimum detectable pressure, is around 80 dB, as shown in Fig. 1(f). The minimum detectable pressure is about 20Pa for a 3-cycle 5MHz excitation with the gain of on-chip amplifiers set to the highest level (60dB).

The results of the acoustic tests of the PZT matrix-on-ASIC conform to the design considerations. Proper sub-array beamforming has been demonstrated, as well as the capability to detect pressures down to 20 Pa, making the approach a promising candidate for future miniature 3D TEE probes.
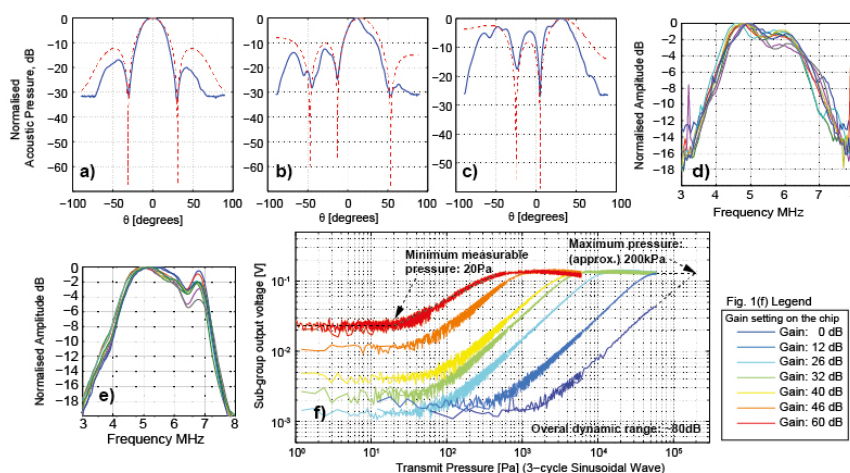
a) - c) Comparison of beam profile for a 3x3 subgroup (solid blue: Measured, dashed red: Theory) for steering angles of 0,17 and 37 degrees.
d) Frequency response of 9 individual elements; e) Frequency Response of the 9 3x3 sub-groups f) Dynamic Range of the chip.

P5C2-2 _____

8:00 am   Dual frequency IVUS array for contrast enhanced intravascular ultrasound imaging

Zhuochen Wang[1], Wenbin Huang[1], Karl Heath Martin[2], Paul A. Dayton[2], Xiaoning Jiang[1]; [1]*North Carolina State University, USA,* [2]*University of North Carolina, USA*

Background, Motivation and Objective

Recent studies suggest that contrast ultrasound for molecular imaging or microvascular imaging for vasa vasorum assessment can be promising in identification of vulnerable plaque. However, conventional intravascular ultrasound (IVUS) transducers with frequency of 20 MHz-60 MHz are not optimized for imaging with microbubble contrast agents due to the less effective micro-bubble excitation at high frequencies. Our prior work has shown that high performance contrast imaging can be achieved using transducers which excite microbubbles near resonance and can receive higher order harmonics. Our group reported initial successes last year in developing a 6.5 MHz/30 MHz single element IVUS transducer and an IVUS array transmitter (8 elements at 2.25 MHz) for contrast enhanced IVUS imaging. In this paper, we demonstrate the capability of a dual-frequency IVUS array for nonlinear contrast detection. The prototype transducer topology consists of a receiving array (32-element, 30 MHz) built on the top of transmitting array (8-element, 2.25 MHz) to achieve super harmonic contrast enhanced imaging.

SATURDAY POSTER

Statement of Contribution/Methods

This dual frequency IVUS array consists of an 8-element 2.25 MHz lead magnesium niobate-lead titanate (PMN-PT) single crystal transmitting array and a 32-element 30 MHz high frequency receiving array. A frequency selective isolation layer and the flex circuit of high frequency receiving array are placed between two PMN-PT layers. The dimension of the transmitting element is $5 \times 0.37 \times 0.3$ mm, and it is $0.5 \times 0.37 \times 0.06$ mm for the high frequency receiving elements. After fabrication, the dielectric loss and capacitance of every element was measured. The prototyped dual-frequency IVUS array was then acoustically characterized using pulse-echo measurements for the receiving array while the transmitting array was evaluated by hydrophone measurements of the pressure field. Contrast tests were performed either in a water bath or in a tissue mimicking phantom by exciting microbubbles flown through a cellulose tube (200 μm Ø) using the 2.25 MHz transmitting array while detecting the microbubble super harmonics using the 30 MHz receiving array. The receiving elements were connected to a Verasonics System (Vantage 256 TM, Verasonics, Inc., Kirkland, WA) for the contrast tests.

Results/Discussion

Initial characterization results show that the capacitance and dielectric loss of the receiving elements are 52.5 ± 3.5 pF and 0.024 ± 0.003, respectively; while those of transmitting elements are 177.7 ± 3 pF and 0.022 ± 0.004, respectively. The center frequency of the receiving array is 28 MHz $\pm$ 1.1 MHz with a bandwidth of 41 % $\pm$ 7%. The transmitting elements can be used to produce acoustic pressure > 3 MPa at 100 V excitation, which is enough to induce non-linear response from microbubbles. The contrast imaging tests using the prototyped dual frequency array is being performed and the details will be reported in the full paper.

P5C2-3

8:00 am   A simulation frame work to optimize volumetric cardiac imaging on a multiplexed system

Carolina Vallecilla[1], Alejandra Ortega[1], Martino Alessandrini[1], Jan D'hooge[1]; *[1]Cardiovascular Imaging and Dynamics, KU Leuven, Leuven, Belgium*

Background, Motivation and Objective

Commercial volumetric cardiac ultrasound systems make use of two-stage beam forming in order to limit the wiring and the number of channels. However, for maximal beam forming flexibility, fully wired systems are preferable but expensive. Multiplexed systems offer an attractive solution with a fully wired matrix probe but limited number of channels. Although such systems allow to capture data from all elements by repeating the transmit event and switching between elements, this process can induce artifacts when imaging moving objects. Similarly, these systems allow to control all array elements on transmit but not fully independent thereby constraining the generated acoustic fields. The aim of this work was therefore to develop a simulation frame work to optimize the transmit multiplexing scheme for cardiac imaging.

Statement of Contribution/Methods

The frame work consists of three steps: 1) definition of the system configuration, 2) an ultrasound simulator, and 3) an objective function to be minimized. In 1) a 32x32 element matrix probe (2.5MHz, 1x1cm2) to be connected to 256 channels using a 1:4 transmit Mux was defined. Hereto, 4 elements were randomly selected from a predefined sub-aperture (4x4 or 8x8) and connected to the same transmit channel. Each element of a group was switched off with a likelihood of 10%. The transmit amplitude and phase of each group was defined as the mean and median respectively of the values used on a fully wired system. This grouping process was repeated until all elements were connected. The defined configuration was used to simulate its transmit field in Field II (in a plane orthogonal to the transmit direction) when focusing at 6 cm. The sum of squared differences of the obtained pressure field with the one from the fully wired configuration was used as a similarity metric. The above process was repeated until a threshold was reached.

Results/Discussion

An example of the time delays for a given configuration, the associated apodization function and the resulting sound field are given in the Figure. With a multiplexed array of 923 elements the transmitted energy lower but focused in a narrower main lobe with a side lobe reduction of 6 dB compared to the full array. Future work focuses on optimizing the multiplexing process for other steering directions. The proposed frame work could easily be modified for other multiplexed-based systems.
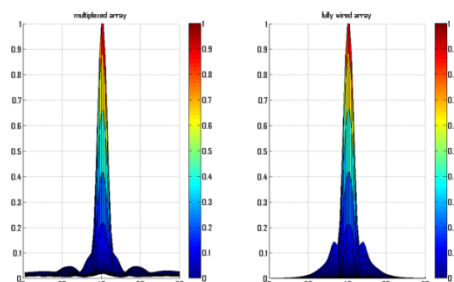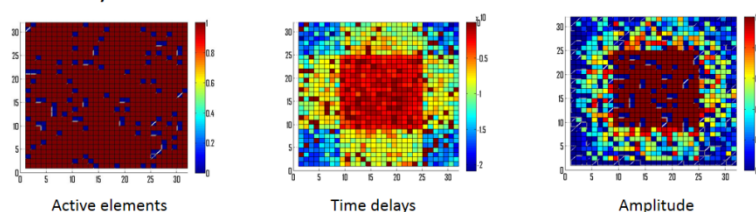
P5C2-4

8:00 am   Press-focused 226MHz Ultrahigh Frequency Ultrasound Transducer for Programmable Particle Manipulation

Ming Qian[1], Ying Li[2], Qifa Zhou[2], K. Kirk Shung[2], Hairong Zheng[1]; *[1]Shenzhen Institutes of Advanced Technology, Chinese Academy of Sciences, China, People's Republic of, [2]NIH Ultrasonic Transducer Resource Center and Department of Biomedical Engineering, University of Southern California, USA*

Background, Motivation and Objective

Noncontact and precise manipulations of micro particles have many biophysical applications. The optical tweezers use a tightly focused optical beam to manipulate particles. However, relatively small trapping force, possible damage to biological samples, and being not applicable to optically opaque particles limit their usage. A single acoustic beam can be used to trap individual particles without damage. To allow precise trapping of particles at the cellular level, highly sensitive ultrahigh frequency (UHF) ultrasonic transducers should be developed so as to reduce the beam width.

SATURDAY POSTER

Statement of Contribution/Methods

A UHF transducer was fabricated using with $LiNbO_3$ single crystal. The backing material of conductive silver epoxy was cast onto a gold-electroplated $LiNbO_3$ plate. After lapping the backing layer, the front side was lapped to 17 mm. The sample was diced into 0.5*0.5 mm^2. A lead wire was connected to the backing layer of using conductive epoxy. The acoustic stack was concentrically assembled in brass housing with an insulating epoxy. The stack was press-focused at focal length of 0.5 mm. Chrome/gold layers were sputtered onto the transducer surface to make connection between the stack and the housing. A thin parylene layer was deposited on the front face to serve as an acoustic matching layer and a protection. The transducer was assembled in an SMA connector for further experiments.

Results/Discussion

The pulse-echo response and frequency spectra of the LiNbO3 transducer are shown in Figure A and B. The peak-to-peak voltage was about 50mV without gain. The focal depth was 0.46mm. Thus, the f-number is less than 1. It was found that the center frequency of the transducer was around 226.6 MHz and the -6 dB bandwidth was determined to be 39.2%. The capability of this 226-MHz UHF transducer in trapping a single microsphere of 5¦lm was demonstrated. Figures C and D showed the experimental setup. The transducer was driven by a sinusoidal burst of 226 MHz, a driving voltage of 30 Vpp, a duty cycle of 0.2% and a pulse repetition frequency of 1 kHz. It was observed that a single 5¦lm microsphere was manipulated along with the movement of the microbeam device at a programmable trajectory. As shown in Fig E, the microsphere moved at a trajectory of ¡°USC¡±. In conclusion, the 226MHz UHF transducer was successfully made and used to trap micro-sized particles to move in programmable trajectory.
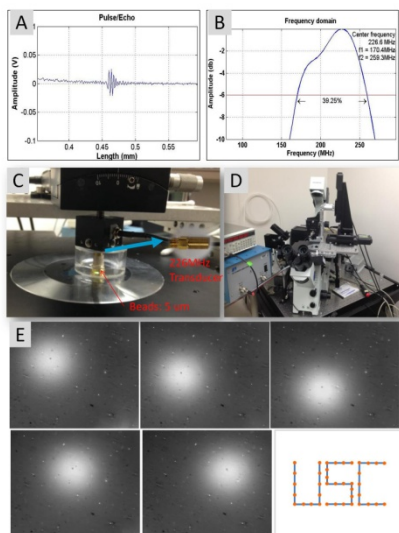
P5C2-5 _____

8:00 am   The Effect of the Transducer Parameters on Spatial Resolution in Plane-Wave Imaging

Zainab Alomari[1,2], **Sevan Harput**[2], Safeer Hyder[2], Steven Freear[2]; [1]*Electronics Engineering College, Mosul University, Mosul, Iraq,* [2]*School of Electronic and Electrical Engineering, University of Leeds, Leeds, United Kingdom*

Background, Motivation and Objective

Plane-Wave imaging (PWI) can produce a complete image after a single transmission of an unfocused ultrasound beam, and therefore can achieve ultrahigh frame rates of thousands frames per second. Many ultrasound imaging applications, such as elastography, require ultrahigh frame rates. However, due to the lack of a focusing point in PWI, it is not possible to derive an expression for the spatial resolution based on the f-number. This work studies the transducer parameters that affect the imaging quality in PWI and summarises their relation with a mathematical expression.

Statement of Contribution/Methods

The parameters whose effect is studied in this work using Field-II are the imaging depth, central frequency, bandwidth and the transducer width and number of elements. The image quality is assessed based on the spatial resolution, which is the minimum distinguishable distance between two points located in the axial and lateral directions. The resolution was measured at the -6dB intensity drop, for an array transducer with number of elements varying from 10 to 256, a frequency range of 1 to 30MHz, bandwidth of 10 to 100%, a total aperture width of 3 to 80mm and an imaging depth of 1 to 200mm. Afterwards, using Matlab curve fitting tool, a mathematical expression was derived that best explains the relation between the resolution and the varying transducer parameters.

Results/Discussion

The results that show how spatial resolution in PWI is affected by each transducer parameter are presented in table 1. From these results, it is concluded that selecting an imaging probe with higher bandwidth, central frequency, number of elements and total width will provide a better lateral resolution in PWI. Despite introducing grating lobes, which may eventually affect the resolution, the inter-element spacing is found to have no direct effect on resolution, where it increased with increasing the transducer width and decreased with increasing the number of elements, and in both cases the lateral resolution was improved.

Parameter	Lateral Resolution Proportional to:	Axial Resolution Proportional to:
Central Frequency (f_0)	$\dfrac{1}{f_0}$	Negligible change
Bandwidth (BW)	Negligible change	$\dfrac{1}{BW}$
Number of elements (N)	$\dfrac{1}{N}$	Negligible change
Total Aperture Width (Wt)	$\dfrac{1}{Wt}$	Negligible change
Imaging Depth (Z)	Z	Negligible change

Table 1. The effect of the Transducer Parameters on Spatial Resolution in PWI

P5C2-6

8:00 am   **Fabrication and Characterisation of Miniature Parabolic Acoustic Lenses**

Erwin J Alles[1], Daniil Nikitichev[1], Adrien E Desjardins[1]; *[1]Department of Medical Physics & Biomedical Engineering, University College London, London, United Kingdom*

Background, Motivation and Objective

Due to its small dimensions, an all-optical ultrasound probe consisting of two optical fibres for ultrasound transmission and reception is well suited for high-frequency interventional imaging. However, the same small dimensions result in a divergent acoustic source, and consequently lead to clutter and loss of sensitivity in 2D images acquired through in-plane probe translation. These limitations can be addressed by focussing the generated ultrasound into the image plane, which can be achieved with miniature (mm-scale) acoustic lenses. For 2D imaging, such lenses preferably have parabolic surfaces, which complicates their fabrication. In this work, two novel methods for fabricating miniature aspherical acoustic lenses are tested: laser cutting and 3D printing.

Statement of Contribution/Methods

The lenses were either laser-cut from PMMA (c = 2750 m/s, α = 0.5 dB/MHz/cm at 20 MHz), or 3D-printed in VeroWhitePlus (VWP, c = 2490 m/s, α = 4.0 dB/MHz/cm). These materials were chosen due to their favourable acoustical properties and compatibility with the fabrication techniques. A genetic algorithm was used in conjunction with an acoustic model to optimise the design of a lens with a fixed focal length of 4.5 mm. Different designs were obtained and fabricated for the two materials, and the resulting lenses were characterised through acoustic field measurements in terms of focus quality, amplitude and bandwidth.

Results/Discussion

The fractional bandwidth achieved through a PMMA lens (109% around 11MHz) was wider than the one achieved through a VWP lens (90% around 10 MHz). In addition, for both lenses a higher pressure was achieved within the focal region compared to that achieved in the absence of a lens, despite the reflection losses at the lens surfaces. The focal width for both lenses measured approximately 0.6 mm at a distance of 8.5 mm from the source fibre, as is visible for a PMMA lens in the figure below. Thus, at a centre frequency of 10 MHz the acoustic energy is effectively confined within a narrow plane using acoustic lenses produced through both laser-cutting from PMMA and 3D printing in VWP. PMMA lenses exhibit lower attenuation despite bubble formation during cutting, while VWP lenses have shapes that follow the lens design more closely. In addition, VWP lenses can in principle be fabricated with more complex curvature, allowing for a wider range of applications.
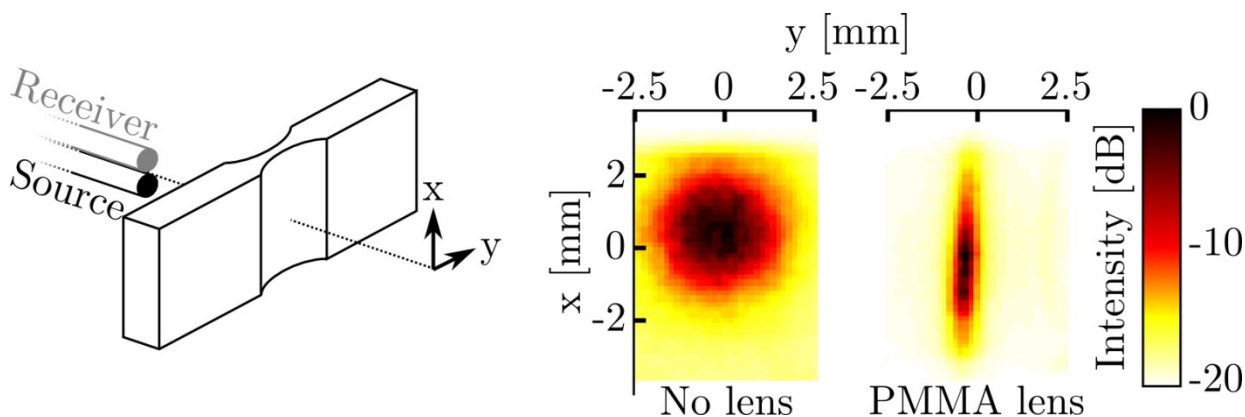
P5C2-7

8:00 am   **Design of linear array transducer using inversion layer for ultrasound harmonic imaging**

Chan Yuk Park[1], Jin Ho Sung[1], Jong Seob Jeong[1]; *[1]Medical Biotechnology, Dongguk University, Gyeonggi-do, Korea, Republic of*

Background, Motivation and Objective

It has been well known that the inversion layer method can increase a center frequency and a bandwidth of the ultrasound transducer by controlling poling direction of piezoelectric materials. There are two kinds of inversion layer methods such as back-side and front-side inversion, and typically LiNbO$_3$ has been used for the performance demonstration. In this study, we applied this technique to the design of novel linear array transducer. In this configuration, both back-side and front-side structures were employed in an identical array transducer, and PZT-5H and PMN-PT were used for inversion layers. By using FEM (finite element method) simulation, the performance of back-side, front-side, and simultaneous activation were demonstrated and compared with each other.

Statement of Contribution/Methods

A 5.5 MHz linear array transducer with 2-2 composite was designed by using PZFlex tool based on FEM analysis. A single element was sub-diced and each part was assigned to back-side and front-side inversion structure. The element pitch was 300 μm, the kerf size was 25 μm, the elevation length was 6 mm, and total thickness of element was 340 μm. Because the ratio of inversion layer was 0.3, the thicknesses of inverted layer and uninverted layer were 102 μm and 238 μm, respectively. Through optimization, the widths of sub-diced elements for back-side and front-side were 75 μm and 175 μm, respectively. Two matching layers with $1.5f_0$ thickness and a 5.9 MRayl backing layer were used, and a flexible PCB was added at the bottom of composite.

Results/Discussion

Figure 1 shows the schematic diagram and the pulse-echo responses of the proposed method. In the case of back-side inversion, the first resonant peak had 5.6 MHz frequency and 36% -6 dB bandwidth of 36%. The second resonant peak has 10.9 MHz frequency and 39% -6 dB bandwidth. In the case of front side inversion, the center frequency was 7.2 MHz and -6 dB bandwidth was 63%. For simultaneous activation of front- and back-side inversion layers, a center frequency was 7.7 MHz and a -6 dB bandwidth was 75%. To obtain $1.5f_0$ center frequency, the thickness of piezoelectric material was 340 μm much thicker than normal case. Thus, the inversion layer method can be applied to the array transducer especially for ultrasound harmonic imaging.
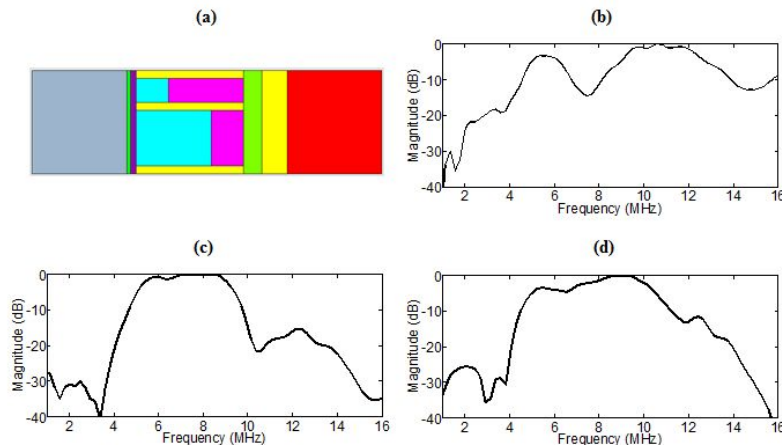
Figure 1. (a) Schematic diagram of the proposed ultrasound transducer, (b) pulse-echo response of back side inversion layer, (c) pulse-echo response of front side inversion layer, (d) pulse-echo response of simultaneous activation of back and front side inversion layers.

P5C2-8 _____

8:00 am   Non-Elevation-Focused Probe (NEFP) Designed for Pure Plane-wave Ultrasound Imaging

Congzhi Wang[1], Ning Guo[1], Yang Xiao[1], Weibao Qiu[1], Hairong Zheng[1]; *[1]Shenzhen Institutes of Advanced Technology, Chinese Academy of Sciences, China, People's Republic of*

Background, Motivation and Objective

Plane-wave ultrasound imaging has been widely used in many frontier research areas in medical ultrasound due to its ultra-high frame rate. To improve its image quality, many novel beamforming methods have been proposed and in-depth studied, such as coherent compounding method and methods based on compressive sensing. However, the influence of the structure and working mode of the ultrasound probe on the image′s lateral resolution and contrast is still rarely studied. Convenient ultrasound probe is always self-focused with an acoustic len in the elevation direction, and thus the acoustic energy distributed in the y-z plane is not uniform. We hypothesized that, if the probe is not focused in the elevation direction, the quality of the image obtained with a kind of ″pure plane-wave″ will be increased.

Statement of Contribution/Methods

To verify our hypothesis, the non-elevation-focused probe (NEFP) was fabricated, and the plane-wave ultrasound images obtained with NEFP were compared with those obtained with the traditional elevation-focused probe (EFP). The experiments were conducted with a ultrasound driven/acquire system (V1, Verasonics, USA) and a general purpose ultrasound imaging phantom (model 525, Dansk Fantom Service, Denmark). Both the NEFP and EFP probes were linear array with 128 elements and the centre frequency is 7.5 MHz. The sampling frequency is 60 MHz and the speed of sound is 1540 m/s. The dynamic range of image displaying is 50 dB.

Results/Discussion

The two images were obtained with coherent compounding method by 9 plane-wave images, as shown in Figure 1(a)(b). The image obtained using NEFP visually has a higher contrast than the one obtained using EFP in the near field. In addition, the image pixels in the x direction were extracted from these images at two depths: 11.6 mm and 89.3 mm, and the lines were plots for a comparison, as shown in Figure 1(c). It is shown that, in both near and far field, the contrast of NEFP image are both a little better than the EFP image, however, the difference of their lateral resolution is unapparent. The results of this study indicates that, the NEFP probe is actually better than EFP probe in some respects, and this may provide us an additional way to enhance the image quality of plane-wave ultrasound imaging technique.

SATURDAY POSTER

(a) EFP   (b) NEFP   (c) Pixels amplitude at different depths
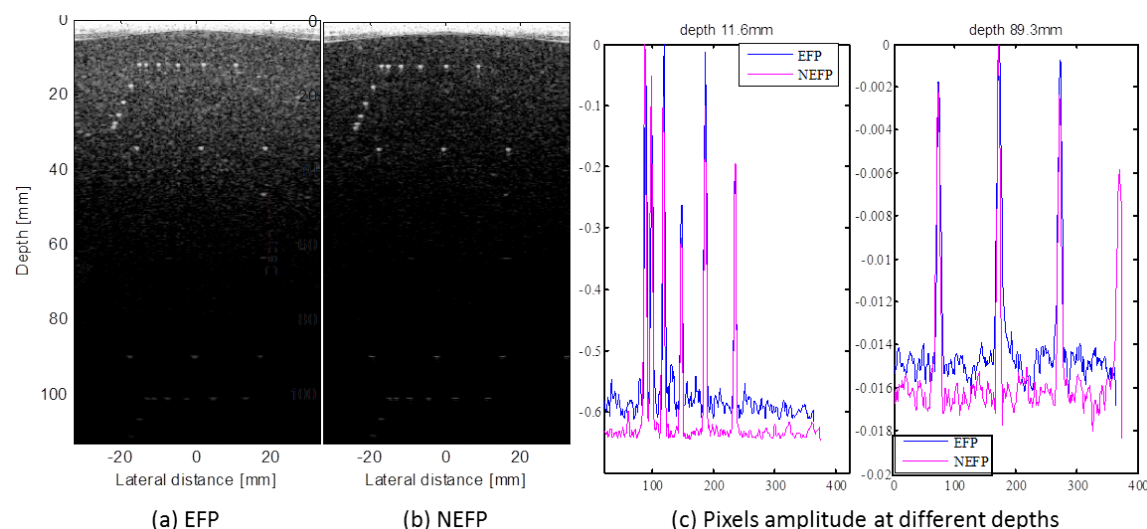
P5C2-9

8:00 am   **An Integrated Convex Ultrasound Endoscope for Digestive Tract Imaging**

Jue PENG[1,2], Zhifei Qin[1,2], Xiaojian PENG[1,2], Tianfu WANG[1,2], Siping CHEN[1,2]; *[1]Department of Biomedical Engineering, School of Medicine, Shenzhen University, National-Regional Key Technology Engineering Laboratory for Medical Ultrasound, Shenzhen, China, People's Republic of, [2]Department of Biomedical Engineering, School of Medicine, Shenzhen University, Guangdong Key Laboratory for Biomedical Measurements and Ultrasound Imaging, Shenzhen, China, People's Republic of*

Background, Motivation and Objective

Endoscopic ultrasound (EUS) is a procedure used to diagnose disorder and stage cancers of the gastrointestinal tract and of nearby organs such as the pancreas, bile ducts, and gallbladder. Although there has been commercial success in the development of electronic echoscope, the present camera in the EUS has no auto-focusing function. It is not convenient for physicians to adjust the focus field and evaluate the region of interest through the whole operation procedure. In this paper, a EUS probe integrating an 8 MHz electrical scanning transducer with a 3D focusing camera module of 5 million pixels is presented. By this means we improve the focus capacities at the short range, so that the image of distortion is minimized and the contrast of the vessel wall and mucosal surfaces is enhanced.

Statement of Contribution/Methods

In this study, we design and fabricate an integrated electronic convex ultrasound endoscope probe operating at centre frequency 8MHz, with 64 elements and the external diameter less than 6.5 mm for digestive tract ultrasound imaging. A curvilinear ultrasound transducer based on PZT ceramic, leaning and facing on one side provides a 180 degree scanning ultrasound view. An auto-focus 5 Mega Pixels CMOS camera module, mounted and leaned at 45 degree angle, provides a 75 degree field of vision. A novel voice coil motor (VCM) for lens focus adjustments is employed. This device not only can change the focus position of the lens but also can adjust the tilting angle of the lens in order to extend the depth of field (DOF). With this new technology, we can evidently improve the image quality of the endoscope.

Results/Discussion

A schematic of an integrated EUS is shown in figure 1. A curvilinear ultrasound transducer based on PZT ceramic, leaning and facing on one side provides a 180 degree scanning ultrasound view. A CMOS camera module, mounted and leaned at 45 degree angle, provides a 75 degree field of vision. The external diameter is designed as 8 mm. Figure 2 shows the actual pulse-echo measurement results of a randomly selected element from the convex ultrasound array. The results show that the BW @-6dB is 83 % at the frequency of 7.88 MHz. The insertion loss close to -42dB was obtained at the average central frequency. A cross talk of less than -36 dB is achieved for the adjacent columns at centre frequency, which ensures a desirable imaging resolution of the EUS.
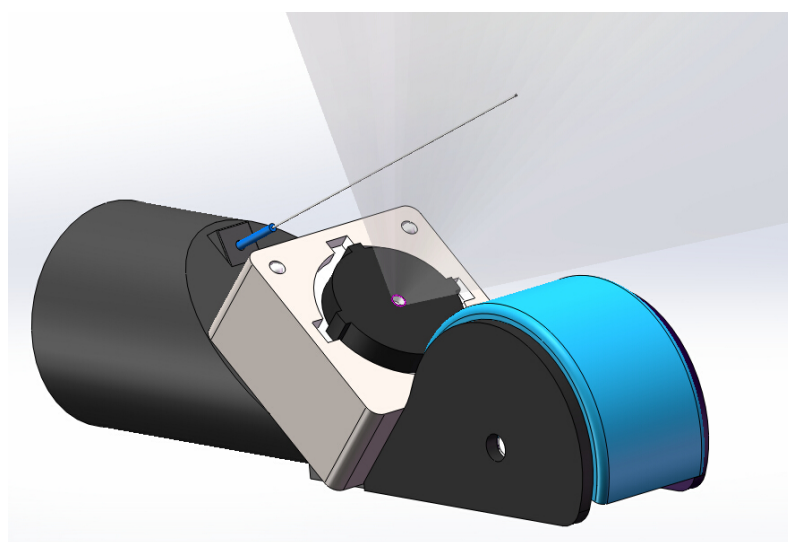
P5C2-10 _____

8:00 am **Fabrication and Performance of a Micro 50-MHz IVUS Transducer Based on a 1-3 Composite with Geometric Focusing**

Xiaohua Jian[1], Zhile Han[1], Weiwei Shao[1], Zhangjian Li[1], Yaoyao Cui[1]; *[1]Suzhou Institute of Biomedical Engineering and Technology, CAS, Suzhou, China, People's Republic of*

Background, Motivation and Objective

Intravascular Ultrasound (IVUS) allows us to see a coronary artery from the inside-out, which has evolved to an important research tool of modern invasive cardiology. In order to get high resolution image, an IVUS transducer usually has a high center frequency (20~50 MHZ). A considerable drawback to current IVUS transducer is that their lateral imaging resolution (200~300 μm) is much lower than their axial resolution (80~100 μm). This is mainly caused by its small dimension, which is extremely limited by the blood vessel. For improving the lateral resolution, a possible method is to make the generated ultrasound wave focusing. A traditional method is to add an acoustic lens, but fabricating a suitable acoustic lens to focus the ultrasound in IVUS imaging is particularly challenging since the IVUS transducer outer diameter is limited (3~9 F), and the focusing length should be small (<10 mm). We have avoided these issues by fabricating a high-frequency flexible 1-3 piezo-composite material. This allows the active transducer to be focused by simply geometrically curving the piezo-composite.

Statement of Contribution/Methods

The first step in the fabrication procedure was to make a high-frequency 1-3 piezo-composite. A grid pattern was diced into a ceramic PZT-5H using a 12 μm blade and a pitch of 60 um. The cuts were then filled with epoxy, and following curing. Then a second set of cuts was made through the center of the PZT pillars to create a composite pattern with 18um pillars and 12 μm kerfs. The composite was filled with epoxy again, and then lapped to the finished thickness of 33 μm. After that, it was electroded by sputtering a chrome/gold layer of 200 Å in thickness. The composite was then mounted on a 5 mm radius PTFE ball as curving jig using wax. Conductive epoxy E-SOLDER 3022 was applied on the composite as the backing material in a PDMS mold. After curing, the composite was heated to remove the PTFE curving ball, and diced in to the size of 0.6 × 0.6 mm. Then the individual piece was placed in a catheter housing, and the center core and mesh wire of a coaxial wire were connected to the piezo-composite upper surface and backing layer respectively with silver conductive. At last, a 9 μm Parylene C layer was coated as its matching layer.

Results/Discussion

The electrical impedance of this transducer was measured with an impedance analyzer E4991A. The measured center frequency is about 52.76 MHz, and its electromechanical coupling coefficient is 0.70. Its acoustic distribution was measured by a 3D scanning tanks UMS III with a 0.2 mm diameter hydrophone. The measured focal length along axial direction is about 5 mm, the diameter of the focal point in the focal plane is about 120 μm. The imaging resolution is tested by imaging a serial of interval distribution tungsten line targets with our homemade IVUS system. According to the results, its axial resolution is 80 μm, and lateral resolution is about 150 μm, which effectively improved the lateral resolution of current IVUS system.

P5C2-11 _____

8:00 am **Evaluation of piezo composite based omnidirectional single fibre transducers for 3D USCT**

Michael Zapf[1], Kai Hohlfeld[2], Gourav Shah[1], Sylvia Gebhardt[3], Hartmut Gemmeke[1], Alexander Michaelis[2,3], Nicole V. Ruiter[1]; *[1]Institute for Data Processing and Electronics, Karlsruhe Institute of Technology, Eggenstein-Leopoldshafen, Germany, [2]Institute of Materials Science, TU Dresden, Dresden, Germany, [3]IKTS, Fraunhofer Institute, Dresden, Germany*

Background, Motivation and Objective

At KIT a 3D Ultrasound Computer Tomography (USCT) medical imaging system for early detection of breast cancer is under development. The system is optimized for imaging using Synthetic Aperture Focusing Technique (SAFT) and has therefore a multistatic setup of 2041 ultrasound transducers with approx. 1MHz 3dB bandwidth and 36° 3dB opening angle for 2.5MHz. The USCT groups transducers in a semi-elliposoidal aperture surrounding a ROI of 10x10x10cm³. To increase the ROI for a next USCT generation, the opening angle of a future transducer design should be increased to approx. 60° while other characteristics should be preserved or even improved.

Statement of Contribution/Methods

The fundamental connection between an ultrasound transducer's emission and reception sensitivity in the azimuth and elevation angle space is the tranducer's aperture size. Simulations showed that approx. half the side length of current generation transducer is required. A circular instead of the current rectangular aperture would result in additional homogenicity.

The established piezo-fibre composite technology can provide circular fibres of required dimensions.

In this work a transducer design is presented which utilizes individual and reproducible dimensioned piezo fibres. The fibres were fabricated from PZT powder using the polysulfone spinning process. 13 fibres were positioned with a mechanical mask and filled with a matrix of epoxy, curing to a rod of 18cm length and 2.3cm diameter. From this rod piezo composite discs were sawed, defining the main resonance frequency by thickness, and then uniformly polarized. Electrical connectivity was achieved with manually wiring via heat curing glue on top and bottom printed circuits. A transducer array was finalized in a cylincrical housing by filling with PU backing material.

Results/Discussion

The electrical performance was evaluated with a phase-impedance analysator for all piezo fibres. Ultrasound characteristics were evaluated quantitatively with a hydrophone in a 3-axis water tank for selected sample transducers.

The presented approach fullfilled the expectation of repoducible positioned transducer arrays, regarding disc thickness and fibres position and size. The fibres' diameters varied ±10μm (approx. 5%), the achieved mean thickness varied by 1.08% standard deviation. The transducers' opening angles were in the expected range, absolute sound pressure was lower (down to 25.9%), bandwith and center frequency were preserved. As expected, the manual bonding process was unreliable and requires future adaption. Most interestingly and to our surprise, the aimed for characteristic of very similar electrical and ultrasound performance of the individual fibres did not materialize, they exposed a great variability. This previously unnoticed effect couldn't been tracked back to polarization or bonding process and is currently unexplained. Therefore this will be further analyzed in a future work.

P5C2-12 _____

8:00 am **Quantifying the effect of dicing on element vibration in ultrasound transducers**

Jovana Janjic[1], Maysam Shabanimotlagh[2], Martin D. Verweij[1,2], Nico de Jong[1,2], Gijs van Soest[1], Antonius F.W. van der Steen[1,2]; *[1]Dept. of Biomedical Engineering, Erasmus MC, Rotterdam, Netherlands, [2]Lab. of Acoustical Wavefield Imaging, Delft University of Technology, Delft, Netherlands*

Background, Motivation and Objective

In ultrasound imaging, one of the challenges of transducer design is to maximize the acoustic energy that is radiated into the medium, which is important for obtaining a high signal-to-noise ratio. The acoustic coupling between a vibrating transducer and the medium is described by the acoustic radiation impedance, which is defined as the complex average pressure amplitude divided by the normal particle velocity amplitude [1]. Subdicing the elements of an ultrasound transducer and extending kerfs into the backing affect the element vibration and thus the acoustic radiation impedance and the output pressure. In this work 2D FEM (PZFlex) simulations are considered and compared to the analytical expression of the radiation impedance for a 2D strip in a rigid baffle.

Statement of Contribution/Methods

The model geometry used in PZFlex is shown in Fig.1a. For all the simulations the frequency of the excitation is constant while the width a of the strip is varying and all the results are plotted relative to ka, with $k=2\pi/\lambda$.

SATURDAY POSTER

The radiation impedance for subdiced and non-subdiced elements is computed from PZFlex simulations by considering the amplitudes of the time varying pressure and velocity at the top surface of the PZT element. In Fig.1b the radiation impedance obtained from PZFlex simulations is compared to the numerical solution (Matlab) computed from the Rayleigh integral [2] that assumes piston-like motion of the elements.

Dicing into the backing is also simulated in PZFlex for an isolated element and the output pressure obtained at the surface of the element is compared for different cutting depths and plotted in Fig.1c, where the cut depth is expressed as the percentage of the PZT thickness.

Results/Discussion

In Fig.1b, for *ka*<3, simulation results are in good agreement with the analytical result, showing that the radiation efficiency drops very quickly for elements width smaller than ½λ. On the other hand, large elements may also radiate less efficiently because of the excitation of spurious modes, leading to reduced radiation impedance. Subdicing improves the radiation impedance up to 40% (at *ka*=6).

The depth of the cut in the backing also affects the output pressure at the front of the transducer. For *ka*>1, an appropriate cut depth may lead to a pressure increase of approximately 10%, while for *ka*<1 the increase can be as high as 30%.
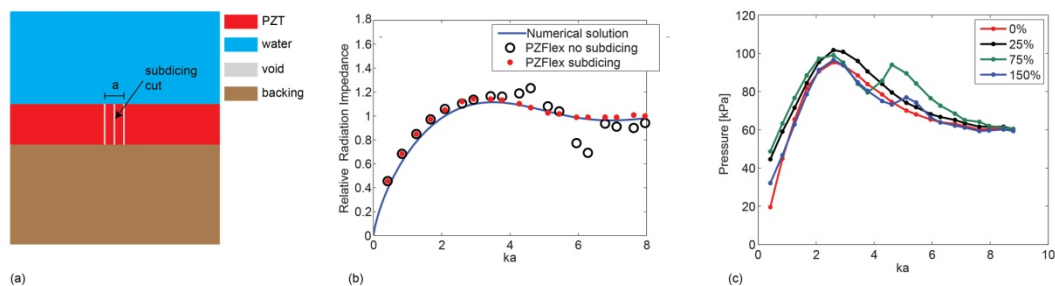
Figure 1. (a) PZFlex 2D model: PZT is 75µm thick and the width *a* varies from 5µm to 95µm with a step of 5µm. (b) Acoustic radiation impedance normalized to water impedance from numerical computation and PZFlex simulations for subdiced and non subdiced element. (c) Effect of cutting into the backing on output pressure.

[1]   D. Blackstock, Fundamentals of Physical Acoustics. Hoboken NJ USA: Wiley-InterScience, 2000, pp 43-44.
[2]   Verweij M.D., Treeby B.E., van Dongen K.W.A. and Demi L. , "Simulation of Ultrasound Fields".
      In: Brahme A. (Editor in Chief.) Comprehensive Biomedical Physics. vol. 2, Amsterdam: Elsevier, 2014, pp. 465-500.

P5C3 - Transducers for Therapy

4th floor

Saturday, October 24, 2015, Posters displayed 08:00 am - 05:00 pm. Authors must be present at their poster from 9:30 - 10:30am (odd number posters) and 14:30 – 15:30pm (even number posters).

Chair: **Christine Démoré**
University of Dundee

P5C3-1 _____

8:00 am **Design and fabrication of a novel three-row dual frequency ultrasound transducer for image-guided drug delivery**

Min Su[1], Shu Xue[1], Yongchuan Li[1], Lili Niu[1], Weibao Qiu[1], Yang Xiao[1], Congzhi Wang[1], Hairong Zheng[1], **Ming Qian[1]**; *[1]Shenzhen Institutes of Advanced Technology, Chinese Academy of Sciences, China, People's Republic of*

Background, Motivation and Objective

Currently, the major treating methods for malignant tumors are radiation treatment and chemo-treatment. It should be noted that there are huge side effects to the human body during the treating process. If there is a way to deliver the drugs to where the disease locates, the regional drug concentration could be greatly enhanced and the side effects could be greatly eliminated. The ultrasound waves can be used for both imaging and acoustic manipulation. Small objects such as particles or microbubbles can be manipulated and moved using the acoustic radiation force effect, and this kind of particle transportation can be guided by ultrasonic imaging at the same time. In this sense, ultrasound is a good tool for image-guided localized drug delivery.

Statement of Contribution/Methods

In this study, a novel three-row dual frequency ultrasound transducer was designed and fabricated for image-guided drug delivery. The middle row was a 128-element linear array and was designed to work at 5.5 MHz, which was used for ultrasonic imaging. The outer two rows were 64-element linear arrays and were designed to work at 1.5 MHz, which is used for generating acoustic radiation force. All the linear arrays were fabricated using 1-3 piezoelectric composite. As shown in Figure A, the outer rows were assembled at an angle of 8.75° so as to focus at a focal depth of 40 mm. Also, the middle row was designed to focus at 40 mm. The pulse echo waveform and the frequency spectrum of the middle and outer rows were tested and plotted.

Results/Discussion

The three rows were assembled in a mould and fixed using epoxy, as shown in Figure B. The completed three-row dual frequency transducer was shown in Figure C. The pulse echo response was acquired using a polished steel reflector placed in a tank of deionized water positioned at the array elevation focal point. A Panametrics 5800 pulser (Olympus) was used to excite array elements individually, and the receiver on the same unit was used to amplify the echoes before displaying them on a digital oscilloscope (Tektronix DPO 4104). The pulse-echo waveform (blue line) and spectrum (black line) of a typical element of the middle row, as shown in Figure D, had a center frequency of 5.5 MHz and a -6dB bandwidth of 79.2%. The response of a typical element of the outer row, as shown in Figure E, had a center frequency of 1.4 MHz and a -6dB bandwidth of 50.2%. Related experiments will be performed later.
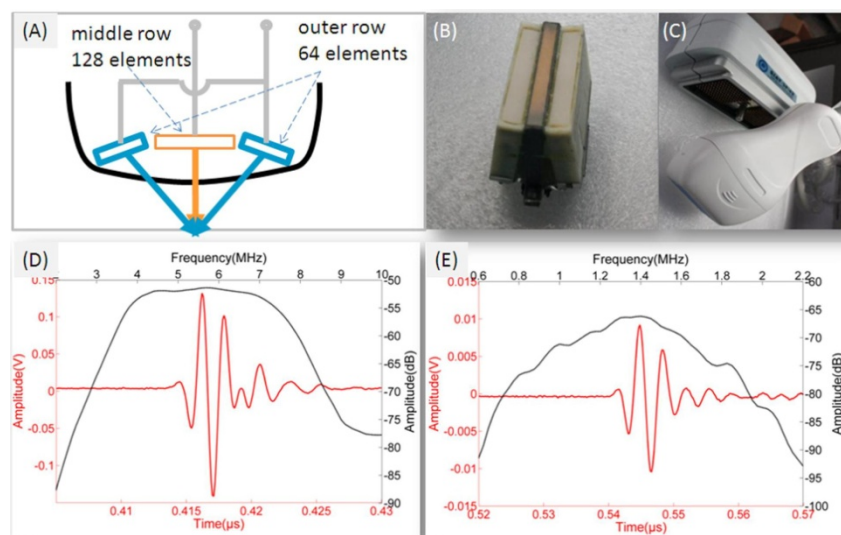
P5C3-2 _____

8:00 am **Sparse spherical HIFU arrays based on Fermat's Spiral**

Mario Ries[1], Martijn de Greef[1], **Pascal Ramaekers[1]**, Chrit Moonen[1]; *[1]Imaging Division, University Medical Center Utrecht, Netherlands*

Background, Motivation and Objective

Phased array High-Intensity Focused Ultrasound (HIFU) transducer systems in form of a spherical cap, which combine electronic and geometric focusing capabilities, have been proposed as early as 1991 by Ebbini et al. The design results in a good on-axis performance, while keeping even for large apertures the required amount of independent RF-channels low. Unfavorable is the occurrence of undesired grating lobes and secondary maxima in the focal plane and the rapid degradation of the focus quality off-axis. Most subsequent designs use a pseudo-random (PR, left img) element arrangement, improving the focus quality both on- and off-axis. However, numerical optimization of the element placement for PR-arrays is generally computationally expensive. Here, we evaluate by simulation the acoustic performance of a phased array element placement in which the azimuthal angle of every element is an integer multiple of the golden angle, whereas their polar angle follows from the algebraic angle – radius relation for Fermat's spiral. Subsequently, we investigate if additional Voronoi tiling allows increasing the active surface of the array, while maintaining the on-axis and off-axis focal point quality.

SATURDAY POSTER

Statement of Contribution/Methods

We evaluated a sparse spherical array (140 mm curvature, 140mm aperture) with an element arrangement according to the generating function of Fermat's spiral in 3D (FS design, center img) and a second derived design with additional Voronoi tiling (VTFS design, right img). The VTFS increases the active surface, while maintaining the favorable properties of the FS (no symmetries). Both designs were compared with two commercial PR-arrays (Philips Sonalleve V1 and V2). The acoustic simulations are based on direct integration of the Rayleigh-Sommerfeld integral in a reference plane and subsequent propagation of the angular spectrum of plane waves, and evaluated the focal point pressure both for on-axis and off-axis sonications.

Results/Discussion

The FS-design shows a comparable performance to the pseudo-random designs, however, optimal element positioning follows algebraically for any combination of transducer aperture and element number, greatly simplifying the design process. The VTFS design improves the pressure in the focus at a given acoustic power by 14%, while maintaining off-axis focal point quality and steering range of the FS-design.

Phased array HIFU transducer with sparse pseudo-random element arrangement

Phased Array with element placement according to Fermat's Spiral

Phased Array combing Fermat's Spiral pattern with additional Voronoi tiling

---
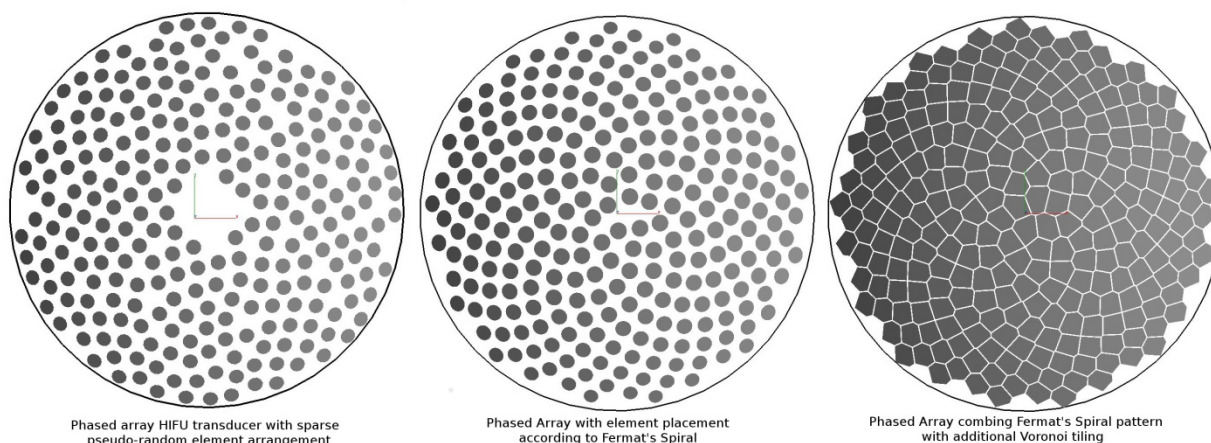
P5C3-3

8:00 am   **Study of Ultrasound Transducer Which Produces Second Harmonic Superimposed Signal**

Zulfadhli Zaini[1], Hayato Jimbo[1], Ryo Takagi[1], Shin Yoshizawa[1], Shin-ichiro Umemura[1]; *[1]Tohoku University, Japan*

Background, Motivation and Objective

Superimposing the second harmonic to fundamental is an approach to efficiently form cavitation bubbles which expedite the treatment with high intensity focused ultrasound (HIFU). However, an air-backed transducer in conventional design is not suitable to generate the second harmonic and fundamental at the same time. In this study, we propose a heavy matching layer approach to solve this problem. We further propose a double matching layer design with an additional lighter layer, to foresee the possibility to increase the performance of the heavy matching layer transducer.

Statement of Contribution/Methods

A finite element code (PZflex) was used to numerically analyze the transducer in the proposed design. A prototype transducer (Imasonic) was fabricated based on one of the designs and its performance was measured and compared with simulation. For the heavy matching layer, an acoustic impedance much closer to that of piezocomposite than the conventional design was chosen. The numerical model had only one piezoceramic pillar surrounded by polymer material with mirror boundary condition on all the four lateral sides, This way, a transducer with infinitely large lateral size can be simulated in a very short computation time.

Results/Discussion

Figure 1 illustrates the simulation result of transducers with a single heavy matching layer, a double matching layer, and a conventional matching layer. The result shows that the heavy matching layer transducer can produce both the second harmonic and fundamental acoustic pressure at a high efficiency for the same drive voltage, while the conventional transducer cannot. It also shows that slight improvement in the bandwidth is expected with the double matching layer over the single heavy matching layer. Figure 2 compares the measured efficiency of the prototype transducer to the simulation result with the single heavy matching layer. The overall agreement demonstrates the validity of the numerical simulation.

Session Chairs

Addison, Robert 5B
Aigner, Robert... 7D
Arnold, Walter 5L, P2B2
Bernassau, Anne P3B1, P3B2
Bosch, Hans 4D
Bouakaz, Ayache 1C, 3B
Bridal, Lori................................... P1B2, P1B6
Byram, Brett... P1A1
Chapelon, Jean-Yves......................................4I
Chow, Yi-Hong 1E
Cochran, Sandy 8C
Cowell, David 8E
Dahl, Jeremy 4C
Dai, Jidong 7C
de Jong, Nico 2D
de Korte, Chris 2E
Degertekin, Levent................................8B
Démoré, Christine P5C1, P5C2, P5C3
D'hooge, Jan.. 2G
Ebbini, Emad 3E, 3K
Emelianov, Stas..1B
Ferrara, Katherine 4H
Fink, Michael...................................P5B1, P5B2
Friend, James 5K
Gallippi, Caterina 3G
Garcia, Damien 2C
Greve, David..................................5D, P2C1
Hall, Timothy.. 3H
Hansen, Hendrik P1B1
Harley, Joel P2A2
Hashimoto, Ken-ya 7B
Hemmsen, Martin......................................P1A6
Hladky, Anne-Christine 8G

Hossack, John 4G, P1B5
Hynynen, Kullervo 3C
Jensen, Jørgen..............................4E, P1B7
Jiang, Xiaoning..8K
Kanai, Hiroshi..P1C1
Kessler, Lawrence 5C
Ketterling, Jeff 5I
Khuri-Yakub, Pierre 5H, P2C3
Kolios, Michael 2J
Konofagou, Elisa 3F
Kudo, Nobuki P1C5
Kuypers, Jan 7E
Lal, Amit 6A
Larson, John 6D, P3C1, P3C2, P3C3
Laude, Vincent 6G
Laugier, Pascal 1I
Li, Meng-Lin P1A4
Liebgott, Herve...2H
Lopata, Richard P1B3, P1B4
Løvstakken, Lasse 2I, P1A7
Mamou, Jonathan..P1A2
Matsukawa, Mami P1C6
Matula, Tom 4J
Mayer, Andreas 6E
Miller, James G..3J
Mischi, Massimo 4K, P1B8
Mulvana, Helen 2A, P1A5
Nakamura, Kentaro...........................5F, P2C2
Naumenko, Natalya P4B2
Nightingale, Kathy...1D
Nikolov, Svetoslav.................................1H, 4F
Nowicki, Andrzej....................................P1C7
O'Donnell, Matthew......................................2K

Oelze, Michael 1G
Oralkan, Omer..8F
Oruklu, Erdal................................ P2A3, P2B1
Palmeri, Mark...3I
Pereira da Cunha, Mauricio......................P4A1
Pitschi, Maximilian P4A2
Ren, Wei 8J
Saniie, Jafar 5E
Schafer, Mark 8A
Schmitz, Georg..3D
Smith, Scott..8H
Takeuchi, Yasuhito.............. P5A1, P5A2, P5A3
Tanaka, Shuji 7A
Tanter, Mickael 2B
Thomenius, Kai P1C3
Tortoli, Piero 1F, 3A
Trahey, Gregg P1A3
Tsujino, Jiromaru 5A, P2A1
van der Steen, Ton.................................1A, 4B
Van Dongen, Koen W.A. 6C
Wagner, Karl......................................P4B1
Wan, Mingxi P1C4
Weihnacht, Manfred.....................................2F
Wu, Tsung-Tsong....................................... 6B
Yen, Jesse 4A
Yong, Yook-Kong P3A1
Yu, Alfred C. H..1J, 1K
Yuan, Jian 8I
Zheng, Hairong P1C2
Zhgoon, Sergei P4A3
Zhou, Qifa..8D, P

Author Index